



Palm Beach, Florida PALM BEACH CONVENTION CENTER

ABSTRACT

As of October 27, 2025





TU: TUTORIAL: 2D MAGNETS – FUNDAMENTALS AND EMERGING FRONTIERS

Chair(s): A. Manchon, *Aix-Marseille University, Marseille,*France

Monday, October 27, 2025

02:30 PM-05:00 PM

Grand Ballroom

TU-01. 2D Magnetic Heterostructures – Skyrmions and Their Applications

Y. Wu

Electrical and Computer Engineering, University of Florida, Gainesville, Florida, United States

This talk will survey the rapidly advancing field of two-dimensional (2D) quantum materials [1-3], with emphasis on emergent magnetism and skyrmion-based phenomena. I will introduce the key principles of magnetism in reduced dimensions—spin interactions, anisotropy, topology, and ordering—and outline experimental and theoretical methods to probe 2D skyrmions, including spectroscopy, microscopy, and multiscale modeling. Breakthroughs in van der Waals magnets such as CrI3, Fe3GeTe2 [4,5], and Fe3GaTe2 will be highlighted, together with opportunities in heterostructures that couple magnetism with superconductivity, spin—orbit interactions, and other correlated states.

I will then explore how skyrmions and related topological textures open pathways for novel device concepts in spintronics, neuromorphic computing [6,7], and quantum technology [8]. Special attention will be given to frontiers such as room-temperature stabilization, electric [9] or optical control, and integration with other quantum platforms [8]. The talk will conclude with a forward-looking perspective on open challenges and prospects for transformative applications in information technology and energy-efficient devices.

- [1] Wang, K.L., Wu, Y., Eckberg, C., Yin, G. and Pan, Q., 2020. Topological quantum materials. *MRS Bulletin*, *45*(5), pp.373-379.
- [2] Zhong, H., Plummer, D.Z., Lu, P., Li, Y., Leger, P.A. and Wu, Y., 2025. Integrating 2D magnets for quantum devices: from materials and characterization to future technology. *Materials for Quantum Technology*, *5*(1), p.012001.
- [3] Zhang, B., Lu, P., Tabrizian, R., Feng, P.X.L. and Wu, Y., 2024. 2D magnetic heterostructures: Spintronics and quantum future. *npj Spintronics*, *2*(1), p.6.

[4] Wu, Y., Zhang, S., Zhang, J., Wang, W., Zhu, Y.L., Hu, J., Yin, G., Wong, K., Fang, C., Wan, C. and Han, X., 2020. Néeltype skyrmion in WTe2/Fe3GeTe2 van der Waals heterostructure. *Nature communications*, *11*(1), p.3860. [5] Wu, Y., Francisco, B., Chen, Z., Wang, W., Zhang, Y., Wan, C., Han, X., Chi, H., Hou, Y., Lodesani, A. and Yin, G., 2022. A van der Waals interface hosting two groups of magnetic skyrmions. *Advanced Materials*, *34*(16), p.2110583. [6] Plummer, D.Z., D'Alessandro, E., Burrowes, A., Fleischer, J., Heard, A.M. and Wu, Y., 2025. 2D Spintronics for Neuromorphic Computing with Scalability and Energy Efficiency. *Journal of Low Power Electronics and Applications*, *15*(2), p.16.

[7] Sosa, L., Wi, M., Barrera, M., Nasrullah, I., Wu, Y., 2025. Simulating pattern recognition using non-volatile synapses: MRAM, ferroelectrics and magnetic skyrmions. *Journal of Magnetism and Magnetic Materials, 630*, p. 173353.
[8] Wu, Y., Balicas, L., Cheng, R. and Zhang, X.X., 2025. Spin excitations and dynamics in 2D magnets: An overview of magnons and magnetic skyrmions. *Progress in Quantum Electronics, 100-101*, p.100564.

[9] Wu, Y., Sofer, Z., Karuppasamy, M. and Wang, W., 2025. Room-temperature ferroelectric control of 2D layered magnetism. *IEEE Transactions on Magnetics*, *61*(4), p. 2500105.

TU-02. 2D van der Waals Magnets: From Fundamental Physics to Applications

J. Park

Seoul National University, Seoul, Korea (the Republic of)

The discovery of magnetism in atomically thin materials has opened an entirely new chapter in the study of low-dimensional quantum matter. Since the first reports of antiferromagnetic van der Waals magnets (FePS3, MnPS3, NiPS3) in 2016, followed by the discovery of ferromagnetic counterparts (Cr2Ge2Te6 and CrI3) in 2017, the field has evolved into one of the most vibrant areas of condensed matter physics. In this talk, I will give a comprehensive overview of the key developments in the field of 2D vdW magnetism, drawing from my recent review [1].

I will begin with the historical and theoretical context, explaining why 2D magnetism was once thought to be impossible, and how recent materials have overcome these constraints [2]. I will then discuss the rapidly expanding family of van der Waals magnets, their underlying spin Hamiltonians, and experimental platforms for probing

magnetic excitations, chirality, and phase transitions. The talk will also highlight surprising phenomena such as magnetic excitons, Floquet-engineered states, and light-induced metastable phases.

To coordinate with the other talks, I will focus mostly on antiferromagnetic van der Waals magnets, unless necessary.

- [1] Je-Geun Park et al., submitted to Rev. Mod. Phys.: https://arxiv.org/abs/2505.02355
- [2] https://sites.google.com/view/vdw-magnetism-origin

TU-03. Epitaxial Growth, Spin-Orbit Torque, and Magnetization Dynamics in 2D Magnets

R. Kawakami

Department of Physics, The Ohio State University, Columbus, Ohio, United States

In the tutorial, I will discuss two interesting aspects of 2D magnets, namely epitaxial growth and magnetization dynamics. First, I will review some of the recent developments in the growth of 2D magnets and related studies of spin-orbit torque based magnetization switching. Together, these can form the basis of a scalable, energy efficient, non-volatile magnetic memory. Second, I will discuss magnetization dynamics in ferromagnet CrGeTe₃ and layered antiferromagnet CrSBr, which both show relatively low damping and precessional dynamics. These dynamics have been investigated using resonance methods as well as time-resolved, optical pump-probe methods. For the tutorial, I will go over the Landau-Lifshitz-Gilbert equations for magnetization dynamics and describe both the ferromagnetic resonance and antiferromagnetic resonance modes. Time-resolved magneto-optic Kerr effect provides a general method for investigating magnetization dynamics. In addition, the magnon-exciton coupling in CrSBr allows one to use a simpler time-resolved reflectivity measurement to probe such dynamics.

SESSION AA: SPIN-OPTOELECTRONICS TOWARDS REAL WORLD APPLICATIONS

Chair(s): Y. Lu, *Institut Jean Lamour, Nancy, France*Tuesday, October 28, 2025
08:30 AM-12:00 PM
Grand Ballroom

AA-01. Controlling the helicity of light by electrical magnetization switching in Spin Light Emitting Diodes

P. Renucci^{1,7}, A. Dainone², N. Figueiredo-Prestes³, M. Morassi⁴, X. Devaux², M. Lindemann⁵, J. George³, H. Jaffrès³, A. Lemaitre⁴, B. Xu^{6,7}, M. Stoffel², L. Lombez¹, D. Lagarde¹, G. Cong¹⁰, T. Ma¹¹, M. Vergnat², X. Marie¹, X. Han⁸, S. Mangin², J. Rojas-Sanchez², J. Wang⁹, M. C. Beard¹², N. Gerhardt⁵, I. Zutic¹³, Y. Lu²

¹Université de Toulouse, INSA-CNRS-UPS, LPCNO, Toulouse, France, ²Institut Jean Lamour, Université de Lorraine, CNRS, UMR 7198, Nancy, Nancy, France, ³Laboratoire Albert Fert, CNRS, Thales, Université Paris-Saclay, Palaiseau, France, ⁴Université Paris-Saclay, CNRS, Centre de Nanosciences et de Nanotechnologies, Palaiseau, France, ⁵Photonics and Terahertz Technology, Ruhr-Universität Bochum, Bochum, France, ⁶Key Laboratory of Semiconductor Materials Science, Institute of Semiconductors, Chinese Academy of Sciences, Beijing, China, ⁷College of Materials Science and Opto-Electronic Technology, University of Chinese Academy of Sciences, Beijing, China, 8Beijing National Laboratory for Condensed Matter Physics, Institute of Physics, University of Chinese Academy of Sciences, Chinese Academy of Sciences, Beijing, China, ⁹Department of Electrical and Computer Engineering, University of Minnesota, Minneapolis, Minnesota, United States, ¹⁰Platform Photonics Research Center, National Institute of Advanced Industrial Science and Technology, Tsukuba, Japan, ¹¹Beijing National Laboratory for Condensed Matter Physics, Institute of Physics, University of Chinese Academy of Sciences, Chinese Academy of Sciences, Beijing, China, ¹²Chemistry and Nanoscience Center, National Renewable Energy Laboratory, Golden, Colorado, United States, ¹³Department of Physics, University at Buffalo, State University of New York, Buffalo, New York, New York, United States

The control of emitted light intensity and charge currents in semiconductor materials is the basis for information transfer and processing. In parallel, the writing and robust storage of information is made possible by magnetic memories, which are implemented using the spin and associated magnetization in ferromagnetic materials. The present work

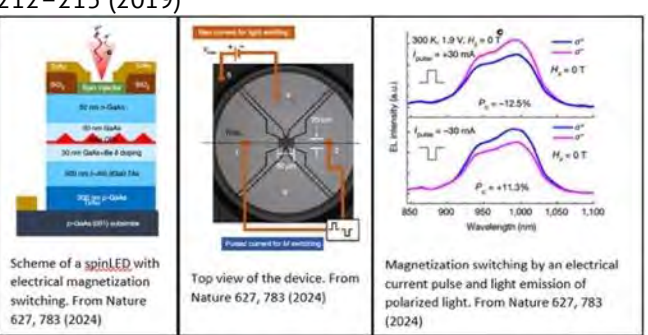
represents an important first step towards the development of devices combining optics, as well as functions as information writing, magnetic storage and optical transfer. This study [1] demonstrates the possibility of modulating magnetic information using electrical pulses while converting them into a circularly polarized light signal in light-emitting diodes (SpinLEDs [2]), at room temperature and zero applied magnetic field. The spin injector is a Cr/Ta/CoFeB/MgO multi-layer and the GaAs-based LED contains p-doped InAs quantum dots. A lateral control charge current generates a vertical spin current through the spin Hall effect, electrically reversing the magnetization of the ferromagnetic part. This switching then determines the spin orientation of the carriers injected vertically into the LED, in which the transfer of angular momentum from the electron spin to the photon controls the circular polarization of the emitted light. Different heavy metals are investigated on top of CoFeB to improve the efficiency and speed of the switching. The results obtained with these on-demand sources of polarized photons pave the way to developments in several fields: chirality analysis of molecules, spincontrolled single-photon sources for quantum technologies, 3D displays, free-space optical communications, and spin laser diodes with high data rates [3].

[1] P. A. Dainone, N. Figueiredo Prestes, P. Renucci, A. Bouché, M. Morassi, X. Deveaux, M. Lindemann, J-M. George, H. Jaffrès, A. Lemaître, B. Xu, M. Stoffel, T. Chen, L. Lombez, D. Lagarde, G. Cong, T. Ma, P. Pigeat, M. Vergnat, H. Rinnert, X. Marie, X. Han, S. Mangin, J-C Rojas-Sanchez, J-P Wang, M.C Beard, N.C Gerhardt, I. Zutic and Y. Lu, Controlling the helicity of light by electrical magnetization switching, Nature 627, 783-788 (2024)

See also News and Views "Electrons flip a switch on optical communications" S. Hiura, Nature 627, 737 (2024) [2] Fiederling, R. et al. Injection and detection of a spin-

polarized current in a light-emitting diode. *Nature* 402, 787–790 (1999).

[3] Lindemann, M. et al. Ultrafast spin-lasers. Nature 568, 212–215 (2019)



AA-02. Efficient generation of spin-polarized light emission with 2D magnetic heterostructure

X. Zhang

Physics, University of Florida, Gainesville, Florida, United States

The advent of two-dimensional(2D) magnetic crystals has enabled both studies of fundamental magnetic interactions in reduced dimensions and novel compact designs for spintronics devices. In this talk, I will present our recent results on a 2D spin-polarized light-emitting-diode composed of a monolayer semiconducting transition metal dichalcogenide (TMD) and a few-layered CrI₃. The valley and spin degrees of freedom are coupled in a monolayer TMD due to the broken inversion symmetry and the large spinorbit coupling. The most common initiation method of the valley/spin index is through the valley-dependent optical selection rule, where the valley- and spin-polarized carriers are selectively excited with different circularly polarized light. Here, we demonstrate an efficient electrical injection of spin-polarized carriers and subsequent valley-polarized electroluminescence in monolayer TMD through the magnetic tunneling junction of CrI₃. The magnetic field dependence of the electroluminescence helicity closely follows the overall magnetization of the few-layered Crl₃. By comparing the case of optical excitation, we conclude that the electrical spin injection has an efficiency of > 70%. Furthermore, the electroluminescence helicity can be modulated and reversed electrostatically by varying the Crl₃ doping level due to the doping-dependent interlayer exchange interactions in Crl₃. Our results establish an efficient device scheme to achieve high efficiency and an electronically tunable spin-polarized 2D light-emitting diode and open up new directions for valleytronics and spintronics.

Dang, J. *et al.* Electrical switching of spin-polarized light-emitting diodes based on a 2D CrI3/hBN/WSe2 heterostructure. *Nature Communications* 15, 6799, doi:10.1038/s41467-024-51287-9 (2024).

^{*} Best Student Presentation Finalist / LB - Late-breaking Poster

AA-03. Room-temperature spin-optoelectronics based on defect-enabled spin amplification

S. Hiura

Hokkaido University, Sapporo, Japan

In recently, spin-optoelectronics has attracted much attention for the development of next-generation information technologies with potential applications in optical communication of electron spin information [1]. Spin-optoelectronics is a new research area of spintronics aiming to utilize the coupling between photon and spin angular momentum, and magnetically controlled optoelectronic devices based on III-V semiconductors can generate, manipulate and detect circularly polarized light. However, the electron spin polarization is rapidly lost in conventional nonmagnetic semiconductors at and above room temperature, which hinders efficient spin-photon interconversion. In this work, we have achieved the highest electron spin polarization of 90% at room temperature by integrating the defect-enabled spin amplification of dilute nitride GaNAs with an InAs quantum dot active layer [2]. The ultrafast spin-amplification dynamics was thoroughly investigated by polarization- and time-resolved photoluminescence in combination with a rate equation analysis [3,4]. We have also demonstrated the roomtemperature operation of spin-polarized light-emitting diodes [5], electric-field-effect spin-optoelectronic devices [6] and polarization-sensitive photodiodes [7] based on defect-enabled spin amplification of GaNAs. Our results indicate that defect-enabled spin amplification is one of the key technologies for practical spin-optoelectronic applications.

- [1] P. A. Dainone, Y. Lu, et al., Nature, Vol. 627, p.783 (2024)[2] Y. Huang, S. Hiura, et al., Nat. Photonics, Vol. 15, p.475 (2021)
- [3] S. Sato, S. Hiura, et al., Appl. Phys. Lett., Vol. 123, p.232405 (2023)
- [4] S. Hiura, et al., Appl. Phys. Lett., Vol. 126, p.052403 (2025)
- [5] K. Etou, S. Hiura, et al., Phys. Rev. Appl., Vol. 19, p.024055 (2023)
- [6] S. Park, S. Hiura, et al., Nanoscale, Vol. 15, p.16784 (2023)
- [7] D. Mineyama, S. Hiura, et al., Appl. Phys. Lett., Vol. 126, p.223507 (2025)

AA-05. Recent Progress in Understanding Polarization Modulation in Spin Lasers

N. Yokota

Research Institute of Electronics, Shizuoka University, Hamamatsu, Shizuoka, Japan

Spin lasers have attracted a considerable number of researchers due to their distinctive spin-related properties [1] and ultrafast polarization modulation [2]. Recent advancements in the field of electrical spin injection into semiconductors [3] have led to promising applications of spin lasers, including potential uses in data communications, optical sensing, and photonic computing. In order to develop a more profound comprehension of the capabilities and requirements of spin lasers, it is imperative to undertake a thorough characterization of polarization modulation in these devices.

This study presents a comprehensive examination of the polarization modulation characteristics of spin lasers, measured through the utilization of optical techniques. In this study, we present a method for measuring high-speed polarization modulation responses in spin lasers [4] and the results of such measurements in InAlGaAs-quantum-well vertical-cavity surface-emitting lasers (VCSELs) operating at telecom wavelengths. Furthermore, our recent observations of polarization bistability of VCSELs under Larmor precession of electron spins [5] are discussed to explore novel collaborations between spintronics and photonics. To elucidate the validity of the observations presented, the results of a simulated study employing the spin-flip model are also presented. The findings of this study serve to facilitate a more profound comprehension and utilization of spin lasers. Moreover, they serve as a source of inspiration for the development of material technologies that relate to the injection, transport, and manipulation of spin-polarized electrons.

- [1] I. Zutić et al., Solid State Commun., Vol. 316, p.113949 (2020)
- [2] M. Lindemann et al., Nature, Vol. 568, p.212 (2019)
- [3] P. A. Dainone et al., Nature, Vol. 627, p.783 (2024)
- [4] N. Yokota et al., Appl. Phys. Lett., Vol. 113, p.171102 (2018)
- [5] N. Yokota et al., APL Photon., Vol. 10, p.016110 (2025)

AA-04. Chiral Induced Spin Selectivity in Lead-Halide Hybrid Semiconductors

M. C. Beard

Chemical and Nanoscience Center, National Renewable Energy, Golden, Colorado, United States

Understanding the interconversion between spin and charge current under chirality induced spin selectivity (CISS) is critical to leverage chiral semiconductors for developing room-temperature control over spin, charge and light. The mix of semiconducting properties and synthetically tunable chirality in chiral metal halide perovskite semiconductors (CMHS) offer a compelling platform. We demonstrated spin injection across chiral halide perovskite/III-V interfaces achieving spin accumulation in a standard semiconductor III-V (Al_xGa_{1-x})_{0.5}In_{0.5}P multiple quantum well (MQW) light emitting diode (LED). The spin accumulation in the MQW is detected via emission of circularly polarized light with a degree of polarization of up to 15%. We also developed simple chiral spin valve operation with CISS enabled magnetoresistance of ~ 300%. The CISS-MR is attributed to the formation of an interfacial spin-selective tunneling barrier induced by spin exchange interactions at the chiral semiconductor/ferromagnetic interface. We also demonstrate inverse CISS via THz generation when a spincurrent is injected across this interface. We discuss the implications of our observations with regard to the underlying CISS mechanism.

SESSION AB: QUANTUM SENSING OF NOVEL MAGNETISM

Chair(s): G. Fuchs, *Cornell University, Ithaca, New York, United States*Tuesday, October 28, 2025

08:30 AM-12:00 PM Ballroom A

AB-01. Imaging and Control of 2D Magnets Revealed by Quantum Sensors

B. Zhou

Physics, Boston College, Chestnut Hill, Massachusetts, United States

The single electron spin of a defect in diamond known as the nitrogen-vacancy (NV) center has emerged as a nanoscale-resolved sensor capable of operation in versatile environments and at diverse interfaces. In this talk, I will highlight our efforts to extend NV quantum sensing to the imaging and control of dynamical magnetization responses

and antiferromagnetic (AFM) states in 2D magnetic materials. We leverage ac dynamical decoupling sequences to detect the ac magnetic susceptibility in few-layer CrBr₃ and probe its domain wall dynamics up to MHz frequency [1]. Moreover, we integrate pulsed optical excitation into a NV sensing sequence to reveal a transient magnetization enhancement in 2D CrCl₃ due to charge transfer driven by exciton recombination dynamics [2]. Finally, we exploit high-sensitivity scanning NV magnetic imaging to resolve nominally degenerate even-layer states in atomically thin CrPS₄. We directly visualize how interfacial exchange coupling at lateral junctions between configurable even-layer (AFM-like) domains and odd-layer (FM-like) regions engenders a tunable lateral exchange bias. NV quantum sensors provide a unique perspective for understanding and controlling 2D magnetism for spintronic technologies.

- 1. X.-Y. Zhang, Y.-X. Wang, B. B. Zhou, *et al.* ac Susceptometry of 2D van der Waals Magnets Enabled by the Coherent Control of Quantum Sensors. *PRX Quantum* 2, 030352 (2021).
- 2. X.-Y. Zhang, T. K. M. Graham, B. B. Zhou, *et al.* Enhanced magnetization by defect-assisted exciton recombination in atomically thin CrCl₃. *Phys. Rev. Materials* 8, 104402 (2024). 3. Y.-X. Wang, T. K. M. Graham, B.B. Zhou, *et al.* Configurable antiferromagnetic domains and lateral exchange bias in 2D CrPS₄. *Nature Materials* (2025).

AB-02. Quantum Sensing with Single Spin Defects in 2D and 1D Materials

<u>T. Li</u>

Purdue University, West Lafayette, Indiana, United States

Spin color centers in hexagonal boron nitride (hBN) have opened new possibilities for quantum sensing with two-dimensional (2D) materials. Recently, we created single spin defects in hBN nanosheets via carbon-13 ion implantation and thermal annealing, revealing both *S*=1 and *S*=1/2 spin states within a single hBN spin defect. We polarized single carbon-13 nuclear spins and demonstrated atomic-scale nuclear magnetic resonance (NMR). We also discovered optically active single spin defects in boron nitride nanotubes (BNNTs), a one-dimensional (1D) van der Waals material. These defects exhibit a spin *S*=1/2 ground state without a fixed quantization axis, enabling orientation-independent magnetic sensing. Using this property, we probed the anisotropic magnetization of a 2D magnet under

orthogonal magnetic fields—challenging for conventional *S*=1 systems like diamond NV centers. These results highlight the potential of hBN and BNNT spin defects for advanced quantum sensing applications.

[1] S. Vaidya, et al. *Advances in Physics: X*, 8, 2206049 (2023).

[2] X. Gao, et al. *Nature*, DOI: 10.1038/s41586-025-09258-7 (2025); preprint: arXiv:2409.01601

[3] X. Gao, et al. Nature Communications, 15, 7697 (2024).

AB-03. Quantum Sensing of Nonlinear Magnonic Dynamics

L. Liu, Z. Hu, Q. Wang

MIT, Cambridge, Massachusetts, United States

Magnon, the quanta of collective excitations of spins inside magnetic materials, own unique properties such as nonlinearity, nonreciprocity, etc, promising useful applications for information processing and transduction in the quantum and classical domains. Probing the dynamics of magnons generally requires high frequency bandwidth --GHz and above, and fine spatial resolution – sub-microns for wavelength matching. In our recent efforts, we have explored new techniques for sensing magnons, allowing us to probe unexpected aspects of nonlinearity. On one hand, we study the multi-photon resonances inside Nitrogen vacancy (NV) centers, which was traditionally utilized as sensors for only static or low frequency magnetic fields. With the mixing of two or more microwave photons, we demonstrate that the intrinsic nonlinear dynamics in NV spins can be used for magnetic sensing across a wide spectrum [1]. Following this, we further show that this capability can be enhanced in hybrid systems formed by NV and ferri- or ferro-magnetic thin films, where the shortwavelength parametric pumping and high order nonlinear magnon scatterings are revealed [2]. Along a different direction, we have also looked into probing the parametric magnonic processes with the usage of the strongly coupled cavity-magnon system. Using either magnon-NV or magnoncavity interactions, we expand the capability in sensing nonlinear resonances in magnetic system and gain new insights onto the quantum characteristics.

1.Z. Hu et al., Phys. Rev. Applied 21, 044057 (2024)

2.Z. Hu et al., Nano. Lett. 24, 15731(2024)

AB-04. Quantum Sensing with Spin Defects: From Spin-Wave Spectroscopy to Symmetry Detection

Boston College, Chestnut Hill, Massachusetts, United States

Solid-state spin defects, such as nitrogen-vacancy (NV) centers in diamond, have become powerful quantum sensors of condensed matter phenomena, particularly in magnetic materials whose spin fluctuations generate broadband electromagnetic noise [1]. In this talk, I will first review progress in the field, including our recent theoretical and experimental work demonstrating that NV center relaxometry can probe spin-wave transport in magnetic systems [2,3]. Building on insights from quantum optics – where cooperative effects among quantum emitters have led to new paradigms for light-matter interactions—I will introduce a general framework for quantum sensing that leverages bath-mediated quantum correlations, extending beyond the traditional single-qubit paradigm [4]. As a direct application, I will show that the relaxation dynamics of a correlated NV ensemble can reveal symmetry breaking in a magnetic bath [5] — suggesting that our approach might enable model-agnostic quantum sensing strategies capable of uncovering properties invisible to current state-of-the-art protocols, which operate solid-state defects as single-qubit sensors.

- [1] F. Casola, T. van der Sar, and A. Yacoby, Probing condensed matter physics with magnetometry based on nitrogen-vacancy centres in diamond, Nat. Rev. Mater. 3, 17088 (2018).
- [2] B. Flebus, and Y. Tserkovnyak, Quantum-impurity relaxometry of magnetization dynamics, Phys. Rev. Lett. 121, 187204 (2018).
- [3] H. Wang, S. Zhang, N. J. McLaughlin, B. Flebus, M. Huang, Y. Xiao, E. E. Fullerton, Y.

Tserkovnyak, and C. R. Du, Quantum sensing of spin transport properties of an antiferromagnetic insulator, Science Advances 1, 8 (2022).

[4] X. Li, J. Marino, D. E. Chang, and B. Flebus, A solid-state platform for cooperative quantum phenomena, Phys. Rev. B 111 6, 064424 (2024), Editors'

Suggestion.

[5] X. Li, and B. Flebus, Cooperative non-reciprocal emission and quantum sensing of symmetry breaking, arXiv:2410.14850 (2024).

SESSION AC: SKYRMIONS AND MAGNETIC TEXTURES RELATED PHENOMENA

Chair(s): C. Chou, *Physics, Massachusetts Institute of Technology, Cambridge, Massachusetts, United States*Tuesday, October 28, 2025
08:30 AM-12:00 PM
Ballroom C

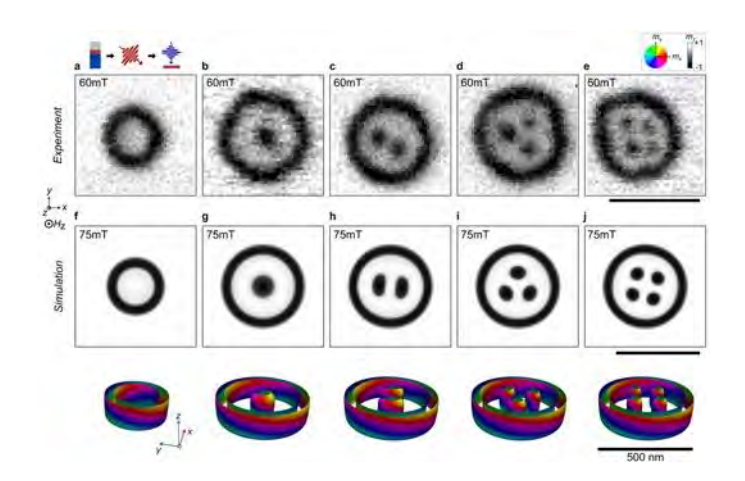
AC-02. Controlled Formation of Skyrmion Bags L. Kern

Department of Materials Science and Engineering, Massachusetts Institute of Technology, Cambridge, Massachusetts, United States

Magnetic skyrmions are widely regarded as prototypical topologically non-trivial spin textures, and have attracted significant interest in both fundamental and applied research¹. Skyrmions are valued for their single-particle character, their robustness and potential applications in spintronics¹. While most studies have focused on conventional π -skyrmions with a simple winding of spins, a broader spectrum of topological spin textures with higher complexity exists^{2,3} and may provide enhanced functionalities, including higher density storage and faster operation4. However, the emergence and potential applications of higher-order spin textures have so far been studied primarily in theoretical simulations^{3,4} and remained largely unexplored in experiments. Here, we report the experimental stabilization of isolated higher-order skyrmion bags-skyrmionium (2π -skyrmion), target skyrmion (3π skyrmion), and skyrmion bags with variable topological charge—in ferromagnetic thin films⁵. We demonstrate that by shaping the anisotropy landscape on the nanometer scale via local ion irradiation, we can predefine preferential nucleation sites for the field- or laser-induced nucleation of these complex spin textures^{5,6}. Notably, ultrafast laser pulses achieve a substantially higher conversion rate transforming conventional skyrmions into higher-order skyrmion bags compared to their formation driven by magnetic fields only. High-resolution x-ray imaging enables direct observation of the resulting skyrmion configurations. Complementary micromagnetic simulations highlight the critical role of the anisotropy defect and its geometry in stabilizing closed-loop domain textures. Importantly, we identify the formation of an intermediate "flower state" as a prerequisite for successful ring closure. Our findings not only expand the experimental accessibility of complex topological spin textures but also offer a robust and tunable approach for incorporating skyrmion bags into future

spintronic devices, both within a unified material platform.

- 1. A. Fert, N. Reyren, V. Cros, Nat. Rev. Mat., 2(7), 1-15 (2017).
- 2. B. Göbel, I. Mertig, O. A. Tretiakov, Physics Reports, 895, 1-28 (2021).
- 3. F. Rybakov, N. Kiselev, Phys. Rev. B 99, 064437 (2019).
- 4. V. M. Kuchkin, K. Chichay, B. Barton-Singer, et al., Phys. Rev. B, 104(16), 165116 (2021).
- 5. L.-M. Kern, V. M. Kuchkin, V. Deinhart, et al., Adv. Mater., 2501250 (2025).
- 6. L.-M. Kern, B. Pfau, V. Deinhart, et al., Nano Lett., 22(10), 4028-4035 (2022).



Variety of stable skyrmion bags (S(0)-S(4)) in experiment and simulation. Figure adapted from Ref. 5.

AC-03. Stabilization of Non-collinear Magnetic Textures in Epitaxial Fe₃GeTe₂/Bi₂Te₃ Heterostructures from Interfacial Strain and Dzyaloshinskii-Moriya Interaction

<u>D. Le</u>¹, E. Thareja¹, Y. K. Luo², M. Phan¹, J. D. Gayles¹

¹Department of Physics, University of South Florida, Tampa, Florida, United States, ²Department of Physics and Astronomy, University of Southern California, Tampa, California, United States

Over the past decade, the development of two-dimensional van der Waals (2D vdW) materials has enabled new opportunities for controlling emergent quantum phenomena in low-dimensional systems. Among them, 2D vdW magnets offer exceptional tunability of magnetic properties via external stimuli such as strain and interfacial effects [1]. When ferromagnetic Fe₃GeTe₂ (FGT) layers are interfaced with antiferromagnetic MnPS₃, a significant and tunable

exchange bias has been observed, modulated by the vdW gap [2]. To stabilize non-collinear magnetic textures widely associated with monolayer FGT, interfacing with materials possessing strong spin-orbit coupling (SOC) is essential to induce interfacial Dzyaloshinskii-Moriya interaction (DMI) [1]. Bi₂Te₃ serves as a promising interfacial material due to its robust topological surface states, which persist at reduced thicknesses [3]. In Fe₃GeTe₂/Bi₂Te₃ heterostructures, interfacial exchange coupling has been shown to enhance both the Curie temperature and the intralayer spin interactions of FGT [4]. However, the role of interfacial strain-arising from epitaxial growth on these magnetic properties remains insufficiently understood [5]. In this work, we study two complementary strain scenarios: (1) strained FGT on unstrained Bi₂Te₃, and (2) strained Bi₂Te₃ on unstrained FGT. In both cases, the topological surface state of five quintuple layers of Bi₂Te₃ remains stable, though it develops a small gap (~0.02 eV) upon interfacing with FGT. We compute the exchange interaction, interfacial DMI, and magnetic anisotropy for each system, demonstrating that non-collinear spin textures can be stabilized within the heterostructure. Our results reveal that both exchange stiffness and magnetic anisotropy increase with the thickness of the FGT layers. Notably, scenario (1) exhibits inplane magnetic anisotropy, while scenario (2) favors out-ofplane anisotropy. We also show that DMI and its interfacial components vary with layer thickness, contributing critically to the stabilization of non-collinear textures. These findings deepen the understanding of interfacial and strain-driven effects in vdW heterostructures and offer valuable insights into the design of spin-texture-based devices.

- [1] Hellman et al. "Interface-induced phenomena in magnetism." Reviews of Modern Physics 89, 025006 (2017). [2] Puthirath et al. "Identifying the Origin of Thermal Modulation of Exchange Bias in MnPS₃/Fe₃GeTe₂ van der Waals Heterostructures." Advanced Materials 36, 2403685 (2024).
- [3] Tang et al. "A comprehensive review on Bi_2Te_3 based thin films: thermoelectrics and beyond." Interdisciplinary Materials 1, 88 (2022).
- [4] Wang et al. "Above room-temperature ferromagnetism in wafer-scale two-dimensional van der Waals Fe_3GeTe_2 tailored by a topological insulator." ACS nano 14, 10045 (2020).
- [5] Zhou et al. "Tuning the Curie temperature of a two-dimensional magnet/topological insulator heterostructure to above room temperature by epitaxial growth." Physical Review Materials 7, 104004 (2023).

AC-04. Efficient Manipulation of Topological Objects in B20 Multilayer Structures

<u>G. M. Pantano</u>, E. Thareja, D. Le, J. D. Gayles Department of Physics, University of South Florida, Tampa, Florida, United States

Classical computers face speed and energy bottlenecks due to the physical separation of memory and processing units; addressing this challenge requires significant leaps in understanding quantum materials to integrate both functions. One promising approach involves leveraging multifunctional quantum materials such as chiral B20 compounds that host various topological phenomena. Among these, CoGe is a nonmagnetic Weyl semimetal where spin-momentum locking and topological protection suppress backscattering, enabling low-dissipation transport for logic circuits. FeGe, with the same crystal structure, supports stable nanoscale skyrmions through the Dzyaloshinskii-Moriya interaction (DMI), allowing highdensity data storage and control using ultralow spin currents. Our work investigates two multilayer heterostructures, (1) CoGe/FeGe/CoGe and (2) FeGe/CoGe/FeGe, to study the interplay between real-space magnetic textures and momentum-space Weyl topology with potential logic-in-memory applications. In (1), spin currents from CoGe exert spin-orbit torque (SOT) on skyrmions in the FeGe layer, controlling their position and tuning properties such as helicity. In (2), the noncollinear spin textures in FeGe gap the Weyl nodes of CoGe, inducing the quantum anomalous Hall effect (QAHE) with dissipationless edge states at cryogenic temperatures. We use first principles calculations and Wannier tight-binding Hamiltonians to determine the bulk and interfacial DMI contributions and calculate the SOT and QAHE. Our results suggest strong interface-driven modifications to the magnetic exchange and transport properties with sensitivity to the interstitial layer thickness and interface orientations ([100], [110], and [111]) in both heterostructures. We further construct phase diagrams to identify the critical width for skyrmion stabilization and QAHE onset. These findings deepen our understanding of interfacial phenomena in B20 multilayers and offer quidance for spintronic device design that integrates high-density storage and fast processing with minimal components and enhanced functionality.

AC-05. Tunable magnetic skyrmions in self-formed 3D wrinkles in freestanding membranes*

<u>Z. Yin</u>^{1,2*}, K. Gu¹, P. Wang¹, H. Meyerheim¹, T. Jiang¹, A. Srivastava¹, S. Parkin^{1,2}

¹NISE, Max Planck Institute of Microstructure Physics, Halle, Germany, ²Department of Physics, Martin-Luther-Universität Halle-Wittenberg, Halle, Germany

Three-dimensional (3D) structures in magnetic materials have recently garnered significant attention [1,2]. The presence of chiral magnetic properties, induced by curvature or torsion, makes materials hosting domain walls and skyrmions with 3D structures promising candidates for 3D spintronic devices. In this study, a freestanding technique is employed to realize 3D architectures in MgO|IrAl|Co_{2.3}Al heterostructures. In these structures, Néel-type skyrmions are stabilized by strain gradient in the Co_{2.3}Al ferromagnetic layer, which is induced by the IrAl templating layer [3]. Upon releasing the membrane in the water by dissolving the sacrificial layer, self-formed 3D wrinkles emerge as a result of strain relaxation.

Here, we present the first observation of Néel-type skyrmions on 3D wrinkles via Lorentz transmission electron microscopy (LTEM) [4]. Our findings reveal that the density of magnetic textures exhibits variations across wrinkles. Finite-element simulations suggest that the local curvature results in variations in strain gradient, which subsequently modulate the Dzyaloshinskii–Moriya interaction (DMI), thereby influencing the skyrmion density.

Additionally, we investigate the influence of the MgO buffer layer thickness on wrinkle formation and the density of magnetic textures. We show that increasing the MgO thickness promotes the formation of more wrinkles and results in a lower density of magnetic textures. X-ray diffraction (XRD) analysis reveals that, the presence of a thicker MgO layer leads to an increased tensile strain, thereby contributing to an enhancement in wrinkle density. Meanwhile, the extracted epitaxy-induced strain gradients, which are comparable in magnitude to the mechanically induced gradient, are found to be decreased with the thicker MgO layer, leading to the lower density of magnetic textures. The density distribution over the wrinkled areas is attributed to the combined effects of epitaxy-induced and mechanically induced strain gradients.

This study demonstrates the ability to tune magnetic skyrmions in both 2D and 3D curved geometries, offering a potential approach for the development of practical 3D skyrmionic devices.

[1] C. Donnelly, A. H-. Rodríguez, C. Abert, K. Witte, Nat. Nanotechnol. 17, 136 (2022). [2] A. M. A. Farinha, S.-H. Yang, J. Yoon, Nature, 639, 67 (2025). [3] P. Wang, R. Saha, Under review (2025). [4] Z. Yin, K. Gu, P. Wang, In preparation (2025).

AC-07. Interlayer Dzyaloshinskii – Moriya interactions in epitaxial Co/Ir/Co/Pt multilayers

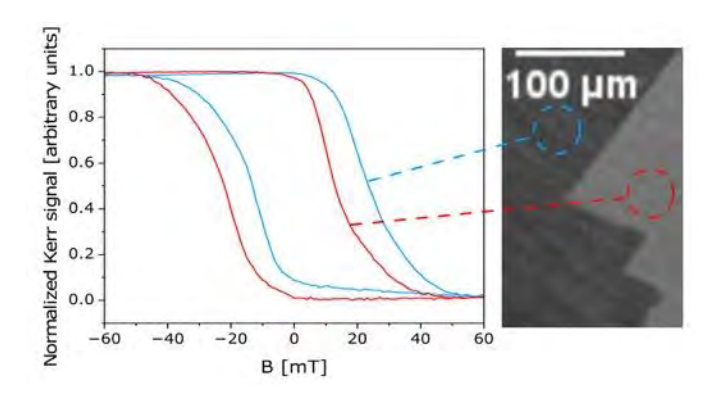
<u>A. Koziol Rachwal</u>, E. Oles, P. Drozdz, A. Kwiatkowski, M. Slezak, T. Slezak

AGH University of Krakow, Krakow, Poland

The Dzyaloshinskii-Moriya interaction (DMI) is an antisymmetric exchange interaction that arises in systems lacking inversion symmetry. Initially demonstrated in ferromagnetic (FM) thin films, DMI describes the coupling between spins mediated by an adjacent paramagnetic heavy metal layer. As DMI favors a specific rotational sense of spin alignment within the FM layer, is inherently chiral in nature. More recently, theoretical predictions¹ and experimental studies² have confirmed the presence of a significant interlayer DMI between neighboring FM layers separated by a non-magnetic spacer. This type of interlayer DMI opens up new avenues for tailoring magnetic textures and improving the functional capabilities of magnetic multilayer structures. In our study we investigated the magnetic properties of epitaxial Co(3nm)/Ir(t_{lr})/Co(d_{Co})/Pt multilayers grown by molecular beam epitaxy on MqO(111). The top FM layer exhibited in-plane magnetization, while variation of the d_{Co} enabled control of perpendicular magnetic anisotropy in the bottom Co layer. For a specific range of Co layer thickness and Ir spacer thickness, where strong antiferromagnetic RKKY interaction is expected, we observed unique magnetic behavior of the bottom Co layer that is sensitive to the magnetic state of the top Co film. Figure 1 (right) shows the polar magnetooptic Kerr effect (PMOKE) microscopy contrast obtained under a perpendicular magnetic field of -16 mT. Prior to the PMOKE measurement, the sample was demagnetized using an inplane magnetic field to induce the formation of in-plane magnetic domains in the top Co layer. PMOKE hysteresis loops measured in two regions—corresponding to antiparallel in-plane domains—are shifted in opposite directions (Figure 1, left), providing clear evidence of interlayer DMI in the system. In my presentation, I will demonstrate how the magnetic properties of $Co(3nm)/Ir(t_{li})/Co(d_{Co})/Pt$ multilayers evolve with changes in t_{lr} and d_{Co} .

^{*} Best Student Presentation Finalist / LB - Late-breaking Poster

- 1. E. Y. Vedmedenko et al., Phys. Rev. Lett. 122, 257202 (2019).
- 2. A. Fernández-Pacheco et al., Nature Mater. 18, 679–684 (2019).



Right: PMOKE microscopy image registered at B_z =-16mT for Co(3nm)/Ir(0.4nm)/Co(1.7nm)/Pt, left: PMOKE hysteresis loops measured for regions of the sample with two antiparallel in-plane domains of top layer.

AC-08. Ab-initio Study of the Topological Hall Effect Caused by Magnetic Skyrmions in Pd/Fe/Ir(111)

<u>A. Kosma</u>¹, P. Rüßmann^{1, 5}, Y. Mokrousov^{1, 2}, S. Blügel^{1, 3}, P. Mavropoulos⁴

¹Peter Grünberg Institut, Forschungszentrum Jülich and JARA, Juelich, Germany, ²Institute of Physics, Johannes Gutenberg-University Mainz, Mainz, Germany, ³Physics Department, RWTH-Aachen University, Aachen, Germany, ⁴Department of Physics, National and Kapodistrian University of Athens, Athens, Greece, ⁵Institute for Theoretical Physics and Astrophysics, University of Würzburg, Würzburg, Germany

The electrical detection of magnetic skyrmions is a key ingredient for the development of spintronic applications that harness the topological protection of these magnetic textures. In this study, we conduct an investigation of the topological Hall effect (THE) arising from stable magnetic skyrmions [1] in the thin film Pd/Fe/Ir(111) [2], based on predictive *ab-initio* simulations. To achieve the formation of stable magnetic skyrmions in this system, we employ non-collinear spin-density-functional theory within the full-potential Korringa-Kohn-Rostoker (KKR) Green function method. The multiple scattering problem is first solved using the KKR method [3], followed by spin-transport calculations performed within the Boltzmann formalism [4] to determine the resistivity and the Hall angle of the

system. We examine how the skyrmions size infuences the Hall angle and explore the effect of additional electron scattering, modeled as random disorder broadening, on the THE.

Our findings reveal that the skyrmion size plays a crucial role, as demonstrated by the study of two different sizes. Furthermore, the degree of sample disorder significantly impacts the results of the Hall angle [5] indicating that different sources of disorder (e.g., impurity atoms) should not be neglected in any quantitative analysis.

- [1] D. Maccariello et al., Nat. Nanotechnology, 13 (2018).
- [2] N. Romming et al., Science, 341, 6146 (2013).
- [3] P. Rüßmann *et al.*, JuDFTteam/JuKKR: v3.6, Zenodo (2022). doi: 10.5281/zenodo.7284738.
- [4] A. Kosma et al., Phys. Rev. B, 102, 144424 (2020).
- [5] A. Kosma et al., Phys. Rev. B, 111, 174412 (2025).

AC-09. Control on the motion of magnetic skyrmions by the interfacial improvement

H. Koizumi¹, W. Zeng², H. Ma², R. Ishikawa³, Y. Suzuki⁴, <u>A. Hirohata^{1, 5}</u>

¹Center for Science and Innovation in Spintronics, Tohoku University, Sendai, Japan, ²College of Engineering, City University of Hong Kong, Hong Kong, Hong Kong, ³ULVAC, Osaka, Japan, ⁴Osaka University, Osaka, Japan, ⁵Max Planck Institute for Chemical Physics of Solids, Dresden, Germany

Magnetic skyrmions have been attracting significant attention as an alternative information career in a racetrack memory and logic thanks to their smaller size and energy for displacement than those for the conventional magnetic domains [1], [2]. They can also be generated and moved not only by a magnetic field and/or an electrical current but also by local heating [3]. However, their speed for operation is known to rely on the Dzalosynskii-Moriya interaction (DMI) at the interface of their hosting media. It is hence important to control the DMI and the resulting operation of skyrmions.

In this study, a medium consisting of MgO/Ta/CoFeB/Ta was deposited by ultrahigh vacuum sputtering, followed by annealing to form a uniform and smooth interfaces. For further improvement in the interfacial quality, a series of pulsed current (0.5 mA for 300 µs up to 2,5000 times) was applied as previously demonstrated in magnetoresistive junctions [4]. Before and after this additional current pulses,

the skyrmion motion was imaged as a movie by magnetooptical Kerr effect (MOKE) as shown in Fig. 1. vies frame by frame, the detailed motion of each skyrmion was revealed as vectorial data to evaluate the influence of the current pulses. We will present a clear difference in their motion and the expected changes in the DMI.

Acknowledgements: This work has been partially supported by JSPS Grants-in-Aid on Home-Returning Researcher Development (No. 22K21362).

- [1] J. Iwasaki et al., Nat. Nanotech. 8, 742 (2013).
- [2] J. Sampaio et al., Nat. Nanotech. 8, 839 (2013).
- [3] Y. Nakatani *et al.*, *Sci. Rep.* 9, 13475 (2019); *ibid.* 11, 8415 (2021).
- [4] W. Frost et al., Sci. Rep. 11, 17382 (2021).

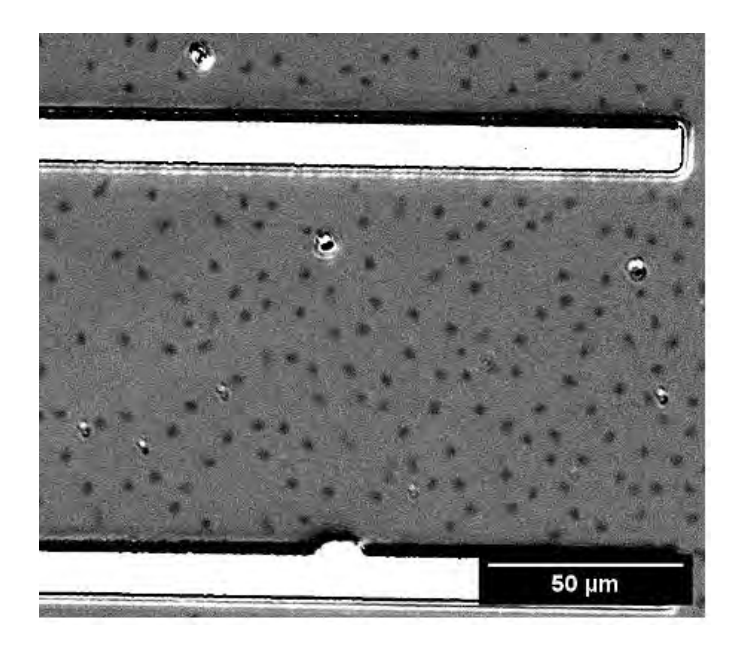


Fig. 1 Magnetic skyrmions (grey dots) imaged between two electrodes for a current application (as appeared as white bars).

AC-11. Voltage-Controlled Magnetic Anisotropy Effects in Skyrmionic Magnetic Tunnel Junctions

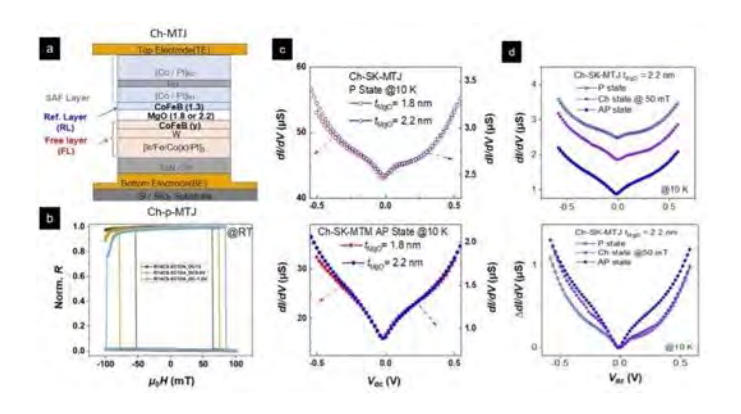
A. Kumar¹, S. Chen², A. Chaturvedi¹, B. Xie¹, J. Lourembam², A. Soumyanarayanan^{1, 2}, <u>J. Zhou</u>²

¹Physics, National University of Singapore, Singapore, Singapore, ²Institute of Materials Research & Engineering (IMRE), Agency for Science, Technology and Research (A*STAR), Singapore, Singapore

Magnetic tunnel junctions (MTJs) are foundational components for spintronic technology, serving as the core of non-volatile memory, sensors, and logic. Perpendicular MTJs (p-MTJs), operating through binary switching between parallel (P) and antiparallel (AP) magnetization states, are robust, but face limitations in scaling bit density and functionality. Integrating magnetic skyrmions topologically protected nanoscale spin textures - enables multi-state MTJ operation, promising high-density, energyefficient cells for memory and reconfigurable neuromorphic computing. Here, voltage-controlled magnetic anisotropy (VCMA) has emerged as a key mechanism for achieving magnetic switching. Well-studied in p-MTJs, VCMA was recently used to switch skyrmionic (SK-) MTJs with ultralow energies [1]. While promising, the role and mechanisms of VCMA in SK-MTJs is unclear, particularly regarding its impact on skyrmion manipulation, stability and electrical readout.

Here, we investigate the electrical characteristics of nanoscale p-MTJs and SK-MTJs fabricated on a 200mmwafer-scale platform [1] (Figure 1). Focusing on the interplay between spin-transfer torque (STT) and VCMA, magnetoresistance (MR(H)) measurements reveal that STT shifts the loop center, whereas VCMA causes a 3-4 times stronger modulation of coercive field (c.f. STT). Next, we demonstrate all-electrical, room-temperature switching among P, AP, and SK states and precise tuning of skyrmion size via VCMA. While positive voltage reduces anisotropy and expands skyrmions, negative voltage enhances anisotropy and shrinks them. Finally, temperaturedependent dynamic conductance (dl/dV) and inelastic tunneling (IET, d^2I/dV^2) spectra reveal that spin-dependent coherent tunnelling is influenced not only by the MgO barrier, and the ferromagnet/MgO interface, but also by the VCMA effects. These findings provide valuable insights for developing SK-MTJs towards scalable, multi-state platforms for next-generation computing technologies.

[1] S. Chen et al., "All-electrical skyrmionic magnetic tunnel junction". Nature (2024) 627, 522. doi: 10.1038/s41586-024-07131-7.



(a-b) Schematic of chiral p-MTJ, MR-H loops of p-MTJ with DC bias. (c) dI/dV spectra of SK-MTJs at P and AP states. (d) Absolute and relative dI/dV spectra for P-, SK- and AP-states.

AC-12. A study on room temperature ferromagnetic Fe₃GaTe₂

R. Jain¹, L. Tsai¹, N. Hai¹, H. Chang¹, R. Sankar¹, Y. Liou², Y. Chen², J. Liang³, <u>S. Lee¹</u>

¹Institute of Physics, Academia Sinica Taiwan, Taipei, Nangang, Taiwan, ²Department of Physics, National Cheng Kung University, Tainan, Taiwan, ³Department of Physics, Fu-Jen Catholic University, Taipei, Taiwan

Ferromagnetic ordering in Fe₃GaTe₂ (FGaT) is stable even above room temperatures which is the most important and interesting aspect of this material. FGaT can potentially host topologically stable skyrmions due to uniaxial (perpendicular) magnetic anisotropy. Skyrmions can be stabilized in non-centrosymmetric magnetic materials due to bulk Dzyaloshinskii-Moriya interaction (DMI), in magnetic multilayers symmetry breaking at the interface results in interfacial DMI which facilitates the creation of skyrmions and in centrosymmetric magnetic materials, strong uniaxial magnetic anisotropy helps in forming the skyrmions [1, 2]. It is reported in literature that skyrmion lattices can be created in FGaT by an optimized magnetic field-cooled method [3]. Geometrical confinement of such systems into micro- or nano-structures can result in the interaction between skyrmion spin configurations and boundaries to bring about a change in topological charge. In this work, single crystal of FGaT was mechanically exfoliated into flakes to study their magnetic and transport properties. Perpendicular magnetic anisotropy of the FGaT was confirmed using SQUID magnetometer at 5K and 300 K. Curie temperature of 356 K was obtained from the

derivative of temperature vs magnetization data.

Temperature dependence of R_{xx} shows a minimum at 35 K suggesting a Kondo-like effect. Electrode leads Ti/Au were patterned on to FGaT flake of ~218 nm thickness in a double cross Hall measurement configuration, using optical lithography and magnetron sputtering. Disks of diameter 2 um and height of ~5 nm were etched in between one of the two pairs of Hall voltage electrodes using electron beam lithography and Ar-ion etching. Magnetic domain imaging using magnetic force microscopy (MFM) shows stripe like domains along with bubble-like structures. Anomalous Hall measurements at different temperatures show that as the temperature is lowered the shape of the curve widens and the switching occurs in two steps in the region with disks and in three steps in the region without disks. This study intends to study correlation in domain structure and magneto-transport behavior of FGaT and the influence of geometrical confinement.

S. Mi, J. Guo, G. Hu, G. Wang, S. Li, Z. Gong, S. Jin, R. Xu, F. Pang, W. Ji, W. Yu, X. Wang, X. Wang, H. Yang, and Zhihai Cheng, Real-Space Topology-Engineering of Skyrmionic Spin Textures in a van der Waals Ferromagnet Fe_3GaTe_2 , Nano Lett. 2024, 24, 13094–13102.

S. Jin, Z. Wang, S. Dong, Y. Wang, K. Han, G. Wang, Z. Deng, X. Jiang, Y. Zhang, H. Huang, J. Hong, X. Wang, T. Xia, S. W. Cheong, X. Wang, Local manipulation of skyrmion lattice in Fe_3GaTe_2 at room temperature, Journal of Materiomics 11, 100865, (2025).

C. Liu, S. Zhang, H. Hao, H. Algaidi, Y. Ma, and X. X. Zhang, Magnetic skyrmions above room temperature in a van der Waals ferromagnet Fe_3GaTe_2 , Adv. Mater. 36, 2311022 (2024).

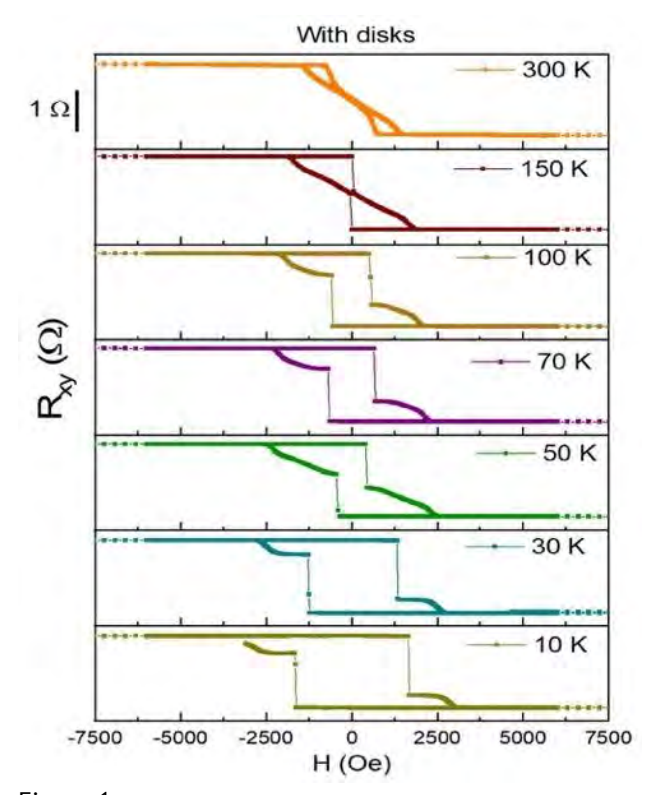
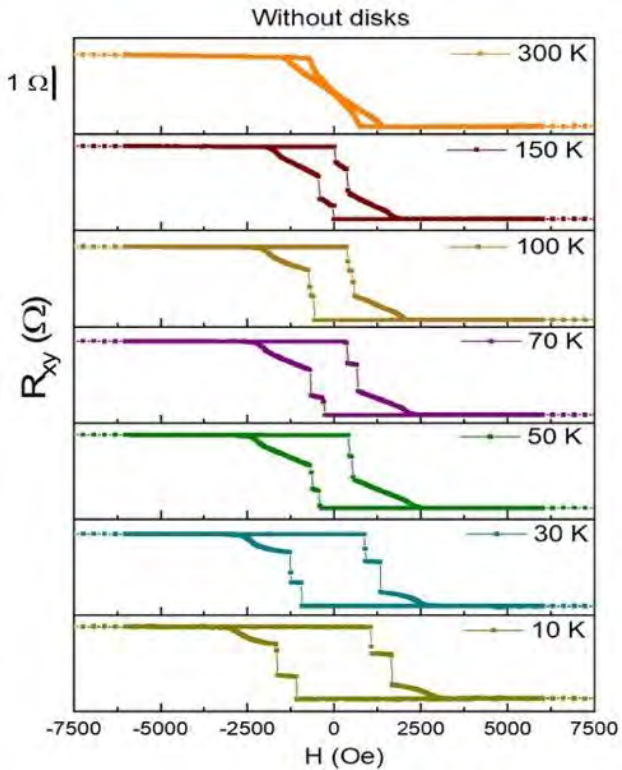


Figure 1



* Best Student Presentation Finalist / LB – Late-breaking Poster

Figure 2

AC-13. Effect of the Dzyaloshinskii-Moriya interaction on the energy dispersion of spin spirals

D. Huang, A. Manchon

Aix-Marseille Université, CNRS, CINaM, Marseille, France

The perpendicular magnetic anisotropy (PMA) and Dzyaloshinskii-Moriya interaction (DMI) are two crucial ingredients that need to be finely tuned to stabilize chiral magnetic textures, such as Néel domain walls, skyrmions, etc. Several recent works have pointed out the possibility of enhancing PMA and DMI through orbital engineering in van der Waals heterostructures such as Co/graphene [1] and FM/h-BN [2]. In addition, it was also demonstrated that DMI can display unconventional symmetries in certain classes of low-symmetry heterostructures, such as in Fe₃GeTe₂ [3, 4], favouring the stabilization of in-plane spin canting. To understand the microscopic origin of DMI in these systems and its influence on the magnetic textures, we built effective tight-binding models of low-symmetry crystals, i.e., adopting D_{3h} and C_{3v} symmetries. By performing symmetry analysis, we construct the general form of the Hamiltonian, including spin-orbit coupling, magnetic exchange, and highorder orbital-momentum coupling based on group theory. We calculate the energy dispersion of spin spirals in these minimal models, which provides evidence of exotic solitons (skyrmions, bimerons, etc.). We explore the interplay between spin-orbit coupling, orbital order, and magnetic exchange on the spin spiral dispersion and discuss the effect of high-order orbital-momentum and spin-spin interactions on noncollinear spin textures.

[1] H. Yang, A. D. Vu, A. Hallal, N. Rougemaille, J. Coraux, G. Chen, A. K. Schmid, and

M. Chshiev, Nano letters 16, 145 (2016).

[2] A. Hallal, J. Liang, F. Ibrahim, H. Yang, A. Fert, and M. Chshiev, Nano Letters 21, 7138 (2021).

[3] S. Laref, K.-W. Kim, and A. Manchon, Physical Review B 102, 060402 (2020).

[4] D. Li, S. Haldar, T. Drevelow, and S. Heinze, Physical Review B 107, 104428 (2023).

SESSION AD: MAGNETOELECTRIC AND MULTIFERROICS I

Co-Chair(s): P. Stevenson, *Physics, Northeastern University,*Boston, Massachusetts, United States and Y.

Takamura, Materials Science and Engineering, University of
California, Davis, Davis, California, United States
Tuesday, October 28, 2025
08:30 AM-12:00 PM
Ballroom B

AD-01. Colossal enhancement of spin transmission through magnon confinement in an antiferromagnet

S. Husain

Department of Materials Science and Engineering, University of California Berkeley, Berkeley, California, United States

Since Felix Bloch's introduction of the concept of spin waves in 1930, magnons (the quanta of spin waves) have been extensively studied in a range of materials for spintronics, particularly for non-volatile logic-in-memory devices [1]. Controlling magnons in conventional antiferromagnets and harnessing them in practical applications, however, remains a challenge. In this talk, I will discuss our recent discovery of magnon confinement that leads to a highly efficient magnon transport in allantiferromagnetic superlattice system which can be controlled electrically [2], making it highly desirable for energy-efficient computation. Leveraging spin-orbit-driven spin-charge transduction, I will discuss the material architecture that permits magnon confinement in ultrathin antiferromagnets, enhancing the output voltage generated by magnon transport by several orders of magnitude in comparison to single layer conterpart [3,4]. I will talk about how this effect may provide a pathway to enable magnetoelectric memory and logic functionalities [5,6]. Additionally, its non-volatility enables ultralow-power logicin-memory processing, where magnonic devices can be efficiently reconfigured via electrically controlled magnon spin currents within magnetoelectric channels.

- [1] V. Baltz, et al., Antiferromagnetic spintronics. Rev. Mod. Phys. 90 (1), 015005 (2018).
- [2] S. Husain, et al. Colossal enhancement of spin transmission through magnon confinement in an antiferromagnet. *arXiv preprint arXiv:2503.23724* (2025). [3] S. Husain, et al., Non-volatile magnon transport in a single domain multiferroic. Nat. Comm. 15 (1), 5966 (2024).
- [4] S. Husain* et al. Symmetry-based phenomenological model for magnon transport in a multiferroic. *Phys. Rev.*

Lett. 134.1 (2025): 016703.

- [5] S. Manipatruni, et al., Scalable energy-efficient magnetoelectric spin-orbit logic. Nature 565 (7737), 35-42 (2019).
- [6] S. Husain et al, Enabling magnetoelectric spin-orbit logic and memory. *Newton* 1.1 (2025).

AD-03. Multiphysics and Multiscale FEM Modeling of Ni-LNO-Ni Magnetoelectric Composites with Self-Bias Behavior D. Bidouba-Sanvany^{1, 2}, T. Huang^{1, 2}, A. Gensbittel^{1, 2}, Y. Zheng³, E. Dandeu³, H. Talleb^{1, 2}, M. Marangolo³ ¹Sorbonne Université, CNRS, Laboratoire de Génie Electrique et Electronique de Paris, Paris, France, ²Université Paris-Saclay, Centrale Supélec, CNRS, Laboratoire de Génie Electrique et Electronique de Paris, Paris, France, ³Sorbonne Université, CNRS, Institut des NanoSciences de Paris, INSP, UMR7588, Paris, France

Research on smart multifunctional magnetoelectric composite (MEC) materials has grown rapidly due to their potential in biomedical devices, energy harvesting, and microsystems. MECs are multiferroic heterostructures combining magnetostrictive and piezoelectric layers; magnetoelectric (ME) coupling occurs indirectly via strainmediated elastic interactions.

Unlike piezoelectric materials, magnetostrictive ones behave nonlinearly. In direct ME mode, a magnetic field H = H_{dc} + H_{ac} (H_{dc} a static bias and H_{ac} a small dynamic component) is applied . This field deforms the magnetostrictive layer, transfers strain to the piezoelectric layer, and generates a voltage across the electrodes. The efficiency of conversion is quantified by the ME coefficient α_E = ($\delta V/t_p\delta H_{ac}$), where t_p is the piezoelectric thickness.

Conventional MECs need a static bias $H_{\rm dc}$ supplied by bulky permanent magnets, hindering miniaturization and integration. To overcome this, self-biased MECs use internal stresses instead of external fields. This study focuses on Ni/LNO/Ni trilayers fabricated by RF sputtering. Residual thermal stress from deposition induces an intrinsic magnetic bias, enabling operation at $H_{\rm dc}$ = 0. This design removes external magnets and allows seamless on-chip integration.

Sputtering enables monolithic fabrication without adhesive layers, improving mechanical coupling and energy conversion efficiency. The residual strain induced in the Ni layers acts as an internal bias, allowing self-biased operation without external magnetic fields. To model this

behavior, a nonlinear multiscale magnetoelastic model is developed and implemented in a Finite Element Method (FEM) framework. Figure 1 presents the experimentally measured magnetization curve of the sputtered Ni (black) layer, while Figure 2 shows the simulated magnetoelectric (ME) coefficient obtained using the proposed FEM model. The self-biased behavior observed by the FEM simulation results are in great concordance with measurement ones. The proposed approach shows promising consistency with experimental observations.

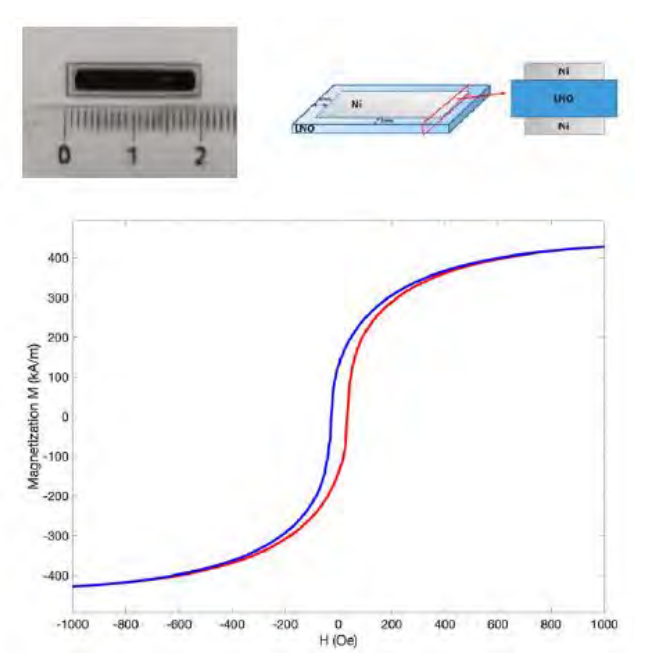


Figure 1 : ME composite and the M(H) measurement curve of the deposited Ni layer

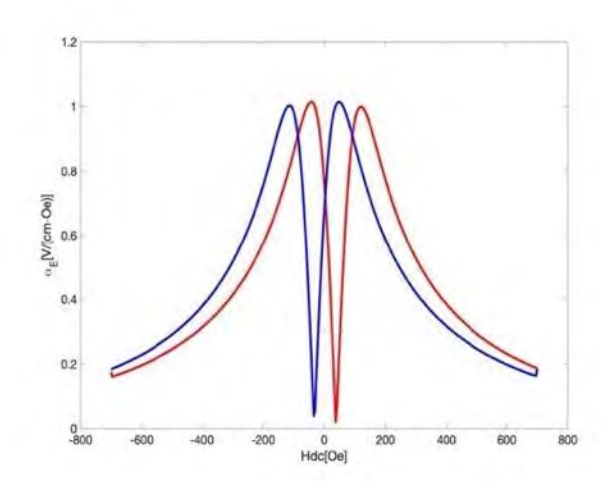


Figure 2 : ME coefficient from the multiphysic FEM simulation

AD-04. Achieving Large and Tunable VCMA in CoFeB/MgO through Electron Depletion with Work-Function-Engineered PtxW1-x Underlayer

Y. Chen¹, T. Peterson², Q. Jia¹, Y. Yang¹, S. Liang³, B. Zink¹, Y. Huang^{4,1}, D. Lyu¹, <u>B. Dixit</u>¹, J. Wang^{1,2,3}

¹ECE, University of Minnesota, Minneapolis, Minnesota, United States, ²School of Physics and Astronomy, University of Minnesota, Minneapolis, Minnesota, United States, ³Chemical Engineering and Materials Science, University of Minnesota, Minneapolis, Minnesota, United States, ⁴National Yang Ming Chiao Tung University, Materials Science and Engineering, Hsinchu, Taiwan

Voltage-controlled magnetic anisotropy (VCMA) is a promising mechanism for advanced magnetic random-access memory (MRAM). The energy barrier of ferromagnetic materials can be modulated by applying an external electric field across the MRAM stack, which lowers the writing current as the energy barrier decreases. However, the relatively low VCMA coefficient remains a bottleneck for practical applications. To explore the intrinsic properties of the VCMA effect, theoretical studies have predicted that a higher VCMA coefficient can be achieved by reducing the electron density at the Fe/MgO interface [1]. Prior experimental work demonstrated that the VCMA coefficient could be enhanced using a high work function Ta/Pd/Ta trilayer underlayer, but the improvement was limited with this structure [2].

In this study, we propose a new high work function alloy design based on Pt_xW_{1-x} [3]. By systematically tuning the Pt composition, we engineered the work function of Pt_xW_{1-} x alloys to effectively deplete electrons from the adjacent CoFeB layer, resulting in a Fermi surface shift at the interface. As shown in Fig. 1, perpendicular magnetic anisotropy (PMA) and the VCMA effect were characterized through anomalous Hall effect (AHE) resistance on microsized gated Hall bar devices. The interfacial anisotropy energy (K_i) and the VCMA coefficients were extracted via linear fits, as summarized in Fig. 2(a). An eight-fold enhancement in the VCMA coefficient was achieved compared to pure W underlayers, with Pt₇₇W₂₃ showing the highest efficiency. Fig. 2(b) displays the distribution of Ki and VCMA coefficients across ten devices for each composition. These results highlight the strong dependence of Ki and VCMA on the underlayer work function.

[1] Zhang, Jia, et al., Physical Review B, vol. 96, pp. 014435 (2017).

^{*} Best Student Presentation Finalist / LB - Late-breaking Poster

[2] Thomas J. Peterson, et al., Journal of Applied Physics, vol. 131, pp. 153904 (2022).

[3] Chen, Yu-Chia, et al., ACS nano vol. 19,pp. 15953-15962(2025).

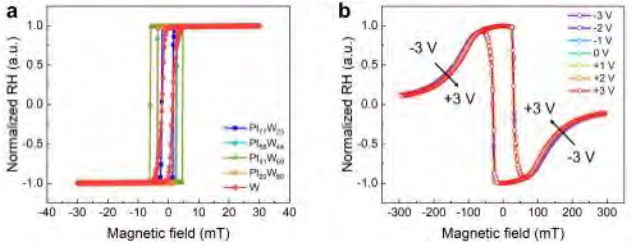


Fig. 1. (a) Normalized AHE resistance measurements for various Pt_xW_{1-x} compositions under an OOP magnetic field. (b) Normalized AHE for $Pt_{77}W_{23}$ case under an IP magnetic field, with varying gate bias voltages.

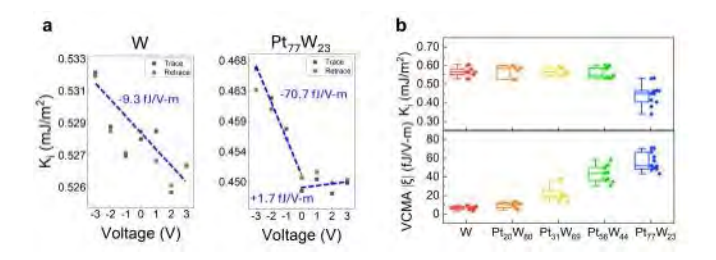


Fig. 2. (a) K_i values derived under gate biases, along with linear fits used to determine the VCMA coefficients. (b) Box plots showing the distribution of Ki and corresponding VCMA coefficients for various Pt_xW_{1-x} underlayer compositions.

AD-05. Interfacial multiferroics of super-orbital-splitting type with colossal interfacial response at room temperature

<u>H. Naganuma</u>¹, K. Nawa², T. Ichinose², K. Amemiya⁴, Y. Sato³, T. Shiraishi³, T. Fukushima²

¹Nagoya University, Nagoya, Aichi, Japan, ²AIST, Tsukuba, Japan, ³Kumamoto University, Kumamoto, Japan, ⁴KEK, Tsukuba, Japan

Magnetoelectric interactions in multiferroic materials have garnered significant interest due to their potential for enabling ultra-low-power, non-volatile magnetic memory devices and highly sensitive magnetic sensors for biosensing. However, practical application of multiferroics has been limited by their low magnetic or charge-order transition temperatures, often below room temperature, and by their weak magnetoelectric responses at ambient conditions. Therefore, realizing magnetoelectric coupling

above room temperature remains a critical challenge in the research field.

In this study, we report the emergence of a novel type of interfacial multiferroics exhibiting colossal magnetoelectric effects at room temperature. This behavior is observed at the interface between antiferromagnetic-based and ferroelectric BiFeO $_3$ and a metallic Co overlayer. Structural and spectroscopic analyses revealed that a thin interfacial layer—approximately 1 nm thick—is formed. X-ray magnetic circular dichroism (XMCD) measurements in KEK-PF indicate the appearance of a strong interfacial magnetic moment, which is electrically controllable via the underlying ferroelectric polarization.

To elucidate the electronic and magnetic structure of this interface, first-principles calculations using FUGAKU were conducted. The calculated XMCD spectra show good agreement with experimental data, suggesting that the interfacial multiferroic layer features a distinct electronic reconstruction driven by oxygen deficiencies 1) and partial substitution of Fe sites with Co atoms. Surprisingly, the interface remains insulating despite these structural modifications—highlighting an unconventional orbital configuration we classify as a "super-orbital-splitting" type. Our findings demonstrate that interfacial engineering can induce emergent multiferroic phenomena unattainable in bulk systems, offering a pathway to develop roomtemperature, tunable magnetoelectric devices. This study opens new avenues in the design of artificial multiferroics through precise atomic-scale control at oxide-metal interfaces.

1) Tomohiro Ichinose, Hiroshi Naganuma, 'Insight into the Mechanism of Magnetoelectric Effects in Rhombohedral $BiFeO_3$ Epitaxial Films with high orientation' Physical Review Materials, 7, 014405 (2023).

AD-06. Double-leaf Riemann surface topological converse magnetoelectricity

Y. Zhou, S. Dong

Southeast University, Nanjing, Jiangsu, China

Electric field control of magnetism in solids, i.e., the converse magnetoelectricity, is highly desired for applications of scalable energy-efficient logic devices. However, it is not only a technical challenge but also a scientific paradox, since in principle the electric and magnetic degrees of freedom obey distinct rules of symmetries. Despite the great progress obtained in the

^{*} Best Student Presentation Finalist / LB - Late-breaking Poster

community of multiferroics during the past decades, the success of magnetoelectricity remains on its way and more alternative approaches with conceptual revolution are urgently needed. Here, by introducing the concept of topology into multiferroics, an exotic magnetoelectric double-leaf Riemann surface is unveiled based on the mechanism of spin-dependent d - p hybridization in a twodimensional magnet: GdI₂ monolayer. Protected by the topology, a 180° spin reversal can be precisely achieved by an electric cycle, leading to a robust and dissipationless converse magnetoelectric function. Such a topological magnetoelectricity allows the nontrivial manipulation of magnetization by ac electric field. In this category, more candidate materials with better performance are designed targetedly, which paves the road to the potential applications with topological magnetoelectrics.

AD-08. Seeing is Believing: Imaging Magnetic Order in Multiferroics

P. Stevenson

Physics, Northeastern University, Boston, Massachusetts, United States

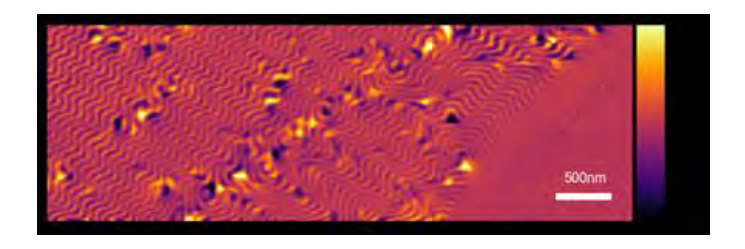
Multiferroic materials have emerged as an exciting platform for exploring the fundamental interactions between spins, offering a rich playground where magnetic, polarization, and strain orders can couple to yield new functionalities, with applications ranging from fundamental physics to lowpower computation. The complex magnetic textures found in these systems are an essential component of their utility, yet the full extent of their complex behavior is often hidden with conventional characterization approaches. Scanning nitrogen vacancy magnetometry (SNVM) has emerged as an exceptionally powerful tool for exploring magnetic materials, combining nanoscale spatial resolution with exquisite sensitivity. In this talk, I will discuss our work using the real-space imaging capabilities SNVM to illuminate the complex behavior of BiFeO₃, a roomtemperature antiferromagnetic multiferroic. Armed with this approach, we are able to directly image magnetoelectric coupling [1], reveal new manifestations of cycloidal ordering [2,3], and uncover robust topological states formed at the intersection of multiple domains.

Beyond BiFeO₃, I will show how composite multiferroic platforms can function as control systems for next-generation spin qubits. These systems offer a route to local, energy-efficient control of qubits, but must be carefully

engineered to suppress nonlinear, multi-magnon processes which degrade qubit performance. The NV center can be used to both characterize different dynamic processes in these devices and image heterogeneity within the materials, providing a direct route to optimizing these systems.

[1] P. Meisenheimer et al., Switching the spin cycloid in BiFeO3 with an electric field, Nat Commun 15, 2903 (2024). [2] P. Meisenheimer et al., Designed Spin-Texture-Lattice to Control Anisotropic Magnon Transport in Antiferromagnets, Advanced Materials, 2404639 (2024)

[3] S. K. Ojha et al, *Morphogenesis of Spin Cycloids in a Non-Collinear Antiferromagnet*, Proc. Natl. Acad. Sci. 122 (17), e2423298122 (2025)



AD-09. Direct Evidence of Non-oxidative Mechanism in Oxygen Based Magnetoionics

T. Bhatnagar-Schöffmann^{2, 3}, P. Schöffmann⁴, A. Resta⁴, <u>A. Lamperti¹</u>, G. Bernard^{2, 3}, A. Kovács⁵, L. Largeau^{2, 3}, A. Durnez^{2, 3}, A. Harouri^{2, 3}, X. Lafosse^{2, 3}, D. Ourdani⁷, M. Syskaki⁶, Y. Roussigné⁷, S. Ono⁸, R. E. Dunin-Borkowski⁵, J. Langer⁶, D. Ravelosona^{2, 3}, M. Belmeguenai⁹, A. Solignac^{9, 3}, L. Herrera Diez^{2, 3}

¹CNR-IMM, Agrate Brianza, MB, Italy, ²C2N, CNRS, Palaiseau, France, ³Université Paris-Saclay, Palaiseau, France, ⁴Synchrotron SOLEIL, Saint-Aubin, France, ⁵Forschungszentrum Jülich GmbH, Jülich, Germany, ⁶Singulus Technology AG, Kahl Am Main, Germany, ⁷CNRS-UPR 3407 Université Sorbonne Paris Nord, Villetaneuse, France, ⁸Central Research Institute of Electric Power Industry, Yokosuka, Japan, ⁹CEA, CNRS, SPEC, Gif-sur-Yvette, France

The convergence of microelectronics and neuroscience in research on artificial synapses opens the potential for magnetoionics, where the magnetic anisotropy of a ultrathin ferromagnet layer is modulated by the ion migration from an adjacent oxide layer by voltage application. In this respect, the understanding of the chemistry at the oxide/ferromagnet interface is the key for direct evidence of

the mechanism at the root of magnetic state change. Here, we report ToF-SIMS and XPS analysis of Ta(5)/CoFeB(1)/Pt(0.09)/MgO(2)/HfO₂(3) (thickness in nm), assketched in Figure 1a, prior and after the exposure to different voltages for several seconds, through ionic liquid gating, as measured by AHE (Figure 1b and c). From ToF-SIMS, after -3.5 V applied for 360 s, a decrease of the OH inside the MgO layer is revealed in the depth profile, implying a depletion of oxydrilic groups, or hydrogen, from pristine MgO (Figure 2a). Concomitantly, ¹⁸O- and Mg⁻ intensity remains unchanged (Figure 2b and c). XPS reinforces this finding by showing a shift in the binding energy of the Mg(2s) edge compatible with Mg(OH)₂ reverting to MgO upon voltage application (Figure 2d), a change that detrimentally impacts on the magnetic anisotropy cyclability, even on sold-state gated stacks. Our study proves the co-existence of complex reversible and irreversible effects at the root of magnetoionics.

Financial support from European Union through Horizon Europe EIC Pathfinder METASPIN project (Grant n. 101098651) is acknowledged.

T. Bhatnagar-Schöffmann et al., Advanced Materials Interfaces 11, 2300955 (2024)

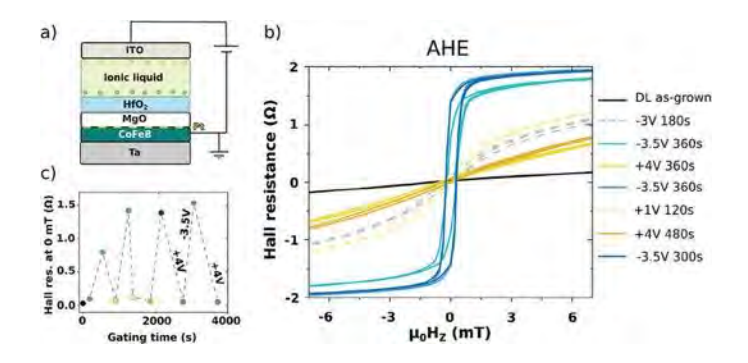


Figure 1. a) Illustration of the structure of the magneto-ionic device, ionic liquid gated. b) AHE hysteresis loops as a function of μ_0H_z for the as-grown stack and after exposure to a sequence of gate voltages. c) Hall resistance at 0 mT for the voltage cycles shown in (b) plus points measured for a +4 V/–3.5 V/+4 V gate voltage application sequence.

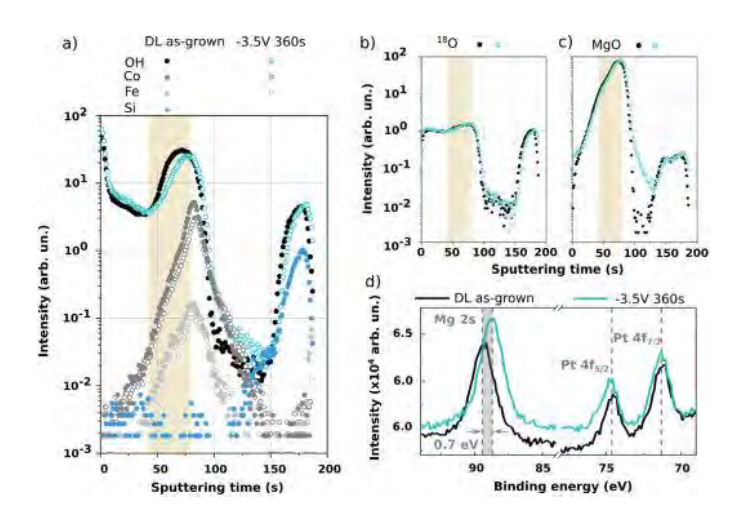


Figure 2. ToF-SIMS measurements before (filled black symbols) and after negative voltage gating (cyan open symbols) for OH (a), 18 O (b) and MgO (c). Co, Fe and Si are also shown in (a). The shaded area corresponds to the position of the MgO layer. d) XPS spectra before and after gating in the binding energy range of the Mg 2s levels and the Pt $4f_{5/2}$ and $4f_{7/2}$ levels.

SESSION AE: NEW APPLICATIONS AND OTHER EMERGING TOPICS I

Chair(s): S. Pollard, *Physics and Materials Science, The University of Memphis, Memphis, Tennessee, United States*Tuesday, October 28, 2025
08:30 AM-12:00 PM
Room 2DE

AE-02. High-Gradient Magnetic Separation of Lithium Iron Phosphate in Lithium Ion Batteries

<u>D. Rogers</u>, P. Andrei, P. Wang *Florida State University, Tallahassee, Florida, United States*

Today's lithium mining practices are not sustainable enough to fuel the rapidly growing global demand for lithium-based

technologies. In the coming years, lithium is expected to be formally labeled a critical element, making the development of new methods for recovering and reusing lithium essential. Extracting lithium iron phosphate (LFP) from discharged batteries is a promising strategy to recover and recycle lithium. In this paper, we demonstrate the effectiveness of a microsphere based high gradient magnetic separation (HGMS) method for isolating LFP particles from discharged lithium ion batteries. The cathode of a LIB contains LFP, conductive carbon, and a polyvinylidene fluoride (PVDF) binder, and the anode contains mostly graphite. The anode and cathode in powder form are mixed in methyl pyrrolidone (NMP). The NMP dissolves the binder, releasing the carbon from the LFP particles. The solution is passed through a packed column of paramagnetic microspheres (280 µm diameter) paced in a 1T magnetic field. The microspheres focus the magnetic field and generate strong magnetic gradients that capture the magnetic LFP particles. The non magnetic components; carbon, binder, and graphite pass through the magnetized column. Once the column is removed from the magnetic field, the microspheres demagnetize and the LFP particles captured in the column are recovered by flushing the system under pressure.

Inductively coupled plasma mass spectrometry (ICP-MS) analysis of the three samples showed that 99% of LFP particles were captured using this method. Scanning electron microscopy (SEM) imaging was also used to image the graphite and binder. Images of the separated solution (Fig 1) give qualitative results that graphite and dissolved binder had passed through the system and separated from the LFP. The ICP-MS and SEM results together show that our HGMS system captures LFP while allowing non magnetic graphite, binder, and carbon black, to pass through.

Quantitative results using thermogravimetric analysis mass spec will give the resulting grade shift after separation and will be demonstrated in the paper.

Zh. Hu, J. Liu, T. Gan, D. Lu, Y. Wang and X. Zheng, *Separation and Purification Technology*, (2022)



Fig. 1: SEM imaging of solution that passed through the column. Graphite (~30 µm) and dissolved binder are visible.

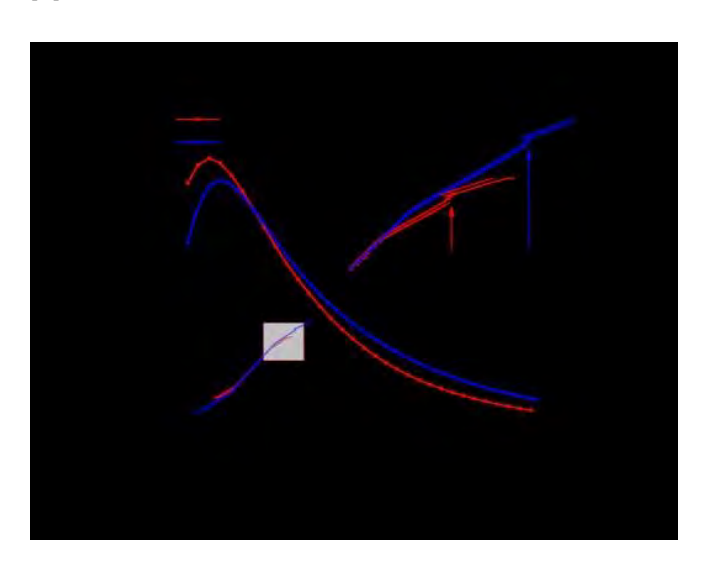
AE-03. Orbital hybridization induced changes to oscillatory dynamics in epitaxial La $_{0.67} Sr_{0.33} MnO_3$ films

H. Chhabra, A. Jaman, I. Garcia, <u>T. Banerjee</u> *University of Groningen, Groningen, Netherlands*

Magnetic materials, such as mixed valence manganite (ABO₃) that possess comparable energy ground states are rich playground for studying emergent functionalities. applicable for unconventional computing. Metal-to-insulator (MIT) phase transition is a rich example of electron correlation effect in such materials, whose electrical control display non-linear characteristics similar to neuronal functionalities in the human brain. I will discuss two examples of such phase transition induced negative differential resistance states in strained epitaxial films of La0.67Sr0.33MnO3 (LSMO) that shows remarkable differences, induced by octahedral distortion, in textured LaAlO3 (LAO) substrates. The wedge disinclination induced by twin boundaries in the LAO substrate leads to spatial inhomogeneity of the magnetization across the film which strongly couples with the electronic transport in such manganites. By engineering the time dynamics of such metastable phases we demonstrate a voltage-tunable oscillator that dynamically oscillates at variable frequencies (kHz to MHz) [1]. In the second example we show how

differences in orbital couplings due to local strain variations can be picked up by designing electrical contacts at different electrode distance (Fig. 1). By varying the magnetic field, we find that the negative differential states shifts to different voltages indicative of changes in the orbital hybridization that locally couples with the electronic states. This enriches the phase space of operation of the voltage tunable oscillators over a wide range of frequencies in the same magnetic film. Such local control of the MIT phase transition stabilized by different transport mechanisms and triggered by voltage shows how orbital hybridization plays an important role in in the design of voltage tunable oscillators for different applications in unconventional computing.

[1] A. Jaman et al., Adv. Funct. Mater., 2419840, 2025



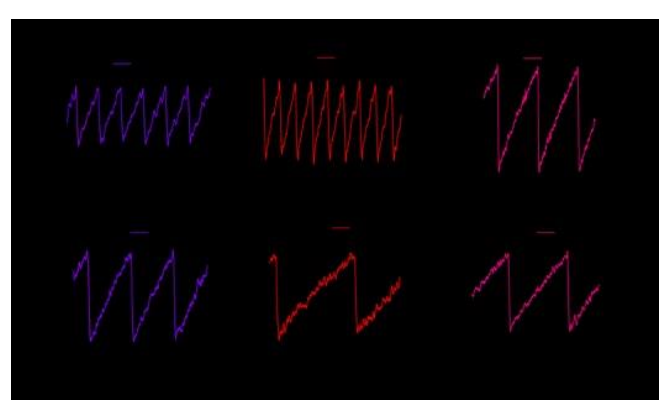


Fig. 1 (left): Spatial variation of the resistance of an epitaxial film of LSMO on a LAO substrate, picked up by different electrodes with varying spacing between them. The

variations in the oscillations with and without a magnetic field are shown in the right.

AE-05. A Workflow for Magnetic Material Discovery: Experimental Database meets Graph Neural Networks B. Schoener¹, Y. Hu², H. Hui¹, Y. Liu¹, T. Wojnar¹, J. Xiong², I. Zutic¹, H. Zeng¹

¹Physics, University at Buffalo, Buffalo, New York, United States, ²Computer Science and Engineering, University at Buffalo, Buffalo, New York, United States

A key difficulty for material discovery using computational methods is the incompatibility between the computational cost of first principles calculations, and the vast space of potential material compositions and structures. Machine learning is capable of bridging this gap by offering the ability to compute material properties at far lower computational cost, often by orders of magnitude, while also maintaining comparable accuracy to first principle techniques. These machine learning models allow for preliminary, large scale screenings of potential materials. However, this method relies on databases such as the Materials Project (MP), which is created using highthroughput first principles calculations. Such a database does not exist for magnetic properties due to the unreliable accuracy of those calculations. Our work has been the development of a magnetic material discovery workflow, leveraging experimental data automatically extracted from research articles. While some groups have implemented these approaches, they are limited to more recent articles which are offered in HTML format. We have applied advanced Optical Character Recognition (OCR) techniques to include older articles that only have an image-based representation such as PDF. This opens up decades worth of articles for data collection. Another advancement our approach makes is in the alignment of entries in the experimental database to material structures in the Inorganic Crystal Structure Database (ICSD). This allows the use of more advanced machine learning architectures such as the Crystal Graph Convolutional Neural Network (CGCNN), where the input requires exact atomic coordinates. These improvements in both data availability and model sophistication allow for greater reliability in our machine learning predictions. A test of this workflow was done on the discovery of new altermagnets, where we first screened the ICSD and MP for new high temperature antiferromagnets and then compared these to current candidates along with certain symmetry constraints. Our

^{*} Best Student Presentation Finalist / LB - Late-breaking Poster

approach opens the door for combining state of the art techniques with magnetic materials discovery.

Funding: NSF DMR-2242796 and UB Center for Advanced Semiconductor Technologies.

- T. Xie and J. Grossman, Physical Review Letters, 120, 145301 (2018)
- Y. Zhang, S. Itani, K. Khanal, Journal of Magnetism and Magnetic Materials, 597, 172001 (2024)
- S. Itani, Y. Zhang, and J. Zang, arxiv:2409.15675 (2024)
- L. Šmejkal, J. Sinova, and T. Jungwirth, Physical Review X, 12, 040501 (2022)

AE-06. Magnetic Tag Recognition via High-Order Projection of Far-Field Measurements

<u>S. Ben Mbarek</u>, S. Amara, G. Setti CEMSE, KAUST, Jeddah, Thuwal, Saudi Arabia

Magnetic tags offer a compelling alternative to existing identification methods owing to their distinctive blend of durability and compatibility with non-line-of-sight detection [1-4]. In this study, we present a method for recognizing and identifying a magnetic tag for a given far-field measurement. The magnetic tag is composed of a 2×2 array of neodymium permanent magnets. The magnetic tag is represented by four current loops located in the x-y plane with the same magnetic moment. Using two distinct magnetization states, that is by magnetization up ('+1') or down ('-1'), the magnetic tag can be used as a magnetic code. Magnetic induction at an observation point is the superposition of the fields relative to all four dipoles using the Biot-Savart law. A direct measurement was used for flux scanning (B_z) above a magnetic tag. Figure 1 shows the experimental setup. The experiments incorporated a Hall axial probe connected to a Gaussmeter HM5100 and secured with a clamp to ensure stability. The magnetic tag was fixed in a stationary position while the Hall probe moved via an X-Y translation stage. The recognition algorithm begins with an input B_z heatmap measured 3 cm above the magnetic tag. Using a downward continuation based on a high-order Taylor expansion, we obtained a B_7 heatmap in a nearer plan. In fact, we used finite differences to calculate the horizontal gradients of B_z to start the downward continuation. These gradients were then subjected to the Hilbert transform in both the x- and ydimensions. To reduce the high-frequency noise, a Gaussian filter was used to stabilize the numerical derivatives. The downward-projected magnetic flux heatmap is compared to

the forward magnetic flux field, and recognition is performed by selecting the configuration that presents the minimum relative error. The results presented in Figure 2 demonstrate that the proposed algorithm can identify distinct magnetic tag signatures, particularly when arranged in intricate designs.

- 1- Goll, Dagmar, et al. "Magnetic Coding of Steel for Industrial Internet Applications." *physica status solidi* (a) 217.17 (2020): 2000160.
- 2- Mitrelias, Thanos, et al. "Magnetic microtags and magnetic encoding for applications in biotechnology." *AIP Conference Proceedings*. Vol. 1025. No. 1. American Institute of Physics, 2008.
- 3- Kohls, Noah D., et al. "Magnetic tags with unique self-assembly patterns for tracking applications." *Journal of Magnetism and Magnetic Materials* 535 (2021): 168045.
 4- Liu, Tingli, et al. "Advancements in magnetic dipole detection: Direct magnetic gradient tensor data versus total magnetic intensity derived calculations." *Measurement* 253 (2025): 117386.

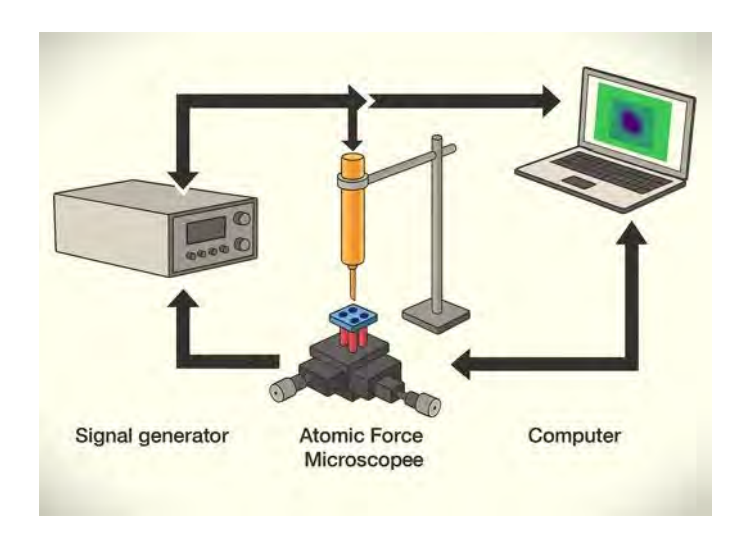
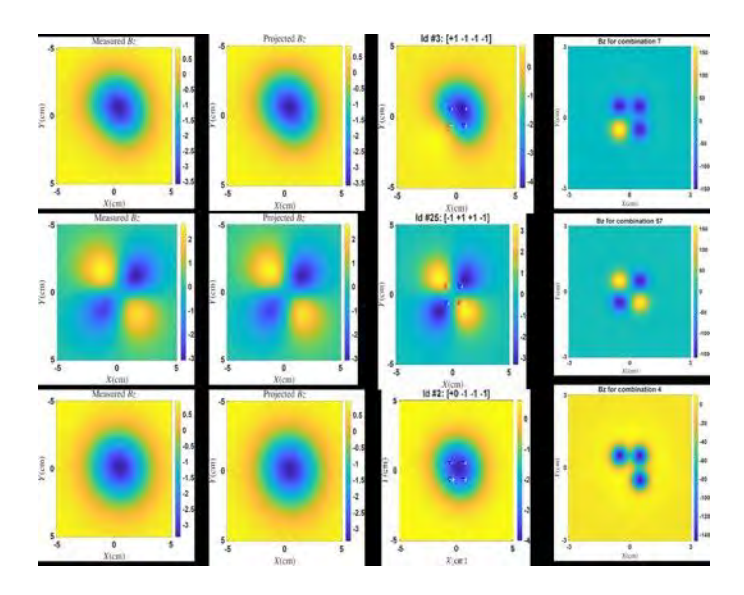


Fig. 1 Experimental setup



Column 1 shows the measured far-field scan of the tag, followed by the projected B_z field used as input to the algorithm, column 3 displays the recognized tag ID, while column 4 presents the near-field scan, revealing the actual ID.

AE-07. Integrating spins and ions for spiontronics <u>G. Miao</u> 1,2

¹Electrical and Computer Engineering, University of Waterloo, Waterloo, Ontario, Canada, ²Institute for Quantum Computing, Waterloo, Ontario, Canada

Iontronics benefits from the controllable motion and detection of ions in electronics devices, and it can naturally couple with spintronics and the conventional charge-based electronics, forming an interesting emerging area - the spiontronics. A vast amount of knowledge can be borrowed from the well-established renewable battery literatures, leading to the engineering of "battery-like" electronics structures. The injection, confinement, transport and extraction of ions in fully solid-state nanostructures can lead to profound changes to the spin states and charge transport properties. For examples, we show that we can regulate a tunnel junction's spin polarization, monitor or turn the magnetism/antiferromagnetism on and off, modulate the spin transports in 2D magnetic materials, and infusing short-term and long-term memories in neural networks, and so on. We also illustrate the actual back-endof-line (BOEL) integration of such foundry forbidden materials on CMOS chips, as a demonstration of principle

for the potential integration of exotic quantum materials with the prevailing semiconductor technologies.

1. Silva G.V.D.O., Ghosh L., Islam R., Araujo C.I.L.D., Miao G.-X., Voltage-Driven All-Solid-State Ionic Control on Co/CoO Antiferromagnet/Ferromagnet Exchange Bias, ACS Nano, 2025.

2. Islam R., Shi Y., de Oliveira Silva G.V., Sachdev M., and Miao G.-X., Volatile and Nonvolatile Programmable Iontronic Memristor with Lithium Imbued TiOx for Neuromorphic Computing Applica, ACS Nano, Volume 18, 22045-22054, 2024.

3. Li Q., Li H., Xia Q., Hu Z., Zhu Y., Yan S., Ge C., Zhang Q., Wang X., Shang X., Fan S., Long Y., Gu L., Miao G.-X., Yu G., and Moodera J.S., Extra storage capacity in transition metal oxide lithium-ion batteries revealed by in situ magnetometry, Nature Materials, Volume 20, 76-83, 2021.
4. Long G., Xue Q., Li Q., Shi Y., Li L., Cheng L., Li P., Zhang J., Zhang X., Guo H., Fu J., Li S., Moodera J.S., and Miao G.-X., Interfacial Control via Reversible Ionic Motion in Battery-Like Magnetic Tunnel Junctions, Advanced Electronic Materials, Volume 7, 2100512, 2021.

=

AE-08. Magnetic Image Recognition Under Environmental Noise: A Machine Learning Approach

S. Amara, D. Divyanshu, S. Ben Mbarek, G. Setti CEMSE, KAUST, Jeddah, Thuwal, Saudi Arabia

Magnetic labelling provides a robust alternative to optical and RFID tagging, particularly in harsh conditions. Leveraging far-to-near field transformation, it enables highresolution magnetic image recognition using unique field signatures. A ResNet-based deep learning classifier enhances robustness against tag variations and noise, making this approach highly suitable for industrial applications where traditional methods fail [1]-[5]. In this work, we studied the case of a 2*2 array of permanent magnets. Each position could have three states: 0 (no magnet), 1 (magnet up), -1 (magnet down). We generated by Matlab the row data of the 34configurations. These images were delivered with different resolutions and at different distances. The algorithm performs targeted finetuning of a pretrained ResNet-18 model (17 convolutional layers and 1 fully connected layer) adapted for magnetic tag classification. Each image is resized to and stochastically perturbed with Gaussian noise (σ^2 [0.005, 0.055]). The network is restructured by removing its original fc_{1000} with fc_{81} . The modified architecture is trained

with 'Adam' optimizer {batch size (β) = 16, learning rate (α)=10⁻⁴, epochs (ϵ) = 15}. Targeted Fine-tuning is then restricted to the hard tag subset (Z), optimizing only the final fc_{81} layer using 'Adam' (β =8, α =10⁻⁵, ϵ =15) to construct a specialized model with improved robustness on difficult class boundaries. Results showed strong generalization performance, confirming that deeper CNN architectures like ResNet are effective for reliable magnetic image recognition. Figure1 shows the overall obtained accuracy using this method. In a second stage, we experimentally scanned the hardest configurations of the 2*2 array using a gaussmeter and an X-Y displacement system. The experimental scans where injected in the algorithm to be tested . Figure2a shows the experimental setup block diagram, and Figure 2b is showing the next running study.

[1] Ahamed, N. et. al. "Tracking and tracing the halal food supply chain management using blockchain, RFID, and QR code," Multimedia Tools and Applications, vol. 83, no. 16, 2024.

[2]K. Bhanushali, et. al., "A 125 um x 245 um Mainly Digital UHF EPC Gen2 Compatible RFID Tag in 55 nm CMOS Process," *IEEE Journal of Radio Frequency Identification*, vol. 5, no. 3, Sept. 2021. Version June 17, 2025.

[3] Olenik, S., Lee, H.S. Güder, F. The future of near-field communication-based wireless sensing. *Nat Rev Mater 6*, 286–288 (2021).

[4] Hess, D.W. (1985). Far-Field to Near-Field Transforms in Spherical Coordinates. *In: Boerner, WM., et al. Inverse Methods in Electromagnetic Imaging.* NATO ASI Series, vol 143. Springer, Dordrecht.

[5] KIM, Woobin, *et al.* Near-field to far-field RCS prediction on arbitrary scanning surfaces based on spherical wave expansion. *Sensors*, 2020, vol. 20, no 24, p. 7199.

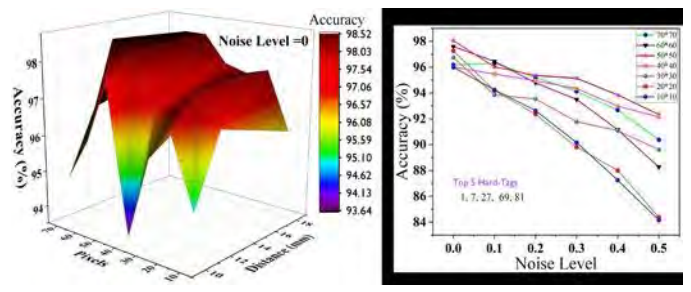


Fig. 1 3D plot for accuracy at different resolution and interspacing distance for Noise level 0. (b) Accuracy vs Noise level for different resolutions.

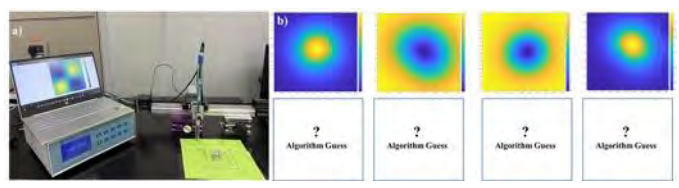


Fig. 2 a) Experimental Setup for Tag Scanning. b) Specific examples for Algorithm testing for configuration recognition using modified ResNEt-18.

AE-10. Exfoliation of Hematene: An Air-Stable Non-van der Waals 2D Material Exhibiting Room-Temperature Ferromagnetism

A. Puthirath Balan^{1, 2, 4}, S. Radhakrishnan^{1, 3}, M. Anantharaman^{1, 4}, C. Tiwary^{1, 5}, A. Pulickel M.¹
¹Rice University, Houston, Texas, United States, ²Johannes Gutenberg University Mainz, Mainz, Germany, ³Intel Corporation, Rio Rancho, New Mexico, United States, ⁴Cochin University of Science and Technology, Kochi, India, ⁵Indian Institute of Technology Khargpur, Kharagpur, India

Hematene, a novel non-van der Waals two-dimensional (2D) material derived from natural hematite (α -Fe $_2$ O $_3$), presents remarkable electronic and magnetic properties, opening new avenues in next-generation electronic and spintronic applications. Unlike conventional 2D materials such as graphene, which originate from van der Waals layered structures, hematene is exfoliated from hematite—a material traditionally regarded as unsuitable for producing ultrathin sheets due to its robust three-dimensional bonding network.

In this work, we report the successful isolation of few-atomthick hematene sheets using an organic solvent-assisted liquid-phase exfoliation technique. [1] The resulting 2D flakes, with a typical thickness of three atomic layers, exhibit properties distinctly different from their bulk counterpart. While bulk hematite is antiferromagnetic, hematene demonstrates room-temperature ferromagnetism, attributed to quantum confinement and surface effects.

The successful isolation of hematene marks a significant milestone in the exploration of non-van der Waals 2D materials, demonstrating that dimensional reduction is feasible even for materials with strong interlayer bonding. [2] This paves the way for a broader class of 2D materials, potentially synthesized via both top-down and bottom-up approaches, with wide-ranging applications in spintronics,

optoelectronics, and flexible electronics.

- [1] Puthirath Balan, A., Radhakrishnan, S., Woellner, C.F.,..., Pulickel M. Ajayan et al. Exfoliation of a non-van der Waals material from iron ore hematite. Nature Nanotech 13, 602 609 (2018)
- [2] Puthirath Balan, A.,...., Pulickel M. Ajayan et al. "Non-van der Waals quasi-2D materials; recent advances in synthesis, emergent properties and applications." Materials Today 58, 164-200 (2022)

AE-11. Characterization of Current-Flux and Current-Force Relationships in Reluctance Actuators for High-Precision Applications

M. Al Saaideh¹, N. Alatawneh^{2,3}, M. Al Janaideh³
¹Memorial University of Newfoundland, St. John's,
Newfoundland, Canada, ²Sacred Heart University, Fairfield,
Connecticut, United States, ³University of Guelph, Guelph,
Ontario, Canada

Reluctance actuators have been increasingly employed in high precision applications, such as Lithography machines, due to their high output power density compared to Lorentz actuators. However, the strong non-linearity between input current and output magnetic force is still a challenging modeling task, which can significantly decrease the control accuracy.

In this work, an experimental characterization of currentforce relationship of a custom made reluctance actuator is presented. A prototype of reluctance actuation system is fabricated using a stationary part, C-core, and a movable Icore. Both cores are constructed of M19 non-oriented electrical steel laminations and placed in an aluminum enclosure, as shown in Fig. 1.

The experimental results of input current versus flux density with a fixed air gap of 0.5 mm show a systematic evolution of hysteresis loop, such that the loop are confined entirely within the major loop borders, as illustrated in Fig.2 (a). The current-force relationship of the same fixed air gap is a butterfly pattern, as shown in Fig. 2(b).

In contrast, when the air gap changes, the current-flux hysteresis loops demonstrate a peculiar evolution, where the increase in the current results in a rotation of the hysteresis loop around the origin, and then the loops cross over each other, as shown in Fig. 2(c). The current-force relationship of the variable air gap is an interleaved butterfly pattern, as shown in Fig. 2(d).

The extraordinary current-flux-force relationships of variable air gap in reluctance actuators highlight the necessity for advanced modelling of hysteresis. Generalized Prandtl–Ishlinskii model is a promising candidate to characterize this strong non-linear behavior. Conclusions of this work will contribute to the development of a reliable control system of reluctance actuators in high precision applications.

- [1] M. Yin, M. Naidjate, N. Bracikowski, Journal of Magnetism and Magnetic Materials, Vol. 602, p. 172174 (2024)
- [2] X. Zhang, L. Lai, L. Zhang, Precision Engineering, Vol. 75, p. 11 (2022)
- [3] E. Barhoumi, F. Wurtz, C. Chillet, IEEE Transactions on Magnetics, Vol. 52, p.2404 (2016)
- [4] M. Al Janaideh, S. Rakheja, and S. Chun-Yi, IEEE/ASME Transactions on Mechatronics, Vol. 16, p. 734 (2011)

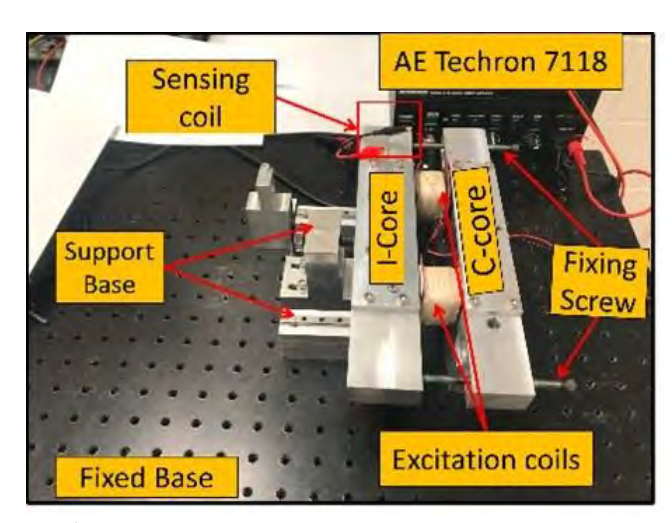


Fig.1: Experimental setup of reluctance actuator system

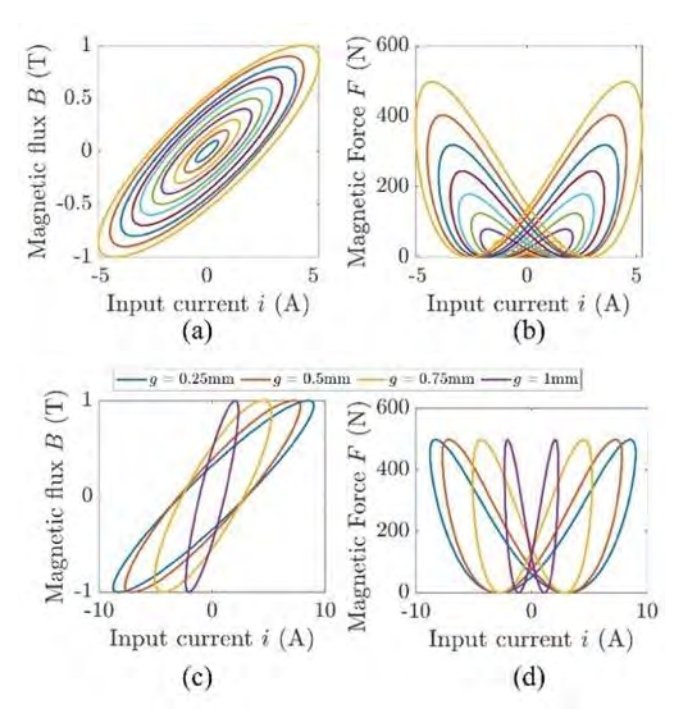


Fig.2: (a) *Current-f*lux and (b) *Current-f*orce characteristics at air gap =0.5 mm (c) *Current-f*lux and (d) *Current-f*orce characteristics at flux of 1T and various air gaps

AE-12. Magnetocaloric properties and magnetic structures in Tb_2CoGe_2

A. Herrero¹, A. Morozkin², E. Apiñaniz³, I. Puente-Orench⁴, A. Garshev^{5, 2}, V. Yapaskurt⁶, <u>A. Oleaga</u>¹

¹University of the Basque Country UPV/EHU, Bilbao,
Spain, ²Department of Chemistry, Moscow State University,
Moscow, Russian Federation, ³Universidad del País Vasco
UPV/EHU, Vitoria-Gazteiz, Spain, ⁴Institute Laue Langevin,
Grenoble, France, ⁵Faculty of Materials Science, Moscow State
University, Moscow, Russian Federation, ⁶Department of
Petrology, Moscow State University, Moscow, Russian
Federation

Rare earth based intermetallic materials are found to be competitive as magnetocaloric materials working in the gas liquefaction regions [1]. What is desirable is a combination of a high magnetic entropy change at the right temperature with a high value of the refrigerant capacity, which can be accomplished by selecting a material with several magnetic transitions close enough to maintain a tableau in the magnetic entropy change, thus expanding the temperature range of application [2]. In this study we present the compound Tb_2CoGe_2 from the R_2TX_2 family (R = Rare

earth; T = Mn, Fe, Co; X = p-block element) which will be compared with $Tb_2CoSi_2[3]$. Interestingly, the substitution of Si by Ge gives a complete turn to the magnetic/magnetocaloric properties.

Figure 1 shows the magnetization as a function of temperature. There is a first transition from the paramagnetic state to an antiferromagnetic one (in the case of $\mathsf{Tb}_2\mathsf{CoSi}_2$ this is ferromagnetic [3]). At lower temperatures T_M , there is a second magnetic transition which leads to complex magnetic states. Besides, there is a metamagnetic transition from an antiferromagnetic to a ferromagnetic state in $\mathsf{Tb}_2\mathsf{CoGe}_2$ with applied field (see inset in Fig 1). The magnetic entropy changes give rise to interesting magnetocaloric effects, as shown in figure 1b, with a table-like effect in the gas liquefaction regions, flat enough to be of interest.

Neutron diffraction measurements have also been carried out, both as a function of temperature and as a function of magnetic field (see figure 2), at ILL in Grenoble, in order to understand the role of rare earth and transition metal type/sublattices in magnetic ordering and resulting magnetic properties of these compounds, paying special attention to the low temperature phases which surely have a complex non-collinear arrangement of spins (incommensurate, canted AFM, etc.). The evolution of the lattice parameters and the magnetic moments at each magnetic site for this compound will be presented.

V. Franco, J.S. Blázquez, J.J. Ipus, J.Y. Law, L.M. Moreno-Ramírez, A. Conde, Prog. Mat. Sci. 93 (2018) 112-232.
 Y. Zhang, J. Alloys Compd. 787 (2019) 1173-1186.
 AV. Morozkin, A.V. Knoto, V.O Yapaskurt, M. Pani, R. Nirmala, Q. Quezado, S.K. Malik, J. Mag. & Mag. Mat. 413 (2016) 97-107

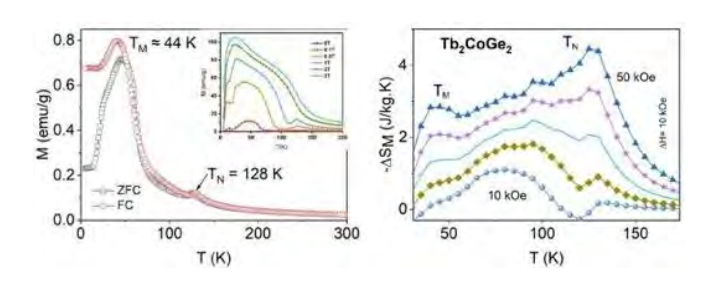


Figure 1. Left: zfc-fc magnetization vs temperature in field of 100 kOe, isofields in inset; right: Magnetic entropy change $-\Delta S_M$ for μ_0H from 1 T to 5 T

^{*} Best Student Presentation Finalist / LB – Late-breaking Poster

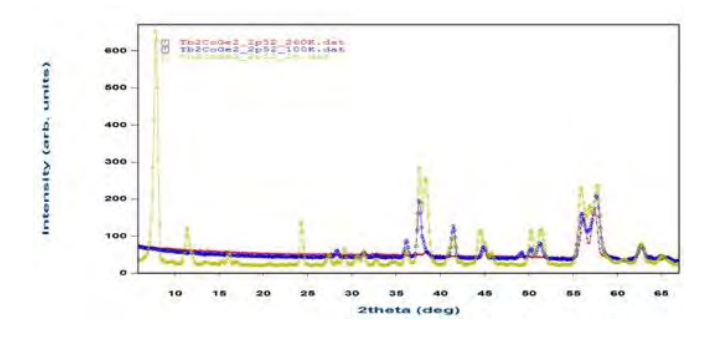


Fig. 2. Neutron diffraction patterns at 2, 100 and 260 K

SESSION AF: SPIN-ORBIT TORQUE AND RELATED PHENOMENA

Chair(s): R. Posti, *Physics, Carnegie Mellon University, Pittsburgh, Pennsylvania, United States*Tuesday, October 28, 2025

08:30 AM-12:00 PM

Room 2BC

AF-01. Symmetry-based Classifcation of Spin Current Origin B. Miao

Nanjing University, Nanjing, China

Spin current and the related spin-orbit torque are crucial for spintronic applications, including magnetic random access memory and spin current logic devices. Various methods have been reported to generate pure spin current, including the spin Hall effect, interface Rashba-Edelstein effect, spin splitting effect etc. Typically, these mechanisms induced phenomena are very similar thus distinguishing them is not straightforward.

Recently, we have developed systematic methods to distinguish different spin-charge conversion mechanisms based on the symmetry analysis and the reciprocal relation of the spin-charge inter-conversion. We identified the Rashba-Edelstein effect in Ag/Bi-ferromagnetic metal interface and solved the debate about the spin transport picture in Ag/Bi interface [1], isolated the anisotropic spin Hall effect and spin splitting effect contributions in RuO_2 [2], observed the anamolus spin Hall effect in Py and realized field-free switching of perpendicularly magnetized YIG with the *z*-polarized spin current [3]. [1] J. Cheng, B. F. Miao, Z. Liu, Phys. Rev. Lett. Vol. 129, p. 097203 (2022)

[2] Z. Q. Wang, Z. Q. Li, L. Sun, Phys. Rev. Lett. Vol. 133, p. 046701 (2024)

[3] M. Yang, L. Sun, Y. L. Zeng, Nat. Commun. Vol. 15, p. 3201 (2024)

AF-02. Observation of Field-Free Orbital Hall Torque Switching in In-Plane Magnetized NiFe/Cr Devices

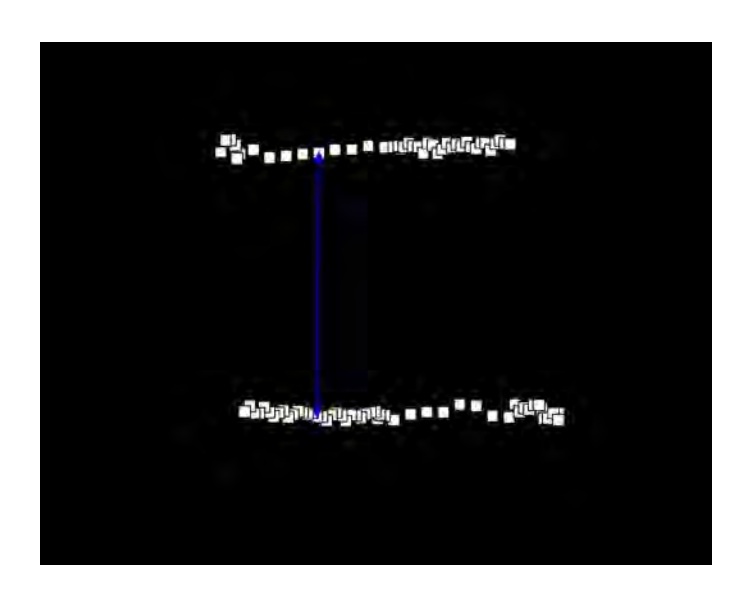
<u>A. Kumar</u>¹, A. Ashokan.K¹, C. Kalouni¹, K. Varshney¹, V. K. Malik², D. Roy¹

¹Physics, Indian Institute of Technology Ropar, Rupnagar, Punjab, India, ²Physics, Indian Institute of Technology Roorkee, Roorkee, Uttarakhand, India

We report field-free magnetization switching in an in-plane magnetized NiFe/Cr bilayer, enabled by orbital Hall torque (OHT). In this system, orbital currents are generated via the orbital Hall effect (OHE) in Cr, a 3d transition metal, and are converted into orbital torque at the NiFe/Cr interface. This torque is sufficient to deterministically switch the magnetization without the assistance of any external magnetic field or heavy-metal layers.

To investigate the efficiency of orbital torque, we systematically varied Cr thickness and performed room-temperature transport measurements. The in-plane magnetic anisotropy was confirmed by M–H loops, while planar Hall effect (PHE) measurements were used to probe the magnetization orientation. The torque efficiency was quantitatively extracted using second harmonic (2ω) Hall measurements, revealing consistent OHT behavior across the Cr thickness range. The switching process was electrically detected using the odd planar Hall voltage (O-PHV), a DC-based readout method that offers clear identification of magnetic states due to its odd symmetry with respect to magnetic field reversal. A robust O-PHV signal of 1.357×10^{-5} V was observed at a switching current of 30 mA.

To the best of our knowledge, this is the first demonstration of field-free switching in an in-plane magnetic system driven by orbital torque alone. Our findings, supported by direct switching measurements (Figure 1), establish a new framework for low-power, scalable orbitronic and spintronic device applications.



AF-03. Orbital Torque and Field-Free Magnetization Switching in a Light-Element-Based SOT Device

G. K. Shukla, S. Isogami

Research Centre for Magnetic and Spintronics Material, National Institute For Materials Science, Tsukuba, Ibaraki, Japan

Orbital torque from the orbital Hall effect (OHE) is gaining attention for next-generation orbitronic devices [1,2]. Unlike heavy-metal-based spin-orbit torque (SOT) systems [3], light metals offer a sustainable alternative, as OHE can generate substantial orbital currents without strong spin-orbit coupling (SOC) [4], which convert to spin currents in adjacent ferromagnets. To date, the OHE has been experimentally verified in only three systems: Cr [2], Ti [5], and Zr [6]. The other major challenge in SOT devices is achieving deterministic magnetization switching without an external in-plane field, called field-free switching (FFS) [7], which has been demonstrated using different techniques [8]. This study aims to fabricate light-element-based SOT devices for energy-efficient switching by harnessing orbital torque and achieving FFS.

A recent SOT device using 2D-MXene Cr_2N shows FFS driven by the OHE from its intrinsic band structure, highlighting the strong potential of 2D materials for OHE-based FFS [9]. Inspired by this discovery, we investigate FFS in a VN-based SOT device: Al_2O_3 substrate // VN(5) / $[Co(0.35) / Pt(0.3)]_3 / MgO(3)$ (in nm), aiming to utilize OHE from the VN layer. The VN has a (111)-oriented FCC structure with alternating V and N layers, resembling the layered nature of 2D-

MXenes. Figure 1(a) shows magnetization switching under various in-plane fields, with full switching under applied field and partial FFS without it, indicating high switching efficiency. The analysis of second harmonic Hall data for three different ferromagnetic layers on $[Co(0.35) / Pt(0.3)]_3$, CoFeB(1.5), and Py(4) (Fig. 1(b)) suggests that the [Co/Pt]₃ device exhibits a damping-like torque efficiency. which is twice that of CoFeB, while Py(4) exhibits the fieldlike behaviour due to small orbital to charge conversion efficiency. The field-free magnetization switching is attributed to broken mirror symmetry at the interface arising from the existence of small in-plane magnetic anisotropy. [1]. Zhao et al. Adv. Electron. Mater. 2024, 2400721 [2]. S. Lee et al. Commun. Phys. 2021, 4, 234. [3]. Song et al. Prog. Mater. Sci. 118 (2021) 100761 [4]. Kontani et al. Phys. Rev. Lett. 102, 016601. [5]. Choi et al., Nature 2023, 619, 52. [6]. Yang et al. Nat Commun 15, 8645 (2024). [7]. Yun et al. Sci. Adv.9, eadj3955(2023). [8]. Zheng et al. Nat Commun 12, 4555 (2021). [9]. P. Kumar et al. Small 2025, 2500626.

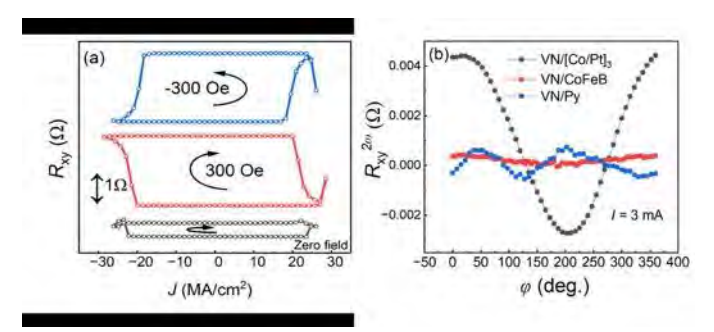


Fig.1. (a) Magnetization switching under zero, 300 Oe and - 300 Oe of in-plane external magnetic fields. (b) $R_{xy}^{2\omega}$ versus in-plane angle φ between the magnetic field and current direction for different ferromagnetic layers.

AF-04. Spin-orbit torque efficiency in IrPt alloy/ferromagnet bilayers

G. Jung¹, S. Lee², S. Ko³, S. Yoon¹, W. Kim¹, H. Jeon¹, H. Cho¹, D. Woo¹, K. Kim³, B. Park⁴, J. Hong², K. Eom¹, S. Lee¹

¹Semiconductor Engineering, Gachon University, Seongnam, Korea (the Republic of), ²Materials Science and Engineering, Yonsei university, Seoul, Korea (the Republic of), ³Physics, Korea Advanced Institute of Science and Technology, Daejeon, Korea (the Republic of), ⁴Materials Science and Engineering, Korea Advanced Institute of Science and Technology, Daejeon, Korea (the Republic of)

Spin-orbit torque (SOT) offers energy-efficient and ultrafast magnetization switching in spintronic devices [1]. Since SOT

^{*} Best Student Presentation Finalist / LB – Late-breaking Poster

originates from spin currents generated by the spin Hall effect (SHE) and/or the Rashba-Edelstein effect, extensive researches has been conducted to find materials capable of efficient charge-to-spin conversion. Recently, the orbital Hall effect has emerged as a promising candidate for generating large SOT, because it can provide larger angular momentum than the SHE. However, since orbital angular momentum cannot directly exert torque on magnetization, it must be converted into spin angular momentum through an orbital-to-spin conversion process enabled by spin-orbit coupling (SOC). This has motivated various approaches to facilitate orbital-to-spin conversion, such as inserting heavy metals (Pt, Ta, or W) or using ferromagnets (Gd or Ni) with strong SOC [2,3]. Nevertheless, orbital-to-spin conversion in alloy-based systems remains unexplored.

In this work, we investigate orbital-to-spin conversion in IrPt alloys, where Ir is theoretically predicted to exhibit significant orbital Hall conductivity [4], and Pt is known to provide efficient orbital-to-spin conversion due to its strong SOC [2]. We prepared IrPt (5 nm)/Co₄₀Fe₄₀B₂₀ (3 nm) bilayers, with the Ir concentration varied from 10 to 90 atomic percent (at%) in 10 at% steps. To evaluate SOT efficiencies and the corresponding orbital-to-spin conversion, harmonic Hall voltage measurements were performed. Fig. 1 shows that the damping-like torque efficiency (ξ_{DLT}) as a function of the Ir concentration. Interestingly, a significant enhancement is observed at Ir₅₀Pt₅₀. This enhancement may be attributed the combined effect of the large orbital Hall conductivity of Ir and the efficient orbital-to-spin conversion by Pt. These results expand our understanding of orbital-tospin conversion in alloy systems and provide new opportunities for energy-efficient spintronic devices based on the orbital degree-of-freedom.

- [1] J. Ryu, S. Lee, K.-J. Lee, et. al., Adv. Mater., Vol. 32, p.1907148 (2020).
- [2] S. Lee, M. G. Kang, D. Go, et. al., Commun. Phys., Vol. 4, p.234 (2021).
- [3] G. Sala and P. Gambardella, Phys. Rev. Research, Vol. 4, p.033037 (2022).
- [4] L. Salemi and P. M. Oppeneer, Phys. Rev. Mater., Vol. 6, p.095001 (2022).

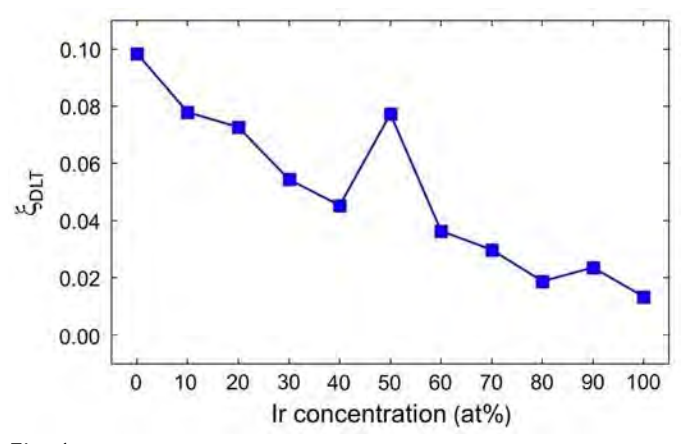


Fig. 1 Damping-like torque efficiencies (ξ_{DLT}) as a function of Ir concentration in IrPt (5 nm)/Co₄₀Fe₄₀B₂₀ (3 nm) bilayers.

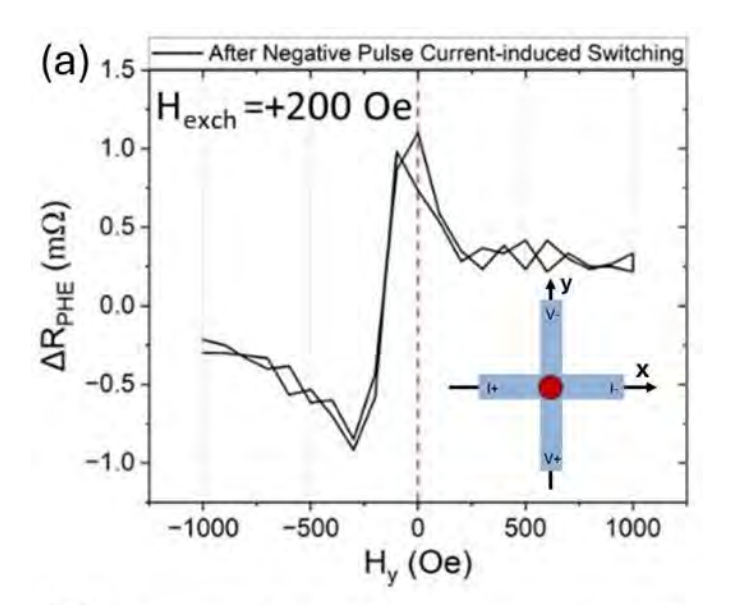
AF-05. Spin-orbit torque switching of both magnetization and exchange bias in Pt/IrMn/CoFeB Hall cross devices Y. Fan, L. Wan, G. Mihajlović, J. Gibbons, J. Katine, T. Santos Western Digital, San Jose, California, United States

Electrical switching of the exchange bias in an exchangebiased free layer of a magnetic tunnel junction in contact with a spin-orbit torque (SOT) layer has shown promise for MRAM applications due to its field-free switching mechanism, scalability, excellent magnetic field immunity, and good endurance [1-4]. Here we utilize the differential planar Hall effect (PHE) [5] to measure the SOT-induced switching of both in-plane magnetization and exchange bias in a Pt/IrMn/CoFeB Hall cross device (Fig. 1 inset), where a patterned IrMn/CoFeB circular dot sits in the center of the Hall cross device and on top of the Pt SOT channel. The initial direction of the exchange bias between the antiferromagnetic IrMn layer and the CoFeB free layer is set by the direction of the in-plane magnetic field applied during anneal after film deposition. During the transport experiment, in addition to the pulse current-induced magnetization switching, the exchange bias switching has been verified by measuring differential PHE versus field loops (Fig. 1a,b), which explicitly show the direction change of the exchange bias achieved by the pulse current and the monostable state of the bit (at H=0 Oe) after the reversal. The Hall cross device structure and the differential PHE method provide an efficient way to explore the currentinduced exchange bias switching mechanism in the IrMnbased material stack, since the initial exchange bias condition and the applied electric current direction in the Hall cross device can be easily tailored. The efficient

^{*} Best Student Presentation Finalist / LB – Late-breaking Poster

switching of exchange bias by electrical current could initiate new strategies toward achieving ultra-low power, magnetically immune, high-performance spintronic memory devices.

- [1] A. Du et al., Nat. Electron. 6, 425-433 (2023).
- [2] A. Du et al., Adv. Electron. Mater. 10, 2300779 (2024).
- [3] W. Cai et al., arXiv:2410.13202 (2024).
- [4] D. Xiong et al., IEEE IEDM 1-4 (2024). doi:
- 10.1109/IEDM50854.2024.10873465.
- [5] G. Mihajlovic et al., Appl. Phys. Lett. 109, 192404 (2016).



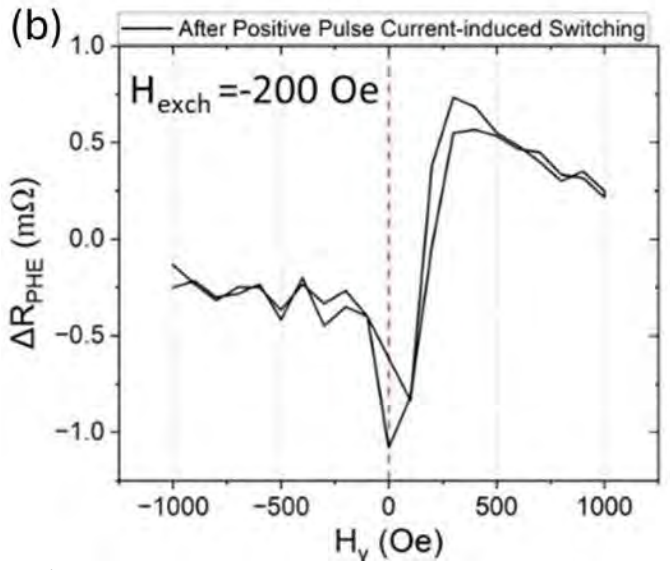


Fig 1. Exchange bias direction measured in the device after negative (a) and positive (b) pulse current-induced switching in the Hall cross device, respectively. Inset: Schematic of the Hall cross device geometry.

AF-06. Spin-Orbital Conversion in Resonantly Excited Magnetization

O. A. Bakare¹, G. T. Street¹, R. E. Maizel¹, C. Klewe², S. Emori¹ Physics, Virginia Tech, Blacksburg, Virginia, United States, ²Lawrence Berkeley National lab, Berkeley, California, United States

Recent work suggests that the dynamics of orbital magnetization, albeit typically much smaller than spin magnetization, can play a critical role in ferromagnets and their heterostructures [1-3]. However, quantifying the relative magnitudes of orbital and spin dynamics remains challenging.

Here, we quantitatively compare the orbital-to-spin moment ratios (μ_L/μ_S) of the equilibrium *static* magnetization [Fig. 1(a)] and the resonantly excited dynamic magnetization [Fig. 1(b)] in Co-based ferromagnets. We used a unique method of ferromagnetic resonance probed by X-ray magnetic circular dichroism (XMCD), that enables direct sum-rule quantification of μ_L/μ_S of the dynamic magnetization [4]. Figure 1(c) summarizes the integrated XMCD spectra of 2.5nm-thick Co capped with Ti, from which we obtain μ_L/μ_S = 0.0988 ± 0.0005 for the dynamic magnetization. This value is \approx 6% greater than 0.0931 ± 0.0015 for the static magnetization of the same sample, measured on the same X-ray synchrotron beamline. We similarly observe ≈5-7% greater μ_L/μ_S for the dynamic magnetization than for the static magnetization, in Co interfaced with Pt and Cu/Pt, as well as Co₉₂Ho₈ [Fig. 2]. This implies that the dynamic magnetization within Co gains an enhanced orbital moment, potentially through the conversion of spin to orbital moment during resonant excitation [3].

Furthermore, $Co_{50}Pt_{50}$ exhibits an even greater relative enhancement of μ_L/μ_S between dynamic and static magnetizations, at $\approx 14\%$ [Fig. 2]. This observation suggests that the strong spin-orbit coupling from Pt may mediate a more efficient spin-orbital conversion within the ferromagnet. Our research provides unique quantitative insights into the fundamental dynamics of spin and orbital moments.

[1] D. Go, K. Ando and A. Pezo, *Phys. Rev. B.*, *111(14)*, L140409 (2025).

[2] H. Hayashi, D. Go and S. Haku, *Nature Electronics.*, *7*(8), 646-652 (2024).

^{*} Best Student Presentation Finalist / LB - Late-breaking Poster

[3] Y. Chen, H. Chen and X. Shen, *Phys. Rev. Lett.*, *134*(13), 136701 (2025).

[4] S. Emori, R. E. Maizel and G. T. Street, *Appl. Phys. Lett.*, *124*(12), 122404 (2024).

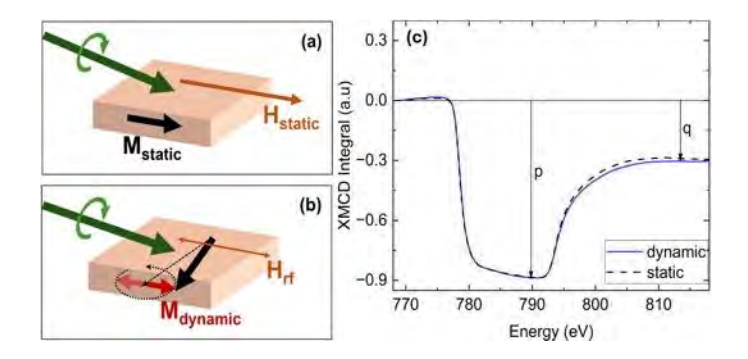


Fig. 1 XMCD measurements with (a) static magnetization, M_{static} ; (b) dynamic magnetization, M_{dynamic} . (c) Static and dynamic integrated XMCD spectra at Co $L_{3,2}$ edges. The moment ratios is computed from the sum-rule formula, $\mu_{\text{L}}/\mu_{\text{S}} = (2/3)(q / (3p - 2q))$.

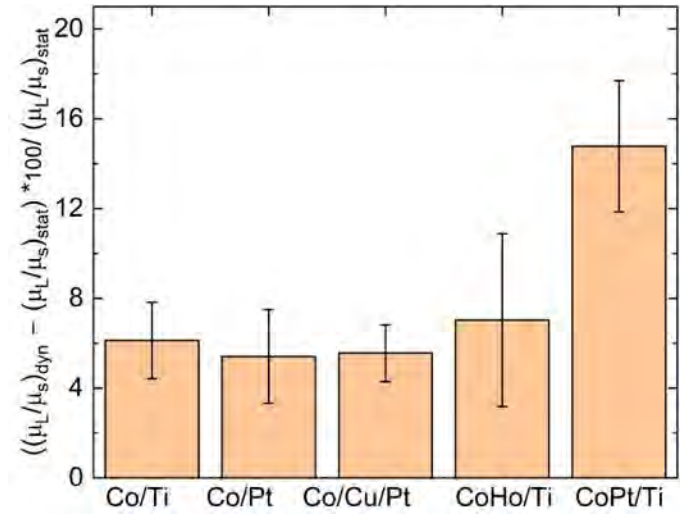


Fig. 2 Relative enhancement of μ_L/μ_S between the dynamic and static magnetizations for different Co-based ferromagnets.

AF-07. Harnessing Spin Reorientation for Energy-efficient Field-free Switching by Orbital Torque

S. Das, B. Jamshed, M. Ramu, <u>S. Piramanayagam</u> School of Physical & Mathematical Sciences, Nanyang Technological University, Singapore, Singapore

Current-induced spin-orbit torque (SOT) has emerged as a promising method for achieving energy-efficient magnetisation switching in advanced spintronic devices. Over the past few decades, researchers have primarily focused on enhancing spin current generation through the spin Hall effect, relying predominantly on the spin degree of freedom of electrons while neglecting their orbital counterparts. However, Orbital Torque (OT) has emerged as an alternative to SOT in recent theoretical studies, due to its potential in making more energy-efficient devices. However, the superiority of OT over SOT is yet to be proven experimentally. Concurrently, magnetisation switching of PMA requires an in-plane magnetic field to break inversion symmetry, which increases power consumption and limits their industrial applications. Moreover, there has not been much research in field-free switching (FFS) on materials systems with orbital torque. In this study, we demonstrated an FFS by tuning the spin reorientation in a series of synthetic antiferromagnetic (SAF) samples. We effectively modified the exchange coupling field and magnetic anisotropy of the SAFs by fine-tuning the magnetic layer thickness. We obtained a magnetisation switching of 96 % in the optimised SAF sample utilising both spin and orbital torque. Additionally, we optimised the orbital Hall layer thickness to further enhance the energy efficiency of our devices. We obtained a 12 % reduction in critical switchina current density and a 21 % enhancement of switching efficiency in the optimised sample compared to the reference sample with a Pt (5 nm) layer. Our study underscores the potential of combining orbital and spin Hall effects, and SAFs to drive next-generation spintronics, combining high-density integration with improved energy efficiency.

- 1. Kammerbauer et. al., Nano Lett. 2023
- 2. YuheYang et. al., Nature Communications (2024) 15:8645
- 3. Rahul Gupta, Chloé Bouard, and Mathias Kläui, Nature Communications (2025) 16:130

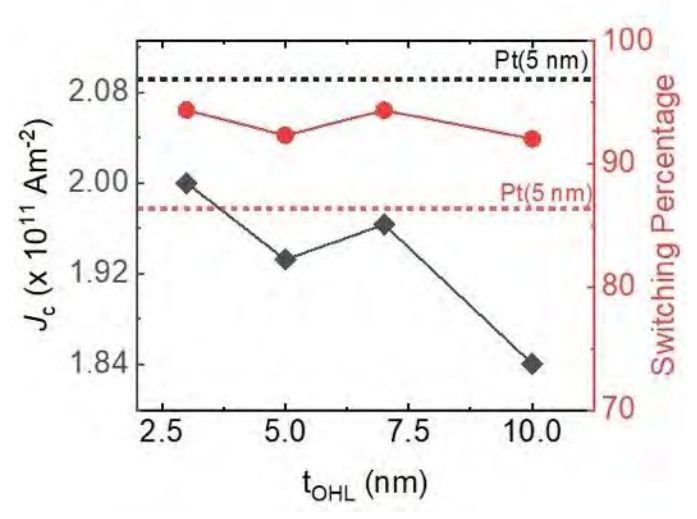


Fig. 1 The figure shows the critical switching current density (black squares) and switching percentage (red circles) as a function of the orbital Hall layer thickness. The dotted line represents the corresponding values of the reference sample with Pt (5 nm) spin Hall layer.

AF-08. Orbital-Spin Hall nano oscillator

R. Gupta^{1, 2}, N. Behera¹, U. Shashank¹, A. Kumar^{1, 3, 4}, S. Ghosh¹, J. choi¹, J. Akerman^{1, 3, 4}

¹Physics, University of Gothenburg, Gothenburg,
Sweden, ²Physics, University of South Florida, Tampa, Florida,
United States, ³Research Institute of Electrical Communication,
Tohoku University, Sendai, Japan, ⁴Center for Science and
Innovation in Spintronics, Tohoku University, Sendai, Japan

The Spin Hall Effect (SHE) offers promising applications in spintronic devices, such as controlling magnetization in magnetic random-access memory (MRAM) [1,2], spin Hall nano-oscillators (SHNOs) [3], spintronic terahertz emitters [4], and magnetic sensors [5]. To further enhance the efficiency and material flexibility of such devices, orbitronics has emerged as a compelling direction by utilizing the orbital angular momentum (OAM) of electrons, which can give rise to sizable orbital currents even in materials with weak intrinsic spin-orbit coupling (SOC). Motivated by this, we adopted an approach based on the orbital Hall effect (OHE) [6-9], which is analogous to the SHE but generates an orbital current from a charge current without requiring high-SOC materials. Theoretical predictions suggest that the charge-to-orbital conversion efficiency can be an order of magnitude higher than the charge-to-spin conversion efficiency, enabling the

development of more efficient devices [10]. For example, this allows for a larger spin-orbit torque (SOT) to switch the magnetization, thereby reducing the switching current required for magnetization reversal in SOT-MRAM and the threshold current for auto-oscillations in SHNOs. In this work, we fabricated nanoscale SHNOs in the form of constriction-type devices with varying constriction widths. We employed a series of bilayer and trilayer stacks comprising both orbital Hall materials and conventional spin Hall materials (e.g., Ta and Pt) as sources of orbital and spin currents, respectively. Power spectral density (PSD) measurements were carried out as a function of the applied DC current, revealing that our oscillator devices incorporating orbital current sources exhibited a ~50% reduction in the auto-oscillation threshold current compared to their SHE-dominated counterparts, as shown in Figure 1 [11]. This significant reduction highlights the potential of orbital torques to improve oscillator device efficiency.

Furthermore, we investigated the sign and magnitude of the effective SOT efficiency in different oscillator devices. Remarkably, we observed that the SOT efficiency in our orbital-SHNOs remained positive, even when the stack included a material with a negative spin Hall conductivity. This observation is in excellent agreement with theoretical predictions regarding orbital-to-spin conversion mechanisms, as well as with the calculated signs of orbital and spin Hall conductivities in our stack [11]. These findings provide compelling experimental evidence for the active role of orbital currents in driving magnetization dynamics and reinforce the potential of orbitronics to complement—or even replace—conventional spintronic approaches in future device architectures.

- [1] J. Sinova et al.; Rev. Mod. Phys., 2015, 87, 1213.
- [2] S. Husain, R. Gupta, et al.; Appl. Phys. Rev., 2020, 7, 041312.
- [3] S. Jiang et al.; Appl. Phys. Rev., 2024, 11, 041309.
- [4] R. Gupta et al.; Adv. Optical Mater., 2021, 9, 2001987.
- [5] S. Koraltan, R. Gupta, et al.; Phys. Rev. App., 2023, 20, 044079.
- [6] D. Go et al.; Phys. Rev. Lett., 2018, 121, 086602.
- [7] S. Ding et al.; Phys. Rev. Lett., 2020, 125, 177201.
- [8] A. Bose, R. Gupta, et al.; Phys. Rev. B, 2023, 107, 134423.
- [9] R. Gupta et al.; Nat. Commun., 2025, 16, 130.
- [10] L. Salemi et al.; Phys. Rev. Mat., 2022, 6, 095001.
- [11] R. Gupta et al.; Under preparation, 2025.

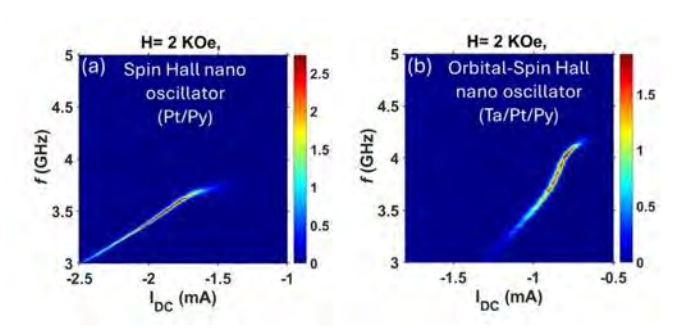


Fig. 1 Power spectral density (PSD) versus applied current $(I_{\rm d.c.})$ for the nano-constrictions in (a) Pt/Py spin Hall nano oscillators and (b) Ta/Pt/Py orbital-spin Hall nano oscillators.

AF-09. Spin-Orbit Torque and Nernst Effects in a Bulk Rashba Channel

J. Ahn^{1,2}, J. Jeon³, S. Cho², S. Lee², O. Lee², H. Koo^{1,2}
¹KU-KIST Graduate School of Converging Science and Technology, Korea University, Seoul, Korea (the Republic of), ²Center for Semiconductor Technology, Korea Institute of Science and Technology, Seoul, Korea (the Republic of), ³Package Manufacturing Technology Group, Samsung Electro-Mechanics, Busan, Korea (the Republic of)

Spin-orbit coupled systems are capable of generating spin torque and driving ferromagnetic switching by converting charge currents into spin currents. While earlier research has largely centered on Rashba spin-orbit coupling in twodimensional electron systems and heavy metal/ferromagnet (HM/FM) bilayers [1,2], there has been growing interest in materials like GeTe that possess strong bulk Rashba-type spin-orbit interactions [3]. In this study, we investigate the spin-orbit torques in GeTe/FM bilayers using harmonic measurement and spin-torque ferromagnetic resonance (ST-FMR). We fabricated GeTe/NiFe bilayer Hall bar devices and performed second harmonic measurement [4]. Defining ϑ as the angle between the channel current and external magnetic field, the second harmonic transverse voltage can be expressed as [5]: $V_{2\omega} = C_1 \cos 2\vartheta \cos \vartheta + C_2 \cos \vartheta$ where C_1 is a function of the field-like torque and C_2 is a function of the damping-like torque and thermoelectric effects. Analyzing the external magnetic field dependence of C_1 and C_2 allows for the extraction of field-like and damping-like torque, respectively. However, accurate determination of dampinglike torque was challenging due to dominant contribution of the thermoelectric effects to $V_{2\omega}$. Especially, the ordinary Nernst effect dominates C_2 , making it difficult to separate

damping-like torque. To overcome this, we employed ST-FMR to reliably estimate damping-like torque in GeTe/NiFe and GeTe/CoFeB bilayer [6]. Using standard ST-FMR analysis models [7], we extracted the spin—orbit torque efficiencies for both systems. In Fig. 1, the measured damping-like torque and field-like torque efficiencies were 0.166 and 0.404 for GeTe/NiFe, and 0.257 and 0.161 for GeTe/CoFeB, respectively. These values are significantly higher than those typically observed in conventional HM/FM bilayers, where the efficiencies generally remain below 0.1 [8]. This indicates that GeTe/FM structures offer notably enhanced spin—orbit torque performance, highlighting their potential for spintronic device applications.

- 1. H. C. Koo, J. H. Kwon and J. Eom, Science, Vol. 325, p.1515 (2009)
- 2. I. M. Miron, K. Garello and G. Gaudin, Nature, Vol. 476, p.189 (2011)
- 3. D. D. Sante, P. Barone and R. Bertacco, Adv. Mater., Vol. 25, p.509 (2013)
- 4. J. U. Ahn, J. Jeon and S. W. Cho, Curr. Appl. Phys., Vol. 49, p.12 (2023)
- 5. C.O. Avci, K. Garello and M. Gabureac, Phys. Rev. B, Vol. 90, p.224427 (2014)
- 6. J. U. Ahn, J. Jeon and S. W. Cho, Phys. Status Solidi B, Vol. 261, p.2300334 (2024)
- 7. C.-F. Pai, Y. Ou and L. H. Vilela-Leão, Phys. Rev. B, Vol. 92, p.064426 (2015)
- 8. A. Manchon, J. Zelezný and I. M. Miron, Rev. Mod. Phys., Vol. 91, p.035004 (2019)

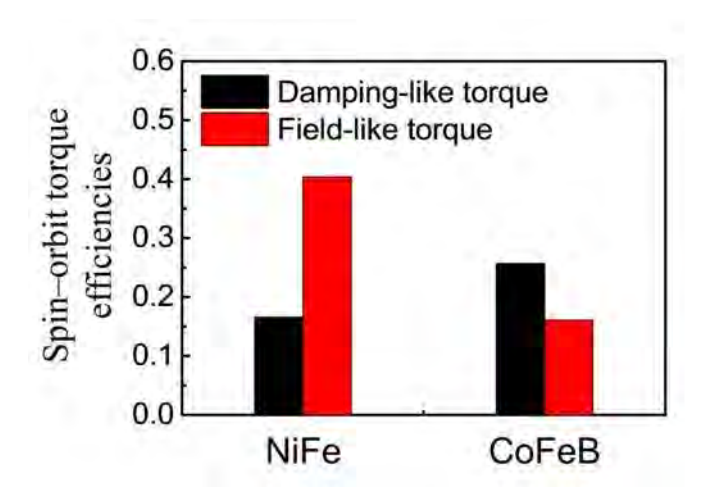


Fig. 1. Spin-orbit torque efficiencies of GeTe/NiFe and GeTe/CoFeB systems

AF-10. Enhancement of damping-like spin-orbit torque efficiency in $RuO_2/\alpha W$ -Ta and RuO_2/Pt systems

Y. Saito¹, S. Ikeda^{1, 2}, S. Karube³, T. Endoh^{1, 4}

¹Center for Innovative Integrated Electronic Systems, Tohoku University, Sendai, Japan, ²Center for Science and Innovation in Spintronics, Tohoku University, Sendai, Japan, ³Institute for Chemical Research, Kyoto University, Kyoto, Japan, ⁴Department of Electrical Engineering, Graduate School of Engineering, Tohoku University, Sendai, Japan

In recent years, spin-orbit torque (SOT) and orbital torque (OT) originating from the spin-Hall effect (SHE), orbital-Hall effect (OHE) and orbital Rashba-Edelstein effect (OREE) have aroused extensive interest among researchers due to their potential applications for spin devices. For realizing these devices, metal electrode with both high SOT and low resistivity (ρ_{xx}) is necessary, which is important to achieve low power consumption SOT switching. As the magnitudes of OHE and OREE are nearly independent of magnitude of spin-orbit coupling of the nonmagnetic layer, a large OT is expected to be obtained by using light metals, which generally have lower ρ_{xx} than heavy metals. However, it is not clear what kind of multilayer structures using light metals, heavy metals and ferromagnetic materials are most preferable for realizing a large SOT with low ρ_{xx} . Moreover, it was reported that oxygen treatment of light elements has a strong effect on SOT due to the OREE in the ferromagnet/Pt/CuO_x system [1]. On the other hand, in the reversed CuO_x/Pt/ferromagnet structure, a decrease in the spin pumping signal was reported, indicating a decrease in the SOT efficiency [2]. These results indicate that we should carefully consider the order of the structures and the signs of OH conductivity (σ_{OH}) and SH conductivity (σ_{SH}) for increasing SOT efficiency.

In this work, we comparatively study the SOT in RuO_2/α -WTa and RuO_2/Pt systems. As a result, using the WTa or Pt as a material on top of RuO_2 , we observed enhancement of the SOT efficiency and perpendicular magnetization of ferromagnet on both WTa and Pt layers (Fig. 1). Moreover, field-free switching for the samples with RuO_2/Pt layers in the thickness range of $t_{Pt} \le 2$ nm has been observed (Fig.2) [3].

In this presentation, we will also show the results of light metal insertions and discuss the correlation between the SOT efficiency and the signs of σ_{OH} and σ_{SH} comparing between RuO₂/WTa and RuO₂/Pt systems, and the possible origin for the observed field-free switching. This work was supported by the CIES Consortium, X-NICS (No. JPJ011438), and JSPS KAKENHI (JP24H00030, JP21K18189).

- [1] S. Ding et al., Phys. Rev. Lett. 125, 177201 (2020).
- [2] E. Santos et al., Phys. Rev. B 109, 014420 (2024).
- [3] Y. Saito et al., Phys. Rev. B 110, 134423 (2024).

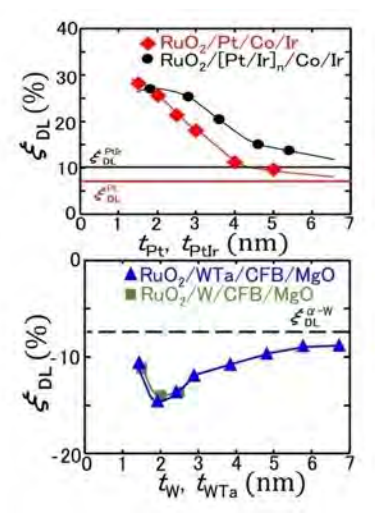


Fig. 1 SOT efficiency as functions of t_{Pt} , t_{Ptlr} , t_{W} and t_{WTa} .

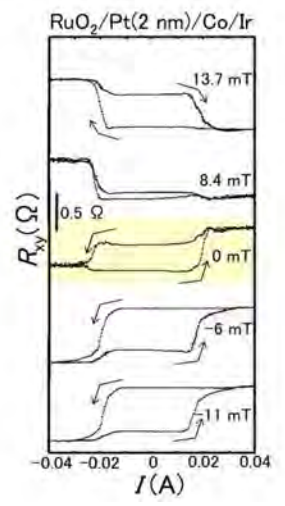


Fig. 2 Current-induced SOT switching.

SESSION AG: ELECTRONIC STRUCTURE AND MAGNETIC EXCITATIONS

Chair(s): C. Beekman, Florida State University, Tallahassee,
Florida, United States
Tuesday, October 28, 2025
08:30 AM-12:00 PM
Room 2A

AG-02. Realistic modeling of transport properties at finite temperature in magnetic materials by local quantization of a Heisenberg model

F. Engelke^{1, 2}, C. Heiliger^{1, 2}

¹Institute for theoretical Physics, Justus Liebig University Giessen, Giessen, Hesse, Germany, ²Center for Materials Research, Justus Liebig University Giessen, Giessen, Hesse, Germany

The quantitative description of the electrical resistivity of a magnetic material remains challenging to this day. Qualitatively, it is well understood that the temperatureinduced lattice and spin disorder determines the temperature dependence of the resistivity. While prior publications reached good agreement with experiment in the so-called supercell or direct approach for non-magnetic materials where the spin-disorder contribution to the resistivity is negligible, an accurate, purely theoretical description of magnetic materials remains elusive. This shortcoming can be attributed to the missing accuracy in the description of the temperature-dependent spin-disorder itself. In this work, we employ a joint approach from abinitio transport calculations and atomistic modeling of the temperature-dependent spin-disorder. Using the example of α -Fe, we demonstrate that the inclusion of quantum mechanical effects using a semiclassical local quantization of the Heisenberg model significantly improves the description of the spin-disorder component to the electrical resistivity (cf. Fig. 1). Compared to previous approaches, this model includes the description of magnetic short-range order effects, enabling us to study temperature effects around and above the Curie temperature, where prior meanfield theory-based approaches inevitably predicted a constant contribution (cf. Fig. 2).

[1] G. White and S. Woods, Philosophical Transactions of the Royal Society of London. Series A, Vol. 251, p. 273 (1959) [2] Y. Liu, Z. Yuan, R. J. H. Wesselink, Physical Review B, Vol. 89, 220405 (2015)

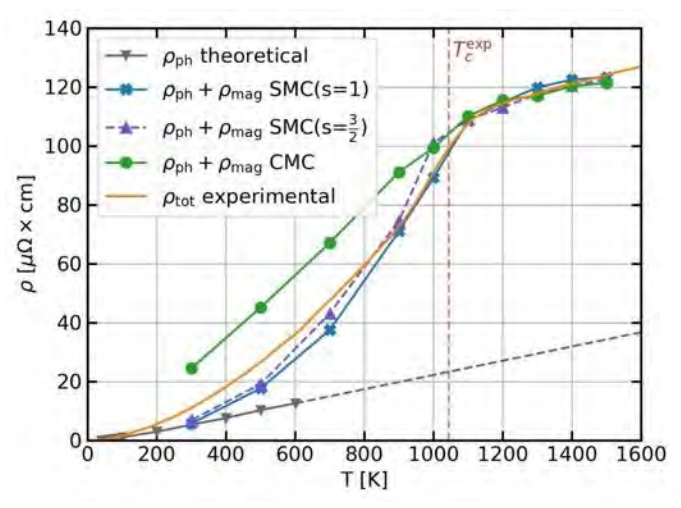


Fig. 1 Comparison of total specific electrical resistivity for classical and semiclassical description with experimental data, under the assumption of Matthiessen's rule. Experimental Data taken from ref. [1]. Theoretical phonon contribution taken from ref. [2].

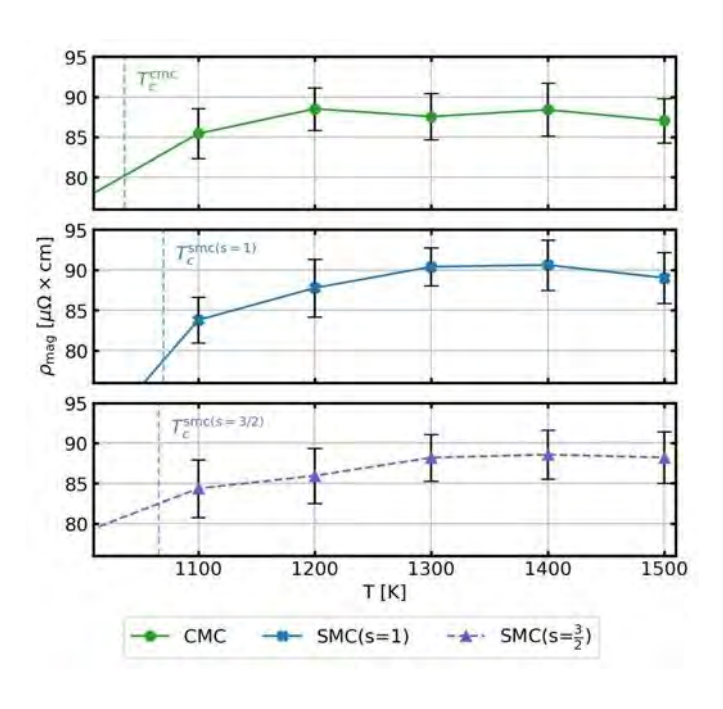


Fig. 2 Comparison of isolated spin-disorder resistivity obtained from CMC and SMC based calculations above the Curie temperature. Error bars indicate statistical uncertainty based on the fitting procedure alone.

AG-03. Observation of multiple flat bands and van-Hove singularities in the distorted kagome metal NdTi₃Bi₄

M. Mondal¹, A. Sakhya¹, M. Sprague¹, B. Ortiz², M. Matzelle³, A. Kumay¹, A. Seal¹, B. Ghosh³, A. Bansil³, M. Neupane¹

¹Physics, University of Central Florida, Orlando, Florida, United States, ²Oak Ridge National lab, Oak Ridge, Tennessee, United States, ³Physics, Northeastern University, Boston, Massachusetts, United States

Kagome materials have attracted enormous research interest recently owing to their diverse topological phases and manifestation of electronic correlation. Here, we present the electronic structure of a distorted ferromagnetic kagome metal, NdTi₃Bi₄, exhibiting a transition temperature of 9 K. Our investigation employs a combination of angleresolved photoemission spectroscopy (ARPES) measurements and density functional theory (DFT) calculations. We discover the presence of two "flat" bands which are found to originate from the kagome structure formed by Ti atoms with major contribution from Ti d_{xv}orbitals. We also observed multiple van-Hove singularities (VHSs) in its electronic structure, with one VHS lying near the Fermi level. The ARPES data reveals the existence of Dirac cone at the K point, a finding which is corroborated by our DFT calculations. These findings present detailed electronic structure capable of hosting correlation-driven phenomenon in this novel ferromagnetic kagome metal.

AG-04. Gapless Topological Behaviors in a Long-Range Quantum Spin Chain

S. Yanq¹, H. Lin¹, X. Yu^{2, 3}

¹Institute for Advanced Study in Physics and School of Physics, Zhejiang University, Hangzhou, Zhejiang, China, ²Department of Physics, Fuzhou University, Fuzhou, Fujian, China, ³Fujian Key Laboratory of Quantum Information and Quantum Optics, College of Physics and Information Engineering, Fuzhou University, Fuzhou, Fujian, China

Topology in condensed matter physics is typically associated with a bulk energy gap. However, recent research has shifted focus to quantum critical points or phases that exhibit nontrivial topological properties. In this work, we explore a cluster Ising chain with long-range antiferromagnetic interactions that decay as a power law with distance. Using large-scale density matrix renormalization group simulations, we unambiguously demonstrate that the nontrivial topology at the critical point

remains stable against long-range interactions, resulting in a topologically nontrivial critical line. Remarkably, even within the gapped region, the interplay between topology and long-range interaction can give rise to a new topological phase featuring algebraic decay correlation and edge modes, similar to gapless topological phases. Hence, we refer to this new phase as the algebraic topological phase, which exhibits nontrivial gapless topological behaviors and arises solely from long-range interactions without any short-range counterpart. This presentation is based on findings published in Communications Physics 8, 27 (2025).

- S. Yang, H.-Q. Lin and X.-J. Yu, Commun Phys., 8, 27 (2025)
 T. Scaffidi, D. E. Parker and R. Vasseur, Phys. Rev. X, 7, 041048 (2017)
- o R. Verresen, R. Thorngren, N. G. Jones and F. Pollmann, Phys. Rev. X, 11, 041059 (2021)

AG-05. Altermagnetism: What can we believe?

<u>P. S. Stamenov</u>, M. T. Stamenova School of Physics and CRANN, Trinity College, Dublin, Dublin, Ireland

Altermagnetism has been promoted as an alternative class of magnetic order to encompass a range of *collinear* antiferromagnets, the crystal time-reversal symmetry breaking in which should support the existence of spontaneous Hall and spin Hall effects.[1] The requirements for a material to belong to the class can be summarized as: (1) collinear antiferromagnet, containing an even number of atoms in the unit cell; (2) lack of inversion symmetry between the magnetic sublattices, due to the presence of non-magnetic ions in their vicinity; (3) sublattices connected by translation and rotation and (4) spin sublattice point group corresponding to the lattice position point group or spin being a good quantum number essentially everywhere.[2]

Experimental evidence for the implications of atermagnetic bandstructures could be: (1) non-vanishing anomalous Hall effect, with vanishing non-collinearity and vanishing net moment; (2) strong non-degeneracy of the spin-resolved band structure close to the Fermi level such as evidenced by SARPES and (3) Fermi-surface cross section measurements by means of quantum oscillations at high magnetic field, i.e. dHvA and ShdH, showing angular dispersions compatible with the ones predicted by symmetry-constrained DFT. All of these should ideally be accompanied by reliable

estimates of the spin components and local fields, as provided by polarized neutron diffraction and muon spin rotation spectroscopy. Unfortunately, there are only few examples, where multiple techniques are deployed on the same samples.

Here we focus on several candidate altermagnets (and candidate collinear antiferromagnets supporting topological fermions near the Fermi level): RuO₂, CrSb, FeS and CuMnAs, by comparing standard relativistic electronic structure calculations within the framework of DFT, using the GGA approximation for the exchange-correlation potential, with SOC. All of these are either metallic or fully-degenerated semiconductors. We compute and match closely the experimental observables: ARPES cross-sections, MCD maps, Berry curvature-induced Hall and spin-Hall effect and angular dispersions of the Quantum Oscillations, without imposing strict altermagnetic symmetry and without introducing Hubbard *U* and *J* terms or adjusting the Fermi level position in any substantial way.

In all of the above example cases, non-negligible noncollinearity of the spin states (distributions) exists, lowering the overall Berry curvature and hence the magnitude of the spontaneous Hall and spin Hall coefficients. SOC results in avoided band-crossings and band-touches, and Fermisurface reconstructions, which have support over substantial regions of k-space, where spin is not a good quantum number. In the specific case of RuO₂, a mounting body of evidence [5] suggests that the available moments and spin splitting are small, and that any magnetic order may only bring about rather small magnetotransport and galvanomagnetic effects, in application [6]. In view of this, we hope that tighter scrutiny of the available experimental data and its matching to model calculations will result in a much more critical approach to new candidate altermagnets (and practical applications of the phenomenon) and possibly reconsideration of some of the ones already in circulation.

[1] L. Smejkal, R. G-Hernandez, T. Jungwirth and J. Sinova *Sci. Adv.*, Vol. 6, eaaz8809 (2020)

[2] L. Smejkal, J. Sinova and T. Jungwirth *Phys. Rev. X*, Vol. *12*, 031042 and 040501 (2022)

[3] O. Fedchenko, J. Minar A. Akashdeep, et. al. *Sci. Adv.*, Vol. *10*, eadj4883 (2024)

[4] Z. Wu, M. Long, H. Chen, et. al. *arXiv*: [cond-mat.matrl-sci], 2503.20621v1 (2025)

[5] M. Hiraishi, H. Okabe, A. Koda, et. al. Phys. Rev. Lett., Vol. 132, 166702 (2024)

[6] H. Chen, Z-A. Wang, P. Qin, et. al. Adv. Mat., 2507764 (2025)

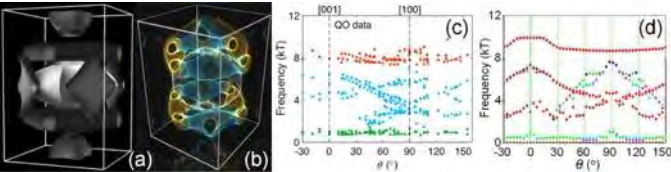


Figure 1. (a) Fermi surface of altermagnetic RuO₂, after [3]. (b) Spin-resolved Fermi surface of non-collinear RuO₂, resulting in ARPES, MCD, AHE and dHvA predictions matching the available experimental data. (c) Quantum Oscillations spectra (Fermi surface extremal sections), measured via dHvA torque in RuO₂, after [4]. (d) Predicted, using the computed FS from (b) dHvA frequencies for (*k*-local, w.r.t. local quantisation axis) spin up. *Note*: The colours in (d) correspond to topological connectivity of the FS sections and do not follow the convention of (c). The spin-down frequencies are similar (courtesy of the relatively small spin splitting) but are not shown here, for reasons of clarity.

AG-06. Electronic and Magnetic Properties of Hole Doped Topological Kagome Metal Thin Films

<u>R. Dutta</u>¹, P. M. Laxmeesha¹, T. Tandon¹, T. D. Tucker¹, S. Sheikh², U. M. Jayathilake², W. Tian³, A. Aczel³, T. Lee⁴, A. X. Gray², S. May¹

¹Department of Materials Science and Engineering, College of Engineering, Drexel University, Philadelphia, Pennsylvania, United States, ²Department of Physics, Temple University, Philadelphia, Pennsylvania, United States, ³Neutron Scattering Division, Oak Ridge National Laboratory, Oak Ridge, Tennessee, United States, ⁴Diamond Light Source Ltd., Didcot, United Kingdom

Topological quantum materials with magnetically active atoms on a kagome sublattice have received tremendous attention due to the possibilities of manifesting the topological band features like linear dispersive Dirac cone (DC) and nondispersive flat bands (FBs), Weyl points, and Van Hove singularity [1-4]. Thus, through positioning the Fermi level (E_F) relative to FB and DC, one can move from nearly massless excitations to correlated electronic phenomena such as magnetism, superconductivity and density waves. Previous work on kagome materials such as FeSn, CsV₃Sb₅, and YMn₆Sb₆ have verified the presence of FB and ordered magnetic states [5-7]. Magnetism and electronic properties within these materials depend on the orbital characteristics in the vicinity of the E_F with respect to the FB. This is best illustrated in electron doped Fe_{1-x}Co_xSn

alloys where antiferromagnetism gets diminished to a spin glass phase as the $E_{\rm F}$ moves above the FB upon Co substitutions [8]. Here, we present topological hole doped kagome FeSn metals where interdependent magnetism and band structures are studied. FeSn (sq. P6/mmm, $T_N \sim 365$ K) exhibits metallic signatures and magnetic spins are aligned in an A-type antiferromagnet (AFM) sublattice. Our recent work [9] using neutron diffraction measurements on hole doped Fe_{1-x}Mn_xSn epitaxial thin films (see Fig.1a) reveals planar A-AFM ordering with decreased T_N below x = 0.3, whereas Fe_{0.7}Mn_{0.3}Sn seemingly exhibits axial A-AFM. From experimental observations and DFT calculations, a relative shift of E_F closer to FB opposite to the $Fe_{1-x}Co_xSn$ system is observed (see Fig.1b). Our results suggest that magnetic order may remain even as the $E_{\rm F}$ is pushed down to the DC and needs better understanding of magnetism at room temperature for spintronics device applications. This research was primarily supported by the U.S. Department of Energy (DOE), Office of Science, Basic Energy Sciences (BES), under Award No. DE-SC0024204.

[1] M. Kang et al., *Nat. Mater.* 19, 163 (2020). [2] Z. Ren et al., *npj Quantum Mater.* 7, 109 (2022). [3] J.-X. Yin et al., *Nature (London)* 612, 647 (2022). [4] I. I. Mazin et al., *Nat. Commun.* 5, 4261 (2014). [5] B. R. Ortiz et al., *Phys. Rev. Materials* 3, 094407 (2019). [6] M. Kang et al., *Nat. Mater.* 19, 163 (2020). [7] M. Li et al., *Nat. Commun.* 12, 3129 (2021). [8] W. R. Meier et al., Phys. Rev. B 100, 184421 (2019). [9] R. Dutta et al., accepted 2nd June 2025, Phys. Rev. Materials.

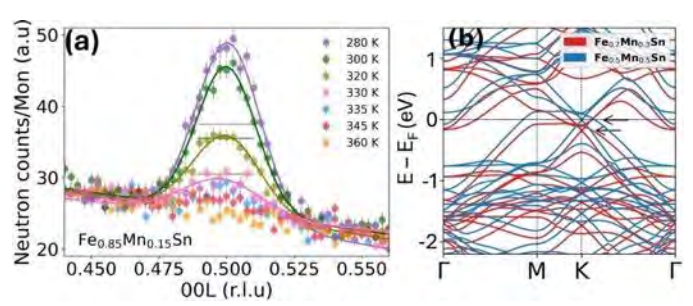


Fig. 1: (a) Temperature dependent neutron diffraction profiles of the (0 0 1/2) reflection in Fe $_{0.85}$ Mn $_{0.15}$ Sn thin film. Horizontal bars indicate instrument resolution. (b) Band structures of Fe $_{1-x}$ Mn $_x$ Sn (x = 0.3, 0.5). Black arrows indicate DC at K point.

AG-08. Beyond Altermagnetism: Unconventional Magnetism O. Liu

Southern University of Science and Technology, Shenzhen, Guanadona, China

With the advancement of antiferromagnetic (AFM) spintronics, magnetic materials with diverse magnetic structures have garnered widespread attention. Of particular interest are "unconventional magnets", which simultaneously exhibit AFM configurations while displaying properties reminiscent of ferromagnets (FMs). Thus, unconventional magnets promise to combine the advantages of both FM and AFM materials, offering, e.g., high storage capacity, low power consumption, electrical manipulation and read-out, and ultrafast dynamics. The rapid evolution of the emerging field of unconventional magnetism has inevitably engendered some degree of conceptual ambiguity and uncertainty, particularly regarding the intricate entanglement between spin-split-AFM (including altermagnets) and anomalous-Hall-AFM. In this talk, we start with symmetry theory describing magnetic geometry—spin group theory [1,2]—to discuss the symmetry design strategies and material pools for these two types of unconventional magnets, aiming to inspire further exploration in the field of unconventional magnetism [3-5]. We also introduce a homemade online program, FINDSPINGROUP (https://findspingroup.com/), which is applied to diagnose the symmetry classification of magnetic materials.

- [1] P. Liu, ..., X. Wan* and <u>OL*</u>, Phys. Rev. X 12, 021016 (2022).
- [2] X. Chen, ..., <u>OL*</u>, Phys. Rev. X 14, 031038 (2024).
- [3] X. Chen, ..., OL*, Nature 640, 349 (2025).
- [4] Y. Zhu, ..., S. Qiao*, <u>OL*</u> and C. Liu*, Nature 626, 523 (2024).
- [5] OL* et al. Nat. Phys. 21, 329 (2025).

^{*} Best Student Presentation Finalist / LB – Late-breaking Poster

SESSION AP: BIOMAGNETISM AND BIOMEDICAL **APPLICATIONS I (POSTER SESSION)**

Chair(s): J. Alonso Masa, CITIMAC, University of Cantabria, Santander, Cantabria, Spain Tuesday, October 28, 2025 09:00 AM-12:00 PM **Exhibit Hall Posters**

AP-01. Temperature Measurement of Magnetic Nanoparticles using Diamond Quantum Sensor for Magnetic Hyperthermia

Y. Arakawa, M. Inoue, S. Yabukami, A. Kuwahata Tohoku University, Sendai, Miyagi, Japan

Magnetic hyperthermia (MH) based on magnetic nanoparticle (MNP) heating is a promising modality for minimally invasive cancer therapy [1]. Critical to the safety of MH is the ability to monitor temperature in vivo in real time to prevent excessive tissue heating. While magnetic signals from magnetic nanoparticles can be utilized to estimate in vivo temperature [2], the determination of absolute temperature is limited by the measurement principle. In this study, we demonstrated absolute temperature measurement during magnetic hyperthermia using a diamond quantum sensor [3-5], which offers high biocompatibility and enables highly sensitive detection. Figure 1 shows the experimental setup for temperature measurement using a diamond quantum sensor under an alternating magnetic field. The temperature of heated MNPs was measured using a diamond sensor, and infrared thermography as a reference temperature. Figure 2 presents the absolute temperature measurement using a diamond quantum sensor based on an optically detected magnetic resonance (ODMR) spectrum under different amplitudes of the magnetic field. We observed a unique ODMR spectrum as a function of magnetic field amplitudes (Fig. 2(a)) and evaluated the zero-field splitting parameters as a quantitative measure of absolute temperature. The experimentally obtained temperatures exhibit strong consistency with the theoretical expression, as well as with both linear [4] and quadratic approximations [5] (Fig. 2(b)). The associated error margin is within 2.0 K. Our results offer a pathway toward absolute temperature monitoring in future less invasive magnetic hyperthermia for cancer therapy.

- [1] H. Petra Kok et al., International Journal of Hyperthermia, 37(1), 711-741 (2020).
- [2] A. Kuwahata et al., AIP Advances 13, 025142 (2023).
- [3] F. Jelezko and J. Wrachtrup, phys. stat. sol. 203, 13:3207 –

* Best Student Presentation Finalist / LB – Late-breaking Poster

3225 (2006).

[4] V. M. Acosta et al., Phys. Rev. Lett. 104, 070801 (2011). [5] K. Ouyang et al., Meas. Sci. Technol. 34, 015102 (2023).

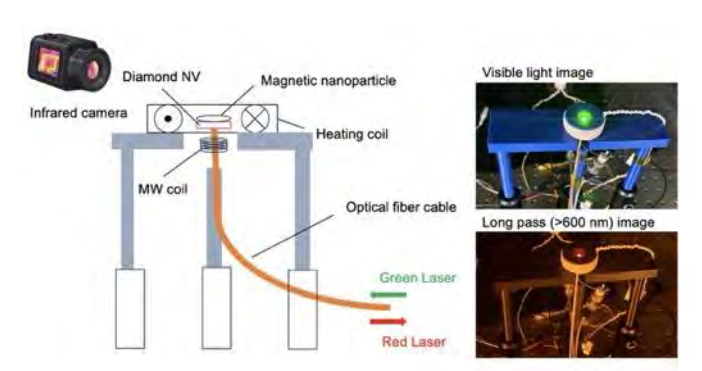


Figure 1. Experimental setup for temperature measurement using diamond quantum sensor under application of alternating magnetic field. Temperature of heated magnetic nanoparticles is measured using diamond sensor and infrared thermography

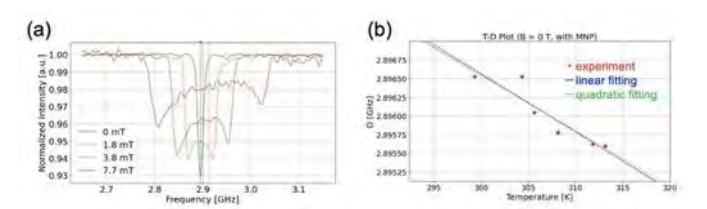


Figure 2. Absolute temperature measurement using a diamond quantum sensor. (a) Optically detected magnetic resonance (ODMR) spectrum obtained under different amplitudes of the applied alternating magnetic field. (b) A quantitative relationship between the absolute temperature and zero-field splitting parameter *D* of diamond NV centers.

AP-02. Gradiometer using single bulk diamond quantum sensor for magnetic field sensing

M. Inoue, Y. Arakawa, S. Yabukami, <u>A. Kuwahata</u> *Tohoku University, Sendai, Japan*

The negatively charged nitrogen-vacancy (NV) center in diamond enables highly sensitive quantum sensing of physical quantities such as magnetic fields and temperature at room temperature [1]. Furthermore, its high biocompatibility has enabled magnetic field sensing in biomedical applications [2–4]. However, such detection typically requires long-time signal averaging, which limits real-time performance. Sensitivity, defined by the signal-tonoise ratio (SNR), can be enhanced by reducing noise contributions. In this study, we aim to demonstrate the principle of sensitivity enhancement through external noise suppression by employing a single diamond and excitation lasers modulated at different frequencies, functioning as a gradiometer.

Figure 1 shows the experimental setup of the proposed gradiometer with a single bulk diamond. Excitation light modulated at 150 Hz (ch1: signal channel) and 1500 Hz (ch2) is delivered through two optical fibers to establish the gradiometer configuration. Red fluorescence emitted from the diamond is collected via a central optical fiber (Figs. 1(a) and 1(b)) and the signal is extracted using a lock-in amplifier. Figure 2 presents the optically detected magnetic resonance (ODMR). In Fig. 2(a), ODMR spectral shifts are observed in the presence of a uniform magnetic field (as a noise) and/or a local magnetic field (as a target signal). In Fig. 2(b), we successfully extracted only the local magnetic field signal even in the presence of the uniform noise field. The results demonstrate the feasibility of constructing a compact gradiometer based on optical separation using multiple modulation frequencies. Future work will focus on the evaluation of magnetic field sensitivity and noise suppression performance.

- [1] F. Jelezko and J. Wrachtrup, phys. stat. sol. 203, 13:3207 3225 (2006).
- [2] A. Kuwahata et al., Scientific Reports 10, 2483 (2020).
- [3] K. Arai et al., Communication Physics 5, 200 (2022).
- [4] J. F. Barry et al., Proc. Natl. Acad. Sci. 114, 6730 (2017).

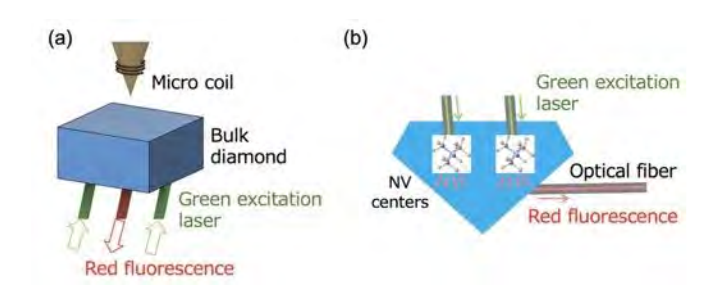


Fig. 1 Gradiometer setup of single bulk diamond, where excitation light modulated at 150 and 1500 Hz via two separate optical fibers (ch1 and ch2). Emitted red fluorescence is collected through center fiber; (a) experimental setup and (b) schematic view.

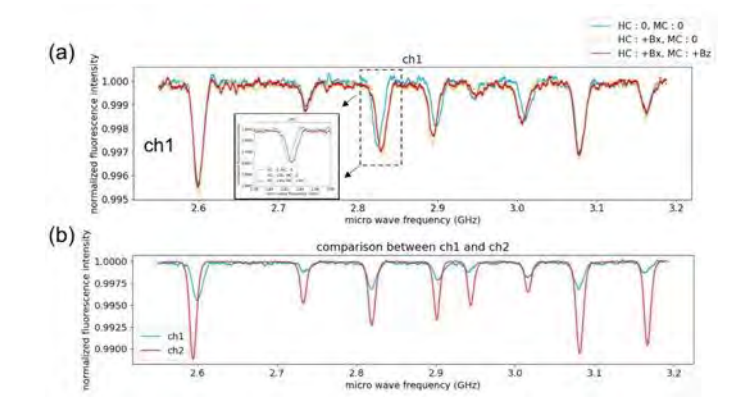


Fig. 2 Measured optically detected magnetic resonance (ODMR) spectrum. (a) spectral shifts occur in response to uniform- (noise) and local- (target signal) magnetic field. (b) Extraction of local magnetic field signal under noise field.

AP-03. Highly sensitive detection of GDF15 in Urine using magnetic nanoparticle aggregation

<u>S. Yabukami</u>^{1, 2}, T. Murayama¹, L. Tonthat¹, K. Okita², T. Abe¹

¹Tohoku University, Sendai, Japan, ²Tohoku-TMIT, Sendai, Japan

There is a substantial demand for the rapid detection of proteins that can serve as biomarkers for diagnosing metastatic cancer, mitochondrial disease, hypertension, and other conditions. We developed a quick and easy detection system of protein in human urine. We clarified the mechanism by which magnetic signals are enhanced through the cross-bridging of magnetic nanoparticles by proteins [1]. The mechanism is the opposite of the phenomenon where the magnetic susceptibility of magnetic

nanoparticle aggregates decreases as the concentration of bacteria increases [2]. This method has the following outcomes in bacterial detection: low cost, rapid evaluation, high sensitivity, and reduced influence of contaminants. Fig. 1 shows the change in magnetic susceptibility as a function of GDF15 concentration, as evaluated using a portable device. The sample consists of magnetic nanoparticles (Nanomag-D with protein A, 500 nmΦ) that were bound to the primary antibody (Anti-GDF15 antibody, Rabbit monoclonal), the secondary antibody (Anti-GDF15 biotinylated antibody, polyclonal), and polystyrene microspheres (7 μmΦ). Then, the antigen-antibody reaction with the antigen protein (GDF15) was carried out by sandwich method. The GDF15 concentrations were from 0 to 10 µg/ml. Increasing the concentration of GDF15 increased the magnetic susceptibility due to increased aggregation of magnetic nanoparticles. Fig. 2 shows the results of evaluating GDF15 in urine samples from nine patients with mitochondrial disease, compared with those obtained using ELISA [3]. The correlation coefficient with ELISA was approximately 0.91 (p≒0.015), showing a high correlation. This method can only evaluate antigens that aggregate with magnetic nanoparticles due to magnetic force, thereby reducing the influence of contaminants present in real human samples and demonstrating the possibility of accurate evaluation.

[1] S. Yabukami, T. Murayama, K. Kaneko, A. Ban, L. TonThat, Y. Ozawa, H. Okamoto, T. Kamei, M. Tanaka, Y. Tanaka, T. Abe, *IEEE Trans. Magn.*, 61, p. 1-1(2025). [2] K. Okita, Y. Pu, L. Tonthat, S. Yabukami, Y. Ozawa, S. Asamitsu, H. Okamoto, T. Kamei, "Novel Method to Measure Bacterium using Magnetic Nanoparticles", *IEEE Magnetics Letters*, vol. 14, p. 3100504 (2023). [3] D.M. Rissin, C.W. Kan, T.G. Campbell, S.C. Howes, D.R. Fournier, L. Song, T. Piech, P.P. Patel, L. Chang, A.J. Rivnak, E.P. Ferrell, J.D. Randall, G.K. Provuncher, R.R. Walt, and D.C. Duffy, *Nature Biotechnology*, 28, p. 595 (2010).

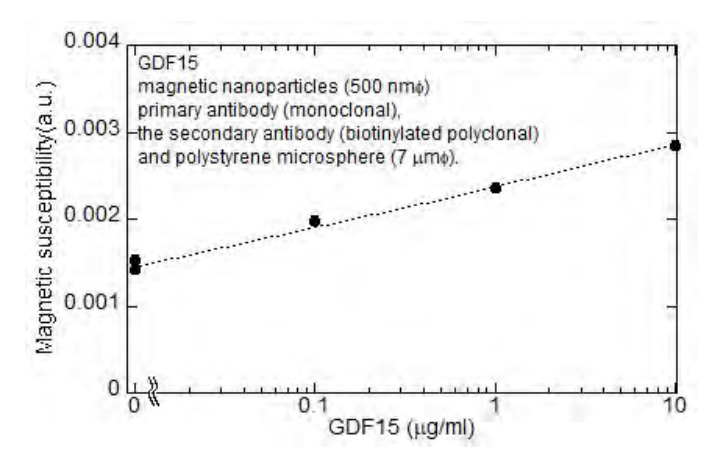


Fig. 1 Magnetic susceptibility versus GDF15 concentration evaluated using a portable device.

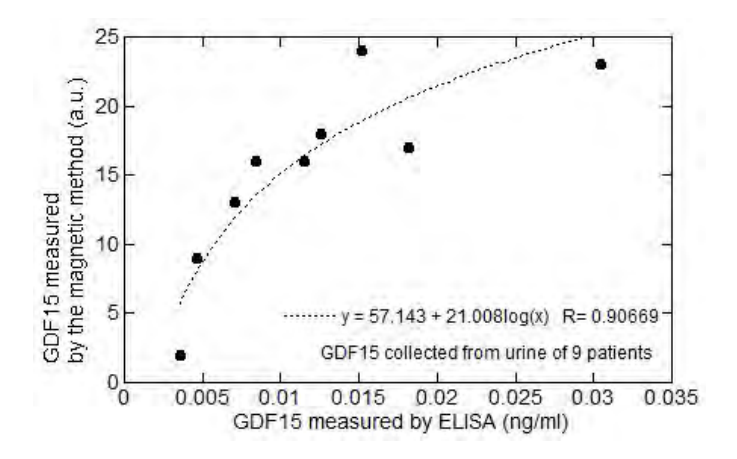


Fig. 2 The evaluated GDF15 in urine samples from mitochondrial disease patients (nine patients) compared with ELISA.

AP-04. Hydrophilic Magnetite Nanoparticles for Biomedical Applications

<u>E. Jaberolansar</u>¹, S. Jan¹, R. Roy Chowdhury¹, D. A. Arena¹, S. Mohapatra², H. Srikanth¹

¹Department of Physics, University of South Florida, Tampa, Florida, United States, ²Morsani College of Medicine, University of South Florida, Tampa, Florida, United States

Magnetic nanoparticles, particularly spinel ferrites, have attracted significant attention for their unique magnetic properties and broad applicability in energy storage and biomedical technologies [1-2]. Here, we investigate magnetite nanoparticles' performance in magnetic hyperthermia and cellular cytotoxicity. Using a thermal decomposition synthesis method, we synthesized two sets of hydro dispersed nanoparticles using Polyethylene glycol (PEG) and Polyethyleneimine (PEI) with two different molecular weights. By fine-tuning the synthesis conditions, quality hydrophilic nanoparticles were obtained. Nanoparticles were investigated for targeted drug delivery and hyperthermia applications after being coated with biocompatible polymer shells. Both sets of nanoparticles were also evaluated for cellular cytotoxicity. Comprehensive magnetic characterization, including magnetization vs temperature (M-T), magnetization vs field (M-H), and RF transverse susceptibility measurements performed for both sets of nanoparticles to determine the magnetic response. AC magnetic hyperthermia experiments, conducted with nanoparticles embedded in Agar (a cell phantom), demonstrated that optimized heating efficiency (Specific Absorption Rate) for cancer therapy is related to the magnetic anisotropy of the nanoparticles that depends on their size, shape, arrangement, and dipolar interactions. Our findings underscore the importance of tailoring nanoparticles' properties to enhance their effectiveness in cell treatment, particularly for hyperthermia-based cancer therapy and targeted drug delivery.

- [1] Lavorato, Gabriel C., et al. "Hybrid magnetic nanoparticles as efficient nanoheaters in biomedical applications." *Nanoscale Advances* 3, 867 (2021).
- [2] Attanayake, Supun B., et al. "Tailoring the Magnetic and Hyperthermic Properties of Biphase Iron Oxide Nanocubes through Post-Annealing." *Crystals* 14, 519, (2024).

AP-05. Measurement of Viscoelastic Properties Using Magnetic Resonance Elastography (MRE) Technique on Brain Phantoms

M. M. William¹, <u>W. Lohr</u>¹, L. Schandler², V. J. Weir³, R. M. Khan⁴, R. L. Hadimani^{2, 1}

¹Biomedical Engineering, Virginia Commonwealth University, Richmond, Virginia, United States, ²Mechanical and Nuclear Engineering, Virginia Commonwealth University, Richmond, Virginia, United States, ³Department of Veterans Affairs, Central Virginia VA Health Care System, Richmond, Virginia, United States, ⁴Clinical Professor of Diagnostic Radiology, Virginia Commonwealth University, Richmond, Virginia, United States

Magnetic Resonance Elastography (MRE), a non-invasive imaging technique that maps tissue stiffness using magnetic fields, radiofrequency coils, and low-frequency vibrations, has become a key tool in brain biomechanics [1], but its broader use is limited by the lack of validated tissue phantoms [2]. Despite decades of research, there is still no known material that accurately replicates the viscoelastic properties of living brain tissue for use in injury simulation or neuromodulation testing. In this study, a PVA/PHY hydrogel phantom was developed to mimic the viscoelastic behavior of brain tissue and validated using both rheometry and MRE. A composite hydrogel was synthesized from polyvinyl alcohol (PVA) and phytagel (PHY) using controlled freeze-thaw cycles to tune viscoelastic behavior. Samples were molded into cylindrical shapes to match the 6-inch liver MRE transducer available at the VA Hospital. Petri dish samples from each batch were first tested using a rheometer to measure storage (G') and loss (G") moduli. The same samples were then tested using MRE to generate spatial stiffness maps. Rheometer results showed G' and G" values consistent with literature for live brain tissue [3]. MRE analysis of larger cylindrical samples revealed internal stiffness gradients and surface artifacts, offering insights not possible with mechanical testing alone. A commercial phantom measured 3.26 kPa, while our hydrogel phantom averaged 18.64 kPa, suggesting that while the hydrogel mimics brain mechanics at small scales, bulk samples suffer from uneven crosslinking. This is the first study to crossvalidate a brain-mimicking phantom using both rheometry and MRE, establishing a foundation for anatomically detailed models for TBI research, MEG calibration, and neuromodulation research.

References

[1] Muthupillai, R., et al. "Magnetic resonance elastography by direct visualization of propagating acoustic strain waves."

Science 269.5232 (1995): 1854-1857.

[2] Chatelin, S., et al. "Biomechanics of brain tissue." Medical Image Analysis 13.4 (2009): 628-639.

[3] Budday, S., et al. "Mechanical properties of gray and white matter brain tissue by indentation." Journal of the Mechanical Behavior of Biomedical Materials 46 (2015):

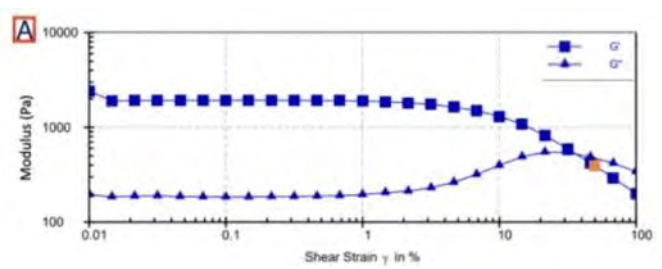


Fig1: G' and G" of the hydrogel measured using rheometer. Showing stable elastic behavior at low strain

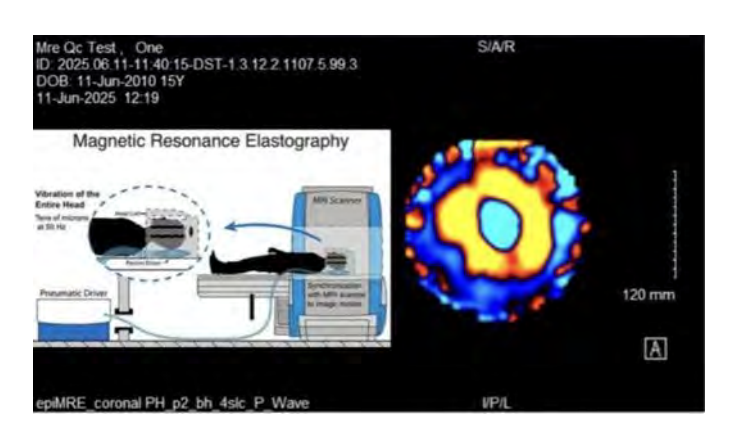


Fig2: MRE wave image of the phantom. Irregular wave patterns and variation in color reflect stiffness inhomogeneity due to uneven cross-linking in the bulk sample

AP-06. Investigation of the Impact of Individualized Neuroanatomy and Functional Connectivity on Primary Motor Cortex Excitability During Transcranial Magnetic Stimulation

M. Paslar¹, <u>T. J. Taylor</u>¹, B. Embree², W. Lohr¹, T. Atalugama², C. L. Peterson¹, R. L. Hadimani^{1, 2}

¹Biomedical Engineering, Virginia Commonwealth University, Richmond, Virginia, United States, ²Mechanical and Nuclear Engineering, Virginia Commonwealth University, Richmond, Virginia, United States

Transcranial magnetic stimulation (TMS) is a non-invasive technique that targets specific brain regions through

localized electric fields. The primary motor cortex (M1) is commonly stimulated due to its reliable elicitation of motor evoked potentials (MEPs), measurable via electromyography (EMG). Typically, the relationship between TMS-induced electric field intensity and motor cortical excitability is assessed through analysis of the MEP recruitment curve. While variability in TMS responsiveness has been associated with cortical oscillatory states, intrinsic brain states, and anatomical factors such as scalp-to-cortex distance, the detailed effects of individualized neuroanatomical and functional connectivity features on TMS outcomes remain unclear.

In this study, we investigated the influence of individualized neuroanatomy and EEG-derived functional connectivity on motor cortex excitability during TMS. We recruited 20 healthy adults (8 women; mean age 28.3 ± 9.4 years), obtaining multimodal datasets including EMG recordings during TMS, resting-state electroencephalography (EEG), and structural magnetic resonance imaging (MRI) [1]. EEG analyses provided insights into the functional connectivity of M1 (Figure 1), while MRI-derived anatomical models enabled accurate computational simulations of TMS-induced electric fields (Figure 2). Our results confirm that the relationship between motor cortex excitability and functional connectivity aligns with established literature [1.2].

By integrating neuroimaging, electrophysiological data, and computational simulations, we expect to significantly improve predictions of individual M1 responses to TMS. These insights may enhance personalized TMS protocols, refine stimulation parameters, and reduce interindividual variability, ultimately improving the efficacy and precision of therapeutic neuromodulation.

1. M. Lee, J. G. Yoon, and S. W. Lee, "Predicting Motor Imagery Performance From Resting-State EEG Using Dynamic Causal Modeling," Front Hum Neurosci, vol. 14, p. 321, 2020, doi: 10.3389/fnhum.2020.00321
2. M. Hamada, N. Murase, A. Hasan, M. Balaratnam, and J. C. Rothwell, "The role of interneuron networks in driving human motor cortical plasticity," Cereb Cortex, vol. 23, no. 7, pp. 1593-605, Jul 2013, doi: 10.1093/cercor/bhs147.

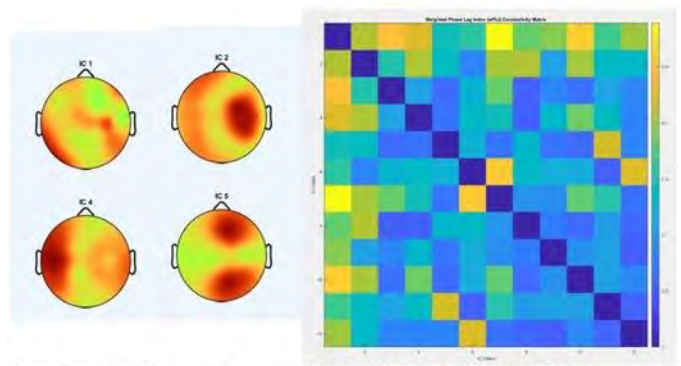


Figure 1: Functional connectivity maps were estimated using resting state EEG data. Selected independent components and the functional connectivity are demonstrated.

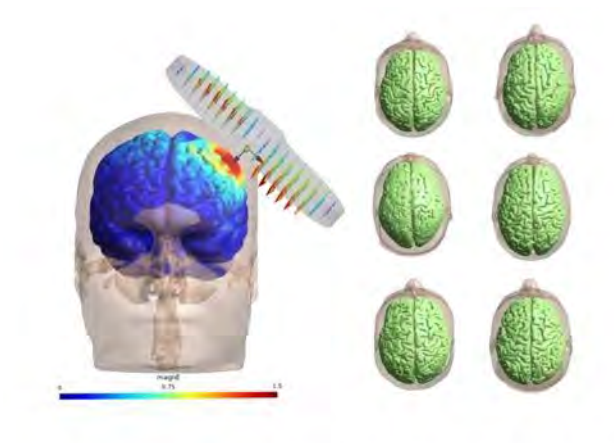


Figure 2: MRI structural images were used to create geometrically accurate simulations of the brain tissue during TMS to estimate the electrical field intensity.

AP-07. Tuning Size, Shape, and Phase Composition for Enhanced Magnetic Hyperthermia in FeO/Fe₃O₄ Nanoparticles and Superclusters

W. Manuel^{1, 2}, <u>D. Luu</u>¹, M. Gili^{1, 2}, D. Brown¹, S. Jan¹, M. Nguyen³, M. Vega², T. Lee³, H. Srikanth¹, M. Phan¹

¹Department of Physics, University of South Florida, Tampa, Florida, United States, ²Materials Science and Engineering Program, College of Science, University of the Philippines Diliman, Philippines, ³Department of Chemistry and the Texas Center for Superconductivity, University of Houston, Houston, Texas, United States

Single-domain magnetic iron oxide nanoparticles (IONPs) have been widely studied in recent years due to their superparamagnetic (SPM) properties, which make them useful for various applications [1,2]. SPM behavior in IONPs is typically observed when their size is below 25 nm while larger particles tend to transition to a ferromagnetic phase.

However, factors such as particle shape and composition also play a significant role [3]. To achieve SPM behavior at larger sizes, single-domain IONPs can be stacked or assembled into structures often referred to as superclusters [4]. These larger SPM IONPs are particularly desirable in biomedical applications because they can help reduce potential toxicity caused by the deep tissue absorption and retention of smaller particles (less than 30 nm) in sensitive areas of the body. In this study, we demonstrate that the magnetic hyperthermia performance of FeO/Fe₃O₄ coreshell spherical and cubic IONPs can be significantly enhanced and optimized through the combined control of particle size, shape, and FeO/Fe₃O₄ phase volume fraction. At a comparable size of around 15 nm, cubic IONPs showed higher specific absorption rate (SAR) values than spherical ones across all tested field strengths. Increasing particle size alone did not result in higher SAR, as variations in the FeO/Fe₃O₄ phase volume fraction significantly influenced the magnetization, thereby impacting SAR performance. Optimal SAR values were achieved through a combined adjustment of particle size and FeO/Fe₃O₄ ratio. Furthermore, assembling spherical IONPs into superclusters led to a SAR increase of over 10%, while superclusters formed from cubic IONPs exhibited an enhancement exceeding 20%. These findings suggest that favorable spin alignment and enhanced inter-particle interactions in cubic core/shell IONP superclusters make them particularly promising for magnetic hyperthermia applications. Overall, our study highlights the importance of morphological control and cluster assembly in optimizing the magnetic heating efficiency of IONPs, emphasizing the potential of phase-tunable core/shell Superclusters in safer and more effective biomedical applications.

- [1] Thong, et al., Multifunctional Nanocarriers of Fe₃O₄@(PLA-PEG)/Cur for MRI, magnetic hyperthermia, and drug delivery, *Nanomedicine* 17, 1677 (2023)
- [2] Attanayake, et al., Superparamagnetic Superparticles for Magnetic Hyperthermia Therapy: Overcoming the Particle Size Limit, ACS Applied Materials and Interfaces 17, 19436 (2025)
- [3] Nemati, et al., Improving the Heating Efficiency of Iron Oxide Nanoparticles by Tuning Their Shape and Size, *The Journal of Physical Chemistry C* 122, 2367 (2018)
- [4] Nguyen, et.al., Fine-Tuning the Superparamagnetic Properties of FeO@Fe₃O₄ Core/Shell Nanoparticles and Superclusters by Controlling Size and Shape, *ACS Applied Materials and Interfaces* 17, 19 (2025)

AP-08. Development of a novel Ferromagnetic Suppression Coil to Increase Focality in TMS Procedures on Small Animals

T. V. Atalugama, W. Lohr, R. L. Hadimani Department of Mechanical and Nuclear Engineering, Virginia Commonwealth University, Richmond, Virginia, United States

Transcranial Magnetic Stimulation is an FDA approved noninvasive neuromodulation technique that stimulates brain regions via a focalized electric field induced by a timevarying current in wire coils placed above the head. This field is often focalized through a "figure 8" coil design where opposing currents are conducted through two closely placed wire coils, doubling field strength at their meeting point. A typical approach to TMS focalization is strengthening this central region, however, undesired stimulation still occurs under the rest of the coil. We present a novel approach to TMS focalization that instead inhibits the electric field in the non-central region by placing two half-moon ferromagnetic suppression coils (FSC) with opposing current on the outer quarters of the figure 8 coil and ferromagnetic cores in their centers. The FSC current opposes that of the figure 8, creating a varying magnetic field to destructively interfere with that of non-central figure 8 regions, while ferromagnetic cores amplify focality. We test this design on a TMS rat phantom.

In Ansys Maxwell 3D, we designed 2 copper TMS coils, a standard figure 8 and a figure 8 with two FSCs attached. Cores were made of permendur, a highly magnetically permeable iron-cobalt alloy. A gray matter box underneath simulated the brain. Eddy current simulations were run at a current of 1000 A varying at 2.5 kHz, and electric field data was recorded. Results showed significantly less induced electric field in regions directly under the FSCs. The figure 8-FSC coil had a similar maximum V/m to the standard coil through the box, but was far more focal. This design thus focalizes coils by inhibiting simulation in non-central regions without greatly sacrificing penetration strength of the focal region. The continuity of the coils implies this effect holds at various currents. Future research entails testing on a simulated rat head, and creating physical FSCs to test on a rat TMS phantom.

Acknowledgements: This research is partly funded by NSF Grant #2349694, # 2304513, and the VCU Presidential Research Quest Fund.

Z. Deng, S. Lisanby and A. Peterchev, Brain Stimulation., Volume 6, Issue 1, p.1-13 (2013)

L. Hernandez-Garcia, T. Hall T, L. Gomez and E. Michielssen, Brain Stimulation, Vol3(4), p.218-225 (2010)
H. Siebner, K. Funke and A. Aberra, Clinical
Neurophysiology., Volume 140, p.59-97(2022)
V. E. Amassian and P.J. Maccabee, Conf Proc IEEE Eng Med
Biol Soc. 2006, p.1620–1623(2006)

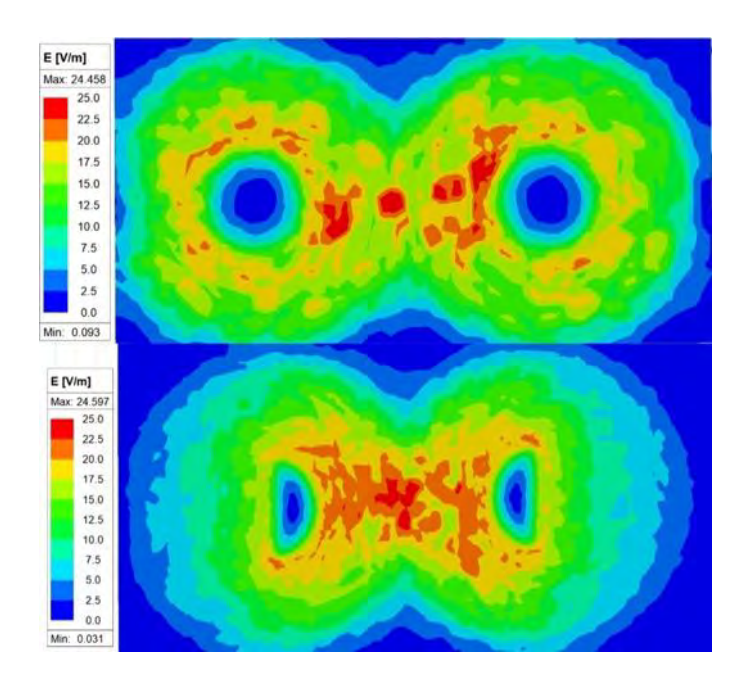


Fig. 1: E Field Strength on top of gray matter for Standard Coil (top) and FSC (bottom).

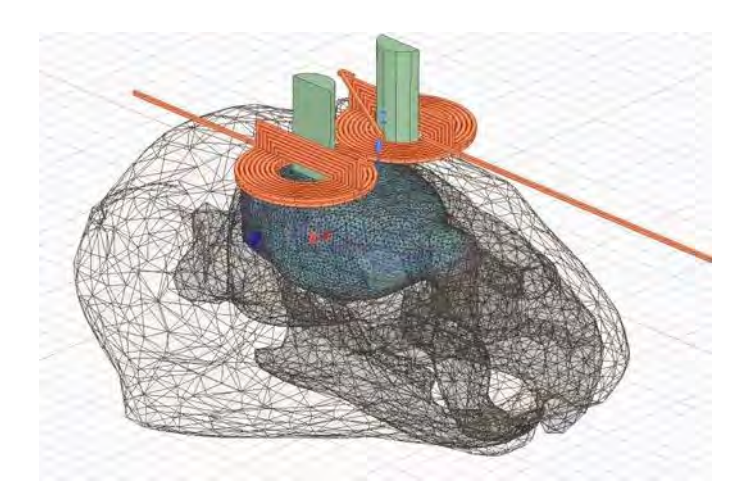


Fig. 2: Figure 8-FSC Coil above Simulation Rat Head.

AP-09-LB. Simulation of Adaptive Magnetic Coils for Directionally Adjustable Targeted Neuromodulation P. Chan¹, J. Pothuganti², G. Licwinko², W. Yu², V. Chen² ¹Indiana University, Bloomington, Indiana, United States, ²Loyola University Chicago, Chicago, Illinois, United States

This study presents simulation results demonstrating the feasibility of modulating both the strength and direction of an induced electric field in neural tissue using a combination of miniaturized stimulation coil modules, each capable of independently adjusting its magnetic field to contribute to a controlled, vectorized overall magnetic field. Recognizing the clinical challenge that optimal stimulation parameters and target orientations are often unknown prior to device implantation, this approach allows for postimplantation adjustment of the electric field without additional surgical intervention. Further investigation is required to assess safety considerations, including thermal effects, and to optimize stimulation parameters for clinical translation. We propose a novel miniaturized modular coil architecture for magnetic field generation in targeted neuromodulation applications. Each coil unit consists of tightly wound enameled copper wire around a resin-printed core, creating compact solenoids that are independently controllable and mechanically modular. These units are arranged in geometrically structured 3D configurations, such as full and partial spheres, concentric rings, layered stacks, or staggered volumes, to support flexible spatial targeting. The design allows dynamic control of polarity and current intensity, enabling constructive or destructive shaping of induced magnetic and electric fields. The strategy is to facilitate spatiotemporal modulation of neural tissue for both invasive and non-invasive stimulation paradigms. Simulations conducted in Ansys are being used to identify optimal geometries, and magnetic field density. We are also using simulations and 3D modeling to explore strategies for further miniaturizing each module, enhancing their applicability while addressing resistive and thermal challenges. We aim to develop a configurable platform for quantitatively evaluating the functional efficacy of our miniaturized modular coil units in vitro using living neuronal cultures.

[1] W. Paulus, "Transcranial electrical stimulation (tES-tDCS; tRNS, tACS) methods," *Neuropsychological rehabilitation*, vol. 21, no. 5, pp. 602-617, 2011.
[2] M. A. Nitsche *et al.*, "Shaping the effects of transcranial direct current stimulation of the human motor cortex," *J.*

Neurophysiol., vol. 97, no. 4, pp. 3109-3117, 2007.

[3] M. Kobayashi and A. Pascual-Leone, "Transcranial magnetic stimulation in neurology," *The Lancet Neurology*, vol. 2, no. 3, pp. 145-156, 2003.

[4] C.-F. Chen and F. Fregni, "Regulating Skin-Electrode Impedance of Multiple-Anodal or Multiple-Cathodal tDCS," *Brain Stimulation: Basic, Translational, and Clinical Research in Neuromodulation*, vol. 10, no. 1, p. e7, 2017.

[5] S. Van Hoornweder, M. Nuyts, J. Frieske, S. Verstraelen, R. L. Meesen, and K. A. Caulfield, "Outcome measures for electric field modeling in tES and TMS: A systematic review and large-scale modeling study," *Neuroimage*, vol. 281, p. 120379, 2023.

- [6] Z.-D. Deng, S. H. Lisanby, and A. V. Peterchev, "Electric field depth-focality tradeoff in transcranial magnetic stimulation: simulation comparison of 50 coil designs," *Brain stimulation*, vol. 6, no. 1, pp. 1-13, 2013.
- [7] C.-F. Chen *et al.*, "Higher-order power harmonics of pulsed electrical stimulation modulates corticospinal contribution of peripheral nerve stimulation," *Scientific reports*, vol. 7, p. 43619, 2017.
- [8] W.-M. Yu, M. A. McCullen, and V. C.-F. Chen, "Accelerating peripheral nerve regeneration using electrical stimulation of selected power spectral densities," *Neural Regeneration Research*, vol. 17, no. 4, pp. 781-782, 2022.
- [9] J. J. Borckardt *et al.*, "A pilot study of the tolerability and effects of high-definition transcranial direct current stimulation (HD-tDCS) on pain perception," *The Journal of Pain*, vol. 13, no. 2, pp. 112-120, 2012.
- [10] M. Alam, D. Q. Truong, N. Khadka, and M. Bikson, "Spatial and polarity precision of concentric high-definition transcranial direct current stimulation (HD-tDCS)," *Physics in Medicine & Biology*, vol. 61, no. 12, p. 4506, 2016.
- [11] S. Collavini, M. Fernández-Corazza, S. Oddo, J. P. Princich, S. Kochen, and C. H. Muravchik, "Improvements on spatial coverage and focality of deep brain stimulation in pre-surgical epilepsy mapping," *Journal of Neural Engineering*, vol. 18, no. 4, p. 046004, 2021.
- [12] J. S. Perlmutter and J. W. Mink, "Deep brain stimulation," *Annu. Rev. Neurosci.*, vol. 29, no. 1, pp. 229-257, 2006.
- [13] H. Ye, V. C.-F. Chen, J. Helon, and N. Apostolopoulos, "Focal suppression of epileptiform activity in the hippocampus by a high-frequency magnetic field," *Neuroscience*, vol. 432, pp. 1-14, 2020. [14] H. Ye, V. Chen, and J. Hendee, "Cellular mechanisms underlying state-dependent neural inhibition with magnetic stimulation," *Scientific Reports*, vol. 12, no. 1, p. 12131, 2022. [15] G. Bonmassar, S. W. Lee, D. K. Freeman, M. Polasek, S. I.

Fried, and J. T. Gale, "Microscopic magnetic stimulation of neural tissue," *Nature communications*, vol. 3, no. 1, p. 921, 2012.

[16] S. W. Lee and S. I. Fried, "Enhanced control of cortical pyramidal neurons with micromagnetic stimulation," *IEEE Transactions on Neural Systems and Rehabilitation Engineering*, vol. 25, no. 9, pp. 1375-1386, 2016.



Fig. 1 Multilayer design boosts magnetic flux density, while custom 3D-printed resin components ensure coil stability.

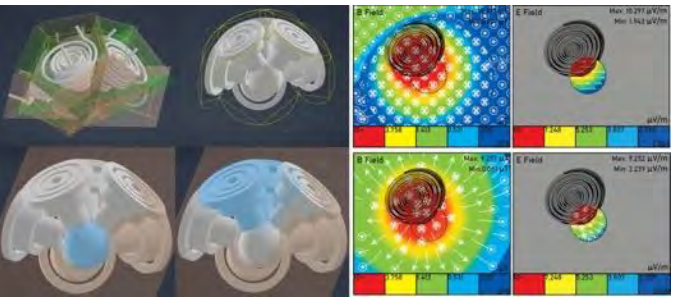


Fig. 2 Simulated coaxial coils in a half-decahedron, spherical target with white matter properties, and 2 coils.

AP-10-LB. Bio-resorbable magnetic tunnel junctions

D. Kim¹, B. Kim², B. Park¹, J. Ahn², H. Yang³
¹Department of Materials Science and Engineering, Korea
Advanced Institute of Science and Technology (KAIST), Daejeon,
Korea (the Republic of), ²School of Electrical and Electronic
Engineering, Yonsei University, Seoul, Korea (the Republic
of), ³Department of Electrical and Computer Engineering,
National University of Singapore (NUS), Singapore, Singapore

Magnetic tunnel junctions (MTJs) play a crucial role in spintronic technologies, especially for data storage and sensors. As a non-volatile memory, MTJs has received substantial interest due to their CMOS compatibility, low power consumption, fast switching, and high endurance. In parallel, bio-resorbable electronics are emerging as a promising solution for temporary operation and secure data disposal in military, intelligence, and biomedical systems, where devices must safely disintegrate under physiological conditions.

In this study, we examine the bio-resorbability of MTJ by

analyzing the dissolution behavior of its nanometer-thick constituent layers in phosphate-buffered saline (PBS) solution at pH 7.4, simulating physiological environments. The MTJ stacks, composed of bio-resorbable materials, exhibit controlled degradation behaviors. A critical feature is that once one of the ferromagnetic layers dissolves, binary information is irreversibly erased within 10 hours of immersion. This unique mechanism, combined with inherent advantages of MTJs, including fast switching speed, low power consumption, non-volatility, and seamless integration with CMOS platforms, makes them particularly well suited for secure memory applications requiring temporary operation and automatic data disposal. The dissolution kinetics can be tuned by adjusting layer thicknesses and further accelerated under physiological conditions such as elevated temperature or mechanical agitation. Overall, our findings confirm the feasibility of integrating MTJ-based memory into bio-resorbable electronic systems [1]. Such devices offer a compelling combination of on-demand data erasure, transient functionality, and biocompatibility, paving the way for their use in secure, short-lived electronics. The ability to modify the dissolution lifetime by materials and thickness selection offers unique advantages for short-lived implantable devices, paving the way for integrating spintronic functionality into next-generation bioresorbable electronics.

[1] D.-J. Kim, B. J. Kim, H. Shin, et al. "Bio-Resorbable Magnetic Tunnel Junctions." *Adv. Mater.* (2025): e07912. https://doi.org/10.1002/adma.202507912

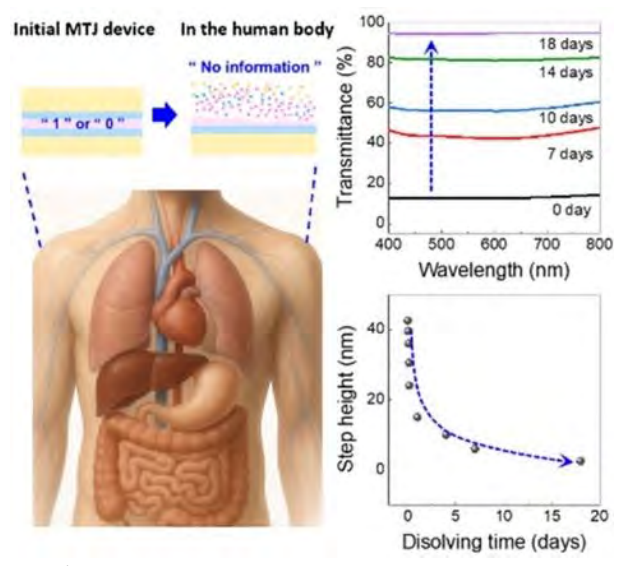


Fig. 1 Bio-resorbable MTJ concept and device structure and dissolution kinetics of the complete MTJ stack

SESSION AQ: INSTRUMENTATION AND MEASUREMENT TECHNIQUES (POSTER SESSION)

Chair(s): K. Islam, *Physics and Materials Science, The University of Memphis, Memphis, Tennessee, United States*Tuesday, October 28, 2025
09:00 AM-12:00 PM
Exhibit Hall Posters

AQ-01. Emergence of Anomalous and Topological Hall Effects in Magnetic Topological Insulator Mn₂BiSbTe₅

A. Saxena^{1, 2}

¹Program on Key Materials, National Cheng Kung University, Tainan, Tainan, Taiwan, ²Physics, National Sun Yat-sen University, Gushan, Kaohsiung, Taiwan

Mn₂BiSbTe₅ is an intrinsic magnetic topological insulator that provides a unique platform for studying the interplay between magnetism and nontrivial band topology. This material is of particular interest for realizing exotic quantum phenomena, such as the quantum anomalous Hall effect (QAHE), axion insulator states, and topological magnetoelectric effects. The presence of both intrinsic magnetism and strong spin-orbit coupling makes Mn₂BiSbTe₅ a compelling candidate for next-generation spintronic and quantum device applications. In this work, we systematically investigate the structural, magnetic, and electronic transport properties of Mn₂BiSbTe₅ using X-ray diffraction (XRD), magnetization, and electrical transport measurements. Rietveld refinement of powder XRD data confirms a well-ordered orthorhombic structure, with precise determination of lattice parameters and atomic positions. Magnetic characterization reveals an antiferromagnetic ordering with a Néel temperature of T_N ~ 19 K, tunable via external perturbations. The delicate balance between interlayer magnetic interactions suggests the potential for engineered topological magnetic phases. Transport measurements provide clear signatures of nontrivial band topology, with the observation of both the Anomalous Hall Effect (AHE) and Topological Hall Effect (THE) as shown in fig.(a) and (b). The presence of AHE confirms significant Berry curvature contributions, while THE indicates the emergence of chiral spin textures such as skyrmions. These findings suggest that Mn₂BiSbTe₅ can host tunable topological states driven by magnetic interactions, offering new opportunities for the exploration of novel quantum phases. Our results establish Mn₂BiSbTe₅ as a promising material for fundamental studies in topological magnetism and highlight its potential for practical applications in quantum and spintronic devices.

AQ-02. High-Precision Iron Loss Evaluation with Reduced Signal Averaging via Bayesian Inference

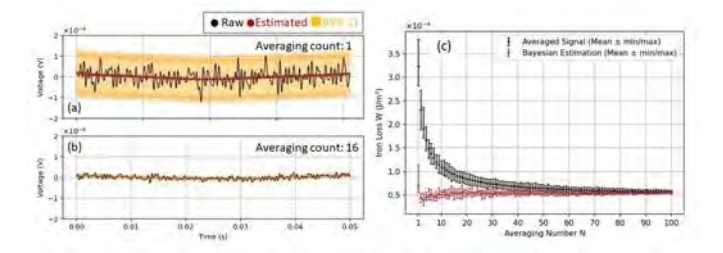
T. Suwa¹, N. Ono^{1, 2}, S. Okamoto^{1, 3, 4}

¹Institute of Multidisciplinary Research for Advanced Materials, Tohoku University, Sendai, Japan, ²Department of Applied Physics, Tohoku University, Sendai, Japan, ³Center for Science and Innovation in Spintronics, Tohoku University, Sendai, Japan, ⁴National Institute for Materials Science, Tsukuba, Japan

With the rapid advancement of power electronics, the demand for precise evaluation of energy losses in soft magnetic materials, particularly iron loss, has grown considerably [1]. Among various measurement techniques, the two-coil method is widely used. In this method, the iron loss W is calculated as the time integral of the product of the input current I(t) and the induced voltage V(t). The induced voltage in the secondary coil is given by $V(t) = i 2\pi f$ M I(t), where f is the excitation frequency, M is the mutual inductance, and I(t) is the primary current. This equation indicates that the voltage amplitude is directly proportional to both the excitation frequency and the current [2]. Therefore, under low excitation frequencies, the induced voltage becomes extremely weak. To ensure a sufficient signal-to-noise ratio, conventional measurements require many signal averages, which in turn prolong the measurement time and thereby limit real-time applicability. To overcome this challenge, particularly the heavy dependence on averaging, we propose a Bayesian inferencebased approach that enables accurate iron loss estimation with significantly fewer signal averages. Figure 1(a) corresponds to a single-shot signal, while Figure 1(b) shows the case with 16 signal averages. The measurements were performed on a Mn-Zn ferrite core at 20 Hz. For each case, the estimated mean (posterior expectation) is shown along with the 95% credible interval (CI). The CI represents the range within which the true value lies with 95% probability under the posterior distribution. Based on these results, the iron loss was calculated, indicating that while approximately 100 signal averages are typically required to obtain a reliable loss value, our proposed method achieves accurate estimation with only about 10 signal averages (Figure 1(c)). This approach is expected to significantly reduce the measurement time while maintaining high estimation accuracy, making it a promising candidate for applications such as real-time loss evaluation, characterization of miniature samples, and analysis under low excitation amplitudes.

[1] D. Neumayr, D. Bortis and J. W. Kolar, CPSS Trans. Power Electron. Appl., Vol. 5, p.251 (2020).

[2] A. J. Hanson, J. A. Belk, S. Lim, C. R. Sullivan and D. J. Perreault, IEEE Trans. Power Electron., Vol. 31, p.7909 (2016).



AQ-03. A Scalable Implementation of a 3D Magnetic Hall Sensor Card for Mapping and Monitoring Applications L. Messner^{1, 2}

¹EP-DT, CERN, Meyrin, Switzerland, ²Biomedical Engineering *Group, Department of Mechatronics, University of Innsbruck,* Innsbruck, Austria

High-energy physics experiments at the Large Hadron Collider (LHC) rely on large, often custom-built magnets to bend particle trajectories and thus allow their identification by calculating their momenta. These magnets necessitate an accurate mapping of the magnetic field. For that, a large number of 3D magnetic field sensors is required, in the order of tens or even hundreds. [1] Since 2002, CERN developed a system to map the magnetic field of the solenoid in the ATLAS experiment. Despite its limitations, the system was applied to multiple magnets in the future. [2] This research presents the development and validation of a new 3D Hall sensor card that overcomes the limitations of the previous design.

The new PCB is designed to meet several key requirements, including CANOpen communication, integration of modern electronics within a compact layout, and reliable performance in strong magnetic fields. These goals are achieved through careful circuit and PCB design (figure 1), supported by robust firmware. Another aspect is the precise and straightforward alignment of three perpendicular Hall elements, ensuring their measurement axes intersect at a single point. This is realized using two support PCBs mounted in milled slots on the main sensor card, as shown in figure 2. To achieve magnetic field measurement accuracy in the order of 10⁻⁴ T, a new calibration procedure based on spherical harmonics is introduced to model both

the sensor card's movement and its voltage response. Experimental results confirm the precise Cartesian alignment of the Hall elements and the stability of the voltage readout in strong magnetic fields, enabling accurate magnetic field measurements. The proposed spherical harmonic model achieves a reconstruction precision of 0.02% for field magnitude and 0.2% for field orientation. validated through rotational calibration in uniform fields of 225mT, 450mT, and 675mT. These results surpass the initial accuracy target of 10⁻⁴ T, demonstrating the card's potential for further optimization and even higher precision.

[1] T. Taylor, The magnets for the LHC experiments. IEEE transactions on applied superconductivity, 10, 342. (2000) [2] M. Aleksa, F. Bergsma, L. Chevalier et al., Results of the ATLAS solenoid magnetic field map. Journal of Physics: Conference Series, 110, 092018. (2008)



Fig.1 PCB of the newly developed 3D Hall sensor card.

48

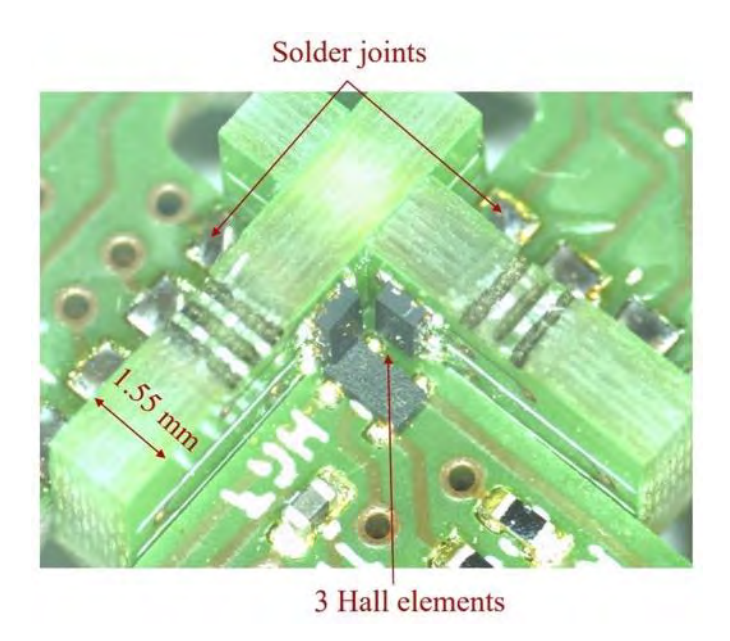


Fig.2 Support PCBs with soldered Hall elements enabling precise 3D Hall element placement when inserted into the sensor card.

AQ-04. Magnetic Orientation of Rod-shaped Diamagnetic Crystals in Rotating Magnetic Fields Based on Real-time Observation and the Analysis of Orientation Conditions

Y. Takeuchi¹, R. Kimoto¹, A. Hamasaki²

¹Muroran Institute of Technology, Muroran, Japan, ²Faculty of science, Shinshu University, Matsumoto, Japan

Controlling diamagnetic crystal orientation is crucial for enhancing metal and ceramic materials, with rotating magnetic fields proving to be vital for complete alignment (1.2). Until now, the mainstream method has been to rotate the sample in a static magnetic field (3); however, we designed and manufactured a quadrupole electromagnet to rotate the magnetic field directions themselves (4). The developed device simplifies the process (simply placing the sample) and does not affect the suspension convection, even during high-speed or repeated rotation. It also enables easy real-time observation of material orientation dynamics. Through direct observations, we investigated the relationship between the magnetic field rotation conditions and the orientation behavior of rod-shaped diamagnetic cellulose crystals in a diamagnetic material. In the experiment, as shown in Fig. 1, we tested one-way clockwise rotation and a pattern alternating between

clockwise and counterclockwise every 90°, while changing the rotation speed of the magnetic field. In each pattern, the magnetic direction was changed continuously by 1° or intermittently by 90°. Here, the rod could not follow the magnetic flux even at 120 seconds per revolution. As shown in Fig. 2, the one-way rotation oriented the crystals faster than the alternating rotations. The absolute value of the magnetic flux vector acting on the crystals was the same for both magnetic-field application patterns; the aforementioned difference is thought to be due to the magnetic saturation of the electromagnet's magnetic poles. Next, it was shown that in the case of one-way rotation, alignment occurred more quickly when the rotation was changed continuously. Until now, although the alignment speed depends on the speed of the rotating magnetic field, there has been no in-depth discussion of other parameters. and new knowledge that will be useful for the development of new materials has been obtained.

[1] T. S. Suzuki, K. Kobayashi and T. Uchikoshi, *International Journal of Applied Ceramic Technology*, 20, 718 (2022)
[2] S. Tanaka, Y. Doshida and H. Shimizu, *IOP Conference Series: Materials Science and Engineering*, 20, 012002 (2011)
[3] S. Horii, M. Yamaki and M. Haruta, *IEEJ Transactions on Fundamentals and Materials*, 132, 397 (2012)
[4] Y. Takeuchi, H. Kawaguchi, and A. Hamasaki, *Applied Physics Express*, 14, 057002 (2021)

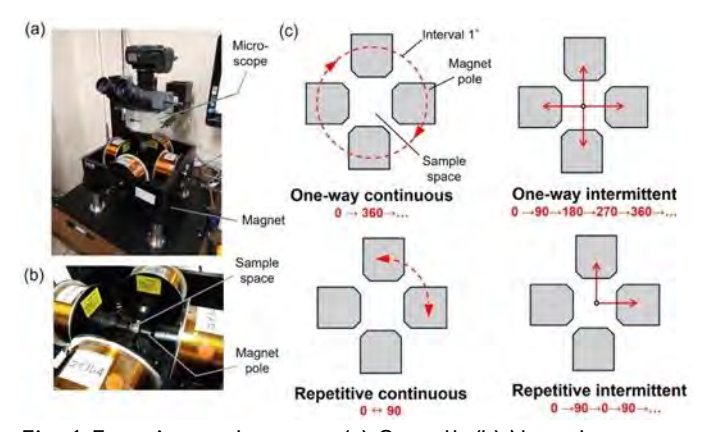


Fig. 1 Experimental system: (a) Overall, (b) Near the electromagnet, (c) Magnetic field application conditions

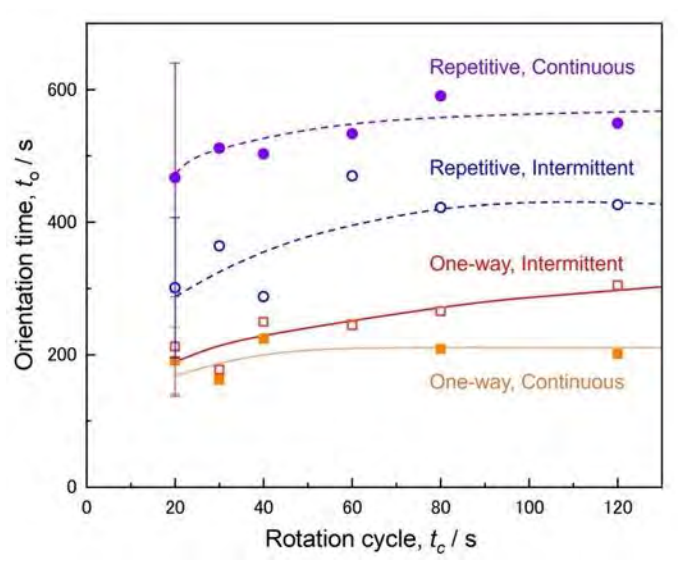


Fig. 2 Orientation time as a function of rotation period under each rotation condition

AQ-05. Red Blood Cell Magnetic Property Monitoring Using Cell Tracking Velocimetry: Applications to Blood Banking and Sickle Cell Disease

L. Nguyen T. Tran¹, K. Paz Gonzalez¹, H. Choe², X. Wu², P. Iyer², K. Wu³, J. Chalmers², <u>J. Gomez-Pastora</u>¹

¹Chemical Engineering, Texas Tech University, Lubbock, Texas, United States, ²Chemical and Biomolecular Engineering, The Ohio State University, Columbus, Ohio, United States, ³Electrical and Computer Engineering, Texas Tech University, Lubbock, Texas, United States

Red blood cells (RBCs) undergo progressive biochemical and morphological changes during storage, collectively termed the "storage lesion," which impacts transfusion efficacy and patient outcomes [1]. Traditional storage quality assessment relies on limited markers like hemolysis and ATP levels, necessitating more comprehensive evaluation methods. RBC magnetic susceptibility, influenced by hemoglobin oxygenation state and cellular integrity, represents a sensitive indicator of storage-related deterioration [2]. Cell tracking velocimetry (CTV) offers a novel approach for realtime, non-invasive assessment of single-cell magnetic properties. This optical technique measures individual cell velocities in controlled magnetic field gradients (191.82 TA/mm²), enabling precise determination of magnetic susceptibility without sample preparation or labeling [3,4]. Unlike bulk magnetometry methods, CTV provides singlecell resolution and can distinguish heterogeneous populations within stored blood products. In this work, we

apply CTV to monitor RBC magnetic properties during extended storage in AS-3 additive solution over 42 days. This technique enabled detection of storage-related changes in magnetic susceptibility at the single-cell level, revealing heterogeneity within stored RBC populations that may not be apparent through conventional bulk analysis methods. This research extends to sickle cell disease (SCD). where altered hemoglobin polymerization affects cellular magnetic properties. Sickle RBCs show distinct magnetic signatures compared to healthy cells, potentially enabling CTV-based assessment of disease severity and treatment response. The technique's sensitivity to single-cell changes makes it particularly valuable for monitoring SCD patients, where cellular heterogeneity is clinically significant. Thus, CTV represents a promising tool for blood banking quality control and SCD monitoring, offering real-time, quantitative assessment of RBC magnetic properties with single-cell resolution. This technology could enhance transfusion safety and provide new insights into RBC pathophysiology during storage and disease states.

[1] T. Yoshida, T. Shevkoplyas and S.S. Yoshida, Transfusion, Vol. 59, p.1450 (2019)

[2] M. Zborowski, L.R. Moore and P.S. Williams, Biophys. J., Vol. 84, p.2638 (2003)

[3] L.R. Moore, M. Zborowski and L. Sun, J. Magn. Magn. Mater., Vol. 293, p.572 (2005)

[4] L.N.T. Tran, K.M. Paz Gonzalez and H. Choe, Micromachines, Vol. 16, p.126 (2025)

AQ-06. Computational Design of a Magnetic Particle Imaging (MPI) Prototype: Effects of Gradient Fields and Nanoparticle Properties on Imaging Performance

S. Mostufa, B. Rezaei, K. Wu

Department of Electrical and Computer Engineering, Texas Tech University, Lubbock, Texas, United States

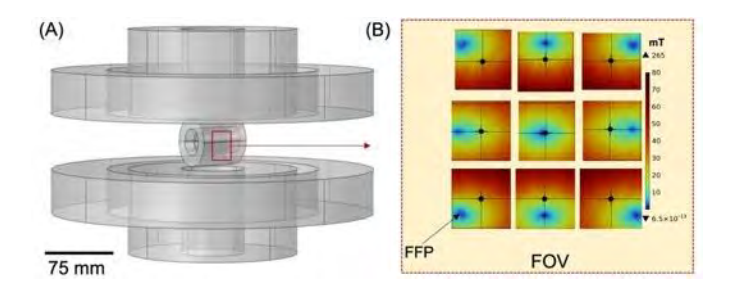
Magnetic particle imaging (MPI) is a non-ionizing biomedical imaging technique that uses dynamic magnetizations of magnetic nanoparticles (MNPs) to generate spatially resolved images [1][2][3]. This work presents a comprehensive computational demonstration of an MPI system, covering coil design and image reconstruction. Finite Element Method (FEM) simulations were conducted in COMSOL Multiphysics to design Maxwell coils for gradient fields, Helmholtz coils for focus fields, and solenoidal coils for drive, receive, and compensation functions. We focused on a 30 mm³ field of view (FOV),

evaluating magnetic field uniformities and amplitudes. A complete 3D MPI system design is shown in Fig. 1(A). Fig. 1(B) illustrates the field-free point (FFP) movement in 2D space, enabled by the interplay of gradient, drive, and focus coils. The compensation and receive coils were optimized to suppress feedthrough signals from the drive field. Magnetization dynamics of MNPs and image reconstruction were modeled in MATLAB using FEM-simulated magnetic field data. We analyzed MNPs with core diameters of 10 nm and 30 nm, using Langevin functions to evaluate the effects of magnetization curve steepness and gradient amplitude. X-space-based image reconstruction with fundamental frequency filtering generated images from a four-point phantom (Fig. 2(A), inset). As shown in Fig. 2(B), MNPs with sharper magnetization curves (30 nm) and a 2.5 T/m gradient field yielded superior image quality, validating the simulation. This study provides a complete 3D simulation framework for MPI system design and investigates the effects of MNP properties and magnetic gradients on imaging performance.

[1] M. Graeser et al., "Human-sized magnetic particle imaging for brain applications," Nat. Commun., vol. 10, no. 1, 2019, doi: 10.1038/s41467-019-09704-x.

[2] Z. W. Tay et al., "Superferromagnetic Nanoparticles Enable Order-of-Magnitude Resolution & Sensitivity Gain in Magnetic Particle Imaging," Small Methods, vol. 5, no. 11, pp. 1–10, 2021, doi: 10.1002/smtd.202100796.

[3] J. Rahmer, A. Halkola, B. Gleich, I. Schmale, and J. Borgert, "First experimental evidence of the feasibility of multi-color magnetic particle imaging," Phys. Med. Biol., vol. 60, no. 5, pp. 1775–1791, 2015, doi: 10.1088/0031-



9155/60/5/1775.

Fig. 1. (A) COMSOL Multiphysics 3D structural design of the 2D scanning MPI system containing the focus, gradient, drive, receive, and compensation coils. (B) Simulated movement of FFP in the 2D FOV.

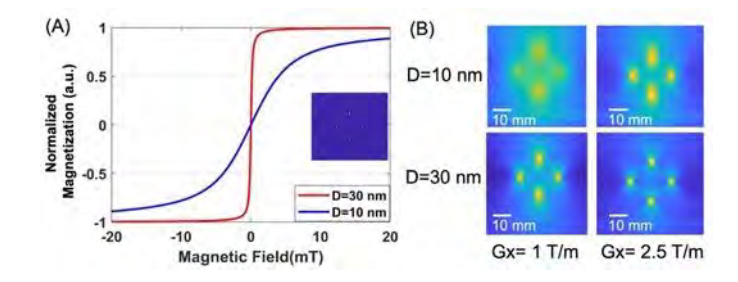


Fig. 2. (A) Langevin-modeled magnetization curves for 10 nm and 30 nm MNPs, highlighting slope differences; the inset shows the four-point phantom. (B) X-space image reconstruction in MATLAB illustrating effects of MNP size and gradient strength.

AQ-07. Design of a Mechanical-part-free Rotational Magnetic Field with Minimal Poles

<u>A. Hamasaki</u>¹, K. Sato², H. Kawaguchi², Y. Takeuchi²
¹Faculty of science, Shinshu University, Matsumoto,
Japan, ²Muroran Institute of Technology, Muroran, Japan

The rotation of the magnetic field direction is an important factor for the magnetic orientation of diamagnetic materials, especially for the case of complete orientation (1,2). Traditionally, rotating fields has involved physically moving samples on turntables (3). We recently developed a rotating magnetic field generator using a quadrupole electromagnet with no moving parts that is intended to be used in conjunction with a heater or similar device (4). However, because the poles are present on four sides, space utilization is limited. When using a bar-shaped electromagnet, the number of poles required to rotate the magnetic flux direction in a 2D plane can theoretically be reduced to three. In this study, we used the finite element method to predict the rotational magnetic field generated by passing the currents shown in the figure through coils A-C for the tripole electromagnet structures shown in Fig. 1(a), a motor without a core, and in Fig. 1(b), a structure with a large opening (called the 120° and 90° types, respectively). In the calculation, we considered the saturation magnetization of the magnetic material used in the core and frame of the electromagnet, and set the saturation magnetic flux density of SS400, a common steel material, to 2.3 Tesla. The total maximum current passing through each bar-shaped electromagnet was set to 6 A. As shown, for both the 120° and 90° types, the magnetic field direction is linear with respect to the current phase, and the magnetic field can rotate at a constant speed (Fig.

2(a)). The magnetic flux density at the center is stable for the 120° type, whereas it fluctuates depending on the current phase, particularly for the 90° type, as shown in Fig. 2(b). This is because more current flows through coil B in the case of the 90° type than through the other coils, resulting in saturation magnetization. At the conference, we will also present the experimental results obtained using the constructed tripole electromagnet.

[1] T. Kimura and M. Yoshino, *Langmuir*, 21, 4805 (2005) [2] C. Tsuboi, K. Aburaya and F. Kimura, *CrystEngComm*, 18, 2404 (2016)

[3] S. Tsukui and T. Kimura, *Japanese Journal of Applied Physics*, 51, 057301 (2012)

[4] Y. Takeuchi, H. Kawaguchi and A. Hamasaki, *Applied Physics Express*, 14, 057002 (2021)

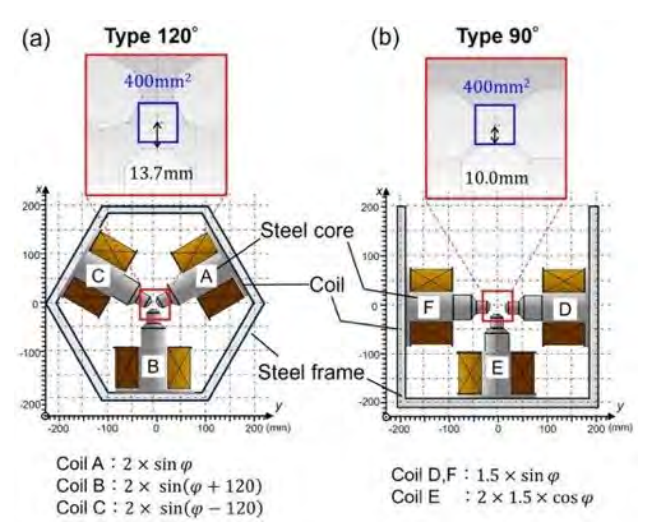


Fig. 1 Tripole electromagnet shapes: (a) 120° and (b) 90° types

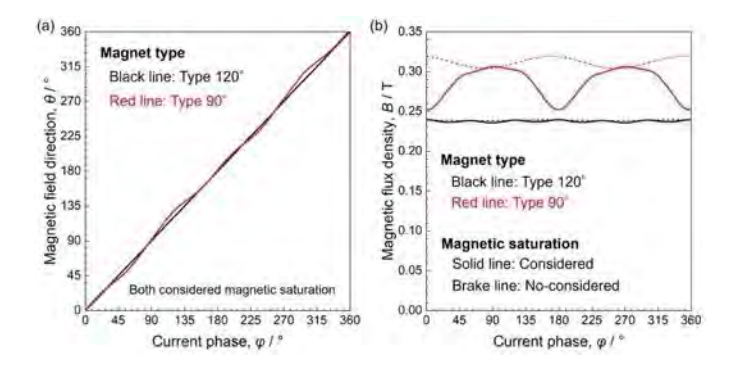


Fig. 2 Relationship between (a) current phase and magnetic field direction and (b) current phase and magnetic flux density

AQ-08. Optimization Method of Interface Exchange-Coupled Magnetic Moment in Iron-Based Dual-Phase Magnetic Materials Based on First-Principles

J. Yuan^{1,2}, <u>D. Zhang</u>^{1,2}, X. Chen^{1,2}, H. Zhou^{1,2}, F. Xiao^{1,2}, F. Yang^{3,4}, Y. Liu^{3,4}, C. Wang^{3,4}, T. Ma⁵, X. Guo⁵, X. Ma⁵

¹School of Electrical Engineering and Automation, Wuhan university, Wuhan, Hubei, China, ²State Key Laboratory of Power Grid Environmental Protection, School of Electrical Engineering and Automation, Wuhan University, Wuhan, Hubei, China, ³China Electric Power Research Institute, Beijing, China, ⁴State Key Laboratory of Advanced Power Transmission Technology, Beijing, China, ⁵State Grid Anhui Electric Power Co., Ltd. Huaibei Power Supply Company, Huaibei, Anhui, China

The performance of Magnetically Controlled Reactors (MCRs) is constrained by traditional core materials' inefficiency in continuous magnetic flux regulation. To overcome this, we investigate a novel α-Fe/ Nd₂Fe₁₄B dualphase composite. This material exploits the synergistic combination of α -Fe's rapid magnetization reversal and Nd₂Fe₁₄B 's high magnetocrystalline anisotropy, enabling easy saturation/demagnetization for efficient, remanencebased MCR inductance control. A critical design challenge remains the lack of theoretical methods for optimizing magnetic properties at heterogeneous interfaces. Addressing this, we propose a first-principles computational strategy: Density Functional Theory (DFT) optimizes the single-phase structures and constructs strained α -Fe(010)/ Nd₂Fe₁₄B (001) heterostructures (Fig. 1a,b) with varied soft/hard layer ratios. High-throughput magnetic moment calculations identify the optimal ratio (10:5) via maximization (Fig. 2a). Subsequent spin-resolved DOS analysis of the optimal structure (Fig. 1c,d) and interfacial spin polarization quantification via PDOS (Fig. 2b) reveal a significantly enhanced magnetic moment of 83.909 µB at the 10:5 ratio. This efficient, reproducible computational methodology resolves the interfacial magnetic moment optimization challenge, providing a reliable theoretical framework for high-performance MCRs and electromagnetic devices.

[1]Niu K, Qiu G, Wang C, et al. Self-intercalated magnetic heterostructures in 2D chromium telluride[J]. Advanced Functional Materials, 2023, 33(2): 2208528.
[2]Yang Z, Lu S, Tian Y, et al. Assessing the magnetic order dependent γ -surface of Cr-Co-Ni alloys[J]. Journal of Materials Science & Technology, 2021, 80: 66-74.
[3]Ren J, Wu M, Li C, et al. Deformation mechanisms in an

^{*} Best Student Presentation Finalist / LB - Late-breaking Poster

additively manufactured dual-phase eutectic high-entropy alloy[J]. Acta Materialia, 2023, 257: 119179.

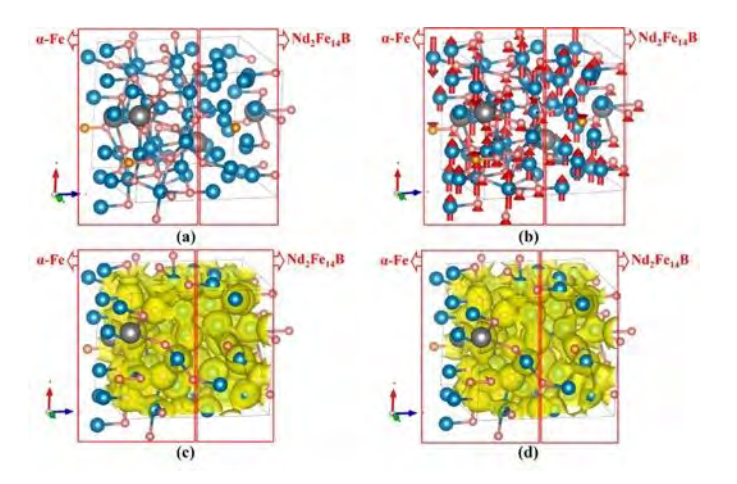


Figure 1. Structural characterization of the α -Fe/ Nd₂Fe₁₄B (10:5) heterostructure. (a) Schematic diagram of the 3D atomic structure; (b) 3D magnetic moment distribution; (c) Charge density map for spin-up states; (d) Charge density map for spin-down states. Atom color code: Orange = Nd, Blue = Fe, Yellow = O, Green = B. Red arrows in (b) indicate magnetic moment magnitude and direction.

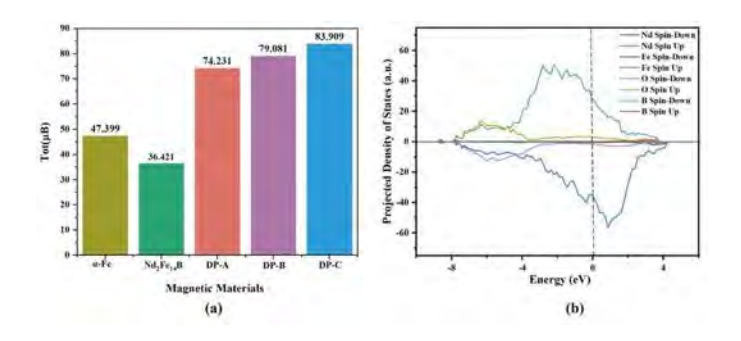
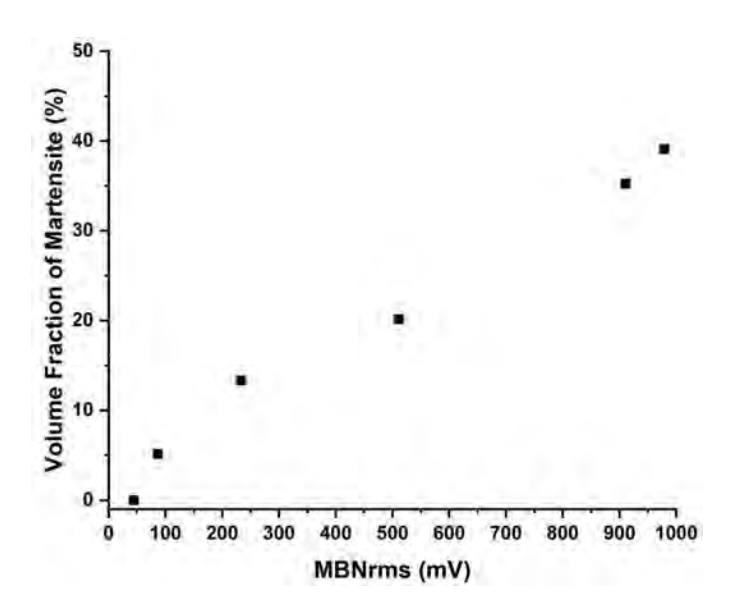


Figure 2. Comparative magnetic properties of α -Fe/Nd₂Fe₁₄B heterostructures. (a) Calculated magnetic moments for varying soft/hard phase thickness ratios: 1:5 (DP-A), 5:5 (DP-B), 10:5 (DP-C); (b) Projected density of states (PDOS) near the Fermi level (E_F=0 eV) for the optimal 10:5 configuration.

AQ-09. Structural Health Monitoring in Austenitic Steels by Means of Determining Martensitic Phases

T. Damatopoulou, X. Vourna, E. V. Hristoforou *National TU of Athens, Athens, Greece*

Austenite steels are important for several demanding sectors in industry, energy, transportation and large research infrastructures. Demanding heat exchangers and critical shaft structures are made of austenitic steel for industrial, energy and transportation applications. Apart from that, critical vessels under pressure are also made of the same steel grade(s). Finally, accelerating rings in large research infrastructures employee austenitic steels. Therefore, the structural health monitoring of this type of steel is of critical importance. Our technology to monitor residual stress in magnetic steels could not be used for structural characterization of austenite steel since they don't present magnetic properties. However, before the failure of the austenite steel, it is transformed into martensite, that has magnetic properties. Therefore, determination of magnetic mass inside the austenite phase declares the beginning of its transformation into martensite, indicating the beginning of its failure. Due to that reason, we have initiated work towards the determination of magnetic mass (martensitic phase) into the austenite steel. This way, the first attempt has been the study of the martensitic phase from 0% up to 45%, that is more or less the threshold after which the austenitic steel will fail. We have ordered austenitic steel grades in the form of 1 mm thin sheets, namely 304, 316, 316L and 316LN steel grades with 1%, 3%, 10%, 20%, 30%, 40% and 45% of martensitic phase and we determined their magnetic response by using our own single sheet tester. The observed dependence of the magnetic response on the amount of austenitic steels has been linear for excitation frequencies from 0.1 Hz up to 1 Hz, indicating the ability of the magnetic response to determine the percentage of the martensitic phase in the austenitic steel. Furthermore, we have determined the response of 3D AMR sensors with respect to the size and the depth of martensitic spheres inside a non-magnetic foam, simulating in fact the austenitic steel. These preliminary results on such a dependence have been proven to be monotonic and are presented in our work (Fig. 1).



AQ-10. Probing the Antiferromagnetic-Ferromagnetic Phase Transition in FeRh using Ultrafast Extreme Ultraviolet High Harmonic Spectroscopy

N. Li, A. Grafov, E. Sawruk, M. Lebrat, H. C. Kapteyn, M. M. Murnane

JILA, University of Colorado, Boulder, Colorado, United States

Ultrafast laser pulses can drive the fastest spin dynamics and phase transitions in magnetic materials, with dynamics ranging from attoseconds on up.[1-6] However, to fully exploit these capabilities for more energy-efficient nanotechnologies, a detailed understanding of the physics underlying nanoscale spin manipulation is required. Ultrafast X-ray pulses make it possible to probe elementspecific spin dynamics in multi-component magnetic systems, providing rich new information not accessible using visible light. In particular, tabletop laser-based high harmonic (HHG) sources are ideal for probing fast spin dynamics since they can probe sub-lattices in a compound, or distinct layers in a structure, simultaneously and with element specificity.[2-4] This makes it possible to capture and distinguish processes such as spin transfer, spin reorientations, spin currents and spin flips, to understand how to manipulate spins using light.

Here we study FeRh, a material that exhibits a first-order antiferromagnetic (AFM) to ferromagnetic (FM) phase transition near room temperature, that has attracted wide interest due to its coupled magnetic and structural responses.^[5] While the dynamics of Fe 3d states during this transition have been extensively studied, the role of Rh 4d

electrons—especially their hybridization-driven magnetic behavior—remains less understood. After excitation of the material using femtosecond laser pulses at different fluences, we probe the resulting AFM-to-FM phase transition at photon energies near the Fe M-edge and the Rh N-edge, to study the respective contributions of Fe and Rh. Preliminary results indicate that Rh exhibits a finite asymmetry even in the nominally non-magnetic AFM state, suggesting the presence of induced spin polarization via Fe-Rh hybridization.

- [1] E. Beaurepaire, J. C. Merle and A. Daunois, Phys. Rev. Lett., Vol. 76, p.4250 (1996)
- [2] P. Tengdin, P. Gentry and A. Blonsky, Sci. Adv., Vol. 6, eaaz1100 (2020)
- [3] W. You, P. Tengdin and C. Chen, Phys. Rev. Lett., Vol. 121, 077204 (2018)
- [4] P. Tengdin, W. You and C. Chen, Sci. Adv., Vol. 4, eaap9744 (2018)
- [5] A. V. Kimel and M. Li, Nat. Rev. Mater., Vol. 4, p.189 (2019)
- [6] G. Li, R. Medapalli and J. H. Mentink, Nat. Commun., Vol. 13, 2998 (2022)

SESSION AR: MAGNETIZATION DYNAMICS (POSTER SESSION)

Co-Chair(s): A. Capua, Electrical Engineering and Applied Physics, The Hebrew University of Jerusalem, Jerusalem, Jerusalem, Israel and B. J. Assouline, Applied Physics, The Hebrew University of Jerusalem, Jerusalem, Israel

Tuesday, October 28, 2025

09:00 AM-12:00 PM

Exhibit Hall Posters

AR-01. Effect of oxygen ion implantation on the interfacial properties of the Pt/Co/Pt multilayer with perpendicular magnetic anisotropy

<u>A. Sharma</u>¹, P. Karmakar², R. Brajpuriya¹, V. Reddy³, A. Gupta¹, M. Gupta³, S. Pathak¹

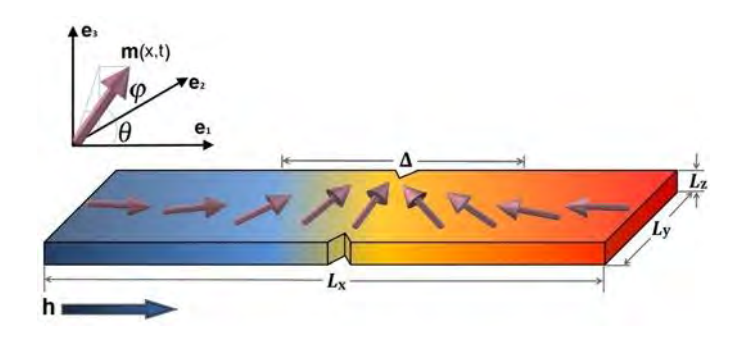
¹Physics, UPES Dehradun, Dehradun, Uttarakhand, India, ²Variable Energy Cyclotron Centre, Kolkata, West Bengal, India, ³UGC DAE CSR, Indore, Madhya Pradesh, India

The interaction of oxygen with cobalt and cobalt-based allovs has been a very important topic in the field of spintronics as it leads to enhanced orbital anisotropy and interfacial Dzyaloshinskii-Moriya interaction (DMI), which are crucial in the context of applications such as magnetic tunnel junctions (MTJs) based data storage and domain wall motion. To understand the complex and interesting relationship between oxygen and ferromagnetic (FM)/heavy metal (HM) interfaces, we studied controlled oxygen ion (O) implantation in a cobalt layer located in a Pt/Co 1.2 /Pt (nm) multilayer with a specific structure. O ions of 6 keV energy were used in this process, which uniformly implanted the ions on both Pt interfaces. This implantation was confirmed by hard X-ray photoelectron spectroscopy (HAXPES) performed at 6 keV energy, which clearly showed that the oxygen ions were incorporated in the cobalt layer in a controlled manner. Under low field regime, the Co/Pt multilayer's domain wall velocity got increased by a significant value because of the oxygen implantation. The main reason for this rise is that the structural and magnetic changes caused by O ion implantation lower the energy barriers. This study is an important step towards using oxygen implantation to tune ferromagnetic interfaces. which could make future spintronic devices work better.

AR-02. Depinning of Domain Walls in a Notched Ferromagnetic Nanostrip: Role of Inertial and Nonlinear Damping Effects

S. Dolui¹, S. Maity¹, S. Dwivedi¹, G. Consolo²
¹School of sciences, National Institute of Technology Andhra
Pradesh, Tadepalligudem, Andhra Pradesh, India, ²Department
of Mathematical and Computer Sciences, Physical Sciences and
Earth Sciences, University of Messina, Messina, Italy

In this work, we investigate theoretically the static and kinetic depinning field of a domain wall in a notched magnetic nanostrip under the generalized framework of the Landau-Lifshitz-Gilbert equation, which combines inertial and nonlinear viscous-dry friction damping effects. We assume a head-to-head transverse domain wall configuration and analyzed its motion subject to an external magnetic field. To deduce the equation ruling the spatiotemporal evoution of the magnetic domain wall, we adopt the Schryer and Walker trial function approach. The results show that static and kinetic depinning fields increase as the dry friction dissipation increases. Moreover, viscous dissipation exhibits a weak dependence on the kinetic depinning field and saturated domain wall velocity, while inertial damping due to the relaxation time of angular momentum significantly impacts the kinetic depinning field, depinning time, and breakdown velocity. Our numerical results are in good qualitative agreement with the recent observations reported in the literature.



Schematics of a ferromagnetic nanostrip with an artificial notch in the form of two symmetrical triangles and reference axes.

AR-03. Modulation of switching dynamics in magnetic tunnel junctions for low-error-rate computational random-access memory

Y. Lv, B. Dixit, J. Wang

Electrical and Computer Engineering, University of Minnesota -Twin Cities, Minneapolis, Minnesota, United States

Al's growth has increased computational demands, especially for neural networks. Traditional von Neumann architectures suffer from a "memory bottleneck" due to the physical separation of logic and memory, which forces constant data movement and leads to reduced performance and higher energy consumption.

To address this, approaches like near-memory computing [1] and in-memory computing [2], [3] have been explored. A recent advancement, "true" in-memory computing, is demonstrated by CRAM [4], [5], where logic operations occur within memory cells, removing external data transfers. CRAM enables random access, high parallelism, and reconfigurable logic [4], [5], all within a digital system, showing strong potential for enhanced performance and energy efficiency [6].

In this work, we introduce a novel approach to optimize MTJ based CRAM by utilizing Voltage-Controlled Magnetic Anisotropy (VCMA) [7]. Through comprehensive numerical and HSPICE simulations, for the first time we demonstrate that incorporating VCMA substantially enhances the steepness of the Switching Probability Transfer Curve (SPTC), thus greatly reducing the logic operation error rate. VCMA coefficient of 200 fJV⁻¹m⁻¹ results in a significant error rate reduction of approximately 61.43% compared to standard CRAM configurations without any VCMA effect. Additionally, the inclusion of VCMA reduces the required logic voltage, further contributing to energy efficiency.

The statistical average outputs of a NAND logic operation of CRAM was analyzed with and without VCMA. The VCMA-enhanced configuration required a lower logic voltage (Vlogic) to achieve optimal error rates. Specifically, the Vlogic decreased from 1.801 V (without VCMA) to 1.458 V (with VCMA), accompanied by a reduction in the error rate from 26.33% to 17.25%. This demonstrates the dual benefit of VCMA in improving logic reliability and reducing energy consumption.

[1] J. T. Pawlowski, in 2011 IEEE Hot Chips 23 Symposium (HCS), May 2011, pp. 1–24.

- [2] S. Matsunaga *et al.*, *Appl. Phys. Express*, vol. 1, p. 091301 (2008).
- [3] J. Borghetti *et al.*, *Nature*, vol. 464, no. 7290, pp. 873–876 (2010).
- [4] J.-P. Wang and J. D. Harms, *US Patent*, US9224447B2 (2015).
- [5] Z. Chowdhury *et al.*, *IEEE Comput. Archit. Lett.*, vol. 17, no. 1, pp. 42–46 (2018).
- [6] M. Zabihi *et al.*, *IEEE Trans. Comput.*, vol. 68, no. 8, pp. 1159–1173 (2019).
- [7] Lv, Yang, Brahmdutta Dixit, and Jian-Ping Wang. *arXiv* preprint arXiv:2505.14829 (2025).

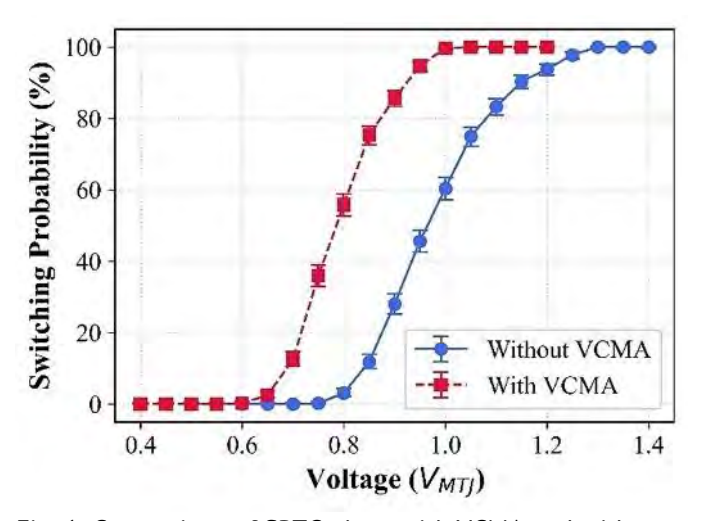


Fig. 1. Comparison of SPTC plots: with VCMA and without VCMA.

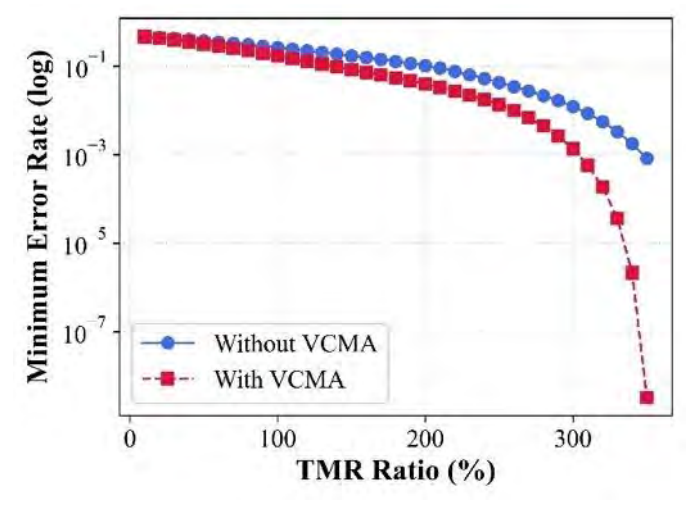


Fig. 2. CRAM error rate vs. TMR ratio, with and without VCMA

AR-04. Nonlinear dynamics of spin waves in L-shaped ferromagnetic nanowires and nanoplatelets under high-power microwave pumping

B. Hussain¹, M. G. Cottam²

¹University of Michigan, Dearborn, Michigan, United States, ²University of Western Ontario, London, Ontario, Canada

There is a strong ongoing interest in the linear and nonlinear properties of spin waves (SW) or magnons in finite-sized magnetic nanostructures. The resulting mode confinement can provide new material capabilities and application developments (e.g., see [1-4]). Nonlinear SW effects are significant, for example, when parallel microwave pumping is applied (e.g., [5,6]). Here we present theoretical results for the SW instabilities induced by microwave pumping in the parallel configuration. Applications are made to ferromagnetic nanoplatelets and nanowires with an asymmetric L-shape cross section. The lack of rotational and reflection symmetries in this shape, in general, influences the characteristics of the SWs and also leads to strong spatial inhomogeneities for the SW amplitudes. We employ a microscopic (Hamiltonian-based) approach like that used in [5,6] for ultrathin films and for nanowires with a microwave pumping field. Particularly, the quantized SW frequencies and their threshold fields are investigated for the onset of a SW-decay instability. We use permalloy with realistic magnetic parameters for the Lshape platelets and wires of varied sizes. The results show significantly modified butterfly curves (for plots of threshold field vs. applied field), as well as more structural features compared to those for thin films.

A typical numerical example is shown in Fig. 1 for the lowest few frequencies of the dipole-exchange SWs obtained for a L-shape platelet plotted versus the applied field B_0 . The static magnetization within the platelet (with size as depicted) is spatially inhomogeneous. The initial dip in the curve for the lowest SW mode is attributed to a realignment of the spins as the applied field increases. More importantly, the separations between the mode frequencies vary with B_0 , resulting in modifications to the threshold microwave fields for the SW instabilities to occur under parallel pumping. Our results for L-shaped structures are compared and contrasted with those predicted for spherical geometries (e.g., [7]).

- [1] G. Gubbiotti (ed.), *Three-Dimensional Magnonics*, 2019, Jenny Stanford Publishing (Singapore).
- [2] H. Yu et al., Nature Comm., 2016, 7, 11255.
- [3] I.A. Golovchanskiy et. al., J. Appl. Phys., 2020, 127, 093903

- [4] T. Brächer, P. Pirro, and B. Hillebrands, *Physics Reports*, 2017, 699, 1.
- [5] H.T. Nguyen and M.G. Cottam, *Phys. Rev. B.*, 2014, *89*, 144424.
- [6] Z. Haghshenasfard and M.G. Cottam, *IEEE Magnetics Lett.*, 2016, *7*, 3705705.
- [7] J. Lim, A. Garg, and J.B. Ketterson, *J. Mag. Magn. Mat.*, 2023, *587*, 171232.

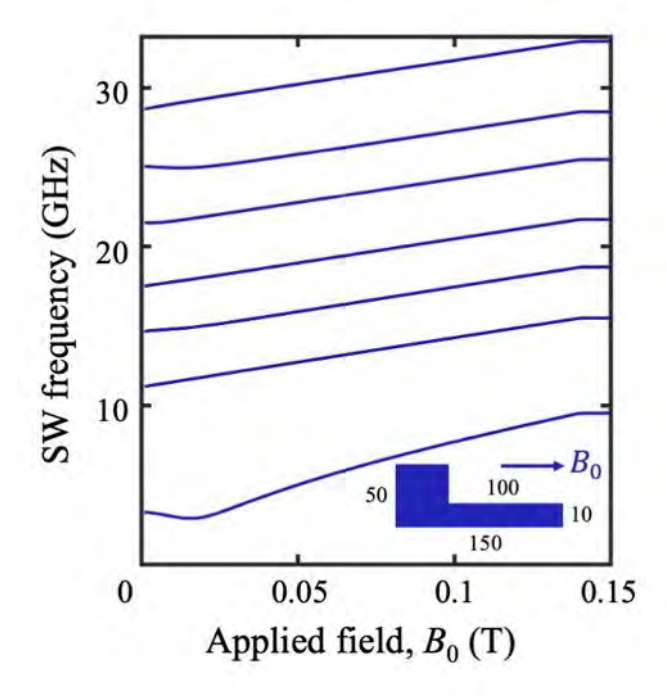


Fig. 1. SW frequencies plotted versus the applied magnetic field for a L-shaped nanoplatelet of permalloy. The inset is a schematic for the geometry (all dimensions shown in nm).

AR-05. Data-Driven Estimation of Magnetic Nanoparticle Properties via Stochastic Langevin Model

E. Azizi¹, H. Zuo², V. K. Chugh³, R. He¹, <u>K. Wu¹</u>
¹Department of Electrical and Computer Engineering, Texas
Tech University, Lubbock, Texas, United States, ²Lubbock High
School, Lubbock, Texas, United States, ³Seagate Technology
LLC, Bloomington, Minnesota, United States

The dynamic magnetization of magnetic nanoparticles (MNPs) arises from coupled Néel and Brownian relaxations, which are influenced by intrinsic particle properties such as size, saturation magnetization, magnetic anisotropy, and damping. While experimental AC magnetization measurements can reveal the collective dynamic behavior of MNP ensembles, extracting accurate particle-specific

parameters from such data remains a challenge due to experimental limitations and model oversimplifications. To address this, we apply a stochastic Langevin model that explicitly captures the time-dependent magnetization response of MNPs under alternating magnetic fields by incorporating both thermal fluctuations and stochastic relaxation processes.[1] This model provides a physically grounded framework for simulating magnetization hysteresis under experimental conditions, enabling parameter estimation through direct data fitting. In this work, we fit the stochastic Langevin model to experimentally measured dynamic hysteresis loops of different MNPs collected at 20 mT and 5 kHz AC field. By coupling the model with Bayesian optimization and Gaussian process regression, we identify optimal values of key magnetic parameters: saturation magnetization, effective anisotropy constant, and Gilbert damping parameter. This approach is demonstrated using four commercial MNP products (SHS30, IPG30, SHP25, and SHP15, from Ocean Nanotech, LLC), yielding high-fidelity fits to experimental data and robust estimation of their magnetic properties. Fig. 1 presents the data fitting results for SHS30 and IPG30 MNPs. The extracted damping parameter values are higher than those typically reported for iron oxide, which is expected, given that these MNPs are suspended in liquid and exhibit combined Néel and Brownian relaxation mechanisms.[2,3] Our framework offers a powerful tool for the quantitative characterization of MNPs under application-relevant dynamic field conditions. [1] Azizi E, Mostufa S, Rezaei B, Xin S, Sun J, Shi Z, Gómez-Pastora J and Wu K 2025 Applying stochastic Langevin function with coupled Brownian-Néel relaxations to study the dynamic magnetizations of nanoparticle tracers in magnetic particle imaging J. Phys. Appl. Phys. 58 135002 [2] Reeves D B and Weaver J B 2015 Combined Néel and Brown rotational Langevin dynamics in magnetic particle imaging, sensing, and therapy Appl. Phys. Lett. 107 223106 [3] Shasha C and Krishnan K M 2021 Nonequilibrium dynamics of magnetic nanoparticles with applications in biomedicine Adv. Mater. 33 1904131

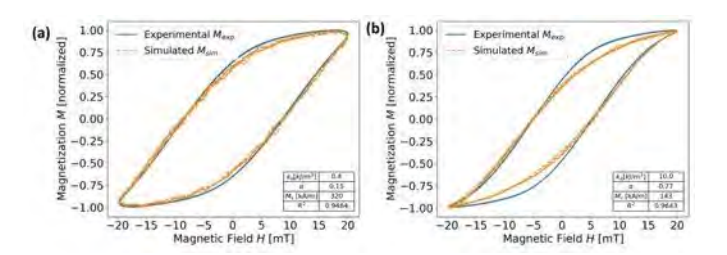


Fig. 1. Data-fitting on normalized AC hysteresis loops of (a) SHS30 and (b) IPG30 MNPs subjected to 20 mT, 5 kHz field.

AR-06. Development of High-sensitive ST-FMR with Amplitude Modulated Magnetic Field

<u>A. Kamiryo</u>¹, T. Horaguchi², T. Manago²
¹Osaka Metropolitan Univ., Sakai, Osaka, Japan, ²Fukuoka Univ., Fukuoka, Fukuoka, Japan

Spin-torque ferromagnetic resonance (ST-FMR) is a versatile method for evaluating the efficiency of spin-current generation induced by the spin Hall effect or analogous mechanisms. In this method, ferromagnetic resonance (FMR), mainly driven by spin torque, is detected as a DC voltage via the rectification through the magnetoresistance. The generation efficiency of the spin current is obtained by analyzing the FMR signal consisting of symmetric and antisymmetric Lorentzian components¹⁾. In the conventional methods, DC voltage is measured directly, which results in the superposition of unwanted thermoelectric voltages and various offset voltages²⁾, leading to a poor signal-to-noise (S/N) ratio. As a result, evaluation of small samples with weak spin Hall effects has been challenging. In this study, we developed a high-precision method by applying magnetic field-modulated differential signal detection³⁾ to ST-FMR. This allows evaluation of materials with weak spin Hall effect and detection of subtle spin torque variations.

A NiFe (15 nm thick)/Pt(10 nm thick) bilayer (5 µm wide, 100 µm long) was fabricated by electron beam lithography and electron beam deposition [Fig. 1(a)]. An AC magnetic field (frequency: 100-1100Hz), much lower than the FMR frequency, was applied along with a swept static magnetic field. The differential voltage signal due to ST-FMR was detected using the lock-in technique. Figure 1(b) shows obtained FMR spectrum. The blue dots are the measured data; the red dashed line is the fitting result by analytical formula. These show good agreement. Notably, the offset voltage and background noise are negligibly small. Compared to conventional methods, the S/N ratio was significantly improved. In the presentation, we will report quantitative comparison in terms of evaluated spin Hall angle and S/N ratio.

- 1) L. Liu et al., Phys. Rev. Lett. 106, 036601(2011).
- 2) M. Aoki et al., Phys. Rev. B 104, 094401(2021).
- 3) S. Tamaru *et al.*, Rev. Sci. Instrum. 89, 053901 (2018)

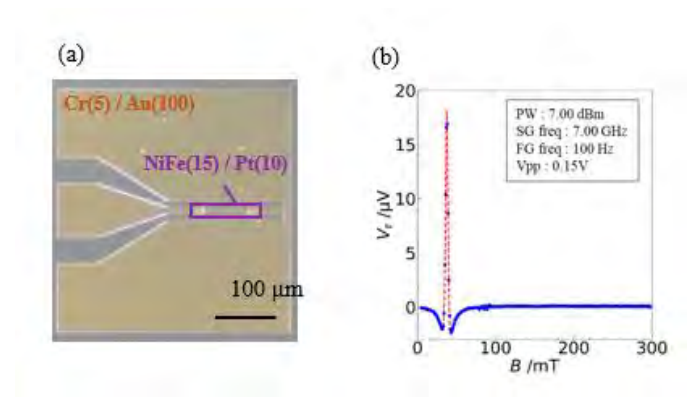


Fig 1 (a) An optical microscope image of the fabricated sample. (b) ST-FMR spectrum measured by the magnetic field modulation method.

AR-07. Dynamic Control and Amplification of Spin Waves via Temporally Modulated Magnetic Fields

K. W. Sobucki, P. Gruszecki

Adam Mickiewicz University, Poznan, Poland

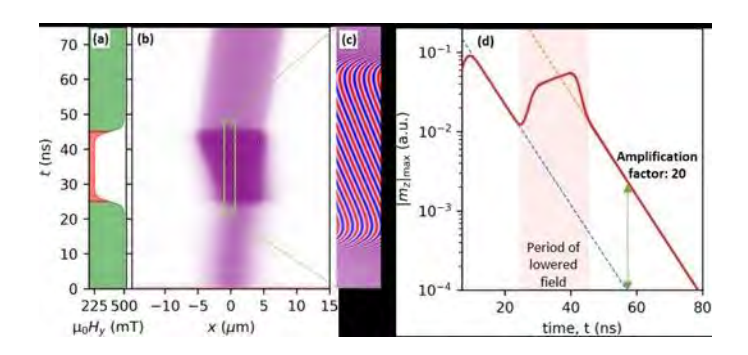
Spin waves (SWs) are propagating oscillations of magnetic moments in magnetic materials, governed by the Landau – Lifshitz equation. As massless and chargeless information carriers, they do not experience Joule heating and offer shorter wavelengths than electromagnetic waves, enabling device miniaturization. However, efficient SW amplification remains a key challenge for practical applications. Time-varying media and effects like temporal reflection and refraction offer promising but underexplored avenues for magnonics [1,2]. In this theoretical study, we propose controlling SW propagation by dynamically modulating the external magnetic field in time and space within ferromagnetic films featuring perpendicular anisotropy and Dzyaloshinskii – Moriya interaction, which induces nonreciprocity.

W

e investigate how such modulation affects SW behavior near the critical bias field marking a transition from uniform inplane magnetization to stripe domains [3]. Micromagnetic simulations using MuMax3 [4] reveal SW reflection and refraction at temporal interfaces. Importantly, temporal modulation of the bias field enables time-domain control and 20-fold SW amplification (Fig. 1). This approach offers a practical route for dynamic SW manipulation using externally driven magnetic fields, such as those generated by coplanar antennas.

Acknowledgements: The research leading to these results has received funding from the National Science Centre of Poland, projects no. PRELUDIUM 2022/45/N/ST3/01844, and SONATA-15 2019/35/D/ST3/03729

- [1] J Toedt and W Hansen, Scientific Reports 11.1 (2021): 7821.
- [2] K Schultheiss et al. Physical review letters 126.13 (2021): 137201.
- [3] J Kisielewski, et al., Physical Review B 107.13 (2023): 134416.
- [4] A Vansteenkiste, et al., AIP advances 4.10 (2014).



(a) Time profile of the uniform bias magnetic field. (b) Space-time evolution of the out-of-plane magnetization component m_z . (c) Zoomed-in view of (b) showing changes in m_z during field modulation. (d) Maximum $|m_z|$ as time function, with the red region marking the interval of reduced magnetic field. The blue dashed line in (b) shows the expected decay of the spin-wave packet without field modulation. In contrast, the simulated field reduction leads to a 20-fold amplification of the spin-wave amplitude, marked by the green arrow.

^{*} Best Student Presentation Finalist / LB - Late-breaking Poster

AR-08. Broadband Magnetization Dynamics and Multiphase Switching in Cobalt Ferrite Nanoparticles Embedded in Activated Carbon

<u>S. Jan</u>¹, R. Roy Chowdhury¹, N. Schulz⁴, A. I. Ojo¹, M. González de la Vega², J. Á. Blanco Rodríguez², P. Gorria^{2, 3}, D. A. Arena¹, H. Srikanth¹

¹University of South Florida, Tampa, Florida, United States, ²Universidad de Oviedo, Oviedo, Spain, ³IUTA, Universidad de Oviedo, Gijón, Spain, ⁴Naval Surface Warfare Center, Panama City, Florida, United States

Magnetic nanocomposites exhibiting broadband dynamic response are critical for advanced electromagnetic, biomedical, and additive manufacturing applications [1, 2]. In this study, we investigate cobalt ferrite (CFO) nanoparticles embedded within a porous activated carbon matrix (CFO@C). Comprehensive structural characterization confirms the formation of quasi-spherical nanoparticles, uniformly dispersed throughout the carbon matrix. Static magnetization measurements reveal broad thermally activated blocking behavior and characteristic wasp-waisted hysteresis loops, indicative of coexisting soft and hard magnetic phases. A Voigt-profile-based fitting approach was employed for the deconvolution of the hysteresis loop data into the respective hard and soft magnetic components. To explore dynamic magnetic response, magnetic hyperthermia measurements were performed in both deionized water and agar media, with specific absorption rate and intrinsic loss power values determined using multiple fitting approaches. Ferromagnetic resonance spectroscopy in the 18 – 30 GHz range revealed an average q-factor of 1.95 and 2.0 for two representative samples, along with broadened linewidths consistent with strong damping behavior. Additionally, transverse susceptibility measurements over 25-320 K provided insights into the evolution of anisotropy fields with temperature. These findings highlight CFO@C as a multifunctional magnetic nanocomposite, thereby positioning it as a promising candidate for integration into broadband EMI shielding systems and additive manufacturing platforms incorporating magnetic nanoparticles for frequency-selective device applications.

1. Jan, S.Q., Schulz, N., Roy Chowdhury, R., Ojo, A.I., Anjum, D.H., Khurshid, H., Arena, D.A. and Srikanth, H., 2025. Magnetization Dynamics in Cobalt-Decorated Cobalt Ferrite Nanocomposites: Implications for High-Frequency Electromagnetic Shielding. *ACS Applied Nano Materials*.

2. Fadel, M., Martín-Jimeno, F.J., Fernández-García, M.P.,

Suárez-García, F., Paredes, J.I., Belo, J.H., Araújo, J.P., Adawy, A., Martínez-Blanco, D., Álvarez-Alonso, P. and Blanco, J.A., 2023. Untangling the role of the carbon matrix in the magnetic coupling of Ni@ C nanoparticles with mixed FCC/HCP crystal structures. *Journal of Materials Chemistry C*, 11(12), pp.4070-4080.

AR-09. Investigation of the magnetic behavior of 11 nm diameter magnetite (Fe_3O_4) nanoparticles encased in a 2 nm coating

T. M. Pekarek¹, K. O'Shea²

¹Physics, Univ. of N. Florida, Jacksonville, Florida, United States, ²Department of Chemistry and Biochemistry, Florida International Univ., Miami, Florida, United States

Humic acid grafted magnetite nanoparticles have emerged as a valuable tool for the remediation of arsenic, phosphorous, and selenium contaminants from water. We report on the magnetic behavior of 11 nm diameter magnetite (Fe₃O₄) nanoparticles encased in a 2 nm coating that form the core of this valuable system. The hysteresis loops observed at 5, 20, and 200 K were 80% saturated in a 0.10 T field. The saturated magnetization from the hysteresis loops is well described by a fit using Block's $T^{3/2}$ law over the entire range from 5 to 320 K. The remnant magnetization was found to decrease by 94% as the temperature increases from 20 to 320 K. The 0.0350 T coercive field at 20 K was found to decrease to 0.0011 T at 320 K. The values of the coercive field between 20 and 140 K were analyzed using Kneller's law $H_c = H_0 \left[1 - (T/T_B)^{\alpha} \right]$, where H_0 is the coercivity at 0 K, T_B is the blocking temperature, and α is a constant. From a fit using Kneller's law, we extracted the values of $H_0 = 0.0713$ T, $T_B = 220$ K, and α = 0.28. The value of α below 0.5 is characteristic of small nanoparticles. The blocking temperature was also independently observed as a broad peak near 220 K in the magnetization data taken in a 0.0100 T field.

*The authors would like to thank M.M. Rashid and A.M. Martin. This research was supported by UNF's Terry Presidential Professorship and by the National Science Foundation (NSF) Grants No. DMR-16-26332 and DMR-14-29428.

AR-10. PETASPIN 2.0: a high-performance CUDA™-native numerical solver for micromagnetic and ferroelectrics calculations

A. Giordano¹, A. Hasan², E. Piccolo³, D. Rodrigues³, M. Carpentieri³, <u>G. Finocchio</u>²

¹Department of Engineering, University of Messina, Messina, Italy, ²MIFT, University of Messina, Messina, Italy, ³Department of Electrical and Information Engineering, Politecnico di Bari, Bari, Italy

With this work we present a new release of the Petaspin solver [1] CUDA™ native, called *Petaspin 2.0*, an effective tool for micromagnetic simulations of ferromagnetic dynamics at mesoscopic scale. This tool can be applied for verifying theoretical models and study new phenomena in the emerging field of spintronics [2,3]. Petaspin 2.0 is a finite difference solver based on the LLG equation, it allows localized parameter definitions at each mesh point. This new version has been migrated from the standard CUDA™ implementation to a CUDA Thrust-based code architecture [4]. The solver provides several integration methods to reproduce the time-domain dynamic including (i) a generalized version of the Adams-Bashforth (AB3M2) method, and (ii) a multistep adaptive step-size method based on the Lagrange formula for polynomial interpolation, the latter significantly reduces the simulation times. The new code architecture supports seamless switching between CPU, GPU and multi-GPU improving scalability. It also abstracts many low-level CUDA implementation details, making development more accessible to non-expert programmers and reducing errors such as out-of-bound memory access through built-in iterators that manage computational scope. Additionally, kernel launches are automatically optimized, delivering performance comparable to custom implementations in most cases. These enhancements streamline development and position the solver as a more efficient and user-friendly tool for micromagnetic simulations. Petaspin provides options to include the standard micromagnetic code such as the exchange, magnetostatic, anisotropy, external, and magnetoelastic fields in the effective field computation. It also supports computation for STT, and other effects that contribute in the LLG equation to determine the dynamics of spintronic systems. Petaspin 2.0 also integrates a ferroelectric solver based on Landau-Ginzburg equation that allows the coupling of ferroelectrics and ferromagnetic materials via strain fields to simulate effectively magnetoelectric multilayer. We will present also new concept of antennas and oscillators based on those

coupling.

ACKNOWLEDGEMENTS

This work was supported under the project by the Italian Ministry of University and Research through the project "SKYrmion-based magnetic tunnel junction to design a temperature SENSor - SkySens" PRIN_20222N9A73_002, project PRIN 2020LWPKH7 (IT-SPIN) and by the PETASPIN association (www.petaspin.com).

- [1] https://www.petaspin.com/
- [2] G. Bertotti, Hysteresis in Magnetism, For Physicists,
 Material Scientists, and Engineers, 1998, Academic Press.
 [3] Jiang Sheng et al., Spin-torque nano-oscillators and their applications, Applied Physics ReviewsVolume 11, Issue 41
 December 2024 Article number 041309
- [4] https://developer.nvidia.com/thrust

AR-11-LB. Chip-Scale Band Engineering in Doped MoS₂ Heterostructure for Spintronic Integration

N. Do¹, H. Ko², U. Palanivel³, S. Kim⁴, J. Kim⁵, H. Kim³, <u>T. Kim</u>¹ Department of Physics, Ewha Womans University, Seoul, Korea (the Republic of), ²SKKU Advanced Institute of Nanotechnology, SKKU, Suwon, Korea (the Republic of), ³Center for Ultrafast Phase Transformation, Sogang University, Seoul, Korea (the Republic of), ⁴Department of Chemistry, Sookmyung Woman's University, Seoul, Korea (the Republic of), ⁵Departement of Physics, Pusan National University, Pusan, Korea (the Republic of)

This work explores van der Waals (vdW) heterostructures based on monolayer MoS_2 doped with transition metals such as Ir, Mn, and Fe, aiming to develop scalable platforms for chip-scale quantum and spintronic technologies. The results suggest that atomic doping may offer a viable route to tune the electronic and magnetic properties of the material, potentially enabling its integration into future spintronic devices.

Low-temperature vertical magnetoresistance and temperature-dependent resistance measurements reveal doping-induced magnetic ordering and correlated changes in band structure. Additionally, for the MoS₂ samples with 6 at.% Fe and Mn doping spin Hall magnetoresistance (SMR) of approximately 0.1% was observed at cryogenic temperatures, indicating the presence of spin-dependent scattering mechanisms and suggesting the emergence of spin-charge interconversion phenomena. Previous studies also suggest that monolayer MoS₂, particularly when doped

or combined in heterostructures, may support spin Hall or spin-dependent transport effects, further highlighting its potential for spin current manipulation [1]. Optical characterizations, including photoluminescence (PL) spectroscopy, further reveal modifications in excitonic behavior and optical bandgap, providing direct evidence of doping-induced electronic structure deformation. In particular, the emergence of mid-gap states was observed, consistent with the presence of dopant-induced defect levels within the bandgap.

The experimental observations are supported by complementary density functional theory (DFT) calculations, which predict dopant-induced band structure shifts, symmetry breaking, and localized states in monolayer MoS₂.[2,3] Scalable fabrication techniques enabled the development of wafer-scale vdW heterostructures with tunable magnetic and optical properties through material and doping control.

These findings establish doped MoS₂ heterostructures as a versatile and practical platform for chip-compatible spintronic and optoelectronic quantum devices.

- [1] K. R. Sahoo et al., Adv. Func. Mater., 2502406, 2025.
- [2] A. Yoshimura et al., Nano Express 1, 01008, 2020
- [3] J. Suh et al., Nat. Commun 9, 199, 2018.

AR-12. Prediction of Magnetocrystalline Anisotropy Constants in FeCoNi Thin Films Using Density of States Features

R. Sudo¹, T. Ueno¹, S. Yamashita^{1, 2}, M. Oogane¹
¹Tohoku University, Sendai, Japan, ²The Max Planck Institute for Chemical Physics of Solids, Dresden, Germany

To achieve low anisotropy fields for high-sensitivity TMR sensors, materials with low magnetocrystalline anisotropy constants (K_1) are desirable. However, accurately evaluating K_1 remains challenging due to difficulties in computing anisotropy energy. The lack of guidelines often leads to inefficient experimental screening. Consequently, data-driven materials discovery using machine learning (ML) has gained attention. The effectiveness of ML strongly depends on the quality of the input features. Since K_1 originates from spin-orbit coupling and details of electronic structure, descriptors such as the density of states (DOS) are promising. They are also easier to obtain than experimental features and provide enhanced interpretability, though their effectiveness remains unverified. We compare the performance of DOS-,

experimental-, and composition-based features for ML prediction of K_1 . A dataset of K_1 values for FeCoNi alloys with 43 compositions (50 nm films on MgO substrates [1]) was used. DOS was computed using first-principles calculations. Input features included DOS at the Fermi level, spin polarization, and DOS-derived statistics. Models using experimental and composition features were also evaluated. Among tested feature sets, the LightGBM model with composition features performed best (MAE = 1.3), followed by experimental (1.4) and DOS-based features (1.7). The DOS-based model achieved 80% accuracy in classifying the sign of K_1 , indicating its utility for screening low K_1 candidates. Although errors appeared near the signreversal at $K_1 = 0$, predictions elsewhere were highly accurate (Fig.1). Notably, 43 data points yielded accuracy comparable to prior studies with 500 bulk FeCoNi compositions [2]. Feature analysis (SHAP, permutation importance, correlation) showed that for experimental features, predictions were driven by composition ratios, whereas in DOS-based models, spin-resolved DOS near the Fermi level contributed most. Similar trends were observed with Random Forest, XGBoost, and MLP. Although DOSbased accuracy was limited, its interpretability highlights the value of improving representation, e.g., via orbitalresolved DOS.

[1] T. Ueno et al., Journal of Magnetism and Magnetic Materials, Vol. 616, p.172841 (2025)
[2] R. Sudo, M. Oogane, 2023 IEEE International Magnetic Conference-Short Papers, (2023)

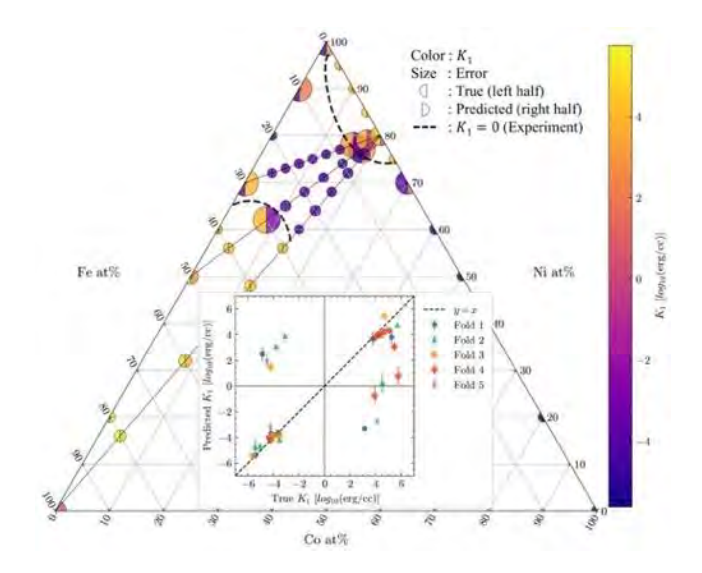


Fig.1 Prediction results of K_1 using LightGBM trained on DOS features.

^{*} Best Student Presentation Finalist / LB - Late-breaking Poster

AR-13. Interpretable Machine Learning for Designing Atomic-Scale Magnets

J. Navratil¹, R. Topolnicki^{2,4}, M. Otyepka^{1,3}, <u>P. S. Blonski^{1,3}</u>
¹Palacky University Olomouc, Olomouc, Czechia, ²University of Wroclaw, Wroclaw, Poland, ³VSB-Technical University of Ostrava, Ostrava, Czechia, ⁴Polish Academy of Sciences, Warsaw, Poland

The growing environmental footprint of the information and communication technology sector, coupled with escalating data storage demands, calls for innovative and sustainable solutions. Atomic-scale magnets (ASMs) based on transition metal (TM) dimers on defective graphene-featuring exceptional magnetic anisotropy energy (MAE) - offer a promising route toward ultrahigh-density, energy-efficient storage. While freestanding systems show potential, practical spintronic applications require graphenesupported ASMs to interface with solid surfaces. Exploring the vast design space of graphene-adsorbed atoms and substrates to achieve high MAE is computationally demanding when relying solely on density functional theory with spin-orbit coupling (DFT-SOC). Machine learning (ML) models trained on scalar-relativistic (SR) DFT data can significantly improve throughput, but a key challenge is ensuring they capture the underlying physics governing MAE—enabling accurate extrapolation beyond the training set.

Here, we present a CatBoost gradient boosting ML model trained on SR-DFT data to predict MAE for graphenesupported TM dimers. The model implicitly captures key physical interactions from second-order perturbation theory (PT2), as confirmed by a complementary model trained directly on PT2-derived contributions. We also develop an ML model to predict SOC energies from the same SR-DFT data, further validating the approach's robustness and ability to capture essential quantum mechanical effects. The model generalizes to TM dimers on defective graphene deposited on MgO, Cu, Ni, and Ir substrates - none included in training—retaining predictive fidelity. It significantly outperforms simpler models such as multivariate linear and Lasso regression. While generalizability may diminish for systems far from the training domain, expanding the descriptor space and refining learning strategies promise broader applicability.

This work highlights ML's potential to decode complex quantum interactions and guides ASM design for sustainable, atomic-scale storage.

J. Navratil, R. Topolnicki, M. Otyepka, P. Blonski, npj Computational Materials 11, 138 (2025)

AR-14. Automated Experimental Platform for Al Driven Magnetic Materials Discovery

A. Huang

MTI Corporation, Richmond, California, United States

The discovery of advanced magnetic materials is vital for next-generation technologies including electric motors, data storage, and spintronic devices. To accelerate this process, we present an automated experimental platform integrated with Al-driven decision-making for magnetic materials discovery. The system enables precise control over multi-source precursor dosing, automated mixing, pellet pressing, and high-temperature processing for rapid synthesis and screening of candidate materials. High-throughput magnetic property characterization is coupled with real-time data analysis and machine learning models. This closed-loop framework enhances efficiency in identifying novel compositions and optimizing key magnetic parameters.

- 1. Materials Genome Initiative Strategic Plan
- 2. An autonomous laboratory for the accelerated synthesis of novel materials
- 3. Accelerated development of hard high-entropy alloys with data-driven high-throughput experiments





SESSION BA: RECENT ADVANCES AND FUTURE CHALLENGES WITH NON-COLLINEAR ANTIFERROMAGNETS

Chair(s): S. Nakatsuji, Department of Physics, University of Tokyo, Tokyo, Tokyo, Japan Tuesday, October 28, 2025 02:00 PM-05:30 PM Grand Ballroom

BA-01. Spin Polarization of Noncollinear Antiferromagnets E. Y. Tsymbal

University of Nebraska-Lincoln, Lincoln, Nebraska, United States

Ferromagnets with high spin polarization are known to be valuable for spintronics—a research field that exploits the spin degree of freedom in information technologies. Recently, antiferromagnets have emerged as promising alternative materials for spintronics due to their stability against magnetic perturbations, absence of stray fields, and ultrafast dynamics. For antiferromagnets, however, the concept of spin polarization and its relevance to the measured electrical response are elusive due to nominally zero net magnetization. Here, we define an effective momentum-dependent spin polarization and reveal an unexpected property of many noncollinear antiferromagnets to exhibit nearly perfect spin polarization in a broad area of the Fermi surface. This property leads to the emergence of an extraordinary tunneling magnetoresistance (ETMR) effect in antiferromagnetic tunnel junctions (AFMTJs). As a representative example, we predict that a noncollinear antiferromagnet Mn₃GaN exhibits nearly 100% spinpolarized states that can efficiently tunnel through lowdecay-rate evanescent states of perovskite oxide SrTiO₃ resulting in ETMR as large as 10⁴% (Fig. 1). Our results uncover hidden functionality of material systems with noncollinear spin textures and open new perspectives for spintronics.

1. D.-F. Shao and E. Y. Tsymbal, npj Spintronics 2, 13 (2024). 2. G. Gurung, M. Elekhtiar, Q. Q. Luo, D.-F. Shao, and E. Y. Tsymbal, Nat. Commun. 15, 10242 (2024).

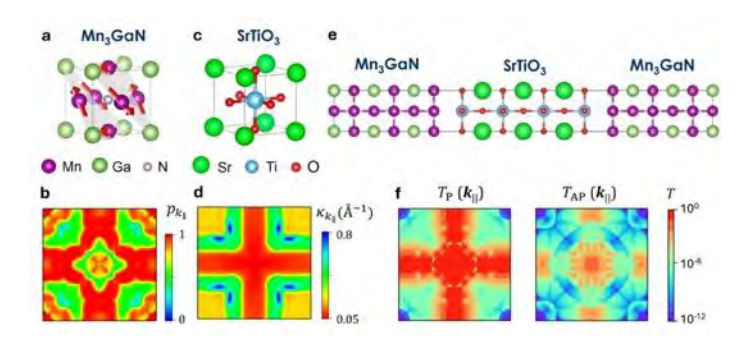


Fig. 1 (a) Atomic and magnetic structure of Mn₃GaN. (b) Spin polarization of Mn₃GaN. (c) Atomic structure of SrTiO₃. (d) Lowest decay rate in SrTiO₃. (e) Atomic structure of Mn₃GaN/SrTiO₃/Mn₃GaN (001) AFMTJ. (f) Transmission for parallel (T_P) and antiparallel (T_{AP}) aligned AFMTJ.

BA-02. Sub-nanosecond electrical switching of non-collinear antiferromagnetic Mn₃Sn through chiral-spin rotation

Y. Takeuchi^{1, 2}, Y. Sato^{3, 4}, Y. Yamane^{3, 5}, J. Yoon^{3, 4}, Y. Kanno^{3,} ⁴, T. Uchimura^{3, 4}, K. De Zoysa^{3, 4}, J. Han¹, S. Kanai^{3, 6}, J. Ieda⁷, H. Ohno^{3, 8}, S. Fukami^{3, 6, 9}

¹WPI-Advanced Institute for Materials Research (WPI-AIMR), Tohoku University, Sendai, Miyaqi, Japan, ²Research Center for Magnetic and Spintronic Materials (CMSM), National Institute for Materials Science (NIMS), Tsukuba, Ibaraki, Japan, ³Laboratory for Nanoelectronics and Spintronics, Research Institute of Electrical Communication (RIEC), Tohoku University, Sendai, Miyaqi, Japan, ⁴Graduate School of Engineering, Tohoku University, Sendai, Miyagi, Japan, ⁵Frontier Research Institute for Interdisciplinary Sciences (FRIS), Tohoku University, Sendai, Miyaqi, Japan, ⁶Center for Science and Innovation in Spintronics (CSIS), Tohoku University, Sendai, Miyagi, Japan, ⁷Advanced Science Research Center, Japan Atomic Energy Agency (JAEA), Tokai, Ibaraki, Japan, 8Center for Innovative Integrated Electronic Systems (CIES), Tohoku University, Sendai, Miyagi, Japan, ⁹Inamori Research Institute for Science (InaRIS), Kyoto, Kyoto, Japan

Efficient electrical manipulation of magnetism is a central topic of spintronics research. Spin-orbit torque (SOT) offers a promising approach, and magnetization switching in ferromagnets and Néel vector rotation of collinear antiferromagnets have been demonstrated. Here we show an unprecedented dynamic behavior in magnetic systems: the chiral-spin rotation driven by SOT in a non-collinear antiferromagnetic Mn₃Sn, yielding the sub-nanosecond switching of the collective spin structure. We deposit stacks of W(2)/Ta(3)/Mn₃Sn(20)/MgO(1.3)/Ru(1)

(in nm) on MqO(110) substrate by sputtering. The W/Ta buffer layer facilitates the epitaxial growth of (1-100)oriented Mn₃Sn [1]. In this configuration, an electric current along the [11-20] direction efficiently and persistently rotate the antiferromagnetic chiral-spin structure by SOT [2], and an application of in-plane magnetic field along the current can stop the persistent rotation, thereby inducing the bidirectional switching [3,4]. The stacks are patterned into Hall devices with Mn₃Sn nanodot and W/Ta channel [Fig. 1] by electron beam lithography and Ar ion milling [5]. We measure a pulse-current-induced switching of a Mn₃Sn nanodot device with the dot diameter of 200 nm. Figure 2(a) illustrates the Hall resistance R_H as a function of current density J_{HM} for pulse width t of 0.3 ns under an in-plane field $\mu_0 H_x$ of 300 mT, confirming a binary switching due to single domain structure [5]. We then evaluate the switching probability P versus J_{HM} at $\mu_0 H_x = 0$ and 300 mT, as shown in Fig. 2(b). We observe a characteristic *P* oscillation between the switched and switched-back states, which is attributed to the coherent spin rotation of Mn₃Sn. In the talk, we discuss more details of the switching dynamics and fundamental difference from ferromagnets in general. Our study highlights the potential of antiferromagnets for high speed and efficient spintronics devices [6]. This work was partly supported by JSPS-KAKENHI, JST-PRESTO, MEXT-X-nics, and RIEC Cooperative Research Projects.

- [1] J.-Y. Yoon et al., Appl. Phys. Express 13, 013001 (2020).
- [2] Y. Takeuchi et al., Nat. Mater. 20, 1364 (2021).
- [3] T. Higo et al., Nature 607, 474 (2022).
- [4] J.-Y. Yoon et al., Nat. Mater. 22, 1106 (2023).
- [5] Y. Sato et al., Appl. Phys. Lett. 122, 122404 (2023).
- [6] Y. Takeuchi et al., Science, in-press.

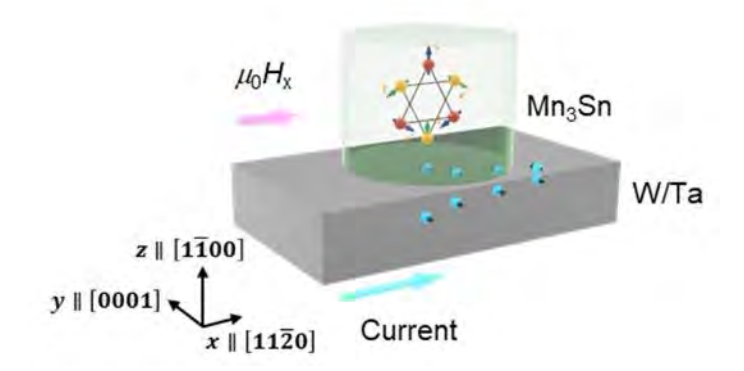


Fig. 1 Schematic illustration of a Mn₃Sn nanodot device.

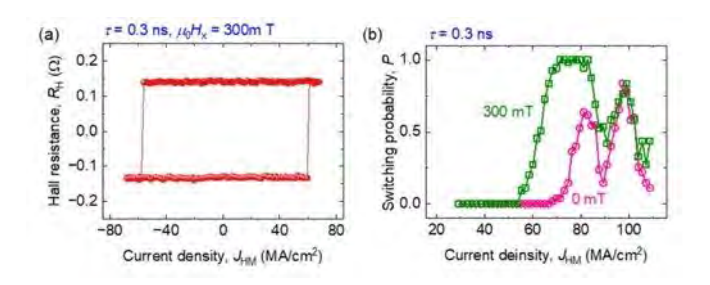


Fig. 2 (a) R_{H} - J_{HM} curve under $\mu_0 H_{\text{x}} = 300$ mT and (b) P- J_{HM} for various H_{x} in a Mn₃Sn nanodot. The nominal dot diameter is 200 nm, and τ is 0.3 ns.

BA-03. Spin-torque-driven GHz magnetization dynamics in the noncollinear antiferromagnet Mn₃Sn

W. Lee¹, S. Hwang¹, H. Ko¹, B. Park¹, K. Lee¹, <u>G. Choi</u>² ¹KAIST, Daejeon, Korea (the Republic of), ²Sungkyunkwan University, Suwon, Korea (the Republic of)

Antiferromagnetic spintronics has recently gained significant attention, and its most attractive feature is ultrafast magnetization dynamics due to the strong exchange coupling. Mn₃Sn is a representative material of noncollinear antiferromagnets, and its unique spin structure gives rise to large reading responses of the anomalous Hall effect, anomalous Nernst effect, and magneto-optic Kerr effect. However, the study of ultrafast dynamics of noncollinear antiferromagnets driven by spin torque, a critical pursuit for writing mechanism, has been largely limited. Here, we report the time-resolved dynamics of Mn₃Sn on a picosecond timescale, driven by an optically induced spin current pulse [1]. Our results reveal that the magnetization of Mn₃Sn tilts immediately after the spin current pulse and subsequently undergoes 70 GHz precession (Fig. 1). This immediate tilting underscores the predominant role of damping-like torque stemming from spin current absorption by Mn₃Sn. We also determine the spin coherence length of Mn₃Sn to be approximately 15 nm. This value significantly exceeds that of ferromagnets, highlighting a distinct spin-dephasing process in noncollinear antiferromagnets. Our results hold promise for ultrafast applications of noncollinear antiferromagnets and enrich our understanding of their spin transfer physics.

[1] W.-B. Lee, S. Hwang, H.-W. Ko, B.-G. Park, K.-J. Lee, and G.-M. Choi, Nature Nanotech. Vol. 20, p. 487 (2025).

^{*} Best Student Presentation Finalist / LB - Late-breaking Poster

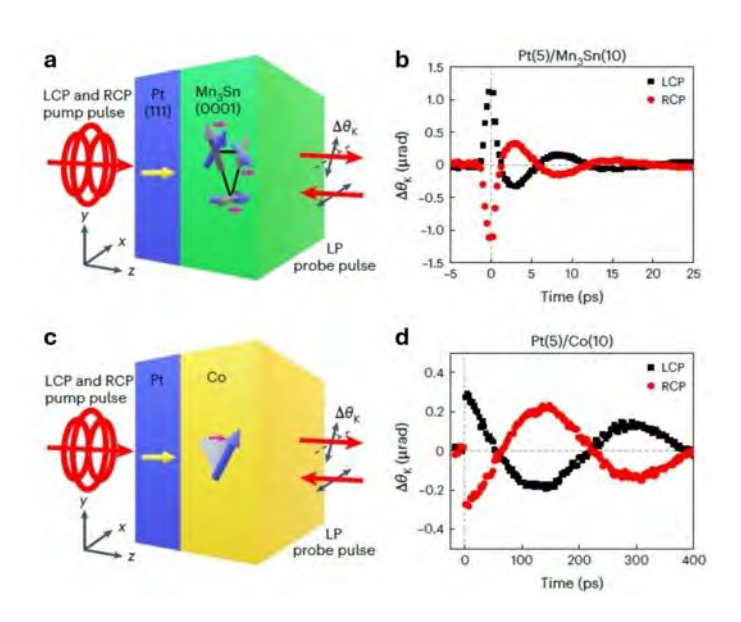


Figure 1. TR-MOKE measurement of spin-torque-driven dynamics. a,c, Schematics of optical spin-orbit torque in Pt(5)/Mn₃Sn(10) (a) and Pt(5)/Co(10) (c) structures. A circularly polarized pump pulse (LCP, left circular polarization; RCP, right circular polarization) generates a short-pulse spin current with z polarization (yellow arrows) at the Pt layer. This spin current exerts spin torque to the magnetic moment (blue arrows) of the Mn₃Sn and Co layers, respectively. A linearly polarized (LP) probe pulse detects the spin-torque-driven ultrafast dynamics in the z direction. b,d, The measured magnetization dynamics of Pt(5)/Mn₃Sn(10) (b) and Pt(5)/Co(10) (e) samples.

BA-04. Observation of antiferromagnetic spin torque diode effect

<u>S. Sakamoto</u>^{1,2}, T. Nomoto^{3,4}, T. Higo^{1,5}, Y. Hibino⁶, T. Yamamoto⁶, S. Tamaru⁶, Y. Kotani⁷, H. Kosaki¹, M. Shiga¹, D. Nishio-Hamane¹, T. Nakamura^{7,8}, T. Nozaki⁶, K. Yakushiji⁶, R. Arita^{3,9}, S. Nakatsuji^{1,5,10}, S. Miwa¹

¹The Institute for Solid State Physics, The University of Tokyo, Kashiwa, Japan, ²Institute for Materials Research, Tohoku University, Sendai, Japan, ³Research Center for Advanced Science and Technology, The University of Tokyo, Meguro, Japan, ⁴Department of Physics, Tokyo Metropolitan University, Hachioji, Japan, ⁵Department of Physics, The University of Tokyo, Bunkyo, Japan, ⁶National Institute of Advanced Industrial Science and Technology (AIST), Tsukuba, Japan, ⁷Japan Synchrotron Radiation Research Institute (JASRI), Sayo, Japan, ⁸International Center for Synchrotron Radiation

Innovation Smart, Tohoku University, Sendai, Japan, ⁹Center for Emergent Matter Science, RIKEN, Wako, Japan, ¹⁰Institute for Quantum Matter and Department of Physics and Astronomy, Johns Hopkins University, Baltimore, Maryland, United States

Spintronics based on ferromagnets has not only revolutionized memory technologies but also enabled the development of microwave devices such as spin-torque oscillators and diodes [1,2]. These microwave spintronic devices operate at magnetization precession frequencies reaching several tens of GHz; however, increasing the frequency often narrows the precession cone angle, thereby weakening the output signal. Antiferromagnets present a promising alternative [3]. In easy-plane antiferromagnets, even slight deviations of magnetic moments from the easy plane generate strong internal exchange fields, supporting high-frequency precession—from GHz to THz—while maintaining significant amplitude. Due to the development of the easy-plane antiferromagnet Mn₃Sn thin films [4-6], recent studies have shown that spin torque can drive switching and continuous rotation—referred to as chiral spin rotation—of the non-collinear triangular spin structure [6— 8]. In this work, we investigate the microwave response of Mn₃Sn and demonstrate the antiferromagnetic spin-torque diode effect [9], in which the interaction between chiral spin rotation and a microwave current generates a rectified DC transverse Hall voltage.

W/Mn₃Sn epitaxial bilayers were fabricated on MgO(110) substrates using molecular beam epitaxy and X-ray magnetic circular dichroism measurements confirmed the magnetic uniformity across the bottom W/Mn₃Sn and top Mn₃Sn/MqO interfaces [10]. Hall bar devices (Mn₃Sn: 7 nm, W: 6 nm) were patterned by standard photolithography and Ar ion etching. A DC bias current and amplitude-modulated microwave current were applied via a bias-tee, and the resulting DC Hall voltages were measured using a lock-in amplifier, as schematically shown in Fig. 1. We observed clear DC Hall voltage peaks at specific magnetic fields under the simultaneous application of microwave and DC currents, when the DC current exceeded the threshold for initiating chiral spin rotation, as shown in Fig. 2. Numerical simulations suggest that these rectified signals originate from the effective modulation of the chiral spin rotation frequency by the microwave spin-orbit torque. This antiferromagnetic spin-torque diode effect is robust at higher frequencies, offering the potential for broadband spintronic functionality beyond the GHz limitations of ferromagnetic systems.

This work was supported by JSPS-KAKENHI, JST-Mirai Program, JST-ASPIRE, X-nics, and Spin-RNJ.

[1] A. Tulapurkar *et al.*, Nature 438, 339 (2005). [2] G. Finocchio *et al.*, Appl. Phys. Lett. 118, 160502 (2021). [3] Y. Zhou *et al.*, Sci. Adv. 10, eadk7935 (2024). [4] J. Yoon *et al.*, Appl. Phys. Express 13, 013001 (2019). [5] S. Sakamoto *et al.*, Phys. Rev. B 104, 134431 (2021). [6] T. Higo *et al.*, Nature 607, 474 (2022). [7] H. Tsai *et al.*, Nature 580, 608 (2020). [8] Y. Takeuchi *et al.*, Nat. Mater. 20, 1364 (2021). [9] S. Sakamoto *et al.*, Nat. Nanotechnol. 20, 216 (2025). [10] S. Sakamoto *et al.*, Phys. Rev. B 110, L060412 (2024).

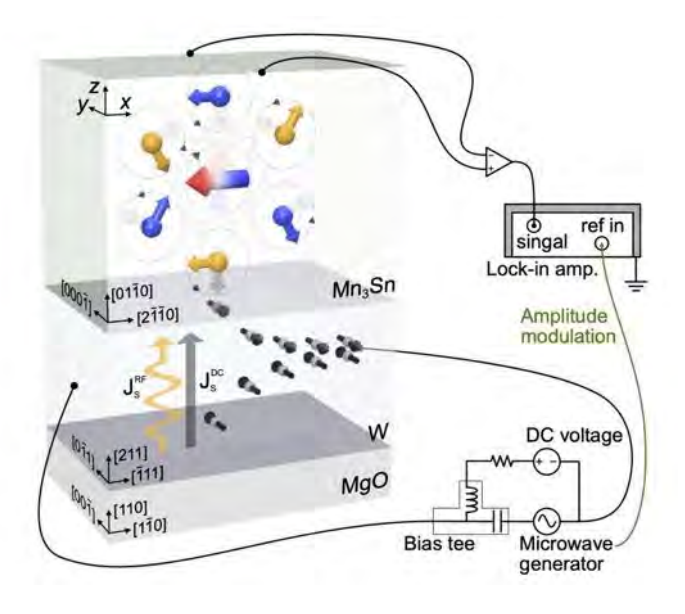


Fig. 1 Experimental setup for spin-torque diode measurements.

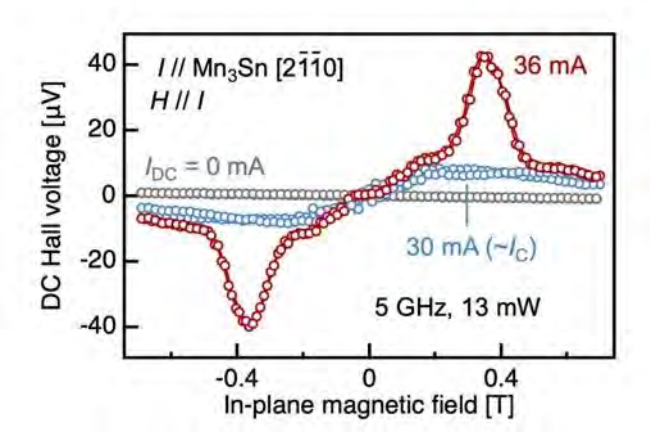


Fig. 2 Diode signals as a function of in-plane magnetic field, measured under various DC currents.

BA-05. Optically induced renormalization of coherent magnons in antiferromagnets.

D. Bossini

University of Konstanz, Konstanz, Germany

The collective dynamical response of a magnetic solid is encoded in the dispersion relation of magnons, which in antiferromagnets (AFs) possess frequency in THz regime. The optical activation of coherent magnons in AFs has been widely reported, even into nonlinear regimes of spin dynamics. The arbitrary optical control of the spectrum of the eigenmodes appearing in the dispersion relation is still lacking. In my talk I will discuss one strategy to achieve this goal. Our approach relies on a resonant optical drive of high-energy magnons, with wavevectors near the edges of the Brillouin zone, in a non-collinear AF. The transient spin dynamics reveals the activation and amplification of coherent low-energy zone-centre magnons, which are not directly driven. Strikingly, the spectrum (frequency, amplitude and lifetime) of these low-energy magnons is renormalized by the coupling with the photoinduced highenergy modes. Shifts of the magnonic eigenfrequencies up to 20% of their ground-state values were observed. Interestingly, cooling down the material (hematite) to the AF collinear phase, the photoinduced spectrum renormalization is drastically different. We rationalise the observation in terms of a resonant scattering mechanism, in which zone-edge magnons couple nonlinearly to the zonecentre modes. Numerical simulations can reproduce the measured frequency renormalization. Our results present a milestone on the path towards an arbitrary tuning of the quasiparticles eigenfrequencies.

67

^{*} Best Student Presentation Finalist / LB – Late-breaking Poster

SESSION BB: BIOMAGNETIC SENSORS: FROM BENCH TO BEDSIDE

Chair(s): R. L. Hadimani, Mechanical and Nuclear Engineering, Virginia Commonwealth University, Richmond, Virginia, United States

> Tuesday, October 28, 2025 02:00 PM-05:30 PM Ballroom A

BB-01. Structure-property relationships in core-shell magnetoelectric nanowires -towards minimally invasive neural stimulation

N. Ferson, <u>J. Andrew</u> Dept. of Materials Sci. & Eng., University of Florida, Gainesville, Florida, United States

Nanostructured composite materials have the potential to overcome challenges in many areas of materials research, which cannot be addressed by more conventional singlephase materials. For example, ferroelectric and ferromagnetic materials can be combined to form composites with enhanced multiferroic or exchange coupling properties. Here, we will present on multiferroic composite nanomaterials prepared using a template assisted approach, generating materials with controllable anisotropy and resultant properties. Electron microscopy and X-ray diffractometry (XRD) were used to investigate the nanowire structure. Magnetoelectric behavior of the nanowires was confirmed via vibrating sample magnetometry (VSM) after poling the nanowires at increasing electric field strengths (0, 50, and 700 kV/cm) and measuring the resultant magnetic hysteresis loops. Magnetoelectric voltage coefficients (a_{ME}) of 1040 mVcm⁻ ¹Oe⁻¹ under zero bias field conditions were obtained using a modified lock-in technique. The a_{ME} of these nanowires is 2.5 times larger than our previously reported a_{ME} for Janus structured cobalt ferrite-barium titanate nanowires and thus provides greater efficiency for in vivo electrical stimulation and does not require an external magnetic bias field. The efficacy of the ME nanowires for use as a neuronal stimulation platform will also be presented. Including in vitro investigations using pheochromocytoma PC12 cells to leverage ME stimulation to induce PC12 cell differentiation in comparison to growth factor mediated differentiation controls. Preliminary experiments using cytotoxicity assays show that cells cultured on collagen-ME nanowire surfaces do not elicit a greater cytotoxicity when compared to collagen controls, indicating ME nanowires are not toxic to PC12 cells.

1. N. D. Ferson, J. R. Ganiban, D. P. Arnold, J.S. Andrew, Tunable synthesis of magnetoelectric CoFe₂O₄− BaTiO₃ core−shell nanowires, *ChemComm*, 14073, 2024. 2. N. D. Ferson, A. M. Uhl, J. S. Andrew, Piezoelectric and Magnetoelectric Scaffolds for Tissue Regeneration and Biomedicine: A Review, *IEEE TransNanoBioSci*, 229, 2020.

BB-02. Magneto-LC Resonance Biosensing Technology for Advanced Biodetection and Diagnostics

M. Phan^{1, 2}

¹University of South Florida, Tampa, Florida, United States, ²VinUniversity, Hanoi, Viet Nam

The integration of highly sensitive sensors with magnetic nanomaterials as biomarkers has led to the development of novel biosensing platforms capable of ultrafast detection of a wide range of targets, including biomolecules, bacteria, cancer cells, and, more recently, real-time physiological monitoring [1]. The ability to simultaneously detect magnetic and dielectric signals from magnetic-core/bioshell nanoparticles significantly enhances the functionality of advanced biosensors. However, most existing biosensors are limited in their ability to perform such dual-mode detection. In this talk, we present a newly developed magneto-LC resonance (MLCR)-based microfluidic biosensing technology [2,3], which demonstrates exceptional sensitivity in detecting both magnetic and dielectric signals from core/shell nanoparticles. Moreover, this technology enables the differentiation of magnetic responses from superparamagnetic (SPM) and ferrimagnetic (FM) nanoparticles of similar sizes, further broadening their applicability in biodetection and real-time diagnostic platforms [4].

- 1. M.H. Phan et al., "Magnetoimpedance Biosensors and Real-Time Healthcare Monitors: Progress, Opportunities, and Challenges," Biosensors 12, 517 (2022).
- 2. M.H. Phan et al., "Novel Magneto-LC Resonance Technology for Real-Time Respiratory Motion Monitoring," US Patent No.: US11607154B2 (2024).
- 3. M.H. Phan et al., "A New Method for Dual Detection of Magnetic and Dielectric Signals from Core/Shell Nanoparticles for Advanced Biodetection and Diagnostics," US Patent Application filled (2025).
- 4. Signal Differentiation of Moving Magnetic Nanoparticles for Enhanced Biodetection and Diagnostics, Biosensors 15, 116 (2025).

BB-03. Wireless Brain-Machine Interface with MagnetoElectric NanoParticles

E. Zhang², P. Liang¹, M. Abdel-Mottaleb³, S. Chen³, M. Shotbolt³, V. Andre³, J. Tian³, A. Scott-Vandeusen³, E. Zhu³, S. Pané², <u>S. Khizroev³</u>

¹Cellular Nanomed, Irvine, California, United States, ²Institute of Robotics and Intelligent Systems, Swiss Federal Institute of Technology, Zurich, Switzerland, ³University of Miami, Coral Gables, Florida, United States

The presentation will give an overview of our research to launch wireless brain-machine interface (BMI) applications of MagnetoElectric NanoParticles (MENPs). Due to the magnetoelectric effect, unlike other nanoparticles, MENPs allow to use magnetic fields to wirelessly induce local electric fields, thus wirelessly and non-invasively or minutely invasively modulating neural activity deep in the brain. Conversely, local electric fields due to neural activity in the vicinity of MENPs can change the nanoparticles' magnetization; in turn, this magnetization change can be detected using magnetometers. As a result, MENPs can offer non-surgical solutions to monitor, in real time, cellular activity such as the brain's electric circuitry and, if necessary, restore its malfunctions by targeted neuromodulation, ideally, at the single-neuron level, without using physical electrodes. In vitro and in vivo experiments have been conducted to demonstrate the technological capabilities of these nanoparticles. Arguably, one of the most outstanding characteristics of these nanoparticles is their capability to control fundamental biological mechanisms without using any bioreagents, instead relying only on properties of the nanoparticles, e.g., their magnetoelectric effect and magnetocrysalline anisotropy. As a result, these properties can serve to enable frequency-dependent "On/Off" switches for activation of desired biological mechanisms. For example, basic studies have demonstrated that the applied magnetic field frequency can be used to distinguish between excitatory and inhibitory activation of targeted neurons. The potential implications of this research are two-fold. First, MENPs allow to conduct research that can help understand the computing architecture of the brain and deepen our understanding of human intelligence. Second, MENPs unlock the possibility of pinpoint treatment of neurological and other brain diseases.

BB-04. Magnetic Nanoparticles and Sensors for Antigen Tests

M. Rivas, M. Salvador, V. Pilati, J. L. Marques, J. C. Martinez-Garcia

Department of Physics, University of Oviedo, Gijón, Spain

At the end of 2020, the terms "antigen test" and "rapid

diagnostic test" (RDT) became popular worldwide. This fast, easy-to-use, and affordable tool became part of our lives to prevent the spread of the SARS-CoV-2 virus. COVID-19 RDTs use gold nanoparticles that produce a binary signal (positive/negative) with moderate sensitivity (there are frequent false negatives). WHO advocates for ongoing research on RDTs to make them more reliable and quantitative, thereby increasing their applicability and efficacy in health prevention and early detection. Magnetism can provide solutions to mitigate these limitations without introducing complexity that could compromise the primary advantages of RDTs. This presentation will demonstrate how substituting traditional gold particles with superparamagnetic ferrite nanoparticles as detection mediators enhances the sensitivity of RDTs [1,2]. We will present a multiband resonant refractometric sensor that enables precise quantification without compromising the inherent advantages of RDTs [3]. I will discuss the specific characteristics of the magnetic particles and the sensor and how they can optimize the magnetic solution to enhance RDT performance.

- [1] M. Salvador et al., "Magnetic Nanoclusters Increase the Sensitivity of Lateral Flow Immunoassays for Protein Detection: Application to Pneumolysin as a Biomarker for Streptococcus pneumoniae."* Nanomaterials 12 (2022): 2044. doi: 10.3390/nano12122044
- [2] V. Pilati et al., "Mn-ferrite nanoparticles as promising magnetic tags for radiofrequency inductive detection and quantification in lateral flow assays." Nanoscale Adv. 6 (2024): 4247–4258.
- [3] J. L. Marqués et al., "New Perspective on Planar Inductive Sensors: Radio-Frequency Refractometry for Highly Sensitive Quantification of Magnetic Nanoparticles." Sensors 23 (2023): 2372. doi: 10.3390/s23052372

BB-05. NV Centers as Quantum Sensors for Biomagnetic Signal Measurement

M. Sekino¹, M. Fushimi¹, A. Kuwahata², M. Hatano³

¹The University of Tokyo, Tokyo, Japan, ²Tohoku University, Sendai, Japan, ³Institute of Science Tokyo, Tokyo, Japan

Diamond nitrogen-vacancy (NV) centers have recently garnered attention as next-generation quantum sensors for biomagnetic measurements. These sensors offer high sensitivity and broad dynamic range without the need for cryogenic cooling. Magnetoencephalography (MEG) and magnetocardiography (MCG), which estimate internal current distributions in the brain and heart, respectively, have relied on superconducting quantum interference devices (SQUIDs). Despite their exceptional sensitivity, SOUID-based systems necessitate cooling systems. Recent advancements in optically pumped magnetometers (OPMs) and NV-based sensors have enabled the development of wearable and portable biomagnetic systems. NV centers in diamond exhibit magnetically sensitive electron spin states that can be initialized and optically read out, allowing for highly sensitive detection of weak magnetic fields. Their solid-state configuration facilitates miniaturization and integration, while the resonance-based detection mechanism enables both high spatial resolution and extensive dynamic range. The authors' group demonstrated MCG measurements in rats using NV sensors, achieving millimeter-scale spatial resolution and confirming signal reproducibility across individuals [1]. The ability to estimate cardiac current distributions at such resolutions has the potential to facilitate the investigation of arrhythmia mechanisms. Furthermore, the integration of NV sensors with magnetic nanoparticles has led to the development of a novel method for sentinel lymph node detection, offering a radiation-free and minimally invasive alternative to conventional radioisotope-based techniques [2]. A compact magnetic probe system employing NV sensors was developed, particularly well-suited for small- to mid-sized medical facilities. The sensitivity of the device has been enhanced, with recent improvements reaching sub-10 pT/Hz^{1/2} levels [3]. The potential applications of this technology are manifold, including real-time brain and heart monitoring in daily life, such as for automotive driver state detection or remote medical diagnostics [4]. However, challenges such as magnetic shielding and noise separation remain. Innovations in active shielding, compact enclosures, and signal processing techniques including machine learning are expected to address these barriers.

- [1] K. Arai, et al. Millimetre-scale magnetocardiography of living rats with thoracotomy. Comm Phys 5, 200, 2022.[2] A. Kuwahata, et al. Magnetometer with nitrogen-vacancy
- center in a bulk diamond for detecting magnetic nanoparticles in biomedical applications. Sci Rep 10, 2483, 2020.
- [3] N. Sekiguchi, et al. Diamond quantum magnetometer with dc sensitivity of sub-10 pT Hz^{-1/2} toward measurement of biomagnetic field. Phys Rev Appl 21, 064010, 2024. [4] N. Sekiguchi, et al. Performance evaluation of a diamond quantum magnetometer for biomagnetic sensing: A phantom study. Appl Phys Lett (in press).

SESSION BC: THERMOELECTRIC, MAGNETIC, AND SUPERCONDUCTING EFFECTS IN HYBRID HETEROSTRUCTURES AND SPIN TEXTURES

Chair(s): Y. Wu, Electrical and Computer Engineering, University of Florida, Gainesville, Florida, United States Tuesday, October 28, 2025 02:00 PM-05:30 PM Ballroom C

BC-01. Single-Molecule Magnets (SMM) Transport Channel Formation Along the Liftoff Produced Exposed Sides of Metal-Insulator-Semiconductor (MIS) Diodes

P. Suh

Mechanical Engineering, University of the District of Columbia, Washington DC, District of Columbia, United States

Single-molecule magnets (SMM) are true mass-producible quantum materials, but their scope as a potential device element is hampered by the limitations of conventional molecular device fabrication methods. In this study, we report a Metal-Insulator-Semiconductor (MIS) templatebased approach to successfully form SMM transport channels between the silicon and ferromagnetic electrodes(Fig.1). MIS cross junction with NiFe/AlOx/p-Silicon and exposed sides were fabricated to set ~ 2 nm physical gap between the NiFe and p-Si electrodes. We have utilized lipoic acid-functionalized SMM, of formula [Mn6(µ3-O)2(H2N-sao)6(lip)2(MeOH)6][Mn6(μ3-O)2(H2Nsao)6(cnph)2(MeOH)6]10MeOHLipoic. SMM was bridged between Si and NiFe along the >10µm long exposed side edges. The current-voltage(I-V) study was performed before and after establishing the SMM channels. Interestingly, despite a difference in initial MIS background I-V, SMMs produced strikingly similar I-V profiles. We modeled the current-voltage data using the tunneling and diode

transport model to compare the conduction channel attributes between two electrodes before and after establishing SMM channels. We also conducted KPFM to observe the SMM impact on electrode surface potential. SMM channels modified the surface potential of NiFe by ≈0.4 V, indicating that SMM is capable of modifying the charge density of the electrode material (Fig.2). MIS testbed offers a new opportunity to harness SMM-like high-potential molecules by connecting them between spin-reservoir and semiconductor.

M. Orts-Arroyo, C. Rojas-Dotti, N. Moliner, and J. Martínez-Lillo, "Lipoic Acid Functionalized Hexanuclear Manganese(III) Nanomagnets Suitable for Surface Grafting," International Journal of Molecular Sciences, vol. 24, no. 10, p. 8645, 2023. [Online]. Available: https://www.mdpi.com/1422-0067/24/10/8645.

P. Tyagi, C. Baker, and C. D'Angelo, "Paramagnetic Molecule Induced Strong Antiferromagnetic Exchange Coupling on a Magnetic Tunnel Junction Based Molecular Spintronics Device," Nanotechnology, vol. 26, p. 305602, 2015.

P. Tyagi, D. F. Li, S. M. Holmes, and B. J. Hinds, "Molecular Electrodes At The Exposed Edge Of Metal/Insulator/Metal Trilayer Structures," J. Am. Chem. Soc., vol. 129, no. 16, pp. 4929 4938, Apr 25 2007. [Online]. Available: ://000245782800030.

P. Tyagi and C. Riso, "Magnetic force microscopy revealing long range molecule impact on magnetic tunnel junction based molecular spintronics devices," Organic Electronics, vol. 75, p. 105421, 2019/12/01/ 2019, doi: https://doi.org/10.1016/j.orgel.2019.105421. Bogani, L., & Wernsdorfer, W. (2008). Molecular spintronics using single-molecule magnets. Nature Materials, 7(3), 179-186

Brinkman, W., R. Dynes, and J. Rowell, Tunneling conductance of asymmetrical barriers. Journal of applied physics, 1970. 41(5): p. 1915-1921

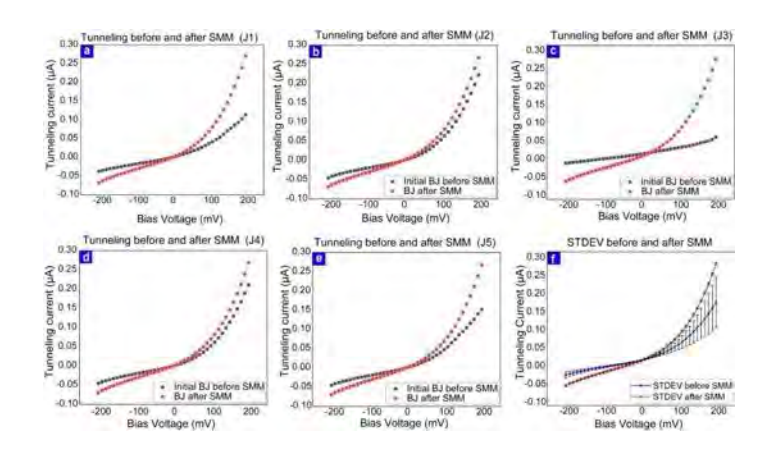


Fig. 1 Standard deviation of the tunneling current before (blue) and after (red) SMM attachment, highlighting the increase in current and the overall improved stability among the junctions after SMM functionalization.

The statistical consistency in current measurements after SMM attachment demonstrates the reliable modification of junction properties.

BC-02. Withdrawn

BC-03. Observation of nonlinear thermoelectric effect at room temperature

Y. Hirata¹, T. Kikkawa^{1,2}, H. Arisawa^{1,3}, E. Saitoh^{1,3,4}
¹Department of Applied Physics, University of Tokyo, Bunkyo-ku, Tokyo, Japan, ²ASRC, JAEA, Tokai-mura, Japan, ³CEMS, RIKEN, Wako-shi, Saitama, Japan, ⁴Beyond Al, University of Tokyo, Bunkyo-ku, Tokyo, Japan

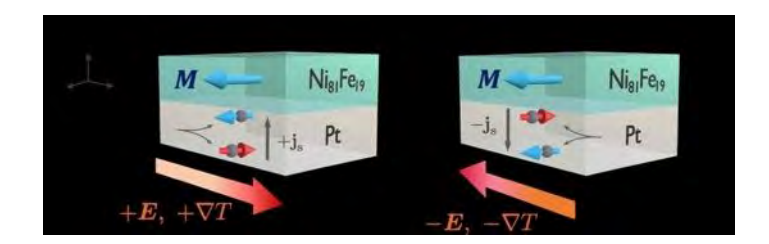
Thermoelectric effects refer to the conversion of a temperature gradient into a voltage. While previous studies have primarily focused on linear thermoelectric effects, a nonlinear thermoelectric effect, proportional to the square of the temperature gradient, has recently been proposed theoretically [1]. Last year, a nonlinear Nernst voltage was experimentally observed in a junction system composed of the type-II superconductor MoGe and the ferromagnetic insulator $Y_3Fe_5O_{12}$ [2]. Although this phenomenon offers a new power generation principle that can convert temperature fluctuations into electricity, it was only observed under the extreme low-temperature conditions (below 5 K) required for MoGe to remain superconducter phase.

In the present study, we successfully observed a nonlinear Seebeck effect at room temperature [3]. Using a double thermal-source lock-in technique, we measured nonlinear Seebeck voltages in a junction composed of ferromagnetic Ni₈₁Fe₁₉ and paramagnetic heavy metal Pt. Under finite temperature gradient, spin current flowing inside Pt is induced due to spin-orbit interaction and deflected toward the interface with Ni₈₁Fe₁₉, resulting in asymmetric magnetization-spin scattering processes relative to the direction of heat flow. By investigating the dependencies on the magnetization direction and sample length, we clarified that the observed nonlinear Seebeck signals originate from this magnetization-induced spin scattering mechanism. In this presentation, we discuss the experimental results in detail and explain the underlying principles of the nonlinear Seebeck effect in comparison with the unidirectional spin Hall magnetoresistance effect [4].

[1] R. Nakai and N. Nagaosa, Phys. Rev. B 99, 115201 (2019).[2] H. Arisawa, Y. Fujimoto, T. Kikkawa and E. Saitoh, *Nat Commun* 15, 6912 (2024).

[3] Y. Hirata, T. Kikkawa, H. Arisawa and E. Saitoh, *under review*.

[4] Avci, C., Garello, K., Ghosh, A. et al. *Nat Phys* 11, 570–575 (2015).



Schematic illustrations of the bilayer system consisting of $Ni_{81}Fe_{19}$ and Pt. The red (blue) arrows denote up (down) spins of the electrons. (Left) When a positive electric field (a positive temperature gradient) is applied in the y direction, the spin Hall (Nernst) current $+j_s$ is induced. (Right) Under a negative electric field (a negative temperature gradient), the direction of spin current is reversed to $-j_s$. The scattering intensity between the electrons and magnetization, therefore, varies depending on the input direction.

BC-14. Chirally Coupled Magnetic Tunnel Junctions resulting from the Dzyaloshinskii-Moriya interaction*

B. Vermeulen^{1, 2*}, J. Chatterjee¹, G. Talmelli¹, Y. Canvel¹, Y. Li¹, S. Rao¹, B. Sorée^{1, 3, 4}, K. Temst^{2, 1}, V. Nguyen¹

¹IMEC, Leuven, Belgium, ²Department of Physics and Astronomy, Quantum Solid-State Physics Division, KU Leuven, Leuven, Belgium, ³Department of Electrical Engineering, ESAT-INSYS Division, KU Leuven, Leuven, Belgium, ⁴Department of Physics, Universiteit Antwerpen, Antwerpen, Belgium

Current-driven domain-wall (DW) logic promises energy-efficient and compact circuits, leveraging non-volatility and majority operations [1]. Fast DW motion and the Dzyaloshinskii-Moriya interaction (DMI) in ferromagnet/heavy metal bilayers enabled current-driven DW logic using magnetic imaging [2]. Advancing toward applications, electrical write/read was achieved by spintransfer torque (STT) and tunnel magnetoresistance (TMR) using magnetic tunnel junctions (MTJs) on 300-mm wafers in nanoscale DW devices [3].

Nevertheless, current-driven DW motion faces challenges such as pinning and Joule heating. To overcome these, we present an approach to couple input and output MTJs via chiral coupling [4]. Micromagnetic simulations reveal that DMI-induced chiral coupling leads to antiparallel alignment of perpendicular MTJs interconnected by an in-plane magnetized free layer [5] (Fig. 1a-d). Furthermore, we show that DMI can directly induce the switching of a region with perpendicular magnetic anisotropy (PMA). STT-switching of the input MTJ induces the output MTJ switching without additional current, enabling current-free information propagation in a compact inverter logic gate. We find that the switching is governed by the interplay between DMI and PMA. Moreover, coupling four MTJs enables compact majority gates providing 'AND' and 'OR' functions [6]. Experimentally, we show that a hybrid free layer (HFL) MTJ stack allows to combine high DMI materials, such as Pt/Co, via interlayer exchange coupling with CoFeB/MgO to preserve MTJ properties [7]. DMI of ~0.7 mJ/m² is obtained from DW dynamics using magnetic imaging and Hall bar loop shift measurements. TMR of 80% and efficient STT switching is obtained in magnetically interconnected 80-nm MTJs (Fig. 2a). Finally, we demonstrate treatments based on Helium ion irradiation and Ion Beam Etching (IBE) to precisely tune the PMA in specific HFL stacks (Fig. 2b-c), paving the way for scalable fabrication of chiral logic devices.

- [1] Vermeulen, B. et al. Micromachines 15, 696 (2024).
- [2] Luo, Z. et al. Nature 579, 214 (2020).
- [3] Raymenants, E. et al. Nat. Elec. 4, 392 (2021).
- [4] Luo, Z. et al. Science 363, 1435 (2019).
- [5] Vermeulen, B. et al. Phys. Rev. Appl. 21, 024050 (2024).
- [6] Nguyen, V.D., Vermeulen, B. et al. US Patent App. US20240023459A1 (2024).
- [7] Vermeulen, B. et al. AIP Adv. 14, 025030 (2024).

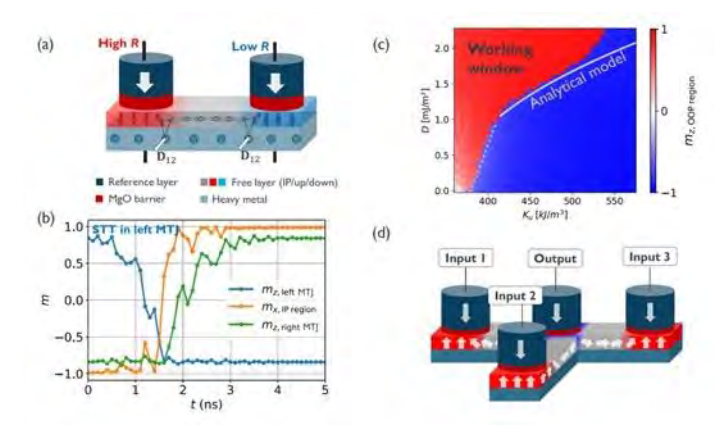


Fig. 1: (a) Chiral inverter. (b) Magnetization switching in chiral inverter. (c) Working window depending on DMI and PMA. (d) Chiral majority gate. [5]

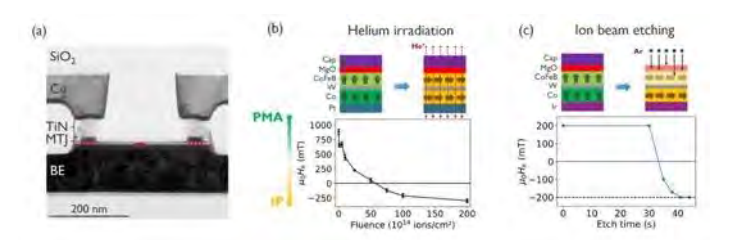


Fig. 2: (a) TEM image of interconnected MTJs. (b-c) PMA to IP conversion by He⁺ irradiation [7] and IBE.

BC-07. Thermally induced spin transport in in situ postannealed NiFe $_2$ O $_4$ thin films with varying lattice parameters and saturation magnetization

F. Meier¹, J. Straßburger¹, J. Biedinger¹, M. Gaerner¹, F. Peters¹, T. Samanta¹, L. Caron¹, O. Gomonay², <u>T. Kuschel</u>^{1, 2}
¹Bielefeld University, Bielefeld, Germany, ²Johannes Gutenberg University Mainz, Mainz, Germany

The ferrimagnetic insulator NiFe $_2O_4$ (NFO) is a prototype thin-film material for spin filtering [1] and spin transport. Here, spin Seebeck effect (SSE) [2,3], spin Hall magnetoresistance [4] and non-local magnon spin transport [5] have been studied in recent years. NFO thin films can be grown by sputtering [6], pulsed laser deposition [7], molecular beam epitaxy [8] or through thermally induced interdiffusion of Fe $_3O_4$ /NiO bilayers [9]. When using lattice-matched substrates such as MgGa $_2O_4$, the magnetic properties of NFO such as switching field or magnetic damping become comparable to the standard spin-transport material $Y_3Fe_5O_{12}$ due to reduction of anti-phase boundaries [10]. With these films, we recently performed SSE-based vectorial magnetometry for magnetocrystalline anisotropy studies [11,12].

While thermally induced spin transport via SSE has been explored in plenty of various materials in the recent decade, fundamental dependencies of SSE on individual material parameters have been studied only rarely. In order to name an example, we prepared NiFe₂O_x thin films and varied the oxygen content x. Thus, we were able to study the SSE dependence on charge conductivity [13]. Within our current investigation, we varied the NFO lattice parameters systematically by in situ post-annealing the NFO films in oxygen atmosphere. We observe a linear dependence of the lattice constant on the annealing temperature. The saturation magnetization $M_{\mbox{\tiny S}}$ detected by superconducting quantum interference device magnetometry also varies but not as systematically as the lattice parameters do.

The SSE measurements reveal a suppression of the SSE with increasing $M_{\scriptscriptstyle S}$ similar to the SSE suppression that has been reported for higher external magnetic field as a consequence of the Zeeman gap in magnon excitation [14]. In addition, a reduced precession cone angle related to larger $M_{\scriptscriptstyle S}$ causes a decreased spin polarization of the thermally induced spin current and, thus, a reduced signal at the spin current detector material Pt. We can further identify a clear $1/M_{\scriptscriptstyle S}$ dependence of the SSE which agrees with the $1/M_{\scriptscriptstyle S}$ term in the Landau-Lifshitz-Gilbert equation, and,

finally, confirms the theory of the longitudinal SSE developed by Rezende et al. [15].

- [1] U. Lüders et al., Adv. Mater. 18, 1733 (2006); Appl. Phys. Lett. 88, 082505 (2006).
- [2] D. Meier, TK et al., Phys. Rev. B 87, 054421 (2013); Nat. Commun. 6, 8211 (2015).
- [3] T. Kuschel et al., Phys. Rev. Lett. 115, 097401 (2015); IEEE Trans. Magn. 52, 4500104 (2016).
- [4] M. Althammer, TK et al., Phys. Rev. B 87, 224401 (2013); Appl. Phys. Lett. 115, 092403 (2019).
- [5] J. Shan, TK et al., Appl. Phys. Lett. 110, 132406 (2017); Appl. Phys. Lett. 113, 162403 (2018).
- [6] C. Klewe, TK et al., J. Appl. Phys. 115, 123903 (2014).
- [7] M. Hoppe et al., Phys. Rev. B 91, 054418 (2015).
- [8] J. Rodewald et al., Phys. Rev. Mater. 4, 064404 (2020).
- [9] O. Kuschel, TK et al., Phys. Rev. B 94, 094423 (2016).
- [10] A. V. Singh et al., Adv. Mater. 29, 1701222 (2017).
- [11] Z. Li, TK et al., Appl. Phys. Lett. 114, 232404 (2019);
- [12] A. Rastogi, TK et al., Phys. Rev. Applied 14, 014014 (2020).
- [13] P. Bougiatioti,TK et al., Phys. Rev. Lett. 119, 227205 (2017); J. Appl. Phys. 122, 225101 (2017).
- [14] T. Kikkawa et al., Phys. Rev. B 92, 064413 (2015); J. Phys. Soc. Jpn 85, 065003 (2016).
- [15] S. M. Rezende et al., Phys. Rev. B 89, 014416 (2014); J. Magn. Magn. Mater. 400, 171 (2016).

Beach¹

BC-09. Distinct element-specific nanoscale magnetization dynamics following ultrafast laser excitation

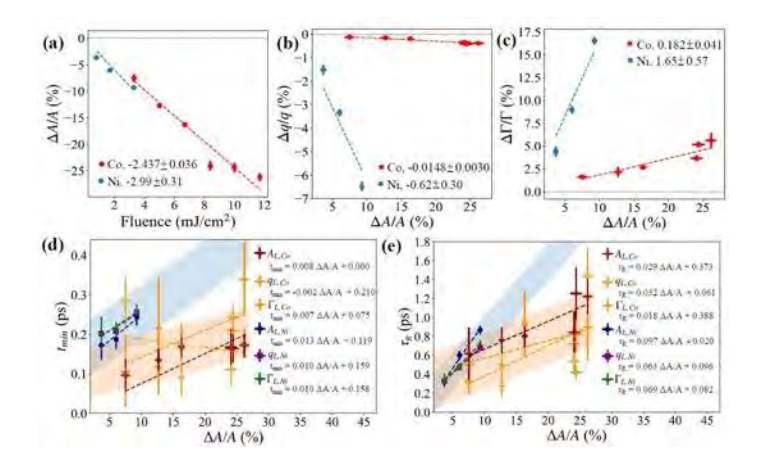
E. Bernard¹, R. Jangid^{1, 2}, N. Zhou Hagström¹, F. Meera¹, J. A. Brock³, M. Pancaldi⁴, D. De Angelis⁴, F. Capotondi⁴, E. Pedersoli⁴, K. Rockwell⁵, M. Keller⁶, S. Bonetti⁷, E. Fullerton³, T. Silva⁶, R. Kukreja¹

¹Materials Science and Engineering, University of California Davis, Davis, California, United States, ²NSLS-II, Brookhaven National Laboratory, Upton, New York, United States, ³Center for Memory and Recording Research, University of California San Diego, San Diego, California, United States, ⁴Elettra Sincrotrone, Trieste, Italy, ⁵Center for Magnetism and Magnetic Nanostructures, University of Colorado Colorado Springs, Colorado Springs, Colorado, United States, ⁶Quantum Electromagnetics Division, NIST, Boulder, Colorado, United States, ⁷Molecular Sciences and Nanosystems, a' Foscari University of Venice, Venice, Italy

The ultrafast optical control of magnetization represents a promising avenue for next-generation memory and data storage devices. While many studies have focused on understanding the rapid transfer of angular momentum, recent measurements have revealed rich physics underlying laser modification of nanoscale magnetic textures, including labyrinthine or stripe domains, skyrmions, etc. We have utilized time-resolved magnetic scattering at the FERMI free electron laser to probe the nanoscale magnetization dynamics in a [Co/Ni/Pt] multilayer following infrared (IR) laser excitation at both the Co and Ni resonant M edges. Changes in the amplitude (A), period (g), and inhomogeneity (Γ) of the labyrinthine- and stripe- like domain scattering patterns are compared for Co and Ni. Surprisingly, Ni exhibited a 10 to 40 times stronger modification of the labyrinthine pattern in reciprocal space than Co for a similar quench of magnetization. Figure 1 demonstrates these results, showing the maximum change in A,q, and Γ as a function of demagnetization amplitude, and quench and recovery time constants. As distortions of the labyrinthine pattern in reciprocal space relate to the modification of domain textures in real space, significant differences in Co and Ni indicate a 3D distortion of the domain pattern in the far-from-equilibrium regime. The modification of exchange interactions at the Co/Pt and Ni/Pt interfaces, magnon dynamics following laser excitation, and the influence of Pt induced Dzyaloshinskii-Moriya interaction (DMI) are considered to explain these distinct dynamics.

Fig.1 caption: Comparison of magnetization dynamics for Co and Ni labyrinthine domains: (a) Fluence dependence of Ni

 $(A_{Ni,L})$ and Co $(A_{Co,L})$. (b) Normalized radial shift $(\Delta q/q)_L$ and (c) width $(\Delta \Gamma/\Gamma)_L$ as a function of demagnetization amplitude $(\Delta A/A)$. For plots (a) to (c), a linear regression model was used with constrained intercepts, and the value of slope, including its error, is reported in the legend. (d) Quench and (e) recovery time constants for both Ni and Co obtained from the temporal fits for $A_{Ni,L}$, $A_{Co,L}$, $q_{Ni,L}$, $q_{Co,L}$, $\Gamma_{Ni,L}$ and $\Gamma_{Co,L}$. The dashed line in all plots indicates the slope fit with a linear regression model.

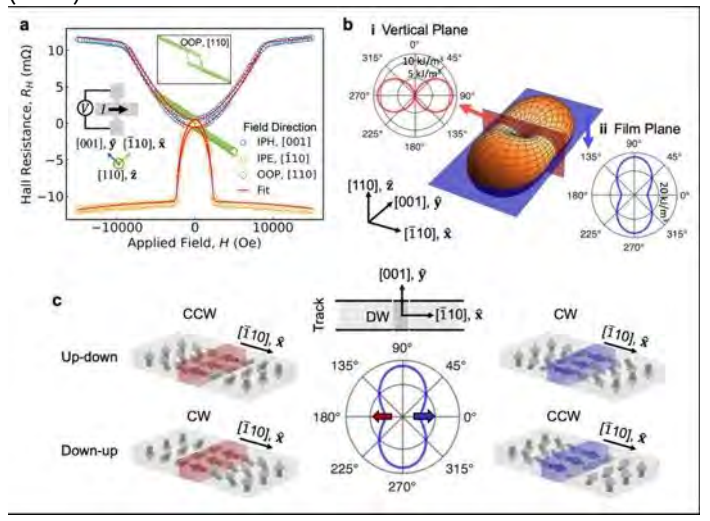


BC-11. Néel Domain Walls with Bistable Chirality in a Perpendicularly Magnetized Ferrimagnetic Insulator Y. Sonq¹, S. Huanq¹, D. Bono¹, J. Sadowski², C. A. Ross¹, G.

¹Massachusetts Institute of Technology, Cambridge, Massachusetts, United States, ²Brookhaven National Laboratory, Upton, New York, United States

Field-free spin-orbit torque-driven domain wall motion in magnetic thin films with perpendicular magnetic anisotropy (PMA) requires the domain walls to have Néel character. Conventionally, Néel domain walls are stabilized by the Dzyaloshinskii-Moriya interaction (DMI) in ultrathin films. Here, in a europium iron garnet thin film with PMA and an additional uniaxial in-plane anisotropy characterized by SMR (Fig a and b), we demonstrate two bistable Néel domain wall states (Fig. c) in the absence of DMI, and the capability to toggle the wall states with an in-plane field pulse and consequently their directions of motion under a current pulse. We present a phase diagram for the bistable Néel domain wall states as a function of in-plane field pulse width and amplitude. By fitting the experimental data to an analytical model of Néel wall reversal through the

nucleation and propagation of Bloch lines, we extract the length of the initial reversed domain wall segment and Bloch line nucleation energy barrier. Current-driven motion of in-plane anisotropy stabilized Néel walls is qualitatively different from that of DMI-stabilized ones owing to the different symmetry of the effective fields that stabilize the Néel configuration. Furthermore, we present a proof of principle demonstration for 2-bit random number generation based on the stochastic reversal of domain wall chirality. These results provide critical insight into the topological energy barrier of Bloch lines and identify paths towards domain wall-based memory and computing devices. Song, Y., Huang, S., Bono, D. et al. Nat Commun 16, 5201 (2025).



Magnetic characterization and DW structure of the film. a, SMR data and modeled fit to extract the anisotropy energies. Transverse Hall resistances are measured as a function of applied field along IP easy (IPE), IP hard (IPH), and OOP directions. b, Surface plot of the measured anisotropy landscape. c, Schematics of DW track configuration for Néel wall stabilization and of fully Néel CCW and CW DW spin structures stabilized in the film by the strong IP anisotropy corresponding to the wall center spins oriented to the left (red arrow) and to the right (blue arrow) for up-down and down-up walls.

BC-12. Meron chirality selection by transverse magnetic fields at reconfigurable domain wall racetrack

V. V. Fernandez^{1,2}, A. Herguedas^{1,2}, C. Quirós^{1,2}, P. Suarez-Blanco¹, C. Fernandez-Gonzalez³, A. Sorrentino³, S. Ferrer³, A. Hierro-Rodriguez/^{1,2}, M. Velez^{1,2}

¹Universidad de Oviedo, OVIEDO, Spain, ²CINN (CSIC-UO), El Entrego, Spain, ³Alba Synchrotron, Cerdanyola del Vallès, Spain

Stochastic domain wall propagation at nanowire bifurcations has been used to design probabilistic spintronic devices [1]. Here, we explore stripe domain bifurcations as possible probabilistic junctions within the reconfigurable domain wall racetracks proposed in ref. [2]. This system is based on the controlled propagation of magnetic textures (vortices and antivortices) within a soft NiFe layer guided by the stripe domain pattern of a hard NdCo₅ layer with weak perpendicular magnetic anisotropy (Fig. 1).

In this bilayer system, vortex/antivortex nucleation in the NiFe layer occurs at the cores of stripe domain bifurcations [3], coupled to the generation of a meron texture and a Bloch point in the NdCo₅ layer. Topological constraints force the propagation of vortices along the central stripe, while antivortices can choose between the two equivalent paths joining at the bifurcation core (Fig. 2) resulting in either CW or CCW chirality of the underlying meron texture.

Magnetic Transmission X-ray microscopy and micromagnetic simulations have been used to study the probability of antivortex propagation along each of the two branches under the effect of *in-situ* magnetic fields applied parallel (H_x) and/or perpendicular (H_y) to the stripe domain pattern. Experimental CW/CCW meron unbalance as a function of magnetic history will be discussed in terms of the main relevant factors suggested by the micromagnetic simulations such as spin precession at the bifurcation core during vortex/antivortex nucleation, Zeeman coupling with transverse fields at the bifurcation core and bifurcation mobility due to magnetic pressure under longitudinal field pulses.

Work supported by Spanish AEI and Asturias Sekuens.

- [1] D. Sanz-Hernandez, et al, Tunable stochasticity in an artificial spin network, Advanced Materials 33, 2008135 (2021).
- [2] V. V. Fernandez, et al, Memory effects on the current-induced propagation of spin textures in NdCo₅/Ni₈Fe₂ bilayers, Phys. Rev. Appl. 23, 014023 (2025). [3] A. Hierro-Rodriguez, et al, Observation of asymmetric distributions of magnetic singularities across magnetic multilayers, Phys. Rev. B 95, 014430 (2017).

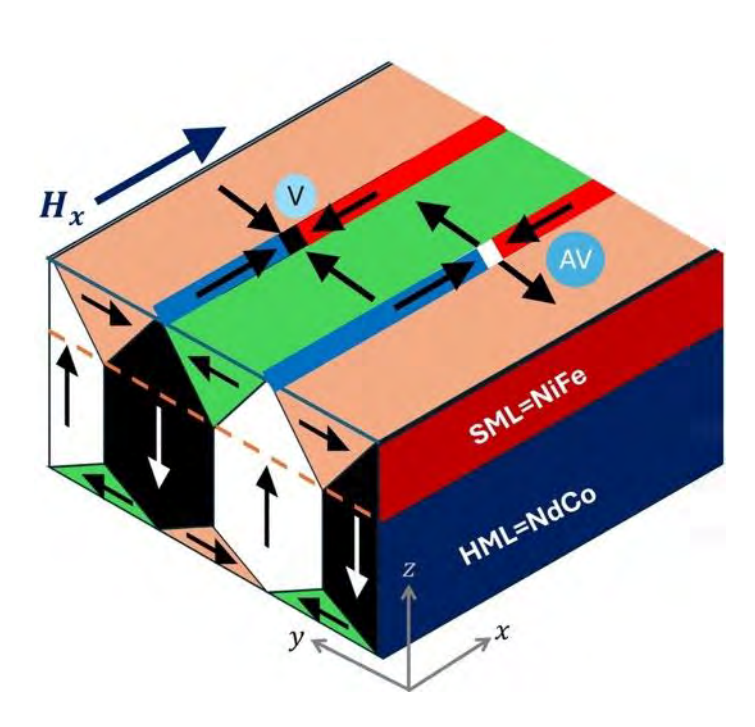


Fig. 1 Reconfigurable domain wall racetrak: vortices (V) and antivortices (AV) propagate on a NiFe layer under the effect of current and/or field pulses, guided by the stripe domains in NdCo layer. These stripe domains can be reoriented at will with an external magnetic field.

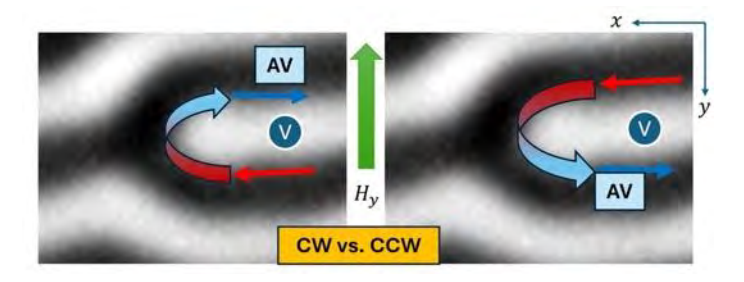


Fig.2 Sketch of Antivortex propagation along the two possible bifurcation branches and the corresponding CW/CCW meron texture under the effect of an H_x field pulse. Transverse H_y allows us to tune the CW/CCW meron probability at each bifurcation core.

BC-13. Vortex Nernst effect in ferrimagnetic insulator/high-temperature superconductor heterostructures

M. Yang, J. Li

Department of Physics, Southern University of Science and Technology, Shengzheng, GuangDong, China

The injection of pure spin current into superconductors is an active research area for the potential realization of lowdissipation spintronics devices. Around the superconducting transition temperature (T_c), pronounced enhancements of the thermoelectric voltage and ferromagnetic resonance linewidth have been reported in the heterostructure composed of ferromagnets and conventional superconductors [1-3]. However, such studies are still lacking in high-temperature superconductors. In this work, we report the successful growth of YBa₂Cu₃O₇(YBCO) epitaxial film on spinel ferrimagnetic insulator Li_{0.5}AlFe_{1.5}O₄(LAFO) film, and thermal transport measurements are performed to check whether pure spin current can be injected into the cuprate. A hysteresis loop in the magnetic-field-dependent transverse thermoelectric voltage is observed only around the superconducting T_c, at which the Vortex Nernst effect (VNE) in a single YBCO layer also predominates. In order to disentangle the contribution from the VNE and spin Seebeck effect (SSE), an insulating MgO layer is inserted at the LAFO/YBCO interface to block spin current injection. Interestingly, the hysteresis transverse thermoelectric signal persists despite the barrier, suggesting that it stems from the modulation of the VNE by the magnetic stray field generated by the ferrimagnetic insulating layer, rather than SSE from spin current. This work highlights that cuprates such as YBCO are not ideal candidates for spin current injection due to their weak spin-orbit coupling. Instead, the Vortex Nernst effect in YBCO can be effectively modulated by the stray field from neighboring ferrimagnetic insulators like LAFO. References:

- [1] K.-R. Jeon et al. Giant Transition-State Quasiparticle Spin-Hall Effect in an Exchange-Spin-Split Superconductor Detected by Nonlocal Magnon Spin Transport, ACS Nano 14, 15874 (2020).
- [2] M. Umeda et al. Spin-current coherence peak in superconductor/magnet junctions, Appl. Phys. Lett. 112, 232601 (2018).
- [3] K.-R. Jeon et al. Enhanced spin pumping into superconductors provides evidence for superconducting pure spin currents, Nat. Mater. 17, 499 (2018).

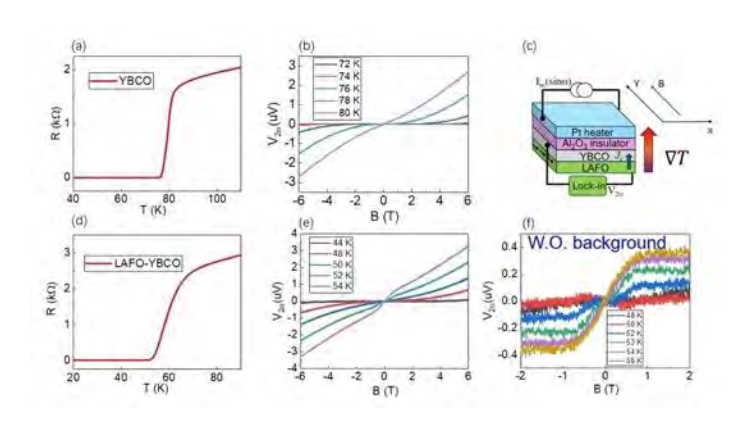


Figure (a), (d): Resistance-temperature curves of pure YBCO and LAFO/YBCO bilayer films; Figure (b), (e): magnetic field dependence of thermovoltage signals of pure YBCO and LAFO/YBCO bilayer films; Figure (c): Measurement geometry of thermovoltage signal; Figure (d): Thermovoltage signal of LAFO/YBCO bilayer film after subtracting VNE background.

SESSION BD: SOFT MAGNETIC MATERIALS I

Co-Chair(s): C. Chinnasamy, Manufacturing Science Division,
Oak Ridge National Laboratory, Knoxville, Tennessee, United
States and P. Kulik, University of Central Florida, Orlando,
Florida, United States
Tuesday, October 28, 2025
02:00 PM-05:30 PM
Ballroom B

BD-01. Iron Nitride Based Nanocomposite Magnet and its Prototype Motor Application

<u>T. Ogawa^{1, 2}</u>, S. Yamamoto³, N. Kobayashi², H. Yamamoto², K. Nakamura¹

¹Graduate School of Engineering, Tohoku University, Sendai, Japan, ²Future Materialz Co. Ltd., Tokyo, Japan, ³Sankei Giken Koqyo Co. Ltd., Tokyo, Japan

Metastable iron nitride nanoparticles, such as α "-Fe₁₆N₂, exhibit high saturation magnetization (~2.2 T) and a semihard magnetocrystalline anisotropy constant (~1 x 10⁶ J/m³) [1]. Their use in nanocomposite bonded magnets, when combined with conventional permanent magnet powders such as the Sm-Fe-N phase, presents new potential for achieving intermediate magnetic properties, namely, high residual magnetization (B_r) and moderate coercivity (H_c) values exceeding those of AlNiCo or ferrite magnets. Our uniquely developed Sm-Fe-N/Fe₁₆N₂ bonded magnet exhibited simultaneous magnetization reversal and a

smooth hysteresis curve as shown in the left side of Fig.1, in contrast to independently reversing behaviors typically observed. This behavior enables the continuous tuning of intermediate magnetic properties as a function of the mixture ratio. At present, we have achieved the maximum B_r of 0.71 T and H_c of 380 kA/m as shown in the right side of Fig.1 by optimizing Fe₁₆N₂ powder mixture ratio to Sm-Fe-N powder and some additives amount to the magnet powder. Also, a conventional 4-pole surfacemounted permanent magnet synchronous motor (PMSM) was experimentally demonstrated using the fabricated anisotropic Sm-Fe-N/Fe₁₆N₂ magnets by the present process, whose B-H curve was shown as black colored data in the right side of Fig.1. As a result, a high efficiency of 89.3% was successfully achieved at a torque of 160 mNm, closely matching the results predicted by three-dimensional finite element simulations (3D-FEM) as shown in Fig.2 [2]. These findings may open new avenues for developing hybrid composite magnet materials with tailored magnetic properties, particularly suited for high-torque, highefficiency motor applications.

[1] T. Ogawa et al., Appl. Phys. Exp. 6 (7), 073007 (2013).

[2] I. Çirozlar et al., J. Magn. Soc. Jpn. 49(2), 32 (2025).

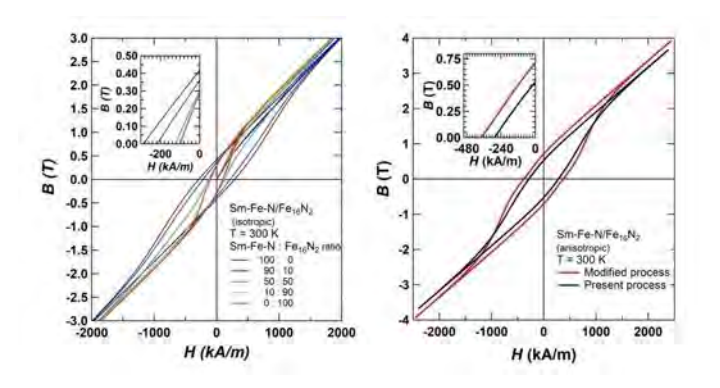


Fig.1 B-H curves for isotropic (left) and anisotropic (right) Sm-Fe-N/Fe₁₆N₂ bonded magnets. The inset shows the expanded area in 2^{nd} quadrant.

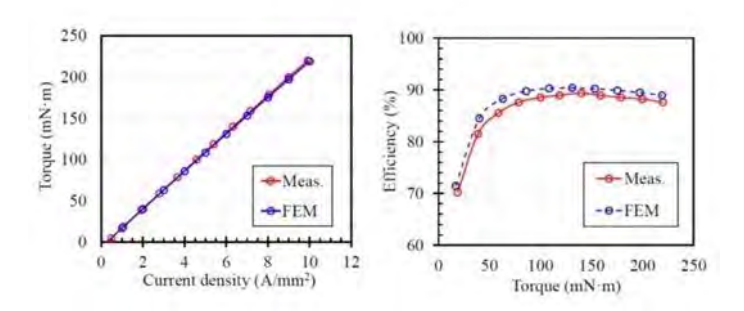


Fig.2 Measured and 3D-FEM calculated torque v.s. current density characteristics (left) and efficiency v.s. torque (right) for PMSM equipped with Sm-Fe-N/Fe₁₆N₂ bonded magnet.

BD-02. Theoretical Investigation of Magnetic Moment Enhancement in (Fe_{1-x}Co_x)₁₆N₂ Compared to Fe_{1-x}Co_x Alloy Y. Asari¹, T. Tabata¹, M. Noujima¹, S. Terada¹, M. Enoki², T. Ogawa³

¹Hitachi, Ltd, Hitachi, Japan, ²Shimane university, Matsue, Japan, ³Tohoku university, Sendai, Japan

It is well known that Fe-Co alloy with body-centered-cubic (bcc) crystal structure exhibit a higher magnetic moment than $\alpha\text{-Fe}$ [1]. However, the practical application of Fe-Co alloys is limited due to the high cost of cobalt. To broaden the use of the excellent magnetic materials, it is essential to reduce the Co content from this alloy. While decreasing the amount of Co can reduce the price of the material, it also leads to a reduction in magnetic moment, as described by the Slater-Pauling curve.

On the other hand, the $\alpha''\text{-Fe}_{16}N_2$ phase, formed by introducing nitrogen into $\alpha\text{-Fe}$, is reported to exhibit a high magnetic moment [2]. Nitrogen incorporation transforms the crystal structure into a body-centered-tetragonal (bct) phase. Since nitrogen occupies interstitial sites distinct from the iron site, it is structurally feasible to introduce both nitrogen and cobalt into $\alpha\text{-Fe}$ simultaneously. Therefore, it is expected that a magnetic material with exceeding the magnetic moment of the conventional Fe-Co alloy can be synthesized by nitriding the Fe-Co alloy.

To date, the magnetic moment of nitrided Fe-Co alloys has been investigated theoretically [3,4], and these studies suggest it may exceed that of conventional Fe-Co alloys. However, since the calculations have been limited to only a few specific cases, the conditions under which the magnetic moment surpasses that of FeCo remain unclear.

In this study, we investigated the magnetic moment of

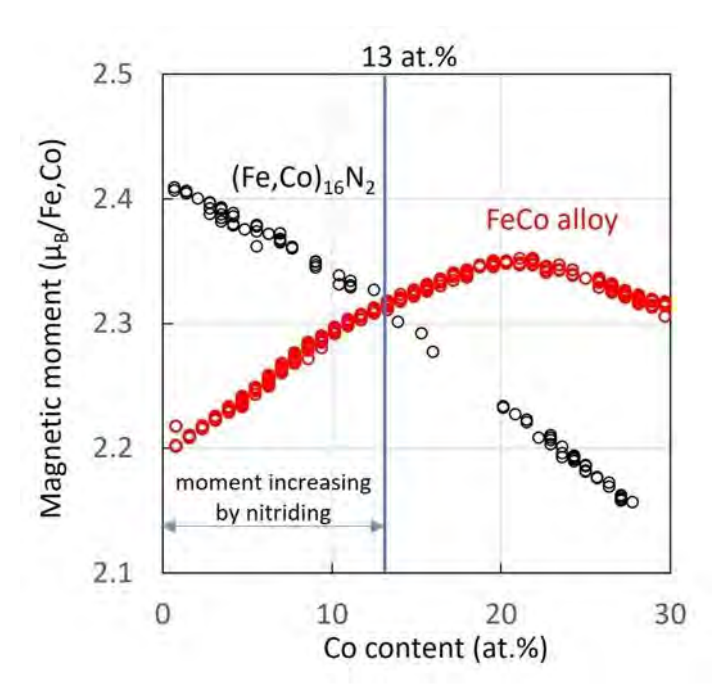
nitrided Fe-Co alloys and identified the compositional range in which it exceeds that of conventional Fe-Co alloys. We constructed a supercell model of $8((\text{Fe},\text{Co})_{16}\text{N}_2)$, comprising a total of 144 atoms, and calculated the electronic structure using the first-principles density functional theory. The magnetic moment was evaluated from the difference in integrated spin densities. We found that nitriding may enhance the magnetic moment when the Co concentration is below 13 at.% as shown in the figure.

This research is partially based on results obtained from Green Innovation Fund Projects / Next-generation Motor Development (JPNP21026) commissioned by the New Energy and Industrial Technology Development Organization (NEDO).

[1] D. I. Bardos, J. Appl. Phys., Vol. 40, p.1371 (1969).[2] Y. Sugita, K. Mitsuoka, M. Komuro, et al., J. Appl. Phys., Vol. 70, p. 5977 (1991).

[3] M. Chandran, et al., J. Appl. Phys. 101, 033912 (2007).

[4] L. Ke, et al., Phys. Rev. B88, 024404 (2013).



Magnetic moment for FeCo alloy (red) and nitrided FeCo (black).

BD-03. Microstructure and permeability of Fe-deficient Ni-Cu-Zn ferrites sintered under reduced oxygen partial pressure

C. Priese, <u>J. Töpfer</u> Ernst-Abbe-Hochschule Jena, Jena, Germany

Fe-deficient Ni-Cu-Zn ferrites are used as soft magnetic materials for multilayer inductors. Fabrication of multilayer inductors is based upon cofiring ferrite layers and screenprinted Aq coils pattern at around 900°C in air. We report here on a study on the effect of oxygen partial pressure on densification, microstructure and permeability of ferrites of composition Ni_{0.30}Cu_{0.20}Zn_{0.52}Fe_{1.98}O_{3.99} during sintering at 900°C. The Fe-deficient ferrites bulk samples were sintered in gas atmospheres with different partial pressure of oxygen in the range of $0 \le logp_{02} \le -5$. The sintered microstructure consists of stoichiometric ferrite grains and copper oxiderich grain boundary phases. We have studied the densification and grain growth during sintering in different p₀₂. It is found, that the density and grain size both show maximum values of 98% and 1.5 µm, respectively, after sintering in $p_{02} = 10^{-2}$ atm. Simultaneously, the permeability at 1 MHz also has a maximum of μ = 350 after sintering at 10⁻² atm. XRD reveals an increase of ferrite lattice parameter, a reduction of the ferrite phase content, and an increase in the copper oxide secondary phase content at more reducing conditions. Similarly, EDX analysis reveals enhanced formation of Cu-oxide grain boundary phases. The variation of permeability is discussed in relation to the ferrites' microstructure. The variation of permeability with grain size was analyzed using the non-magnetic grain boundary model. Formation of intra-crystalline porosity in larger grains and of non-magnetic Cu oxide grain boundary phases with different composition are key factors which affect the permeability of Ni-Cu-Zn ferrites. We have also studied ferrite multilayer samples made from

We have also studied ferrite multilayer samples made from stacking, laminating and sintering of ferrite tapes. The sintering behavior and microstructure formation of bulk and multilayer ferrites are compared. It is found, that ferrite multilayer inductors with Ag coil metallization which were co-fired at 900°C and $p_{02} = 10^{-2}$ atm exhibit a defect-free microstructure and high permeability. The results are significant for finding optimum sintering protocols for ferrite multilayer inductors.

BD-04. Nd₂Fe₁₇N₃ with planar magnetocrystalline anisotropy for sub-terahertz broadband absorbers

<u>S. Abe</u>¹, J. Akamatsu¹, N. Mitsui¹, N. Imaoka¹, S. Okada², K. Ozaki²

¹Nichia Corporation, Anan, Japan, ²National Institute of Advanced Industrial Science and Technology (AIST), Nagoya, Japan

The demand for sub-terahertz electromagnetic wave absorption materials intended for 6G systems is growing. $Nd_2Fe_{17}N_3$ exhibits large planar magnetocrystalline anisotropy and high saturation magnetization and would absorb electromagnetic waves in the microwave region owing to its natural resonance [1–6].

In this study, we measured the complex permeability of $Nd_2Fe_{17}N_3$ up to the sub-terahertz frequency range for the first time, using a 3- μ m single-crystal $Nd_2Fe_{17}N_3$ powder prepared through our reduction-diffusion method without any subsequent pulverization [6].

The prepared powder was characterized by its spherical shape and absence of secondary phases, such as α -Fe. Subsequently, $Nd_2Fe_{17}N_3$ powder coated with phosphate was mixed with a thermoplastic polyamide elastomer to obtain a 1-mm thick sheet containing 60 vol% of the powder. The sheets were then processed into the desired shape and their complex permeabilities were evaluated using a impedance analyzer and a network analyzer.

Fig. 1 shows the frequency dependence of the imaginary permeability (μ ") of the Nd₂Fe₁₇N₃ powder. As the figure shows, μ " is above zero within the extremely wide bandwidth from 1 to 330 GHz.

Fig. 2 shows the demagnetization curves of Nd₂Fe₁₇N₃ measured along the directions parallel and perpendicular to the aligned field using a vibrating sample magnetometer. The saturation magnetization calculated using the law of approach to saturation approximation (LASA) was 1.71 T. Furthermore, the anisotropy field H_{a2} estimated by extrapolating the magnetization curves obtained using LASA was about 16 T. The natural resonance frequencies of Nd₂Fe₁₇N₃ calculated based on H_{a2} and the corresponding field H_{a1} obtained from the literature [1] were within the range of 21–150 GHz. The natural resonance frequencies of the material predicted from its demagnetization curves significantly differed from the values shown in Fig. 1. Thus, at frequencies above 150 GHz, the resonance phenomena in Nd₂Fe₁₇N₃ will occur through mechanisms other than natural resonance.

[1] N. Imaoka, M. Tada, T. Nakagawa, and M. Abe, "Powder Compacts of $Nd_2Fe_{17}N_x$ exhibiting μ " > 1 at 1–18 GHz," *Abst. of the 53rd Annual Conference on Magnetism and Magnetic Materials*, Austin, USA, November 2008, p. 36.

[2] N. Imaoka, M. Abe, T. Nakagawa, and M. Tada, EP patent 2 146 357, March 18, 2010.

[3] L. Fa-Shen, W. Fu-Sheng, Z. Dong, Q. Liang, Z. Wen-Liang, "Microwave Magnetic Properties of $Nd_2Fe_{17}N_{3-\delta}$ with Planar Anisotropy", *Chinese Phys. Lett.* vol. 25, No. 3, pp. 1068–1070, 2008.

[4] Y. Wang, P. Zhang, K. Li, T. Xin, W. Yang, S. Liu, J. Han, H. Du, C. Wang, Z. Luo, J. Yang, "Tunable magnetic properties and microwave absorbing properties of $(Nd_{1-x}Y_x)_2Fe_{17}N_{3-\delta}$ ", Journal of Magnetism and Magnetic Materials, Vol. 613, 1 February 2025

[5] P. Wang, J. Zhang, G. Wang, B. Duan, T. Wang, and F. Li, "Preparation and study of $Ce_2Fe_{17}N_3$ microflakes with easy-plane anisotropy and high working frequencies", *Appl. Phys. Lett.*, vol.116, March 2020

[6] J. Akamatsu, S. Abe, M. Abe, K. Iwai, S. Yamanaka, S. Tada, and N. Imaoka, US patent 20250014791 A1, January 9, 2025

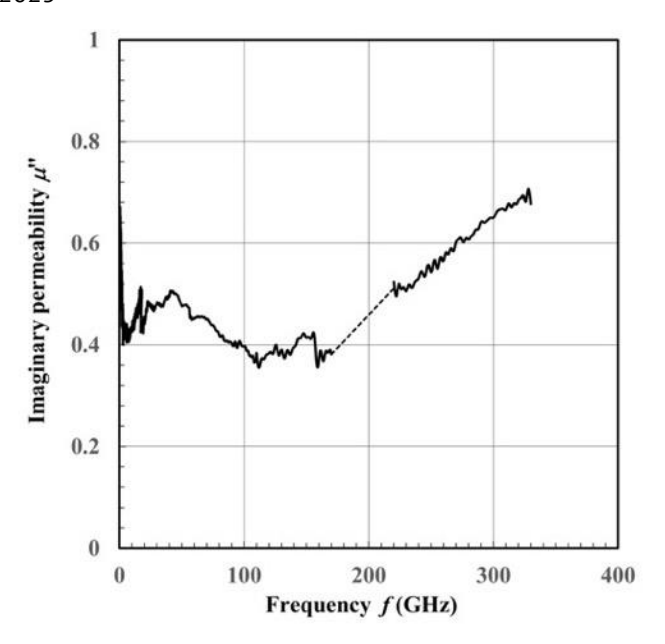


Fig. 1 Frequency dependence of μ " of the Nd₂Fe₁₇N₃ powder

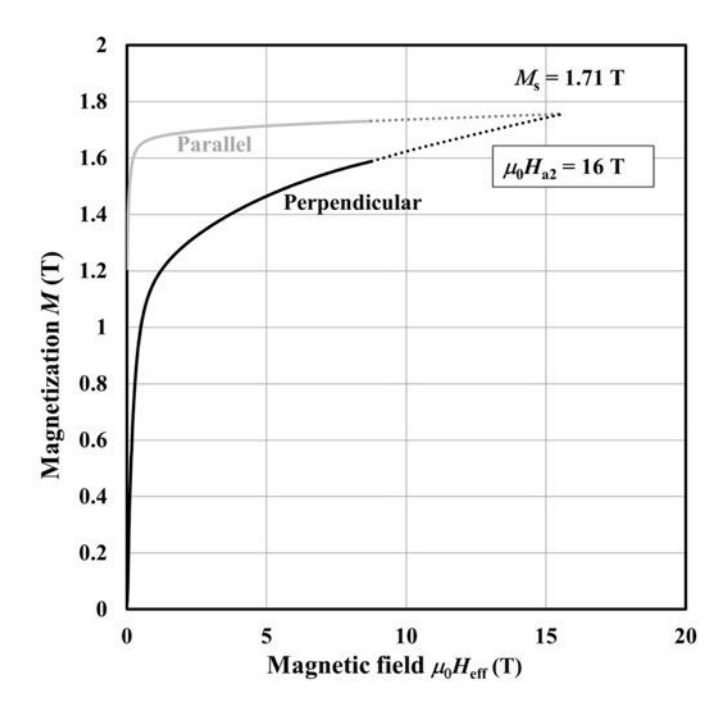


Fig. 2 Demagnetization curves of the $Nd_2Fe_{17}N_3$ powder along the directions parallel and perpendicular to the aligned field

BD-05. Role of Dipolar Interactions on the Determination of Effective Magnetic Anisotropy in Biopolymer coated Eu doped Magnetite Nanoparticles

K. Hazarika, D. P. Borah

Department of Science and Humanities, National Institute of Technology, DIMAPUR, Nagaland, India

Numerous research groups have contributed to a better understanding of the physical mechanisms governing self-heating studies in single-domain magnetic nanoparticles (SDMNPs) for magnetic fluid hyperthermia (MFH) applications. However, the role of all relevant parameters concerning magnetic relaxation still sparks debates among researchers. In this study, we conduct a comprehensive experimental analysis on the magnetic relaxation of SDMNPs with effective anisotropy, assessing the impact of particle-intrinsic factors and experimental conditions on self-heating efficiency in both noninteracting and interacting systems, with a particular focus on the dipolar interaction effect. Our study resolves prior conflicting reports on interaction effects in both agglomerated and less

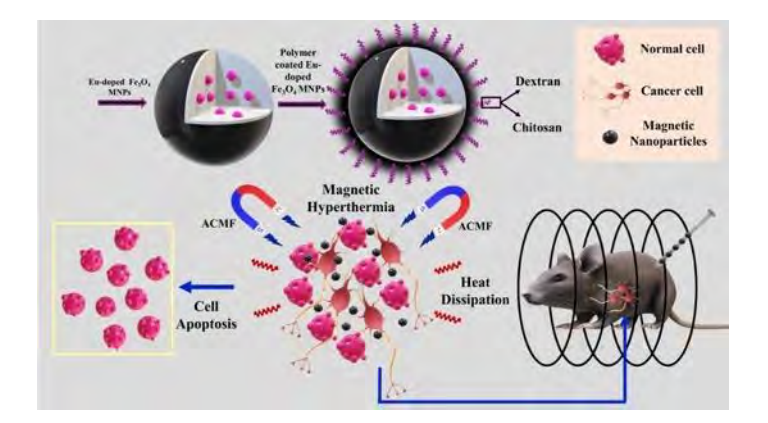
agglomerated setups for MFH applications. We discuss an analytical approach and its thermal interpretation, which are both focused on nanoparticle design and selecting experimental conditions to achieve optimal heating. The results indicate that polymer (Chitosan/Dextran) coated MNPs with low Eu doping exhibit improved characteristics and hold promise as potential application candidates due to their high specific absorption rate (SAR) values. Analyzing these profiles, we can obtain more profound insights into temperature variations, structure, morphology, and selfheating efficiency during magnetic hyperthermia experiments.

[1] Valdés D P, Lima, E, Zysler R D, Goya G F and De Biasi E 2021 Role of Anisotropy, Frequency, and Interactions in Magnetic Hyperthermia Applications: Noninteracting Nanoparticles and Linear Chain Arrangements *Phys. Rev. Appl.* 15 1–18

[2] Hazarika K P and Borah J P 2023 RSC Advances parameter tuning, and self heating in magnetic nanoparticles *RSC Adv.* 13 5045–57

[3] Naha P C, Hsu J C, Kim J, Shah S, Bouché M, Si-Mohamed S, Rosario-Berrios D N, Douek P, Hajfathalian M, Yasini P, Singh S, Rosen M A, Morgan M A and Cormode D P 2020 Dextran-Coated Cerium Oxide Nanoparticles: A Computed Tomography Contrast Agent for Imaging the Gastrointestinal Tract and Inflammatory Bowel Disease *ACS Nano* 14 10187–97

[4] Kurihara Y, Yokota H and Takahashi M 2022 Water-Dispersible Carboxymethyl Dextran-Coated Melamine Nanoparticles for Biosensing Applications *ACS Omega*



BD-06. Advanced In-Situ Friction Stir Forging of Soft Magnetic Composites for Axial-Flux Electric Motor Applications

R. Kalsar¹, H. Das¹, S. Shukla¹, L. Li¹, T. Ajantiwalay¹, J. Haag¹, T. P. Chhetri¹, B. Gwalani², V. Joshi¹, <u>C. Chinnasamy³</u>

¹Pacific Northwest National Laboratory, Richland, Washington, United States, ²North Carolina State University, Raleigh, North Carolina, United States, ³Manufacturing Science Division, Oak Ridge National Laboratory, Knoxville, Tennessee, United States

Soft magnetic composites (SMCs) are gaining prominence in high-frequency, high-flux applications such as axial-flux electric motors, due to their superior magnetic performance under dynamic conditions. In response to the demand for more energy-efficient and advanced manufacturing processes, this study investigates in-situ friction stir forging (I-FSF) as a novel, energy-efficient, single-step consolidation process for Fe-3.5Si soft magnetic powders. During I-FSF, a thermally induced oxide layer forms on individual powder particles, serving as an interparticle electrical insulation barrier. This enhances the composite's effective electrical resistivity, significantly reducing eddy current losses. Compared to conventional sintering, I-FSF offers enhanced densification kinetics, reduced diffusion distances, and enables near-net-shape fabrication of dense components. The processed SMC specimens exhibited tensile strengths exceeding 600 MPa while maintaining high saturation magnetization, highlighting a favorable balance of mechanical and magnetic performance. These results position I-FSF as a viable and sustainable route for manufacturing advanced SMCs, supporting the development of next-generation axial-flux electric motors with improved energy efficiency and structural reliability.

BD-07. Minnealloy Fabrication for High Power Transformers A. S. Padgett¹, S. R. Bishop¹, J. D. Boissiere¹, C. R. Riley¹, P. F. Weck¹, S. Percival¹, D. Bosomtwi¹, A. R. Marotta¹, D. Richards¹, W. Echtenkamp², J. Wang²

¹Sandia National Laboratories, Albuquerque, New Mexico, United States, ²University of Minnesota, Minneapolis, Minnesota, United States

Industry, telecommunications, and electrical grid technology rely on transformers; the cores for many of these transformers contain critical materials [1] that are susceptible to availability and supply chain risks. A rareearth and critical material free alternative called Minnealloy, α "-Fe₁₆NC, which has a larger saturation magnetization (≥ 2.47 T) than grain oriented electrical steel and a magnetic coercivity (197 A/m bulk phase, ~5 A/m engineered) comparable to amorphous metals is being developed to supplant legacy transformer core materials [2,3]. Minnealloy's small coercivity and enormous magnetic flux density result in low losses and more power transferred per cycle than any existing transformer core material for a given mass or volume [4,5,6,7,8]. In this talk, we will discuss our progress on fabricating Minnealloy via: meltatomization and cryomilling, electrodeposition, and spraypyrolysis. We will present the magnetic saturation, magnetic coercivity, electrical conductivity, and complex permeability from 20 Hz to 2 MHz on melt-atomization fabricated pressed powder transformer cores and compare them to pressed powder Minnealloy cores fabricated by meltspinning. Finally, calorimetry measurements will be presented and compared with our predictions from density functional theory.

Sandia National Laboratories is a multimission laboratory managed and operated by National Technology & Engineering Solutions of Sandia, LLC, a wholly owned subsidiary of Honeywell International Inc., for the U.S. Department of Energy's National Nuclear Security Administration under contract DE-NA0003525.

[1] D. J. Bauer, R. T. Nguyen, and B.J. Smith, "Critical Materials Assessment," U.S. Department of Energy, DOE/EE-2756 (2023)

[2] H. Giselher, *Acta Mater.*, vol. 61, p. 718 (2013)

[3] F.C. Li, T. Liu, J.Y. Zhang, *Mater. Today Adv.*, vol. 4 (2019)

[4] M. D. Mehedi, Y. Jiang, P. K. Suri, D. J. Flannigan, *J. Phys. D: Appl. Phys.*, vol. 50, no. 37 (2017)

[5] X. Zhang and J-P Wang, Appl. *Phys. Lett.*, vol. 114, iss. 15 (2019)

[6] G. Guo, J. Liu, and JP Wang, *TMS 2020 149th Supplemental Proceedings*, p. 1841 (2020)

[7] W. Echtenkamp, A. S. Padgett, S. R. Bishop, *AIP Adv.*, vol. 15, iss. 3, p. 035008 (2025)

[8] J. Zhu, and J-P Wang, *AIP Adv.*, vol. 14, iss. 1, pp. 015031 (2024)

BD-08. Co-sputtered FeCo-AlN Thin Films with Ultra-high Resistivity for High-Frequency Integrated Magnetics

R. Anjum, G. Wei, A. Masood, <u>R. Sai</u> Integrated Power and Energy Systems, Tyndall National Institute, Cork, Ireland

The evolution of high-frequency on-silicon integrated voltage regulators escalates the development of magnetic thin films that are ultra-low lossy at and beyond 100 MHz. Eddy-current loss dominates at such a high frequency – necessitating an ultra-high resistivity soft magnetic thin film. Nanogranular thin films [1] hold the key for next-gen power and RF applications, where reduced losses preferred to enhanced permeability. Here, we report a set of nanogranular magnetic thin films based on co-sputtered FeCo-AlN and FeCoB-AlN compositions. These films exhibit process-tuned resistivity, in-plane magnetic isotropy and beyond-GHz ferromagnetic resonance frequency – making them ideal for efficient and miniaturized on-silicon magnetics applications.

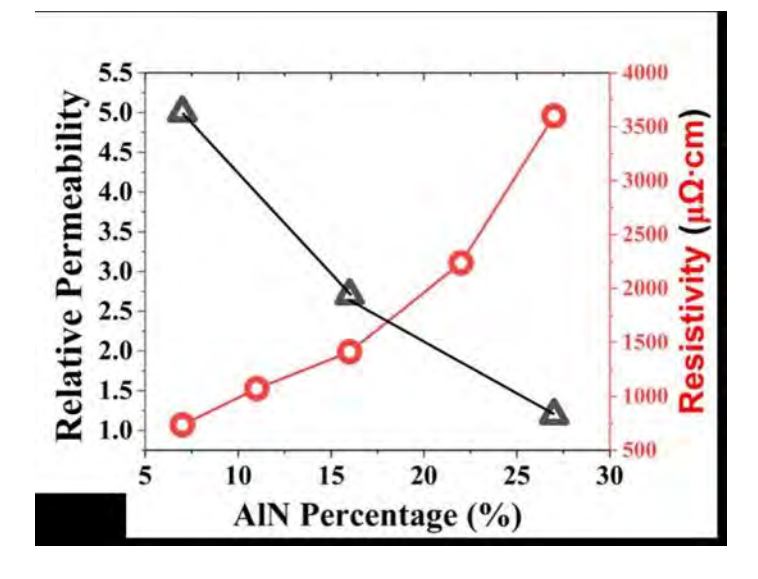
Through a delicate manipulation of dielectric concentration, significant control was attained over film morphology, grain size, magnetic, and electric properties. For instance, inplane isotropic behaviour with μ_r of 5 up to several hundreds of MHz was observed in FeCo-AlN (7%) sample. The amount of AlN percentage is found to play a key role in controlling the resistivity. The resistivity increases significantly with increasing AlN concentration with insignificant grain size variation. The 7% AlN exhibits relatively low ρ of 735 $\mu\Omega$ cm with a grain size of 30 nm, whereas, increasing the AlN concentration up to 27% led to a gradual yet significant increase of resistivity up to 3600 $\mu\Omega$ cm, which is 36x higher than similarly co-sputtered CoZrTa-SiO₂ nanogranular thin film [2], while the grain size decreases only to 13 nm. The insulating AlN phase severely impede electrical conductivity owing to reduced number of grain boundaries that hinders carrier transport.

The isotropic FeCo-AlN and FeCoB-AlN films, with moderate permeability and exceptionally high resistivities ranging

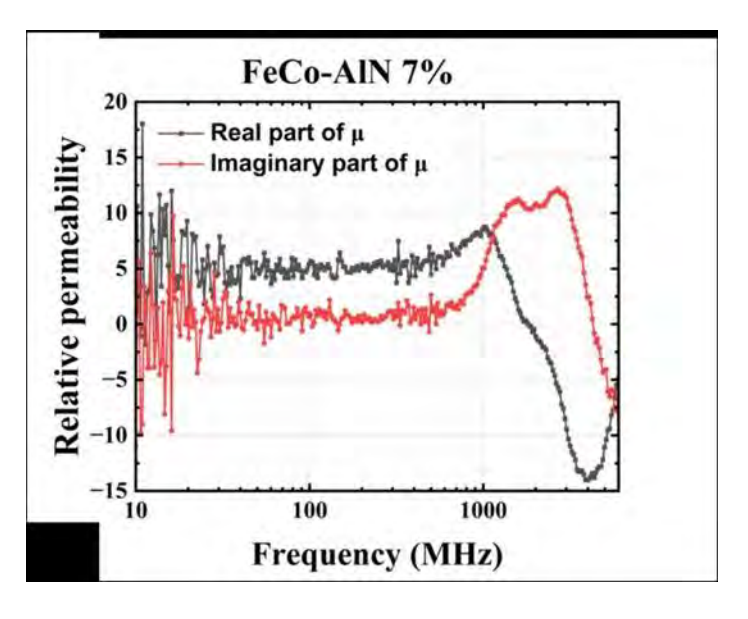
^{*} Best Student Presentation Finalist / LB - Late-breaking Poster

from 500 to 3600 $\mu\Omega cm$ provide several options of low-lossy high-frequency on-silicon magnetic core for various applications such as thin-film micro inductors, GHz-range electromagnetic interference (EMI) suppressors, and monolithic magnetic-core RF inductors.

[1] H. Kijima-Aoki, et. al., "Shape effect of Co nanoparticles on the electric and magnetic properties of Co – SiO₂ nanogranular films," AIP Adv., vol. 12, p. 035229, 2022. [2] D. Cronin, et al., "Soft magnetic nanocomposite CoZrTaB-SiO₂ thin films for high-frequency applications," J. Appl. Phys., vol. 127, no. 24, 2020.



Electrical resistivity and relative permeability of films vs AlN concentration(%).



Frequency dispersion of permability of FeCo-AlN(7%) sample

BD-09. Bipolar Faraday Rotation Garnets for Integrated Magnet-free Isolators on Si

P. Liu¹, B. Moghal², B. Stadler^{2, 1}

¹Chemical Engineering and Materials Science, University of Minnesota, Minneapolis, Minnesota, United States, ²Electrical and Computer Engineering, University of Minnesota, Minneapolis, Minnesota, United States

Magneto-optical garnets with ~0.5 mm thickness have long filled the need for industrially relevant optical isolators. However, artificial intelligence (AI) is driving photonic data needs toward monolithic [1,2] or transfer-printed [3] integration, where integrated bipolar garnets (positive (ϑ_F) and negative Faraday rotation $(-\vartheta_F)$) will be needed to meet the need using magnet-free designs [4]. Here, we deposited garnet onto silicon by sputtering and systematically studied Ce doping (Ce/Ce+Tb = R_2) and rare-earth content (Ce+Tb/Fe = R_1). Mr/Ms values of 0.50 to 0.70 were measured, which are suitable for field-free isolators in tiny photonic devices. Faraday rotation of -830±100°/cm was found for $R_2 \ge 0.2$ -0.25. (Fig.1), which is similar to the value but opposite in sign to undoped TbIG. Furthermore, a two-step anneal was found to lower the annealing temperature from 900°C to 800°C. A first anneal of 400°C can increase the Faraday rotation of films annealed at 800°C by ~33%. Using these results, simulated nonreciprocal phase shifting (NRPS) was calculated as the difference in forward and backward propagation constants ($\beta_{forward} - \beta_{backward}$) for garnet claddings on silicon-on-insulator waveguides.[5,6] Fig.2 shows the three different MZI isolator designs with positive (ϑ_{E}) or/and

negative FR garnet claddings.[4,7–8] The last design with alternating garnet segments having bipolar FR indicates that sub-mm scale magnet-free Si-integrated MZI isolators can be achieved.

- 1. P.-H. Liu, B. K. Moghal, and B. J. H. Stadler, "Effect of composition and two-step annealing on Ce-doped terbium iron garnets on Si," Opt. Mater. Express, OME 15(7), 1407 1418 (2025).
- 2. SY Sung, X Qi, BJHStadler Appl Phys Lett 87 (2005)
- 3. K Srinivasan, A Schwarz, JC Myers, NC Seaton, BJH Stadler ACS Appl Nano Mater 4 (2021)
- 4. K. Srinivasan and B. J. H. Stadler, "Push-pull non-reciprocal phase shifting," United States patent US12055756B2 (August 6, 2024).
- 5. M. Li, Y. Zhao, S. Dai, W. Yu, J. Li, T. Lin, Z. Zhang, and J. Liu, "Compact and low loss magneto-optical waveguide isolator for TE mode based on lithium niobate on insulator," Optics Communications 495, 127088 (2021).
- 6. S. Yamamoto and T. Makimoto, "Circuit theory for a class of anisotropic and gyrotropic thin film optical waveguides and design of nonreciprocal devices for integrated optics," Journal of Applied Physics 45(2), 882–888 (1974).
- 7. T. Mizumoto and Y. Naito, "Nonreciprocal Propagation Characteristics of YIG Thin Film," IEEE Transactions on Microwave Theory and Techniques 30(6), 922–925 (1982).
- 8. F. Auracher and H. H. Witte, "A new design for an integrated optical isolator," Optics Communications 13(4), 435–438 (1975).

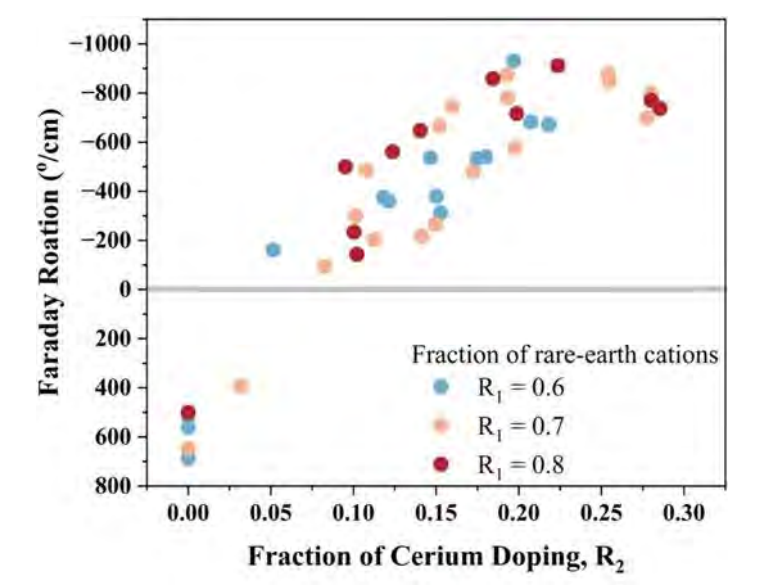


Fig. 1 Faraday rotation of all the garnet films at 1550 nm as a function of R_1 and R_2 .

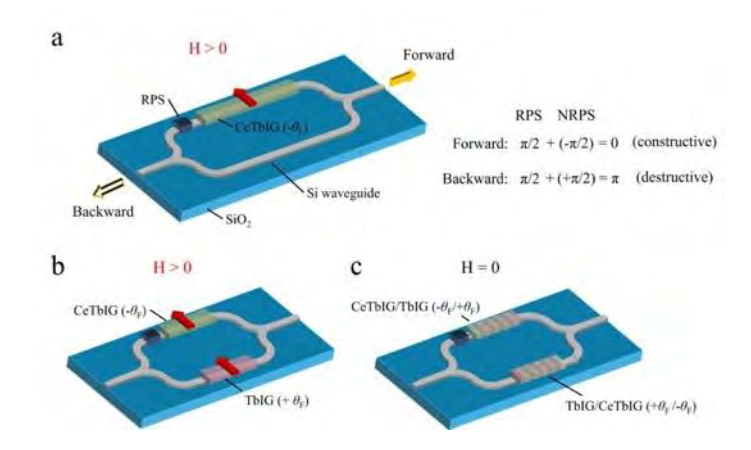


Fig. 2 Schematics of MZI isolator with (a) one nonreciprocal branch of CeTbIG $(-\theta_F)$ thin film, (b) two nonreciprocal branches of respective CeTbIG $(-\theta_F)$ and TbIG $(+\theta_F)$ thin film, and (c) two branches of alternative CeTbIG and TbIG segment thin films. Both (a) and (b) require an external unidirectional magnetic field (H > 0), whereas (c) operates without a fixed magnetic field (H = 0). Reciprocal phase shifters (RPSs) are included to ensure constructive interference in the forward direction and destructive interference in the backward direction.

BD-10. Micromagnetic Modeling of Gap-Controlled Permeability in Realistically Structured Soft Magnetic Materials

J. Duan, V. Lomakin

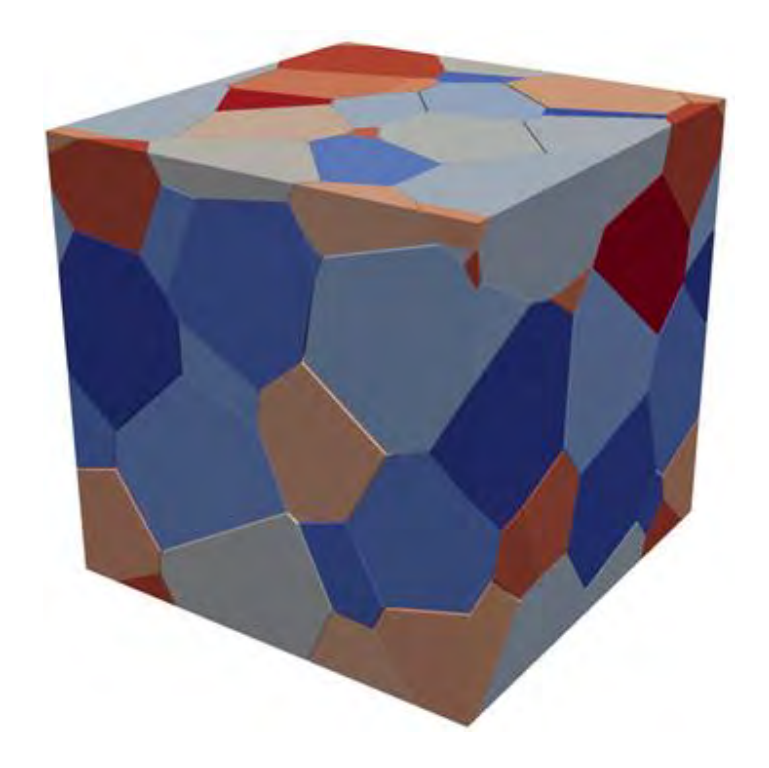
University of California San Diego, San Diego, California, United States

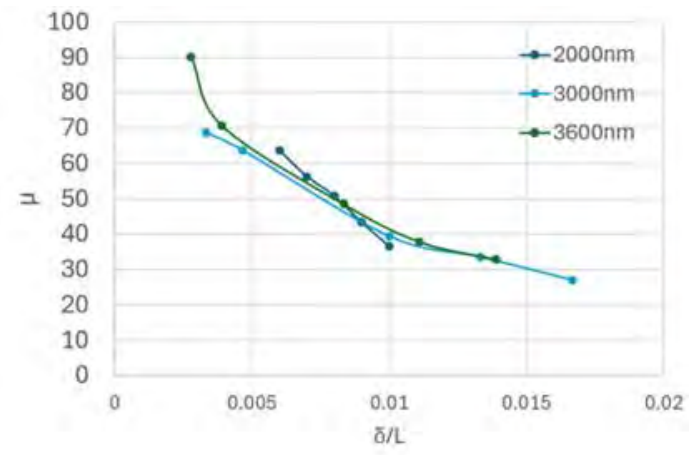
We present a study of the effective magnetic permeability in granular structured soft magnetic materials, focusing on the role of inter-grain gaps and their ratio to grain size. Using a finite element framework micromagnetic framework, we perform fully dynamic micromagnetic simulations that capture the effects of magnetization dynamics and geometrical constraints. The granular models are constructed with physically realistic geometries that mimic observed microstructures in transmission electron microscopy (TEM) and scanning electron microscopy (SEM) images of commercially available NiZn ferrite materials. These realistic grain shapes and configurations ensure the modeled results are representative of structures achievable through modern fabrication processes.

Our main contribution lies in the systematic analysis of permeability behavior as a function of the normalized gap size between grains. The granular models consist of single-domain ferrite grains with cubic anisotropy, separated by thin non-magnetic or weakly magnetic gaps. Periodic boundary conditions (PBCs) are employed in all directions to emulate bulk material behavior while preserving the microstructural fidelity. We compute the effective permeability using harmonic field excitation and extract the real and imaginary components of the permeability tensor from the steady-state response.

Figure 1a shows the periodic unit cell used in the simulations, composed of closely packed grains with submicron gap widths. Each grain is modeled with micrometer-scale dimensions and separated by air or insulating material representing inter-granular boundaries. Figure 1b presents the effective permeability versus the ratio of gap width to grain size. The permeability remains nearly invariant across a certain range of ratios, and provides an insight into material design, suggesting that effective permeability can be preserved despite the grain size.

These findings advance the understanding of structureproperty relationships in soft magnetic materials and offer guidance for engineering low-loss ferrite components with relaxed tolerances in gap uniformity.





^{*} Best Student Presentation Finalist / LB – Late-breaking Poster

BD-11. Engineering High Thermal Stability in Zr/Nb-doped CoFeB for High Power Conditioning in Extreme Environments

M. F. Mancias¹, N. M. Bruno², V. Keylin², A. Leary², K. Chinnathambi³, R. D. Noebe², K. Srinivasan¹
¹Electrical and Computer Engineering, Boise State University, Boise, Idaho, United States, ²Materials and Structures Division, NASA Glenn Research Center, Cleveland, Ohio, United States, ³Boise State Center for Materials Characterization, Boise State University, Boise, Idaho, United States

Cobalt- and iron-based nanocrystalline soft magnetic cores for inductors and transformers are known to enable highpower-high-frequency conversion that are critical for allelectric propulsion and energy distribution systems [1-4]. However, in extreme environments, such as Martian and Venus surfaces, temperatures can fluctuate from -65 °C to 464 °C, respectively [5]. Therefore, applications in space require soft magnetic alloys to possess a high saturation induction and low permeability to handle high-power, while also maintaining a high temperature stability. Our work focuses on lowering permeability and expanding the operating temperature by strain-annealing and Zr/Nb doping of Co₆₀Fe₂₀B₂₀ alloy, respectively. Recent work on Fe_{72.5}Nb₂Mo₂Cu₁Si_{15.5}B₇ amorphous nanocomposite ribbons reveal that a two-step strain annealing process can reduce permeability by at least an order of magnitude while retaining a high saturation magnetization [6]. Yet, achieving high-temperature stability requires increased primary crystallization temperature (T_{x1}) without compromising magnetic performance. Sputtered Zr-CoFeB thin films, from differential scanning calorimetry (DSC) and in-situ annealing in TEM, indicate that increased Zr concentration (5-20 at.%) increases T_{x1} from 770 K (in undoped CoFeB) to above 900 K in the doped alloy, as shown in Figure 1. Magnetic measurements show that a large saturation magnetization of 800 emu cc⁻¹ was retained despite alloy composition change. Additionally, Co₅₇Fe₁₉B₁₉Nb₅ melt-spun ribbons with similar post-processing as [6] demonstrated high saturation induction with varying, lower permeabilities, as shown in Figure 2. Core loss measurements also pointed to losses <15 W/kq. These results illustrate promise in co-doping of CoFeB alloys with Zr and Nb and motivate further studies into the underlying mechanisms and alloy microstructure to develop high temperature, efficient soft magnetic materials.

[1] G. Herzer and H. R. Hilzinger, *Phys. Scr.*, vol. 1988, no. T24, p. 22, Jan. 1988

[2] R. Hasegawa, J. Magn. Magn. Mater., vol. 304, no. 2, pp.

187-191, Sep. 2006

[3] A. Leary, "The Impact of Soft Magnetic Materials in Electrified Aircraft Applications," Sep. 12, 2023. [Online].

[4] "Moon-to-Mars Architecture Definition Document (ESDMD-001)", Exploration Systems Development Mission Directorate, NASA, April 2023

[5] "Solar System Temperatures - NASA Science." [Online].[6] N. M. Bruno *et al.*, *J. Magn. Magn. Mater.*, vol. 603, p. 172280, Aug. 2024

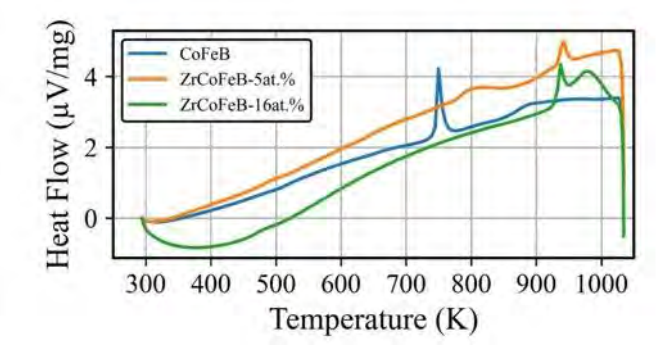


Fig. 1: Differential scanning calorimetry curves for undoped and Zr-doped CoFeB.

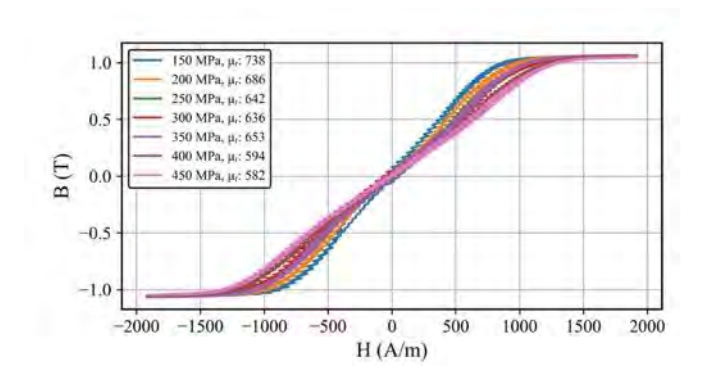


Fig. 2: BH loops of Nb-doped CoFeB ribbons under varying levels of strain annealing.

BD-12. Soft magnetic properties of Fe-Co-B-Si-Cu nanocrystalline alloys at high temperatures

<u>I. Skorvanek</u>¹, J. Marcin¹, B. Kunca¹, P. Svec jr.², P. Svec² ¹Institute of Experimental Physics, SAS, Kosice, Slovakia, ²Institute of Physics, SAS, Bratislava, Slovakia

The growing technological demand for soft magnetic materials capable of operating at high temperatures has intensified research into FeCo-based nanocrystalline alloys. In this study, we investigated the influence of different thermal processing on the structure and high temperature soft magnetic properties of (Fe₆₄Co₂₁B₁₀Si₅)₉₉Cu₁ ribbons prepared by planar flow casting. Special attention was given to the ultra-rapid annealing (URA), which involves compressing samples between pre-heated massive copper blocks. This approach enables the synthesis of nanocrystalline soft magnetic alloys with a reduced content of non-magnetic elements, offering an attractive combination of high saturation magnetic flux density (B_s) and low coercivity (H_c) [1,2]. A description of our URA setup is available in a previous publication [3].

As-quenched ribbons were annealed for 0.5 seconds at 490 °C, which was determined as optimal URA treatment. For comparison, the pieces of ribbon were subjected to conventional annealing (CA) in a vacuum furnace for 30 minutes at 370 °C. Our results revealed that the high heating rate and short processing duration of URA promoted the formation of finer nanocrystalline grains, typically ranging from 15 to 17 nm, compared to CA. This grain refinement significantly improved magnetic softness, reducing coercivity from 210 A/m in CA-treated samples to 3 A/m in URA-processed ribbons. URA samples exhibited $B_{\rm s}$ value of 1.85 T.

The primary focus of this study was to characterize the soft magnetic behavior of URA ribbons at elevated temperatures. Hysteresis loops were measured from room temperature (RT) up to 425 °C using a quasi-static Förster-type B–H loop tracer. Reference hysteresis loops were recorded at RT after each high-temperature cycle to monitor possible irreversible changes in the microstructure during thermal exposure. The results in Fig. 1 demonstrate that the URA-processed ribbons maintain excellent stability of coercivity from RT up to 250 °C, which highlights their strong potential for use in magnetic components operating in high temperature environments.

Acknowledgements: This work was supported by the projects APVV-23-0281, VEGA 2/0148/23 and JRP NOMAGRAD

- 1. K. Suzuki et al., Appl. Phys. Lett. 110, 012407 (2017)
- 2. B. Kunca et al., J. Alloy. Compd. 911, 16503 (2022)
- 3. B. Kunca et. Al., J. Magn. Magn. Mater. 591, 171679 (2024)

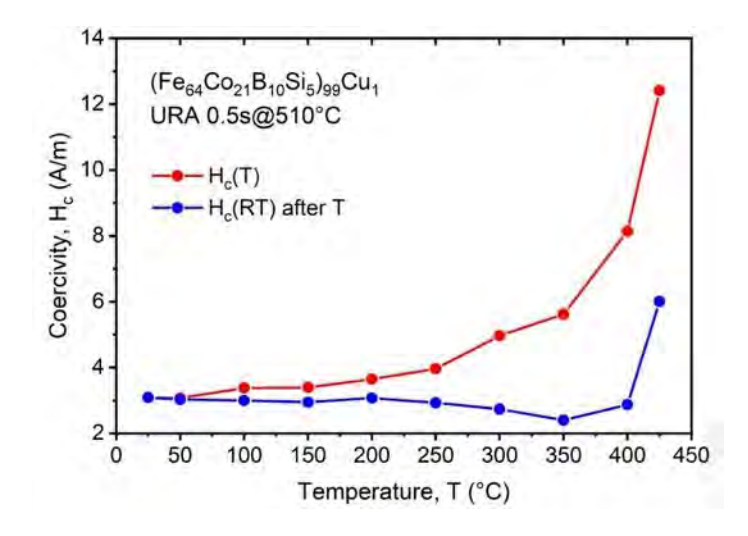


Figure 1:

BD-13. Fabrication of soft magnetic cores composed of amorphous Fe-B particles for next-generation magnetic passive components

<u>S. Ajia</u>¹, C. Masumoto¹, Y. Kodama¹, T. Miyazaki², S. Muroga¹, Y. Endo^{1, 3}

¹Department of Electrical Engineering, Tohoku University, Sendai, Japan, ²School of Engineering, Tohoku University, Sendai, Japan, ³CSIS, Tohoku University, Sendai, Japan

Fe-based soft magnetic materials have been widely used for passive components because of their low coercivity and large saturation magnetization. However, the eddy current limits the Fe-based soft magnetic alloy powder for applying in the high frequency range [1]. For this challenging, the particle size of soft magnetic powder is needed to be submicron size, and with amorphous state [2, 3]. Herein, we synthesized amorphous Fe-B particles capable with controlled particle size ranging from nano-meter to submicron size, fabricated soft magnetic composite (SMC) core, and further evaluated their high frequency magnetic properties.

Fig. 1(a) shows the XRD patterns of as-synthesized (Fe-B_AS) and annealed Fe-B (Fe-B_AN) particles. After heat-treatment at 400°C for 1 min, the Fe-B particles maintained an amorphous state, and their coercivity decreased (not shown). SMC cores using Fe-B particles were fabricated, demonstrating spherical particle with size of 0.9 \sim 1.5 μ m

(Fig. 1(b), (c)). On the other hand, SEM image of SMC of CIP showed deformed and aggregated particle from its spherical counterparts (Fig. 1(c)).

Fig. 2 demonstrated the core loss (P_{cv}/f) for all SMC cores measured in the frequency range between 100 kHz - 5 MHz under B_m of 1 mT. The P_{cv}/f of SMC cores using Fe-B particle was almost constant in the frequency range up to 5 MHz, while the P_{cv}/f of that of CIP powders gradually increased from 200 kHz, and steeply increased after 1 MHz. Such low P_{cv}/f of SMC using Fe-B particles may be attributed by combination of their smaller particle size and relatively high resistivity originated from the amorphous state of the particles.

Therefore, the combination of microstructure and magnetic properties of Fe-B particles makes it possible for next-generation magnetic passive components in MHz range. This study was supported by KAKENHI 24K21602; MEXT-Program for Creation of Innovation Core Technology for Power Electronics No. JPJ009777 and MEXT, No. JP011438; CSIS of Tohoku University.

[1] B. Zhou, et. al., J. Pgys. D: Appl. Phys. 50, 475001 (2017).
[2] Y. Shimada, et. al., IEEE Trans. Magn. 45, 4298 (2009).
[3] K. Murata, et. al., T. Magn. Soc. Jpn. (Special Issues)., 5, 1-5 (2021).

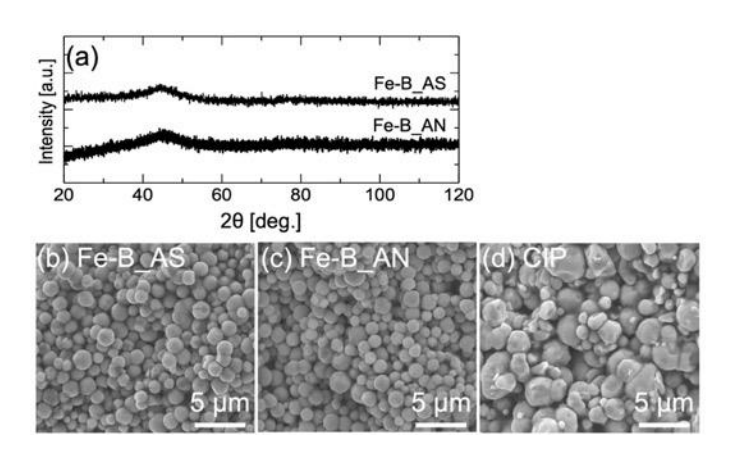


Fig. 1 (a) XRD patterns of Fe-B_AS and Fe-B_AN particles. Cross-sectional SEM images of cores made of (b) Fe-B_AS, (c) Fe-B_AN, and (d) CIP powder.

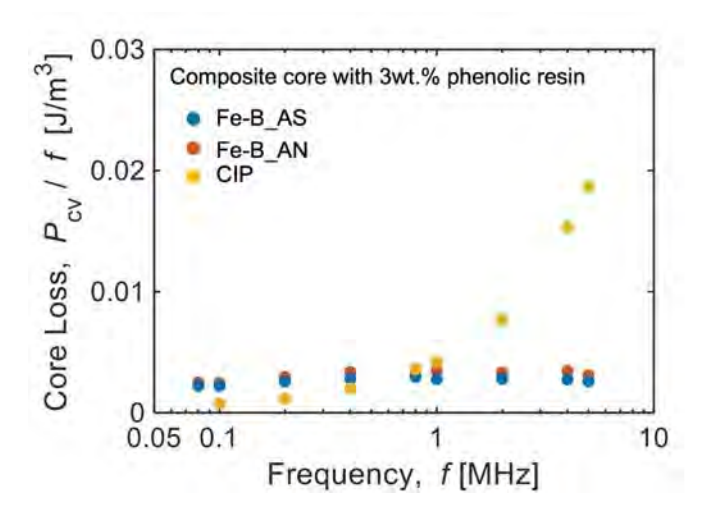


Fig. 2. Core loss of composite cores of Fe-B_AS and Fe-B_AN, comparing with that of CIP.

SESSION BE: MAGNETO-OPTIC AND MAGNETO-CALORIC MATERIALS AND DEVICES

Co-Chair(s): A. Biswas, *Ames National Laboratory, Ames, Iowa, United States* and M. Khan, *Physics, Miami University, Oxford, Ohio, United States*Tuesday, October 28, 2025
02:00 PM-05:30 PM

Room 2DE

BE-01. High-efficiency Optical Training of Spin Textures in 2D Magnets

C. Gong

University of Maryland, College Park, Maryland, United States

The emergent two-dimensional (2D) layered magnets [1, 2] provide ideal platforms for atomically thin magneto-optical devices. Though many have envisioned that 2D magnets can enable efficient control of magnetism by various external stimuli, true breakthroughs remain lacking. For example, circularly polarized pulses from ultrafast lasers with power density of ~107 uW/um² have been commonly employed for optical switching of magnetization in both traditional magnetic thin films and 2D layered magnets [3]. We proposed a new scheme [4] by optically modifying the magnetic phase transition kinetics, through which we achieved efficient control of magnetic domain formations by ultralow-power optical incidence on 2D magnets during zero-field cooling process. Our results show the continuous wave laser of only tens of uW/um² can effectively alter the domain behaviors. Specifically, the linearly polarized light

can enlarge the formed domains of both spins, while the circularly polarized light can lead to single domains with the spin orientation determined by optical helicity. The mechanism underlying such optical training of spin textures in 2D magnets relates to the optically excited spin polarized electrons as "magnetic seeds" for guiding the formation of single domains, which resembles chemical synthesis of using crystalline seeds to promote the single crystal growth. The high-efficiency optical training of 2D magnets potentially opens new avenues towards low-power spintronics and photonics.

- 1. C. Gong, et al. Nature 546, 265-269 (2017).
- 2. C. Gong, X. Zhang. Science 363, eaav4450 (2019).
- 3. P. Zhang, et al. Nature Materials 21, 1373-1378 (2022).
- 4. T. Xie, et al. Nature Physics (2025). DOI: https://doi.org/10.1038/s41567-025-02928-3.

BE-03. Stochastic magnetic tunnel junction arrays for infrared sensing

<u>A. Deka</u>², U. Singh¹, L. Bauer¹, M. Mousa¹, B. Prasad³, Z. Jacob¹

¹ECE, Purdue University, West Lafayette, Indiana, United States, ²Birck Nanotechnology Center, Purdue University, West Lafayette, Indiana, United States, ³Indian Institute of Science, Bangalore, India

Stochastic magnetic tunnel junctions (MTJ) are attractive for probabilistic computing due to their low energy barrier. This energy barrier of <10k_BT at room temperatures (k_B is Boltzman's constant and T is temperature) is of the same order of energies as long wave infrared (LWIR) photons emitted by objects near room temperature. Therefore, such MTJs can be used to detect LWIR at room temperatures, which otherwise require highly specialized cryocooled detectors. We recently demonstrated detection of LWIR using such an uncooled spintronic bolometer (ref 1). The wavelength of absorbed IR radiation is controlled using nanoplasmonic antennas over the MTJ, which leads to an increase in temperature near the transduction layer. Effectively, this increase in temperature changes the count rate of the stochastic MTJ which enables us to convert the LWIR absorption into a readable electrical signal.

Modern practical bolometers prefer a high-speed CMOS compatible scalable pixel array for thermal imaging that operates at room temperature. In this presentation I will talk about our prototype demonstration of fabrication and

readout from a stochastic MTJ-based bolometer array containing 4 pixels (ref 2). As shown in Fig.1, our prototype shows an experimentally measured Noise Equivalent Differential Temperature (NEDT) of <1 K. This demonstrates that our uncooled spintronic bolometer array can detect a < 1°C temperature change in an object at room temperature. This is an important development for efficient thermal imaging at room temperatures, without the need for cryogens.

- 1. L. Bauer, A. Deka et al. Nano Letters *25* (14), 5599-5608, 2025.
- 2. U. Singh, A. Deka et al., Stochastic spintronic arrays for long wave infrared bolometry (to be submitted)

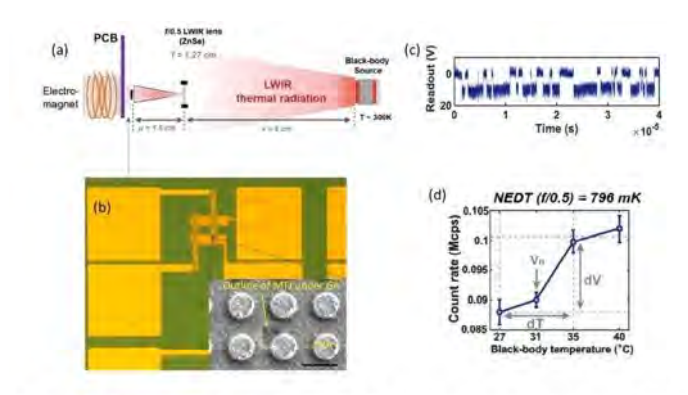


Figure 1 (a) Experimental setup to detect LWIR. (b) Bolometer array is loaded on the PCB for measurements. (c) A readout signal from one pixel when blackbody source is at 27°C. (d) Count rate vs blackbody temperature used for estimation of Noise Equivalent Differential Temperature (NEDT) = 0.796°C.

BE-04. Multi-Lanthanide Metal-Organic Frameworks: From Multifunctional Magnetic Materials to Quantum Applications

E. Bartolomé¹, X. Liu¹, A. Arauzo³, Z. Li², J. Giner-Planas¹

¹Institut de Ciència de Materials de Barcelona (ICMAB),
Barcelona, Spain, ²Shandong Provincial Key Laboratory of
Monocrystalline Silicon Semiconductor Materials and
Technology, Dezhou University, Dezhou, China, ³Condensed
Matter Physics, Instituto de Nanociencia y Materiales de Aragón
(INMA)-Universidad de Zaragoza, Zaragoza, Spain

Lanthanide-based Metal-Organic Frameworks (Ln-MOFs) are emerging as versatile platforms for numerous applications, in information storage and processing, luminescence, thermometry, magnetic refrigeration etc. Recently, we achieved the unprecedented synthesis of multivariate carborane-based MOFs incorporating tunable combinations of multiple lanthanides in controlled ratios [1], opening new directions in the study of "complex magnetic materials" and the design of new materials with tailored functionalities [2,

3]. Here, we highlight the potential of our strategy through selected examples, including: the first MOF containing eight different Ln ions (Dy, Tb, Gd, Ce, Yb, Eu, La, Y) [1]; multifunctional {GdLn} (Ln=Tb, Eu, Tb/Eu) MOFs combining magnetocaloric effect (MCE), Single-Molecule Magnet (SMM) and luminescent properties [4]; {Nd/Yb} magnetic and NIR emissive MOFs; and a {Gd₃} "quMOF" shaping a record 512-level qudit for Quantum Computing [5] (Figure 1). Magneto-thermal properties were studied by dc/ac magnetometry, heat capacity, pulsed EPR and XAS-XMCD; the latter was key for characterizing the spectroscopic, magnetocaloric, and magnetic properties of individual Ln ions in these multivariate MOFs.

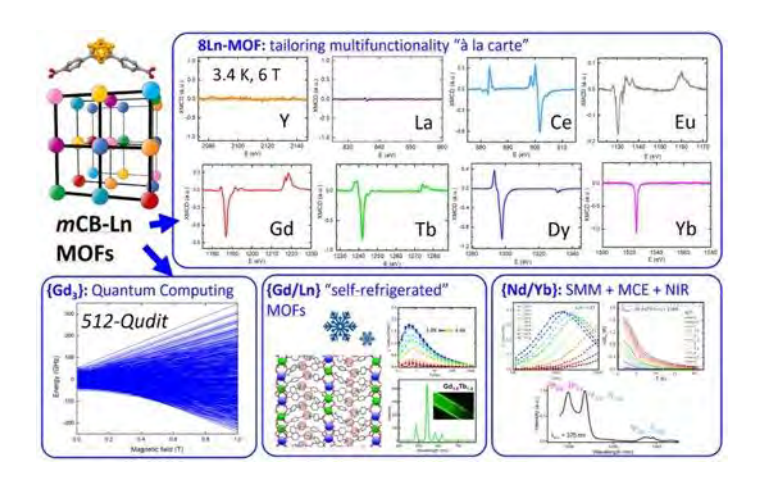
[1] E. Bartolomé*, José Giner Planas* et al., Adv. Func. Mat., vol. 33, p. 1 (2023)

[2] C. Roscini*, J. Giner Planas* *et al., Chem. Mater.*, vol. 34, p. 4795 (2022)

[3] J. Giner Planas*, E. Bartolomé* et al., Dalton Trans., vol., 53, p. 8969 (2024)

[4] J. Giner Planas*, E. Bartolomé* et al., J. Mater. Chem. A, vol., 12, p. 21971 (2024)

[5] E. Bartolomé,* J. G. Planas*, et al., ACS Appl. Mat.&Interf., accepted, in press (June 2025)



Multi-lanthanide carborane-based MOFs enabling a range of multifunctional magnetic molecular materials

BE-07. Theoretical Modeling of Magnetocaloric Effect During Hexagonal-Orthorhombic Phase Transition

<u>A. Kosogor</u>^{1, 2, 3}, D. Böhm¹, T. Schrefl¹
¹University for Continuing Education Krems, Krems,
Austria, ²Faculty of Physics, University of Vienna, Vienna,
Austria, ³V.G. Baryakhtar Institute of Magnetism of the NAS of
Ukraine, Kyiv, Ukraine

The first-order magnetostructural phase transition from a paramagnetic hexagonal phase to a ferromagnetic orthorhombic phase is characteristic of many magnetic solids and is considered promising for achieving a giant magnetocaloric effect (MCE) [1]. Understanding the thermodynamics of this transition is essential for controlling phase stability, minimizing hysteresis, and predicting the entropy change associated with the transition.

A general theoretical framework is presented to describe the hexagonal—orthorhombic phase transition using a Landau-type phenomenological model. The elastic free energy is expanded in terms of order parameters expressed through the strain components [2]. The elastic energy includes contributions from both shear and deviatoric strains, as well as volume changes, with temperature-dependent coefficients determining the stability limits of each phase.

The framework enables computation of heat flow and entropy change associated with the structural transition by relating the evolution of free energy to temperature. Using model functions for the temperature-dependent elastic coefficients, it is possible to simulate the thermal behavior of the system, including latent heat and entropy change [3]. The magnetic subsystem is incorporated by introducing a magnetoelastic coupling and magnetic free energy term for second-order paramagnetic –ferromagnetic transitions. This allows the computation of magnetic-field induced entropy change and adiabatic temperature change during magnetostructural phase transition. Moreover, this approach enables a separation of magnetic and structural contributions to MCE, supporting a deeper understanding of magnetostructural coupling mechanisms.

Acknowledgement: This research was funded by the European Innovation Council, funded by the European Union, through project CoCoMag (Grant No. 101099736).

- [1] N.T. Trung et al., Appl. Phys. Lett. 96, 172504 (2010).
- [2] V.A. Chernenko et al., Metals 3, 237 (2013).
- [3] A. Kosogor et al., Phys. Stat. Sol. (b), 252, 2758 (2015).

BE-08. From Concept to Operation: Design Strategies, Experimental Evaluation, and Engineering Challenges across Three Generations of a Magnetocaloric Air Conditioner* G. Fidelis Peixer^{2*}, A. Lorenzoni², P. Vitor de Faria², D. D.

Reif³, A. T. Dias Nakashima², C. Silva Teixeira³, J. A. Lozano², J. Riso Barbosa Jr.^{1, 2}

¹Craft & Hawkins Department of Petroleum Engineering, Louisiana State University, Baton Rouge, Louisiana, United States, ²POLO - Research Laboratories for Emerging Technologies in Cooling and Thermophysics,, Federal University of Santa Catarina, Florianópolis, Santa Catarina, Brazil, ³Lab3M - Laboratory of Magnetism and Magnetic Materials, Federal University of Santta Catarina, Blumenau, Santa Catarina, Brazil

Heating, refrigeration, and air conditioning (HVAC) systems account for 7.8% of global greenhouse gas emissions and 20% of global electricity consumption. Moreover, the demand for air conditioning is expected to triple by 2050. Magnetocaloric technology has emerged as a promising alternative, with the potential to eliminate the use of volatile fluids and reduce energy consumption. This study presents the design strategies, experimental evaluation, and key insights from the development and operation of a pilotscale magnetocaloric air conditioner. The system was designed and optimized using artificial neural networks (ANNs) and genetic algorithms (GAs) (Peixer et al., 2023a), and incorporates a rotor-stator magnetic circuit (Cattelan et al., 2024), La(Fe,Mn,Si)13Hz refrigerants (Döring et al., 2024), and tube-fin heat exchangers (Peixer et al., 2022). A photo of the system is shown in Fig. 1. Three prototype generations were designed and commissioned (Peixer et al., 2023b; Peixer et al., 2024), each incorporating modifications based on operational constraints. The performance evaluation, shown in Fig. 2, highlights this prototype as achieving one of the highest cooling capacities and temperature spans reported in the literature. Additionally, it is the only system reported to successfully refrigerate a cold room without emulating the thermal load using electric heaters. The first-generation prototype delivered the best performance, achieving the temperature spans required for air conditioning (22 °C to 35 °C), although its cooling power was limited to a peak of 480 W. While magnetocaloric systems show considerable potential, losses in auxiliary components and the limited durability of magnetocaloric materials remain major challenges. These results underscore both the progress made and the obstacles that must still be overcome to advance this technology.

A.M. Döring, C. de Amorim et al. J. Magn. Magn. Mater., Vol. 591, p.171721 (2024)

G.F. Peixer, S.L. Dutra et al., Ann. Acad. Bras. Cienc., Vol. 94 (2022)

G.F. Peixer, M. Nakashima, et al., Appl. Therm. Eng., Vol. 227, p.120368 (2023a)

G.F. Peixer, M.C. Silva, A. M. Lorenzoni, et al., Int. J. Ref., Vol. 151, p.1 (2023b)

G.F. Peixer, A.M. Lorenzoni, et al., Int. J. Ref. (2024)

L.F. Cattelan, G.F. Peixer, et al., IEEE Trans. Magn. (2024)

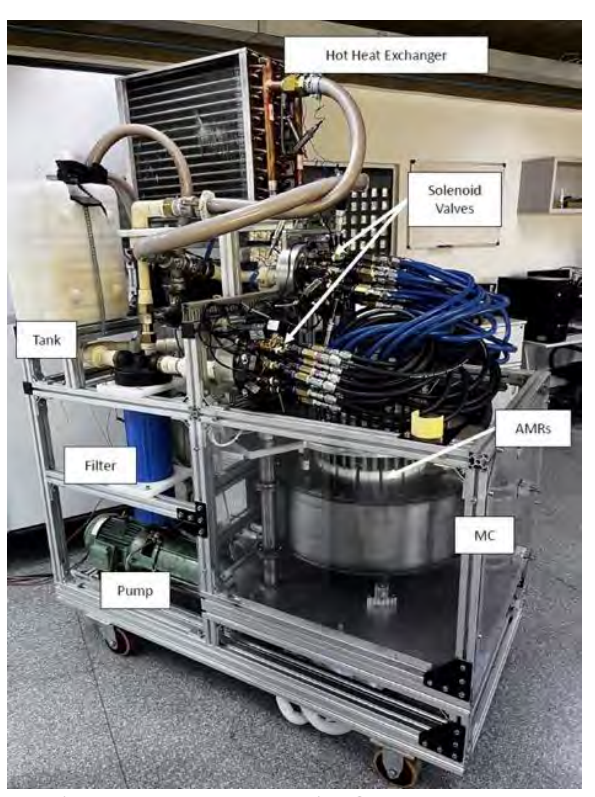


Fig. 1 The Magnetocaloric Air Conditioner and its main components.

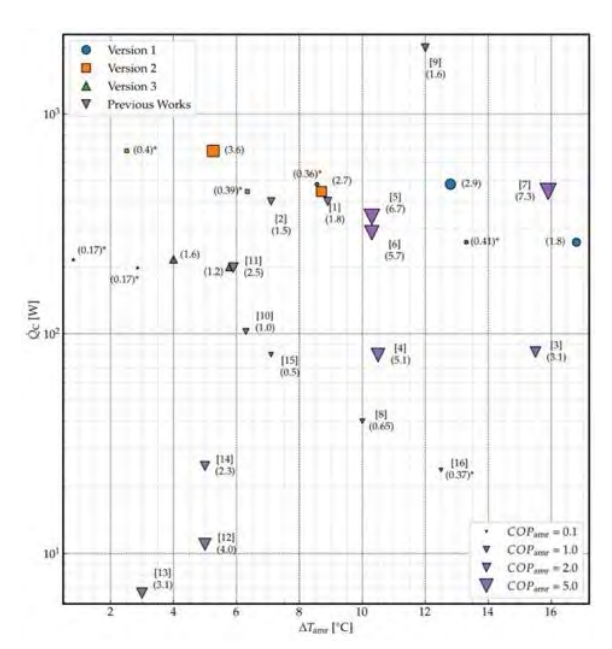


Fig. 2 Comparisson between the performance of the 3 versions of the system and selected prototypes presented in the literature (references omitted for the sake of word limitation).

BE-10. Magnetic and magnetocaloric properties of the new $Gd_3Co_{1+x}Ni_{1-x}$ solid solution

A. Herrero¹, A. Provino^{2, 3}, I. Aseguinolaza¹, S. De Negri², D. Peddis^{2, 4}, P. Manfrinetti^{2, 3}, <u>A. Oleaga</u>¹

¹University of the Basque Country, Bilbao, Spain, ²Department of Chemistry, University of Genova, Genova, Italy, ³CNR, Institute SPIN, Genova, Italy, ⁴CNR, Institute of Structure of Matter, Genova, Italy

A comprehensive analysis of the crystallographic, magnetic, and magnetocaloric properties of the new rare-earth based $Gd_3Co_{1+x}Ni_{1-x}$ intermetallic compound (with $x=0.1,\,0.2,\,0.3,\,$ and 0.4) has been performed. This novel solid solution adopts the orthorhombic Y_3Co_2 -type structure (oP20-Pnnm) [1], which has not previously been reported for any compound other than the prototype.

The compound exhibits a second-order magnetic phase transition from a paramagnetic to a ferromagnetic state (PM-FM), confirmed by positive slopes in Arrott plots, the absence of magnetic hysteresis, the existence of universal curves and the behavior of the magnetocaloric n exponent. Increasing the Co content leads to a higher Curie temperature (Tc), shifting the peak of the magnetic entropy change to higher temperatures. This demonstrates the tunability of the working temperature region from

approximately 177 K (for $Gd_3Co_{1.1}Ni_{0.9}$) to 186 K (for $Gd_3Co_{1.4}Ni_{0.6}$). Analysis of the critical behavior indicates that the critical exponents are close to the 3D Heisenberg model, suggesting short-range order isotropic magnetic interactions. The reliability of the determined critical exponents is robustly supported by a correct scaling of magnetocaloric properties.

Regarding the magnetocaloric properties, the Gd₃Co_{1+x}Ni_{1-x} family exhibits competitive performance. For an applied magnetic field change of $\mu_0\Delta H = 5$ T, the magnetic entropy change peaks ($|\Delta S^{pk}_{M}|$) range between 7.81 and 8.40 J kg⁻¹ K⁻¹, and the refrigerant capacity values are approximately 600 J kg⁻¹. Crucially, the magnetocaloric properties remain well preserved across the different compositions, despite the shift in T_c. This allows for a significant tuning of the working temperature region by almost 40 K (from 147 K for Gd₃Ni₂ to 186 K for Gd₃Co_{1.4}Ni_{0.6}) solely by adjusting the Co/Ni concentration. These results underline the potential of the Gd₃Co_{1+x}Ni_{1-x} family as a promising candidate for efficient and sustainable magnetocaloric refrigeration technologies, allowing the precise selection of the working temperature by compositional tuning without affecting the overall magnetocaloric properties.

[1] J. M. Moreau, E. Parthé, D. Paccard. *Acta Crystallogr. B* (1975) 31, 747-749.

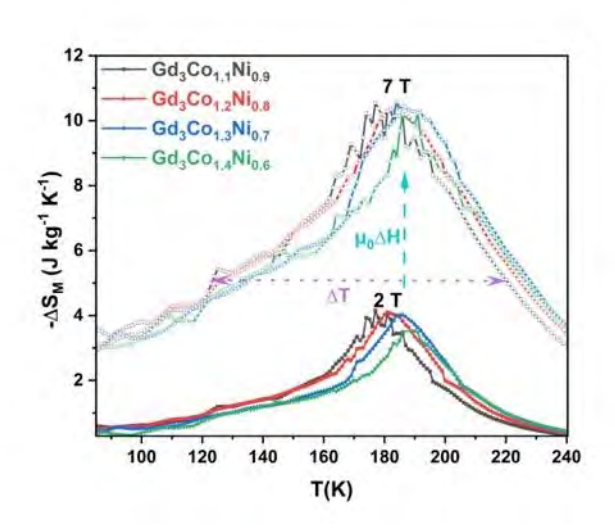


Fig. 1: Magnetic entropy change for $Gd_3Co_{1+x}Ni_{1-x}$ with $\mu_0\Delta H$ = 1-6.9 T.

BE-13. Magnetocaloric Properties of $Gd_{1-x}Er_xNiAl$ Alloys near Hydrogen Liquefaction Temperatures

P. Chaitanya¹, <u>A. Kumar</u>², L. Patra^{3, 4}, J. P. Nunez¹, E. R. Canavan⁵, B. Liao⁴, M. J. Dipirro⁵, Y. Mudryk², R. L. Hadimani¹ Department of Mechanical and Nuclear Engineering, Virginia Commonwealth University, Richmond, Virginia, United States, ²Ames Laboratory, Iowa State University, Ames, Iowa, United States, ³Department of Mechanical Engineering, Georgia Institute of Technology, Atlanta, Georgia, United States, ⁴Department of Mechanical Engineering, University of California, Santa Barbara, Santa Barbara, California, United States, ⁵Cryogenics and Fluids Branch, Code 552, NASA Goddard Space Flight Center, Greenbelt, Maryland, United States

The rare-earth intermetallic GdNiAl offers a tunable magnetic transition, which can be tailored via Er substitution. We investigate the magnetocaloric properties of $Gd_{1-x}Er_xNiAl$ (x = 0, 0.20, and 0.50) alloys for potential application in cryogenic magnetic refrigeration near hydrogen liquefaction temperatures. Structural analysis confirms that the alloys crystallize in the hexagonal ZrNiAltype structure across all compositions. Systematic tuning of the Curie temperature (T_c) from 57 K for x=0 to 33 K for x=0.50 is observed with increasing Er concentration, enabling control over the operational window for refrigeration. All compositions undergo a 2nd-order magnetic phase transition, as verified by modified Arrott plots. Interestingly, the magnetic entropy change (ΔSm) measured under applied fields demonstrates a substantial magnetocaloric effect (MCE) across all samples and reveals an enhancement in Δ Sm with Er substitution. At x = 0.5, a maximum ΔSm of ~12 J/kgK is observed at 23 K, compared to $\sim 10 \text{ J/kgK}$ at 57 K for x = 0, making these alloys particularly suitable for hydrogen liquefaction applications. Numerical modeling employing mean-field theory and scaling analysis accurately reproduces experimental trends and predicts a peak Δ Sm of ~14 J/kgK at 5 T for x = 0, slightly exceeding the experimental value of ~11 J/kgK. This agreement validates the theoretical framework. We conclude that Er substitution in GdNiAl enables effective tuning of both T_C and magnetocaloric performance, underscoring the suitability of Gd_{1-x}Er_xNiAl as promising candidates for adiabatic demagnetic refrigeration and deepspace cryogenic systems.

RLH acknowledges funding support by the NASA Grant #80NSSC24PB625. LP and BL acknowledge the funding support from the NASA Early Career Faculty program under

the award number 80NSSC21K1812. These samples were prepared at Ames National Laboratory and supported by DMSE, BES, Office of Science, U.S. DOE. Ames Lab is operated for the DOE by Iowa State University under Contract No. DE-AC02-07CH11358.

- [1] Agurgo Balfour E, Ma Z, Fu H, et al. Table-like magnetocaloric effect in Gd56Ni15Al27Zr2 alloy and its field independence feature. *Journal of Applied Physics*. 2015;118(12):123903. doi:10.1063/1.4931765
- [2] Dembélé SN, Ma Z, Shang YF, et al. Large magnetocaloric effect of GdNiAl2 compound. *Journal of Magnetism and Magnetic Materials*. Published online May 2015. doi:10.1016/j.jmmm.2015.05.005
- [3] Mudryk Ya, Paudyal D, Pecharsky V, Gschneidner K. Low-temperature crystal structure and magnetic properties of Gd_{5}Ge_{3}. *Physical Review B*. 2012;85(1). doi:10.1103/PhysRevB.85.014116
- [4] Korte BJ, Pecharsky VK, Gschneidner KA Jr. The correlation of the magnetic properties and the magnetocaloric effect in (Gd1–xErx)NiAl alloys. *Journal of Applied Physics*. 1998;84(10):5677-5685. doi:10.1063/1.368830

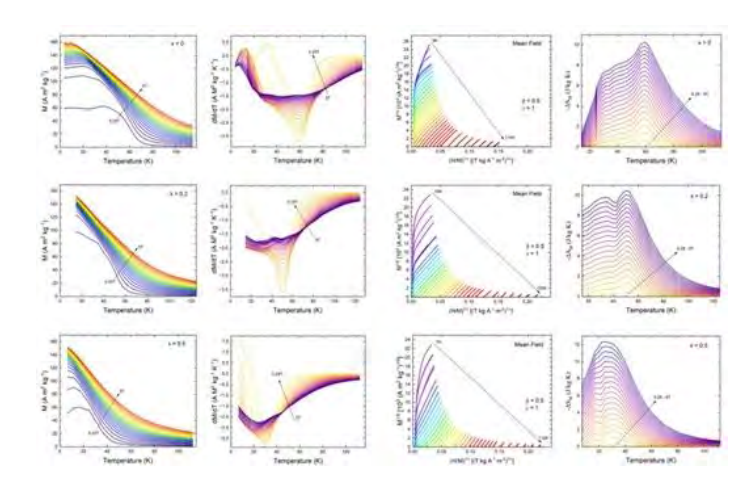


Fig. 1 (a)-(c) Magnetization at different fields, (d)-(f) temperature derivative of the magnetization. (g)-(i) The modified Arrott plots (j)-(l) normalized Δ Sm vs temperature.

SESSION BF: STT-MRAM AND SOT-MRAM AND RELATED DEVICES

Chair(s): D. Kim, Department of Materials Science and Engineering, KAIST, Daejeon, Korea (the Republic of) Tuesday, October 28, 2025 02:00 PM-05:30 PM Room 2BC

BF-01. Energy Efficient Spintronic Devices for Memory and Computing by New Materials, New Physics and Voltage Control

J. Wang^{1, 2, 3}, Y. Yang¹, Y. Chen¹, Q. Jia¹, S. Lee¹, T. Low¹, O. Benally¹, B. Dixit¹, D. Sousa¹, T. Peterson³, D. Lyu¹, M. Odlyzko⁴, J. Garcia-Barriocanal⁴, G. Yu⁴, G. Haugstad⁴, Y. Fan¹, Y. Huang¹, Y. Lv¹, S. Liang², B. Zink¹, Z. Cresswell²
¹Electrical and Computer Engineering, University of Minnesota, Minneapolis, Minnesota, United States, ²Chemical Engineering and Materials Science, University of Minnesota, Minneapolis, Minnesota, United States, ³Physics, University of Minnesota, Minneapolis, Minnesota, United States, ⁴Characterization Facility, University of Minnesota, Minneapolis, Minnesota, United States

Spin-orbit torque (SOT) is a promising mechanism for nextgeneration memory and logic devices that could surpass traditional CMOS technology. However, the low SOT efficiency and the need for an external magnetic field in existing materials have limited industrial adoption. To overcome these challenges, we proposed and experimentally demonstrated new SOT materials and voltage-controlled device architectures. In this talk, I will first focus on Ni₄W, a newly identified unconventional SOT material with high efficiency and intrinsic field-free switching capability. These properties arises from Ni₄W's low crystalline symmetry, which enables spin polarization along multiple directions and breaks the system's symmetry. Epitaxial Ni₄W thin films with high crystalline quality were grown using magnetron sputtering. Harmonic Hall measurements revealed a Y-spin SOT efficiency of 0.73 and a Z-spin efficiency of 0.02 at room temperature—among the highest for unconventional SOT materials reported [1]. We further demonstrated deterministic field-free switching of perpendicular magnets with 40% lower current density than Pt.

In the second part of the talk, I will introduce our work on voltage-controlled spintronic devices, utilizing a newly proposed electron-depletion-based voltage-controlled magnetic anisotropy (ED-VCMA) and a recently demonstrated new switching mechanism: voltage-controlled

* Best Student Presentation Finalist / LB – Late-breaking Poster

exchange coupling (VCEC). VCMA is a well-known solution for achieving low switching current by reducing the energy barrier of the ferromagnetic material through the application of an additional electric field. By applying electron depletion physics with a work-function-engineered underlayer, the VCMA coefficient can be further enhanced [2]. VCEC is a mechanism by which an applied voltage modulates both the direction and strength of interlayer magnetic exchange interactions. By integrating VCEC into a superparamagnetic magnetic tunnel junction (MTJ), we demonstrate device-level bipolar switching with an associated power consumption of only 40 nW, about two orders of magnitude lower than that of spin-transfer torque (STT) switching [3].

- [1] Y. Yang et al., Advanced Materials, p. 2416763 (2025).
- [2] Y.-C Chan et al. ACS nano 19.16, 15953-15962. (2025).
- [3] Q. Jia et al., Nano Letter, 25 (23), 9181-9188 (2025).

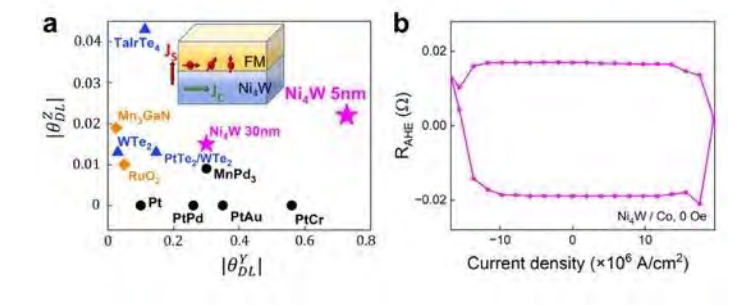


Fig. 1. (a) Summary of conventional () and out-of-plane () SOT efficiencies of Ni₄W and state-of-the-art SOT materials. The inset shows the generation of spins along all X, Y, and Z directions by Ni₄W. (b) Deterministic field-free switching of a perpendicular magnet at room temperature using the multi-directional spin components of Ni₄W.

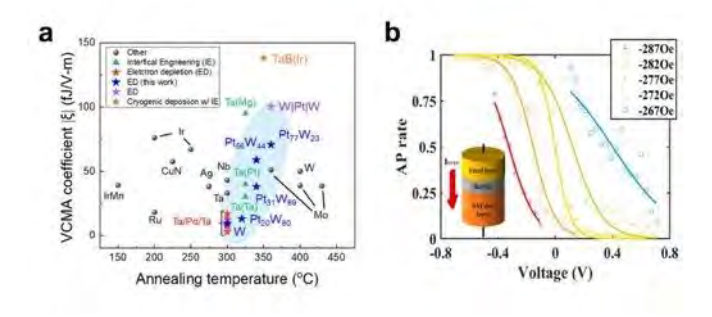


Fig. 2. (a) Benchmarking of the VCMA coefficients in the PMA CoFeB/MgO system with various underlayer materials. (b) The antiparallel (AP) switching rate of the stochastic signal manipulated by VCEC. The inset illustrates the VCEC-integrated superparamagnetic MTJ (sMTJ) structure.

BF-02. Large Voltage-Controlled Magnetic Anisotropy in 3X-nm Perpendicular Magnetic Tunnel Junctions

<u>J. G. Athas</u>¹, C. Duffee¹, T. Neuner¹, N. Davila², J. Katine², P. Khalili Amiri¹

¹Electrical and Computer Engineering, Northwestern University, Evanston, Illinois, United States, ²Western Digital Corporation, San Jose, California, United States

Voltage-controlled magnetic anisotropy (VCMA) enables highly energy-efficient switching in perpendicular magnetic tunnel junctions (pMTJs), but reliable low-voltage switching by VCMA in sub-50 nm devices remains challenging [1,2]. We present the first statistical study of 20 CoFeB/MgO-based 3X-nm pMTJs exhibiting large VCMA coefficients (mean $\xi\approx 106$ fJ/Vm), high tunneling magnetoresistances, and robust switching performance across a single wafer. Devices were patterned into 30 to 36 nm diameter circles and subjected to sub-nanosecond voltage pulses. Bidirectional switching was achieved with pulses as short as 450 ps, and three devices exhibited write error rates (WER) below 10^{-3} (Fig. 1).

The voltage-induced modulation of anisotropy energy was quantified using two independent methods: (i) Using experimentally measured switching threshold voltages and (ii) using direct dwell-time-based energy barrier analysis under varying DC bias. Both approaches yielded consistent large ξ values. Average switching voltages were below 2 V, and measured write energies as low as 7 fJ were measured (Fig. 2).

Endurance testing up to 2×10^{10} switching cycles showed no degradation in TMR or resistance states. The switching data fits well with a single-domain reversal model [3]. This work demonstrates the viability of 3X-nm high-VCMA coefficient pMTJs for memory and probabilistic computing applications, establishing reproducible high-performance switching behavior at scaled dimensions.

[1] Y. Shao, V. Lopez-Dominguez, and P. Khalili Amiri,
Communications Materials, Vol. 3, p. 87 (2022)
[2] Y. Shao and P. Khalili Amiri, Advanced Materials
Technologies, Vol. 8, p. 2300676 (2023)
[3] P. Khalili Amiri, P. Upadhyaya, and K. L. Wang, Journal of applied Physics, Vol. 113, p. 013912 (2013)

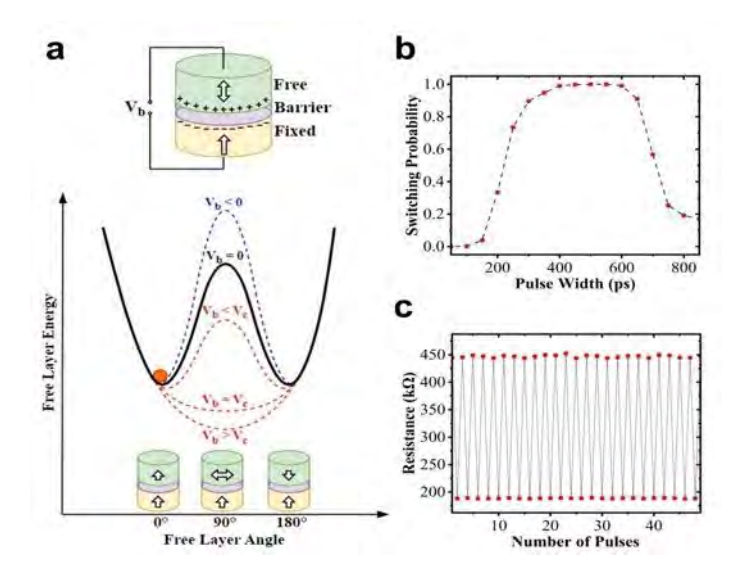


Fig. 1, (a) Illustration of a VCMA MTJ energy diagram under different applied voltages. (b) Measured switching probability at different voltage pulse durations. Each data point consists of 10³ switching attempts. (c) Measured resistance after 50 consecutive voltage pulses, each with a duration of 500 ps.

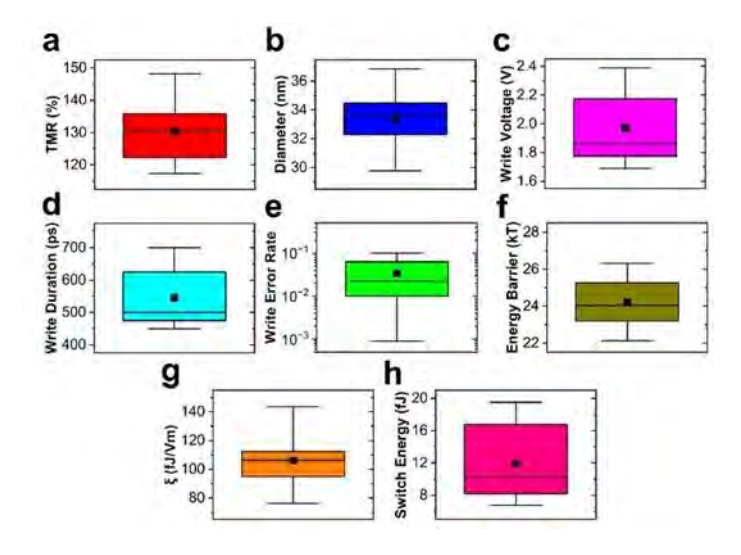


Fig. 2, Box and whisker diagram of device statistics across 20 different VCMA MTJs. The measured characteristics include (a) TMR, (b) diameter, (c) write voltage amplitude and (d) width, (e) WER, (f) energy barrier, (g) calculated VCMA coefficient for > 90% switching success, and (h) switching energy.

BF-03. Improved VCMA Coefficients in Perpendicular MRAM Measured With Device-Level Spin-Torque Ferromagnetic Resonance

R. V. Chopdekar, H. J. Richter, J. Li, T. Santos Western Digital Research Center, Western Digital Corporation, San Jose, California, United States

To reduce energy and switching time needed to reverse the free layer in magnetic random access memory (MRAM) devices, alternatives to spin-transfer torque such as voltage control of magnetic anisotropy (VCMA) have been explored in recent years. Upon application of voltage, charge accumulation or depletion at the ferromagnet-insulator interface modifies the electron occupancy of interfacial d orbitals of different symmetries, which results in a modulation of magnetic anisotropy energy (MAE). Insertion of atoms at the interface have increased the VCMA coefficient, shown in both theory and in experiment [1-5]. VCMA as an assist mechanism in switching of spin-orbit torque based devices has also been proposed [6], necessitating the use of a top-pinned MRAM structure, but it is not clear if microstructural differences between toppinned and bottom-pinned devices affect VCMA-induced free layer switching.

Using spin-torque ferromagnetic resonance (ST-FMR) [7], we have characterized the effect of heavy metal insertion layers (e.g. Ir and Pt-Ir alloy) at the interface between the MgO barrier and the free layer, in both bottom-pinned and toppinned 75 nm diameter perpendicular MRAM devices. Blanket film FMR measurements show that addition of heavy metal dusting increases damping by up to a factor of two, but inhomogeneous line broadening remains less than 100 Oe, indicating that macroscopic free layer uniformity is similarly high for all samples. An example ST-FMR dataset is shown in Fig. 1, in which the Pt-Ir insertion layer significantly increases the change in resonance frequency per applied voltage. We have measured a doubling of the VCMA coefficient with Pt-Ir insertion, and the improvement of VCMA coefficient is comparable for bottom- and toppinned devices. This confirms that heavy metal insertion is effective for boosting VCMA coefficient, independent of any growth-order induced microstructural non-idealities for the two different film stacking orders.

- 1. T. Nozaki et al., NPG Asia Mater. 9, e451 (2017)
- 2. Y. Jibiki et al., Appl. Phys. Lett. 114 082405 (2019)
- 3. R. Carpenter et al., IEDM21-394 (2021)
- 4. A. Khandelwal, R. V. Chopdekar et al., APL Mater. 13 061119 (2025)

5. B. Prasad et al. (manuscript in preparation)
6. Y.C. Wu et al., Phys. Rev. Appl. 15 064015 (2021)
7. H. J. Richter, G. Mihajlović, R. V. Chopdekar et al., J. Appl. Phys. 136 113902 (2024)

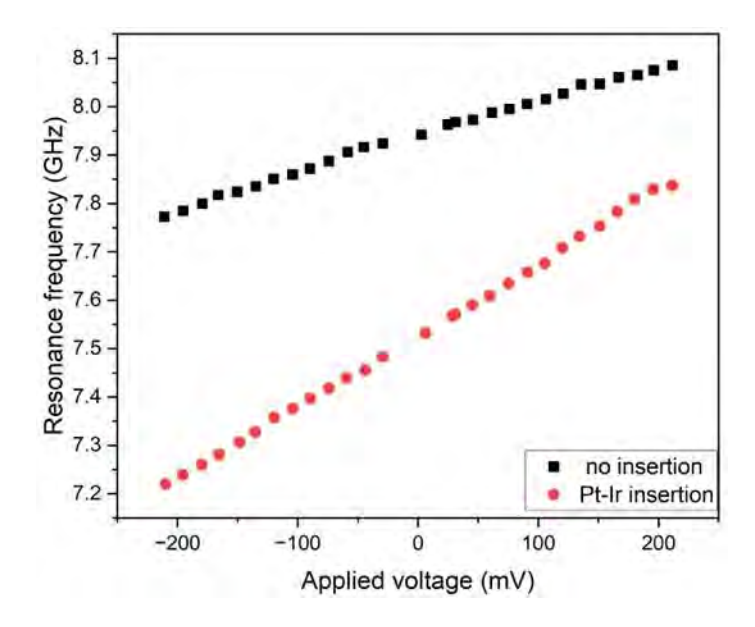


Fig. 1 – Change of ferromagnetic resonance peak for two bottom-pinned MRAM devices as a function of applied bias as measured with ST-FMR, indicating higher VCMA coefficient with heavy metal insertion.

BF-04. Spin transfer torque switching in double magnetic tunnel junctions based on dual MgO layers

W. Jung, G. Mihajlović, <u>R. V. Chopdekar</u>, J. Lille, M. Grobis, T. Santos

Western Digital, San Jose, California, United States

The double magnetic tunnel junction (DMTJ) has been proposed as an alternative spin transfer torque (STT) magneto-resistive random access memory (MRAM) design that can achieve lower write currents than a conventional single MTJ (SMTJ) having one reference layer (RL) [1]. A DMTJ cell consists of two RLs, one below (RL1) and one above (RL2) the free layer (FL) (Fig.1a). For antiparallel magnetization orientations of the RLs, the spin torques exerted on the FL add constructively, resulting in reduction of the switching current I_c.

While up to 2X lower I_c has been reported for DMTJs [2], the challenge has been to achieve simultaneously low I_c and high tunnel magnetoresistance ratio (TMR). Reducing resistance and TMR of the top tunnel junction by employing

a thin MgO2 improves total TMR, but as reported in [2], doing so results in less effective I_c reduction. Alternatively, replacing MgO2 by a low-resistance non-MgO spacer layer can reduce I_c while minimizing TMR dilution [3], but the FL has a low coercive field H_c and thus low thermal stability due to absence of interfacial perpendicular anisotropy from MgO2. An additional challenge for the DMTJ structure is to achieve sufficient stability of RL2, due to lack of proper seeding and roughness as grown on top of the FL and MgO2.

In this talk we will present fabrication of DMTJ cells with electrical diameter of about 65nm and with MgO2 having much lower RA than MgO1 (refer to Fig.1a). Our DMTJs exhibit high overall TMR > 120% while still showing very efficient 2X reduction of $I_{\rm c}$ compared to SMTJ (Fig.1c). We demonstrate $H_{\rm c}$ values > 2kOe for the FL at room temperature and excellent magnetic stability of RL2, with pinning field exceeding 6kOe (Fig.1b). Our experimental study and analysis of switching shows that $I_{\rm c}$ in such DMTJs is the result of combined STT effects of individual RLs, with tunneling and spin-valve-like contributions adding constructively. Our work shows that efficient reduction of $I_{\rm c}$ can be achieved in DMTJs with dual MgO barriers where one of the barriers has significantly lower RA to enable high TMR [4].

- 1) D. C. Worledge and G. Hu, MRS Adv. 8 (2023) 131.
- 2) G. Hu et al., 2021 IEDM (2021) 2.5.1.
- 3) G. Hu et al., 2022 IEDM (2022) 10.2.1.
- 4) G. Mihajlović et al., Appl. Phys. Lett. 126 (2025) 022403.

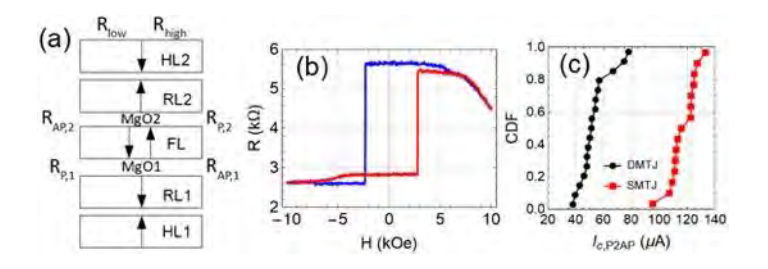


Fig 1. (a) Illustration of magnetic and MgO layers in DMTJ. (b) R vs H measured for an exemplary DMTJ cell. (c) Switching currents for SMTJ and DMTJ.

BF-05. Perpendicular Magnetic Tunnel Junction with Co-Nibased Synthetic Antiferromagnet

W. Skowronski¹, M. Cierpial¹, D. Maslanka¹, K. Gubala¹, J. Mojsiejuk¹, K. Grochot¹, J. Wrona², J. Langer², T. Nan³

¹Institute of Electronics, AGH University of Krakow, Krakow, Poland, ²Singulus Technologies, Kahl am Main, Germany, ³School of Integrated Circuit, Tsinghua University, Beijing, China

Magnetic tunnel junctions (MTJ)s used currently in storage applications are characterized by perpendicular magnetic anisotropy (PMA), which enhances thermal stability, enables small footprint of the memory device and reduces the critical current density needed for the magnetization switching using spin-transfer torque (STT) effect [1]. Fixing the reference magnetic layer typically requires perpendicular synthetic antiferromagnetic (SAF) structure, which involves Pt- or Pd-based materials to obtain sufficiently large anisotropy field of a few hundreds of mT. Yet, Pt and Pd are among the least abundant materials in the world, therefore, there is a need for alternative ways to create a reliable reference magnetic structure. In the current work, we present an alternative way to design the MTJ structure, which does not involve any less-abundant material. The reference layer is based on Ni-Co superlattice [2], coupled via 0.9 nm thick Ru spacer resulting in strong antiferromagnetic coupling. The full structure contains buffer/SAF/RL/MgO/FL/capping. Both free and reference layers (FL, RL) are based on FeCoB alloy, which ensures small magnetization damping and high PMA energy with an additional atomically thin W interlayer [3] within synthetic FL. On the wafer-level, ferromagnetic resonance measurement enabled determination of the magnetic anisotropy fields of $\mu_0H_K = 145$ and 223 mT, for FL and RL, respectively, as well as magnetization damping of α = 0.011-0.013, both showing high potential for storage application.

Test devices were fabricated using electron beam lithography and lift-off process with circular cross section between 500 and 80 nm in diameter. MTJs showed the TMR of up to 140%, thermal stability exceeding $\Delta > 50$ depending on the pillar size and thickness of the FL. Using current pulses down to 5 ns in length, the switching current density J < $3\times10^6 \text{A/cm}^2$ was measured [4].

Acknowledgements

Project supported by the National Science Centre, Poland grant no. 2021/40/Q/ST5/00209, Excellence initiative-research university programme of the AGH University of Krakow and Funded by the European Union under

^{*} Best Student Presentation Finalist / LB - Late-breaking Poster

NICKEFFECT project, GA number 101058076

- [1] S. Ikeda et al. Nat. Mater. 2010, 9, 721
- [2] Daalderop et al. Phys. Rev. Lett. 1992, 68, 682
- [3] W. Skowronski et al. Sci. Reports 2017, 7, 10172
- [4] M. Cierpial et al. Sci. Reports submitted 2025

BF-06. Electrical Detection of Synthetic Antiferromagnet States via Tunnel Magnetoresistance

<u>D. Giuliano</u>^{1, 2}, B. Vermeulen^{1, 2}, V. Kateel¹, G. Talmelli¹, M. Gama Monteiro¹, S. Rao¹, C. Fleischmann^{1, 2}, K. Temst^{2, 1}, V. Nguyen¹

¹Imec, Leuven, Belgium, ²Physics and Astronomy, KU Leuven, Leuven, Belgium

Synthetic antiferromagnets (SAFs), composed of two magnetic layers antiferromagnetically coupled via a non-magnetic spacer, are promising materials for spintronics applications due to their fast switching, thermal stability, and resilience to external perturbations [1,2]. They have been studied for enabling spin-orbit torque (SOT) switching [1] and efficient domain wall and skyrmion motion [2,3]. However, electrically detecting SAF magnetic states at the nanoscale remains a key challenge.

The antiparallel alignment of SAF sub-layers results in a reduced net magnetization, limiting the effectiveness of conventional techniques such as Hall bar measurements [4], particularly in nanoscale devices with low magnetic signals.

Here, we present a tunnel magnetoresistance (TMR)-based method to electrically detect SAF states independently of net magnetization. By integrating a Co/Ru/Co SAF with a CoFeB/MgO magnetic tunnel junction (MTJ) free layer, we achieve selective TMR sensitivity with a ratio of 90% to a single SAF sub-layer (M1 in Fig. 1a).

While blanket measurements confirm the expected SAF switching behavior (Fig. 1b), fabricated 100 nm MTJs (Fig. 2a) show unconventional switching characteristics (Fig. 2b). In addition to the reference layer switching at negative fields due to the antiparallel alignment with the hard layer, the SAF free layer reverses before zero field. We show that this behavior is driven by the antiparallel exchange coupling. By varying the thickness of the M1 Co layer, we investigate the evolution of the coupling field, extracted from minor loop measurements (Fig. 2c), which agree with blanket data (Fig. 2d), confirming our approach.

This work provides a robust and scalable approach to probe SAF states electrically and offers insights into SAF switching mechanisms, paving the way for their integration into future spintronic technologies.

[1] H. Fan, M. Jin, Y. Luo et al., Advanced Functional Material, Vol. 33, p. 2211953 (2023).

[2] S. H. Yang, K.-S. Ryu, S. Parkin et al., Nature Nanotechnology, Vol. 10, p. 221 (2015).

[3] V. T. Pham, N. Sisodia, I. Di Manici et al., Science, Vol. 384, p. 6693 (2024).

[4] J. C. Jeon, A. Migliorini, J. Yoon et al., Science, Vol. 386, p. 315 (2024).

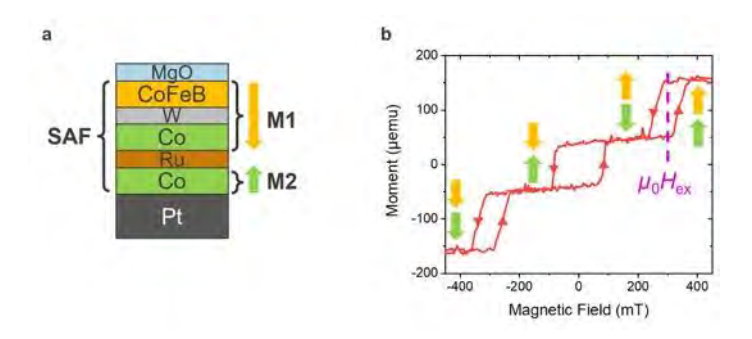


Fig.1: (a) Schematic of the SAF-HFL stack. (b) VSM hysteresis loop showing antiparallel coupling.

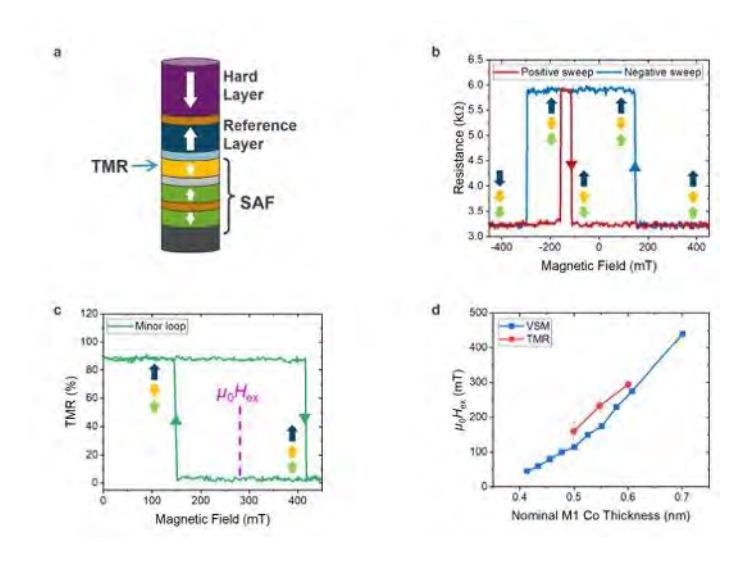


Fig. 2: (a) MTJ with a SAF-based free layer. (b) TMR loop showing selective detection of the M1 SAF sub-layer. (c) Minor TMR loops from zero to saturation revealing the exchange coupling field. (d) Exchange coupling field extracted from VSM and minor loops.

BF-07. Multi-level spin-orbit torque magnetic nanoarray for process-in-memory applications

D. Koh, M. Kang, D. Kim, B. Park

Materials Science and Engineering, Korea Advanced Institute of Science and Technology (KAIST), Daejeon, Korea (the Republic of)

The advancement of data-driven technologies has increased energy and time consumption in data transfer between processors and memory units, limiting further improvement in device performance. To address this challenge, processin-memory (PIM) architecture has emerged, alleviating data transfer overhead through in-memory computation. In this work, we propose a multi-level nanoarray spin-orbit torque (SOT) device for PIM applications. In a Hall bar structure composed of multiple ferromagnetic islands, the SOT switching current varies depending on the size or shape of each ferromagnetic island. This enables precise control over discrete multi-level states through input current modulation, demonstrating analog PIM functionality. Furthermore, we present logic operations using the same device, with pulse currents as digital inputs and multi-level resistances as digital outputs, making it suitable for digital PIM applications. Notably, multilevel SOT switching can operate with nanosecond current pulses, without requiring an external magnetic field, highlighting its potential for ultrafast, energy-efficient PIM platforms.

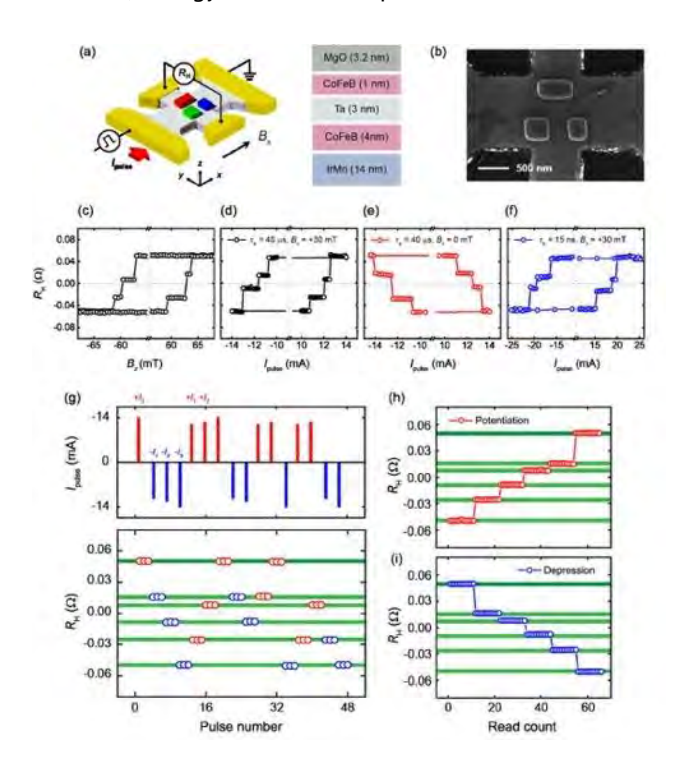


Figure 1. Multi-level SOT switching in a nanoarray device. (a) Schematic of the SOT switching setup with a nanoarray magnetic stack. (b) SEM image of the device.

(c) $R_{\rm H}$ vs. $B_{\rm z}$ curve. (d-f) SOT switching curves for different pulse widths ($\tau_{\rm p}$ = 40 us or 15 ns) and in-plane fields ($B_{\rm x}$ = 0 or +30 mT). (g) Discrete $R_{\rm H}$ states induced by pulses I_1 = 11.3 mA, I_2 = 12.3 mA, and I_3 = 14.0 mA under 40 µs and +30 mT. Top: pulse sequence. Bottom: corresponding $R_{\rm H}$ changes. (h, i) Synaptic modulation via pulse sequences: (h) potentiation ($-I_3$, + I_1 , - I_2 , + I_2 , - I_1 , + I_3), (i) depression (+ I_3 , - I_1 , + I_2 , - I_2 , + I_1 , - I_3).

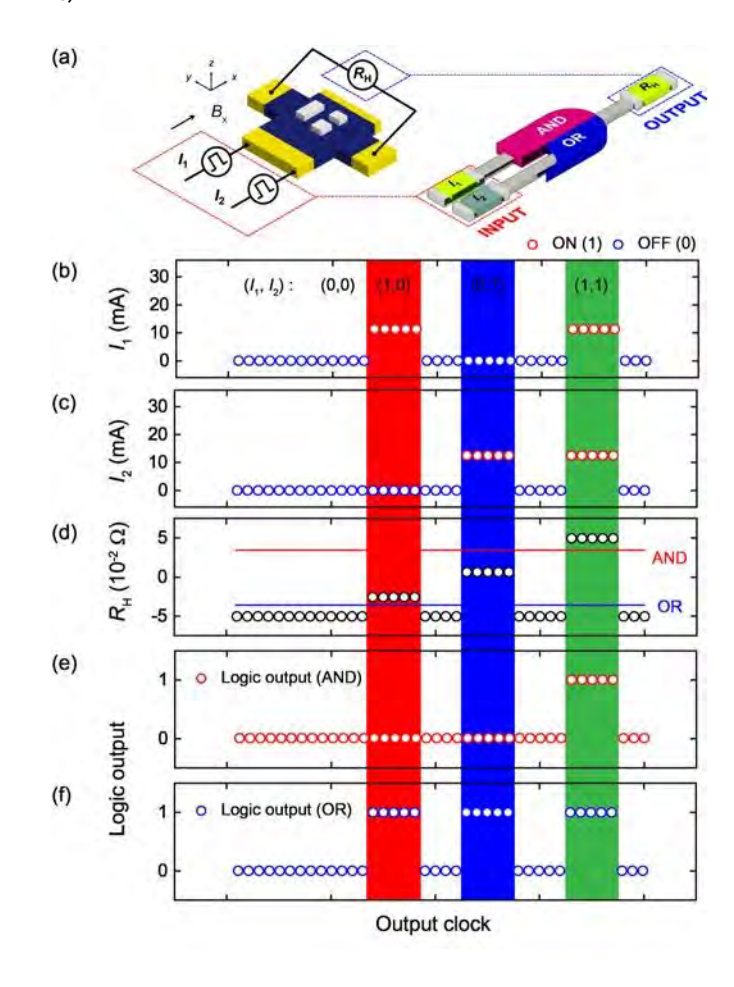


Figure 2 | Logic operations using a multi-level SOT nanoarray device. (a) Schematic showing two parallel input currents (I_1 , I_2) controlling the output R_H . (b, c) Applied pulse amplitudes for digital inputs: I_1 = 11.3 mA, I_2 = 12.3 mA. Colored regions indicate logic states: white (0,0), red (1,0), blue (0,1), green (1,1). (d) Resulting R_H for each input combination; $R_{H,ref}$ set to 0.035 Ω for "AND" and -0.035 Ω for "OR." (e, f) Logic outputs for "AND" (e) and "OR" (f) under τ_p = 40 μ s and B_x = +30 mT.

BF-08. Domain Wall Leaky-Integrate-Fire Dendrites with Spatiotemporally Varied Inputs for Event-Based Sensing

H. Jin¹, F. Chance², C. H. Bennett², S. G. Cardwell², J. Incorvia¹ ¹Chandra Family Department of Electrical and Computer Engineering, University of Texas at Austin, Austin, Texas, United States, ²Sandia National Laboratories, Albuquerque, New Mexico, United States

Spiking neural networks (SNNs) are versatile tools that emulate bio-inspired computing between artificial neurons and synapses; but, artificial dendrite functions have only recently been studied [1, 2]. Dendrites are neuronal interconnects with time-dependent responses to electronic and ionic inputs. Since mimicking such behavior in CMOS requires large area and energy overhead costs, spintronic dendrites arise as a promising candidate for scalable, backend-of-the-line compatible SNNs [3, 4]. Our previous work shows that by using shape anisotropy-driven motion of domain walls (DWs), inherent time-dependent effects can be engineered into DW racetracks with tunable leakage and integration [5].

Here, we design a perpendicular spin orbit torque (p-SOT) DW-based dendrite using spatiotemporally varied input signals and show the designed device can implement eventbased sensing for selective firing. These bio-inspired event sensors provide asynchronous measurements, encoding spike timing and location data, and present a smaller footprint than a combination of multiple neurons. By implementing an input setup that only allows for unidirectional current (see Fig. 1), inputs upstream to the DW are unable to excite or inhibit DW motion. The addition of multiple input regions along the length of the DW track results in an input scheme that can integrate and fire only under specific spatiotemporally varied sequences. To demonstrate, we conduct MuMax micromagnetic simulations with 4 inputs spaced evenly along a trapezoidal Pt/CoFeB/MgO p-SOT racetrack [6]. Due to the DW selectively integrating in response to downstream inputs, only 2 of 24 total combinations of sequential inputs result in firing (see Fig. 2), showing high directional selectivity to downstream signals similarly seen in biological synapses. Given the results of our simulations, we conclude that we have effectively designed a DW-LIF dendrite that exhibits event-based firing for emergent neuromorphic accelerators with low area consumption and high tunability. SNL is managed and operated by NTESS under DOE NNSA contract DE-NA0003525.

- [1] Chance, F. S., Abbott, L. F., & Reyes, A. D. Neuron, 35(4), 773-782 (2002).
- [2] Liu, S., Akinwande, D., Kireev, D., & Incorvia, J. A. C. Nano Letters, 24(24), 7211-7218 (2024).
- [3] Aamir, S. A., Müller, P., Hartel, A., Schemmel, J., & Meier, K. ESSCIRC Conference 2016: 42nd European Solid-State Circuits Conference, 71-74 (2016).
- [4] Li, K.-S., Shieh, J.-M., Chen, Y.-J., Hsu, C.-L., Shen, C.-H., Hou, T.-H., Lin, C.-P., Lai, C.-H., Tang, D. D., & Yuan-Chen Sun, J. 2023 International Electron Devices Meeting (IEDM) (2023).
- [5] Leonard, T., Zogbi, N., Liu, S., Rogers, W. S., Bennett, C. H., & Incorvia, J. A. C. ACS Nano, 19(3), 3470-3477 (2025). [6] Vansteenkiste, A., Leliaert, J., Dvornik, M., Helsen, M., Garcia-Sanchez, F., & van Waeyenberge, B. AIP Advances, 4(10), 107133 (2014).

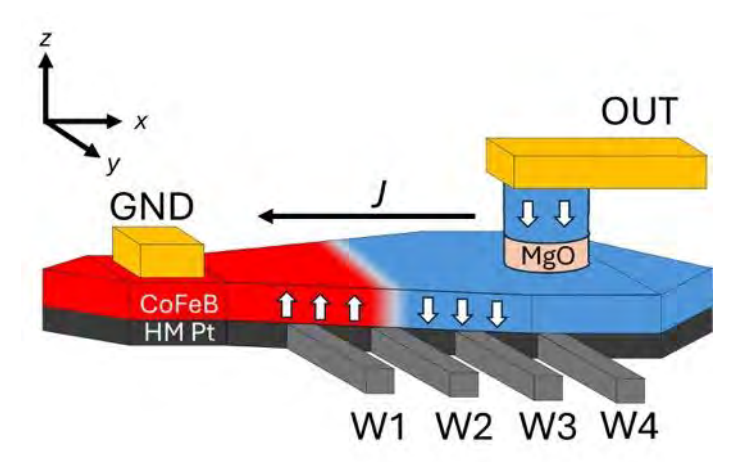


Fig. 1) DW-LIF dendrite with inputs regions W1-4 and MTJ readout, GND-OUT.

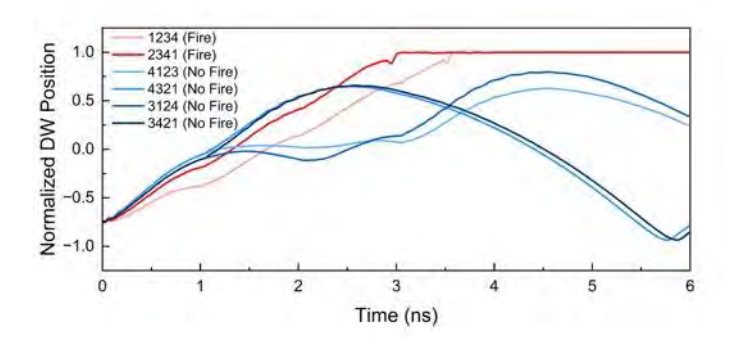


Fig. 2) Firing inputs (red) vs. non-firing inputs (blue).

101

BF-09. Standby Magnetic Immunity Calculator

<u>A. Talapatra</u>¹, F. Schlaphof¹, P. Scharf¹, M. Mansueto¹, D. Sanchez Hazen¹, J. Müller¹, S. Soss², A. Zaka¹
¹GlobalFoundries, Dresden, Germany, ²GlobalFoundries, Malta, New York, United States

The standby magnetic immunity (SMI) of spin-transfer torque (STT) magneto-resistive random-access memory (MRAM) arises due to the undesired bit flip under the presence of an external magnetic field (H_{ext}) which reduces the magnetic energy barrier (E_b) of the free layer of the magnetic tunnel junction (MTJ). The evaluation of SMI requires the estimation of the external magnetic field experienced by the MRAM chip, and the corresponding exposure time. Micromagnetic simulations can predict the values of E_b as a functions of a 3D-applied magnetic field. We have performed simulations with the Magnumfe micromagnetic simulator [1] considering a standalone free layer along with a measured value of the coupling field due to the reference layer and synthetic antiferromagnet. We use the energy minimization following the string method. The values from the model have been compared with the hardware (HW) data measured in-house at GlobalFoundries within the field range of 0.19T-0.23T, as shown in Fig. 1. Micromagnetic simulations show the transition from AP-P state via domain wall propagation. The maximum difference between the median HW data and the simulated data is below 5%. However, the extrapolation of the HW data in the low-field (<0.19T) regime (below the measurable bit-errorrate (BER)) following the analytical domain wall model [2] provides an overly conservative prediction of E_b in the lowfield regime. The simulated E_b at a specific magnetic field and temperature can be converted to the BER corresponding to various field exposure times, as shown in the 2D plot of Fig. 2, using the Arrhenius equation. This provides us the platform to build a machine-learned (ML) model with a graphical user interface (GUI) enabled SMI calculator for specific mission profiles. The advantages of using the GUIbased ML model include faster turnaround time, large statistics including process variabilities, and free from analytical fitting.

- 1. C. Abert, L. Exl, F. Bruckner et al., J. Magn. Magn. Mater. 345, 29 (2013).
- 2. S. Srivastava, K. Sivabalan, J. Kwon et al., *Appl. Phys. Lett.* 114, 172405 (2019).

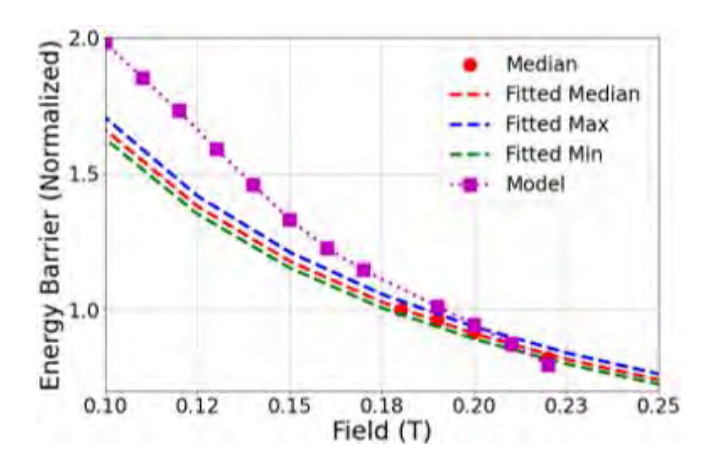


Fig.1 Normalized energy barrier at room temperature as a function of perpendicular magnetic field: comparison of HW, fitted and simulated data.

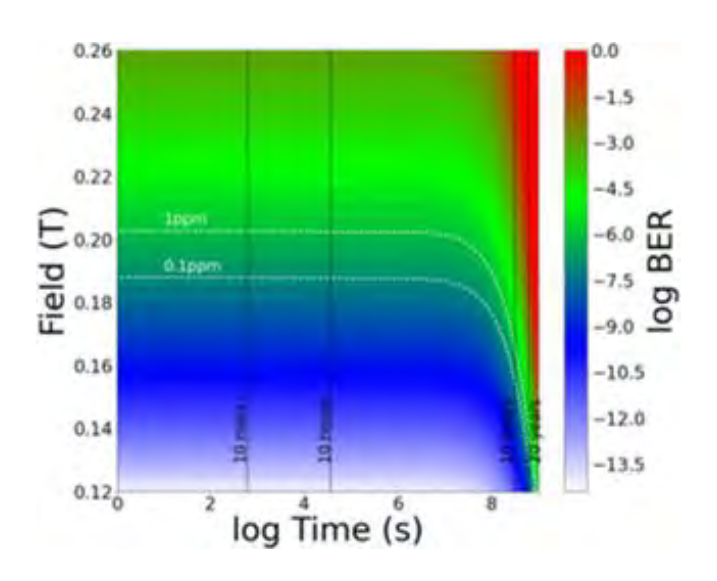


Fig. 2 2D plot for BER with field and exposure time.

BF-10. Harnessing GHz Frequency Spin-Orbit Torque for Spin-Wave Amplification in Cobalt Nanomagnets P. Pal¹ R. Fabiha² A. Mondal¹ S. Bandyonadhyay² A.

<u>P. Pal</u>¹, R. Fabiha², A. Mondal¹, S. Bandyopadhyay², A. Barman¹

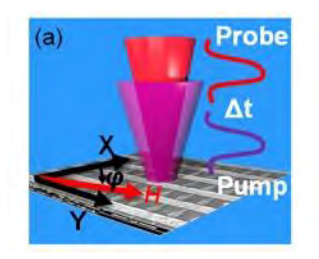
¹Department of Condensed Matter and Materials Physics, S. N. Bose National Centre for Basic Sciences, Kolkata, West Bengal, India, ²Department of Electrical and Computer Engineering, Virginia Commonwealth University, Richmond, Virginia, United States

Spin-orbit torque (SOT) driven by the spin Hall effect has emerged as a powerful mechanism for manipulating

magnetization dynamics at ultrafast timescales. In this work, we demonstrate a novel approach for achieving resonant amplification and spectral filtering of spin-wave (SW) modes in a single-domain nanomagnet using an alternating current-induced SOT (ac-SOT). The experimental platform consists of a ferromagnetic nanomagnet placed in contact with a heavy metal nanostrip, into which a tunable GHz-frequency ac charge current is injected. The resulting alternating spin current exerts a time-varying SOT on the magnetization, selectively coupling to and amplifying a targeted SW mode when the excitation frequency matches the intrinsic mode frequency.

This resonant energy transfer leads to more than a ten-fold increase in the amplitude of specific SW modes, with the amplification factor being tunable via the amplitude of the ac charge current. Additionally, a significant reduction in the spectral linewidth of the amplified modes is observed, indicating enhanced coherence and spectral purity. These features are especially advantageous for magnonic applications involving analog signal processing, spin-wave-based filtering, and high-fidelity information transmission in the GHz regime.

Our findings open up a new pathway for utilizing ac-SOT in mode-selective magnonics, where energy-efficient control of spin dynamics is crucial. The ability to both amplify and purify the spectral characteristics of spin waves in a controllable and selective manner may significantly impact future development of integrated magnonic devices and circuits for ultrafast, low-power computing technologies.





(a) Schematic of the experimental setup for time-resolved magneto-optical Kerr effect (TR-MOKE) measurements. The sample is oriented within the x-y plane, while the two-color pump-probe beam is aligned along the z-axis to investigate the magnetization dynamics. (b) Schematic illustrating the ac-SOT mechanism, where spin current (*I*_s) is generated by the passage of ac current through the Pt strip, driving magnetization dynamics in the adjacent nanomagnets.

SESSION BG: HARD MAGNETIC MATERIALS I: SM-BASED AND RARE EARTH FREE MAGNETS

Chair(s): H. Parmar, *Critical Materials Institute Hub, Ames*National Laboratory, Ames, Iowa, United States
Tuesday, October 28, 2025
02:00 PM-05:30 PM
Room 2A

BG-01. High Entropy Thin Films with High Magnetic Anisotropy and Tunable Magnetic Order

W. Beeson¹, D. Bista¹, D. Bhattacharya¹, H. Zhang^{2, 3}, S. Krylyuk², N. Naushin⁴, A. T. N'Diaye⁵, R. Kukreja⁴, A. Davydov², G. Yin¹, <u>K. Liu</u>¹

¹Physics Department, Georgetown University, Washington, District of Columbia, United States, ²National Institute of Standards and Technology, Gaithersburg, Maryland, United States, ³Theiss Research, Inc, La Jolla, California, United States, ⁴University of California, Davis, Davis, California, United States, ⁵Lawrence Berkeley National Lab, Berkeley, California, United States

High entropy alloys (HEAs) have opened up an exciting platform for materials discovery. The vast number of electronic structures afforded by entropy-stabilization has the potential to achieve rare-earth-free high magnetic anisotropy materials. They also offer an exciting platform to explore novel magnetic phases as they often house competing exchange interactions in combination with random site disorders.

We have achieved enhanced magnetic anisotropy in a series of sputtered HEA thin films using rapid thermal annealing (RTA). Thin films of FeCoNiMnCu sputtered on thermally oxidized Si/SiO₂ substrates are magnetically soft, with a coercivity ~ 10 Oe. After post-deposition RTA, the films exhibit a single face-centered-cubic (fcc) phase, with an almost 40-fold increase in coercivity, resulting from microstructural changes and strain-induced anisotropy enhancement. Addition of Pt reduces the symmetry of the cubic fcc lattice to an intermetallic tetragonal $L1_0$ phase of (FeCoNiMnCu)Pt. Atomic resolution STEM high-angle annular dark-field (HAADF) images taken along the [001] and [110] zone-axis, not only reveal the 4-fold and 2-fold symmetry, respectively, but also illustrate the striking chemical ordering of the $L1_0$ phase (Fig. 1). This intermetallic phase is confirmed to host high magneto-crystalline anisotropy, with 3 orders of magnitude coercivity increase. An effective uniaxial anisotropy of 2×10⁶ erg/cm³ is extracted [1].

We have also demonstrated high magnetic anisotropy in rare-earth and precious metal-free C16-ordered high entropy boride films. Films of (FeCoNiMn)₂B exhibit clear C16 chemical ordering after RTA. A combinatorial fabrication process was employed, leading to the discovery of novel boride compositions exhibiting high coercivity and anisotropy. This was supported by DFT calculations, which predicted anisotropy energies up to 9×10⁶ erg/cm³. These high entropy borides could be well-suited for applications such as magnetic recording media or magnetic tunnel junctions.

Furthermore, we have demonstrated a sensitive and tunable magnetic order in sputtered single-layer FeCoNiMnAl_x films, as a function of non-magnetic Al addition, along with an unexpected exchange bias (EB) effect. Thin films of 50 nm FeCoNiMn exhibit a fcc phase, and a large EB of over 500 Oe after field-cooling to 5 K. The EB is increased to 930 Oe through a small addition of 6 at.% Al. Further Al addition to 11 at.% results in a body-centered-cubic (bcc) phase, coinciding with a large increase in the saturation magnetization, decrease of EB to 50 Oe (Fig. 2). The change in magnetic order is mediated by the switching of Mn ground state from antiferromagnetic (AF) to ferromagnetic (FM), which is supported by first-principles calculations and experimentally confirmed via X-ray magnetic circular dichroism. These results open up new HEA strategies for explorations of novel magnetic phases [2].

This work has been supported in part by the NSF (ECCS-2151809, ECCS-2429995, DMR-1828420, DMR-2145893), 5E Advanced Materials, NIST (70NANB22H101/MML22-1014), DOE (DE-AC02-05CH11231) and the ACCESS Program.

[1] W. B. Beeson, D. Bista, H.R. Zhang, S. Krylyuk, A. Davydov, G. Yin, and Kai Liu, Adv. Sci. 11, 2308574 (2024). [2] W. B. Beeson, D. Bista, N. Naushin, A. T. N'Diaye, R. Kukreja, G. Yin, and Kai Liu, Adv. Funct. Mater. 35, 2424741 (2025).

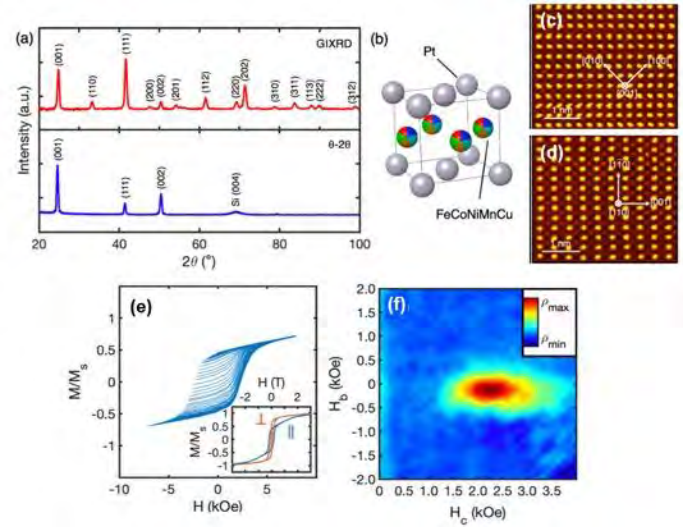


Fig. 1. (a) (Top) GIXRD and (bottom) θ -2 θ XRD scans for (FeCoNiMnCu)Pt films after RTA at 600 °C for 60 s. (b) Schematic crystal structure of L1 $_0$ (FeCoNiMnCu)Pt. (c,d) Atomic resolution HAADF-STEM images taken along the [001] and [110] zone-axis, respectively, showing the chemical ordering of the L1 $_0$ structure on the FeCoNiMnCu and Pt sites. (e) In-plane family of FORCs and (f) corresponding FORC distributions for (FeCoNiMnCu)Pt films after RTA at 600°C for 60 s.

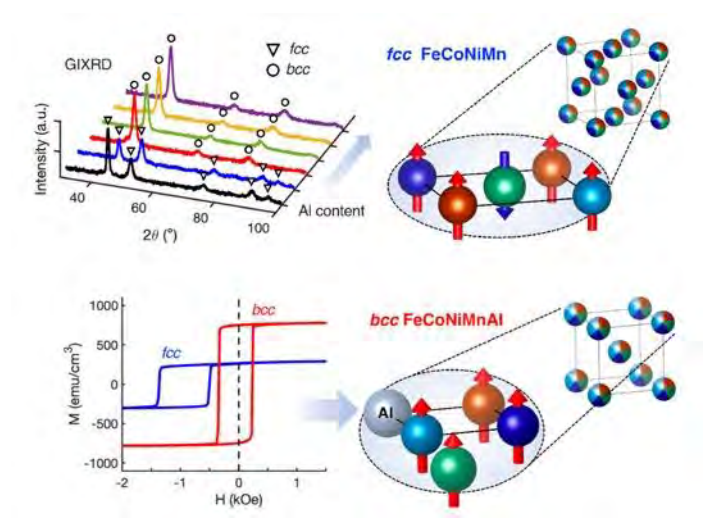


Fig. 2. Non-magnetic Al addition provides a sensitive handle to switch the magnetic order in high entropy $FeCoNiMnAl_x \ thin \ films \ via \ fcc \ to \ bcc \ phase \ transformation.$ Films with fcc structure exhibit a large exchange bias, while bcc films exhibit enhanced FM properties, reflecting the magnetic ground state of Mn which switches from AF to FM.

BG-02. Investigation of the phase formation and thermal stability of the L1₀ phase in the MnAlCu system

H. Baldino¹, N. Schnitzer^{2, 3}, Z. Monem⁴, S. Rego⁵, D. Hedlund⁵, D. Heiman^{6,7}, B. Cui⁸, L. Li⁴, D. Muller^{3,9}, P. Kulik^{1,5} ¹Material Science and Engineering, University of central Florida, Orlando, Florida, United States, ²Material Science and Engineering, Cornell University, Ithaca, New York, United States, ³Kavli Institute at Cornell for Nanoscale Science, Cornell University, Ithaca, New York, United States, ⁴Mechanical and Aerospace Engineering, University of Central Florida, Orlando, Florida, United States, ⁵Electrical and Computer Engineering, University of Central Florida, Orlando, Florida, United States, ⁶Physics, Northeastern University, Boston, Massachusetts, United States, ⁷Plasma science and Fusion center, Massachusetts Institute of Technology, Cambridge, Massachusetts, United States, ⁸Division of Critical Materials, Ames National Laboratory, Ames, Iowa, United States, 9School of Applied and Engineering Physics, Cornell University, Ithaca, New York, United States

The MnAl system ferrimagnetic L1₀ phase has shown promise as a commercially viable material if its metastability can be resolved. Recent work has shown that Cu [1,2], Ga [3], and V [4] may be MnAl L1₀stabilizers. Focusing on the Cu literature, very little work has explored the impact of greater than 4 at. % addition of Cu with some of the results from higher Cu addition showing an increased thermal stability [1,2]. The MnAlCu system contains an ϵ phase immiscibility gap in the 3-6 at. % Cu range, substituting for Mn, creating two different τ -phases [5]. It is possible that the τ_2 -phase formed from the ϵ_2 -phase has improved thermal stability. To better understand the τ_2 phase, samples of MnAl with 8-9 at. % Cu additions were investigated to determine structural properties, phase transformations, microstructures and magnetic properties. The samples were investigated using x-ray diffraction at various temperatures, differential scanning calorimetry, optical as well as electric microscopy techniques and magnetic characterization techniques. The addition of Cu in this high degree is seen to deepen or kinetically slow the eutectoid reaction of $\varepsilon \rightarrow \beta$ -Mn+ v_2 down to at least 453 K with the ε_2 -phase transforming, through a two-step martensitic mode of transformation, to the τ_2 -phase. Transmission electron microscopy images show alternating twin boundary domain size indicative of self-modulating Bain strain. The ε_2 -phase unit cell volume is about 1.5% smaller with Cu than without. The τ_2 -phase shows a partial decomposition at 750 K, martensite precipitation event, and transforms entirely to the ε -phase at 1225 K, Figure 1.

* Best Student Presentation Finalist / LB – Late-breaking Poster

Magnetic characterization shows a striped domain pattern, consistent with the martensitic plate microstructure and similar magnetocrystalline anisotropy constant to that of Cu-free τ -MnAl. These results offer insight into the mechanisms by which the MnAl τ phase can be modified to improve its phase formation ability and increase its thermal stability towards a potential commercial application.

- [1] H. Baldino, Northeastern University (2024)
- [2] M. Sanchez, L. Amaya, L. Giron, Heliyon, vol 11 (2025)
- [3] T. Mix, F. Bittner, K-H. Muller, Acta Materialia, Vol 128, pp. 160-165 (2017)
- [4] Z. Xiang, X. Zhang, X. Wang, Intermetallics, Vol 116 (2020)
- [5] C. Müller, H. Stadelmaier, B. Reinsch, Z.Metallkd, Vol 88, pp. 620-624 (1997)

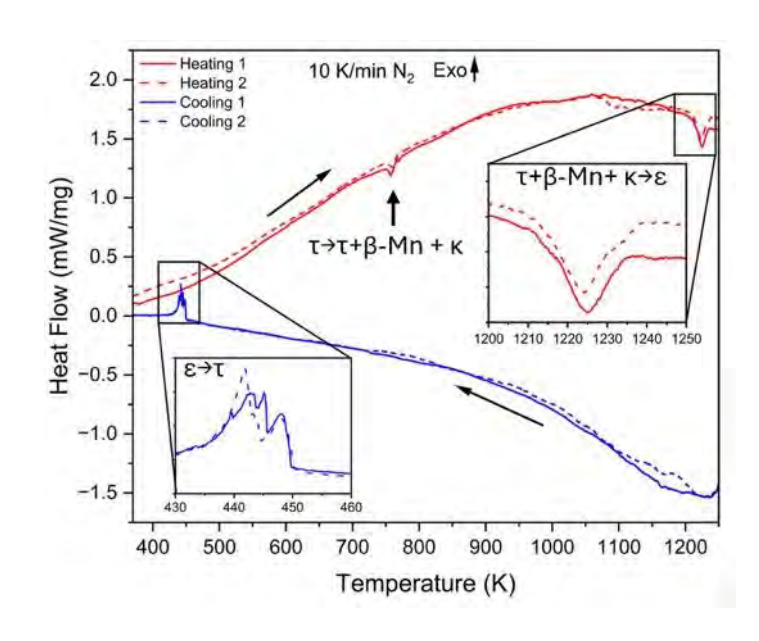


Figure 1. Differential calorimetry measurements of MnAlCu8 single crystals with associated phase transformation inferred from T-XRD.

BG-03. A New Approach in Sintered Mn-Bi Magnets via Silane Coupling Agent

 $\underline{\mathsf{Y.Song}}^{1,2}$, B. Zhang^{1,3}, X. Zheng^{1,3}, C. Choi¹, K. Jong-Woo¹, K. Lee², J. Park¹

¹Nano Materials Research Division, Korea Institute of Materials Science, Changwon, Gyeongsangnam-do, Korea (the Republic of), ²School of Materials Science and Engineering, Ulsan National Institute of Science and Technology (UNIST), Ulsan, Korea (the Republic of), ³Division of Materials Science and Engineering, Pusan National University, Busan, Korea (the Republic of)

The increasing demand for sustainable, rare-earth-free technologies has renewed interest in Mn–Bi permanent magnets due to their promising magnetic properties, particularly the positive temperature coefficient of coercivity, which is advantageous for motor applications. However, their practical use is hindered by low bulk density and degradation of coercivity (H_c) during the sintering process.

In this study, we propose a strategy to address both limitations by employing a silane coupling agent coating technique. While conventional sintering is typically conducted within the stability range of the low-temperature phase between 300 and 355 °C, we demonstrate that the Mn-Bi low-temperature phase (LTP) remains stable even after heat treatment at temperatures up to 446 °C of high temperature phase (HTP). This expanded processing window enabled the fabrication of sintered magnets with high relative density of ~97%, as shown in Fig. 1(a). To counter the associated coercivity loss due to grain growth at elevated temperatures, we applied a silane coupling agent containing epoxy functional groups. Upon heating, the agent formed a siloxane network at particle interfaces, effectively suppressing grain coarsening and improving H_c , as shown in Fig. 1(b). Microstructural analysis

This approach offers a promising pathway for advancing Mn–Bi sintered magnets by achieving both high density and enhanced coercivity.

confirmed the role of the coupling agent in maintaining fine

grain morphology.

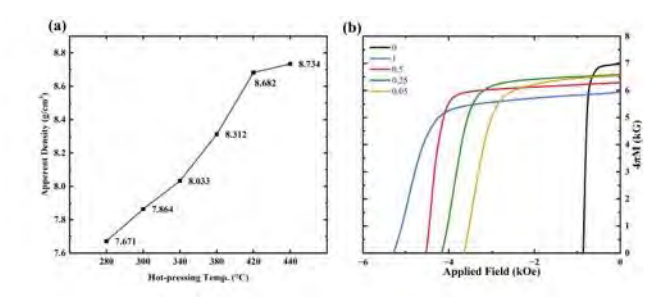


Fig. 1 Apparent densities at different hot-pressing temperatures; (b) Demagnetization curves for various silane coupling agent coating amounts.

BG-04. A Material Processing Perspective on Exchange-Spring Permanent Magnets

T. Lamichhane

Engineering & Physics, University of Central Oklahoma, Edmond, Oklahoma, United States

Exchange coupling between hard and soft magnetic layers enhances the magnetic energy density in exchange-spring permanent magnets, an area with high potential for rare-earth-free permanent magnets design. Despite successes in thin film technology, realizing exchange-spring coupling in bulk polycrystalline magnets remains challenging due to intricate material synthesis requirements. This paper examines the current advancements in both thin-film and bulk polycrystalline exchange-spring systems, comparing successful material systems and their processing technologies. Special attention is given to the potential for critical rare-earth-free exchange-spring systems, such as La-and Ce-based compounds, with significant implications for renewable energy and automotive applications.

^{*} Best Student Presentation Finalist / LB – Late-breaking Poster

BG-05. Enhancing Magnetic Performance of AlNiCo Permanent Magnets via Magnetic Field-Assisted Directed Energy Deposition

<u>O. Bishop^{1, 2}</u>, A. R. Duong¹, I. M. Smith³, E. E. Carpenter³, K. Snyder², R. Barua¹

¹Mechanical and Nuclear Engineering, Virginia Commonwealth University, Richmond, Virginia, United States, ²Commonwealth Center for Advanced Manufacturing, Disputanta, Virginia, United States, ³Chemistry, Virginia Commonwealth University, Richmond, Virginia, United States

Global supply chain disruptions and geopolitical tensions have intensified efforts to develop rare-earth-free permanent magnets. AlNiCo alloys are a promising alternative due to their thermal stability, corrosion resistance, and use of domestically available elements. However, conventional additive manufacturing (AM) methods, such as Directed Energy Deposition (DED), typically yield poor magnetic properties in as-built parts due to limited control over the microstructure. This study explores Magnetic Field-Assisted DED as a strategy to improve magnetic performance during fabrication, reducing reliance on post-processing and lowering overall energy demands

In this study, AlNiCo powders were deposited via a Directed Energy Deposition (DED) system integrated with a customdesigned Halbach array capable of generating static magnetic fields up to 1600 Oe at the build surface. A design-of-experiments approach was employed to systematically vary laser power, scan speed, powder mass flow rate, and toolpath orientation. Microstructural and magnetic analyses revealed that grain morphology and phase segregation could be modulated through the interplay of thermal gradients and magnetic field effects. Increased energy density led to enlarged melt pools, promoting grain coarsening and secondary phase evolution. The applied magnetic field induced anisotropic grain alignment, enhancing ferromagnetic phase orientation and resulting in coercivity values up to 570 Oe and saturation magnetization exceeding 115 emu/g-comparable to those of conventionally heat-treated samples fabricated without magnetic assistance. Additionally, magnetic field application improved powder catchment efficiency by approximately 20% and influenced part geometry through dynamic toolpath-field interactions.

These findings position Magnetic Field-Assisted DED as a scalable and energy-efficient pathway for manufacturing rare-earth-free AlNiCo magnets with tailored

microstructures and high magnetic performance directly in the as-built state.

- [1] Duong et al., "Processing-Driven Microstructure Control in Additively Manufactured Alnico Permanent Magnets" JOM (submitted, under review
- [2] White et. al., "Processing of alnico magnets by additive manufacturing." *Applied Sciences* 9, no. 22 (2019): 4843. [3] S. Dussa, Saikumar, *J. of Mag. Magn. Mat.* 609, 172490, 2024

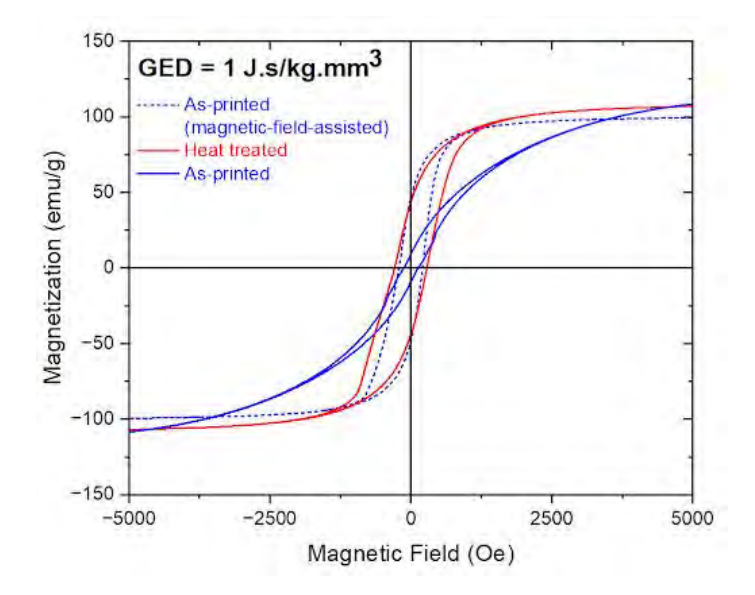


Figure 1: Hysteresis curves reveal that the as-built samples produced in this study achieve magnetic performance comparable to heat-treated counterparts and significantly surpass that of untreated, as-printed samples.

BG-06. Magnetic Behavior of Co(Mo) Nanoparticles

S. Dhapola^{1, 2}, D. Sagar³, A. Kashyap³, J. Shield^{1, 2}
¹Mechanical and Materials Engineering, University of Nebraska-Lincoln, Lincoln, Nebraska, United States, ²Nebraska Center for Materials and Nanoscience, University of Nebraska-Lincoln, Lincoln, Nebraska, United States, ³School of Physical Sciences, Indian Institute of Technology, Mandi, Himanchal Pradesh, India

Extended solid solubility in immiscible systems can forge a path towards creating new magnetic materials with increased anisotropy. HCP solid solution alloys with solute concentrations well beyond equilibrium limits were formed in Co(Mo) nanoparticles. Nanoparticles with Mo compositions of 0,18 & 35 at.% Mo were fabricated by Inert

Gas condensation (IGC). All Co(Mo) nanoparticles investigated are ferromagnetic. Varying processing parameters such as sputtering power & aperture sizes led to a wide variation in coercivity of nanoparticles, ranging from 265 to 1600 Oe, which were dependent on nanoparticle size. Magnetic behavior also depended on composition (Fig 1). For 18 at.% Mo, HRTEM images showed predominantly single-crystalline hcp structures. For 35 at. % Mo, HRTEM images showed poorly crystalline structures. The higher coercivity with higher Mo dissolution into the hcp Co can be correlated to the magnetocrystalline anisotropy enhancement caused by 4d dissolution into hcp Co [1]. Density Functional Theory corroborated this, showing an increase in K but dramatic decrease in Ms beyond dilution effects.

Skomski R, Sharma V, Balamurugan B, Shield J E, Kashyap A, and Sellmyer D J, "Anisotropy of Doped Transition-Metal Magnets" Proc. REPM'10, Eds.: S. Kobe and P. McGuinness, Jozef Stefan Institute, Ljubljana, p. 55-60, (2010).

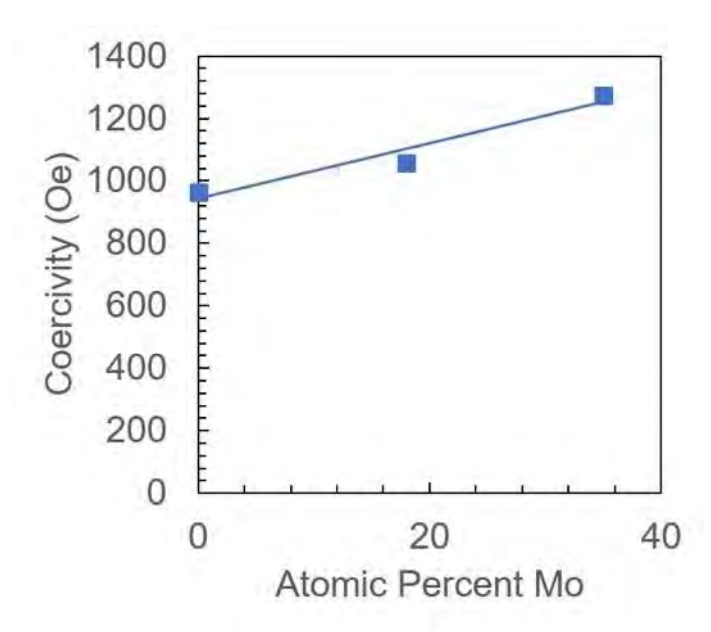


Fig.1 Coercivity at constant nanoparticle size (6-8nm) are composition dependent.

BG-07. The Possibility of New Complex Magnet Materials J. Snyder

northwestern, EVANSTON, Illinois, United States

Magnets are needed for numerous applications including essential consumer electronic components, electric motors that power industry and the future of transportation as well as generating and transforming most electric power. Strong magnets reduce the size and weight of electric motors and generators and improve efficiency. The maximum magnetic field produced by a magnet is determined by the Saturation Magnetization Bs, related to the density of unpaired spins. Most magnets are iron-based alloys or oxides that have at most about 2 unpaired spins per atom. Given that there are many atoms with 5 or more unpaired spins higher Bs should be possible.

Many applications require permanent magnets with high coercivity Hc as well as high Bs where the best metric is the maximum B x H product. Since the almost accidental discovery of Nd2Fe15B-based magnets in 1980s, no new magnet material has exceeded its performance. Despite the expense and concern for sourcing Nd, Nd2Fe15B dominates 60% of the magnet market proving the importance of strong magnets. Nd2Fe15B has a crystal structure and chemistry much more complex than the metal alloys and oxides most frequently used and studied. Nd2Fe15B is mostly Fe with Bs similar to metallic Fe. The dilute non-metal boron is coordinated to Iron like a subnitride, suboxide or subcarbide that then forms layers with the rare earth Nd. This inherently anisotropic structure enables high BHmax. To find an entirely new structure for an even more powerful magnet such structural features should be examined and searched for using advanced AI, machine learning techniques that can identify millions of new complex structures like Nd2Fe15B. Combining this with advanced, high throughput computation of Bs and MagnetoCrystalline Anisotropy Energy the discovery of new Complex Magnet Materials should now be possible.

BG-08. Investigation on magnetic properties of anisotropic nanocrystalline Sm-Co-Cu magnets

<u>K. Park</u>¹, Y. Hirayama¹, Y. Akita²

¹Multi-Material Research Institute, National Institute of Advanced Industrial Science and Technology (AIST), Nagoya, Japan, ²AISIN Corporation, Kariya, Japan

Permanent magnets are used in a wide range of fields, including electronics, industrial and automotive motors [1].

^{*} Best Student Presentation Finalist / LB - Late-breaking Poster

Recently, with the promotion of carbon neutrality and green transformation, electrification has been accelerating in various fields, including automobiles and industrial machinery. Consequently, there is a strong demand for highperformance permanent magnets. In particular, the development of anisotropic permanent magnets with higher remanence and coercivity has become a critical issue. In our previous study, an isotropic nanocrystalline Sm-Co magnet exhibiting a huge coercivity of 5 T was successfully consolidated from Sm-Co alloy nanopowder synthesized by the induction thermal plasma (ITP) process [2]. X-ray diffraction (XRD) analysis revealed that the Sm-Co nanopowder contained 36 wt% of the SmCo₅ phase, which possesses a high anisotropy field. In this study, Cu was doped to increase the SmCo₅ phase content and achieve a magnetically harder nanopowder. The addition of Cu to the Sm-Co alloy system lowers the solidus line temperature, thereby promoting phase formation within a narrower compositional range without any phase separation [3]. Sm-Co-Cu nanopowder was prepared by the ITP process with mixed raw powders in an atomic ratio of Sm:Co:Cu = 1:4.75:0.25. XRD analysis revealed that the Sm-Co-Cu nanopowders contained approximately 60 wt% of the SmCo₅ phase, about 1.6 times higher than that of the Cufree Sm-Co nanopowder. The anisotropic Sm-Co-Cu bulk magnet showed the enhanced crystallographic alignment of SmCo₅ phase compared to that of Sm-Co magnet without Cu doping. The alignment degree of the anisotropic Sm-Co-Cu magnet was estimated to be approximately 87%, based on XRD pole figure measurements. Furthermore, the Sm-Co-Cu bulk magnet exhibited improved coercivity of 1.6 T and anisotropic magnetic behavior, compared to the Sm-Co bulk magnet. This study suggests the potential of rare-earth alloy nanopowders for fabricating high-performance anisotropic permanent magnets.

[1] Y. Ghorbani, I. Ilankoon, N. Dushyantha, G.T. Nwaila, Resources, Conservation and Recycling, Vol. 212, p.107966 (2025).

[2] K. Park, Y. Hirayama, J. Wang, M. Kobashi, Scripta Materialia, Vol. 218, p.114847 (2022)

[3] A. Perry, Journal of the Less Common Metals, Vol. 51, p.153-162 (1977)

BG-09. Exploring stable sites and compositional ranges in $Sm_2Fe_{17}M_x$ (M = H, C, N) using neural network potentials Y. Tatetsu

Health Informatics, Meio University, Nago, Okinawa, Japan

This study systematically investigates the stable structures and compositional limits of $Sm_2Fe_{17}M_x$ (M=H, C, N; x=0-10), a promising material for powerful permanent magnets. We utilized CHGNet [1] and Matlantis [2] computational tools, both based on neural network potentials, in conjunction with the cluster expansion method from ATAT [3]. This approach allowed us to identify stable occupation sites across various concentrations of M atoms, deepening our understanding of how elemental additions influence material stability.

Specifically, we thoroughly examined the stable occupation sites, which are reported to be 3b, 9e, and 18g Wyckoff positions, for H, C, and N atoms within the Sm₂Fe₁₇ host lattice at various concentrations. Although the absolute energy values differ between Matlantis and CHGNet, both methods exhibit good agreement in predicting the qualitative trends. Contrary to the general trend observed for other sites, the addition of M atoms at the 9e site tends to result in the most stable formation energy across all M elements investigated. For Sm₂Fe₁₇N_x, our calculations suggest that the most stable range for nitrogen addition is approximately up to x = 3. This finding is in good agreement with experimental reports indicating that the $Sm_2Fe_{17}N_x$ structure is maintained beyond approximately x =3, demonstrating that our calculations effectively explain the experimental results for nitrogen addition [4]. The energy trends as a function of concentration were analyzed to clarify the impact of each element's introduction on structural stability and to define the maximum concentration that can be stably incorporated. These insights provide crucial fundamental information for designing high-performance magnetic materials within the $Sm_2Fe_{17}M_x$ system.

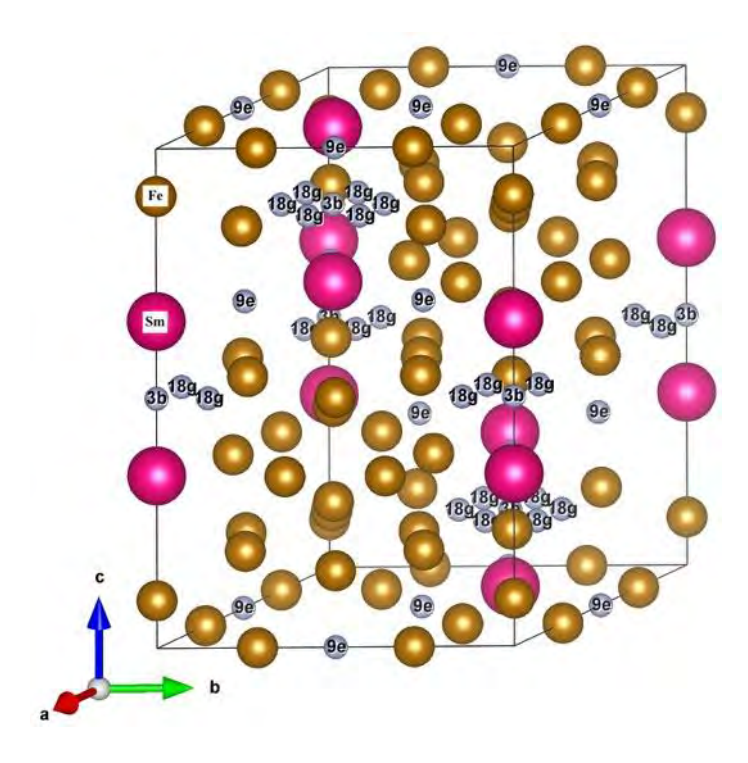
Moving forward, we plan to compare the results obtained in this study with those from density functional theory (DFT) to further validate the accuracy and applicability range of neural network potential-based calculations. Our presentation will include a detailed discussion on these computational results and their comparison with DFT calculations, as well as an in-depth consideration of the stable sites for C and H.

[1] B. Deng, et al., Nature Machine Intelligence 5, 1031 – 1041 (2023).

[2] S. Takamoto, et al., Nat Commun 13, 2991 (2022).

[3] A. van de Walle, et al., Calphad Journal 42, 13-18 (2013).

[4] T. W. Capehart, R. K. Mishra and F. E. Pinkerton, Appl. Phys. Lett., 13, 58 (1991).



BG-10. Microstructure – Magnetism Correlation in SmCo₅-Based Materials via Solid-State Design Strategies

<u>F. Ishrak</u>, M. Lastovich, M. Uddin, F. Tsai, B. Gwalani Materials Science and Engineering, North Carolina State University, Raleigh, North Carolina, United States

SmCo₅ is widely recognized for its exceptional magnetic hardness and high-temperature stability, yet its brittleness and processing limitations hinder scalable integration into structural or application-specific magnet designs. This study presents a systematic research progression aimed at overcoming these limitations through solid-state material design strategies.

Initially, a single-step magnet fabrication method was developed using high-shear consolidation of $SmCo_5$ and Sm_2Co_7 powders. This approach leveraged thermomechanical activation to induce phase transformation and defect-assisted domain pinning, yielding magnets with refined grain structures and enhanced coercivity. In parallel, spark plasma sintering (SPS) was used to investigate

exchange coupling in SmCo $_5$ systems modified with Fe. While Fe additions improved saturation magnetization, they introduced soft magnetic phases such as FeCo and Sm $_2$ Co $_1$ 7, requiring precise control to avoid coercivity degradation. Building on this foundation, the current phase of research targets low-density, high-coercivity Al–SmCo $_5$ composites. Here, aluminum acts as a ductile, non-magnetic binder that promotes structural integrity while enabling magnetic decoupling through particle isolation and interfacial control. Solid stir extrusion is employed to embed SmCo $_5$ within the Al matrix, yielding magnetically active regions without percolating soft paths. Magnetic force microscopy and SQUID measurements confirm the emergence of domain isolation and high coercivity (>13 kOe), alongside improved mechanical toughness.

This work defines a coherent research pathway: from single-step magnet synthesis, to exchange-engineered SPS systems, to scalable Al-based magnet composites. It demonstrates that coercivity and toughness can be codesigned via microstructural control in solid-state processed Sm-Co systems. These materials are well-suited for site-specific, lightweight magnetic components in aerospace, energy, and advanced structural applications.

BG-11. Improvement of Thermal Stability of TbCu $_7$ Sm-Fe phase by Addition of Zr and Y in Synthesis of the Fine Powder with Low-temperature Reduction-Diffusion S. Okada

Multi-Material Research Institute, National Institute of Advanced Industrial Science and Technology (AIST), Nagoya, Aichi, Japan

TbCu⁷-type Sm-Fe-N is an attractive material due to its high saturation magnetization (1.7 T)[1]. However, since the TbCu₇-type Sm-Fe-N is a metastable phase, its synthesis process is currently limited to non-equilibrium processes, resulting in only isotropic powders being available. To synthesize anisotropic TbCu₇-type powder, we focused on the reduction-diffusion (R-D) process. In conventional R-D process, heating to temperatures above the melting point of Ca (approx. 850°C) is required, which limits synthesis to the stable phase Th₂Zn₁₇-type Sm-Fe fine powder. Meanwhile, by adding LiCl molten salt, which dissolves Ca, we successfully reduced the R-D temperature to approx. 600°C, enabling the synthesis of the TbCu₇-type Sm-Fe-N anisotropic powder[2, 3]. However, due to the low R-D temperature, particle growth was insufficient, and the particles formed were mainly agglomerated. Furthermore,

the estimated Fe/Sm ratio is approx. 8.5, which is insufficient for achieving high saturation magnetization. To address these issues, this study investigated the effects of adding Zr and Y, which are promising elements to stabilize the metastable phases and increase in the Fe/Sm ratio[4, 5]. Aqueous solutions of selected elemental nitrates were prepared, and spray pyrolysis was performed to synthesize oxide powders. The oxide powders were reduced with hydrogen, mixed with Ca and LiCl, and subjected to R-D treatment. After washing with water and dehydrogenation, the samples were evaluated by XRD measurement. As shown in Fig. 1(a), when no additive elements are present, a peak corresponding to the Th₂Zn₁₇ phase at around 49° begins to appear at an RD temperature of 650°C, and as shown in Fig. 1(b), the c/a value decreases. On the other hand, in the presence of Zr or Y additives, no formation of the Th₂Zn₁₇ phase is observed in the XRD pattern or c/a values even at 750°C. Additionally, a noticeable increase in c/a is observed when Zr is added. It was found that the addition of Zr and Y contributes to the stabilization and increase in iron concentration of the TbCu₇ phase also in the reduction diffusion method.

[1] S. Sakurada et al., Journal of Applied Physics, 79, 4611 (1996) [2] S. Okada, and K. Takagi, Journal of Rare Earths, 40, 1126 (2022) [3] S. Sato et al., Journal of Alloys and Compounds, 929, 167280 (2022) [4] H. Suzuki, AIP Advances, 7, 56208 (2017) [5] M. Hagiwara et al., Journal of Magnetism and Magnetic Materials, 465, 554 (2018)

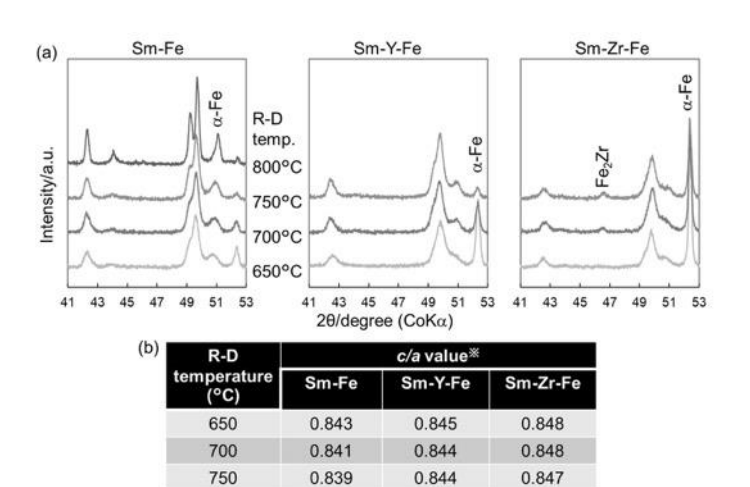


Fig.1 (a) XRD patterns of the synthesized samples and (b) the estimated c/a of the samples by Rietveld analysis

*c/a values were estimated with TbCu₇ crystalline structure

BG-12. High coercivity TbCu₇-type Sm-Fe-N powder prepared by induction thermal plasma process

<u>Y. Hirayama</u>, Z. Liu, W. Yamaguchi National Institute of Advanced Industrial Science and Technology, Nagoya, Japan

TbCu₇-type Fe-rich Sm-Fe-N has extremely high intrinsic properties that surpass those of Nd₂Fe₁₄B [1, 2]. The important point is that Fe/Sm exceeds 8.5, which realizes high magnetization. Anisotropic powder of TbCu₇-type SmFe has been synthesized by low-temperature reduction diffusion [3] and thermal plasma method [4]. Neither method has succeeded in synthesizing so-called Fe-rich TbCu₇-type Sm-Fe with Fe/Sm=8.5 or more. Therefore, in this study, we attempted to synthesize Fe-rich TbCu₇-type Sm-Fe by substituting Y with Sm. Sm-Y fine powder with a D₉₉ particle size under 10 µm was obtained by ball milling for 15 hours in IPA. In addition, the Sm-H fine powder with a D₉₉ of 2.7 µm was obtained by hydrogenating Sm metal at 550 °C and then subjecting it to a jet mill. Fe, Sm-Y, and Sm-H mixed powders with an atomic ratio of Sm:Y: Fe = 0.7: 0.3: 3 were used as raw material powder for the thermal plasma process. The nanopowder obtained by thermal plasma was annealed at 700 °C for 3, 10 and 48 hours. Then, the nitriding was performed under nitrogen flow at 400 °C for 30 minutes. The phase of the powders was evaluated by powder X-ray diffraction (XRD) experiments using the Lab XRD facility (Empyrean, Malvern Panalytical, Co-Kα). SEM and TEM were used for microstructural analysis. The magnetic property was measured using a VSM (DynaCool, Quantum Design, Inc.) with a maximum applied field of 9 T at room temperature.

The average particle size of the Sm-Y-Fe powder obtained by the thermal plasma process was 94 nm. The XRD profiles showed that all peaks originating from the $TbCu_7$ structure were shifted to lower angles after nitridation, confirming the volume expansion caused by introducing nitrogen. The peak positions also suggested that the Fe/Sm (at%) ratio was greater than 8.5, indicating that Fe-rich Sm-Fe-N was successfully prepared. The coercivity increased from 0.6 to 1.8 MA/m with increasing the annealing time from 3 to 48 hours. This 1.8 MA/m is the highest coercivity for the $TbCu_7$ -type Sm-Fe-N compound. Therefore, this study demonstrated that substituting Sm with Y makes it possible to produce Fe-rich $TbCu_7$ -type Sm-Fe-N nanopowder using the induction thermal process.

[1] S. Sakurada, A. Tsutai, T. Hirai, Y. Yanagida, M. Sahashi, S. Abe, T. Kaneko, Structural and magnetic properties of

^{*} Best Student Presentation Finalist / LB - Late-breaking Poster

rapidly quenched $(R,Zr)(Fe,Co)_{10}N_x$ (R=Nd,Sm), J. Appl. Phys. 79(8) (1996) 4611-4613.

[2] A.R. Dilipan, D. Ogawa, H. Sepehri-Amin, P. Tozman, T. Hiroto, K. Hono, Y.K. Takahashi, Excellent intrinsic magnetic properties in the TbCu7-type Sm-Fe-N compound, Acta Mater. 274 (2024) 119996.

[3] S. Okada, K. Takagi, Novel synthesis of single-crystalline TbCu7-type Sm-Fe powder by low-temperature reduction-diffusion process using molten salt, Journal of Rare Earths 40(7) (2022) 1126-1133.

[4] Y. Hirayama, Z. Liu, W. Yamaguchi, K. Takagi, K. Ozaki, Preparation of Sm-Fe-N Hard Magnetic Nanopowder From Micrometer-Sized Sm-H and Fe Mixed Powder, IEEE Transactions on Magnetics 59(11) (2023) 1-4.

BG-13. First-Principles Prediction of Permanent Magnetism in SmFe₁₁Ti

B. Narangerel¹, M. Adiya¹, <u>D. Odkhuu^{1,2}</u>
¹Department of Physics, Incheon National University, Incheon, Korea (the Republic of), ²Institute of Physics and Technology, Mongolian Academy of Sciences, Ulaanbaatar, Mongolia

Despite the excellent permanent magnetic performance of SmFe₁₂, its structural instability limits practical applications. The presence of Ti stabilizes the SmFe₁₁Ti phase; however, it rapidly degrades the permanent magnetic performance. Using systematic density functional theory, density functional perturbation theory, Monte Carlo, and micromagnetic simulations, we investigate the partial replacement of Ti with a metal element that can improve the intrinsic permanent magnetic properties of SmFe₁₁Ti phase without degrading structural stability. Our calculations demonstrate that among the substitutional metal elements, the simple metal Al is the most optimal. More specifically, Sm(Fe,Al)_{11.5}Ti_{0.5} phase exhibits a saturation magnetization $\mu_0 M_s$ up to 1 T and a uniaxial magnetocrystalline anisotropy K_u up to 6 MJ/m³ at room temperature, leading to the theoretical energy product, anisotropy field, and hardness parameter, superior to the widely investigated SmFe₁₁Ti phase. The enhanced hard magnetism is attributed to the changes in the energy level of the strong spin-orbit-coupled Sm 4f electrons. Furthermore, similar improvements with other simple metal and metalloid substitute elements (Ga, Si, and Ge) are corroborated in the present prediction. Finally, these theoretical results have been partly confirmed by experimental characterizations.

SESSION BP: MAGNONICS I: SPIN WAVES & SPIN DYNAMICS (POSTER SESSION)

Chair(s): J. Zhou, *Institute of Materials Research and Engineering, A*STAR, Singapore, Singapore*Tuesday, October 28, 2025
02:30 PM-05:30 PM
Exhibit Hall Posters

BP-01. Magnetic field dependence of dipole-exchange spin waves in square ferromagnetic nanorings

<u>A. Frost</u>¹, B. Hussain¹, M. G. Cottam²
¹University of Michigan, Dearborn, Michigan, United
States, ²University of Western Ontario, London, Ontario, Canada

Ferromagnetic nanorings have been of ongoing interest due to the competing vortex and onion states, their switching behavior, and device applications [1-3]. As well as circular rings, other shapes have attracted attention. Here we focus on square nanorings (which have received relatively less attention [4,5]) by presenting a theoretical analysis for the role of an in-plane external magnetic field in manipulating the frequencies and spatial intensities of the quantized spin waves (SWs). The calculations involve dividing the geometry into small cubic cells, each with an effective spin and size chosen to be less than the so-called exchange correlation length. The cells interact via short-range bilinear exchange and long-range dipole-dipole interactions, and they have a Zeeman energy in the applied field B_0 . The first step is to determine the equilibrium orientations of the spins for the spatially inhomogeneous magnetization. Then a dynamic matrix approach is employed to extract the SW properties, following the approach in [6] for circular nanorings. By contrast with circular nanorings, it is found that the magnetization process follows a two-stage process as B_0 is increased, with consequences for the SW dynamics. Some typical results are shown in Figs. 1 and 2. The profile of the scaled magnetization M/M_0 versus B_0 , where M_0 is the saturation magnetization, is illustrated in Fig. 1. At small B_0 a vortex state occurs, followed by an abrupt transition to a partially magnetized onion state. Then, as B_0 is increased further, M/M_0 increases in a spin reorientation transition with full magnetization attained here at around 0.15 T. The corresponding behavior for the frequencies of the lowest few SW modes is given in Fig. 2.

- [1] C.A.F. Vaz et al., J. Phys. Condens. Matter, 2007, 19, 255207.
- [2] M. Zhu et al., J. Appl. Phys., 2013, 113, 17B905.
- [3] C.D. Moreira et al., J. Mag. Magn. Mat., 2017, 443, 252.

- [4] S. Mamica et al., J. Appl. Phys., 2012, 112, 043901.
- [5] C. Banerjee et al., J. Appl. Phys., 2014, 116, 163912.
- [6] B. Hussain and M.G. Cottam, Nanomaterials, 2024, 14, 1594.

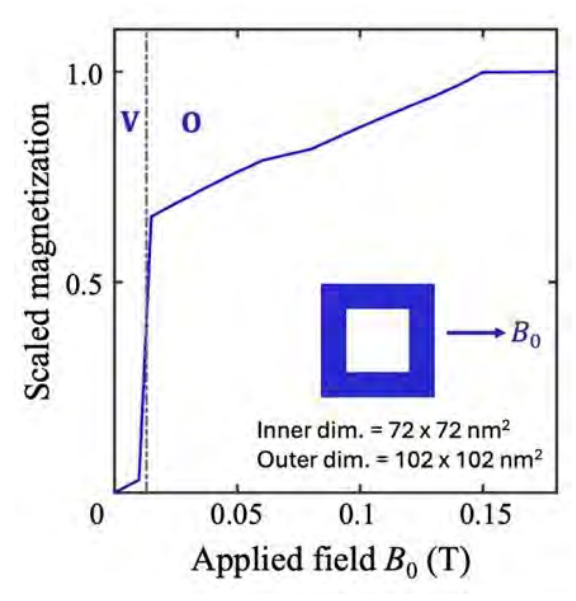


Fig. 1. Plot of scaled magnetization M/M_0 versus applied magnetic field, for a square nanoring of permalloy. The vertical line represents the transition field between the vortex (V) and onion (O) magnetic states. Saturation in the magnetization is achieved at 0.15 T

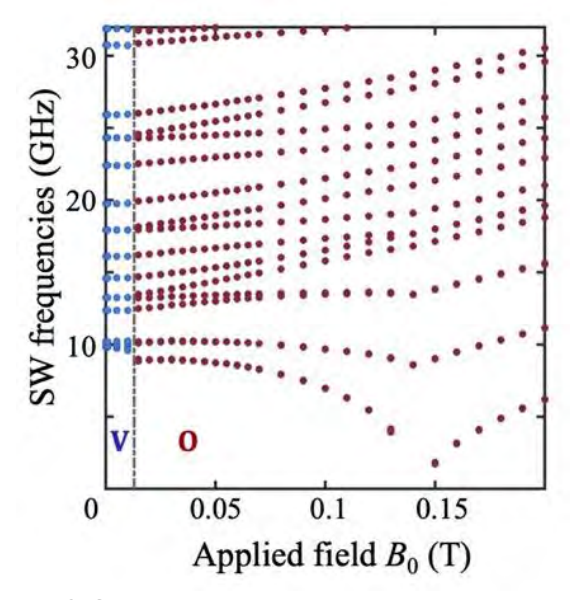


Fig. 2. SW frequencies plotted versus B_0 for the nanoring in Fig.1, showing the vortex (V) and the onion (O) states. The large dip for the lowest SW mode at 0.5 T can be attributed to a spin reorientation to saturated magnetization.

BP-02. Nanoscale Quantum Imaging of Caustic Spin-Wave in YIG Film

T. Zheng, E. Zhang, B. Yang, J. Zhu
Department of Electrical and Computer Engineering, Carnegie
Mellon University, Pittsburgh, Pennsylvania, United States

Quantum sensing with nitrogen-vacancy (NV) centers in diamond has emerged as a powerful tool for nanoscale magnetic imaging, enabling the study of dynamic magnetic phenomena beyond the optical diffraction limit. In particular, caustic spin-wave propagation, arising from anisotropic dispersion relations, has attracted considerable interest due to its potential applications in magnon transport and spin-wave based computing. Compared with conventional methods such as Brillouin light scattering or inductive detection, scanning NV magnetometry can directly image spin-wave amplitude, phase, and polarization at room temperature with nanoscale spatial resolution and high sensitivity.

In this work, we employ a scanning NV-center probe to image caustic spin-wave beams emitted from a single slit in a 109 nm-thick yttrium iron garnet (YIG) film. With the NV sensor positioned approximately 100 nm above the YIG film, we map the stray fields generated by surface spin-wave propagating under localized in-plane excitation. The measured spin-wave beam patterns (Fig. 1) reveal realspace caustic spin-wave propagation, providing clear evidence of anisotropic wave propagation. The corresponding Fourier transform (Fig. 2) of the wave mapping shows an anisotropic distribution of wavevectors at a fixed excitation frequency, reflecting the underlying dispersion relation. Different slit geometries are systematically varied and the same analysis techniques are applied to extract detailed characteristics of the caustic spin wave propagation in the YIG film.

The study here demonstrates the scanning NV magnetometry as a versatile platform for resolving caustic spin-wave beams and their underlying anisotropic dispersion at the nanoscale. This capability opens new opportunities to study spin-wave directionality, transport, scattering, and coherent control in magnonic systems.

- 1. T. Schneider, A. A. Serga and A. V. Chumak, *Phys. Rev. Lett.*, 104, p.197203 (2010)
- 2. R. Gieniusz, H. Ulrichs and V. D. Bessonov, *Appl. Phys. Lett.*, 102, p.102409 (2013)
- 3. I. Bertelli, J. Carmiggelt and B. Simon, *Sci. Adv.*, 6, p.eabd3556 (2020)

4. B. G. Simon, R. Buchanan and R. E. Camley, *Nano Lett.*, 22, p.9198 (2022)

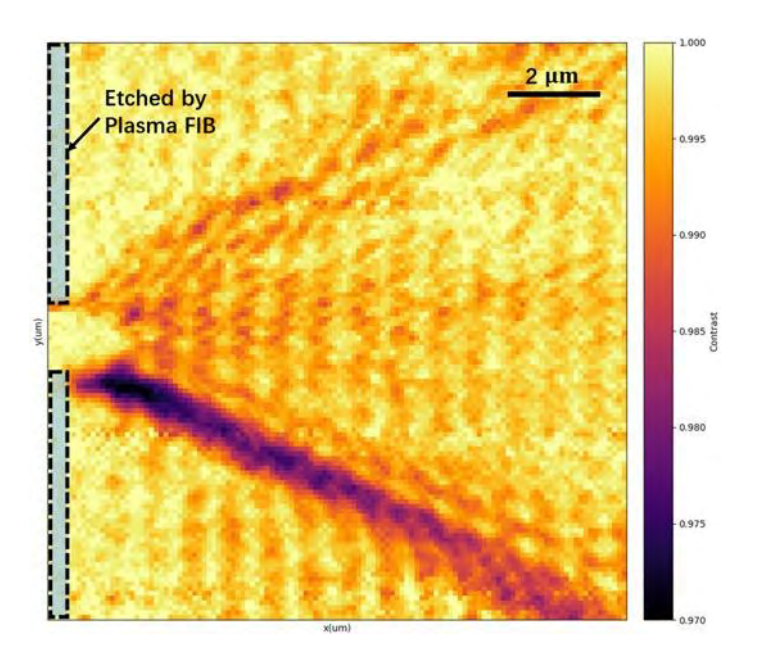


Fig. 1. Spatial map of spin-wave propagation through a single slit in a 109 nm-thick YIG film. Spin waves are driven by a RF wire at 2.66 GHz (matching the NV center's ground-state spin resonance) under a 10 mT bias field along the y-axis. Dashed lines indicate the etched region.

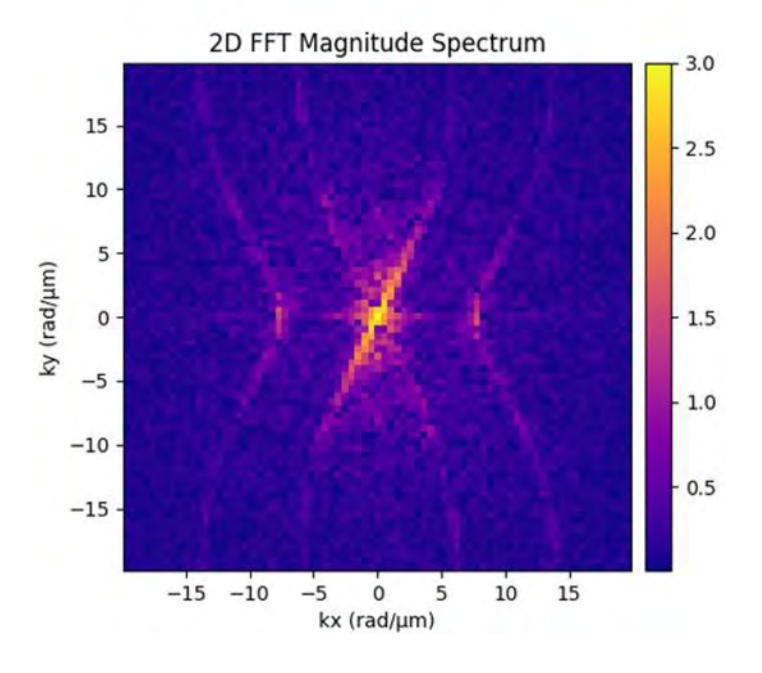


Fig 2. 2D Fourier transform of the spin-wave contrast image in Fig. 1.

BP-03. Dynamic Spin-Wave Characterization in Ferrimagnetic Insulators: Time-Resolved Imaging and Frequency Domain Analysis

Suzuki², R. Knut⁴, D. A. Arena¹
¹Department of Physics, University of South Florida, Tampa, Florida, United States, ²Department of Physics, Stanford University, Stanford, California, United States, ³Helmholtz-Zentrum Berlin, Berlin, Germany, ⁴Department of Physics and Astronomy, Uppsala University, Uppsala, Sweden

V. Ganepola Arachchige¹, Z. Ishraque¹, S. Alaei², S. Wintz³, Y.

We employ time-resolved scanning transmission X-ray microscopy (TR-STXM) using the MAXYMUS at the BESSY II synchrotron, combined with X-ray Magnetic Circular Dichroism (XMCD), to investigate the spin-wave dynamics and magnetic properties of the ultra-low damping spinel ferrite MgAl_{0.5}Fe_{1.5}O₄ (MAFO), which can be grown on single-crystal spinel substrates, a capability that arises from the availability of MgAl₂O₄ as the only commercially available spinel substrate [1]. Using TR-STXM, we visualize the spin-wave amplitude and phase dynamics across a range of frequencies: 6.57 GHz, 8.57 GHz, 9.28 GHz, 10.07 GHz, and 13.5 GHz. An example is presented in Fig. 1.

Our analysis focuses on identifying Damon-Eshbach modes and exploring field-driven transitions to backward volume spin waves. Spin waves were measured at gigahertz frequencies along the Damon-Eshbach geometry, and transitions to backward volume modes were observed as the external magnetic field was increased. These spin-wave dispersions and transitions demonstrate the strong sensitivity of spin dynamics to the external magnetic field.

These findings enhance our understanding of superexchange interactions in ferrimagnetic oxides and their role in determining spin-wave propagation and damping properties. This approach extends methods used in earlier studies to a new class of materials, with considerable potential implications for spintronic applications.

[1] S. Emori, T. Nan, A. M. Belkessam, *et al.*, APL Mater., Vol. 6, p. 111103 (2018)

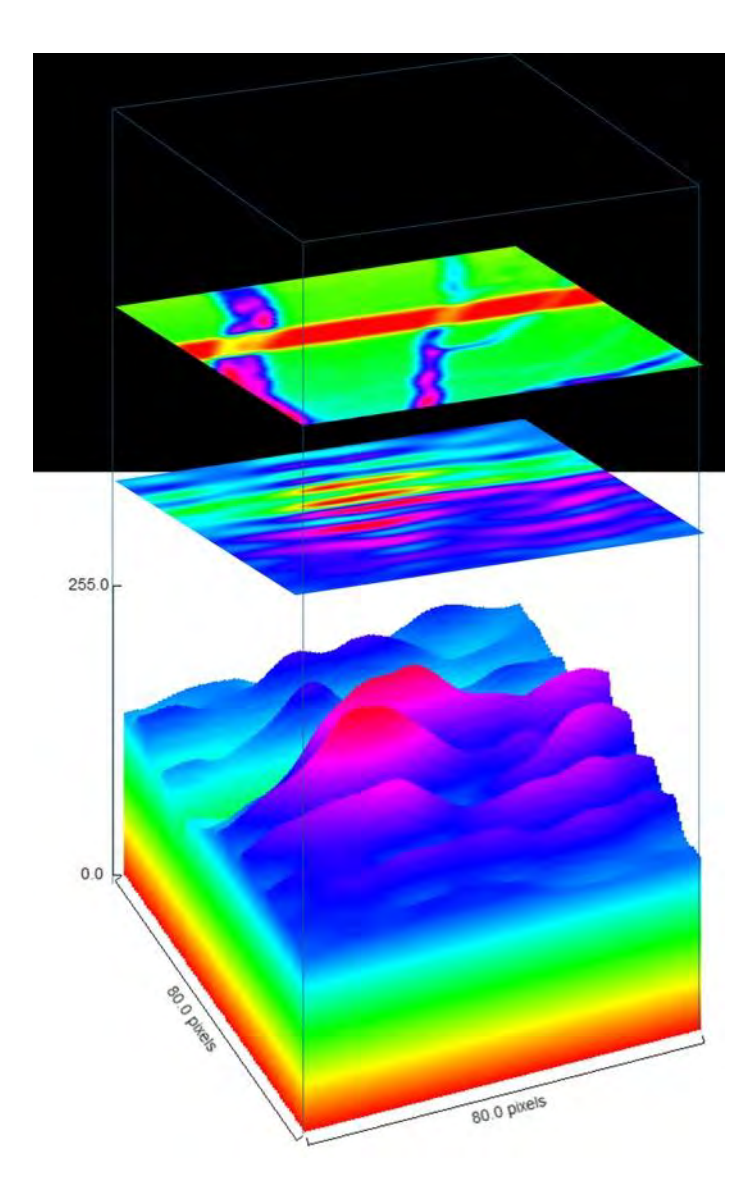


Fig. 1. Three-dimensional visualization of spin-wave at 13.57 GHz using TR-STXM.

BP-04-LB. Ultra-small fine particle inspection system for LIB cathode by HTS SQUIDs

S. Tanaka¹, P. Polkotuwa², T. Ohtani²

¹Institute for Research on Next-generation Semiconductor and Sensing Science (IRES2), Toyohashi University of Technology, Toyohashi, Aichi, Japan, ²R & D Division, Nikka Densok Limited, Kawagoe, Saitama, Japan

Fires caused by small metallic contaminants, particularly stainless steel or nickel exceeding 20 µm in diameter, becoming mixed into lithium-ion batteries (LIB) during manufacturing have become a significant issue. It is known that these small metallic foreign particles act as nuclei, causing dendrites to form inside the battery during use. We have been developing inspection systems utilizing high-temperature superconducting SQUIDs (HTS SQUIDs) over the years. This time, we fabricated planar SQUID gradiometers and magnetometers based on our own design, mounted them in an 8-channel special cryostat, and inspected actual LIB cathodes, achieving unprecedented results.

The inspection system consists of a 0.3 T horizontal magnetization permanent magnet and a cryostat for SQUIDs installed in a four-layer permalloy magnetic shield box. The cryostat is equipped with four gradiometers and four magnetometers, enabling continuous operation for 8 hours through liquid nitrogen cooling.

A LIB cathode sheet (100 mm wide × 200 mm long) placed on the sample transfer device passes through the permanent magnet to become magnetized, and then the magnetization of the metallic contaminant is detected by the SQUID sensor. The LIB cathode features a 5-micronthick coating of lithium cobalt oxide material on AL foil. The automatic inspection system is designed and manufactured for factory operation, ensuring high reliability and adequate electromagnetic noise attenuation (Fig.1). The stand-off distance between the SQUID sensor and the cathode sheet during inspection was set to approximately 4 mm. For metallic contaminant samples, stainless steel pieces and nickel pieces cut using FIB (Focused Ion Beam) were prepared.

The gradiometer inspection results showed a signal-to-noise ratio (SNR) of 5 or higher, enabling clear signal waveforms to be obtained as small as $\Phi 30~\mu m \times L30~\mu m$ (Stainless steel) and $\Phi 25~um$ nickel \times L26 μm (Fig.2). On the other hand, the magnetometer yielded favorable results with signal peak values approximately three times higher than the gradiometer. However, at a position 50 mm from the edge of the cathode sheet, distinguishing signals from

metallic contaminants became difficult due to interference from the edge signal. The magnetometer is effective for inspecting long cathode sheets, while the gradiometer is more effective for short cathode sheets.

These automatic inspection results using actual cathode sheets are the world's first and can be considered useful.

[1] Saburo Tanaka, Takeyoshi Ohtani, Kanji Hayashi, "Comparison of the Performance of Metal Contaminant Detection Using an Optically Pumped Magnetometer With an HTS SQUID", IEEE Transactions on Applied Superconductivity, 35, (2025), 1600204_1-5. (doi: 10.1109/tasc.2024.3507748)

[2] K. Hayashi, R. Ohtani;, Y. Tottori, S. Ariyoshi, and S. Tanaka, "Flux Noise Reduction of HTS-SQUIDs via Introduction of Antidots", IEEE Transactions on Applied Superconductivity, 33, (2023), No.5 1600704_1-4. (doi: 10.1109/TASC.2023.3249648)



Fig. 1 Inspection System.

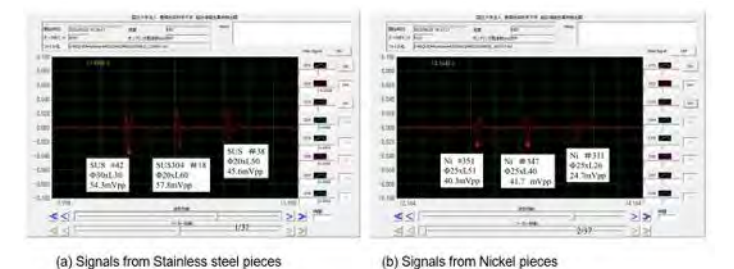


Fig.2 Signal waveforms detected by a SQUID gradiometer.

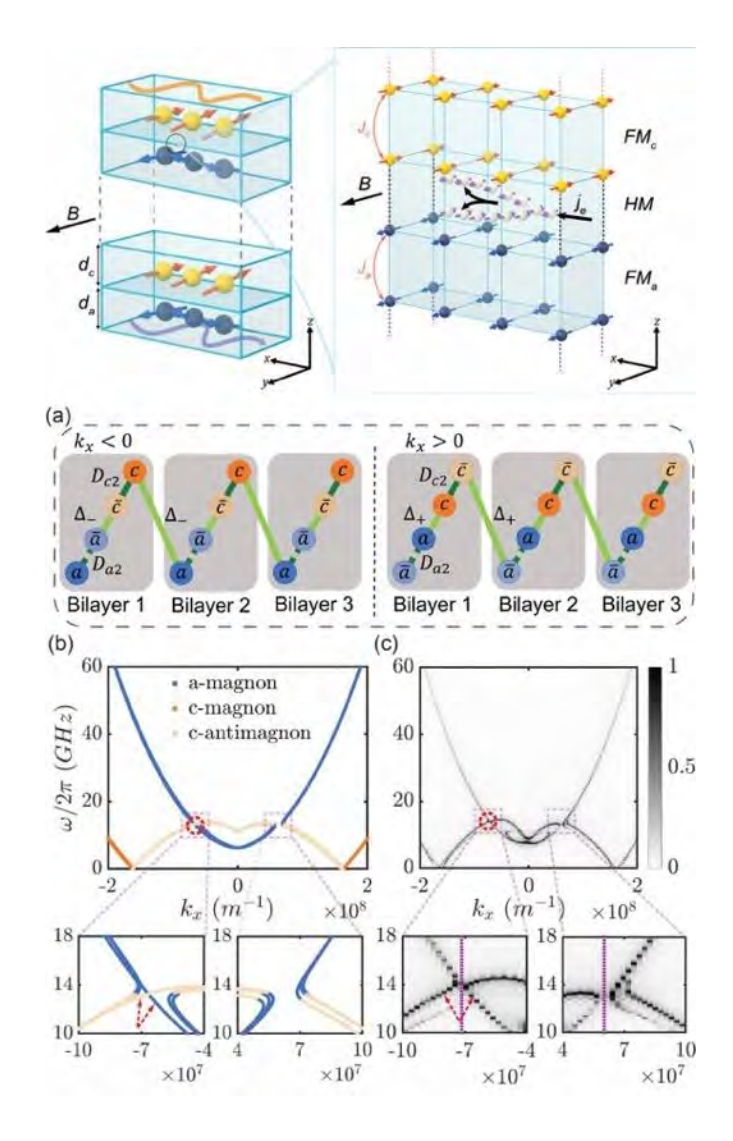
BP-05-LB. Tunable Coupling, Topology, and Chirality by Antimagnons in Magnetic Multilayer

Y. Liu¹, Z. Chen², Q. Shao¹

¹Electronic Engineering, The Hong Kong University of Science and Technology, Hong Kong, Hong Kong, ²Physics, The Hong Kong University of Science and Technology, Hong Kong, Hong Kong

Realizing novel topological states in magnonic systems unlocks robust, low-power spin-wave devices. In this letter, we show that incorporating left-handed spin waves (antimagnons) fundamentally reorganizes band topology, and enables tunable spin-wave coupling and chirality. We proposed a two-dimensional Su-Schrieffer-Heeger like model, the 2D-SSH4 chain, where dipolar interactions between magnons and antimagnons generate topological bands with nonzero Chern numbers. This framework explains the origin of topological surface states in ferromagnetic multilayer and shows they share the same topological origin as classic magnetostatic surface spin waves. Our model also offers a straightforward framework for designing more complex magnetic multilayer connected by dipolar interactions, such as antiferromagnetic/ferromagnetic multilayer. In these dipolar-coupled multilayers, both coherent and dissipative interlayer spin-wave couplings together with the layer resolved chirality, are tunable via external magnetic fields and spin torques. Our results provide a practical platform for topological magnonics, enabling control of magnon chirality and coupling in future devices.

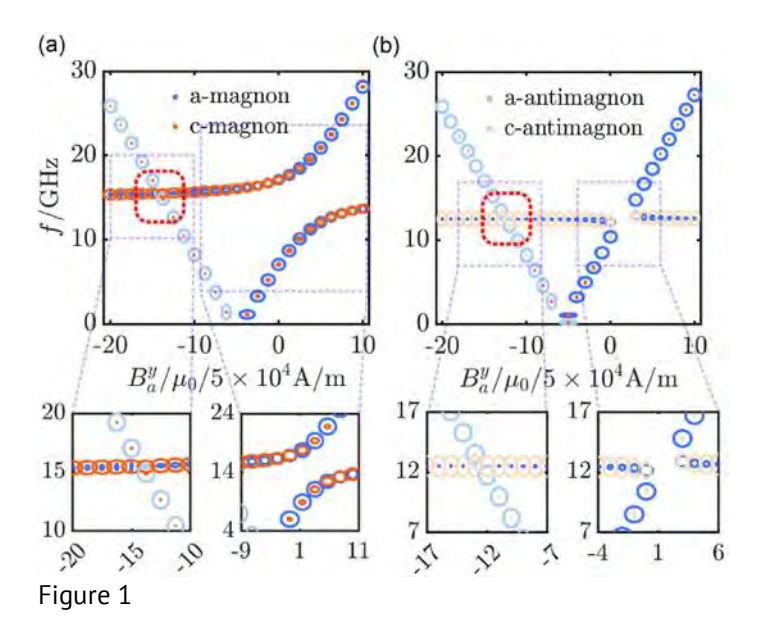
- [1] Z. Hu, L. Fu, and L. Liu, Tunable magnonic chern bands and chiral spin currents in magnetic multilayers, Phys. Rev. Lett. 128, 217201 (2022).
- [2] P. M. Gunnink, J. S. Harms, R. A. Duine, and A. Mook, Zero-frequency chiral magnonic edge states protected by nonequilibrium topology, Physical Review Letters 131, 126601 (2023).
- [3] K. Yamamoto, G. C. Thiang, P. Pirro, K.-W. Kim, K. Everschor-Sitte, and E. Saitoh, Topological characteri zation of classical waves: The topological origin of magne tostatic surface spin waves, Phys. Rev. Lett. 122, 217201 (2019). [4] B. Z. Rameshti, S. V. Kusminskiy, J. A. Haigh, K. Us ami, D. Lachance-Quirion, Y. Nakamura, C.-M. Hu, H. X. Tang, G. E. Bauer, and Y. M. Blanter, Cavity magnonics, Physics Reports 979, 1 (2022).



Model of antiparallel FM multilayer.

- (a) Illustration of the 2D-SSH4 chian for antiparal lel case. Magnon (denoted as a,c) and antimagnon (denoted as bar_a, bar_c) states of the layers are coupled via interlayer (light green, Δ _±) and intralayer (dark green, D2) dipolar interactions, with the much weaker intralayer interaction (Da2) indicated by dash dark green lines.
- (b) Calculated band structure for three antiparallel FM-bilayer unit cells;
- (c) Simulated counterpart for two unit cells.

Red circles and red ar rows indicate nonreciprocal topological surface states between the level-attraction anticrossing bulk states.



Tunable coupling and chirality in an antiparallel FM bilayer for traveling spin wave at kx = 6.8×10^7 1/m.(a) B_yc/ μ 0 = 0 A/m (b)B_yc/ μ 0 = -8.5×10^5 A/m. Spin wave chirality is shown as ellipses. There are two types of interlayer dipolar coupling, where spin waves hybridize: (a) level repulsive anticrossings as coherent (same chirality) coupling, whereas (b) level-attractive anticrossings as dissipative (opposite chirality) coupling. Red dashed boxes highlight intrinsic surface states of each uncoupled layer – degenerate modes with no observable splitting.

BP-06. Magnon Superlattices around Skyrmions in Frustrated Magnets

<u>A. Hullahalli</u>^{1,2}, C. Panagopoulos¹, C. Psaroudaki² ¹Nanyang Technological University, Singapore, Singapore, ²École Normale Supérieure, Paris, France

Magnetic skyrmions are topologically nontrivial spin textures typically studied in chiral magnets, which are known to exhibit complex magnon dynamics. We consider here skyrmions stabilized in frustrated magnets, in which both skyrmions and magnons possess fundamentally different properties. We identify a novel crystal-like localization of magnon modes around isolated skyrmions (see Figure), emerging due to strong interference effects caused by the comparable length scales of skyrmions and extended magnon states in the frustrated system. These magnon superlattices have tunable periodicity and exhibit complex structure related to the internal magnetization

^{*} Best Student Presentation Finalist / LB - Late-breaking Poster

dynamics of the skyrmion. In addition, long-ranged interactions between skyrmions and an additional 'helicity' degree of freedom introduce nonlinear interaction dynamics between skyrmions, leading to a topologically nontrivial band related to helicity within the first magnon gap and reshaping the higher energy modes.

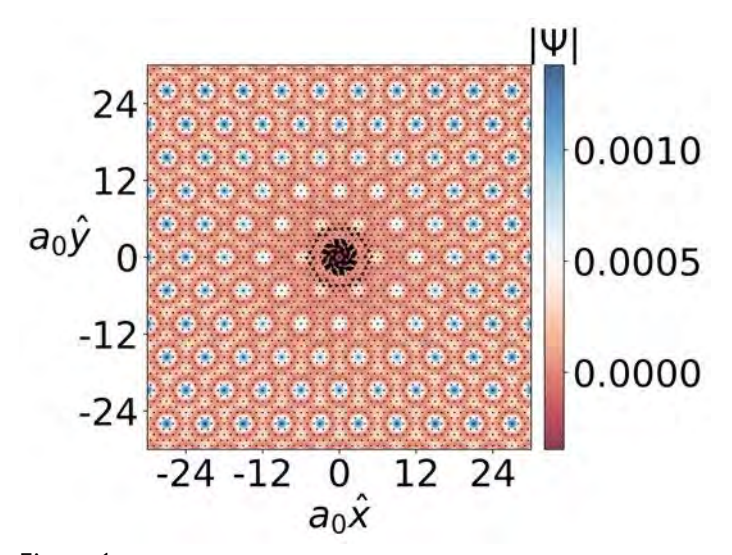


Figure 1

BP-07. Role of interfacial Dzyaloshinskii-Moriya interactions on dipole-exchange spin waves in ferromagnetic nanoribbons

<u>S. Hussain</u>¹, B. Hussain², M. G. Cottam³
¹Orange Coast College, Costa Mesa, California, United States, ²University of Michigan, Dearborn, California, United States, ³University of Western Ontario, London, Ontario, Canada

magnetic materials was introduced many decades ago [1,2],

Although the concept of antisymmetric exchange in

it typically provided only a small effect on the spin waves (SWs). The situation changed with the discovery of an interfacial Dzyaloshinskii-Moriya interaction (DMI), occurring at interfaces between a magnetic material and certain heavy metals (e.g., Fe/Ir). This enhancement has revitalized the interest of DMI in the SW dynamics of magnetic nanostructures (e.g., see [3,4]). Here we report on novel SW theoretical results obtained in finite-width ferromagnetic nanoribbons (or nanostripes) with DMI. We employ a microscopic (or Hamiltonian-based) approach that includes Heisenberg exchange interactions, magnetic dipole-dipole interactions, DMI, and Zeeman effects of a static magnetic field applied out of the plane of the ribbon. This methodology is analogous to that utilized in

earlier SW studies of DMI in magnetic nanorings [5]. It allows us to calculate the discrete spectrum of quantized bulk SWs, which have a propagating character with wave vector k along the length of the nanoribbon and behave as standing modes across the width. In addition, we find for some values of the parameters that there may be localized edge SWs whose amplitudes decay with distance from the lateral edges of the ribbon. Some examples of dispersion relations are shown in Figs. 1 and 2 for cases with and without the DMI, respectively, when the exchange is dominant. The asymmetry between positive and negative k in Fig. 2 clearly shows the mode nonreciprocity. We find that the dipole-dipole interactions lead to a shift in the SW energies.

[1] I. Dzyaloshinskii, J. Phys. Chem. Solids, Vol. 4, p.241, (1958).

[2] T. Moriya, Phys. Rev., Vol. 120, p.91 (1960).

[3] J.-H. Moon et al., Phys. Rev. B, Vol. 88, p.184404 (2013). [4] R. Camley and K. E. Livesey, Surf. Sci. Reports, Vol. 78, p.100605 (2023).

[5] B. Hussain and M. G. Cottam, J. Appl. Phys., Vol. 132, p.193901 (2022).

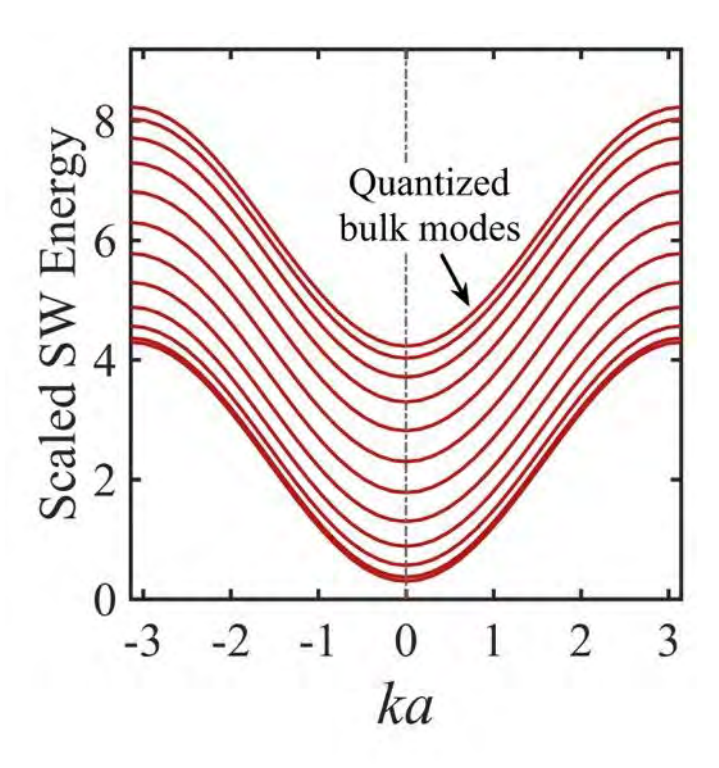


Fig. 1. Energies (in units of SJ, for spin S and exchange constant J) for the discrete SWs plotted versus ka where k is the wave vector along the ribbon (a = lattice parameter). In this case, there is no DMI, and so the modes are symmetric

in the positive and negative k directions.

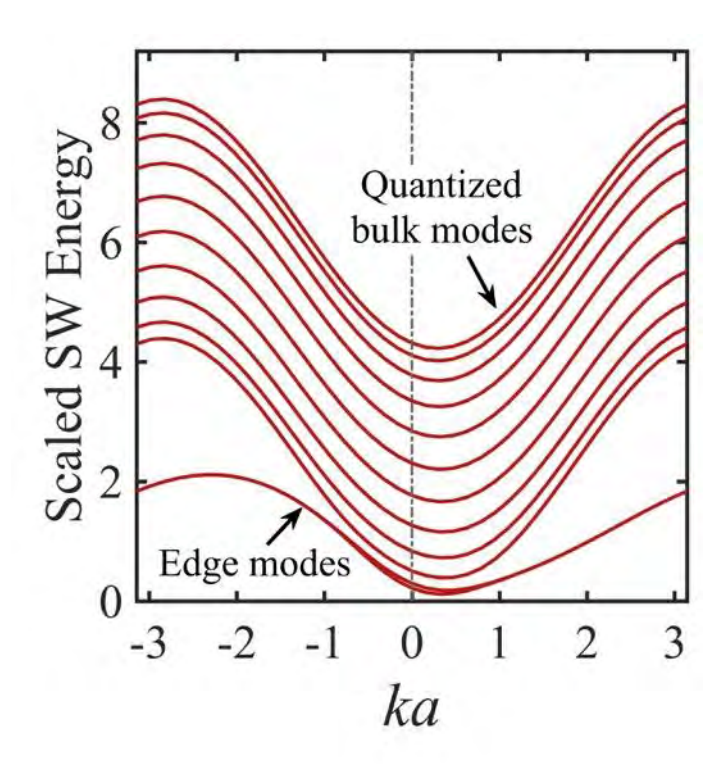


Fig. 2. As in Fig. 1, but for the case of nonzero DMI of magnitude $J_{DM} = 0.3J$ and with the introduction of edge exchange perturbations ($J_E = 0.2J$). There is now an asymmetry between SW propagation in the positive and negative k directions, as well as localized edge SWs split off from the region of quantized bulk modes.

BP-09. Simulating Magnon Dispersion of Layered Antiferromagnets

<u>T. Jeffrey</u>, E. Stimpson, J. Sklenar Physics & Astronomy, Wayne State University, Detroit, Michigan, United States

Synthetic antiferromagnets (SAFs) are ferromagnetic slabs of material that are coupled antiferromagnetically using a non-magnetic spacer layer. These materials are currently of broad interest to the magnonics community because of the rich set of magnon-magnon interactions that can be engineered into a SAF. Most studies have focused on magnons at the long wavelength limit, k=0. In general, there is a gap in our understanding of how magnon-magnon interactions behave at finite magnon wavelengths in a SAF. To study finite wavenumber effects, we use micromagnetic simulations to measure the dispersion of both optical and

acoustic magnons. The SAF structure is built in Mumax3 and models a traditional AFM bilayer with a size of $100\mu m^2$. The system is set to relax in the presence of a static uniform field until it reaches a ground state. A spatially non-uniform field pulse is applied, and the magnetization of the system is recorded as the waves propagate. The polarity of the pulse is used to couple to either optical or acoustic magnons. A spectral analysis of the micromagnetic system reveals a continuous spectrum of magnon modes (as seen in Figure 1) which can be used to reconstruct the magnon dispersion relationships within the SAF system. Our work will lay a foundation for better understanding of magnonmagnon interactions in layered AFM in the finite-wavelength limit.

TJ. and J.S. acknowledge support from the National Science Foundation under DMR-2328787.

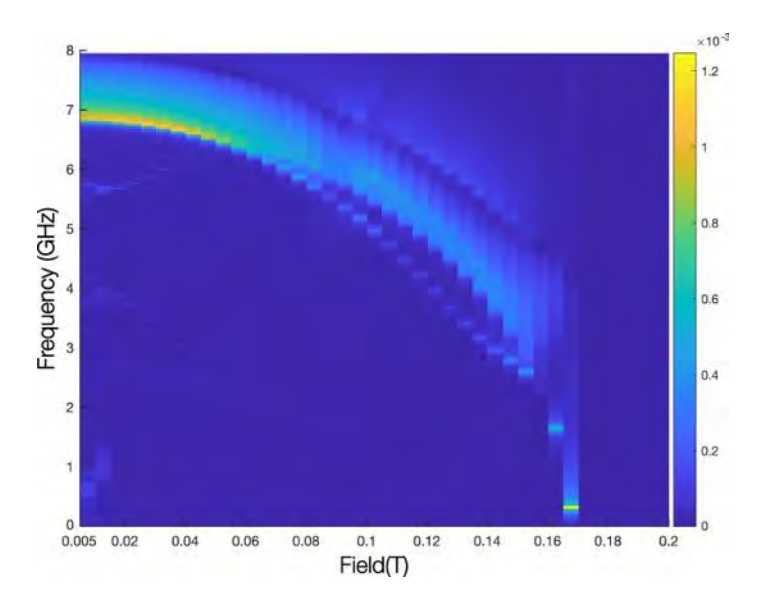


Fig. 1. Visualization of the optical magnon spectrum in field-frequency space. The band is comprised of finite wavelength modes with corresponding wavelengths from the long-wavelength limit to approximately a few hundred nanometers. Colormap indicates amplitude of magnon in arbitrary scale.

BP-10. Observation of breathing magnetic domain wall at ferromagnetic nanowires

S. Ahn

Postech, Pohang, Korea (the Republic of)

The thermal fluctuation in a geometrically constrained magnetic domain wall (CDW) is critical to understand switching behaviors of CDWs as inputs for a random variable generator for probabilistic computing [1]. Here, we elucidate the effect of thermal magnetization fluctuation on its oscillatory behavior by considering the thermal fluctuation of the 2D magnetization (m) vector [2]. Fig. 1(a) shows noise spectra in magnetization components (m_x and m_v) at specific frequencies of 4 kinds of modes—the red region indicates the highest magnetization fluctuation at each mode as shown in the inset of Fig. 1(b). Fig. 1(b) shows noise spectra in m_x and m_y at specific frequencies under H_T =-150 Oe corresponding to maximum downward field. Compared to Fig. 1(a) indicating the oscillatory depinning behavior, peaks at 1.52 (Mode 1) are relatively strengthened, whereas peaks at 2.28 (Mode 2), 3.58 (Mode 3), and 4.52 GHz (Mode 4) are comparatively weakened. Especially, the m_x and m_y show stepwise reductions at Mode 1 and Mode 3 with increasing H_T in the negative direction as shown in Fig. 2(b). It is clearly seen that the behavior of thermal magnetization fluctuations at mode 1 and mode 3 of Fig. 2(b) follows that of depinning field from notches as shown in Fig. 2(a). Especially, Such behaviors correspond to oscillatory tilting-angle(φ) behavior of the magnetization m with respect to H_T (not shown). The oscillation of tilting angle(ϕ) induces the breathing domain wall mode [3]. The tilting angle(φ) behavior is confirmed by a micromagnetic simulation at 300 K.

- [1] K. Everaert et al., Appl. Phys. Lett. 122 (2023) 211902.
- [2] N. Smith, J. Appl. Phys. 90 (2002) 5768.
- [3] M. Mori et al., J. Phys.: Condens. Matter 26 (2014) 255702.

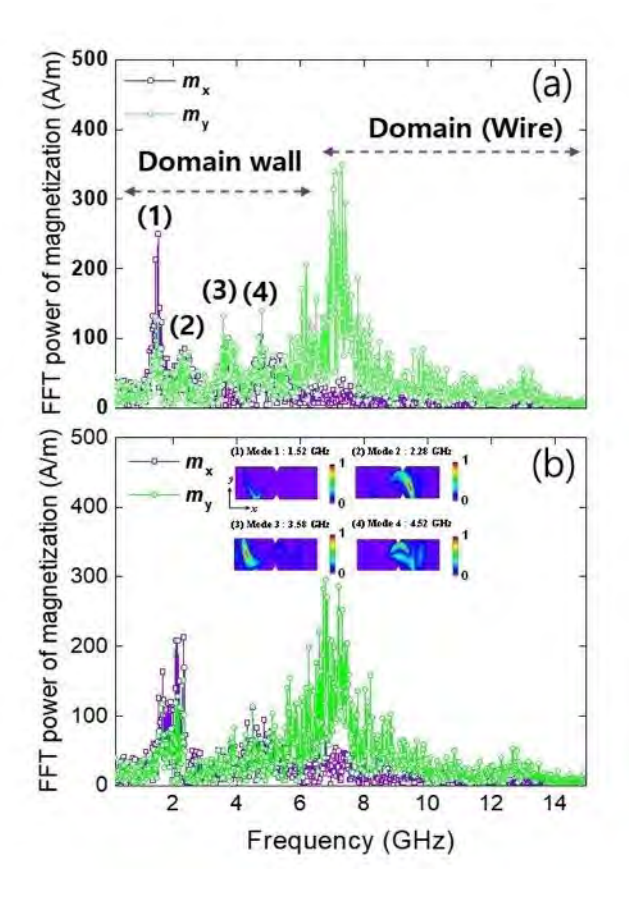


Fig. 1 (a) Noise spectra in magnetization components (m_x and m_y) under (a) H_T = 0 Oe (No external field) and (b) H_T =-150 Oe. Inset: 4 modes(schematics) at specific frequencies under H_T = 0 Oe.

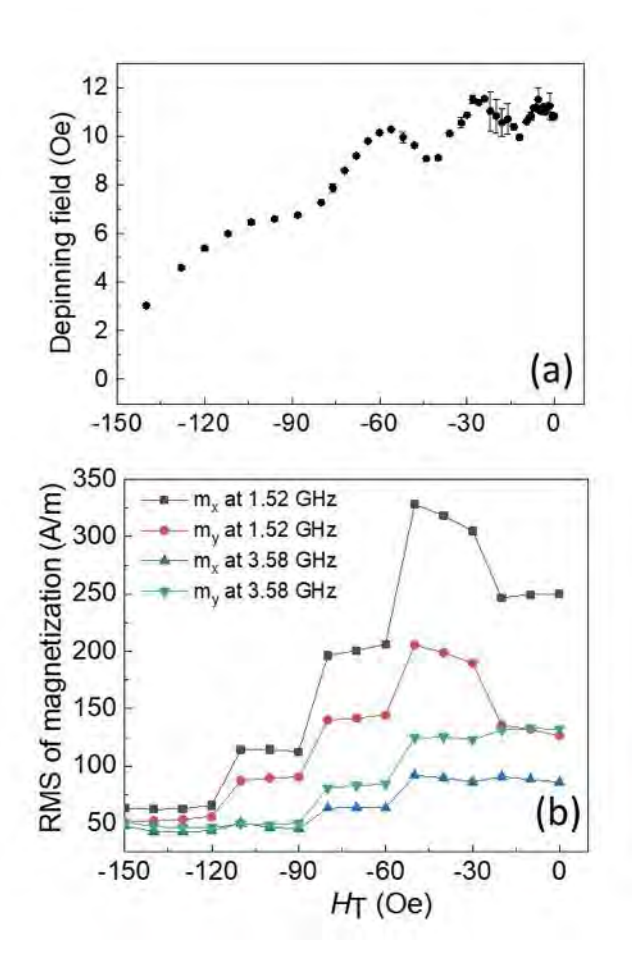


Fig. 2 (a) Depinning field with respect to H_T (exp.) (b) RMS values of m_x and m_y of DWs at specific frequency of 1.52 and 3.58 GHz with respect to H_T .

SESSION BQ: TRANSFORMERS AND POWER ELECTRONICS I (POSTER SESSION)

Chair(s): H. Matsumori, *Nagoya Institute of Technology, Nagoya, Japan*Tuesday, October 28, 2025
02:30 PM-05:30 PM
Exhibit Hall Posters

BQ-01. Structural Design of a Common-Mode Inductor with Metal Casing for Improved High-Frequency Performance

Y. Ueda¹, H. Matsumori¹, K. Nagayoshi²
¹Electrical and Mechanical Eng., Nagoya Institute of Technology, Nagoya, Aichi, Japan, ²Toyota industries corporation, Nagoya, Aichi, Japan

In recent years, power converters used in electric vehicles have required higher power density. However, in on-board chargers (OBCs), EMI filters often occupy considerable volume [1], primarily due to the degradation of highfrequency performance caused by the parasitic capacitance (EPC) between the windings of the common-mode (CM) inductor. This necessitates additional filtering components. A conventional approach, shown in Fig. 1, places a capacitor equal to four times the EPC between the center tap of bifilar windings and ground to cancel the EPC [2]. However, this method requires special winding configurations and additional components, increasing cost and complexity. This paper proposes a novel approach to cancel EPC by intentionally introducing opposing parasitic capacitance, referred to as cancellation capacitance, between the inductor winding and a surrounding metal casing. The CM inductor is designed to meet the inductance required by the EMI attenuation target. From this inductance value, the necessary magnetic core and winding parameters are derived, which in turn define the EPC of the CM inductor [3, 4]. Based on the obtained EPC, the metal casing is then designed to introduce a cancellation capacitance that offsets the EPC. The cancellation capacitance is determined through circuit simulations that include parasitic elements, and the casing geometry is adjusted accordingly. Using this method, a 22-turn inductor (Fig. 2) [5] is applied to evaluate performance. The left-hand panel within the CM attenuation section of Fig. 2 shows that a casing with 2-5 times the EPC improves attenuation, whereas excessive capacitance (e.g., 8EPC) degrades performance. The right-hand panel within the same section compares simulation and experimental results for the 5EPC and no-casing conditions. The measurements confirm improved CM attenuation with the casing, aligning

closely with the simulation.

This study demonstrates that the proposed method effectively maintains high-frequency performance. The final paper will provide detailed explanations of the casing design process, cancellation capacitance simulation, and experimental validation.

[1]M. J. Kasper, J. A. Anderson, G. Deboy, Y. Li, M. Haider and J. W. Kolar, "Next Generation GaN-based Architectures: From 240W USB-C Adapters to 11kW EV On-Board Chargers with Ultra-high Power Density and Wide Output Voltage Range" PCIM Europe 2022; International Exhibition and Conference for Power Electronics, Intelligent Motion, Renewable Energy and Energy Management, pp. 1-10, (2022)

[2]Shuo Wang, Fred C. Lee and Jacobus Daniel van Wyk: "A Study of Integration of Parasitic Cancellation Techniques for EMI Filter Design With Discrete Components", IEEE Transactions on Power Electronics, Vol.23, No.6, pp.3094-3102 (2008)

[3]Szymon Pasko, Boguslaw Grzesik, Fabian Beck, "Attenuation of Nanocrystalline and Ferrite Common Mode Chokes for EMI Filters", Electronics, Vol. 14, No.1, June 2010. [4]Shotaro Takahashi, Keiji Wada, "Simple Method for Estimation of Stray Capacitance of Toroidal Inductors by Considering an Insulation between Winding and Core," IEEJ Transactions on Industry Applications, vol. 142, no. 1, pp.33-40, 2022.

[5]Nippon Chemi-Con Corp. "FW series core"

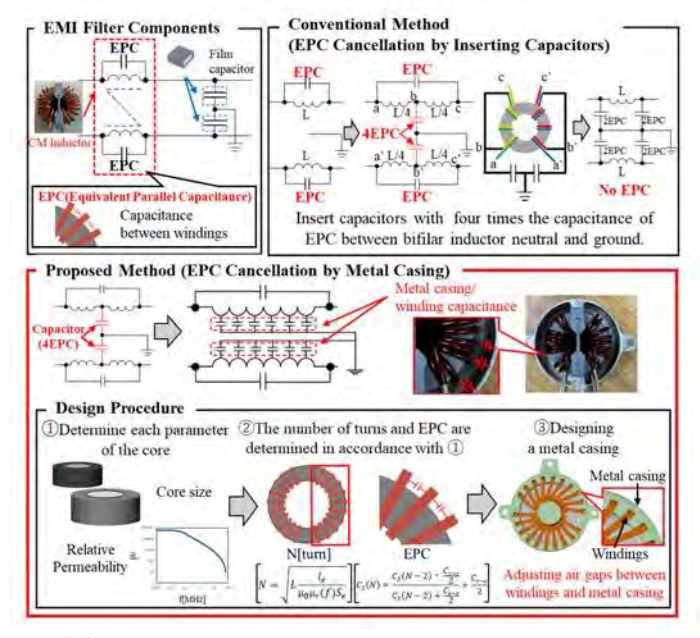


Fig. 1 Overview of this paper

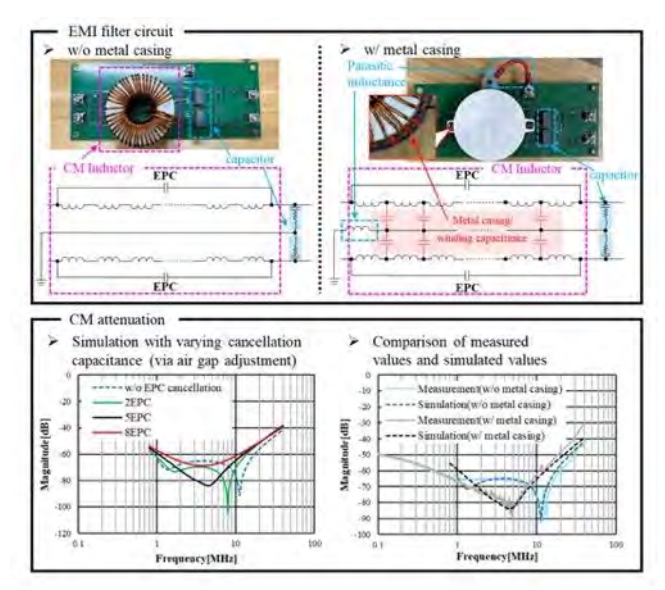


Fig. 2 EMI filter circuits and CM attenuation characteristics

BQ-02. A Study on volume reduction and power density improvement of motor using PCB stator

<u>Y. Lim</u>, D. Choi, Y. Lee, J. Lee, W. Kim *Electrical Engineering, GACHON UNIVERSITY, Seongnam-si, Gyeonggi-do, Korea (the Republic of)*

This paper proposes an AFPM with SSSR structure using PCB stator to improve the power density of RFPM. With the sophistication of modern industry, the demand for

high-performance motors is growing rapidly, especially in next-generation industries such as electric vehicles, drones, and robots, which require high power density characteristics.

Axial Flux Motor(AFPM) can be designed with shorter axial lengths than Radial Flux Motor(RFPM) under the same volume conditions because the torque is proportional to the cube of the rotor diameter, which is advantageous for improving power density through thinning and lightweighting. However, conventional AFPM have structural limitations in core design utilizing laminated steel plates. To improve this, recent research has focused on PCB Stator AFPM, which utilize a PCB(Printed Circuit Board) as a stator. PCB Stator implements the winding pattern on the substrate, which provides a high degree of freedom in winding design compared to conventional processes. It is a coreless type structure in which the stator core is deleted, so there is no stator iron loss and zero cogging can be realized[1]. This paper studied AFPM with PCB stator to

reduce the volume of existing RFPM and improve the power density by utilizing the characteristics of PCB motor. Since various topology configurations are possible depending on the configuration of rotor and stator and the magnetization arrangement of permanent magnets, we compared the performance of two structures of AFPM, SSDR(Single-Stator Double-Rotor) and SSSR(Single-Stator Single-Rotor)[2], [3]. While maintaining the same performance as a conventional RFPM, the efficiency trade-off points for varying the winding pattern end turns and applying a magnet overhang structure were identified. While the SSDR is designed with the minimum magnet thickness that can be fabricated at the target volume, the SSSR has an efficiency margin based on the target efficiency from previous studies, which allows for further reduction in magnetization to reduce the volume. Finally, we derived a model of SSSR with higher power density than SSDR and verified its performance through finite element method(FEM).

[1]D. -W. Nam, M. -K. Hong, N. -R. Jo, D. -H. Jung and W. -H. Kim, "Design of Coil Patterns for an Axial Flux Permanent Magnet Synchronous Motor With PCB Stator," in *IEEE Access*, vol. 13, pp. 12936-12944, 2025.

[2]H. H. Heimes, S. Biegler, R. Pandey, L. Heetfeld, S. Dünnwald and L. Jansen, "Development and comparison of various continuous duty cooling concepts for the stator of an SSDR Axial-flux motor," 2023 First International Conference on Cyber Physical Systems, Power Electronics and Electric Vehicles (ICPEEV), Hyderabad, India, 2023.
[3]Choi, D.-H.; Han, H.-S.; Hong, M.-K.; Jung, D.-H.; Kim, W.-H. Design for Loss Reduction in a Compact AFPM Electric Water Pump with a PCB Motor. Energies 2025.

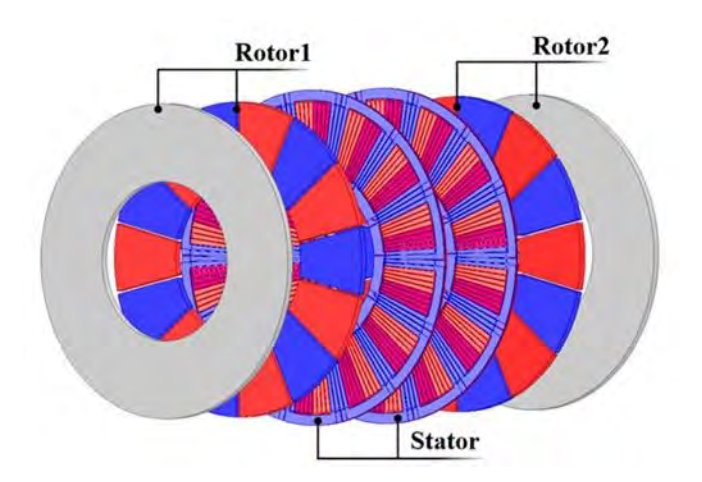


Fig. 1. PCB Stator AFPM SSDR

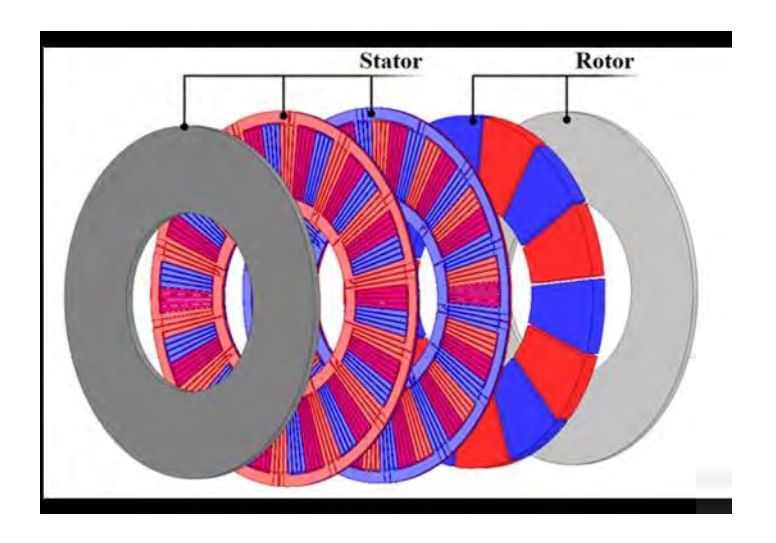


Fig. 2. PCB Stator AFPM SSSR

BQ-03. Thin-film YIG-based Tunable Inductors at Microwave Frequencies

<u>S. Sultana</u>, D. Hedlund, P. Kulik University of Central Florida, ORLANDO, Florida, United States

The continuous miniaturization of electronic components has led to a high demand for compact, high-performance power devices in recent years. This has driven interest in thin-film magnetic materials. In this work, we present a yttrium iron garnet (Y3Fe5O12 YIG) thin-film inductor exhibiting a strong inductive response from 1.8 GHz to 3 GHz, demonstrated through finite element method simulations. The inductor coils were modeled using a 2 µm thick aluminum layer on a 10 µm YIG layer supported by a 500 µm gadolinium gallium garnet (GGG) substrate. YIG has high magnetic permeability, the lowest Gilbert damping factor at microwave frequencies, and offers negligible electrical skin effect due to its insulating nature. In contrast, conventional inductors suffer from significant conduction losses at high frequencies. Moreover, the magnetic film improves the overall inductance by enhancing the magnetic field induced by the current flowing through the inductor coils.

The proposed structure (figure 1) achieved an inductance of 48 nH with no applied bias. Under an out-of-plane magnetic bias of 3000 Oe, it attained a quality factor (Q) of 5.5 for an inductance density of 1.44nH/mm². This magnetic thin-film

^{*} Best Student Presentation Finalist / LB – Late-breaking Poster

on-chip inductor can also be tuned (figure 2) within the ultra-high band (0.03 to 3 GHz) frequencies by introducing variations of an applied magnetic bias, making them suitable to be used in adaptive RF systems and tunable filters.

Additionally, YIG exhibits excellent magnetic stability from cryogenic temperatures up to ~550 K (~277°C), allowing YIG-based devices to maintain consistent performance across wide temperature ranges and under radiation exposure. Even though in some cases, YIG inductors might have a larger footprint due to having a biasing circuit integrated, they will out-perform semiconductor or ferritecore inductors in a high-frequency application and under harsh environmental conditions.

Gardner, D. S., Schrom, G., Paillet, F., Jamieson, B., Karnik, T., & Borkar, S. (2009). Review of on-chip inductor structures with magnetic films. *IEEE Transactions on Magnetics*, *45*(10), 4760–4766. https://doi.org/10.1109/TMAG.2009.2030590 K. I. Arai, M. Yamaguchi, H. Ohzeki and M. Matsumoto, "Application of YIG film to thin film inductors," in *IEEE Transactions on Magnetics*, vol. 27, no. 6, pp. 5337-5339, Nov. 1991, doi: 10.1109/20.278831

Wang, G., Liu, H., Wu, H., Li, X., Qiu, H., Yang, Y., Qu, B., Ren, T. L., Han, X., Zhang, R., & Wang, H. (2016). Epitaxial yttrium iron garnet film for fabrication of high frequency on-chip inductors. *Applied Physics Letters*, *109*(16).

https://doi.org/10.1063/1.4964642

Hao, W., Li, X., Pan, Z., Maio, R., Yue, Z., Yang, C., & Wang, A. Z. (2024). Advances and Perspectives in Magnetic-Integrated Inductors for RF ICs. *IEEE Transactions on Materials for Electron Devices*, 1–15.

https://doi.org/10.1109/tmat.2024.3410166 Désiré, A., Kriga, A., Youssouf, M., Siblini, A., Chatelon, J. P., Blanc-Mignon, M. F., Payet-Gervy, B., Piot, A., Dufeu, D., & Rousseau, J. J. (2013). Fabrication and characterization of micro-inductors deposited on magnetic thin and thick layers. *Advanced Electromagnetics*, *2*(3), 44–50. https://doi.org/10.7716/aem.v2i3.210

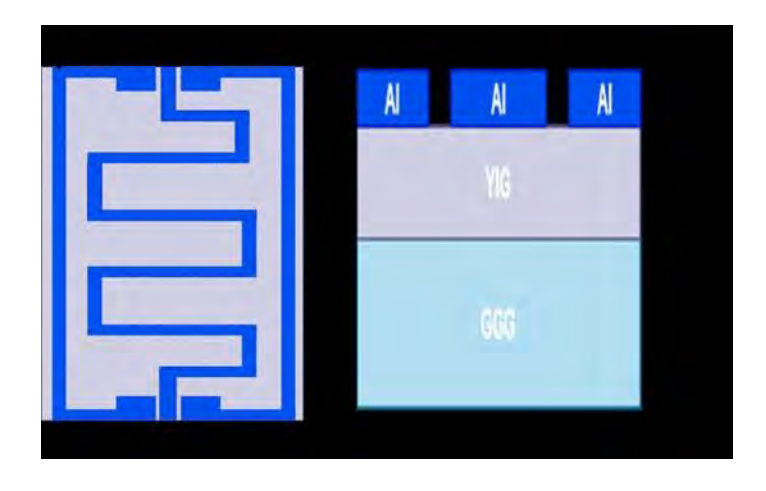


Figure-1: (a) YIG thin-film inductor (b) Cross-sectional view of the inductor

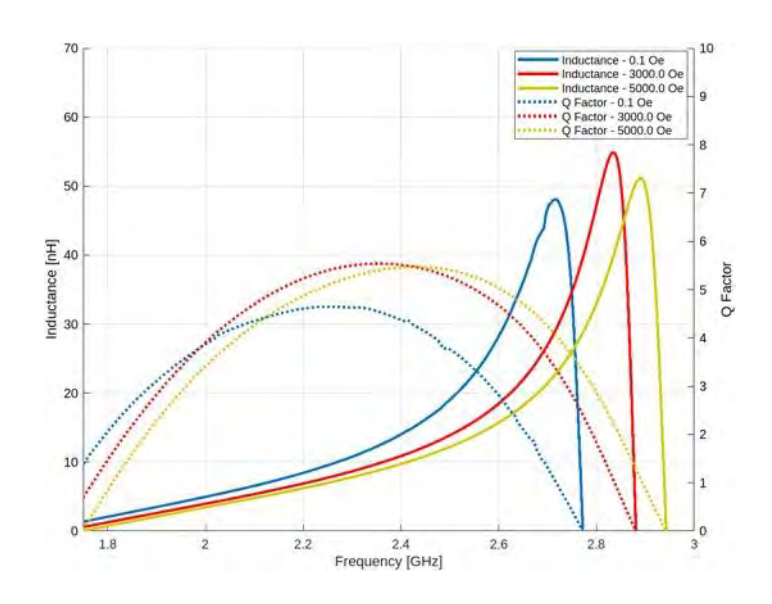


Figure-2: Magnetic tunability of inductance and Q factor

BQ-04. New Slim Microspeaker Design for Smartwatches with Halbach Array Magnetic Circuit

Y. Jeong¹, J. Park¹, D. Xu², S. Hwang¹
¹Department of Mechanical Engineering, Pusan National
University, Busan, Korea (the Republic of), ²School of
Mechatronic Engineering and Automation, Shanghai University,
Shanghai, China

Recent wearable device development has focused not only on functionality but also on user comfort and wearability[1]. As smartwatches have become a key fashion item, a slimmer design has become essential for wearability. Since the speaker is usually mounted vertically on the side, its width becomes a critical constraint on the overall device thickness. Therefore, minimizing the speaker width without compromising the acoustic performance is a key challenge in next-generation smartwatch speaker design[2].

This study proposes a novel speaker design that significantly reduces the width while improving the sound pressure level (SPL). Fig. 1 shows the 3D and cross-sectional views of the prototype and new type designs. The pure acoustic component size of the prototype is 20.34 mm × 4.65 mm × 3.73 mm, while the new type is designed as 24.32 mm × 3.46 mm × 3.5 mm. The total volume and width were reduced by 17% and 26%, respectively.

The primary difference is the structure of the magnetic circuits. The prototype employed a conventional three-magnet structure with an additional top magnet. In contrast, the new type introduces a novel magnetic structure inspired by the circular Halbach array, designed to increase the magnetic flux passing through the coil[3]. This allows the use of more permanent magnets and a significant reduction in the thickness of the bottom steel yoke. Moreover, because of the limited space for side diaphragms and center magnet, a bobbin structure, commonly used in loudspeakers, was adopted.

The force factor, a key parameter of speaker performance, defined as the product of the magnetic flux density and total coil length, was measured as 0.448 N/A and 0.569 N/A for the prototype and new type, respectively. For SPL measurements, the B&K setup is employed and Fig. 2 shows the SPL experimental results from 100 Hz to 20 kHz. The new type achieved an average SPL improvement of 1 dB across the low frequency range (100–1k Hz), demonstrating enhanced acoustic performance despite the reduced width.

These results validated the effectiveness and practicality of the proposed design.

[1] S. H. Chuah, P. A. Rauschnabel and N. Krey, *Computers in Human Behavior*, Vol. 65, p.276-284 (2016)

[2] Ki-Hong Park, Zhi-Xiong Jiang and Sang-Moon Hwang, *Applied Sciences*, Vol. 10, p.8902 (2020)

[3] R. Bjørk, C. R. H. Bahl and A. Smith, *Journal of Applied Physics*, Vol. 104, 013910 (2008)

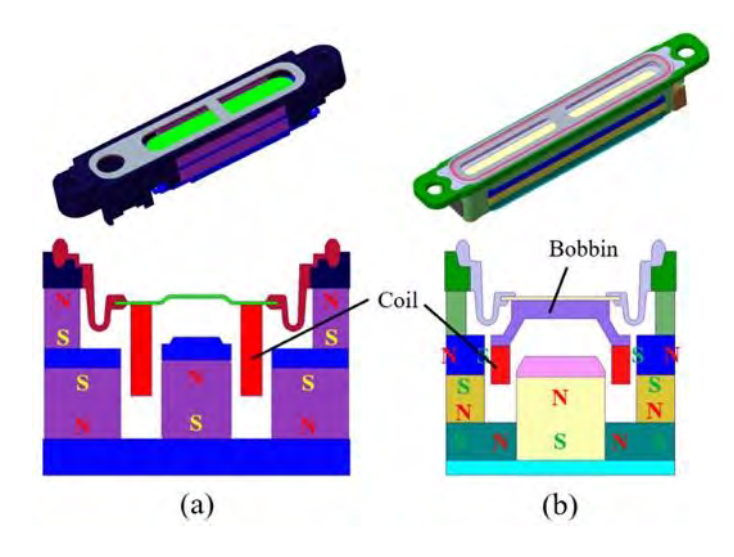


Fig. 1 3D and cross-sectional view: (a) prototype and (b) new type

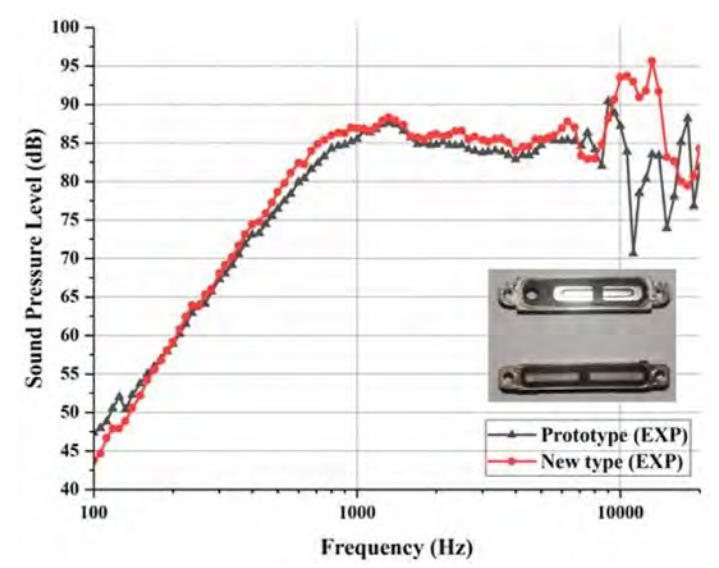


Fig. 2 SPL comparison between the Prototype and New design.

BQ-05. A Heating Power Optimization Method for Electro-Thermal Multi-Energy Flexible Generator Based on Composite Anisotropic Materials

 $\underline{J. Yuan}^{1,3}$, H. Wang^{1,3}, B. Peng^{1,3}, H. Zhou^{1,3}, X. Chen², Q. Wang²

¹School of Electrical Engineering and Automation, Wuhan University, Wuhan, Hubei, China, ²Electric Power Research Institute China Southern Power Grid, Guangzhou, China, ³State Key Laboratory of Power Grid Environmental Protection, School of Electrical Engineering and Automation, Wuhan University, Wuhan, Hubei, China

To address decentralized winter heating and unstable wind power output, integrated permanent magnet wind turbines with eddy-current heaters have emerged as a solution^[1]. Optimizing thermal output is critical, and modifying heating element materials offers significant potential. Typical materials present a trade-off: high-conductivity metals like aluminum or copper suffer from low permeability, limiting magnetic flux and heat generation, while ferromagnetic materials like steel 1010 enable strong flux but are hindered by low conductivity. Existing enhancement methods like slotting in stator near magnets increase complexity, weaken structural integrity, and can exacerbate torque ripple^[2].

This work pioneers the implementation of an aluminum-steel 1010 dual-layer stator structure within the equipment, contrasting it conceptually with the traditional single-material design in Fig.1(a). Fig.1(b) highlights the superior magnetic circuit characteristics offered by the bilayer compared to a monolithic high-conductor material. Subsequent finite-element analysis, employing a 2 mm aluminum layer and 4 mm steel layer, rigorously validated the structure's effectiveness; the resultant magnetic flux density and power distribution within the stator are presented in Fig.1 (c). Crucially, the analysis detailed in Fig.2(b) shows that this structural innovation dramatically boosted heat generation by 209.64%, elevating output from 3.32 kW to 10.28 kW, while achieving a substantial 68.36% reduction in torque ripple, down to 0.56%.

Further optimization explored the layer combinations while maintaining the established thicknesses, comparing the performance of copper/aluminum outer layers paired with either standard steel-1010 or the advanced soft magnetic alloy Hiperco 50, chosen due to its superior saturation flux density and enhanced permeability within critical non-saturated operating regimes shown in Fig.2(a). Simulation results unequivocally revealed that the copper-Hiperco 50 configuration delivers optimal performance, pushing

thermal power output to 14.61 kW and minimizing torque ripple to 0.51%.

[1] TUDORACHE T, TRIFU I and MELCESCU L, et al. Numerical analysis of an electro-thermal wind generator[C]/2017 9th International Conference on Electronics, Computers and Artificial Intelligence(ECAI).IEEE, 2017: 1-4.

[2]Peng B, Yuan J, Wang H, et al. Electromagnetic Parameter Design and Finite Element Analysis of aNovel Dual-Stator Electric-Thermal Output Machine[C]//2024 1EEE 21st Biennial Conference on Electromagnetic Field Computation (CEFC).IEEE,2024:01-02.

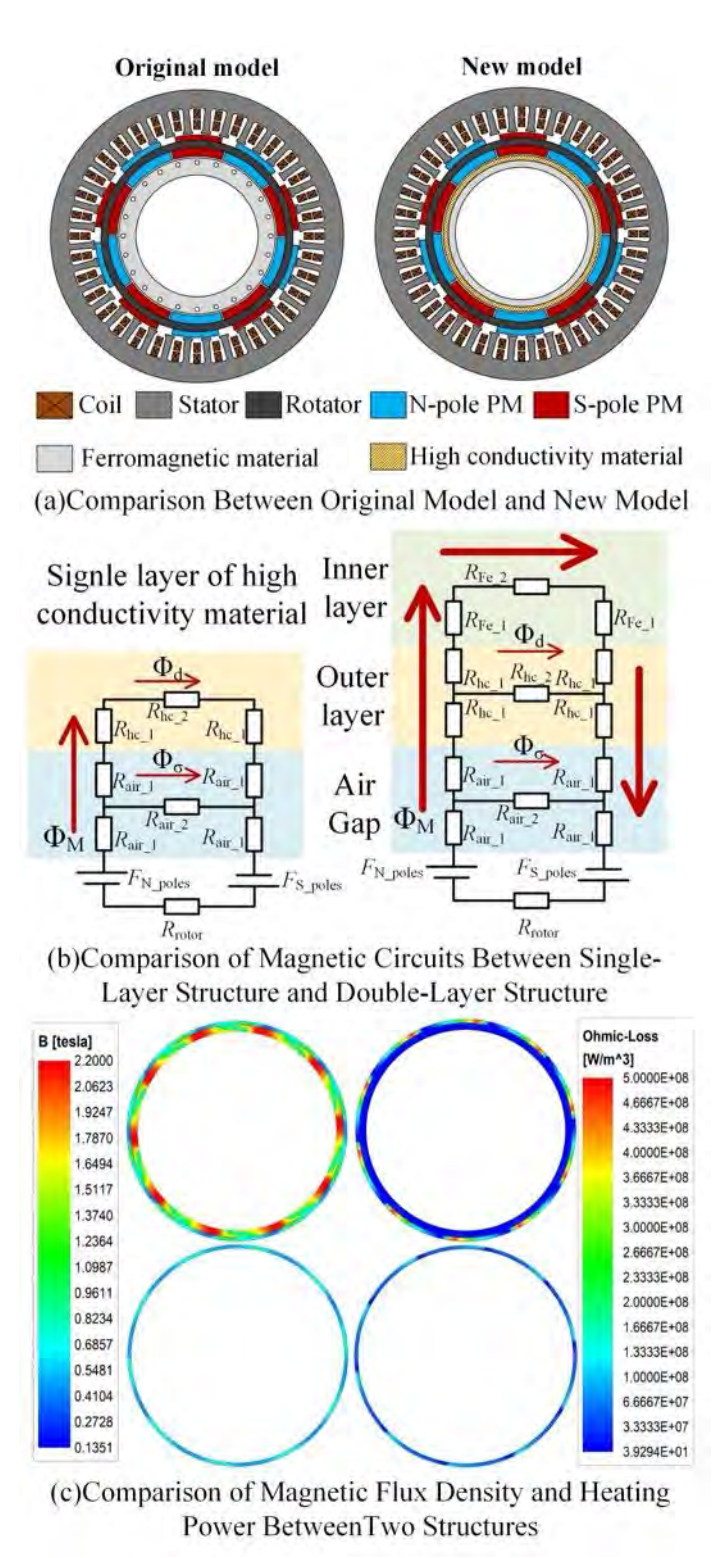
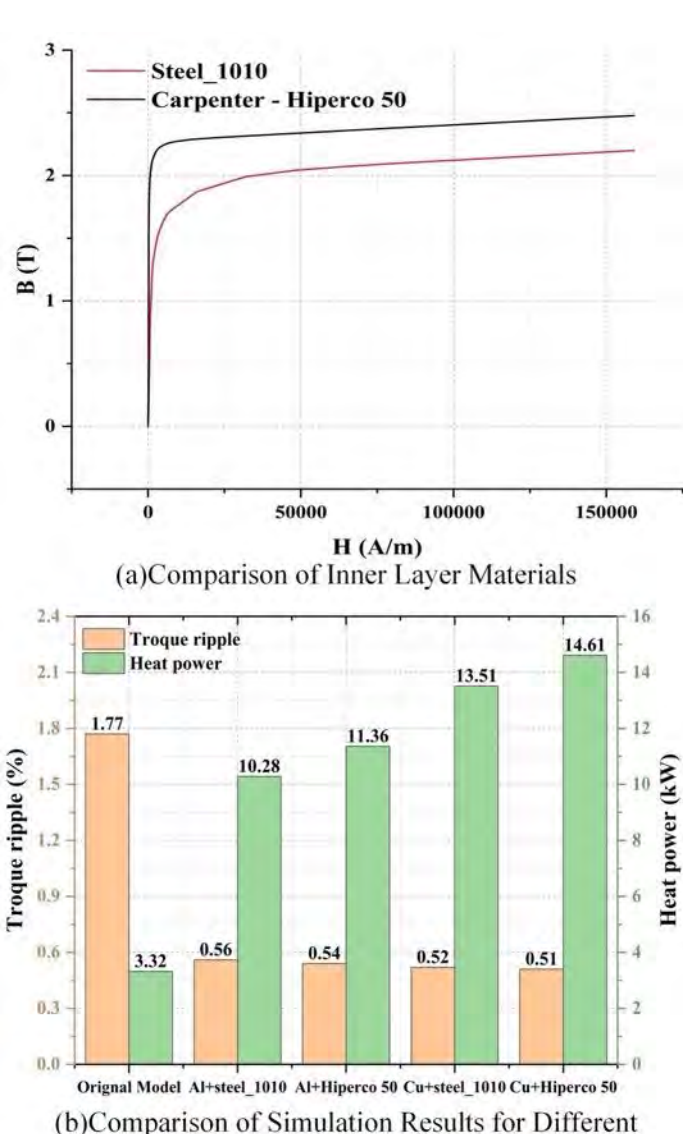


Fig. 1 New Structure of the Equipment and Its Optimization Effect



Combinations

Fig. 2 Comparison of Material Properties and Simulation Results of Key Performance

BQ-06. Configuration of Transmitter and Receiver of Wireless Power Transfer System while Driving for Electric Vehicles (EVs)

K. Hidaka¹, F. Sato¹, O. Ito¹, S. Miyahara¹, S. Sasaki²
¹Tohoku Gakuin University, Sendai, Miyagi, Japan, ²Hikaridenshi
.CO,LTD., Osaki, Miyagi, Japan

Research on wireless power transfer technology for EVs in motion is being actively conducted along with the electrification of internal combustion engines has been promoted. we assumed that the power transfer occurred within the 85[kHz] band following SAE International J2954⁽¹⁾ and determined the optimal coil size through simulation, considering the power transfer efficiency between the coils.

Fig. 1 shows the model of wireless power transfer during driving in this study. A rectangular coil was used on the transmitter side to ensure stable power supply in the direction of vehicle travel, and a square coil was used on the receiver side to facilitate the penetration of the vertical magnetic flux generated by the transmision coil. Using the electromagnetic field simulation software Ansys Maxwell 3D, we quantify the variation in the power feed efficiency that arises from the combination of outer dimensions and inner dimensions of the transmitter and receiving coils

The coupling coefficients are analyzed for the following combinations of transmitting and receiving coils.the coupling coefficients are analyzed from the combination of the transmitter and receiving coils when the width of the transmision coil is varied from 0.5 to 1.5[m] at 0.25[m] intervals and the length is varied from 5 to 15[m] at 5[m] intervals, while the outer dimensions of the receiving coil is fixed at 0.5[m] and the inner dimensions is varied from 0.05 to 0.45[m] at 0.05[m] intervals.

It is known that the power supply efficiency between the transmitting and receiving coils in electromagnetic inductivity is as shown in the following equation. (2) $\eta = 1/(1+2/\alpha(1+\alpha)^{\alpha}(1/2)) \ [\%] \ ^*\alpha = k^2 Q_1 Q_2$

Fig. 2 shows the variation of power supply efficiency with coil size ratio. The average values demonstrate that the highest power transfer efficiency is obtained when the ratio of the inner dimensions to outer dimensions of the receiving coil is 3:5. as for the power transmission coil, it was confirmed that a coil with an aperture of approximately $11[m^2]$ and a width of up to 1.25[m] tends to ensure a power feed efficiency of 80[%].

- (1) Guangyao Yu, Thiago Batista Soeiro, Jianning Dong, Study of Back-end DC/DC Converter for 3.7 kW Wireless Charging System according to SAE J2954, 2021 IEEE 15th International Conference on Compatibility, Power Electronics and Power Engineering (CPE-POWERENG), (2021)
- (2) Akira Saito, Yutaro Oishi, Satoshi Miyahara, Study on Wireless Power Transfer System for EVs while Driving Using Continuous Repeater Power Transmission Coil, IEEJ Transactions on Fundamentals and Materials Vol.143 No.4 pp.173-179 (2022)

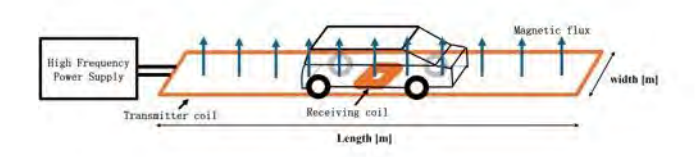


Fig.1 Overview of wireless power transfer system for EVs while driving

		Power Transfer Efficient n[%] Reciever Coil Outer Dimensions and Inner Dimensions								
	1									
		1:10	1:5	3:10	2:5	1:2	3:5	7:10	4:5	9:10
Transmitter Coil Width : Length [m]	0.5:5	88.6	88.9	89.0	89.1	88.9	89.2	87.7	86.4	81,
	0.5:10	84.8	85.1	85.2	85.5	85.2	85.6	83.7	82.0	76.
	0.5:15	82.2	82.6	82.7	83.0	82,6	83.2	80.9	79.1	72.
	0.75 : 5	86.9	87.2	87.4	87.6	87.5	88.0	86.4	85.3	80.6
	0.75:10	82.6	83.0	83.2	83.6	83.3	84.0	82,0	80.6	74.1
	0.75:15	79.7	80.2	80.4	80.8	80.5	81.3	79.1	77.4	70.5
	1:5	83.8	84.2	84.4	84.8	84.5	85.2	83.4	82.0	76.
	1:10	79.0	79.5	79.8	80.2	79.9	80.7	78.4	76.8	70.
	1:15	75.7	76.2	76.5	76.9	76.6	77.5	75.0	73.2	65.5
	1.25:5	80.8	81.2	81.5	81.8	81,6	82.3	80.2	78.7	72.4
	1.25 ; 10	75.3	75.8	76.1	76.6	76.2	77.1	74.6	72.7	65.4
	1.25 : 15	71.7	72.3	72.6	73.1	72.7	73.7	70.9	68.9	60.9
	1.5:5	77.8	78.3	78.6	79.0	78.7	79.5	77.1	75.4	68.5
	1.5:10	71.7	72.4	72.6	73.1	72.8	73.8	70.9	68.9	60.9
	1.5:15	67.7	68.4	68.7	69.3	68.9	69.9	66.9	64.6	56.0
Average		79.2	79.7	79,9	80.3	80.0	80.7	78.5	76,8	70.3

Fig.2 Variation in Power Transfer Efficiency Due to Coil Size Ratio

BQ-07. Research on a Nanocrystalline Amorphous-Based Magnetically Saturated Bridge Arm Coupled Reactor Applied in MMC-HVDC Systems

J. Yuan, W. Zhang, H. Zhou, J. L. Liu, Y. Sun, J. Liu, <u>D. Zhang</u> *Wuhan University, Wuhan, China*

The bridge arm reactor, a critical component in Modular Multilevel Converter High-Voltage Direct Current (MMC-HVDC) systems, is connected in series within converter arms. It acts as the AC interface for power transfer, suppresses arm circulating currents, and limits fault current rise [1]. Conventional air-core reactor, however, exhibit fixed inductance that cannot optimally balance these functions. Although a magnetically saturated bridge arm coupled reactor (MAR) using silicon steel was proposed to enhance current suppression via magnetic saturation and mutual inductance coupling [2], its high saturation point, low B-H curve slope variation, and limited demagnetization permeability constrain performance. This paper proposes a nanocrystalline amorphous-based MAR (NMAR) comparing material properties and performance against silicon steel designs.

In Fig. 1, the proposed NMAR comprises silicon steel, nanocrystalline amorphous, permanent magnets, excitation windings, and four sets of working windings. Within this configuration, the nanocrystalline amorphous replaces silicon steel as the core material within working column. The permanent magnets and excitation windings collectively establish the bias magnetic flux. The four working winding sets are bridged in pairs to enable mutual coupling. Under steady conditions, paired windings inversely couple, reducing their inductance. During circulating currents, they couple in the same direction, summing their inductance. Under short circuit faults, fault current desaturates the nanocrystalline core, rapidly raising the inductor's reactance.

Finite element electromagnetic field simulations of RLC discharge modeling MMC DC faults in Ansys were performed for both reactor materials. In Fig. 2, at 10ms post-fault, the MMC-HVDC arm short-circuit current using NMAR was only 1.2 kA, representing a 36.8% improvement compared to the magnetic saturation coupled reactor using silicon steel. Furthermore, the *B* on its desaturated core was also lower than that of the silicon steel reactor.

[1] C. Zhao, Q. Fan and S. Li. "Operation Method of MMC Capacitance Reduction Under Arm Inductor Switching Control." IEEE Transactions on Power Delivery, Vol. 36, p.418-428 (2021).

[2] J. Yuan, W. Zhang and Y. Sun. "Topological Design of a Novel Magnetically Saturated Bridge Arm Reactor with Controllable Inductance." 2024 IEEE 21st Biennial Conference on Electromagnetic Field Computation (CEFC), Jeju, Korea, p.1-2 (2024).

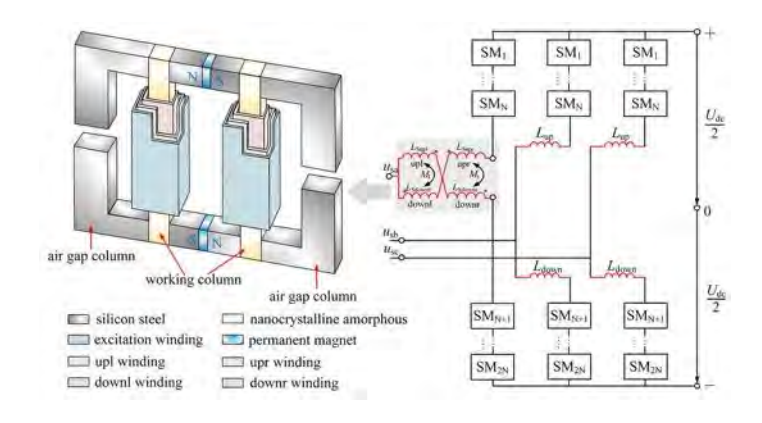


Fig. 1Configuration of NMAR Topology in MMC

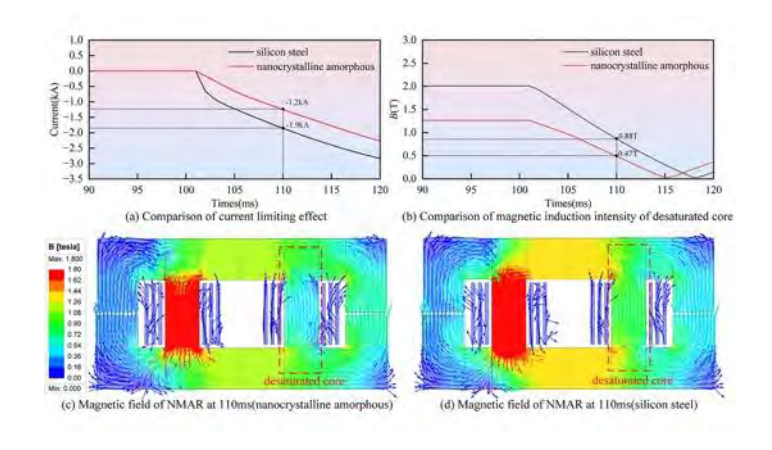


Fig. 2 Comparative Analysis of Electromagnetic Distribution Characteristics for Two Materials under Short Circuit Conditions

BQ-09. Design and Analysis of Nanocrystalline Core for Low-Temperature-Rise Anode Saturation Reactor

X. Li^{2,1}, J. Yuan^{2,1}, H. Zhou^{2,1}, Z. Mo¹, Y. Wang¹, J. Hou^{2,1}

¹School of Electrical Engineering and Automation, Wuhan
University, Wuhan, China, ²State Key Laboratory of Power Grid
Environmental Protection, School of Electrical Engineering and
Automation, Wuhan University, Wuhan, China

With the rapid development of high-voltage direct current transmission projects and the continuous increase in converter valve capacity, thyristors, as the core switching elements of converter valves, are facing severe risks due to the rate of current change. Although the Anode Saturation Reactor (ASR) can provide transient inductance to suppress the current rate of change and protect the thyristors, its core loss is relatively high under the excitation of periodic nonsinusoidal pulses, and heat accumulates within the low thermal conductivity insulating layer [1]. The local temperature rise effect of the ultra-thin silicon steel ASR may cause material thermal aging, becoming a bottleneck that limits the reliability of the converter valve system [2]. To address these issues, this paper proposes the use of nanocrystalline material (Metglas-2605S3A) to construct a new type of Anode Saturation Reactor (NC-ASR). Due to its excellent low-loss characteristics, nanocrystalline materials can significantly reduce the energy consumption of the equipment. However, due to their relatively low magnetic saturation point, the saturation time is significantly shortened, failing to meet the strict requirements for saturation time needed to protect the thyristors. Therefore, this paper uses the original saturation time and the initial rate of current change as evaluation criteria. Based on the magnetic performance parameters of nanocrystalline materials, the core size of the NC-ASR is redesigned through a capacitor discharge circuit coupling simulation. The structure of the ASR and the capacitor discharge waveform before and after replacing the core material are shown in Figure 1. The results of the electromagnetic-thermal-fluid multiphysics simulation indicate that the NC-ASR achieves significant improvements in loss and temperature rise, while ensuring the protection performance of the thyristor: its saturation time and initial rate of current change are almost identical to those of the ultra-thin silicon steel ASR, with the core loss reduced to 71% of the original value and the steady-state average core temperature decreased by 8.3%.

[1] Mo, Zuoquan, et al. "Valve reactor for HVDC system: Electrical, thermal and vibrational properties." *International Journal of Electrical Power & Energy Systems* 161 (2024):

110149.

[2] Wang, Yifan, et al. "Simulation analysis on magnetic core loss characteristic of valve reactor in UHVDC system." *AIP Advances* 14.2 (2024).

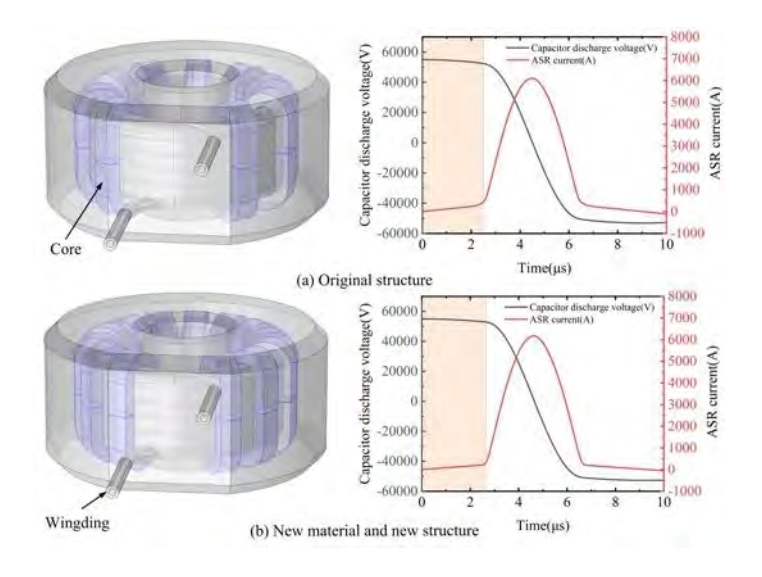


Fig. 1 ASR Model and Capacitor Discharge Waveform

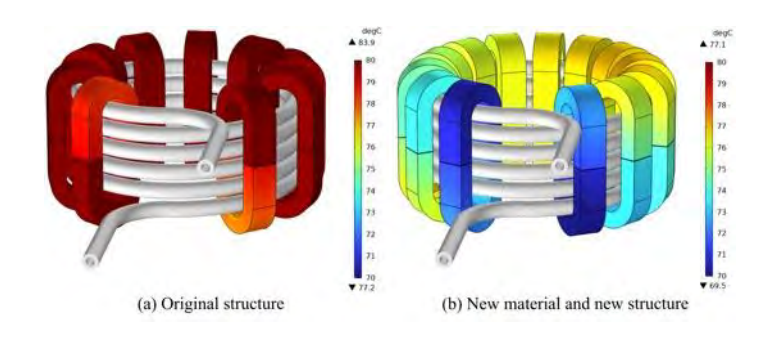


Fig. 2 Steady state temperature of iron core

130

BQ-10. Research on Adjustment Range Expansion of Orthogonal Controllable Reactors Based on Low-Saturation-Point Core Materials

J. Hou^{1,2}, J. Yuan^{1,2}, H. He^{1,2}, G. Ma^{1,2}, <u>X. Li</u>^{1,2}, H. Liu^{1,2}, H. Zhou^{1,2}

¹State Key Laboratory of Power Grid Environmental Protection, Wuhan University, Wuhan, China, ²School of Electrical Engineering and Automation, Wuhan University, Wuhan, China

With the continuous development of the power system, its volatility has been increasingly enhanced, and adjustable reactors are playing an increasingly critical role in the power system^[1].

This paper proposes a planar-type orthogonal controllable reactor topology, as shown in Fig. 1(a). The reactor is configured with two AC windings (positioned on the outer side) and two DC windings (located on the inner side). As illustrated in the magnetic circuit analysis of Fig. 1(b), the magnetic fluxes of the AC and DC windings intersect in the orthogonal region. By adjusting the magnitude of the DC current, the saturation level of the orthogonal region can be altered, thereby enabling the regulation of the inductance value^[2].

The inductance adjustment range is a critical performance indicator for controllable reactors. To enhance this indicator, the saturation of the orthogonal region is facilitated by changing the materials used in this region. While the core region of the reactor is made of 300130. three materials with distinct saturation points – 300130, Metglas2605S3A, and NANO-1—are selected for the orthogonal region to investigate their effects on improving inductance adjustment characteristics. The BH curves of the three materials are shown in Fig. 2(a): NANO-1 reaches saturation at approximately 1T (the lowest saturation point), Metglas2605S3A saturates at around 1.4T, and 30Q130 saturates at approximately 1.8T. When the DC current varies, the simulated inductance characteristic curves of the orthogonal region are presented in Fig. 2(b). Owing to NANO-1's minimum saturation point, the orthogonal region exhibits the most pronounced saturation effect, achieving the optimal inductance adjustment performance with a range of 29.68%. This demonstrates that materials with lower saturation points can significantly enhance the inductance adjustment characteristics of this reactor type, thereby opening a new application pathway for lowsaturation-point materials.

[1]Z. Keju, W. Xin and B. He, IEEE Access, Vol. 10, p. 31377-31384 (2022).

[2]J. Yuan, X. Zheng and F. Chen, *IEEE Transactions on Power Delivery*, Vol. 37, p. 4527-4538 (2022).

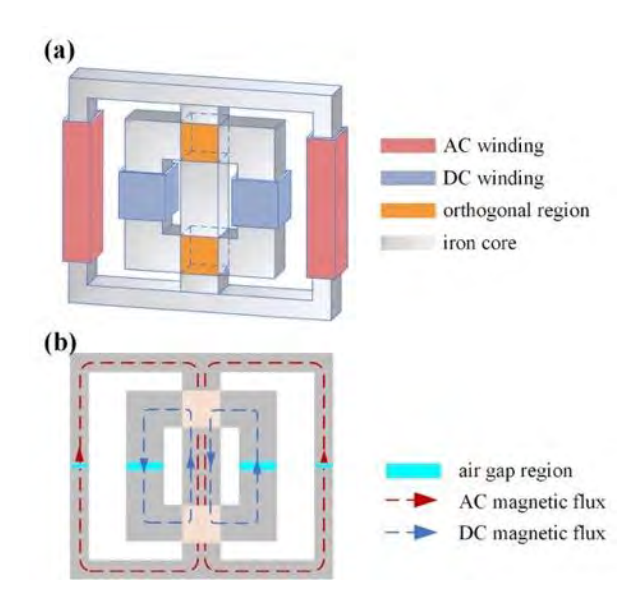


Fig1. Structure and magnetic circuit of planar orthogonal controllable reactor

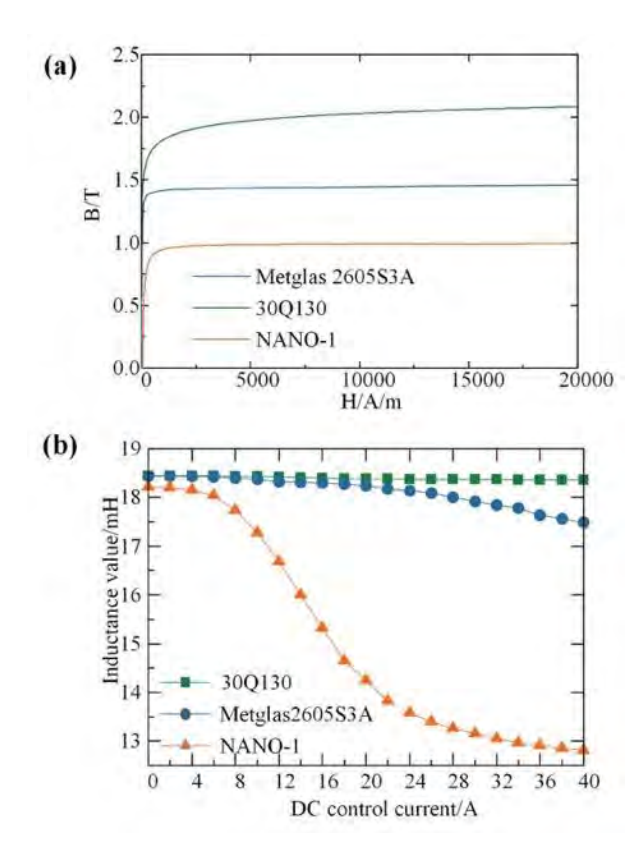


Fig2. BH curves of three materials and inductance regulation characteristics of orthogonal region with three materials

SESSION BR: ENERGY ASSISTED MAGNETIC RECORDING & MAGNETIC SENSORS (POSTER SESSION)

Co-Chair(s): N. A. Natekar, Western Digital, San Jose,
California, United States and T. Kubota, Advanced Spintronics
Medical Engineering, Tohoku University, Sendai, Miyagi, Japan
Tuesday, October 28, 2025
02:30 PM-05:30 PM
Exhibit Hall Posters

BR-01. Magnetization dynamics: maxwell equation based approach

K. Rivkin

RKMAG Corporation, Pacific Grove, California, United States

Today magnetization dynamics problems are modeled either by solving the Landau-Lifshitz equation, often with Fourier transform based calculation of the demagnetization field, or by solving the Walker equation, which is essentially a combination of linearized Landau-Lifshitz and Maxwell equations.

We propose that for a number of practical scenarios there is an approximation of Maxwell equations which produces a relatively simple formulation of the magnetization dynamics which accounts for the nonlinear effects and can be solved using simple Finite Difference Time Domain (FDTD) technique without the need for Fourier transform or Finite Elements calculations.

We demonstrate its performance for a basic domain wall motion problem as well as for a full scale magnetic write modeling, with more than 1,000 times speedup compared to any conventional micromagnetic solver.

BR-02. Cubic Anisotropy Media for Microwave Assisted Magnetic Recording

S. Greaves¹, Y. Kanai²

¹RIEC, Tohoku University, Sendai, Japan, ²Niigata Institute of Technology, Kashiwazaki, Japan

Microwave assisted magnetic recording (MAMR) offers a way to switch the magnetisation of recording medium grains with higher coercivity (H_c) than can be switched by a head field alone. The resonance frequency of a grain depends on the angle between the magnetisation and the easy axis. In grains with cubic anisotropy the variation of resonance frequency as the magnetisation reverses should be less that that of a grain with uniaxial anisotropy. Thus, in this work we compare the response of grains with uniaxial or cubic anisotropy to high frequency (HF) magnetic fields, and

consider the use of cubic anisotropy media in a MAMR system.

Fig. 1 shows the coercivity on the left and right sides of the hysteresis loop for single grains with uniaxial and cubic anisotropy. A 1 kOe, circular high frequency (HF) field was applied during the hysteresis loop calculation. Without the HF field (the zero frequency point in fig. 1) H_c was about 20 kOe for both grains. With the HF field, H_c of the cubic anisotropy grain could be reduced by a larger amount than that of the uniaxial anisotropy grain, with minimum H_c values of 3.2 kOe and 11.1 kOe for the cubic and uniaxial grains, respectively. The rate of H_c reduction with increasing HF field frequency was the same for both grains, but the critical frequency, above which the HF field became ineffective, was higher for the cubic anisotropy grain.

Next, composite recording media with hard and soft magnetic layers were optimised for MAMR. In one case both the hard and soft layers had uniaxial anisotropy; in the other case the hard layer had cubic anisotropy and the soft layer had uniaxial anisotropy. Both optimised media had graded anisotropy soft layers, with $K_{\rm u}$ decreasing towards the surface of the media. Fig. 2 shows that the peak SNR was about 1 dB higher for the optimised composite media with cubic/uniaxial anisotropy. The written track width was almost the same in both media.

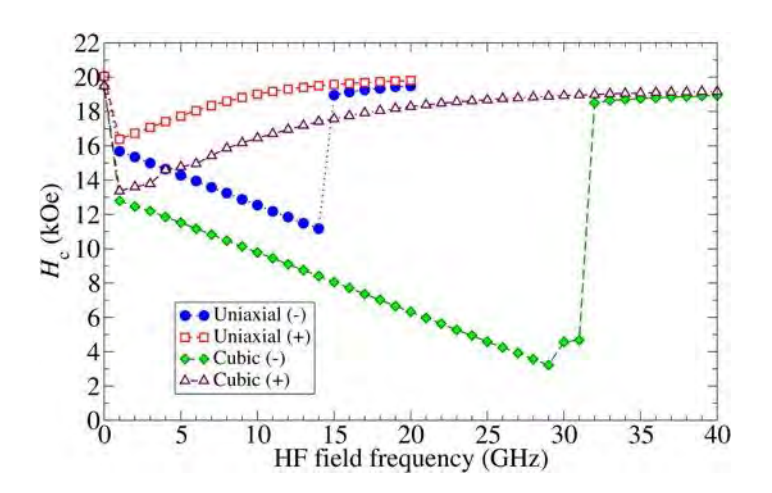


Fig. 1. H_c vs. HF field frequency for single grains with uniaxial or cubic anisotropy. 1 kOe circular HF field."+/-" = H_c on right/left sides of MH loop.

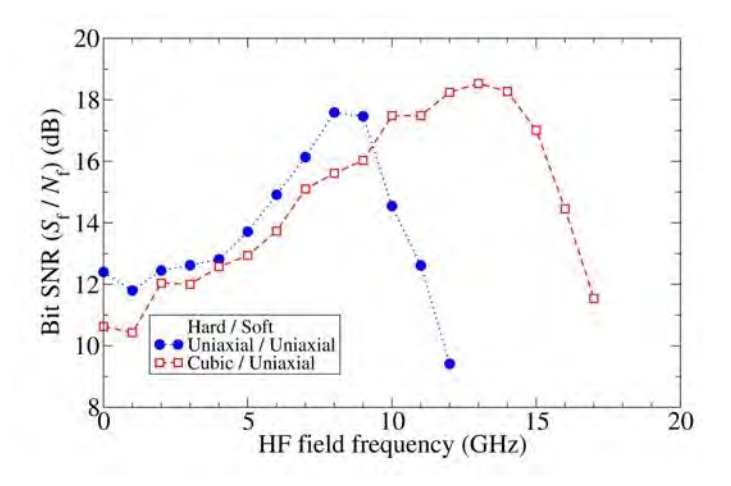


Fig. 2. SNR of tracks written on composite media with either uniaxial anisotropy, or cubic anisotropy hard layers and uniaxial anisotopy soft layers.

BR-03. Plasmonic Nanoantennas for Helicity-Dependent All-Optical Switching

T. E. McCormack, J. Scott, W. R. Hendren, N. Kuninski, R. M. Bowman

Centre for Quantum Materials and Technologies, Queen's University Belfast, Belfast, Antrim, United Kingdom

All-optical control of ferrimagnetic multilayers opens a path toward next-generation magnetic storage. The discovery by Stanciu et al. [1] of deterministic magnetisation switching in synthetic GdFeCo using circularly polarised light sparked interest in ultrafast magnetic dynamics and their integration into recording media. Replacing traditional field-driven writing with all-optical switching (AOS) points to recordbreaking data recording rates with lower energy demands. A helicity-dependent AOS (HD-AOS) system could, in principle, write data on sub-picosecond timescales at nanometre scales. A key challenge is concentrating incident light into deep sub-wavelength volumes while maintaining strong circular polarisation. This necessitates an optical element that focuses light beyond the diffraction limit and preserves or induces helicity. This study addresses this by designing a plasmonic antenna that employs localised surface plasmon resonances (LSPRs) to tailor ultrafast laser light for AOS applications.

We present a device concept simulated via finite element method (FEM) in COMSOL Multiphysics: a nanoscale gold cross antenna with four-fold (C4v) symmetry. Inspired by prior work on polarisation control with plasmonic nanoantennas [2], this design allows excitation with

^{*} Best Student Presentation Finalist / LB – Late-breaking Poster

controlled polarisation and precise tuning of geometry, material permittivity, and wavelength. This reveals rich plasmonic behaviour, including strong local field enhancements—ideal for energy deposition into recording media—and high circularity, quantified via Stokes parameter analysis. Notably, the antenna shows quarter-wave plate behaviour, converting linearly polarised light to circularly polarised light and vice versa.

We will complement the FEM approach with finite difference time domain (FDTD) simulations using Ansys Lumerical. This will provide time-resolved insight into the antenna's response under realistic ultrafast laser pulses instead of ideal plane waves, and yield time-dependent fields critical to preserving or inducing helicity into the AOS media [3].

- 1. Stanciu, C. D. *et al.* All-Optical Magnetic Recording with Circularly Polarized Light. *Phys. Rev. Lett.* 99, 047601 (2007).
- 2. Biagioni, P., Huang, J. S., Duò, L., Finazzi, M. & Hecht, B. Cross Resonant Optical Antenna. *Phys. Rev. Lett.* 102, 256801 (2009).
- 3. Biagioni, P. *et al.* Near-field polarization shaping by a near-resonant plasmonic cross antenna. *Phys. Rev. B* 80, 153409 (2009).

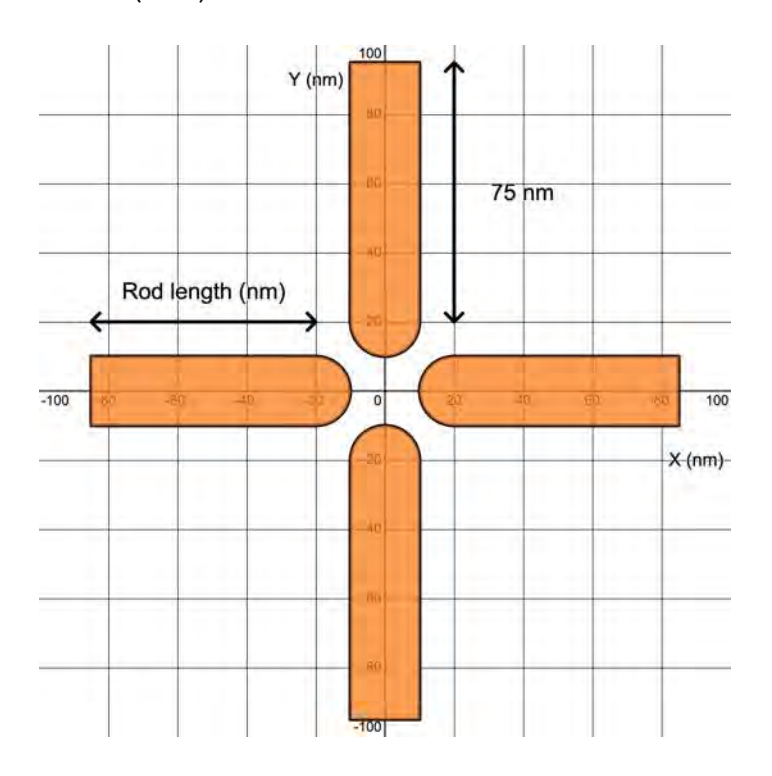


Fig. 1. Antenna design illustrating rods of variable length

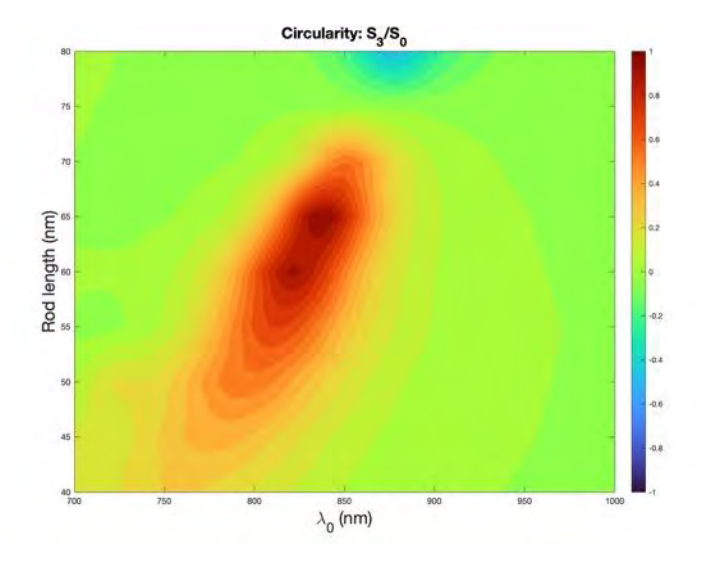


Fig. 2. Degree of circular polarisation with varying antenna x-axis rods and wavelength

BR-04. Effect of rare earth metal substitution in FePt-C granular films on magnetic properties and nanostructure K. Tham¹ D. Miyazaki¹ S. Saito²

K. Tham¹, D. Miyazaki¹, S. Saito²

¹Tanaka Precious Metal Technologies, Tsukuba, Japan, ²Tohoku University, Sendai, Japan

The L1₀ type FePt phase has been utilized as the heat assisted magnetic recording (HAMR) medium material due to its high uniaxial crystalline magnetic anisotropy energy of 5×10⁷ erg/cm³ at room temperature and moderate Curie temperature (T_c) of 750 K. To obtain a granular structure, the research of adding grain boundary material, such as carbon into FePt thin films have been widely conducted. During writing process in HAMR, FePt granular film is heated by a laser close to or above T_c to reduce the switching field. The heat energy will dissipate and lead to the thermal damage. Thus, reducing T_c of the granular film is guite essential. Substitution of FePt in the granular films with non-magnetic metals such as Mn^{1,2)}, Cu³⁻⁶⁾, Ru⁷⁾, and $Rh^{8,9}$ is one of practical ways for controlling T_c . However, excessive substitution of FePt with non-magnetic metals will reduce the saturation magnetization (M_s^{film}). Therefore, we perform experiment of substituting FePt with rare earth (RE) metals which has low T_c and high magnetic susceptibility¹⁰⁾. In this paper, we will report the evaluation result of nanostructure and magnetic properties of those granular films.

Fig. 1 shows *M-H* loops of FePt-C granular films substituted with typical RE metals Tb, Gd, and Ho. Film structure is

^{*} Best Student Presentation Finalist / LB – Late-breaking Poster

shown in the inset. Smaller hysteresis without degradation in $M_s^{\rm film}$ can be observed with substitution of any RE metals. Fig. 2 shows in-plane XRD profiles for FePt-C granular films shown in figure 1. Grain diameter (GD) evaluated by Scherrer's equation¹¹⁾ is also shown on the right side of the graph. For all films, mainly, the (110), (200), and (220) diffractions from L1₀-FePt phase are observed, indicating that FePt grains have c-plane sheet texture. Concerning (001) diffraction, there is no significant change which suggests that the ratio of FePt grains with their c-axes parallel to film normal of the granular films is close to that of without RE metal substitution. GD shows reduction of more than 20% from 7.6 nm for any RE metals substitution.

- 1) A. Z. Menshikov et al., *J. Magn. Magn. Mater.*, 65, 159 (1987).
- 2) D. B. Xu et al., J. Appl. Phys., 109, 07B747 (2011).
- 3) J. Ikemoto et al., IEEE Trans. Magn., 44, 3543 (2008).
- 4) Y. Ogata et al., J. Magn. Soc. Jpn., 34, 209 (2010).
- 5) J. Wang et al., J. Appl. Phys., 109, 123916 (2011).
- 6) D. A. Gilbert et al., Appl. Phys. Lett., 102, 132406 (2013).
- 7) T. Ono et al., Appl. Phys. Express, 9, 123002 (2016).
- 8) T. Hasegawa et al., J. Appl. Phys., 106, 103928 (2009).
- 9) D. Xu et al., J. Appl. Phys., 116, 143902 (2014).
- 10) J. Jensen and A. R. Mackintosh: Rare Earth Magnetism, Oxford (1991).
- 11) P. Scherrer, Mathematisch- 270 Physikalische Klasse, 2, 98, (1918).

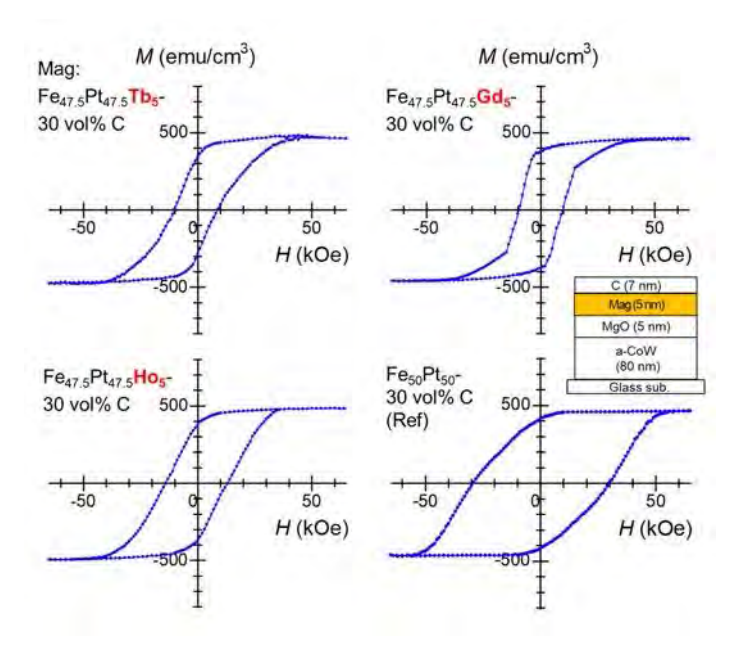


Fig. 1 *M-H* loops of FePt-C granular films substituted with typical rare earth metals Tb, Gd, and Ho. Film structure is shown in the inset.

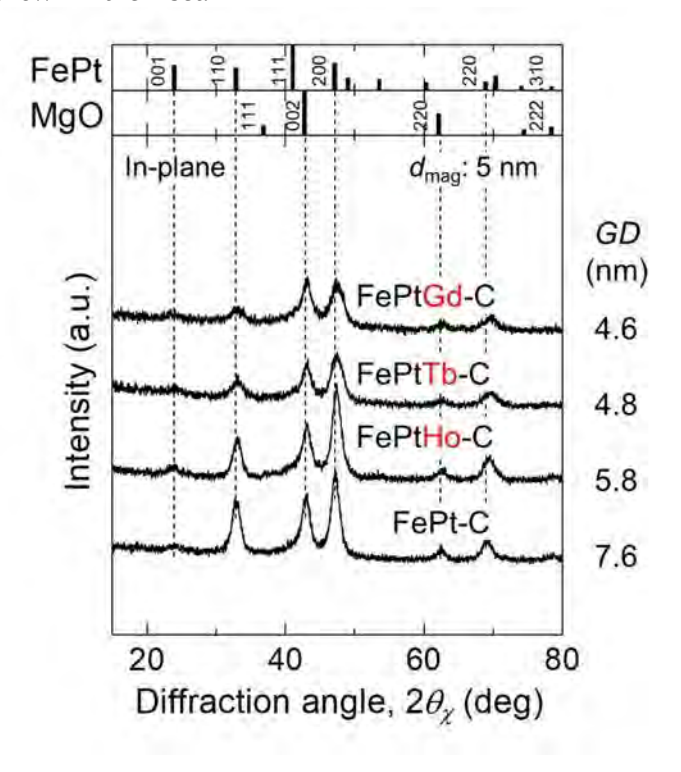


Fig. 2 In-plane XRD profiles of FePt-C granular films shown in figure 1

BR-05. FePt granular films with rare earth metal oxides as ferromagnetic grain boundary materials

D. Miyazaki¹, K. Tham¹, S. Saito²

¹1Tanaka Precious Metal Technologies, Tsukuba, Ibaraki, Japan, ²Tohoku University, Sendai, Miyagi, Japan

The heat assisted magnetic recording medium uses a granular film composed of c-axis oriented L1₀ type FePt magnetic grains that have a high uniaxial crystalline magnetic anisotropy energy of $5\times10^7 \mathrm{erg/cm^3}$ and moderate Curie temperature (T_c) of 750 K. During a recording process, a transition position is determined when the medium is cooled from T_c to below the freezing temperature where the anisotropy field becomes beyond the capability of local head field. Grain-to-grain of T_c variation (σT_c) will directly translate into significant degradation signal-to-noise ratio, limiting the areal recording density [1-3]. It is reported that σT_c of FePt-C granular films with the same grain size is significantly reduced when magnetic oxide grain boundary

material (GBM) is added [4]. Based on our previous research in CoPt granular films with rare earth metal (REM) oxide GBMs, the granular films show strong magnetic exchange coupling, indicating that REM oxide GBMs are magnetic materials [5, 6, 7]. Therefore, to reduce σT_c we conducted an experiment of adding REM oxide GBMs to FePt granular films.

Fig. 1 shows in-plane XRD profile of FePt granular films with various REM oxide GBMs. The (110), (200), and (220) diffractions of the $L1_0$ -FePt phase are observed, respectively, which reveals that mainly the FePt magnetic grains have c-plane sheet texture. Also, the (001) diffraction can be hardly observed. These results suggest that the ratio of FePt grains with their c-axes parallel to film normal is quite low.

Fig. 2 shows in-plane TEM images of FePt granular films with various REM oxide GBMs. The grain size of the FePt granular films is considerably small for REM oxide GBMs. Most of the grains are well separated with the average grain size of less than 5 nm, especially with Sm_2O_3 and CeO_2 addition, suggesting that REM oxide is effective to reduce the grain size. In the conference, we report the detail of σT_c with REM oxide GBMs.

- [1] J. G. Zhu et al, J. Appl. Phys., 115 (2014)
- [2] H. Li et al., IEEE Trans. Magn., 49, 3658 (2013)
- [3] H. Li et al., J. Appl. Phys., 115, 17B744 (2014)
- [4] B. Zhou et al., Appl. Phys. Lett., 113, 082401 (2018)
- [5] K. K. Tham et al., IEEE Trans. Magn., 55, 3200305 (2019)
- [6] K. K. Tham et al., AIP Adv., 10, 015027 (2020)
- [7] K. K. Tham et al., *IEEE Trans. Magn.*, 57, 3200604 (2021)

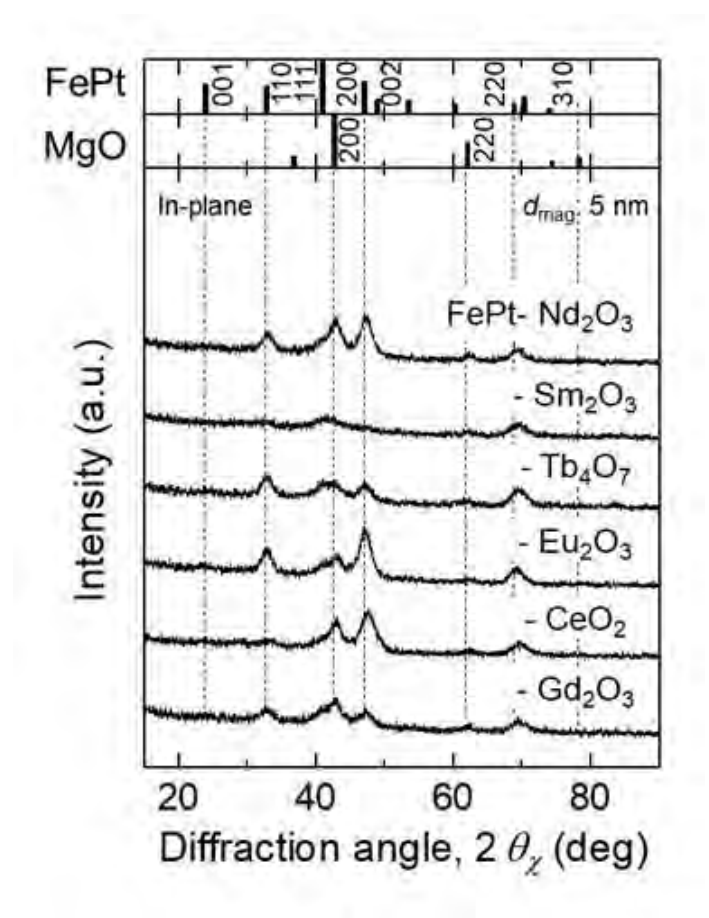


Fig. 1 In-plane XRD profile of FePt granular films with various REM oxide GBMs.

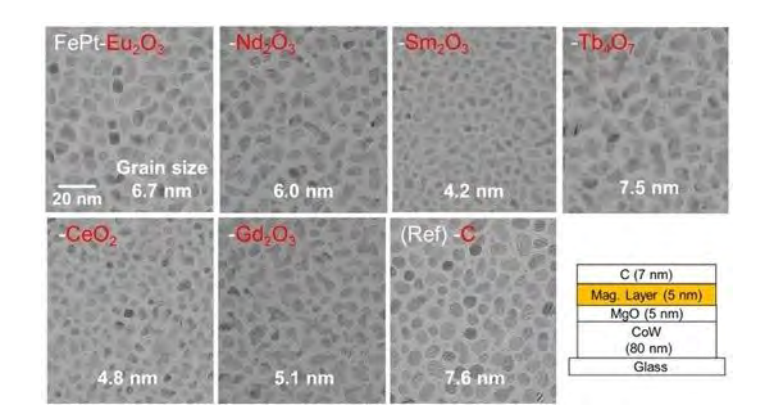


Fig. 2 In-plane TEM images of FePt granular films with various REM oxide GBMs. Film structure is shown in the inset.

BR-06. Thermally Activated Magnetic Switching in Films with Perpendicular and Random Anisotropies

<u>D. Alharbi</u>^{1, 2}, M. Guy¹, M. Davis¹, F. Bakhshizadeh¹, F. Efe¹, A. Lisfi¹

¹Physics, Morgan State University, Baltimore, Maryland, United States, ²Physics, The Catholic University of America, Washington DC, District of Columbia, United States

The increasing interest in magnetic media with perpendicular anisotropy is driven by fundamental science and technological demands such as data storage. Perpendicular magnetic media with small grains size and narrow switching field distribution have demonstrated their superior performance of high recording capacities. However, the media magnetic stability is compromised by the reduction of the grain size due to the thermal switching driven by the competition between thermal and magnetic anisotropy energies [1]. In this paper, we elucidate the thermal stability of two types of films with perpendicular and random anisotropies. The perpendicular anisotropy films consist of epitaxially strained CoFe₂O₄ heterostructures, which were deposited by pulsed laser deposition from a polycrystalline target on (100) MgO substrate. The randomly oriented anisotropy films are based on chemically ordered FePt in L₁₀ phase, which were sputtered on a glass substrate. Magnetic relaxation measurements were performed with VSM under two different methods. (1) Direct measurement of the magnetization time dependence at constant applied magnetic field. (2) Measurement of hysteresis loops at different sweep rates of applied magnetic field in the range of 10-5000 Oe/s. As depicted by Fig. 1 the time dependence measurements reveal a logarithmic decay of the magnetization over time and small magnetic viscosity weakly dependent on the external applied field. The investigation results will be presented and discussed based on the structural domains resulting from the epitaxy and the granular structure of the randomly oriented anisotropy films, the demagnetizing field imposed by the measurement geometry, the thermally activated irreversible process and the magnetization reversal mechanism in the granular and the epitaxial structures. [1] Vassil Skumryev, Stoyan Stoyanov, Yong Zhang, George Hadjipanayis, Dominique Givord and Josep Noqués Nature 423, 850-853 (2003)

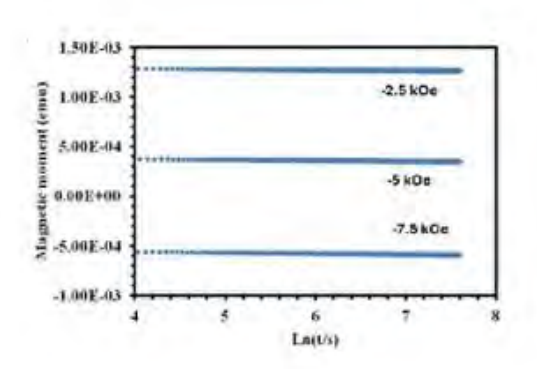


Fig. 1 Magnetization time dependence of $CoFe_2O_4$ film measured along the easy axis (film plane normal) at 3 different applied fields (-7.5 kOe, -5 kOe and -2.5 kOe).

BR-07. A Frequency-Tunable Copper Coil-Based Microfluidic Sensor for High-Throughput Screening and Magnetic Biomarker Detection

<u>D. Brown</u>¹, W. Manuel^{1, 2}, D. Luu¹, M. Gili^{1, 2}, M. Vega², M. Phan¹

¹Department of Physics, University of South Florida, Tampa, Florida, United States, ²Materials Science and Engineering Program, College of Science, University of the Philippines, Diliman, Philippines

Functionalized magnetic nanoparticles (MNPs) are widely used for chemically labeling antibodies and DNA/RNA probes. Quantifying these MNPs is crucial for detecting biomarkers associated with early-stage cancers and various pathogens. Among available materials, magnetite is a preferred choice due to its biocompatibility, ease of surface functionalization, and favorable magnetic properties [1]. However, current challenges include the lack of a costeffective, user-friendly, point-of-care (POC) detection method that offers rapid and high-fidelity results [2,3]. To address this, we have developed a frequency-tunable, copper coil-based microfluidic sensor that integrates a speed-adjustable micropump and a vector network analyzer (VNA). The system operates by generating frequencydependent signals, analyzing both S11 (reflected) and S21 (transmitted) parameters. A permanent magnet is used to concentrate MNPs at the coil detection site, significantly enhancing both sensitivity and signal-to-noise ratio (SNR) a key yet often overlooked metric in biosensing. Our results demonstrate an SNR exceeding 40 dB for larger sample masses (>5 mg) and around 26.7 dB for smaller masses (~1

mg). This performance is attributed to changes in the coil's parasitic capacitance and inductive properties caused by dielectric variations induced by the MNPs at different frequency ranges. Compared to conventional giant magnetoimpedance-based biosensors, our biosensor offers superior sensitivity and SNR. Furthermore, its design supports high-throughput screening and multiplexed analyte detection, making it a promising platform for next-generation biomedical diagnostics.

[1] P.Q. Thong et al., Multifunctional Nanocarriers of Fe₃O₄@(PLA-PEG)/Cur for MRI, magnetic hyperthermia, and drug delivery. *Nanomedicine* 17, 1677 (2023).
[2] K.Y. Hwang et al., Signal Differentiation of Moving Magnetic Nanoparticles for Enhanced Biodetection and Diagnostics. *Biosensors* 15, 116 (2025).
[3] T. Kavetskyy et al., Magnetoimmunoassay of cancer

[3] T. Kavetskyy et al., Magnetoimmunoassay of cancer biomarkers: Recent progress and challenges in biomedical analysis. *Microchemical Journal* 167, 106320 (2021).

BR-08. Highly Sensitive Magnetic Sensor Using Superparamagnetic Tunnel Junctions with Stochastic Magnetization Reversal

R. Hirama¹, T. Kubota², M. Endo², K. Fujiwara³, S. Sasaki⁴, H. Yutaka⁴, L. Sakai⁴, M. Hosomi⁴, M. Oogane¹
¹Department of Applied Physics, Graduate School of Engineering, Tohoku University, Sendai, Miyagi Prefecture, Japan, ²Department of Advanced Spintronics Medical Engineering, Graduate School of Engineering, Tohoku University, Sendai, Miyagi Prefecture, Japan, ³Spin Sensing Factory Corporation, Sendai, Miyagi Prefecture, Japan, ⁴Sony Semiconductor Solutions, Minato ku, Tokyo, Japan

Magnetic tunnel junctions (MTJs) exhibit stochastic magnetization reversal at room temperature when the device size is scaled down to the nanoscale. The probabilistic dynamics of magnetization can be observed as resistance fluctuations through the tunnel magnetoresistance (TMR) effect. The behavior is especially prominent in superparamagnetic tunnel junctions (SMTJs) [1], which are attracting considerable attention as promising devices for unconventional computing applications, such as probabilistic and neuromorphic systems [2]. In this work, we demonstrate for the first time the operation of SMTJs as highly sensitive magnetic sensors utilizing their probabilistic magnetization reversal characteristics. The MTJ multilayer stack, with the structure Ta (5)/ Ru (10)/ IrMn (10)/ CoFe (3)/ Ru (0.9)/ CoFeB(3)/ MgO/ Co₇₅Fe₂₅ (0.4)/

CoFeB (0.8)/ Ru (0.4)/ Ta(5)/ Pt (5)/ Ru (5) (thickness in nm), was deposited on a thermally oxidized Si substrate using DC/RF magnetron sputtering. The multilayer was patterned into an elliptical shape with a minor axis of 100 nm and a major axis of 120 nm using electron beam lithography and Ar ion milling. Subsequently, the device was annealed at 330 °C for 1 hour under an in-plane magnetic field of 1.0 T applied along the major axis of the ellipse. Time-domain signals were measured from the fabricated SMTJs, from which the dwell times and state probabilities were obtained through analysis, as shown in Fig. 1 and 2, respectively. The state probability *P* was modulated by the applied magnetic field H, and the resulting magnetic field sensitivity, defined as $S_H = \partial P/\partial H$, reached a high value of approximately 60 %/mT at a bias current $I = 146 \mu A$. This strong sensitivity, arising from the magnetic field dependence of P. demonstrates the potential of SMTJs as high sensitivity magnetic sensors based on a novel operational principle.

[1] J. Z. Sun *et al.*, Phys. Rev. B 107, 184433 (2023).[2] B. Cai *et al.*, Appl. Phys. A 129, 236 (2023).

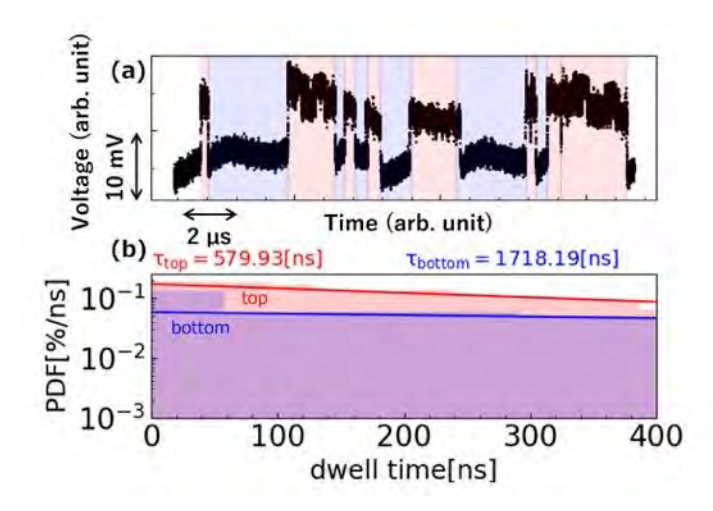


Fig. 1 (a) Time-domain signal of the fabricated SMTJ. The two states are classified using red and blue segments. (b) Probability density function (PDF) of the dwell times for each state.

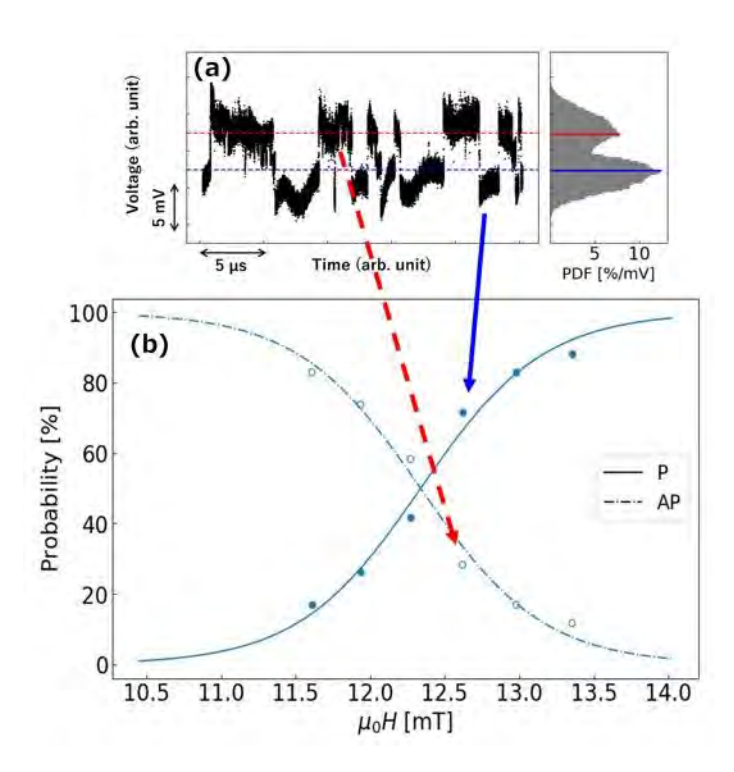


Fig. 2 (a) PDF of the voltage obtained from the time-domain signal. (b) Magnetic field dependence of P (dots) and the fitting curves (solid lines) for each state.

BR-09. Methods for Quantifying Parameter Estimation Uncertainty in Eddy Current Testing of Coated Steel Sheets

M. Koll¹, D. Wöckinger¹, G. Bramerdorfer¹, N. Gstöttenbauer², S. Scheiblhofer², S. Schuster², J. Reisinger²

¹Institute of Electric Drives and Power Electronics, Johannes
Kepler University, Linz, Austria, ²voestalpine Stahl GmbH, Linz, Austria

This paper aims to investigate different computationally efficient frameworks for evaluating parameter estimability in eddy current testing (ECT) of metallic coated steel sheets. ECT is used in industry for the non-destructive testing of electrically conductive components. For selected applications, advanced and highly accurate EC models for the induced voltage in coils [1,2] have been developed and estimation approaches can be used to determine the parameters of interest [3,4].

The focus is set on modelling metal-coated layered steel sheets under ECT using a differential coil system (Fig. 1), and utilizing a sinusoidal multi-frequency approach. The study proposes different structured methods to quantify the

uncertainty associated with material parameter estimates and highlights their differences, advantages and draw backs. The Cramér-Rao Lower Bound [5] is used to quantify practical parameter estimability based on a noise model, a linear EC signal model, and the Fisher information matrix (FIM) [6].

Assuming nonlinear magnetic behavior of the steel sheet, no explicit analytical model exists and its derivation is challenging. Instead, finite element-based analyzes can be used, but applying the FIM is computationally intensive due to the large number of nodes required for high-frequency EC problems. For structural identifiability analysis, the directional derivatives with respect to the parameters can still be used, but this method becomes impractical when dealing with a large number of parameters and practical or statistical identifiability analysis [7], e.g., n-layer sheet. Due to the extensive number of parameters and estimators to be analyzed, a computationally efficient method based on the FIM is presented, utilizing Monte Carlo experiments and histograms to investigate their practical estimability. For instance, Fig. 2 shows exemplary results of the normalized standard deviation of the coating thickness estimate for a simple two-layer sheet based on the FIM. The final paper gives a detailed overview about the structural and practical identifiability of the parameters of a three-layer sheet.

- [1] D. Dodd Luquire; Spoeri, Oak Ridge National Laboratory, 1969.
- [2] T. Theodoulidis und E. Kriezis, *Journal of Materials Processing Technology*, Bd. 161, Nr. 1, S. 343–347, 2005.
- [3] J. C. Moulder, E. Uzal, und J. H. Rose, *Review of Scientific Instruments*, Bd. 63, Nr. 6, S. 3455–3465, 1992.
- [4] M. Koll, COMPEL, 2024.
- [5] C. Rao, Calcutta mathematical society, 1945.
- [6] S. M. Kay, "Fundamentals of statistical signal processing: Estimation theory," 1993.
- [7] R. C. Smith, "Uncertainty quantification: theory, implementation, and applications", SIAM, 2024.

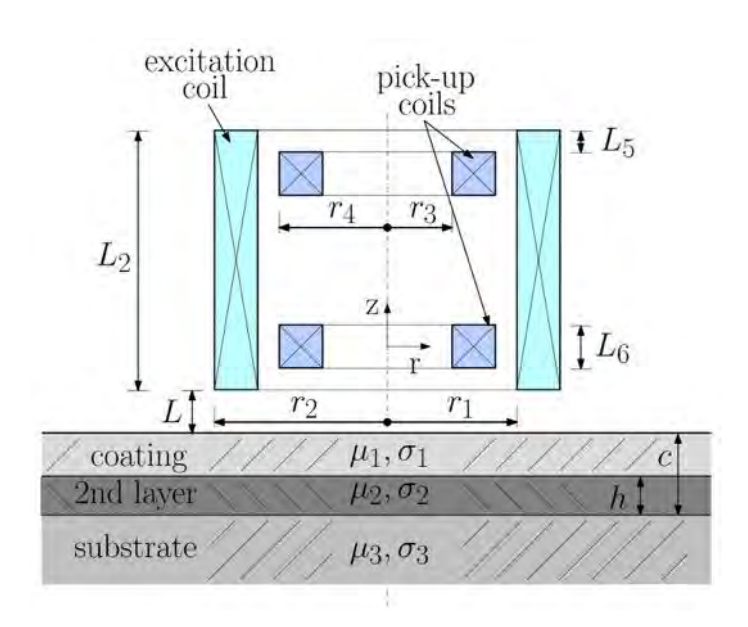


Fig. 1. Used differential coil system.

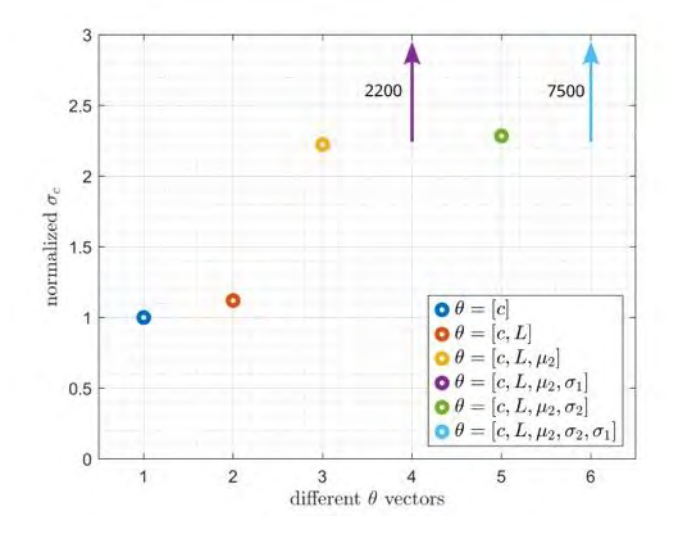


Fig. 2. Normalized std. deviation of coating thickness for different estimators.

BR-10. Electromagnetic Material Characteristics of Steels Used for Hot-dip Galvanization and their Impact on the Coating Thickness Estimation Bias in Eddy Current Testing

M. Koll¹, D. Wöckinger¹, M. Peer¹, C. Dobler¹, G. Bramerdorfer¹, N. Gstöttenbauer², S. Scheiblhofer², S. Schuster², J. Reisinger²

¹Institute of Electric Drives and Power Electronics, Johannes Kepler University, Linz, Austria, ²voestalpine Stahl GmbH, Linz, Austria

The precise coating thickness determination of metalliccoated steel sheets is crucial in industrial applications. Typically for eddy current (EC) testing, coils, e.g., the differential coil shown in Fig. 1, are needed to measure the induced voltage, which is then used to infer parameters of the coated sheets. A model-based estimation approach based on a well-known analytical model is applied to estimate the unknown coating thickness by employing a multi-frequency method as discussed in [1-4]. Generally, the coating thickness estimation of linear substrate materials does not require exact knowledge of the substrate materials properties. However, if the substrate material is magnetically nonlinear, the linear model-based estimation approach can still be applied, but yields systematic errors in the estimated coating thickness. This bias is studied with Monte Carlo experiments based on FEAs, followed by a thickness estimation using the linear EC model. The model and the estimation approach will be presented in detail. Therefore, it is necessary to characterize steels commonly used in continuous hot-dip galvanizing processes and to assess the impact of the material behavior's nonlinearity on coating thickness estimation. This deviations in the thickness estimation depend on the coating thickness, the air gap, and the electromagnetic properties of the sheet material. The worst-case bias in thickness estimation is quantified.

This conference contribution presents the magnetic properties of industrially relevant steel grades used in hot-dip galvanization, including titanium-stabilized interstitial-free steel, dual-phase steel, and micro-alloyed steel. The commercial off-the-shelf coated sheets undergo a chemical pickling process to remove the coating. Thus, the same microstructure of the steels can be ensured as expected during eddy current inline measurements after hot-dip galvanizing, while accounting for the thermal and mechanical effects of annealing and forming.

The material's electrical properties are characterized using the van der Pauw method [5], while the DC magnetization properties are determined by quasi-static ring core measurements.

[1] D. Dodd Luquire; Spoeri, OAK RIDGE NATIONAL LABORATORY, 1969.

[2] T. Theodoulidis und E. Kriezis, *Journal of Materials Processing Technology*, Bd. 161, Nr. 1, S. 343–347, Apr. 2005. [3] J. C. Moulder, E. Uzal, und J. H. Rose, *Review of Scientific Instruments*, Bd. 63, Nr. 6, S. 3455–3465, Juni 1992. [4] M. Koll, *COMPEL*, 2024.

[5] L. J. van der Pauw, Philips *Research Reports*. Band 13, Nr. 1, 1958, S. 1–9.

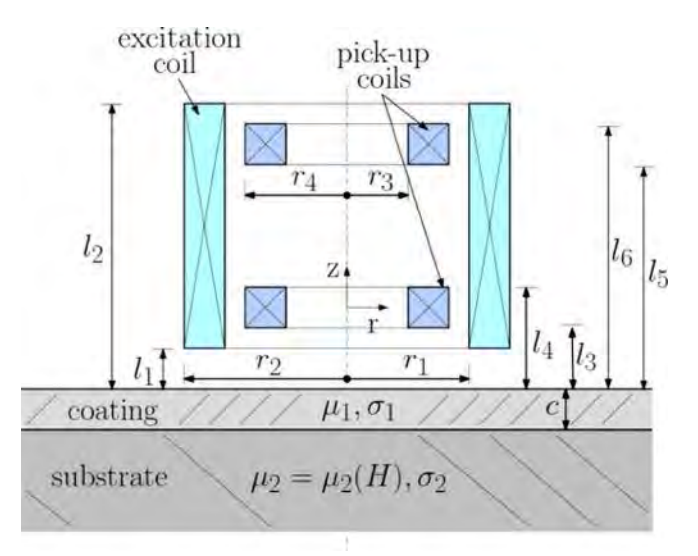


Fig. 1. Illustration of the used ECT setup.



Fig. 2. Ring samples.

BR-11. Variable Exploration of Micromagnetic Simulations of Concentration Detection Range of Large Area Low Aspect Ratio GMR Sensors in Biomedical Diagnostics

R. A. Mendonsa, S. Liang, J. Wang University of Minnesota, Minneapolis, Minnesota, United States

Biosensors using MNPs and GMR sensors [1] are a technology that promises zeptomole concentration detection capabilities [2]. Most works focused on stripe sensors, but large area low aspect ratio sensors, have shown to have linear response capabilities [3] and use the phenomenon of reverse nucleation sites [4]. Previous works in this area [5] have shown that the capability of GMR large area low aspect ratio sensors saturate over a couple orders of magnitude, and also shows that change in properties of the MNP's can change the sensitivity of the system. This study aims to use micromagnetic simulations to explore different methods to extend the range of this sensing system, by focusing on the GMR sensor shape with different aspect ratio as well as explore the effect of the spacing between the nanoparticles to the surface of the free layer of the sensor Fig. 1. These are features that can be easily designed into the system. Examples of such features being explored are shown in Fig. 2. Further, methods to speed up simulation and sensitivity analysis, by comparing features of the reverse nucleation sites are also explored.

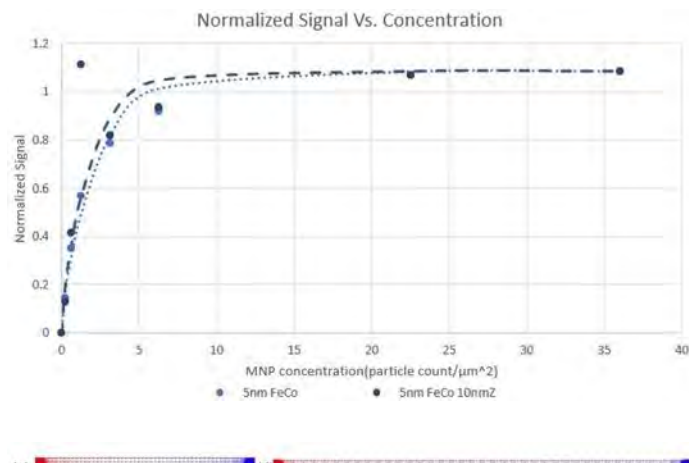
Baselt, David R., et al. "A biosensor based on magnetoresistance technology." Biosensors and Bioelectronics 13.7-8 (1998): 731-739.

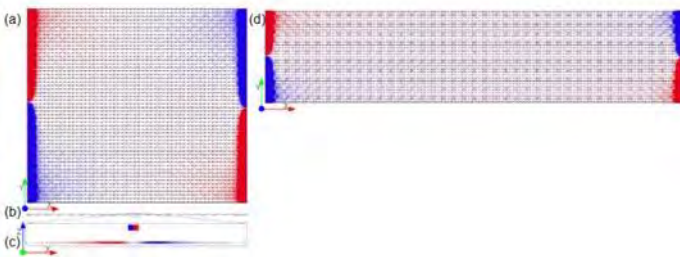
Srinivasan, B. et al. A detection system based on giant magnetoresistive sensors and high-moment magnetic nanoparticles demonstrates zeptomole sensitivity: potential for personalized medicine. Angew. Chem. Int. Ed. 48, 2764–2767 (2009).

Su, Diqing, Kai Wu, and Jian-Ping Wang. "Large-area GMR bio-sensors based on reverse nucleation switching mechanism." Journal of Magnetism and Magnetic Materials 473 (2019): 484-489.

Feng, Yinglong, et al. "Localized detection of reversal nucleation generated by high moment magnetic nanoparticles using a large-area magnetic sensor." Journal of Applied Physics 122.12 (2017).

Mendonsa, Riyan, et al. "Micromagnetic Simulations of Concentration Detection Capability of Large-Area and Low-Aspect-Ratio GMR Sensors in Biomedical Diagnostics." IEEE Transactions on Magnetics (2025).





BR-12. Tuning TMR magnetic sensors using ion irradiation E. Monteblanco, Y. Sassi, M. Deroo, M. Grelier, M. Drouhin, D. Gouéré, <u>D. Ravelosona</u>

R&D, Spin-Ion Technologies, Ile de France, Palaiseau, France

We have developed a unique manufacturing process based on ion irradiation to tailor the structural properties of ultrathin magnetic materials at atomic scale and enhance their performance, in particular for MRAM, magnetic sensors and neuromorphic computing applications.

The importance of TMR sensors increases in industries ranging from speed, position, and distance measurement to rotation and current detection. As the performance of these devices strongly depends on the properties of interfaces (AF coupling, RKKY,, anisotropy,....), ion beam irradiation is a key tool to finely tune the magnetic properties of the sensor layers [1].

Here, we will demonstrate the ability of ion irradiation to tune properties of two different TMR magnetic sensors stacks: a standard MTJ stack (i) Ta/AF₁/SyF/MgO/CoFeB/Ta and a double pinned MTJ stack (ii)Ta/AF₁/SyF/MgO/CoFeB/AF₂/Ta as seen in figure 1. We will show different important results including (i) tunability of exchange bias for both the AF₁/FM

and AF₂/FM layers (figure 2(a)), (ii) the tunability of sensitivity and linear range of the sensor (figure 2(b)), (iii) the increase of the SyF stability and (iv) the tunability of magnetic anisotropy (H_k).
[1] G. Masciocchi et al. APL 121, 182401, (2022)

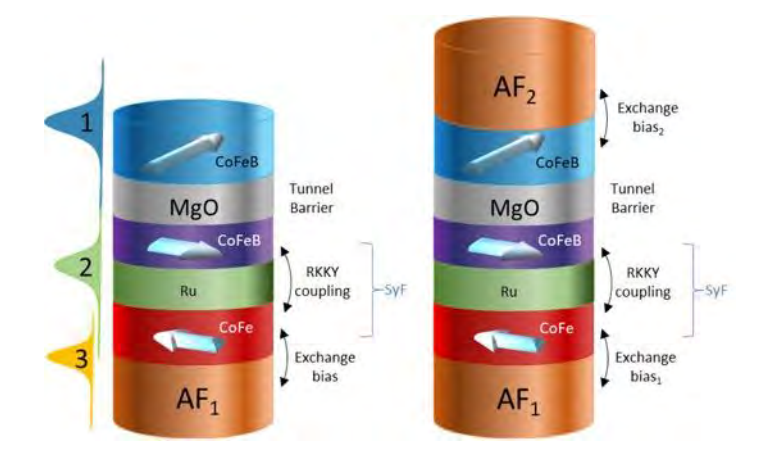


Fig. 1. Schematic of the standard and double pinned XMR sensor, comprising a bottom SAF pinned layer, an insulated barrier, and a top free layer or pinned layer.

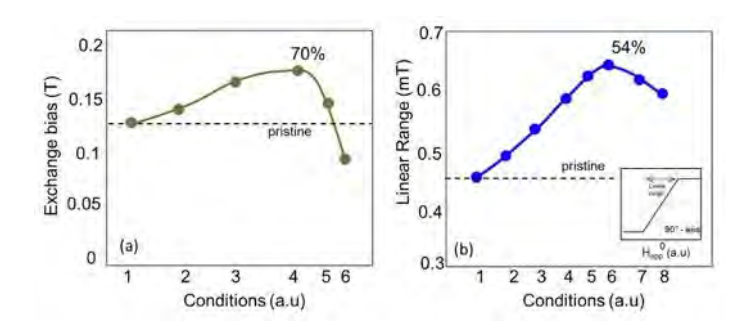


Fig. 2 Depending on the irradiation process, both the exchange bias field in either the bottom or top layer (a) and the linear range (b) can be tuned.

BR-13. Noise-Robust Method Using Sparsity for Locating a Crack in a Steel Rod Based on the Fourier Coefficients of the Leakage Magnetic Flux

K. Shiku¹, N. Shigematsu², Y. Kuwahara², Y. Gotoh³, T. Nara¹ ¹The University of Tokyo, Bunkyo-ku, Japan, ²Neturen Co., Ltd., Hiratsuka Kanagawa, Japan, ³Oita University, Oita-shi, Japan

Magnetic flux leakage testing for a steel rod is crucial before the induction hardening, since cracks can extend during the process. Especially, locating the crack both in the rod's axial and circumferential directions is required for filing it efficiently. An array of magnetic sensors is often used to measure the leakage magnetic flux (LMF) [1]. However, calibration of the numerous sensor elements is complex. In contrast, we proposed the Fourier coils, which directly measure the circumferential first-order Fourier cosine and sine coefficients of the LMF, thereby enabling the estimation of crack circumferential position with only two coils [2,3]. However, due to the strong noise and weak LMF signal, the proposed method was unable to detect a tiny hole-shaped crack, such as one with a depth less than 100 µm and a diameter less than 1 mm in a about 10 mm diameter rod, which may occur during the manufacturing process.

This study presents a noise-robust method for locating tiny cracks using the developed sensor unit, as shown in Fig. 1, which comprises a ring-shaped permanent magnet, vokes. and the Fourier coils. The magnet and yokes strongly magnetize the specimen by constructing the magnetic circuit. The measured signal is processed using a noiserobust method based on the sparsity of the signal, modeling it as being generated by a small number of dipoles. We measured the signal ten times as the rod moved with a velocity of 0.6 m/s. Fig. 2 shows the means and standard deviations of the estimation results of the hole-shaped crack with a diameter of 694 µm and depth of 66 µm in the 9 mm diameter rod. The maximum error in the means was 21 degrees. Oscillatory estimation errors can be caused by the excessive width of the developed Fourier coils and misalignment in the center position of the rod, the Fourier coils, or the permanent magnet. Developing narrower coils, improving the precision of the center position, and devising a calibration method to correct its misalignment are future areas of work.

[1] Z. Zhou and Z. Liu, IEEE Transactions on Industrial Electronics., Vol. 68, pp. 2543–2553 (2021). [2] K. Shiku, T. Nara, and Y. Gotoh, IEEE Transactions on Magnetics., Vol. 59, pp. 1–5 (2023). [3] K. Shiku, M. Kuromizu, Y. Gotoh, et al., IEEE Transactions on Magnetics., Vol. 60, pp. 1–5 (2024).

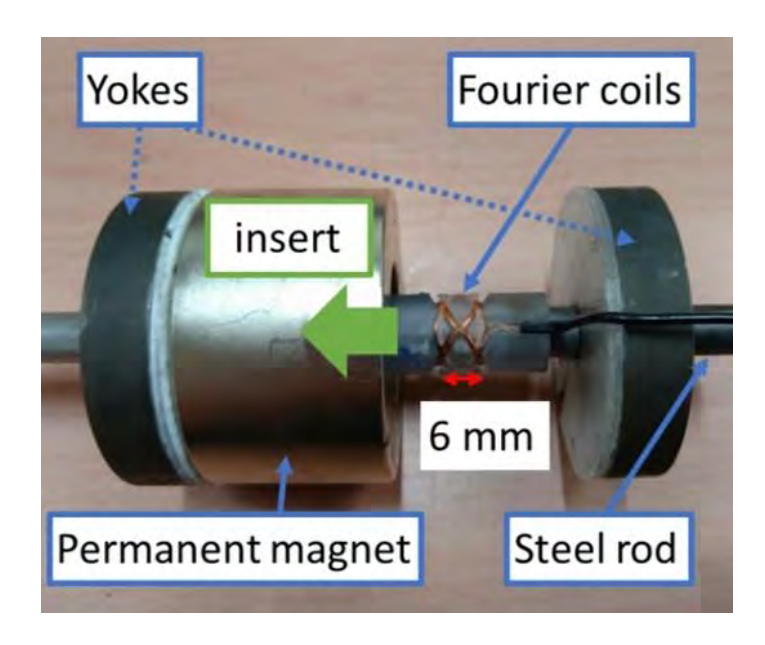


Fig.1 Sensor unit and specimen. The Fourier coils were inserted in the direction of the green arrow to be placed at the center of the permanent magnet.

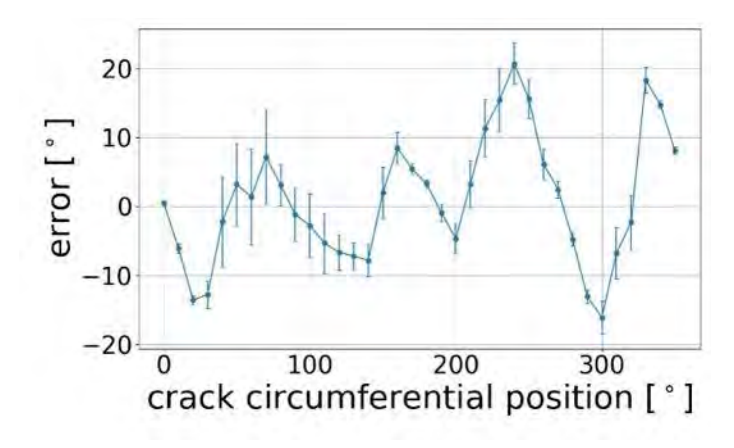


Fig.2 Estimation results of the crack circumferential position

XA: COMMEMORATING 50 YEARS OF THE MAGNETIC TUNNEL JUNCTION

Chair(s): T. Santos, Western Digital, San Jose, California, United
States
Tuesday, October 28, 2025
06:30 PM-08:00 PM
Grand Ballroom

XA-01. A Perspective on Magnetic Tunnel Junctions and Tunnel Magnetoresistance – The Journey

J. S. Moodera

Physics, Plasma Science and Fusion Center, MIT, Cambridge, Massachusetts, United States

The electron tunneling phenomenon has richly contributed to our understanding of various branches of physics over the years. Spin-polarized tunneling (SPT) was discovered in 1971 by Meservey and Tedrow. In a series of elegant experiments, they laid the foundation to a new field of research. SPT uses the superconducting state to probe spin dependent features of the electron density of states of superconductors, magnetic materials and magnetic semiconductors. Here the tunneling electrons' spin polarization is sensed using a spin split superconducting Al as the detector. This discovery is one of the major driving forces initializing the field of spintronics, and related breakthroughs since the seventies. Magnetic tunnel junctions (MTJs) are structures where the spin source and the detector happen to be ferromagnetic (FM) layers with their uneven spin distribution at the Fermi level. Here the tunneling current is dependent on the relative orientation of the magnetizations of the source and detector. Following the SPT knowledge, M. Jullière in 1975 put forward a simple model for FM-I-FM tunneling and magnetoresistance assuming the tunneling of up and down spin channels contribute independently to the current. The 1995 discovery of large and clear tunnel magnetoresistance (TMR) with MTJs at room temperature, signaled the breakthrough pivotal to transforming the computer/information storage industry and sensor technology. With extensive technological developments, it has geared up for a similar revolution in nonvolatile memory, in-memory computing as in neuromorphic computing, and artificial intelligence. Furthermore, MTJs have shown the potential to develop low power and fast electronics needed for processing, nonvolatile storage and computation - ability to advance into comprehensive package containing all electronic devices and components. This overview talk will cover the field starting from the

origin of TMR to its current status.

"Spin Polarized Tunneling" – A chapter by J. S. Moodera and R. Meservey in "Magnetoelectronics" Ed. by M. Johnson (Elsevier Academic Press 2004)

"Frontiers in Spin Polarized Tunneling", J. S. Moodera, G-X. Miao and T. S. Santos, Physics Today (April 2010) p46 'Tunneling path toward spintronics', Guo-Xing Miao, Markus Münzenberg and Jagadeesh S Moodera, Rep. Prog. Phys. 74, 036501 (2011)

"Magnetoresistive Random Access Memory: Present and Future", S. Ikegawa, F. B. Mancoff, J. Janesky and S. Aggarwal, IEEE Tran. on Electron Devices, vol. 67, no.4, 1407-1419 (2020)

"Spin-transfer torque magnetoresistive random access memory technology status and future directions", Daniel C. Worldege and Guohan Wu, Nature Reviews Electrical Engineering Vol 1, 730-747 (2024)

"A multifunctional standardized magnetic tunnel junction stack embedding sensor, memory and oscillator functionality", Chavent, A. et al., J. Magn. Magn. Mater. 505, 166647 (2020)

"Opportunities and challenges for spintronics in the microelectronics industry." Dieny, B. et al. Nat. Electr. 3, 446–459 (2020).

"Neuromorphic spintronics", J. Grollier, D. Querlioz, K. Y. Camsari, K. Everschor-Sitte, S. Fukami & M. D. Stiles, Nat. Electr. 3, 360–370 (2020)

"Weighted spin torque nano-oscillator system for neuromorphic computing"T. Böhnert, Y. Rezaeiyan, M. S. Claro, L. Benetti, A. S. Jenkins, H. Farkhani, F. Moradi & R. Ferreira, Communications Engineering vol 2, Article no.: 65 (2023)

"Neuromorphic computing with spintronics", C. H. Marrows, J. Barker, T. A. Moore & T. Moorsom, npj Spintronics volume 2, Article no.: 12 (2024)

XA-02. Advances in magnetic tunnel junctions for giant tunnel magnetoresistance: Interface engineering and novel materials toward future applications

H. Sukegawa

Research Center for Magnetic and Spintronic Materials, National Institute for Materials Science (NIMS), Tsukuba, Japan

Fifty years have passed since the discovery of the tunnel magnetoresistance (TMR) effects, and thirty years since the realization of a room-temperature TMR effect exceeding 10%. Today, magnetic tunnel junctions (MTJs) are

United States

indispensable elements in spintronics applications. Refinement in MTJ fabrication techniques and the discovery of new materials have accelerated their development, especially leading to significant increases in TMR ratios. Since MTJs can directly convert magnetic information into electrical signals, the magnitude of the TMR ratio is critical to the efficiency of this conversion. Thus, increasing TMR ratios has remained a central challenge in MTJ developments. In this session, I will review the history of room-temperature TMR ratios, the current status of MTJ technology, and future perspectives.

TMR ratios exceeding 600% have been reported in CoFeB/MgO/CoFeB MTJs, which are widely used in spintronic applications. However, progress stalled for many years after this record was set. To overcome this limitation, we revisited the basic Fe/MgO/Fe single-crystal MTJ structure and focused on improving barrier interface quality [1]. Finally, we achieved a new record of 631% at room temperature using a single-crystal CoFe/MgO/CoFe(001) MTJ [2]. We also found that TMR oscillation phenomena, where TMR significantly oscillates as a function of barrier thickness, became more prominent as the TMR ratio increased [1,2]. The origins of TMR oscillation have not been fully understood for a long time, but recent theoretical advances have shown that considering "the superposition of Δ_1 and Δ_2 wave functions" provides a good explanation that matches experimental data [3].

Rapid progress is also being made regarding barrier materials. We have demonstrated that spinel oxides, such as MgAl₂O₄, enable large TMR ratios [4,5]. More recently, we reported that Ga-based barriers (MgGaO) can effectively reduce barrier height [6]. Furthermore, we successfully stabilized a five-cation oxide, LiTiMgAlGaO, as an MTJ barrier [7]. This material is an example of a "high-entropy oxide," demonstrating the potential application of complex oxides in spintronic devices.

In summary, improvements in barrier interface quality and the development of novel barrier materials open up new possibilities for designing next-generation MTJs with enhanced TMR and advanced functionality. These advances not only deepen our fundamental understanding but also support the development of future spintronic technology for memory, logic, and sensing devices.

- [1] T. Scheike et al., Appl. Phys. Lett. 118, 042411 (2021).
- [2] T. Scheike et al., Appl. Phys. Lett. 122, 112404 (2023).

- [3] K. Masuda et al., Phys. Rev. B 111, L220406 (2025).
- [4] R. Shan et al., Phys. Rev. Lett. 102, 246601 (2009).
- [5] T. Scheike et al., Appl. Phys. Lett. 120, 032404 (2022).
- [6] R. R. Sihombing *et al.*, Appl. Phys. Lett. 126, 022407 (2025).
- [7] R. R. Sihombing et al., Mater. Today 88, 12 (2025).

XA-03. Perpendicularly magnetized magnetic tunnel junctions for Spin-Transfer-Torque MRAM applications G. Hu, M. G. Gottwald, C. Safranski, P. L. Trouilloud, L. Rehm, S. Brown, J. Bruley, C. Heinsohn, G. Kim, J. Kim, J. Liang, M. Robbins, P. Hashemi, D. Worledge IBM T J Watson Research Center, Yorktown Heights, New York,

Magnetic tunnel junctions (MTJs) are the fundamental building blocks of spin-transfer torque magneto-resistive random-access memory (STT-MRAM). Specifically, perpendicular MTJs (pMTJs), which utilize perpendicular magnetic anisotropy (PMA), have been instrumental in the commercialization of STT-MRAM due to their superior switching efficiency compared to devices with in-plane magnetic anisotropy (IMA). This presentation begins with a brief overview of the discovery and development of CoFeBbased pMTJs with low resistance-area product (RA $\sim 10~\Omega$ μm²), which are foundational to all current STT-MRAM products [1]. We then discuss the performance requirements and status of four major STT-MRAM applications: standalone memory, embedded non-volatile memory (eNVM), non-volatile working memory, and last-level cache [2]. The first two have already reached commercial deployment [3 -4]. Continued optimization of conventional CoFeB-based single MTJ devices is expected to meet the demands of next-generation embedded MRAM for non-volatile working memory. However, extending STT-MRAM to last-level cache (LLC) applications will require breakthroughs in materials and device structures to meet stringent requirements for switching current, speed, and endurance.

In the second part of the presentation, we will highlight our recent progress in lowering the switching current and enhancing high-speed switching performance of STT-MRAM devices aimed at last-level cache (LLC) applications. By utilizing a novel double spin-torque MTJ (DS-MTJ) device structure, we achieved up to a 2x reduction in switching current and reliable sub-nanosecond switching. This was accomplished by harnessing spin torques from both the top and bottom interfaces of the free layer in DS-MTJs with a

second reference layer [5-6]. Furthermore, we developed magnetic ordered-alloys with low moment and strong bulk PMA as replacements for conventional CoFeB-based free layer materials. STT-MRAM devices based on these new materials showed superior device properties, exhibiting high coercivity ($H_c > 8 \text{ kOe}$), high energy barrier ($E_b > 80 \text{ k}_B T$), and sub-5 nanosecond switching simultaneously, overcoming the fundamental trade-off between high energy barrier and high-speed switching found in CoFeB-based devices using interface PMA [7].

- 1. D. C. Worledge, et al., "Switching distributions and write reliability of perpendicular spin torque MRAM," 2010 IEEE International Electron Devices Meeting (IEDM), 2010, pp 12.5. 1-12.5. 4
- 2. D. C. Worledge and G. Hu, "Spin-transfer torque Magnetoresistive random access memory technology status and future directions," Nature Reviews Electrical Engineering 2, p71 (2025)
- 3. S. Aggarwal, et al., "Demonstration of a Reliable 1 Gb Standalone Spin-Transfer Torque MRAM For Industrial Applications," 2019 IEEE International Electron Devices Meeting (IEDM), 2019, pp. 2.1.1-2.1.4
- 4. K, Lee, et al., "1Gbit High Density Embedded STT-MRAM in 28nm FDSOI Technology," 2019 IEEE International Electron Devices Meeting (IEDM), 2019, pp. 2.2.1-2.2.4
- 5. G. Hu et al., "Double spin-torque magnetic tunnel junction devices for last-level cache applications," 2022 IEEE International Electron Devices Meeting (IEDM), 2022, pp. 10.2.1-2.2.4
- 6. C. Safranski et al., "Reliable Sub-nanosecond MRAM with Double Spin-torque Magnetic Tunnel Junctions," 2022 Symposium on VLSI Technology, 2022, T01-4
- 7. M. Gottwald et al., "First demonstration of high retention energy barriers and 2 ns switching, using magnetic ordered-alloy-based STT MRAM devices," 2024 Symposium on VLSI Technology, 2024, T10-4

^{*} Best Student Presentation Finalist / LB - Late-breaking Poster

SESSION CA: BEYOND POLYCRYSTALLINE FILMS: TEXTURED MATERIALS FOR HIGH-PERFORMANCE SPINTRONIC DEVICES

Chair(s): P. Khalili Amiri, Northwestern University, Evanston,
Illinois, United States
Wednesday, October 29, 2025
08:30 AM-12:00 PM
Grand Ballroom

CA-01. Integration of highly textured, and epitaxial, materials into 300 mm MRAM manufacturing

S. Mertens¹, M. Ben Chroud¹, X. Piao², K. Sankaran¹, T. Tran¹, N. Jossart¹, A. Palomino Lopez¹, N. Franchina Vergel¹, M. Gama Monteiro¹, S. Rao¹, <u>R. Carpenter¹</u>

'imec, Leuven, Belgium, 'The Institute for Solid State Physics, University of Tokyo, Kashiwa, Japan

Perpendicularly anisotropy Spin-Transfer Torque Magnetic Random Access Memory (STT-MRAM) has now been in production as an e-flash replacement for a few years. Despite this, next generation applications have yet to be found due to the large switching currents/current densities (I_{sw}/J_{sw}), too low Tunnel Magnetoresistance Ratio (TMR, < 300%), insufficient retention (Δ), and large switching energy. In addition to this, these are often in competition with each other limiting the ability to engineer the system without trade-offs.

In literature, there are a number of new material classes that are proposed to tackle.0 these. However, they typically rely on specific substrates (single crystal MgO, Sapphire etc.), deposition techniques (Pulsed laser deposition, Molecular beam epitaxy etc.), and process conditions (temperatures >400°C etc.) that are not compatible with industrial manufacturing of memories.

In this invited talk, we will describe some of the boundary conditions of the memory manufacturing process. For example, the thermal budget requirements for Cu interconnect crystallisation as well as typical stresses that the films must withstand. in addition to this, the key challenges for next-generation MRAM, such as reducing the current to enable scaling of the drive transistors, will be covered in order to give context to the direction of material development that is required.

These areas will form the context for our research into industrially compatible processes that can enable highly textured, or epitaxial, MgO compatible systems. For the former, we will present a method of fabricating highly

textured TiN and Cr seed layers directly onto a Si/SiO₂ wafer. These seed layers are used to create a high-quality Free-Layer and MgO tunnel barrier in a so-called 'MTJ First' design. In the case of the Cr seed layer, we will also show that the texture of the Cr seed layer can be maintained on a W bottom contact, where the Cr forms a so-called bottom electrode. This is critical for the fabrication of the scaled devices, 60nm with a centre to centre separation of 200nm, for which the electrical data will be shown. For the latter, we will show an alternative technique to the NiAl epitaxy on Si described in [2] using a CVD Ge seed layer. The advantage of this system is that the epitaxy process requires the Ge native oxide, therefore removing the requirement of HF cleaning in close coupling with the deposition of the thin films, or 1200°C degas of the Si surface. Furthermore, we will show magnetic measurements where a 30nm layer of Fe shows the typical magnetocrystalline easy/hard axes in line with the Si substrate orientation, with near-bulk values of magnetisation. In addition, we will show we can achieve an epitaxial 1nm Fe layer with perpendicular anisotropy. Finally we will present Voltage Control of Magnetic Anisotropy in hall bar devices.

- [1] M Ben Chroud *et al.* 2024 *J. Phys. D: Appl. Phys.* 57 135309
- [2] K. Yakshuji et al. Appl. Phys. Lett. 115, 202403 (2019)

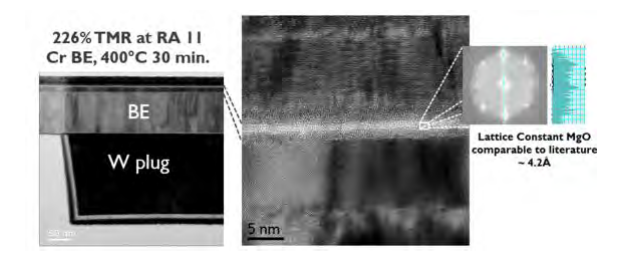


Fig.1 TEM image post thin-film deposition showing the crystallinity of our Magnetic Tunnel Junction (MTJ), fabricated on a textured seed layer depositing on a standard W electrode.

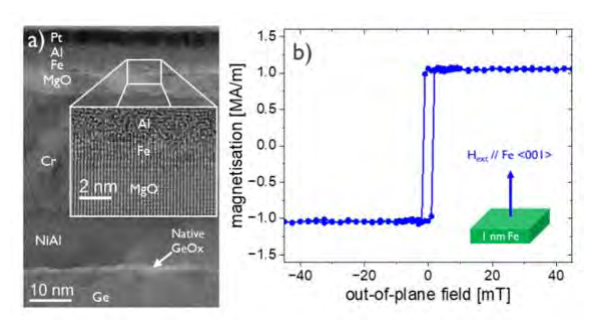


Fig. 2 TEM image (left) showing the epitaxial relation of the MgO/Fe alongside a hysteresis loop (right) for 1nm of Fe, measured perpendicular to the plane.

CA-02. Epitaxial magnetic Weyl semimetals for efficient magnetic reading and writing

C. Chou, Z. He, L. Liu
MIT, Cambridge, Massachusetts, United States

The majority of spintronic devices are conventionally made from polycrystalline metals and insulators, where the averaged material properties from an ensemble of randomly oriented crystal grains determine the final properties. Recently, with the discovery of novel quantum materials, it becomes critical to incorporate highly textured or epitaxial thin films into spintronic devices to fully exploit the unconventional physical effects. For example, in a recent work, we developed fully epitaxial magnetic tunnel junctions (MTJs) based on a ferromagnetic Weyl semimetal Co₂MnGa and correlate the tunneling magnetoresistance (TMR) with the Weyl semimetallic phase (Fig. 1) [1]. We find that the TMR becomes enhanced with the improvement of the chemical ordering of Co₂MnGa electrodes, providing insights on further enhancing TMR via semimetal engineering. The capability of correlating the crystalline texture with spin transport property also allows us to obtain large TMR from an MTJ based on antiferromagnetic (AFM) Weyl semimetal. In this related work, we experimentally develop single-sided antiferromagnetic MTJs consisting of one AFM electrode (Mn₃Sn) and one ferromagnet (FM) electrode (CoFeB), where the spin polarized tunneling transport from AFM is detected by the FM layer (Fig. 2) [2]. The high TMR ratio obtained in this asymmetric AFM MTJ is consistent with theoretical understanding on the spin splitting band structure along low symmetrical crystalline orientation of this AFM. Besides reading, we also see that the textured crystalline orientation can play an important role in determining the writing performance of AFM

materials. Due to the interplay between spin sublattices and spin orbit torque, efficient magnetic switching only occurs when the AFM Mn₃Sn is grown with its basal plane oriented perpendicular to the substrate surface [3]. Finally, in addition to epitaxially grown materials, we also investigate magnetic transistors using single-crystalline CrSBr—a van der Waals antiferromagnetic semiconductor—as the channel material [4]. We observe large magnetoresistance in the transistor channel current with a strong dependence on gate voltage, consistent with our magnetic transistor theory. Furthermore, we show that the anisotropic crystal structure enables highly energy-efficient control of the channel current. The capabilities of correlating crystal orientation with spin transport, as well as tailoring epitaxial thin film growth in practical stack structures bring in new opportunities for developing next generation of spintronic devices.

- [1] Z. He, et al., Phys. Rev. Appl. 22, 044024 (2024).
- [2] C.-T. Chou, et al., Nat Commun 15, 7840 (2024).
- [3] J.-Y. Yoon et al., Nat. Mater. 22, 1106 (2023).
- [4] C.-T. Chou, et al., arXiv preprint arXiv:2505.09019 (2025)

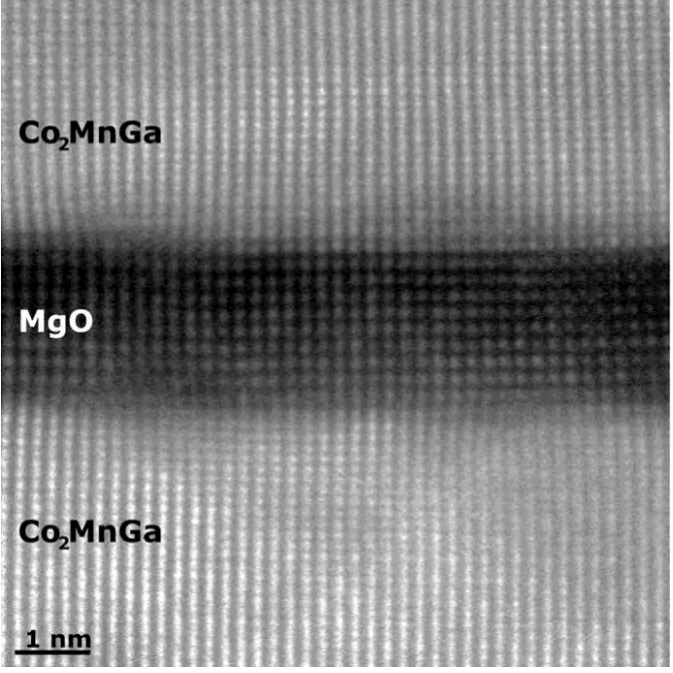


Fig. 1 Scanning transmission electron microscopy image of epitaxial stack of a Co₂MnGa-based tunnel junction.

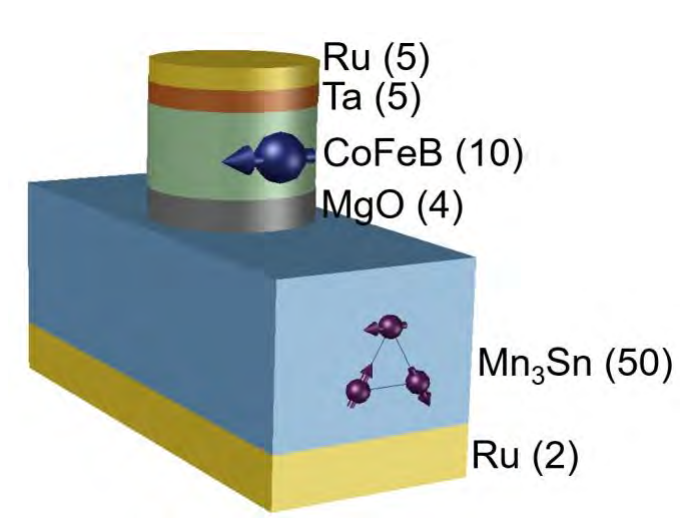


Fig. 2 Schematics of the device structure of Mn₃Sn-based tunnel junctions

CA-03. Ultrafast and Chiral Spin Dynamics in Engineered Heusler Architectures: From Synthetic Antiferromagnets to Monolayer Tunnel Junctions

P. C. Filippou

Research, IBM, San Jose, California, United States

Spintronic based devices are used across a wide range of commercial applications, providing memory, storage and sensing solutions. Additionally, they are actively explored for emerging applications in probabilistic computing, neuromorphic hardware and RF technologies. The device's operating performance, in the heart of these applications, inherently dependents on the materials' properties constituting the spintronic device. We show how ordered Heusler alloys can now be utilized for their advantageous magnetic properties in spintronic devices. A framework is required to bring structured alloys - chemically ordered and with the desired crystal structure/texture- on CMOS compatible substrates.

Bridging complex, highly textured ordered materials with device applications opens a new pathway of exploration and commercialization in next generation spintronic devices with improved performance. We demonstrate a comprehensive approach to advancing spintronic technologies using atomically engineered ferrimagnetic Heusler compounds. By leveraging chemical templating techniques, we achieve atomically ordered ultrathin Mn₃Z (Z = Ge, Sn, Sb) films with strong perpendicular magnetic

anisotropy, even with room temperature growth [1]. These layers enable high-speed magnetic tunnel junctions with fast (sub nanosecond), low-current switching and high thermal stability, suitable for MRAM [2]. Further, by introducing appropriate chemical templating layers, we demonstrate spin orbit torque generation [1] and ordered Heusler alloy based synthetic anti-ferrimagnets showing oscillatory interlayer exchange coupling [3]. Our work establishes a versatile platform for low-moment, dipole-free, and scalable spintronic devices based on tetragonal Heusler ferrimagnets enabled via the chemical templating layer technique [4].

1.Filippou P. Ch. *et al.* Chiral domain wall motion in unit-cell thick perpendicularly magnetized Heusler films prepared by chemical templating. *Nature Communications* 9, 4653 (2018). 2.Garg C., Filippou P. Ch. *et al.* Ferrimagnetic Heusler tunnel junctions with fast spin-transfer torque switching enabled by low magnetization. *Nat. Nanotechnol.* 1–6 (2025) . 3.Filippou P. Ch. *et al.* Heusler-based synthetic antiferrimagnets. *Science Advances* 8, (2022). 4.Faleev S. V., Filippou P. Ch. *et al.* Half-Metallic Full-Heusler and Half-Heusler Compounds with Perpendicular Magnetic Anisotropy. *physica status solidi (b)* 260, (2023).

CA-04. Withdrawn

CA-05. Epitaxial Noncollinear Antiferromagnetic Devices for Microwave Spintronics

S. Nakatsuji

Department of Physics and Astronomy, Johns Hopkins University, Baltimore, Maryland, United States

Antiferromagnets have attracted great interest for their potential to enhance the operation speed to THz regime. Many materials have been studied for new ferromagnetic like responses including altermagnets. Among them, the most prominent effects coming from spin-split bands have been demonstrated in the noncollinear antiferromagnets such as Mn3X systems. In contrast to altermagnets, in the noncollinear and noncoplanar antiferromagnets, the timereversal symmetry (TRS) is macroscopically broken by spin texture itself, leading to the nonrelativistic spin-split band and the unconventional transport phenomena including anomalous Hall effect, anomalous Nernst effect, X-ray magnetic circular dichroism and anisotropic TRS-odd spin current or magnetic spin Hall effect [1]. The noncollinear spin splitting in the momentum space generates the strongly anisotropic spin polarized current and anisotropic tunnelling magnetoresistance even in the case of all antiferromagnetic tunnelling junction [2]. Our recent work on the noncollinear antiferromagnets Mn3X has demonstrated such anisotropic large responses using the epitaxially grown thin film devices [2-5]. We will present recent advances in terms of spin-orbit torque switching and tunneling magnetoresistance using the epitaxially grown thin films of Mn3Sn [2,3]. If time permits, we will also discuss the spin current driven domain wall propagation with a record-high mobility seen in single crystalline devices based on the chiral antiferromagnet Mn3Ge [4].

This work is made in the collaboration with M. Asakura, X. Chen, T. Higo, K. Kondou, T. Matsuda, T. Matsuo, M. Raju, K. Tanaka, H. Tsai, Miwa group at ISSP, UTokyo, T. Nomoto and R. Arita at UTokyo, Broholm group at IQM, and Tchernyshyov group at JHU. This work was partially supported by JST-MIRAI Program (PMJMI20A1), JST-ASPIRE (JPMJAP2317) and by DOE, Office of Science, Basic Energy Sciences under Award No. DE-SC0019331.

[1] S. Nakatsuji and R. Arita, Annual Review of Condensed Matter Physics 13, 119 (2022).
[2] X. Chen, T. Higo, K. Tanaka, T. Nomoto, H. Tsai, H. Idzuchi, M. Shiga, S. Sakamoto, R. Ando, H. Kosaki, T. Matsuo, D. Nishio-Hamane, R. Arita, S. Miwa, and S. Nakatsuji, Nature 613, 490 (2023).

[3] T. Higo, K. Kondou, T. Nomoto, M. Shiga, S. Sakamoto, X. Chen, D. Nishio-Hamane, R. Arita, Y. Otani, S. Miwa, and S. Nakatsuji, Nature 607, 474 (2022).

[4] M. Wu, T. Chen, T. Nomoto, Y. Tserkovnyak, H. Isshiki, Y. Nakatani, T. Higo, T. Tomita, K. Kondou, R. Arita, S. Nakatsuji, and Y. Otani, Nature Communications 15, 4305 (2024).

[5] S. Sakamoto et al., Nature Nanotechnology 20, 216 (2025).

^{*} Best Student Presentation Finalist / LB – Late-breaking Poster

SESSION CB: FUTURE READ HEAD TECHNOLOGIES

Chair(s): S. Hernandez, Seagate Technology, Bloomington,
Minnesota, United States
Wednesday, October 29, 2025
08:30 AM-12:00 PM
Ballroom A

CB-01. Reader Technology for Ultra-High Capacity HDDsA. Grier

Seagate Technology, Derry, United Kingdom

Rapid data growth is driving an increasing demand for high-capacity storage. Hard disk drive (HDD) technology is advancing with innovation in read, write, and media technologies. Heat-Assisted Magnetic Recording (HAMR) has been a key enabler, allowing HAMR HDDs to achieve areal densities of 3TB+ per disk and demonstration of 6.5TB per disk in lab conditions [1].

This presentation will focus on the critical role of reader technology in supporting ultra-high capacity HDDs as areal density continues to scale to 10TB per disk and beyond. It will review the scaling of current readers including performance and dimensional scaling requirements. A wide range of new device proposals have been considered for future reader sensors [2], and some of these configurations/material developments will be summarized. Two-Dimensional Magnetic Recording (TDMR) arrangements such as Multiple Sensor Magnetic Recording (MSMR) with multiple readers can play a role in enhancing areal density capabilities of readback systems [3]. The principles of multiple reader architectures and related reader design considerations will also be reviewed.

[1] Seagate, https://www.seagate.com/blog/the-nanomarvels-enabling-the-ai-era (2025)
[2] G. Albuquerque et al., IEEE Transactions on Magnetics, Vol. 58, 2 (2022)

[3] C. Rea et al., IEEE Transactions on Magnetics, Vol. 53, 11 (2017)

CB-02. Ultra Narrow Readers – Challenges and Outlook<u>H. G. Zolla</u>, G. Baiao De Albuquerque, J. L. Grab, J. Liu, C. Yu, J. M. Freitag, I. Andoni, X. Liu, Y. Hong *Western Digital, San Jose, California, United States*

The hard disk drive (HDD) industry is transitioning from conventional, purely magnetic recording to heat assisted magnetic recording (HAMR). Much of the technology underlying this transition focuses on the performance and reliability of optics, plasmonics, write heads and recording media.

Increases in areal density, enabled by HAMR, reduce track pitch more than linear bit length [1] thus requiring read elements which are narrower than any previously produced. Trackwidth reduction plus side reading, head-media spacing loss, mechanical tolerances and process variation will eventually push physical track width to 12nm and below. Today's magnetic tunnel junction (MTJ) based read elements suffer scaling limitations at these dimensions. Such limitations include increased noise due to higher electrical resistance as well as decreased signal and stability due to reduced physical dimension.

This paper discusses the performance challenges mentioned above as well as patterning challenges associated with fabricating MTJs in the 12nm and narrower regime. This will be followed by a description of a novel read element design based on the inverse spin Hall effect (iSHE). iSHE devices are more complicated to fabricate and utilize since they have separate current and voltage paths requiring four terminals, whereas MTJs require only two. However, we expect such readers will offer improved scaling and performance over MTJ-based devices in the sub-12nm regime.

[1] S. Hernandez et al, "High Areal Density HAMR Demonstration" Presented at TMRC 35, Berkeley, CA (5-7 Aug 2024) paper B1.

CB-03. Sub-10 nm Reader Design Using Lateral Spin Valve Structure

R. H. Victora^{1, 2}, R. Hao¹

¹ECE, U. Minnesota, Minneapolis, Minnesota, United States, ²Physics, U. Minnesota, Minneapolis, Minnesota, United States

We present a new magnetic reader design using a lateral spin valve (LSV) structure that features a sensing end less than 10 nm thick [1]. As shown in Fig. 1, the left ferromagnet (FM1) injects spin-polarized electrons into the nonmagnetic channel, e.g. aluminum (Al). These spins diffuse within the channel to the right side, then enter the synthetic antiferromagnetic free layer (SAF-FL) to modify its internal magnetizations by spin-transfer torque. The SAF-FL/TB/PL forms a magnetic tunnel junction, whose tunneling magnetoresistance is detected. The right applied voltage drives more spins into the SAF-FL for magnetization switching, and also reduces shot noise at Al/SAF-1 interface by restricting back diffusion of spins. Micromagnetic simulations show that SNR > 20 dB can be achieved for a pseudorandom binary sequence with a minimum bit length 0.5 ns.

Further, we calculate gigahertz spin transport in a thin Al channel by solving the time-dependent spin drift-diffusion equation [2][3]. An integral solution for transmitted spin polarization is provided. A frequency-dependent spin transport length is found that shows high-frequency spin signals transmit much less efficiently than low-frequency spin signals. An applied electric field (E-field) along the channel is shown to improve transmission. In Fig. 2, at a transmission distance of z = 500 nm, with a reasonable spin diffusion length (l_s), e.g. D = 30 cm²/s and $l_s = 318$ nm, transmitted signal strength doubles as E-field goes from 0 to -1 kV/cm. On the other hand, if l_s is too small, e.g. D = 10 cm²/s and $l_s = 106$ nm, overwhelming spin scatterings occurring during spin transport decreases the signal strength to zero, and a realistic E-field cannot help.

[1] R. Hao and R. H. Victora, J. Magn. Magn. Mater. vol. 593, p. 171852 (2024).

[2] Z. G. Yu and M. E. Flatte, Phys. Rev. B 66, 235302 (2002).

[3] Z. G. Yu and M. E. Flatte, Phys. Rev. B 66, 201202 (2002).

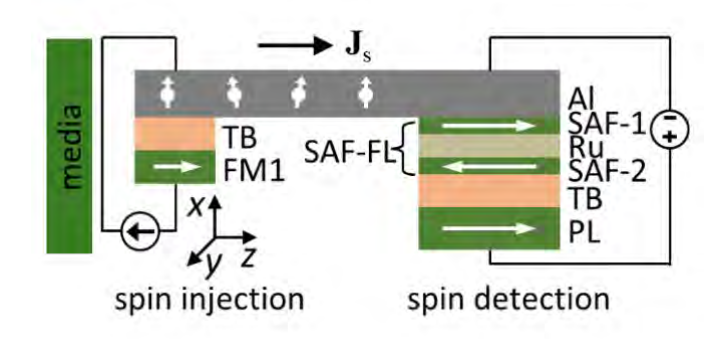


Fig. 1 Our magnetic reader design using LSV structure [1]. J_s : spin current. TB: nonmagnetic insulator as a tunnel barrier. SAF-FL consists of two FM layers (SAF-1, SAF-2) and a nonmagnetic layer, e.g. ruthenium (Ru), in between. PL: FM with pinned magnetization.

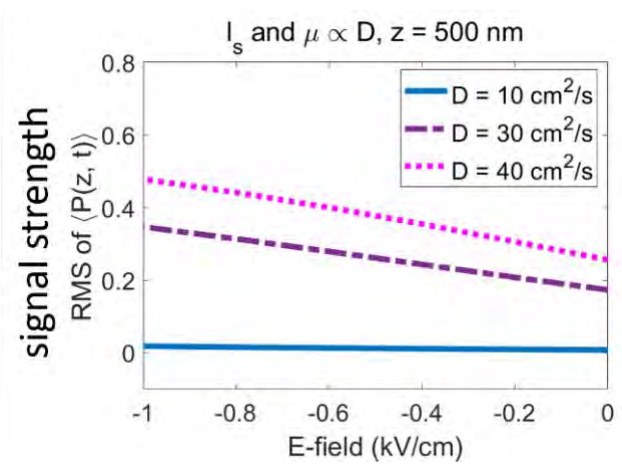


Fig. 2 Transmitted signal strength in Al channel under an applied electric field. μ : electron drift mobility. P(z, t): electron spin polarization in Al, t: time. is average of P(z, t) over 40 samples.

CB-04. Tailoring MTJs for future applications: Barrier interfaces engineering and new spinel barrier materials

T. Scheike^{1, 2}, H. Sukegawa¹

¹NIMS, Tsukuba, Ibaraki, Japan, ²AIST, Tsukuba, Ibaraki, Japan

Magnetic tunnel junctions (MTJs) are the backbone of spintronics applications utilizing the relative orientation of the two ferromagnetic (FM) electrodes' moments – separated by an insulating barrier – for, i.e., data storage or magnetic sensing. CoFeB/MgO/CoFeB MTJs became the standard in read head sensors thanks to their large tunnel magnetoresistance (TMR), high sensitivity, lower power consumption, and thermal robustness which paved the way

must shrink in size (<10 nm) leading to a series of drawbacks, i.e., increased noise, lower TMR, thermal stability, and increased resistance. Thin MgO barriers (~1 nm) are necessary to avoid higher resistance, however, pinholes and defects lead to significant reduction of the TMR and breakdown of the MTJs at lower applied voltages. Reaching the limit of standard CoFeB/MgO/CoFeB multilayers, and absence of suitable alternative candidate materials, exploration of new materials for next generation applications are of increasing importance. In this talk, I will focus on the development of spinel-based oxides for MTJ barrier applications and importance of interface engineering. With the introduction of the prototype spinel material, MqAl₂O₄ (Fig.1a), H. Sukegawa et al. have reported large TMR tunable over a wide range of resistance area (RA) by a barrier post-oxidation method [1]. It was also found that spinel ordering of the barrier is not necessary and large TMR is obtained even when a cationdisordered spinel barrier with a rocksalt structure is used (Fig. 1b). This makes spinel-based barrier oxides highly tunable by, i.e., changing the composition ratio or replacing the cations with a different element allowing for adjusting barrier height or lattice matching at the electrode/barrier interface. We have previously shown that using MgGa₂O₄ instead of MgAl₂O₄ with the same barrier thickness can reduce the RA by over one order of magnitude (Fig. 1c) while keeping large TMR ~120% because of the reduced barrier height [2]. Recently, an increased TMR >150% was demonstrated by inserting ultrathin MgO layers at the bottom and top Fe/MgGa₂O₄ interfaces to suppress Ga diffusion [3]. The importance of interface engineering was further demonstrated in standard single-crystal Fe/MgO/Fe,

for hard disk drives (HDD) areal storage densities exceeding

2 Tb/in². However, as HDD densities scale further, MTJs

insertion a significant increase of TMR was obtained when CoFe insertion layers were used and Mg was inserted at the bottom interface (Fig. 1d), resulting in up to 631% TMR. A strong reduction (increase of) RA (TMR) is observed after CoFe is inserted at the bottom interface. In CoFeB/MgAl₂O₄/CoFeB MTJs the insertion of CoFe and MgO at the bottom interface is necessary to promote the

CoFeB/MgAl₂O₄/CoFeB MTJs [4-6]. In Fe/MgO/Fe MTJs

Co₂FeAl/MqAlO/CoFe and poly-crystalline

at the bottom interface is necessary to promote the crystallinity of $MgAl_2O_4$ barrier. These examples further show that non-stoichiometry of the oxide barriers due to mixing with insertion layers does not interfere with their good tunneling properties.

The presented research was partly supported by JSPS KAKENHI Grant Nos. 22H04966, 23K26535, 24K00948, and

24H00408 and is partly based on results obtained from a project, JPNP16007, commissioned by the New Energy and Industrial Technology Development Organization (NEDO) and MEXT Program: Data Creation and Utilization-Type Material Research and Development Project (Grant No. JPMXP1122715503[HS1]).

- [1] H. Sukegawa et al., Appl. Phys. Lett. <u>105</u>, 092403 (2014).
- [2] H. Sukegawa et al., Appl. Phys. Lett. <u>110</u>, 122404 (2017).
- [3] R.R. Sihombing *et al.*, Appl. Phys. Lett. <u>126</u>, 022407 (2025).
- [4] T. Scheike et al., Appl. Phys. Lett. <u>122</u>, 112404 (2023).
- [5] T. Scheike et al., Appl. Phys. Lett. <u>105</u>, 242407 (2014).
- [6] Ikhtiar et al., Appl. Phys. Lett. 112, 022408 (2018).

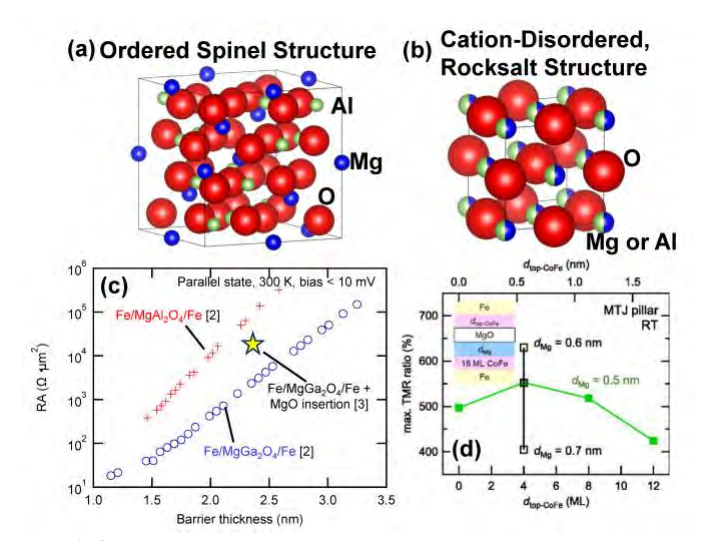


Fig. 1 Ordered (a) and cation-disordered (b) spinel structure; (c) RA reduction by use of a MgGa $_2$ O $_4$ barrier [2,5]; (d) Change of TMR with CoFe (Mg) insertion at top (bottom) Fe/MgO interface for Fe/MgO/Fe [4].

CB-05. Potential and challenges of anomalous Hall sensors for future read head technology

<u>T. Nakatani</u>, P. D. Kulkarni, M. Manikketh, R. Toyama, H. Suto, K. Masuda, N. Suwannaharn, T. Sasaki, H. Iwasaki, Y. Sakuraba

National Institute for Materials Science, Tsukuba, Japan

The development of energy-assisted magnetic recording technologies will significantly increase the areal recording density of hard disk drives to multi-terabits/in². This advancement requires improvements in read head technology because current tunnel magnetoresistance (TMR) read heads are reaching their limits in terms of

performance. These limitations mainly result from their multilayered spin-valve structure and relatively high electrical resistance. A promising alternative is the anomalous Hall effect (AHE) read head.[1] As shown in Fig. 1, the AHE read head functions as a Hall cross device. A bias current is applied in the x direction (between the NiFe side shields), and the magnetization of the sensing layer, which corresponds to the free layer of TMR heads, rotates in the zx plane. The Hall voltage (V_H) is detected in the y direction (between the top and bottom shields). Since AHE heads consist mainly of a single sensing layer, they offer advantages over TMR heads, such as higher resolution and reduced thermal magnetic noise. Our simulation-based studies [1] have highlighted the benefits of AHE heads, including improved SNR due to giant AHE in topological magnets, and symmetric transfer curves. However, there are also challenges, such as output voltage reduction due to bias current shunting and Hall voltage leakage through adjacent NiFe shields. We will discuss AHE head structures that can mitigate this issue. Our recent experimental investigation focused on

spatial resolution and signal-to-noise ratio (SNR)

developing polycrystalline thin films with giant AHE, particularly for the Co-Mn-Al (CMA) alloy system. The study of the bulk single-crystalline Co₂MnAl Heusler alloy reported record-high AHE resistivity (ρ_{yx}) of 36.9 $\mu\Omega$ cm at room temperature. Such a giant value of ρ_{vx} is believed to stem from an intrinsic AHE mechanism originating from its electronic band structure. However, previously reported values for thin films were up to 22 $\mu\Omega$ cm. [3] We explored the compositional dependence of ρ_{yx} in the CMA system using combinatorial sputtering technique, which enables us high-throughput investigations. Figure 2 shows the contour plot of ρ_{vx} for 30-nm-thick CMA films directly deposited on a thermally oxidized Si substrate and annealed at 500 °C. High ρ_{vx} values above 26 $\mu\Omega$ cm were obtained for Al-rich off-stoichiometric composition. We also fabricated uniformcomposition CMA films within a substrate using a conventional sputtering technique. We obtained ρ_{vx} values above 30 $\mu\Omega$ cm for Al-rich off-stoichiometric compositions, surpassing all prior reports for thin films at room temperature.

- [1] T. Nakatani et al., Appl. Phys. Lett. 124, 070501 (2024).
- [2] P. Li et al., Nat. Commun. 11, 3476 (2020).
- [3] R. Modak et al., APL Mater. 9, 031105 (2021).

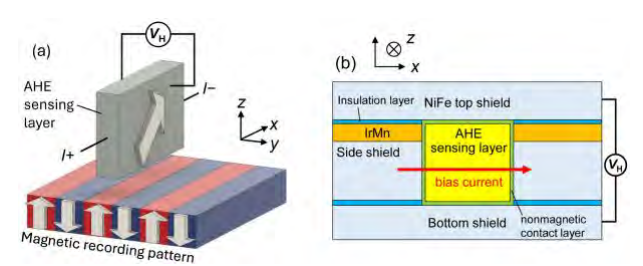


Fig. 1 Schematics of (a) the working principle and (b) the structure from air bearing surface of AHE read head.

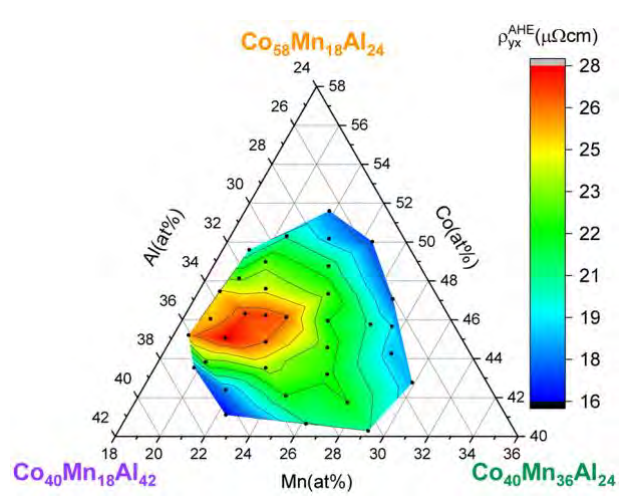


Fig. 2 Ternary contour plot of the variation of ρ_{yx} for Co-Mn-Al composition.

SESSION CC: MAGNETO-TRANSPORT AND MAGNETO-OPTICS OF HIGHER ORDERS IN MAGNETIZATION

Chair(s): T. Kuschel, *Bielefeld University, Bielefeld, Germany*Wednesday, October 29, 2025
08:30 AM-12:00 PM
Ballroom C

CC-01. Angle-dependent magneto-transport of higher order in magnetization

M. Althammer^{1, 2}

¹Walther-Meißner-Institut, Garching, Germany, ²TUM School of Natural Sciences, Physics Department, Technical University of Munich, Garching, Germany

Magneto-transport phenomena—such as anisotropic magneto-resistance (AMR) and the anomalous Hall effect (AHE)—have been central to the study of magnetically

ordered materials for decades. While amorphous and polycrystalline systems often exhibit behavior that can be described by relatively simple models, single-crystalline materials reveal a significantly more complex response due to the influence of crystal symmetry [1]. These symmetry constraints not only shape the form of the magneto-transport response but also permit higher-order contributions with unconventional dependencies on magnetization, many of which have been experimentally observed [2].

In this presentation, I will first discuss how crystal symmetry governs magneto-transport behavior. I will then explore its connections to optical phenomena such as the magneto-optical Kerr effect, as well as to quantum geometric properties of the electronic band structure. These insights will be illustrated through representative experimental results, with a focus on epitaxial ferromagnetic thin films—an ideal platform for investigating symmetry-driven effects [3,4]. The talk will conclude with a review of recent advances in non-linear magneto-transport experiments. Time permitting, I will also briefly touch on the role of crystalline symmetry in shaping the magneto-thermopower response.

- [1] R. R. Birss, *Symmetry and Magnetism* (North-Holland, Amsterdam, 1966)
- [2] P. K. Muduli et al., Phys. Rev. B 72, 104430 (2005)
- [3] W. Limmer et al., Phys. Rev. B 77, 205210 (2008)
- [4] C. Bihler et al., Phys. Rev. B 78, 045203 (2008)

CC-02. Quadratic and Cubic Magneto-optic Kerr Effect in Thin Films Depending on Structural Domain Twinning and Crystal Orientation

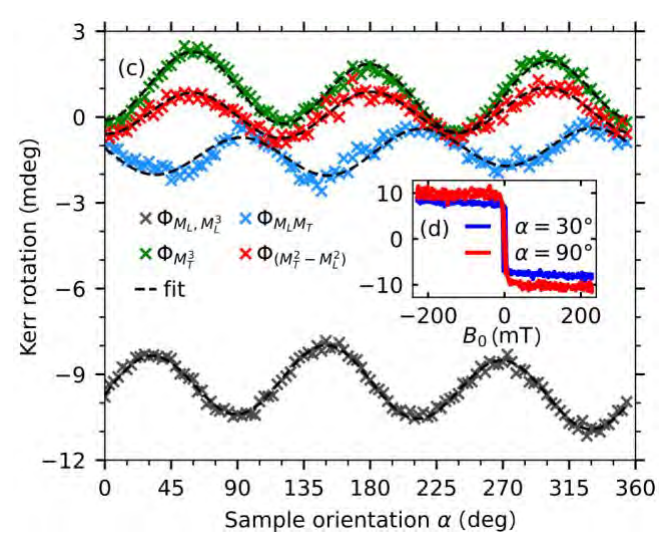
<u>J. Hamrle^{1, 2}, M. Gaerner⁴, R. Silber³, M. Schäffer⁴, M. Veis¹, T. Kuschel⁴</u>

¹Faculty of Mathematics and Physics, Charles University, Prague, Czechia, ²Faculty of Nuclear Sciences and Physical Engineering, Czech Technical University, Prague, Czechia, ³Department of Materials Engineering and Recycling, VSB -Technical University of Ostrava, Ostrava, Czechia, ⁴Faculty of Physics, Bielefeld University, Bielefeld, Germany

Magneto-optic Kerr effect (MOKE) is a well-established method to investigate magnetic materials. The most commonly used MOKE is linear MOKE (LinMOKE), for which the strength of MOKE is linearly proportional to the magnetization (\sim M_i). MOKE proportional to the quadratic form of magnetization (\sim M_iM_j) is called quadratic MOKE

(QMOKE) [1]. QMOKE has been utilized to study antiferromagnets [2] or to investigate spin-orbit torques in insulating structures [3]. The MOKE effects proportional to the cubic form of magnetization (~M_iM_iM_k) are called cubic MOKE (CMOKE). CMOKE can be understood as an anisotropy of LinMOKE and it has been discussed rarely so far [4, 5]. The LinMOKE, OMOKE, and CMOKE depend not only on magnetization orientation but also on crystal symmetry, surface orientation of the crystal, and the sample orientation. Therefore, for example, surfaces (001) and (111) can have different MOKE responses. Here, we provide a theoretical background for the phenomenological description of QMOKE and CMOKE for (111) and (001) oriented cubic crystal structures, and compare the results with experimental data collected on Ni(111) and Ni(001) thin film samples. CMOKE manifests as a three-fold angular dependence in Ni(111) thin films, while for Ni(001), a fourfold angular dependence of CMOKE is predicted. The dependence on the incidence angle changes from one crystal orientation to another. Furthermore, the strength of the CMOKE is also sensitive to the degree of twinning of the Ni(111) thin film [5]. Finally, ab-initio calculated LinMOKE, QMOKE, and CMOKE spectra are presented.

- [1] R. Silber et al., Phys. Rev. B 100, 064403 (2019).
- [2] V. Saidl et al., Nat. Photonics 11, 91 (2017).
- [3] M. Montazeri et al., Nat. Commun. 6, 8958 (2015).
- [4] A. V. Petukhov et al., J. Appl. Phys. 83, 6742 (1998).
- [5] M. Gaerner et al., Phys. Rev. Applied 22, 024066 (2024).



Dependence of LinMOKE+CMOKE ($\Phi_{ML,ML}^3$, Φ_{MT}^3) and QMOKE (Φ_{MLMT} , Φ_{MT}^2 - $_{ML}^2$) contributions on sample orientation α for Ni(111) thin film at a wavelength 635 nm [5].

CC-03. Magneto-optical-Kerr-effect measurement of spinorbit torques with two magnetic layers

X. Fan

University of Denver, Denver, Colorado, United States

Ferromagnets can generate transversely polarized spin currents with both conventional and unconventional symmetries, driven by the interplay between magnetization and spin-orbit coupling [1]. A common platform for investigating spin current generation involves trilayers composed of two ferromagnetic films separated by a spacer, where one ferromagnet acts as the spin current source and the other as the detector. However, the simultaneous presence of both ferromagnets complicates the independent identification of magnetization perturbations caused by spin-orbit torque (SOT).

In this talk, I will present how the magneto-optical Kerr effect (MOKE) can be used to disentangle the SOT effects on each individual ferromagnetic layer. The MOKE signal from a metallic ferromagnetic film consists of two independent components: Kerr rotation and Kerr ellipticity. Due to the finite optical penetration depth [2], these components differ for the two ferromagnetic layers—even when they are made of the same material—providing a layer-specific signature. By analyzing both Kerr rotation and ellipticity, we extract the SOT-induced magnetization tilting in each layer. We demonstrate this method in a multilayer film substrate/3Py/6Cu/15IrMn/2CoFe/5SiO₂. Here the numbers are nominal thicknesses in nanometers. In this film, there are two ferromagnetic layers, Py and CoFe. The CoFe is exchange coupled to IrMn, which gives rise to an exchange bias field acting on the in-plane magnetization. Due to the Cu spacer, the Py does not experience an exchange bias. Both the Py and CoFe layers experiences spin-orbit torques, partially generated from the IrMn. The damping-like spinorbit torques tilts the magnetization, which is measured by MOKE. The Kerr rotation and Kerr ellipticity are shown in Fig. 1(a). Both curves exhibit hysteresis of CoFe and Py, which are signatures of the damping-like torques [3]. After the extrapolation, the magnetization tilting from the CoFe and Py layers are shown in Fig. 1(b). The signals from the two magnetic layers are decoupled.

We further apply this approach to quantify the notable self-spin-orbit torque in a spin valve structure, highlighting the technique's versatility and sensitivity.

- [1] A. Davidson et al., Physics Letters A, 384, 126228 (2020)
- [2] W. Wang et al., Nature Nanotechnology 14, 819 (2019)
- [3] X. Fan et al., Applied Physics Letters, 109, 122406 (2016)

CC-04. Application of Q-MOKE in Magnetometry

E. Schmoranzerová, Z. Sadeghi, V. Wohlrath, J. Kimák, P. Kubascik, L. Nadvornik, P. Nemec, T. Ostatnicky Department of Chemical Physics and Optics, Charles University, Prague, Czechia

When discussing the "magneto-optical effect", one typically imagines a change in polarization upon reflection or transmission in a magnetized material. These effects serve as sensitive tools for detecting magnetic order and small variations within it.

Conventionally, magneto-optical effects linear in magnetization, such as Kerr and Faraday effects, are used in magnetometry due to their relative strength. However, they are limited to systems with broken PT symmetry, ruling out a major part of compensated materials. The quadratic-in-magnetization effects (Q-MOKE, Voigt, or Cotton-Mouton effects) provide an ideal complement. Although weaker, these effects are not subject to the same symmetry requirements and can be used in antiferromagnetic [1], ferrimagnetic [2], and other types of magnetically ordered materials.

In this invited talk, we will present our approach for study and, importantly, application of quadratic magneto-optical effects. Our methods are based on analyzing the dependence of measured signals on the initial light polarization. We are able to perform sensitive magnetometric measurements to extract weak magnetic anisotropies of complex systems, such as YIG or FeRh [3,4], in a manner compatible with cryogenic temperatures. We highlight the importance of tuning experimental parameters, such as the light wavelength [3], and, most importantly, we address the issue of the anisotropy of quadratic magneto-optical effects [5]. Our combined theoretical and experimental approach allows us to extract both the magnetic anisotropy and the anisotropy of the quadratic MO effects themselves from a single set of data. as we show on the example of a ferromagnetic semiconductor GaMnAs [5].

With this knowledge of the quadratic MO response, we were able to optimize our time-resolved magneto-optical experiments, which can resolve different MO effects. The combination of particular signals — for example, polar Kerr and quadratic Voigt effects — provides sensitivity to both inplane and out-of-plane components of the laser-induced magnetization dynamics [6,7]. These results demonstrate the power of quadratic magneto-optical techniques as a versatile tool for investigating spin structures and their ultrafast dynamics in a wide range of magnetic materials.

- [1] K. Yang et al., Phys. Rev. Mat., Vol. 3, p.124408 (2019)
- [2] A. Akhbar et al., Optics Express, Vol. 25, p.30551(2017)
- [3] E. Schmoranzerová et al., Phys. Rev. B, Vol. 106, p.104434 (2022)
- [4] Z. Sadeghi et al., in preparation
- [5] V. Wohlrath et al., J. Phys. D: Appl. Phys., Vol. 58, p.155001(2025)
- [6] N. Tesarová et al., Appl. Phys. Lett., Vol. 100, p.102403 (2012)
- [7] E. Schmoranzerová et al., New J. Phys., Vol. 25, p.033016 (2023)

CC-05. Multipolar Anisotropy in Anomalous Hall Effect from Spin-Group Symmetry Breaking

Z. Liu¹, M. Wei¹, D. Hou², Y. Gao¹, Q. Niu¹
¹Department of Physics, University of Science and Technology of China, Hefei, Anhui, China, ²University of Science and Technology of China, Hefei, Anhui, China

The traditional view of the anomalous Hall effect (AHE) in ferromagnets is that it arises from the magnetization perpendicular to the measurement plane and that there is a linear dependence on the latter. Underlying such a view is the thinking that the AHE is a time-reversal symmetry breaking phenomenon and can therefore be treated in terms of a power series in the magnetic order. However, this view is squarely challenged by a number of recent experiments, urging for a thorough theoretical investigation on the fundamental level. We find that for strong magnets, it is more appropriate and fruitful to regard the AHE as a spingroup symmetry breaking phenomenon where the critical parameter is the spin-orbit interaction strength, which involves a much smaller energy scale. In collinear ferromagnets, the spin-orbit coupling breaks the ∞2' spin rotation symmetry, and the key to characterizing such symmetry breaking is the identification of spin-orbit vectors which transform regularly under spin-group operations. Born out of our framework is a rich multipolar relationship between the anomalous Hall conductivity and the magnetization direction, with each pole being expanded progressively in powers of the spin-orbit coupling strength. For the leading order contribution, i.e., the dipole, its isotropic part corresponds to the traditional view, and its anisotropic part can lead to the in-plane AHE where the magnetization lies within the measurement plane. Beyond the dipolar structure, the octupolar structure offers the leading order source of nonlinearity and hence introduces

unique anisotropy where the dipolar structure cannot. Our theory thus offers a unified explanation for the in-plane AHE recently observed in various ferromagnets, and further extends the candidate material systems. It can also be generalized to study the anomalous Hall effect in crystals with any periodic spin structure and to study the nonlinear Hall effect and the spin Hall effect. Our theory lays the ground for decoding the coupling between various transport and optical phenomena and the magnetic orders.

- 1. Z. Liu, M. Wei and D. Hou, arXiv:2408.08810
- 2. W. Peng, Z. Liu and H. Pan, arXiv:2402.15741

SESSION CD: MAGNETOELECTRIC AND MULTIFERROICS II

Chair(s): S. Husain, *Material Science and Engineering*, *University of California, Berkeley, Berkeley, California, United States*Wednesday, October 20, 2025

Wednesday, October 29, 2025 08:30 AM-12:00 PM Ballroom B

CD-01. Magneto-Ionic Vortices: Paving the Way for Secure, Reconfigurable and Energy-Efficient Devices

<u>I. Spasojević</u>¹, Z. Ma¹, A. Barrera², F. Celegato³, A. Magni³, S. Ruiz Gómez⁴, M. Foerster⁴, A. Palau², P. Tiberto³, K. Buchanan⁵, J. Sort¹

¹Physics Department, Autonomous University of Barcelona, Bellaterra, Barcelona, Spain, ²Instituto de Ciencia de Materiales de Barcelona (ICMAB), Bellaterra, Spain, ³Advanced Materials and Life Science Division, Istituto Nazionale di Ricerca Metrologica, Torino, Italy, ⁴ALBA Synchrotron, Cerdanyola del Vallès, Spain, ⁵Physics Department, Colorado State University, Fort Collins, Colorado, United States

The exponential rise of Big Data is driving a dramatic increase in energy consumption by information technologies¹. One reason is that most memory systems utilize electric currents to write data, which inherently dissipates energy through Joule heating². Electric-field control of magnetic properties has emerged as a sustainable leading strategy to address this issue. Among the diverse voltage-driven mechanisms for the tuning of magnetism (e.g. electrostatic charging, strain-mediated multiferroic coupling or electrochemical reactions³), control of magnetism through electric-field-induced ion motion (magneto-ionics) is rapidly gaining momentum. Magneto-ionics provides unprecedented non-volatile control of coercivity, anisotropy, exchange bias or magnetization,

ultimately enabling conversion between magnetic and non-magnetic states^{4,5}. However, despite the pressing need for strategies to control magnetic states at the nanoscale, magneto-ionics has been studied mainly in continuous thin films, leaving nanoscale magnetic architectures underexplored.

In this talk, we will demonstrate in-situ probing of magnetic properties and associated ion dynamics in nanometer-scale patterned structures, revealing dynamically evolving spin configurations that strongly depend on the voltage gating duration (Fig. 1). More precisely, we will introduce a so far unexplored nanoscale magnetic object: magnetic vortex controlled by electric-field-driven ion motion, termed magneto-ionic vortex or, for simplicity, "vortion"⁶. Vortions are generated within initially paramagnetic FeCoN nanodots via voltage-driven gradual extraction of N³⁻ ions. What distinguishes vortions from conventional magnetic vortex states is that their key properties such as magnetization amplitude, nucleation and annihilation fields, coercivity, remanence and anisotropy, can be controlled and fine-tuned post-synthesis in an analog, reversible and energy-efficient manner⁶. This obviates the need for energy-demanding methods like laser pulses or spin-torque currents. Such tunability is made possible by taking advantage of a so far overlooked aspect of N³⁻ magneto-ionics: the occurrence of a planar ion migration front (Fig. 2a,b), which allows precise, post-synthesis control of the magnetic layer's thickness. Consequently, we demonstrate voltage-mediated transitions between paramagnetic, single-domain, and vortion states (Fig. 2c), unlocking a new paradigm for energy-efficient control of magnetism at the nanoscale.

This unprecedented level of control over magnetic properties at the nanoscale and at room temperature opens new horizons for the development of advanced magnetic devices with functionalities that can be tailored at the postsynthesis stage, therefore providing enhanced flexibility, needed to meet specific technological demands. Magnetoionic states induced within patterned units enable transformative potential for neuromorphic devices⁷, analog computing, multi-state data storage, and, crucially, hardware-level data security. In the face of escalating Big Data challenges, where conventional software defenses increasingly fail, our work reveals how the unique tunability and non-volatility of patterned magneto-ionic systems can be strategically exploited to create robust, self-protected magneto-ionic hardware security primitives.8 These findings pave the way for a new class of hardware security solutions rooted in emergent magnetic phenomena.

- [1] N. Jones, Nature 561, 163-166 (2018).
- [2] J. Puebla et al., Commun. Mater. 1, 24 (2020)
- [3] C. Song et al. Prog. Mater. Sci. 87, 33-82 (2017).
- [4] U. Bauer et al., Nat. Mater. 14, 174-181 (2015).
- [5] J. De Rojas et al., Nat. Commun. 11, 5871 (2020).
- [6] I. Spasojevic et al., Nat. Commun. 16, 1990 (2025).
- [7] P. Monalisha et al., Small Sci. 4, 2400133 (2024).
- [8] I. Spasojevic et. al., submitted.

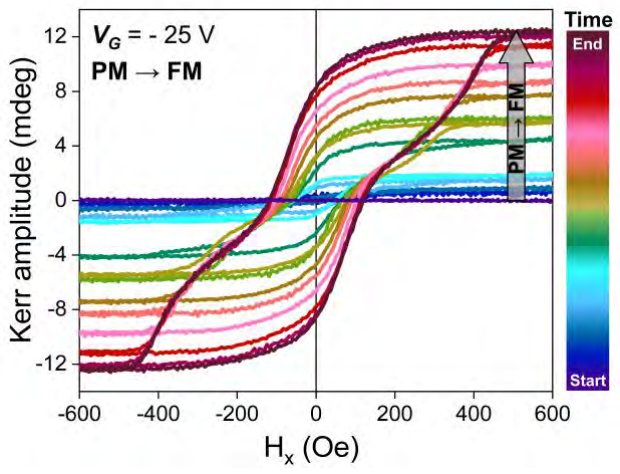


Fig. 1 MOKE hysteresis loop evolution of FeCoN nanodots under negative gating, showing the transition from a paramagnetic (PM) state to ferromagnetic (FM) singledomain and magneto-ionic vortex states with increasing actuation time.

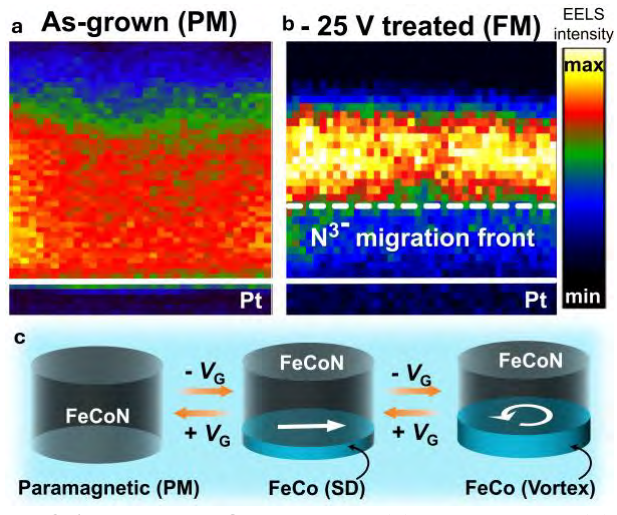


Fig 2. Nitrogen EELS mapping of (a) as-grown and (b) voltage-treated nanodots, showing a planar nitrogen migration front and magnetic phase nucleation at the magneto-ionic unit's base. (c) Schematic of magnetic state transitions between paramagnetic, single domain, and vortex states.

CD-03. Boosting magneto-ionics in Ta/CoFeB/Pt/MgO/HfO $_2$ by interfacial atomic intermixing through Ne $^{\scriptscriptstyle +}$ irradiation

S. Chen^{1, 2, 7}, E. Monteblanco², M. Deroo², Z. Ma³, <u>A. Cataldo</u>⁴, A. Lamperti⁴, A. Solignac⁵, S. Ono⁶, E. Menéndez³, J. Sort³, D. Ravelosona²

¹Centre de Nanosciences et de Nanotechnologies, Palaiseau, France, ²Spin-Ion Technologies, Palaiseau, France, ³Departament de Física, Universitat Autònoma de Barcelona, Cerdanyola del Vallés, Spain, ⁴IMM-CNR, Agrate Brianza, Italy, ⁵Institut Rayonnement-Mati` ere de Saclay, CEA-Saclay, Gif-sur-Yvette, France, ⁶International Center for Synchrotron Radiation Innovation Smart, Tohoku University, Sendai, Japan, ⁷Hangzhou International Innovation Institute, Beihang University, Hangzhou, China

Magneto-ionics is an emerging approach of voltagecontrolled magnetism, facilitated by the voltage-driven ion migration and electrochemical reactions. Moreover, magneto-ionics in general can be used to emulate brain functionalities, thereby offering new computing paradigms beyond the conventional von Neumann architecture. The heavy metal (HM)/ferromagnet (FM)/metal-oxide (MO)based magneto-ionic system is an ideal candidate for efficient magnetization reversal in the voltage-controlled magnetic memory and logic devices. As the magneto-ionic system scales down, the interfacial and crystalline structure plays a crucial role in the magneto-ionic response. Here, Ne⁺ ion irradiation/implantation is utilized to tune the magnetic properties and boost the magneto-ionic effect in the asgrown Ta(5 nm)/CoFeB(1 nm)/Pt(0.09 nm)/MgO(2 nm)/HfO2(3 nm) system through interfacial atomic intermixing and modification of crystalline structure. By performing a systematic study of ion energy (5 keV, 15 keV, and 25 keV) and fluence (2.5×10¹³ ions/cm² - 2.0×10¹⁴ ions/cm²), we demonstrate an increase in perpendicular magnetic anisotropy (PMA) maximal by 94 %. Additionally, we observe an ion-fluence-dependent magneto-ionic response across all the energies, contrasting with the absence of such effect in the as-grown state. These results pave the way to further use the Ne+ irradiation/implantation to tailor the magnetic properties and enhance the magnetoionic performance in the magnetic stacks with ultrathin films.

CD-04. Exploring the Full Magneto-ionic Oxidation Spectrum in Pt/CoFeB/HfO₂

I. Benguettat- El Mokhtari¹, R. Pachat¹, V. Poree², A. Lamperti³, Y. Roussigné⁴, M. Syskaki⁵, J. Wrona⁵, G. Bernard¹, A. Cataldo^{3, 6}, A. Resta², A. Nicolau², S. Ono⁷, S. Cherif⁴, J. Langer⁵, D. Ravelosona¹, M. Belmeguenai⁴, A. Solignac⁸, L. H. Diez¹

¹Centre de Nanosciences et de Nanotechnologies, CNRS, Université Paris-Saclay, Palaiseau, France, ²Synchrotron SOLEIL, Saint-Aubin, France, ³CNR-IMM, Agrate Brianza, Italy, ⁴Laboratoire des Sciences des Procédés et des Matériaux, CNRS-UPR, Villetaneuse, France, ⁵Singulus Technologies AG, Kahl am Main, Germany, ⁶Department of Chemistry, Materials and Nanotechnology, Politecnico di Milano, Milan, Italy, ⁷Central Research Institute of Electric Power Industry, Kanagawa, Japan, ⁸SPEC, CEA, CNRS, Gif-sur-Yvette Cedex, France

Voltage-controlled magnetic anisotropy (MA) via ion migration - known as magneto-ionics - has become a compelling strategy for non-volatile and energy-efficient control of magnetic properties in ultrathin films [1-4]. While most studies have focused on tuning a limited portion of the oxidation landscape, targeting the transition from in-plane anisotropy (IPA) to perpendicular magnetic anisotropy (PMA), the ability to exploit the entire oxidation spectrum remains unspoiled [4-5]. This work addresses this challenge by investigating a Pt (5 nm)/Co₆₀Fe₂₀B₂₀ (0.7 nm)/HfO₂ (2 nm) heterostructure gated by ionic liquid [EMI]⁺[TFSI]⁻. Using voltage-driven oxygen ion migration, we access and control three distinct magnetic states: under-oxidized IPA, PMA, and over-oxidized IPA [6].

Magnetic characterization via anomalous Hall effect (AHE) reveals that a gate voltage of -2.3 V applied for 300 s drives the system from an as-grown IPA state into a PMA state. A subsequent voltage of -2.4 V for 360 s results in an over-oxidized IPA state (Fig. 1). These states are non-volatile for at least 60 days and exhibit clear hysteretic behavior. X-ray photoelectron spectroscopy (XPS) complemented by synchrotron-based X-ray absorption spectroscopy (XAS) at the Co and Fe L_3 edges shows a reduction in the metallic Co and Fe components by ~ 30% and ~ 50%, respectively, confirming voltage-driven oxidation (Fig. 2).

The full IPA \rightarrow PMA \rightarrow IPA cycle is repeatable over at least 10 voltage cycles, proving a robust reversibility. Such results show accessible intermediate oxidative states between IPA

and PMA transitions and push the capabilities of magnetoionic devices for multi-state memories.

Financial support from European Union through Horizon Europe EIC Pathfinder METASPIN project (Grant n. 101098651) is acknowledged.

- [1] R. Pachat, D. Ourdani and J. van der Jagt, Phys. Rev. Applied 15, 064055 (2021)
- [2] T. Bhatnagar-Schöffmann, P. Schöffmann and A. Resta, Advanced Materials Interfaces 11, 2300955 (2024)
- [3] T. Da Câmara Santa Clara Gomes, T. Bhatnagar-Schöffmann and S. Krishnia, Phys. Rev. Applied 21, 024010 (2024)
- [4] A. Fassatoui, J. P. Garcia and L. Ranno, Phys. Rev. Applied 14, 064041 (2020)
- [5] T. Bhatnagar-Schöffmann, A. Kovàcs and R. Pachat, Applied Physics Letters 122, 042402 (2023)
- [6] I. Benguettat-El Mokhtari, R. Pachat and V. Porée, Applied Physics Letters 126, 232402 (2025)

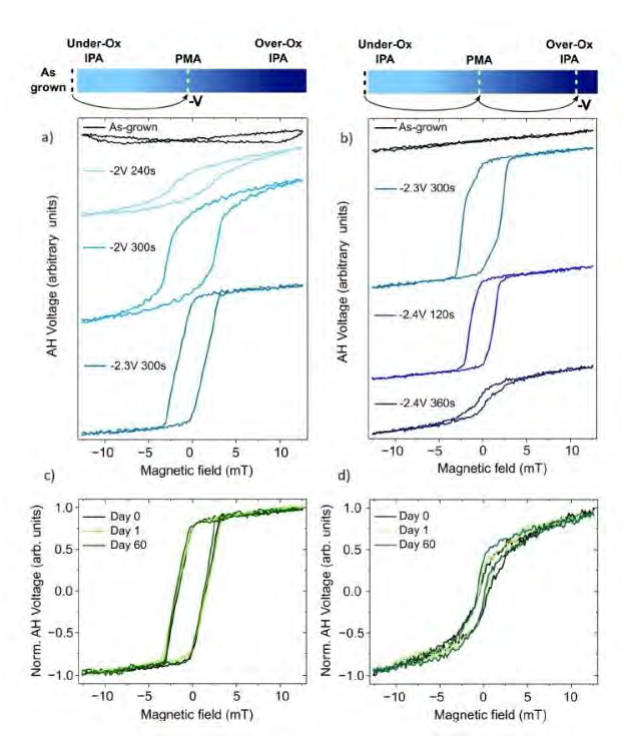


Figure 1 – Panels a) and b) show evolution of MA under V-measured by AHE. The color scale illustrates the gate-induced changes in MA. Panels c) and d) show the time evolution of the final magnetic states in a) and b), respectively.

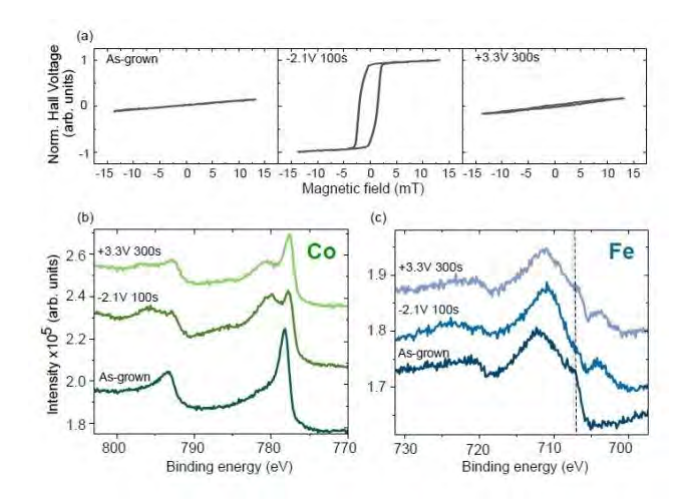


Figure 2 – Panel a) hysteresis loops for the as-grown and bias application. XPS spectra of Co (panel b) and Fe (panel c) for as-grown and after gating under -2.1V for 100s, and subsequent +3.3V for 300s.

CD-05. Theoretical and experimental investigation of magnetic order in Mn₂PtIn

C. Sadler¹, M. Pulse², A. Venner², M. Anas², P. Kharel², P. Shand¹, <u>P. Lukashev</u>¹

¹Physics, University of Northern Iowa, Cedar Falls, Iowa, United States, ²South Dakota State University, Brookings, South Dakota, United States

We present the results of a combined experimental and computational investigation of electronic, magnetic, and structural properties of Mn₂PtIn, a Heusler compound exhibiting tetragonal crystal structure and potential noncollinear magnetic order. Our calculations indicate that this alloy will likely crystallize in tetragonal structure with c/a ratio of around 1.3, although the cubic structure cannot be ruled out as well. The magnetic alignment that corresponds to the lowest energy tetragonal phase is non-collinear, with a large canting angle of around 30° and a magnetization value of 0.70 $\mu_B/f.u.$ At the same time, in the cubic phase the magnetic alignment is ferrimagnetic, with a smaller magnetization value of around 0.30 μ_B/f.u. The noncollinearity in the tetragonal phase of Mn₂PtIn originates from the competition of nearest and next-nearest-plane exchange couplings. Experimentally, this material has been synthesized using the arc-melting technique. The x-ray diffraction pattern can be indexed with a tetragonal crystal structure (space group /-4m2). The unit cell parameters, determined from Rietveld refinement, are a = b = 4.323 Åand c = 6.743 Å. In the thermomagnetic curve, a magnetic

transition is observed near 350 K. Magnetization isotherms reveal high-field (3T) magnetization values of 1.28 $\mu_B/f.u.$ at 100 K and 0.57 $\mu_B/f.u.$ at 300 K. We will also discuss the electrical transport properties of the arc-melted bulk Mn_2PtIn in this presentation.

This research is supported by the *National Science Foundation* (NSF) under Grant Numbers 2003828 and 2003856 via DMR and EPSCoR. Mohd Anas is supported by DOE EPSCoR (DE-SC0024284) grant.

CD-06. Scale-dependent thermodynamic control of metalinsulator transition in $La_{0.67}Sr_{0.33}MnO_3$

<u>I. Bhaduri</u>^{1, 2}, S. Snijder¹, T. Banerjee^{1, 2}
¹Zernike Institute for Advanced Materials, University of Groningen, Groningen, Netherlands, ²Groningen Cognitive Systems and Materials Center, University of Groningen, Groningen, Netherlands

Volatile resistive switching materials have attracted significant interest due to their potential applications in neuromorphic systems as artificial neurons, selectors, or nociceptors [1].

La_{0.67}Sr_{0.33}MnO₃ (LSMO) is a mixed-valence manganite that undergoes a temperature-dependent transition from a ferromagnetic metal to a paramagnetic insulator. This transition can also be electrically triggered via Joule heating [2] and recent studies have shown that it proceeds through the formation of a paramagnetic, insulating filament transverse to the current flow [3]. This is accompanied by a characteristic N-type negative differential resistance (NDR) in voltage-controlled measurements and a hysteretic response in current-controlled measurements.

In this work, we electrically characterize LSMO devices with lateral dimensions ranging from 50 to 200 microns, grown on SrTiO $_3$ (001) substrates. We show that by scaling the device dimensions, and thereby altering their resistance, we can control the thermal dynamics governing filament propagation. Less resistive devices exhibit a sharper N-type NDR and a wider hysteresis, indicating faster filament propagation due to more efficient heating. Furthermore, we find that smaller, more resistive devices require less power to trigger the transition.

Our work demonstrates that device scaling is an effective way of manipulating the thermal dynamics of the MIT in LSMO, thus providing an avenue for controllably engineering the volatile resistive switching properties.

- [1] D. Kim et al., Appl. Phys. Lett., Vol. 121, p. 010501 (2022)
- [2] A. Jaman *et al.*, Front. Nanotechnol., Vol. 5, p. 1121492 (2023)
- [3] P. Salev et al., Nat. Commun., Vol. 12, p. 5499 (2021)

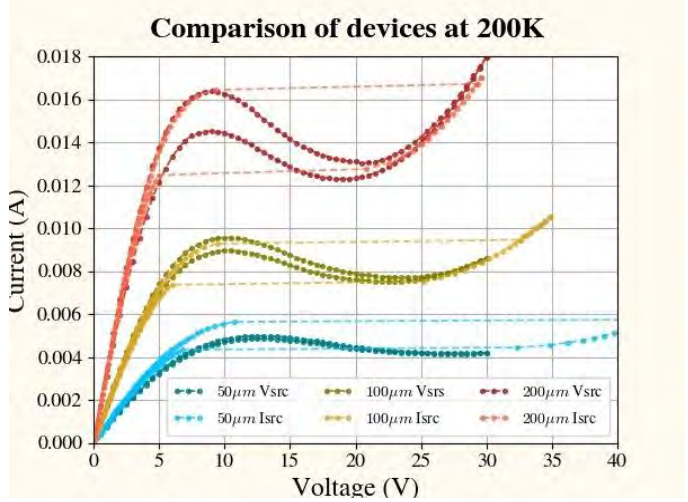


Fig 1: Voltage-controlled and current-controlled measurements at 200 K for three devices of varying width.

CD-08. Tailoring Magnetic Spin Textures in La_{0.7}Sr_{0.3}MnO₃-based Micromagnets

D. Sasaki^{2,1}, B. Achinuq², T. Sahoo¹, I. Nihal¹, E. Teano¹, M. Frame¹, I. Snowden¹, S. Retterer³, <u>Y. Takamura</u>¹

¹Materials Science and Engineering, University of California, Davis, Davis, California, United States, ²Advanced Light Source, Lawrence Berkeley National Laboratory, Berkeley, California, United States, ³Center for Nanophase Materials Sciences, Oak Ridge National Laboratory, Oak Ridge, Tennessee, United States

The development of next-generation computing devices based on spintronics and magnonics requires an understanding of how magnetic spin textures can be tailored in patterned magnetic materials. Within the wide range of magnetic materials available, complex oxides such as ferromagnetic (FM) $La_{0.7}Sr_{0.3}MnO_3$ (LSMO) and antiferromagnetic (AF) $La_{1-x}Sr_xFeO_3$ (LSFO) provide an ideal platform for tailoring magnetic spin textures when

lithographically patterned as nano/micromagnets. This unique tunability arises due to the strong interactions between charge, spin, lattice, and orbital degrees of freedom. In this talk I will demonstrate how an intricate interplay exists between shape, magnetoelastic, domain wall, and magnetocrystalline anisotropy energies as well as exchange coupling interactions at LSMO/LSFO interfaces, and therefore, the resulting AF and FM spin textures can be controlled using parameters such as the LSMO and LSFO layer thicknesses, micromagnet shape, and temperature.[1] These spin textures are imaged using x-ray photoemission electron microscopy (X-PEEM) for a variety of shapes (circles, squares, triangles, and hexagons with their edges oriented along different low index crystallographic directions) with and without their core regions removed (aka donut structures, Fig. 1(a) and (b)). LSMO nanomagnets were also patterned into artificial spin ice (ASI) structures,[2] where large arrays of nanomagnets are arranged into geometries where all the magnetic interactions cannot be satisfied simultaneously. While one might expect shape anisotropy to dictate Ising states in the nanomagnets, the unique combination of magnetic parameters associated with LSMO enables the formation of both Ising and complex spin textures (CSTs) based on the nanoisland width and spacing. These CSTs consist of single and double vortices (Fig. 1(c)) and alter the nature of dipolar coupling between nanomagnets, giving rise to exotic physics in the ASI lattices. These studies demonstrate that complex oxide provide a unique platform for engineering FM and AF spin textures for next generation spin-based devices.

[1] Y. Takamura et al., PRL, 111, 107201 (2013), M.S. Lee, Y. Takamura et al., ACS Nano, 10, 8545 (2016); M.S. Lee, Y. Takamura et al., JAP, 127, 204901 (2020)
[2] R.V. Chopdekar, Y. Takamura, et al., PR Materials, 1, 024401 (2017); D. Sasaki, Y. Takamura, et al., PR Applied, 17, 064057 (2022); D. Sasaki, Y. Takamura, under review.

CD-09. Voltage-driven fluorine motion for novel organic spintronic memristor

Y. Lu¹, A. Nachawaty¹, T. Chen¹, F. Ibrahim², Y. Wang³, Y. Hao¹, K. Francesca⁴, P. Tyagi¹, A. Da Costa⁴, A. Ferri⁴, C. Liu³, X. Li³, M. Chshiev², S. Migot¹, L. Badie¹, W. Jahjah⁵, R. Desfeux⁴, J. Le Breton⁵, P. Schieffer⁵, A. Le Pottier⁵, T. Gries¹, X. Devaux¹

¹Institut Jean Lamour, Nancy, France, ²SPINTEC, Grenoble, France, ³University of Science and Technology of China, Hefei, China, ⁴Univ. Artois, Lens, France, ⁵Univ. Rennes, Rennes, France Integrating tunneling magnetoresistance (TMR) effect in memristors is a long-term aspiration because it allows to realize multifunctional devices, such as multi-state memory and tunable plasticity for synaptic function. However, the reported TMR in different multiferroic tunnel junctions is limited to 100%. Here, we demonstrate a giant TMR of -266% in La_{0.6}Sr_{0.4}MnO₃(LSMO)/poly(vinylidene fluoride)(PVDF)/Co memristor with thin organic PVDF barrier [1]. Different from the ferroelectricity-based memristors [2], we discover that the voltage-driven F motion in the junction generates a huge reversible resistivity change up to 106% with ns timescale. The removing F from PVDF layer suppresses the dipole field in the tunneling barrier, thereby significantly enhances the TMR. Furthermore, the TMR can be tuned by different polarizing voltage due to the strong modification of spin-polarization at the LSMO/PVDF interface upon F doping. The combining of high TMR in the organic memristor paves the way to develop highperformance multifunctional devices for storage and neuromorphic applications.

- [1] A. Nachawaty, et al. Voltage-Driven Fluorine Motion for Novel Organic Spintronic Memristor. *Adv. Mater.* 36, 2401611 (2024).
- [2] S. Liang, et al. Ferroelectric control of organic/ferromagnetic spinterface. *Adv. Mater.* 28, 10204 (2016).

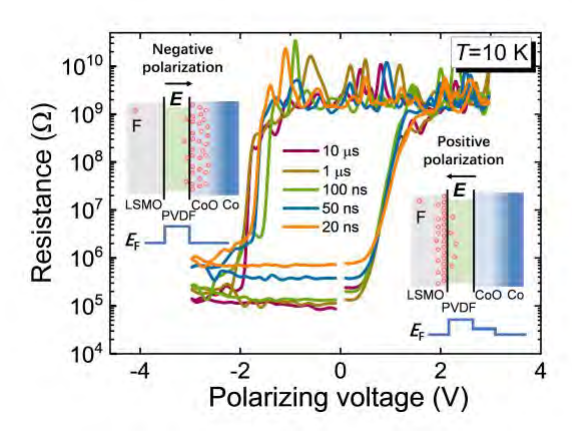


Fig. 1 We discover the voltage-driven F motion in the $La_{0.6}Sr_{0.4}MnO_3(LSMO)$ /poly (vinylidene fluoride) (PVDF) /Co junction, which can generate a huge reversible resistivity change up to $10^6\%$ with ns timescale upon polarizing voltage. The removing F from PVDF layer also significantly enhances the tunneling magnetoresistance, paving the way to develop multifunctional organic spintronic memristor for storage and neuromorphic applications.

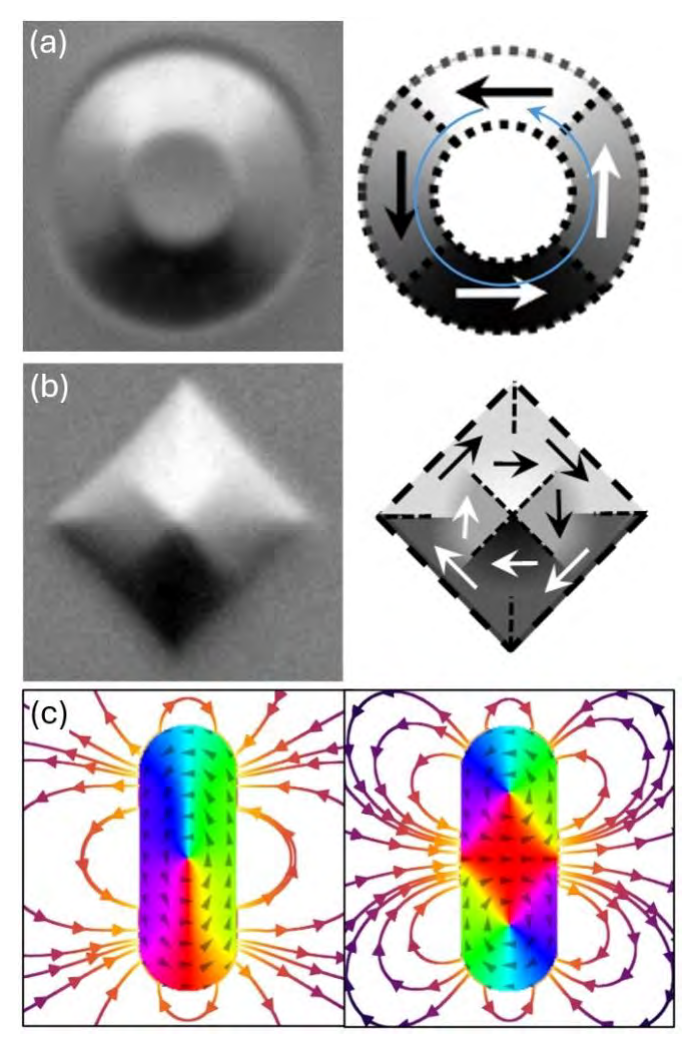


Fig. 1: (a) and (b) X-PEEM images and domain schematics for FM LSMO micromagnets with 2 micron diameter showing the diversity of spin textures that can be observed. (c) Magnetization maps and stray field profiles for single- and double-vortex CSTs observed in LSMO-based ASIs.

CD-10. Energy-Efficient Control of Probabilistic Switching in sMTJs via Voltage-Controlled Exchange Coupling: Experiment and Simulation*

Q. Jia^{1*}, O. Benally¹, B. Zink¹, D. Zhang¹, Y. Lv¹, S. Liang¹, D. Lyu¹, Y. Chen¹, Y. Yang¹, Y. Huang², J. Wang¹

¹University of Minnesota, Minneapolis, Minnesota, United States, ²National Yang Ming Chiao Tung University, Hsinchu, Taiwan

Superparamagnetic magnetic tunnel junctions (sMTJs) are promising components for energy-efficient probabilistic computing. In our recent work ([Q. Jia et al., Nano Lett., (2025)]), we demonstrated voltage-controlled exchange coupling (VCEC) as a novel mechanism to induce switching in sMTJs with only 40 nW power consumption, nearly two orders of magnitude lower than conventional spin-transfer torque (STT) control. While VCEC modifies the magnetic energy landscape via a voltage-induced effective exchange field, its switching dynamics have not been rigorously compared to STT. Here, we present macromagnetic simulations that directly compare VCEC and STT-driven dynamics in sMTJs. Our results reveal that VCEC not only reproduces similar probabilistic output control as STT but also enables operation in systems with enhanced damping without incurring additional energy costs. These findings position VCEC as a compelling low-power alternative for stochastic magnetic control in probabilistic hardware systems.

- [1] Q. Jia *et al.*, "Energy-Efficient Stochastic Signal Manipulation in Superparamagnetic Tunnel Junctions via Voltage-Controlled Exchange Coupling," *Nano Lett.*, May 2025, doi: 10.1021/acs.nanolett.4c06306.
- [2] Q. Jia *et al.*, "Ultrafast and Directional Magnetization Control via Voltage-Controlled Exchange Coupling," May 05, 2025, *arXiv*: arXiv:2504.06509. doi: 10.48550/arXiv.2504.06509.
- [3] D. Zhang *et al.*, "Bipolar Electric-Field Switching of Perpendicular Magnetic Tunnel Junctions through Voltage-Controlled Exchange Coupling," *Nano Lett.*, vol. 22, no. 2, pp. 622–629, Jan. 2022, doi: 10.1021/acs.nanolett.1c03395.
 [4] B. R. Zink *et al.*, "Ultralow Current Switching of Synthetic-Antiferromagnetic Magnetic Tunnel Junctions Via Electric-Field Assisted by Spin–Orbit Torque," *Adv. Electron. Mater.*, vol. 8, no. 10, p. 2200382, 2022, doi: 10.1002/aelm.202200382.

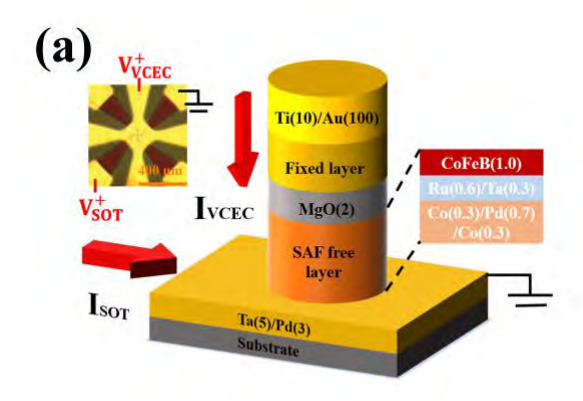


Fig. 1. Schematic of the VCEC-sMTJ device structure and current flow directions, with a top-view microscope image inset (top left). Adapted from Nano Lett., 2025.

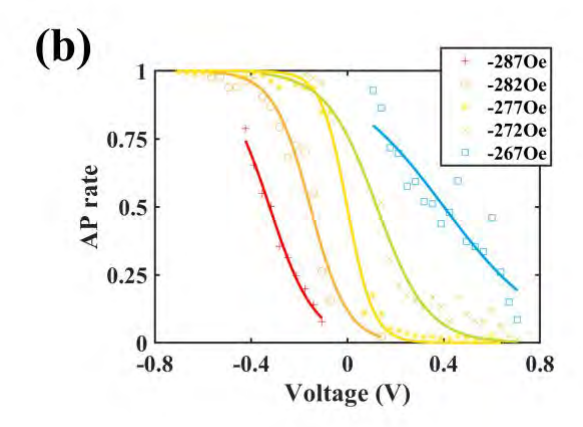


Fig. 2. AP-to-P switching in sMTJs under VCEC, demonstrating ~40 nW power consumption. Adapted from Nano Lett., 2025.

SESSION CE: ALTERMAGNETISM & ANTIFERROMAGNETISM - THIN FILMS AND OTHER SYSTEMS

Chair(s): R. Gupta, *Institute of Physics, University of Gothenburg, Gothenburg, Sweden*Wednesday, October 29, 2025
08:30 AM-12:00 PM
Room 2DE

CE-01. Collective excitations in altermagnetic α -MnTe A. De la Torre Duran

Northeastern University, Burlington, Massachusetts, United States

Altermagnetism is a recently identified magnetic phase that unites the spin-polarized electronic bands of ferromagnets with the compensated magnetic order of antiferromagnets via unconventional symmetry operations. Here, we present a combined x-ray magnetic circular dichroism (XMCD) and circular dichroism resonant inelastic X-ray scattering (CD-RIXS) study in thin films of the altermagnetic α -MnTe [1]. We reveal that the momentum and polarization dependence of the low-energy magnonic and phononic excitations are consistent with the chiral split nature of excitations in gwave altermagnets. Additionally, by looking at the highenergy charge excitations, we show that the electronic structure in MnTe is susceptible to epitaxial strain. All together, our data reveals a unique magnetophononic coupling in MnTe and demonstrates that substrate strain engineering opens a pathway toward next-generation magnonic and spintronic devices.

S. Bey et al., arXiv:2409.04567 (2024)

CE-03. Magnetoelastic stabilization of 180° domain walls in a collinear antiferromagnet

<u>A. Koziol Rachwal¹</u>, M. Szpytma¹, P. Drozdz¹, E. Madej², D. Wilgocka-Slezak², A. Kwiatkowski¹, E. Oles¹, M. Slezak¹, T. Slezak¹

¹AGH University of Krakow, Krakow, Poland, ²Jerzy Haber Institute of Catalysis and Surface Chemistry Polish Academy of Sciences, Krakow, Poland

Antiferromagnetic (AFM) spintronics offers promise for future data storage due to ultrafast dynamics and resilience to external magnetic fields. 1 Key to their application is understanding domain formation in AFMs, where conventional magnetostatic interactions do not drive domain wall (DW) formation. Here, we study domain evolution in collinear, fully compensated CoO films grown on MgO(001), with thicknesses of 5 nm and 10 nm. Using magneto-optical birefringence and XMLD-PEEM, we observe a transition from 90° orientational domains in 5 nm films (Fig. 1a) to 180° AFM domains in 10 nm films (Fig. 1b). The 180° domains are separated by worm-like DWs. Optical contrast arising from the Voigt effect exhibits sin(2φ) dependence (Fig. 1 c), confirming Néel vector alignment along [110] directions. In 10 nm CoO, domain walls show inplane spin orientation, as confirmed by XMLD-PEEM contrast and its absence with out-of-plane x-ray polarization. DW widths range from 150-200 nm. Notably, thermal cycling across the Néel temperature leads to renucleation of domains without correlation to previous patterns, indicating weak pinning and minimal influence of local defects. This contrasts with previous findings in NiO² and CuMnAs,³ where defect-driven DW formation dominates. Our findings reveal that AFM DWs in CoO emerge from intrinsic mechanisms and are stabilized by strain-induced effects rather than extrinsic defects. The observed transition fo domain structure with thickness highlights the critical role of magnetoelastic coupling in stabilizing DWs. These insights provide a pathway for controlled AFM domain engineering in thin-film devices.

Acknowledgements

This work was supported by Grant No. 2020/38/E/ST3/00086 funded by the National Science Centre, Poland.

- 1. V. Baltz et al. "Antiferromagnetic spintronics". In: Rev. Mod. Phys. 90, 015005 (2018).
- 2. Hendrik Meer et al.,: Advanced Functional Materials 33.21, 2213536 (2023).

3. Sonka Reimers et al., Nature Communications 13, 724 (2022).

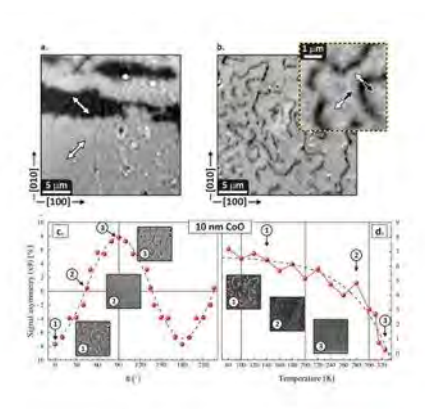


Fig. 1 The birefrignence images of 5nm and 10nm of CoO (a and b, respectively) collected for light polarization parallel to [100] direction of CoO. (c) Evolution of the room temperature birefringence contrast as a function of azimuthal angle φ for CoO layer with a thickness of 10nm. Inserts in (c) show birefringence images for selected φ angles.

CE-04. Two-dimensional antiferromagnets with non-relativistic spin splitting switchable by electric polarization <u>H. Mavani</u>, K. Huang, K. Samanta, E. Y. Tsymbal *Department of Physics and Astronomy, University of Nebraska, Lincoln, Lincoln, Nebraska, United States*

Altermagnetic materials have recently aroused huge scientific interest due to their spin-split electronic structure that allows using them in next-generation spintronics devices [1]. For these applications, switching the antiferromagnetic (AFM) Néel vector is required to perform digital operations. While it is potentially possible to reverse the Néel vector of altermagnets using spin-transfer or spinorbit torques [2], these operations are energy costly due to a large current density that is required to produce these torques. In this work, using the concept of polar stacking [3], we design two-dimensional (2D) antiferromagnets exhibiting non-relativistic spin splitting (NRSS), where switching the Néel vector is not required for spintronic applications. Using the spin-space group approach and firstprinciples calculations, we demonstrate that polar stacking of 2D van der Waals (vdW) antiferromagnets MPX_3 (M = Mn, V; X = S, Se) and 1T-CrTe₂ produces NRSS in their band structures. We predict that NRSS may have either altermagnetic or non-altermagnetic origins and elucidate

symmetry conditions under which NRSS becomes switchable by electric polarization. Figure 1 illustrates the polar-stacked VPS₃ bilayer as a representative system exhibiting d-wave altermagnetism with the sign of NRSS reversible by electric polarization. We argue that the NRSS switching can be detected by linear or nonlinear anomalous Hall effects, depending on the magnetic group symmetry of the system. Motivated by the recent experimental success in achieving ultrafast, fatigue-free ferroelectric switching of polar-stacked 3R-MoS₂[4] and BN [5] bilayers, we argue that the electric-field control of NRSS in polar-stacked AFM bilayers represents a viable route toward energy-efficient spintronic devices.

- [1] L. Šmejkal, et al., Phys. Rev. X 12, 040501(2022).
- [2] L. Han et al., Sci. Adv. 10, eadn0479 (2024).
- [3] E. Y. Tsymbal, Science 372, 1389 (2021).
- [4] R. Bian, et al., Science 385, eado1744 (2024).
- [5] K. Yasuda, et al., Science 385, eadp3575 (2024).

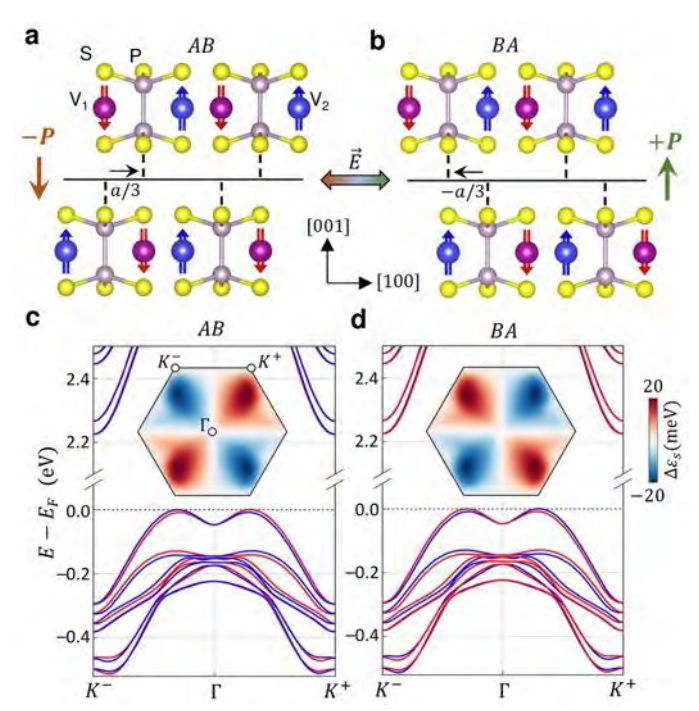


Fig. 1: Altermagnetism in polar-stacked VPS₃ bilayer. (a,b) Side view of the polar ground states AB (a) and BA (b), exhibiting opposite electric polarization. (c,d) Spin-polarized band structures and nonrelativistic spin splitting energy $\Delta \varepsilon_s = \varepsilon(s, k_x, k_y) - \varepsilon(-s, k_x, k_y)$ for the highest valance band of the AB (c) and BA (d) stackings.

CE-05. Structure and Magnetotransport in Altermagnetic MnTe Thin Films

S. Bey¹, M. Zhukovskyi³, T. Orlova³, S. Fields², V. Lauter⁴, H. Ambaye⁴, A. Ievlev⁵, S. P. Bennett², X. Liu¹, B. A. Assaf¹¹Physics and Astronomy, The University of Notre Dame, Notre Dame, Indiana, United States, ²Materials Science and Technology Division, U.S. Naval Research Laboratory, Washington, District of Columbia, United States, ³Integrated Imaging Facility, The University of Notre Dame, Notre Dame, Indiana, United States, ⁴Neutron Sciences Directorate, Oak Ridge National Laboratory, Oak Ridge, Tennessee, United States, ⁵Center for Nanophase Materials Science, Oak Ridge National Laboratory, Oak Ridge, Tennessee, United States

MnTe has emerged as a prominent platform for experimental studies of altermagnetism. Achieving high quality growth of thin films is an important next step towards realizing altermagnets in spintronics devices. In light of early works studying MnTe [1,2], we must achieve a mature understanding of how sensitive altermagnetism is to structural and chemical modifications. In this work, we present new perspectives into the growth mechanism and surface structure of epitaxial MnTe films grown by MBE on GaAs(111). These features are revealed through transmission electron microscopy (TEM), and polarized neutron reflectivity (PNR). We demonstrate that an interfacial misfit dislocation at the substrate-film interface is effective at relaxing lattice strain. We also report how the surface chemistry is modified by oxidation through a combination of TEM and PNR [3]. Next, we report on the sensitivity of MnTe films to in-plane field cooling via magnetotransport measurements where field-cooling (FC) reliably tunes the magnitude and polarity of the AHE [4]. We explore this unexpected tunability further by studying changes in PNR as a function of field cooling. The tunable anomalous Hall effect in MnTe offers a promising platform for future device applications and serves as a powerful tool to probe the underlying physics governing this new class of materials. Altogether, this work provides valuable insight towards understanding how structural, chemical and magnetic tuning can be utilized to control emerging altermagnetic materials.

Funding: NSF-2313441

[1] Phys. Rev. Lett., 130, 3, 036702 (2023)

[2] Nature, 636, 348 (2024)

[3] Bey, et al. arXiv:2504.12126 (2025) - accepted Phys. Rev. Mater.

[4] Bey, et al. arXiv:2409.04567 (2024)

CE-06. Probing altermagnetic band splitting and magnetic order in epitaxial CrSb thin films

N. Samarth^{1, 2}

¹Dept. of Physics and Dept. of Materials Science and Engineering, The Pennsylvania State University, University Park, Pennsylvania, United States, ²Argonne National Lab, Lemont, Illinois, United States

Altermagnets are a newly identified family of collinear antiferromagnets with momentum-dependent spin-split band structure of non-relativistic origin, derived from spingroup symmetry-protected crystal structures [1,2]. Among candidate altermagnets, CrSb is attractive for potential applications because of a large spin-splitting near the Fermi level and a high Neel transition temperature of around 700 K [3-5]. We use molecular beam epitaxy to synthesize CrSb (0001) thin films on SrTiO₃ (111)/Sb₂Te₃ with thicknesses ranging from 10 nm to 100 nm [6]. Structural characterization, using reflection high energy electron diffraction, scanning transmission electron microscopy, and X-ray diffraction, demonstrates the growth of epitaxial films with good crystallinity. Polarized neutron reflectometry shows the absence of any net magnetization in the CrSb layers, consistent with antiferromagnetic order. *In vacuo* angle resolved photoemission spectroscopy (ARPES) measurements carried out with photon excitation energy between 20 eV - 100 eV probe the band structure in film thicknesses down to 10 nm. These ARPES measurements show a three-dimensional momentum-dependent band splitting of up to 0.7 eV with q-wave symmetry, consistent with that seen in prior studies of bulk single crystals. The distinct altermagnetic band structure required for potential spin-transport applications survives down to the 10 nm thin film limit at room temperature. We also describe DC and RF electrical transport measurements aimed at probing chargespin interconversion in these thin films, potentially using strain to break the constraints imposed by the q-wave symmetry.

This work is done in collaboration with S. Santhosh, P. Corbae, W. J. Yanez-Parreno, S. Ghosh, C. J. Jensen, A. V. Fedorov, M. Hashimoto, D. Lu, J. A. Borchers, A. J. Grutter, T. R. Charlton, Saurav Islam, A. Richardella, K. A. Mkhoyan, C. J. Palmstrøm, and Y. Ou.

Primary support for this project was provided by the Penn State Two-Dimensional Crystal Consortium-Materials Innovation Platform (2DCC-MIP) under NSF Grant No. DMR-2039351. We also acknowledge the Penn State MRSEC Center for Nanoscale Science via NSF award DMR 2011839,

NSF Grant No. DMR-2309431, and the University of California, Santa Barbara NSF Quantum Foundry through Q-AMASE-i Program via Award No. DMR-1906325.

- 1. Mazin, I.: Editorial: Altermagnetism—a new punch line of fundamental magnetism. *Phys. Rev. X* <u>12</u>, 040002 (2022).
- 2. Smejkal, L., Sinova, J., Jungwirth, T.: Emerging research landscape of altermagnetism. *Phys. Rev. X* <u>12</u>, 040501 (2022).
- 3. Zeng, M., *et al*: Observation of spin splitting in room-temperature metallic antiferromagnet CrSb. *Adv. Sci.* <u>11</u>, 2406529 (2024).
- 4. Ding, J., et al: Large band splitting in g-wave altermagnet CrSb. Phys. Rev. Lett. 133, 206401 (2024).
- 5. Reimers, S., *et al.*, : Direct observation of altermagnetic band splitting in CrSb thin films. *Nat. Commun.* <u>15</u>, 2116 (2024).
- 6. Santhosh. S., et al., (2025) arXiv:2505.00239

CE-07. Robust Biaxial Anisotropy and Electrical Switching of $LaFeO_3$ Epitaxial Thin Films

J. Lanier, J. Michel, D. Russell, J. Flores, B. Liu, J. Hwang, <u>F. Yang</u>

The Ohio State University, Columbus, Ohio, United States

Antiferromagnetic (AFM) spintronics has generated considerable interest since the demonstration of electrical switching of AFMs. AFMs with robust biaxial anisotropy, accessible spin-flop fields, and high Néel temperatures are ideal for AFM spintronics. Currently, AFM research has been mostly focused on binary AFMs, while the large family of complex oxide AFMs have been much less unexplored. We show the growth of high quality LaFeO₃ epitaxial films (Fig. 1) down to 1 nm thickness on SrTiO₃(001). Using angulardependent spin-Hall magnetoresistance (SMR) characterization of Pt/LaFeO₃ bilayers, we observe (1) a robust and accessible spin-flop field of 1-3 T, (2) a squareshaped transverse SMR with 90-degree wide plateaus at 2-5 T, indicating a clear biaxial anisotropy, and a saw-toothshaped longitudinal SMR with well-defined subtle features; and (3) decreasing magnitudes and sinusoidal shape of SMR at higher fields up to 14 T. The clear biaxial anisotropy persists down to 2-nm LaFeO₃ and AFM ordering is detected in 1-nm LaFeO₃ at 25 K. Our experimental SMR results can be precisely simulated by a macrospin model, which captures all the subtle details [1]. We pattern two Hall bars with the current channel along SrTiO₃ [100] (AFM hard axis) and [110] (easy axis), which show switched shapes of square and saw-tooth SMR between longitudinal and transverse SMR. Our model accurately explains the shape switching as well as the fine features of these two samples. We also perform electrical switching of the Néel vector between two easy axes (Fig. 2), where each channel of the cross is at 22.5° in between the two easy axes for both electrical switching and detection, which exhibit clean and reversable switching in Pt/LaFeO₃ bilayers [2]. This work indicates that LaFeO₃ and other AFM perovskites are promising candidates for AFM spintronic applications such

indicates that LaFeO₃ and other AFM perovskites are promising candidates for AFM spintronic applications such as memory, magnonics, and altermagnetism, which will greatly expand the scope of the field of AFM spintronics. This work was primarily supported by the Department of Energy under Grant No. DE-SC0001304.

- 1. J. Lanier, J. Michel, J. Flores, and F. Y. Yang, "Robust Biaxial Anisotropy and Switchable Néel Vectors in LaFeO₃ Epitaxial Films," *Nano Lett.* 25, 4667 (2025).
- 2. J. Lanier, *et al.* "Electrical Pulse Switching and Imaging of Antiferromagnetic Spins in Perovskite Epitaxial Films," in preparation.

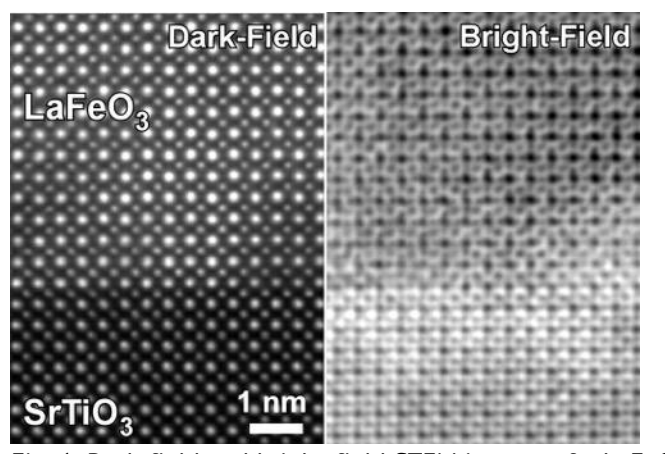


Fig. 1. Dark-field and bright-field STEM images of a LaFeO $_3$ film on SrTiO $_3$.

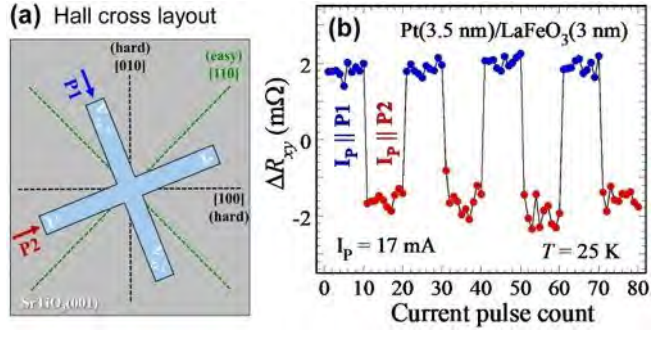


Fig. 2. (a) Schematic of a Hall cross. (b) Electrical switching of a Pt/LaFeO₃ bilayer.

^{*} Best Student Presentation Finalist / LB - Late-breaking Poster

CE-08. High-temperature anomalous Hall and magnetoresistance effects driven by frustrated spin fluctuations in the antiferromagnetic metallic delafossite PdCrO₂

Y. Tao¹, P. Jain¹, Y. Zhang¹, F. Tutt¹, D. Phelan², C. Balz³, S. Hatt⁴, E. Zappala⁴, J. Neuefeind³, S. Rosenkranz², B. Frandsen⁴, <u>C. Leighton¹</u>

¹University of Minnesota, Minneapolis, Minnesota, United States, ²Argonne National Lab, Argonne, Illinois, United States, ³Oak Ridge National Lab, Oak Ridge, Tennessee, United States, ⁴Brigham Young University, Provo, Utah, United States

Metallic delafossite oxides are of exceptional current interest due to their ultraclean metallic transport [1,2]. In the case of PdCrO₂, this arises in a triangular-lattice antiferromagnet, creating an extraordinary opportunity to study frustrated magnetism in a clean metal [1]. Here, we combine a new chemical vapor transport crystal growth approach [2] with magnetic, thermodynamic, magnetotransport, and neutron scattering measurements to elucidate the striking anomalous Hall effect in antiferromagnetic PdCrO₂ [1,3,4]. The unconventional anomalous Hall effect and a large (>1000%) positive magnetoresistance effect are shown to exhibit complex temperature dependencies, persisting to almost seven times the Néel temperature. For the first time, these effects are directly compared to elastic neutron scattering, inelastic neutron scattering, and neutron magnetic pair distribution function data, establishing a clear link between anomalous magnetotransport properties and directly probed shortrange spin fluctuations. The latter are shown to occur over a notably broad temperature range due to geometrical magnetic frustration. Connecting to recent experimental and theoretical developments [3-5], these findings are interpreted in terms of a temperature-dependent interplay between chiral spin order and chiral spin fluctuations, significantly elucidating the high-temperature anomalous magnetotransport in such compounds.

Work at the University of Minnesota supported primarily by the Department of Energy through the University of Minnesota Center for Quantum Materials.

1. A.P. Mackenzie, Rep. Prog. Phys. 80, 032501 (2017). 2. Y. Zhang, F. Tutt, G.N. Evans, P. Sharma, G. Haugstad, B. Kaiser, J. Ramberger, S. Bayliff, Y. Tao, M. Manno, J. Garcia-Barriocanal, V. Chaturvedi, R.M. Fernandes, T. Birol, W.E. Seyfried Jr., and C. Leighton, Nat. Commun. 15, 1399 (2024). 3. H. Takatsu, S. Yonezawa, S. Fujimoto, and Y. Maeno, Phys. Rev. Lett. 105, 137201 (2010)

4. H. Jeon, H. Seo, J. Seo, Y.H. Kim, E.S. Choi, Y. Jo, H.N. Lee, J.M. Ok and J.S. Kim, Comms. Phys. 7, 162 (2024).

5. H. Ishizuka and N. Nagaosa, Sci. Adv. 4, eaap9662 (2018).

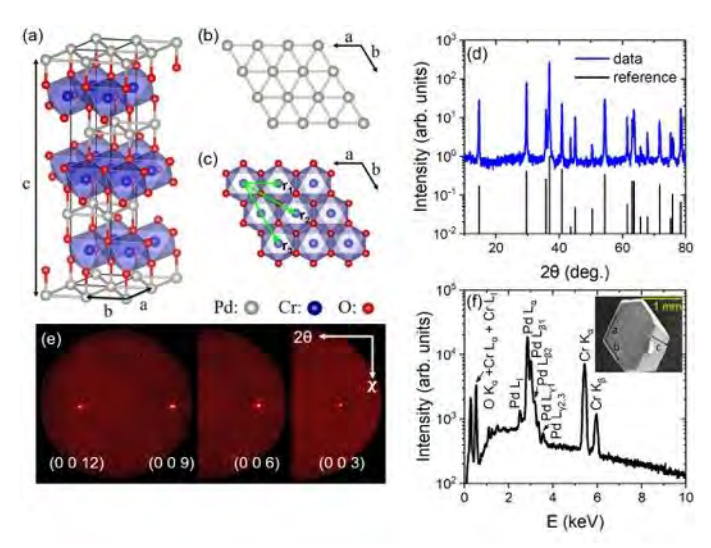


Fig. 1: PdCrO₂ crystal structure (a-c), powder x-ray diffraction (d), single-crystal X-ray diffraction (e), and energy dispersive X-ray spectrsocopy (f). Inset: Crystal image.

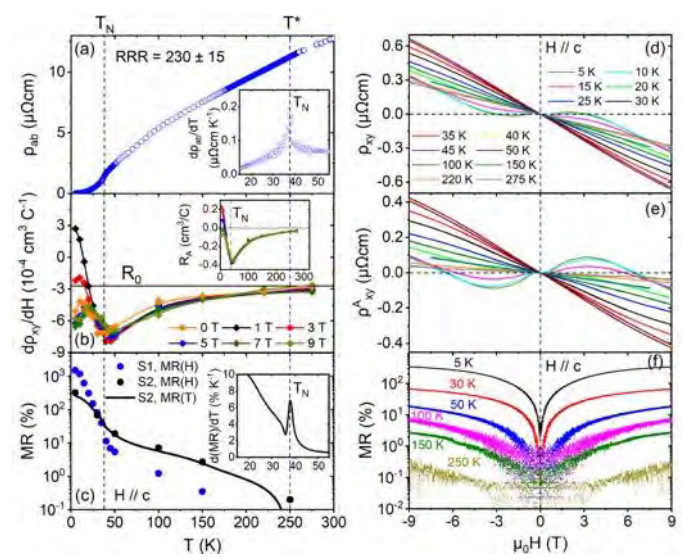


Fig. 2: (a-c) Temperature dependence of the a-b plane resistivity (a), field-derivative of Hall resistivity (b), and magnetoresistance (c) in single-crystal $PdCrO_2$. The insets show the derivative of the resistivity, anomalous Hall effect, and derivative of magnetoresistance, respectively. (d-f) Magnetic field dependence of the raw Hall resistivity (d), anomalous Hall resistivity (e), and magnetoresistance (f) at various temperatures.

169

CE-09. Nanoscale Magnetic Structure Imaging of an Atomically Thin 2D Antiferromagnet

J. Katoch¹, A. Tiwari¹, A. Smekhova², S. Patil², R. Bandapelli¹, Z. Cui¹, I. Kao¹, R. Posti¹, F. Kronast², <u>S. Singh</u>¹

¹Physics, Carnegie Mellon University, Pittsburgh, Pennsylvania, United States, ²Helmholtz-Zentrum Berlin für Materialien und Energie, Albert-Einstein-Straße, Berlin, Germany

Antiferromagnetic (AFM) materials are predicted to play a crucial role in conceptualized spintronics devices, such as ultrafast magnetic memory device and magnonic devices for generation, transmission, and detection of high frequency signals. The van der Waals (vdW) based AFMs display highly intriguing properties, such as thickness-dependent magnetic ground state, electric field tunability, enhancement of interlayer AFM exchange coupling in the ultra-thin limit, and tunable magnon-magnon coupling, to name a few. And a comprehensive understanding of magnetism in AFM systems is needed for spintronics device applications. Layered CrSBr is a unique system to study AFM order. In CrSBr, the magnetic moments lie in the plane defined by Cr layers. The moments are aligned ferromagnetically within the layer, but nearby layers are antiferromagnetically coupled. We will report on experiments, wherein we employ photoemission electron microscopy (PEEM) paired surfacesensitive X-ray Magnetic Circular/Linear Dichroism (XMCD/XMLD) to perform layer-dependent domain imaging of CrSBr. We will discuss detailed thickness, temperature, and externally applied magnetic field dependent magnetic domain imaging of atomically thin samples of CrSBr.

SESSION CF: LOW-DIMENSIONAL SYSTEMS, MOLECULAR AND ORGANIC MAGNETS

Chair(s): J. Hanson-Flores, *Physics, University of Central Florida, Orlando, Florida, United States*Wednesday, October 29, 2025
08:30 AM-12:00 PM
Room 2BC

CF-01. Quantum and Nonlinear Magnonics

G. Fuchs

Applied and Engineering Physics, Cornell University, Ithaca, New York, United States

As we progress more deeply into the second quantum revolution, a natural question we ask is – is there a role for magnonics in quantum information platforms? Building on a

decade of foundational work on this progress, I will discuss my take on this question and our efforts to develop new the roles for magnonics in quantum and classical technologies. For quantum technologies, a major challenge is mitigating loss, since loss is the enemy of quantum coherence. Building on our efforts to establish a scalable cavity magnonics platform based on the ultra-low loss organicbased magnet vanadium tetracyanoethylene V[TCNE]_x [1], I'll discuss our approach to a cavity-magnonics implementation of the optomechanical-type nonlinear Hamiltonian [2]. Using this nonlinear interaction, we theoretically show how driving magnons that are coupled to a microwave electromagnetic resonator can enable resonator cooling and quantum squeezing. This approach can work with any low-loss magnetic material, here we describe it implementation with vttrium iron garnet (YIG) and V[TCNE]x. Finally, I'll describe our recent working using scanning NV center probes to understand nonlinear frequency generation in magnetic spin textures. We correlate the efficiency of harmonic generation with the local spin texture of Ni₈₁Fe₁₉/Pt bilayers at low magnetic field. We find that harmonic generation is both highly local and chiral in nature.

[1] Adv. Sci. 11, 2310032 (2024)

[2] Phys. Rev. B 111, 134440 (2025)

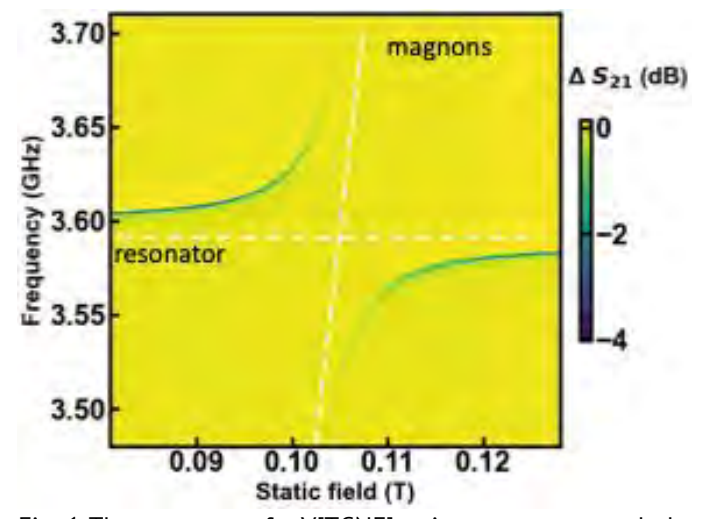


Fig. 1 The spectrum of a V[TCNE]_x microstructure coupled to a lumped-element superconducting resonator with cooperativity exceeding 1000.

CF-02. Low-Lying Excitations, Magnetic Irreversibilities and Griffith's Phase in Quasi-two-dimensional Manganite M. Verma, Y. Bitla

Physics, Central University of Rajasthan, Ajmer, Rajasthan, India

Magnetism in low-dimensional systems like twodimensional materials (2DM), artificial heterostructures and van der Waals (vdW) monolayers is an active area of research. However, the magnetic properties of typical quasitwo-dimensional (Q2D) materials, which lack vdW bonding, remain relatively unexplored. A detailed bulk magnetization study of an archetype Q2D $La_{1.4}Sr_{1.6}Mn_2O_7$ manganite over a broad temperature range reveals a series of transitions from 3D ferromagnetic (FM) to Q2D FM at 101 K, Q2D-2D FM at 232 K and 2D FM-paramagnetic phase at 361 K. There are two weak intermediate transitions in 2D FM state due to intergrowths that get suppressed with magnetic field. The compound has strong uniaxial anisotropy and a gap in the spin-wave spectrum. For the first time, we show an evidence of antiferromagnetic clusters in the Griffith's phase. These properties are governed by the interplay of inter-bilayer (J'), intra-bilayer (J₁), in-plane (J₁) interactions and magnetocrystalline anisotropy related to spin-lattice and dipolar interactions. Furthermore, the compound shows a notable magnetocaloric effect across a broad temperature range, underscoring its potential for cryogenic magnetic refrigeration applications. This study constructs a wide temperature T-H phase diagram for Q2D La_{1.4}Sr_{1.6}Mn₂O₇ compound.

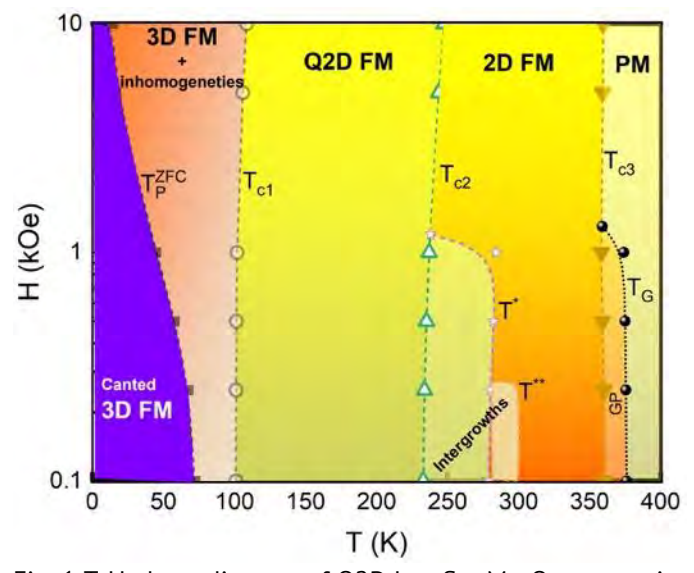


Fig. 1 T-H phase diagram of Q2D La_{1.4}Sr_{1.6}Mn₂O₇ manganite.

CF-03. Enhanced Coercivity and Spin-Glass Behavior in SiO_2 -Coated Fe_5C_2 Nanorods

P. Joshi¹, H. Abbas¹, T. Karki¹, J. Mohapatra¹, X. Liu², P. Liu¹

¹Physics, The University of Texas at Arlington, Arlington, Texas, United States, ²Ames Laboratory, Critical Materials Institute, Ames, Iowa, United States

Rod-shaped Fe_5C_2 and SiO_2 -coated Fe_5C_2 nanocrystals were synthesized via a solution-based chemical method (Fig. 1a). Structural analysis confirmed the monoclinic phase of Fe₅C₂ with space group C2/c. Zero-field-cooled (ZFC) and fieldcooled (FC) magnetization curves revealed distinct magnetic behaviors: uncoated Fe₅C₂ exhibited a low-temperature FC plateau indicative of strong dipolar interactions, while Fe₅C₂@SiO₂ showed a monotonic increase in FC magnetization, suggesting reduced dipolar interactions due to SiO₂ surface passivation (Fig. 1b). Isothermal remanent magnetization (IRM) and DC demagnetization (DCD) measurements supported this trend, with δM plots confirming weaker dipolar interactions in the coated sample. Bloch's law analysis of temperature-dependent saturation magnetization showed a smaller Bloch constant for Fe₅C₂ and a larger value for Fe₅C₂@SiO₂, reflecting enhanced surface disorder and reduced exchange coupling in the latter. Notably, Fe₅C₂@SiO₂ demonstrated increased coercivity, attributed to decreased dipolar interaction and elevated surface anisotropy. Kneller's law analysis yielded higher blocking temperatures for Fe₅C₂@SiO₂ (583 K) than Fe₅C₂ (549 K), highlighting the impact of surface modification on magnetic relaxation. These findings illustrate how SiO₂ coatings effectively modulate dipolar interactions, enhance coercivity, and promote spin-glasslike behavior in Fe₅C₂ nanocrystals.

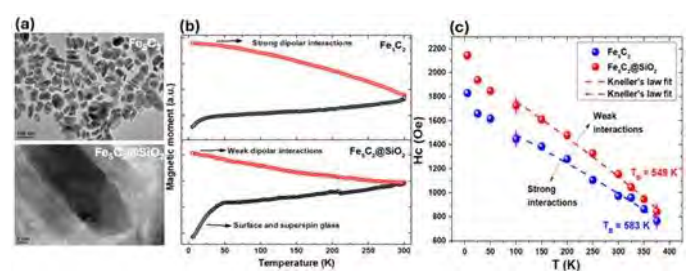


Figure 1: (a) TEM images for Fe_5C_2 and $Fe_5C_2@SiO_2$ nanocrystals. (b) ZFC and FC magnetization curves at dc field of 100 Oe for Fe_5C_2 and $Fe_5C_2@SiO_2$ nanocrystals, (c) Coercivity vs temperature for Fe_5C_2 and $Fe_5C_2@SiO_2$ nanocrystals with Kneller's law fit.

CF-04. Field-induced breathing magnetic domain wall at ferromagnetic nanowires

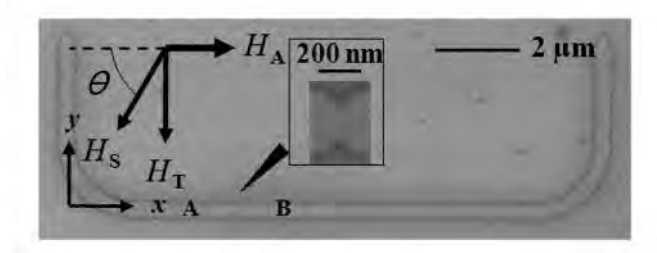
S. Ahn

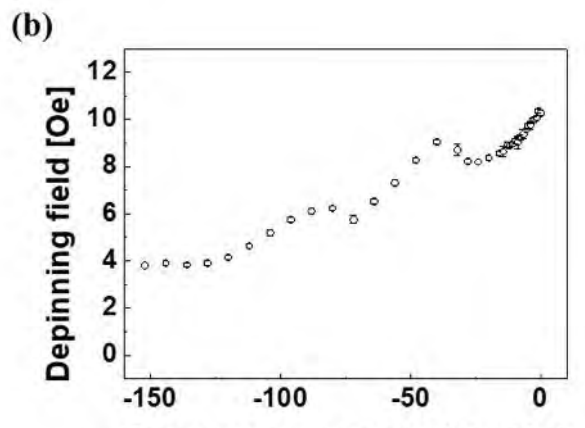
Postech, Pohang, Korea (the Republic of)

The Breathing behavior of a geometrically constrained magnetic domain wall (CDW) is critical to understand switching behaviors of CDWs as inputs for a random variable generator for probabilistic computing [1]. In the previous study, we have found that the CDW shows firstly an oscillatory depinning behavior under a magnetic field H_T transverse to the nanowire [2]. In this study, we elucidate the relation of breathing magnetic domain wall with its oscillatory behavior by considering the 2D magnetization (m) vector. Figure 1(b) shows the oscillatory depinning behavior of CDW at constraints like double notches in the ferromagnetic nanostructures as shown in Fig. 1(a). Especially, the depinning behavior shows oscillatory reductions at each specific field with increasing H_T in the negative direction. To understand such oscillatory reductions, tilting angle(ϕ) — the angle magnetization at the constraints from the easy plane—has been calculated by micromagnetic simulations with respect to H_T . Figure 2 shows that the tilting angle follows oscillatory reductions with respect to H_T like the Fig.1(b). It is clearly seen that the oscillatory behavior of depinning field corresponds to that of tilting angle with respect to H_T . Considering simulated CDW patterns (inset) of Fig.2, a width of the CDW is vibrated depending on H_T , which means that it is called as 'breathing mode'[3]. Furthermore, the breathing mode has been reported as current or voltage-induced phenomenon so far but this result is from the external field of H_T . Therefore, the oscillation of tilting angle(φ) resulted in the breathing CDW, which is the first demonstration of field-induced breathing behavior of CDW in the ferromagnetic nanowire.

[1] K. Everaert *et al.*, Appl. Phys. Lett. 122 (2023) 211902.
[2] S.-M. Ahn *et al.*, J. Nanosci. Nanotechnol. 11 (2011) 6472.
[3] M. Mori et al., J. Phys.: Condens. Matter 26 (2014) 255702.

(a)





Transverse magnetic field [Oel

Fig. 1 (a) Scanning electron micrograph of a U-shaped 300-nm-wide Permalloy nanowire structure with double notches. Positions A and B on the wire correspond to the positions of the MOKE measurement. Inset: High-resolution image of the notch. The arrows indicate the directions of the magnetic fields H_S , H_A , and H_T , respectively. (b) Depinning field with respect to H_T .

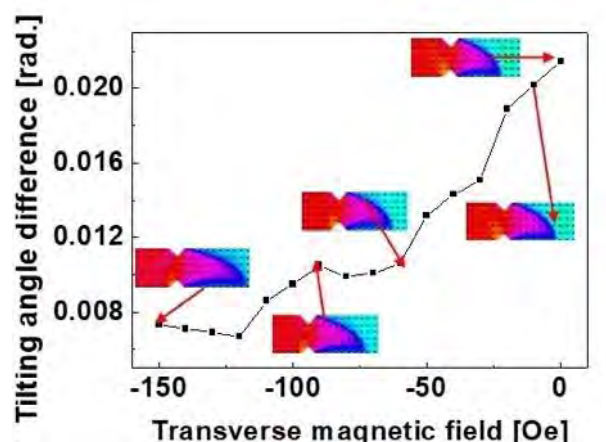


Fig. 2 Tilting-angle(ϕ) with respect to H_T . Inset: Simulated patterns at specific fields pointed by red arrows.

CF-05. Electron Spin Resonance Measurement of a Single Molecule Magnet Terbium Phthalocyanine (TbPc2) Using Scanning Tunneling Microscopy

T. Komeda

Tohoku University, Sendai, Japan

Electron spin resonance (ESR) and nuclear magnetic resonance (NMR) are the primary techniques used to determine the spin properties of molecules and solids. Moreover, in recent studies on applying spins to the quantum gubit of quantum information processes, they play a central role in reading and writing the spin state. However, the conventional ESR/NMR requires a large number of molecules for detection, and the instruments are large, which is a setback for the quantum computer application. For the medical use of NMR, MRI is an indispensable technique. However, the resolution is typically no smaller than mm. To overcome these issues, the development of ESR/NMR measurement by electron attracts attention. Especially, if the tunneling current can provide the ESR/NMR information, the spatial resolution can be reduced to the atomic size.

In this report, we investigate whether scanning tunnelling microscopy and spectroscopy (STM/STS) can provide the atomic-scale structural configuration and spin state with the same accuracy as conventional electron spin resonance (ESR). The experiment was done in UHV conditions at a temperature of 400 mK. RF signal and outer magnetic field are introduced to the tunneling junction between the spinpolarized tip and the Au(111) substrate. NaCl film of several monolayers is inserted as a thin interface layer. The doubledecker phthalocyanine complex of

bis(phthalocyaninato)terbium(III) (TbPc2) molecule was used as the magnetic molecule, which has the π radical at the phthalocyanine ligand as well as 4f spins of the center metal.

The schematic illustration is in Fig. 1, with STM images of the TbPc2 molecule. As shown in Fig. 1(d), a sharp resonance feature is observed as an enhancement of the tunnelling current. The resonance condition shows a Zeeman condition with q~2.0 representing the Pc ligand's delocalized unpaired pai orbital spin. We will discuss the possibility of the application for other areas of research. R. Kawaguchi, K. Hashimoto, T. Kakudate, K. Katoh, M. Yamashita, T. Komeda, Nano Lett., 23 (2023) 213-219.

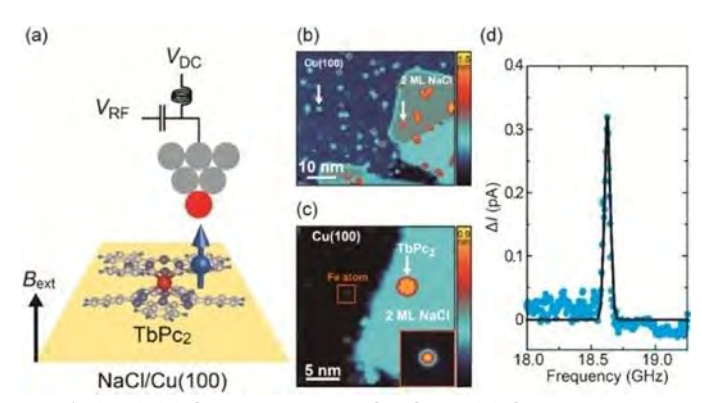


Fig 1: (left) (a) Schematics of ESR-STM. (b) Single-molecule magnet TbPc2 film and (c) isolated TbPc2 on NaCl film.

CF-06. Development and Characterization of Magnetite **Reinforced Nanocomposites for Electromagnetic Responsiveness and Smart Material Applications**

D. Di Napoli, S. Vattathurvalappil Aerospace Engineering, King Fahd University of Petroleum and Minerals, Dhahran, Saudi Arabia

Nanocomposite materials have garnered significant attention in advanced materials science due to their unique ability to exhibit multifunctional properties, particularly in the realm of magnetism and electromagnetic responsiveness. This study focuses on the development and characterization of acrylonitrile butadiene styrene (ABS) polymer matrix reinforced with ferromagnetic iron oxide (Fe3O4) nanoparticles. The primary objective was to investigate the electromagnetic properties of the nanocomposite and evaluate its potential for use in smart materials, sensors, and actuators. The nanocomposite was fabricated using a melt-mixing process, wherein Fe3O4 nanoparticles were incorporated into the ABS thermoplastic matrix at varying concentrations ranging from 10 to 20 wt%. The mixture was then extruded into long, continuous fibers to facilitate testing and analysis. Initial experimental testing demonstrated the material's responsiveness to electromagnetic stimulation. A 12V DC Arduino-controlled electromagnet was used to generate a magnetic field, with the field intensity regulated through pulse-width modulation (PWM). The fibers exhibited significant magnetic receptiveness, as evidenced by their ability to be pulled and displaced both laterally and vertically in response to the applied magnetic field. The results indicated that increasing the concentration of Fe3O4 nanoparticles enhanced the material's sensitivity to electromagnetic stimulation,

173

highlighting its potential for applications requiring precise control over magnetic interactions. In conclusion, this research underscores the potential of Fe3O4-reinforced ABS nanocomposites as a versatile and innovative material system for electromagnetic sensitivity.

CF-07. Integrated Numerical and SAXS Investigation of Ultra-Small SPIONs Magnetophoresis and Separation in High Field and Gradient Fields

X. Wu¹, H. Choe¹, P. Iyer¹, B. Yunker¹, I. H. Karampelas², K. Wu³, J. Chalmers¹, <u>J. Gomez-Pastora³</u>

¹The Ohio State University, Columbus, Ohio, United States, ²Nemak, Sheboygan, Wisconsin, United States, ³Texas Tech University, Lubbock, Texas, United States

The magnetophoretic separation of magnetic nanoparticles (MNPs) in liquid media poses significant challenges as particle size decreases, due to the increasing dominance of Brownian motion over magnetic forces. In this study, we investigate the magnetically induced transport and separation behavior of superparamagnetic iron oxide nanoparticles (SPIONs) in the 5–30 nm size range, using two high field and gradient magnetic sorter and in situ small-angle X-ray scattering (SAXS).

Numerical simulations performed in COMSOL Multiphysics model the magnetic force fields and particle trajectories within two magnetic separation systems, capturing the interplay between radial and axial magnetophoretic components. These simulations predict that even ultrasmall SPIONs (<15 nm) can undergo directed migration under sufficiently strong magnetic gradients, even in the absence of particle-particle interactions. Experimentally, SAXS measurements were conducted under applied field conditions to track SPION spatial redistribution and structural behavior in real time. The SAXS results confirm particle migration aligned with the simulated field-driven trajectories, while also revealing distinct size-dependent behavior: particles ≥30 nm exhibited reversible aggregation via dipole-dipole interactions, while smaller particles (<15 nm) remained well-dispersed, consistent with superparamagnetic behavior.

Additionally, SPIONs exhibited unexpected axial migration after removal from the magnetic field, indicating the influence of residual axial field components, which were

also captured by the simulation. The combined SAXS and modeling results establish that effective magnetophoresis and size-selective separation of ultra-small SPIONs are achievable using permanent magnet-based quadrupole fields, provided sufficiently high field gradients are maintained. These findings contribute to a mechanistic understanding of nanoscale particle dynamics in magnetic separators and inform the rational design of next-generation systems for biomedical purification, targeted delivery, and nanoscale materials recovery.

CF-09. Efficient Fe_3O_4 @CuS nanocomposites for enhanced removal of organic dyes from wastewater

J. Gupta^{2,1}, K. C. Barick¹

¹Chemistry Division, Bhabha Atomic Research Centre, Navi Mumbai, Maharashtra, India, ²School of Advanced Sciences and Languages, VIT Bhopal University Bhopal, Sehore, Madhya Pradesh, India

Magnetic nanocomposites have garnered significant interest due to their promising applications in wastewater treatment. In this context, Fe₃O₄@CuS nanocomposites were synthesized via a two-step chemical method. The developed nanocomposites have been thoroughly analyzed using a range of advanced characterization techniques, including Xray diffraction (XRD), Fourier-transform infrared spectroscopy (FTIR), X-ray photoelectron spectroscopy (XPS), scanning electron microscopy (SEM), transmission electron microscopy (TEM), UV-visible absorption spectroscopy, and a physical properties measurement system. XRD analysis confirmed the coexistence of the magnetite phase of Fe₃@O₄ and the covellite phase of CuS (Fig. 1a), while XPS data supported these findings by verifying the presence of both components. SEM-based elemental mapping analysis also confirmed the presence of Fe, Cu, S, and O (Fig. 1b). TEM images revealed Fe₃O₄ nanoassemblies comprising discrete particles of approximately 5-6 nm in size, with CuS nanoparticles visible on the Fe₃O₄ surface (Fig. 1c). Moreover, the Fe₃@O₄-CuS nanocomposites exhibited superparamagnetic behavior at room temperature. Moreover, zeta potential measurement revealed a reduction of surface charge, providing additional evidence of CuS incorporation onto Fe₃O₄. The catalytic performance of the Fe₃O₄@CuS nanocomposites was evaluated for the degradation of organic dyes – including methylene blue, Rose Bengal, and methyl orange-under dark conditions and in the presence of H₂O₂. Impressively, the photocatalysts achieved a degradation efficiency of 99%

within just 8 minutes. These findings highlight the remarkable environmental remediation potential of the Fe_3O_4 @CuS nanocomposites.

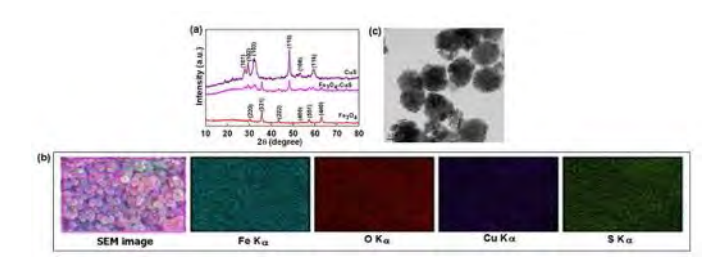


Figure 1

CF-10. Emergence of the Verwey Transition in Fe₅C₂@Fe₃O₄ Core−Shell Nanocrystals Below 5 nm Thickness

<u>H. Abbas</u>, J. Mohapatra, P. Joshi, T. Karki, P. Liu *Physics, The University of Texas at Arlington, Arlington, Texas, United States*

Finite-size effects profoundly alter or even suppress strongly correlated magnetic and electronic phenomena by introducing strain, modifying density, and disrupting intrinsic electronic correlations. A noticeable example is the Verwey transition—a metal-insulator transition in Fe₃O₄ that typically vanishes below the superparamagnetic threshold (~16 nm) due to surface spin disorder and structural inhomogeneity [1, 2]. In this work, we demonstrate the emergence of the Verwey transition in Fe₅C₂@Fe₃O₄ core-shell nanocrystals with sub-5 nm shell thicknesses. Magnetization measurements under 100 Oe reveal the Verwey transition near 125 K in both zero-fieldcooled and field-cooled curves, confirming the formation of a magnetite shell. This behavior arises from the controlled oxidation of Fe₅C₂ nanoparticles via carbon monoxide released from metal carbonyl precursors, yielding a stoichiometric Fe₃O₄ shell. The Verwey transition becomes sharper and more pronounced with increasing shell thickness, highlighting the critical role of interfacial structure and particle size. Simultaneously, overall magnetization decreases due to the lower net moment of the ferrimagnetic Fe₃O₄ shell compared to the Fe₅C₂ core. A gradual increase in coercivity with shell thickness indicates enhanced exchange anisotropy and diminished interparticle interactions. These results highlight the potential of nanoscale shell engineering to revive and tailor emergent correlated phenomena in core-shell structure.

- 1. Mitra, A., J. Mohapatra, and M. Aslam, Magnetic and electronic properties of anisotropic magnetite nanoparticles. Materials Research Express, 2024. 11(2): p. 022002.
- 2. Mohapatra, J., et al., Size-dependent magnetic and inductive heating properties of Fe3O4 nanoparticles: scaling laws across the superparamagnetic size. Physical Chemistry Chemical Physics, 2018. 20(18): p. 12879-12887.

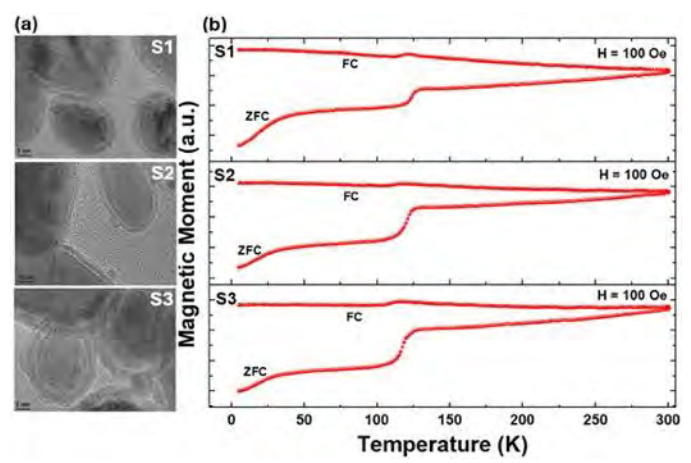


Figure 1: (a) TEM images for $Fe_5C_2@Fe_3O_4$ core-shell nanoparticles with 3 nm (S1), 4, nm (S2) and 5 nm (S3) Fe_3O_4 shell thicknesses, and (b) ZFC-FC magnetization curves measured with applied magnetic field of 100 Oe for all samples.

CF-11. Magnetic Properties of Fe₃O₄ Membranes Transferred from a SrTiO₃ substrate by Etching a BaO Sacrificial Layer

D. Matsubara¹, T. Takeda², M. Tanaka^{1,3,4}, S. Ohya^{1,3,4}
¹Department of Electrical Engineering and Information Systems, The University of Tokyo, Bunkyo-ku, Tokyo, Japan, ²Department of Chemical System Engineering, The University of Tokyo, Bunkyo-ku, Tokyo, Japan, ³Center for Spintronics Research Network (CSRN), The University of Tokyo, Bunkyo-ku, Tokyo, Japan, ⁴Institute for Nano Quantum Information Electronics, The University of Tokyo, Bunkyo-ku, Tokyo, Japan

Strain engineering using transferred epitaxial thin films has emerged as a promising route for tuning physical properties in functional oxides, with potential applications in flexible devices [1]. Fe $_3$ O $_4$ is a ferrimagnetic oxide [Fig. 1(a)] exhibiting rich properties: high Curie temperature $T_c \approx 850$ K [2] and its metal-insulator transition known as the Verwey transition (VT) [3]. In a previous study, Sr $_3$ Al $_2$ O $_6$ (SAO) has been used as a water-soluble sacrificial layer to transfer Fe $_3$ O $_4$ thin films [4]; however, the composition control of SAO is difficult, and the process requires long-time

immersion in water (≤ 1 day), which can degrade the film quality. Here, we demonstrate a rapid and reliable transfer process using BaO, which is an easy-to-grow binary compound, as a sacrificial layer. It readily dissolves in water only within ~1 hour. We grew a heterostructure composed of Fe_3O_4 (50 nm) /BaO (4 nm) on a SrTiO₃ (STO) (001) substrate by molecular beam epitaxy and successfully transferred the Fe_3O_4 film onto a SiO_2/Si substrate [Fig. 1(b)-(d)]. The temperature dependence of the magnetization exhibited a peak at the VT temperature (118 K) (Fig. 2), 2 K lower than that reported for Fe₃O₄ thin films on STO substrates [5]. This decrease can be attributed to enhanced superexchange interactions along the direction perpendicular to the substrate due to strain release. This facilitates the suppression of three-Fe-site quasiparticles called trimerons [6] - regarded as the origin of the VT - at lower temperatures. Our results highlight the effectiveness of BaO for high-quality film transfer of Fe₃O₄, enabling the investigation of intrinsic physical properties of thin films free from epitaxial strain.

- [1] D. Du, J. Hu and J. K. Kawasaki, Appl. Phys. Lett. Vol. 122, p.170501 (2023)
- [2] L. Néel, Annales De Physique, Vol. 12, p.137(1948)
- [3] E. J. W. Verwey, Nature, Vol. 114, p.327 (1939)
- [4] F. An, K. QU, G. Zhong *et al.*, Adv. Funct. Mater. Vol. 30, p.2003495 (2020)
- [5] J. A. Moyer, R. Gao, P. Schiffer *et al.*, Sci. Rep. Vol. 5, p.1 (2015)
- [6] J. P. Attfield, Chem. Mater. Vol. 34, p.2877 (2022) This work was supported by JSPS KAKENHI, JST ERATO, and the Spintronics Research Network of Japan (Spin-RNJ).

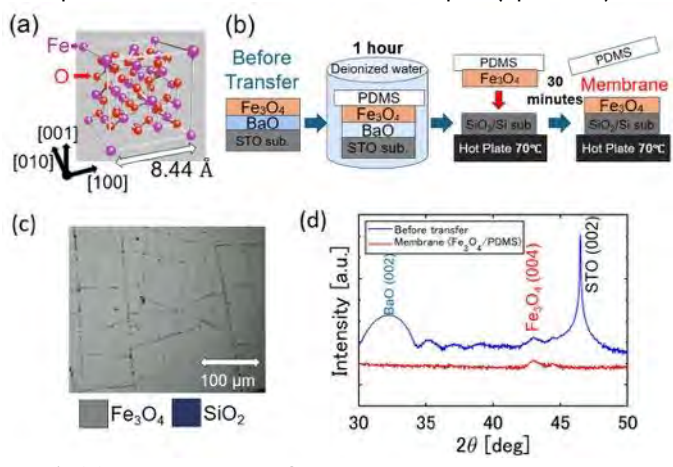


Fig. 1. (a) Unit cell of Fe_3O_4 , which has an inverted cubic spinel structure. (b) Schematic illustrations of the film transferring method. (c) Optical microscope image of the Fe_3O_4 membranes transferred onto a SiO_2/Si substrate. (d)

Out-of-plane x-ray diffraction patterns before (blue) and after (red) transfer.

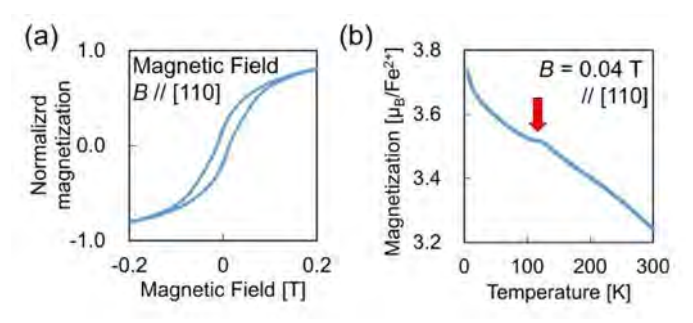


Fig. 2. (a) Normalized magnetization curve at 300 K and (b) temperature dependence of the magnetization measured for the transferred Fe_3O_4 membranes.

SESSION CG: MAGNETIC MICROSCOPY AND IMAGING

Chair(s): J. Fullerton, Argonne National Laboratory, Lemont,
Illinois, United States
Wednesday, October 29, 2025
08:30 AM-12:00 PM
Room 2A

CG-01. Scanning NV magnetometry in a closed-cycle cryostat

<u>M. Bacani</u>¹, C. Schäfermeier¹, G. Puebla-Hellmann², J. Rhensius², K. Karrai¹, A. Morales²
¹attocube systems GmbH, Haar by Munich, Germany, ²QZabre AG, Zurich, Switzerland

The ability to measure magnetic fields on the nanometre scale at cryogenic temperatures is crucial for understanding magnetism on the quantum level, as well as for designing materials for novel data storage devices or quantum computers. Nitrogen vacancy (NV) centres in diamond have proven to be a robust means of harnessing quantum sensing for such applications. We have developed an instrument to measure the magnetic stray field of a sample with nanometre resolution from 2 K - 300 K and that accepts samples without additional preparation, especially without the need to prepare a microwave line on the sample. The instrument features a software interface for controlling and synchronising all included optical, mechanical and electronic devices, which analyses the acquired information in real time. We present the key features and measurement results achieved with atomic force microscopy (AFM) tips

hosting an NV centre and a fully remote controllable microscope platform. We show sensitivity of 3 μ T/ sqrt(Hz), low noise AFM tip control and optically detected resonance scans in a closed-cycle cryostat [1].

[1] C. Schäfermeier et al., arXiv:2502.16599 (2025)

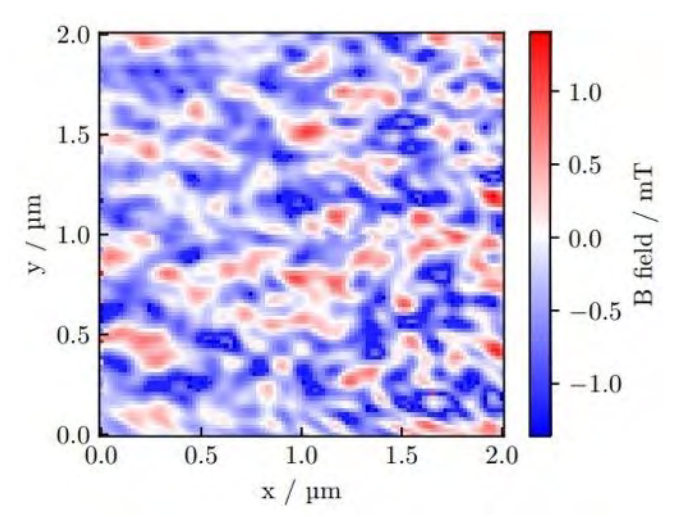


Fig. 1: Stray magnetic field of a Ir/Fe/Co/Pt multilayer sample measured by means of CW-ODMR at 2.9 K. The NV tip was set to a constant offset of 50 nm above the sample. The pixel-pixel distance is 20 nm. No post-processing was performed.

CG-02. Spin structure imaging with ptychography in antiferromagnetic CuMnAs

<u>D. M. Burn</u>¹, K. Edmonds², P. Wadley², C. Parmenter³, R. Campion², B. Daurer¹, S. S. Dhesi¹

¹Diamond Light Source, Didcot, Oxfordshire, United Kingdom, ²School of Physics and Astronomy, University of Nottingham, Nottingham, United Kingdom, ³Nanoscale and Microscale Research Centre, University of Nottingham, Nottingham, United Kingdom

The anti-parallel alignment of magnetic moments in antiferromagnetic (AFM) materials results in zero net magnetization and hence leads to insensitivity to external magnetic fields. Combined with properties including high dynamic precessional frequencies, this makes AFM materials a key area of research at the forefront of innovation for future technological devices [1]. CuMnAs is a particularly interesting example of an AFM material where the antiparallel magnetic moments form inversion partners, enabling current-induced magnetic switching and potential ultrafast memory applications [2].

X-ray based imaging techniques have been used to explore domain and domain wall structures in AFM materials where spin structure can be resolved due to X-ray Magnetic Linear Dichroism (XMLD). Most work to date has used Photo-Emission Electron Microscopy (PEEM) as the imaging technique, comparing horizontal and vertically polarised x-rays to give spin structural contrast imaging with strong surface sensitivity [2,3,4].

Here we demonstrate imaging of CuMnAs lamellae using ptychography, an emerging soft x-ray imaging technique based on the high coherent flux available from next generation synchrotron sources. In combination with XMLD, we show high resolution imaging of the AFM spin structure which extends throughout the entire sample thickness. Analysis of the XMLD as a function of linear polarisation angle reveals the orientation of the spin structure within the domains along with the chirality of the rotation of the spin structure within the domain walls. Furthermore, the results highlight the presence of topological defect features, which correlate with other features of the AFM spin structure such as changes in the chirality along the length of domain walls. We will discuss their origins of these features and the interplay with other properties in the material such as crystalline defects and strain.

- [1] T. Jungwirth et al. Nature Nanotechnol. 11, 231 (2016).
- [2] P. Wadley et al., Science 351, 587 (2016).
- [3] P. Wadley, et al. Nature Nanotechnol. 13, 362 (2018).
- [4] S. Reimers et al., Nat Commun. 13, 724 (2022)

CG-03. Magnetic Patterning By Light He⁺ Ion Irradiation For New Generation Reference Samples

Y. Sassi¹, K. Bouzehouane², A. Finco³, S. Collin², F. Godel², N. Reyren², V. Cros², E. Monteblanco¹, D. Ravelosona¹

¹Spin-Ion Technologies, Centre de Nanosciences et Nanotechnologies (C2N), Palaiseau, France, ²Laboratoire Albert Fert, CNRS, Thales, Université Paris-Saclay, 1 avenue Augustin-Fresnel, Palaiseau, France, ³Laboratoire Charles Coulomb, Université de Montpellier, CNRS, Montpellier, France

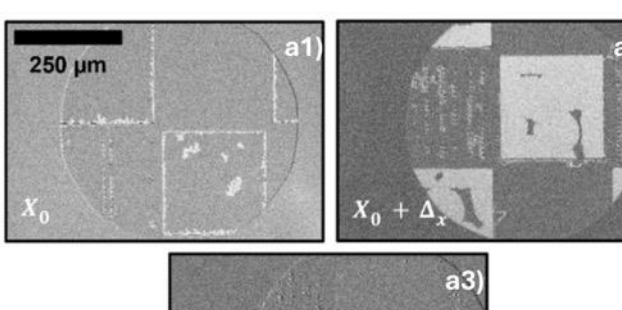
With the latest improvement in magnetic sensitive local measurement techniques, there is a crucial demand for cutting-edge reference samples. Such samples are mandatory for accurate quantitative measurements for near-field or optical imaging. The ideal reference sample should validate a flat surface, and a locally controlled magnetic state, while ensuring high reproducibility above all.

In this study, we rely on magnetic patterning by light He⁺ ion irradiation through a mask to develop such samples. Magnetic patterning by irradiation has already been widely used, for example for reducing pinning effects for DW motion [1], for precisely measuring magnetic moments of ultra-thin films [2] or for skyrmion nucleation and motion [3].

By combining the advantages of light He⁺ ion irradiation (no structural damage, fine tuning of magnetic properties, etc.), together with a fine-tuned lithography process, we demonstrate the capability to precisely and locally control the magnetic anisotropy. It enables us to observe a continuous change from high PMA to an IP state, with a unique large-scale irradiation (Fig. 1). Surface sensitive techniques, such as scanning NV-center magnetometer, have confirmed that the roughness is maintained below 1 nm. A distinct boundary between the irradiated and non-irradiated area is found (Fig. 2). Such an achievement allows for an accurate calibration of any NV probe.

Financial support from a government grant managed by the ANR Equipex+ E-Diamant "21-ESRE-0031" and as part of the France 2030 investment plan from PEPR SPIN ANR-22-EXSP 0008 (SPINCHARAC) are acknowledged.

- [1] C. Balan, et al., Small, 2023, 19, 2302039
- [2] T. Hingant, et al., *Physical Review Applied*, 2015, 4, 014033
- [3] L.M. Kern, et al., Nano Letters, 2022, 22, 4028-4035



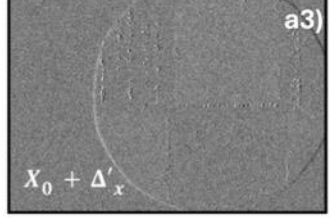


Figure 1: Polar-MOKE images acquired on a sample, after a unique He+ irradiation exposure through a specific patterning. The images are taken at different positions corresponding to different anisotropy strength, due to the

patterning, with respectively: a1) high-PMA, a2) low-PMA and a3) IP oriented. The images are obtained after a 5mT pulse field of 1 μ s along the z-axis.

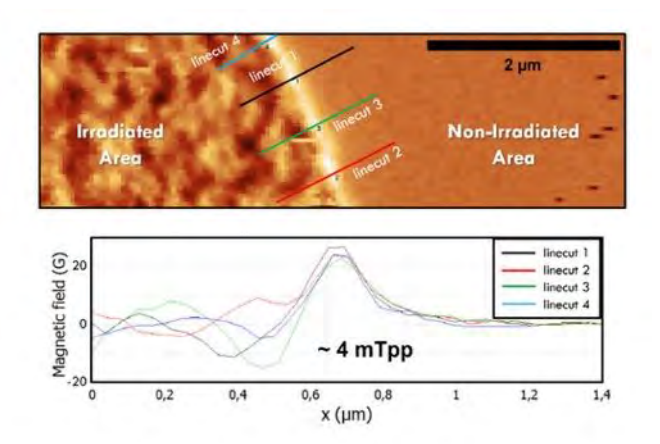


Figure 2: NV-center magnetometer image of the frontier between an irradiated and a non-irradiated area, with its corresponding line cuts. The amplitude of the signal is in agreement with the micromagnetic simulation.

CG-04. A Sensitive MOKE and Optical Hall Effect Technique at Visible Wavelengths: Insights Into The Gilbert Damping N. Am-Shalom, N. Bernstein, B. J. Assouline, A. Capua

Institution of Electrical Engineering and Applied Physics, The Hebrew University of Jerusalem, Jerusalem, Israel

It is well known that the anomalous Hall effect displayed in ferromagnets is much stronger than the ordinary Hall effect measured on non-magnetic metals. Similarly, the magneto optical Kerr effect (MOKE) is orders of magnitude stronger than the optical Hall effect (OHE) which is vanishingly small [1].

We present an ultrasensitive MOKE technique that is based on a large-amplitude modulation of the externally applied magnetic field (Fig.1). When combined with a crosspolarized optical geometry optimized for maximal extinction, the result is a substantial improvement in signal-to-noise ratio even for materials with vanishingly small optical Hall responses such that the OHE becomes measurable for non-magnetic metals at optical wavelengths. We demonstrated the technique on thin films of Pt, Ta, Cu, Al and Au, where we find partial agreement with the Lorentz-Drude model suggesting that a more detailed model of the plasma dynamics is required. [2] The improved sensitivity revealed an intriguing trend: the amplitude of the measurement noise scales with the spin-

orbit coupling (SOC) strength of the tested metal. Heavier metals like Pt and Ta exhibited higher noise levels, whereas lighter ones like Al and Cu remained quieter. This is manifested by a remarkable correlation between the noise amplitude and the Gilbert damping enhancement associated with these metals [3] (Fig. 2). This correlation might enable rapid characterization of the Gilbert damping in normal and magnetic materials and can lead to a deeper understanding of the connection between spin-orbit interaction and optical radiation. The short optical cycle of the technique which mitigates the influence of carrier scattering, is expected to facilitate the research of band structure physics.

[1] S. E. Schnatterly, "Magnetoreflection Measurements on the Noble Metals", Physical Review 183, 664 (1969).
[2] L. Uba, S. Uba, and V. N. Antonov, "Magneto-optical Kerr

spectroscopy of noble metals", Physical Review B 96, 235132 (2017).

[3] H. L. Wang, C. H. Du, Y. Pu, R. Adur, P. C. Hammel, and F. Y. Yang, "Scaling of Spin Hall Angle in 3d, 4d, and 5d Metals from Y3Fe5O12/Metal Spin Pumping", Physical Review Letters 112, 197201 (2014).

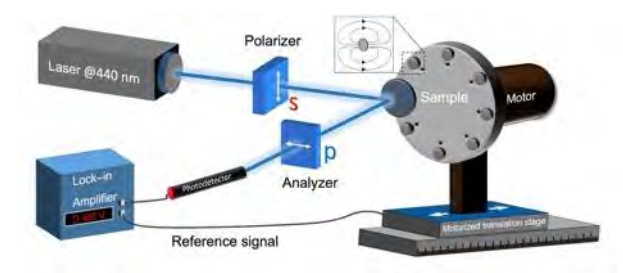


Fig. 1 The experimental setup. Inset: illustration of the magnetic field lines of a single magnet.

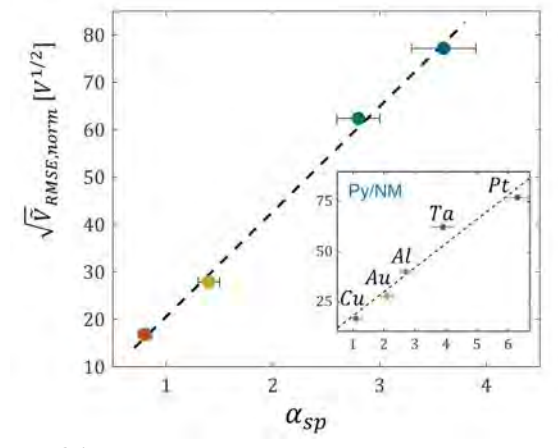


Fig. 2 Noise amplitude and spin pumping enchancment correlation. The heavier metals shows significantly stronger noise signals.

CG-05. 3D Vector Ptycho-Tomographic Imaging of Topological Structures in FeGd Multilayer

<u>I. Binnie</u>¹, H. Fang¹, B. Shearer¹, T. Feggeler^{5,4}, A. Oh^{6,7}, S. Yazdi¹, E. Cating-Subramanian¹, S. Montoya², E. Fullerton², D. Shapiro⁴, J. Miao³, H. C. Kapteyn¹, M. M. Murnane¹

¹University of Colorado Boulder, Boulder, Colorado, United States, ²University of California San Diego, San Diego, California, United States, ³University of California, Los Angeles, Los Angeles, California, United States, ⁴Lawrence Berkeley National Lab, Berkeley, California, United States, ⁵Brookhaven National Lab, Upton, New York, United States, ⁶Vanderbilt University, Nashville, Tennessee, United States, ⁷Columbia University, New York, New York, United States

The ability to directly image three-dimensional topological spin structures such as skyrmions has important implications for both spintronic-based innovation and fundamental physics of magnetism. Such structures often exist in thin films, which present a significant imaging challenge. Here, we describe a computational imaging method for mapping a 3D vector magnetic field with fewnm resolution using coherent soft x-rays, and present the resulting reconstruction of dipole-stabilized topological features in an FeGd multilayer thin film.

The experiment is based on soft x-ray vector ptychotomography and is performed at the COSMIC beamline at the Advanced Light Source synchrotron. Vector ptychotomography uses the coherent diffraction based iterative phase retrieval technique known as ptychography to generate 2D projections in a complete tomographic tilt series with broad solid angle sampling. Each projection is collected with both left and right circularly polarized light, then the difference image is taken to display magnetic contrast through X-ray magnetic circular dichroism (XMCD). The projections are then used as inputs to an iterative tomography algorithm to reconstruct the scalar and vector sample signals. We have adapted this technique to the case of a thin film with topological spin structure. We developed a system of milled fiducial marks that allow for projection registration in the tomography algorithm that is otherwise challenging to execute with a thin film sample.

The resulting 3D reconstruction of the FeGd multilayer (figure 1, 2) reveals with few-nm resolution the magnetic structure of a dipole-stabilized lattice with skyrmions, antiskyrmions, and other topological features, providing a direct experimental verification of simulated topologies.

^{*} Best Student Presentation Finalist / LB – Late-breaking Poster

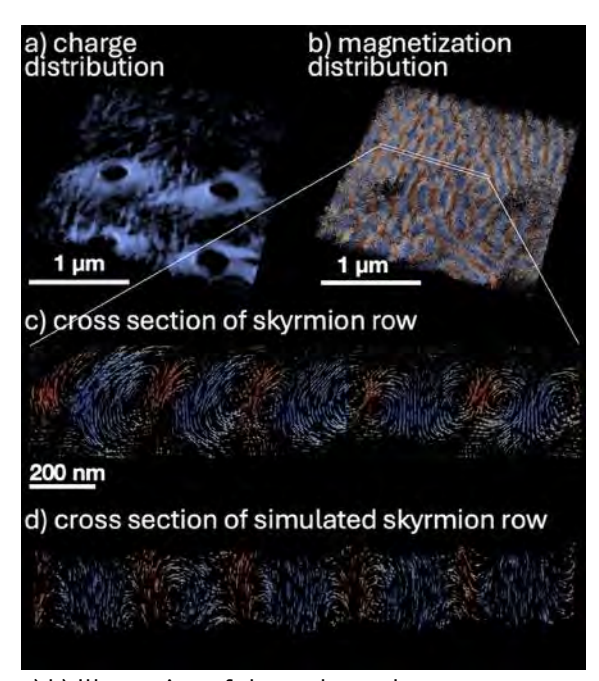
[1] A. Rana, J. Miao, M. Murnane et al., Nature Nanotechnology, Vol. 18, p.227-232 (2022)

[2] M. Pham, Y. Yuan, J. Miao et al., arXiv:2004.10445 (2020).

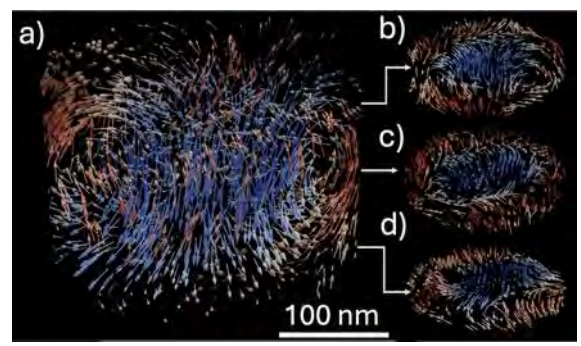
[3] B. Shearer, H. Kapteyn, M. Murnane et al., Optics Express, Vol. 33, p.717-735 (2025)

[4] R. Desautels, L. DeBeer-Schmitt, D. Gilbert et al., Physical Review Materials, Vol. 3, 104406 (2019)

[5] S. Montoya, P. Fischer, B. McMorran et al., Physical Review B, Vol. 95, 224405 (2017)



- a),b) Illustration of the scalar and vector reconstructions, respectively. The scalar image shows milled fiducial holes with clear edges. Red-blue arrows in the vector image indicate z-component of the field.
- c) Cross section of a row of skyrmion tubes, which compares with d), the simulated cross section, showing consistent vortex structures.



a) A single reconstructed antiskyrmion column. Red-blue indicates field z-component.

b-d) Layers of the antiskyrmion column

CG-06. Unveiling Hidden Spatio-Magnetic Phases in Quantum Materials through Quantitative Magnetic Imaging and Transport*

M. Sim^{1*}, G. Krishnaswamy¹, G. Ji Omar¹, M. Pardo-Almanza², Y. Fujisawa², X. Chen³, H. Tan³, Y. Okada², A. Ariando¹, A. Soumyanarayanan^{1, 3}

¹Department of Physics, National University of Singapore (NUS), Singapore, Singapore, ²Quantum Materials Science Unit, Okinawa Institute of Science and Technology (OIST), Okinawa, Japan, ³Institute of Materials Research and Engineering (IMRE), A*STAR, Singapore, Singapore

Magnetic quantum materials, such as ultrathin transition metal chalcogenides and oxides, have emerged as fascinating platforms to explore magnetism, chirality, topology, and their interplay with spin-charge interconversion. Interfacial chiral interactions in such systems may stabilize topological spin textures such as magnetic skyrmions[1-3], which are expected to contribute an additional component to Hall transport signals—known as topological Hall effect (THE)[4].

While large unconventional Hall "bumps" (beyond conventional and anomalous Hall components) have been reported across such materials, their origin is hugely debated. In particular, imaged spin texture densities are several orders of magnitude lower than that required to produce such THEs. Conversely, a compelling alternative mechanism describing these humps across materials remains to be established.

In this work, we employ variable-temperature magnetic force microscopy (MFM) to investigate nanoscale magnetism in epitaxially grown magnetic thin films—chalcogenide $Cr_{1+\delta}Te_2$ and oxide heterostructure $SrRuO_3/SrIrO_3$. We develop and implement a robust, quantitative MFM analysis framework to identify and track field- and temperature-dependent evolution of local magnetic order, and independently, spin textures. These methods transcend conventional image interpretation protocols and uniquely enable spatially resolved insights on the subtle evolution of coexisting magnetic phases.

Notably, in both cases, our investigations reveal strong correlations between the spatially varying magnetic phases unmasked by our technique, and the measured Hall transport—under varying magnetic fields and temperature conditions. These findings deepen our understanding of the complex magnetic landscape in quantum materials and

^{*} Best Student Presentation Finalist / LB - Late-breaking Poster

provide a path towards disentangling anomalous and topological contributions in Hall transport. This nanoscale perspective also offers a new route to unravel subtle emergent magnetic phenomena in low-dimensional systems, which can host a zoo of unconventional phases.

- [1] M. Gibertini et al., *Nature Nanotechnology*, 14, 408-419 (2019)
- [2] J. Matsuno et al., Science Advances, 2, e1600304 (2016)
- [3] K. Yasuda et al., *Nature Physics*, 12, 555-559 (2016)
- [4] P. Bruno et al., Physical Review Letters, 93, 096806 (2004)

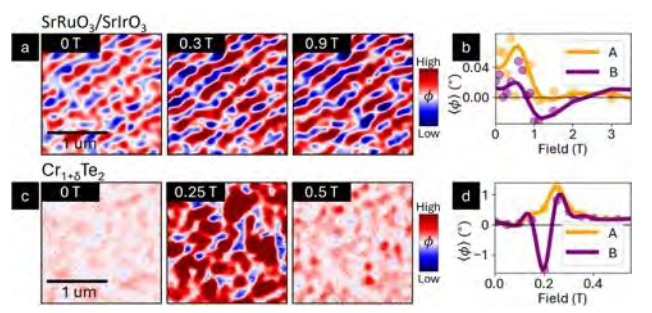


Fig. 1 MFM images and corresponding spatially averaged MFM phases for distinct regions A and B with varying field for (a-b) $SrRuO_3(5 UC)/SrIrO_3(10 UC)$ at 20 K and (c-d) $Cr_{1+\delta}Te_2$ (40 nm) at 100 K.

CG-07. Probing Magnon Dynamics with Microwave-Based Ultrafast Electron Microscopy

C. Liu, S. Reisbick, Y. Zhu

Condensed Matter Physics, Brookhaven National Lab, Upton, New York, United States

Magnons, collective excitations of spin order, are central to advancing energy-efficient spintronic and magnonic technologies. In this presentation, we report a breakthrough in visualizing dipole-exchange spin waves in a ferromagnetic film, enabled by a novel laser-free ultrafast Lorentz electron microscope we developed. This system incorporates a microwave-driven ultrafast electron pulser, providing high spatiotemporal resolution without the complexity of laser synchronization.

Using a topological spin texture in permalloy, involving vortex-antivortex pairs and various intricate domain walls generated by GHz electromagnetic fields, we directly image the generation, propagation, reflection, and interference of spin waves. Notably, we observe that antivortex cores act as preferential sources of spin-wave emission, which strongly correlates with oscillatory motion of adjacent domain walls

[1]. These findings provide new insights into magnon dynamics in complex spin textures and establish a platform for exploring reconfigurable spin-wave interactions via spin-transfer torque, with broad implications for next-generation spintronic devices.

[1] Liu, C., Ai, F., Reisbick, S., Zong, A., Pofelski, A., Han, M.-G., Camino, F., Jing, C., Lomakin, V., Zhu, Y., "Correlated spinwave generation and domain-wall oscillation in a topologically textured magnetic film", Nature Materials, 24, 406–413 (2025).

CG-09. 3D spin wave microscopy

K. Rivkin

RKMAG Corporation, Pacific Grove, California, United States

We propose a method of monitoring internal properties of a magnetic sample by means of focusing or beaming volume spin waves with the consequent analysis of their scattering on internal inhomogenuities. It is accomplished by subjecting the sample's surface to a magnetic field with a specific spatial profile which can be created by a neighboring ferromagnet, which establishes a network of surface spin wave sources with a functionality similar to a phase array lens whose properties can be adjusted to focus on an arbitrary location inside the sample or to produce a Gaussian beam which maintains its shape over long distances. Modeling demonstrates that such methods allow for 3D visualization of material inhomogenuities, domain walls and other related phenomena with up to 100-200nm resolution.

CG-10. Mechanochemical Synthesis of Strontium Hexaferrite Magnets from Mill Scale Waste

<u>N. Gunduz Akdogan^{1, 3}, D. Kalkavan¹, D. Celebi^{1, 2}, O. Akdogan^{1, 2}</u>

¹NANOTerial Technology Co., Istanbul, Turkey, ²Bahcesehir University, Istanbul, Turkey, ³Piri Reis University, Istanbul, Turkey

Strontium is widely used in the permanent magnet industry and is considered a critical raw material due to the heavy reliance on its supply. In this study, mill scale, an iron-rich industrial waste, was used as an alternative iron source to synthesize $SrFe_{12}O_{19}$ with a mechanochemical approach. To improve its magnetic performance, various oxides (Al_2O_3 , Cr_2O_3 , Co_3O_4 , and La_2O_3) were introduced as dopants. These

oxides are known to affect particle morphology and magnetic anisotropy. X-ray diffraction (XRD) analysis confirmed that the $SrFe_{12}O_{19}$ phase was successfully formed using precursors obtained from the mill scale. Scanning electron microscopy (SEM) showed that the synthesized powders were homogeneous and had particle sizes below 10 microns. Thermogravimetric analysis (TGA) revealed an increase in the Curie temperature in doped samples. Vibrating sample magnetometry (VSM) analysis demonstrated significant improvements in remanent magnetization, coercivity, and magnetic anisotropy, particularly in the Co_3O_4 -doped sample, as illustrated in Fig. 1. These results highlight the effectiveness of oxide doping in enhancing the magnetic performance of recycled strontium hexaferrite.

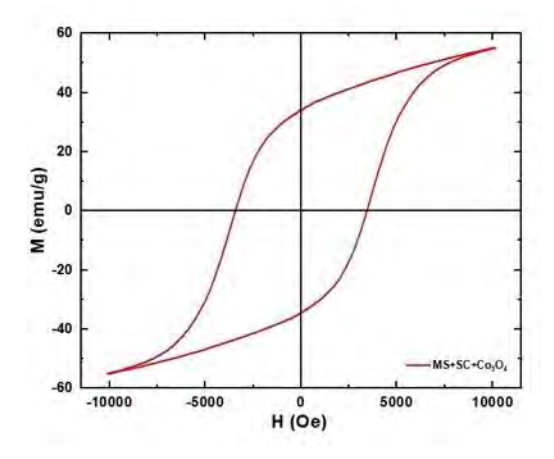


Fig.1 Hysteresis loop of Co₃O₄ doped SrFe₁₂O₁₉ sample.

CG-11. Nanoscale imaging and control of altermagnetism in MnTe

O. Amin¹, A. Dal Din¹, E. Golias², Y. Niu², A. Zakharov², S. Fromage¹, C. Fields^{1, 3}, S. Heywood¹, R. Cousins⁴, F. Maccherozzi³, J. Krempaský⁵, H. Dil^{6, 5}, D. Kriegner⁷, B. Kiraly¹, R. Campion¹, A. Rushforth¹, K. Edmonds¹, S. S. Dhesi³, L. Šmejkal^{8, 9, 10}, T. Jungwirth^{7, 1}, P. Wadley¹ ¹University of Nottingham, Nottingham, United Kingdom, ²MAX IV Laboratory, Lund, Sweden, ³Diamond Light Source, Didcot, United Kingdom, ⁴Nanoscale and Microscale Research Centre, Nottingham, United Kingdom, 5Photon Science Division, Paul Scherrer Institut, Villigen, Switzerland, ⁶Institut de Physique, École Polytechnique Fédérale de Lausanne, Lausanne, Switzerland, ⁷Institute of Physics, Czech Academy of Sciences, Prague, Czechia, 8 Max Planck Institute for the Physics of Complex Systems, Dresden, Germany, 9Max Planck Institute for Chemical Physics of Solids, Dresden, Germany, 10 Institute of Physics, Johannes Gutenberg University, Mainz, Germany

The α -phase of MnTe is a g-wave altermagnet exhibiting a spontaneous anomalous Hall effect (AHE) [1], sizable anisotropic spin-splitting of the electronic bands [2], and an x-ray magnetic circular dichroism (XMCD) response [3]. While the spin-polarisation is inherently of nonrelativistic origin, the associated measurable effects depend on the orientation of the compensated magnetic order (Néel vector) relative to the crystal axes. Thus, tailoring the magnetic domain state is pertinent to controlling the altermagnetic output. Here, I present our recent work [4], using x-ray photoemission electron microscopy to produce real-space maps of the altermagnetic domain structure in MnTe films with nanoscale resolution. We highlight, in fabricated microstructures, the formation of single domains, pinned domain walls, and exotic vortex textures, dictated by field-cooling. This provides a convenient way to control the altermagnetic state and paves the way to designing nextgeneration spintronic devices based on these materials.

- [1] Gonzalez Betancourt, R. D., et al. "Spontaneous anomalous Hall effect arising from an unconventional compensated magnetic phase in a semiconductor." *Physical Review Letters* 130.3 (2023): 036702.
- [2] Krempaský, Juraj, et al. "Altermagnetic lifting of Kramers spin degeneracy." *Nature* 626.7999 (2024): 517-522.
- [3] Hariki, A., et al. "X-ray magnetic circular dichroism in altermagnetic α -MnTe." *Physical Review Letters* 132.17 (2024): 176701.
- [4] Amin, O. J., et al. "Nanoscale imaging and control of altermagnetism in MnTe." *Nature* 636.8042 (2024): 348-353.

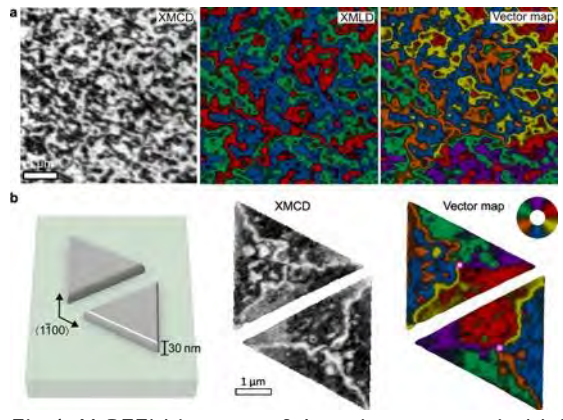


Fig.1: X-PEEM images of domain structure in MnTe. a) Unpatterned film imaged using XMCD (left), XMLD axis map (middle), combined XMCD-XMLD vector map (right). b) In patterned triangle microstructures, the edge-induced anisotropy stabilises the formation of an isolated vortex. The vortex chirality is determined by the triangle orientation.

SESSION CH: FAST AND EFFICIENT SWITCHING

Co-Chair(s): X. Fan, *Division of Natural Sciences and*Mathematics, University of Denver, Denver, Colorado, United
States and Satoshi Sugimoto, NIMS, Tsukuba, Japan
Wednesday, October 29, 2025
08:30 AM-12:00 PM
Room 1BC

CH-01. Ultrafast Creation of Magnetization Through the Targeted Excitation of Circularly-polarized Phonons

T. Zalewski^{1, 2}, A. V. Boris³, A. Kirilyuk^{1, 2}, C. S. Davies^{1, 2}

¹HFML-FELIX, Radboud University, Nijmegen,
Netherlands, ²Institute for Molecules and Materials, Radboud
University, Nijmegen, Netherlands, ³Max Planck Institute for
Solid State Research, Stuttgart, Germany

The interaction between ultrashort light pulses and the crystal lattice has recently emerged as a powerful approach for controlling magnetic order in materials. While optical phonons are typically viewed as linearly polarized, recent studies have revealed that circular ionic motions - circularly-polarized phonons - can carry angular momentum [1]. These phonons serve as channels for angular momentum transfer, enabling the generation of large effective magnetic fields when driven at resonance by farinfrared pulses. Such fields have been theoretically predicted to reach tens of tesla [2], and experimental detection of around 1 T has been demonstrated in paramagnetic CeF₃ [3].

In this work, we leverage the wavelength tunability of the free-electron lasers at the FELIX facility to selectively drive optical phonon modes in CeF $_3$ at resonance across the broad spectral range of 21-42 μ m. It allows for selective excitation of polarized phonon modes with highly narrowband pump pulses, while the emergent transient magnetization is probed using synchronized 150-fs-long pulses of wavelength 520 nm. As shown in Fig. 1, excitation at a pump wavelength of 31 μ m induces a measurable ultrafast rotation of polarization, providing clear evidence of an emergent magnetization, consistent with the results presented in Ref. [3].

By comparing the spectral response of the magneto-optical signals with the frequency-dependent permittivity obtained through infrared ellipsometry, we gain insights into phonon coupling mechanisms and selection rules.

The ability to tune the excitation wavelength is crucial for mapping out the spectral response of chiral phonons, deepening our understanding of their coupling mechanisms, and paving the way toward exploring similar effects in other 4f rare-earth trihalides or 3d transition-metal oxide magnets [4].

T.Z. and C.S.D. acknowledge support from the European Research Council ERC Grant Agreement No. 101115234 (HandShake), and A.K. acknowledges support from the European Research Council ERC Grant Agreement No. 101141740 (INTERPHON).

- [1] C. Dornes, et al., Nature 565, 209 (2019).
- [2] D. M. Juraschek, T. Neuman, and P. Narang, Phys. Rev. Res. 4, 013129 (2022).
- [3] J. Luo, et al, Science (80). 382, 698 (2023).
- [4] S. Chaudhary, D. M. Juraschek, M. Rodriguez-Vega, and G. A. Fiete, Phys. Rev. B 110, 094401 (2024).

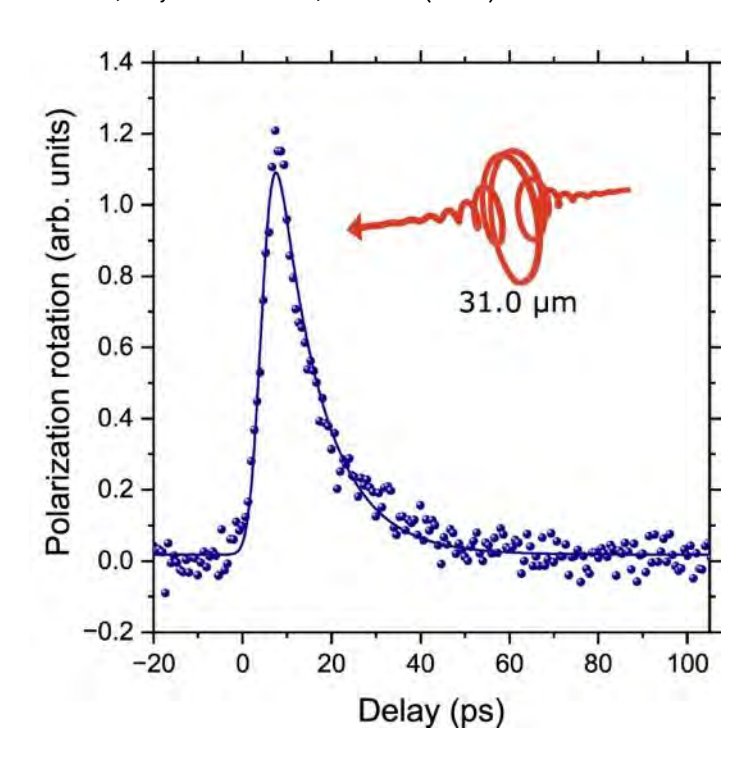


Fig. 1 Polarization rotation in CeF $_3$ induced by a circularly-polarized far-infrared pulse of wavelength 31 μ m, measured at a base temperature of about 5 K.

CH-03. Strain-Assisted Magnetization Reversal in Nanomagnets

S. Sarker¹, M. F. Chowdhury¹, M. J. Gross⁵, M. Rajib¹, P. S. Keatley⁶, R. Hicken³, C. A. Ross⁴, J. Atulasimha¹,²¹ ¹Mechanical & Nuclear Engineering Department, Virginia Commonwealth University, Richmond, Virginia, United States, ²Electrical & Computer Engineering Department, Virginia Commonwealth University, Richmond, Virginia, United States, ³Department of Physics and Astronomy, University of Exeter, Exeter, United Kingdom, ⁴Department of Materials Science and Engineering, Massachusetts Institute of Technology, Boston, Massachusetts, United States, ⁵Electrical Engineering and Computer Science Department, Massachusetts Institute of Technology, Boston, Massachusetts, United States, ⁶Electromagnetic and Acoustic Materials Department, University of Exeter, Exeter, United Kingdom

Strain-mediated manipulation of magnetization orientation—whether static [1, 2] or dynamic [3], such as through surface acoustic waves (SAWs)—has been shown to be energy-efficient. Here, we demonstrate through simulation that applying SAWs to an elliptical nanomagnet (110 nm × 100 nm × 5 nm) enables magnetization reversal in a Co-based nanomagnet with a magnetostriction constant of λ_s = 30 ppm. Starting from a relaxed magnetization orientation along the easy axis (+X direction) of an elliptical nanomagnet, the application of 1 GHz SAW pulse train for 6 ns (i.e., 6 repetition cycles) causes the magnetization to switch to the opposite easy axis direction (-X direction) as shown in Fig. 1. The SAWs trigger magnetization dynamics via inverse magnetostriction or the Villari effect, that over multiple cycles help the magnetization overcome the energy barrier between the two easy axis directions of the elliptical nanomagnet. Such reversal for a different strain configuration has also been shown by other simulations [4]. To study the magnetization dynamics experimentally, we have fabricated interdigitated transducers (IDTs) on a lithium niobate (LiNbO₃) piezoelectric substrate to apply surface acoustic waves (SAWs) to elliptical magnets of Co and BiYIG films. We have previously shown static strain control of magnetic anisotropy in BiYIG [5] which offers moderate magnetostriction but potentially lower damping. Fig. 2(a) shows the fabricated IDTs on the LiNbO₃ substrate, and Fig. 2(b) displays the presence of distinct magnetic domains in the BiYIG sample, as observed using single Nitrogen Vacancy (NV) scanning microscopy. We plan to directly probe both the SAW and the magnetization dynamics in birefringence and Kerr measurements

respectively on the substrate and in the magnetic materials to validate our numerical predictions.

Acknowledgement: We acknowledge NSF ECCS 2152601 (NSF-UKRI grant) for funding this study

- [1] N. Lei, T. Devolder and G. Agnus, Nat. Commun., 4, 1378 (2013)
- [2] N. D'Souza, M.S. Fashami and S. Bandyopadhyay, Nano Lett., 16, 2, 1069-1075, 2016
- [3] V. Sampath, N. D'Souza and D. Bhattacharya, Nano Lett., 16,9, 5681-5687 (2016)
- [4] R. Peng, J. Hu and K. Momeni, Scientific Reports, 6, 27561 (2016)
- [5] W. Misba, M.J. Gross and D. Gopman, arXiv:2501.00980 (2025)

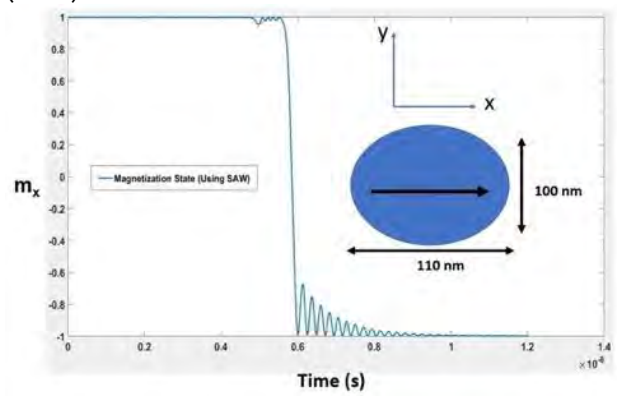


Fig. 1 Magnetization reversal in an elliptical nanomagnet with SAW-assisted strain of 1 GHz frequency

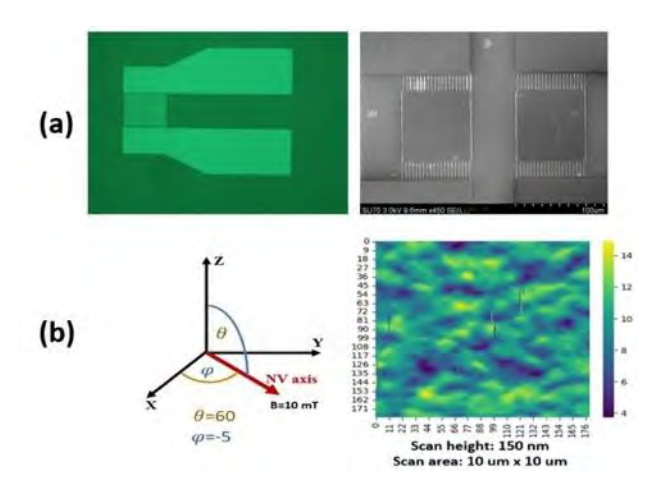


Fig.2 (a) Fabricated IDT on a lithium niobate (LiNbO₃) piezoelectric substrate for applying SAWs, (b) Magnetic domains observed in a BiYIG sample using NV microscopy

CH-04. Origin of Enhanced Switching Efficiency by Increasing Magnetic Anisotropy Field in Accelerated STT-Switching and High-Retention MTJ (AccelHR-MTJ)

<u>S. Itai</u>, K. Koi, H. Maekawa, R. Takashima, M. Toko, Y. Lee, M. Nakayama

Frontier Technology R&D Institute, KIOXIA Corporation, Yokohama, Japan

Latest cutting-edge technologies like AI increase demands for high-speed and high-density nonvolatile memory. STT-MRAM is one of the promising candidates. Recently, 64Gb cross-point STT-MRAM with 20nm MTJ was reported [1,2]. Moreover, we demonstrated the 14nm MTJ with highretention and high-speed switching called Accelerated STT-Switching and High-Retention MTJ (AccelHR-MTJ) [3]. AccelHR-MTJ has a stacked storage layer with a High-Retention Layer (HRL) and a Switching Accelerating Layer (SAL) (Fig. 1a). Switching current I_c of MTJ is generally proportional to thermal stability factor Δ . However, simulations show increasing effective magnetic anisotropy field of HRL ($H_k^{\text{eff}}_{HRL}$) leads to larger Δ while keeping I_c constant in AccelHR-MTJ [3]. But the mechanism of this behavior unique to AccelHR-MTJ is not clear. In this study, we clarify the origin of enhanced switching efficiency by increasing $H_k^{\text{eff}}_{HRL}$ in AccelHR-MTJ. We analyze the time evolution of magnetizations and dissipated energy (E_{dis}) [4,5] by micromagnetic simulations. This E_{dis} analysis is applied to the STT switching in MTJ for the first time. We propose a new model for enhanced switching efficiency that the increased $H_k^{\text{eff}}_{HRI}$ reduces the fluctuation of HRL at the 1st stage of switching and the disturbance to SAL via exchange coupling (Fig. 1b). The simulation confirms that increasing $H_k^{\text{eff}}_{HRL}$ suppresses the in-plane magnetizations of HRL $(m_{IP \text{ HRL}})$, which mean the fluctuation of HRL at the 1st stage of switching (Fig. 2a). We also revealed that E_{dis} in SAL over E_{dis} in HRL increases with increasing $H_k^{eff}_{HRL}$ (Fig. 2b). This result suggests that the energy from STT is utilized more efficiently for the SAL switching. In summary, the reduced fluctuation of HRL is the origin of enhanced switching efficiency by increasing $H_k^{eff}_{HRL}$ in AccelHR-MTJ, which is a key element in future nonvolatile memory.

[1] H. Aikawa, *et al.*, 2024 IEEE International Electron Devices Meeting (IEDM), 20-1.

[2] K. Hatsuda, *et al.*, 2025 IEEE International Solid-State Circuits Conference (ISSCC), 30-6.

[3] M. Nakayama, *et al.*, 2023 International Electron Devices Meeting (IEDM), 2023, 31-1.

[4] B. Behin-Aein, S. Salahuddin and S. Datta, IEEE Transactions on Nanotechnology, 8, 505 (2009). [5] G. Carlotti, *et al.*, Physica B, 435,4 (2014).

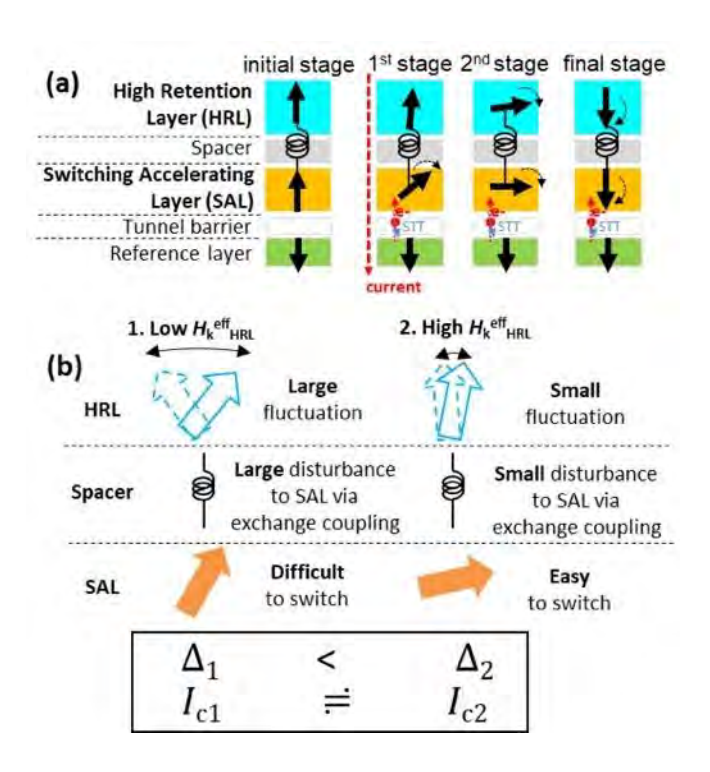


Fig.1 (a) Conceptual view of AccelHR-MTJ's reversal process. (b) Our new model of $H_{\rm k}^{\rm eff}_{\rm HRL}$ dependence of switching process.

185

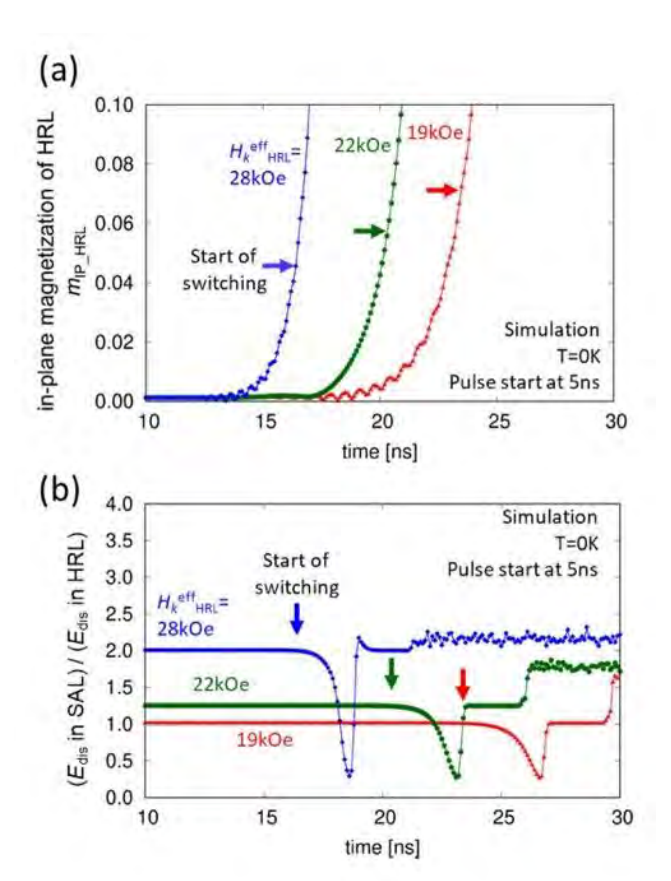


Fig.2 (a) $m_{\rm IP, HRL}$ vs time at the 1st stage of switching for various $H_k^{\rm eff}_{\rm HRL}$. (b) $H_k^{\rm eff}_{\rm HRL}$ dependence of $E_{\rm dis}$ in SAL over $E_{\rm dis}$ in HRL. In both of figures, arrows show the time when the perpendicular magnetizations of SAL have decreased by 2%.

CH-05. Magnetostrictive $Fe_{(100-x)}$ Al_x thin films on Flexible Substrates: correlation between microstructural and magneto-dynamic properties

P. Kumar^{1, 2}, P. Kumar¹, V. Sharma³, M. K. Khanna⁴, <u>B. K. Kuanr</u>¹

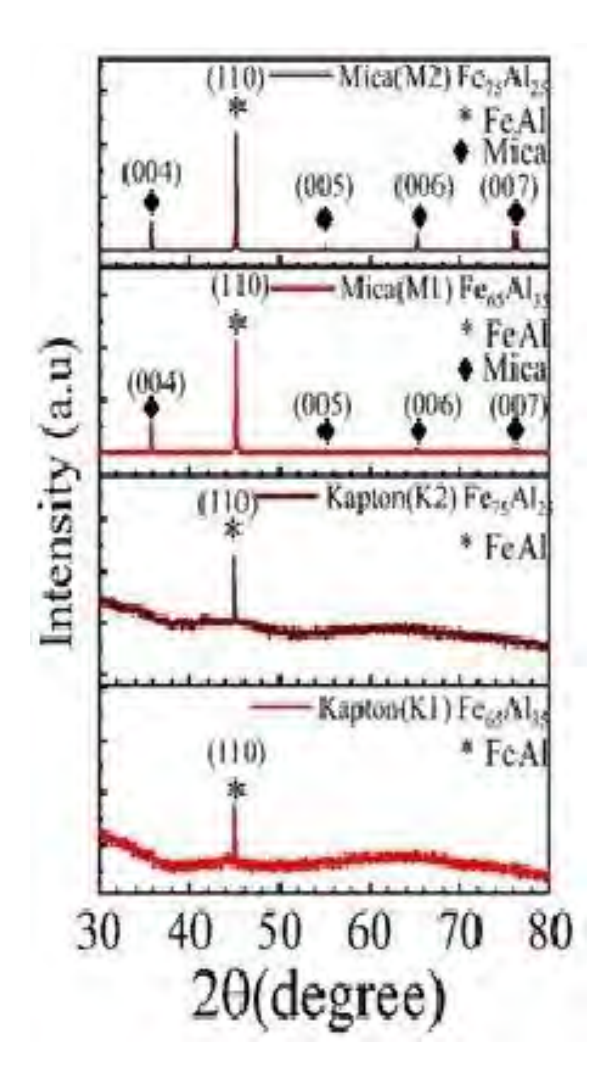
¹Special Centre for Nanoscience, Jawaharlal Nehru University, New Delhi, Delhi, India, ²Department of Physics, Motilal Nehru College, University of Delhi, South Campus, New Delhi, Delhi, India, ³Department of Physics, Northeastern University, Boston, Massachusetts, United States, ⁴Department of Electronic Science, University of Delhi, South Campus, New Delhi, Delhi, India

 $Fe_{(100-x)}Al_x$ thin films, composed of iron (Fe) and aluminum (Al), represent an intriguing class of materials with unique magnetic, electrical, and mechanical properties. These thin films are well studied for their potential applications in

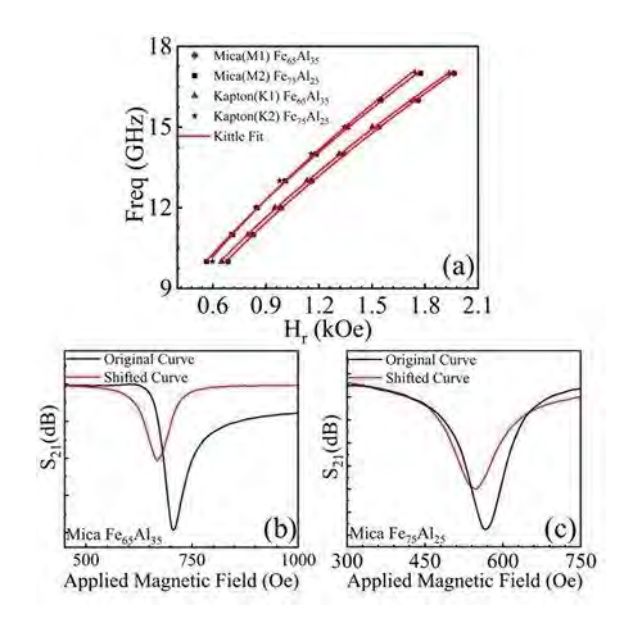
spintronics, magnetic sensors and storage, and protective coatings[1]. In this investigation, using co-sputtering FeAl thin films of two different compositions Fe₆₅Al₃₅ and Fe₇₅Al₂₅ were deposited on two different flexible substrates: Kapton (marked K1, K2) and mica (M1, M2). The XRD plots (Fig. 1) of all films confirms the formation of a disordered ferromagnetic A2 phase. From ferromagnetic resonance (FMR) experiments effective magnetization (M_{eff}) were determined from Hr vs frequency plot (Fig. 2(a)). Almost same values are obtained (14.60 kOe and 14.53 kOe) both for M1 and K1 films. As the Fe concentration increases M_{eff} increased to 16.09 kOe and 17.04 kOe for M2 and K2, respectively. The value of M_S increases as the Fe concentration increases obtained as obtained from the B-H loops. These are 1292 and 1355 emu/cc for M2 and K2 respectively.

To determine the magnetostrictive effect, bending strain was applied. This investigation has been performed using a flexible bended microstrip line-based FMR. Figure 2(b-c) displays FMR spectra obtained by applying stress. The value of the isotropic magnetostriction coefficient (λ) is related as $K_U \approx 1.5 \lambda \sigma_{xx}$ and $H_U = 2K_U/M_s$ (where each term has its usual meaning) [2]. The determined λ is observed to increase in Fe concentration for Kapton and decrease for mica. Their values are 27.57 PPM and 29.59 PPM for K1 and K2, respectively. For mica, the λ values are 29.90 PPM and 27.88 PPM for M1 and M2, respectively. Our research has demonstrated that the magnetization of FeAl deposited on flexible substrates can be controlled by magnetostriction. The observed left shift of FMR spectra is due to tensile stress. Similarly, with compressive stress, we have observed right shift of FMR spectra, which was possible only with flexible substrates.

1. M. Gueye, F. Zighem, M. Belmeguenai, M. S. Gabor, C. Tiusan, and D. Faurie, J Phys D; Appl Phys 49, (2016).
2. M. Gueye, B. M. Wague, F. Zighem, M. Belmeguenai, M. S. Gabor, T. Petrisor, C. Tiusan, S. Mercone, and D. Faurie, Appl Phys Lett 105, (2014).



XRD pattern of different compositions of FeAl on flexible Mica and Kypton Substrate



(a) Hr Vs Freq plot of FeAl films on Mica and Kapton (b-c) shift in Hr position of FMR on Mica for FeAl (75:25 and 65:35)

CH-06. Pt-Transition Metal Synthetic Ferrimagnets for All Optical Switching

<u>J. Scott</u>¹, M. Dabrowski², C. Sait², W. R. Hendren¹, N. Kuninski¹, T. E. McCormack¹, D. M. Burn³, D. G. Newman², P. S. Keatley², A. T. N'Diaye⁴, T. Hesjedal⁵, G. van der Laan³, R. Hicken², R. M. Bowman¹

¹Queen's University Belfast, Belfast, United Kingdom, ²University of Exeter, Exeter, United Kingdom, ³Diamond Light Source, Didcot, United Kingdom, ⁴Lawrence Berkeley National Laboratory, Berkeley, California, United States, ⁵University of Oxford, Oxford, United Kingdom

Synthetic ferrimagnets (SFI), two ferromagnetic (FM) layers with different magnetic moments exchange coupled antiferromagnetically via the RKKY interaction across a non-magnetic spacer, are of interest as a feasible media for all optical switching (AOS) [1,2], demonstrated to be a robust, ultrafast and efficient process with which to write data [3]. SFi are especially promising for applications of data storage as properties of the constituent layers can be tailored independently to tune the AOS mechanism.

Design of the magnetic properties of SFi structures requires knowledge and control of the magnetization, M(T), and anisotropy, K(T), of each FM layer, and the strength of the

exchange coupling between them, $J_{ij}(T)$. We show it is possible to engineer the magnetic properties of series of Ni, Pt, Ir and Co based SFi, fabricated by magnetron sputtering and exhibiting perpendicular magnetic anisotropy (PMA) [4,5]. The tuneability of these structures (through variation of deposition conditions and layer thickness) provides an ideal system with which to investigate the effect of M(T), K(T), $J_{ij}(T)$ and Gilbert damping, α , on reversal mechanisms within SFis, with the added benefit of distinct magnetic species for element/layer specific characterization. Pump/probe experiments have revealed multi-pulse, helicity independent AOS [4], up to 330K in Ni/Pt multilayer SFi [5].

PMA in Ni₃Pt thin films is thought to arise at interfaces between Pt platelets in a Ni matrix, induced via heated deposition [6]. We show it is possible to produce a similar effect through a fine Ni/Pt multilayer, sputtered at room temperature. While the Ni₃Pt alloy layer and Ni/Pt multilayers alone are observed to have nominally the same FM behaviour, swapping the Ni₃Pt alloy layer for the Ni/Pt multilayer in the SFi results in unidirectional AOS, behaviour not observed elsewhere.

- [1] S. Mangin et al, Nature Materials, 13, 286-292 (2014)
- [2] J-W. Liao et al, Adv. Sci, 6, 1901876 (2019)
- [3] A.V. Kimmel and M. Li, Nat. Rev. Mater, 4, 189-200 (2019)
- [4] M. Dabrowski et al, Nano. Lett. 21, 9210-9216 (2021)
- [5] C.R.J. Sait et al, Phys Rev B, 109, 134417 (2024)
- [6] D. Vasumathi et al, J.Magn.Magn.Mater 223, 221-223 (2000)

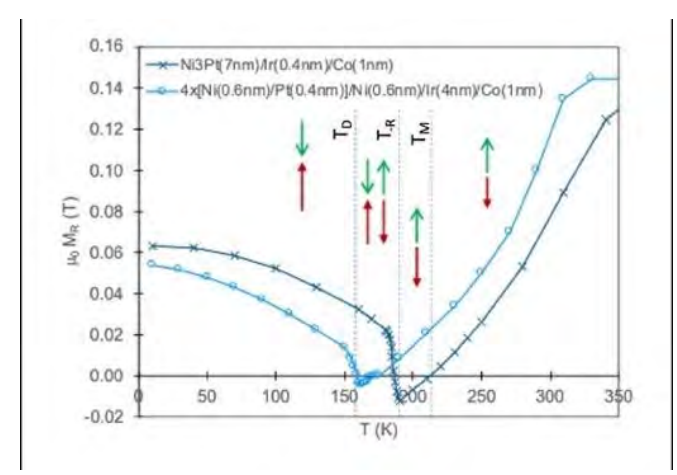


Fig. 1 M_R vs T of N_{i3} Pt and Ni/Pt multilayer based SFi (samples saturated at +0.5T before remanence measurement), showing similar temperature dependent behaviour, with three distinct regions. Green arrows denote the orientation of the Co layer, red the NiPt based layer

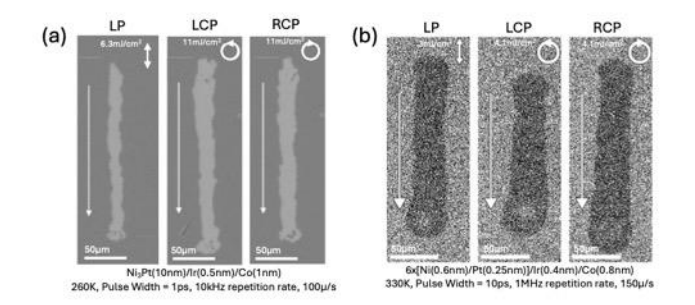


Fig. 2 Wide field Kerr microscopy showing helicity independent AOS in (a) Ni₃Pt alloy [4] and (b) Ni/Pt multilayer SFi [5]

CH-07. Tracking and Characterization of Domains in $Nd_2Fe_{14}B$ Micro-Magnets

<u>F. Lasthofer</u>¹, O. Hrushko¹, A. Kosogor¹, T. Schrefl¹, S. Raznjevic², K. Zuzek Rozman², V. Sršan², S. Šturm²
¹University for Continuing Education Krems, Wr. Neustadt, Austria, ²Jozef Stefan Institute, Ljubljana, Slovenia

Permanent magnets, particularly Neodymium-Iron-Boron (NdFeB), play a vital role in clean energy technologies by enabling efficient energy conversion in electric vehicles and wind turbines. A challenge in NdFeB magnets lies in the gap between their theoretical and actual coercivity. Advancing the understanding of how grain structures influence magnetic domain behavior is key to improving magnet performance. To facilitate a direct comparison between experimental domain images obtained via Lorentz electron microscopy and micromagnetic simulations, we developed a methodology for characterizing and tracking domain patterns during the magnetization of micro-magnet samples.

The left column of Figure 1 presents simulated magnetic domain images of a granular $Nd_2Fe_{14}B$ sample (1.3 × 1.3 μm^2 , 10 nm thick) in the demagnetized state and under an applied field of μ_0H = -0.28 T. The grain boundaries are modeled as weakly ferromagnetic (magnetic polarization Js = 0.27 T, exchange constant A = 4.6 pJ/m). Simulations were performed using a finite element micromagnetic solver [1]. We implement a postprocessing workflow that segments and labels simulated magnetic domains. First the data is mapped onto a binary mask for +z and -z domains. Then, these regions are labeled and analyzed using geometric features such as area, perimeter, eccentricity, and solidity, with the help of the scikit-image library [2]. To track domain

regions across consecutive images, we apply a hybrid approach combining Intersection over Union (IoU) [3] with graph-based labeling methods. The right column of Figure 1 shows the labeled domains following segmentation. Table 1 summarizes selected domain characteristics for two representative domains as a function of the applied field. This work was funded by the European Union under the Horizon Europe grant 101129888 (GREENE).

- [1] T. Schrefl, S. A. Pathak, A. Petrocchi, https://mammos-project.github.io/mammos/ (2025)
- [2] S. Van der Walt, J. L. Schönberger, J. Nunez-Iglesias, PeerJ., Vol. 2, p. e453 (2014).
- [3] M. Everingham, L. Van Gool, C. K. Williams, International journal of computer vision., Vol. 88, p. 303 (2010).

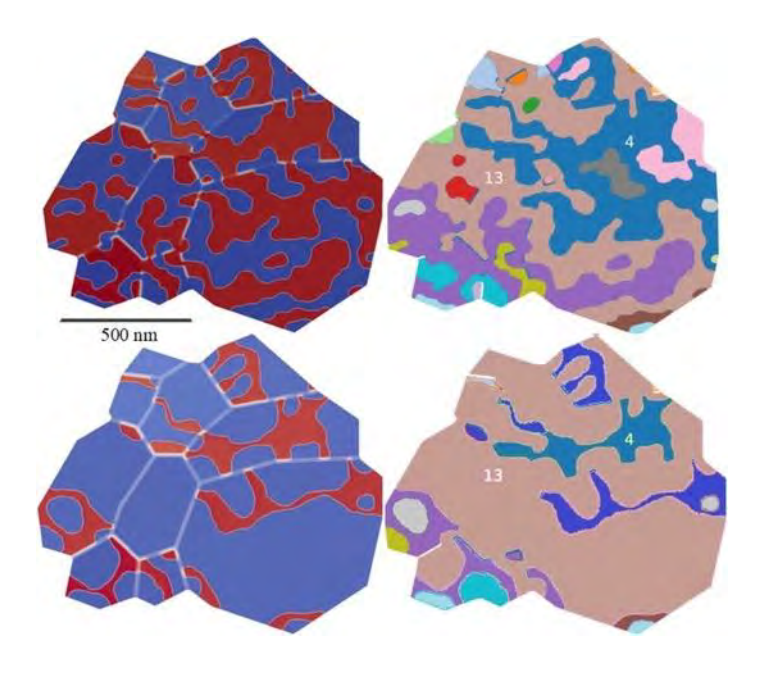


Fig.1 Left: Computed domain patterns for zero applied field and an external field of μ_0H = -0.28 T. Right: Labelled domains as identified by the domain tracking method.

Domain ID	μ ₀ Η (T)	Area (pixel)	Perimeter (pixel)	Eccentricity	Solidity
4	-0.16	53479	3658	0.71	0.47
4	-0.28	15897	1221	0.96	0.44
4	-0.40	4626	978	0.97	0.20
13	-0.16	135211	5933	0.79	0.60
13	-0.28	207226	6202	0.62	0.72
13	-0.40	246988	4958	0.58	0.85

Tab. 1 Computed domain characteristics for an initially updomain (domain ID 4) and an initially-down domain (domain ID 13).

CH-08. Self-modulation instability in high-power ferromagnetic resonance of BiYIG nanodisks

I. N. Yemeli¹, <u>S. Perna</u>², D. Gouéré⁴, A. Kolli¹, M. Muñoz³, A. Anane⁴, M. d'Aquino², H. Merbouche¹, C. Serpico², G. de Loubens¹

¹SPEC, CEA, CNRS, Université Paris-Sarclay, Gif-sur-Yvette, Paris, France, ²Department of Electrical Engineering and Information Technology, University of Naples Federico II, Naples, Italy, ³Institute de Tecnologías Fisicas y de la Información (CSIC), Madrid, Spain, ⁴Laboratoire Albert Fert, CNRS, Thales, Université Paris-Sarclay, Palaiseau, France

Nonlinear magnetization dynamics in confined nanostructures is a phenomenon that promises the realization of fast and energy efficient ICTs [1]. Ferromagnetic resonance (FMR) is a consolidated investigation technique that uses a uniform RF field oscillating at a frequency close to Kittel's value to bring the magnetization out of the equilibrium. For low RF power, FMR is used to characterize the material parameters, while for high power, it brings the magnetization in a deep nonlinear dynamic where foldover and spin wave instability appear[2].

In this work, we investigate the FMR of BiYIG nanodisk uniformly magnetized along the symmetry axis of the disk subject to a DC field in the same direction, where the out of plane anisotropy almost compensates the shape anisotropy of the sample[3]. Our investigation is based on magnetic resonance force microscope (MRFM), on micromagnetic simulations and normal modes analysis[3].

We find, that the control plane (DC field vs RF field) can be divided in three regions according to the observed regime: the first for very low RF field amplitude, where the magnetization oscillations are synchronous to the RF field (P-mode). The spectrum of the transverse magnetization is single peaked (SP) and then this region is labeled accordingly. The second region for intermediate value of RF field, where there is coexistence between a chaotic attractor and the P-mode. The third region is characterized by high RF fields and the chaotic attractor is the only possible dynamics. The spectrum of the chaotic magnetization dynamics exhibits multiple peaks (MP) equally spaced on the top of a continuous spectrum (C). This region is labeled with MP-C and the region of coexistence is labeled MP-C/SP.

In the figure below[4], we show the MRFM data (a), the results of micromagnetic simulations (b), the phase diagram in the control plane (c) and the number of normal modes (NM) significantly in a certain dynamic state (d).

^{*} Best Student Presentation Finalist / LB - Late-breaking Poster

The possibility to excite such a large number of NM in a deep nonlinear dynamical state suggests the potential use of this phenomenon for novel computation schemes.

This work is supported by Italian Ministry of University and Research, PRIN2020 funding program, Grant No. 2020PY8KTC.

- [1] A. V. Chumak *et al.*, *IEEE Trans. on Magn.*, vol. 58, no. 6, pp. 1-72, (2022)
- [2] G. Bertotti, et al., Phys. Rev. Lett. 87, 217203 (2001)
- [3] I. Ngouagnia Yemeli, et al., arXiv:2503.07159 [cond-mat.mes-hall]
- [4] S. Perna, et al, J. Magn. Magn. Mater., 546, (2022)

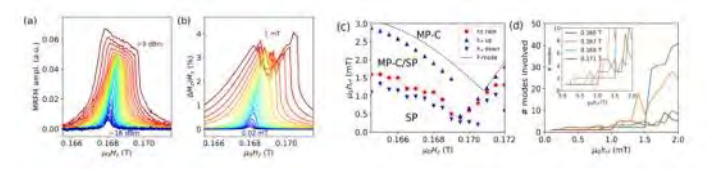


Fig. 1

CH-09. A Physically Unclonable Function Implemented with Defective Magnetic Tunnel Junctions

<u>J. W. Huber</u>¹, R. Rahman², S. Bandyopadhyay¹
¹Electrical and Computer Engineering, Virginia Commonwealth University, Richmond, Virginia, United States, ²Electrical and Computer Engineering, Virginia Commonwealth University, Richmond, Virginia, United States

Mobile and embedded devices are increasingly called upon to authenticate or be authenticated by another party for trust. Physically unclonable functions (PUFs) are a promising way to enable authentication via the physical characteristics of a device which are unpredictable and impossible to anticipate, duplicate or hack. Here, we show that the time it takes to switch the resistance state of a magnetic tunnel junction (MTJs) from high to low, or vice versa, with a fixed current exerting spin transfer torque on the soft layer's magnetization is very sensitive to fabrication defects incurred during manufacturing. Hence, if a chain of MTJs is subjected to a fixed switching current pulse of a fixed pulse width, the number of MTJs in the chain that will switch from one resistance state to the other will vary randomly from sample to sample because of the random manufacturing defects. Hence the series resistance of the MTJs in the chain will act as a "fingerprint" or "biometric" of the chain. This can implement a PUF. We have used MuMax3 simulations of the Landau-Lifshitz-Gilbert-Langevin equations in the presence of random thermal noise at room temperature to extract the histograms of switching time distribution of MTJs with six different defect morphologies and we also obtained the switching probability as a function of current pulse width for a fixed current amplitude. These results confirm the viability of using this construct to realize a PUF. We have also calculated the intra- and inter-Hamming distances for the PUF.

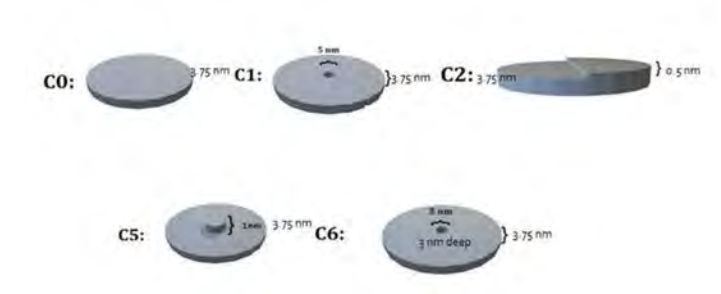


Fig. 1 Different shape morphologies of elliptical disk soft layers considered in the simulations. The average thickness is 3.75 nm in all cases. These defects are incurred during fabrication. These different morphologies result in different threshold currents.

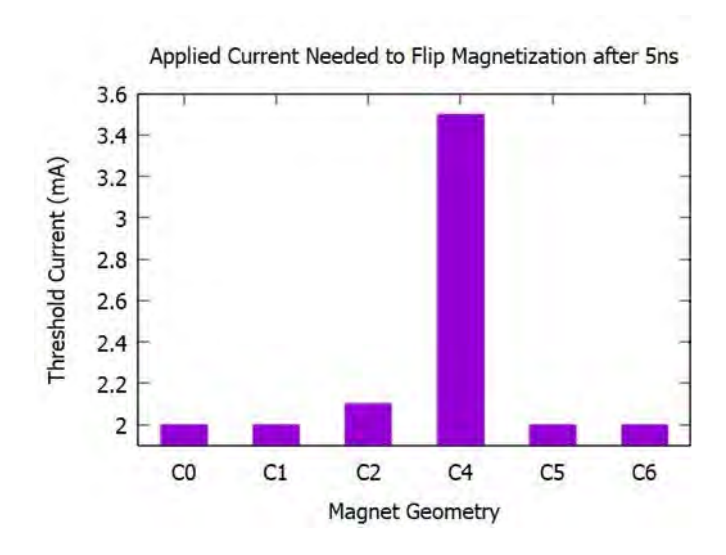


Fig. 2 Threshold currents for various defect morpholgies in the soft layer of the MTJ considered. The thresholds can be significantly affected by defects and this makes the switching current of the MTJ a "biometric" of the device.

CH-10. Exploring Low Sheet Resistance Materials for Enhanced Ferromagnetic Resonance Signals

N. Kuninski, J. N. Scott, W. R. Hendren, T. E. McCormack, R. M. Bowman

CQMT, Queen's University Belfast, Belfast, United Kingdom

Broadband Ferromagnetic Resonance (FMR) is a powerful technique for investigating the dynamic magnetic properties of thin films, including the gyromagnetic ratio and the Gilbert damping parameter [1]. These parameters are essential for understanding the behaviour of magnetic materials and their applications. FMR enables differentiation between intrinsic and extrinsic damping [2], making it invaluable for material characterisation. Accurate extraction of these properties is crucial for studying phenomena like all-optical switching (AOS), a promising data storage technology with transformative potential for information technology [3].

Characterising individual layers within magnetic multilayers, with perpendicular magnetic anisotropy [3] is crucial for advancing our understanding of AOS. However, some of these layers can be sub-nanometre thick [4], making FMR measurements with a good signal-to-noise (S/N) ratio particularly challenging. Various strategies have been proposed to address this issue, either by enhancing data analysis techniques or by modifying the experimental setup to improve the S/N ratio. In this work, a different approach is explored: the introduction of low sheet resistance buffer layers [5] between the sample and the substrate. It is claimed that these layers increase the magnetic component of the detected signal via eddy current shielding effects within the buffer material [5].

This study will compare both the static and dynamic magnetic properties of a range of materials in the out of plane FMR direction, building on the work presented in [5], where only the static magnetic properties were assessed using a vibrating sample magnetometer, and resonance peak positions were identified. Notably, the Gilbert damping parameter was not examined in that work and will be addressed in the present study. In study [5] Au was used, as observed in Figure 1, signal enhancement works for Ag as well with a minor shift in resonance position, interesting with Au it seems to majorly shift the resonance of the 1nm Fe layer, this will be investigated further.

[1] H. Maier-Flaig, et al.; Rev. Sci. Instrum., 2018, 89, 073901.

- [2] C. Bilzer, et al.; J. Appl. Phys., 2007, 101, 074505
- [3] M. Dabrowski et al.; Nano Lett., 2021, 21, 9210-9216.
- [4] O. Yildirim, et al.; Scripta Materialia, 2022, 207, 114285.
- [5] H. Glowinski, et al.; J. Appl. Phys., 2014, 116, 053901.

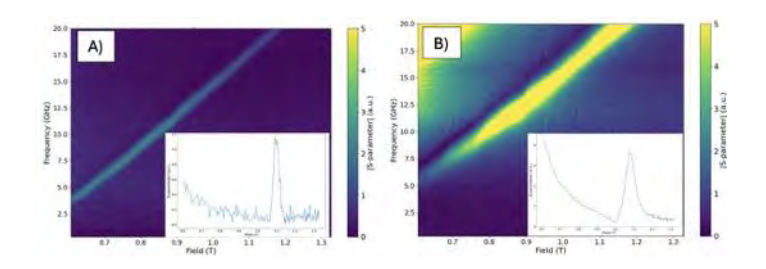


Figure 1. A) FMR contour plot of 6nm Ag, 1nm of Fe, B) FMR contour plot of 60nm Ag, 1nm Fe. Inset in A) and B) Show a peak in field sweep at 17.7GHz

CH-11. The role of the magnetic part of the optical field in the optical control of the magnetization

B. J. Assouline, A. Capua

Applied Physics, Hebrew University of Jerusalem, Jerusalem, Jerusalem, Israel

The magnetic part of light typically receives less attention as compared to the electric part, due to the significantly slower response of the magnetization (~ 10 GHz) compared to the rapid oscillations of optical radiation (400-800 THz). However, recently we have reported on a new mechanism whereby the optical magnetic field may control the magnetization state by merely considering the optical magnetic field in the Landau-Lifshitz-Gilbert (LLG) equation [1]. The principle behind the interaction is that the magnetization is incrementally affected within each optical cycle, such that a significant net torque can build up over the entire pulse duration in typical experimental conditions, as depicted in Fig. 1. We find the strength of the interaction to be determined by $\eta = \alpha \gamma H/\text{fopt}$, where fopt is the optical frequency, α is the Gilbert damping, H is the amplitude of the optical magnetic field and γ is the gyromagnetic ratio.

Here we further elaborate on the principles of the interaction. We show that the torque is proportional to the optical fluence, where its out-of-plane (in-plane) component is dependent (independent) on α , as seen experimentally [2]. We show that the interaction reproduced experimental observations in the signle- and multi-pulse regimes, as well as the CW regime. Finally, our results indicate that the magnetic component of light also contributes to the

Faraday effect, which is generally attributed solely to the electrical component of the optical radiation. Our findings provide an additional perspective to the important interaction between light and spins that has been pioneered by the magnetism community.

[1] Assouline, Capua Phys. Rev. Research 6, 013012[2] G.-M. Choi, et al., Nature Communications, 8 (2017)15085

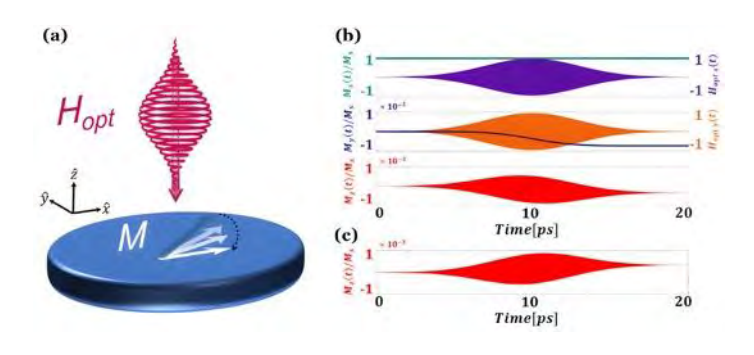


Figure 1. (a) Schematic illustration of magnetization dynamics induced by a CP pulse. (b) Dynamics induced by an 800 nm RCP Gaussian pulse for $\alpha=0.035$ and $\eta=2.5\times10-4$. Top, middle and bottom panels depict the temporal evolution of the x, y and z components of the magnetization and the optical magnetic field in normalized units. (c) LCP pulse.

SESSION CQ: BIOMAGNETISM AND BIOMEDICAL APPLICATIONS II (POSTER SESSION)

Co-Chair(s): P. Kumar, IMS RIKEN Center for Integrative Medical Sciences, Yokohama, Japan and D. A. Arena, Physics, University of South Florida, Tampa, Florida, United States Wednesday, October 29, 2025 09:00 AM-12:00 PM Exhibit Hall Posters

CQ-01. Application of the FDTD Method to Analysis of Light Scattering in Suspensions of Crystals with Magnetic Anisotropy

Y. Takeuchi¹, T. Yamada¹, H. Kawaguchi¹, A. Hamasaki²
¹Muroran Institute of Technology, Muroran, Japan, ²Faculty of science, Shinshu University, Matsumoto, Japan

Understanding light-scattering properties is vital for particle characterization and diverse fields such as bioscience and materials science (1.2). Recently, it was discovered that anisotropic crystals such as cellulose, uric acid, and guanine

are regularly oriented in magnetic fields with strengths comparable to those of permanent magnets and electromagnets (3-5). This discovery is expected to lead to the development of innovative optical devices such as focusing lenses and medical diagnostic equipment (6). However, understanding the light-scattering properties of magnetically oriented crystal groups is difficult with experimental methods alone. Therefore, we applied the finite-difference time-domain (FDTD) method to reproduce light-scattering properties, validating our approach against experimental results.

Fig. 1 shows the calculated scattering intensity distribution in a model that detects incident light from the X axis, magnetic field directions from the Y axis, and scattered light from the XY plane, for one scatterer with a length of approximately 5 µm. When the long axis of the scatterer was oriented perpendicular to the magnetic field, the crystals in Case A were energetically unstable and oriented in the direction of Case B or C. The scattered light intensity from the XY plane decreased at that time. Fig. 2 shows the temporal change in the scattered light intensity when an experiment was conducted under the same conditions as in the numerical calculation, using a material with similar magnetic orientation. When a magnetic field was applied, the light intensity decreased, and when the magnetic field was stopped, the scattered light intensity almost recovered to its original value. The numerical calculation also predicted a decrease in the scattered light intensity, which agreed with the experimental results. Thus, it will be easier to design devices and pursue functionality by supporting the control of anisotropic crystal orientation through an external magnetic field by using numerical analysis with the FDTD method.

[1] J. Rodriguez-Loya, M. Lerma and J. L. Gardea-Torresdey, *Micromachines*, 15, 24 (2023)

[2] D. R. Prasad, N. R. Prasad and N. Prasad, *Engineered Science*, 33, 1332 (2025)

[3] Y. Miyashita, M. Iwasaka and T. Kimura, *Journal of Applied Physics*, 115, 17B519 (2014)

[4] Y. Takeuchi, Y. Miyashita and Y. Mizukawa, *Applied Physics Letters*, 104, 024109 (2014)

[5] M. Iwasaka, Y. Miyashita and Y. Mizukawa, *Applied Physics Express*, 6, 037002 (2013)

[6] M. Iwasaka and H. Asada, *Scientific Reports*, 8, 16940 (2018)

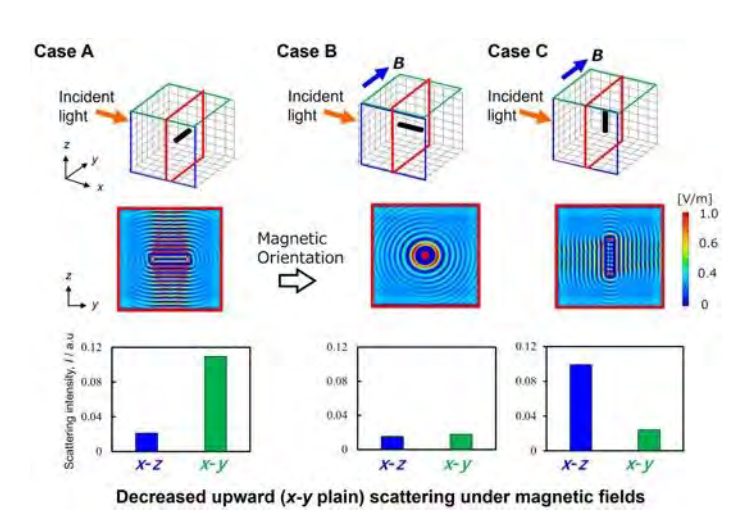


Fig. 1 The simulation results. Top: Numerical model, Middle: Scattering distribution seen from the YZ plane, Bottom: Scattering components on each plane

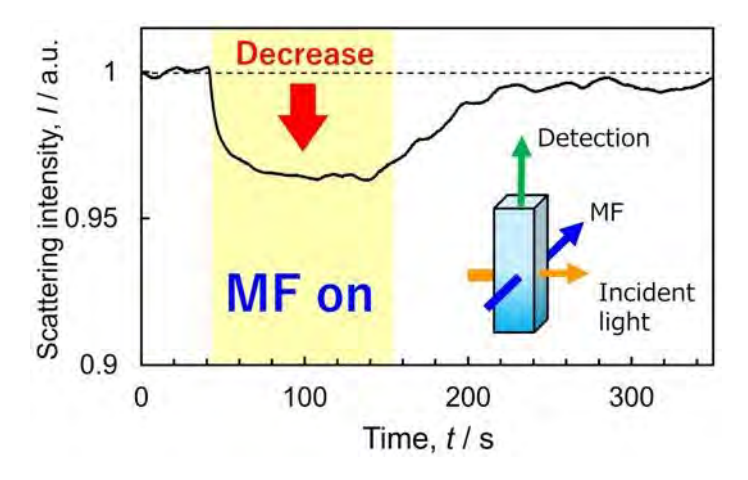


Fig. 2 Light intensity versus time

CQ-02. Temperature-Dependent Agglomeration Dynamics of Magnetic Nanoparticles: Implications for Diffusion and Spatial Control in Magnetic Hyperthermia

<u>B. Cheng</u>, J. Sakurai, S. Hata, C. Oka Micro-Nano Mechanical Science and Engineering, Nagoya University, Nagoya, Japan

In magnetic hyperthermia therapy (MHT) using magnetic nanoparticles (MNPs), the agglomeration state of MNPs is critically influenced by temperature [1], directly impacting their diffusion behavior and complicating the precise spatial control of heating. To investigate this, we first analyzed heat-induced agglomeration dynamics via dynamic light scattering (DLS). Number-weighted distributions revealed a significant transition from larger (Peak 1) to smaller agglomerates (*Peak 2*) with increasing temperature. accompanied by a decrease in the mean radius from 47.5 nm ($r_{s,25}$) to 38.9 nm ($r_{s,45}$), indicating intense competition between thermal perturbation and magnetic interactions within the therapeutic temperature window (Fig. 1). To probe how this deagglomeration affects diffusion within a biomatrix, we designed acrylamide hydrogels (pore size $\xi \approx 1200$ nm, as determined by SEM). MNP dispersions were deposited into wells formed on the hydrogels, and inplane concentration profiles evolving over time were recorded by optical microscopy as grayscale values. By tracking the temporal evolution of the normalized full width at half maximum (σ) of spatial Gaussian distributions of grayscale, we derived the diffusion coefficient (D). Results demonstrate a distinct increase in D with rising temperature (Fig. 2(a)). Crucially, D exhibited a 5.13% greater increase than the D_{ideal} calculated with $r_{s,25}$ (Fig. 2b). The increase in D at 45°C is more consistent with that of D_{ideal} using $r_{s,45}$, quantitatively confirming that agglomerate disruption may lead to enhanced thermal diffusion indicating non-linear expansion of heating zone during MHT. Results highlight the need to include temperature-

Results highlight the need to include temperature-dependent agglomeration in MHT diffusion models. Future studies will incorporate alternating magnetic fields during diffusion analysis and explore wider ξ and temperature ranges to improve predictions.

[1]B. Cheng et al, Alexandria Engineering Journal., Vol. 96, p.72 (2024)

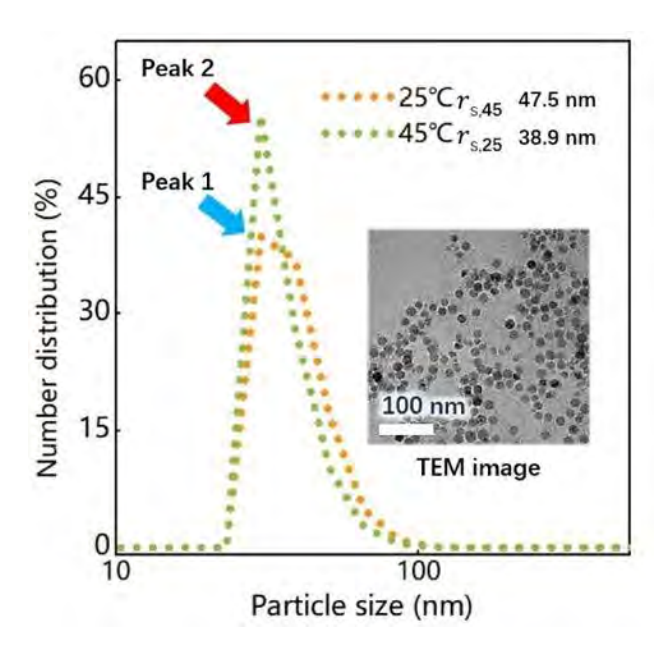


Fig. 1 Results of DLS analysis at 25 and 45°C and TEM image of MNPs.

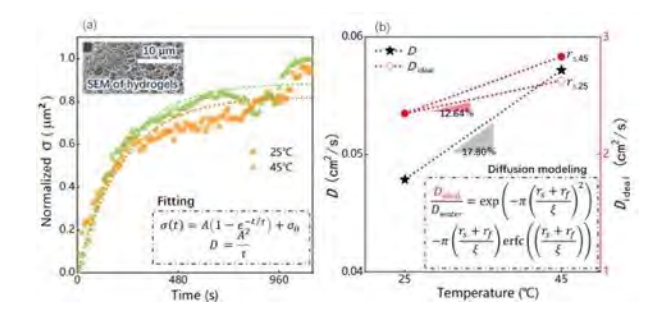


Fig. 2 (a) Normalized σ vs time, fitting equation for calculation of D, and SEM image of hydrogel. A and τ are saturation value and time constant, respectively. (b) D with D_{ideal} . D_{water} is diffusion coefficient in water obtained by DLS, r_{f} = 3.18 nm calculated by Flory's model.

CQ-03. Automated TMS E-Field Mapping of Brain Phantom using Collaborative Robot

L. Schorr¹, W. Lohr², R. L. Hadimani¹

¹Mechanical and Nuclear Engineering, Virginia Commonwealth University, Richmond, Virginia, United States, ²Biomedical Engineering, Virginia Commonwealth University, Richmond, Virginia, United States

Transcranial magnetic stimulation needs precise positioning between the magnetic coil and the desired stimulation site for effective treatment. For clinician administered treatment, which is the most commonly used method, this is achieved by pulsing different locations and measuring the MEPs; the motor cortex will be the location with the highest MEPs. This process is both time-consuming and non-exact, leading to significant potential improvement in both efficiency and effectiveness with an automated method. This is enabled by the utility of collaborative robots with integrated force-torque sensors, as they can approach the head and automatically stop.

For this experiment, a figure-of-eight butterfly coil was attached to the end of a collaborative robot and used to stimulate a brain phantom. For ideal treatment, it is crucial that the coil is aligned normal to the head. With brain scan data, this is trivial with neuronavigation, but without it, another method is required. The robot can measure the force in all directions and gradually adjust the orientation of the coil until there is no force in the x or y directions, which indicates that the coil is normal to the phantom. The induced electric field will be measured by tri-axial probes within the phantom, which the robot can use to identify the location with the highest E-field strength. The robot is moved close to the expected motor cortex location and travels in increments of 1 mm in all directions, using the E-field measurements to identify the true location. The readings were then compiled into a heatmap, shown in Fig.

From the heatmap shown, any sort of pattern is unclear. There are several variables that could be affecting the readings; first is that only a single channel (z axis) of the probe is being measured. Ideally, all three axes would be read and the E-field would be normalized. Second, the grid is based off of a point in robot space, prior to the orientation adjustment algorithm. This means that the spacing between the readings is not true as plotted, as the grid is projected onto the phantom. Despite these, this is a remarkable improvement to the traditional style of mapping.

R. Sparing, D. Buelte, I. G. Meister, T. Paus, and G. R. Fink, "Transcranial magnetic stimulation and the challenge of coil placement: A comparison of conventional and stereotaxic neuronavigational strategies," vol. 29, no. 1, pp. 82–96. X. Ding, J. Guo, Z. Ren, and P. Deng, "State-of-the-art in perception technologies for collaborative robots," vol. 22, no. 18, pp. 17 635–17 645.

A. Giuffre, C. K. Kahl, E. Zewdie, J. G. Wrightson, A. Bourgeois, E. G. Condliffe, and A. Kirton, "Reliability of robotic transcranial magnetic stimulation motor mapping," vol. 125, no. 1, pp. 74–85.

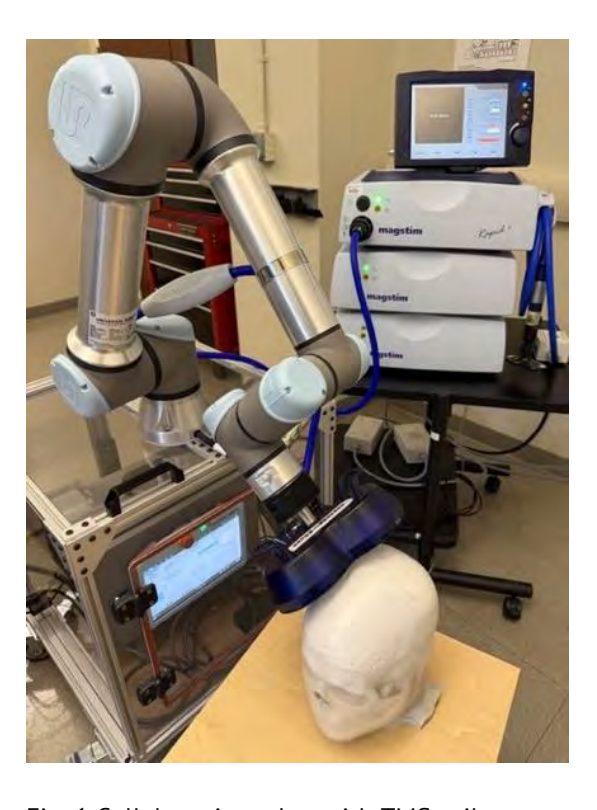


Fig. 1 Collaborative robot with TMS coil

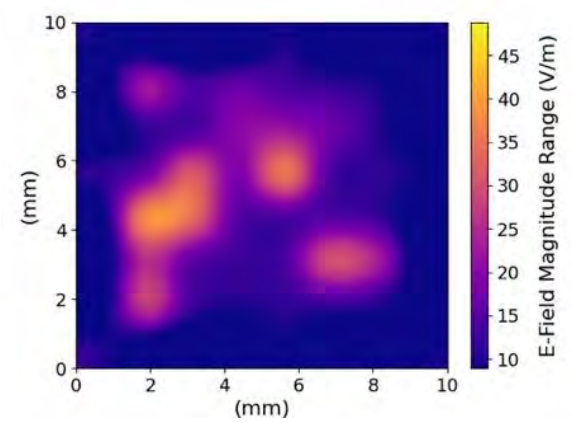


Fig. 2 E-field heatmap

CQ-04. Shape-Directed Magnetic and Hyperthermic Properties of Hydrothermally Synthesized $Mn_{0.5}Zn_{0.5}Fe_2O_4\text{-}$ based Magnetic Fluid

H. H. Patel¹, K. Parekh¹, P. Kopcansky², M. Rajnak²
¹Dr. K. C. Patel Research and Development Centre, Charotar University of Science and Technology, CHARUSAT Campus, Changa, Gujarat, India, ²Institute of Experimental Physics, SAS, Watsonova 47, 040 01, Košice, Slovakia

Nanometer-sized magnetic nanoparticles (MNPs) possess unique properties such as high saturation magnetization, biocompatibility, and low toxicity, making them valuable in industrial, environmental, and biomedical applications. Especially in the biomedical field, Magnetic fluid hyperthermia (MFH) is a promising cancer therapy due to its minimal side effects and relatively easy treatment approach compared to other therapies. MFH involves heat generation from MNPs under an alternating magnetic field, aiming to achieve therapeutic temperatures (42-46 °C) with minimal MNP concentration and exposure time, while staying within the safe field-frequency threshold (5×10° A/m•s). Controlling the hyperthermia temperature is crucial to avoid overheating, which can be achieved by utilizing MNPs with a low Curie temperature (T_c); the MNPs will function as a temperature control switch. The Mn_{0.5}Zn_{0.5}Fe₂O₄, with its low T_c and high pyromagnetic coefficient, makes it a compelling candidate for hyperthermia applications.

This study investigates the morphology-dependent magnetic and thermal properties of hydrothermally synthesized Mn_{0.5}Zn_{0.5}Fe₂O₄ MNP-based magnetic fluid. Various particle shapes, including flower, cube, octahedral, ring, and rod, were synthesized to evaluate their structural, magnetic, and heating properties. Magnetic measurements (M vs. H) were conducted at 300 K and 5 K, along with temperature-dependent magnetization under a 1 T field. Curie temperatures were determined using Bloch's law fitting. The results of the study are shown in Fig. 1. To assess the potential in hyperthermia applications, all samples were subjected to alternating magnetic field exposure in induction heating experiments. A strong dependence of heating efficiency on particle shape was observed, with the rod-shaped (Rods-2) MNPs demonstrating the highest specific absorption rate (SAR) and fastest temperature rise. These findings highlight the importance of nanoparticle morphology in tailoring magnetic behavior and enhancing heating efficiency for MFH applications.

^{*} Best Student Presentation Finalist / LB – Late-breaking Poster

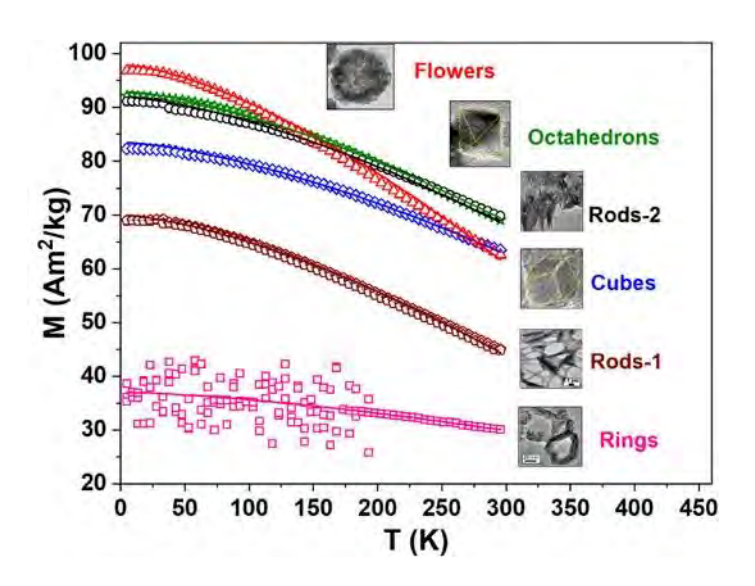


Figure 1: M versus T curve measured at an applied field of 1 T for $Mn_{0.5}Zn_{0.5}Fe_2O_4$ with different shapes: flower, cube, octahedron, ring, and rods.

CQ-05. Wireless Temperature Measurement based on Magnetic Harmonic Signal during Magnetic Heating Operation for Hyperthermia

<u>A. Kuwahata</u>, A. Yamazaki, R. Shinohara, S. Yabukami *Tohoku University, Sendai, Japan*

Magnetic hyperthermia (MH) using magnetic nanoparticles (MNPs) and alternating magnetic fields (AMFs) offers a minimally invasive cancer treatment [1-3]. Real-time in vivo temperature monitoring and AMF power control are vital to avoid overheating and ensure safety. However, no existing system allows temperature monitoring during high-intensity AMF exposure. Here, we present a MH system enabling wireless in vivo temperature monitoring based on magnetic harmonic signals during heating.

Figure 1 shows the magnetic properties of concentrated MNPs (28–112 mg/mL Fe). With increasing concentration, the hysteresis loops broaden (Fig. 1(a)), and the loop area at fourfold concentration is about four times larger (Fig. 1(b)). These results indicate that higher MNP concentrations improve both heating efficiency and temperature sensing accuracy. Figure 2 presents a feasibility study of wireless temperature monitoring during magnetic hyperthermia. By using a noise-resistant signal—the phase of the third harmonic—we achieved a temperature accuracy of 0.07°C (Fig. 2(a)). To reduce noise from the heating magnetic field, we implemented real-time on/off control on the order of

seconds for monitoring/heating system (Figs. 2(b) and (c)). Magnetic signals are acquired during the off-phase, while temperature monitoring continues during heating. This system enabled stable temperature control with a deviation of 0.45°C from the target temperature (Fig. 2(d)). This satisfies the ±1°C accuracy requirement for magnetic hyperthermia therapy, demonstrating its potential for clinical theranostic application.

- [1] A. Kuwahata *et al.*, AIP Advances 13, 025142 (2023). [2] A. Shikano *et al.*, *T. Magn. Soc. Jpn. (Special Issues)* 6, 100-104 (2022).
- [3] Y. Adachi et al., AIP Advances 14, 015144 (2024).

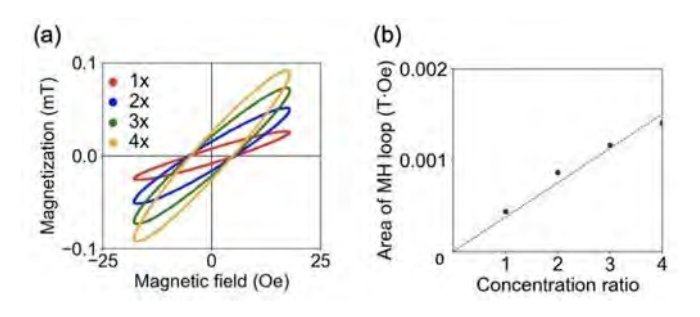


Fig. 1 AC magnetic measurements of highly concentrated magnetic nanoparticles: x1 (28 mg/mL Fe), x2 (56 mg/mL Fe), x3 (84 mg/mL Fe), and x4 (112 mg/mL Fe). (a) Measured AC hysteresis loops at 200 kHz and (b) Hysteresis loop areas for different Fe.

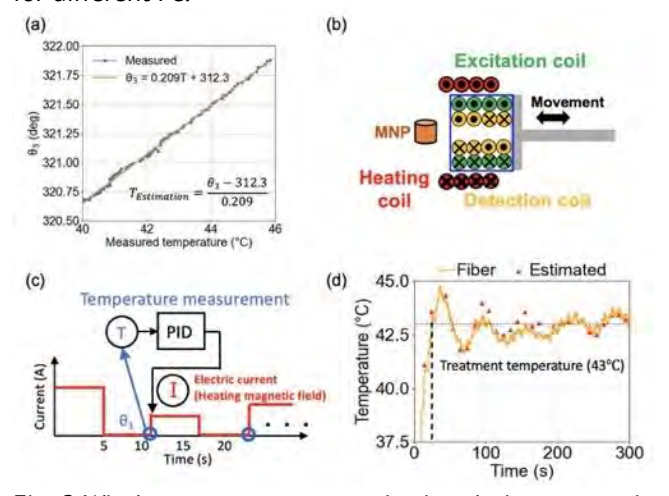


Fig. 2 Wireless temperature monitoring during magnetic hyperthermia. (a) Accuracy of wireless temperature measurements based on magnetic harmonic signals. (b) Monitoring/heating system. (c) PID control using magnetically measured temperature for maintaining a constant treatment temperature. (d) Demonstration of temperature stability in the magnetic hyperthermia system.

CQ-06. Iron Oxide Magnetic Nanoparticles Synthesized by Wet Ball Milling: Evaluation of Hyperthermia Properties

<u>S. Mostufa</u>¹, B. Rezaei¹, I. H. Karampelas², J. Gomez-Pastora³, K. Wu¹

¹Department of Electrical and Computer Engineering, Texas Tech University, Lubbock, Texas, United States, ²Nemak USA, Inc., Sheboygan, Wisconsin, United States, ³Department of Chemical Engineering, Texas Tech University, Lubbock, Texas, United States

Magnetic nanoparticles (MNPs) have gained considerable attention for biomedical applications, particularly in magnetic hyperthermia, where exposure to an alternating magnetic field (AMF) can effectively induce localized heating to trigger tumor cell apoptosis [1]. In this study, we synthesized MNPs using a mechanical ball milling approach, using iron (Fe) powder and water as precursors. The milling was conducted in a stainless-steel jar at 200 rpm using 3 mm stainless steel balls for up to 56 hours. X-ray diffraction (XRD) analysis (Figure 1(A)) confirmed a progressive transformation of the particles into magnetite (Fe₃O₄) with increasing milling time. Particle characterization using dynamic light scattering (DLS) and transmission electron microscopy (TEM), shown in Figure 1(B), revealed the hydrodynamic and morphological properties of the milled nanoparticles. Finally, we measured the magnetic hyperthermia using 30 mT (=23.9 kA/m),101.5 kHz AMF for 20 min in a 1 mL vial, adhering to the clinical safety threshold of 5×10^9 A/m/s [2][3]. We compared the magnetic hyperthermia performance of particles milled for 15 and 56 hours at 10 mg/mL, as well as 56-hour milled particles at both 10 mg/mL and 20 mg/mL concentrations (Figure 1(C)). The results demonstrate that the 56-hour milled particles exhibit superior heating efficiency and can achieve temperatures change up to 30 °C, highlighting their potential as effective and safe agents for magnetic hyperthermia.

[1] W. Jiao, T. Zhang, M. Peng, J. Yi, Y. He, and H. Fan, "Design of Magnetic Nanoplatforms for Cancer Theranostics," Biosensors, vol. 12, no. 1, pp. 1–21, 2022, doi: 10.3390/bios12010038.

[2] S. Dutz and R. Hergt, "Magnetic nanoparticle heating and heat transfer on a microscale: Basic principles, realities and physical limitations of hyperthermia for tumour therapy," Int. J. Hyperth., vol. 29, no. 8, pp. 790–800, 2013, doi: 10.3109/02656736.2013.822993.

[3] R. Hergt and S. Dutz, "Magnetic particle hyperthermiabiophysical limitations of a visionary tumour therapy," J. Magn. Magn. Mater., vol. 311, no. 1 SPEC. ISS., pp. 187–192, 2007, doi: 10.1016/j.jmmm.2006.10.1156.

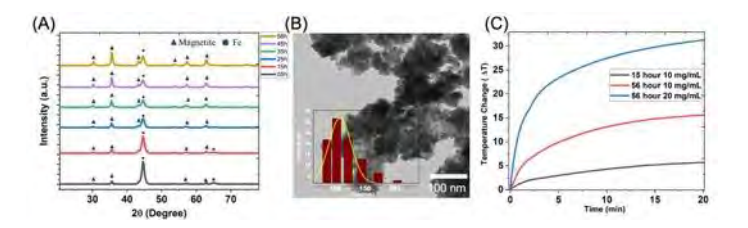


Figure 1. (A) XRD crystallographic analysis demonstrates the progressive formation of magnetite in the ball-milled particles over time, from 5 to 56 hours. (B) TEM image and DLS measurement of MNPs after 56 hours of milling. (C) Magnetic hyperthermia performance of MNPs milled for 15 and 56 hours at concentrations of 10 mg/mL and 20 mg/mL. Greater magnetite content and higher particle concentration are associated with enhanced heat generation.

CQ-07. PEG-Functionalized Spherical and Cubic Iron Oxide Nanoparticles for Magnetic Hyperthermia in Serum-Based Environments

B. Rezaei¹, S. Mostufa¹, I. H. Karampelas², J. Gomez-Pastora³, <u>K. Wu</u>¹

¹Department of Electrical and Computer Engineering, Texas Tech University, Lubbock, Texas, United States, ²Nemak USA, Inc., Sheboygan, Wisconsin, United States, ³Department of Chemical Engineering, Texas Tech University, Lubbock, Texas, United States

Magnetic hyperthermia is a promising, minimally invasive cancer treatment that utilizes heat generated by magnetic nanoparticles under an alternating magnetic field (AMF) to selectively destroy tumor cells [1, 2]. The ability to reach therapeutic temperatures (42–46 °C) within the tumor while minimizing damage to healthy tissues makes it a compelling strategy in oncology. Particle shape and size significantly influence heating efficiency by affecting magnetic anisotropy and energy dissipation. In this study, we compare the hyperthermia performance of iron oxide nanoparticles (IONPs) with varying shapes (cubic, spherical) and sizes (8, 12, and 35 nm). Here, we showcase the hyperthermia performance of 8 nm spherical (Fig. 1 (A)) and 35 nm cubic (Fig. 1 (B)) IONPs dispersed in fetal bovine serum (FBS), a physiologically relevant medium. Both types were synthesized via controlled hydrothermal methods and functionalized with polyethylene glycol (PEG) to enhance colloidal stability and biocompatibility. Heating

performances of IONPs (Fig. 1(C)) were characterized under an AMF of 30 mT (23.9 kA/m) and 101.5 kHz for 30 minutes in a 1 mL vial, within the clinical safety threshold of 5 × 10^9 A/m/s [3]. Our results show that 35 nm cubic IONPs exhibit superior heating efficiency compared to their spherical counterparts, attributed to their higher magnetic anisotropy and better hysteresis losses. These findings highlight the critical role of particle shape, size, and surface modification in optimizing magnetic hyperthermia agents for clinical translation.

[1] C. Caizer, "Magnetic/Superparamagnetic hyperthermia in clinical trials for noninvasive alternative cancer therapy," *Magnetic Nanoparticles in Human Health and Medicine: Current Medical Applications and Alternative Therapy of Cancer*, pp. 430-463, 2021.

[2] B. Rezaei *et al.*, "Investigation on the Magnetic Hyperthermia Performance of Commercial Iron Oxide Magnetic Nanoparticles," *IEEE Transactions on Magnetics*, 2025.

[3] S. Dutz and R. Hergt, "Magnetic nanoparticle heating and heat transfer on a microscale: Basic principles, realities and physical limitations of hyperthermia for tumour therapy," *International Journal of Hyperthermia*, vol. 29, no. 8, pp. 790-800, 2013.

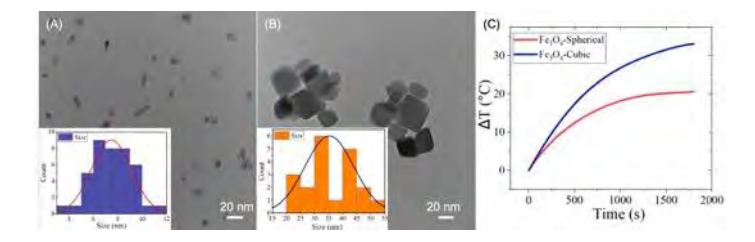


Fig. 1. TEM image and particle core size distribution of (A) spherical and (B) cubic Fe_3O_4 MNPs. (C) Magnetic hyperthermia performance of IONP samples at concentrations of 7 mg/mL.

CQ-08. Magnetic Orientation of Monosodium Urate Crystals in Microspaces: Implications for Gout Diagnosis

A. Hamasaki¹, Y. Takeuchi²

¹Faculty of science, Shinshu University, Matsumoto, Japan, ²Muroran Institute of Technology, Muroran, Japan

Gout is characterized by accumulation of crystals and inflammation in the joints. It has a high recurrence rate and a significant treatment discontinuation rate, highlighting

the need for the continuous suppression of recurrence (1). Current diagnostics, such as serum uric acid measurements performed only at medical institutions, are insufficient for continuous home risk evaluation (2). We are researching "magnetic orientation," in which monosodium urate (MSU) crystals, the cause of gout, are aligned under a permanent magnet's field (3). By externally irradiating near-infrared light and applying a magnetic field, we aimed to evaluate crystalinduced light-intensity changes, thus realizing a noninvasive gout diagnostic device for home use (4). Crystals can exist in microscopic areas of the joints of the fingers and feet. Therefore, to examine the orientation behavior of the crystals in a microspace, a thin-layer cell (Fig. 1), whose thickness could be adjusted at will, was placed in an electromagnet, and the transmitted light intensity of a crystal suspension was measured. Crystals with lengths of approximately 15 µm were artificially created, and sapphire was used as the window material for the cell. When the thickness of the film in the space where the crystal suspension was injected was narrowed from 800 µm to 50 µm, the change in light intensity became smaller, as shown in Fig. 2, but this was mainly due to a relative decrease in the number of crystals present in the light path. However, the orientation speed remained almost unchanged. Thus, although the orientation speed was affected when the crystals and solvent were affected by the surface, they behaved the same as in the bulk case, even in a space with a width of 50 µm. This shows that it is possible to orient the crystals using a magnetic field, even in a narrow space inside the body, provided there are no specific adsorption points.

[1] V. Beslon, P. Moreau and A. Maruani, *Journal of General Internal Medicine*, 33, 358–366 (2018).

[2] Y. Takeuchi, Y. Sugawara and T. Sugawara, *IEEE Transactions on Magnetics* 50, 11 (2014).

[3] Y. Takeuchi and M. Iwasaka, *IEEE Transactions on Magnetics* 52, 7 (2016).

[4] Y. Yang, Y. Song and X. Bo, *Nature Biotechnology* 38, 217–224 (2020).

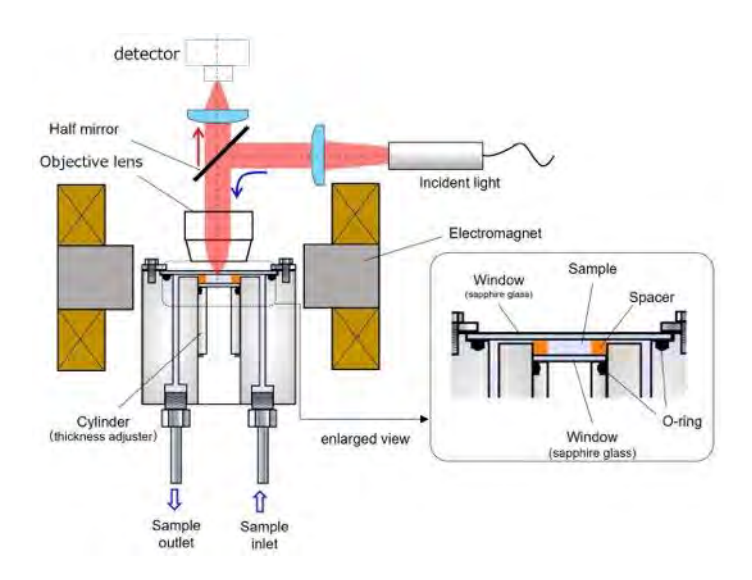


Fig. 1 Observation system of microspace under microscope

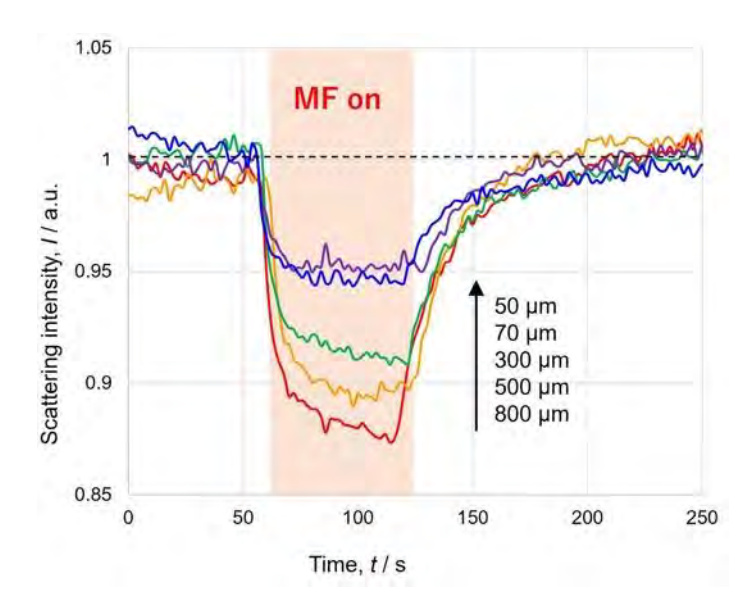


Fig. 2 Scattering intensity versus time with varying film thicknesses

CQ-09. Anatomical and Conductive Rhesus Macaque Head Phantom for E-field sensing in Transcranial Magnetic Stimulation.

W. Lohr¹, T. Atalugama², M. Basker², R. L. Hadimani²
¹Biomedical Engineering, Virginia Commonwealth University, Richmond, Virginia, United States, ²Mechanical and Nuclear Engineering, Virginia Commonwealth University, Richmond, Virginia, United States

Transcranial magnetic stimulation (TMS) is an increasingly used neuromodulation technique that allows both assessment and modulation of neural circuits. It holds promise for a range of therapeutic and research applications, including those involving nonhuman primates (NHPs), which serve as valuable translational models due to their neuroanatomical and functional similarities to humans. Despite growing interest in preclinical TMS studies, particularly involving NHPs, the availability of accurate, anatomically realistic, and reproducible phantom models remains extremely limited. Researchers working with live NHPs are all too familiar with the logistical and ethical hurdles involved in gaining approval from the Institutional Animal Care and Use Committee (IACUC) which is timeconsuming, resource-intensive, and restrictive. To help reduce the dependency on live animal subjects while enabling robust experimental design, we present the design, fabrication, and validation of a novel head phantom modeled after the rhesus macaque.

This phantom (Fig1) was developed using magnetic resonance imaging (MRI) data from an NHP to replicate head geometry and incorporate anatomy including skin, skull, and brain analogs. Brain equivalent tissue was created using a composite material composed of polydimethylsiloxane (PDMS) and carbon nanotubes (CNTs), selected for their ability to mimic the electrical conductivity of brain matter. This material combination offers conductive medium suitable for repeated stimulation and measurement.

To capture the electric field (E-field) distributions induced by TMS, triaxial dipole probes (TDPs) were strategically embedded within the brain region of the phantom. These probes are capable of resolving the full vector components of the E-field at multiple spatial locations, enabling detailed 3D field mapping when stimulated using a standard figure-of-eight TMS coil. Measured data will be compared to results from FEM simulations conducted in Sim4Life (Fig2).

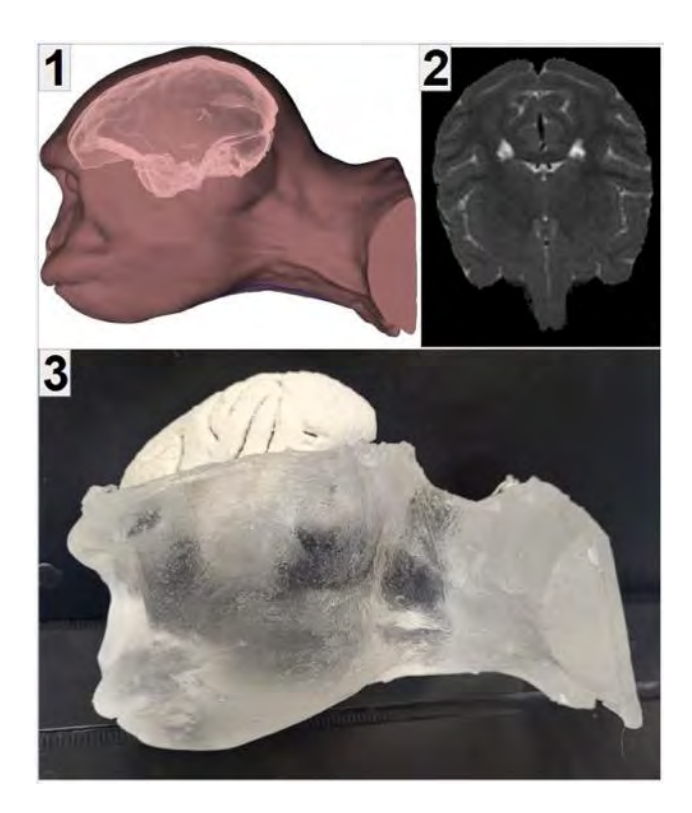


Fig 1: Phantom Pipeline. 1) MRI 2) STL 3) head phantom

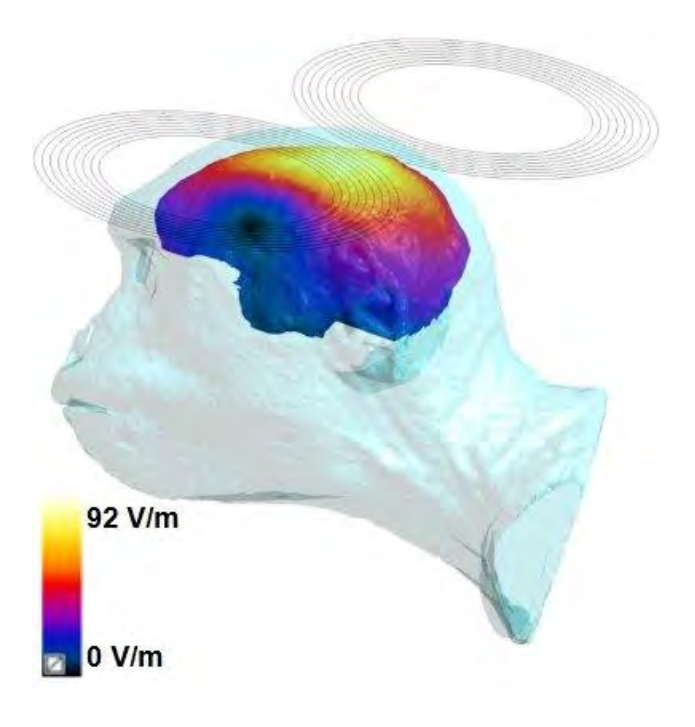


Fig 2: E field simulation of macaque phantom showing peak stimulation of 92 V/m

SESSION CR: SOFT MAGNETIC MATERIALS II (POSTER SESSION)

Chair(s): N. Alatawneh, Sacred Heart University, Trumball,
Connecticut, United States
Wednesday, October 29, 2025
09:00 AM-12:00 PM
Exhibit Hall Posters

CR-01. Analysis of Domain Wall Pinning and Anomalous Eddy Current Losses via Multiscale Magnetic Simulations

<u>Y. Shima</u>¹, T. Yamazaki¹, S. Tamaru², C. Mitsumata³, A. L. Foggiatto¹, M. Kotsugi¹

¹Department of Materials Science and Technology, Tokyo University of Science, Tokyo, Japan, ²National Institute of Advanced Industrial Science and Technology, Tsukuba, Ibaraki, Japan, ³University of Tsukuba, Tsukuba, Ibaraki, Japan

Iron losses are one of the key factors determining the performance of soft magnetic materials and reducing them is crucial for enhancing the performance of power-electronics devices to meet the surging energy demand [1]. Among the components that constitute iron losses, anomalous eddy current losses that become pronounced under high-frequency magnetic fields remain insufficiently understood due to the complex dynamics of domain wall motion. In this study, we aim to elucidate the relationship between domain wall dynamics and anomalous eddy current losses by performing multiscale magnetic simulations based on the coupled Maxwell-LLG equations [2], focusing on domain wall pinning phenomena in a single domain wall.

Finite element method-based multiscale simulations were carried out using the Micromagnetics Module [3, 4] and the AC/DC Module of COMSOL Multiphysics, modeling a single domain wall within an amorphous alloy (Fig. 1). Material parameters for the amorphous alloy were set as follows: saturation magnetization $M_{\rm s}=9.57\times10^5$ A/m, exchange stiffness $A=1.0\times10^{-11}$ J/m, and anisotropy constant $K_{\rm x}=3.0\times10^5$ J/m³. Simulations were conducted with an external magnetic field of up to $\mu_0H=50$ mT at a frequency of 100 MHz.

Figure 2 shows the color maps of the *x*-component of magnetization and the current density obtained from the coupled simulations. The domain wall was pinned and distorted at the pinning site, and upon depinning we observed a localized enhancement of current density both in the vicinity of the pinning site and along the domain wall.

These findings suggest that the rapid motion of the domain wall driven by the need to release the locally elevated magnetic energy caused by its distortion contributes directly to the increase in anomalous eddy current losses. In the presentation, we will include a detailed analysis of the magnetic energy and carry out a quantitative discussion of how variations in domain-wall curvature and velocity, depending on the pinning-site type, correlate with the observed losses.

- [1] Silveyra, Josefina M., *et al.*, Science 362, no. 6413 (2018): eaao0195.
- [2] Shima, Y., *et al.*, Journal of Applied Physics., 137.12 (2025)
- [3] Yu, Weichao, Jin Lan, and Jiang Xiao, Physical Review Applied., 13.2 (2020): 024055
- [4] Hua, Chensong, Kai Wu, and Weichao Yu., Woodhead Publishing, pp. 37-80., (2024)

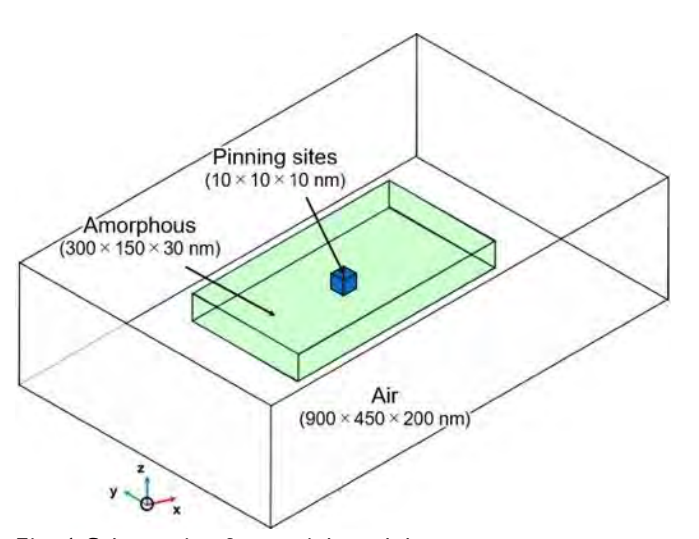


Fig. 1 Schematic of material model.

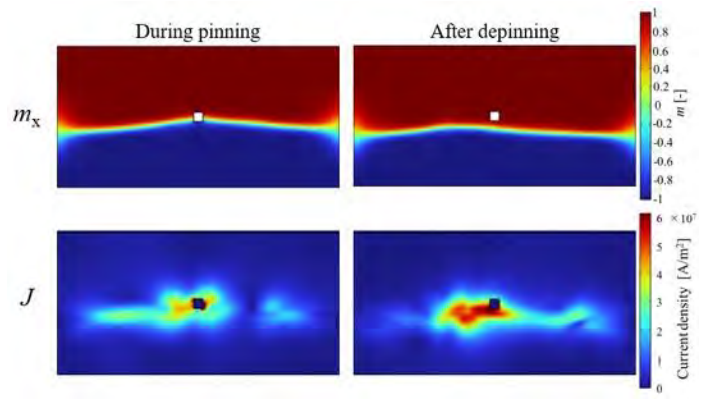


Fig. 2 *x*-component of magnetization and current density during pinning and after depinning.

CR-02. *Ab initio* study of promising antiferromagnetic aluminides for magnetocaloric applications

H. Aihemaiti¹, E. Dastanpour¹, A. Bergman², L. Vitos^{1, 2}

¹Material Science and Engineering, KTH Royal Institute of Technology, Stockholm, Sweden, ²Department of Physics and Astronomy, Uppsala university, Uppsala, Sweden

The electronic structure, phase stability, and magnetic properties of binary alloys containing 3d magnetic transition elements (Cr, Mn, Fe, Co, Ni) with Al are investigated using Density Functional Theory (DFT). Our results confirm that among all five aluminides, the ordered B2 phase is more stable than the disordered body-centered cubic structure. Of these studied elements, cobalt shows the highest tendency to form a stable B2 phase with aluminum. The AlCo and AlNi compounds are non-magnetic in the B2 structure, while AlFe is found to be weakly magnetic, in line with previous DFT calculations. Direct ab initio total energy calculations and magnetic simulations based on Heisenberg Hamiltonian built from ab initio exchange interactions predict an antiferromagnetic ground state for B2 AlCr. The Al(Cr_{1-x}Co_x) system undergoes an antiferromagnetic-to-ferromagnetic transition with Co level near 22 at. %. The ferromagnetism of B2 Al(CrCo) is largely attributed to Cr atoms [1]. The present findings contribute to a deeper understanding of the phase stability and magnetic properties of AlX binary alloys, offering insights into the formation mechanisms of the B2 structure with 3d magnetic transition metals. The predicted ferromagnetic B2 Al(CrCo) system is a promising candidate for magnetocaloric materials resembling the well-known B2 FeRh prototype [2].

- 1. H. Aihemaiti, E. Dastanpour and L. Vitos, First-principles study of phase stability and magnetic properties of B2 AlCr, AlMn, AlFe, AlCo and AlNi aluminides, Phys Rev Mater (under review) (2025).
- 2. G. Shirane, R. Nathans and C. W. Chen, Magnetic moments and unpaired spin densities in the Fe-Rh alloys, Phys. Rev. 134, A1547 (1964).

^{*} Best Student Presentation Finalist / LB - Late-breaking Poster

CR-03. Influence of Annealing Treatment on Magnetic Properties of Submicron Sized Amorphous Fe-Co-B Particles

<u>K. Sato</u>¹, K. Wakabayashi¹, S. Ajia¹, T. Miyazaki¹, S. Muroga¹, Y. Endo^{1, 2}

¹Graduate School of Engineering, Tohoku University, Sendai, Miyagi, Japan, ²Center for Science and Innovation in Spintronics, Tohoku University, Sendai, Miyagi, Japan

Submicron sized Fe-Co based alloy particles are focused on one of the candidates as magnetic materials for next-generation inductors because they have the high saturation magnetization and can suppress the eddy current loss in the frequency range near GHz.

Until now, we have reported that the submicron sized amorphous Fe-Co-B particles synthesized by aqueous solution reduction method showed excellent high frequency magnetic properties, but that their coercivity became high¹⁾. Therefore, their static magnetic properties must be improved to use as magnetic materials for the inductors. To address this issue, the annealing treatment is one of effective methods because it was reported that the coercivity of submicron sized Fe-B particles synthesized by the same method decreased from 40 Oe to 23 Oe by annealing treatment²⁾. Herein, we investigated the influence of annealing treatment on magnetic properties of submicron sized amorphous Fe-Co-B particles synthesized by aqueous solution reduction method.

As shown in Fig.1, in case of the as-synthesized particles, they were spherical with smooth surfaces. Their median size was approximately 470 nm with the size distribution of 390 – 640 nm. In contrasts, in case of the annealed particles, both the median size and the size distribution were almost similar to those of as-synthesized particles, but the surface was different from that of as-synthesized particles: it was rough. The reason for this may be that the structure changed for $T_a \ge 400$ °C.

As can be seen in Fig. 2, for $T_a \le 250$ °C, H_c significantly decreased from 80 Oe to 10 Oe with the increase of T_a owing to the internal stress release. On the other hand, for $T_a \ge 250$ °C, H_c increased with the increase of T_a because the structure changed with the increase of annealing temperature, i.e. not only amorphous phases but also the bcc-Fe-Co phases appeared.

Therefore, these results demonstrate that Fe-Co-B particles annealed at around 250 °C remained in amorphous state, and that their soft magnetic properties can be improved markedly.

- 1) K. Sato et al., Abstracts of the 175 th Fall Meeting of JIMM., p.399 (2024)
- 2) C. Masumoto et al., T. Magn. Soc. Jpn. (Special Issues), Vol.9, p.7-11 (2025)

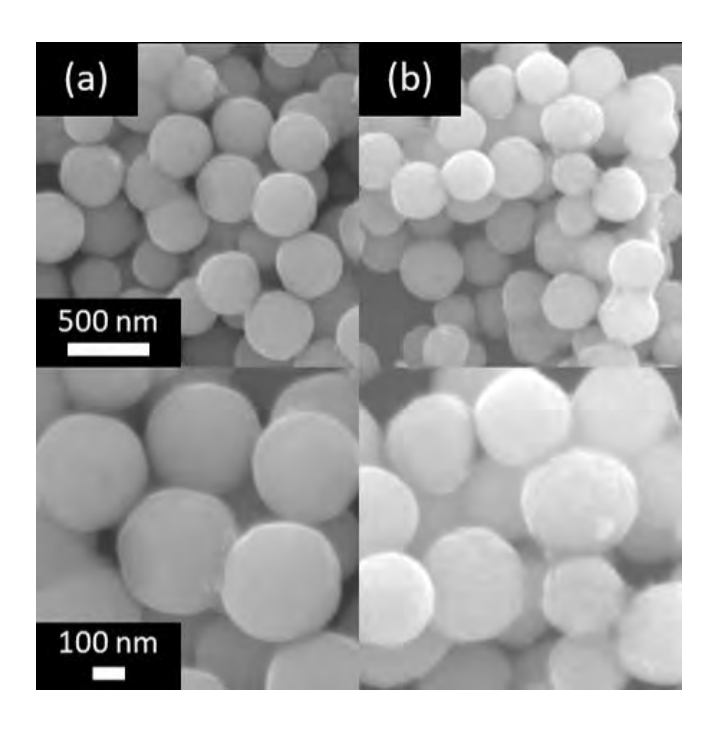


Fig.1 SEM images of (a) as-synthesized and (b) annealed (400 °C) Fe-Co-B particles.

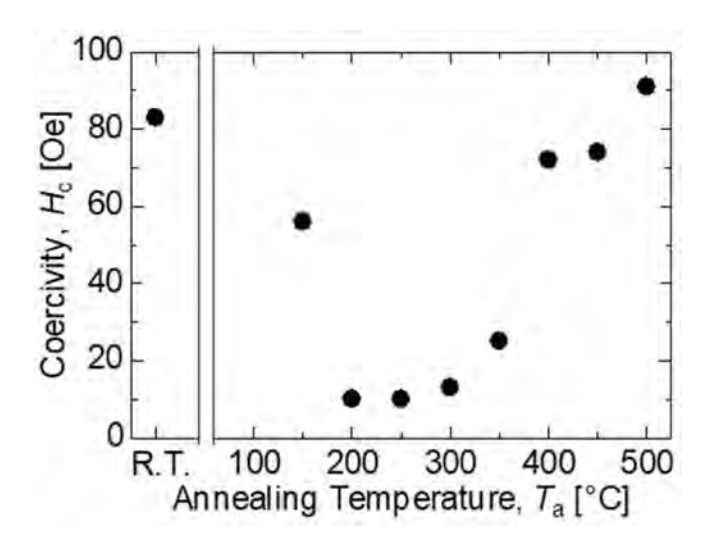


Fig.2 Annealing temperature dependence of coercivity for Fe-Co-B particles.

CR-04. 120 °C Si-O insulating shell formation on iron nanoparticles synthesized from micron-size magnetite by gas-solid reaction

<u>A. Nishikura</u>, M. Miyazawa, H. Nakashinden, M. Tobise, S. Saito

Tohoku University, Sendai, Japan

Inverters for power electronics require inductors with large excitation amplitude and high-frequency response. Thus, inductors' cores must have high saturation magnetic flux density, low hysteresis loss and low eddy current loss. As core material, iron-rich soft magnetic particles are promising because of their high saturation magnetization and low loss. While for suppressing eddy currents, resin coating on particles is often used though, it tends to be thick, inhomogeneous and low heat resistivity. Hence, we formed insulating shells on iron nanoparticles by a gas-solid reaction.

Adding Si and Al to bcc-Fe is important for introducing soft magnetic properties and forming shell. There are several reports on shell formation to FeAl powder, thus, we focus on FeSi powder. Micron-size magnetite (Fe, Si)₃O₄ was selected as raw powder. Samples were obtained by reducing the raw powder in hydrogen, followed by oxidation in dry air. Fig. 1 shows images of a sample observed by (a) scanning transmission electron microscope (STEM) and (b) high-angle annular dark field (HAADF). Reaction conditions were 600 °C reduction for 2 h and 120 °C oxidation for 1 h. It can be seen from (a), particle size is ca. 40 nm; from (b), a dark area covers a bright area. These mean nanoparticles with coreshell structure were obtained by present gas-solid reaction. Fig. 2 shows frequency f dependence of (a) the real and (b) imaginary parts of impedance Z of sample synthesized by 550 °C reduction for 2 h and oxidation for 1 h. The sample was measured without binder resin. Re[Z] changes 400 times at 120-130 °C and 4.5 times at 130-140 °C, which means particles take core-shell and oxide. Im[Z] decreases with a constant slope for 1/f in the high f, which means appearance of capacitivity. Assuming Measured object is homogeneous structure, effective saturation magnetization, resistivity and relative dielectric constant of the nanopowder are 176 emu/g, 47.1 Ω cm and 51.5. The gassolid reaction allowed the iron nanoparticles to have relatively high magnetization and resistance with capacitivity.

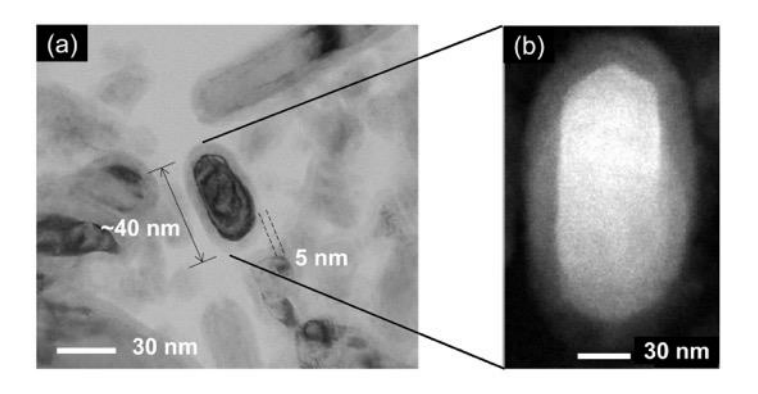


Fig. 1 Images of nanoparticles obtained by (a) STEM and (b) HAADF.

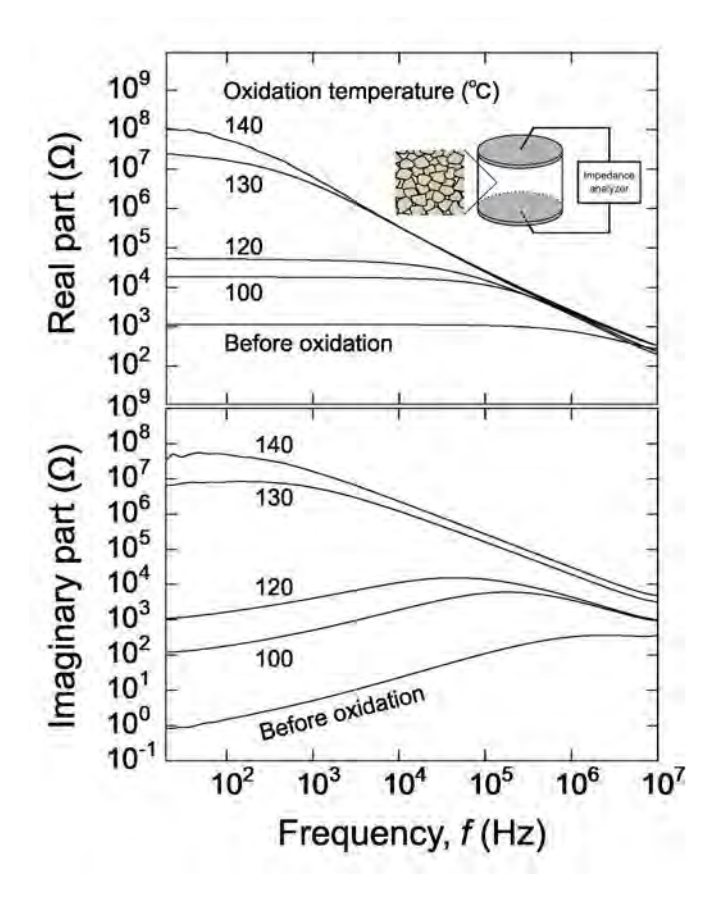


Fig.2 Frequency dependence of (a) the real and (b) imaginary parts of impedance of nanopowder.

CR-05. Additive manufacturing of soft ferrite components B. Capraro¹, S. Bachmann², R. Wachs², H. Lauterbach³, O. Horst³

¹Fraunhofer Institute for Ceramic Technologies and Systems IKTS, Hermsdorf, Thuringia, Germany, ²Tridelta Weichferrite GmbH, Hermsdorf, Thuringia, Germany, ³QSIL Metals Hermsdorf GmbH, Hermsdorf, Thuringia, Germany

In recent years, a wide variety of processes for the additive manufacturing of complex components have become established on the market. Most of these processes are powder-bed-based. The advantage of these processes is the great freedom in design, but the surface quality, structure, and precision, as well as the ability to print intricate, finely structured details, often fall short of the requirements of industrial applications.

Three-dimensional screen printing is an extension of traditional screen printing, in which only one layer or a few layers are deposited. Screen printing is an established industrial manufacturing process used worldwide in the electronics industry, solar industry [1], and, for example, in the production of ceramic sensors [2]. Three-dimensional screen printing combines the advantages of traditional screen printing with the complexity of powder-bed-based additive manufacturing processes. It is particularly interesting due to the optional screen change. This allows complex components with special functions to be printed. Freely overprinted channels without additional support structures represent a special feature of the process. In the traditional process chain to produce soft-ferritic components, the raw material is already in a water-bound emulsion before pressing. This is used to adjust the rheological properties of the emulsion with the help of suitable additives to create a printable paste. This paste is the basis for what are probably the world's first printing tests with soft ferritic powders using 3D screen printing. The poster shows the results of the realization of complex soft ferritic components and compares the magnetic performance of screen-printed components with conventionally manufactured ones. The field emission scanning electron microscopy (FE-SEM) images show no significant differences in the microstructure between these components (Tab. 1). After adjusting the sintering regime, slightly lower power losses were measured for the additively manufactured components. This can be further improved by adjusting the ferrite particle size and the printing process parameters as well as further optimizing the sintering regime.

- [1] Ansgar Mette, PhD thesis, New Concepts for Front-Side Metallization of Industrial Silicon Solar Cells, Fraunhofer Institute for Solar Energy Systems, Freiburg im Breisgau, 2007
- [2] Stefan Stolz, PhD thesis, Screen Printing of Electrically Conductive Ceramics for the Development of Heat able Ceramic Micro components, Faculty of Applied Sciences, Albert Ludwig University of Freiburg im Breisgau, 2002

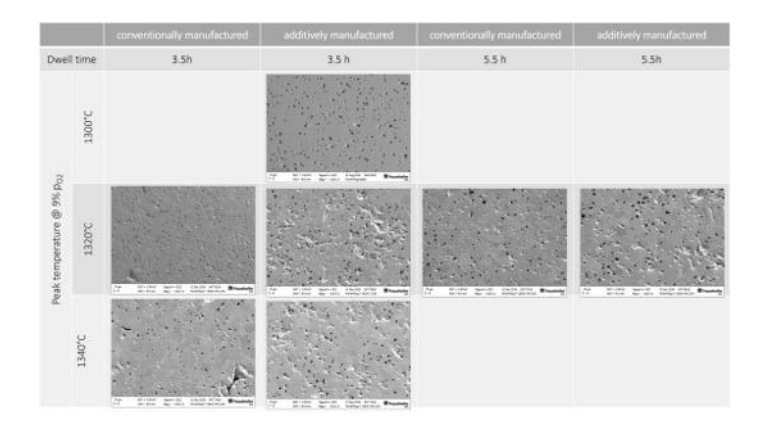


Figure 1

CR-06. Research on High Thrust Density Permanent Magnet Vernier Linear Electric Machine for Gravity Energy Storage Systems Based on High Saturation Magnetic Flux Density Materials

J. Yuan, Q. Wu, H. Zhou School of Electrical Engineering and Automation, Wuhan University, Wuhan, China

With the development of new power systems, the demand for new energy storage technologies is gradually increasing. Gravity energy storage (GES) technology has received widespread attention due to its advantages of environmental friendliness, long life and flexible siting, etc. GES can be categorized into linear motor (LM) type and rotary motor (RM) type. Compared with RM-GES, LM-GES has the advantages of high efficiency, fast response speed and high structural integration. The core unit of LM-GES is LM, and the primary performance requirement of GES for LM is to have large thrust, while the magnetic field modulation type permanent magnet vernier linear motor (PMVLM) is the typical representative of realizing large thrust. Since the core of the traditional PMVLM is made of silicon steel, its saturation flux density is around 1.8T, and the core flux density directly affects the thrust performance, which will limit the upper limit of thrust enhancement. To address this limitation, the core flux density characteristics of the

conventional structure are first analyzed (Fig. 1(b)), and it is found that the larger flux density region is located at the tooth tips and necks of the core teeth, which can reach up to 2.18T. In response to this phenomenon, this paper proposes a solution that integrates a high saturation flux density (HSFD) tooth sleeve (TS) and magnetic core (MC) as shown in Fig. 1(a), in which the TS and the MC both adopt the Carpenter-Rotelloy 8 with HSFD. In Fig. 1(b), the maximum magnetic density of the PMVLM with TS only is up to 2.67T, and that of the PMVLM with TS and MC at the same time is up to 2.76T, which breaks through the limitation of the traditional silicone steel material. Comparative analysis of the average thrust and core loss is shown in Fig. 2(a) and (b), which indicates that the new scheme does not cause an increase in core loss, while there is a more significant increase in thrust. In addition, the noload induced voltage and flux linkage of the new scheme and the conventional scheme are also analyzed, as shown in Fig. 2(c) and (d), which further validate the advantages of the new scheme.

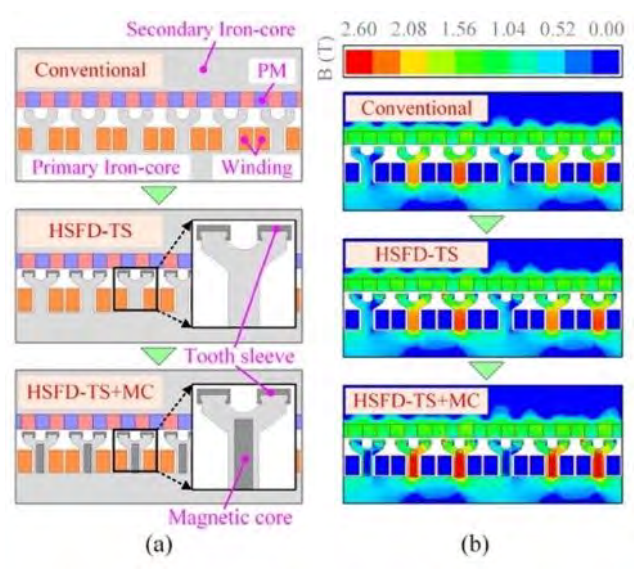


Fig.1 PMVLM structure and flux density analysis

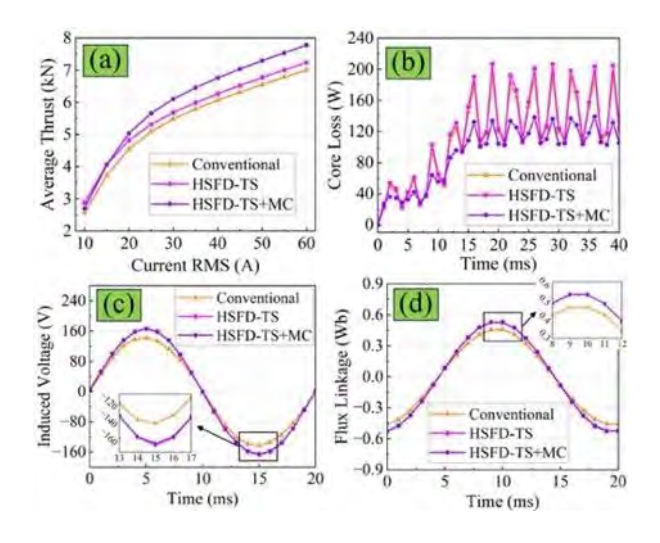


Fig.2 Comparative analysis of performance

CR-07. Giant Magnetization and Low Anisotropy in Zn-Doped Cobalt ferrite

<u>F. Bakhshizadeh</u>¹, F. Efe¹, D. Alharbi^{1, 2}, M. Guy¹, M. Davis¹, A. Lisfi¹

¹Physics, Morgan State University, Baltimore, Maryland, United States, ²Physics, The Catholic University of America, Washington DC, District of Columbia, United States

Cobalt ferrite is one of the most important magnetic oxides of the spinel family due to its large magnetostriction (-590 ppm) and high anisotropy (0.33 MJ/m³) [1-2]. The high anisotropy is believed to be generated by Co ions, which tend to occupy octahedral sites in the regular inverted structure. However, despite its highly magnetic constituents (Fe³⁺ and Co²⁺), its magnetization is relatively low (80 emu/q) due to the antiferromagnetic order within its lattice unit. To make this material attractive to technology applications such as sensing and actuating and enhance its performance, it is important to reduce its anisotropy, increase its magnetization and suppress hysteresis from its magnetic response to external fields. To achieve these goals, we launched a thorough investigation to study the effects of substituting cobalt with zinc on the magnetic properties of the Zn-dope ferrite. The material of interest (Co_{1-x}Zn_xFe₂O₄) was prepared with ball milling in the form of a powder with different Zn concentrations (x=0.2, 0.4, 0.5). Samples were compacted and annealed at different temperatures up to 1400 °C, while another set of samples was quenched from high temperatures. The prepared samples were the subject of structural and chemical analyses with AFM, XRD, XPS and Raman scattering,

whereas their magnetic properties were characterized by using VSM, MFM and torque magnetometer. This study reveals that the investigated material manifests enhanced properties, which consist of the following. (1) A giant magnetization of 98 emu/g was observed in quenched samples from 1400 °C. (2) The hysteresis loss is fully suppressed in the Zn-doped ferrite annealed at temperatures above 1200 °C. (3) A substantial drop in anisotropy is seen upon increasing the Zn concentration as illustrated by the magnetization curves portrayed in Fig. 1. All the investigation results will be discussed in detail in the presentation.

[1] R. M. Bozorth, Elizabeth F. Tilden, and Albert J. Williams, "Anisotropy and Magnetostriction of Some Ferrites." Phys. Rev. 99, 1788 – Published 15 September, (1955)
[2] A. Lisfi, C. M. Williams, L. T. Nguyen, J. C. Lodder, A. Coleman, H. Corcoran, A. Johnson, P. Chang, A. Kumar, and W. Morgan, "Reorientation of magnetic anisotropy in epitaxial cobalt ferrite thin films", PHYSICAL REVIEW B 76, 054405 (2007)

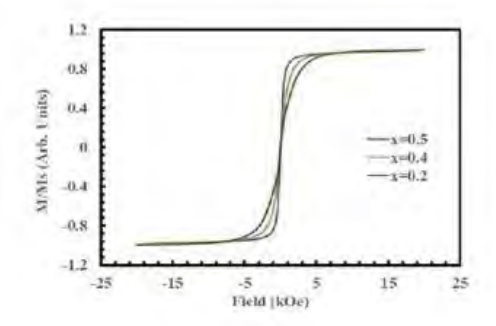


Fig. 1 Magnetization curves of $Co_{1-x}Zn_xFe_2O_4$ with 3 different Zn concentrations (0.2, 0.4 and 0.5) measured at fields between -20 kOe and +20 kOe. Note that the magnetization saturation field is largely reduced upon increasing the Zn concentration, which illustrates a substantial decrease in magnetic anisotropy.

CR-08. Magnetostriction of Iron-Based Binary Alloys

T. Fukuzaki, T. Inoue, T. Kanematsu, T. Yoshimoto Nidec Product Technology R&D Center, NIDEC CORPORATION, Kawasaki, Kanagawa, Japan

Relative permeability is one of the most important properties for determining the magnetic flux path within a motor's magnetic circuit design. Magnetostriction, on the other hand, is a magnetic phenomenon that causes changes in a material's dimensions during the magnetization process. There is a close relationship between magnetostriction and relative permeability. Our research investigates a variable magnetic flux motor that utilizes magnetostrictive materials in which the relative permeability changes with the stress induced by centrifugal force. To facilitate this, we are developing materials with large magnetostriction. We have prepared materials exhibiting large magnetostriction using iron-based binary alloys and have investigated their underlying magnetostrictive mechanisms. Alloy ingots with nominal compositions of $Fe_{1-x}M_x$ (x = 0-0.2) were prepared by arc melting. M represents an element that forms a solid solution with iron; specifically, Si, Al, Ge, Ga, Ni, Co, and V were selected for this study. Magnetostriction was measured by the strain gauge method using a single-plate DC magnetization measurement system for field strengths up to 20,000 A/m. Fig. 1 shows the magnetostriction as a function of the lattice constants for Fe-Co, Fe-V, Fe-Al, and Fe-Ga alloys. The magnetostriction of Fe-V, Fe-Al, and Fe-Ga alloys increased with increasing lattice constants. These results suggest that increasing the lattice constants decreases the interatomic energy among iron atoms, thereby influencing magnetostriction. Conversely, the magnetostriction of Fe-Co alloys did not show a direct correlation with the lattice constants. The magnetostriction of Fe-Co alloys is primarily determined by the magnetic anisotropic energy because Co atoms significantly influence the magnetic anisotropic energy of iron atoms. This suggests that magnetostriction is determined by the interplay between the interatomic energy and the magnetic anisotropic energy among iron atoms.

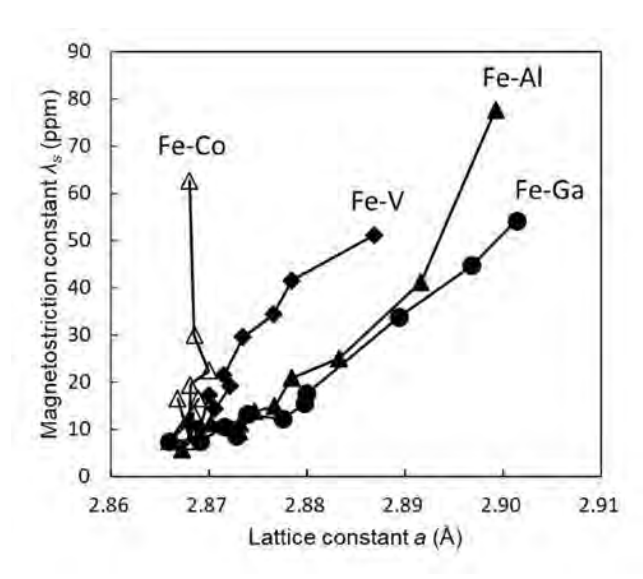


Fig. 1 Magnetostriction as a function of the lattice constants for Fe-Co, Fe-V, Fe-Al and Fe-Ga alloys.

CR-09. Magnetometry of Buried Nanolayers by Hard X-ray Photoelectron Spectroscopy

<u>A. Hloskovsky</u>¹, C. Schlueter¹, G. Fecher²
¹Photon Science, DESY, Hamburg, Germany, ²Max Planck
Institute for Chemical Physics of Solids, Dresden, Germany

Magnetic circular dichroism (MCD) effect has a $\cos(\theta)$ dependence where θ is the angle between light polarization and sample magnetization. This yields direct information about the magnetization direction with respect to the polarization of the synchrotron X-ray beam for both, ferromagnetic or antiferromagnetic materials. Extracting quantitative information about absolute values of local magnetic moments is very challenging, because of complicated structure of photoelectron spectra. For example, the 4eV Co satellite cannot be explained by the solid-state calculations. The satellite obviously exhibits strong dichroism. This may be an indication of a correlationinduced satellite of majority spin nature in Co. Very recently, X-ray standing wave technique [1] was successfully combined with MCD-HAXPES measurements on HM/CoFeB/HM (HM=heavy metal) sample. Achieved depth resolution was sufficient to differentiate between the top and bottom interfaces of a 10nm thick CoFeB layer. Depth selective magnetic information was obtained by varying the angle of incidence across the angle of incidence θ =0.6. [1] P Vishwakarma, M Nayak, VR Reddy, A Gloskovskii, W Drube, A Gupta, Appl. Surf. Sci. 590 (2022) 153063

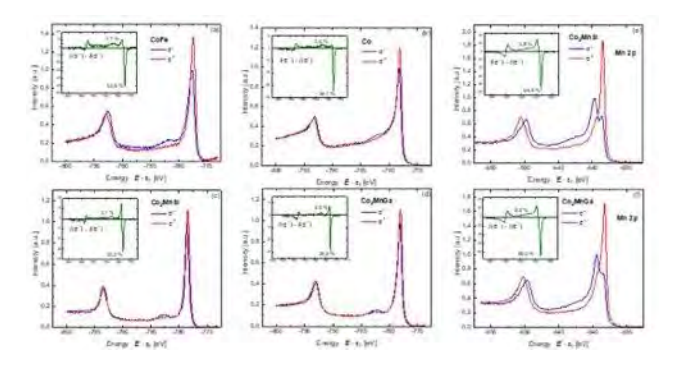


Fig. 1: Polarization-dependent core-level spectra for Co 2p excitations of CoFe (a), Co (b), Co2MnSi (c), Co2MnGa (d) and Mn 2p excitations of Co2MnSi (e), and Co2MnGa (f) thin films. Insets show dichroism in the HAXPES spectra.

CR-10. Fabrication and Evaluation of Magnetic anisotropy of Co-based Heusler alloy $Co_2FeAl_xSi_{1-x}$ epitaxial thin films

T. Hojo^{1,2}, H. Hamasaki², M. Tsunoda^{3,4}, M. Oogane^{2,5}
¹Department of Advanced Spintronics Medical Engineering,
Graduate School of Engineering, Tohoku University, Sendai,
Miyagi, Japan, ²Department of Applied Physics, Graduate School
of Engineering, Tohoku University, Sendai, Miyagi,
Japan, ³Department of Electronic Engineering, Graduate School
of Engineering, Tohoku University, Sendai, Miyagi,
Japan, ⁴Research Center for Green X-Tech, Green Goals
Initiative, Tohoku University, Sendai, Miyagi, Japan, ⁵Center for
Science and Innovation in Spintronics (Core Research Cluster)
Organization for Advanced Studies, Tohoku University, Sendai,
Miyaqi, Japan

For the development of highly sensitive tunnel magnetoresistance (TMR) sensors, it is essential to explore materials that simultaneously exhibit low magnetic anisotropy and high TMR ratio [1]. In our previous work, we demonstrated that the magnetocrystalline anisotropy constant K_1 can be tuned by adjusting the Al/Si composition in Co-based Heusler alloy $\text{Co}_2\text{FeAl}_x\text{Si}_{1-x}$ (CFAS as follows) thin films [2]. In this study, we report on the investigation of the annealing temperature dependence of K_1 for the compositions near the K_1 = 0 region.

The stacking structure of Cr (60 nm)/ Ag (20 nm)/ CFAS (50nm)/ Ta (3 nm) were deposited on MgO (001) single crystal substrate by magnetron sputtering. After deposition, annealing process was carried out at temperatures T_a from 300 to 600 degrees. Structural and magnetic properties of the CFAS layers were evaluated using XRD and VSM,

respectively. The magnetocrystalline anisotropy constant K_1 was determined by the in-plane angular dependence of the magnetic resonance field using FMR measurements.

The Cr layer functioned as a buffer layer to mitigate lattice mismatch and the Aq layer prevented diffusion of Cr atoms into the CFAS layer during annealing. In our samples, Cr/Ag buffer layers exhibited epitaxial growth along the (001) orientation. From the magnetization curve of CFAS, no reduction in saturation magnetization was observed for any sample after annealing, suggesting that Cr diffusion into the CFAS layer did not occur. XRD 2theta/omega profiles showed high (001) orientation and at least B2 ordering of the CFAS layer in all samples. Figure 1 shows the annealing temperature dependence of K_1 of the samples with various Al/Si composition The results indicate that K_1 is influenced not only composition but also by annealing temperature. This behavior is likely due to changes in the degree of B2 and L2₁ ordering induced by annealing. The technique for realizing Co-based Heusler alloy thin film with $K_1 \sim 0$ by controlling the composition and annealing temperature is important for dramatically increasing the sensitivity of TMR sensors.

[1] T. Nakano et al., Appl. Phys. Lett. 126, 160503 (2025)[2] T. Hojo et al., J. Magn. Magn. Mater. 601, 172144 (2024)

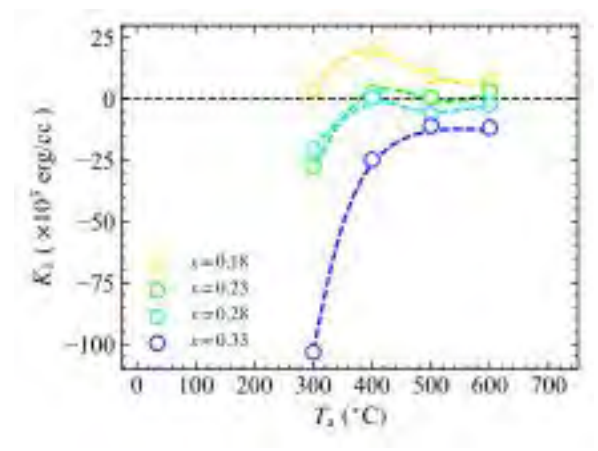


Figure 1 Annealing temperature dependence of K_1 in CFAS thin films with various Al/Si compositions.

CR-11. Enhancement of microwave absorption and resonance linewidth through large specific surface area of magnesium substituted Zn-Ni Ferrites

S. Kaushik¹, M. Dabla¹, P. Kumar¹, M. Sharma^{1, 2}, <u>B. K. Kuanr</u>¹

Special Centre for Nanoscience, Jawaharlal Nehru University,
New Delhi, Delhi, India, ²Department of Physics, Deshbandhu
College, University of Delhi, New Delhi, Delhi, India

Magnetic nanomaterials those exhibit reduced agglomeration and high surface area are attractive for various microwave applications. A lightweight and large specific surface area nanostructure plays a significant role in enhancing microwave absorption. We report the correlation between microstructural, magneto-dynamic and microwave absorption properties (K_u-band (12 GHz - 18 GHz)) of $Mq_xZn_{0.8-x}Ni_{0.2}Fe_2O_4$ ferrites (x=0.0,0.2,0.4,0.6). XRD pattern of the compositions matched with the space group Fd-3m of cubic spinel ferrite crystal structure [Fig.1(A)]. Mg²⁺ are considerably diffused into the ferrite crystal without sign of intermediate or secondary phases. From Rietveld refinement lattice parameters and crystallite size were observed to decrease with Mg substitution. The small ionic radius of Mq²⁺ compared to Zn²⁺reduced crystallite size, lattice constant and cell volume [1]. The decrease in cell volume increased surface area that affect magnetic properties and enhancing microwave absorption (RL: Reflection Loss). Mg substitution also increases in FMR linewidth and M_s value. The rise of M_s results in increase of permeability (μ) in ferrites. With increasing Mg content, permittivity (ε)decreases because Mg²⁺ replaces Fe³⁺ in tetrahedral sites, diminishing Fe²⁺/Fe³⁺ pairs in Octahedral sites [2]. Decreasing ϵ' and increasing μ' promotes impedance matching and improves the microwave absorption. We have observed maximum RL of -60.66 dB at 16.68 GHz, normalized impedance (Z=1.002) and attenuation constant (1070) for absorber thickness of 1.5mm [Fig. 2(C)] with 0.4 formula unit of Mg²⁺ substituted Zn-Ni Ferrites, that exhibit a low ε'' and a high μ'' . In addition, the ratio of μ' to ε' observed to be close to 1 which is a criterion for impedance matching delivering large RL. Hence, Mg_xZn_{0.8-} _xNi_{0.2}Fe₂O₄ nanoparticles can be good material to be studied for the various applications like shielding, attenuation, and the fabrication of electromagnetic induction-based flexible absorbing sheets.

[1] M. A. Darwish *et al.*, "Impact of the Mg/Zn ratio on features of structural and magnetic properties in A-site stoichiometric nanosized spinel ferrites," *J. Alloys Compd.*, vol. 968, no. August, p. 172278, 2023, doi:

^{*} Best Student Presentation Finalist / LB - Late-breaking Poster

10.1016/j.jallcom.2023.172278.

[2] C. B. N. K. and W. Madhuri, "Microwave assisted solid state reaction method: Investigations on electrical and magnetic properties NiMgZn ferrites," *Mater. Chem. Phys.*, vol. 181, pp. 432–443, 2016, doi: 10.1016/j.matchemphys.2016.06.079.

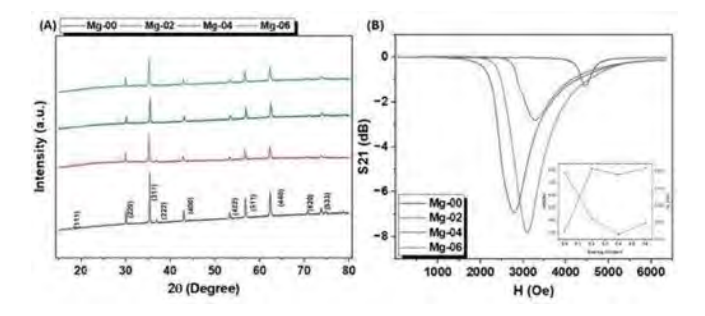


Fig. 1 (A) XRD and (B) FMR results

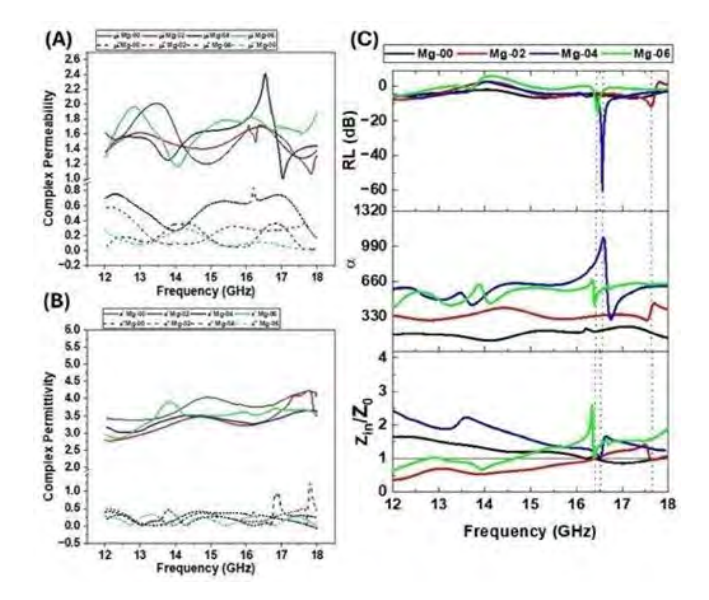


Fig. 2 (A) Permeability (B) Permittivity (C) RL, α and Z_{in}/Z_0

CR-12. Normalized switching field distribution for the thin film of Co

J. Hidalgo Gonzalez¹, S. P. Sánchez¹, <u>A. E. Oropesa</u>¹, J. Matutes²

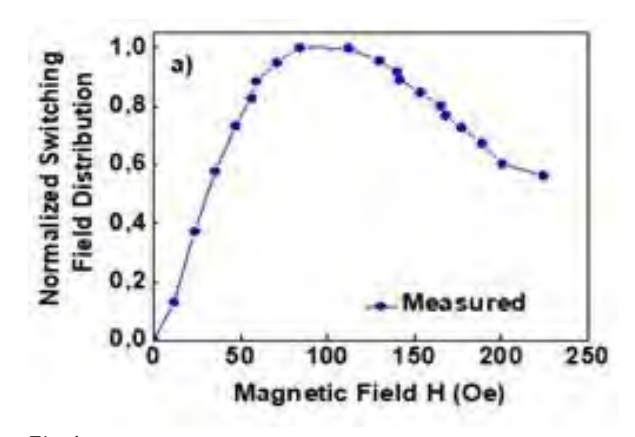
¹Universidad Autonoma de San Luis Potosi, San Luis Potosí, Mexico, ²Centro de Investigación en Materiales Avanzados, Chihuahua, Chihuahua, Mexico

Thin films of Co were obtained by electrodeposition at room temperature. The magnetic properties of thin films were measured at room temperature. Normalized SFDs for the thin film of Co were measured with an applied magnetic field perpendicular to the film plane. It is important to comment that thin films measured perpendicular to the film plane are actual important because these can present ferromagnetic interactions that in spin-pumping experiments produce a coupling in their excitation modes [1,2]. It is seen that the thin film of Co presents a SFD narrower that is important due to that it could be extend the magnetic recording to densities beyond 1 Tb/in². Normalized reduced effective anisotropy $\Delta N = /M$ for thins films with thickness different was determined. Modified IRM (1-2m_r) and m_d remanence curves as a function of magnetic field for thin films Co were measured with an applied magnetic field perpendicular to the film plane. The plot Modified IRM (1-2m_r) and m_d remanence curves show that they were not coupled curves and confirm the existence of magnetic interactions between the particles such that these were not coupled curves.

J. B. S. Mendes, R. O. Cunha, O. Alves Santos, P. R. T. Ribeiro, F. L. A. Machado, R. L. Rodriguez-Suarez, A. Azevedo, and S. M. Rezende. Large inverse spin Hall effect in the antiferromagnetic metal Ir20Mn80. PHYSICAL REVIEW B 89, 140406(R) (2014).

Atakan Tekgül, Mürsel Alper, Hakan Kockar. Simple electrodepositing of CoFe/Cu multilayers: Effect of ferromagnetic layer thicknesses. Journal of Magnetism and Magnetic Materials 421 (2017) 472–476.

^{*} Best Student Presentation Finalist / LB – Late-breaking Poster



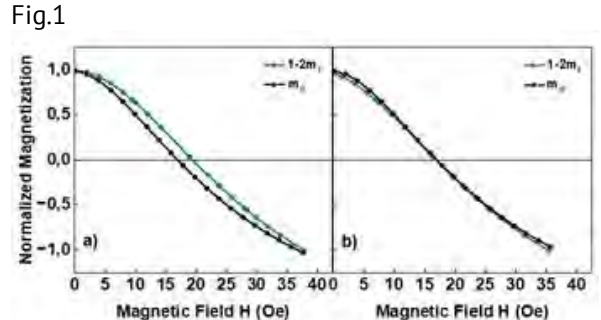


Fig 2.

CR-13. Exploring Interfacial Effects in Transition Metal Dichalcogenide / Ferrimagnetic Alloy Heterostructure L. Ramos, D. A. Arena, A. I. Ojo, H. Rodríguez Gutiérrez, Y. Wadumesthri

Physics, University of South Florida, Tampa, Florida, United States

Ferrimagnetic materials and 2-dimensional transition-metal dichalcogenide (TMDs) materials have recently attracted attention as promising candidates for spintronics applications due to their tunable magnetic properties [1] and proximity effect [2], respectively. We are particularly interested in the magnetic behavior of the WSe2/FeCoGd heterostructure system, as there is limited research on the effect of TMDs seed layer on the magnetic properties of FeCoGd.

In this study, we explore the influence of film thickness and specific TMD substrates on the magnetic properties of amorphous ferrimagnetic FeCoGd alloy thin films. A set of FeCoGd thin films in the range of 4-32nm, with a composition of Fe $_{73}$ Co $_{8}$ Gd $_{19}$, were fabricated using the magnetron sputtering technique on various substrates: Si, Si/WSe2bilayer, and Si/WSe2monolayer. A 5 nm capping layer of Ta was deposited to protect the films from oxidation and contamination. Structural analysis via X-ray

diffraction (XRD) confirmed the amorphous nature of the FeCoGd films, while energy-dispersive spectroscopy (EDS) verified their elemental composition. Raman spectroscopy was employed on Si/WSe2/FeCoGd, revealing the characteristic WSe2 peak at ~250cm⁻¹ and demonstrating that the sputtering process preserved the properties of the WSe2 seed layer. Magnetic properties were assessed using a vibrating-sample magnetometer (VSM).

Our findings reveal a soft magnetic phase, in-plane magnetic anisotropy, and tunability of the saturation magnetization and coercive field of FeCoGd thin films with varying thickness and substrate, as shown in Figures 1a & 1b. Additionally, a proximity effect of WSe2 on FeCoGd is observed, where both the saturation magnetization and coercivity depend on the WSe2 seed layer. Out-of-plane Magneto-Optical Kerr Effect (MOKE) measurements were employed to investigate the perpendicular magnetic anisotropy (PMA) as a function of thickness, revealing that the coercivity along the hard axis, and thus the PMA [3], is modulated by the presence of the WSe2 layer. These results demonstrate the potential of 2D WSe2 and amorphous ferrimagnetic FeCoGd alloy thin film heterostructures for tailoring magnetic properties in spintronic device applications.

- [1] K. Wang, L. Wu, Z. Xu, Z. Lu, R. Xiong, Extraordinary Hall effect of sputtered amorphous ferrimagnetic GdFeCo alloy films, Mater. Today Commun. 35 (2023) 106023
- [2] N. Zibouch, A. Kuc, J. Musfeldt, T. Heine, Transition-metal dichalcogenides for spintronic applications, Ann. Phys. 526 (2014) 201400137
- [3] M. Ding, S. Poon, Tunable perpendicular magnetic anisotropy in GdFeCo amorphous films, J. Magn. Magn. Mater. 339 (2013)

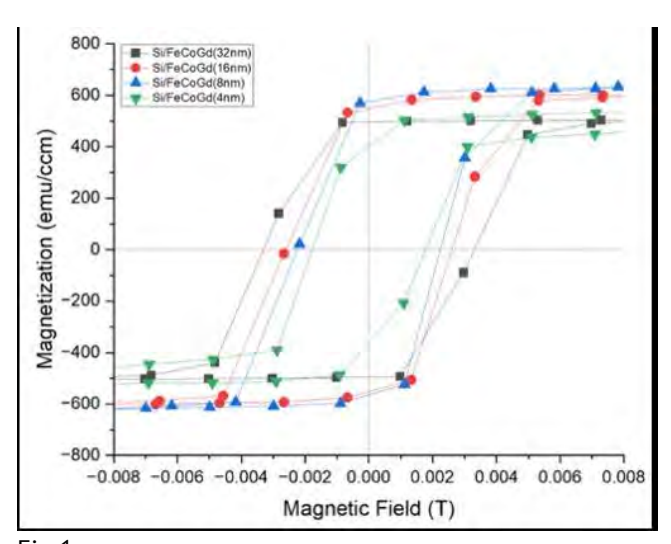


Fig 1a.

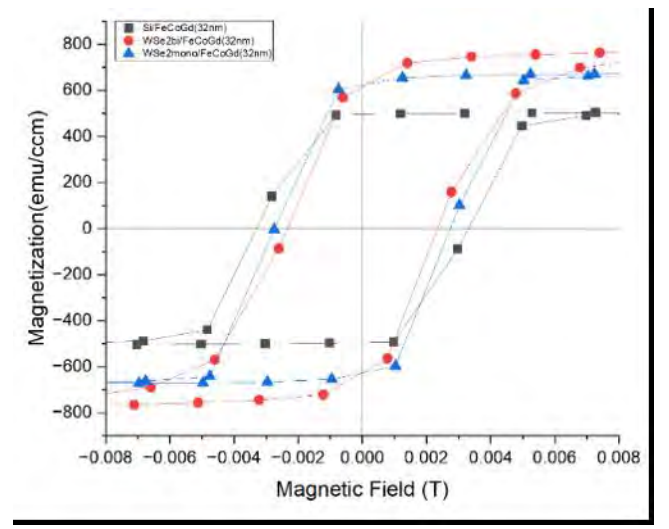


Fig 1b.

CR-14. Epitaxial CoFeMnGe Thin Films with Low Gilbert Damping: A Promising Quaternary Heusler Alloy for Spintronics

R. Roy Chowdhury, V. Mishra, A. I. Ojo, <u>R. Huligerepura Shankaregowda</u>, P. Sharma, D. DeTellem, H. Srikanth, D. A. Arena, S. Witanachchi, M. Phan *Department of Physics, University of South Florida, Tampa, Florida, United States*

Quaternary Heusler alloys (QHAs) are emerging as promising materials for spintronic applications due to their enhanced compositional flexibility, reduced structural disorder, and potential for high spin polarization, high Curie temperatures, and low Gilbert damping [1]. In this study, we investigate the temperature-dependent magnetic and spin dynamic properties of equimolar CoFeMnGe (CFMG) thin films—an epitaxial QHA system grown on (001)-oriented single-crystal MgO substrates with thicknesses of approximately 5, 30, and 40 nm. X-ray diffraction confirms a cubic structure, with in-plane lattice parameters, a, b, c = 5.742 Å, 5.749 Å, 5.751 Å, respectively, with a lattice mismatch of $\sim 3 - 4\%$ with respect to MgO substrate. Magnetometry reveals a high Curie temperature exceeding 400 K and soft ferromagnetic behavior, with an in-plane (IP) easy axis and out-of-plane (OOP) hard axis. The 30 nm film exhibits a saturation magnetization (M_S) of ~ 5.55 μ_B /f.u. at 10 K and 4.85 $\mu_{\rm R}/{\rm f.u.}$ at 300 K. Transverse magnetic susceptibility measurements display asymmetric bipolar scans (Fig.1), indicating anisotropy dispersion rather than uniaxial single-domain behavior. The effective magnetic anisotropy field decreases steadily with increasing temperature (inset, Fig.1). Temperature-dependent IP ferromagnetic resonance (FMR) measurements over a wide range of frequencies 18-40 GHz reveal q factors of ~ 2.11 at 10 K and 2.08 at 300 K. The effective Gilbert damping constants (α_{eff}) for the 30 nm film are ~ 2.23 × 10⁻³ at 10K and 2.03 × 10⁻³ at 300 K (Fig.2), which are substantially lower than those reported for the isostructural CoFeMnSi alloy [2]. Micromagnetic simulations reveal a multidomain ground state configuration with domain sizes ~ 95-140 nm. The combination of low damping, soft magnetic behavior, and high thermal stability positions CFMG thin films as a strong candidate for next-generation spintronic devices.

[1] K. Inomata, N. Ikeda, N. Tezuka, R. Goto, S. Sugimoto, M. Wojcik, and E. Jedryka, "Highly spin-polarized materials and devices for spintronics", *Sci. Technol. Adv. Mater.* 9, 014101 (2008).

[2] L. Bainsla, R. Yilgin, M. Tsujikawa, K. Z. Suzuki, M. Shirai, and S. Mizukami, "Low magnetic damping for equiatomic CoFeMnSi Heusler alloy", *J. Phys. D: Appl. Phys.* 51, 495001 (2018).

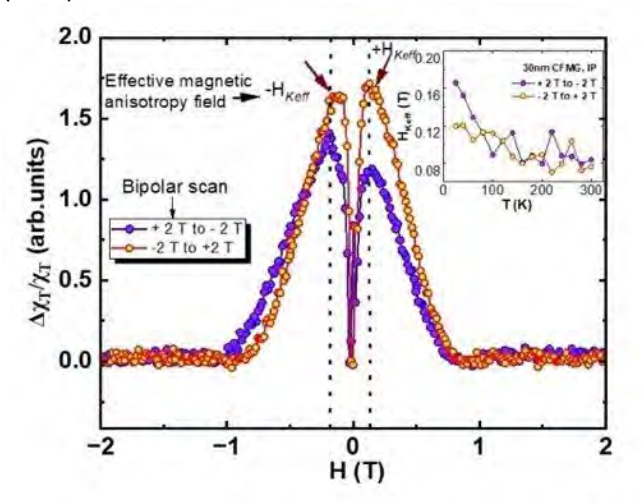


Fig.1 Magnetic field dependence of transverse susceptibility (inset shows temperature dependence of effective magnetic anisotropy field in 30nm CFMG)

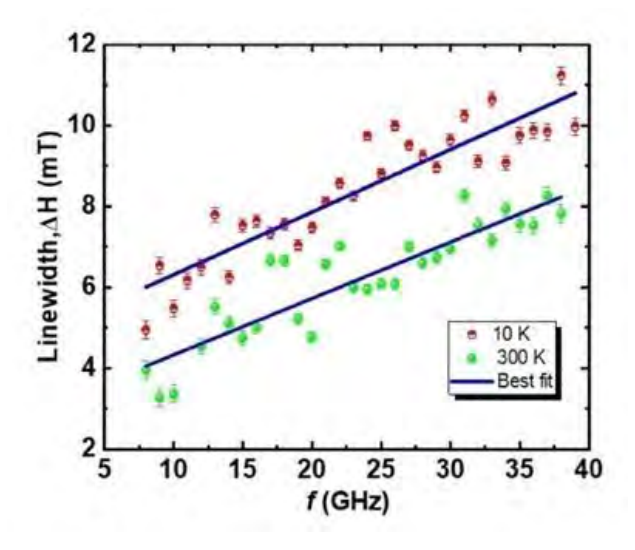


Fig.2 Linear fit of the frequency dependence of line width, ΔH , at 10K and 300 K from FMR.

SESSION DA: PERSPECTIVE OF PROBABILISTIC COMPUTING WITH MAGNETIC TUNNEL JUNCTIONS

Chair(s): G. Finocchio, *University of Messina, Messina, Italy*Wednesday, October 29, 2025
02:00 PM-05:30 PM
Grand Ballroom

DA-01. Advanced Designs of Stochastic Magnetic Tunnel Junctions for Spintronic Probabilistic Computing S. Kanai^{1, 2, 3}

¹Laboratory for Nanoelectronics and Spintronics, Research Institute of Electrical Communication, Tohoku University, Sendai, Miyagi, Japan, ²WPI-Advanced Institute for Materials Research (WPI-AIMR), Tohoku University, Sendai, Miyagi,

Japan, ³Graduate School of Engineering, Tohoku University, Sendai, Miyagi, Japan

Probabilistic computing has attracted significant attention due to its potential to efficiently solve computationally demanding non-deterministic polynomial-time (NP) problems [1,2]. Leveraging intrinsic stochastic behaviors of nanoscale magnetic devices, probabilistic computing offers substantial computational efficiency advantages over traditional CMOS-based deterministic architectures [3–6]. Among candidate devices, stochastic magnetic tunnel junctions (s-MTJs) have emerged as promising, enabling high calculation speeds through parallelized bit updates and exceptional energy efficiency via spontaneous thermally activated magnetization switching at low energy barriers [1,2]. This work examines advanced s-MTJ device designs crucial for probabilistic computing applications, focusing on the time-domain response (dictating calculation speed) and the time-averaged response (determining computational precision).

Recent theoretical study revealed that key device parameters—particularly switching speed—depend not only on the energy barrier height but also strongly on the direction of magnetic anisotropy. Devices with an in-plane magnetic easy axis exhibit significantly faster stochastic switching than those with perpendicular anisotropy, due to accelerated magnetization precession facilitating quicker increases in free energy and thus faster thermal activation [7]. Guided by this insight, experimental relaxation times as short as 8 ns have been achieved without spin-transfer torque (STT) in in-plane s-MTJ [8], offering practical guidelines for optimizing device structures and materials for improved time-domain performance in probabilistic computing.

Practical probabilistic devices must also withstand external magnetic fields of ~1 mT [9]. Under external fields, conventional s-MTJs experience Zeeman energy changes, causing undesirable magnetization pinning that disrupts stochastic operation. Synthetic antiferromagnetic (SAF) structures integrated into s-MTJ free layers significantly enhance robustness against external magnetic disturbances by compensating for Zeeman effects [10]. By optimizing ferromagnetic layer thicknesses around the Ru spacer layer, which antiferromagnetically couples adjacent magnetic layers, SAF-based devices experimentally show markedly reduced sensitivity to external magnetic fields compared to single-layer structures [10]. Furthermore, reducing junction diameters from about 100 nm to around 40 nm decreases relaxation time and notably enhances robustness against external magnetic fields, achieving susceptibility below 0.1 mT⁻¹. Smaller junctions also exhibit significantly reduced bias-voltage sensitivity (~0.5 V-1 at 40 nm), approximately 100 times lower than conventional s-MTJs [11]. Innovative designs, including double-free-layer (DFL) s-MTJs without fixed reference layers, have been proposed [12] and experimentally validated [13]. These structures effectively suppress STT-induced biases between top and bottom free layers, further reducing voltage-dependent switching variability. The precise engineering of DFL architecture ensures stable stochastic switching behaviors independent of voltage fluctuations. Such combined structural and interfacial strategies optimized for time-averaged response establish reliable stochastic operations for accurate probabilistic computation under practical conditions. In conclusion, comprehensive theoretical analyses and rigorous experimental validations have clarified critical parameters and provided engineering guidelines for designing advanced s-MTJ devices for probabilistic computing. Continuous refinement of these characteristics and integration strategies holds great potential for practical deployment in complex, large-scale probabilistic computing systems, enabling efficient solutions to increasingly challenging computational problems. This research was supported by JSPS KAKENHI, JST-CREST, JST-PRESTO, JST-ASPIRE, MEXT X-NICS, and cooperative projects of RIEC.

- [1] K. Y. Camsari et al., Phys. Rev. X 7, 031014 (2017).
- [2] W. A. Borders et al., Nature <u>573</u>, 390 (2019).
- [3] N. Singh et al., Nat. Commun. 15, 2685 (2024).
- [4] A. Grimaldi et al., IEDM, 22.4.1 (2022).
- [5] N. Singh et al., IEDM 2023, San Francisco, USA (2023).
- [6] N. Singh et al., IEDM 2024, San Francisco, USA (2024).

- [7] S. Kanai et al., Phys. Rev. B <u>103</u>, 094423 (2021).
- [8] K. Hayakawa et al., Phys. Rev. Lett. 126, 117202 (2021).
- [9] B. Dieny *et al.*, IEEE Electron Devices Magazine $\underline{2}$, 52–59 (2024).
- [10] K. Kobayashi et al., Phys. Rev. Appl. <u>18</u>, 054085 (2022).
- [11] K. Kinoshita et al., arXiv:2505.05316 (2025).
- [12] R. Ota et al., Appl. Phys. Lett. <u>125</u>, 022406 (2024).
- [13] K. Selcuk et al., Phys. Rev. Appl. 21, 054002 (2024).

DA-02. Solving Combinatorial Optimization Problems with Stochastic Actuated Magnetic Tunnel Junction

A. D. Kent

Physics, New York University, New York, New York, United States

Can stochastic magnetic tunnel junction arrays solve complex optimization problems better than existing methods? The first part of this talk addresses this question by presenting the Sherrington-Kirkpatrick (SK) spin-glass model, which is a complex problem with a known solution in the thermodynamic limit. Remarkably, we show by numerical modeling that coupled macrospins emulating the SK model and evolving according to Landau-Lifshitz Gilbert dynamics can get closer to the true ground state energy than state-of-the-art numerical methods and discuss the possible reasons [1]. In the second part of my talk, I will present our work on stochastic magnetic tunnel junctions based on perpendicular magnetic tunnel junctions. In contrast to superparamagnetic MTJs, we experiment with magnetically stable MTJs and actuate them with nanosecond pulses to make them behave stochastically [2]. We denote this a stochastic magnetic actuated random transducer (SMART) pMTJ device because a pulse generates a random bit stream on-demand, much like a coin flip. SMART-pMTJs produce truly random bit streams at high rates while being more robust to environmental changes, such as their operating temperature and device-to-device variations, compared to other stochastic nanomagnetic devices [3,4]. By interfacing a pMTJ to an FPGA, we have generated over 1 trillion bits at rates greater than 100 MHz that pass multiple statistical tests for true randomness, including all the NIST tests for random number generators with only one XOR operation [5,6]. Finally, I will discuss opportunities to advance the science and applications of stochastic MTJs toward the goals of having better sources of random numbers and addressing complex optimization problems.

- [1] Dairong Chen, Andrew D. Kent, Dries Sels and Flaviano Morone, "Solving combinatorial optimization problems through stochastic Landau-Lifshitz-Gilbert dynamical systems," Phys. Rev. Research 7, 013129 (2025) [2] L. Rehm, C. Capriata, S. Misra, J. Smith, M. Pinarbasi, B. Malm, and A. D., Kent, "Stochastic magnetic actuated random transducer devices based on perpendicular magnetic tunnel junctions," Phys. Rev. Appl. 19, 024035 (2023)
- [3] L. Rehm, M. G. Morshed, S. Misra, A. Shukla, S. Rakheja, M. Pinarbasi, A. W. Ghosh, and A. D. Kent, "Temperature-resilient true random number generation with stochastic actuated magnetic tunnel junction devices," Appl. Phys. Lett. 124, 052401 (2024)
- [4] Md Golam Morshed, Laura Rehm, Ankit Shukla, Yunkun Xie, Samiran Ganguly, Shaloo Rakheja, Andrew D. Kent, Avik W. Ghosh, "Reduced sensitivity to process, voltage and temperature variations in activated perpendicular magnetic tunnel junctions based stochastic devices," arXiv:2310.18781
- [5] A. Dubovskiy, T. Criss, A. Sidi El Valli, L. Rehm, A. D. Kent, A. Haas, "One Trillion True Random Bits Generated With a Field-Programmable Gate Array Actuated Magnetic Tunnel Junction," IEEE Magnetics Letters 15 (2024)
- [6] Ahmed Sidi El Valli, Michael Tsao, J. Darby Smith, Shashank Misra, and Andrew D. Kent. "High-Speed Tunable Generation of Random Number Distributions Using Actuated Perpendicular Magnetic Tunnel Junctions," Appl. Phys. Lett. 126, 212403 (2025)

DA-03. Probabilistic Computing with Voltage-controlled Magnetic Tunnel Junctions and Digital CMOS

P. Khalili Amiri

Northwestern University, Evanston, Illinois, United States

Probabilistic (p-) computing is a physics-inspired approach to solving certain computing problems more efficiently than deterministic von Neumann machines. A key requirement for p-computing is the realization of fast, compact, and energy-efficient p-bits. While stochastic magnetic tunnel junctions (S-MTJs) have been used for this purpose, this approach has scaling challenges due to the need for digital-to-analog converters and precise control of a small energy barrier across many devices. Here we demonstrate an alternative p-bit design based on voltage-controlled perpendicular magnetic tunnel junctions (V-MTJs) that use the voltage-controlled magnetic anisotropy (VCMA) effect [1]. The V-MTJs are stable (with large energy barriers) in the absence

of voltage and generate random bits on-demand when a voltage pulse is applied [2]. We discuss perspectives for application-specific integrated circuits (ASICs) based on integration of digital CMOS and V-MTJs for p-computing. We report an ASIC fabricated in 130 nm foundry CMOS, which implements integer factorization as a representative hard optimization problem. The ASIC uses stochastic bit sequences read from an adjacent V-MTJ chip driven by 10 ns voltage pulses. We experimentally demonstrate the chip's functionality on up to 24-bit problems and provide projections for designs in advanced nodes [3].

- [1] Y. Shao et al., Communications Materials 3, 87 (2022)
- [2] Y. Shao et al., Nanotechnology 34, 495203 (2023)
- [3] C. Duffee et al., arXiv:2412.08017 (2024)

DA-04. Ising machine based on Magnetic Tunnel Junctions E. Raimondo^{1, 3}, A. Grimaldi², R. Tomasello², M. Chiappini¹, A. Giordano³, M. Carpentieri², G. Finocchio³

¹Istituto Nazionale di Geofisica e Vulcanologia, Rome, Italy, ²Politecnico di Bari, Bari, Italy, ³University of Messina, Messina, Italy

Ising machines (IMs) have emerged as a promising hardware-oriented approach for solving combinatorial optimization problems (COPs) [1-2], by mapping these problems onto an Ising model and searching for the ground state of the corresponding Ising Hamiltonian. Several implementation of IM have been proposed, including quantum annealers, simulated bifurcation machines, coherent Ising machines, oscillator-based Ising machines (OIMs), and probabilistic Ising machines (PIMs). Among these, OIMs and PIMs have been successfully realized using a range of physical technologies. Notably, spintronic-based solutions – particularly those based on magnetic tunnel junctions (MTJs) – have attracted growing interest due to their intrinsic scalability, energy efficiency, and compatibility with standard CMOS fabrication processes [2-5].

However, hardware implementations inevitably introduce variability across devices. In this work, we focus on PIMs and analyze the impact of device-level non-idealities, specifically variations in the sigmoidal response of probabilistic bits (p-bits). These deviations are primarily modeled as variations in the slope of each p-bit's sigmoid curve. We evaluate how such variability affects the success probability across several COP instances and compare three widely used energy minimization algorithms: simulated

annealing (SA), parallel tempering and simulated quantum annealing (SQA). Our results demonstrate that SQA consistently outperforms the others, exhibiting remarkable robustness to hardware-induced variability [6]. Building upon MTJ-based implementation of both probabilistic and oscillator-based IMs, we propose a unified architecture, called collective IM (CoIM). This architecture integrates the PIM and OIM paradigms using a single MTJ device, configured as a spin-torque nano-oscillator (STNO). By tuning external parameters, the STNO can operate in either a probabilistic or deterministic regime. In the deterministic regime, achieved by applying large amplitude AC currents, thermal noise facilitates stochastic phase synchronization, enabling phase locking into either in-phase or anti-phase states, producing the stable, coherent phase dynamics characteristic OIMs. In contrast, at lower AC current amplitudes, thermal fluctuations dominate, leading to weak frequency-locking and random phase transitions - known as phase slips - between the two states. Furthermore, applying an additional AC signal near the STNO's precession frequency fo induces first-harmonic injection locking. This breaks the phase symmetry and biases the oscillator's phase toward one of the two stable states, resulting in a sigmoidal phase distribution characteristic of PIM. Interestingly, at frequencies of AC current above 2fo, the sigmoidal behavior partially changes, revealing a previously unreported physical phenomenon. By sweeping the AC at 2f across these regimes, naturally emulates a hardware-embedded SA process.

In benchmark tests – such as the 100-node Max-Cut problem "gka1d" – the CoIM exhibits faster convergence compared to standalone PIM or OIM implementations. These results highlight the advantages of an hybrid architecture that combines both probabilistic and deterministic dynamics within a unified spintronic platform.

Acknowledgements: This work has been supported by project number 101070287 — SWAN-on-chip — HORIZON-CL4-2021-DIGITAL-EMERGING-01, the projects PRIN 2020LWPKH7, PRIN_20225YF2S4, PRIN20222N9A73, PON Capitale Umano (CIR_00030), funded by the Italian Ministry of University and Research (MUR), and by the PETASPIN association (www.petaspin.com). R.T. acknowledge support from Project PE0000021.

- [1] N. Mohseni, Nat. Rev. Phys. 4, 363 (2022).
- [2] T. Zhang, IEEE Trans. on Nano., 23, 704-717 (2024).
- [3] K. Y. Camsari, Phys. Rev. X 7, 031014 (2017).

- [4] G. Finocchio, J. Magn. Magn. 521, 167506 (2021).
- [5] A. Grimaldi, Phys. Rev. Appl. 17, 024052 (2022).
- [6] E. Raimondo, arXiv:2503.13015 (2025)

DA-05. On-chip Training of Stochastic Multilayer Spintronic Neural Networks

P. Talatchian
SPINTEC, Grenoble, France

Developing energy-efficient AI systems requires the integration of on-chip learning within physical neural networks. Stochastic spintronic neurons, particularly coupled superparamagnetic tunnel junctions (SMTJs)[1-3], provide a promising hardware platform due to their thermally induced stochastic magnetization fluctuations, which inherently emulate binary stochastic neurons at the nanoscale. In this work, we present the first experimental demonstration of a binary classification task performed using a network of SMTJs. Our approach leverages the intrinsic stochasticity of SMTJs to process binary inputs and produce classification outcomes. The network architecture is designed to exploit the probabilistic switching behavior of SMTJs.To facilitate network learning, we implement a local rule inspired by Equilibrium Propagation [4-5], allowing us to avoid the energy-intensive data shuffling typically required in neural network training. By interfacing SMTJ arrays with electronic control circuits, we demonstrate the network's ability to learn and classify binary patterns in real time. Our experimental results showcase the robust performance of SMTJ-based networks in performing binary classification tasks, highlighting the potential of spintronic neurons for implementing on-chip learning in hardwarebased neural networks. This advancement paves the way for scalable, low-power neuromorphic and Ising-based systems capable of real-time processing and training.

- [1] P. Talatchian, M. W. Daniels, A. Madhavan *et al.*, Phys. Rev. B, 104, 054427 (2021).
- [2] M. W. Daniels, A. Madhavan, P. Talatchian *et al.*, Phys. Rev. Appl. 13, 034016 (2020).
- [3] L. Soumah, L. Desplat, N.-T. Phan *et al.*, Phys. Rev. Appl. 24, L011002 (2025).
- [4] B. Scellier and Y. Bengio, Front. Comput. Neurosci. 11, p24 (2017).
- [5] J. Peters and P. Talatchian, arXiv :2503.22810, (2025).

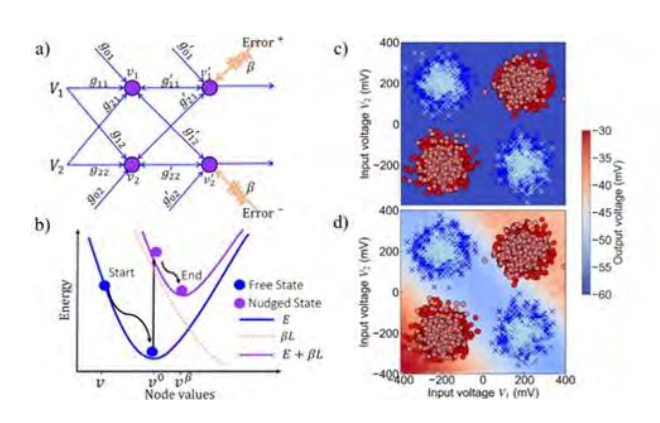


Figure 1. (a) Schematic of the SMTJ-based neural network architecture, consisting of two input voltage nodes (V1, V2) and their corresponding output values (v'1-v'2). The network connectivity is defined by the conductance matrix (g_{ij}) , which determines the weighted interactions between nodes. The learning process is guided by the error signal (BL) applied to the output nodes. (b) Energy landscape illustrating the free (blue curve) and nudged states (purple curve) following error-driven learning The nudging term (B) modulates the energy landscape, guiding the system from the initial (start) to the final (end) state. (c) The experimental output voltage intensity as a function of the input voltages (V1, V2), highlighting the separation between dataset clusters to be classified before at the initial state, and (d) after on-chip local training.

SESSION DB: ADVANCING MAGNONICS: UNLOCKING THE POTENTIAL OF THE THIRD DIMENSION

Chair(s): G. Gubbiotti, *IOM-CNR*, *Perugia, Italy*Wednesday, October 29, 2025
02:00 PM-05:30 PM
Ballroom A

DB-01. Magnon control in dipolar 3D multilayered artificial spin-ice hybrid systems

R. Sultana¹, R. Negrello², V. Bhat¹, M. T. Kaffash¹, H. Carfagno³, T. C. Dion⁴, K. D. Stenning⁵, A. Vanstone⁵, H. Holder⁵, G. Alatteili⁶, V. Martinez⁶, T. Kimura⁴, R. Oulton⁵, H. Kurebayashi⁷, W. Branford⁵, E. Iacocca⁶, M. Doty⁸, Y. Ji¹, J. Gartside⁵, F. Montoncello², G. Gubbiotti⁹, <u>B. Jungfleisch¹</u> Department of Physics and Astronomy, University of Delaware, Newark, Delaware, United States, ²Università di Ferrara, Ferrara, Italy, ³Department of Materials Science and Engineering, University of Delaware, Newark, Delaware, United States, ⁴Solid

State Physics Laboratory, Kyushu University, Fukuoka, Japan, ⁵Dept of Physics, Blackett Laboratory, Imperial College London, London, United Kingdom, ⁶Center for Magnetism and Magnetic Nanostructures, University of Colorado Colorado Springs, Colorado Springs, Colorado, United States, ⁷London Centre for Nanotechnology, University College London, London, United Kingdom, ⁸Department of Materials Science and Engineering, University of Delaware, Newark, Delaware, United States, ⁹5Istituto Officina dei Materiali del Consiglio Nazionale delle Ricerche (IOM-CNR), Perugia, Italy

As the carbon footprint and associated energy costs of traditional computing platforms continue to increase, finding alternative, more efficient computational architectures is imperative. Magnonic systems based on the elementary quanta of spin waves - magnons, offer a potential solution. However, to create efficient magnonic computing elements, we need to understand how to effectively control magnons at the nanoscale. This can be achieved by strongly interacting artificial spin ice (ASI) systems, which are magnetic metamaterials where magnetic domains can be mapped onto a spin-lattice model [1]. These systems have recently emerged as functional material platforms for reconfigurable magnonics, including twodimensional magnonic crystals, in which the desired magnon band structure is engineered, a similar approach to that taken in photonics [1].

Here, we couple ASI structures made of CoFeB or NiFe stadium-shaped nanoelements to continuous NiFe film underlayers to understand how the presence of the ASI affects the spin-wave properties in the film underlayer. We present a combined experimental and numerical study of the spin-wave dispersion in the ASI/film hybrid structures [2,3]. The spin-wave dispersion, measured by wavevector resolved Brillouin light scattering spectroscopy, consists of a rich number of modes with either stationary or propagating character [3]. Micromagnetic simulations unveil the details of the dynamic coupling between the ASI lattice and film underlayer. The ASI lattice facilitates dynamics of the film, either specific wavelengths or intensity modulation peculiar to the modes of the ASI elements imprinted in the film. Our results demonstrate that propagating spin waves can be modulated at the nanometer length scale by harnessing dynamic mode coupling in the vertical direction, i.e., the out-of-plane direction, of suitably designed structures. These findings also significantly enhance our understanding of three-dimensional, multilayered artificial spin-ice systems [4,5].

Work on the NiFe ASI/NiFe film systems was supported by the U.S. Department of Energy, Office of Basic Energy Sciences, Division of Materials Sciences and Engineering under Award No. DE-SC0020308. It was partially supported by NSF through ENG-1839056. Research on the CoFeB ASI/NiFe film and multilayer ASI systems was supported by the U.S. Department of Energy, Office of Science, Office of Basic Energy Sciences under Award Number DE-SC-0024346.

[1] R. Sultana, A. K. Mondal, V. S. Bhat, et al., arXiv:2504.06548 (2025).

[2] F. Montoncello, M. T. Kaffash, H. Carfagno, et al., J. Appl. Phys. 133, 083901 (2023).

[3] R. Negrello, F. Montoncello, M. T. Kaffash, et al., APL Mater. 10, 091115 (2022).

[4] T. Dion, K. Stenning, A. Vanstone, et al., Nat. Commun. 15, 4077 (2024).

[5] V. S. Bhat and M. B. Jungfleisch, Appl. Phys. Lett. 126, 022406 (2025).

DB-02. Three-dimensional Control and Imaging of Spin Waves in Nanostructured Thin Films

V. Levati¹, M. Vitali¹, D. Girardi¹, S. Finizio², C. Donnelly³, J. Raabe², M. Panzeri¹, R. Silvani⁴, M. Madami⁴, D. Breitbach⁶, P. Pirro⁶, R. Bertacco¹, V. Russo¹, A. Li Bassi¹, G. Corrielli⁷, R. Osellame⁷, F. Maspero¹, A. Del Giacco¹, N. Pellizzi¹, I. Biancardi¹, P. Florio¹, S. Tacchi⁵, D. Petti¹, E. Albisetti¹

¹Politecnico di Milano, Milano, Italy, ²PSI, Villigen, Switzerland, ³Max Planck Institute, Dresden, Germany, ⁴Università di Perugia, Perugia, Italy, ⁵CNR-IOM, Perugia, Italy, ⁶RPTU Kaiserslautern-Landau, Kaiserslautern, Germany, ⁷CNR-IFN, Milano, Italy

In the field of magnonics, harnessing the third dimension has become one of the most desired capabilities for introducing new functionalities. To this goal, understanding and manipulating spin-waves in three-dimensional nanostructured systems are crucial. Here, we discuss two recent advancements in the field: the imaging of spin waves in 3D using Soft X-Ray Laminography (TR-SoXL) [1], and the three-dimensional control of magnetism in crystalline Yttrium Iron Garnet via direct laser irradiation [3]. The experimental visualization of propagating spin waves in three-dimensions has been elusive, due to the need of combining nanoscale spatial resolution in 3D, and time resolution in the GHz frequency range. We use TR-SoXL, to

image in three-dimensions spin waves emitted by nanoscale spin textures and study their propagation in a synthetic antiferromagnets. We reconstruct propagating spin waves in three-dimensions, and map the distribution of the SW modes throughout the volume. We observe complex depth-dependent SW profiles, giving rise to three-dimensional interference patterns.

Then, we introduce a new methodology based on phase nanoengineering [2] for direct three-dimensional nanostructuring of crystalline YIG thin film [3]. We show that by irradiating single-crystal YIG films with a focused UV laser, (Figure 1) we drive a giant stable enhancement of the perpendicular magnetic anisotropy, in nanoscale regions confined in three-dimensions and whose extension within the volume of the system can be finely controlled. By harnessing these three-dimensional anisotropy profiles, we demonstrate a fine tuning of the spin-wave band structure, and spatial localization of the spin-wave modes within the volume, realizing proof-of-principle magnonic materials and magnonic crystals (Figure 2).

[1] Girardi et al. Nature Communications, Vol 15, p. 3057 (2024).

[2] V. Levati et al., Advanced Materials Technologies, Vol 8, p. 2300166 (2023).

[3] V. Levati et al., arXiv:2409.17722 (2024).

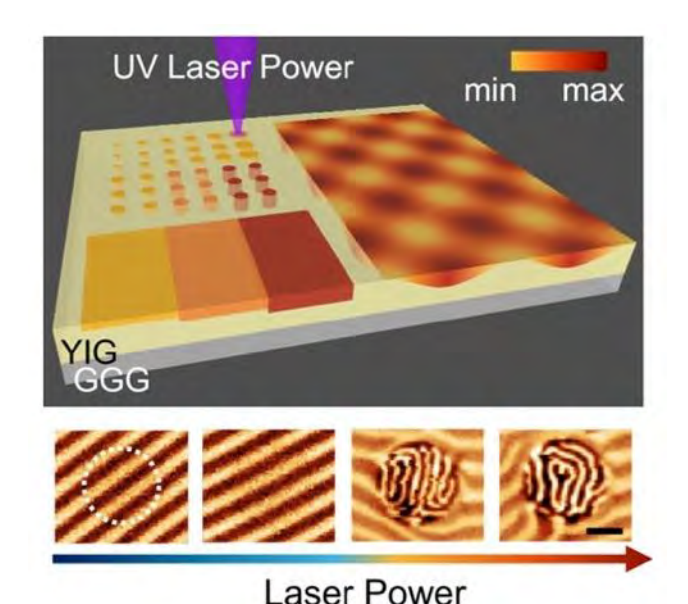


Fig. 1 Sketch of the laser irradiation process and of the three-dimensional magnetic properties profiles induced in YIG (top panel). Magnetic force microscopy images of the domain structure of YIG increasing the laser power from left to right. Scale bar 2 um.

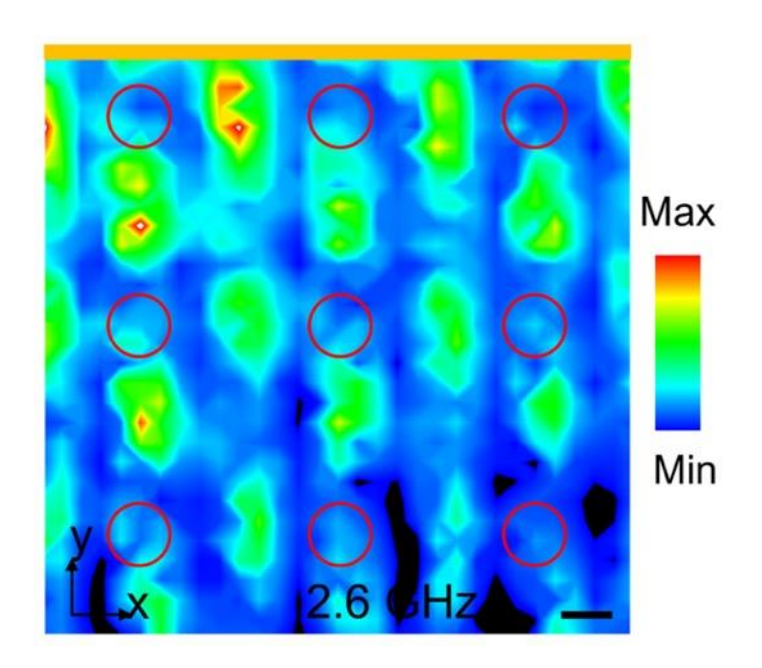


Fig. 2 Spatial map of the spin-wave intensity in a 3D magnonic crystal measured via Brillouin Light Scattering microscopy. Irradiated regions are marked by red circles.

Microwave antena in yellow. Scale bar 500 nm.

DB-03. Micromagnetic Simulation of High-Frequency Modes in Interconnected Nanowire Arrays

R. Hertel

Université de Strasbourg, CNRS, Institut de Physique et Chimie des Matériaux de Strasbourg, Strasbourg, France

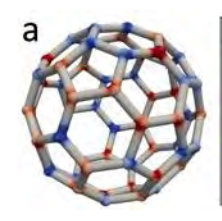
Advances in nanofabrication now allow the creation of fully three-dimensional (3D) magnetic nanoarchitectures with complex geometries and tunable properties [1]. Among such systems, extended arrays of interconnected soft-magnetic nanowires have recently emerged as a promising class of artificial magnetic materials. These structures exhibit key features of three-dimensional artificial spin ices, including a broad variety of nearly degenerate magnetization states and defect-like micromagnetic textures at the wire junctions. Due to their connectivity and geometric complexity, they are promising for applications in 3D magnonics. We investigate high-frequency magnetization dynamics in such systems by means of advanced finite-element micromagnetic simulations tailored for magnonic studies. Specifically, we employ frequency-domain simulation techniques that compute the system's linear response to

harmonic excitations around a given equilibrium configuration [2]. This method allows for the direct calculation of the resonance spectrum with high resolution and efficiency, even for large and geometrically complex structures.

The simulations cover various geometries of interconnected nanowires, including buckyball-type structures [3], cubic arrays, diamond-type crystals [4], and gyroid networks. In all cases, we observe distinct resonance peaks in the computed absorption spectra, which can be attributed to characteristic micromagnetic configurations and geometric features. Notably, the magnetization structure at the nanowire junctions plays a decisive role in shaping the spectrum. At higher frequencies, standing spin-wave modes confined within individual nanowires emerge.

The strong sensitivity of the resonance behavior to local magnetic and geometric details highlights the potential of these 3D nanoarchitectures for tunable and reconfigurable magnonic functionalities. The results also illustrate the utility of frequency-domain finite-element micromagnetic methods in addressing the challenges posed by complex 3D geometries and large-scale simulations. Beyond these systems, we are extending our studies to other 3D magnonic geometries with nontrivial topology, such as Möbius-shaped nanostructures [5], which will also be briefly discussed in the presentation.

- [1] A. Fernandez-Pacheco et al., Nature Communications, 8, 15756 (2017)
- [2] M. d'Aquino and R. Hertel, J. Appl. Phys., 133, 033902 (2023)
- [3] R. Cheenikundil, J. Bauer, M. Goharyan et al., APL Materials, 10, 081106 (2022)
- [4] R. Cheenikundil, M. d'Aquino, R. Hertel, arXiv:2312.08415 (2023)
- [5] A. Thonikkadavan, M. d'Aquino, R. Hertel, arXiv:2508.15463 (2025)



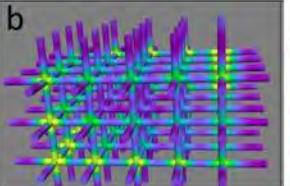




Fig.1: Simulated high-frequency magnetic oscillations in different types of interconnected nanowire arrays. (a) Buckyball geometry, (b) regular cubic array of nanowires, (c) artificial diamond-type magnetic lattice of nanowires. The

typical length of the nanowires is around 100 nm, and the total size of the objects is in the micron range. Standing spin-wave patterns are observed in the nanowires, in addition to oscillations localized at the vertex sites.

DB-04. Nonreciprocal magnonics in 3D nanostructures

F. Brevis¹, L. Körber², B. Mimica-Figari¹, R. Gallardo¹, A. Kákay³, <u>P. Landeros</u>¹

¹Departamento de Física, Universidad Técnica Federico Santa María, Valparaíso, Chile, ²Institute of Molecules and Materials, Radboud University, Nijmegen, Netherlands, ³Institute of Ion Beam Physics and Materials Research, Helmholtz-Zentrum Dresden-Rossendorf, Dresden, Germany

Three-dimensional magnonics is a research field that focuses on the spin-wave control in magnetic materials, going beyond the well-known two-dimensional limit. It has been recently demonstrated that spin waves in magnetic films can exhibit nonreciprocal behavior when a symmetrybreaking mechanism is artificially introduced [1], meaning that the propagation of spin waves differs depending on the direction of propagation. Over the past decade, nonreciprocal magnonic systems have been proposed and successfully realized experimentally, with some exhibiting frequency shifts on the order of several GHz [2], such as the ferromagnetic bilayer or the ultrathin ferromagnetic film in contact with a high spin-orbit coupling layer. Nonetheless, for more complex magnonic systems, such as graded films, bilayers, multilayers, curved shells, and nanotubes, or in cases where the equilibrium magnetization is nonuniform, numerical methods are required to estimate the frequency shift among counterpropagating spin waves [3-5]. Consequently, given the relevance of nonreciprocal and unidirectional wave propagation for magnon-based technological devices (such as magnonic diodes, circulators, and isolators), there is a pressing need for novel approaches to predict the existence of spin-wave nonreciprocity. One of these approaches [4-5] involves the toroidal moment, which arises from the multipole expansion of the vector potential [6-7]. In ferromagnetic systems lacking external electric or polarization currents, the volume-bound current (the curl of the magnetization) can generate a texture-based toroidal moment.

The significance of the toroidal moment has been recently established in the context of nonreciprocal magnonics [6]. It will be discussed in various scenarios, such as the current-induced spin-wave Doppler shift in thin films, different

magnetic textures (such as conical-helical, skyrmionic, meron, and bimerons), magnetization-graded films, magnetic bilayers, and films with interfacial and bulk DMI. The toroidal moment accounts for the spatial symmetry breaking of the magnetization in such a way that, if the wave vector has a nonzero projection along the toroidal moment, nonreciprocal spin-wave propagation is permitted, with physical origin on the magnetostatic interaction [5,8].

- [1] B. Flebus et al., J. Phys.: Condens. Matter 36, 363501 (2024).
- [2] G. Gubbiotti et al., J. Phys.: Condens. Matter 37 143502 (2025)
- [3] R. A. Gallardo, P. Alvarado-Seguel, and P. Landeros, Phys. Rev. B 105, 104435 (2022).
- [4] L. Körber et al., Phys. Rev. B 106, 014405 (2022).
- [5] L. Körber, Ph.D. thesis, Sachsische Landesbibliothek, Staats- und Universitatsbibliothek Dresden.
- [6] V. Dubovik and V. Tugushev, Phys. Rep. 187, 145 (1990).
- [7] N. Spaldin, M. Fiebig, and M. Mostovoy, J. Phys. Condens. Matter 20, 434203 (2008).
- [8] F. Brevis et al., Phys. Rev. Applied 24, 024058 (2025).

DB-05. Nonreciprocal Magnons in Programmable 3D Ferromagnetic Screws and Tubular Nanonetworks Created by Atomic Layer Deposition

D. Grundler^{1, 2}

¹Institute of Materials (IMX), Ecole Polytechnique Fédérale de Lausanne (EPFL), Lausanne, Vaud, Switzerland, ²Institute of Electrical and Micro Engineering (IEM), Ecole Polytechnique Fédérale de Lausanne (EPFL), Lausanne, Vaud, Switzerland

Chiral magnets possess unique three-dimensional (3D) spin helices. They give rise to nonreciprocal transport phenomena enabling energy efficient data transmission. However progress in applications is hindered by typically low critical temperatures. We report on the creation and exploration of artificial chiral magnets (ACMs) operating at room temperature. Using atomic layer deposition of highquality ferromagnetic Ni [1,2] we prepare tubular screws from thin conformal shells around polymeric nanotemplates and observe nonreciprocal magnon transport at room temperature by means of inelastic light scattering microscopy and micromagnetic simulations. Controlling their toroidal moments and magnetochiral effects via 3D geometrical handedness and field-dependent spin orientation, we obtain ACMs with programmable nonreciprocity at zero magnetic field [3]. Ferromagnetic Ni

shells on 3D woodpile lattices of polymer nanorods have already shown incoherent surface magnon modes which exhibited unconventionally high resonance frequencies [2]. In recently performed inductive measurements and micromagnetic simulations we have identified an unconventional phase evolution of edge magnon modes when coherently excited by a microwave field [4]. Our experiments and findings are a major step in functional 3D nanomagnetism at room temperature and 3D nanomagnonics based on a mass production compatible deposition technology. Cooperations with M. Xu, AJ.M. Deenen, H. Guo, M. Hamdi, K. Lenz, M. Golebiewski, R. Narkowicz, J. Lindner, and M. Krawczyk are gratefully acknowledged. Our work is funded by SNSF via grant 197360.

- 1. M.C. Giordano, K. Baumgaertl, S. Escobar Steinvall et al., ACS Appl. Mater. Interfaces, Vol. 12, p. 40443 (2020) 2. H. Guo, A.J.M. Deenen, M. Xu et al., Adv. Mater., Vol. 35, p. 2303292 (2023)
- 3. M. Xu, AJ.M. Deenen, H. Guo et al., arXiv:2404.19153v2, https://doi.org/10.48550/arXiv.2404.19153
- 4. H. Guo, K. Lenz, M. Golebiewski et al., arXiv:2506.16103, https://doi.org/10.48550/arXiv.2506.16103

SESSION DC: NANOPARTICLES, 3D, AND OTHER STRUCTURED MATERIALS

Chair(s): M. Charilaou, *Physics, University of Louisiana at Lafayette, Lafayette, Louisiana, United States*Wednesday, October 29, 2025
02:00 PM-05:30 PM
Ballroom C

DC-01. Creating Topological Spin and Stray Field Textures with Coupled 3D Magnetic Nanohelices

<u>J. Fullerton</u>¹, N. Leo², J. Jurczyk³, C. Donnelly⁴, D. Sanz Hernandez⁵, L. Skoric⁶, N. Mille⁷, S. Stanescu⁷, D. MacLaren⁸, R. Belkhou⁷, A. Hierro-Rodriguez/⁹, A. Fernández-Pacheco³, C. Phatak^{1,10}

¹Materials Science Division, Argonne National Laboratory, Lemont, Illinois, United States, ²Department of Physics, University of Loughborough, Loughborough, United Kingdom, ³Institute of Applied Physics, TU Wien, Vienna, Austria, ⁴Max Planck Institute for Chemical Physics of Solids, Dresden, Germany, ⁵Laboratoire Albert Fert, CNRS, Thales, Université Paris-Saclay, Palaiseau, France, ⁶University of Cambridge, Cambridge, United Kingdom, ⁷Synchrotron SOLEIL, Saint-Aubin, France, ⁸SUPA, School of Physics and Astronomy, University of Glasgow, Glasgow, United Kingdom, ⁹Depto. Fisica, Universidad de Oviedo, Oviedo, Spain, ¹⁰Department of Materials Science and Engineering, Northwestern University, Evanston, Illinois, United States

With recent advancements in nanofabrication techniques, it is now possible to 3D nano-print functional, magnetic structures with a precisely designed 3D geometry [1]. Through this geometric control, we can affect the formation and stability of intricate spin and stray field textures and gain insights for future applications in spintronic devices with increased efficiency and new functionalities [2,3]. Nanohelices represent a key structure in the field of 3D nanomagnetism owing to their intrinsic geometric curvature and chirality [4]. Here, we discuss nanostructures formed of multiple coupled magnetic nanohelices which induce topologically nontrivial magnetic textures due to their patterned geometry and tuned by external field sequences [2,3].

First, we report formation of fractional skyrmion tubes in intertwined magnetic helices with x-ray magnetic ptychography [2]. We show how 3D geometric patterning can influence the magnetic energy landscape and investigate the fundamental interplay between magnetic and geometric chirality. By applying a minor loop sequence, we show how the coupling between geometric and magnetic chirality can be locally broken and recovered. Notably, having the magnetic chirality oppose that of the geometry directly leads to the formation of higher order topological states, representing a mechanism for skyrmion tube formation based purely on 3D geometric effects.

Furthermore, we show that nanostructures formed by several interwoven helical nanowires can create controllable topological stray field patterns by reconfiguring the magnetic state of the nanostructure [3]. By applying external magnetic fields, the magnetization of the nanostructure can be reconfigured, creating corresponding arrangements of magnetic charges in 3D space. These charges lead to unique forms of the emanating stray field localized in the gaps of the nanostructure. The work presented here shows how 3D nanostructures can be utilized in the creation of not only topological spin textures, but also complex nanoscale magnetic fields.

- [1] L. Skoric, et. al., Nano Lett., 20, 184 (2020).
- [2] J. Fullerton et al., Adv. Funct. Mater. 2025, 2501615
- [3] J. Fullerton et al., Nano Lett. 2025, 25, 13, 5148-5155

[4] J. Fullerton et al., *Nano Lett.* 2024, 24, 8, 2481–248 [5] This work was funded by the US Department of Energy, Office of Science, Office of Basic Energy Sciences, Materials Science and Engineering Division. Work performed at the Center for Nanoscale Materials, a U.S. Department of Energy Office of Science User Facility, was supported by the U.S. DOE, Office of Basic Energy Sciences, under contract no. DE-AC02-06CH11357.

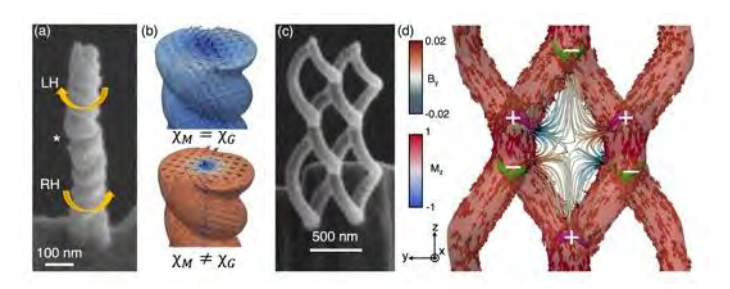


Fig 1: (a) A double helix nanostructure fabricated by FEBID [2]. (b) Micromagnetic simulations where the magnetic (χ_M) and geometric (χ_G) chiralities either match (top) or oppose (bottom) each other. (c) An interwoven cobalt nanostructure formed of multiple nanohelices [3]. (d) A micromagnetic simulation of the magnetization and resulting stray field in center gap in a single domain state. The magnetization is colored by the M_z component while the stray field is colored by the B_y component, and the purple and green isosurfaces represent areas of maximum and magnetic charge created by the diverging and converging magnetization.

DC-02. Unconventional Spin Textures in 3D Magnetic Möbius Bands

<u>C. Langton</u>¹, D. Bhattacharya¹, B. Fugetta¹, Z. Chen¹, O. Bezsmertna⁴, D. W. Raftrey^{2, 3}, J. Sands^{2, 3}, S. Satapathy², C. Fernandez-Gonzalez⁵, A. Sorrentino⁵, D. Makarov⁴, P. Fischer², G. Yin¹, K. Liu¹

¹Department of Physics, Georgetown University, Washington, District of Columbia, United States, ²Materials Sciences Division, Lawrence Berkeley National Laboratory, Berkeley, California, United States, ³Department of Physics, University of California Santa Cruz, Santa Cruz, California, United States, ⁴Institute of Ion Beam Physics and Materials Research, Helmholtz-Zentrum Dresden-Rossendorf, Dresden, Germany, ⁵MISTRAL Beamline, ALBA Synchrotron Light Facility, Barcelona, Spain

Three-dimensional (3D) nanomagnetic structures provide a fertile ground for stabilizing unconventional spin

configurations [1–3]. In particular, curvature can intricately modify the energy landscape and govern magnetic characteristics, including topology and chirality. In this study, we have fabricated a prototypical 3D topological nanostructure, magnetic Möbius bands, using two-photon polymerization, followed by sputtering of magnetic films with either in-plane or perpendicular magnetic anisotropy (PMA).

The in-plane Möbius bands consisted of a Fe/Ta film (Fig. 1). Magnetometry and first-order reversal curve (FORC) analysis revealed distinct magnetization reversal behaviors for inplane vs. out-of-plane fields. Micromagnetic simulations indicated that curvature promotes domain wall formation near the twist of the Möbius band, followed by guided propagation along the structure. Magnetic imaging using X-ray transmission microscopy confirmed such domain wall formation (Fig. 1, inset). Magneto-transport measurements across individual bands have been performed to further elucidate this behavior.

The second set of Möbius bands consisted of a Co/Pd multilayer thin film stack, which exhibits both PMA and Dzyaloshinskii–Moriya interaction (DMI), resulting in complex labyrinth domain structures on a flat surface. Magnetic soft X-ray nanotomography has been performed on the MISTRAL beamline at the ALBA light source. A full 3D magnetic reconstruction will be presented demonstrating a close correlation between spin arrangements and the local curvature. Magnetometry and FORC analysis further corroborate the tomography findings. Together, these studies offer a powerful platform for exploring the interplay between spin textures and curvature in 3D nanomagnetic systems, highlighting how geometry influences domain structure and spin configuration across distinct material systems.

Acknowledgement: NSF (DMR-2005108, DMR-2320636, ECCS-2429995), U.S. DOE-BES DE-AC02-05-CH11231 (NEMM FWP), Ministry of Research and Innovation of Spain, Generalitat de Catalunya, and FEDER (ALBA).

- [1] Fischer et. al., APL Mater. 8 (1), 010701 (2020).
- [2] Pylypovskyi et. al., Phys. Rev. Lett. 114, 197204 (2015).
- [3] Raftrey et. al., arXiv:2506.05938 (2025).

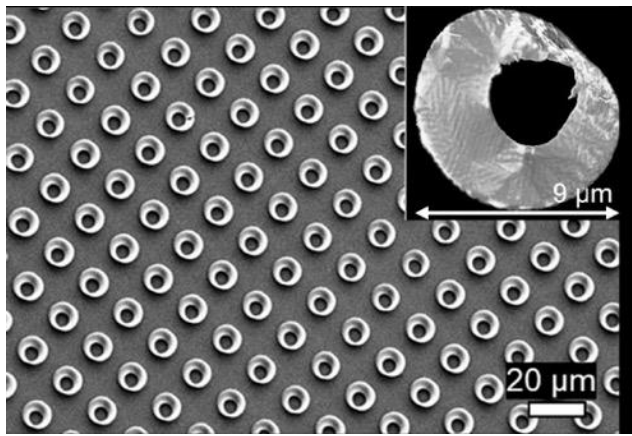


Fig. 1. SEM image of Fe-coated Möbius bands. Inset: XMCD image of magnetic domains, bright/dark regions are parallel/antiparallel to X-ray incidence.

DC-03. Characterizing fragile magnetic textures in three dimensions using Scanning NV magnetometry

P. Rickhaus¹, A. van den Berg², <u>J. Lenz</u>¹, S. Ladak²
¹Qnami AG, Basel, Switzerland, ²School of Physics and Astronomy, Cardiff University, Cardiff, United Kingdom

Scanning NV magnetometry (SNVM) is a sensitive and non-invasive magnetic characterization technique. However, its operation principle is based on rastering a surface, making it intrinsically challenging to characterize three dimensional textures. Here, we discuss mitigation strategies that allow using the high spatial resultion, sensitivity and non-invasivness of SNVM [1] in the third dimension. Motivated by the current interest in three dimensional magnetic structures, we will demonstrate the investigation of magnetic monopoles in 3D artificial spin-ice structures [2]. We will show how we identify topological solitons and monopolar fields in these structures, while preserving the fragility of the states.[3] For the exploration of the highly divergent monopole defects, we vary the NV flying distance [4] and confirm our findings by micromagnetic simulations.

[1] P. Rickhaus, O. V. Pylypovskyi, G. Seniutinas, et.al. Nano Lett., 24, 42, 13172–13178 (2024)

[2] A.v.d. Berg, P. Rickhaus, F.Barrows, C.Nisoli, S. Ladak, *in preparation* (2025)

[3] A. May et al., Nature Communications, 12, 1, 3217, (2021)[4] U. Celano, P. Rickhaus, C. Bran, et.al., Nanoscale, 16, 16838-16843 (2024)

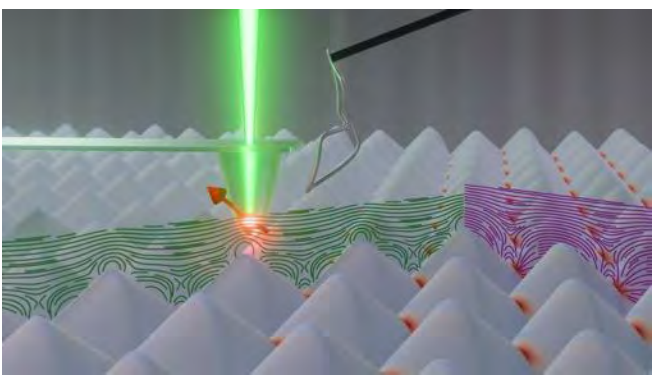


Fig. 1

DC-04. Effect of curvature on chirality and magnetic configuration in perpendicular Co/Pd multilayer films

D. Bhattacharya¹, <u>C. Langton</u>¹, D. W. Raftrey², B. Fugetta¹, S. Satapathy², O. Bezsmertna³, A. Sorrentino⁴, D. Makarov³, G. Yin¹, K. Liu¹, P. Fischer²

¹Physics, Georgetown University, Washington, District of Columbia, United States, ²Materials Sciences Division, Lawrence Berkeley National Laboratory, Berkeley, California, United States, ³Helmholtz-Zentrum Dresden-Rossendorf e.V., Institute of Ion Beam Physics and Materials Research, Dresden, Germany, ⁴ALBA light source, Cerdanyola del Vallès, Spain

Introducing curvature into magnetic nanostructures has recently emerged as a promising design strategy, as it enables control over local magnetic interactions and spin textures at sub-micron length scales [1-3]. Here, we report curvature-induced modification of magnetic configuration in a Co/Pd multilayer thin film with perpendicular magnetic anisotropy (PMA), deposited on an interconnected network of Cu nanowires (NWs) with diameters down to 50 nm and lengths up to 6 µm [4]. The NW networks were fabricated via electrodeposition and drop-cast onto 50 nm-thick silicon nitride membranes. Subsequently, the membrane was coated by a Pd (7)/[Co (0.4)/Pd (0.6)]₂₀/[Co (0.7)/Pd (0.6)]₂₀/Ta (2.5) (thicknesses in nm) multilayer via sputtering. The resulting sample contained both planar and curved regions, allowing a comparative study of curvature-induced effects on spin textures. To visualize the 3D spin arrangement, magnetic soft X-ray nanotomography was performed at the full-field transmission soft X-ray microscope on the MISTRAL beamline at the ALBA light source. Figure 1 shows full vector reconstruction of a curved section of the film over a single NW. In the curved regions, the magnetization was found to deviate from the out-of-plane direction, aligning instead with the local surface normal. The overall domain orientation was also influenced by the underlying NW-defined curvature and the domains preferentially

aligned along the long axis of the NWs. Furthermore, the chirality of the domain walls (DWs) was strongly affected by curvature. In particular, Néel DWs were promoted, and the effective DMI contribution was found to be approximately one-third of the intrinsic DMI of the Co/Pd multilayer (Fig. 2). These results will spur future experimental exploration of curvature-stabilized topological spin textures and 3D curved racetrack memory technologies.

Acknowledgement: NSF DMR-2005108, NSF ECCS-2429995, US DOE BES DE-AC02-05-CH11231 (NEMM FWP), DFG (MA5144/22-1, MA5144/33-1), ERC 3DmultiFerro (101141331).

- 1. Volkov et. al., Sci. Rep., 8 (1), 866 (2018).
- 2. Farinha et. al., Nature, 639 (8053), 67 (2025).
- 3. Fischer et. al., APL Mater. 8 (1), 010701 (2020).
- 4. Raftrey et. al., arXiv:2506.05938 (2025).

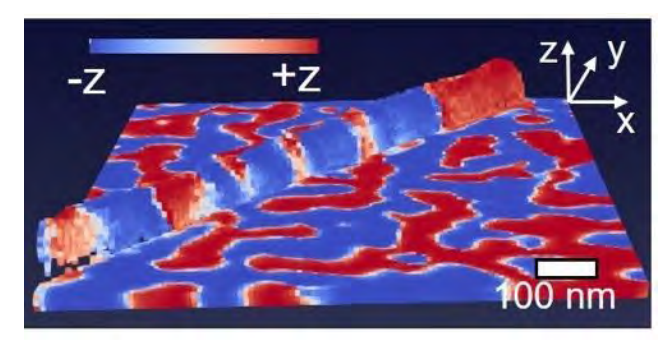


Fig. 1. *z*-component of the full vector reconstruction of curved film over a Cu nanowire.

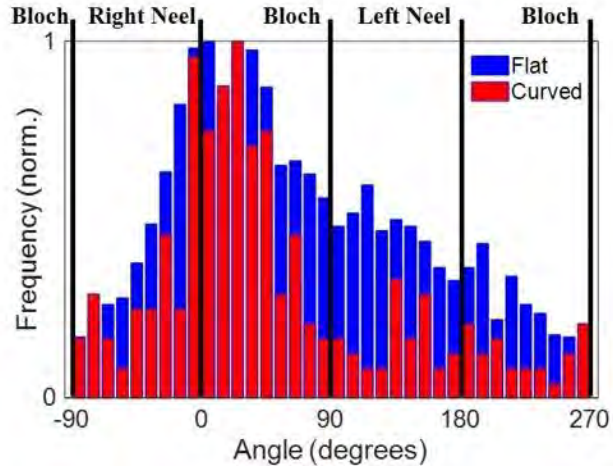


Fig. 2. Histograms of angle between DW magnetization and normal vector, flat and the curved region overlaid on top of each other.

DC-05. Nonlinear Dynamics and Frequency Comb Generation in Macroscopic Artificial Spin Ice

R. Peroor, L. A. Scafuri, E. Iacocca, D. A. Bozhko
Department of Physics and Energy Science, University of
Colorado Colorado Springs, Colorado Springs, Colorado, United
States

Nonlinear dynamics in physical systems can give rise to a variety of complex phenomena, such as frequency combs. First observed in optical systems [1], they have since been observed in many systems, including micromechanic [2, 3] and magnetic [4, 5]. Artificial spin ices (ASIs) are systems of interacting magnetic elements that offer a versatile platform for studying linear and nonlinear dynamics. One way to expand the capabilities of such systems is by augmenting the magnetic degree of freedom with a mechanical one. The most accessible arrangements for experimental studies are macroscopic mechano-magnetic models [6, 7].

In this work, we demonstrate the formation of a frequency comb in a square lattice of a macroscopic mechanomagnetic artificial spin ice (macro-ASI) [8]. The system comprises 60 bar magnets mounted on mechanical hinges, constrained to rotate in a single plane and interact with each other through their magnetic fields (Fig. 1). The relative motion of magnetic poles results in the temporal modulation of dipole-dipole interactions.

Our results demonstrate a striking similarity between the dynamics of the macroscopic system and the nanoscopic ASIs when driven by a harmonic external field. However, when the macro-ASI system is driven with a substantial external field magnitude, a nonlinear amplitude and phase modulation emerges, resulting in a frequency comb spectrum (Fig. 2). These dynamics are due to a metastable condition, i.e., a Hopf bifurcation, evidenced by numerical simulation [8]. One special feature of this macro-ASI system is that all these complex behaviors happen at low frequencies, making them visible to the naked eye. Our results also suggest that nonlinear phenomena could be enhanced in nanoscale systems using microresonators decorated with magnetic materials to dynamically modulate their coupling.

This material is based upon work supported by the National Science Foundation under Grant No. 2205796 (L.S. and E.I.) and Grant No. DMR-2338060 (R.R.P. and D.A.B). The support from the IEEE Magnetics Society in the frame of "The Game of Magnets" project is gratefully acknowledged.

^{*} Best Student Presentation Finalist / LB - Late-breaking Poster

[1] T. Fortier and E. Baumann, Commun. Phys., Vol. 2, p.153 (2019).

[2] J. S. Ochs et al., Phys. Rev. X., Vol. 12, p.041019 (2022).

[3] M. H. J. de Jong et al., Nat. Commun., Vol. 14, p.1458 (2023).

[4] G.-T. Xu et al., Phys. Rev. Lett., Vol. 131, p.243601 (2023).

[5] T. Hula et al., Appl. Phys. Lett., Vol. 121, p.112404 (2022).

[6] P. Mellado et al., Phys. Rev. Lett., Vol. 109, p.257203 (2012).

[7] E. Olive and P. Molho, Phys. Rev. B, Vol. 58, p.9238 (1998).

[8] R. R. Peroor et al., Phys. Rev. Appl., Vol. 23, p.044010 (2025).

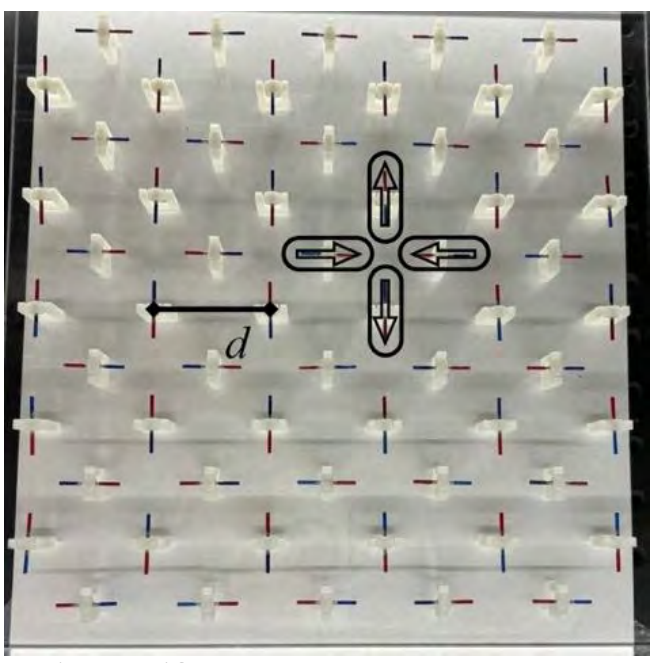


Fig. 1. Macro-ASI

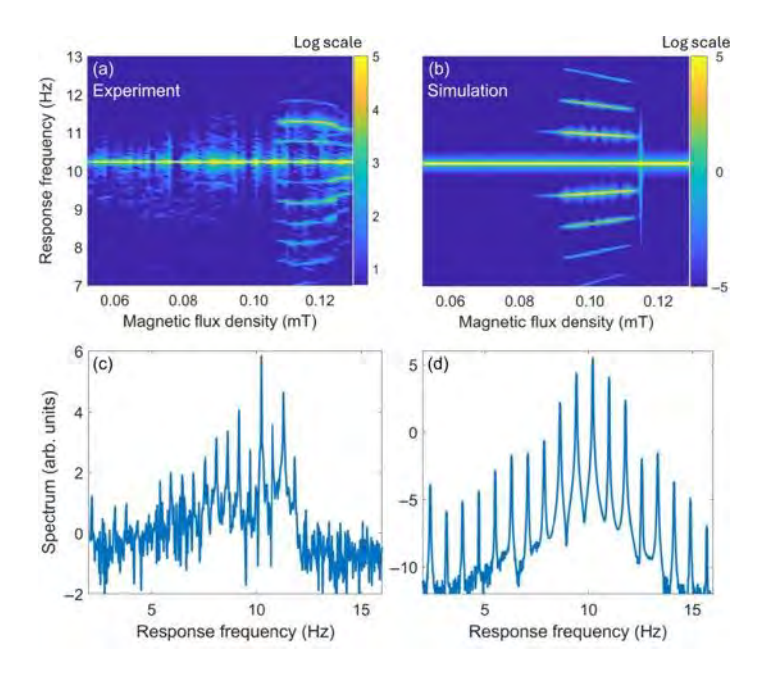


Fig. 2. Magnetic spectrum showing the emergence of a comb in experiments and simulations.

DC-06. Perturbing the Pyrochlore Structure: Local structure and Magnetic tuning in doped rare earth titanate compound R. Sain¹, M. Sahoo³, C. Upadhyay²

¹School of Materials Science and Technology, IIT (BHU), Varanasi, UTTAR PRADESH, India, ²School of Materials Science and Technology, IIT (BHU), Varanasi, UTTAR PRADESH, India, ³Surface and Sensors Studies Division, Materials Science Group, Indira Gandhi Centre for Atomic Research, Kalpakkam, Kalpakkam, India

Competing interactions and constraints to the local crystalline geometries of 3-dimensional systems have long been known to arise an exotic magnetic ground state in various compounds. In 3-dimensional geometrically frustrated structures, pyrochlores offer an ideal playground to study these ground states. Fig. 1 presented an antiferromagnetically coupled spin example of geometrical frustration in 2- and 3-dimensional systems. Where the one frustrated spin site in 2D and two spin sites in 3D systems are depicted by question marks [1, 2]. Pyrochlore compound, RE $_2$ Ti $_2$ O $_7$ (RE = Dy, Ho) is a dipolar spin ice compound, where local spins freeze into a "2-in/2-out" arrangement due to the ferromagnetic exchange interactions in the presence of strong crystal-field-induced Ising anisotropy along the local cubic <111> axis [3]. Dy- and Ho-based pyrochlore oxide

compounds are of great interest due to exchange interactions and strong dipolar interactions, which are fundamental for their magnetic properties and ordering behaviour. Previously, with decreasing temperature. There are two types of disorder considered at both sites of pyrochlore structure, one with magnetic substation and another with the non-magnetic ion substitution. In this work, we have investigated the correlation of magnetic interaction and local structure tuning due to non-magnetic ion substitution at a non-magnetic site in the pyrochlore compound RE₂Ti₂O₇. This is expected to impact the exchange interactions, dipolar and crystal electric field of RE ions. We have shown that the maximum dopant concentration at Ti sites, the magnetic state of the rare earth titanate compound, is robust. Low-temperature X-ray diffraction, dc susceptibility, and magnetic field-dependent ac susceptibility data are utilized to discuss the crystal structure and spin dynamics. The following results will be discussed in detail in correspondence to the magnetic behaviour of other rare earth-based pyrochlore oxides. Fig. 1. An antiferromagnetically coupled spin presented two prototypical examples of geometrical frustration in 2- and 3-dimensional systems. Frustrated spin sites are depicted by question marks (red colour).

- 1. Gardner JS, Gingras MJ, Greedan JE, *Reviews of Modern Physics*, 82(1): p. 53-107 (2010)
- 2. Bramwell, S.T. and M.J. Gingras, *Science*, 294(5546): p. 1495-1501 (2001)
- 3. Samarakoon, Anjana M., et al., *Physical Review Research* 4.3: 033159 (2022)

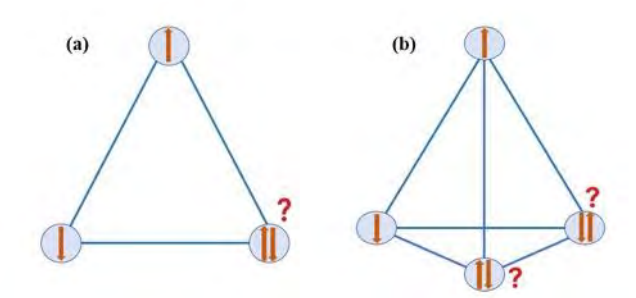


Fig. 1

DC-07. Complex Evolution of Magnetic Anisotropies in Magnetosomes of Magnetotactic Bacteria

D. Gandia¹, L. Marcano^{2, 3}, L. Gandarias^{4, 5}, A. G. Gubieda⁴, A. García-Prieto¹², L. Fernández Barquín⁶, J. Espeso⁶, E. M. Jefremovas^{7, 8, 9}, I. Orue¹⁰, A. Abad⁴, A. García-Arribas¹¹, M. Fernandez Gubieda¹¹, J. Alonso Masa⁶ ¹Ciencias, Universidad Pública de Navarra, Pamplona, Spain, ²Física, Universidad de Oviedo, Oviedo, Spain, ³CIC biomaGUNE, Donostia, Spain, ⁴Inmunología, Microbiología y Parasitología, Universidad del País Vasco (UPV/EHU), Leioa, Spain, ⁵Aix-Marseille Institute of Biosciences and Biotechnologies (BIAM), Aix-Marseille Université, CNRS, Saint-Paul-lez-Durance, France, ⁶CITIMAC, Universidad de Cantabria, Santander, Spain, ⁷Institute of Physics. Johannes Gutenberg University of Mainz, Mainz, Germany, 8Physics and Materials Science, University of Luxembourg, Grand Duchy of Luxembourg, Luxembourg, 9Institute for Advanced Studies, Luxembourg, Luxembourg, ¹⁰SGlker, Universidad del País Vasco (UPV/EHU), Leioa, Spain, ¹¹Electricidad y Electrónica, Universidad del País Vasco (UPV/EHU), Leioa, Spain, ¹²Física Aplicada, Universidad del País Vasco (UPV/EHU), Bilbao, Spain

Magnetosomes synthesized by magnetotactic bacteria (MTB) represent exceptional model systems for studying nanoscale magnetic phenomena due to their high crystallinity, uniform size, and chain-like arrangement [1,2]. In this work, we investigate the thermal evolution of magnetic anisotropies in magnetosomes produced by two MTB species—

Magnetospirillum gryphiswaldense and Magnetovibrio blakemorei—which synthesize Fe₃O₄ nanoparticles of similar size but different morhphologies: cuboctahedral and truncated hexa-octahedral, respectively (Fig.1). Static magnetization measurements (M vs T, M vs H) from 5 to 300 K, combined with simulations based on a dynamic Stoner—Wohlfarth model, reveal a complex interplay between shape, dipolar, and magnetocrystalline contributions to the total anisotropy [3].

At room temperature, shape anisotropy dominates, with the elongated *M. blakemorei* magnetosomes showing an effective uniaxial anisotropy constant of ~25 kJ/m³-more than twice that of *M. gryphiswaldense*. Below the Verwey transition (~110 K), the uniaxial anisotropy increases nonmonotonically, driven by the emergence of a magnetocrystalline component which significantly affects the magnetic behavior (Fig.2). By isolating each anisotropy contribution, we demonstrate that the Verwey transition in these magnetosomes, contrary to what happens in the bulk, is gradual rather than abrupt, pointing to a progressive cubic-to-monoclinic structural transformation.

These results highlight the potential of magnetosomes as precise nanoplatforms to probe and model complex magnetic behaviors, with implications for biomedical applications and emerging areas such as bioencoded magnonics [4].

- 1. D. Gandia, L. Gandarias, L. Marcano et al., Nanoscale., Vol. 12, p. 16081 (2020)
- 2. I. Orue, L. Marcano, P. Bender et al., Nanoscale., Vol. 10, p. 7407 (2018)
- 3. D. Gandia, L. Marcano, L. Gandarias et al., ACS Omega, Vol. 10, p. 16061 (2025)
- 4. B. W. Zingsem, T. Feggeler, A. Terwey et al. Nature Communications, Vol. 10, p. 4345 (2019)

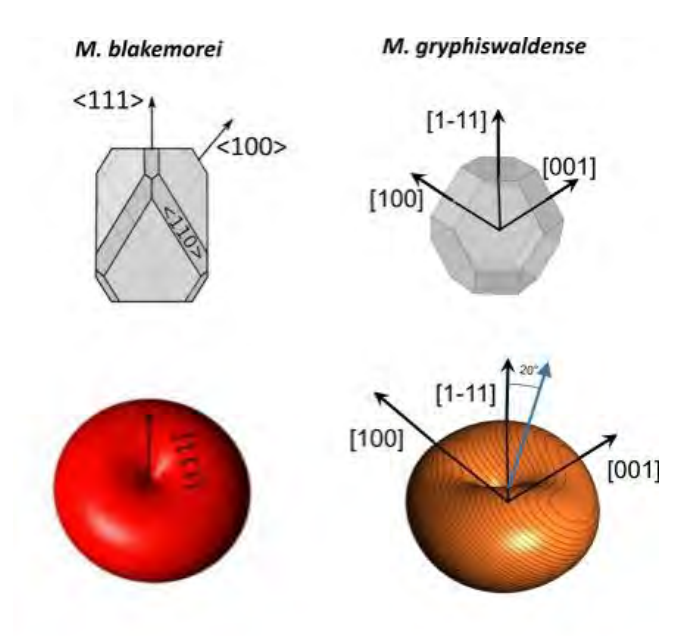


Fig. 1 Schematic morphology and shape anisotropy energy landscape of magnetosomes from *M. blakemorei* and *M. gryphiswaldense*.

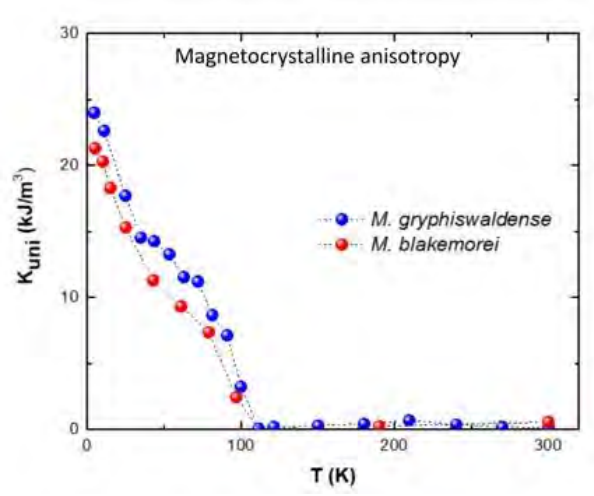


Fig. 2 Temperature dependence of the magnetocrystalline effective uniaxial anisotropy constant.

DC-10. All-Oxide Hybrid Spinel Core@Shell Nanoparticles: A Seed-Mediated Approach Toward Magneto-Optical Theranostics

<u>S. Jan</u>¹, R. Das², R. Roy Chowdhury¹, A. I. Ojo¹, Y. Wadumesthri¹, H. Rodríguez Gutiérrez¹, H. Srikanth¹, D. A. Arena¹

¹Department of Physics, University of South Florida, Tampa, Florida, United States, ²SEAM Research Centre, South East Technological University, Waterford, Ireland

Hybrid epitaxial quantum dots based on II-VI materials (e.g., CdSe@CdS) have been extensively studied for their quantum confinement effects and optoelectronic properties. Here, we report the successful synthesis and characterization of a new class of hybrid all-oxide spinel nanoparticles (HSNPs) composed of a luminescent (ZGO) spinel core and a magnetic (FO) spinel shell. The core NPs were synthesized using a solvothermal method, followed by shell growth via thermal decomposition by employing the seed-mediated approach. Structural analyses via X-ray diffraction confirm the preservation of the spinel phase in both core and core@shell architectures with no impurity phases, supported by TEM imaging that reveals clear core@shell morphology. Raman and photoluminescence (PL) spectroscopy confirmed the retention of ZGO optical signatures in the core@shell system. Additionally, magnetometry studies revealed a broad Verwey transition (around 110 K), indicative of finite-size effects in the FO shell 1. MH loops exhibited non-vanishing coercivity up to 350 K, indicating robust magnetic order. Bloch law fitting of saturation magnetization versus temperature yielded an

exponent of 1.93, deviating from bulk behavior (3/2) and consistent with nanoscale magnetic confinement. These findings demonstrate the successful integration of optical (ZGO) and magnetic (FO) functionalities in a single hybrid nanostructure. Neutron scattering studies are planned to probe the magnetic structure and refine our core@shell models at the nanoscale ². These findings position ZGO@FO HSNPs as promising candidates for multifunctional nanoplatforms in bioimaging, magnetic hyperthermia, and magnetically guided drug delivery.

1. Das, R.; Kalappattil, V.; Phan, M.-H.; Srikanth, H., Magnetic anomalies associated with domain wall freezing and coupled electron hopping in magnetite nanorods. J. Magn. Magn. Mater. 2021, 522, 167564.

2. Kons, C.; Krycka, K. L.; Robles, J.; Ntallis, N.; Pereiro, M.; Phan, M.-H.; Srikanth, H.; Borchers, J. A.; Arena, D. A., Influence of hard/soft layer ordering on magnetization reversal of bimagnetic nanoparticles: Implications for biomedical/theranostic applications. ACS Appl. Nano Mater. 2023, 6 (13), 10986-11000.

DC-11. Nanostructuring effects on the Verwey Transition in Fe_3O_4 Nanoparticles

R. Gautam¹, W. Pitt³, R. Harrison², <u>K. Chesnel¹</u>
¹Physics, Brigham Young University, Provo, Utah, United States, ²Chemistry, Brigham Young University, Provo, Utah, United States, ³Chemical Engineering, Brigham Young University, Provo, Utah, United States

Magnetite (Fe₃O₄) nanoparticles provide a platform for a wide range of applications in nanotechnologies and medicine, such as targeted drug delivery and magnetic hyperthermia. Controlling the magnetic properties of the nanoparticles is crucial for optimal use in these applications. However, nano-structuration often leads to the alteration of the physical properties compared to bulk Fe₃O₄. Here, we report the alteration and vanishing of the magneto-crystalline Verwey transition in Fe₃O₄ nanoparticles under 150 nm, depending on their size, shape and spatial arrangement. Synthesized via an organic solution-based method, our nanoparticles' size ranges from 5 to 125 nm and their shape varies from spherical to partially faceted. When deposited on substrates, the nanoparticles either remain detached or form cluster or chains. X-ray diffraction (XRD) confirms phase-pure, crystalline particles with a cubic inverse spinel structure. Vibrating sample magnetometry (VSM) allowed us to

establish the Verwey transition via field cooling (FC/ZFC) measurements as well as via temperature-dependent hysteresis. We found that the magnitude of Verwey transition and Verwey temperature T_V not only depend on particle size but also shape and arrangement. Specifically, T_V and the magnitude of the transition are reduced compared to the bulk value (125 K) and decrease when the particle size decreases, before completely vanishing. The cutoff size depends on various parameters, such as particle morphology surface spin disorder, anisotropy, and crystallographic imperfections. Also, we found that the Verwey transition is incompatible with superparamagnetism. To summarize these findings, we generated a phase diagram as illustrated in Fig.1, using particle size as the order parameter.

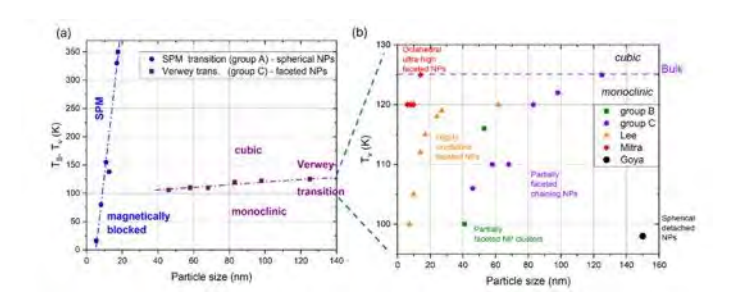


Fig. 1 Overview of the observed magnetic transitions in 5-150 nm Fe $_3$ O $_4$ NPs. (a) Plot of the superparamagnetic transition T $_B$ for our small spherical SPM NPs and of the Verwey transition T $_V$ for our larger partially faceted NPs (b) Zoomed-in view on the Verwey transition, plotting T $_V$ for our Fe $_3$ O $_4$ NPs against results in the literature for highly faceted NPs.

DC-12. Dynamics of magnetic fluctuations in Fe₃O₄ nanoparticles

K. Chesnel, J. Rackham BYU, Provo, Utah, United States

Magnetic nanoparticles (NPs) provide an ideal support for developing a wide range of nanotechnologies and biomedical applications, such as drug-delivery, gene delivery, hyperthermia, or contrast agents for MRI.[1] Magnetite (Fe₃O₄) NPs are good candidates for these applications due to their non-toxicity and long-life in the bloodstream. To optimize these applications, it is crucial to well control the magnetic response of individual NP when manipulating a collection of them via a magnetic field. In

particular, it is useful to identify any interparticle magnetic correlations that may cause the magnetic response to deviate from superparamagnetism, induce superferromagnetism and magnetic hysteresis. To that end, we have studied the magnetic response of 5 - 100 nm Fe₃O₄ NPs and its dependence on NP size, using magnetometry [2] and spin muon resonance [3]. However, this information remains macroscopic or spatially averaged. Here we show how nanoscale spatial information on interparticle magnetic correlations can be obtained via x-ray resonant magnetic scattering (XRMS) [4] as illustrated in Figure 1. By tuning the energy of the x-rays to resonant edges of Fe and comparing opposite polarization helicities, we have extracted information about the local inter-particle magnetic orders within NP assemblies of various sizes.[5] We fitted the XRMS data using a model based on chains of NPs.[6] The data fitting shows ferromagnetic ordering when an external magnetic field is applied, and the emergence of antiferromagnetic ordering, competing with magnetic randomness, when the field is brought back near the coercive point (zero net magnetization). We studied how these correlations depend on particle size and found an enhancement of magnetic couplings and antiferromagnetic orders for bigger particles. [7]

- 1. Frey et al., Chem. Soc. Rev. 2009, 38, 2532-2542 (2009)
- 2. Klomp et al., IEEE Trans. Mag. 56, 2300109 (2020)
- 3. Frandsen et al., Phys. Rev. Matter 5, 054411 (2021)
- 4. Kortright et al., Phys. Rev. B 71, 012402 (2005)
- 5. Chesnel et al., Magnetochemistry 4, 42-58 (2018)
- 6. Rackham et al., AIP Advances 9, 035033 (2019)
- 7. Rackham et al., Phys. Rev. B 108 (10), 104415

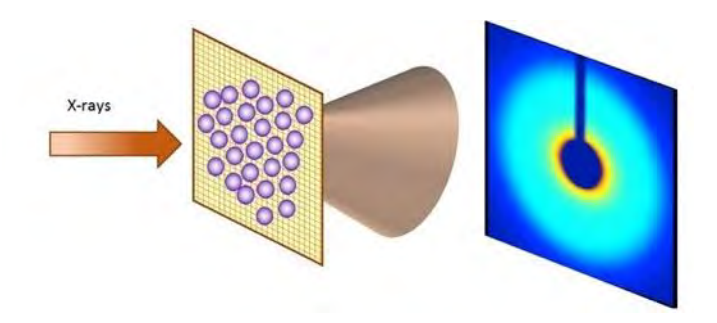


Figure 1: Layout of the x-ray resonant magnetic scattering (XRMS) measurement of a nanoparticle assembly.

SESSION DD: ND2FE14B AND MEASUREMENT TECHNIQUES

Co-Chair(s): A. Lisfi, *Physics, Morgan State University,*Baltimore, Maryland, United States and Y. Hirayama, National
Institute of Advanced Industrial Science and Technology (AIST),
Nagoya, Japan

Wednesday, October 29, 2025 02:00 PM-05:30 PM Ballroom B

DD-01. Unveiling Buried Magnetic Nanodomains: High-Resolution Phase Mapping in Thin Films with Synchrotron Radiation

A. Lengyel¹, D. G. Merkel¹, G. Bazso¹, A. I. Chumakov², D. L. Nagy¹, G. Hegedus¹, Z. E. Horvath³, N. M. Nemes⁴, M. A. Gracheva³, E. O. Szilagyi¹, S. Sajti¹, A. Deak³, L. Illes³, A. Nemeth¹, F. Maccari⁵, I. Radulov⁵, M. Major^{1, 5}, Z. Zolnai³, S. Graning⁶, K. Sajerman⁷, T. Vaczi¹, P. Petrik³, D. Mukherjee³, S. Lenk⁷, D. Bessas², G. Z. Radnoczi³

¹HUN-REN Wigner Research Centre for Physics, Budapest, Budapest, Hungary, ²European Synchrotron Radiation Facility, Grenoble, France, ³HUN-REN Centre for Energy Research, Budapest, Budapest, Hungary, ⁴Universidad Complutense de Madrid, Madrid, Spain, ⁵Technische Universität Darmstad, Darmstad, Germany, ⁶Eotvos Lorand University, Budapest, Budapest, Hungary, ⁷Budapest University of Technology and Economics, Budapest, Budapest, Hungary

Nuclear resonance scattering (NRS) is an exceptionally powerful tool for the characterization of magnetic phases and microenvironments. By leveraging the latest developments of the European Synchrotron Radiation Facility, depth-selective/high-resolution magnetic mapping of iron-rhodium (FeRh) thin layer (in a multiferroic composite) was performed during temperature-, magneticand electric field-induced metamagnetic phase transitions. NRS experiments revealed that different depths of the homogenous FeRh layer not only exist in different magnetic states, but also responds differently to external stimuli. It was found that both temperature and magnetic field induce a vertically homogeneous antiferromagnetic-toferromagnetic transition, whereas the electric field produces an oriented transformation. The direct probing of the microenvironments within a single nanostructure was enabled only by the recent installation of the nanofocus system at the nuclear resonance beamline. Surprisingly, the smaller patches were found to favor the antiferromagnetic state more than the larger ones during heating. Since no significant differences in the lattice parameters were observed, the usual initial strain couldn't be the primary

cause of the observed behavior. A plausible explanation could be the formation of an oxide layer on the surface, which may constrain the FeRh lattice and inhibit its thermal expansion. Since the magnetic transition in FeRh is coupled to lattice expansion, this constraint could suppress the transition altogether. However, it is also possible that if the patches fall below a critical size, they cannot house multidomain magnetic structures; and in single domain state their stray magnetic field would require too much energy to allow the magnetic transition.

In addition, multiple methods, such as localized heat treatment by laser or masked heavy ion implantation, were tested for producing various magnetic nanostructures within the chemically homogeneous alloy. NRS also showed that the implantation creates cone-like structures within the thin film. Collectively, the results offer critical insight into the mechanisms driving the FeRh-based multiferroics and highlight the potential of the NRS.

D. G. Merkel, G. Hegedus ... A. Lengyel: A Three-Dimensional Analysis of Magnetic Nanopattern Formation in FeRh Thin Films on MgO Substrates: Implications for Spintronic Devices, ACS APPLIED NANO MATERIALS, 5:4 pp. 5516-5526., 11 p. (2022) doi: 10.1021/acsanm.2c00511

A. Lengyel, G. Bazsó ... D.G. Merkel: Synergy effect of temperature, electric and magnetic field on the depth structure of the FeRh/BaTiO3 composite multiferroic, *MATERIALS SCIENCE AND ENGINEERING B*, 285,115939, 8 p. (2022) doi:10.1016/j.mseb.2022.115939

D.G. Merkel, K. Sajerman ... A. Lengyel: Laser irradiation effects in FeRh thin film, *MATERIALS RESEARCH EXPRESS*, 10:7, 076101, 7 p. (2023) doi:10.1088/2053-1591/ace4a3

A. Lengyel ... G. Hegedus, D. G. Merkel: Nuclear resonance scattering study of metamagnetic transition in nanosized FeRh structures (under publication) (2025)

DD-03. Accurate Saturation Magnetization Measurement Method for Fe-based Alloy Foils

<u>T. Tabata</u>, Y. Asari, M. Noujima, S. Terada Research & Development Group, Hitachi Ltd., Hitachi, Ibaraki, Japan

To enhance the power density of electric motors, improving the saturation magnetization ($\mu_0 M_s$) of electrical steel sheets is a key development objective. In addition, thinning of these sheets has been promoted to reduce eddy current

losses, and sheets with a thickness below 100 µm have already been commercialized. Therefore, it is essential to accurately evaluate the $\mu_0 M_S$ of thin bulk foil materials. Vibrating Sample Magnetometers (VSMs) are widely used to measure $\mu_0 M_S$. However, evaluation using VSMs is affected by factors such as sample shape, working gap, and dimensional deviations relative to the standard Ni reference shape. The shape dependence of measurement values has not yet been fully clarified [1][2]. This issue is particularly critical for thin materials, where even slight dimensional variations can significantly influence the results. In this study, to establish a precise measurement method, we investigated the effects of dimensional differences. We prepared a standard Ni plate and pure iron plates with varying dimensions and aspect ratios, and examined how these differences affect the measured $\mu_0 M_S$. The results revealed that superconducting VSMs, in which the magnetic field and sample vibration directions are parallel, and normal-conducting VSMs, in which these directions are perpendicular, exhibit opposite trends in the effect of the sample aspect ratio on the measured $\mu_0 M$. This discrepancy arises because the relative distance to the detection coil changes in opposite ways depending on whether the aspect ratio is aligned with the magnetic field direction in the two VSM types. Therefore, to compare results from different VSMs, it is necessary to correct the measured values for dimensional deviations relative to the standard Ni sample. These findings highlight the importance of accounting for the specific characteristics of each VSM when interpreting measurement results and developing precise evaluation methods.

This research is partially based on results obtained from Green Innovation Fund Projects / Next-generation Motor Development (JPNP21026) commissioned by the New Energy and Industrial Technology Development Organization (NEDO).

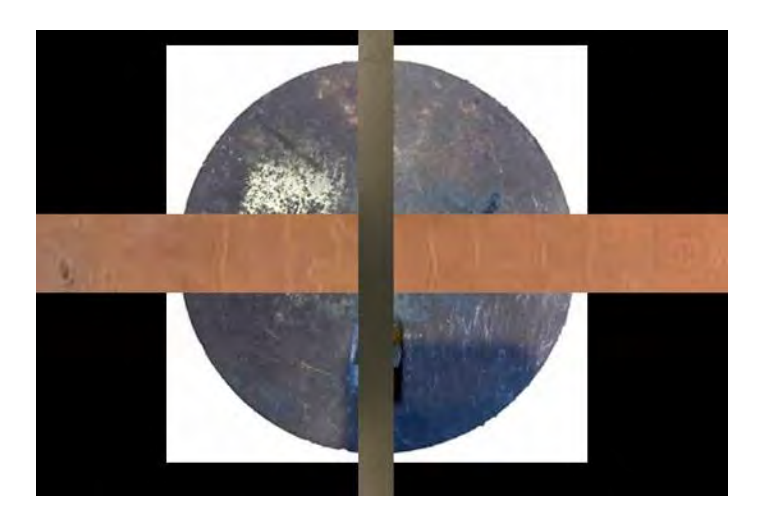
[1] J. Lindemuth, J. Krause and B. Dodrill, IEEE Transactions on Magnetics, Vol. 37, No. 4, p.2752 (2001)

[2] A. Zieba and S. Foner, Rev. Sci. Instrum, Vol. 53, No. 9, p.1344 (1982)

DD-05. New steel coupons hosting residual stresses for steel health monitoring calibration

T. Damatopoulou, E. V. Hristoforou *National TU of Athens, Athens, Greece*

Steel coupons are plates of various steel grades, in which residual stresses have been induced and maintained to be used as transfer standards to calibrate the response of magnetic sensors with respect to these residual stresses. The monotonic and non-hysteretic dependence of these sensors on residual stresses, permits the measurement and monitoring of the distribution of residual stresses in the under-test steel, thus allowing for the structural conditioning and possibly the corresponding failure time prognosis. Our group has initiated the principle of steel coupons using autogenous welding to generate residual stresses on the surface and in the bulk of various steel grades. However, these steel coupons suffered issues of repeatability, difficulty in preparation and phase transformation. Therefore, we have initiated work towards the development of new types of stress coupons, that will be advances in different aspects. These new steel coupons are presented for the first time in this paper. Bearing in mind the experience concerning the challenges of induction heating, namely the fast and somehow non-controllable temperature increase at the heated area, we decided to use a much simpler technology, namely the normal Joule heating process via a stove eye, equipped with a precise thermostat. Fig. 1 illustrates the actual set-up, the temperature of which is controlled by a thermostat with a maximum uncertainty of ± 1 °C, while the range of temperatures for proper quenching can be in the order of ±10°C. A cast iron substrate offers a uniform temperature distribution. The required temperature profile can reach the required temperature in some minutes after setting it on top of the copper plate, which is considered as a safe time window to avoid temperature homogenization in the steel coupon. As soon as the required temperature profile is reached, the steel coupon in inserted in water or oil bath to undergo a quenching process. This way, a Standard draft can be prepared to be applied in a related standard's organization, like ASTM or IEEE.

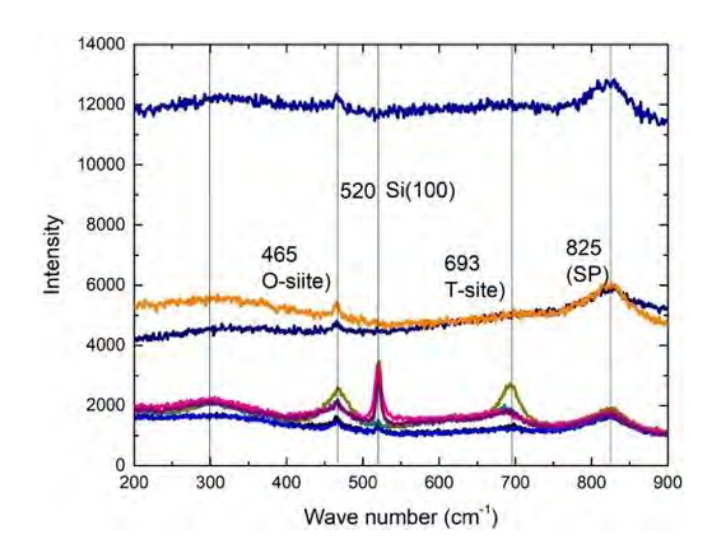


DD-06. Raman Spectroscopic and Computational Investigation of Gold-Coated CoFe $_2$ O $_4$ Thin Films

T. Lamichhane

Engineering & Physics, University Of Central Oklahoma, Edmond, Oklahoma, United States

Magnetic nanoparticles and thin films have attracted considerable interest over recent decades due to their versatile applications in high-density magnetic recording, data storage, spintronics, solar cells, sensors. Among these, cobalt ferrite (CoFe₂O₄) has emerged as a prominent material, valued for its excellent electromagnetic performance, chemical stability, mechanical hardness, and high cubic magnetocrystalline anisotropy. here, we investigate the structural, magnetic, and vibrational properties of cobalt ferrite thin films coated with gold, using Raman spectroscopy and computational methods. The gold coating enhances surface conductivity and stability while influencing the material's vibrational modes and magnetic anisotropy. Raman spectra revealed the suppression of key Raman-active modes, including 693 cm⁻¹ (A₁g) and 465 cm⁻¹ ¹ (F₂g), post gold coating, reflecting restricted Fe-O vibrations at tetrahedral and octahedral sites. Firstprinciples calculation based on Density Functional Theory (DFT) corroborate these findings, showing metallic bonding at the Au/CoFe₂O₄ interface and enhanced magnetic moments of surface atoms. Thus, this combined experimental and computational investigation highlights the tunable properties of gold-coated CoFe₂O₄ films for advanced technological applications.



DD-07. Measuring Magnetic Exchange using Magnetometry and Atomistic Simulations

C. Swindells^{1, 2}, W. K. Peria¹, J. Barker³, J. J. Wisser¹, M. Schneider¹, M. Pufall¹, H. T. Nembach¹

¹NIST, Boulder, Colorado, United States, ²Electrical Engineering, CU Denver, Denver, Colorado, United States, ³School of Physics and Astronomy, University of Leeds, Leeds, United Kingdom

Exchange stiffness is a fundamental parameter underpinning many magnetic phenomena. The emergent response arising from this local interaction governs key device-level metrics such as domain wall velocity¹ and switching probabilities in MRAM cells^{2,3}, while any micromagnetic simulator requires it to produce accurate results. However, open questions remain regarding how best to quantify exchange stiffness in magnetic thin films. Measuring exchange in samples a few nanometers thick is difficult – usually it is inferred from a global material property. State of the art neutron scattering measurements, typically the gold standard in extracting exchange, are not feasible on the nanoscale due to the low sample volume and polycrystalline films. Another common method is to fit a Bloch T^{3/2} relation to the temperature profile of the magnetization; however, this is only valid at low temperatures⁴ and relies on several parameters not easily defined in real thin films. While fitting the spin wave dispersion obtained using Brillouin Light Scattering (BLS)⁵ can overcome these issues, it is not a technique readily available to most. To be able to quantify exchange in a timely and effective manner, we require a method that is compatible with existing measurement techniques. Here, we show a method to determine the exchange parameter, by using atomistic simulations^{6,7} to

quantitatively model temperature dependent magnetization data obtained using a magnetometer. For a simple, thin CoFeB system, we explore the landscape of three fitting parameters, exchange, moment and the anisotropy constant, and show how the resultant exchange stiffness for thin film systems is drastically reduced compared to bulk values. We compare these results to parameters obtained using BLS⁷ to determine the impact of the assumed lattice structure on the exchange determination. This method to quickly determine key material parameters from unpatterned films has significant implications for both future simulations and accelerated device development.

This work was performed with funding from the CHIPS Metrology Program, part of CHIPS for America, National Institute of Standards and Technology, U.S. Department of Commerce.

- [1] D. Kumar et al., Phys. Rep. 958 (2022)
- [2] T. Santos et al., J. Appl. Phys. 128, 113904 (2020)
- [3] G. Mihajlović Appl. Phys. Lett. 117, 242404 (2020)
- [4] J. Barker et al Phys. Rev. B 100, 140401(R) (2019)
- [5] G. Riley et al., Appl. Phys. Lett. 120, 112405 (2022)
- [6] J. Barker et al Electron. Struct. 2 044002 (2020)
- [7] J. Barker, JAMS, GitHub repository, https://github.com/stonerlab/jams (2025)

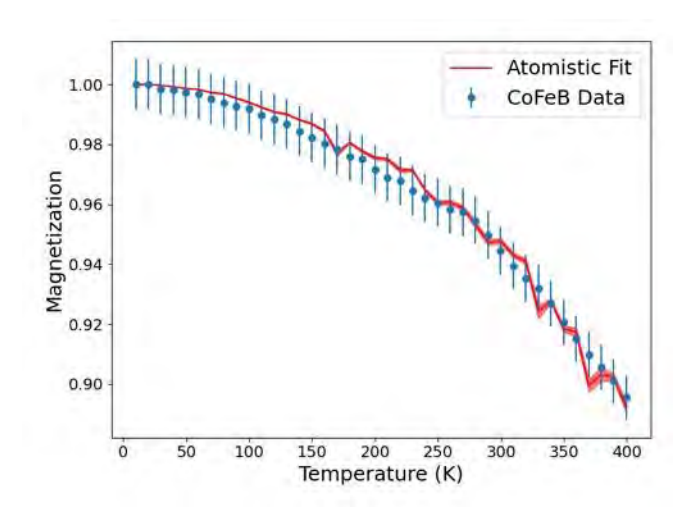


Fig.1 Example atomistic fit to data

DD-08. Mechanical Strengthening of Nd-Fe-B Sintered Magnets via Microstructure Engineering

<u>B. Cui</u>, X. Liu, W. Tang, I. Nlebedim, J. Cui Ames National Laboratory, Ames, Iowa, United States

Rare-earth permanent magnets (REPMs), primarily Nd-Fe-B and Sm-Co sintered magnets, exhibit exceptional magnetic

properties. They are widely used in wind turbines, electric and hybrid vehicles, telecommunications, consumer electronics, industry automation, medical devices, data storage, and magnetic sensors. However, sintered REPMs are inherently brittle. The brittleness can lead to high magnet failure rates and material waste during manufacturing, especially when machining thin or narrow magnets. Moreover, extra precautions are necessary for applications involving high stress, vibration, or mechanical shock. Therefore, developing mechanically robust sintered REPMs with high magnetic performance is of considerable scientific and technical importance.

This work focuses on novel strengthening strategies for improving the mechanical properties, particularly flexural strength, of Nd-Fe-B sintered magnets while maintaining their magnetic properties. These strategies mainly include grain size and grain boundary engineering. Fracture in Nd-Fe-B magnets is dominated by an intergranular mode, where the grain boundary phases (GBPs) represent the weakest link. Our micromechanical modeling and experimental results show that the fracture strength of Nd-Fe-B magnets is influenced by factors such as matrix grain size, the crystal structure and chemical composition of the GBPs and additives, and their distribution and volume fractions. The mechanical strength increases as the matrix grain size increases. Additionally, by enhancing the fracture toughness, content, and dispersion of ductile metallic GBPs with high fracture toughness, the mechanical strength of Nd-Fe-B magnets can be significantly improved. These microstructure engineering approaches help impede the initiation and propagation of microcracks, resulting in a substantial increase in the magnet's flexural strength. Notably, a simultaneous enhancement of both flexural strength (σ) and intrinsic coercivity (H_{ci}) was achieved in ductile GBP-modified Nd-Fe-B sintered magnets. For example, σ increased from 333 MPa to 480 MPa and H_{ci} rose from 14.4 kOe to 16.6 kOe, while maintaining 90% of the maximum energy product (BH)_{max}.

DD-10. Relationship between Nd-rich phase and oxygen content for additive-free sintering with regenerated powder from magnet sludge waste

D. Kim¹, V. Galkin²

¹Korea Institute of Materials Science, Changwon, Korea (the Republic of), ²Daegu Gyeongbuk Institute of Science and Technology, Daegu, Korea (the Republic of) Nd-Fe-B-based magnets are widely applied in many fields such as electrical devices, generators, and electric motors due to their outstanding magnetic property [1]. The conventional Nd-Fe-B sintered magnet production generates up to 30-40 % waste, most of which is a sludge produced during cutting or machining operations. Since this sludge is so oxidized, it cannot be used for direct remelting or sintering. Typical recycling methods based on hydrometallurgy have several disadvantages, such as the use of hazardous chemicals, the difficulty of boron recycling, and the separate production of iron and rare earth elements. Therefore, reduction-diffusion (RD) process is emerging and gaining significant attention nowadays for recycling of magnet sludge [2]. On the other hand, regenerated Nd-Fe-B powder by RD poses difficulties in sintering without rare earth (RE) hydride additives due to oxidation or loss of the Nd-rich phase during the washing

Here, the effect of different washing methods such as conventional water washing, acetic acid washing, and novel wet ball milling (WBM) washing on the Nd-rich phase and oxygen content of RD powders was studied. The WBM washing involves low energy ball milling in organic liquid media, which simplified the removal of impurities from the RD powder. In addition, different CaH₂/sludge ratios and temperature for heat treatment were examined for process optimization. The powder after WBM washing showed that oxygen content was decreased compared to water washing and Nd-rich phase remained compared to acidic washing, which resulted in successful densification during sintering and the formation of Nd-rich areas in sintered body. The regenerated powder possessed coercivity (Hc) of 7.0 kOe, squareness (Mr/Ms) of 0.95, and (BH)max of 20.0 MGOe and additive-free sintered body demonstrated a coercivity of 25.3 kOe and (BH)max of 33.3 MGOe, which is comparable to the magnets made from acidic acid-washed powder with the essential addition of more than 10 wt% of REHx reported in other paper [3].

[1] O. Gutfleisch, M.A. Willard, E. Brück, C.H. Chen, S.G. Sankar and J.P. Liu, Adv. Mater., Vol.23, p.821 (2011)
[2] H. Xu, Q. Lu, Y. Li, W. Liu, X. Yi, Y. Wang and M. Yue, JALCOM, Vol.909, p.164744 (2022)
[3] X. Yin, M. Liu, B. Wan, Y. Zhang, W. Liu, Y. Wu, D. Zhang

[3] X. Yin, M. Liu, B. Wan, Y. Zhang, W. Liu, Y. Wu, D. Zhang and M. Yue, J. of Rare Earth, Vol.36, p.1284 (2018)

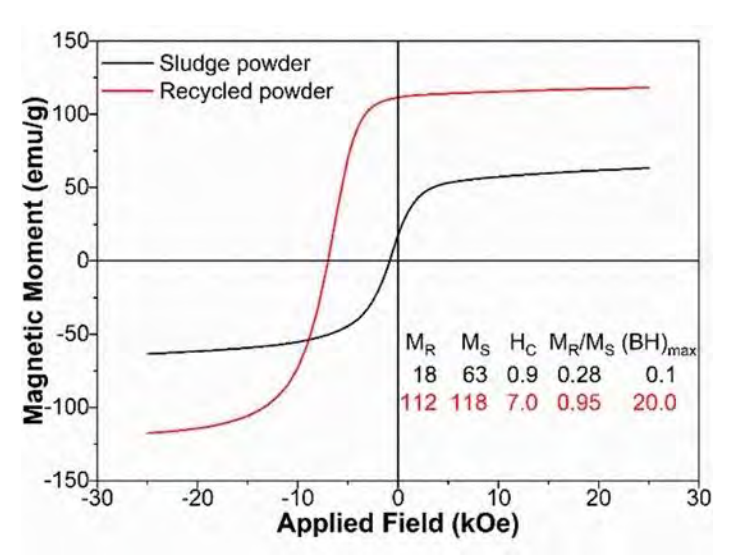


Figure 1. Room temperature demagnetization curves for initial magnet sludge powder and regenerated powder

DD-11. Correlation of Coercivity, Microstructure, and Surface Defects in HDDR-Processed Nd-Fe-B Powders for Bonded Magnet Applications

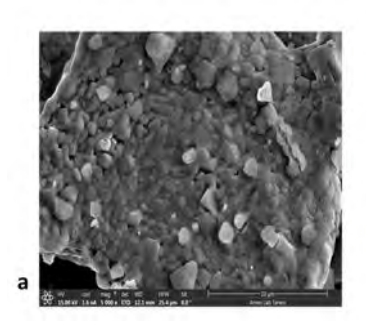
X. Liu¹, M. K. Kesler², Z. Tener³, M. J. Kramer⁴, I. Nlebedim¹
¹Division of Critical Materials, Ames National Laboratory, Ames, Iowa, United States, ²Materials Science and Technology Division, Oak Ridge National Laboratory, Oak Ridge, Tennessee, United States, ³Savannah River National Laboratory, Aiken, South Carolina, United States, ⁴Division of Materials Science and Engineering, Ames National Laboratory, Ames, Iowa, United States

This work relates to the need for a deeper understanding and controlling of surface defects in Hydrogenation-Disproportionation-Desorption-Recombination (HDDR)-processed powders, particularly for applications in recycling and the production of high-performance bonded magnets. A key challenge in optimizing HDDR-processed Nd-Fe-B powders is understanding the impact of surface defects on their magnetic properties, particularly coercivity. This study investigates the influence of surface defects on coercivity and microstructure in HDDR powders using scanning electron microscopy (SEM), X-ray diffraction (XRD), magnetic measurements, and micromagnetic simulations.

We observed that coercivity decreases as particle size reduces, with SEM revealing surface defects and the detachment of Nd₂Fe₁₄B grains and Nd-rich phases from the

particles surface (Fig. 1a). Micromagnetic simulations show that demagnetization begins at the surface (Fig.1b), where these defects are most concentrated which leads to reduced coercivity. The reduction in coercivity for smaller HDDR particles is attributed to an increased specific surface area, which creates more sites for magnetic domain nucleation during magnetization reversal. The understanding from our work can be leveraged to address materials criticality through recycling of sintered Nd-Fe-B magnets into bonded magnets, beneficial for reclaiming REEs. By addressing the role of surface defects in coercivity degradation, this study provides insights for improving both new powder production and recycling strategies, ultimately leading to enhanced performance of bonded magnets and contributing to more sustainable practices in the rare earth supply chain.

This work was supported by the Critical Materials Innovation Hub funded by the U.S. Department of Energy, Office of Energy Efficiency and Renewable Energy, Advanced Materials and Manufacturing Technologies Office (AMMTO). The work was performed in Ames National Laboratory, operated for the U.S. Department of Energy by Iowa State University of Science and Technology under Contract No. DE-AC02-07CH11358.



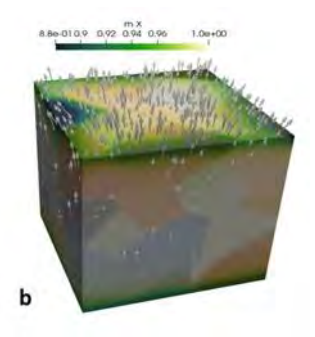


Fig.1 (a) SEM image and (b) micromagnetic simulated magnetization distribution (at a remanent state) of HDDR-process Nd-Fe-B particle

DD-12. Critical Rare Earth Lean Nd-Ce-Fe-B Permanent Magnets Powder via Wet Chemical Process

<u>H. Parmar</u>, M. Broders, C. I. Nlebedim, X. Liu Division of Critical Materials, Ames National Laboratory, Critical Materials Innovation Hub, Ames, Iowa, United States

NdFeB permanent magnets are the strongest magnets and are widely used in many applications. Nevertheless, their

growing demands lead to strain on the supply of rare earth elements, including Nd, Pr, Dy and Tb. Hence, Ce can be applied to produce magnetic materials. Also, it is much less utilized coproduct of Pr/Nd mining [1]. However, Ce-Fe-B has far inferior intrinsic magnetic properties than Nd-Fe-B. It was shown theoretically that Ce-Fe-B magnetic property can be improved by partial replacement of Ce by Nd or Pr. In addition, the calculation also shows that the magnetic property is improved in nanoscale particles [2]. Conventional sintering techniques are unable to produce the required ideal nanostructure. Hence, bottom-up synthesis techniques, such as chemical synthesis is a promising approach to produce such nanostructures. In this work, we have adopted chemical based synthesis process to make rare earth-iron-boron oxides followed by reduction diffusion using calcium as reductants. We have successfully prepared a series of Ce-Nd-Fe-B nanoparticles with varied Nd content. The typical coercivity increased significantly, from 0.7 kOe to 9.1 kOe, as Nd content increased from 0 to 100%.

This work was supported by the Critical Materials Innovation Hub funded by the U.S. Department of Energy, Office of Energy Efficiency and Renewable Energy, Advanced Materials and Manufacturing Technologies Office (AMMTO). The work was performed in Ames National Laboratory, operated for the U.S. Department of Energy by Iowa State University of Science and Technology under Contract No. DE-AC02-07CH11358.

A. K. Pathak et al., "Cerium: An unlikely replacement of dysprosium in high performance Nd-Fe-B permanent magnets," Adv. Mater., vol. 27, no. 16, pp. 2663–2667, Apr. 2015.

X. B. Liu et al., "Theoretical Correlation of Elemental Distribution of Nd and Pr in Ce-Fe-B Microstructure With Hard Magnetic Properties, IEEE Transactions on Magnetics, vol. 57, no. 2, Feb. 2021

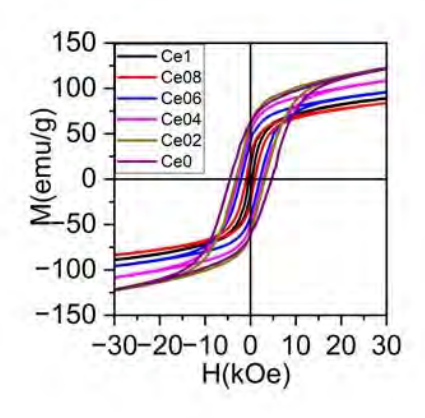


Fig. 1 Hysteresis loop of particles synthesized with a range of Nd substitution from 0% to 100% in Ce-Fe-B.

DD-13. Tailoring Nd-Fe-B Microstructure via LPBF like Cooling in Melt Spinning

A. Paul^{1, 2}, J. Shield^{1, 2}

¹Mechanical and Materials engineering, University of Nebraska-Lincoln, Lincoln, Nebraska, United States, ²Nebraska Center for Materials and Nanoscience, University of Nebraska-Lincoln, Lincoln, Nebraska, United States

Additive manufacturing (AM) of permanent magnets like Nd-Fe-B offers the opportunity to develop complex, net-shaped magnetic components with minimal post-processing and low material loss. The complex solidification inherent to laser powder bed fusion (LPBF) necessitates the development of new alloy compositions compatible with LPBF. High throughput alloy development using proxy processes that mimic the thermal environment during layerwise laser melting is essential. While melt spinning offers high cooling rates and directional heat flow similar to LPBF, traditional melt spinning with copper wheels (thermal conductivity ~400 W/mK) overestimates the cooling rate compared to LPBF. We optimized Nd-Fe-B alloys using a stainless steel (SS 304) wheel whose thermal conductivity (~16 W/mK) is closer to that of Nd-Fe-B (~7-10 W/mK) to better replicate solidification behavior in LPBF. To understand and quantify cooling rate differences, we conducted a 2D transient heat flow simulation. The results show approximate matching of cooling rates, with SS (304) at 20 m/s and Cu at 10 m/s both yielding ~3×10⁵ K/s. To experimentally verify this, an optimized ternary $Nd_{18}Fe_{74.5}B_{7.5}$ alloy was melt-spun at 10 m/s on both wheels. Magnetic measurements showed comparable coercivities of

18.8 kOe on Cu and 18.3 kOe on SS (Fig. 1), and SEM confirmed near-identical microstructures, validating the simulation. To further explore cooling rate effects, the same alloy was processed on SS wheels at speeds from 9 m/s to 12 m/s in 1 m/s steps. A drop in coercivity was observed, from 18 kOe at 12 m/s to 11.6 kOe at 9 m/s (Fig. 2), highlighting the sensitivity of this system to cooling rate. These findings offer a thermally realistic pathway for engineering Nd-Fe-B alloys for LPBF.

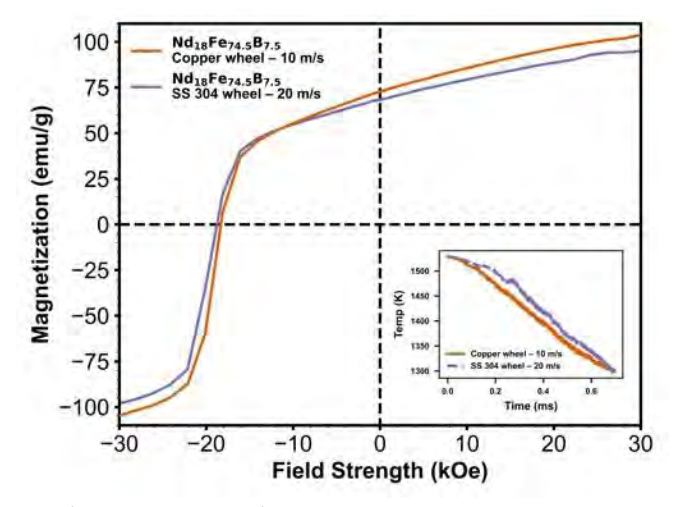


Fig. 1 M–H curves of $Nd_{18}Fe_{74.5}B_{7.5}$ ribbons produced using Cu and SS304 wheels. (Inset) Simulated cooling profiles of Nd-Fe-B ribbons processed on Cu (10 m/s) and SS 304 (20 m/s) wheels using 2D transient thermal analysis.

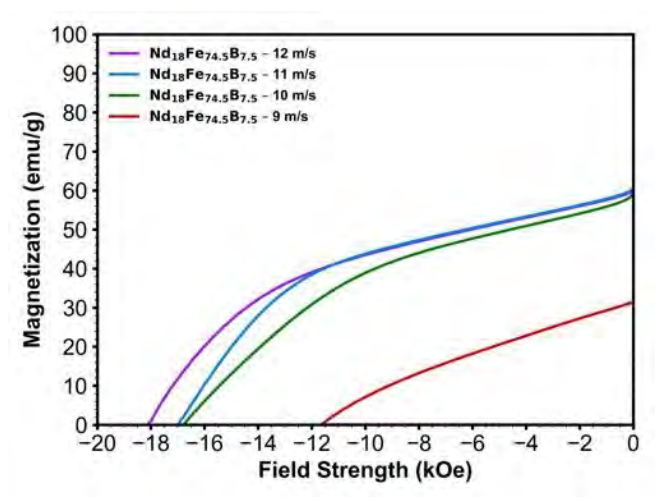


Fig. 2 Second quadrant M–H curves of $Nd_{18}Fe_{74.5}B_{7.5}$ ribbons processed on SS 304 wheels at speeds ranging from 12 m/s to 9 m/s.

DD-14. Dy-Free Sintered Nd-Fe-B Magnets Enhanced by Pr-Al-Cu Alloy via Different Grain Boundary Engineering Techniques.

<u>W. Tang</u>¹, J. Wang¹, Y. Varma², C. Pan¹, J. Cui^{1,2}
¹Ames National Laboratory, Ames, Iowa, United
States, ²Materials Science and Engineering, Iowa State
University, Ames, Iowa, United States

Nd₂Fe₁₄B-based magnets are primary candidates for applications such as wind turbine generators, industrial pumps, and electric vehicles (EVs). Heavy rare earth elements like Dy up to 10 wt% may be required for the magnets capable of operating at 200°C. Unfortunately, Dy is scarce, expensive, and subject to supply chain risks. Consequently, the development of Dy-lean or Dy-free Nd-Fe-B magnets capable of high-temperature (HT) operation is of significant interest to the EV industry. Microstructure engineering technique by grain boundary diffusion (GBD) is an effective method to develop Dy-lean or Dy-free HT magnets. GBD methods can be classified into two types: (1) Blending GBD: Grain boundary modifying alloys are blended with primary Nd-Fe-B alloy powder before sintering [1-3]. (2) Surface GBD: The GBD alloy is applied to the surface of sintered magnets in final shape through methods like dip coating, evaporation deposition, etc. [4-6]. In this study, a Pr-Al-Cu alloy was used as a GBD material and diffused into Nd-Fe-B sintered magnets using both blending and surface GBD methods. The magnetic properties and microstructure of the magnets were systematically evaluated by varying the amount of Pr-Al-Cu. Table 1 and Figure 1 present the magnetic properties and partial demagnetization curves of the magnets for comparison. For blending GBD, increasing Pr-Al-Cu content enhanced coercivity (Hci) but reduced remanence (Br) and maximum energy product ((BH)_{max}). The best compromise between H_{ci} and (BH)_{max} was achieved with 7.5 wt.% Pr-Al-Cu. On the other hand, the surface diffusion method yielded a magnet with a high H_{ci} of 21.3 kOe using only 1.5 wt.% PrAlCu, outperforming the 10 wt.% Pr-Al-Cu blending diffusion magnet (H_{cj} =19.2 kOe). However, the surface diffusion magnet exhibited lower (BH)_{max} (33.1 MGOe) due to poor squareness in its demagnetization curve. The benefits and trade-offs of two GBD methods are compared and discussed based on the resulting microstructural and magnetic properties of the magnets.

[1] W. Tang, J. Wang, C. C. Pan, M. C. Kang, L. Zhou, M. J. Kramer, J. Cui, and I. E. Anderson, IEEE Trans. Magn., 2024, 9, 2100505.

[2] F. M. Wan, Y. F. Zhang, J. Z. Han, S. Q. Liu, T. Liu, L. Zhou, J. B Fu, D. Zhou, X. D. Zang, J. B. Yang, Y. C. Yang, J. Chen, and Z.W. Deng, J. Appl. Phys. 2014, 115, 203910.

[3] M. Yan, W. Chen, J. Y. Jin, Y. S. Liu, H. S. Chen, S. P. Ringer, J. J. Xu, Y. L. Hou, M. Yue, X. L. Liu, Acta Materialia, 2022, 231, 117873.

[4] Z. W. Liu, J. Y. He, R. V. Ramanujan, Materials & Design, 2021, 209, 110004.

[5] H. Sepehri-Amin, T. Ohkubo, K. Hono, Acta Mater. 2013, 61. 1982.

[6] K. Loewe, C. Brombacher, M. Katter, O. Gutfleisch, Acta Mater. 2015, 83, 248.

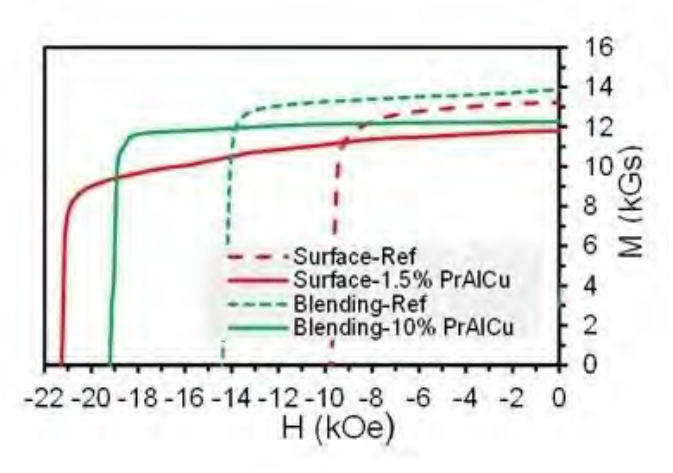


Fig. 1 Demagnetization curves of magnets diffused by Pr-Al-Cu $\,$

alloy through blending and surface GBD methods

Method	wt. %	Ms (kGs)	Br (kGs)	H _{cj} (kOe)	(BH) _{max} (MGOe)
~0.5	14.1	13.0	15.5	39.2	
~1.5	12.8	11.8	21.3	33.1	
Blending diffusion	0	14.1	13.9	14.5	45.3
	3	13.7	13.6	16.4	46.5
	5	13.1	12.9	17.1	41.2
	7.5	12.7	12.6	18.0	39,1
	10	12.3	12.2	19.2	37.2

Table 1 Magnetic properties of the magnets diffused by PrAlCu alloy through blending and surface GBD methods

SESSION DE: MAGNETIC GROUND STATES, PHASE TRANSITIONS AND MAGNETO-ELASTIC PHENOMENA

Co-Chair(s): N. J. Jones, *Physical Metallurgy and Fire*Performance Branch, Naval Surface Warfare Center, Carderock

Division, Bethesda, Maryland, United States and H.

Chi, University of Ottawa, Ottawa, Ontario, Canada

Wednesday, October 29, 2025

02:00 PM-05:30 PM

Room 2DE

DE-01. Tuning Magnetic Properties of FeGa Magnetostrictive Thin Films Using Light or Electric Fields

<u>P. Tiberto</u>¹, G. Barrera¹, F. Celegato¹, M. Coisson¹, G. Pradhan¹, D. Martella²

¹Advance Materials and Life Sciences, INRIM, Torino, Italy, ²Department of Chemistry "Ugo Schiff", Università di Firenze, Torino, Italy

Composite magnetic heterostructures with multi-responsive behavior to environmental stimuli play a crucial role in various applications, particularly in sensing and actuation systems. The integration of FeGa magnetostrictive layers with both rigid piezoelectric (PMN-PT) and flexible (Kapton, soft photo-responsive polymer) substrates represents a significant advancement in multifunctional materials, offering unprecedented control over magnetic properties through strain-mediated interactions. The ability to tune magnetism via mechanical deformation and external stimuli (i.e. magnetic fields, light, and electric fields) opens new avenues for innovative device architectures and applications.

Magnetoelectric materials hold great potential for sensor applications due to their ability to manipulate magnetic states using electric fields, thereby enhancing energy efficiency. Specifically, when FeGa layers are deposited on rigid PMN-PT piezoelectric substrates, anisotropic in-plane strains induced by electric fields (0-8 kV/cm) reorient magnetic anisotropy in 5 µm elliptical FeGa microstructures, as evidenced by hysteresis shifts in MOKE measurements [1]. Conversely, the combination of a 30 nm magnetostrictive FeGa layer with soft photo-responsive polymers—specifically, a liquid crystalline network (LCN) containing azobenzene – enables fine tuning of the film magnetic properties through light irradiation, eliminating the need for an external magnetic field. The photoactuation mechanism induces mechanical stress on the magnetostrictive FeGa thin film, causing magnetic domain rearrangement due to uniaxial stress anisotropy [2]. The

effect of light on magnetisation and electrical resistance are reported in Fig.1 a and b respectively.

This mechanically induced control over magnetism presents an alternative, energy-efficient approach for switching and modulating magnetic properties without relying on traditional magnetic components, addressing the growing demand for novel tuning mechanisms in advanced functional materials. <!--![endif]---->

[1] G. Pradhan et al., J. Phys. Mater. 7 (2024) 015016[2] G. Barrera et al., Adv. Sci. 11 (2024) 2408273

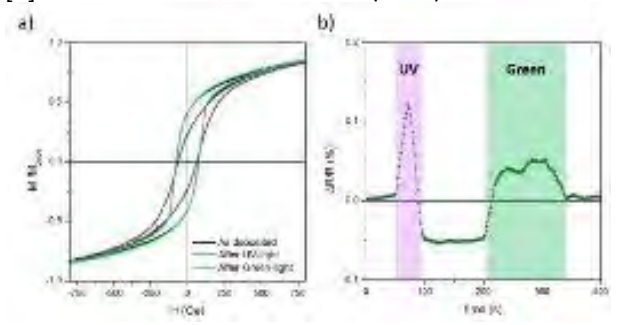


Figure 1: Hysteresis loop of the FeGa/LCN sample in asdeposited state and after UV and green light irradiation time; b) evolution of the $\Delta R/R$ curve.

DE-03. Ultra-Flexible Magneto-Elastic Diaphragm for Low-Power Actuation Applications

K. Moussi, <u>S. Ben Mbarek</u>, S. Amara, G. Setti King Abdullah University of Science and Technology (KAUST), Thuwal, Saudi Arabia

We report the design, fabrication, and experimental validation of an ultra-flexible magneto-elastic diaphragm tailored for low-power actuation in compact soft robotic and biomedical systems. The diaphragm is composed of a biocompatible silicone elastomer (Ecoflex 00-20) embedded with neodymium-based magnetic powder (MQP-15-7-20065), forming a soft composite with tunable magnetomechanical properties.

A custom molding process was developed using 3D-printed negative molds to produce circular diaphragms with a well-defined thickness of $150~\mu m$ and edge curvature (Fig. 1A-B). The structure retains high mechanical flexibility while enabling magnetic responsiveness suitable for actuation under low field excitation. Finite Element Modeling (FEM) was employed to simulate magnetic flux distribution, membrane deformation, and stress concentration, with results confirming strong agreement with experimental data (Fig. 1C-D).

Electromagnetic actuation testing was conducted using a 600-turn copper coil (0.5 mm wire diameter, 30 mm inner diameter), producing a peak out-of-plane deflection of 6.7 mm under a 19 mT magnetic field at 5 mm distance (Fig. 2). The diaphragm's performance remained stable across excitation frequencies from 1 to 5 Hz. A strong correlation was observed between the magnetic field and membrane displacement, as confirmed by both experimental and FEM data.

The developed diaphragm offers a low-energy, compact actuation platform suitable for magnetically driven micropumps, wearable drug delivery devices, and soft robotics. Its robustness, reversibility, and responsiveness to low magnetic fields make it a promising building block for next-generation biomedical actuators.

K. Moussi and J. Kosel, J. Microelectromechanical Syst*ems*, vol. 27, no. 5, (2018).

Z. Liao, O. Zoumhani and C. M. Boutry, Materials, 16, 3802, (2023).

D. Ficai, M. Gheorghe, et al., Micromachines, 13, 351, (2022).

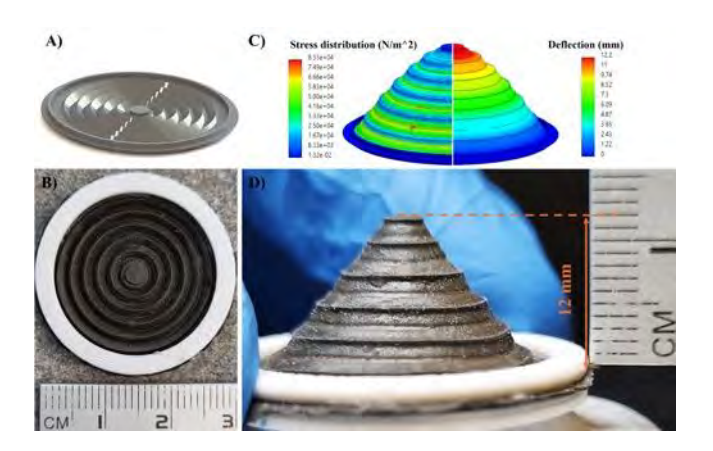


Fig. 1. Fabrication, simulation, and characterization of the magneto-elastic diaphragm. A) 3D schematic of diaphragm design. B) Photo of the fabricated diaphragm. C) FEM showing the diaphragm stress distribution and displacement. D) Manual deflection measurement (12 mm peak).

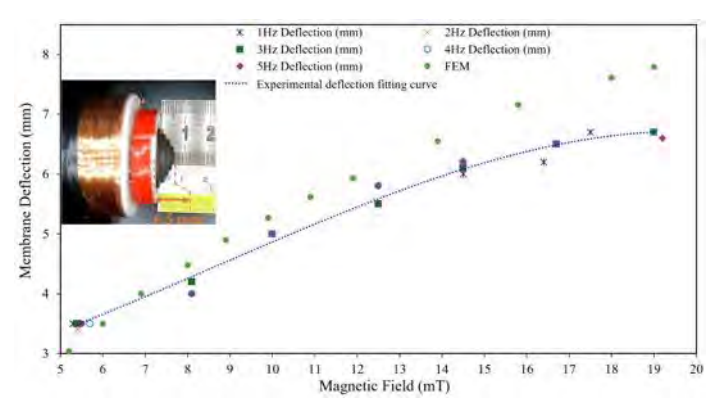


Fig. 2. Deflection versus magnetic field at multiple frequencies (1–5 Hz). Inset: photograph showing 6.5 mm diaphragm deflection at 17 mT.

DE-04. Heterogeneously Integrated Lithium Niobate-Yttrium Iron Garnet Heterostructures for Magnetoelectric Devices

A. R. Will-Cole¹, L. Hackett¹, M. Miller¹, T. Friedmann¹, S. Arterburn¹, S. Herrera¹, M. Eichenfield²

¹Sandia National Laboratories, Albuquerque, New Mexico, United States, ²University of Arizona, Tucson, Arizona, United States

Yttrium iron garnet (YIG) is a best-in-class magnetic insulator for spintronic applications, primarily due to its ultralow Gilbert damping, which facilitates long spin wave decay lengths. 1-8 These properties make it attractive for acoustic driven magnetic resonance whereby surface acoustic waves drive and couple with magnetic spin waves. 9,10 However, the magnetic film properties of YIG are contingent upon epitaxial growth and microstructural perfection, which poses significant challenges for integration with state-of-the-art piezoelectric materials, like lithium niobate (LN). In this study, we circumvent epitaxial constraints by instead leveraging heterogenous integration through wafer bonding and subsequent substrate handle removal. We successfully integrated 5 µm thick Y-cut LN films onto the surface of YIG films, which were grown via liquid phase epitaxy on gadolinium gallium garnet (GGG) substrates. 11-12 In this LN/YIG/GGG heterostructure, sufficient acoustic velocity mismatch between the LN and YIG layers enables effective waveguiding and thus low propagation loss within the piezoelectric film but still provides strong strain coupling to spin waves in the YIG near the interface. Thus, we were able to demonstrate surface acoustic wave (SAW) delay devices on these heterostructures. The acoustic propagation losses were comparable to those of Y-cut LN

films on silicon in the two orthogonal propagation directions, with an interdigital transducer (IDT) insertion loss near the 6 dB physical limit for bidirectional IDTs. We also developed wide bandwidth SAW devices utilizing a linear taper of the interdigital transducer target wavelength, achieving fractional bandwidths of up to 35% and minimal insertion losses of -17 dB for 250 µm delay lengths. We performed radiofrequency transmission measurements over a swept vector in-plane magnetic field and observed acoustic driven magnetic resonance despite the YIG being buried beneath the LN film - a first demonstration in LN/YIG to the best of our knowledge. This study highlights heterogenous integration as a viable approach to engineer magnetoelectric devices that exhibit excellent piezoelectric and magnetic properties, circumventing epitaxial growth constraints.

[1] A. A. Serga, A. V. Chumak, and B. Hillebrands, J. Phys D: Appl. Phys., 43, 264002 (2010). [2] A. V. Chumak, V. I. Vasyuchka, A. A. Serga, and B. Hillebrands, *Nature Phys.*, 11, 453-461 (2015).[3] Y. Kajiwara, K. Harii, S. Takahashi, J. Ohe, K. Uchida, M. Mizuguchi, H. Umezawa, H. Kawai, K. Ando, K. Takanashi, S. Maekawa, and E. Saitoh, Nature, 464, 262-266 (2010).[4] M. Sparks, Ferromagnetic-Relaxation Theory, New York, NY, USA: McGraw-Hill, (1964).[5] E. G. Spencer, R. C. LeCraw, and A. M. Clogston, Phys. Rev. Lett., 3, 32-33, (1959).[6] J. Ding, T. Liu, H. Chang, and M. Wu, *IEEE* Magnetics Letters, 11, 5502305 (2020).[7] H. Yu, O. d'Allivy Kelly, V. Cros, R. Bernard, P. Bortolotti, A. Anane, F. Brandl, R. Huber, I.Stansinopoulos, and D. Grundler, Sci. Rep., 4, 6848 (2014).[8] S. Maendl, I. Stasinopoulos, and D. Grundler, Appl. Phys. Lett., 111, 012403, (2017).[9] M. Küß, M. Albrecht, and M. Weiler, Chiral Magnetoacoustics, Frontiers in Physics, 10, (2022). DOI: 10.3389/fphy.2022.981257[10] B. Luo, A.R. Will-Cole, C. Dong, Y. He, X. Liu, H. Lin, R. Huang, X. Shi, M. McConney, M. Page et al., Nat Rev Electr Eng 1, 317 – 334, (2024). DOI: 10.1038/s44287-024-00044-7[11] C. Dubs, O. Surzhenko, R. Thomas, J. Osten, T. Schneider, K. Lenz, J. Grenzer, R. Hübner, and E. Wendler, Phys. Rev. Mater., 4, 024416, (2020).[12] A.R. Will-Cole, J.L Hart, V. Lauter, A. Grutter, C. Dubs, M. Lindner, T. Reimann, N.R. Valdez, C.J. Pearce et al, Phys. Rev. Materials, 7, 054411, (2023).

DE-05. Multimodal Magnetoactive Elastomers for Magnetic and Touch Sensing with Stylus Functionality

Y. Sekertekin^{1, 2}, S. Sonkusale^{1, 2}

¹Electrical and Computer Engineering, Tufts University, Medford, Massachusetts, United States, ²Sonkusale Research Laboratory, Medford, Massachusetts, United States

Magnetoactive elastomers (MAEs), primarily consisting of magnetic particles embedded within elastomeric matrices, exhibit remarkable multimodality, including magnetoresistance, magnetocapacitance and magnetomechanical, which vary depending on the fillers1. The integration of these properties in both isotropic and anisotropic MAEs for interactive electronics without additional circuitry, such as capacitive styluses, has not been thoroughly investigated². This study uniquely illustrates the performance of multimodal isotropic and anisotropic MAEs, which consist of soft silicone elastomer and identical dual fillers (carbon black, 3.6% and cobalt, 33%), for magnetoresistance, magnetocapacitance, magnetomechanical, piezoresistance and capacitive coupling (stylus) features. Magnetoresistance/capacitance were characterized using impedance spectroscopy at 1 kHz (0-300 mT), and piezoresistivity was investigated at 10 Hz through compression tests. Magnetomechanical sensitivity was quantified by measuring bending angles under magnetic fields (0-150 mT), and the stylus functionality was shown by measuring capacitance between the MAE stylus tip and a commercial touchscreen at 100 kHz under applied forces. The MAEs' size is 15x15x1 mm for the magnetoresistance/capacitance/mechanical tests, and 5x5x2 mm for piezoresistivity and stylus tests. Fig. 1 confirms that enhanced magnetoresistance/capacitance responses in the MAEs are attributed to engineered conductivity and permittivity from the filler networks³. Magnetomechanical testing revealed greater bending responses in the anisotropic MAE (58° at 150 mT vs. 50° for the isotropic), emphasizing alignment-enhanced responsiveness⁴. In Fig. 2, the piezoresistivity of isotropic MAE shows consistent 36.25%N⁻¹ sensitivity⁵, and notably, the anisotropic MAE exhibited an efficient stylus performance (41.33% pF.N⁻¹), reliably activating touchscreens at minimal forces (<0.1 N)6. The filler network within the elastomer enhances interfacial polarization, enabling sufficient charge exchange to function effectively as passive styluses.

1. S. Hu, Y. Xiang, Z. Sun et al., Composites Part A: Applied Science and Manufacturing 163 (2022).

- 2. D. Chen, A. Song, X. Hu et al., IEEE Access 7, 15125-15139 (2019).
- 3. V. G. Shevchenko, G. V. Stepanov and E. Y. Kramarenko, in Polymers (2021), Vol. 13.
- 4. L. Cestarollo, S. Smolenski and A. El-Ghazaly, ACS Applied Materials & Interfaces 14 (16), 19002-19011 (2022).
- 5. D. Zhao, J. Cui, X. Dai et al., Journal of Applied Polymer Science 138 (12) (2021).
- 6. H. Nam, K.-H. Seol, J. Lee et al., Sensors 21 (14), 4776 (2021).

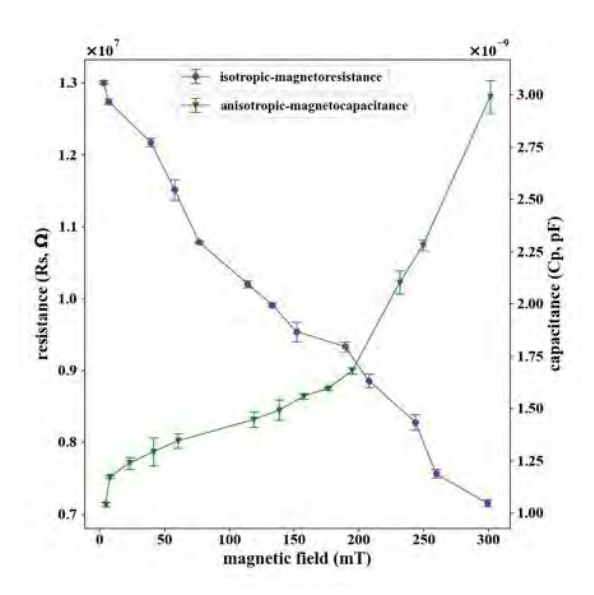


Fig. 1 Magneto-resistance/capacitance properties of the isotropic and anisotropic MAEs

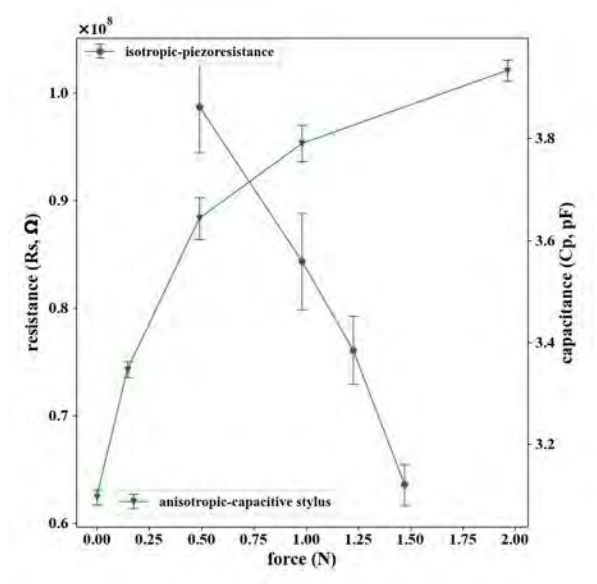


Fig. 2 Piezoresistivity and capacitive coupling of the isotropic and anisotropic MAEs

DE-06. Selective readout of isolated superconducting hybrid magnonic circuit

P. Pal^{1, 2}, U. Welp¹, R. Divan³, V. Novosad¹, A. Hoffmann², Y.

¹Materials Science Division, Argonne National Laboratory, Lemont, Illinois, United States, ²Department of Materials Science and Engineering and Materials Research Laboratory, University of Illinois Urbana-Champaign, Champaign, Illinois, United States, ³Center for Nanoscale Materials, Argonne National Laboratory, Lemont, Illinois, United States

Hybrid magnonic systems, which exploit the coherent coupling between microwave photons and collective spin excitations in magnetic materials, are gaining significant interest for multifunctional microwave and quantum devices. In this work, we have demonstrated a versatile experimental platform that enables selective detection of hybrid magnon-photon modes using a dual-resonator design integrated with spatially separated YIG spheres.

The system consists of two superconducting microwave resonators—one mounted in-plane and the other mounted vertically, each precisely engineered and individually shielded using copper enclosures to suppress cross-talk and spurious background transmission. The in-plane superconducting resonator is inductively coupled to two spatially separated single-crystal YIG spheres mounted at specific locations along its length. One of these YIG spheres is positioned near a vertically mounted superconducting $\lambda/4$ resonator, enabling strong coupling between the vertical resonator and the magnon mode of the YIG sphere. At the opposite end of the in-plane resonator, a vertical loop antenna is positioned for microwave excitation and inductive readout. Importantly, this antenna is not coupled to any YIG sphere, allowing it to selectively probe the inplane resonator without directly exciting the vertical resonator. This configuration enables a spatially controlled and mode-selective measurement scheme, where different resonant subsystems can be independently addressed via different ports.

We demonstrate selective excitation and readout of two individual resonators using microwave drives from two vertical ports. By comparing S11, S22, and S21 measurements across varying magnetic fields, we clearly distinguish the resonances of each resonator. Strong magnon-photon coupling and port-dependent anticrossing confirm mode-selective hybrid magnonic detection,

enabling high-fidelity characterization for reconfigurable microwave devices.

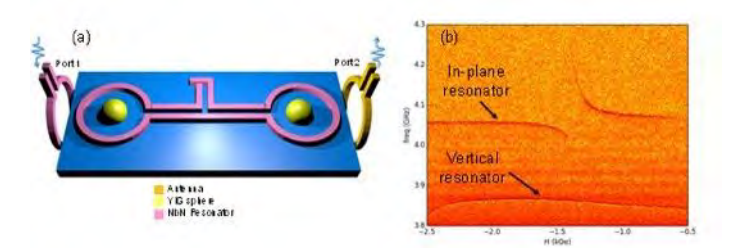


Fig. 1 (a) Schematic of the device structure. (b) Full power spectrum of the S21 parameter of the hybrid circuit showing magnon-photon mode anticrossing and another resonator mode.

DE-07. Tailored Ferromagnetic Resonance in Thick Film YIG via Ion-Implantation Technique

H. Baldino¹, D. Hedlund², K. Collins³, P. Ström⁴, D. Heiman^{5,6}, R. Peroor⁷, E. Abels⁷, D. A. Bozhko⁷, M. Page³, M. Newburger³, P. Kulik^{1, 2}

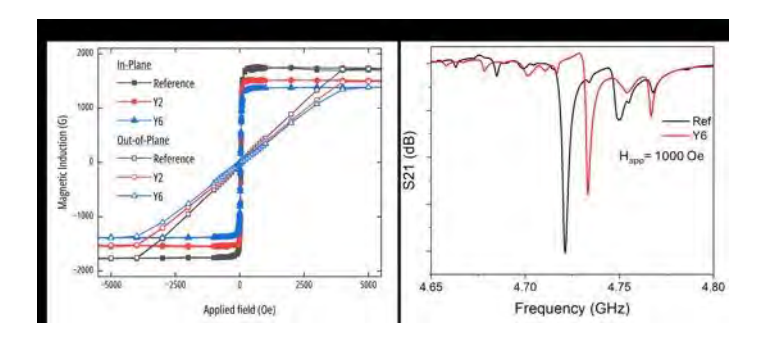
¹Material Science and Engineering, University of Central Florida, Orlando, Florida, United States, ²Electrical and Computer Engineering, University of Central Florida, Orlando, Florida, United States, ³Materials and Manufacturing Directorate, Air Force Research Laboratory, WPAFB, Ohio, *United States*, ⁴*Physics and Astronomy*, *Uppsala University*, *Uppsala, Sweden, ⁵Physics Department, Northeastern* University, Boston, Massachusetts, United States, ⁶Plasma Science and Fusion Center, Massachusetts institute of technology, Cambridge, Massachusetts, United States, ⁷Department of Physics and Energy Science, Center for Magnetism and Magnetic Nanostructures, University of Colorado, Colorado Springs, Colorado, United States

Recent years have shown a revitalized interest in yttrium iron garnet (Y₃Fe₅O₁₂, YIG) films for use in tunable electronic devices. However, tuning the properties of single crystal YIG films is difficult to achieve during the film growth stage without significant loss in the quality of the RF properties compared to undoped films [1]. Here we report the first Ho doping of YIG thick films by ion-implantation with the retention of the high-quality RF properties of the YIG films. The Ho implantation was conducted at 210 keV with an ion fluence range of 10^{13} cm⁻² to 10^{15} cm⁻² on thick film stacks consisting of high RF quality 10 µm liquid phase epitaxially grown YIG on GGG. To understand how the Ho cations move in the structure during the ion implantation process, ferromagnetic resonance (FMR) was measured on the

240

samples in the as-implanted state, as well as following a stabilization anneal. The direct implantation shows up to 30% reduction in the saturation magnetization of the films and a positive resonant frequency shift for a given applied field, Figure 1. We note that there is no degradation in the FMR linewidth from the ion implantation process in Figure 1b. We further utilize Brillouin light scattering (BLS) microscopy to study the spatial uniformity of the implantation and to understand the impact of ion-implantation on the magnon dispersion. Comparison to geometry dependent FMR spectra helps to understand how ion fluency impacts the different magnon modes. Through this analysis, we demonstrate that magnetic tunability of YIG films is achievable post growth without loss of RF quality.

[1] A. Arsad, A. Zhudi, N. Ibrahim, Applied Sciences, Vol 13 (2023)



(a) Magnetic hysteresis curve of the YIG reference, Y2 (10¹³ cm⁻² ion fluence), and Y6 (10¹⁵ cm⁻² ion fluence). Filled symbols represent in-plane whereas open symbols represent out of plane. (b) Reference sample and Y6 sample ferromagnetic resonance under an applied field of 1000 Oe.

DE-08. An exploration of field-induced ground states and phase transitions in pyrochlores using torque magnetometry C. Beekman^{1, 2}

¹Physics, Florida State University, Tallahassee, Florida, United States, ²National High Magnetic Field Laboratory, Tallahassee, Florida, United States

Geometrically frustrated systems have an inherent incompatibility between the lattice geometry and the magnetic interactions, resulting in macroscopically degenerate ground-state manifolds. The single-ion anisotropy and magnetic interactions in these systems give rise to unusual non-collinear spin textures. In classical spin ices this leads to Pauling states and emergent quasiparticle

excitations equivalent to magnetic monopoles. There is an enticing potential of using these monopoles for the development of new quantum information applications. The effective spin correlation strength (Jeff) determines the relative energies of the different possible spin-ice states. I will review our recent work in which we benchmarked capacitive torque magnetometry as a unique tool to characterize metamagnetic transitions in spin-ice Ho₂Ti₂O₇ single crystals, which allows extraction of J_{eff} and the magneto-chemical potential of monopole formation [1]. Our work shows that the spin ice state that features antiferromagnetic alignment of spin chains, is more stable (i.e., has a higher Jeff) than one would predict from the dipolar spin ice model based on nearest neighbor exchange. Torque magnetometry has allowed us to put bounds on beyond-nearest-neighbor interaction energy scales. I will also review experimental results on thin film counterparts of this spin ice, which show that strain and disorder in the films play important roles in determining their magnetic properties [2], effectively destabilizing the formation of these antiferromagnetically aligned spin chains for some, but not all, thin films. Lastly, I will briefly highlight some very recent torque magnetometry data on the quantum spin ice candidate Pr₂Hf₂O₇. My group has successfully grown these films on various substrates. In short, torque magnetometry is a unique tool for exploring field-induced ground states and phase transitions in (quantum) spin ices.

Beekman acknowledges the support of the National Science Foundation, under Grant No. NSF DMR-1847887 (CAREER). Use of National High Magnetic Field Laboratory user facilities was supported by NSF Cooperative Agreements No. DMR-1157490, No. DMR-1644779, and the state of Florida.

- [1] N. Anand et al., Nat. Com. 13, 3818 (2022)
- [2] K. Barry et al., Phys. Rev. Mater. 3, 084412 (2019)

DE-10. Effect of Si Concentration on the Crystal Structure and Magnetic Ground State of Mn₂FeAl_{1-x}Si_x Heusler Alloys S. Saha¹, A. K. Khorwal¹, Y. Bitla¹, A. K. Patra^{1, 2}

¹Department of Physics, Central University of Rajasthan, Ajmer, Rajasthan, India, ²School of Physics, University of Hyderabad, Hyderabad, Telangana, India

The rapidly growing field of antiferromagnetic (AFM) spintronics demands new AFM materials with promising properties [1]. Mn₂FeAl having a β -Mn crystal structure (space group $P4_132$) shows AFM ground state with spin-glass

^{*} Best Student Presentation Finalist / LB - Late-breaking Poster

(SG) behavior [2], whereas Mn₂FeSi with an XA-type structure (space group *F-43m*) shows a purely AFM nature [3]. This study explores the phase formation and corresponding magnetic ground states of a series of Heusler alloys between the two parent alloys, Mn₂FeAl and Mn₂FeSi (Fig. 1). A series of polycrystalline samples of $Mn_2FeAl_{1-x}Si_x$ (x = 0.4, 0.6, 0.8) are prepared using arcmelting, and their crystal structure and magnetic properties are studied using X-ray diffraction and magnetic measurements, respectively. The lowest Si content alloy adopts a β-Mn crystal structure similar to Mn₂FeAl, while the highest Si content alloy mainly exhibits an XA-type structure with a minor β-Mn phase, closely resembling the XA-type structure of Mn₂FeSi (Fig. 1). These alloys display AFM character (16 K \leq T_N \leq 19.5 K) (Fig. 2). The typical SG signatures as observed in parent Mn₂FeAl such as bifurcation in zero-field-cooled and field-cooled magnetization curves, exponential decay of temperaturedependent coercivity and remanence, frequency-dependent shift in ac susceptibility peak temperature, and magnetic relaxation and memory effect below the characteristic temperature are present in x = 0.4 sample, indicating the presence of a low-temperature SG phase (Fig. 2). In contrast, the alloys with higher Si content (x = 0.6, 0.8) display unconventional SG features where at least one of these signatures is absent. This is likely due to the emerging XA phase with increasing Si content. The results suggest a structural evolution from β-Mn-type to XA-type with increasing Si, and concomitant magnetic phase from an AFM ground state with pronounced SG behavior to a predominantly AFM state with reduced SG features, consistent with both the end parent members, Mn₂FeAl and Mn₂FeSi [S. Saha, et al. under review].

[1] A. Dal Din, O. J. Amin, P. Wadley, et al. *npj Spintronics*, Vol. 2, p.25 (2024)
[2] Shubhra Dash, A. V. Lukoyanov, Nancy, et al. *Journal of Magnetism and Magnetic Materials*, Vol. 513, p.167205 (2020)
[3] Anil Aryal, Said Bakkar, Hassana Samassekou, et al. *Journal of Alloys and Compounds*, Vol. 823, p.153770 (2020)

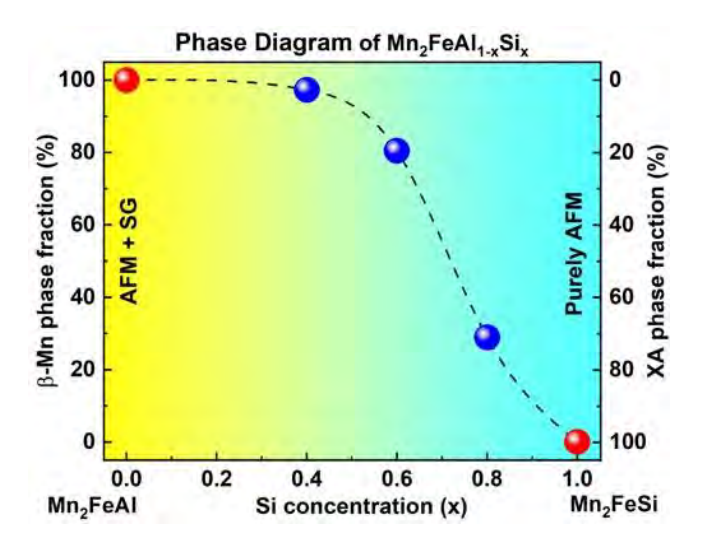


Fig. 1 Evolution of crystal structure and magnetic ground state in $Mn_2FeAl_{1-x}Si_x$

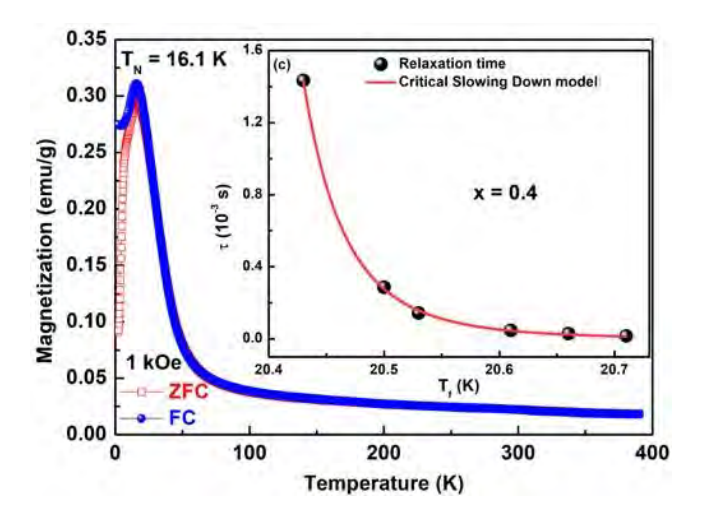


Fig. 2 Antiferromagnetic ground state with spin-glass features of x = 0.4 alloy

SESSION DF: SPIN INJECTION, PUMPING AND TRANSFER TOROUES

Chair(s): D. Qu, Center for Condensed Matter Sciences, National Taiwan University, Taipei, Taiwan Wednesday, October 29, 2025 02:00 PM-05:30 PM Room 2BC

DF-01. Self-generated Spin-orbit Torques Driven by Magnonic Spin Dissipation in Antiferromagnet/Ferromagnet Bilayer

<u>W. Choi</u>^{1,2}, J. Ha^{1,3}, M. Jung¹, S. Kim¹, H. Koo^{1,4}, O. Lee¹, B. Min¹, H. Jang^{2,5}, A. Shahee⁶, J. Kim⁷, M. Kläui⁶, J. Hong³, K. Kim⁸, D. Han¹

¹Center for Semiconductor Technology, Korea Institute of Science and Technology, Seoul, Korea (the Republic of), ²Department of Materials Science and Engineering, Seoul National University, Seoul, Korea (the Republic of), ³Department of Physics and Chemistry, Daegu Gyeongbuk Institute of Science and Technology, Daegu, Korea (the Republic of), ⁴KU-KIST Graduate School of Converging Science and Technology, Korea University, Seoul, Korea (the Republic of), ⁵Research Institute of Advanced Materials, Seoul National University, Seoul, Korea (the Republic of), ⁶Institute for Physics, Johannes Gutenberg University, Mainz, Germany, ⁷Department of Physics, Kunsan National University, Kunsan, Korea (the Republic of), ⁸Department of Physics, Yonsei University, Seoul, Korea (the Republic of)

Controlling magnetization in ferromagnets (FMs) with high energy efficiency is central to spintronic applications. Conventional spin-orbit torque (SOT) systems rely on injecting spin currents via heavy metals or interfacial spin-orbit coupling (SOC) [1].

Recent studies suggest that intrinsic spin currents (ISCs) generated within FMs—once considered negligible—can significantly contribute to SOTs [2, 3]. Despite this, evaluating the impact of ISC remains challenging, due to difficulty separating its contribution from dominant external spin sources in typical heterostructures.

To address this, we employ a bilayer system comprising an FM and an antiferromagnetic insulator (AFI), where charge transport remains symmetric while spin transport becomes asymmetric due to selective spin dissipation at the FM/AFI interface [4]. In this configuration, we demonstrate that magnonic spin dissipation within the AFI enables the conversion of ISC into sizable SOTs, without relying on external spin injection.

Through harmonic Hall measurements [5], we reveal that

the SOT efficiency strongly depends on the alignment between ISC spin polarization and the AFI's Néel vector. Furthermore, SOTs persist even in thick AFI layers, underscoring the role of magnon dissipation. Temperature-and thickness-dependent studies further confirm the correlation between AFI magnon dissipation and self-torques driven by ISCs in the FM.

Finally, we demonstrate magnetization switching purely driven by this mechanism, providing direct evidence that ISCs and magnon dissipation alone can generate sufficient torque. These findings offer a pathway toward energy-efficient spintronic devices harnessing internal spin sources and engineered dissipation.

- 1. Sinova, J. *et al.* Spin Hall effects. Rev. Mod. Phys. 87, 1213–1260 (2015).
- 2. Amin, V. P. et al. Intrinsic spin currents in ferromagnets. *Phys. Rev. B* 99, 220405 (2019).
- 3. W, Wang. *et al.* Anomalous spin-orbit torques in magnetic single-layer films. Nat. Nanotechnol. 14, 819–824 (2019).
- 4. Kim, K.-W. Park, B.-G. & Lee, K.-J. Spin current and spin-orbit torque induced by ferromagnets. npj Spintron. 2, 8 (2024).
- 5. Avci, C. O. *et al.* Interplay of spin-orbit torque and thermoelectric effects in ferromagnet/normal-metal bilayers. Phys. Rev. B 90, 224427 (2014).
- 6. Choi, W.-Y. *et al.* Magnetization switching driven by magnonic spin dissipation. Nat. Commun. (Accepted).

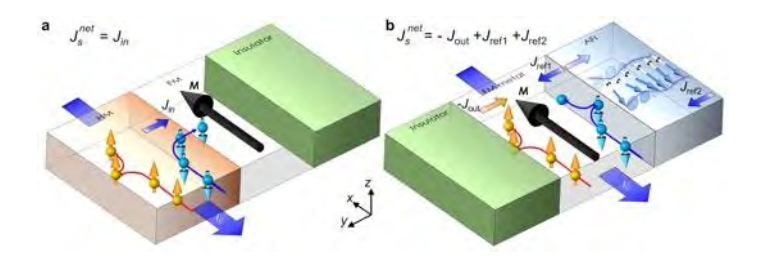


Fig 1. Schematic illustration of SOT mechanism. a, Conventional SOT from HM via SHE. b, In AFI/FM, ISC in FM leads to net spin angular momentum via asymmetric spin dissipation in AFI, enabling SOT in FM metal layer without external spin sources.

DF-02. Temperature gradient-driven motion of magnetic domains in a magnetic metal multilayer by entropic forces L. Huangala L. Barker L. Kailas S. Hair S. Connell G.

L. Huang^{1, 2}, J. Barker¹, L. Kailas¹, S. Hait¹, S. Connell¹, G. Burnell¹, <u>C. Marrows</u>¹

¹University of Leeds, Leeds, United Kingdom, ²University of Sheffield, Sheffield, United Kingdom

Spin textures, such as domain walls [1] (DWs) and skyrmions [2], have been shown to move in response to both spin currents and entropic forces arising from temperature gradients. The spin currents arise from the flow of magnons [3,4,5] (electrons [6]) induced by the spin(-dependent) Seebeck effect [3]. This current of angular momentum exerts spin transfer torques on spin textures that causes them to move towards the hot end of the gradient [4]. On the other hand, entropic forces arise since the temperature gradient leads to gradients in the micromagnetic parameters that determine the energy of the spin texture [7], which can either enhance or oppose this effect [8].

We studied the displacement of magnetic domains under temperature gradients in perpendicularly magnetized Ta/[Pt/Co₆₈B₃₂/Ir]×10/Pt multilayer tracks with microfabricated Pt heaters/thermometers by magnetic force microscopy (MFM) [9]. Subtracting out the effects of the Oersted field from the heating current reveals the pure temperature gradient-driven motion, which is always towards the heater. An example is shown in Figure 1. The larger the thermal gradient along the track (owing to proximity to the heater or larger heater currents), the larger the observed displacements of the domains, up to a velocity of around 1 nm/s in a temperature gradient of 20 K/µm. Quantitative estimates of the strength of different driving mechanisms [9] shows that entropic forces [7] dominate over spin Seebeck [4] and spin-dependent Seebeck [6] effects.

- [1] W. Jiang, P. Upadhyaya, Y. Fan, et al. Phys. Rev. Lett. 110, 177202 (2013).
- [2] Z. Wang, M. Guo, H.-A. Zhou, et al., Nature Electron. 3, 672 (2020).
- [3] D. Hinzke and U. Nowak, Phys. Rev. Lett. 107, 027205 (2011).
- [4] A. A. Kovalev and Y. Tserkovnyak, Phys. Rev. B 80, 100408 (2009).
- [5] P. Yan, X. S. Wang, and X. R. Wang, Phys. Rev. Lett. 107, 177207 (2011).
- [6] L. Yi, D. Yang, M. Liu, et al., Adv. Funct. Mater. 30, 2004024 (2020).

- [7] F. Schlickeiser et al., Phys. Rev. Lett. 113, 097201 (2014).[8] E. Raimondo, et al., Phys. Rev. Applied 18, 024062 (2022).
- [9] L. Huang, J.Barker, L. Kailas, S. Hait, S. D. A. Connell, G. Burnell, and C. H. Marrows, arXiv:2506.09628 [cond-mat.mes-hall].

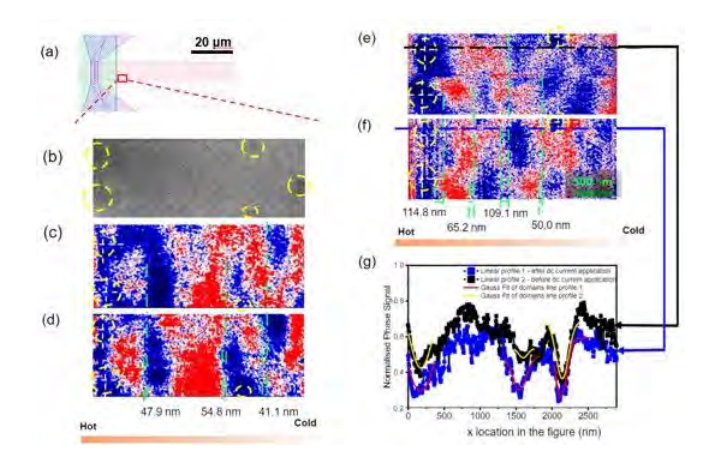


Fig 1: MFM imaging of thermally-induced domain motion. (a) Schemetic of magnetic track (red) spanned by electrically isolated (green) Pt heater/thermometer (purple). (b) MFM image when the track is fully saturated in +700 Oe. The dark regions in the dashed yellow circles are defects on the track surface. (c) and (d) are the MFM images in +30 Oe before and after a +30 mA current was applied to the heater, respectively. Dashed green lines indicate position of the leading edge of the reverse domains. (e) and (f) MFM images in +30 Oe before and after a -30 mA current was applied to the heater, respectively. Dashed blue and black lines indicate the positions of the line profiles that are shown in (g).

DF-03. Dependence of Current-Induced Switching Threshold on Composition Gradient Width in Si/Al-Integrated Perpendicular Magnetic Films

<u>S. Takagi</u>¹, K. Yamanoi¹, Y. Nozaki^{1,2}
¹Dept. of Phys., Keio Univ., Yokohama, Kanagawa, Japan, ²Center for Spintronics Research Network, Keio Univ., Yokohama, Kanagawa, Japan

Compositionally graded interfaces of common elements such as silicon (Si) and aluminum (Al), despite their inherently weak spin-orbit interaction and small spin Hall effect, have recently been shown to generate spin-orbit torque (SOT) efficiencies comparable to those of heavy metals [1]. This unexpected enhancement emerges only

within a narrow interfacial thickness range (1-2 nm), indicating that nanoscale compositional gradients can act as novel spin current sources [1-3].

Here, we demonstrate current-induced magnetization switching in perpendicular magnetic films integrated with Si/Al composition gradient materials, aiming to establish their viability as spin current generation channels for SOT-MRAM applications. A Pt/Co/Pt trilayer with strong perpendicular anisotropy was deposited on the Si/Al composition gradient structure. As shown in Fig. 1, electrical measurements using the anomalous Hall effect under an inplane magnetic bias field revealed a pronounced dependence of the switching threshold current on the gradient thickness, consistent with prior reports on spin torque efficiency [1].

To avoid interfacial atomic mixing between Al and Pt, which can degrade SOT performance of Si/Al composition gradient material via spin Hall torque cancellation in Pt/Co/Pt trilayer, we further employed a Pt-free perpendicular magnet: GdFeCo. We show that a

Ta(10)/Al(10)/Gd₂₅(Fe₉₀Co₁₀)₇₅(10)/Ta(10) (thickness in nm) stack grown on Si substrates exhibits robust perpendicular magnetization and is suitable for integration with Si/Al gradient layers (Fig. 2). Comparative analysis of both Pt-based and Pt-free systems highlights the impact of interfacial design on spin current generation and reveals the optimal gradient thickness for minimizing switching current. These findings offer a new materials design strategy for efficient and sustainable spintronic devices.

[1] T. Horaguchi et al., Sci. Adv., 11, eadr9481 (2025).[2] H. Nakayama et al., Phys. Rev. B, 107, 174416 (2023).[3] H. Nakayama et al., Adv. Electron. Mater., 11, 2570021 (2025).

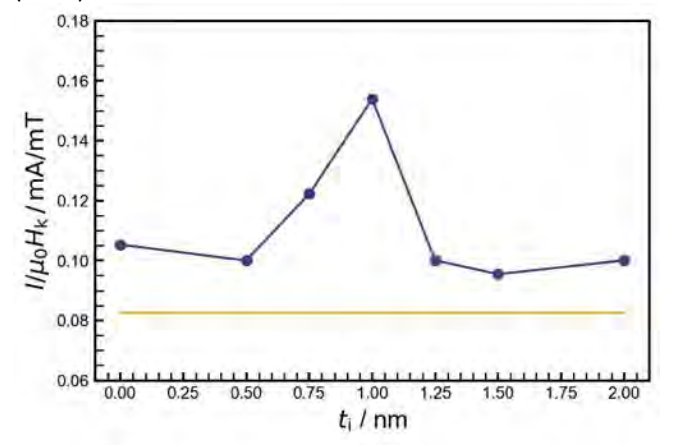


Fig. 1. Dependence of the switching current on the gradient width of Si/Al composition-graded materials (purple), compared with the switching current induced by spin current generated from a 2 nm Pt layer (orange).

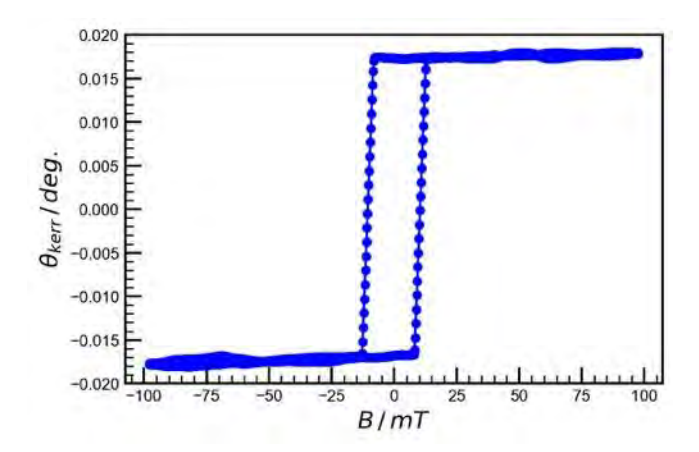


Fig. 2. Polar magneto-optical Kerr effect hysteresis loop of an as-grown $Ta(10)/Al(10)/Gd_{25}(Fe_{90}Co_{10})_{75}(10)/Ta(10)$ (thicknesses in nm) multilayer film.

DF-04. Dissipationless Spin-orbit Torque in Magnetic Insulators

S. Ahmad¹, F. Mahfouzi², P. Haney², <u>F. Xue</u>¹

¹Department of Physics, University of Alabama at Birmingham, Birmingham, Alabama, United States, ²PML, National Institute of Standards and Technology, Gaithersburg, Maryland, United States

Spin-orbit torque (SOT) has emerged as a leading approach for all-electrical control of magnetization, by harnessing spin-orbit coupling to convert charge currents into spin currents. In conventional metallic heterostructures, a charge current flowing through a heavy metal generates a transverse spin current via the spin Hall effect; this spin current then diffuses into an adjacent ferromagnet, exerting a torque that drives magnetization dynamics. Such observations have firmly established the view that SOT relies on mobile conduction electrons.

In this talk, we challenge that assumption by demonstrating a dissipationless SOT in a purely insulating ferromagnet. Using a minimal model of an inversion-symmetry-breaking magnetic insulator, we show that the time-reversal-even component of SOT remains finite within the band gap, despite the absence of any bulk carriers. In addition, we find that the in-gap torque is nonzero even in the topologically

^{*} Best Student Presentation Finalist / LB – Late-breaking Poster

trivial ferromagnetic insulator with Chern number 0. So this dissipationless in-gap torque is not directly related to the electron topology. However, we also find that the in-gap torque in a topologically nontrivial state is much larger than that in a topologically trivial state with the same gap. We conclude by discussing how these in-gap torques arise in real-space nonequilibrium Green 's-function calculations, and outline the implications for designing energy-efficient, insulator-based spintronic devices.

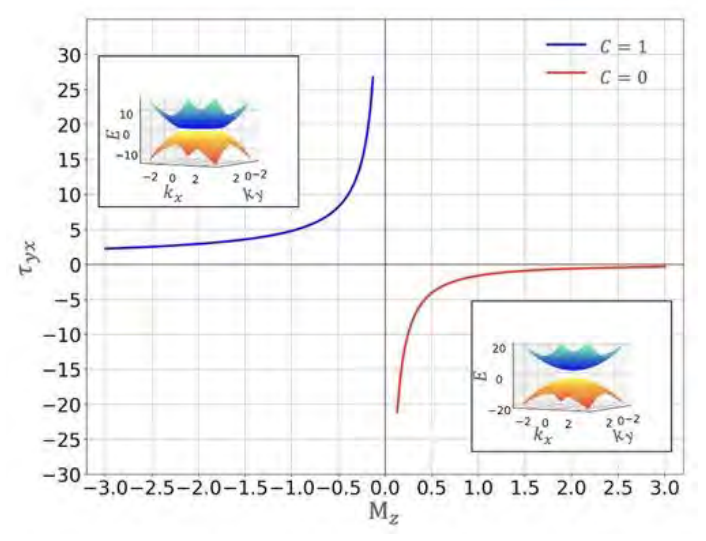


Fig. 1 The spin-orbit torkance as a function of the gap in a Chern insulator with the magnetization in the z-direction. The applied electric field is in the x-direction and the only nonzero torkance is in the y-direction. The blue line indicates the Chern phase, where the gap is negative, while the red line indicates the trivial phase, where the gap is positive. The insets show the band structures of the Chern phase and the trivial phase.

DF-05. Effect of Interfacial DMI on Write Error Rate Anomalies of STT-MRAM Devices

P. Das¹, M. Rajib¹, J. Atulasimha^{1, 2}

¹Department of Mechanical and Nuclear Engineering, Virginia Commonwealth University, Richmond, Virginia, United States, ²Department of Electrical and Computer Engineering, Virginia Commonwealth University, Richmond, Virginia, United States

Spin-transfer torque (STT) is used to switch magnetization in commercial spin transfer torque random access memory (STT-RAM). Recent work suggests that the reliability of STT switching appears to be impacted by interfacial Dzyaloshinskii–Moriya interaction (DMI), which potentially

leads to non-monotonic behavior of switching error vs. voltage/current applied to switch STTRAM as discussed in Ref 1, 2. In this work, using micromagnetic simulations, we studied the effect of DMI on the degradation of STT switching and its potential role in causing the Write Error Rate (WER) anomaly known as the "ballooning effect" observed in perpendicular-Magnetic Tunnel Junctions (p-MTJs) [1,2]. All the simulations are performed on 20 nm diameter p-MTJs for different DMI strengths in the presence of room temperature thermal perturbation. We observed (Fig. 1) that, without DMI, the switching is smooth and uniform with minimal distortion. In contrast, the presence of DMI creates distortion in the spin configuration, which leads to switching delay. We also found that higher DMI (3 mJ/m²) forms distorted inhomogeneous spin configurations that persist beyond the STT pulse. Such a distorted configuration (Fig 1) prevents magnetization from switching to the desired final state. Even at higher current densities, high DMI can cause persistent switching failures, leading to a "ballooning" like effect observed in earlier experimental studies from other groups, as shown in our simulations in Fig 2. Our results highlight the manner in which DMI can disrupt STTdriven switching and emphasize the need to limit interfacial DMI for achieving reliable performance in STT-MRAM devices at the nanoscale; while the same DMI can have a beneficial effect in voltage control of magnetic anisotropy (VCMA) based switching of p-MTJs mediated by a skyrmion state [3, 4].

We acknowledge Virginia VIPC CCF Commercialization grant and Virginia Commonwealth University Commercialization grant and discussions with Dr. Jonathan Z. Sun on the simulation results and their analysis.

- 1. Y. Zhang, J. Zhao and J. Z. Sun, *IEEE Trans. Magn.*, 54, 9300104 (2018)
- 2. A. Lyle, Y. Zhang and J. Z. Sun, *Appl. Phys. Lett.*, 109, 032403 (2016)
- 3. D. Bhattacharya and J. Atulasimha, *ACS Appl. Mater. Interfaces*, 10, 17455 (2018)
- 4. M. M. Rajib, W. A. Misba and J. Atulasimha, *Sci. Rep.*, 11, 20914 (2021)

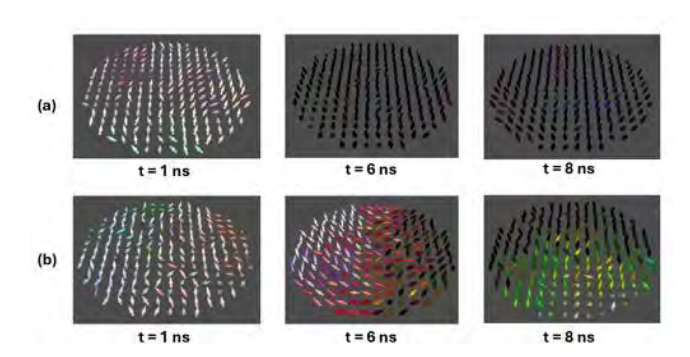


Fig. 1. Magnetization states observed at 1 ns, 6 ns, and 8 ns for DMI values of (a) 0 mJ/m² and (b) 3 mJ/m².

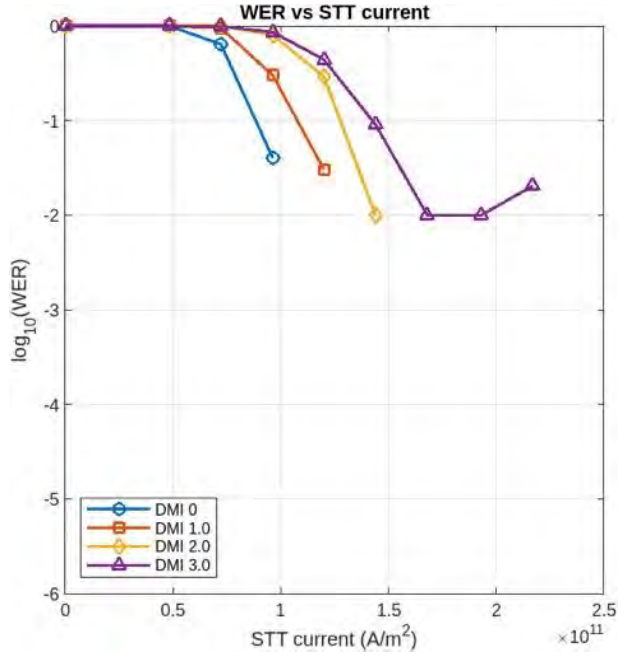


Fig. 2. Write Error Rate (WER) as a function of STT current for varying DMI strengths.

DF-06. Influence of Device Structure on RF Oscillation Properties in Spin Hall Nano Oscillators

<u>H. lida</u>^{1, 2}, K. De Zoysa¹, Y. Yoshida^{1, 2}, A. Sud³, A. Lagarrigue¹, T. Dohi¹, A. Kumar^{4, 5}, A. A. Awad^{1, 4}, S. Kanai^{1, 6}, J. Akerman^{1, 4}, S. Fukami^{1, 5}, H. Ohno^{5, 7}

¹LNS, RIEC, Tohoku Univ., Sendai, Japan, ²Graduate School of Engineering, Tohoku Univ., Sendai, Japan, ³FRIS, Tohoku Univ., Sendai, Japan, ⁴Physics department, Univ. of Gothenburg, Gothenburg, Sweden, ⁵CSIS, Tohoku Univ., Sendai, Japan, ⁶WPI-AIMR Tohoku Univ., Sendai, Japan, ⁷CIES, Tohoku Univ., Sendai, Japan

Nanoconstriction-based spin Hall nano-oscillators (SHNOs), typically consisting of heavy metal (HM)/ferromagnet (FM) bilayers^[1], have attracted significant attention due to their potential applications in next-generation information devices, including broadband RF field generators and neuromorphic devices [2]. Although extensive research has been conducted on material systems and array structures for efficient and stable operations, quidelines for the geometric design of nanoconstrictions remain unclear. Here, we report the oscillation properties of the SHNO with different nanoconstriction structures and discuss the underlying physics in terms of the maximum oscillation power (P_{max}). A stack with Si substrate/Pt(5)/Py(4,5,6)/MgO(2)/Ta(1) (thickness in nm) is processed into nanoconstriction device with different constriction widths (w) ranging from 80 - 300 nm through the electron beam lithography. Figure 1 shows the measurement circuit and the scanning electron microscopy (SEM) image of the nanoconstriction. Oscillations are excited by applying DC under an in-plane external magnetic field (m_0H_{ext}) of 80 mT with an angle of 80 degrees with respect to the direction of the applied current and detected by a spectrum analyzer. With these inplane fields, the oscillations localize to the edges of the constriction^[3]. P_{max} is defined as the peak amplitude of the Lorentzian fit to the measured power spectral density. We observe non-monotonic behavior of P_{max} vs. w [Fig. 2], which may be attributed to the consequence of the overlap of edge-localized modes and the junction resistance. The present finding lays the foundation for designing an efficient SHNO device.

We thank F. Shibata, R. Nomura, I. Morita, M. Musya, and R. Ono for their technical support. This work was supported by JSPS Kakenhi, JST PRESTO, and JST ASPIRE. H. Iida acknowledges financial support from GP-Spin at Tohoku University.

[1] V. Demidov *et al.*, Appl. Phys. Lett. 105, 172410 (2014). [2] T. Chen, *et al.*, Proc. IEEE 104, 1919–1945 (2016). [3] M. Dvornik, *et al.*, Phys. Rev. Appl. 9, 014017 (2018).

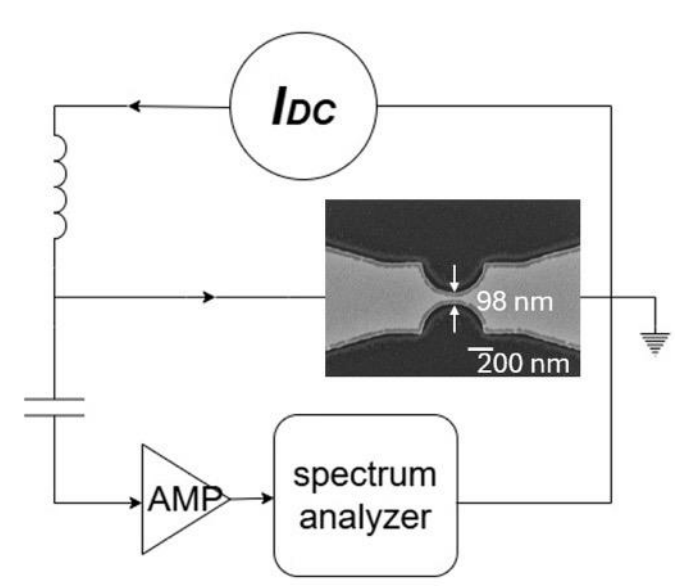


Fig. 1: Measurement circuit with SEM image of nanoconstriction

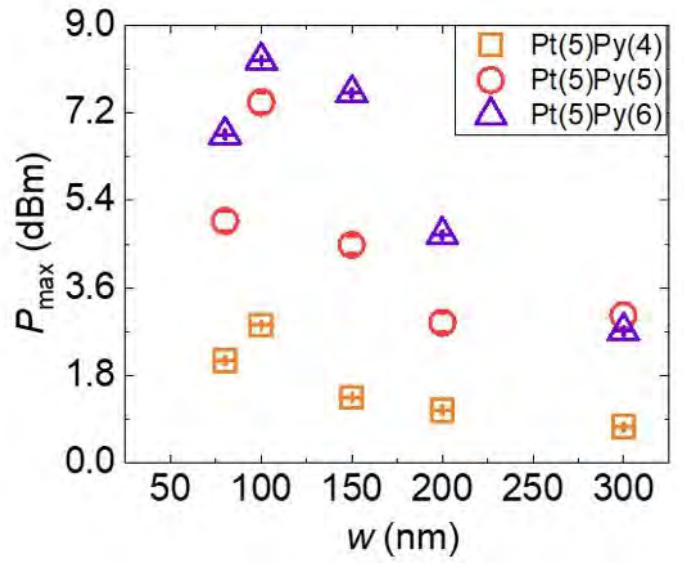


Fig. 2: Constriction width *w* dependence of maximum output power *P*max of SHNO

DF-07. Magnetotransport Signatures of Spin Transfer Beyond the Semiclassical Regime

G. T. Street, S. Emori

Physics, Virginia Tech, Blacksburg, Virginia, United States

Semiclassical spin transfer can suppress or amplify thermal magnetic fluctuations, depending on whether incident spins s are parallel or antiparallel to the time-averaged

magnetization $\langle M \rangle$ (Fig.1ab). Higher magnetic fields and lower temperatures reduce baseline thermal magnetization fluctuations, leading to a weaker spin transfer effect. Yet, recent studies suggest a nonclassical spin transfer for s antiparallel to $\langle M \rangle$, that modifies the magnetization in the absence of thermal fluctuations [1]. In this regime, incident spins entangle with local moments; thus, a spin flip triggers a corresponding moment flip, effectively shrinking $\langle M \rangle$ [2]. Here, we search for such nonclassical spin transfer through DC magnetotransport in a Pt|Co bilayer, where a DC current in Pt injects *y*-polarized spins into *y*-magnetized Co (Fig. 1c).

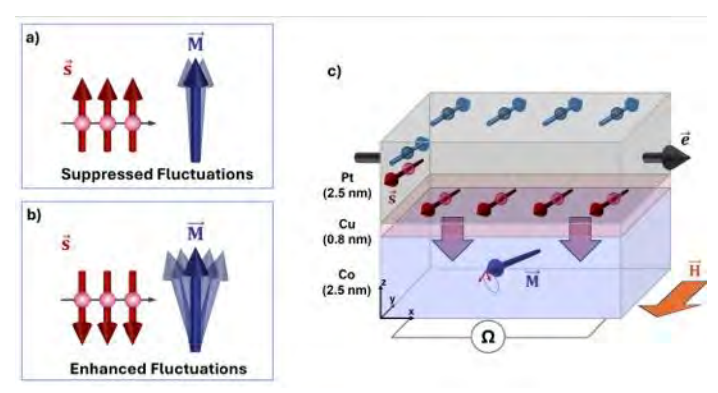
Following Ref. [3], we quantify the unidirectional magnetoresistance, ΔR, under various fields and temperatures that set the baseline fluctuations. Conventionally, ΔR at high DC density ~10¹¹ A/m² captures change in $\langle M \rangle$ from semiclassical spin transfer on thermally fluctuating moments (Fig. 1ab). However, across various fields, ΔR increases with field strength (Fig. 2a) contrary to semiclassical spin-transfer theory that predicts smaller current-induced effects for more rigid magnetizations. At 8K, thermal fluctuations are further minimized, yet ΔR persists at even greater magnitudes (Fig. 2b). Our surprising observations of enhanced ΔR under reduced thermal fluctuations rule out semiclassical spintransfer mechanisms. Instead, our work may point to significant underlying quantum contributions to DC magnetotransport [2] in prototypical spin-orbit bilayers.

[1] A. Zholud, S. D. Watel, and S. Urazhdin, *Phys. Rev. Lett.*, Vol. 119, p. 257201 (2017).

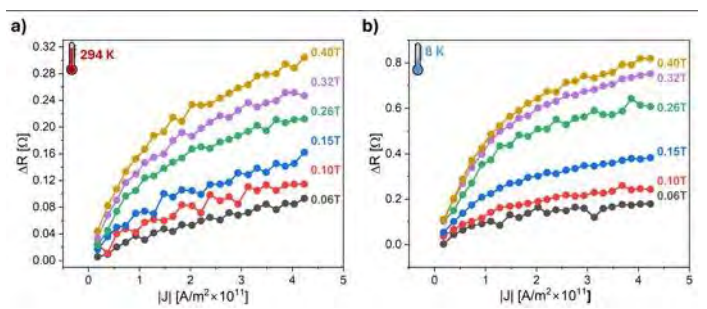
[2] P. Mondal, U. Bajpai, and B. K. Nikolić, *Phys. Rev. B.*, Vol. 99, p. 094431 (2019).

[3] T.-Y. Chang, C.-L. Cheng, and C.-F. Pai, *Phys. Rev. B*, Vol. 104, p. 024432 (2021).

^{*} Best Student Presentation Finalist / LB – Late-breaking Poster



(a) Spins incident parallel to local magnetization suppress thermal fluctuations. (b) Spins incident antiparallel enhance thermal fluctuations. (c) Spins injected from the spin-Hall Pt layer into the magnetized Co layer below. Longitudinal resistance probes changes in the local magnetization.



Unidirectional magnetoresistance ΔR at various fields, at (a) 294 K and (b) 8 K.

Switching Due to Spin Berry Curvature Generated by Minute

DF-08. Single-Layer Spin-Orbit-Torque Magnetization

Spontaneous Atomic Displacement in Weyl Oxide SrRuO₃ H. Horiuchi¹, Y. Araki², Y. K. Wakabayashi³, J. Ieda², M. Yamanouchi⁴, Y. Sato⁵, S. Kaneta-Takada¹, Y. Taniyasu³, H. Yamamoto³, Y. Krockenberger³, M. Tanaka^{1,6,7}, S. Ohya^{1,6,7} ¹Department of Electrical Engineering and Information Systems, The University of Tokyo, Bunkyo-ku, Tokyo, Japan, ²Advanced Science Research Center, Japan Atomic Energy Agency, Tokaimura, Ibaraki, Japan, ³NTT Basic Research Laboratories, NTT Corporation, Atsugi-shi, Kanagawa, Japan, ⁴Division of Electronics for Informatics, Graduate School of Information

Science and Technology, Hokkaido University, Sapporo-shi, Hokkaido, Japan, ⁵Research and Education Institute for Semiconductors and Informatics, Kumamoto University, Chuoku, Kumamoto, Japan, ⁶Center for Spintronics Research Network

(CSRN), The University of Tokyo, Bunkyo-ku, Tokyo, Japan, ⁷Institute for Nano Quantum Information Electronics, The University of Tokyo, Bunkyo-ku, Tokyo, Japan

Enhancing the efficiency of spin-orbit torque (SOT)-induced magnetization switching is a key objective in spintronics. Increasing spin Berry curvature (SBC), which reflects band topology as the spin counterpart of Berry curvature, is a promising route, as it enhances the intrinsic spin Hall effect (SHE) and thus the SOT. Breaking crystalline inversion symmetry (IS) in ferromagnetic layers is expected to amplify SBC significantly, which will enable single-layer SOT magnetization switching. Despite this potential, SOTinduced magnetization switching has so far been realized mostly using ferromagnet/heavy-metal bilayers. Here, we demonstrate SOT-induced partial magnetization switching in a single layer of ferromagnetic Weyl oxide SrRuO₃ (SRO) with a small current density of $\sim 3.1 \times 10^6$ A cm⁻² [1], which is one order of magnitude smaller than that needed for conventional bilayer structures [Fig. 1(a)]. We have prepared the SRO film on a SrTiO₃ (STO) substrate using machinelearning-assisted molecular-beam epitaxy [2]. Our transmission electron microscopy analysis suggests that the film has a seemingly perfect, defect-free periodic lattice. However, detailed analysis reveals small oxygen octahedral rotations (OORs) with angles of ~5° near the SRO/STO interface [Fig. 1(b)]. SRO exhibits linear band crossings in the symmetric bulk state [3]. Our tight-binding calculations indicate that a strong SBC is induced around small gaps generated at band crossings due to the OOR (Fig. 2). Consequently, a pronounced intrinsic SHE arises near the interface, enabling the efficient switching. The results indicate that a minute atomic displacement in single-crystal films can induce large intrinsic SOTs that are useful for spin-orbitronics devices.

[1] H. Horiuchi et al., Adv. Mater. 2416091 (2025). [2] Y. Wakabayashi et al., APL Mater. 7, 101114 (2019). [3] Y. Chen et al., Phys. Rev. B 88, 125110 (2013). This work was partly supported by Grants-in-Aid for Scientific Research, JST CREST, JST ERATO, and Spintronics Research Network of Japan (Spin-RNJ).

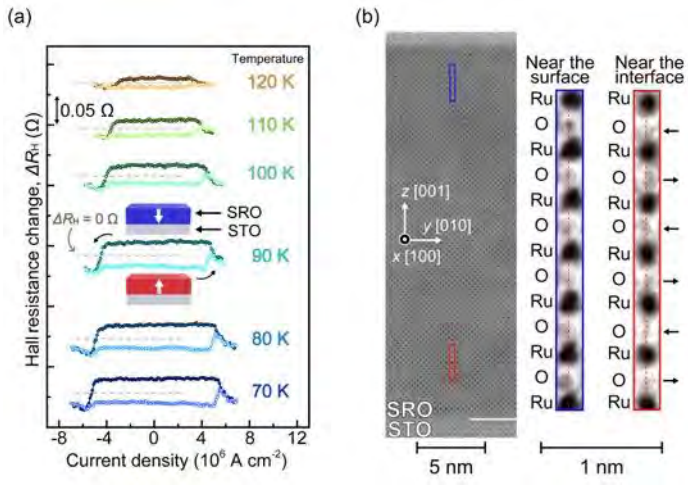
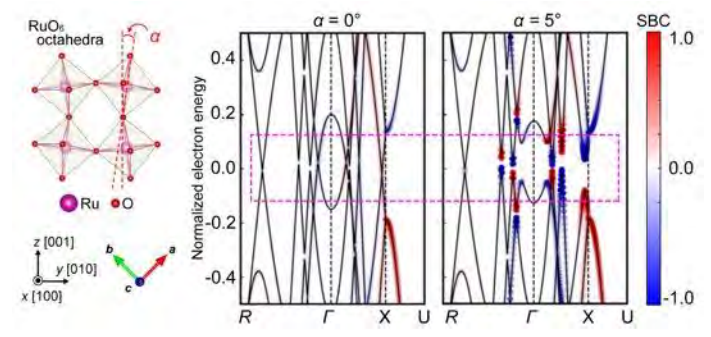


Figure 1 (a) SOT switching loops obtained at various temperatures, where the Hall resistance is proportional to the magnetization perpendicular to the substrate. (b) Annular bright-field scanning transmission electron microscopy image of the SRO/STO sample. Near the interface, O atoms are displaced alternately along the ±y directions, providing evidence of OOR.



Band structure and normalized SBC, whose value is indicated by color scale, calculated for different OOR angles (α) .

DF-09. Spin Pumping and Inverse Spin Hall Effect in Chiral **Polymers**

S. Li, S. Jeon, Y. Chen, M. Yoo, A. Hoffmann, Y. Diao University of Illinois Urbana Champaign, Urbana, Illinois, **United States**

We studied the chirality-induced spin polarizations in chiral polymers by measuring the inverse spin Hall voltages(V_{ISHE}) generated in chiral P(g₄2T-TT) by spin pumping. Specifically, we deposited a 10 nm ferromagnetic layer(Py; Ni80Fe20) on top of right-handed P(q₄2T-TT). We then applied a RF current in GHz range to excite the magnetization dynamics of Py while sweeping a magnetic field along the chiral axis of the polymer at the same time. As shown in Fig.1, a large DC voltage V_{ISHE} is detected when the Py is at resonance during field sweep. We extracted the symmetric and asymmetric components from V_{ISHE} by fitting using Lorentzian functions, and the symmetric component contains information about chirality-induced spin polarizations [1]. We then studied the angular dependency of the symmetric component by rotating the magnetic field and collecting V_{ISHE} at different angles between the magnetic field and the chiral axis. As shown in Fig.2, we observed the largest symmetric components when the field is parallel and anti-parallel with the chiral axis, but with opposite signs for the two angles, indicating chiralityinduced spin polarizations along the chiral axis. We also performed similar measurements on the left-handed P(q₄2T-TT), and we observed a sign change in the symmetric component compared to that from the right-handed polymer, further confirming the chirality-related origin behind the observed inverse spin Hall voltages.

[1] D. Wei, et.al., Nature Communications 5, 3768 (2014)

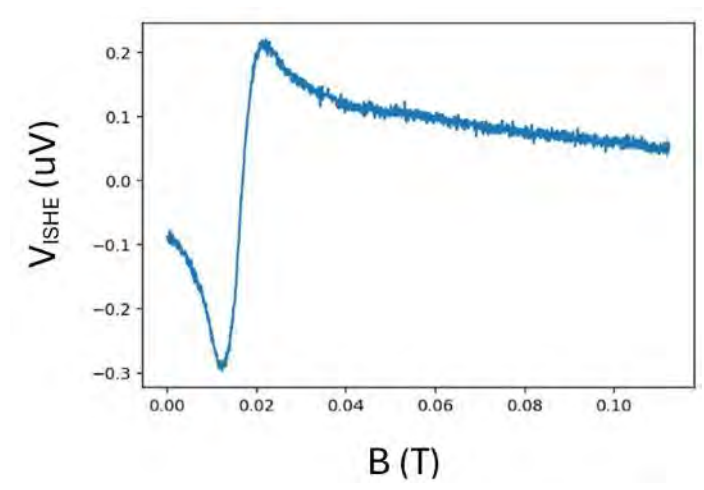


Fig.1 V_{ISHE} when field is along the chiral axis

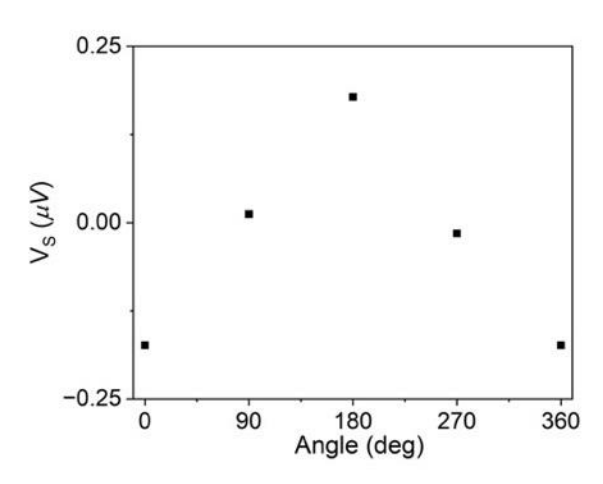


Fig.2 Symmetric component Vs as a function of angle between magnetic field and chiral axis

DF-10. Unconventional spin polarization unleashed by Fermi surface modulation

<u>S. Sugimoto</u>², Y. Araki¹, J. Ieda¹, S. Kasai², Y. K. Takahashi² ¹Japan Atomic Energy Agency, Tokai, Japan, ²National Institute for Materials Science, Tsukuba, Japan

Current-induced spin-orbit torque (SOT) at thin film interfaces plays a critical role in modern spintronics. Besides the conversion efficiency, manipulation of current-induced spin polarization components has also been developed to improve all-electric operations of solid-state non-volatile memories. The unconventional out-of-plane (z) and in-plane (x) polarizations remove geometrically invariant points in magnetization switching processes¹, and enable zero-field SOT switching². In ordinary thin film heterostructures, such unconventional spin polarization is prohibited by spatial symmetries, and hence additional symmetry breaking is necessary in device configurations³).

Here, we propose a brand-new protocol to meet such demands by engineering Fermi surface symmetry at interface. A topological insulator Bi_2Te_3 shows the hexagonal warping structure reflecting the threefold rotational symmetry C_{3V} of crystal. Such a discrete rotational symmetry allows the out-of-plane spin components in response to current, unlike the SOT under continuous rotational symmetry $C_{\omega V}$ (Fig. 1a). By fabricating an atomic-scale thickness modulation, we realize the symmetry lowered down to the trivial C_1 structure (Fig. 1b), in a simple heterostructure device for the first time. Such an asymmetric Fermi surface enables all the three components of current-induced spin polarization.

We demonstrate this type of Fermi surface manipulation

protocol with Bi₂Te₃ (001)/CoFeB sputtered heterostructures⁴⁾. Our ST-FMR measurement results show considerable improvements in the unconventional SOT efficiencies characterized by the nonreciprocal spectra in comparison with the conventional W/CoFeB heterostructure (Fig.1c and d). These results indicate the out-of-plane and on-plane SOT components comparable to the champion values reached in previous experiments so far. Such remarkable improvement of unconventional SOT components will enable zero-field SOT switching without designing complex device structures.

- 1) I. M. Miron et al., Nature (London), Vol. 476, p189 (2011)
- 2) S. Fukami et al., Nat. Nanotechnol., Vol. 11, p621 (2016)
- 3) D. MacNeill et al., Nat. Phys., Vol. 13, p300 (2017)
- 4) S. Sugimoto et al., Commun. Phys., Vol. 8, p100 (2025)

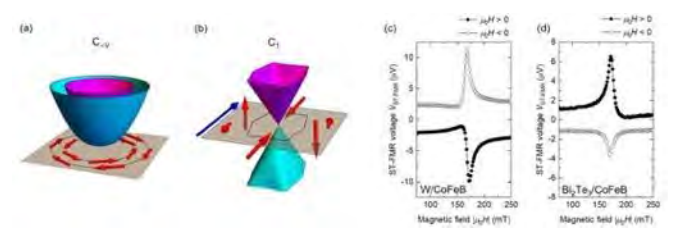


Fig. 1 Schematic images of (a) $C_{\infty V}$ and (b) C_1 symmetries of Fermi surface. Reciprocal and nonreciprocal ST-FMR spectra for (c) W/CoFeB and (d) wedge-shaped $Bi_2Te_3/CoFeB$ heterostructures.

DF-11. Increased Rectified Voltage in Magnetic Tunnel Junction with Pseudo Spin Valve Structure for Wireless Signals Energy Harvesting

<u>K. Kino</u>^{1, 2}, H. Chiku^{1, 2}, T. Dohi², T. Shinoda^{1, 2}, S. Kanai^{1, 2, 3}, H. Ohno^{1, 3, 4}, S. Fukami^{1, 2, 3}

¹RIEC, Tohoku Univ., Sendai, Japan, ²Graduate School of Engineering, Tohoku Univ., Sendai, Japan, ³WPI-AIMR, Tohoku Univ., Sendai, Japan, ⁴CSIS, Tohoku Univ., Sendai, Japan Establishing energy harvesting technologies from ambient wireless signals holds a potential for achieving a low carbon emission society. Toward this end, magnetic tunnel junctions (MTJs) have been used to demonstrate the energy harvesting from a 2.4 GHz WiFi band wireless signal [1,2]. For practical applications, however, improving the conversion efficiency from rf input to dc output is required. For this purpose, this study employs MTJs with a pseudospin-valve (PSV) structure (Fig. 1(a)). Compared with the spin-valve (SV) MTJs used in the previous work [1,2], where reference layer has virtually fixed magnetization with synthetic antiferromagnetic coupling and exchange bias

(Fig. 1(b)), the PSV MTJs have been reported to show higher tunneling magnetoresistance (TMR) with higher temperature annealing stability [3], showing promise for higher conversion efficiency.

PSV and SV MTJs are deposited by sputtering and annealed at 450°C and 300°C, respectively, in a vacuum. Figure (2)(a) shows the TMR ratios of the PSV and SV MTJs as a function of magnetic field, indicating that the TMR ratio of the PSV MTJ is higher than that of the SV MTJ. We investigate the rectified voltage through the ferromagnetic resonance (FMR) [4]. Figure 2(b) shows the maximum voltage vs. input rf power. We find that the PSV MTJs exhibit significantly higher sensitivity, which can be attributed to the higher TMR ratio. This work provides a route for improving the conversion efficiency for wireless signals energy harvesting applications.

We thank H. Yang, R. Sharma, and A. Jiang of the Nat'l Univ. Singapore for fruitful discussion. This work was partly supported by JSPS Kakenhi and MEXT X-NICS.

[1] R. Sharma *et al.*, Nat. Commun. 12, 2924 (2021). [2] R. Sharma *et al.*, Nat. Elec. 7, 653 (2024). [3] S. Ikeda. *et al.*, Appl. Phys. Lett. 93, 082508 (2008). [4] A. A. Tulapurkar *et al.*, Nature 438, 339 (2005).

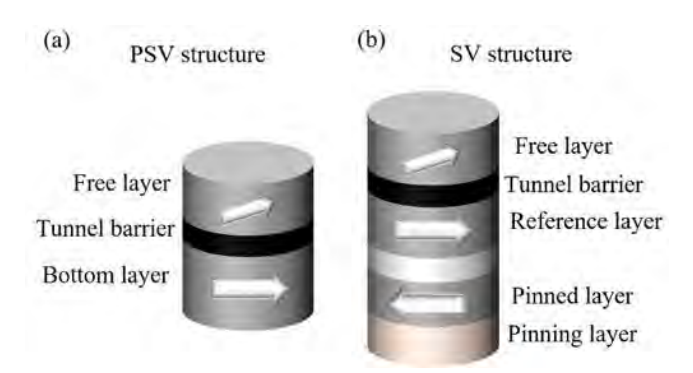


Fig. 1. (a) PSV and (b) SV structures. Arrows indicate magnetization directions in each layer.

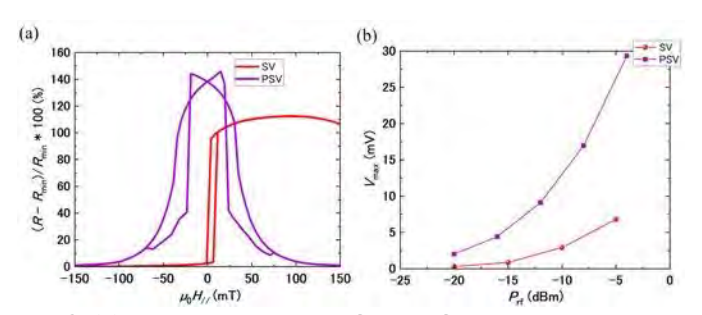


Fig. 2. (a) The TMR ratios of PSV and SV as a function of magnetic field. (b) The maximum rectified voltage (V_{max}) dependence on input rf power (P_{rf}) at 2.5 GHz.

SESSION DG: MAGNETIC SENSORS, HIGH FREQUENCY DEVICES, AND POWER ELECTRONICS I

Co-Chair(s): N. Alatawneh, Sacred Heart University, Trumbull,
Connecticut, United States and N. Schulz, Naval Surface
Warfare Center, Panama City Division, Panama City Beach,
Florida, United States
Wednesday, October 29, 2025
02:00 PM-05:30 PM
Room 2A

DG-01. Magnetic Field Detection from an Ingestible Device using a Tunnel Magnetoresistance Sensor

T. Kubota¹, H. Wagatsuma², K. Fujiwara², M. Endo¹, T. Hojo^{1, 3}, M. Ishida¹, N. Nakasato^{1, 6}, H. Ono², H. Fukushima², S. Kumagai², H. Matsuzaki², K. Yokoi⁴, S. Oyagi⁴, R. Otsuka⁴, I. Yamane⁴, D. Canlas⁵, J. Komaili⁵, S. Pathare⁵, J. Withrington⁵, T. Thompson⁵, J. Jinno⁴, K. Onishi⁴, Y. Ando^{1, 3}

¹Advanced Spintronics Medical Engineering, Tohoku University, Sendai, Miyagi, Japan, ²Spin Sensing Factory Inc., Sendai, Japan, ³Department of Applied Physics, Tohoku University, Sendai, Miyagi, Japan, ⁴Otsuka Pharmaceutical Co., Ltd., Tokyo, Japan, ⁵Otsuka Precision Health Inc., Hayward, California, United States, ⁶Graduate School of Medicine, Tohoku University, Sendai, Japan

Tunnel magnetoresistance (TMR) sensors exhibit highly sensitive magnetic field detection and a large dynamic range enabling magnetic-shield less measurements, which are increasingly used in various applications including biomagnetism and industrial devices[1,2]. The high sensitivity of TMR sensors enables the detection of various signals stemming from electric phenomena including those from ingestible devices. Although the ingestible devices, such as capsule endoscopes and digital medicine[3], provide internal bodily information via electrical voltage measurement requiring skin contact, magnetic field-based approaches present a promising alternative for non-contact data transmission[4].

In this work, we evaluated the magnetic signals from ingestible event marker (IEM) chips used for digital medicine. A TMR sensor comprising a linear series array of 74 tunnel junctions was used[1]. Two rectangular magnetic flux concentrators were placed on both sides of the array. The IEM chip is a self-powered device which is activated when it is dipped into ionic liquids (e.g. saline, hydrochloric acid) [3]. For a measurement, an IEM was placed on a circular container (dia. 135 mm) filled with 200 ml saline. Magnetic signal was detected using the TMR sensor, and electric voltage was subsequently measured using

^{*} Best Student Presentation Finalist / LB – Late-breaking Poster

electrodes dipped in the saline. No magnetic shield was employed for the IEM measurements.

The sensor output dependence as a function of external alternating field amplitude is shown in Fig. 1. The frequency band of the alternating field is 10 kHz which is used for IEM. Based on the linear fit shown in Fig. 1, the slope yielded a sensitivity of about 5000 V/T for the TMR sensor. Fig. 2(a) shows typical magnetic signals from an IEM chip. Clear magnetic signals with an amplitude range on the order of ten nano Tesla were observed in the 10 kHz band. The experimental result supports the potential for the noncontact monitoring devices using highly sensitive TMR sensors. Further details regarding the signal's distance dependence will be presented.

[1] M. Oogane *et al.*, Appl. Phys. Express vol.14, p.123002 (2021).

[2] T. Nakano *et al.*, Appl. Phys. Lett. vol.126, p.160503 (2025)

[3] H. Hafezi *et al.*, IEEE Trans. Biomed. Eng. vol.62, p.99 (2015).

[4] Patent application JPA2025-056510

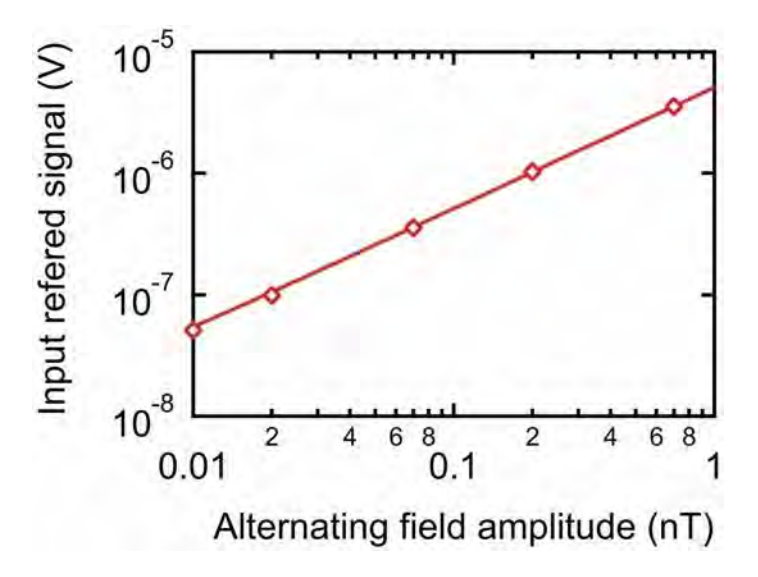


Fig. 1 Alternating field amplitude dependence of the input referred signal of a TMR sensor at the 10 kHz band.

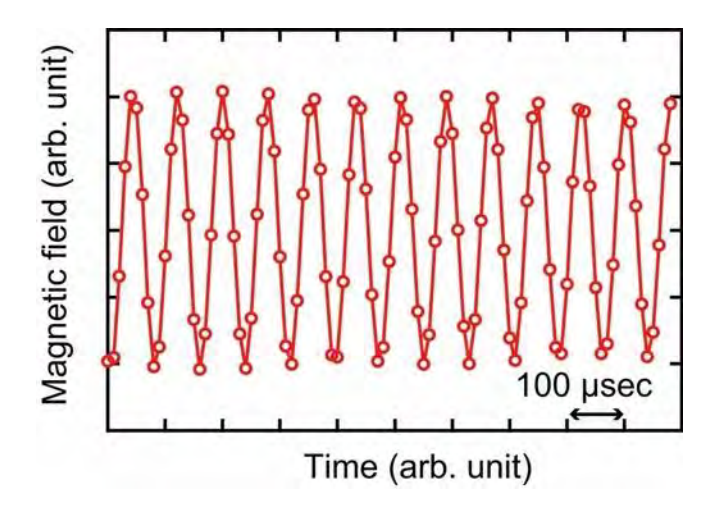


Fig. 2 Time-domain magnetic signal of an IEM chip.

DG-02. Enhancement of Exchange bias in NiFe-IrMn Planar Hall bilayer thin films for rotary sensing applications

K. S. Narasimhan, P. Anil Kumar

Physics, Indian Institute of Science, Bangalore, Bangalore, Karnataka, Karnataka, India

Exchange bias is a magnetic phenomenon extensively exploited in the design and development of various magnetic devices, particularly those involving thin films. occurs at the interface between ferromagnetic (FM) and antiferromagnetic (AFM) materials, manifesting as a shift in the hysteresis loop of the ferromagnetic material when cooled in a magnetic field through the Néel temperature of the antiferromagnet. The essence of exchange bias is in the exchange interaction at the FM-AFM interface, which leads to an increased coercivity and a shift in the magnetic field axis. One common approach is through the careful selection and engineering of the FM and AFM materials. The choice of materials, their crystallographic texture, and the interface quality directly influence the strength of the exchange interactions. Our study focuses on systematic enhancement of the unidirectional anisotropy (exchange bias) of the Planar Hall Magneto resistive thin film configuration to be used as an angle sensor at higher field levels. Rique, J. N., Beck, F., de Andrade, A. M. H., Kern, P. R., Siqueira, J. v., & Carara, M. (2015). Exchange bias in bilayer and multilayer NiFe/IrMn. IEEE Magnetics Letters, 6. https://doi.org/10.1109/LMAG.2015.2397396

Kern, P. R., de Siqueira, J. v, Escobar, O., Silva, D., Marcos, A., & de Andrade, H. (n.d.). Exchange Bias Effect in Multilayers of NiFe/IrMn/Ta Tunneling View project Angular

^{*} Best Student Presentation Finalist / LB - Late-breaking Poster

Dependence of Exchange Bias in Ferromagnetic/Antiferromagnetic Bilayers View project. https://doi.org/10.13140/RG.2.2.36108.77446

Dobrynin, A. N., Warin, P., Vorobiev, A., & Givord, D. (2021). On the origin of positive exchange bias and coercivity enhancement in proximity to the blocking temperature. Journal of Magnetism and Magnetic Materials, 520. https://doi.org/10.1016/j.jmmm.2020.166707

Elzwawy, A., Piskin, H., Akdogan, N., Volmer, M., Reiss, G., Marnitz, L., Moskaltsova, A., Gurel, O., & Schmalhorst, J. M. (2021). Current trends in planar Hall effect sensors: Evolution, optimization, and applications. In Journal of Physics D: Applied Physics (Vol. 54, Issue 35). IOP Publishing Ltd. https://doi.org/10.1088/1361-6463/abfbfb

Kohn, A., Kovács, A., Fan, R., McIntyre, G. J., Ward, R. C. C., & Goff, J. P. (2013). The antiferromagnetic structures of IrMn 3 and their influence on exchange-bias. Scientific Reports, 3. https://doi.org/10.1038/srep02412

Sankaranarayanan, V. K., Yoon, S. M., Kim, D. Y., Kim, C. O., & Kim, C. G. (2004). Exchange bias in NiFe/FeMn/NiFe trilayers. Journal of Applied Physics, 96(12), 7428–7434. https://doi.org/10.1063/1.1815048

Neamtu, J., Volmer, M., & Neamtu, M. C. (n.d.). Spin-valve structures with anisotropic magneto-resistance (AMR) for planar Hall effect (PHE) sensing applications. In OPT OELECTRONICS AND ADVANCED MATERIALS-RAPID COMMUNICATIONS (Vol. 12, Issue 9).

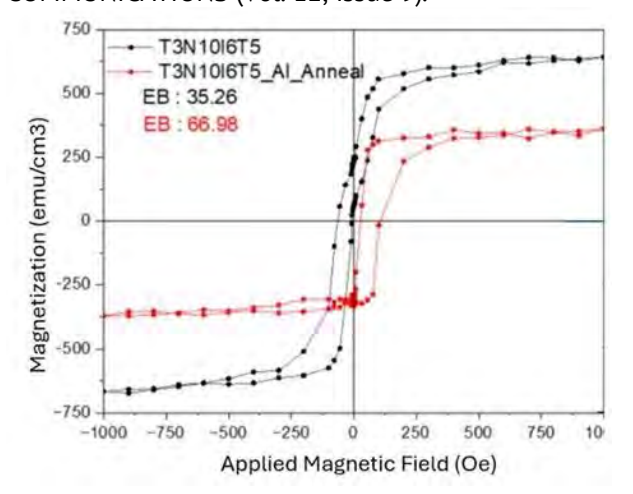


Fig. 1 The graph represents the typical magnetization characteristics of NiFe10IrMn5 thin film before and after magnetic annealing

DG-03. Plasmonically-enhanced Digital Spintronic Detector based on Stochastic Magnetic Tunnel Junctions

<u>S. Gupta</u>, Z. Yang, J. Shalabi, A. Deka, L. Bauer, Z. Jacob *Purdue University, West Lafayette, Indiana, United States*

Infrared detection at room temperature is increasingly critical for advanced applications in imaging, autonomous navigation, defense and medicine applications [1]. However, existing high-sensitivity infrared detectors require cooling for operation. To address this, we introduce the Spintronic Ultrafast Nanoscale Bolometer (SUN Bolometer), a novel detection platform that leverages thermally mediated stochastic spin transitions in magnetic tunnel junctions (MTJs) for ultrafast, room-temperature infrared sensing [2]. In SUN Bolometer, incident infrared radiation induces localized heating, resulting in thermally activated spin transitions. The spin state is related to the MTJ magnetoresistance, enabling digital readout. The system exhibits Poissonian detection statistics, thereby supporting high-fidelity, time-resolved measurements with enhanced signal-to-noise ratios. To optimize performance in the longwave infrared (LWIR) spectrum, we incorporate engineered metal-insulator-metal (MIM) plasmonic metasurfaces on top of the MTJ stack. These metastructures enhance electric field and direct thermal energy directly into the active magnetic region, significantly enhancing both spin sensitivity and detection efficiency. By coupling nanoscale heat transport with stochastic magnetization governed by Néel-Arrhenius statistics, SUN-B establishes a fast, sensitive approach to IR photodetection. This work lays the foundation for the development of ultrafast, roomtemperature magnetic sensors for future applications in IR imaging and probabilistic and spin-based computing architectures.

- 1. R.K. Bhan, V. Dhar. Opto-Electronics Review, Vol. 27(2), p.174-193 (2019)
- 2. L. Bauer, A. Deka, M. Mousa, S. Gupta et al. Nano Lett., Vol. 25 (14), p.5599–5608 (2025)

DG-05. Area-Efficient Perpendicular Magnetic Tunnel Junction Detectivity Enhancement using Vertical Flux Concentrators

Z. Ali¹, H. Naganuma², P. Wallace³, S. X. Wang¹, A. Poon¹
¹Electrical Engineering, Stanford University, Stanford, California, United States, ²Nagoya University, Nagoya, Japan, ³Stanford University, Stanford, California, United States

Biomagnetic sensing techniques, such as magnetoencephalography (MEG) and magnetocardiography (MCG), offer significant clinical and informational advantages over their bioelectric counterparts, such as electroencephalography (EEG) and electrocardiography (EKG) [1, 2]. However, magnetic fields measured outside the body are minuscule and require bulky measurement technologies (e.g. SQUIDs, OPMs) that preclude miniaturization for wearable sensing [3].

Magnetic tunnel junction (MTJ) sensors are a promising alternative technology, but they face two key limitations. First, while most MTJ sensors measure in-plane fields, magnetic fields *radial* to the body are more information-rich than tangential fields [4, 5]. Second, individual MTJ sensors do not possess the requisite detectivity to measure biomagnetic fields. Since the spatial resolution of most biomagnetic signals is ~1 cm [1], researchers have explored approaches that trade device area for enhanced detectivity, but none have attained sufficient detectivity to measure biomagnetic fields without averaging [6].

In this work, we first introduce a new flux concentrator architecture, which we call a vertical flux concentrator (vFC), intended to address these challenges. We show, using COMSOL simulations, that this flux concentrator design amplifies fields in the perpendicular direction and attains improvements in device detectivity comparable to a planar flux concentrator while using over two orders of magnitude less spatial area. We next design a new perpendicular MTJ (pMTJ) material stack which, when fabricated, exhibits a TMR ratio of 150%, the highest for a pMTJ sensor in the literature. Lastly, we use a plasma focused ion beam to fabricate a tall, high-aspect ratio T-bar vFC by etching it out of a permalloy thin film (Fig. 1). This vFC is then integrated with a pMTJ, improving its detectivity by up to 40x while occupying a spatial area of only 150 um² (Fig. 2). Our findings indicate that by fabricating these vFC+pMTJ devices into a massive array, we can achieve single-shot, wearable, biomagnetic sensing.

- 1. M. Hämäläinen, R. Hari, and O. Lounasma, Rev. Mod. Phys. Vol.65, pp. 413-497 (1993).
- 2. J. Lévy, M. Zhang, and J-R. King, arXiv:2502.17480. (2025).
- 3. E. Boto, R. Bowtell, and M. Brookes, PLOS One. (2016).
- 4. J. Iivanainen, M. Stenroos, and L. Parkkanen, Neurolmage. Vol. 147, pp. 542-553 (2017).
- 5. U. Marhl, A. Jodko-Wladzinska, and V. Jazbinsek, PLOS One. (2022).
- 6. A. Kanno, N. Nakasato, and Y. Ando, Scientific Reports. (2022).

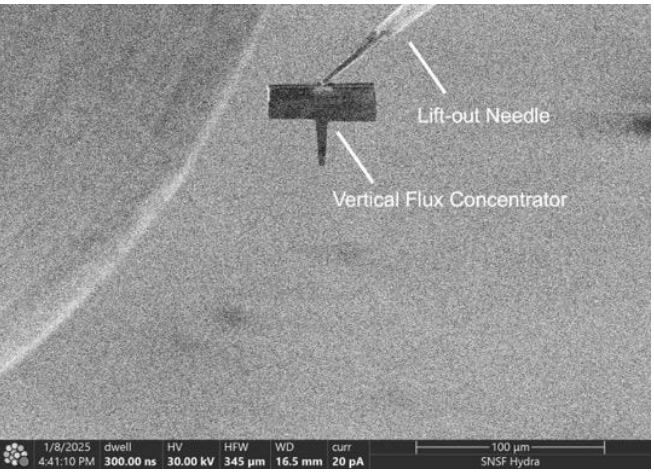


Fig. 1: SEM image of vFC being lowered by lift-out needle onto pMTJ.

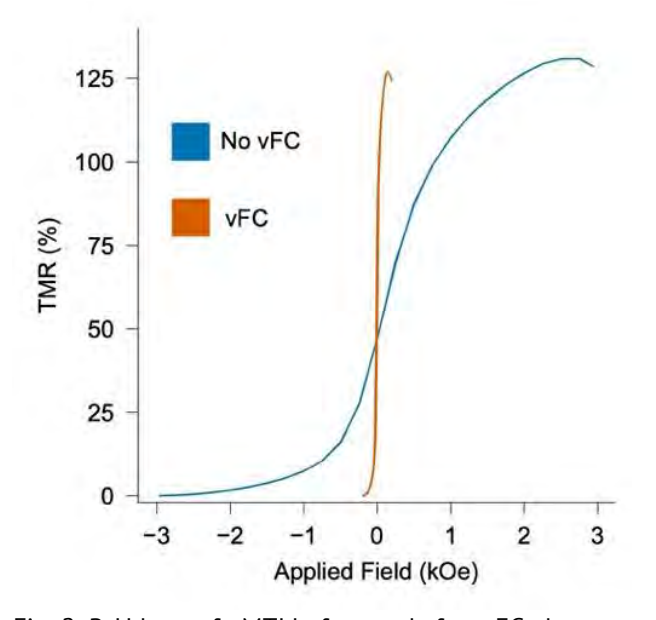


Fig. 2: R-H loop of pMTJ before and after vFC, demonstrating 40x enhancement in sensitivity.

DG-06. Noise Reduction and Dynamic Range Enhancement of Pulse-Driven GMI Sensors via Optimized Anti-Aliasing Filtering

S. Idachi, T. Uchiyama

Department of Electronics, Nagoya university, Nagoya, Aichi, Japan

This study proposes a method to enhance the dynamic range of pulse-driven Giant Magneto-Impedance (GMI) sensors by introducing an optimized anti-aliasing filter (AAF).

While negative feedback is a commonly used technique to linearize the sensor response and improve dynamic range[1,2], it has been observed that increasing the feedback strength beyond a certain point no longer yields further improvements[3]. We confirmed that the primary limitation in expanding the dynamic range arises from the circuit noise floor, which is predominantly determined by aliasing noise in the sampling circuit of GMI sensors.

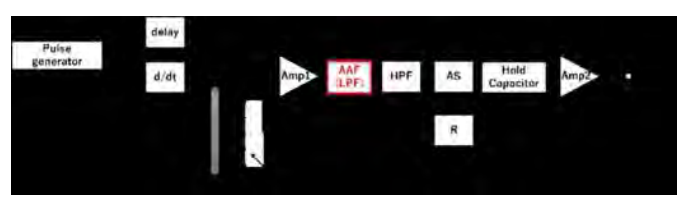
To address this limitation, we introduce a low-pass AAF with a carefully selected cutoff frequency that effectively suppresses aliasing noise while preserving the sensor's intrinsic voltage bandwidth (Fig. 1). Theoretical calculations and experimental validation demonstrated that the reduction in circuit noise achieved by the filter closely matches the predicted suppression rate, derived from the buffer amplifier's noise characteristics and the filter's bandwidth.

Implementation of an AAF with a 31.2 MHz cutoff frequency reduced the circuit noise by approximately 50%, resulting in a 6 dB improvement in dynamic range (Fig. 2). The measurable magnetic field range increased from approximately 20 μ T to 160 μ T. Additionally, replacing the buffer amplifier with the low-noise ADA4899 further reduced the 10 Hz noise floor by 58%.

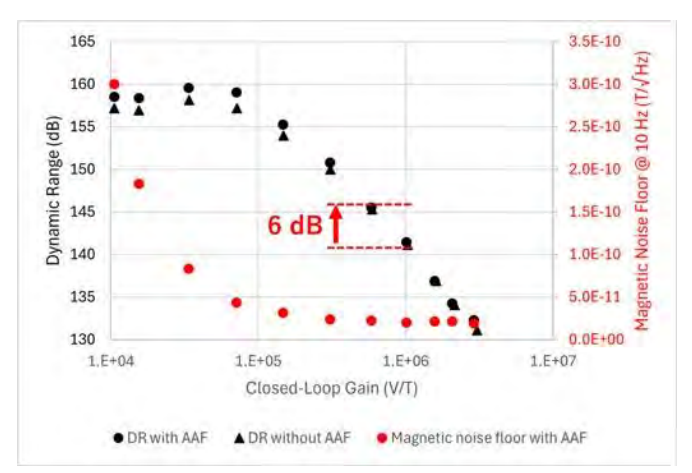
We also confirmed that applying an appropriately designed AAF is particularly critical under high-feedback conditions, where the absence of filtering can lead to severe degradation in dynamic range. Although amplifier noise was effectively mitigated, residual noise contributions from excitation pulses and sampling jitter remained.

Overall, these results demonstrate that systematic noise analysis, combined with targeted filter design, can significantly enhance the performance of GMI sensors, enabling their application in highly sensitive magnetic field measurements, such as biomagnetic signal detection in the picotesla range.

- [1] T. Takiya and T. Uchiyama: *IEEE Trans. Magn.*, 53(11),1 (2017).
- [2] S. Gudoshnikov, N. Usov, A. Nozdrin, M. Ipatov, A. Zhukov and V. Zhukova: *Phys. Status Solidi a*, 211(5), 980 (2014).
 [3] S. Idachi and T. Uchiyama: *Journal of Magnetics*, 29(2), 253 (2024).



Insertion of Anti-Aliasing Filter (AAF) in GMI Sensor circuit



Effect of AAF on Dynamic Range and Noise Floor at 10 Hz

DG-07. High Frequency Transformer Integrated with SiC MOSFETs for Smart Transformer

<u>J. Lu</u>, W. Yao, N. Subhani, A. Seagar, Y. Zhu School of EBE, Griffith University, Gold Coast, Queensland, Australia

The paper presents a novel compact structure of High-Frequency Transformer (HFT) integrated with SiC MOSFETs [1]. This compact structure of HFT integrated with SiC MOSFETs can be applied to Smart Transformer (ST) for renewable energy resources and fast EV charging systems. The HFT can be used in the isolated phase-shift dual active bridge (PS-DAB) converter, inductor-inductor-capacitor (LLC) resonant converter, bidirectional PS-DAB converter, and

capacitor-inductor-inductor-capacitor (CLLC) resonant converter. These DC/DC converters are mainly considered for the integration of HFT with SiC MOSFETs [2,3]. The applications of the high power HFT integrated with SiC MOSFETs are focused on various power supplies used in Solid State Transformer (SST), Uninterruptible Power Supply (UPS), battery energy storage in DC and AC Microgrids, Vehicle to Grid (V2G) bi-directional EV battery charging systems, and other power supplies used in renewable energy systems and fast EV charging systems[4,5,6]. The HFT structure utilizes distributed ferrite cores to create a large central space for accommodating SiC semiconductor devices and their associated drives. SiC semiconductor devices, including MOSFETs, Schottky diodes, and MOSFET modules, can be used in this novel compact structure of HFT. The optimized architecture of HFT and heatsink structure is considered for the thermal management of SiC devices. Several prototype HFTs are used to demonstrate the basic structure of the power supply in the package. The FEM based electromagnetic simulation and DC-DC converter experiment results are presented in this paper.

[1] S. Yao, J. Lu, A. Seagar, F. Bai, and F. Taghizadeh, Integration of Novel High-Frequency Transformer with Silicon-Carbide Schottky Diodes. IEEE Magnetics Letters, vol. 13, 2022

[2] Z. Guo, D. Sha, Introduction. In New Topologies and Modulation Schemes for Soft-Switching Isolated DC-DC Converters, Eds. CPSS Power Electronics Series; Springer: Singapore, 2020; pp. 1-16.

[3] N.H. Baars, J. Everts, H. Huisman, J. L. Duarte, E.A. Lomonova. A 80-kW Isolated DC-DC Converter for Railway Applications. IEEE Transactions on Power Electronics 2015, 30, 6639-6647, doi:10.1109/TPEL.2015.2396006.

[4] F. Xue, R. Yu, A.Q. Huang. A 98.3% Efficient GaN Isolated Bidirectional DC–DC Converter for DC Microgrid Energy Storage System Applications. IEEE Transactions on Industrial Electronics 2017, 64, 9094-9103, doi:10.1109/TIE.2017.2686307.

[5] S. Inoue, H. Akagi. A Bidirectional Isolated DC-DC Converter as a Core Circuit of the Next-Generation Medium-Voltage Power Conversion System. IEEE Transactions on Power Electronics 2007, 22, 535-542, doi:10.1109/TPEL.2006.889939.

[6] A. Nabih, R. Gadelrab, P.R. Prakash, Q. Li, F.C. Lee. High Power Density 1 MHz 3 kW 400 V-48 V LLC Converter for Datacenters with improved Core Loss and Termination Loss. In Proceedings of the 2021 IEEE Applied Power Electronics Conference and Exposition (APEC), Phoenix, AZ, USA, 2021; pp. 304-309.

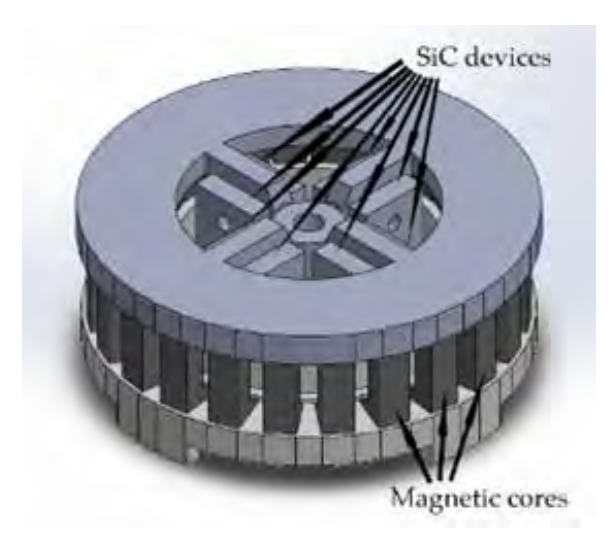


Fig. 1. High-Frequency Transformer Integrated with SiC devices.

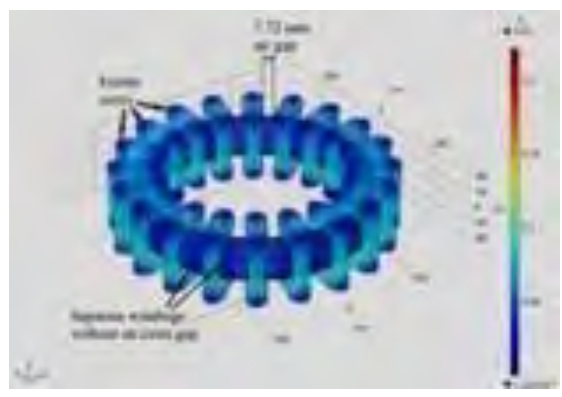


Fig. 2 FEM simulation result of Magnetic field distribution.

DG-08. Influence of heat-treatment on structure and magnetic properties of 10 µm-thick Fe-1,2,3wt.%Si foils S. Ajia¹, T. Takasu¹, S. Muroga¹, Y. Endo^{1,2}

¹Department of Electrical Engineering, Tohoku University, Sendai, Japan, ²CSIS, Tohoku University, Sendai, Japan

Fe-Si steels have been widely used for various applications because of their low coercivity and large saturation magnetization [1,2]. However, for low Si content, the eddy current loss in the high frequency range remains as a challenge. Much more efforts have been made for producing high Si content to 6.5wt.% [3,4], which has both near zero magnetostriction and high permeability. On the other hand, the reduction of sheet thickness is one of the promising approaches for lowering the eddy current loss in the high

frequency range. Herein, 10 µm-thick Fe-1,2,3wt.%Si foils were prepared, and we investigated the effect of heattreatment on the magnetic softness, magnetostriction and high frequency properties of Fe-1, 2,3wt.%Si foils in detail. The coercivity (H_c) of each Fe-Si foil was summarized in Fig. 1(a) with annealing temperature (T_a). In each Fe-Si foil, H_c showed a decreasing tendency as T_a increased. H_c value of as-made Fe-3wt.%Si was reduced from 5.9 Oe at room temperature (300 K) to about 3.1 Oe for $T_a = 773$ K. Thus, the low H_c might result from the strain release and the refinement of grain size of Fe-Si foil by heat-treatment. Fig. 1(b) showed the change of saturation magnetostriction (λ_s) with T_a . λ_s of as-made Fe-Si foil increased with the increase of Si content, whose value was 2.3, 7.1, and 8.1 ppm for 1,2,3wt.%Si, respectively. As T_a increased, λ_s decreased to 0.85, 4.4 and 7.6 ppm for 1,2,3wt.%Si, respectively. Combined with the decreasing H_c and λ_s , consequently, the permeability of Fe-Si foils was increased with the increase of T_a as shown in Fig. 1(c). The resultant high μ_i may be derived from the relaxation of localized strain and lowered magnetocrystalline anisotropy arose from microstructure evolution by annealing.

Therefore, the improved soft magnetic properties of Fe-1.2.3wt.%Si foils after heat-treatment makes the 10 μ m-thick Fe-Si foils promising candidates to apply in next-generation power electronic devices.

This study was supported by MEXT-Program for Creation of Innovation Core Technology for Power Electronics No. JPJ009777 and MEXT, No. JP011438; CSIS of Tohoku University;

- [1] M. Kawano, *et.al.*, Kawasaki Steel Technical. Report, 48, 47-52 (2003)
- [2] O. Gutfleisch, et. al., Adv. Mater. 23(7), 821–842 (2011). [3] Y. Zhang, *et.al.*, J. Magn. Magn. Mater. 451, 187-192
- [4] G. Ouyang, *et.al.*, J. Magn. Magn. Mater. 481, 234-250 (2019).

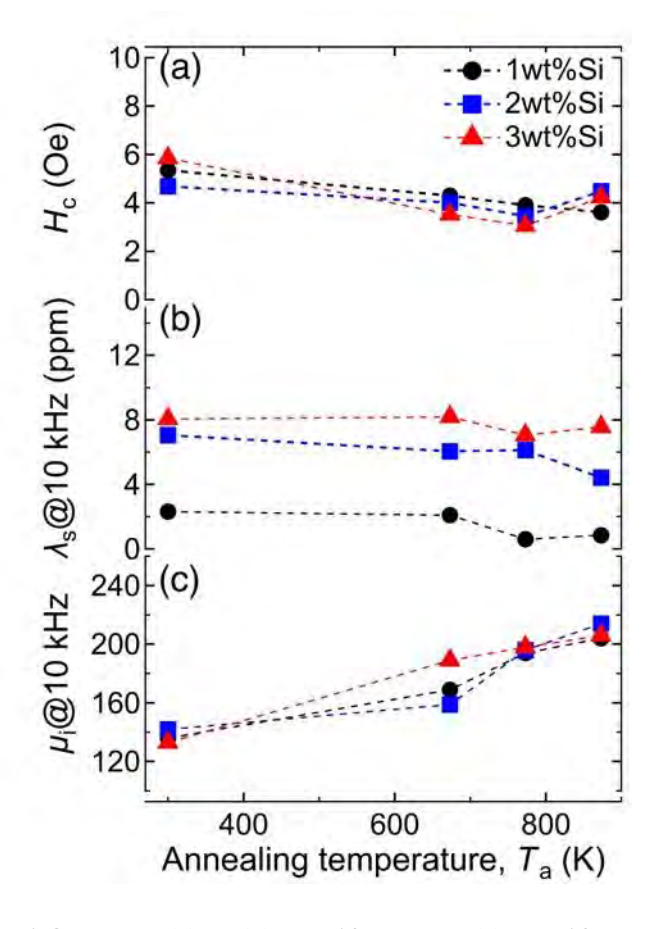


Fig. 1 Change in (a) H_c , (b) λ_s at 10 kHz, and (c) μ_i at 10 kHz with T_a for 10 μ m-thick Fe-1,2,3wt.%Si.

DG-09. An Optimized Design of a Dual Rotor Axial Flux Switched Reluctance Electrical Machine

M. Trapanese

Dipartimento di Ingegneria, Palermo University, Palermo, Italy

This paper introduces and explores an innovative configuration of a dual rotor axial flux switched reluctance electrical machine, aimed at achieving enhanced performance, flexibility, and design efficiency. In the initial sections, the fundamental operating principles of the proposed machine architecture are thoroughly examined, with a focus on both its functionality as a generator and its behavior in motor operation. This dual analysis provides a comprehensive understanding of the machine's capabilities across a broad range of applications.

The performance characteristics of the machine are subsequently analyzed under various operating conditions, allowing for a detailed assessment of its dynamic response, efficiency, and adaptability. A key feature of the proposed design is the presence of two rotors that are mechanically independent from one another. These rotors are mounted on separate shafts, which can be controlled independently, offering a significant degree of mechanical decoupling. This configuration is particularly advantageous in motor mode, where the machine can effectively serve as a mechanical differential. Such a capability has the potential to simplify the architecture of the powertrain system, leading to reductions in both cost and mechanical complexity [1].

To enhance the overall efficiency and effectiveness of the machine, an optimized design methodology has been employed. This methodology is grounded in a parametric design approach, focusing specifically on the magnetic circuit of the machine. The electromagnetic behavior has been meticulously analyzed using a parametric finite element model (FEM), which enables a detailed investigation of the machine's magnetic performance under different loading scenarios. The optimization process was guided by two primary objectives: maximizing the power density output while simultaneously minimizing losses. This design strategy ensures that the machine achieves a high level of performance without compromising energy efficiency, making it suitable for a wide range of advanced applications.

A final comparison with a traditional axial flux machine is presented

1) Jack Gillies; Tim Lambert; Ali Emadi et al, "Axial-Flux Switched Reluctance Motor Design for a Light Electric Vehicle Application" proceedings of 2022 IEEE Transportation Electrification Conference & Expo (ITEC)

DG-10. Microwave-Driven Magnetic Dynamics in Low-Temperature Synthesized Hexaferrites: A Static-to-Dynamic Perspective

K. Rana^{1, 2}, M. Tomar¹, A. Thakur^{3, 2}
¹Department of Physics and Astrophysics, University of Delhi, Delhi, New Delhi, India, ²Innovative Science Research Society, Shimla, Himachal Pradesh, India, ³Physics, Amity University, Gurugram, Haryana, India

M-type Barium hexaferrites are indispensable for microwave absorption, but their performance depends critically on cation substitution and synthesis conditions. This study reports the low-temperature synthesis of cobalt-substitute Barium hexaferrites (BaCo_xFe_{12-x}O₁₉,(x = 0.0-1.0 in steps of 0.2) via conventional co-precipitation method, systematically investigating the impact of doping on structural, magnetic, and electromagnetic properties. XRD confirmed M-phase formation with lattice shrinkage (a= 5.88 to 5.92 Å, c= 23.40 to 23.37 Å) and crystallite growth (29.56 to 45.02 nm) with dopant. VSM revealed non-monotonic magnetization trends, with specific magnetization (σ_s) peaking at 66.44 emu/g (x = 0.0) and coercivity (H_c) maximizing at 37890e (x = 0.8), attributed to increased anisotropy. Vector Network Analyser measurements at Xband (8-12 GHz) showed optimal microwave absorption for x = 0.2 ($\epsilon' = 9$, $\mu' = 1.8$) and x = 0.8 ($\epsilon' = 11$, $\mu'' = 0.3$), suggesting strong dielectric and magnetic loss mechanisms. The x = 0.8 composition, with its high H_c and balanced ε/μ , emerges as a promising candidate for radar-absorbing materials (RAM) and 5G shielding. This work demonstrates a low-energy route to tailor hexaferrites for high-frequency applications, bridging the gap between synthesis efficiency and functional performance.

Y.Lu, M. Akhtar and N. Yousaf, Journal of Alloys and Compound.,994, 174627 (2024).

Z. Yang, S. Wei and X. Wang, Journal of Magnetism and Magnetic Materials.,610, 172519 (2024).

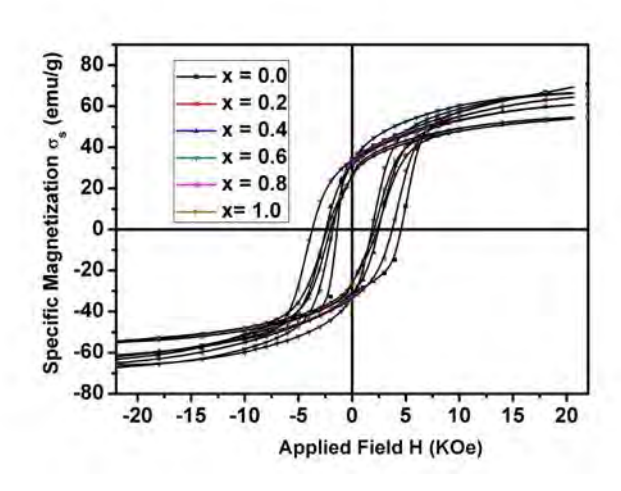


Fig. 1 Static magnetic properties of cobalt substituted M-type barium hexaferrite $BaCo_xFe_{12-x}O_{19}$.

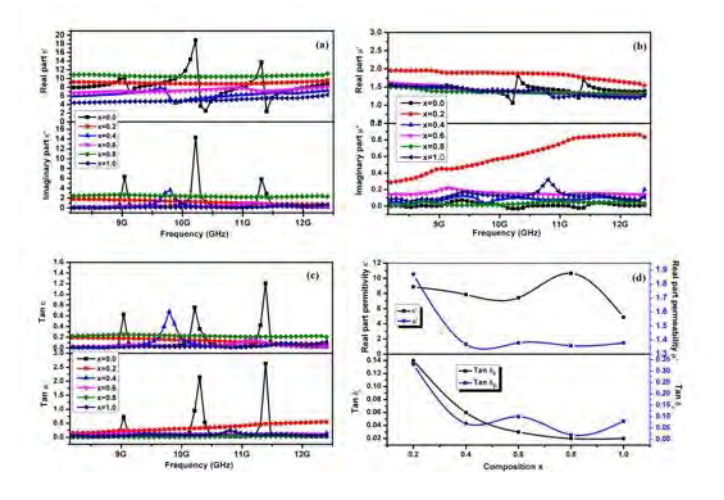


Fig. 2 Frequency-dependent electromagnetic parameters of $BaCo_xFe_{12-x}O_{19}$ at X-band (8–12 GHz): (a) Real (ϵ ') and imaginary (ϵ ") permittivity, (b) real (μ ') and imaginary (μ ") permeability, (c) dielectric (tan δ_e) and magnetic (tan δ_m) loss tangents and (d) variation of real permitivity (ϵ '), permeability (μ ') and tangent losses with composition x.

DG-11. Magnetic Bias-Driven Modulation of Graphene for Tunable Gyrotropic and Magnetoplasmon Devices

S. Amanatiadis¹, T. Ohtani², T. Zygiridis³, N. V. Kantartzis¹, <u>Y. Kanai</u>⁴

¹Aristotle University of Thessaloniki, Thessaloniki, Greece, ²1-17-134, Omachi, Asahikawa, Japan, ³University of Western Macedonia, Kozani, Greece, ⁴Niigata Institute of Technology, Kashiwazaki, Japan

Time-varying media have recently attracted the attention of the research community due to their unique features, such as frequency generation. In this context, graphene is an ideal candidate for such applications because of its inherent ability to be controlled via the application of an external bias. As a result, the time variation of this bias directly affects the surface conductivity of graphene, thereby altering its electromagnetic response. When considering the use of magnetic fields as a bias, various interesting phenomena arise, including gyrotropy when interacting with a plane wave and magnetoplasmons when a surface wave propagates. The primary objective of this work is to investigate the interaction of graphene with propagating waves under the temporal variation of the magnetic bias. This will enable the design of non-conventional plasmonic structures that can be used in modern devices, such as dynamic metasurfaces and THz waveguides.

The initial phase of our analysis focuses on evaluating the resonant characteristics of the graphene structures in relation to the magnetic bias to provide valuable insights into the expected behavior. Depending on the type of interaction with graphene – either a plane wave or a surface wave—the resonances are determined using quasi-normal modes or supported propagating modes, respectively, through the numerical simulation of the corresponding eigenvalue problem. A suitable modulation scheme is then applied to the magnetic bias of graphene to achieve the desired scattering of the plane wave or waveguiding on microstrips. The former generates gyrotropic effects, which, when combined with time modulation, allow for tunable shifts in linear polarization and scattering direction. In the latter case, magnetoplasmons emerge with adjustable propagation of the asymmetric edge modes, while frequency up-conversion of the plasmonic waves occurs. Both scenarios are examined via thorough full-wave numerical analyses, using a modified FDTD scheme to accurately model the time-varying magnetic bias on graphene.

[1] Ramaccia, D., Alu, A., Toscano, A., & Bilotti, F. (2021). Temporal multilayer structures for designing higher-order transfer functions using time-varying metamaterials. *Applied Physics Letters*, *118*(10).

[2] Sounas, D. L., & Caloz, C. (2012). Gyrotropy and nonreciprocity of graphene for microwave applications. *IEEE transactions on microwave theory and techniques*, 60(4), 901-914.

[3] Salehi, M., Rahmatian, P., Memarian, M., & Mehrany, K. (2022). Frequency conversion in time-varying graphene microribbon arrays. *Optics Express*, *30*(18), 32061-32073.

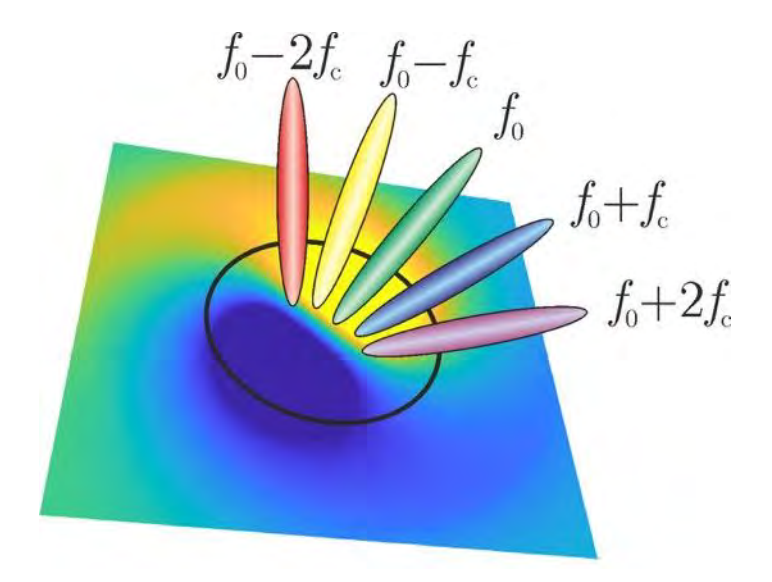


Fig. 1 Frequency generation due to time-modulated magnetic bias on graphene

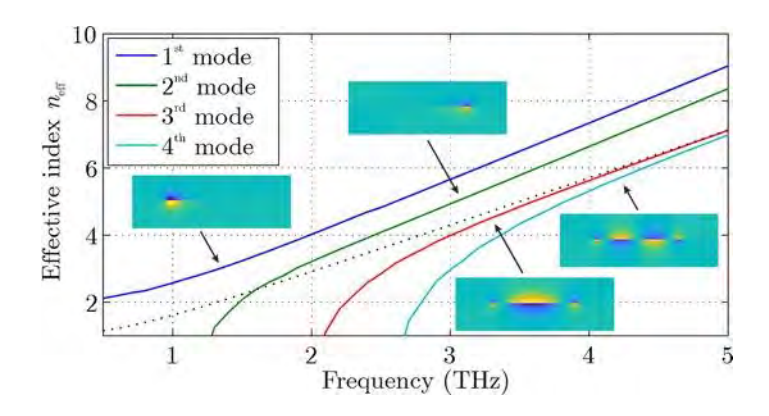


Fig. 2 Dispersion diagram and mode distribution of magnetoplasmon propagation on graphene microstrip

DG-12. Optimization of Magnetoelastic Ribbons for Mass Sensors and Development of Novel Applications in Hydrogel Gelation Time Control

M. Shaji¹, I. Tapon¹, J. Vilas-Vilela^{1, 2}, A. Lasheras¹, L. Pérez-Álvarez^{1, 2}, <u>A. Lopes</u>¹

¹University of Basque Country, Leioa, Spain, ²BCMaterials, Leioa, Spain

Magnetoelastic resonators have attracted growing interest due to their remarkable versatility and sensitivity in detecting diverse physical and biological parameters. They are particularly appealing due to their low cost and wireless detection capabilities¹. Over the years, several parameters have been optimized to improve their performance, including their composition, geometry², and crystallization³. However, these parameters have mostly been studied independently and not in combination.

More recently, we have combined the optimization of each of these parameters, along with ribbon thickness, and compared the performance of these optimized samples with traditionally used ones. The results showed more than double the sensitivity compared to conventional samples. This advancement could have a significant impact on applications involving the detection of mass variations. Furthermore, we are successfully testing these ribbons in monitoring also viscoelastic processes, particularlly during hydrogel gelation. Hydorgels are (colocar alguma coisa sobre a os hydrogeis, muito geal e curta). One of the crutial parameters to be determined is its gelation time, that is currently assessed subjectively using the tube inversion method, which is time-consuming and inaccurate. Using magnetoelastic sensors, we were able to determine the gelation time of polyacrylamide under differnet conditions. Magnetoelastic sensors showed to be fast, simple and precise method in the determination of the gelation processes.

¹P. G. Saiz, R. Fernández de Luis, A. Lasheras, M. I. Arriortua, and A. C. Lopes, Magnetoelastic Resonance Sensors: Principles, Applications, and Perspectives, ACS Sens. 2022, 7, 1248–1268

² P. G. Saiz, R. Fernández de Luis, A. Lasheras, M. I. Arriortua, A. C. Lopes, Enhanced mass sensitivity in novel magnetoelastic resonators geometries for advanced detection systems, Sensors & Actuators: B. Chemical 296 (2019) 126612

³A. Lasheras, J.S. Garitaonandia, I. Quintana, J.L. Vilas, A. C. Lopes, Development of nanocrystallized magnetoelastic

sensors with self-biased effect and improved mass sensitivity, Sensors and Actuators Reports 8 (2024) 100251

DG-13. High-frequency Magnetic Levitation of Macroscopic Masses

V. Sharma¹, M. Simon², R. Candler^{1,3}

¹Department of Electrical and Computer Engineering, University of California, Los Angeles, Los Angeles, California, United States, ²Department of Physics and Astronomy, University of California, Los Angeles, Los Angeles, California, United States, ³California NanoSystems Institute, University of California, Los Angeles, Los Angeles, California, United States

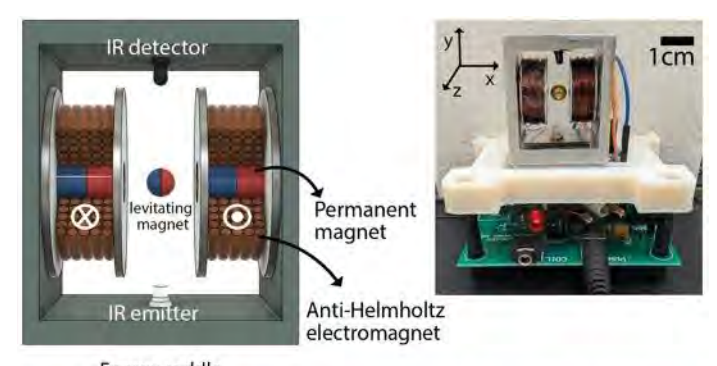
Miniature inertial sensors are pervasive in applications ranging from image stabilization in cameras to automotive safety. Yet, high-performance inertial sensors capable of GPS independent navigation remain elusive, and energy lost through mechanical anchors fundamentally limits sensor performance [1]. To eliminate anchor loss, we are working on miniature levitated systems that could be the basis for inertial sensors (accelerometers and gyroscopes). Existing work on levitation for sensors has either focused on larger masses at low frequency (milliHertz for gravity probe B) or small masses at high frequency (atom trapping) [2]. This work achieves the largest mass× frequency product for a room-temperature levitator to date, nearly 20X better than prior demonstrations (Fig. 1).

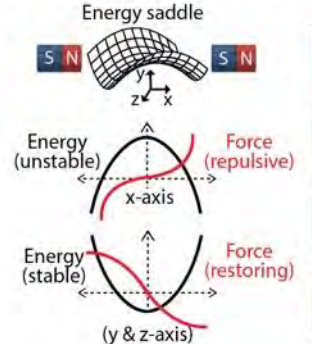
Our levitator consists of two cylindrical NdFeB magnets in a split-pole setup and two electromagnets in anti-Helmholtz configuration (Fig. 1). Levitation of a NdFeB mass has been maintained continuously for over five hours with no observed limitation in time. The residual displacement of the levitated mass is $50~\mu m$, approximately $1/100^{th}$ its diameter. The system maintained trapping through acceleration of 6g during testing, showing strong confinement and mechanical robustness (Fig. 2). The entire system is compact and consumes only 1.5 W of power. Notably, the trap frequency is independent of the levitated mass because the magnetic restoring force scales with volume of the levitating magnet, allowing heavier objects to be trapped without sacrificing the bandwidth.

- [1] Senkal, D., & Shkel, A. (2020). John Wiley & Sons, Inc., IEEE Press.
- [2] Buchman, S., Lipa, J. A., et al. (2015). Classical and Quantum Gravity, 32(22), 224004.
- [3] Melo, B., Cuairan, M. T., et al. (2024). Nature

Nanotechnology, 19(9), 1270-1276.

- [4] Hofer, J., Gross, R., Higgins, G. et al. (2023). Physical Review Letters, 131(4).
- [5] Simon, M. D., Heflinger, L. O., & Geim, A. K. (2001). American Journal of Physics, 69(6).
- [6] Hebestreit, E., Frimmer, M., et al. (2018). Physical Review Letters, 121(6).
- [7] Monteiro, F., Ghosh, S., Fine, A. G., & Moore, D. C. (2017). Physical Review A, 96(6).





Lev Type	Ref	mass × freq (g · Hz)
Electrostatic	[2] [3]	0.63 5e-9
Magnetic	[4] [5] This work	1.3e-3 1.9 44
Optical	[6] [7]	4e-10 3e-6

Fig. 1. Magnetic levitation setup. Permanent magnets provide passive stabilization of the levitating mass along the y- and z-axes, which can be viewed as virtual springs that determine trap frequency when combined with the mass of the levitating magnet. Electromagnets actively control stability along the x-axis. The table shows that our system operates in a previously unexplored regime

behavior.

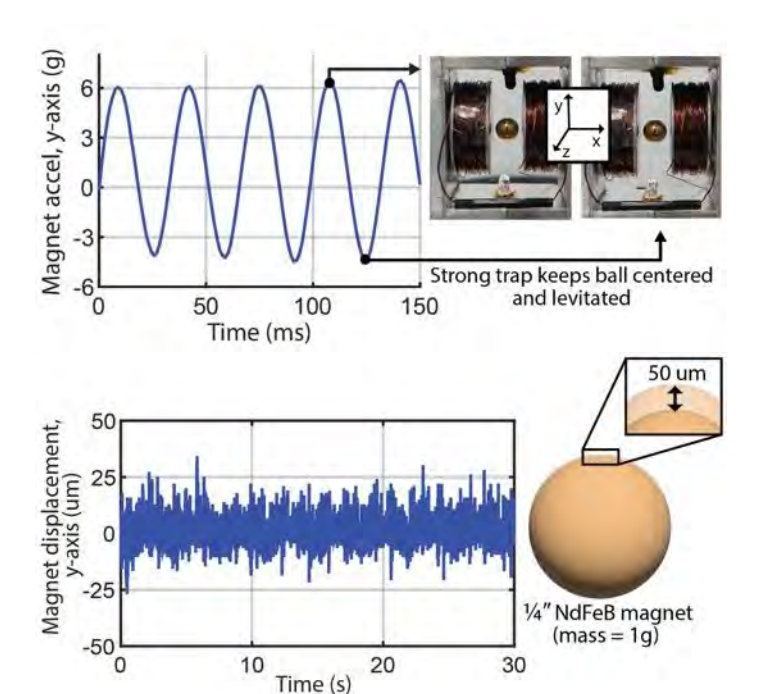


Fig. 2. (Top) Acceleration survival test measured on a shaker table (1 g = 9.81 m/s^2). The two images are frames extracted from a levitation video demonstration. (Bottom) Measured residual displacement (under no acceleration) of the levitated magnet using Keyence displacement sensor

SESSION DQ: MAGNETO-CALORIC, MAGNETOELECTRIC, AND **MULTIFERROIC MATERIALS AND DEVICES (POSTER** SESSION)

Chair(s): K. Srinivasan, *Electrical and Computer Engineering*, Boise State University, Boise, Idaho, United States Wednesday, October 29, 2025 02:30 PM-05:30 PM **Exhibit Hall Posters**

DQ-01. Structural, Magnetic, and Magnetocaloric Properties of Pseudo-binary (Er_{1-x}Yb_x)₂In

A. Kumar, A. Thayer, P. Singh, <u>A. Biswas</u>, Y. Mudryk Ames National Laboratory, Ames, Iowa, United States

Binary R2In compounds (where R is a rare-earth element) have recently attracted considerable interest due to their intriguing magnetic properties, including non-hysteretic first-order transitions and giant cryogenic magnetocaloric effects (MCE).1-6 While binary R2In systems have been extensively studied, 1-6 pseudobinary compounds of the general formula (R1-xRx')2In, where multiple rare-earth ions these systems is key to understanding the relationship between composition, phase stability, and magnetism. In this study, we focus on the pseudobinary series of rare earth intermetallics (Er1-xYbx)2In with x = 0, 0.5, 1.1.5, and 2. Using a newly developed structural descriptor symmetry induced lattice distortion 7 – we explain how Yb substitution drives a structural transformation from the hexagonal Ni2In-type structure (observed in Er2In) to the orthorhombic Co2Si-type structure at $x \ge 1.5$. No temperature-induced structural transitions are observed across the series. Er2In exhibits a paramagnetic-toferromagnetic transition at $T_c \approx 46$ K. Yb substitution introduces significant magnetic frustration, suppressing T_C and stabilizing a glassy magnetic state. Both Er2In and intermediate composition Er1.5Yb0.5In show large, reversible MCE near 46 K and 10 K, respectively. The magnetic field dependence of magnetic entropy change and specific heat studies further confirm the absence of longranged ordering in Yb-substituted samples, underscoring the critical influence of structural disorder on magnetic

(R, R') coexist, remain largely unexplored. Investigating

Acknowledgment: This work was performed at Ames National Laboratory and was supported by the Division of Materials Science and Engineering of the Office of Basic Energy Sciences, Office of Science of the U.S. Department of Energy (DOE). Ames National Laboratory is operated for the U.S. DOE by Iowa State University under Contract No. DE-AC02-07CH11358.

- 1. F. Guillou et al., Nature Communications 9, 2925 (2018).
- 2. A. Biswas et al., Physical Review B 101, 224402 (2020)
- 3. A. Biswas et al., ECS Journal of Solid State Science and Technology 11, 043005 (2022).
- 4. A. Biswas et al., Physical Review Materials 6, 114406 (2022).
- 5. W. Liu et al., Applied Physics Letters 119, 022408 (2021).
- 6. W. Cui et al., Journal of Materials Science & Technology 101, 80 (2022).
- 7. P. Singh et al, arXiv:2503.03120 (2025).

263

DQ-02. The Effect of Ti Addition on the Magnetic and Magnetocaloric Properties of Drop-casted Ni₂Mn_{0.55}Cu_{0.35}Fe_{0.10}Ga Heusler alloy

K. Schaeffer¹, H. A. Adedo¹, J. R. DeFeo², V. Yenugonda², A. Lamichhane¹, A. Pathak², M. Khan¹

¹Physics, Miami University, Oxford, Ohio, United States, ²SUNY Buffalo State University, Buffalo, New York, United States

The Cu doped intermetallic system Ni₂Mn_{1-x}Cu_xGa is a derivative of the Ni₂MnGa Heusler alloy that exhibits a first order martensitic phase transition near 200 K in a ferromagnetic state. The martensitic and ferromagnetic phase transition temperatures in this system can be precisely controlled by Cu doping. For $x \approx 0.25$, a completely coupled martensitic and ferromagnetic transition occurs at $T_M = T_C^A \approx 310 \text{ K}$. A large entropy changes of - 64 J/Kg K have been reported to accompany the transition [1]. $Ni_2Mn_{0.55}Cu_{0.35}Fe_{0.10}Ga$ is a Fe doped derivative of Ni_2Mn_{1-} _xCu_xGa where the second order ferromagnetic transition occurs in the martensitic state and first order martensitic transition occurs in a paramagnetic state. The separation between the two transitions is 30 K while heating and 21 K during cooling. One of the drawbacks of Ni₂Mn_{1-x}Cu_xGa and its derivatives is that they are inherently brittle and suffers from crystalline instability over multiple thermal cycles [2]. In this study, we introduced 1wt% and 2wt% of Titanium (Ti) to Ni₂Mn_{0.55}Cu_{0.35}Fe_{0.10}Ga. The addition was intended for the Ti atoms to occupy the interstices between the host atoms in the lattice without changing the alloy stoichiometry. The XRD measurements indicate that the samples exhibit cubic structures at room temperature. The Ti addition significantly improved the crystalline stability while also effecting the phase transition temperatures. Both Ti added Ni₂Mn_{0.55}Cu_{0.35}Fe_{0.10}Ga samples exhibited the first order coupled magnetostructural phase transition near room temperature. The transitions were accompanied by a large peak entropy change of - 46.5 J/kg K. The results will be presented and discussed in details in this presentation.

The work at State University of New York (SUNY), Buffalo State University, was supported by the National Science Foundation Award No. DMR-2213412.

[1] S. Stadler, M. Khan, J. Mitchell, and N. Ali, Appl. Phys. Lett. 88, 192511 (2006).

[2] H. Adedo, J. R. DeFeo, V. Yenugonda, S. Rahman, A. K. Pathak, and M. Khan, AIP Adv. 15, 3 (2025)

DQ-03. A study of martensitic phase transitions in the paramagnetic state in Fe doped $Ni_2Mn_{0.65-x}Cu_{0.35}Fe_xGa$ Heusler alloys prepared by drop-casting

<u>A. Lamichhane</u>¹, J. R. DeFeo², H. A. Adedo¹, V. Yenugonda², K. Schaeffer¹, A. Pathak², M. Khan¹

¹Physics, Miami University, Oxford, Ohio, United States, ²Physics, SUNY Buffalo State University, Buffalo, New York, United States

The Heusler alloy Ni₂MnGa and many of its' stoichiometrically altered derivatives exhibit the first order martensitic phase transition in a ferromagnetic state. The magnetocaloric effect is one of the numerous functional properties, which is associated with this phase transition. The orbital hybridization and localized Mn moments influence the martensitic and ferromagnetic transitions in these Heusler alloys, which can be tuned via stoichiometric manipulation and doping [1, 2]. When Mn is partially replaced by Fe in Ni₂Mn_{1-x}Fe_xGa, martensitic transition (T_M) decreases while ferromagnetic transition (TA_C) increases with increasing Fe [1]. While in the Cu doped Ni₂Mn_{1-x}Cu_xGa system T_M increases while T^A_C decreases with increasing Cu concentration and a completely coupled martensitic and ferromagnetic transition occurs at $T_M = T_C^A \approx 310 \text{ K}$ for $x \approx$ 0.25. A large entropy changes of - 64 J/Kg K have been reported to accompany the transition [2, 3, 4]. Here, we present a study on the phase transitions and magnetic properties of a series of drop casted Ni₂Mn_{0.65-x}Cu_{0.35}Fe_xGa Heusler alloys (x \leq 0.05 \leq 0.25). X-ray diffraction, dc magnetization, electrical resistivity, and scanning electron microscopy (SEM) measurements were conducted on the samples. All samples exhibited the tetragonal phase at room temperature, and the phase singularity was confirmed via backscattered electron SEM. The temperature dependence of magnetization and electrical resistivity data revealed completely decoupled second order magnetic phase transition and first order structural phase transition across all samples with the martensitic transition occurring in the paramagnetic state. The temperature dependence of the magnetic entropy changes was in agreement with the other experimental data. In this presentation, the experimental results will be presented and discussed in details.

The work at State University of New York (SUNY), Buffalo State University, was supported by the National Science Foundation Award No. DMR-2213412.

[1] D. Kikuchi, T. Kanomata, Y. Yamaguchi, H. Nishihara, K. Koyama, and K. Watanabe, J. Alloys Compd. 383, 184 (2004).

[2] M. Belesi, L. Giebeler, C. G. F. Blum, U. K. Rössler, B. Büchner, and S. Wurmehl, Phys. Rev. B 91, 134415 (2015).
[3] S. K. Sarkar, P. D. Babu, A. Biswas, V. Siruguri, M. Krishnan, et al., J. Alloys Compd. 670, 281 (2016).
[4] D. Zhao, T. Castán, A. Planes, Z. Li, W. Sun, and J. Liu, Phys. Rev. B 96, 224105 (2017).
[5] S. A. Agbo, S. Bhatt, and M. Khan, Intermetallics 138, 107322 (2021).

DQ-04. Magnetocaloric Effect in PrNi_{2-x}Co_x Alloys: Simulation and Experimental Approaches

R. Duarte de Melo, C. L. Rodrigues, A. Gomes Instituto de Física, Universidade Federal do Rio de Janeiro, Rio de Janeiro, Rio de Janeiro, Brazil

The magnetocaloric effect (MCE) has attracted significant attention due to its potential applications in magnetic refrigeration technology [1]. Binary and pseudobinary compounds, such as RTm₂ and R_xR'_{1-x}Tm₂ (where Tm represents transition metals, Al, or B, and R and R' are rare earth elements), have emerged as promising candidates, exhibiting a wide range of MCE values [2,3]. Previous studies [4] have investigated the substitution of Ni for Co in PrNi₂ alloys as a strategy to enhance magnetism in an otherwise paramagnetic material. The PrNi_{2-x}Co_x series demonstrated that it is possible to induce magnetic ordering in this paramagnetic system and to increase the Curie temperature (Tc). These alloys exhibit a notably broad Tc range, which is particularly relevant for applications such as hydrogen liquefaction.

In this study, we investigate the magnetocaloric properties of the $PrNi_{2-x}Co_x$ series, aiming to amplify the MCE and explore the advantages of its wide operating temperature range. Using computational methods, we developed a mean-field Hamiltonian to describe the magnetic system, calculated eigenvalues and eigenstates for the partition function, and derived magnetic isotherms, Gibbs free energy, and magnetic entropy change under applied magnetic fields. The self-consistent algorithm provided valuable predictions of Tc values. To validate our computational approach, we synthesized selected samples with x = 0, 1.2, and 2, and compared the experimental results with the simulations.

[1] Gschneidner Jr.et al. Recent Developments in Magnetic Refrigeration. Materials Science Forum, 315-317, 69–76 (1999).

[2]Alho, B. P. et al. Magnetic and magnetocaloric properties in Gd 1-y Pr y Ni 2 compounds. Journal of Magnetism and Magnetic Materials, 449, 308-312. (2018)

[3] Ribeiro, P. O. et al. Theoretical investigations on the magnetocaloric and barocaloric effects in TbyGd(1-y)Al2 series. Journal of Alloys and Compounds, 563, 242-248 (2013).

[4] Ermolenko, A. S. et al. Compositional genesis of ferromagnetism in alloys PrNi2–Co. Journal of Magnetism and Magnetic Materials, 490, 165489 (2019).

DQ-05. Colloidal Synthesis and Size-Dependent Magnetic Properties of Discrete MnNiSb Nanoparticles for Thermomagnetic Waste Heat Recovery

<u>F. Amoo</u>², S. Brock², J. Sklenar¹, V. Ostapyuk², T. Jeffrey¹

¹Physics and Astronomy, Wayne State University, Detroit,
Michigan, United States, ²Chemistry, Wayne State University,
Detroit, Michigan, United States

Bulk MnNiSb is a ferromagnetic compound with a large magnetocaloric effect and a high Curie temperature (754K), which may be useful in converting low and medium-grade waste heat to electricity. While the bulk properties of MnNiSb have been established, the effect of size on critical factors that underscore the efficiency of the magnetic heat recovery process, including thermal hysteresis, Curie temperature, and magnetic entropy, is unknown. In the present work, a solution phase methodology was developed for the formation of discrete colloidal MnNiSb nanoparticles using dimanganesedecacarbonyl, bis(1,5cyclooctadiene)nickel(0), and triphenylantimony as the main reaction components, and reacting at 230 °C. The resultant MnNiSb nanoparticles, as evidenced by both powder X-ray diffraction and transmission electron microscopy, exhibit the cubic well-ordered half-heusler phase, characterized by the existence of (111) and (200) reflections, a diameter of approximately 10 nm, and low polydispersity. The assynthesized MnNiSb nanoparticles are ferromagnetic at room and high temperatures, with a Curie temperature of 850 K. Current efforts are focused on performing hightemperature, field-dependent magnetization measurements to verify whether the Curie temperature is indeed ~850 K and to confirm the nature of the observed transition. Future studies will investigate the effect of particle size on magnetic entropy changes to gain a deeper understanding of how nanoscale dimensions affect magnetocaloric

performance parameters, including the magnitude of entropy change, transition sharpness, and hysteresis behavior—all factors that are critical for applications in thermomagnetic heat recovery.

DQ-06. Topological Magnetic Texture Stabilization in ϵ -Fe₂O₃ Thin Films

<u>D. DeTellem</u>, S. Witanachchi, M. Phan Department of Physics, University of South Florida, Tampa, Florida, United States

Multiferroic materials, which exhibit both ferroelectric and magnetic ordering, offer the potential to combine the fast, energy-efficient switching of electric fields with the nonvolatile data storage capabilities of magnetic systems [1]. Such a combination could not only enhance the energy efficiency and robustness of current memory technologies but also enable the development of novel device components for advanced computing. However, no known material yet satisfies all the stringent requirements necessary to fully realize this potential. Within this context, magnetic vortices and antivortices represent intriguing topological magnetic states that have been proposed for various functional applications [2,3]. Antivortices, in particular, present a unique challenge due to the difficulty of stabilizing them, which has limited experimental progress. The stabilization of such topological features within a multiferroic system would be of significant interest, both fundamentally and technologically [3]. One promising candidate is ε-Fe₂O₃, a multiferroic material that exhibits both magnetism and ferroelectricity well above room temperature. In this study, we grew thin films of ε-Fe₂O₃ under various growth conditions and carried out a comprehensive structural, magnetic, and ferroelectric characterization using a suite of techniques, including atomic force microscopy (AFM), magnetic force microscopy (MFM), piezoresponse force microscopy (PFM), in-plane and out-of-plane X-ray diffraction (XRD), and vibrating sample magnetometry (VSM). Using extensive micromagnetic simulations, we developed a model to explain the magnetic domain behavior observed in films grown on substrates such as SrTiO₃ (STO), which promote triaxial crystallite domain growth. Our results demonstrate a clear dependence of domain size and coercivity on grain size and the magnetic anisotropy constant. This correlation provides a framework for interpreting the experimentally observed MFM images. Notably, our simulations reveal the presence of topological magnetic states in piezo force microscopy thin films - the

first experimental evidence of such states in this material and we identify these features in the MFM data.

- [1] Khan, et al., The future of ferroelectric field-effect transistor technology, *Nature Electronics* 3, 588 (2020) [2] Drews, et al., Current- and field-driven magnetic antivortices for nonvolatile data storage, *Appllied Physics*
- [3] Xue, et al., Stable antivortices in multiferroic ε -Fe₂O₃ with the coalescence of misaligned grains, *Nature Communications* 16, 440 (2025)

Letters 94, 062504 (2009)

DQ-07. Assembly of Magnetic Tunnel Junctions with Chiral Nanographenes

<u>C. Fang</u>, W. Niu, J. Deka, S. Parkin Max Planck Institute of Microstructure Physics, Halle (Saale), Sachsen-Anhalt, Germany

Chirality-Induced Spin Selectivity (CISS) is an emergent phenomenon whereby chiral molecules act as efficient spin filters, selectively transmitting electrons of a particular spin orientation. This quantum mechanical coupling between molecular geometry and spin introduces new opportunities for spintronic device engineering, especially for materials that operate efficiently under ambient conditions. A central challenge in advancing CISS-based spintronics lies in experimentally verifying spin filtering in structurally defined, laterally extended molecular systems, using standard solid-state device techniques that yield reproducible and robust spin-dependent transport signals under ambient conditions to demonstrate the potential applications in spintronics.

Here, we present direct experimental evidence of the CISS effect in helical nanographenes (NGs), using magnetoresistance (MR) measurements in magnetic tunnel junctions. The device architecture included a bottom electrode CoFeB (4 nm)/MgO (2.5 nm) ferromagnetic contact, orthogonally patterned and electrically isolated by an AlOx layer to confine current to the junctions. NG, a synthetically tailored chiral molecule, was spin-coated to form a thin, uniform layer serving as a spin-filter interface. Different from previous works, the ferromagnet layer grown directly on the substrate offers a better performance of the magnetic properties. Both enantiomeric devices showed MR values around 1 % at room temperature, with minimal variation over the 10–400 K temperature range, indicating robust and reproducible spin selectivity.

Our findings establish laterally extended chiral

nanographenes as effective, thermally stable spin filters and validate CISS as a viable spintronic mechanism at room temperature with set ferromagnet electrode at the bottom. These results represent a demonstration of CISS in $\pi\text{-}$ conjugated carbon-based materials and confirm the viability of using molecular chirality as an effective mechanism for spin control in solid-state systems.

[1] B. Bloom et al. Chem. Rev. 124(4), 2014
[2] S. Ham et al. Micromachines 15(4), 528, 2024
[3] S. Yang et al., Nat. Rev. Phys. 3, 328, 2021
[4] W. Niu et al. Angew. Chem. Int. Ed. 63, e202319874, 2024

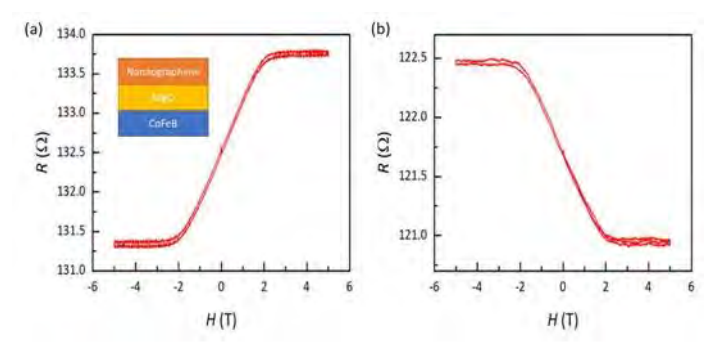


Fig. 1 Magnetoresistance of the magnetic tunnel junctions with NG with opposite chirality. Inset shows the device structure.

DQ-08. Magnetic and Transport Properties of ordered LaSrMnRuO₆ double perovskite thin Films

A. Kumar^{1, 2}, D. Palai³, D. Samal³, P. Santhosh^{1, 2}
¹Department of physics, IIT Madras, Chennai, Tamilnadu, India, ²Functional oxide Research Group, IIT Madras, Chennai, Tamilnadu, India, ³Department of physics, Indian Institute of Physics, Bhubaneswar, Odisha, India

Bulk LaSrMnRuO $_6$ (LSMRO) double perovskites has an orthorhombic structure with a *Pnma* space group and Mn/Ru disorder at the B-site [1]. XPS measurement reveals mixed valency of Mn (+2, +3) and Ru (+4, +5) in the system. M-T measurement on bulk sample shows that ZFC curve displays two transitions in 100 Oe field at ~223 K, followed by a cluster glass transition at ~32 K. Also, at 5 K, the magnetic moment lacks saturation at 70 kOe field, which is less than theoretically predicted value of B-site ordered sample i.e for Mn $^{3+}$ and Ru $^{4+}$ [2]. Therefore, the ordered double perovskites are considered to be better for improving magnetic and transport properties such as Curie temperature and

magnetization, etc [3]. In this work, we have fabricated epitaxial LSMRO thin films STO (111) substrate using the pulsed laser deposition technique. We observed the (111) and (333) superlattice peaks at ~19 and ~61 angle in the xray pattern of the film, respectively, for various thicknesses [Fig.1], which indicates B-site ordering. From the XRR data fit, the average roughness is 0.9, 1.09 nm, corresponding to 32.4 nm and 66.4 nm thin films, were found, respectively. RSM measurement around the (330) asymmetric plane confirms compressive strain in the thin films. From ZFC magnetic measurement, we observe transitions at ~207 K, followed by a peak at ~200 K for the 66.4 nm film, and ~197 K, followed by a peak at ~190 K for the 32.4 nm film [Fig.2]. There were no peaks observed corresponding to the cluster glass transition in bulk. Further, magnetic memory measurement at 20 K and 90 K halt temperature confirms the absence of any glassy transition. Also, at 5 K, an increase in magnetisation was observed in both thin films compared to bulk, which also confirms an increase in B-site ordering. Further, a thorough analysis of structural, magnetic, and transport properties will be presented [4].

1. P. M. Woodward, J. Goldberger, M. W. Stoltzfus, H. W. Eng, R. A. Ricciardo, P. N. Santhosh, and P. Karen, J. Am. Cerum. Soc. 96 (6), 1796 (2008).

2. Manuscript to be submitted

3. J. E. Kleibeuker, E. M. Khoi, E. D. Jones, T. M. Yu, B. Sala, B. A. MacLaren, D. Kepaptsoglou, D. H. Maldonado, Q. M. Ramasse, L. Jones, J. Barthel, I. MacLaren, and J. L. M. Driscoll, NPG Asia Material 9, 406 (2017).

4. Manuscript under preparation.

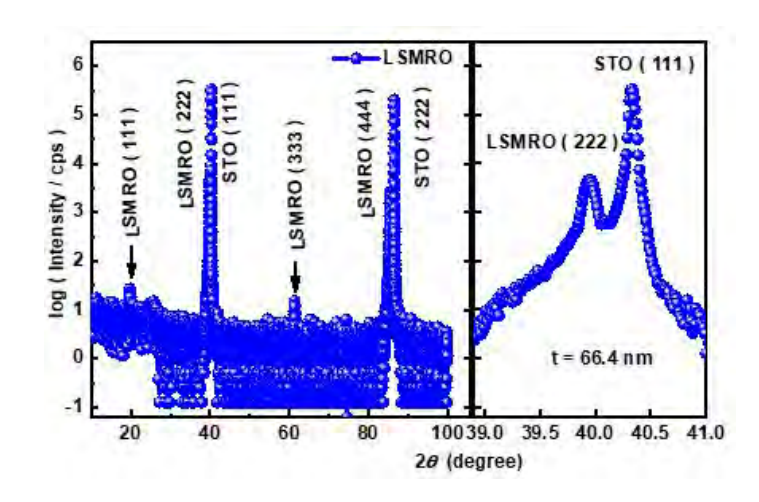


Fig. 1 XRD patterns of LSMRO thin film on STO (111) of 66.4 nm thickness

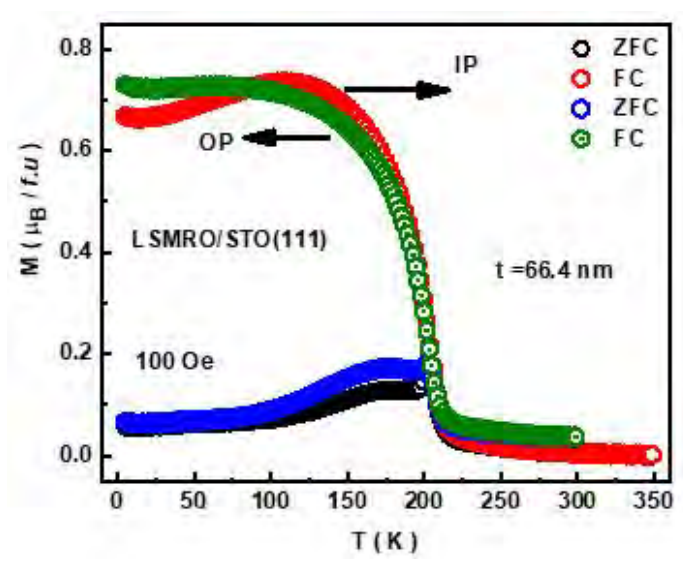


Fig. 2 Thermal variation of magnetization under ZFC and FC protocol in 100 Oe, 1000 Oe, and 10 kOe magnetic fields for 66.4nm film

DQ-09. Doped yttrium iron garnet magnetic nanoparticles with high Zn concentration for potential magneto-electric applications

R. Mohammed¹, V. Grynko^{1, 2}, J. Rado¹, A. Alexandrov¹, A. Hodgson¹, H. Chumak³, M. Popov³, V. Batarchuk^{1, 2}, A. Reznik¹, Y. Shepelytskyi^{1, 2}, M. S. Albert^{1, 2, 4}

¹Lakehead University, Thunder Bay, Ontario, Canada, ²Thunder Bay Regional Health Research Institute, Thunder Bay, Ontario, Canada, ³Taras Shevchenko National University of Kyiv, Kyiv, Ukraine, ⁴Northern Ontario School of Medicine, Thunder Bay, Ontario, Canada

Current- and photo-induced magnetoelectric effect (ME) enable power-efficient rapid tuning of microwave devices ¹⁻³. While yttrium iron garnet (YIG) is the most used magnetic material, its high resistivity limits effective induced ME harvesting ⁴⁻⁶. We conducted a comprehensive evaluation of high Zn^{2+} concentration effect on structural, electrical, and magnetic properties of nanocomposite YIG:Zn (Y₃Fe₅₋ $_xZn_xO_{12}$, x=0-1) to make it suitable for ME-based devices.

YIG:Zn samples were synthesized via sol-gel by dissolving stochiometric amount of yttrium, iron, and zinc nitrates in ethylene glycol with citric acid as a chelating agent. The obtained nanoparticles were pressed into pellets of ~3 mm thickness and annealed at 1000°C for 2h. YIG:Zn samples were characterized using X-ray diffraction (XRD), Raman spectroscopy, conductivity measurements, and magnetic

resonance measurements using vector network analyzer (VNA).

XRD and Raman spectra confirmed formation of YIG at [Zn²+]≤0.4. Doping beyond x=0.4 promoted yttrium iron perovskite phase, while samples with x≤0.3 retained mainly garnet structure. The blue shift in Raman peaks suggests Fe⁴+ creation in tetrahedral sites due Zn doping. Electrical conductivity increased up to three orders of magnitude compared to pure YIG, reaching 22.3mS/m for [Zn²+]of 0.4. This boost was attributed to electron hopping between Fe³+ and Fe⁴+ states in YIG:Zn. Ferromagnetic (FMR) and domain resonances were observed for YIG:Zn samples with [Zn²+]<0.6with external magnetic field normal to resonators' surface. The results showed a quasilinear rise in resonance frequency and a linear increase in FMR linewidth with [Zn] increase.

This work demonstrates the potential of heavily-doped YIG with Zn for future ME applications and offer insights into tailoring ferrite properties for next-gen ME devices.

- 1) Ramesh, R.; Spaldin, N. A. *Nanosci. Technol.* 2009, *6*, 20–28.
- 2) Shepelytskyi, Y.; Li, T. and Grynko, O, *Appl. Phys. Lett.* 2021, *119* (6), 062401.
- 3) Clin, M.; Rivera, J. P. and Schmid,
- H, Ferroelectrics 1990, 108 (1), 213-218.
- 4) Serga, A. A., Chumak, A. V. and Hillebrands, B. J. Phys. D. Appl. Phys. 2010, 43 (26), 264002.
- 5) Yang, X.; Gao, Y. and Wu, J, *IEEE Microw. Wirel. Components Lett.* 2014, *24* (3), 191–193.
- 6) Sun Y and Wu M. Solid State Phys. Adv. Res. Appl. 2013; 64: 157 91

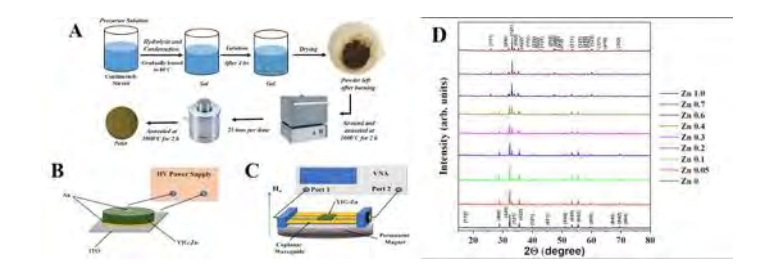


Fig.1 (A) Sol-gel synthesis of YIG:Zn samples. (B) Conductivity and (D) Magnetic resonance measurement setup. (D) XRD patterns of YIG:Zn nanoparticles.

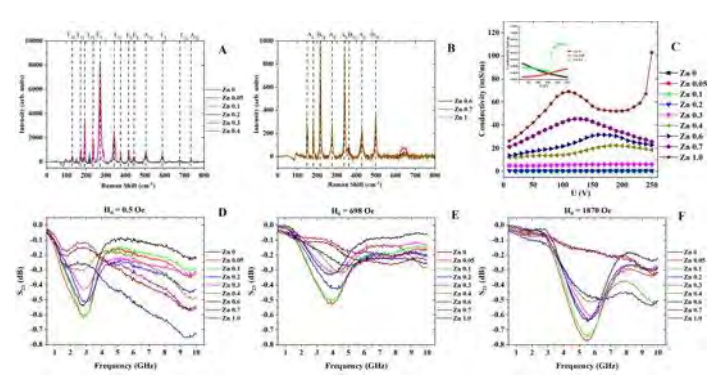


Fig. 2: Raman spectra of YIG:Zn with garnet (A) and perovskite (B) phases. (C) Conductivity curves of YIG:Zn under 0–250 V bias. Transmission coefficient vs. frequency for YIG:Zn resonators at magnetic fields of 0.5 Oe (D), 698 Oe (E), and 1870 Oe (F).

DQ-10. Experimental and computational study of nearly half-metallic $V_2\text{CoGa}$

P. Kharel², <u>C. Sadler</u>¹, C. Brown², M. Anas², P. Shand¹, P. Lukashev¹

¹Physics, University of Northern Iowa, Cedar Falls, Iowa, United States, ²Chemistry, Biochemistry and Physics, South Dakota State University, Brookings, South Dakota, United States

We present the results of a comprehensive computational and experimental study of electronic, magnetic, and structural properties of V2CoGa, a Heusler alloy that exhibits nearly half-metallic electronic structure in an ordered crystal structure. Our calculations indicate that this alloy crystallizes in inverted cubic structure. The magnetic alignment is ferrimagnetic, due to the anti-aligned magnetic moment of two vanadium sub-lattices. The calculated magnetization value is 1.97 $\mu_B/f.u$ at the equilibrium lattice constant of 5.898 Å. Our calculations indicate that V2CoGa retains its high spin polarization values of around 90% under mechanical pressure. At the same time, this material exhibits strong tendency toward A2-type atomic disorder, which has a strong detrimental effect on spin polarization values. Experimentally, arc-melted samples crystallize in the predicted inverted cubic structure with A2-type disorder. To optimize the crystal structure, the samples were annealed at various temperatures. The cubic phase is preserved up to 700 °C, while annealing above this temperature leads to phase separation. X-ray diffraction patterns, analyzed using Rietveld refinement for a cubic crystal structure (space group F-43m), yields a lattice parameter of 5.929 Å, consistent with theoretical predictions. Thermomagnetic

measurements reveal a magnetic transition near room temperature (295 K). Above the transition, the DC susceptibility follows Curie—Weiss behavior, with a calculated effective magnetic moment of 3.6 per formula unit. Given the detrimental effect of A2 disorder on spin polarization, minimizing this disorder is essential to realize the full potential of V2CoGa as a high-spin-polarization material.

This research is supported by the *National Science Foundation* (NSF) under Grant Numbers 2 The 003828 and 2003856via DMR and EPSCoR. Mohd Anas is supported by DOE EPSCoR (DE-SC0024284) grant.

SESSION DR: MAGNETORESISTANCE, SPIN TORQUE, AND SPIN INJECTION IN HETEROSTRUCTURES AND FILMS (POSTER SESSION)

Co-Chair(s): A. Chaurasiya, *Physics, University of Gothenburg, Gothenburg, Sweden* and G. Yu, *Institute of Physics, Chinese Academy of Sciences, Beijing, China* and Dong-Jun Kim, *KAIST, Daejeon, Korea (the Republic of)*Wednesday, October 29, 2025
02:30 PM-05:30 PM
Exhibit Hall Posters

DR-01. Magnetization switching by a laser induced thermocurrent in a GdFeCo/Pt hetero-structure film

<u>S. Sumi</u>¹, M. Mohammadi¹, K. Tanabe¹, H. Awano¹, Y. Nakatani²

¹Toyota Technological Institute, Nagoya, Japan, ²University of Electro-Communications, Tokyo, Japan

A magnetic wire is one of the attractive candidates for high capacity memories and logic devices with low power consumption [1]. We reported that the wire of rare-earth transition metal (RE-TM) amorphous alloy show a current induced domain wall motion (CIDWM) with a faster wall speed of more than 1000 m/sec and a current induced magnetization switching (CIMS) with a lower current density of 5.5 MA/cm² [2, 3]. However, the domain creation method in the wire is one of the key technologies for their applications. It was known that a laser irradiation generated a large thermo-electronic motive force [4, 5]. In this paper, we demonstrate a magnetization switching by a laser induced thermo-current (laser induced CIMS) in a GdFeCo/Pt hetero-structure film.

The film of SiN 10 nm/Pt 5 nm/GdFeCo 10 nm/SiN 10 nm was fabricated on a thermally oxidized silicon substrate using a sputtering system. The film showed a perpendicular anisotropy. Figure 1 shows experimental setup for the laser induced CIMS. The GdFeCo/Pt hetero-structure film was irradiated by a 3.6 mW laser spot of 1 μ m diameter under applying with an in-plane field. The laser induced CIMS was observed using a MOKE microscope.

Figure 2 shows a MOKE image of the laser induced CIMS. A laser spot was scanned across a domain wall along the left hand direction with a field of -1, +1 and zero KOe (see red arrows). Under -1 and +1 KOe, the magnetization switching was occurred only in a down spin aria (white region) and an up spin aria (black region), respectively. On the other hand, under zero KOe, there were no changes. The results show that the laser induced CIMS may be caused by localized current which was generated by the laser irradiation[4]. We demonstrated the magnetization switching by a laser induced thermo-current in a GdFeCo/Pt hetero-structure film. The method can create a CIMS domain by laser. The laser induced CIMS is one of the attractive methods to create the domains in the magnetic wire.

This research was supported by KAKENHI (No. 25K01273), Japan.

- [1] S. S. P. Parkin et al., Science 320, 190 (2008).
- [2] D. Ngo et al., APEX Vol. 4, No. 9, 093002(2011).
- [3] K. Asari et al., AIP Advances 7, 055930 (2017).
- [4] T. Suzuki, et al., Joint MMM-Intermag2019 FK-06 (2019).
- [5] S. Isogami, et al., Acta Mat. 286, 120734 (2025).

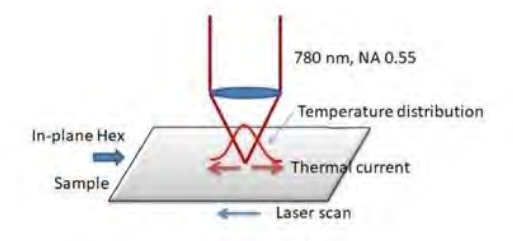


Fig. 1 Experimental setup for magnetization switching by a laser induced thermo-current.

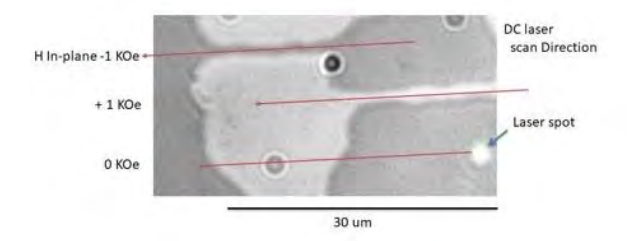


Fig. 2 Polarized microscope image of magnetization switching by a laser induced thermo-current.

DR-02. NIST SP 800-90B Compliant Perpendicular Magnetic Tunnel Junction Based True Random Number Generator O. Jia¹, S. Egan², Y. Lv¹, J. Wang¹

¹Univerisity of Minnesota, Minneapolis, Minnesota, United States, ²Deep Science Ventures, London, United Kingdom

True random number generators (TRNGs) are essential for applications such as hardware security and cryptographic protocols. Stabilized spin-transfer torque-perpendicular magnetic tunnel junctions (STT-pMTJs) have emerged as a promising candidate for TRNGs due to their rapid switching speed and low energy consumption. The switching speed could be controlled by the voltage amplitude, enabling high-quality bit generation with adjustable frequency. In previous studies, the quality of the generated bits is evaluated by NIST 800-22 standards, which are now considered outdated and insufficient for modern cryptographic requirements. In this work, we demonstrate a pMTJ-based TRNG with a low resistance-area (RA) product of 3.5 Ω µm² and tunnel magnetoresistance (TMR) ratio of 105%. The magnetization switching occurs in 2.70 ns with a probability of 50% at a current density of 3.38×10⁷ A/cm². The generated bits achieve NIST SP 800-90B compliance with only a single XOR whitening step.

- [1] I. T. L. Computer Security Division, "Decision to Revise NIST SP 800-22 Rev. 1a | CSRC," CSRC | NIST. Accessed: May 22, 2025. [Online].
- [2] M. Sönmez Turan, et al. "Recommendation for the Entropy Sources Used for Random Bit Generation," National Institute of Standards and Technology, NIST Special Publication (SP) 800-90B, Jan. 2018.

^{*} Best Student Presentation Finalist / LB – Late-breaking Poster

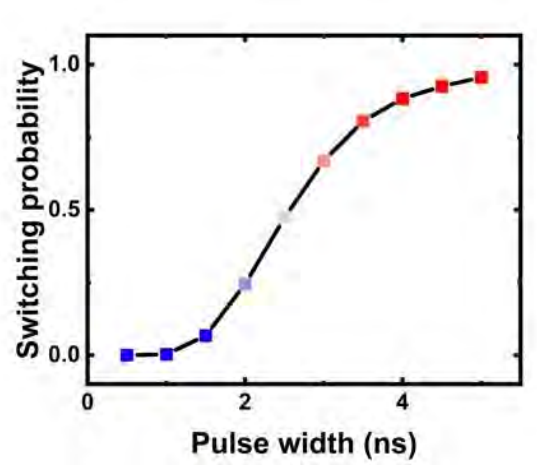


Fig. 1. Switching probability vs. perturbation pulse width of the pMTJ under a fixed voltage of 1.19V. The test is performed at room temperature.

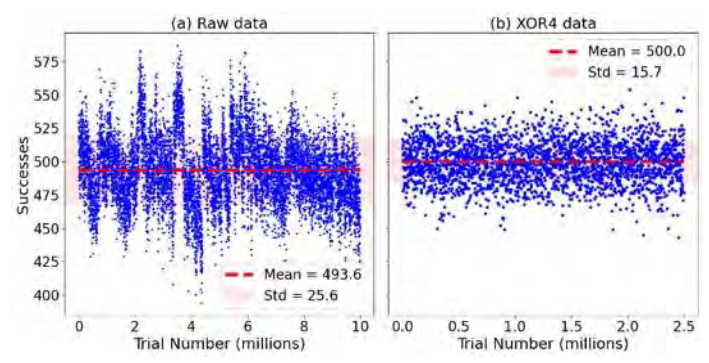


Fig. 2. (a) Number of successful switching attempts over 1000 trials for sequential samples of the raw bitstream. Visible clustering indicates that p is not constant for each set of switching attempts. (b) Number of 1's over 1000 values of the XOR4 bitstream.

DR-03. Influence of In-Plane Geometry design on Spin Transport in NiFe Thin Films

D. Han, J. Lee, K. Son

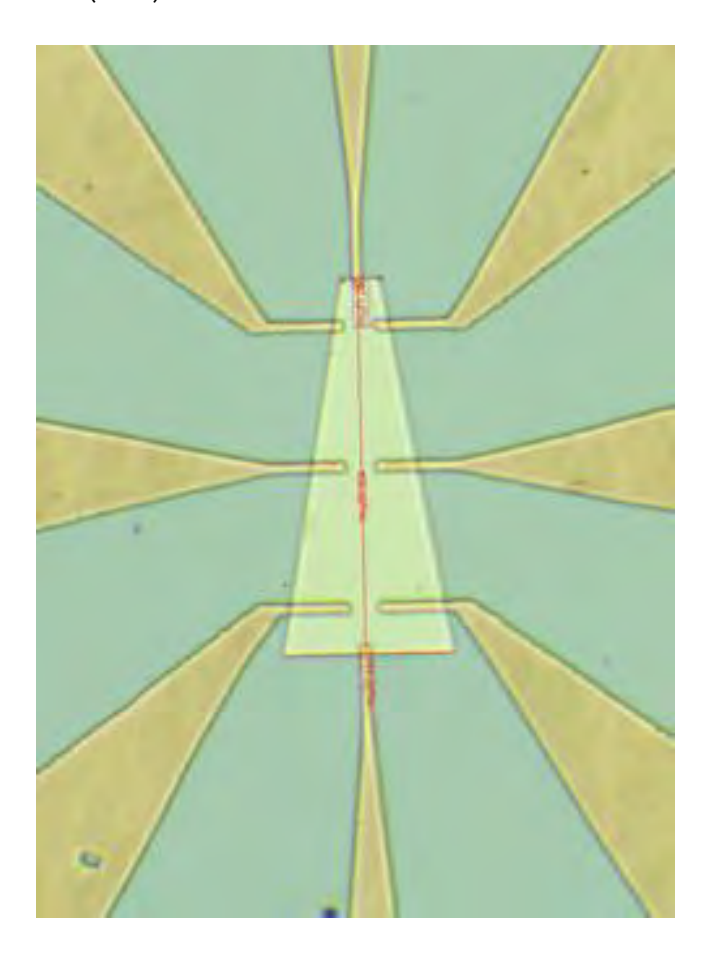
Physics education, Kongju National University, Gongju, Korea (the Republic of)

Field-free magnetization switching is a key step toward the development of energy-efficient spintronic devices. Achieving deterministic magnetization reversal without external magnetic fields requires breaking both the mirror symmetry with respect to the current direction and the symmetry of the magnetic anisotropy. Introducing asymmetry in the in-plane geometry of ferromagnetic layers presents a promising route to induce deterministic in-plane

switching. Such shape-induced asymmetry not only alters the magnetization energy landscape but also affects the local current distribution in the ferromagnetic layer. In this study, we examine how the in-plane geometrical design of NiFe thin films influences their spin transport mechanisms, emphasizing the interplay between macroscopic geometric anisotropy and spin-dependent transport phenomena. Angular-dependent AMR and PHE measurements revealed distinct easy and hard axes for each geometry, accompanied by notable asymmetry and nonlinearity in the responses. These trends were consistently observed in magneto-optical Kerr effect (MOKE) measurements. Also, harmonic Hall measurements in NiFe/ Ta bilayer structures exhibit geometry-dependent spin-orbit torque behavior.

These findings demonstrate the effectiveness of geometric engineering in tuning magnetic anisotropy and transport behavior, and offer insights for realizing deterministic inplane magnetization reversal in field-free spin-orbit torque devices.

Yu, G., Upadhyaya, P., Fan, Y. et al. Nature Nanotech 9, 548–554 (2014)



DR-04. Electrical detection of a minimal spin accumulation in silicon

Y. Koshino¹, M. Goto³, R. Ohshima², M. Shiraishi², Y. Ando¹ ¹Osaka Metropolitan University, Osaka, Japan, ²Kyoto University, Kyoto, Japan, ³Tokyo University of Science, Tokyo, Japan

We have demonstrated room-temperature operation of silicon (Si)-based spin MOSFETs [1] and spin logic devices [2], using ferromagnetic tunnel contacts. These contacts hold potential not only for logic devices but also for quantum computing devices, particularly in Si quantum dots, which can maintain quantum entanglement at relatively high temperatures and are compatible with CMOS technology. However, current spin readout schemes in Si quantum devices require cryogenic temperatures below 1 K due to the small Zeeman energy (tens of µeV), which is vulnerable to thermal disturbance. In contrast, ferromagnetic tunnel contacts especially those consisting of half-metallic materials can provide energy splitting of several hundred meV for the minority spins, offering potential for highertemperature spin detection. A key challenge remains in sensitivity in spin detection, as the number of spins involved in quantum devices is orders of magnitude smaller than in conventional spintronic devices.

In this study, we evaluated the detection limit of spin accumulation voltage using a three terminal Hanle measurement. This method applies current between two ferromagnetic tunnel contacts while measuring voltage at the spin extraction side. It improves signal to noise ratio by avoiding magnetization reversal and suppressing noise, which mainly generated at the contact under spin injection. Measurements were carried out at 30 K, because carrier freeze-out occurs in Si below 10 K. Hanle signals were clearly observed for injection currents down to 1 µA. Given the electrode area of 21 µm × 0.3 µm, the current density at 1 μ A is 1.6 × 10⁵ A/m². Assuming scaling to a 50-nm-square electrode, slightly larger than a typical Si quantum dot, this corresponds to a spin transport current of ~0.4 nA, which is within the tolerable range for Si quantum dot operation. These results suggest that ferromagnetic tunnel contacts are promising candidates for spin detection in Si quantum dots under practical conditions.

[1] T. Tahara et al., Appl. Phys. Express. 8, 113004(2015),

[2] R. Ishihara et al., Phys. Rev. Appl. 13, 044010(2020),

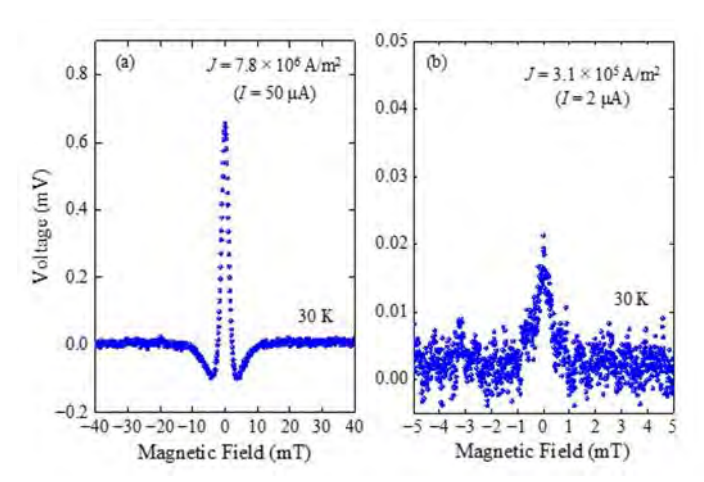


Figure 1 Difference in the three-terminal Hanle signal between antiparallel and parallel configurations measured at 30K. Injection current is (a) 50 µA and (b) 2 µA, respectively.

DR-05. Electrochemical Deposition Optimization of Fe-Co-**B/Ta Magnetic Multilayers for Spintronics**

A. S. Poulo, T. Lamichhane, J. A. Torres, M. Goodman, L. Cosgrove, J. Le Chin, H. Kluck Graham Engineering and Physics, University of Central Oklahoma, Oklahoma City, Oklahoma, United States

Fe1-xCoxB is a versatile spintronics medium with high thermal stability and diverse magnetic properties such as high-magnetization, high-permeability, low coercivity and tunable magnetization direction. It is coupled with several metal and nonmetal oxides to form spintronics plate forms required for diverse technological applications. In this study we will present the structural and magnetic properties of electrochemically deposited Fe1-xCoxB thin film and its magnetic multilayer Fe1-xCoxB/Ta on Si-(100) wafers. We will utilize the concept of design of experiment (DOE) to optimize the input parameters for the targeted film thickness and investigate their correlation with microstructure and magnetic properties.

- 1. Sheng, Z., Development of Magnetostrictive Fe-Co-B Alloys for High-Frequency Sensors and Magnetoelectric Composites. 2015, Auburn University: United States --Alabama. p. 304.
- 2. Belashchenko, K.D., et al., Origin of the spin reorientation transitions in (Fe1-xCox)2B alloys. Applied Physics Letters, 2015. 106(6).
- 3. Vieyra, M., T. Meydan, and F. Borza, X-ray diffraction

analysis and magnetic behavior of amorphous Fe15Co17Ni58B10 nanowires obtained by electrochemical deposition. Journal of Applied Physics, 2007. 101(9).

DR-06. Solid-phase epitaxy of $Co_2Fe_{0.4}Mn_{0.6}Si$ full-Heusleralloy thin films utilizing (001)-textured MgO barrier

K. Watanabe¹, T. Nakano^{1,2}, M. Oogane^{1,3}
¹Department of Applied Physics, Graduate School of
Engineering, Tohoku University, Sendai, Japan, ²Research
Center for Green X-Tech, Green Goals Initiative, Tohoku
University, Sendai, Japan, ³Center for Science and Innovation in
Spintronics, Tohoku University, Sendai, Japan

Co-based full-Heusler alloys, such as $Co_2(Fe,Mn)Si$ (CFMS), are promising spintronic materials due to their predicted half-metallicity and coherent tunneling compatibility with MgO barriers, as demonstrated by TMR ratios over 400% at room temperature in fully epitaxial CFMS/MgO/CFMS MTJs [1]. While most studies have focused on single-crystalline MTJs, we aim to fabricate (001)-textured CFMS thin films on Si/SiO_2 substrates using a solid-phase epitaxy approach for practical applications. Inspired by the crystallization process in CoFeB/MgO systems [2], we have applied a similar method to CFMS/MgO and investigated the crystalline structures and magnetic properties at various annealing temperatures.

All samples were prepared by ultra-high vacuum DC magnetron sputtering. The film stack is: Si/SiO_2 subs./TaB (5)/ $Co_2Fe_{0.4}Mn_{0.6}Si$ (15)/MgO (1.8)/Ta (5) (in nm). Post-deposition annealing was performed at 300-500 °C under a 1 T magnetic field in an annealing furnace. Its crystalline structure and magnetic properties were characterized by x-ray diffractometer (XRD) and vibrating sample magnetometer, respectively.

Figure 1 shows out-of-plane XRD patterns of the asdeposited and 500 °C-annealed films. The as-deposited film shows no crystalline peaks, while a B2 (002) peak appears after 500 °C annealing. Figure 2 shows magnetization curves of the films. The saturation magnetization significantly increased from 444 emu/cm³ to 975 emu/cm³ upon annealing, where the latter is close to the bulk value [3]. These results suggest the solid-phase epitaxy of the CFMS films from amorphous to (001)-texture thanks to the (001)-textured MgO template. The developed thin-film fabrication technique for highly ordered Heusler alloys using solid-phase epitaxy is a promising method for easily fabricating MTJs with high TMR.

This work was supported by SIP project, BRIDGE project,

SCOPE project, NEDO leading project, CSIS, CIES, the AIE-WISE Program, and MEXT Initiative to Establish Next-generation Novel Integrated Circuits Centers (X-nics) Grant Number JPJ011438.

[1] H. Liu *et al.*, J. Phys. D: Appl. Phys. 48, 164001 (2015)[2] D. D. Djayaprawira *et al.*, Appl. Phys. Lett. 86, 092502 (2005)

[3] T. Kubota *et al.*, Materials Transactions, 57, No. 6, 773-776 (2016)

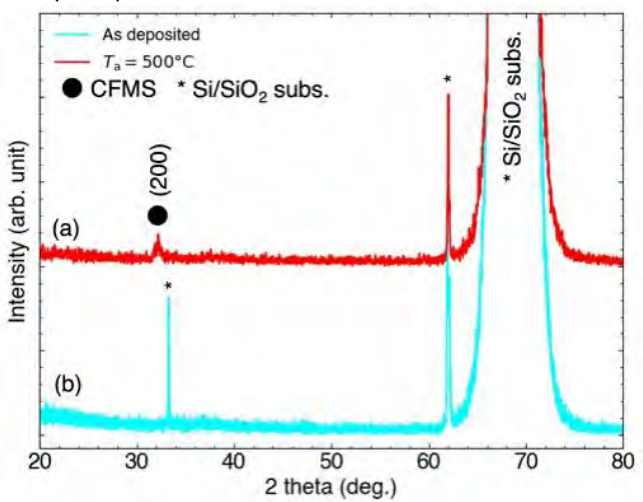


Figure 1. Out-of-plane XRD patterns of (a) 500 °C-annealed and (b) as-deposited CFMS/MgO films.

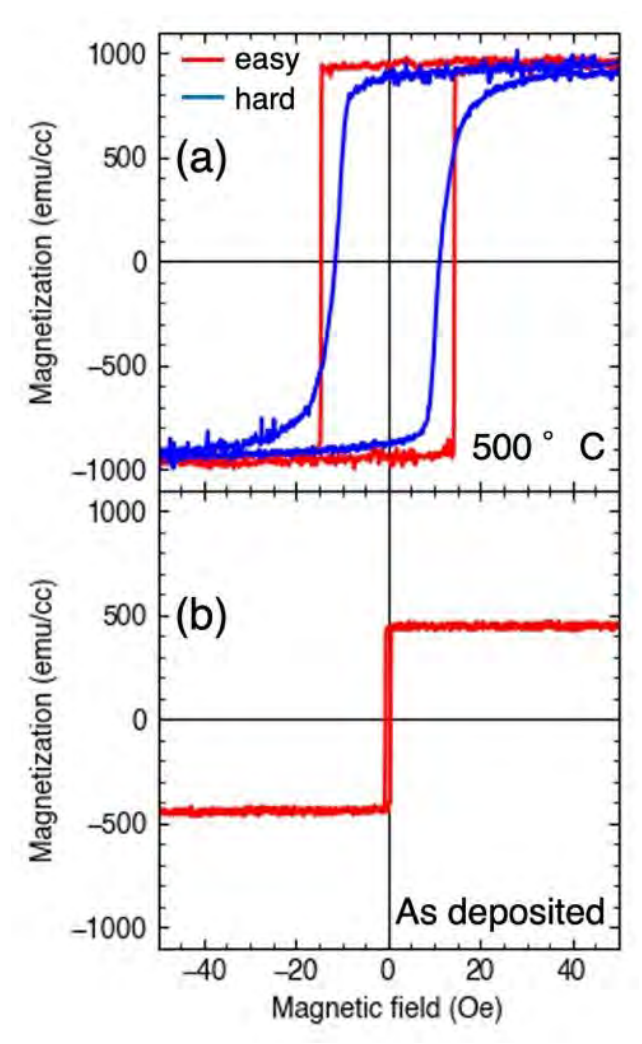


Figure 2. Magnetization curves of (a) 500 °C-annealed and (b) as-deposited CFMS/MgO films.

DR-07. Fabrication of Fcc(111)-Oriented MTJs on Bcc(110)-Oriented FeAlSi Films for TMR Sensors Application

D. Amiie¹, T. Hojo¹, M. Oogane^{1, 2}

¹Graduate school of Engineering, Tohoku Univ., Sendai-shi, Miyagi-ken, Japan, ²Tohoku Univ. CSIS, Sendai-shi, Miyagi-ken, Japan

Magnetic tunnel junction (MTJ)-based tunnel magnetoresistance (TMR) sensors enable high-sensitivity magnetic field detection and are expected to realize applications in the medical field. However, the sensitivity of current TMR sensors remains insufficient for practical use to detect weak bio-magnetic field. Recently, it has been suggested that MTJs with fcc(111)-orientation can significantly improve sensitivity of TMR sensors [1]. In this study, we fabricated fcc(111)-oriented MTJs on bcc(110)oriented FeAlSi epitaxial thin films to obtain both high TMR because of fcc(111)-orientation and low magnetic anisotropy due to soft magnetic properties of FeAlSi. The multilayer films were deposited using an ultrahigh vacuum sputtering system capable of fabricating highquality multilayer structures. A schematic of the fabricated structure is shown in Fig. 1. The multilayers were subsequently patterned via photolithography and evaluated using a two-terminal DC measurement method. Figure 2 shows the magnetoresistance curve of the fabricated MTJ device. A TMR effect with a TMR ratio of 7% was observed for the first time in the (111)-oriented MTJ formed on a (110)-oriented FeAlSi film. Additionally, a resistance linearly changed near zero magnetic field, reflecting the linear magnetization response originating from the (110)-oriented FeAlSi layer. The observed linear signal change with respect to the magnetic field is useful for TMR sensor applications.

This work was supported by the SIP project, the X-nics project, the SCOPE project, CSIS, CIES and the AIE-WISE Program.

[1] K.Masuda, H.Itoh, and Y.Miura, Phys. Rev. B, Vol. 101, p. 144404 (2020)

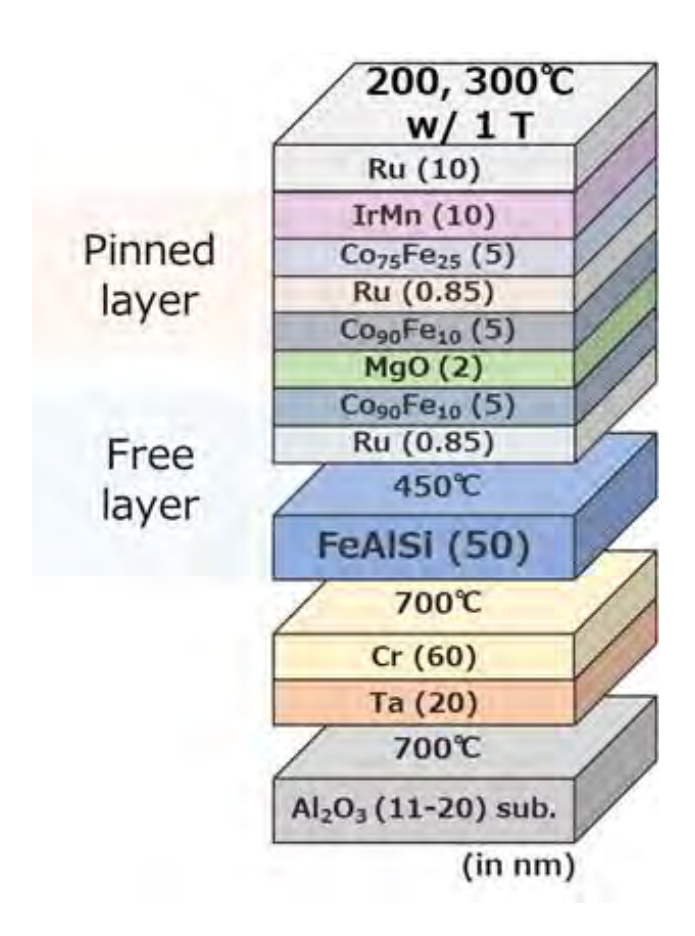


Fig.1 Stacking structure of the fabricated MTJ sample

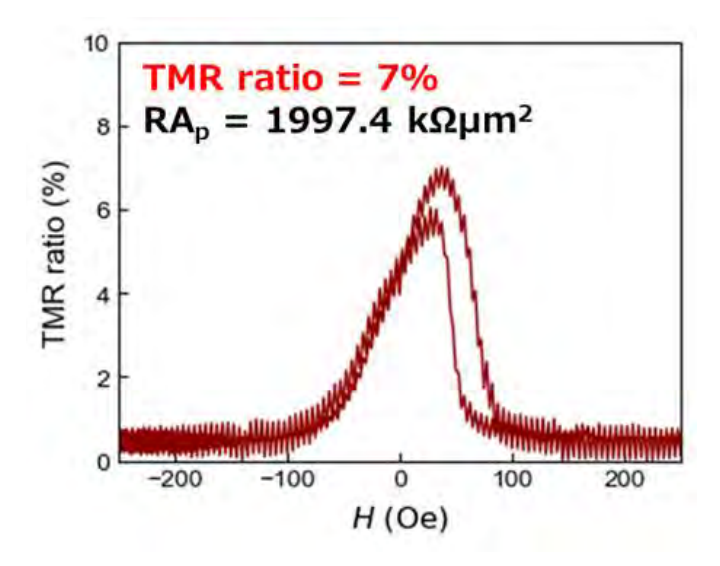


Fig.2 Magnetoresistance curve of the fabricated (111)-oriented MTJ on a (110)-oriented FeAlSi film, showing TMR ratio of 7% and a linear response near zero field.

DR-08. Suppression of Electrical 1/f Noise in Magnetic Tunnel Junctions with Mg-Al-O Barriers

S. Nii¹, <u>C. Zhang</u>¹, H. He¹, Y. Wang¹, T. Hojo¹, T. Nakano^{1, 2}, M. Oogane^{1, 3}

¹Department of Applied Physics, School of Engineering, Tohoku Univ., Sendai, Japan, ²Green X-tech, Tohoku Univ., Sendai, Japan, ³CSIS, Tohoku Univ., Sendai, Japan

Tunnel magnetoresistance (TMR) sensors using magnetic tunnel junctions (MTJs) are highly sensitive devices with growing applications in biomedical areas. These applications often require detection of magnetic field within sub-100 Hz frequency range, where electrical 1/f noise becomes a major issue. This noise originates from charge trapping and detrapping at the tunnel barrier or its interfaces. While MgO is widely, it tends to exhibit high 1/f noise due to the interfacial defects with Fe-based electrodes.3 Magnesium aluminum oxide (MAO) is a promising alternative, owing to its close lattice match with Fe.4 Existing investigations often focused on TMR evaluations. A comprehensive analysis of their lowfrequency noise characteristics remains absent. We here directly compares the electrical 1/f noise of MgO- and MAObased MTJs.

The MTJ structrues used are MgO(001) substrate/ Cr(60)/ Fe(50)/ Mg(0,2)/ MgO or MAO(2)/ Fe(5)/ IrMn(10)/ Cr(5) (thickness in nm), in which MqO or MAO barriers are deposited by electron beam evaporation, while the remaining layers are fabricated using sputtering. MTJs with MgO barriers (MgO-MTJs) exhibit TMR ratios of 140–180%, while those with MAO barriers (MAO-MTJs) achieved 60-100%, which are sufficient for noise measurements. The power spectra density of MgO and MAO-MTJs is measured to assess their electrical 1/f noise characteristics. The Hooge parameter, a key indicator of 1/f noise, is evaluated for both device types. 5 Hooge parameter for MgO-MTJs is at the middle value of 5.74×10⁻⁸ mm², while MAO-MTJs demonstrate a significantly lower value of 5.69×10⁻⁹ mm², indicating the reduced noise with MAO barriers. To investigate the origin of this noise reduction, scanning transmission electron microscopy imaging is used to compare the lattice defect density between MgO and MAO. The analysis reveals that MAO barriers have significantly fewer interfacial defects at Fe/barrier interfaces—about 1% compared to 4% in MgO-suggesting that improved lattice matching and interface quality in MAO are responsible for the reduced noise. These findings provide valuable insights into material selection for the development of low-noise

TMR magnetic sensor technologies.

This work was partially supported by the X-nics project, and CSIS, and CIES at Tohoku University, SIP project and BRIDGE project of Cabinet Office, JSPS KAKENHI 24K17316, and research grants of Hirose Foundation.

References: [1] T. Nakano *et al.*, Appl. Phys. Lett 126, 160503 (2025). [2] M. B. Weissman, Rev. Mod. Phys. 60, 537 (1988). [3] D. Herranz *et al.*, Appl. Phys. Lett 96, 202501 (2010). [4] H. Sukegawa *et al.*, Appl. Phys. Lett. 96, 212505 (2010). [5] F. N. Hooge *et al.*, Rep. Prog. Phys. 44, 497 (1981).

DR-09. Thickness-dependence of the anomalous Hall effect in magnetic heterostructures

E. M. Ababneh¹, N. Boyd², X. Fan², V. Amin¹

¹Indiana University Indianapolis, Indianapolis, Indiana, United States, ²University of Denver, Denver, Colorado, United States

In this work, we characterize how the strength of the anomalous Hall effect in a ferromagnetic layer can be modulated by changing the thickness of neighboring, nonmagnetic layers. We focus exclusively on the skew-scattering contribution to the anomalous Hall effect and model transport using the semiclassical Boltzmann equation, where we include spin-dependent scattering at layer boundaries. A key finding of this study is that the anomalous Hall conductivity can undergo sign reversal when changing a neighboring layer's thickness, even if the ferromagnetic layer is unchanged. Our results shed light on the role of interlayer scattering on charge-to-spin conversion in magnetic heterostructures.

DR-10. The effect of argon plasma exposure on in-plane uniaxial anisotropy in WS₂/Py bilayers

<u>K. Islam</u>, H. Pokhrel, S. Pollard Physics and Materials Science, The University of Memphis, Memphis, Tennessee, United States

Interfaces between thin ferromagnetic films and 2D materials such as transition metal dichalcogenides have garnered considerable attention due to their anisotropic magnetic properties. Recently, a variety of works have explored induced uniaxial in-plane anisotropy in these systems ¹⁻³. However, reports of the strength, or even the presence of an induced anisotropy, has varied significantly. It was proposed that this is largely the result of varying quality of the underlying TMD layer, with mechanically

exfoliated single crystal materials exhibiting the strongest anisotropy. To confirm the role of TMD quality and to explore potential opportunities in which to control this anisotropy, we investigate the effect of exposure to an argon plasma on CVD-grown WS₂ with a subsequently sputter deposited Py layer. WS₂ quality before and after plasma exposure was evaluated by Raman spectroscopy as well as optical imaging. Magneto-optical Kerr measurements reveal induced uniaxial anisotropy when Py is grown on WS₂ prior to plasma exposure, which is eliminated by inserting copper layer, confirming the role of the WS₂ underlayer. Following exposure to an Ar-plasma, anisotropy is completely quenched. This is a result of plasma-induced defects at the WS₂/Py interface. We further find significantly enhanced easy-axis coercivity following plasma exposure and variations in domain nucleation and propagation. Our findings introduce potential strategies for tuning magnetic anisotropy for future magnetic devices.

- ¹ V. Thiruvengadam, et al., ACS Appl Nano Mater 5(8), 10645–10651 (2022).
- ² W. Zhang, et al., APL Mater 4(3), (2016).
- ³ L. Jamilpanah, et al., J Magn Magn Mater 514, 167206 (2020).

DR-11. Large Spin Nernst Effect in Ni₇₀Cu₃₀ Alloy

W. Li^{1,2}, C. Lin¹, G. Guo^{1,3}, S. Huang^{1,4}, D. Qu^{2,4}
¹Department of Physics, National Taiwan University, Taipei, Taiwan, ²Center for Condensed Matter Sciences, National Taiwan University, Taipei, Taiwan, ³Physics Division, National Center for Theoretical Sciences, Taipei, Taiwan, ⁴Center of Atomic Initiatives for New Materials, National Taiwan University, Taipei, Taiwan

The interconversion between heat, spin, and charge plays an important role in spin-caloritronics. The spin Seebeck effect (SSE) enables longitudinal heat-to-spin conversion in ferromagnetic insulators (FMIs), while the spin Hall effect (SHE) facilitates transverse charge-to-spin conversion in non-magnetic (NM) metals—both of which have been extensively studied. In contrast, the experimental exploration on the spin Nernst effect (SNE), which is the thermal counterpart of the SHE, that generates transverse spin currents from a temperature gradient in NM metals, remains limited and is confined to 5*d* metals. One of the main challenges is the sensitive detection of the nanovolt-scale voltages against the background noises.

In this study, with a home-built refined voltage measurement technique, that is capable of detecting nanovolt-scale voltage, we investigate the SNE in 3d alloy Ni₇₀Cu₃₀ in its non-magnetic state. NiCu is a material with a sizable spin Hall angle [1] and a large Seebeck coefficient -both advantageous for detecting SNE. We confirm its nonmagnetic behaviors using vibrating sample magnetometry, along with anomalous Hall and anomalous Nernst effect measurements. From the spin Hall magnetoresistance (SMR) measurement, we show Ni₇₀Cu₃₀ has a spin Hall angle of 1.9 %. From the spin Nernst magneto-thermopower measurement, which is the thermal counterpart of SMR, we show that Ni₇₀Cu₃₀ exhibits a remarkably large SNE, with a spin Nernst angle (ϑ_{SN}) up to -71.7 %, nearly nine times greater than that of platinum $(\vartheta_{SN} = -8.2\%)$ [2]. The large spin Nernst effect in the Ni₇₀Cu₃₀ alloy can be understood from the ab initio calculations, where the Cu doping shifts the Fermi level of Ni to the steepest slope in the spin Hall conductivity, thus the maximum value of spin Nernst conductivity. These findings deepen our understanding of SNE and highlight Ni₇₀Cu₃₀ as a promising candidate for high-performance spin caloritronic applications.

[1] P.-H. Wu, D. Qu, Y.-C. Tu, Y.-Z. Lin, C. L. Chien, and S.-Y. Huang, Phys. Rev. Lett. 128, 227203 (2022).
[2] W.-Y. Li, C.-H. Lin, G.-Y. Guo, S.-Y. Huang, D. Qu, Phys. Rev. B 111, 054421 (2025).

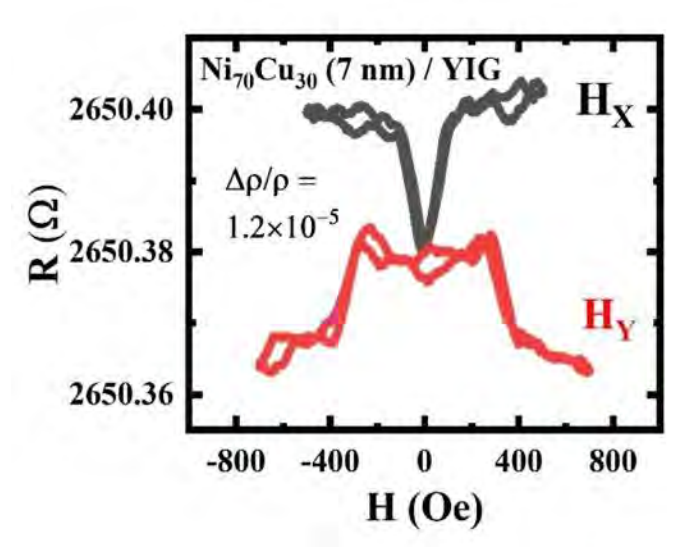


Fig. 1 Spin Hall magnetoresistance in $Ni_{70}Cu_{30}$ (7 nm) / YIG sample

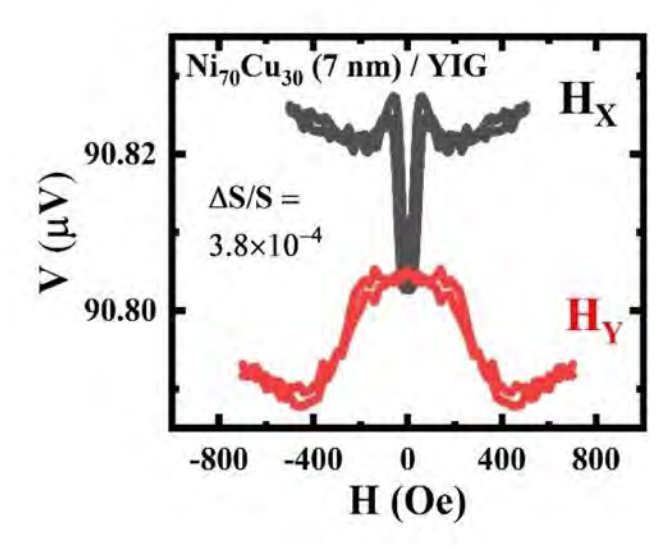


Fig. 2 Spin Nernst effect induced magneto-thermopower in Ni₇₀Cu₃₀ (7 nm) / YIG sample

DR-12. High-throughput ab initio study of magnetoelastic coupling and magnetostriction in cubic intermetallic compounds

H. Abdelhafiz¹, F. Mahfouzi², N. Kioussis³, K. Belashchenko¹
¹Department of Physics and Astronomy, University of Nebraska-Lincoln, Lincoln, Nebraska, United States, ²Physical
Measurement Laboratory, National Institute of Standards and
Technology, Gaithersburg, Maryland, United
States, ³Department of Physics and Astronomy, California State
University, Northridge, California, United States

A p-bit is the building block for probabilistic computing, offering a hardware platform bridging the gap between classical and quantum logic [1]. A compelling physical realization of a p-bit is a low-barrier nanomagnet, where thermal fluctuations induce spontaneous switching between two magnetic states. The switching time depends on the energy barrier E_B, making low E_B essential for high-speed operation. However, nanoscale magnetic elements typically have sizable magnetic anisotropies induced by random strain via magnetostriction. Therefore, utilizing cubic magnetic materials with low magnetostriction may help reduce the energy barriers and improve p-bit performance. Here we perform a high-throughput density functional theory (DFT) study of magnetostriction in more than 200 cubic compounds forming L2₁, C1_b, D0₃, B2, and L1₂ ordered phases. Using the VASP code, we calculate both independent magnetoelastic coupling parameters (B1 and B₂).

^{*} Best Student Presentation Finalist / LB - Late-breaking Poster

We identify several compounds —such as Fe $_3$ Si, MnNiSb and Co $_2$ ZrAl— with exceptionally low magnetostriction, making them candidates for GHz-rate, thermally driven p-bit operation. While experimental data is scarce, our results align well with available experimental data. Remaining discrepancies can be attributed to the sensitivity of magnetostriction to electronic structure and magnetic moment.

This work was supported by NSF Grant No. DMR-2324203.

[1] K. Y. Camsari, B. M. Sutton, and S. Datta, Appl. Phys. Rev., vol.6, p.011305 (2019)

DR-13. MTJ-Based Neuromorphic Circuit for Analog Machine Learning

<u>S. Louis</u>¹, A. N. Slavin¹, C. Trevillian¹, H. Bradley¹, D. Hanna¹, M. Abramson², I. Krivorotov², V. Tyberkevych¹

¹Oakland University, Rochester, Michigan, United States, ²University of California, Irvine, California, United States

Magnetic tunnel junctions (MTJs) are nanoscale spintronic devices composed of two ferromagnetic layers separated by an insulating barrier. MTJs are CMOS-compatible and widely used commercially in magnetic memory and sensor technologies, with over 10^8 devices manufactured annually. In this work, we demonstrate a practical analog artificial neuron by pairing a spin-valve/magnetic tunnel junction (SV/MTJ) device with an NMOS transistor. This SV/MTJ-nMOS neuron supports fully analog machine learning and is compatible with conventional electronic systems and neural network architectures.

In a recent theoretical study [1], it was shown that an SV/MTJ device can function as a biologically plausible spiking neuron, replicating fundamental behaviors observed in biological neurons, such as response latency, synaptic integration, refraction, inhibition, adaptation, and spiketrain generation. By integrating this SV/MTJ neuron with an NMOS transistor, both input and output signals become voltage-based. This configuration allows straightforward implementation of synaptic weights through voltage-controlled amplifiers, thus enabling seamless integration into fully analog neural networks.

To validate system-level performance, we constructed a three-neuron SV/MTJ-nMOS neural network in LTspice, complete with supporting circuitry [2]. A feedforward

backpropagation algorithm was employed, performing all learning and synaptic weight adjustments entirely in the analog domain using spike timing (time-encoded signals). The XOR logic gate, a standard neural network benchmark, was used to assess learning effectiveness. After approximately 30 training epochs, the network reliably converged, performing XOR classification successfully. The complete training cycle required less than 2 us of simulation time. These results confirm the potential of the SV/MTJ-nMOS neuron circuit for fast, low-power, fully analog machine learning, compatible with standard electronic design and established neural network frameworks.

[1] S. Louis, H. Bradley, C. Trevillian, A. Slavin and V. Tyberkevych, IEEE Magn. Lett., Vol. 15, p. 1–5 (2024) [2] S. Louis, H. Bradley, A. Litvinenko and V. Tyberkevych, arXiv preprint arXiv:2503.20813 (2025)

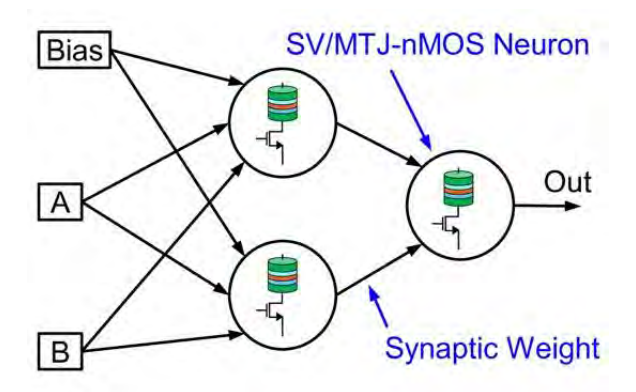
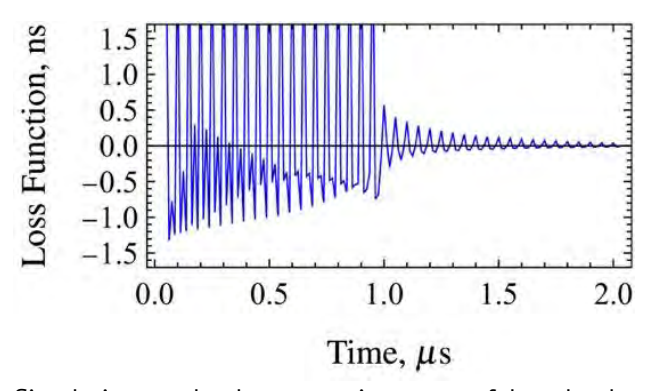


Figure 1 Neural network implemented with SV/MTJ-nMOS neurons and analog synapses.



Simulation results demonstrating successful analog learning of the XOR logic function in an SV/MTJ-based three-neuron network.

DR-14. Solution of advanced classification tasks including MNIST dataset using spin wave based multiler AI system with nonlinear activation functions

K. Rivkin

RKMAG Corporation, Pacific Grove, California, United States

We demonstrate that by applying a non-uniform DC magnetic field to a soft, low damping magnetic material such as YIG, one can create a layout of scatterers capable of approximating the most important components of practical AI algorithms, including vector-matrix mulitplication as well as Relu and Sigmoid activation functions.

It is therefore possible to convert many existing AI computing setups and algorithms to a such spin wave based implementation. We demonstrate a particular setup capable of performing classifications tasks on the basis of MNIST dataset, with the performance matching some of the best conventional (CMOS) based implementations, but with significant power and cost advantages.

^{*} Best Student Presentation Finalist / LB – Late-breaking Poster

SESSION EA: COMPACT EUV SOURCES: EXCEPTIONAL NEW TOOLS FOR ULTRAFAST SPIN DYNAMICS

Chair(s): D. A. Arena, *Physics, University of South Florida,*Tampa, Florida, United States

Thursday, October 30, 2025

08:30 AM-12:00 PM

Grand Ballroom

EA-01. Probing Spin Textures and Dynamics using Ultrafast EUV and Soft X-Ray Sources

M. M. Murnane

JILA and Physics, University of Colorado, Boulder, Colorado, United States

Ultrafast laser pulses can drive the fastest spin dynamics and phase transitions in magnetic materials, on timescales ranging from attoseconds on up. Ultrafast extreme UV (EUV) and soft X-ray pulses make it possible to probe elementspecific spin dynamics and spin textures in multicomponent magnetic systems, providing rich new information not accessible using visible light. In particular, tabletop laser-based high harmonic (HHG) sources are ideal for probing fast spin dynamics since they can probe sublattices in a compound, or distinct layers in a structure, simultaneously and with element specificity. This makes it possible to capture and distinguish processes such as spin transfer, spin reorientations, spin currents and spin flips, to understand how to manipulate spins using light. These new light source capabilities are addressing a decades-long challenge: although ultrafast lasers could quench or switch the magnetic state of materials,[1] the underlying microscopic mechanisms were not well understood. Very recently, through a careful comparison of extensive experimental data acquired using HHG probes, we have addressed several open questions and through extensive comparison between data and simulations, we developed some of the most comprehensive validated theories to date.

We will also present recent advances in full field imaging of 3D spin textures in topological magnetic materials such as metalattice, skyrmion and nanoparticle samples. By combining coherent short wavelength light sources with vector ptychotomography imaging techniques, high resolution imaging of 3D spin textures with ~10nm spatial resolution are now possible.

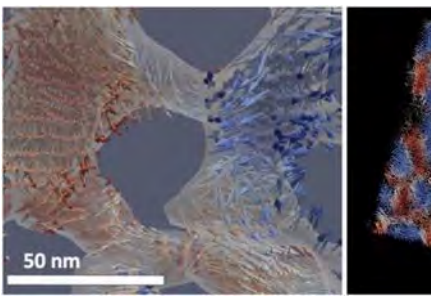
Finally, the ability to create polarization- and phasestructured visible and short wavelength beams (spin and orbital angular momentum, SAM and OAM) makes it possible to enhance contrast, to implement unique excitations and probes of chiral structures in magnetic materials and nanostructures.

Beaurepaire, E., Merle, J. C., Daunois, A. & Bigot, J. Y. Ultrafast spin dynamics in ferromagnetic nickel. Physical Review Letters 76, 4250 (1996).

Ryan, S. A. et al. Optically controlling the competition between spin flips and intersite spin transfer in a Heusler half-metal on sub-100-fs time scales. Science Advances 9, eadi1428 (2023).

Tengdin, P. et al. Direct light-induced spin transfer between different elements in a spintronic Heusler material via femtosecond laser excitation. Science Advances 6, eaaz1100 (2020).

Rana, A. et al. Three-dimensional topological magnetic monopoles and their interactions in a ferromagnetic metalattice. Nature Nanotechnology 18, 227 (2023). Lu, X. et al. Visualizing Magnetic Order in Self-Assembly of Superparamagnetic Nanoparticles, in press, ACS Applied Nano Materials (2025).



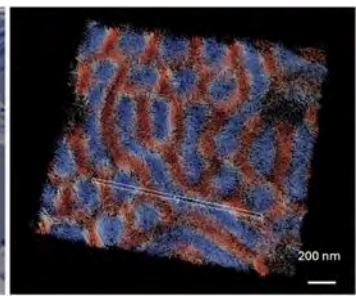


Fig. 1 Experimentally extracted 3D spin texture of magnetic metalattices and skyrmion with ~10nm spatial resolution using coherent soft X-ray vector ptychotomography.

EA-03. Magnetization Dynamics in Transition Metal Films with Low Perpendicular Magnetic Anisotropy

<u>B. Vodungbo</u>¹, E. Jal¹, M. Hennes³, R. Delaunay¹, J. Milano², F. Fortuna⁵, M. Marangolo³, M. Eddrief³, J. Dubois^{1, 4}, G. Lambert⁴

¹Laboratoire de Chimie Physique – Matière et Rayonnement, Sorbonne Université – CNRS, Paris, France, ²Instituto de Nanociencia y Nanotecnologia, CNEA – CONICET, Bariloche, Argentina, ³Institut des Nanosciences de Paris, Sorbonne Université – CNRS, Paris, France, ⁴Laboratoire d'Optique Appliquée, ENSTA – CNRS – École Polytechnique, Palaiseau, France, ⁵Institut des Sciences Moléculaires d'Orsay, Université Paris-Saclay – CNRS, Orsay, France

Above a critical thickness, in the order of tens to hundreds of nanometers, transition metal thin films with low perpendicular magnetic anisotropy (PMA) present a stripe domains structure [1]. Compared to high PMA thin films such as Co/Pt multilayers, in which such a stripe domains structure can also be observed albeit with a lot smaller critical thickness (few nanometers), the domains are not fully magnetized out of plane and the transition between adjacent domains is not very steep. This gives rise to more complex magnetic structures, with magnetic caps at the domains extremities for example, which could be exploited for spintronics applications [2]. For these potential applications, it is fundamental to be able to control the magnetic structure. One way to realize this control is to use optical excitation of the system [3]. Moreover, using the shortest laser pulses possible, in the femtosecond range, opens up the possibility to realize ultrafast devices. Here, we will report on the magnetization dynamics induced by a near infrared (NIR) femtosecond laser pulse in different types for transition metals based thin films. To probe the nanometric magnetic structure of these systems we used high order harmonics (HHG) of NIR femtosecond laser in resonance with the Fe, Co and Ni $M_{2,3}$ absorption edges between 50 and 70 eV (about 20 nm). Indeed, resolving the magnetic structure requires very short wavelengths which cannot be reach in the NIR or visible range. At resonant energies, the magnetic domains structure acts as a diffraction grating and recording the diffracted orders on a CCD camera allow us to retrieve time-resolved informations on this structure. We have pioneered this type of experiment for the study of ultrafast magnetization dynamics in high PMA systems by following the demagnetization of Co/Pt multilayers in a transmission geometry [4]. The films we want to study here are much too thick, between 100 and 300 nm, for conducting a transmission experiment at the $M_{2,3}$ absorption edges. Fortunately, we have recently shown that it is possible to conduct similar experiments in reflection geometry and to study films of arbitrary thickness [5]. This has the advantage to enhance the sensitivity to surface structures which may arise in low PMA films.

[1] N. Saito, H. Fujiwara and Y. Sugita, *Journal of the Physical Society of Japan*, Vol. 19, p.1116-1125 (1964)
[2] L.-C. Garnier, M. Marangolo and M. Eddrief, *Journal of Physics: Materials, Vol.* 3, p.024001 (2020)
[3] C. D. Stanciu, F. Hansteen and A. V.
Kimel, *Physical Review Letters, Vol.* 98, p.207401 (2007)
[4] B. Vodungbo, J. Gautier and G. Lambert, *Nature*

Communications, Vol. 3, p. 999 (2012) [5] M. Hennes, G. Lambert and V. Chardonnet, Applied Physics Letters, Vol. 120, p.072408 (2022)

EA-04. Electron dynamics in two-dimensional semiconductors and spinel ferrites at the NSF-NeXUS user facility

R. Kawakami

NSF-NeXUS and Department of Physics, The Ohio State University, Columbus, Ohio, United States

The NSF-NeXUS facility at Ohio State University will bring capabilities for ultrafast x-ray science to the user community. A high-power laser (800 W) with a high repetition rate (100 kHz - 2 MHz) is used to produce femtosecond-scale extreme ultraviolet (EUV) pulses via gasphase high harmonic generation. These are directed toward three beamlines for time-resolved x-ray reflection/absorption spectroscopy (XRS/XAS), angleresolved photoemission spectroscopy (ARPES), and scanning tunneling microscopy (STM). In addition to discussing the capabilities of the facility, I will mention two types of scientific studies that could be performed at the facility in the near future. First, our group participated in timeresolved ARPES experiments on two-dimensional semiconductors, including studies on monolayer WS₂ and twisted bilayers of transition metal dichalcogenides. Here, ARPES is combined with real-space photoemission electron microscopy (PEEM) to measure the electronic band structure of small, exfoliated flakes and throughout the full Brillouin zone. Following the generation of excitons by an optical pump pulse, the electron dynamics is mapped out in energy and momentum space by a time-delayed ARPES EUV probe pulse. Second, our group was involved in a time-resolved XRS study of electron dynamics in spinel ferrites CoFe₂O₄ and NiFe₂O₄. Following the excitation of electrons by an optical pump pulse, their dynamics are probed by XRS using a time-delayed broadband EUV probe pulse. The element-specific nature of the measurement tracks the dynamics as the electrons hop among the Co, Ni, Fe, and O sites.

EA-05. Revealing domain wall stability during ultrafast demagnetization with subwavelength EUV imaging

<u>H. Chang</u>¹, S. Zayko¹, T. Schmidt², O. Kfir³, M. Sivis^{1,4}, J. H. Mentink⁵, M. Albrecht², C. Ropers^{1,4}

¹Max Planck Institute for Multidisciplinary Sciences, Göttingen, Germany, ²Institute of Physics, University of Augsburg, Augsburg, Germany, ³School of Electrical Engineering, Tel Aviv University, Tel Aviv, Israel, ⁴4th Physical Institute, University of Göttingen, Göttingen, Germany, ⁵Institute for Molecules and Materials, Radboud University, Nijmegen, Netherlands

Ultrafast manipulation of nanoscale magnetic domains plays an important role in the development of next-generation information storage and spintronics. Although experiments with X-ray scattering have suggested photoinduced domain wall broadening occurring at subpicosecond timescales and domain wall displacement at extreme velocities, direct, real-space observation of domain dynamics in such a regime has so far remained elusive due to the requirement to simultaneously reach nanometer and femtosecond spatiotemporal resolution. Using a high-harmonic, circularly polarized extreme ultraviolet source, we demonstrate subwavelength imaging of magnetic domains during photoinduced demagnetization of Co-based thin films. With 13.5 nm spatial resolution, we further achieve nanometer precision in locating domain walls and determining their widths. Thus, we show that for TbCo and Co/Pd thin films, the domain walls remain stationary for demagnetization levels up to 60%, where local stochastic switching of domains emerges and becomes significant for stronger excitations. Our results stipulate an upper limit for the magnitude of net spin transport across the domain walls during ultrafast demagnetization. Our technique allows extraction of local material properties during ultrafast processes and can be readily generalized to study spatiotemporal dynamics in condensed matter with extreme resolution.

- [1] Chang et al. arxiv: 2504.17917.
- [2] Zayko et al. Nat. Commun. 12, 6337 (2021)
- [3] Kfir et al. Sci. Adv. 3, eaao4641 (2017)
- [4] Pfau et al. Nat. Commun. 3, 1100 (2012)
- [5] Jangid et al., Phys. Rev. Lett. 131, 256702 (2023)

SESSION EB: ALTERMAGNETIC MATERIALS

Chair(s): Q. Liu, *Physics, Southern University of Science and Technology, Shenzhen, Guangdong, China*Thursday, October 30, 2025
08:30 AM-12:00 PM
Ballroom A

EB-01. Altermagnetic electronic and magnetic structure explored in MnTe

P. Wadley¹, T. Jungwirth^{1, 2}, O. Amin¹
¹School of Physics and Astronomy, University of Nottingham, Nottingham, Nottinghamshire, United
Kingdom, ²nanospintronics, Institute of Physics ASCR, Praha, Czechia

Altermagnetism is a newly identified class of magnets which combines properties from both ferromagnets and antiferromagnets, making them highly promising candidates for spintronic applications^[1,2]. We recently demonstrated the spin split nature of the altermagnetic electronic band structure in MnTe^[3]. In this work, we demonstrate that the unique resultant properties of altermagnets can be used to image them in unprecedented details, and also to control them in unique ways.

Utilising a combination of x-ray spectroscopy and microscopy We will show unique symmetries in the electronic band structure and also unique ways of imaging the realspace magnetic order. We can image all 6 domain types in a single instrument ,revealing merons and their vorticity. In addition, we utilise a combination of patterning and field cooling to nucleate single domains of our choosing from the micron to nanoscale. We also show generation and control of the position and vorticity of single vortices. These experiments showcase the unique properties of altermagnets and also provide a platform for the next stages of research and application^[4].

References

- 1. Smejkal, L., Sinova, J. & Jungwirth, T. *Beyond Conventional Ferromagnetism and Antiferromagnetism*: A Phase with Nonrelativistic Spin and Crystal Rotation Symmetry. Physical Review X 12, 031042 (2022).
- 2. Smejkal, L., Sinova, J. & Jungwirth, T. *Emerging Research Landscape of Altermagnetism. Physical Review* X 12, 040501 (2022).

Altermagnetic lifting of Kramers spin degeneracy 3. J. Krempaský, L. Šmejkal, P. Wadley, et al Nature 626, 517 – 522 (2024) https://doi.org/10.1038/s41586-023-06907-7

Altermagnetism imaged and controlled down to the nanoscale 4. O. J. Amin, A. Dal Din, P. Wadley et al Nature 636, pages348–353 (2024)

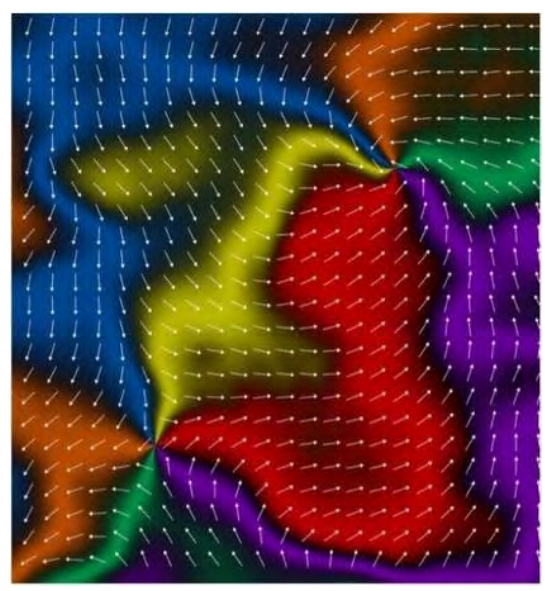


Fig. 1 Altermagnetic domain structure in open space showing a vortex antivortex pair

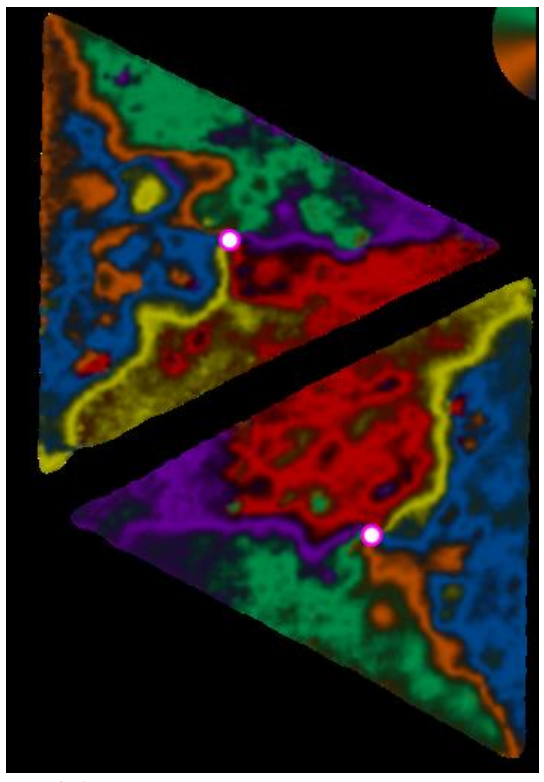


Fig. 2 Altermagnetic domain structure in micro-fabricated field-cooled triangles showing single vortices with opposite vorticity

EB-02. Mn₅Si₃: A Case Study in Altermagnetic Materials

L. Michez¹, J. Rial², M. Leiviska³, H. Reichlova³, D. Kriegner³,

A. Badura³, I. Kounta¹, M. Petit¹, G. Skobjin⁴, S. Beckert⁶, E. Schmoranzerova⁵, O. Gomonay⁷, A. Thomas⁶, R. Lopes

Seeger², L. Smejkal⁷, J. Sinova⁷, S. Goennenwein⁴, T. Jungwirth³, V. Baltz²

¹CINaM-CNRS, Aix Marseille University, Marseille, France, ²Univ. Grenoble Alpes, CNRS, CEA, Grenoble INP, Spintec, Grenoble, France, ³Institute of Physics, Czech Academy of Science, Prague, Czechia, ⁴Fachbereich Physik, Universität Konstanz, Konstanz, Germany, ⁵Faculty of Mathematics and Physics, Charles University, Prague, Czechia, ⁶Leibniz-Institut für Festkörperund Werkstoffforschung, Dresden, Germany, ⁷Institut fur Physik, Johannes Gutenberg Universität, Mainz, Germany

To date, only a few altermagnetic materials have been experimentally confirmed [1]. This is due to challenges in material growth, particularly for those that exhibit altermagnetism only in thin-film form or under strain (Fig. 1) [2], and the difficulty in proving their altermagnetic nature. Among the candidates, Mn₅Si₃ stands out due to its composition of light elements with weak relativistic spinorbit coupling, which allows its altermagnetic properties to be linked to non-relativistic spin physics. Remarkably, Mn₅Si₃ exhibits a significant anomalous Hall effect (AHE) despite having zero magnetization (Fig. 2) [2,3]. Its hexagonal cell structure features four out of six possible Mn₂ sites predicted to display alternating magnetic dipolar ordering (Fig. 1), resulting in a checkerboard arrangement of opposite-spin sublattices with three possible configurations for the magnetic atoms. Direct evidence of altermagnetic order using techniques like ARPES has been elusive due to the requirement for perfect crystal order. In this presentation, we will explore an alternative approach by relating the anisotropy of the AHE to the local anisotropy arising from electric multipoles [4], a hallmark to altermagnetism. Our findings are supported by transport measurements, structural and magnetic characterizations, and a theoretical model involving atomic site-dependent anisotropy and bulk Dzyaloshinskii-Moriya interaction for a single variant, thereby unambiguously demonstrating the altermagnetic character of Mn₅Si₃[5].

[1] L. Bai *et al.*, Adv. Funct. Mater. Vol. 34, p.2409327 (2024)[2] I. Kounta *et al.*, *Phys. Rev. Materials* Vol. 7, p.024416 (2023)

[3] H. Reichlova *et al.*, *Nature Communications Vol. 15, p.4961* (2024)

[4] M. Leiviskä *et al.*, *Physical Review B Vol.* 109, *p.224430* (2024)

[5] J. Rial et al., Physical Review B Vol. 110, p.L220411 (2024)

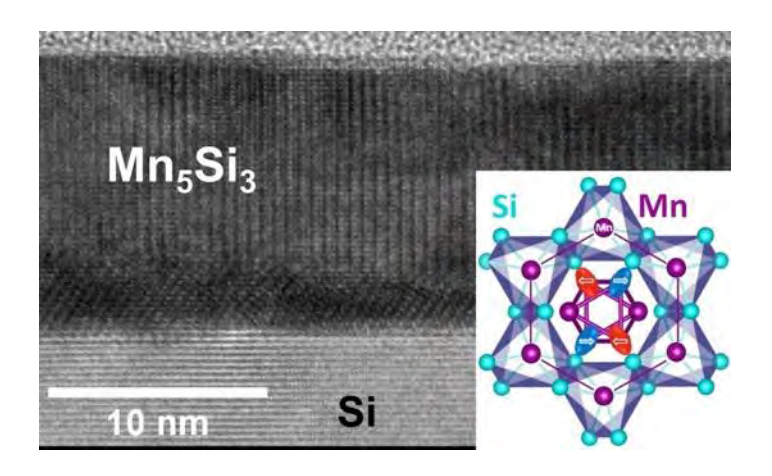


Fig. 1 High-Resolution TEM cross-section of a 13-nm thick Mn5Si3 thin film grown on Si(111). Inset: Magnetic and crystalline structure of Mn5Si3 seen along the c-axis, showing the 4 magnetic Mn atoms in the unit cell.

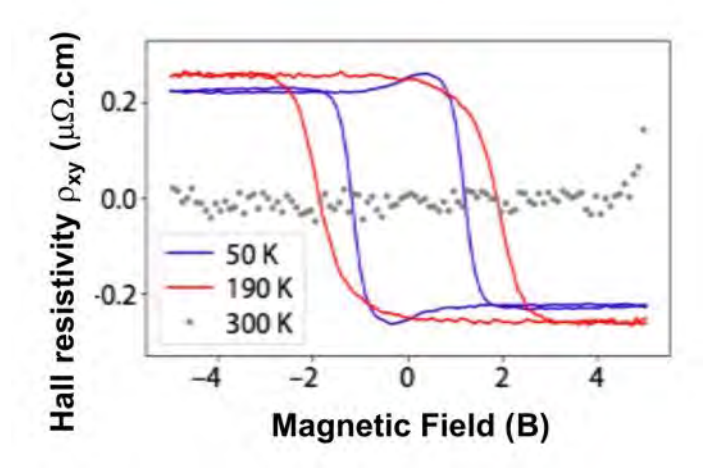


Fig. 2 Anomalous Hall resistivity measured at 50 K, 190 K and 300 K.

EB-03. Three-dimensional mapping of the altermagnetic spin splitting in CrSb

Y. Liu, G. Yang

Physics, Zhejiang University, Hangzhou, Zhejiang Province, China

Altermagnetism, a kind of collinear magnetism that is characterized by a momentum-dependent band and spin splitting without net magnetization, has recently attracted considerable interest. Finding altermagnetic materials with large splitting near the Fermi level necessarily is crucial for spintronic applications and emergent phenomena. Here, using synchrotron-based angle-resolved photoemission spectroscopy (ARPES), spin-resolved ARPES and model calculations, we uncover a large altermagnetic splitting, up to ~1.0 eV, near the Fermi level in CrSb. We verify its bulktype g-wave altermagnetism through systematic threedimensional k-space mapping, which unambiguously reveals the altermagnetic symmetry and associated nodal planes. Spin-resolved ARPES measurements further verify the spin polarizations of the split bands near Fermi level. Tightbinding model analysis indicates that the large altermagnetic splitting arises from strong third-nearestneighbor hopping mediated by Sb ions. The large band/spin splitting near Fermi level in metallic CrSb, together with its high TN (up to 705 K) and simple spin configuration, paves the way for exploring emergent phenomena and spintronic applications based on altermagnets. Finally, we will present our recent progress on other related altermagnetic materials and thin films.

Guowei Yang*, Zhanghuan Li*, Sai Yang, Jiyuan Li, Hao Zheng, Weifan Zhu, Ze Pan, Yifu Xu, Saizheng Cao, Wenxuan Zhao, Anupam Jana, Jiawen Zhang, Mao Ye, Yu Song, Lun-Hui Hu, Lexian Yang, Jun Fuji, Ivana Vobornik, Ming Shi, Huiqiu Yuan, Yongjun Zhang*, Yuanfeng Xu* and Yang Liu*, Three-dimensional mapping of the altermagnetic spin splitting in CrSb, Nature Communications 16, 1442 (2025).

SESSION EC: MODELING AND MACHINE LEARNING

Chair(s): F. M. Abel, *Physics, United States Naval Academy, Annapolis, Maryland, United States* and Selma Amara, *King Abdullah University of Science and Technology, Thuwal, Saudia Arabia*

Thursday, October 30, 2025 08:30 AM-12:00 PM Ballroom C

EC-01. Theory of Magnetization Dynamics Beyond the Landau-Lifshitz-Gilbert Equation

C. M. Webb, S. Zhang

Physics, University of Arizona, Tucson, Arizona, United States

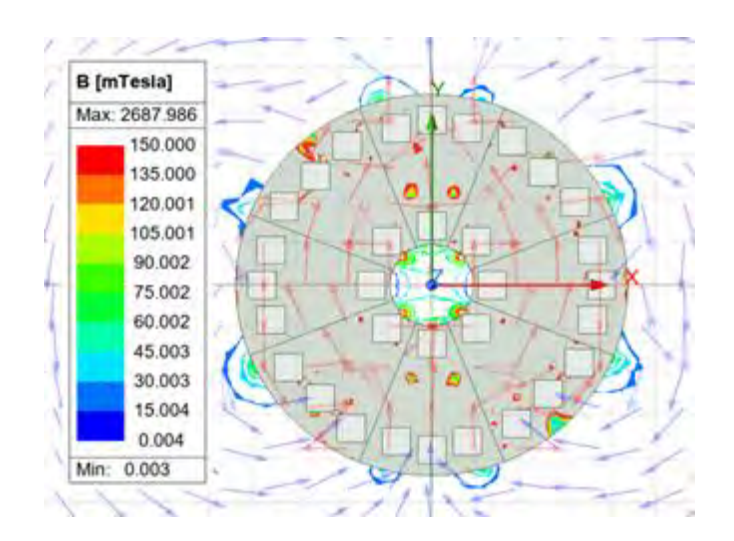
The phenomenological Landau-Lifshitz-Gilbert (LLG) equation has long been a cornerstone of spintronics, widely employed to model magnetization dynamics in ferromagnetic systems. While the LLG equation accurately captures nanosecond-scale dynamics driven by spin torques, spin pumping, and external magnetic fields, recent experimental investigations have pushed the study of magnetization dynamics into the terahertz regime. In this high-frequency domain, an additional term-often referred to as the nutation or inertial term—is introduced to extend the conventional LLG framework. Although several theoretical arguments have been proposed to justify this inertial term, its microscopic origin remains under debate. In this work, we present a microscopic derivation of the inertial LLG equation using spin wave theory combined with a non-Markovian quantum master equation that accounts for magnon-phonon coupling. We demonstrate that coherent interactions between magnons and an external system, such as a phonon bath, are essential for the emergence of high-frequency nutation dynamics. Moreover, our analysis reveals that the full dynamical equation includes additional terms of comparable magnitude to the conventional nutation term. In the fully Markovian limit – where system memory effects vanish—the standard LLG equation with longitudinal damping is recovered.

EC-02. Reduction of materials criticality in hybrid manufacturing of Halbach arrays using sintered NdFeB magnets and additively manufactured soft magnet frames

L. Cosgrove, T. Lamichhane

Engineering & Physics, University of Central Oklahoma, Edmond, Oklahoma, United States

Using sintered magnets cubes and additively manufactured PLA and steel frames, we report enhancement mechanism of lateral magnetic field inside cylindrical dipolar magnets inserted Halbach arrays introducing nested Halbach rings with eight sections for the construction simplicity. The inner Halbach was designed with 8 dipolar NdFeB N48 magnets and outer Halbach ring was designed with tightly fitted similar 24 cubes. The increase in lateral magnetic field was only 5% with the introduction of the second ring with the 8 magnets. About 27% of the axial field was increased when 16 identical steel cubes were added in the outer ring. Interestingly, the increase in lateral field with 8 dipolar magnets cubes and 16 steel cubes was equal to all 24 magnet cubes in the outer Halbach rings. We also compared the influence of pattern of dipolar magnetization in each section. The same set up with one-inch magnet cubes was manufactured to study the influence of thickness of the slabs. This demonstrates the true potential of reduction of criticality of high-quality materials in industrial manufacturing using 3D printing. Finally, the results are validated using Ansys Maxwell and COMSOL Multiphysics simulations and optimal geometries for the potential enhancement of the field is predicted.



EC-03. Exploration of Novel Fe₃Pt Structures for Application as Magnetic Materials: A Density Functional Theory Study N. L. Lethole

Physics, University of Fort Hare, Alice, Eastern Cape, South Africa

The exploration of Fe-Pt alloys has garnered significant attention due to their promising applications in various fields such as magnetic materials, spintronics and nanotechnology. These alloys are characterized by large magnetocrystalline anisotropy suitable for ultrahigh density magnetic storage media and the Invar effect and giant magnetostriction [1,2]. Magnetic, electronic and other properties of various compositions on these alloys have been reported over the years. For example, the equiatomic P4/mmm-FePt possesses large uniaxial magnetocrystalline anisotropy energy between 2.9 and 4.1 eV along the easy axis [001], while the I4/mmm-Fe₃Pt shows thermoelastic martensitic transformations from an fcc parent phase to ferromagnetic bcc martensite, at a Curie temperature of 1043 K [3,4]. Research indicates that the magnetism of Fe-Pt alloys is intrinsically linked to Fe composition, suggesting that variations in Fe content influences their behavior [5,6]. The present study aims to explore four novel structures of Fe₃Pt alloys, aiming to provide an understanding their structural, magnetic, electronic, and mechanical characteristics. We employed the Density Functional Theory (DFT) technique for our analysis.

Our study reveals that in addition to the well reported Pm-3m-Fe₃Pt and I4/mmm-Fe₃Pt, there exist additional Fe₃Pt phases that exhibit excellent properties. The calculated enthalpies formations were found to be negative in all the structures, indicating thermodynamic stability and formation under experimental synthetic conditions. Moreover, the computed magnetic moments are in the range 3.24 to 3.61 Bohr magneton, which is comparable to 3.24 of the widely reported P4/mmm-FePt alloy. The analysis of the electronic structure revealed strong magnetism due to the presence of asymmetry in the spin up and down states of the density of states (DOS) plots. The Fe d states are dominant around the Fermi level. Moreover, all structures, save P63mmc-Fe₃Pt showed excellent mechanical stability, hardness and resistance to compression in the elastic region 0% ≤ Strain ≤ 10%. This due to satisfying the Born necessary stability conditions, large bulk modulus and strong linear relationship fit of > 0.94.

[1] T. Kakeshita, T. Takeuchi and S. Muto, Appl. Phys., Lett. 77 (2000) 1502

- [2] D. Odkhuu and S.C. Hong, J. Appl. Phys., 107, 09A945
- [3] N. Lethole, H. Chauke and P. Ngoepe, Materials, 15, 5679 (2022)
- [4] Y. Shi, M. Lin, X. Jiang and S. Liang, J. Nanomat., 2015, 467873 (2015)
- [5] B. Thacker, M. Solanki and R. Kharatmol, Phys. Status Solidi B, 262, 2400160 (2025)
- [6] K. Aledealat, B. Aladerah and A. Obeidat, Physica B, 651, 414615 (2023)

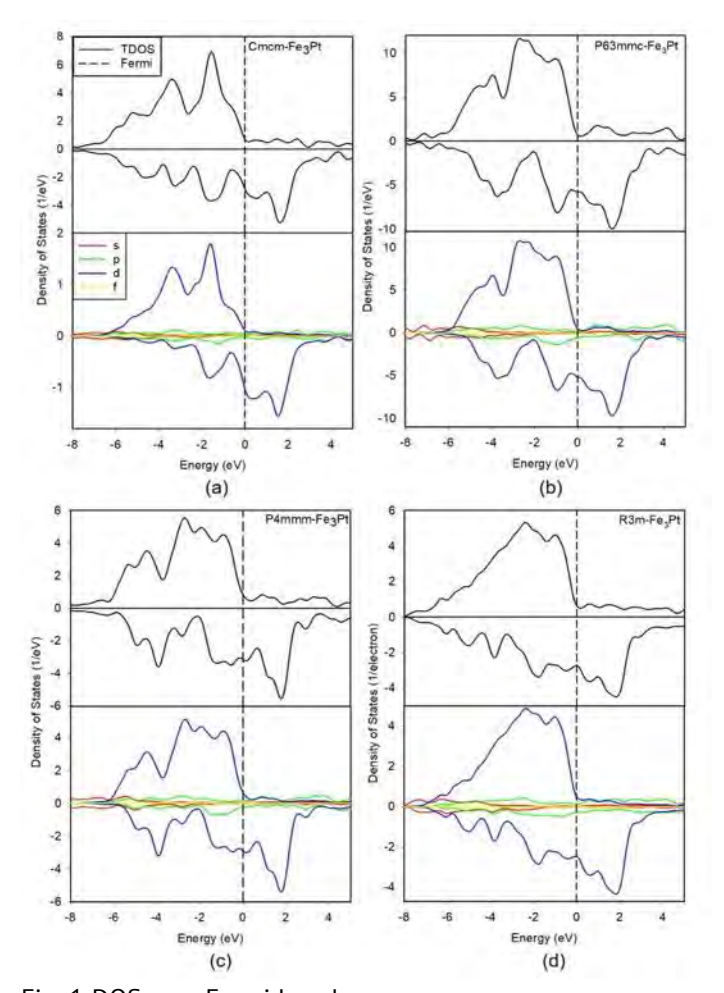


Fig. 1 DOS near Fermi Level

EC-04. Field-assisted thermal fluctuation in non-collinear antiferromagnet Mn₃Sn

S. Oian, A. Shukla, S. Rakheja

Electrical and Computer Engineering, University of Illinois Urbana Champaign, Champaign, Illinois, United States=

Non-collinear chiral antiferromagnets (AFMs)[1, 2], such as Mn₃Sn, have attracted significant attention due to their unique magneto-transport properties[3-5]. Previous studies[6] have explored the dynamics of the magnetic octupole moment moct in strained Mn₃Sn[7] under external magnetic fields and spin-orbit torques at 0 K. However, thermal noise plays a significant role in its prospective applications in high density memory and computation devices. Recent work[8] presented a theoretical analysis of the relaxation time of moct, along with its electrical tunability. However, the role of the external field, crucial for the manipulation of Mn₃Sn, remains insufficiently explored. In this work, we present a comprehensive theoretical analysis of its influence in low energy barrier ($\leq 5 \text{ k}_B\text{T}$) Mn₃Sn systems. Firstly, a Hamiltonian analysis reveals that the orientation of the external magnetic field relative to the easy axis (y axis) in the Kagome plane determines the mode of energy barrier symmetry breaking, as illustrated in Fig. 1. Furthermore, we first offer the theoretical escape time of the magnetic octupole moment (moct) between two stable states using the harmonic transition-state theory. Complementary numerical simulations based on coupled Landau-Lifshitz-Gilbert (LLG) equations show excellent agreement with the theoretical predictions in Fig. 2. The escape time's dependence on field orientation aligns with the energy barrier symmetry shown in Fig. 1. Our analysis further predicts the temporal evolution of moct, accounting for back-and-forth switching between the two states. These precise characterizations of Mn₃Sn's thermal behavior enable its effective manipulation for advanced applications in THz random number generation and probabilistic computing.

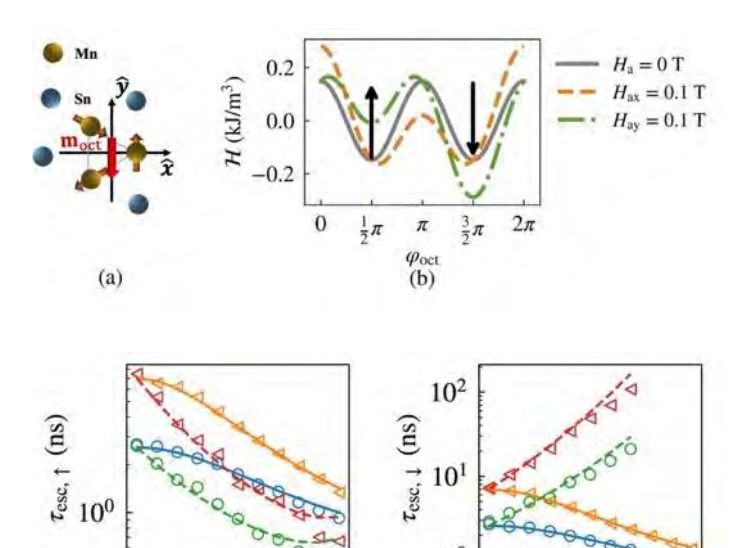
Figure 1(a) crystal structure of Mn₃Sn. (b) Hamiltonian with field along different orientations. The state with m_{oct} in the energy well of φ_{oct} = $\pi/2(3\pi/2)$ is defined as up(down) state as denoted.

Figure 2 Escape as a function of external field. Circle(triangular) marker represents energy barrier = $3(4) k_BT$ and solid(dashed) lines represents $H_{ax}(H_{ay})$. Simulations in (b) are partially restricted to 80 mT due to computational limit.

[1] A. Shukla, S. Qian, and S. Rakheja, "Spintronic devices and applications using noncollinear chiral

antiferromagnets," Nanoscale Horizons, 2025.

- [2] B. H. Rimmler, B. Pal, and S. S. P. Parkin, "Non-collinear antiferromagnetic spintronics," Nature Reviews Materials, vol. 10, no. 2, pp. 109-127, 2024, doi: 10.1038/s41578-024-00706-w.
- [3] S. Nakatsuji, N. Kiyohara, and T. Higo, "Large anomalous Hall effect in a non-collinear antiferromagnet at room temperature," Nature, vol. 527, no. 7577, pp. 212-5, Nov 12 2015, doi: 10.1038/nature15723.
- [4] J. Dong et al., "Tunneling Magnetoresistance in Noncollinear Antiferromagnetic Tunnel Junctions," Phys Rev Lett, vol. 128, no. 19, p. 197201, May 13 2022, doi: 10.1103/PhysRevLett.128.197201.
- [5] M. Ikhlas et al., "Large anomalous Nernst effect at room temperature in a chiral antiferromagnet," Nature Physics, vol. 13, no. 11, pp. 1085-1090, 2017, doi: 10.1038/nphys4181.
- [6] A. Shukla, S. Qian, and S. Rakheja, "Impact of strain on the SOT-driven dynamics of thin film Mn_3Sn ," Journal of Applied Physics, vol. 135, no. 12, 2024, doi: 10.1063/5.0179669.
- [7] J. Y. Yoon et al., "Handedness anomaly in a non-collinear antiferromagnet under spin-orbit torque," Nat Mater, vol. 22, no. 9, pp. 1106-1113, Sep 2023, doi: 10.1038/s41563-023-01620-2.
- [8] S. T. Konakanchi et al., "Electrically Tunable Picosecondscale Octupole Fluctuations in Chiral Antiferromagnets," arXiv preprint arXiv:2501.18978, 2025.



20 40 60 80 100 $H_{ax(y)}$ (mT)

(a)

20 40 60 80 100

 $H_{ax(y)}$ (mT)

(b)

^{*} Best Student Presentation Finalist / LB - Late-breaking Poster

EC-05. Synchronization of spin transfer torque oscillators via magnetoelastic interactions

E. Savostin^{1, 2}, V. Lomakin^{3, 2, 1}

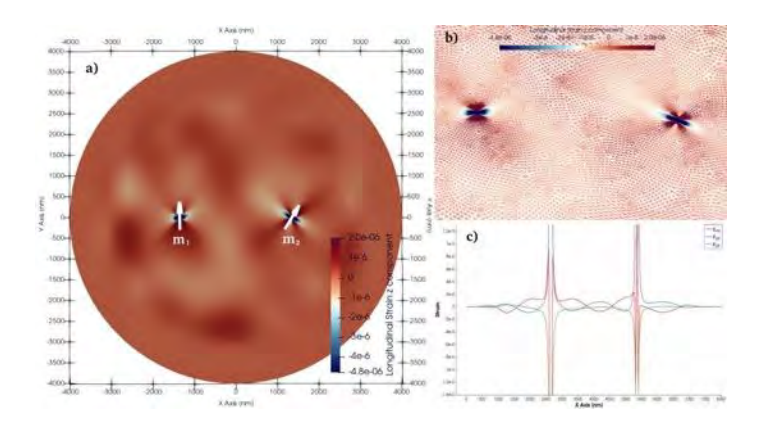
¹Program in Materials Science and Engineering, University of California San Diego, San Diego, California, United States, ²Center for Memory and Recording Research, University of California San Diego, San Diego, California, United States, ³Department of Electrical and Computer Engineering, , University of California San Diego, San Diego, California, United States

Spin-torque transfer oscillators (STTOs) are nanoscale spintronic devices capable of generating high-frequency magnetization dynamics through sustained spin-transfer torque. Synchronization of multiple STTOs is a key requirement for enhancing output power, narrowing spectral linewidths, and enabling neuromorphic and microwave signal-processing applications. In this work, we demonstrate a novel mechanism for STTO synchronization mediated by magnetoelastic interactions. We consider a structure where two or three STTOs, each of 40 nm radius, are embedded within a 3 nm-thick ferromagnetic film and separated by distances corresponding to one or one-half the acoustic wavelength in the material.

Using the theory of magnetoelasticity in cubic ferromagnets, we show that oscillating magnetization generates spatially non-uniform strain fields, which propagate through the medium and act back on other oscillators via the inverse magnetostrictive effect. This two-way coupling leads to spontaneous phase-locking of the STTOs. We employ finite element method (FEM) simulations to model both the spin dynamics and elastic wave propagation in the multilayer structure. Our simulations show that both in-phase and phase-shifted synchronization regimes can be obtained, depending on the relative spin current strengths and oscillator separation.

The results demonstrate that elastic fields can mediate long-range, tunable, and robust synchronization of STTOs without requiring direct magnetic or electrical coupling. This work opens a pathway toward scalable, mechanically connected spintronic networks for neuromorphic computing and high-coherence on-chip microwave sources. Ai, F., & Lomakin, V. (2024). Spin-wave assisted synchronization in 2D arrays of spin torque oscillators (arXiv:2408.11343). arXiv. https://doi.org/10.48550/arXiv.2408.11343

A. Slavin and V. Tiberkevich, "Nonlinear Auto-Oscillator Theory of Microwave Generation by Spin-Polarized Current," in *IEEE Transactions on Magnetics*, vol. 45, no. 4, pp. 1875-1918, April 2009, doi: 10.1109/TMAG.2008.2009935.



EC-06. Wave equation formulation for spin wave propagation in thin magnetic films

K. Rivkin

RKMAG Corporation, Pacific Grove, California, United States

We demonstrate that for all cases involving saturated thin magnetic films, including in-plane and out-of-plane configurations, the Walker equation can be transformed into the Helmholtz wave equation. Therefore, mathematical description of spin wave propagation becomes very similar to that of optical waves, given a specific definition of magnetic refractive index, whose value is determined first and foremost by the non-uniformity of magnetic properties such as external bias field, saturation magnetization and so on.

We compare micromagnetic results with those obtained by solving the wave equation in both linear and non-linear regimes, concluding there is a near perfect match between the two, except a set of cases where both the wavelength of a spin wave and thickness of magnetic material are comparable to the exchange length and some of the basic assumptions behind the magnetostatic approach are no longer valid. We demonstrate how the definition of magnetic refractive index can be altered in order to avoid the resulting divergence from micromagnetic results. Of special interest is the non-linear component of the refractive index, which under most circumstances increases with the spin wave amplitude, leading to a self focusing like phenomena.

EC-07. Temperature and Thickness Dependence of Gilbert Damping in CoFe thin films: Atomistic Study

P. Sharma¹, E. Sampson², G. Luepke¹
¹Applied Science, William and Mary, Williamsburg, Virginia, United States, ²Physics, William and Mary, Williamsburg, Virginia, United States

Engineering Gilbert damping in metallic ferromagnets is key for enhancing the next-generation spintronic devices for applications like magnetic memory, spin-torque oscillators, and ultrafast switching. Gilbert damping helps in quantifying the energy relaxation rate of the magnetization precession. The higher value leads to the faster relaxation rate to equilibrium which enhances the magnetic switching, and ultrafast dynamics. Conversely, lower value of the damping is essential in energy efficiency, spin-wave propagation and so on. As a result, understanding the effects of several other parameters on the Gilbert damping parameter is crucial. CoFe thin films are one of the potential candidates with low gilbert damping, high magnetic moment, excellent interfacial compatibility, and high spin polarization. Previous studies on CoFe films have explored Gilbert damping by varying alloy composition, impurity levels, strain relaxation, defects, and magnetization orientation^{1,2}. However, the investigation of the effects of film thickness and temperature on the damping parameter remains unexplored in terms of atomistic understanding. In this study, we investigated the temperature and thickness dependence of the Gilbert damping parameter (α) in CoFe thin films with MgO layer and with emphasis on both bulk and interfacial damping using an atomistic spin dynamics (ASD) framework. ASD simulations are driven by the interatomic exchange interactions and other important parameters involved which were derived from the density functional theory (DFT) calculations enabling accurate modeling of magnetization relaxation. The strong dependence of the effective damping parameter for film thickness was observed. This work provides atomistic insight into the physical origin of the damping parameter in ultrathin films.

- 1. Yi Li, et.al. Phys. Rev. Letters 122, 117203 (2019)
- 2. H. Xia, et. al. Phys. Rev. B 104, 024404 (2021)

EC-08. Machine Learning Force-Field Models for Large-Scale Dynamical Simulations of Itinerant Electron Magnets

<u>G. Chern</u>¹, S. Zhang¹, Y. Fan¹, K. Shimizu²
¹Physics, University of Virginia, Charlottesville, Virginia, United States, ²RIKEN Center for Emergent Matter Science, Saitama, Japan

Itinerant frustrated magnets, governed by electronmediated spin-spin interactions, often exhibit intricate noncollinear and non-coplanar spin textures. Among these, magnetic vortices and skyrmions are particularly notable for their fundamental importance in magnetism and their potential applications in spintronics [1]. Accurate dynamical modeling of such complex spin structures in itinerant systems poses significant computational challenges. Crucially, the local effective magnetic fields -- analogous to interatomic forces in molecular dynamics -- originate from exchange interactions mediated by itinerant electrons and must therefore be computed quantum mechanically. As a result, dynamical simulations require solving the electronic structure problem for each instantaneous spin configuration at every time step. Repeated evaluation of these quantum forces can render large-scale LLG simulations computationally prohibitive.

Here we present a machine-learning (ML) force-field framework for LLG dynamics simulations of itinerant electron magnets, with an emphasis on the general theory and implementation of symmetry-invariant representations of spin configurations. The linear scalability of our ML approach relies fundamentally on the locality principle, which in our case means the magnetic field acting on a local spin depends predominantly on its immediate neighborhood; as summarized in Fig. 1. A deep-learning neural network (NN) model is developed to encode the complicated dependence of the exchange field on the neighborhood spin configurations [2-5], an architecture similar to those pioneered in ML-based ab initio molecular dynamics methods [5,6]. An efficient magnetic descriptor is presented based on group-theoretical bispectrum method for incorporating the spin-rotation and lattice point-group symmetries into the ML models. We show that LLG simulations driven by local fields predicted by trained ML models accurately reproduce characteristic non-collinear spin textures, including the 120\$^\circ\$ order, tetrahedral order, and skyrmion crystal phases on the triangular lattice. Our work highlights the promising potential of ML models for large-scale spin dynamics of itinerant magnets.

[1] U. K. Roßler, A. N. Bogdanov, and C. Pfleiderer, Nature Vol. 442, 797 (2006).

[2] P. Zhang, G.-W. Chern, Phys. Rev. Lett. 127, 146401 (2021).

[3] P. Zhang, G.-W. Chern, npj Computational Materials 9, 32 (2023).

[4] X. Cheng, S. Zhang, P. C. H. Nguyen, S. Azarfar, G.-W. Chern, and S. S. Baek, Phys. Rev. Research 5, 033188 (2023). [5] Y. Fan, S. Zhang, and G.-W. Chern, Phys. Rev. B 110, 245105 (2024).

[6] J. Behler and M. Parrinello, Phys. Rev. Lett. 98, 146401 (2007).

[7] A. P. Bartok, M. C. Payne, R. Kondor, and G. Csanyi, Phys. Rev. Lett. 104, 136403 (2010).

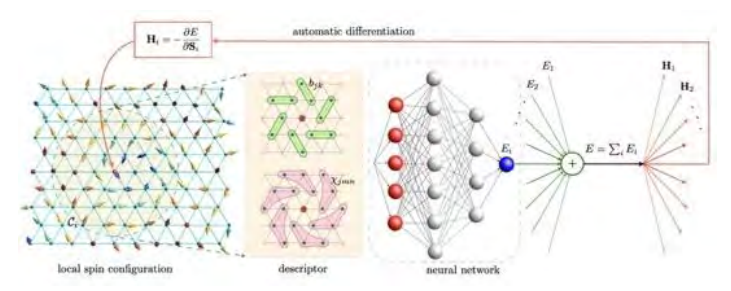


Fig. 1

EC-11. Micromagnetic Simulations of Magnon-Phonon Coupling Dynamics

<u>F. Millo</u>¹, A. Sharma¹, D. Stoeffler², J. Duquesne¹, P. Rovillain¹, M. Marangolo¹

¹Physics, Sorbonne University, Paris, Ile-de-France, France, ²Physics, Strasbourg University, Strasbourg, France

Recently, the coupling between magnons and phonons has been intensively studied in different types of geometries for various spintronic applications. The magnon-phonon coupling is possible by two phenomena called magnetoelasticity and magnetorotation, where the former links the elastic degrees of freedom with magnetization dynamics [1] and the latter links the lattice rotations that phonons cause to the shape anisotropy of the magnetic film [2, 3]. Experimental and theoretical calculations have been performed for thin magnetic films deposited on top of a piezoelectric substrate where certain limitations are imposed into the magnetoelastic (F_{mel}) and magnetorotation (F_{mrot}) energy terms. However, no micromagnetic simulations have been shown so far to incorporate these two phenomena altogether.

In this talk, we will demonstrate that our micromagnetic simulations (mumax3 [4]) of magnon-phonon coupling

dynamics reflects the experimental measurements performed in Fe/GaAs [5] and CoFeB/LiNbO $_3$ [6] geometries. We implemented the additional energy density:

 $F_{mel+mrot} = (B_{\mu\nu}\epsilon_{\mu\nu} - \mu_0 M^2 \omega_{\mu\nu}) m_{\mu} m_{\nu}$

where μ,ν are dummy indices representing coordinates; $B_{\mu\nu}$ [Jm⁻³] are the magnetoelastic constants; μ_0 [Hm⁻¹] is the free magnetic permeability; M_s [Am⁻¹] is the saturation magnetization; m_μ are the reduced magnetization vector elements; $\epsilon_{\mu\nu}$ is the symmetric strain tensor and $\omega_{\mu\nu}$ is the skew-symmetric lattice rotation tensor.

In a nutshell, we will show that the magnon-phonon coupling dynamics is well described by our modified mumax3 version when the above additional energy density term is taken into consideration. The present approach serves as a step forward to a better comprehension of the magnon-phonon coupling dynamics.

Acknowledgements

The authors acknowledge the French National Research Agency (ANR) under contract No ANR-22-CE24-0025 (SACOUMAD).

[1] C. Kittel., Phys. Rev., 1958, vol. 110, 836-841.

[2] S. Maekawa et al., *AIP Conference Proceedings*, 1976, *vol.* 29, pp. 542–543.

[3] M. Xu et al., Sci. Adv., 2020, vol. 6, p. eabb1724.

[4] A. Vansteenkiste et al., AIP Advances, 2013, vol. 4, p.107133.

[5] P. Rovillain et al., *Phys. Rev. Applied*, 2022, *vol. 18*, p. 064043.

[6] F. Millo et al., AIP Advances 15, 045230 (2025)

EC-12. Micromagnetic modelling and simulation of inertial spin waves in ferromagnetic nanodots

M. d'Aquino, <u>S. Perna</u>, C. Serpico Department of Electrical Engineering and Information Technology, University of Naples Federico II, Naples, Italy

The study of ultra-fast magnetization processes is a central issue in spin dynamics for its potential application to future generations of nanomagnetic and spintronic devices[1]. In the last decades, after the pioneering experiment[2] revealing subpicosecond spin dynamics, the investigation of ultra-fast magnetization processes has increasingly attracted the attention of many research groups stimulating the production of considerable research. The advent of intense high-frequency magnetic field sources has recently allowed for the direct detection of non-thermal, ultrafast

magnetization processes in the THz range, which made it possible to demonstrate the spin nutation in ferromagnets experimentally[3] and thereby confirm the presence of inertial effects in magnetization dynamics theoretically predicted several years ago[4]. From the theoretical point of view, inertial magnetization dynamics can be modeled by augmenting the classical Landau-Lifshitz-Gilbert (LLG) precessional dynamics with a torque term taking into account angular momentum relaxation[3,4] proportional to the second time- derivative of magnetization. Such a torque transforms the classical LLG equation into a wave-like equation, meaning that inertia leads to wave propagation phenomena with finite speed. In particular, when magnetic systems of nano- and micro-scale are considered, the issue of the emergence of inertial spin waves oscillating at THz frequency arises. In this paper, by combining analytical theory and full micromagnetic simulations of inertial LLG (iLLG) dynamics, we demonstrate the possibility to excite ultra-short inertial spin waves (see Fig. 1) that propagate with finite speed in a confined ferromagnetic nanodot[5]. The nanodot is driven by the action of THz fields with amplitude similar to those achievable with state-of-the art THz experimental setups.

This work is supported by Italian Ministry of University and Research, PRIN2020 funding program, Grant No. 2020PY8KTC.

- [1] B. Dieny et al., Nature Electronics 3, 446 (2020).
- [2] E. Beaurepaire et al., Physical Review Letters 76, 4250 (1996).
- [3] K. Neeraj et al., Nature Physics 17, 245 (2021).
- [4] M.-C. Ciornei et al., Physical Review B 83, 020410 (2011).
- [5] M. d'Aquino et al., Physical Review B 107 (14), 144412 (2023).

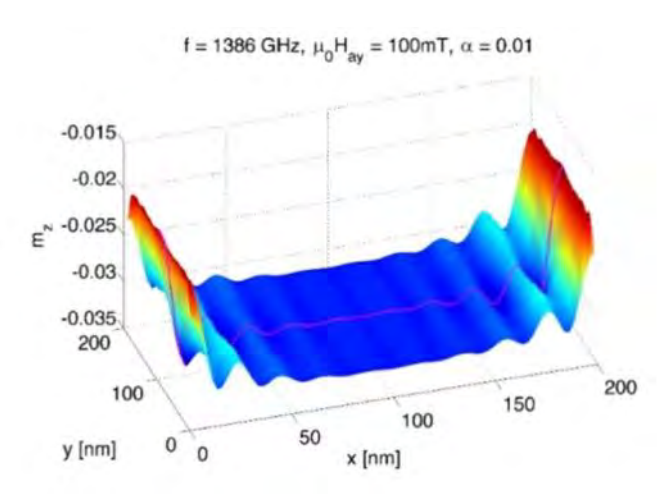


Figure 1: Snapshot of steady-state out-of-plane ac magnetization response (normalized by saturation magnetization) at driving frequency f = 1386 GHz. The color code represents the value of out-of-plane magnetization at each spatial location, ranging from minimum (blue) to maximum (red).

EC-14. Interlayer and interfacial Dzyaloshinskii-Moriya interaction in magnetic trilayers: First-principles and micromagnetic calculations

E. Y. Vedmedenko

Physics, University of Hamburg, Hamburg, Germany

We determine the Dzyaloshinskii-Moriya interaction within and between two magnetic cobalt layers separated by a nonmagnetic spacer through ab initio calculations. We investigate different materials for the nonmagnetic layer, focusing on the experimentally realized Co/Ag/Co system [1,2]. We compare the resulting interactions with the Levy-Fert model and observe a good overall agreement between the model and the ab initio calculations for the dependence on the atomic positions. Additionally, we derive a formula for the strength of the interlayer isotropic exchange interaction depending on the position of the atoms in the nonmagnetic layer and compare it to the first-principles results.

It will also be shown how the IL-DMI changes the magnetic order and FMR-signal within the magnetic planes [3]. The combination of the described phenomena opens up new avenues for the design of three-dimensional race-tracks combining IF- and IL-DMI and paves the way for enhancements of the DMI strength.

[1] J. A. Arregi, P. Riego, A. Berger, and <u>E.Y. Vedmedenko</u>, Nature Commun. 14, 6927 (2023).

[2] T. Matties, L. Rózsa, L. Szunyogh, R. Wiesendanger, and E. Y. Vedmedenko, Phys. Rev. Research 6, 043158 (2024).

[3] <u>E. Y. Vedmedenko</u> and M. Kostylev, Phys. Rev. Appl. 23, 014047 (2025).

SESSION ED: SPIN-CHARGE INTERCONVERSION AND MAGNETOTRANSPORT

Chair(s): M. H. Guimaraes, *University of Groningen, Groningen, Netherlands*Thursday, October 30, 2025
08:30 AM-12:00 PM
Ballroom B

ED-01. Advancing Transistors via Spin-to-Charge Current Conversion in 3D and 2D Ferroelectric Chalcogenides C. Rinaldi

Physics, Politecnico di Milano, Milano, Italy

By 2040, information and communication technology will absorb more than 50% of the electrical energy produced yearly. Devices and architectures beyond the traditional CMOS transistor are needed for electronics to switch greener. A remarkable pathway was suggested by Intel in the work titled "Beyond CMOS computing with spin and polarization" [1]. Spin-based logic-in-memory devices might be the next-generation computing paradigm. The non-volatility of ferroic materials is energetically beneficial, and the information processing through spin Hall [2] or Rashba-Edelstein effects conveniently scales with the geometrical dimension of the device, increasing with the packing densities. However, the performance of existing prototypes is nowadays far from applications [3], indicating the need for further material development.

Ferroelectric Rashba semiconductors such as germanium telluride (GeTe) offer an intrinsic link of ferroelectricity and Rashba-type spin-orbit coupling [4]. As a major consequence, the ferroelectric polarization of epitaxial thin films of GeTe can be reliably switched back and forth by electrical gating and used to reverse the sizeable spin-to-charge conversion by the spin Hall effect [5]. We discuss doping and alloying strategies in germanium telluride as promising routes to tailor ferroelectricity, electrical conductivity, electronic band structure, and spin-to-charge current conversion. We present the development of scalable, energy-efficient, and non-volatile ferroelectric

spin-orbit logic devices, in which information is stored in the ferroelectric state and processed through polarizationdependent spin-to-charge conversion. Finally, we outline future perspectives in the field, focusing on emerging 2D chalcogenides such as tellurene and GeTe-rich GeTe-SbTe lamellae we recently investigated [6].

GeTe and related compounds may represent a viable path towards spintronic-based transistors with ultralow power consumption, facilitated by the monolithic integrability with silicon.

- [1] S. Manipatruni et al., Nature Physics 14, 338 (2018)
- [2] V. T. Pham et al., Nature Electronics 3, 309 (2020)
- [3] D. C. Vaz et al., Nature Communications 15, 1902 (2024)
- [4] C. Rinaldi et al., Nano Letters, 18, 2751 (2018)
- [5] S. Varotto, C. Rinaldi *et al.*, Nature Electronics 4, 740 (2021)
- [6] S. Cecchi, C. Rinaldi *et al.*, Advanced Science 11, 2304785 (2024)

ED-02. Orbital-to-Spin Conversion Material Exploration for Improving SOT-MTJ Performances

M. Biagi¹, C. C. Capriata¹, L. Hutin², B. Viala², R. Sousa¹, K. Garello¹

¹SPINTEC, CEA, Grenoble, Isere, France, ²Leti, CEA, Grenoble, Isere, France

SOT-MRAM technology is currently based on Heavy Metals (HM) with large resistivity [1]. However, recently predicted orbital effects [2] could offer the possibility to integrate lighter elements with lower resisivity, potentially reducing the power consumption and/or increasing the efficiency of SOT-MRAM devices. This work aims to clarify whether orbital-to-spin conversion mechanisms can be regarded as a promising solution for improving current SOT-MRAM technology. In this talk, I report the results of our study on the characterization of various orbital/HM/FeCoB material systems. In this conversion scheme, an orbital source material is topped by a heavy metal, which acts as an "active" conversion layer capable of both converting orbital currents and generating spin currents to control the magnetization of the ferromagnet. I systematically quantify the damping-like efficiency by harmonic Hall voltage methods [3] in both as-deposited and annealed systems, varying the thickness of the HM and/or the orbital source (e.g., Ru-based system in Fig. 1). I compare the results to reference HM/FeCoB bilayer, and I discuss the impact of the orbital layer insertion and annealing on the efficiency. In

addition, I tentatively separate the spin and orbital contributions in the orbital samples by means of a simple current distribution model. The distinct behaviors of the HMs employed as conversion layer are also discussed. Finally, I present the application of the best orbital material solutions to fabricate 3-terminal SOT-MTJ devices, demonstrating proof-of-concept switching using orbital torques in sub-ns regime (e.g. for Ru-based system in Fig. 2), and benchmarking their performances against standard SOT material systems.

- [1] Viola Krizakova et al., Journal of Magnetism and Magnetic Materials, 562, 169692 (2022)
- [2] Dongwook Go et al., Physical Review Letters, 121, 086602 (2018)
- [3] Kevin Garello, et al., Nature Nanotechnology, 8, 587 593 (2013).

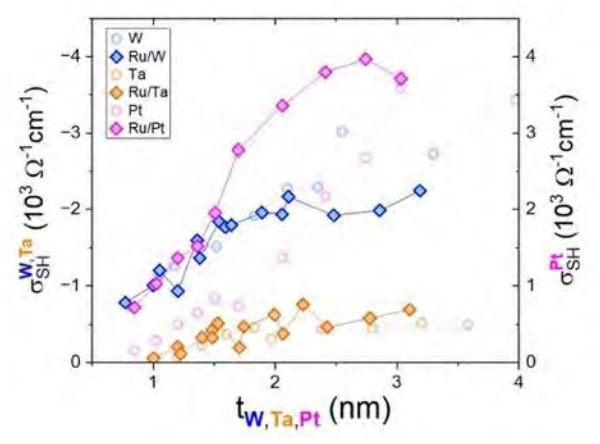


Fig. 1 Spin Hall conductivity as a function of Heavy Metal (HM) layer thickness for Ru(3)/HM/FeCoB orbital systems compared to reference HM/FeCoB systems.

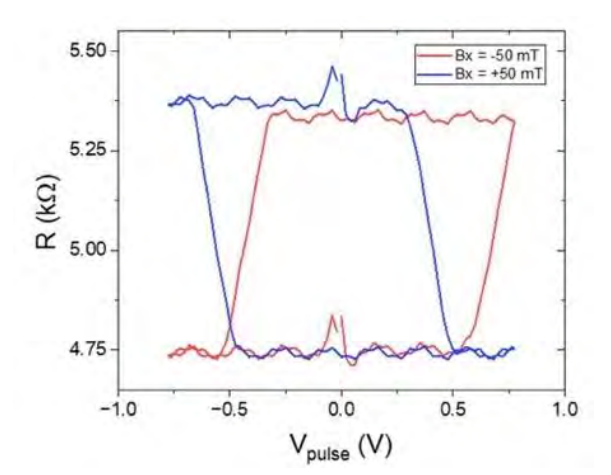


Fig. 2 Sub-ns swiching for Ru(3)/W(1.5) 3-terminal SOT-MTJ device for 0.5 ns pulse width..

ED-04. Interfacial orbital transmission and mechanical torque in metals

C. Sun, A. Manchon

Aix-Marseille Université, CNRS, CINaM, Marseille, France

Orbital transport in metals has attracted significant attention lately [1]. Whereas experimental evidence of orbital transport continues to accumulate, the propagation of the orbital moment in metals remains poorly understood. Indeed, most models so far focus on the orbital transport properties in the bulk of metals (e.g., [2]), disregarding the orbital transmission at interfaces. Such a transmission coefficient is crucial to develop phenomenological models of orbital torque and interpret experiments [3]. We theoretically study the transmission of the orbital current across a metallic interface using a model Hamiltonian with spherical crystal field, (L.k)², adapted to t_{2a} orbitals close to Γ point [4]. It is found that when the orbital moment is injected in the metal, it strongly oscillates due to its interaction with the crystal field, generating a quadrupolar moment, and reduces to a constant value away from the interface. The orbital transmission, oscillation period, and long-range value all vanish upon increasing the crystal field. It is interesting to emphasize that, contrary to spin, the oscillation of the orbital moment is not similar to spin precession: e.g., the oscillation of L_x is not accompanied by the creation of L_{v,z} components, but rather by the creation of the $\{L_v, L_z\}$ quadrupole. The penetration of the orbital moment into the metallic layer induces a mechanical torque that is computed by solving the continuity equation of the orbital transport.

- [1] Go et al., Orbitronics: Orbital currents in solids, Europhys. Lett. 135, 37001 (2021).
- [2] Xiaobai Ning, A. Pezo, Kyoung-Whan Kim, Weisheng Zhao, Kyung-Jin Lee, Aurelien Manchon, Orbital diffusion, polarization, and swapping in centrosymmetric metals, Physical Review Letters 134, 026303 (2025).
- [3] Xiaobai Ning, Henri Jaffrès, Weisheng Zhao, Aurélien Manchon, Phenomenology of orbital torque, pumping, and mixing conductance in metallic bilayers, arXiv:2412.08340.
- [4] Chi Sun, Aurelien Manchon, unpublished.

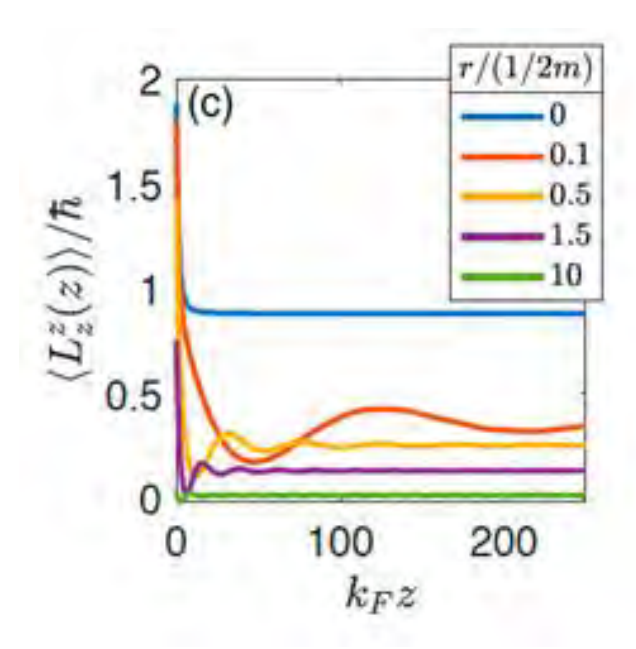


Figure 1: Profile of the orbital moment penetrating the metallic layer for different crystal field parameter values (r).

ED-05. Anisotropic orbital Hall effect in an epitaxial titanium

S. Karube¹, Y. Yahaqi², Y. Saito³, R. Hisatomi¹, Y. Shiota¹, T. Ono1

¹Kyoto University, Uji, Kyoto, Japan, ²NEC corporation, Minatoku, Tokyo, Japan, ³Tohoku University, Sendai, Miyagi, Japan

In recent years, it has been theoretically suggested that orbital angular momentum can be transported in solids[1], and numerous experimental reports have followed[2,3]. The flow of orbital angular momentum is termed "orbital current," and the phenomenon that generates it is the "orbital Hall effect." Unlike the spin Hall effect, the conversion of charge current to orbital current is a nonrelativistic effect not requiring spin-orbit interaction. Supporting this, finite orbital Hall angles have been reported even in materials with weak spin-orbit coupling, such as 3d transition metals[2-4]. However, most experimental studies have used polycrystalline metals, with little investigation into the role of band structure or crystal orientation in epitaxial films.

In this context, we used epitaxial Ti thin films with specific crystal orientations to explore the orbital Hall effect, leveraging the negligible spin-orbit interaction in Ti to isolate the orbital contribution. We epitaxially grew Ti(1100) films on sapphire M-plane substrates and deposited polycrystalline Ni to detect orbital torque. Harmonic Hall measurements were performed at room temperature. In the Ti(1-100) plane, applying an electric field along the [0001] and [0010] directions yielded damping-like torque efficiencies of different magnitudes (Fig. 1). These results qualitatively match theoretical predictions of orbital Hall conductivity anisotropy and reflect the underlying band structure (Fig. 2). Based on this anisotropy, we conducted additional experiments on magnetization reversal driven by orbital torque and successfully detected differences in reversal current density. We discuss these orbital Hallrelated phenomena in epitaxial Ti in detail. This work was supported by the JSPS KAKENHI (JP24H00030) and the JST PRESTO (JPMJPR22B4).

[1] B. A. Bernevig et al, Phys. Rev. Lett. 95, (2005) 066601.

[2] Y. -G. Choi et al, Nature 619, (2024) 52.

[3] H. Hayashi et al, Commun. Phys. 6, (2023) 32.

[4] L. Salemi et al, Phys. Rev. Mater. 6, (2022) 095001.

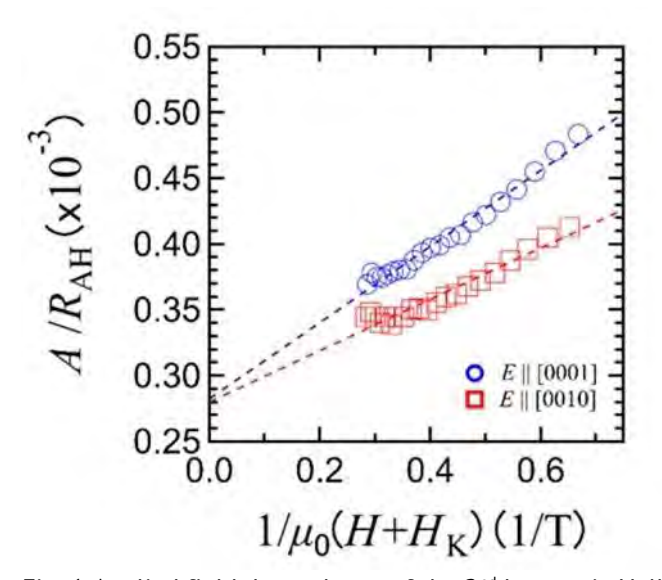


Fig. 1 Applied field dependence of the 2nd harmonic Hall resistance A relating to damping-like torque and thermal contribution divided by anomalous Hall resistance R_{AH} .

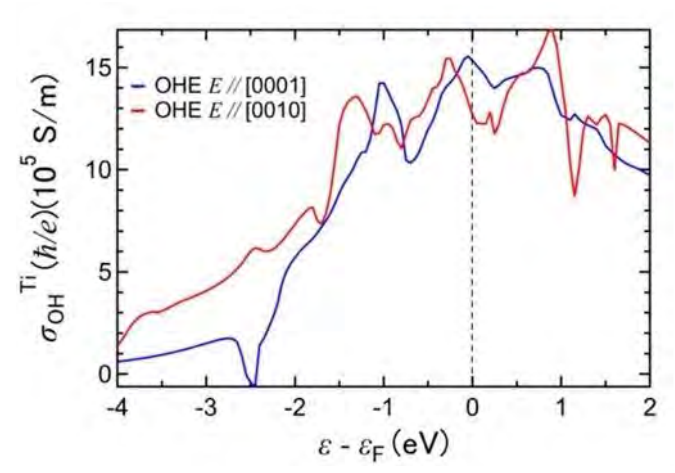


Fig. 2 Calculated orbital Hall conductivity as a function of electron energy based on Fermi energy.

ED-06. Absence of large spin-charge conversion in Bi₁₋ _xSb_x alloys

R. Zhang, W. Lin

Key Laboratory of Quantum Materials and Devices of Ministry of Education, School of Physics, Southeast University, Nanjing, China

Large spin Hall conductivity is calculated in Bi_{100-x}Sb_x alloys [1] and spin Hall angle as large as 52 has been experimentally reported [2]. However, most experiments are in the hertostructures with magnetic metals, where spurious effects of charge current may dominate [3,4]. We deposited Bi and $Bi_{100-x}Sb_x$ alloy layers by dc and rf magnetron sputtering onto ferrimagnetic insulator Y₃Fe₅O₁₂ (YIG). Two types of YIG substrates were used: 0.5-mm-thick polycrystalline YIG slab and 5-µm-thick single crystalline YIG(111) film grown by liquid-phase-epitaxy on GGG(111) substrates. X-ray diffraction indicates (012) and (003) texture in the Bi and $Bi_{100-x}Sb_x$ films. We show that spin current is thermally injected into the Bi_{100-x}Sb_x layer via the longitudinal spin Seebeck effect in YIG, without complications from charge currents. The spin diffusion length of Bi_{100-x}Sb_x alloy increases with Sb concentration. Notably, the inverse spin Hall voltage is not detectable in all the Bi and Bi_{100-x}Sb_x alloys, indicating negligibly small spin Hall angle (< 10⁻⁴), in contrast to those results of large spin Hall angle with magnetic metals. Despite of large spinorbit coupling in Bi and Bi_{100-x}Sb_x alloys, the problem of spin-charge conversion in such materials need more serious theory investigation.

[1] C. Sahin and M. E. Flatté, Phys. Rev. Lett. 114, 107201 (2015).

[2] N. H. D. Khang, Y. Ueda and P. N. Hai, Nat. Mater. 17, 808 (2018).

[3] D. Yue, W. Lin, J. Li, et al, Phys. Rev. Lett. 121, 037201 (2018).

[4] D. Yue, W. Lin, and C. L. Chien, Appl. Phys. Lett. 9, 050904 (2021).

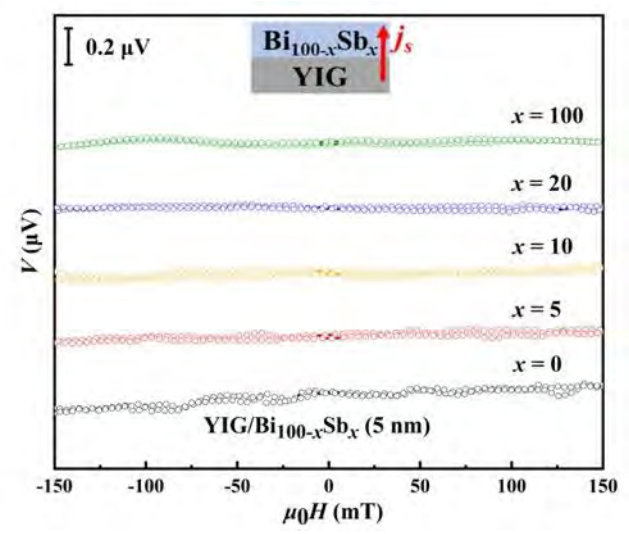


Fig.1 Field dependence of transverse voltage in the $YIG/Bi_{100-x}Sb_x(5 \text{ nm})$ with various Sb concentrations.

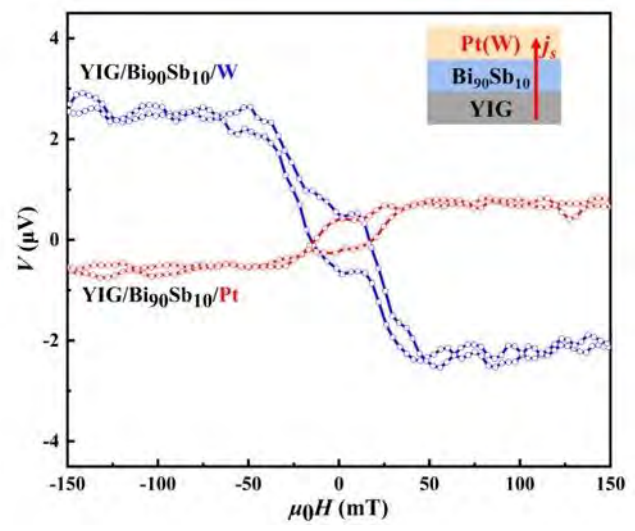


Fig.2 Field dependence of transverse voltage in YIG/Bi $_{90}$ Sb $_{10}$ (2 nm)/Pt(3 nm) and YIG/Bi $_{90}$ Sb $_{10}$ (2 nm)/W(3 nm)

ED-07. Antiferromagnetic spin dynamics revealed by effective magnetization increase on exchange-coupled ferromagnet

C. Gonzalez-Fuentes¹, P. Landeros², J. W. Gonzalez³, S. Oyarzún⁴, R. Rodriguez¹, R. Gallardo²

¹Instituto de Física, Pontificia Universidad Católica de Chile, Santiago, RM, Chile, ²Departamento de Física, Universidad Técnica Federico Santa Maria, Valparaiso, V, Chile, ³Departamento de Física, Universidad de Antofagasta, Antofagasta, Antofagasta, Chile, ⁴Departamento de Física, Universidad de Santiago, Santiago, RM, Chile

We made a broadband ferromagnetic resonance (FMR) study of strong and weak exchange-coupled IrMn $_3$ /NiFe bilayers varyng the IrMn $_3$ layer thickness t_{AF} between 0 and 4.5 nm, mapping the effective magnetization M_{eff} and rotatable anisotropy field (H_{ra}) across the paramagnetic to antiferromagnetic phase transition.

We found a 4.5% increase of the $M_{\rm eff}$ value upon the formation of antiferromagnetic (AF) order on IrMn₃ without change in the volumetric magnetic moment of NiFe as shown in Fig. 1. Theoretical calculations show that this is a dynamical effect arises from the FMR mode's hybridization with the AF layer's lowest resonance mode (Fig. 2 inset). Overall, $M_{\rm eff}$ follows a linear relation with the interfacial exchange between NiFe and IrMn₃ as shown in Fig. 2, resembling but having the opposite effect than interface perpendicular magnetic anisotropy on FMR dynamics.

Our findings reveal that $M_{\rm eff}$ is a more specific indicator of antiferromagnetic excitations on FMR when compared to the homogeneous resonance field shift effects, such as magneto-crytalline anisotropies and non-zero out-of-plane magnon wavevector.

We believe our findings will substantially benefit exploring antiferromagnetic materials with the widely accessible FMR technique.

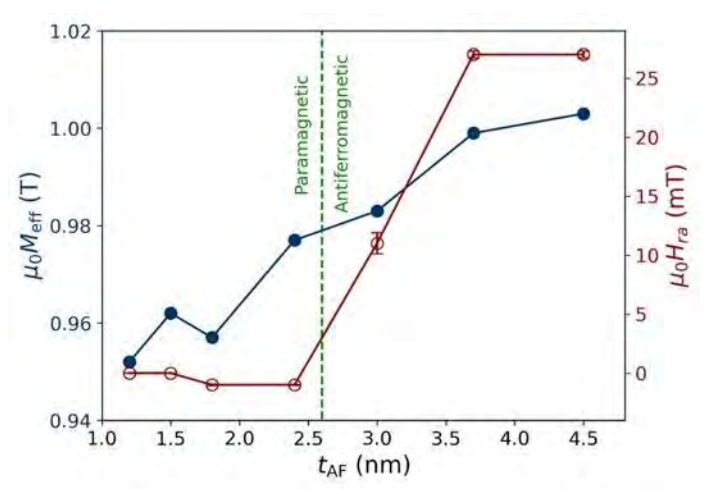


Figure 1 M_{eff} and H_{ra} variation across the paramagnetic to antiferromagnetic phase transition of IrMn₃

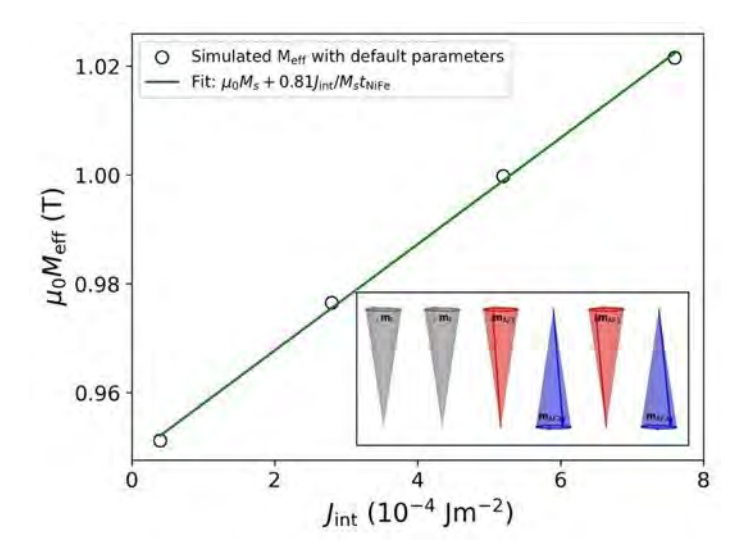


Figure 2 Simulated $M_{\rm eff}$ value vs $J_{\rm int}$ for a NiFe/IrMn₃ bilayer. Inset: schematic of the near-interface spin oscillations for the fundamental eigenmode of the AF/FM thin film system.

ED-08. Field-free spin-orbit torque switching via spinreorientation in synthetic antiferromagnets

<u>B. Jamshed</u>, M. Ramu, D. Kumar, H. Rahaman, S. Das, S. Piramanayagam

School of Mathematics and Physics, Nanyang Technological University, Singapore, Singapore, Singapore

Spin-orbit torque (SOT) driven magnetization switching offers an energy-efficient method for electrical control of magnetization, making it a promising candidate for nextgeneration non-volatile memory and spin logic applications. However, conventional SOT devices with a perpendicular magnetic anisotropy require an in-plane magnetic field to break inversion symmetry, which hinders device scalability and increases power consumption, limiting their practicality for mass fabrication. In this study, we have demonstrated field-free magnetization switching of a ferromagnet by utilizing spin re-orientation, obtained via synthetic antiferromagnetic (SAF) coupling. By tuning the thickness of one of the ferromagnetic layer (single layer Co) in SAF structure, we effectively modified the exchange coupling and its magnetic anisotropy, facilitating spin re-orientation. We observed spin re-orientation until Co thickness of 2.8 nm, which appears to be a large value for spin reorientation. We observed a maximum switching efficiency of 82% in our optimized samples for a Co thickness of 2.4 nm. We performed angular-dependent anomalous Hall measurements to further explore the origin of field-free switching in our sample. This study highlights an interesting strategy for achieving field-free switching in SAF samples through spin reorientation.

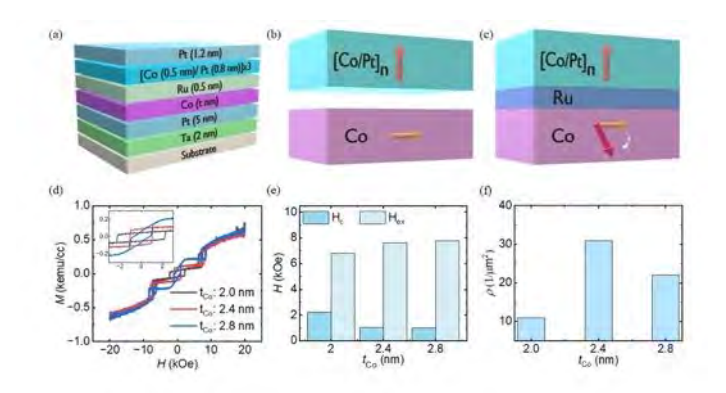


Fig. 1

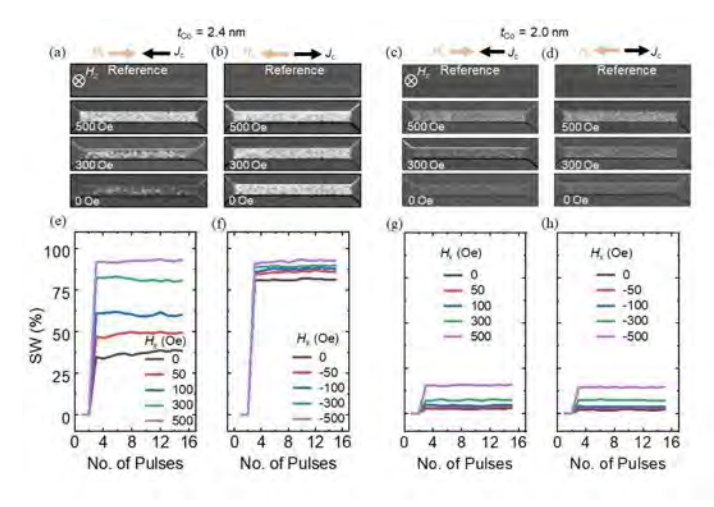


Fig. 2

ED-09. Distortion-Aware Magnetic Symmetry Groups: A Versatile Framework for Identifying Altermagnets and Predicting their Unconventional Properties

M. D. Kitcher, B. Lee, G. Beach

Materials Science and Engineering, Massachusetts Institute of Technology, Cambridge, Massachusetts, United States

Altermagnetism is a newly defined phase of collinear magnetism which exhibits both crystal-compensated magnetic order and non-relativistic spin splitting [1]. In altermagnets, crystallographic rotations connect opposite spin sublattices, separating them from antiferromagnets and ferromagnets under the spin group classification scheme [2]. While their unique symmetry permits non-relativistic piezomagnetism that is odd in the Néel vector (N) [3], other altermagnetic properties of interest, such as the odd-in-N anomalous Hall effect, are mediated by spin-orbit coupling (SOC) [4]. Consequently, the symmetries of such effects must be determined using the magnetic point groups (MPGs), which do not differentiate between altermagnetic and purely relativistic phenomena [5]. Moreover, the prerequisite breaking of time-translation (*Tt*) and parity-time (PT) symmetries is usually provided by an alternating local crystal environment which also modulates the altermagnetic properties [3, 5]. In this presentation, we introduce a new symmetry-driven approach to describing altermagnetism, leveraging a recently developed symmetry formalism [6] which accounts for the presence of distortions in a crystal with respect to a parent structure. By assigning a distortion-aware magnetic point group (DA-MPG) to a material, we can determine if it hosts a nonrelativistic coupling between antiferromagnetic order and staggered

distortions that breaks both *Tt-* and *PT-*symmetries. Moreover, we can use DA-MPGs to predict the symmetries of SOC-mediated altermagnetic properties in a material and distinguish them from purely relativistic effects based on their symmetry-allowed couplings with the distortions. We discuss a case study in which our framework predicts the presence of altermagnetic order parameters—as well as their associated SOC-mediated effects—that scale linearly with the corresponding distortions of the non-magnetic atoms. Our work provides valuable insights into the nature of altermagnetism and the distinction between altermagnetic and purely relativistic phenomena in the presence of SOC. Furthermore, this study demonstrates that DA-MPGs are powerful tools for designing, identifying, and characterizing altermagnets.

- 1. Šmejkal, L. et al., *Phys. Rev. X* 12, 040501
- 2. Šmejkal, L. et al., *Phys. Rev. X* 12, 031042
- 3. Bhowal, S. and Spaldin, N., Phys. Rev. X 14, 011019
- 4. Gonzalez Betancourt, R.D. et al., *Phys. Rev. Lett.* 130, 036702
- 5. Šmejkal, L. et al., *Sci. Adv.* 6, eaaz8809(2020)
- 6. VanLeeuwen, B., Gopalan, V., *Nat. Commun.* 6, 8818 (2015).

ED-10. Observation of D'yakonov-Perel'-type Magnon Spin Relaxation in Uniaxial Antiferromagnetic Insulators

Q. Gao^{1,4}, A. Cong², B. Liang³, M. Yang¹, J. Liu¹, S. Wu³, K. Shen², J<u>. Li</u>¹

¹Southern University of Science and Technology, Shenzhen, China, ²Beijing Normal University, Beijing, China, ³Fudan University, Shanghai, China, ⁴Quantum Science Center of Guangdong–Hong Kong–Macao Greater Bay Area (Guangdong), Shenzhen, China

Long-distance transport of magnon spin currents in antiferromagnetic (AFM) insulators is essential for the development of magnonics [1-3], however, their relaxation mechanisms remain elusive. Here, we report that the D'yakonov-Perel'-type magnon spin relaxation mechanism governs the spin current transport in two prototypical uniaxial AFM insulators, Cr_2O_3 and alpha-Fe₂O₃. Three key pieces of evidence will be presented. (1) An over 450% enhancement of the first-harmonic non-local resistance induced by a magnetic field is observed prior to the spin-flop transition, which cannot be fitted by an established magnon-gap-closure model but is well-interpreted by our model incorporating D'yakonov-Perel'-type magnon spin

relaxation. (2) We find that the magnon spin diffusion length in Cr_2O_3 increases by 35% at 35 K, from 0.63 micrometer at zero magnetic field to 0.85 micrometer above 1.00 Tesla, consistent with the D'yakonov-Perel'-type magnon spin relaxation model. (3) Temperature dependence of the zero-field magnon spin diffusion length in both AFM insulators can be qualitatively explained very well through our model. This work presents a promising approach to effectively control magnon spin relaxation, paving the way for applications that leverage long-distance spin current transport in AFM insulators.

- [1] L. J. Cornelissen, et al., Nat. Phys. 11, 1022 (2015).
- [2] R. Lebrun, et al., Nature 561, 222 (2018).
- [3] DK. de Wal, et al., Phys. Rev. B 107, L180403 (2023).

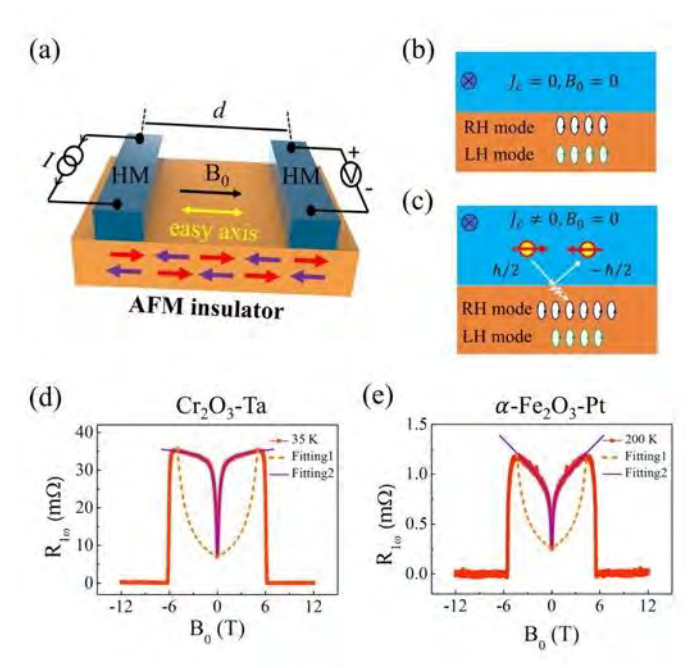


Fig. 1. (a) Schematic of the measurement setup. HM represents heavy metal. (b) and (c) Magnon population beneath the spin current injector in the absence (b) and presence (c) of a charge current at zero magnetic fields. (d) and (e) First-harmonic non-local resistance in the Cr_2O_3 -Ta device at 35 K (d) and the alpha- Fe_2O_3 -Pt sample at 200 K (e).

ED-11. Disentangling thermal contributions to the spin-orbit torque switching of a chiral antiferromagnet

<u>T. Matsuo</u>^{4,1}, T. Higo^{4,2,3}, H. Tsai⁴, D. Nishio-Hamane⁴, T. Matsuda⁵, K. Kondou⁵, S. Miwa⁴, Y. Otani^{4,6}, S. Nakatsuji^{4,1,7}
¹Johns Hopkins University, Baltimore, Maryland, United States, ²JST-PRESTO, Tokyo, Japan, ³Keio University, Yokohama, Japan, ⁴The University of Tokyo, Tokyo, Japan, ⁵Osaka University, Osaka, Japan, ⁶RIKEN, Saitama, Japan, ⁷CIFAR, Toronto, Ontario, Canada

The switching of noncollinear antiferromagnetic order by spin-orbit torque (SOT), most extensively studied in the Weyl antiferromagnet Mn₃Sn [1-6], is promising for future spintronics applications due to the promise of magnetic random-access memory (MRAM) that can be operated at terahertz timescales. Two distinct SOT switching mechanisms have been identified in previous studies: an intrinsic mechanism where the magnetic dynamics are directly induced by the SOT [5, 6]; and a temperatureassisted mechanism where the switching phenomenon is triggered by first raising the antiferromagnet close to its Neel temperature, then cooling it under a finite SOT [3, 4]. These two mechanisms have important implications for applicability in memory storage: it is theoretically predicted that the intrinsic mechanism can achieve switching on the picosecond timescale by relying on the terahertz order antiferromagnetic dynamics [2], while the temperatureassisted limits the speed required for switching to timescales characteristic of the heating and cooling of the device, which can be limited to tens of nanoseconds or longer depending on the device size [3,4, 7]. As such, a required condition for antiferromagnetic SOT-MRAM is that switching must be achieved via an intrinsic mechanism. Therefore, one must be able to distinguish the specific mechanism under which an antiferromagnetic system is switched by SOT. In this study, we prepare Mn₃Sn/Ta/AlO_x heterostructures grown on Si/SiO₂ substrates where the amount of Joule heating during switching is controlled by the sample dimensions. Through a systematic comparison of these devices, we discuss the conditions under which switching under an intrinsic mechanism can be achieved as well as how to identify the mechanism responsible for SOT switching.

- [1] Nakatsuji, Kiyohara, Higo. *Nature* 527, 212-215 (2015)
- [2] Tsai, Higo et al. Nature 580, 608-613 (2020)
- [3] Pal et al. Sci. Adv. 8, eabo5930 (2022)
- [4] Krishnaswamy et al. Phys. Rev. Appl. 18, 024064 (2022)
- [5] Higo, Kondou et al. Nature 607, 474-479 (2022)

- [6] Yoon et al. Nat. Mater. 22, 1106-1113 (2023)
- [7] Yoo et al. APL Mater. 12, 081107 (2024)

ED-13. Chiral Magnets

R. Winkler^{1, 2}, U. Zülicke³

¹Physics, Northern Illinois University, DeKalb, Illinois, United States, ²Materials Science Division, Argonne National Laboratory, Lemont, Illinois, United States, ³School of Chemical and Physical Sciences, Victoria University of Wellington, Wellington, New Zealand

We discuss a new class of magnetic systems, chiral magnets [1]. Ordinarily, one speaks of chirality when a system exists in two versions (enantiomorphs) that are mirror images of each other and are not superposable by any rotation. The lack of mirror symmetries is then synonymous with noninvariance under improper rotations iC, where i denotes spatial inversion and C a proper rotation. Discussing also asymmetry with respect to improper rotations involving time inversion ϑ , which are of the form ϑC and $i\vartheta C$, we obtain the complete set of enantiomorphisms embodied in the 122 magnetic crystal classes. In addition to the usual kind, which we call electrochirality because it arises from the interplay of electric multipolar order, we identify magnetochirality and antimagnetochirality as new categories of chirality characterized by two distinct enantiomorphs. Multichiral systems also exist, where improper rotations iC, ∂C and $i\partial C$ each map the system onto a distinct enantiomorph, yielding four distinct enantiomorphs. Finally, parachiral systems can always be mapped onto each other by improper rotations of the form iC, ∂C and $i\partial C$, i.e., they do not support distinct enantiomorphs. The five categories of chirality identified here yield a complete classification where any physical system belongs to exactly one category.

As an example, Figs. 1 and 2 show α -Fe₂O₃ and Cr₂O₃, which are both variations of the corundum structure. α -Fe₂O₃ in Fig. 1 is magnetochiral (and altermagnetic); the enantiomorphs are invariant under iC, but not under ∂C and $i\partial C$, as illustrated in the upper part of the figure. Cr₂O₃ is antimagnetochiral, invariant only under $i\partial C$.

We discuss implications of our classification for magnetically ordered systems and identify the distinct nonreciprocal phenomena associated with each category. [1] R. Winkler and U. Zülicke, Standard model of

electromagnetism and chirality in crystals (2024), arxiv:2405.20940.

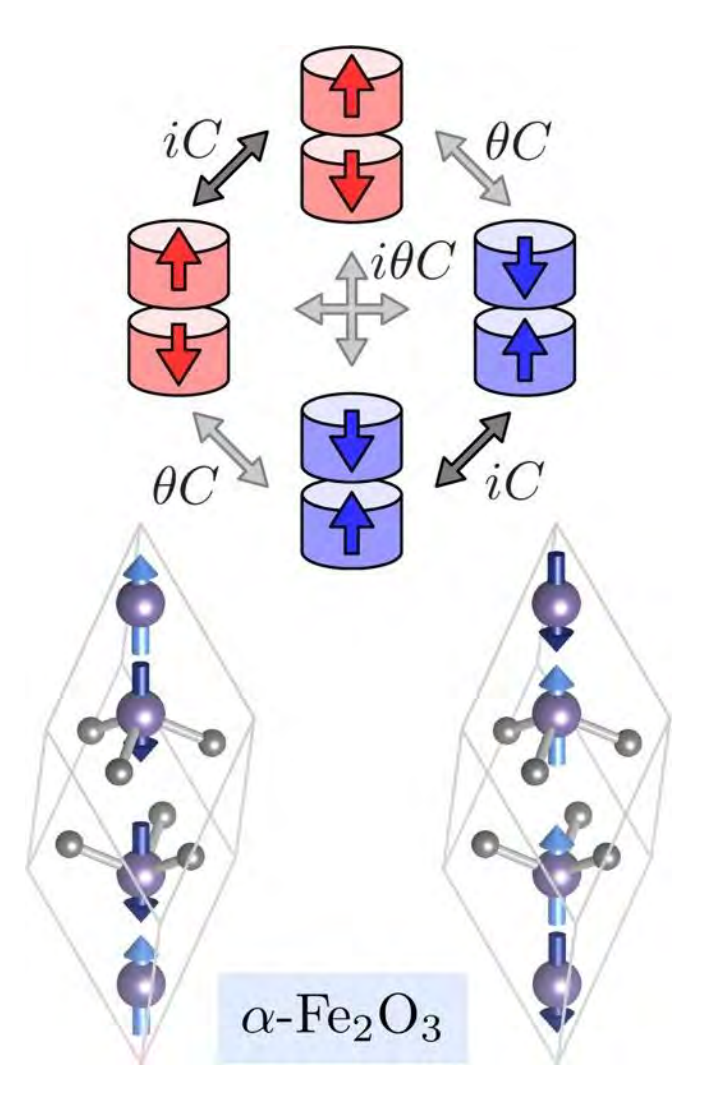


Fig. 1: The enantiomorphs of magnetochiral altermagnetic α -Fe₂O₃ are invariant under iC, but mapped onto each other under ∂C and $i\partial C$, see upper part.

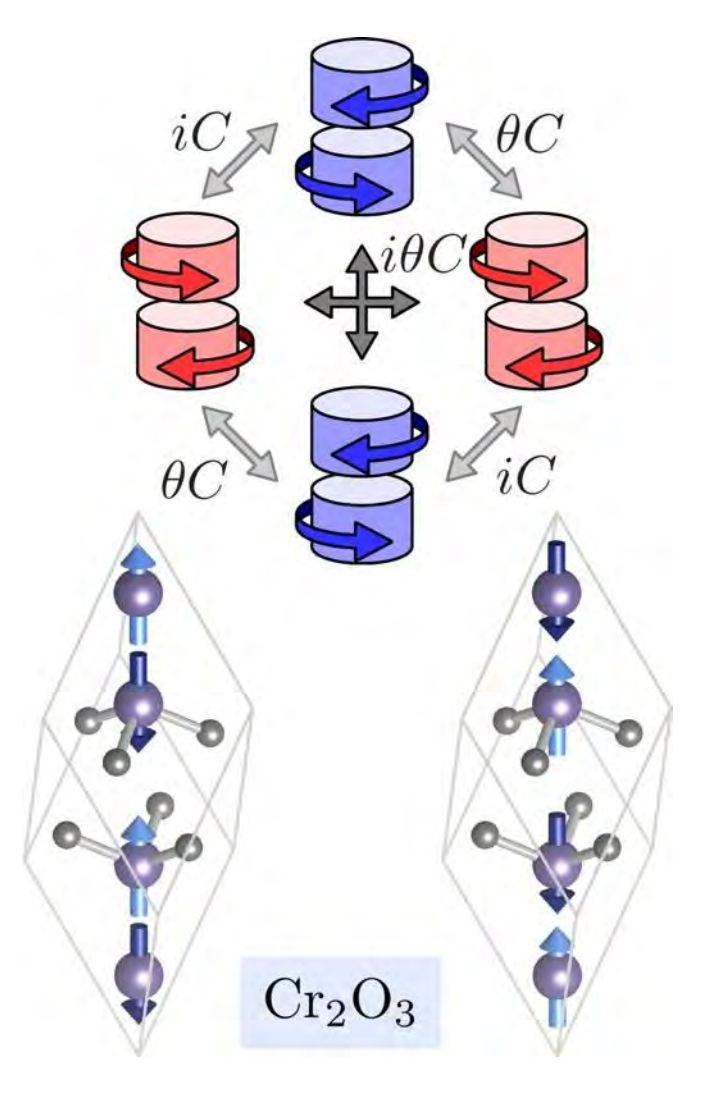


Fig. 2: The enantiomorphs of antimagnetochiral Cr_2O_3 are invariant under $i\partial C$, but mapped onto each other under iC and ∂C , see upper part.

SESSION EE: MAGNONICS II: CRYSTALS & DEVICES

Chair(s): R. Hertel, *Insitut de Physique et Chimie des Matériaux de Strasbourg, Centre National de la Recherche Scientifique*,

Strasbourg, France
Thursday, October 30, 2025
08:30 AM-12:00 PM
Room 2DE

EE-02. Magnon-magnon interaction stimulated by the vertical dynamic coupling in a hybrid magnonic crystal

R. Sultana¹, M. T. Kaffash¹, G. Gubbiotti², Y. Ji¹, B. Jungfleisch¹, F. Montoncello³

¹Department of Physics and Astronomy, University of Delaware, Newark, DE 19716, Delaware, United States, ²CNR-Istituto Officina dei Materiali (IOM), Unità di Perugia, Perugia I-06123, Italy, ³Department of Physics and Earth Sciences, University of Ferrara, Ferrara I-44121, Italy

We present a joint experimental and numerical investigation of the spin-wave properties in a hybrid magnonic crystal [1] consisting of CoFeB artificial spin ice (ASI) made of elliptical macrospins deposited onto a NiFe film, with a 5 nm nonmagnetic Al₂O₃ spacer. Brillouin light scattering (BLS) was exploited to measure the applied field and wavevector frequency dependence of the spin dynamics to highlight the role of interlayer dipolar coupling [2,3]. Experimental results were interpreted by micromagnetic simulations. We demonstrate that the contrast in saturation magnetization M_S enhances the strength of a dynamic coupling between the ASI edge modes and the film backward modes at different wavelengths. This leads to a distinct, remarkable hybridization, which was predicted in the simulations and detected in the BLS experiments as a triplet in the spectra. Such a magnon-magnon interaction was found to be robust with respect to wide magnetic field variations. Figure 1 shows the anti-Stokes side of the BLS spectra for the CoFeB ASI sample compared to the ASI/Al₂O₃/NiFe-film hybrid one: a single broad peak (due to two modes, the simulated profile of which is shown at the bottom of panel (b)) becomes a triplet in the hybrid structure (three simulated modes in the top of panel (b)). The effect is not only shown with reference to the dispersion relation at a fixed applied field, but also as a function of the applied field, in the frequency-field curves, encompassing the whole field range of the hysteresis cycle. This thorough study allows to characterize the dynamic coupling in its diverse aspects, demonstrating that the ability to engineer and manipulate spin-waves through ASI configurations opens new avenues, as magnonic

waveguides of new conception, and the development of advanced magnon-spintronic technologies, with promising applications in computing, communication, and signal processing.

[1] G. Gubbiotti, Three-Dimensional Magnonics: Layered, Micro- and Nanostructures (Jenny Stanford Publishing, Singapore, 2019)

https://www.jennystanford.com/9789814800730/three-dimensional-magnonics/.

- [2] R. Negrello, F. Montoncello, M. T. Kaffash, M. B. Jungfleisch, and G. Gubbiotti, APL Materials 10, 091115 (2022).
- [3] F. Montoncello, M. T. Kaffash, H. Carfagno, M. F. Doty, G. Gubbiotti, and M. B. Jungfleisch, J. Appl. Phys. 133, 083901 (2023).

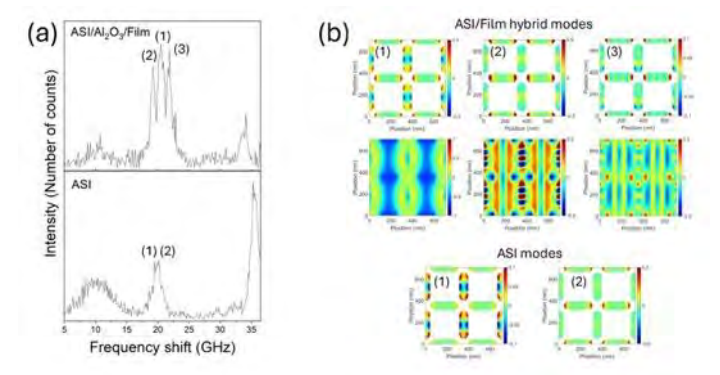


Fig. 1: (a) BLS spectra showing the splitting of an ASI peak into three peaks in the hybrid structure. (b) Simulated modes profiles: isolated ASI modes involved in the hybridization (bottom), forming the single unresolved peak in the BLS spectra; triplet of ASI/film hybrid modes (top) corresponding to the triplet in the spectra.

EE-03. Scalable and Programmable Spin Hall Nano-Oscillator Networks: From Phase-Tunable Synchronization to Networks of 100,000 nano-oscillators

A. Kumar^{1,2}, A. Chaurasiya¹, V. Gonzalez¹, N. Behera¹, R. Khymyn¹, A. A. Awad^{1,2}, J. Akerman^{1,2}
¹Department of Physics, University of Gothenburg, Gothenburg, Sweden, ²RIEC and CSIS, Tohoku University, Japan, Sendai, Japan

The mutual synchronization of spintronic oscillators is a powerful phenomenon. It not only enhances the spectral performance of these devices for wireless communication and signal processing but also opens new opportunities for

early demonstrations using spin torque nano-oscillators (STNOs) in nanopillar and nanocontact geometries confirmed synchronization feasibility, scalability has remained limited to a maximum of eight oscillators [1,2]. primarily due to challenges in achieving controllable coupling and scalable interconnectivity. In this work, we report significant advances using nanoconstriction spin Hall nano-oscillators (NC-SHNOs), which provide a scalable, programmable, and CMOScompatible platform for building massively interconnected oscillator networks. SHNOs employ simple heavymetal/ferromagnet (HM/FM) bilayers and utilize spin-orbit torques (SOTs) to drive persistent magnetization autooscillations. Thanks to in-plane current flow and easy nanofabrication, they allow precise tuning of frequency with applied current, magnetic field, and device geometry. Previously, our group demonstrated mutual synchronization of NC-SHNOs in one-dimensional chains and twodimensional arrays, but the number of synchronized oscillators was limited due to restricted coupling control and considerable thermal dissipation [3,4]. Interestingly, SHNOs with perpendicular magnetic anisotropy (PMA), particularly in W/CoFeB/MqO trilayers, now enable the generation and manipulation of propagating spin waves (PSWs), which can act as a natural carrier of phase information over micrometer distances [5]. In the present work, we first demonstrate a robust variablephase mutual synchronization in SHNOs mediated by PSWs [6]. Electrical measurements and phase-resolved µ-BLS confirm that SHNO pairs can synchronize in both in-phase and anti-phase modes, tunable via applied field angle and current. Constructive and destructive interference patterns in the power spectral density (Fig. 1) directly reflect coherent PSW-mediated coupling. This level of phase control is absent in in-plane magnetized systems (W/NiFe), underscoring the advantage of the generation of PSWs in PMA-based SHNOs. Micromagnetic simulations further reveal that the dispersion characteristics of the emitted PSWs are critical to understanding the observed phase behavior and their control.

unconventional computing and energy harvesting [1]. While

Building on this, we have successfully scaled SHNO arrays to over 100,000 synchronized oscillators [7] using high-SOT W-Ta/CoFeB/MgO multilayers patterned into sub-20-nm NCs [8]. These densely packed networks yield an output power exceeding 9 nW and a quality factor greater than one million. Moreover, they exhibit long-range coherence and collective dynamics suitable for wave-based computing paradigms such as reservoir computing and Ising machines.

Importantly, the SHNO platform supports additional modes of individual tunability through voltage-controlled magnetic anisotropy (VCMA) and memristive gating, offering spatially localized and energy-efficient control over individual oscillators, an essential capability for truly programmable hardware.

Through a combination of experimental innovation and modeling, our results position SHNO networks as a strong candidate for next-generation spintronic systems, capable of solving complex computational problems and generating highly coherent microwave signals. The ability to control synchronization phase and scale beyond 100,000 oscillators marks a new benchmark in the field.

- [1] A. Kumar *et al.*, Book: Nanomagnets as Dynamical Systems: Physics and Applications, pp 143-182 (2024) [2] R. Sharma et al., Nature Communications 12, 2924 (2021).
- [3] A. A. Awad *et al.*; Nature Physics 13, 292 (2017). & A. Kumar *et al.*; Nano Letters 23, 6720 (2023).
- [4] M. Zahedinejad *et al.*; Nature Nanotechnology 15, 47 (2020).
- [5] H. Fulara et al., Science Advances 5 (9), eaax8467 (2019).
- [6] A. Kumar et al.; Nature Physics 21, 245-252 (2025).
- [7] N. Behera, A. K. Chaurasiya, A. Kumar *et al.*, arxiv 2501.18321 (2025).
- [8] N. Behera et al., Advanced Materials 36, 2305002 (2024).

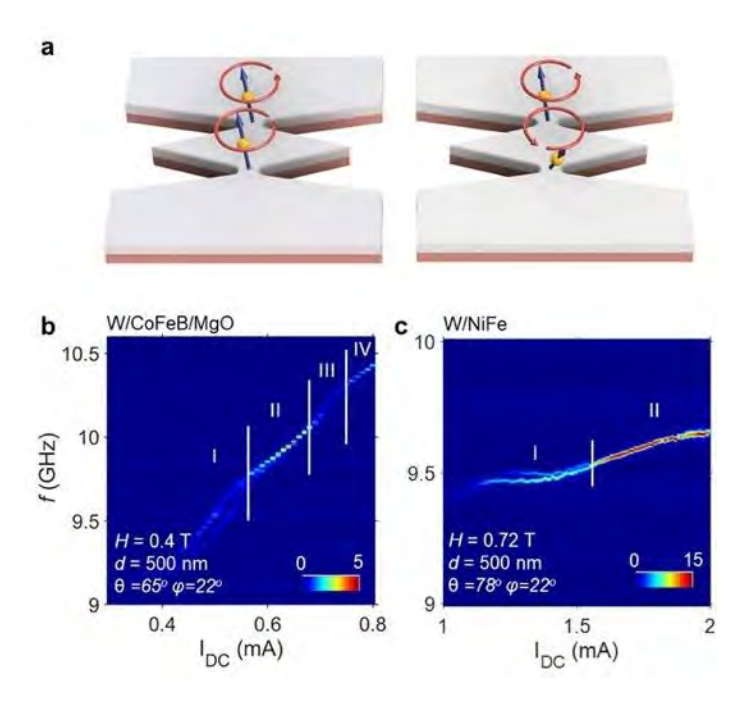


Figure 1. (a) Schematic of in-phase and out-of-phase mutual

synchronization between two NC-SHNOs. Power spectral density as a function of applied current (I_{DC}) for two mutually synchronized NC-SHNOs fabricated using (b) PMA based W/CoFeB/MgO thin films and (c) in-plane magnetized W/NiFe thin films.

EE-04. Strong coupling between spin waves and microwave photons in a superconducting resonator

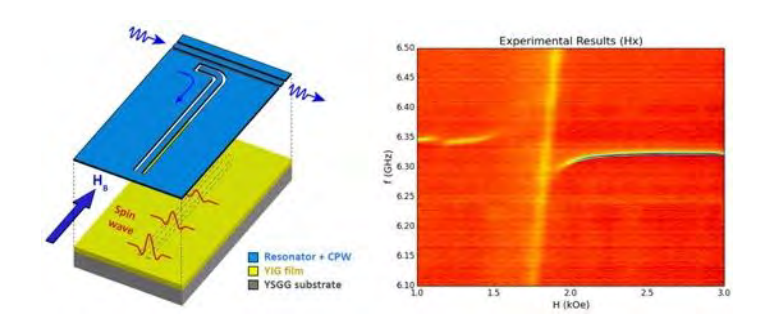
Y. Li¹, J. Lim², T. Polakovic³, C. Kiehl^{1,4}, R. Divan⁵, U. Welp¹, C. Phatak¹, J. Zuo², A. Hoffmann², V. Novosad¹

¹Materials Science Division, Argonne National Laboratory, LEMONT, Illinois, United States, ²Materials Science Engineering, University of Illinois at Urbana Champaign, Urbana, Illinois, United States, ³Physics Division, Argonne National Laboratory, LEMONT, Illinois, United States, ⁴Physics Department, Carthage College, Kenosha, Wisconsin, United States, ⁵Center for Nanoscale Materials, Argonne National Laboratory, LEMONT, Illinois, United States

Hybrid magnonic systems have recently emerged as a new promising direction that exploits the advantages of magnon excitations for processing quantum information [1]. In particular, propagating spin waves demonstrate intrinsic nonreciprocity and wavelength matching to optical light. The unique properties of spin waves make them potential for implementing on-chip microwave isolators and microwave-to-optic transducers with a major benefit of frequency tunability by magnetic field. In this work, we develop a novel hybrid magnonic system with superconducting resonators directly fabricated on top of yttrium iron garnet (YIG) films to achieve coherent coupling with spatially nonuniform spin waves. The YIG films are grown on Y3Sc2Ga3O12 (YSGG) substrate, which eliminates rare-earth elements compared with the commonly used Gd3Ga5O12 (GGG) substrate and thus exhibit zero magnetism at cryogenic temperature [2]. This is crucial for achieving high quality factor for the superconducting resonator fabricated on top. With this new hybrid system, we demonstrate strong coupling between spin waves in the YIG film and photons of the resonator. The small antenna width of the superconducting resonator down to 500 nm allows us to coherently couple to the spatially nonuniform spin wave modes, with a frequency shift from the uniform mode matching well with the width of the antenna and eventually the wavelength of the spin waves. Our results provide a new circuit platform for integrating propagating magnonics with cryogenic superconducting quantum circuits and developing future quantum magnonic

functionality with spin wave engineering.

Work at Argonne and UIUC was supported by the U.S. DOE, Office of Science, Basic Energy Sciences, Materials Sciences and Engineering Division under contract No. DE-SC0022060. Use of the Center for Nanoscale Materials (CNM), an Office of Science user facility, was supported by the U.S. Department of Energy, Office of Science, Office of Basic Energy Sciences, under Contract no. DE-AC02-06CH11357.



Left: schematic of NbN nanowire resonator fabricated on a YIG/YSGG film. Right: mode anticrossing between spin waves and microwave photons of the superconducting resonator.

EE-05. Experimental Observation of Magnetic Rogue Waves K. H. McAllister¹, M. Copus¹, C. Abbott¹, M. Elo², J. Netzer², E. Iacocca¹, R. E. Camley¹, D. A. Bozhko¹

¹Department of Physics and Energy Science, University of Colorado Colorado Springs, Colorado Springs, Colorado, United States, ²Tabor Electronics, Inc., Nesher, Israel

Rogue waves (RWs) are large-amplitude waves localized in time and space and appearing from an incoherent background. Since their discovery in the ocean, RWs have been studied in many systems. In a laboratory setting, RWs have been produced by a time-reversal process, e.g., in water [1, 2]. In contrast to water, magnetic systems lack time-reversal symmetry, and the possibility of creating magnetic RWs through time reversal had been previously studied only theoretically [3-6].

Here we present the first experimental observation of 2D magnetic rogue waves (MRWs), formed in a spin-wave environment [3-6]. The experiment is performed in a 13 μ m-thick film of single-crystal Yttrium Iron Garnet (YIG) magnetized out-of-plane to ensure isotropic forward volume wave geometry. The excitation and recordings necessary for the time-reversal method were performed by means of a near-field microwave scanning microscope (Fig. 1). The

number of recording antennas was limited to four, located in the corners of the sample. After the reversed-in-time recorded waveforms are played back, the distinct peak forms at the location of the initial excitation (Fig. 2). Additionally, we demonstrate that MRWs could be created at an arbitrary location on the film. The observed localization of the MRWs is limited by the range of wavelengths excitable by the antennas, as well as the limited number of excitation sources. We also discuss the transition from the linear to the nonlinear regime. Such on-demand creation of dynamic magnetization landscapes may have applications in spin-wave computing [7-8] and nonlinear spin-wave physics.

This material is based upon work supported by the National Science Foundation under Award No. DMR-2338060 as well as the Graduate Research Fellowship Program under Grant No. 1842494 (K.H.M.). This work was supported by the U.S. Department of Energy, Office of Basic Energy Sciences under Award Number DE-SC0024339 (supporting micromagnetic simulations).

- [1] A. Przadka et al., Physical Review Letters., Vol. 109, p.064501 (2012)
- [2] A. Chabchoub and M. Fink, Physical Review Letters., Vol. 112, p.124101 (2013)
- [3] M. G. Copus and R. E. Camley, Physical Review B., Vol. 102, p.220410 (2020)
- [4] X. W. Jin et al., Chaos, Solitons and Fractals., Vol. 185, p.115171 (2024)
- [5] A. V. Yurov and V. A. Yurov, Symmetry., Vol. 10, p.82 (2018)
- [6] F. Zhao et al., Annals of Physics., Vol. 327, p.2085 (2012)
- [7] A. V. Chumak et al., IEEE Transactions on Magnetics., Vol. 58, p.1 (2022)
- [8] N. Zenbaa et al., Nature Electronics., Vol. 8, p.106 (2025)

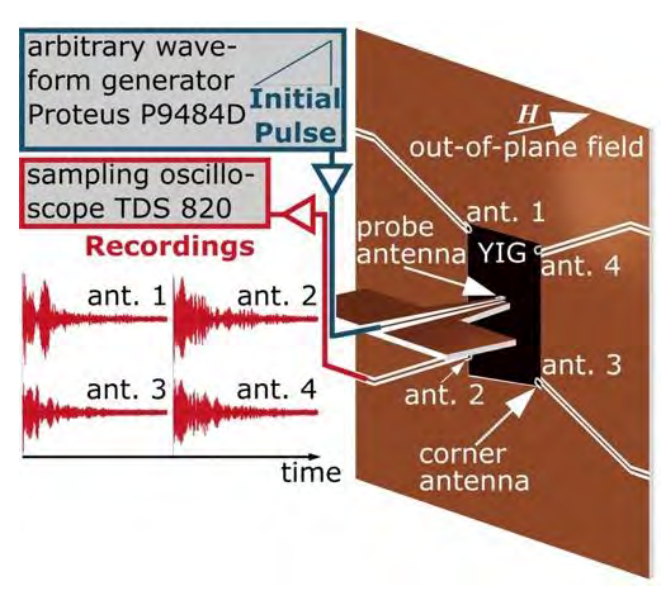


Fig. 1. Experimental setup

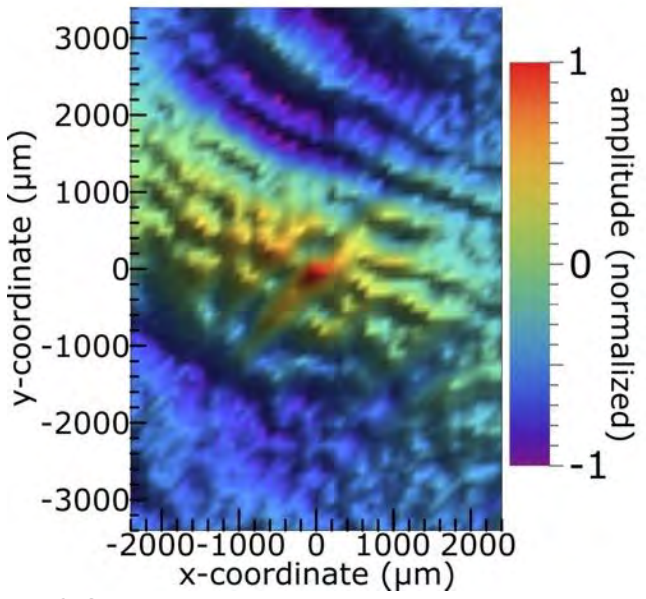


Fig. 2. Spin-wave amplitude across the sample when the MRW appears

EE-06. Monolithic magnetic MEMS integration on a magnonic device

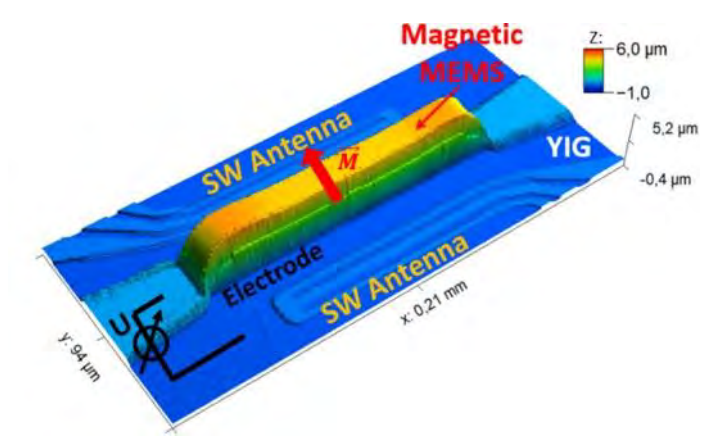
<u>S. Mantion</u>¹, R. Lebrun¹, H. Merbouche², I. Boventer¹, P. Che¹, J. Ben Youssef³, P. Bortolotti¹, P. Martins⁴, A. Anane¹
¹Laboratoire Albert Fert, CNRS, Thales, Université Paris-Saclay, Palaiseau, France, ²Service de Physique de l'État Condensé, CEA, CNRS, Université Paris-Saclay, Gif-sur-Yvette, France, ³LabSTICC, CNRS, Université de Bretagne Occidentale, Brest, France, ⁴Thales Research and Technology, Palaiseau, France

Spin waves offer several attractive properties for the development of innovative microwave devices [1], such as scalability, frequency tunability, potential non-reciprocal and non-linear behaviours. Here, we present our works towards the development of magnonic analog microwave devices. We will first present our strategy to optimize their microwave properties, taking the example of magnonic delay lines. Via a combination of analytical models [2], numerical models and measurements via propagative spin wave spectroscopy (PSWS) using Vector Network Analyzers (VNA), we can successfully optimize their frequency operation, bandwidth and insertion losses. In a second part, we present a strategy to achieve reconfigurable on-chip magnonic delay lines based on MEMS (Micro-Electro-Mechanical Systems) technology [3]. For this purpose, we developed a process allowing the monolithic integration of magnetic MEMS on a YIG delay line (Fig. 1). The magnetic MEMS membrane is suspended above the YIG delay line in the form of a "bridge". By applying a voltage between the magnetic MEMS membrane and an electrode placed onto the surface of the magnonic medium, one can move the magnetic MEMS closer to the YIG surface. The stray field experienced by the YIG is hence locally modified by a few mT, thus changing the spin wave group velocity. First characterization of such effect was performed by PSWS, effectively demonstrating propagation delay tunability (signal phase shift) with virtually zero stand-alone power (Fig. 2). Such approaches hold promising opportunities for the optimized development of reconfigurable, integrated and low-power magnonic devices.

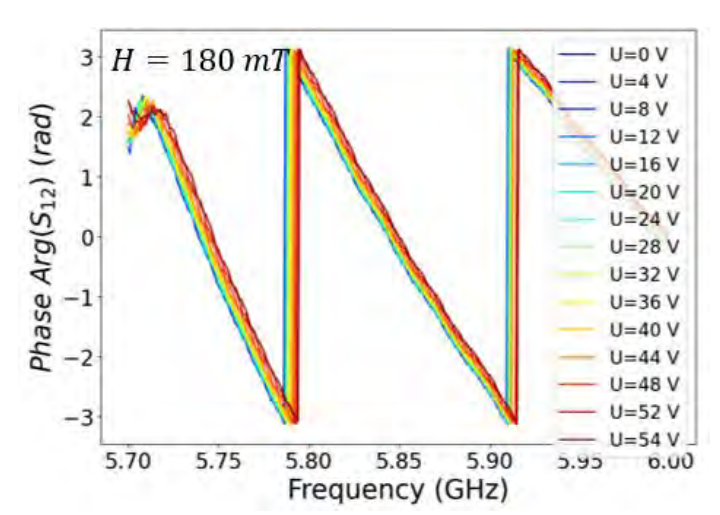
The financial fundings from the European Union's Horizon research and innovation programme under grant agreement No 101070536 (M&MEMS), and No 101070417 (SPIDER), and from a government grant operated by the French National Research Agency as part of the France 2030 program, reference ANR-22-EXSP-0004 (SWING) are

gratefully acknowledged.

- [1] A.V. Chumak, P. Kabos, M. Wu, et al. Advances in Magnetics Roadmap on Spin-Wave Computing. IEEE Transactions on Magnetics 58, 1–72 (2022)
- [2] H. Merbouche, PhD thesis. Université Paris-Saclay (2021)
- [3] F. Maspero, S. Cuccurullo, G. Pavese, et al., 2023 IEEE International Magnetic Conference Short Papers (INTERMAG Short Papers) (2023)



3D optical profilometer image of a YIG delay line combined with a suspended magnetic MEMS membrane.



VNA measurement of the phase shifted spin wave signal with applied voltages between the magnetic MEMS and the electrode (relative MEMS height displacement).

EE-07. Polarization Selective Quantum Sensing of Spin Wave

<u>E. Zhang</u>^{1, 3}, T. Zheng^{1, 3}, B. Yang^{1, 3}, S. Nallan^{1, 3}, M. Ku², J. Zhu^{1, 3}

¹Electrical and Computer Engineering, Carnegie Mellon University, Pittsburgh, Pennsylvania, United States, ²University of Delaware, Newark, Delaware, United States, ³Data Storage System Center, Carnegie Mellon University, Pittsburgh, Pennsylvania, United States

Quantum sensing based on nitrogen-vacancy (NV) centers in diamond has seen significant progress over the past decade, enabling precise magnetic field measurement at nanoscale, with broad applications across multiple disciplines. However, the inherent sensitivity to the polarization of oscillating magnetic field in the spin-triplet system has been largely ignored.

In this work, we employ an in-house-built quantum sensing magnetometry, harness the polarization-selective response of NV centers to detect circularly polarized stray fields from spin waves. Our result shows anisotropic propagation of spin wave in magnetic thin film and its unsymmetric stray field distribution near the film surface. Moreover, by introducing a reflective boundary, we demonstrate polarization selective imaging of standing spin wave through quantum sensing, representing the first direct visualization of such modes via polarization contrast. These results advance polarization-resolved quantum sensing of magnetic field, provide new insights into chiral spin-wave dynamics, and expanding the application of NV-based magnetometry to the detection of dynamic, high-frequency, and polarization-dependent magnetic phenomena.

[1] T. P. M. Alegre, C. Santori, G. Medeiros-Ribeiro, and R. G. Beausoleil, "Polarization-selective excitation of nitrogen vacancy centers in diamond", doi: 10.1103/PhysRevB.76.165205.

[2] M. Kostylev, "Non-reciprocity of dipole-exchange spin waves in thin ferromagnetic films," *J Appl Phys*, vol. 113, no. 5, 2013, doi: 10.1063/1.4789962.

[3] B. G. Simon *et al.*, "Directional Excitation of a High-Density Magnon Gas Using Coherently Driven Spin Waves," *Nano Lett*, vol. 21, no. 19, pp. 8213–8219, 2021, doi: 10.1021/acs.nanolett.1c02654.

[4] T. X. Zhou *et al.*, "A magnon scattering platform," *Proc Natl Acad Sci U S A*, vol. 118, no. 25, pp. 1–6, 2021, doi: 10.1073/pnas.2019473118.

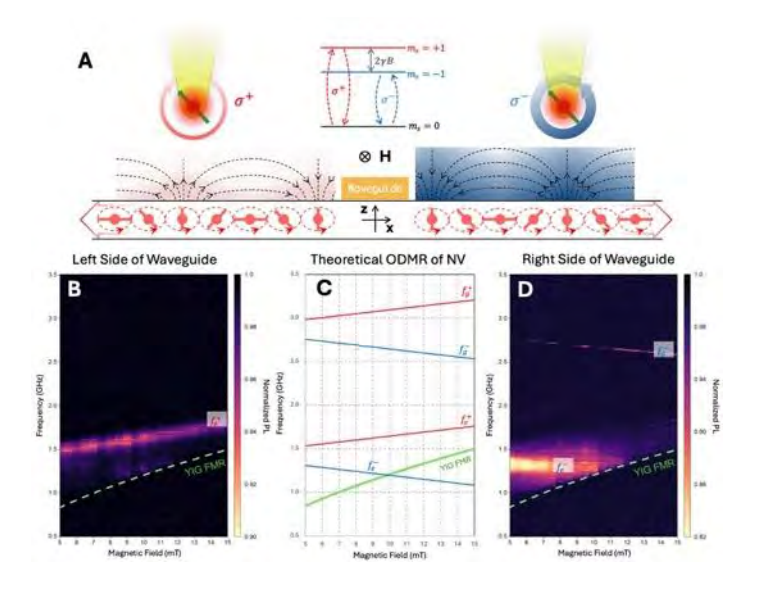


Fig. 1 Sensing circular polarized stray field from spin wave. (A) A single NV probe is positioned on the left and right side of the RF waveguide. The spin precession in the YIG film is illustrated by arrows with circles. The resulting right-handed (red) and left-handed (blue) circularly polarized stray field selectively drive NV center's ESR transitions. The inset above shows the polarization selective excitation of NV center. (B, D) ODMR spectra of the NV center when positioned on the left and right sides of the waveguide. (C) Theoretical ESR transition frequencies as a function of external magnetic field.

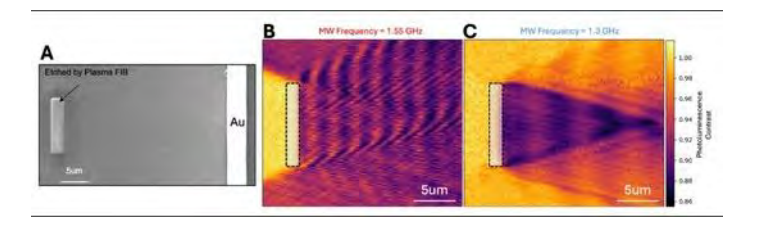


Fig. 2 Polarization selective spatial imaging of incident and reflected spin wave. (A) SEM image of the artificially created reflection boundary, defined by a rectangle region etched into the YIG film using FIB. (B-C) Spatial imaging of incident (B) and reflected (C) spin wave by tuning the RF driving frequency to match NV center's ESR transition frequencies.

EE-08. Sustained Amplification of Coherent Spin-waves by Parametric Pumping with Surface Acoustic Waves

P. Dhaqat¹, A. Jander¹, C. Rivard²

¹Electrical Engineering and Computer Science, Oregon State University, Corvallis, Oregon, United States, ²Intel Corp., Hillsboro, Oregon, United States

Devices using spin waves to carry information hold promise for application in energy-efficient computing and radio-frequency signal processing [1,2]. However, the attenuation of spin-waves has been a limitation in realizing these devices. In this work, we demonstrate the amplification of a coherent spin-wave by parametric pumping with a surface acoustic wave (SAW). A sustained gain of 6 dB is achieved with an acoustic pump power below the onset of parametric instability.

Spin and acoustic waves are generated in an yttrium-irongarnet film using transducers as shown in Fig. 1a. After passing through the SAW beam, the spin-wave is detected at an opposing transducer. Plotted in Fig. 1b is the gain in the spin-wave signal as a function of the SAW power. The gain increases with pump power of up to 10 dBm, beyond which parametric instabilities set in. Conserving momentum in the parametric interaction, a second "idler" spin-wave is generated and propagates away at a distinct angle from the signal spin-wave, to be detected at a third transducer. The idler wave confirms the parametric interaction. As expected, its strength is proportional to both the input spin-wave power and the pump power (Fig. 1c). The results shown in Fig. 1 are for 1GHz forward volume spin-waves pumped by a 2 GHz SAW at 30° angle of incidence. We present a comprehensive study of SAW pumping at different angles of incidence, and link theory [3] and micromagnetic modelling results [4] with experimental data.

Parametric pumping by SAWs offers practical advantages for realizing spin-wave amplifiers. Pumping with a traveling acoustic wave selectively amplifies specific spin-wave modes and wavevectors, as dictated by energy and momentum conservation. Efficient SAW transducers can be fabricated in compact form and are already common in modern communication systems. The ability to amplify spin waves opens doors to use of media compatible with standard integrated circuit manufacturing (e.g., metallic magnetic films), bringing spin-wave devices closer to application.

- [1] A.V. Chumak, et al., *IEEE Transactions on Magnetics*, 2022, 58, 1-72.
- [2] M. Hansen, et al., IEEE Magnetics Letters, 2020, 11, 1-5.
- [3] I. Lisenkov, et al., *Physical Review B*, 2019, 99, 184433.
- [4] C. Rivard, et al., *IEEE Magnetics Letters*, 2024, 15, 5500205.

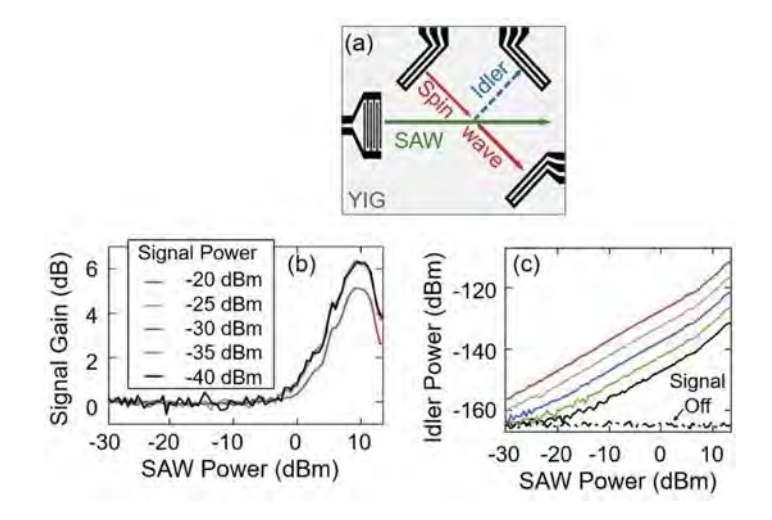


Fig. 1. (a) Illustration of the experimental device. (b) Amplification of spin-waves of varying signal levels as a function of acoustic pump power. (c) Corresponding idler power.

EE-09. Quantum Micromagnetic Theory of Magnons in Finite Nanostructures

C. Serpico, <u>S. Perna</u>, M. d'Aquino Department of Electrical Engineering and Information technology, University of Naples Federico II, Naples, Italy

We present a quantum field theoretical extension of micromagnetics for the study of magnon excitations in finite-size ferromagnetic nanostructures with arbitrary shapes and spatially nonuniform ground states [1]. The formalism is based on the introduction of a quantum micromagnetic Hamiltonian incorporating exchange, Dzyaloshinsky-Moriya, anisotropy, magnetostatic, and Zeeman interactions. The nonuniform ground state is handled by locally aligning the quantization axis of the magnetization operator with the classical ground state, obtained via minimization of the classical micromagnetic energy functional [2].

Expanding the Hamiltonian in the large-spin limit, quadratic terms in the transverse components of the quantum

^{*} Best Student Presentation Finalist / LB - Late-breaking Poster

magnetization operator are retained, leading to a quantum version of the linearized Landau-Lifshitz equation. The resulting eigenvalue problem is diagonalized using generalized Walker-type normalization conditions [3], originally introduced for uniform magnetization [4] and extended here to spatially nonuniform configurations including Dzyaloshinsky-Moriya interactions. This procedure yields discrete magnon modes and associated creation annihilation operators that fully describe the magnon spectrum.

The theory is applied to compute quantum thermal fluctuations of magnons in thin ferromagnetic nanodisks, both for in-plane magnetized and skyrmionic ground states. Numerical results, obtained via a frequency-domain micromagnetic eigensolver [5], reveal strong spatial inhomogeneities in magnon fluctuations at low temperatures, with significant boundary effects and mode localization near skyrmion cores. These findings are relevant for future developments in quantum magnonics and spin based quantum information processing.

This work is supported by Italian Ministry of University and Research, PRIN2020 funding program, Grant No. 2020PY8KTC.

- [1] C. Serpico, S. Perna, M. d'Aquino, Phys. Rev. B 111, 184410 (2025).
- [2] W. F. Brown, Micromagnetics, Interscience (1963).
- [3] D. L. Mills, J. Magn. Magn. Mater. 306, 16 (2006).
- [4] L. R. Walker, Phys. Rev. 105, 390 (1957).
- [5] M. d'Aquino, C. Serpico, G. Miano, C. Forestiere, J. Comput. Phys. 228, 6130 (2009).

EE-11. Bringing Light into the Landau-Lifshitz-Gilbert Equation: Consequences of its Fractal Non-Markovian Memory Kernel for Optically Induced Magnetic Inertia and Magnons

F. Reyes-Osorio, B. Nikolić

Physics and Astronomy, University of Delaware, Newark, Delaware, United States

The Landau-Lisfhitz-Gilbert (LLG) equation has been the cornerstone of modeling the dynamics of localized spins, viewed as classical vectors of fixed length, within nonequilibrium magnets. When light is employed as the nonequilibrium drive, the LLG equation must be supplemented with additional terms that are usually

conjectured using phenomenological arguments for direct opto-magnetic coupling between localized spins and (real or effective) magnetic field of light. However, direct coupling of magnetic field to spins is 1/c smaller than coupling of light and electrons; or both magnetic and electric fields are too fast for slow classical spins to be able to follow them. Here, we displace the need for phenomenological arguments by rigorously deriving an {\em extended} LLG equation via Schwinger-Keldysh field theory (SKFT). Within such a theory, light interacts with itinerant electrons, and then spin current carried by them exerts spin-transfer torque onto localized spins, so that when photoexcited electrons are integrated out we arrive at a spin-only equation. Unlike the standard phenomenological LLG equation with local-in-time Gilbert damping, our extended one contains a non-Markovian memory kernel whose plot within the plane of its two times arguments exhibits fractal properties. By applying SKFT-derived extended LLG equation, as our central result, to a lightdriven ferromagnet as an example, we predict an optically induced magnetic inertia term. Its magnitude is governed by spatially nonlocal and time-dependent prefactor, leading to excitation of coherent magnons at sharp frequencies in and outside the band of incoherent (or thermal) magnons.

R. Mondal, L. Rozsa, M. Farle, et al., Inertial effects in ultrafast spin dynamics, J. Magn. Magn. Mater. 579, 170830 (2023)

A. M. Lomonosov, V. V. Temnov, and J.-E. Wegrowe, Anatomy of inertial magnons in ferromagnetic nanostructures, Phys. Rev. B 104, 054425 (2021)

- U. Bajpai and B. K. Nikolic, Time-retarded damping and magnetic inertia in the Landau-Lifshitz-Gilbert equation self-consistently coupled to electronic time-dependent nonequilibrium Green functions, Phys. Rev. B 99, 134409 (2019)
- F. Reyes-Osorio and B. K. Nikolic, Gilbert damping in metallic ferromagnets from Schwinger-Keldysh field theory: Intrinsically nonlocal, nonuniform, and made anisotropic by spin-orbit coupling, Phys. Rev. B 109, 024413 (2024)

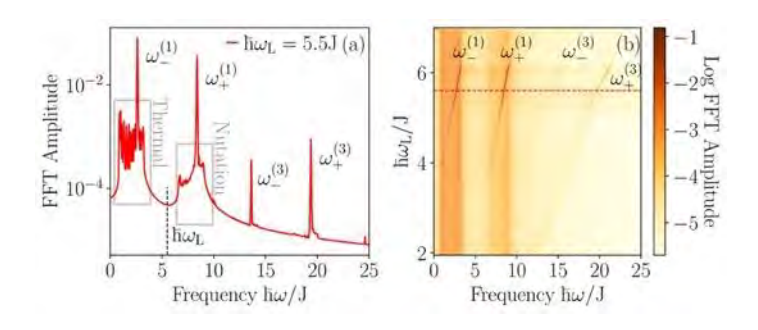


Fig. 1 (a) Magnon spectrum of a chain of localized spins $S_n(t)$ interacting with itinerant electrons. The dynamics of $S_n(t)$ is computed from our SKFT-derived extended LLG equation with time-dependent damping and inertia parameters. The nonequilibrium drive for electrons is CW light of frequency ω_L =5.5J. The four sharp peaks in panel (a) are optically excited coherent magnons obtained only under nonequilibrium conditions. Panel (b) shows spectra for a range of ω_L , revealing a linear relation between the frequency of optically excited coherent magnon peaks and ω_L .

EE-12. Spontaneous Emergence of Phase Coherence in a Quasiparticle Bose-Einstein Condensate

M. Koster², M. R. Schweizer², T. B. Noack², V. I. Vasyuchka², B. Hillebrands², M. Weiler², A. A. Serga², G. von Freymann^{2, 3}, <u>D.</u> A. Bozhko¹

¹Center for Magnetism and Magnetic Nanostructures, University of Colorado Colorado Springs, Colorado Springs, Colorado, United States, ²Department of Physics and Research Center OPTIMAS, RPTU Kaiserslautern-Landau, Kaiserslautern, Germany, ³Fraunhofer Institute for Industrial Mathematics ITWM, Kaiserslautern, Germany

Bose-Einstein Condensate (BEC), first predicted by Albert Einstein in 1932 [1], represents a macroscopic quantum state characterized by the spontaneous emergence of coherence among bosons occupying the lowest energy state. While extensively studied in systems ranging from liquid helium [2] to ultracold atomic gases [3], BEC has also been realized in ensembles of quasiparticles, including magnons [4], the quanta of spin-wave excitations in magnetic materials.

Magnon BECs exhibit hallmark features of coherence, typically inferred from spatial phase-sensitive phenomena such as interference patterns [5], supercurrents [6], and

Josephson oscillations [7]. However, a direct time-domain measurement of the condensate phase relative to an external reference has remained elusive.

In this work, we demonstrate a method for the direct measurement of the absolute phase of a magnon BEC, enabling us to observe the emergence of spontaneous coherence in real time. We show that a freely evolving magnon gas undergoes condensation into a spatially uniform precessional mode with minimal energy and a well-defined global phase. This observation provides definitive confirmation of the spontaneous phase coherence postulated for quasiparticle condensates and establishes a new experimental platform for studying macroscopic quantum phenomena in magnetic systems. Our results not only deepen the fundamental understanding of magnon condensates but also pave the way toward phase-coherent magnonic devices for microwave information processing applications.

This research was funded by grant DMR-2338060 from the National Science Foundation of the United States as well as the Deutsche Forschungsgemeinschaft (DFG, German Research Foundation) in the framework of TRR 173 - Grant No. 268565370 Spin+X (Project B04).

- [1] A. Einstein, Quantentheorie des einatomigen idealen Gases. Zweite Abhandlung, 245–257 (John Wiley & Sons, Ltd, 2005).
- [2] O. Penrose and L. Onsager, Phys. Rev., Vol. 104, P. 576 (1956).
- [3] M. H. Anderson et al., Science, Vol. 269, P. 198 (1995).
- [4] S. O. Demokritov et al., Nature, Vol. 443, P. 430 (2006).
- [5] P. Nowik-Boltyk et al., Sci. Rep., Vol. 2, P. 482 (2012).
- [6] D. A. Bozhko et al., Nat. Phys., Vol. 12, P. 1057 (2016).
- [7] A. J. E. Kreil et al., Phys. Rev. B, Vol. 104, P. 144414 (2021).

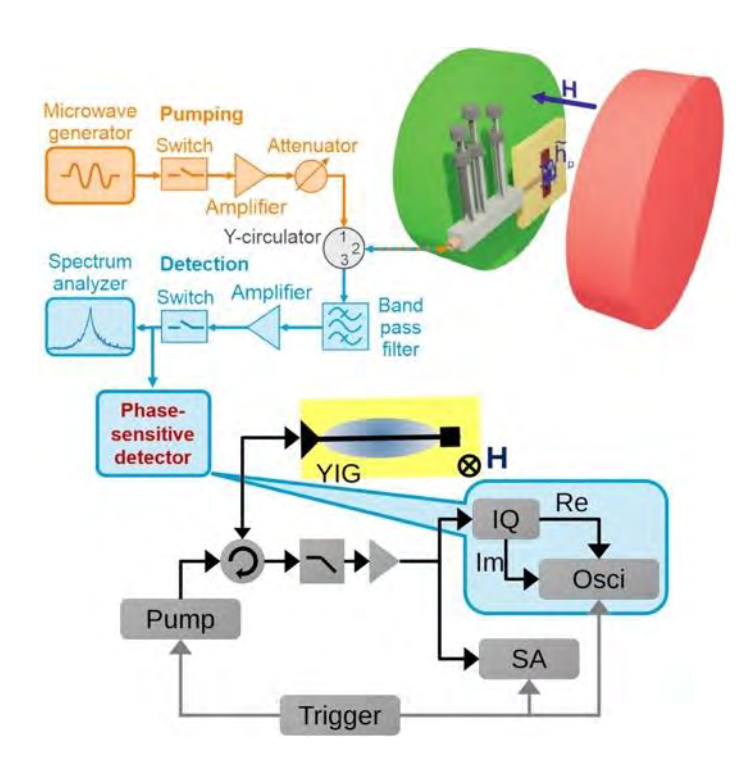


Fig. 1. Experimental setup and microwave circuitry used to generate and detect magnon BEC.

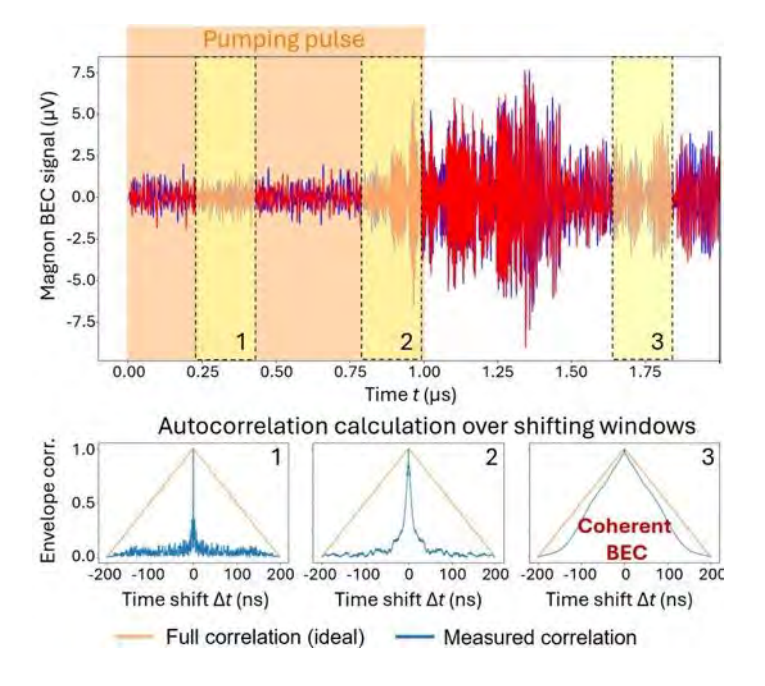


Fig. 2. The reconstructed time-domain magnetization dynamics and autocorrelation of the signal at different

times demonstrate the emergence of coherence after the pumping pulse termination.

EE-13. Squeezed Vacuum and Entanglement in Nonperturbative Cavity Magnonics with Soft Magnons

T. Chiba^{1, 2}, R. Suzuki², T. Otaki², H. Matsueda^{2, 3}
¹Department of Information Science and Technology, Graduate School of Science and Engineering, Yamagata university, Yonezawa, Japan, ²Department of Applied Physics, Graduate School of Engineering, Tohoku university, Sendai, Japan, ³Center for Science and Innovation in Spintronics, Tohoku university, Sendai, Japan

One of the fundamental physics underpinning the recent advancement of quantum information technology is — polariton—which is strongly (coherently) coupled electromagnetic waves and matter in a cavity. In particular, the polariton state that satisfies $g/\omega_{c(m)} \ge 1$ is referred to as the deep-strong coupling (DSC) [1], where ω_c and ω_m are the characteristic (angular) frequencies of the electromagnetic wave and the matter, respectively, and g is the coupling strength. Due to the excitation number nonconserving interaction in the DSC regime, the polariton modes are strongly squeezed, leading to the emergence of a nontrivial ground-state characterized by virtual excitations and nonclassical correlations. Such ground-states have been observed so far only in superconducting quantum circuits in extremely low temperatures [1].

In this study, we reveal DSC phenomena in a cavity magnonics system [2,3] in which coherent magnetization dynamics (magnon) of an easy-axis ferromagnet is coupled to a microwave magnetic field (photon) of a single LC resonator, as shown in Fig. 1(a). Based on the minimal quantum mechanical model, we show that a nontrivial frequency shift, which is characterized by an asymmetric Rabi-like splitting with $q/\omega_c \approx 1$ at the original modes crossing point, emerges in the DSC regime (see Fig. 1(b)). Also, we formulate a connection between the frequency shift and the virtual particle number as well as the entanglement entropy at the ground-state, thereby enabling experimental access to these quantum resources. Furthermore, using soft magnons [4] in an easy-axis ferromagnet, we demonstrate that these quantum quantities diverge at the critical magnetic field where the excitation gap vanishes, i.e., $\omega_{\rm m}$ = 0.

[1] P. Forn-Díaz *et al.*, Rev. Mod. Phys. 91, 025005 (2019).

[2] T. Chiba et al., Appl. Phys. Lett. 124, 012402 (2024).

[3] K. Mita, T. Chiba *et al.*, Phys. Rev. Appl. 23, L011004 (2025).

[4] G. E. W. Bauer et al., Phys. Rev. B 108, 064431 (2023).

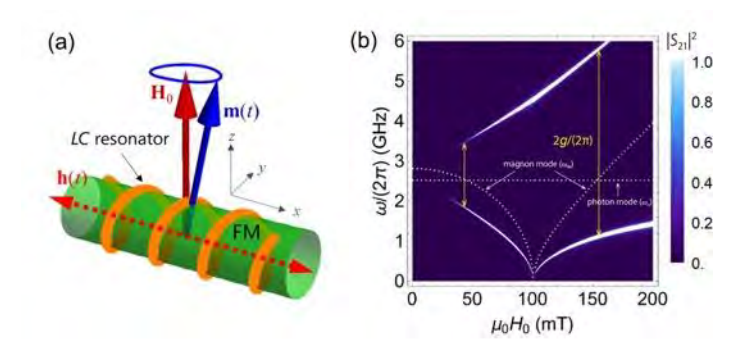


Fig. 1 (a) A model of cavity magnonic systems in which h(t) is a microwave magnetic field (photon) in a single LC resonator and m(t) is coherent magnetization dynamics (magnon) in a ferromagnet (FM) under an external magnetic field H_0 . (b) Calculated transmission amplitude $|S_{21}|^2$ of the hybridized modes as functions of an input frequency $\omega/(2\pi)$ and an external magnetic field μ_0H_0 . Here a ferromagnet is assumed to be $Y_3Fe_5O_{12}$ with millimeters scale rod shape [3]. Soft-magnon-like polariton emerges around $\mu_0H_0=100$ mT.

SESSION EF: SPIN AND MAGNETISM IN VAN DER WAALS LAYERED MATERIALS

Chair(s): P. de Faria Junior, *Department of Physics, University*of Central Florida, Orlando, Florida, United States
Thursday, October 30, 2025
08:30 AM-12:00 PM
Room 2BC

EF-01. Gate-tunable in-plane spin lifetime anisotropy via proximity-induced spin-orbit coupling in low-symmetry graphene-based heterostructures

<u>J. F. Sierra</u>¹, J. Svetlik^{1, 2}, W. Savero-Torres¹, L. Camosi¹, F. Herling¹, T. Guillet¹, K. Xu³, J. Reparaz³, V. Marinova⁴, D. Dimitrov^{4, 5}, S. O. Valenzuela^{1, 6}

¹Catalan Institute of Nanoscience and Nanotechnology (ICN2), CSIC and The Barcelona Institute of Science and Technology (BIST), Barcelona, Spain, ²Universitat Autònoma de Barcelona, Barcelona, Spain, ³Institut de Ciència de Materials de Barcelona, ICMAB-CSIC, Barcelona, Spain, ⁴Institute of Optical Materials and Technologies, Bulgarian Academy of Science, Sofia, Bulgaria, ⁵Institute of Solid State Physics, Bulgarian Academy of Sciences, Sofia, Bulgaria, ⁶Institució Catalana de Recerca i Estudis Avançats (ICREA), Barcelona, Spain

Van der Waals materials, with their atomically thin nature, enable the design of two-dimensional heterostructures where proximity effects can tailor electronic, magnetic, optical, and spin transport properties, which are key for next-generation spintronic applications [1]. Interfacial interactions between magnetic and non-magnetic layers are especially critical. For instance, transition metal dichalcogenides like WS2 can induce valley-Zeeman and Rashba spin-orbit coupling (SOC) in graphene, leading to phenomena such as spin lifetime anisotropy between spins pointing in and out of the graphene plane, the spin Hall effect, and inverse spin galvanic effect [2-4]. Yet, the intrinsic threefold symmetry of the heterostructure yields isotropic in-plane spin dynamics. In this talk, I will present spin dynamics experiments probing proximity-induced SOC in graphene combined with low-symmetry pentagonal PdSe₂. I will highlight recent results demonstrating in-plane spin lifetime anisotropy, along with gate-tunable SOC at room temperature that significantly modulates in-plane spin lifetimes [5].

- [1] J.F. Sierra et al., Nature Nanotechnology 16, 856 (2021).
- [2] M. Gmitra and J. Fabian, Phys. Rev. B 92, 155403 (2015).
- [3] L.A. Benítez, J. F. Sierra *et al.*, Nature Physics. 14, 303 (2018).

[4] L.A. Benítez *et al.*, Nature Materials 19, 170 (2020). [5] J. F. Sierra, J. Svetlik *et al.*, Nature Materials 24, 876 (2025).

EF-02 is now **VP2-08**

EF-02. Large-Scale Epitaxial Growth of Fe₃GaTe₂/Graphene van der Waals Heterostructures with Above-Room-Temperature Ferromagnetism

<u>T. Shinwari</u>¹, K. Khan¹, H. Lv¹, A. Kassa¹, F. Munnik², S. Josephy³, A. Trampert¹, V. Ukleev⁴, C. Luo⁴, F. Radu⁴, J. Herfort¹, M. Hanke¹, J. J. Lopes¹

¹Paul-Drude-Institut für Festkörperelektronik, Leibniz-Institut im Forschungsverbund Berlin e.V, Berlin, Germany, ²Helmholtz-Zentrum Dresden-Rossendorf, Institute of Ion Beam Physics and Materials Research e.V, Dresden, Germany, ³QZabre AG, Neunbrunnenstrasse 50, 8050, Zürich, Switzerland, ⁴Helmholtz Zentrum Berlin for Materialien und Energie, Albert-Einstein Straße 15, 12489, Berlin, Germany

Fe₃GaTe₂ (FGaT), a two-dimensional (2D) layered ferromagnetic metal, exhibits a high Curie temperature (T_c) ~ 360 K along with strong perpendicular magnetic anisotropy (PMA), making it a promising material candidate for next-generation energy-efficient magnetic devices [1-2]. However, the vast majority of studies on FGaT to date have been limited to millimeter-sized bulk crystals and exfoliated flakes, which are unsuitable for practical applications and integration into device processing [3]. Also, its combination with other 2D materials to form van der Waals heterostructures has only been achieved by flake stacking. Consequently, the controlled large-scale growth of FGaT and related heterostructures remains largely unexplored. In this work, we demonstrate a breakthrough in the highquality, large-scale growth of epitaxial FGaT thin films on single-crystalline graphene/SiC templates using molecular beam epitaxy. Structural characterization confirms the high crystalline quality of the continuous FGaT/graphene van der Waals heterostructures [1]. Temperature-dependent magnetization and anomalous Hall measurements reveal robust PMA with an enhanced T_c well above room temperature, reaching up to ~400 K [1]. Furthermore, X-ray absorption and X-ray magnetic circular dichroism spectra provide insight into the spin and orbital magnetic moment contributions, further validating the high T_c and robust PMA [1]. These findings are highly significant for the future development of high-performance spintronic devices based on 2D heterostructures, with potential applications in nextgeneration data storage, logic processing and quantum technologies [4,5].

- 1. T. Shinwari, K. I. A. Khan, M. Lopes, et al. "Above-room-temperature ferromagnetism in large-area epitaxial Fe₃GaTe₂/graphene van der Waals heterostructures." *arXiv* preprint arXiv:2505.06128 (2025).
- 2. S. Wu, Z. He, S. Li, et al. "Robust ferromagnetism in wafer-scale Fe_3GaTe_2 above room-temperature." *Nature Communications* 15.1 (2024): 10765.
- 3. Zhang, Bingyu, et al. "2D Magnetic heterostructures: spintronics and quantum future." *npj Spintronics* 2.1 (2024): 6
- 4. A. M. Ruiz, D. L. Esteras, J. J. Baldoví, et al. "On the origin of the above-room-temperature magnetism in the 2D van der Waals Ferromagnet Fe_3GaTe_2 ." *Nano Letters* 24.26 (2024): 7886-7894.
- 5. N. Kajale, T. Nguyen, D. Sarkar, "Field-free deterministic switching of all-van der Waals spin-orbit torque system above room temperature," Sci. Adv., vol. 10, p. eadk8669, Mar. 2024.

EF-03. Control of magnetic order in quasi-2D magnets by external perturbations: microscopic understanding

K. Carva, K. Pokhrel, S. Ray, P. Qureshi DCMP, Charles University, Prague, Czechia

Magnetic van der Waals materials offer a playground for external manipulation of its magnetic order. A highly interesting connection between the formation of helimagnetic order and breaking of both inversion and rotational symmetry of the lattice has been recently discovered in single-layer Ni dihalides [1]. Here we examine how the magnetic order in NiBr $_2$ is affected by pressure. We find a unique enhancement of the Néel temperature from 44 K at ambient pressure to ~100 K at 3 GPa. Contrary to the Nil $_2$ case, the phase transition to helimagnetism rapidly shifts to lower temperatures with increasing pressure. We show that the interlayer exchange interaction plays here a key role in the selection of the most favorable magnetic order [2].

Magnetic interactions have also been modified by strong phonon population excited in a controlled way, so that even the magnetic order is changed [3]. We investigate microscopic aspects of nonlinear spin-phonon interactions leading to magnetic order modifications. We have evaluated magnetic exchange interactions as well as magnetic anisotropy under the influence of specific non-equilibrium phonon populations for quasi-2D magnet CrBr₃, employing first principles calculation methods. The resulting

modifiction of phase transition temperature is revealed by spin dynamics methods. We also study the change of magnetic interactions in this system under pressure, and find under which conditions are our predictions in agreement with experimental data.

- [1] Song et al., Nature 602 (2022), 7898.
- [2] Qureshi et al., arXiv:2506.04933
- [3] D. Afanasiev, et al., Nature Materials 20, 607 (2021).

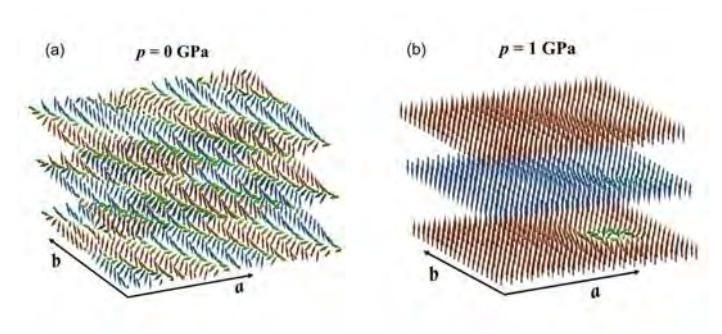


Fig. 1 $NiBr_2$: a. Helimagnetic order at ambient pressure. b. AFM order at 1 GPa, with FM alignment within layers and AFM coupling between them.

EF-05. Nitrogen-Vacancy Magnetometry of Edge Magnetism in Pristine and Fe Implanted WS₂ Flakes

I. Fescenko¹, R. Kumar², T. Gas-osoth^{5, 3, 4}, Y. Wang^{5, 3}, S. Lamichhane⁵, T. Li⁵, A. Erickson⁵, T. Delord², C. Cress⁶, N. Proscia⁶, S. LaGasse^{6, 7}, S. Liou⁵, X. Hong⁵, J. Fonesca⁶, T. An³, C. Meriles², <u>A. Laraoui</u>⁵

¹University of Latvia, Riga, Latvia, ²CUNY-City College of New York, New York, New York, United States, ³Japan Advanced Institute of Science and Technology, Nomi, Japan, ⁴University of Phayao, Mae Ka, Thailand, ⁵University of Nebraska-Lincoln, Lincoln, Nebraska, United States, ⁶US Naval Research Laboratory, Washington, District of Columbia, United States, ⁷Laboratory for Physical Sciences, College Park, Maryland, United States

Two-dimensional (2D) magnets are of significant interest both as a platform for exploring novel fundamental physics and for their potential applications in spintronic and optoelectronic devices [1]. Here, we investigate the magnetic properties of tungsten disulfide (WS₂) multilayered flakes at room-temperature using wide-field quantum

diamond microscopy [2-4]. Recent magnetic bulk measurements have indicated a weak ferromagnetic response in WS₂ [5] and theoretical predictions suggested that the edges of such flakes exhibit magnetization when at least one edge of a flake is partially hydrogenated [6]. In this study, we examine pristine and Fe-implanted WS₂ thin flakes of 45-160 nm thickness, exfoliated from bulk WS2 and transferred to nitrogen-vacancy (NV)-doped diamond substrates. We provide the first direct evidence of edgelocalized stray magnetic fields, growing linearly with the applied magnetic field and reaching up to 4.7 µT at higher magnetic fields [7]. Simulations using alternative magnetization models favor the presence of edge magnetization aligned along an axis slightly tilted from the normal to the flake's plane, a departure from theoretical predictions that we attribute to the presence of the externally applied field [7].

Acknowledgement. We acknowledges support from the Latvian Quantum Initiative under European Union Recovery and Resilience Facility project no.

(2.3.1.1.i.0/1/22/I/CFLA/001), the National Science Foundation Awards OIA-2044049, 2328822, 2025298, and 2203904, the University of Nebraska-Lincoln Grand Challenges catalyst award entitled "Quantum Approaches addressing Global Threats", and from the Department of Defense Award DOD-W911NF-25-1-0134.

- 1. C. Gong et al., Science 363(6428):eaav4450 (2019).
- 2. I. Fescenko, A. Laraoui, et *al.*, Phys. Rev. Appl. 11, 034029 (2019).
- 3. A. Laraoui, et al., App. Phys. Lett. 121, 060502 (2022).
- 4. S. Lamichhane, I. Fescenko, A. Laraoui, et *al.*, ACS Nano 17, 8694 (2023).
- 5. J. Luo, et al., App. Phys. Lett. 124, 033104 (2024).
- 6. N. Huo, et al., Appl. Phys. Lett. 104, 202406 (2014).
- 7. I. Fescenko, A. Laraoui, et *al.*, Advanced Functional Materials, under print (2025).

EF-06. Impacts of alloying and finite thickness on ferromagnetism in kagome Fe₃Sn₂ heterostructures

S. May¹, P. M. Laxmeesha¹, R. Dutta¹, T. Tandon¹, A. Velic¹, R. K. Rai², E. A. Stach², S. Sheikh³, U. M. Jayathilake³, A. X. Gray³, T. Charlton⁴, C. Jensen⁵, J. Borchers⁵, A. J. Grutter⁵

¹Materials Science and Engineering, Drexel University, Philadelphia, Pennsylvania, United States, ²Materials Science and Engineering, University of Pennsylvania, Philadelphia, Pennsylvania, United States, ³Department of Physics, Temple University, Philadelphia, Pennsylvania, United States, ⁴Oak Ridge National Laboratory, Oak Ridge, Tennessee, United States, ⁵NIST Center for Neutron Research, National Institute of Standards and Technology, Gaithersburg, Maryland, United States

Kagome metals have generated significant interest as material platforms that host both flat bands and Dirac points, thus potentially exhibiting characteristics of both strongly correlated and topological materials. Fe₃Sn₂ is one such material, in which Fe atoms form a kagome sublattice within Fe₃Sn bilayers that alternate with Sn₂ monolayers along the c-axis. Recent work on Fe₃Sn₂ single crystals has shown the presence of Dirac cones and flat bands below the Fermi level, as well as the presence of non-Fermi liquid behavior and unconventional Hall effects [1-4]. In aiming to better understand the role of band structure on magnetic order in Fe₃Sn₂, we have used molecular beam epitaxy to synthesize epitaxial films in which Mn and Co were substituted for Fe to hole and electron dope the material, respectively. The heterostructures were grown on (0001)oriented Al₂O₃ substrates with Fe (or Co) buffer layers to realize continuous films and avoid island growth. We find that Co is immiscible in Fe₃Sn₂ leading to phase separation into a different kagome phase of (Fe,Co)Sn and (Fe,Co). In contrast, Fe_{3-x}Mn_xSn₂ retains the structure of Fe₃Sn₂ up to x=1, while remaining ferromagnetic at room temperature. Valence band spectra obtained using hard x-rays and density function theory both confirm that substitution of Mn pushes the Fermi level down as expected for hole doping, confirming alloying as a route to tune the Fermi level relative to the flat band and topological band crossings. We have also synthesized Fe₃Sn₂/CoSn superlattices, in which the ferromagnetic Fe₃Sn₂ is interfaced with paramagnetic kagome CoSn metal. These superlattices allow us to probe the effects of finite thickness on magnetism in Fe₃Sn₂ down to the single Fe₃Sn monolayer and Fe₃Sn₂ bilayer limit. Polarized neutron reflectometry was used to depth profile magnetization across a series of superlattices in which the Fe₃Sn₂thickness is varied. The evolution of magnetization

within Fe_3Sn_2 as a function of thickness will be presented, providing new insights into magnetism down to the single kagome monolayer limit. This research was primarily supported by the U.S. Department of Energy, Office of Science, Basic Energy Sciences, under Award No. DE-SC0024204.

[1] L. Ye, et al., *Nature* 555, 638 (2018); [2] Z. Lin, et al., *Phys. Rev. Lett.* 121, 096401 (2018); [3] Q. Du, et al., *Phys. Rev. Lett.* 129, 236601 (2022); [4] S. A. Ekahana et al., *Nature* 627, 67 (2024).

EF-07. Spin Waves in a Bilayer Kagome Ferromagnet Fe $_3$ Sn $_2$ Y. Soh

Paul Scherrer Institut, Villigen, Switzerland

Magnetic metals with kagome structure can host various topologically non-trivial spin or electronic states, providing an extraordinary platform for studying the fundamental physics of quantum materials. The metallic kagome ferromagnet Fe₃Sn₂, which has large spin-orbital coupling, shows considerable interplay between magnetism and nontrivial electronic states. The material is a host of anomalous bulk properties, including a first-order spin reorientation transition(1), an anomalous planar Hall effect(2), and field tunable electronic states (3, 4). Recently, anomalous quasiparticles showing marginal Fermi liquid behavior and fractionalization have been observed in this system (5). Using Magnetic Circular Dichroism Resonant Ineslatic X-ray scattering (MCD RIXS) and X-ray absorption spectroscopy (XAS), we report a flat spin wave band with large (compared to elemental iron) orbital moments in Fe₃Sn₂(6). The flat mode energy is consistent with the high Curie temperature (~640 K) as well as the strong acoustic mode dispersion. Our results unveil that the defining units of this very popular topological metal are a triangular lattice of octahedral iron clusters rather than weakly coupled kagome planes. The spin waves are strongly damped when compared to elemental iron, opening the topic of interactions of topological bosons (spin waves) and fermions (electrons) with the very specific target of explaining boson lifetimes.

- 1. K. Heritage *et al.*, Images of a First Order Spin Reorientation Phase Transition in a Metallic Kagome Ferromagnet. *Advanced Functional Materials* 30, (2020).
- 2. N. Kumar, Y. Soh, Y. Wang, J. Li, Y. Xiong, Anomalour Planar Hall Effect in a kagome ferromagnet. *arXiv:2005.14237*, (2020).
- 3. M. Yao et al., Switchable Weyl nodes in topological

Kagome ferromagnet Fe3Sn2. *ArXiv e-prints*. 2018. 4. N. Kumar, Y. Soh, Y. Wang, J. Li, X. Y., Tuning the electronic band structure in a kagome ferromagnetic metal via magnetization. *Phys Rev B* 106, 045120 (2022). 5. S. A. Ekahana *et al.*, Anomalous electrons in a metallic kagome ferromagnet. *Nature* 627, 19 (2024). 6. W. Zhang *et al.*, Spin waves and orbital contribution to ferromagnetism in a topological metal. *Nature Communications* 15, 8905 (2024).

EF-09. Intrinsic Non-linear Hall Effect

F. Xue, S. Ahmad

Physics Department, University of Alabama at Birmingham, Birmingham, Alabama, United States

The intrinsic nonlinear Hall effect has recently garnered significant attention as a distinct physical phenomenon with its own symmetry properties, rather than as a mere second-order correction to the linear anomalous Hall effect. While the anomalous Hall effect arises solely from broken time-reversal symmetry, the intrinsic nonlinear Hall effect requires the simultaneous breaking of both time-reversal and spatial inversion symmetries. Previous semiclassical theory has shown that this effect originates from the quantum metric of the band structure and typically relies on the presence of a metallic Fermi surface. As such, the intrinsic nonlinear Hall effect provides deeper insight into the geometric and topological properties of electronic band structures in magnetic metallic systems.

In this work, we introduce a derivation of the intrinsic nonlinear Hall conductivity using the density matrix formalism. A key finding is the existence of a Fermi-sea contribution in addition to the well-known Fermi-surface contribution associated with the quantum metric. In

nonlinear Hall conductivity using the density matrix formalism. A key finding is the existence of a Fermi-sea contribution in addition to the well-known Fermi-surface contribution associated with the quantum metric. In insulating systems, where the chemical potential lies within the energy gap and the Fermi-surface contribution vanishes, the Fermi-sea terms become particularly important. We demonstrate this using a simple two-band model of a Chern insulator, where the intrinsic nonlinear Hall effect remains nonzero even when the linear anomalous Hall conductivity vanishes. We further examine an antiferromagnetic insulator in which the combination of time-reversal and inversion symmetry forbids the linear anomalous Hall effect but allows a finite intrinsic nonlinear Hall effect. Finally, we discuss how contributions to the nonlinear Hall conductivity depend on the underlying material properties, highlighting new opportunities for nonlinear transport in insulating

systems.

Nandy, S., & Sodemann, I. (2019). *Symmetry and quantum kinetics of the nonlinear Hall effect. Physical Review B*, 100(19), 195117.

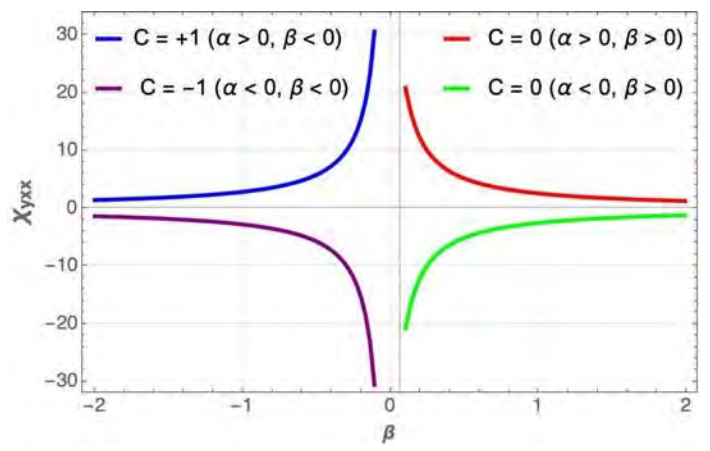


Fig. 1 Plot of Non-linear Hall conductivity with variable gap parameter for Chern and trivial insulator phases.

EF-08. Engineering Magnetic Transition Metal Chalcogenide-Based Quantum Interfaces

H. Chi

University of Ottawa, Ottawa, Ontario, Canada

Significant progress has been made in conceptualizing geometric aspects of condensed matter [1]. Intertwining topology and magnetism at interfaces leveraging disparate quantum features, offers an exciting arena for novel magnetic phenomena towards disruptive energy efficient memory/logic technologies. The extraordinary correlations among charge, spin, orbital and lattice degrees of freedom, renders magnetic transition metal chalcogenides (TMCs) promising for exotic topological phenomena. We highlight here two TMCs, namely, ferromagnetic chromium telluride and antiferromagnetic manganese telluride. Cr₂Te₃ is an emerging platform for exploring spin-orbit driven Berry phenomena. A unique temperature and strain modulated sign reversal of the anomalous Hall effect has been uncovered, resulting from nontrivial Berry phenomena [2,3]. The versatile interface tunability of Cr₂Te₃, hybridized with topological insulator (TI), offers new routes for topological devices [4]. When proximitized with TI, MnTe favorably opens up an exchange gap in magnetic TI natural heterostructure, displaying spin-orbit-torque switching [5]. The discovery-rich magnetic interfaces are key in advancing

quantum materials in the field of topological spintronics.

The research is supported by the Army Research Office (ARO), Canada Research Chairs (CRC) Program, and the Natural Sciences and Engineering Research Council of Canada (NSERC).

[1] H. Chi and J. S. Moodera, Progress and prospects in the quantum anomalous Hall effect, *APL Mater.* 10, 090903 (2022).

[2] H. Chi et al., Strain-tunable Berry curvature in quasi-two-dimensional chromium telluride, *Nat. Commun.* 14, 3222 (2023).

[3] S. Kwon, Y. Liu, H. Chi, G. Yin, M. R. Neupane, and R. K. Lake, Evolution of Berry phase and half-metallicity in Cr_2Te_3 in response to strain, filling, thickness, and surface termination, *Phys. Rev. B* 109, 134430 (2024).

[4] Y. Ou et al., Enhanced ferromagnetism in monolayer Cr_2Te_3 via topological insulator coupling, *Rep. Prog. Phys.* 88, 060501 (2025).

[5] O. A. Vail et al., Proximity Magnetism in Mn(Bi,Sb)₂Te₄–(Bi,Sb)₂Te₃/MnTe Natural Heterostructures (2025).

Interfacial exchange coupling

Topological insulator surface

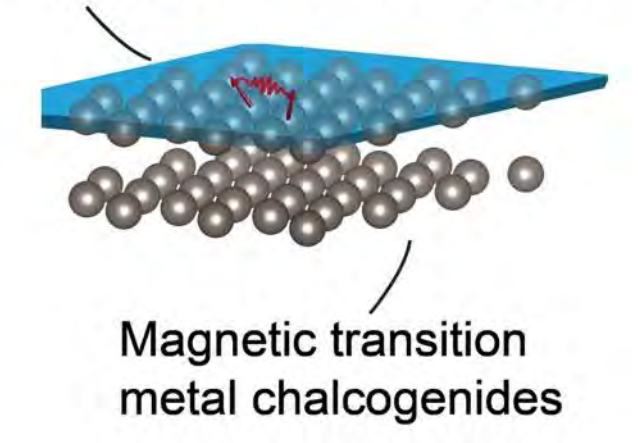


Fig. 1 Interfacial Exchange Coupling

EF-10. Studying the Effect of Nb Doping on the Magnetic Properties of CrTe₂ Crystals

D. R. Lawati¹, J. Kumar¹, P. Karki², K. Prasad², M. A. Elekhtiar¹, S. Lamichhane¹, B. Tiwari¹, K. Huang¹, Z. Hubble², J. Watt³, S. Liou¹, E. Y. Tsymbal¹, J. Wang², K. Ambal², <u>A. Laraoui¹</u> ¹University of Nebraska-Lincoln, Lincoln, Nebraska, United States, ²Wichita State University, Wichita, Kansas, United States, ³Los Alamos National Laboratory, Albuquerque, New Mexico, United States

Two-dimensional (2D) magnets opened new opportunities for the fundamental investigation of magnetism and potential for miniaturized spintronic devices [1-2]. Recently, CrTe₂ has attracted significant attention due to several compelling properties, such as the high Curie temperature (T_c) [3]. Here, we study the effect of Nb doping on the magnetic properties of mm-sized bulk CrTe₂ crystals grown using indirect synthesis methods. The high crystal quality of $Cr_{1-x}Nb_xTe_2$ (x = 0 - 0.2) was verified through a combination of characterization techniques, including X-ray diffraction (XRD), scanning electron microscopy, electron transmission microscope, and energy dispersive X-ray spectroscopy. XRD confirmed the dissolution of Nb into the CrTe2 crystal structure, leading to a change in the lattice parameter, and causing a shift in XRD peak position [4]. The bulk magnetic properties of $Cr_{1-x}Nb_xTe_2$ (x = 0 - 0.2) crystals were measured using vibrating-sample magnetometer. superconducting quantum interference device magnetometer, and ferromagnetic resonance (FMR) spectroscopy. All doped crystals process ferromagnetism with T_c of ~350 K for pristine crystals decreasing to ~295 K for Cr_{0.8}Nb_{0.2}Te₂ crystals [4]. The saturation magnetization decreases from ~140 mT for x = 0 to ~38 mT for x = 0.2. FMR measurements on $Cr_{1-x}Nb_xTe_2$ (x = 0 - 0.2) crystals reveal a decrease of FMR frequency down to ~ 1 GHz and an increase of Gilbert damping constant a to ~ 0.16 for x = 0.2 in comparison to the pristine (x = 0) CrTe₂ crystals with an FMR frequency above 4 GHz and a damping constant a of ~0.08. These changes were explained by the modification of the magnetic anisotropy and magnetic moment upon Nb doping, verified by Quantum ESPRESSO calculations [4]. These results extend the application of Cr_{1-x}Nb_xTe₂ to magnonics [5].

We acknowledge the support of the National Science Foundation Awards OIA-2044049 and 2328822, the UNL Grand Challenges catalyst award entitled Quantum Approaches addressing Global Threats, and by the Nebraska Nanoscale Facility: National Nanotechnology Coordinated Infrastructure and the Nebraska Center for Materials and

Nanoscience (and/or NERCF), which are supported by NSF FCCS under Award 2025298.

- 1. C. Gong, et al., Nature 546, 265-269 (2017).
- 2. B. Huang, et al., Nature 546, 270-273 (2017).
- 3. X. Zhang, et al., Nature Communications 12, 2492 (2021).
- 4. D. Lawati, et *al.*, to be submitted to Advanced Materials (2025).
- 5. A. V. Chumak and H. Schultheiss, J. Phys. D: Appl. Phys. 50 300201(2017).

EF-11. Fe₃GeTe₂ single crystals with varying Fe content probed by x-ray spectroscopy

<u>D. Backes</u>¹, R. Fujita², L. Veiga¹, D. Mayoh³, G. Wood³, S. S. Dhesi¹, G. Balakrishnan³, G. van der Laan¹, T. Hesjedal² ¹Diamond Light Source, Didcot, United Kingdom, ²Claredon Laboratory, University of Oxford, Oxford, United Kingdom, ³Department of Physics, University of Warwick, Coventry, United Kingdom

The discovery of 2D magnetism motivated an intense search for 2D magnets with high transition temperatures [1, 2]. Fe₃GeTe₂ is a promising candidate, exhibiting 2D ferromagnetism with strong perpendicular anisotropy and a transition temperature of around 225 K [3]. A well-known problem is that the magnetic properties of such van der Waals magnets can show large variations. These variations occur between flakes exfoliated from different single crystals but also when exfoliated from different parts of the same single crystal [4]. Furthermore, their small lateral size of only a few tens of micrometers reduces the number of applicable characterization techniques. Spectroimaging techniques, such as x-ray photoemission electron microscopy, are limited in accessibility and the measurement process is very timeconsuming. Hence, establishing a pre-characterization method for the base materials, i.e., the Fe₃GeTe₂ crystals, that can help to optimize the materials parameters and improve their homogeneity is desirable.

We present a spectroscopic study of the magnetic properties of Fe₃₋₆GeTe₂ single crystals with varying Fe content, achieved by tuning the stoichiometry of the crystals [5]. We carried out x-ray absorption spectroscopy and analyzed the x-ray circular magnetic dichroism spectra using the sum rules, to determine the orbital and spin magnetic moments of the materials. We find a clear reduction of the spin and orbital magnetic moment with increasing Fe deficiency. Magnetic susceptibility measurements show that the

reduction in magnetization is accompanied by a reduced Curie temperature. Multiplet calculations reveal that the Fe²⁺ state increasingly mixes with a higher valence state when the Fe deficiency is increased. This effect is correlated with the weakening of the magnetic moment. As single crystals are the base material for exfoliation processes, our results are relevant for the assembly of 2D magnetic heterostructures.

- [1] B. Huang et al., Nature 546, 270 (2017)
- [2] C. Gong et al., Nature 546, 265 (2017)
- [3] Z. Fei et al., Nat. Mater. 17, 778 (2018)
- [4] M. D. Watson et al., New J. Phys. 15, 103016 (2013)
- [5] D. Backes et al., Nanotechnology 35, 395709 (2024)

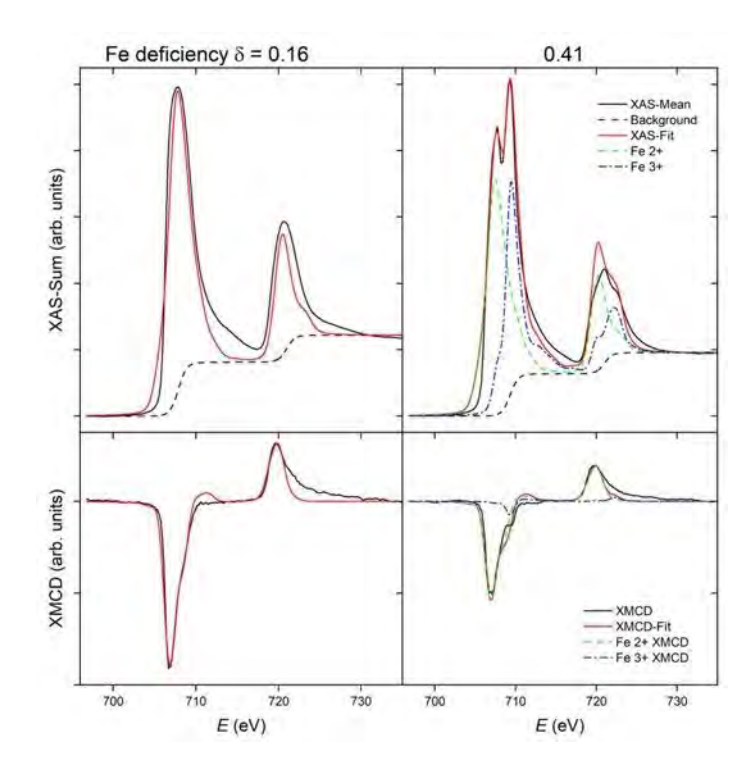


Fig. 1 Experimental and calculated XAS and XMCD spectra for two different Fe contents. The fits (redlines) are superpositions of the calculated Fe^{2+} (green dashed lines) and Fe^{3+} (blue dashed lines) spectra.

SESSION EG: ADVANCED MAGNETIC RECORDING TECHNOLOGIES

Chair(s): A. Venugopal, Seagate Research, Seagate Technology,
Edina, Minnesota, United States
Thursday, October 30, 2025
08:30 AM-12:00 PM
Room 2A

EG-01. Quantifying Erasure and Interference from Adjacent Tracks in Heat-Assisted Magnetic Recording

<u>S. Zheng</u>, W. R. Eppler, J. Loven, J. Gadbois Seagate Technology, Bloomington, Minnesota, United States

Areal density of heat-assisted magnetic recording has passed 3 Tbpsi with track spacing close to 25 nm. This spacing is comparable to the width of the thermal bubble created by the near field transducer and the effective width of the reader. As a result, erasure and interference from adjacent tracks have significant impact on the quality of the center data track and limit further areal density growth. To quantify the interference, a spin stand test utilizing synchronous writing has been developed and was able to resolve two interference components with different phase and explain the lack of correlation between background interference and reader width [1].

In this paper, the test has been extended to quantify erasure and interference of foreground adjacent tracks. The results show that side reading interference from foreground tracks is dominated by the in-phase component, 2 to 7 dB higher than that from background tracks, and strongly correlates with reader width at a sensitivity of -0.6 dB/nm as shown in Fig. 1. Erasure from repeated adjacent track writes reduces the signal power of the main track by 0.3 dB and increases the spatial noise by 0.4 dB for every decade of number of writes. The down track resolution increases with repeated adjacent track erasure, suggesting the erasure dominates at track edge. Measurements of two types of media with similar areal density show different adjacent track erasure under repeated writes, as shown in Fig. 2. This difference needs to be accounted for when comparing the areal density capability.

[1] X. Zheng, W. R. Eppler, and J. Loven, "Quantifying side reading in heat-assisted magnetic recording," IEEE Trans. Mag., vol. 61, no. 4, pp. 1-5, April 2025, Art no. 3200305.

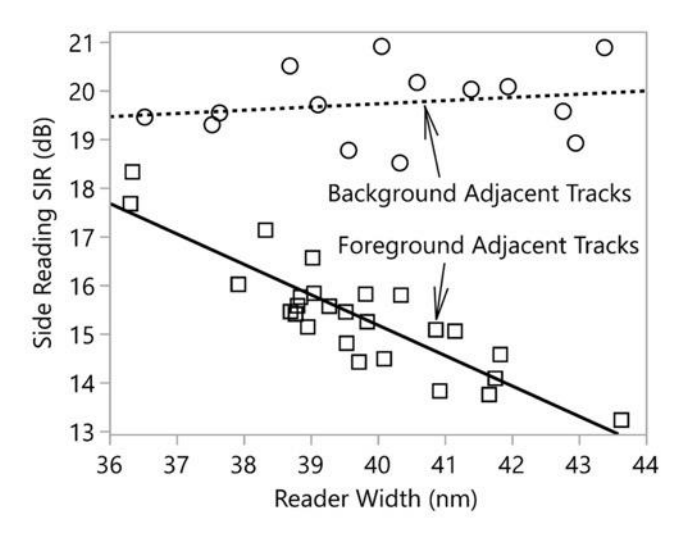


Fig. 1. Side reading signal-to-interference ratio (SIR) as a function of effective reader width for adjacent tracks on the background (circles) and foreground (squares) of the center data track. The dashed line represents the trend for background tracks; the solid line represents the trend for foreground tracks with a slope of -0.6 dB/nm.

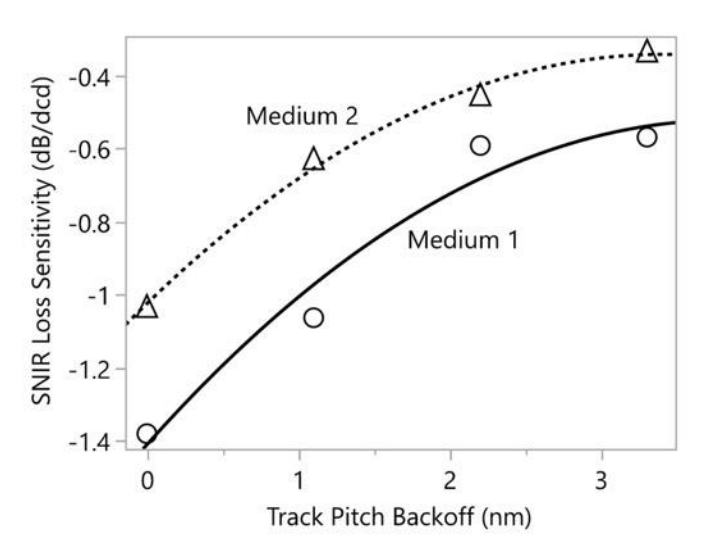


Fig. 2. Total signal to noise and interference ratio (SNIR) loss from adjacent track erasure (ATE) for every decade of number of writes as a function of track pitch backoff for two different medium designs.

EG-02. Detection of In-Plane Magnetized Grains with a Magnetoresistive Head

Y. Chen, R. H. Victora

University of Minnesota, Minneapolis, Minnesota, United States

In Heat-Assisted Magnetic Recording (HAMR) media, MgO underlayers are widely used to promote the perpendicular magnetic anisotropy of FePt grains. However, polycrystalline MgO introduces grain misalignments, resulting in in-plane magnetization components that degrade signal quality and are difficult to detect [1,2]. In this work, we propose a novel detection method based on micromagnetic simulation and a 45° magnetoresistive (MR) read head. This geometry enables sensitivity to both perpendicular and in-plane magnetization.

By simulating the media response with realistic in-plane anisotropy [3], we show that the magnetostatic field from an adjacent track (Track 1) introduces cross-track asymmetry. This breaks the symmetry of in-plane magnetizations and generates detectable playback signals in Track 2. Our simulations demonstrate that even a modest fraction (20%) of in-plane magnetized grains can be identified through the readback signal, and the sensitivity improves as the in-plane anisotropy decreases.

This method allows identification of noise sources in FePt HAMR media without relying on expensive microscopy. It provides a cost-efficient approach to media evaluation during development and testing.

- [1] Wang, Jian, et al. "Magnetic in-plane components of FePt nanogranular film on polycrystalline MgO underlayer for heat-assisted magnetic recording media." Acta Materialia 177 (2019): 1-8.
- [2] Zhang, Li, et al. "L10-ordered high coercivity (FePt) Ag C granular thin films for perpendicular recording." Journal of Magnetism and Magnetic Materials 322.18 (2010): 2658-2664.
- [3] Wang, J., et al. "Effect of MgO underlayer misorientation on the texture and magnetic property of FePt-C granular film." Acta Materialia 91 (2015): 41-49.

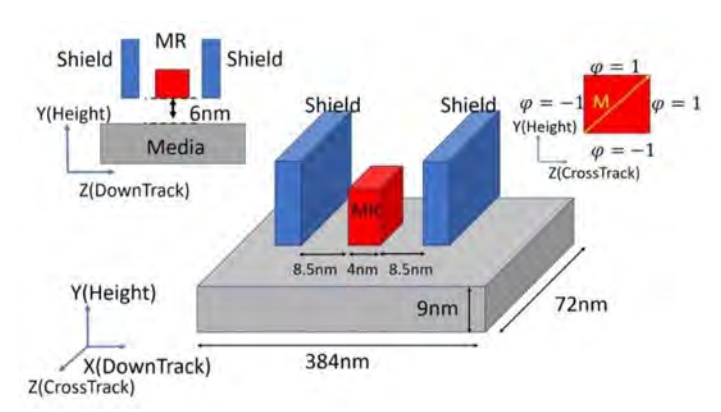


Fig 1. The configuration of media (grey), read head (red), and shield(blue). The magnetization of the head is set by properly defining the potential at its surfaces.

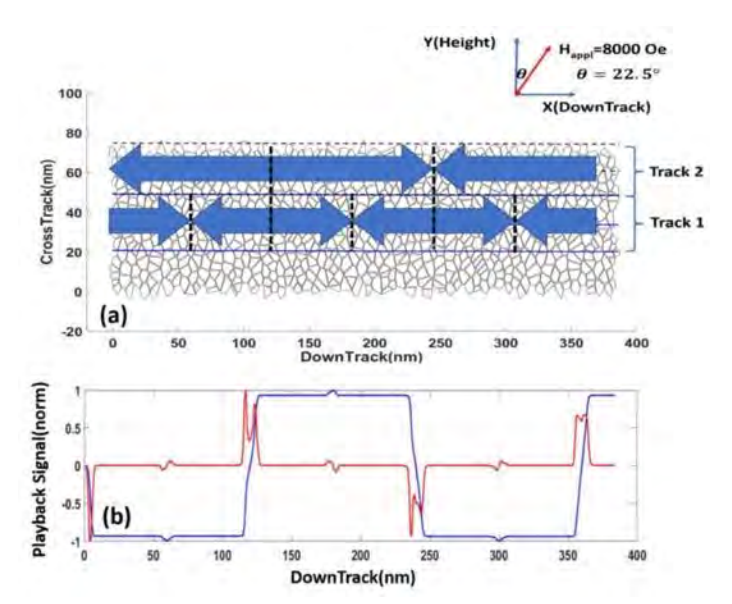


Fig 2. (a) Track 1, located at the center, is first written with a single-tone signal '101010,' featuring a bit length (BL) of 60 nm. Then Track 2, positioned adjacent to Track 1, is written with the inverse signal '010' with a BL of 120 nm. (b) Normalized playback signal from Track 2 with a 20% proportion of in-plane magnetized FePt grains. Blue curves represent original playback signals and red curves represent differentiated playback signals. Smaller peaks arise due to reduced anisotropy, the magnetostatic field from Track 1, and moving the reader along Track 2.

EG-03. The impact of in-plane grains on Heat Assisted Magnetic Recording performance and THMap metrics

N. A. Natekar, P. Jubert, T. Olson, A. Goncharov, R. Brockie, K. Tanahashi

Western Digital, San Jose, California, United States

The dominant noise source in the HAMR process is media noise, which impacts SNR, jitter and recording density [1-4]. One source of media noise is grains with easy axes pointing in-plane; these in-plane grains occur randomly and independently of the fabrication parameters [5-7]. While their presence has been established in literature through experiments, there is less understanding of how these grains impact HAMR performance and THMap metrics. We show the impact of in-plane grains in Fig. 1. ADC is reduced by 30 Gbpsi for every 1% increase in in-plane grains, due to jitter increasing, LFSNR decreasing, and reader SNR (HeSNR) decreasing. Degradation in both LFSNR and jitter indicates in-plane grains impact the entire bit.

Using micromagnetics, we compare the readback signal's mean and variance from THMap runs to an analytical model in Fig.2 (a) and (b) respectively. The analytical model predicts the signal mean and variance based on binomial statistics and is an excellent predictor of the signal variance in absence of magnetostatic interactions (MSI). The presence of MSI reduces signal mean and increases signal variance when the applied field is high, since anticorrelations due to MSI lead to magnetizations pointing away from the applied field direction. For a lower applied field, the signal mean increases and variance decreases slightly, as the anti-correlated magnetizations align grains in random directions like the default orientation. In the presence of MSI, the analytical formulation fits the signal mean. However, we require a new approach to fit the variance data. Signal variance has a significant dependence on the magnitude of the MSI field. Additional correlation length analysis illuminates the dependence of the correlation length on the MSI field magnitude and can be used to explain the relationship between signal variance and MSI scaling as the number of in-plane grains varies. Future work will include improvement of the analytical model and identification of techniques to mitigate impact of in-plane grains.

- [1] J.-G. (Jimmy) Zhu and H. Li, doi: 10.1063/1.4867607.
- [2] N. A. Natekar, Z. Liu, S. Hernandez, and R. H. Victora, doi: 10.1063/1.5007072.
- [3] J. Hohlfeld, P. Czoschke, P. Asselin, and M. Benakli, doi: 10.1109/TMAG.2018.2872758.

[4] C. Vogler, C. Abert, F. Bruckner, D. Suess, and D. Praetorius, doi: 10.1063/1.4953390.

[5] J. Wang et.al, doi: 10.1016/j.actamat.2019.07.017.

[6] H. Sepehri-Amin et.al, doi:

10.1016/j.scriptamat.2016.12.018.

[7] S. Wicht et.al, doi: 10.1063/1.4943936.

[8] N. A. Natekar et.al., doi:

10.1109/TMRC62973.2024.10713977

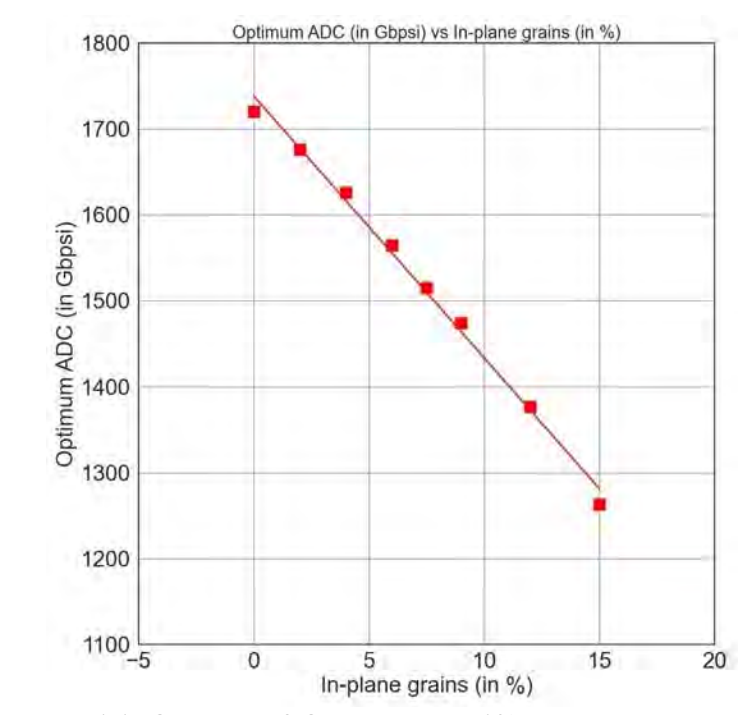


Fig. 1 ADC drop by 30 Gbpsi for every 1% rise in in-plane grains

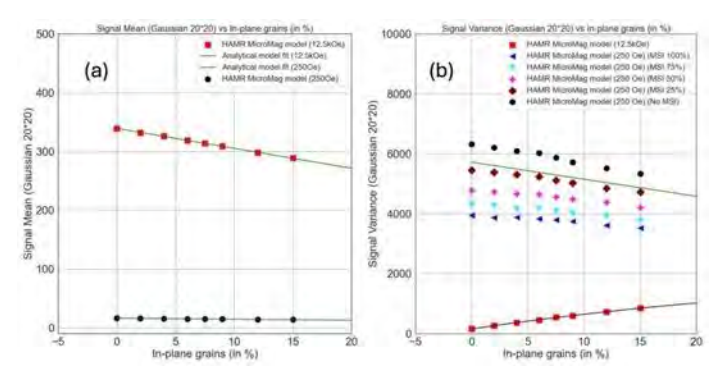


Fig. 2 Readback signal (a) mean and (b) variance (for different magnetostatic fields) calculated for a Gaussian reader 20nm*20nm

EG-04. Dependence of Microstructure and Grain Density on Nucleation Layer Thickness in L1₀ FePt-hBN Granular Thin Films

<u>J. Chang</u>^{1, 2}, A. K. Gribik^{1, 2, 3}, O. R. Peterson^{1, 2, 4}, B. L. Reese^{1, 2}, D. E. Laughlin^{1, 2, 5}, J. Zhu^{1, 2, 5}

¹Data Storage Systems Center, Carnegie Mellon University, Pittsburgh, Pennsylvania, United States, ²Materials Science and Engineering, Carnegie Mellon University, Pittsburgh, Pennsylvania, United States, ³Computational and Chemical Sciences, Carlow University, Pittsburgh, Pennsylvania, United States, ⁴Physics, Kenyon College, Gambier, Ohio, United States, ⁵Electrical and Computer Engineering, Carnegie Mellon University, Pittsburgh, Pennsylvania, United States

The rapid advancement of artificial intelligence and supercomputing is driving the demand for higher-density data storage. Heat-assisted magnetic recording (HAMR) has emerged as a solution with a significant increase in hard disk drive (HDD) areal density of data storage. Prior work on FePt-hexagonal BN (hBN) granular media demonstrated improved grain isolation and the growth of high-aspectratio, columnar grains that are essential for achieving ultrahigh areal densities [1]. While it has been shown that BN volume fraction and growth temperature can vary FePt grain density, the impact of the initial growth stage on the microstructure of the recording media remains unclear [1, 2]. The initial growth stage consists of two steps: deposition of a thin FePt nucleation layer, followed by co-sputtering of FePt with amorphous BN (aBN), which enables lateral grain growth prior to confinement by the subsequent crystallization of hBN. In this study, we systematically investigated microstructural changes in FePt-hBN films as a function of both the FePt nucleation layer thickness and the FePt-aBN layer thickness. We show that for a constant FePt nucleation layer thickness and an increase in FePt-aBN layer thickness from 0.73 to 0.85 nm, the average grain diameter remained relatively constant. However, the standard deviation increased from ±28% to ±54% due to the presence of more interconnected grains. A thicker FePt-aBN layer resulted in a lower degree of L10 ordering, represented by the diffracted intensity ratio $I_{(001)}/I_{(002)}$, which decreased from 2.16 to 2.09. Subsequently, a reduction in the out-of-plane coercivity from 34.4 to 30.4 kOe was observed. The comparison of microstructural data across samples revealed that the FePt nucleation layer thickness primarily influences the grain diameter, while the FePt-aBN layer controls the interconnections between grains and the overall grain shape. Relevant structural, microstructural, and magnetic data will be presented for samples with initial growth stage

thicknesses from 0.8 to 1.5 nm. In summary, the study showed the initial growth stage has substantial influence on the final grain size and size distribution.

¹C. Xu, B. S. D. C. S. Varaprasad, D. E. Laughlin and J.-G. Zhu, IEEE Trans. Mag., Vol. 59, p.1-5 (2023)

² I. Suzuki, J. Wang, Y. K. Takahashi and K. Hono, J. Magn. Magn. Mater., Vol. 500, (2020)

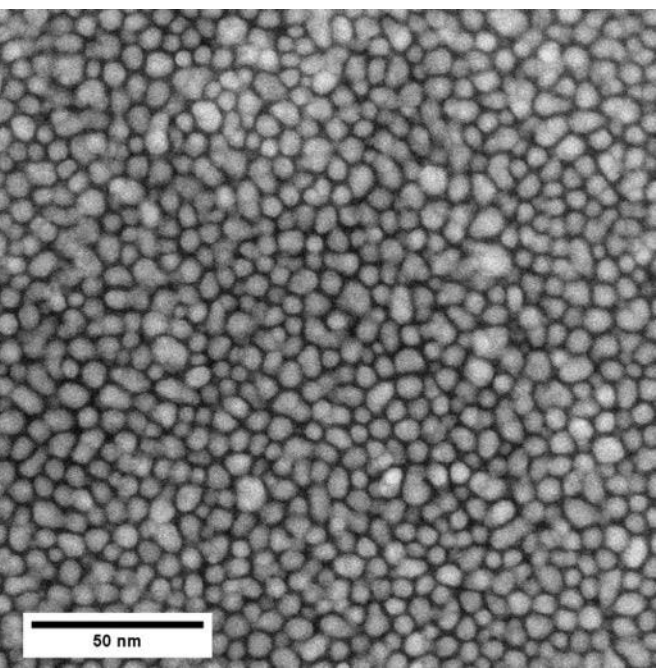


Fig. 1 Plane-view STEM HAADF image of FePt granular thin film.

EG-05. Microstructure and Magnetic properties of high-density $L1_0$ -FePt grains on an electrically conductive (Mg,Ti)O underlayer for HAMR media.

<u>D. Angayarkanni Ramamurthy</u>¹, H. Sepehri-Amin¹, I. Suzuki¹, Y. K. Takahashi^{1, 2}

¹Research Centre for Magnetic and Spintronic Materials, national Institute for Materials Science, Tsukuba, Ibaraki, Japan, ²Research Institute of Electrical Communications, Tohoku University, Sendai, Tohoku, Japan

Heat-assisted magnetic recording (HAMR) is an advanced technology in hard disk drives that has enabled giant data storage capacity or areal recording density (ARD) beyond 4 Tb/in². Chemically ordered L1₀ FePt has been used as a HAMR media due to their high magnetic anisotropy constant (Ku) of 6.6 MJ/m³. The microstructure and magnetic properties of the L10 FePt-X media is primarily governed by segreant materials (X) and underlayer. FePt-X (X=C and BN)

on MgO underlayer has proven to show epitaxial grain growth. However, the MgO underlayer requires a longer deposition time due to their electrically insulating nature. An alternate is to use electrically conductive (MgTi)O with a crystal structure similar to MgO. In previous studies, FePt-C deposited in (MgTi)O resulted in larger grains with irregular grain morphology [1]. In this study, we investigated the microstructure, interface, and magnetic properties of epitaxially grown FePt-X (X= C and BN) on MgO substrate and (Mq,Ti)O underlayer [2]. 6 nm thick FePt-C 40 vol.% and FePt-BN 25 vol.% (FePt-C and FePt-BN) layers were deposited individually on MqO substrate and (Mq,Ti)O underlayer (MTO) using magnetron sputtering. Figure 1 shows the plane view TEM images of FePt-C and FePt-BN deposited on MgO substrate and MTO. Figure 2 shows the respective magnetization curves of these thin films. FePt-C grown on MTO shows larger average grain size (D) of 11.1 nm with a lower grain density of 3.4 Tgrains/in². On the other hand, the FePt-BN on MTO shows smaller D of 6.6 nm with high grain density of 9 Tgrain/in². However, the FePt-BN grown on both MgO and MTO show low coercivity of ~ 2 T, when compared to the FePt-C on MgO ~ 4 T. The differences in microstructure and magnetic properties were elucidated through extensive TEM analysis. Overall, incorporating BN as a segregant for L1₀ FePt, one can easily achieve a desirable microstructure with smaller grains and high grain density on an electrically conductive (Mg,Ti)O underlayers, suitable for high storage capacity HAMR media, with the expense of low coercivity.

[1] B.S.D.C.S. Varaprasad, Y.K. Takahashi, A. Ajan, K. Hono, J. Appl. Phys. 113 (2013) 203907.

[2] A. R. Dilipan, H. Sepehri-Amin, I. Suzuki, Y. K. Takahashi, Available at SSRN 5195401.

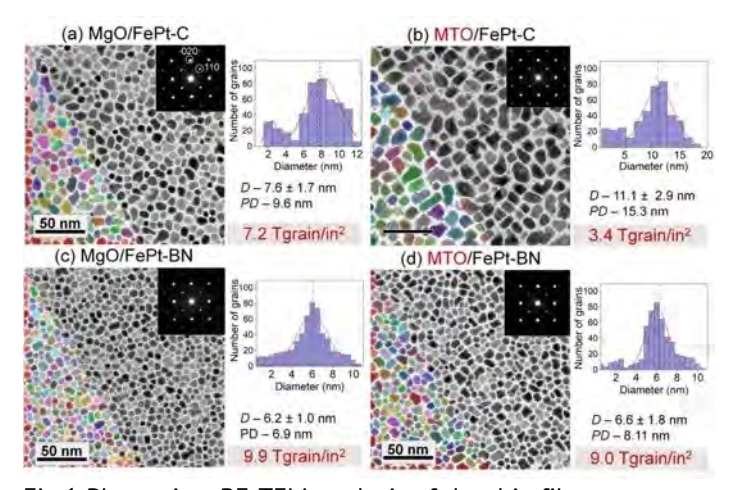


Fig.1 Plane-view BF-TEM analysis of the thin films

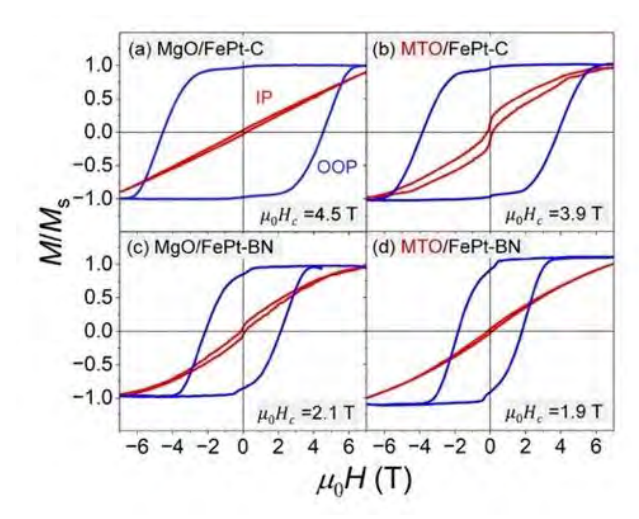


Fig. 2 In-plane and out-of-plane magnetization curves of the thin films

EG-06. Thermal spin-torque heat-assisted magnetic recording

<u>S. Isogami</u>¹, Y. Sasaki¹, Y. Fan², Y. Kubota³, J. Gadbois², K. Hono¹, Y. K. Takahashi¹

¹NIMS, Tsukuba, Japan, ²Seagate Technology, Minneapolis, Minnesota, United States, ³Seagate Technology, Fremont, California, United States

Heat-assisted magnetic recording (HAMR) has emerged as a promising technology for enhancing the recording density of hard disk drives [1,2]. To achieve lower power consumption than the current HAMR for next-generation, a more efficient writing with less laser power would be indispensable. An advanced HAMR concept is developed to address such specification, and the write ability has been demonstrated in multilayer media stacks comprising the structures of antiferromagnetic MnPt and ferromagnetic FePt layers with the magnetic easy axis oriented perpendicular to the film plane (Fig. 1). The concept is based on two distinct switching mechanisms: thermally activated (TA) and spin-transfer-torque (STT) assisted magnetization switching. The latter is driven by an out-ofplane temperature gradient (ΔT) in the MnPt/FePt multilayer which is referred as thermal spin-torque (TST) HAMR media [3]. The hybrid mechanism with TA and STT can be separated by the pump-probe measurements [4], and it is found that the STT dominates the mechanism for coercivity modulation in the short delay time regime. These results suggest that lower laser power consumption is achievable owing to the contribution of STT assisted switching in the TST-HAMR media.

[1] D. Weller et al., Phys. Status Solidi A 210, 1245 (2013); J. Vac. Sci. Technol. B 34, 060801 (2018).

- [2] K. Hono et al., MRS Bull. 43, 93 (2018).
- [3] S. Isogami et al., Acta Materialia 286, 120743 (2025).
- [4] C. Xu et al., Appl. Phys. Lett. 96, 092514 (2010).

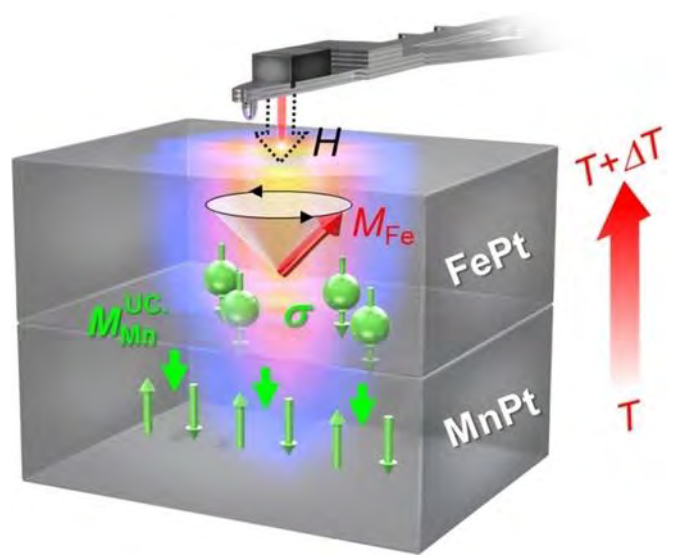


Fig. 1 Schematic illustration of spin-torque HAMR, where M_{Fe} , H, ΔT , σ , and $M_{\text{Mn}}^{\text{UC.}}$ represent the magnetization of Fe, mangeitc field applied from writing head, temperature difference, spin-polarization, and induced magnetic moment of Mn.

EG-07. Vector Recording: Advancing Areal Density in Heat-Assisted Magnetic Recording with Innovative Reader Designs

K. Hosen¹, R. H. Victora^{1, 2}

¹Department of Electrical and Computer Engineering, University of Minnesota Twin Cities, Minneapolis, Minnesota, United States, ²Department of Physics, University of Minnesota Twin Cities, Minneapolis, Minnesota, United States

The hard disk drive (HDD) industry continues to demand higher data storage capacity, driving the exploration of advanced technologies like heat-assisted magnetic recording (HAMR). HAMR enables higher KBPI and KTPI, achieving areal densities up to 4 Tb/in² [1], [2]. However, scaling the reader to access shorter bit lengths and narrower track widths limits further increases in BPI and TPI. While two-dimensional magnetic recording (TDMR) offers some relief by improving ADC and partially relaxing reader scaling constraints, it remains insufficient to meet

long-term storage demands. Vector recording is a technique that employs two readers to sense magnetic fields both parallel and perpendicular to the recording layer (Fig. 1) [3]. In this configuration, two bits in adjacent tracks create four magnetic states (++, --, +-, -+). Standard TDMR can distinguish only three of these, failing to differentiate between + - and - + (Fig. 1b). Our vector reader, when combined with a conventional reader, resolves all four states (Fig. 2), enabling a 21% increase in areal density without reducing reader dimensions. To address vector reader biasing limitations, we also introduce alternative reader designs that bias the heads at 45° and 135°, yet offer comparable performance. These designs overcome scaling constraints and support high TPI data recovery, pushing ADC beyond current TDMR capabilities.

[1] R. H. Victora and P. Huang, "Simulation of heat-assisted magnetic recording using renormalized media cells," IEEE Trans. Magn., vol. 49, no. 2, pp. 751–757, Feb. 2013. [2] M. T. Kief and R. H. Victora, "Materials for heat-assisted magnetic recording," MRS Bull., vol. 43, no. 2, pp. 87–92, 2018.

[3] M. F. Erden, W. Eppler, S. Granz, and S. Hernandez, "Vector recording: A new read process at ultra-high tpis," presented at the IEEE TMRC Conference, 2023.

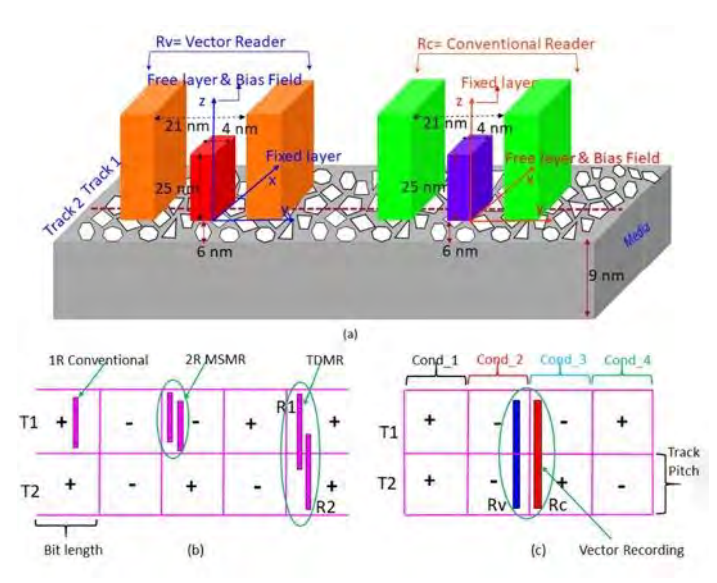


Fig. 1. (a) 3D schematic diagram of two readers with respective filed orientation. (b) Different types of read head architectures [2]. (c) Reading strategy of vector recording.

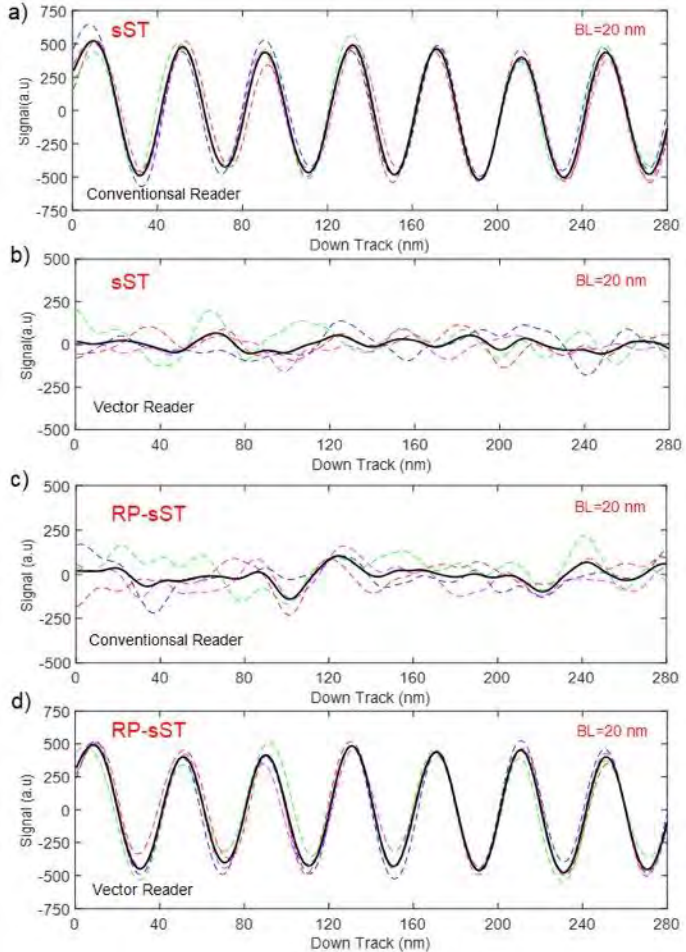


Fig. 2. Readback signals of conventional (Rc) and vector (Rv) reader for different single tone writing patterns at the track edge; a) Rc with same single tone ST on both track (sST), b) Rv with sST, c) Rc with ST with reverse polarity on T1 and T2 (RP-sST), d) Rv with RP-sST.

EG-08. First-principles exploration of Cu-X spacers to enhance magnetoresistance in CPP-GMR read head for next generation HDD

K. Simalaotao^{1,2}, I. Kurniawan², Y. Miura^{3,2}, Y. Sakuraba^{1,2}
¹Graduate School of Pure and Applied Sciences, University of Tsukuba, Tsukuba, Ibaraki, Japan, ²Research Center for Magnetic and Spintronic Materials, National Institute for Materials Science, Tsukuba, Ibaraki, Japan, ³Faculty of Electrical Engineering and Electronics, Kyoto Institute of Technology, Kyoto, Kyoto, Japan

The commercialization of heat-assisted magnetic recording (HAMR) in hard disk drives (HDDs) marks a key milestone in write technology, enabling higher areal density. Advancements in read-head technology are now crucial to unlock the full potential of next-generation HDDs. Currentperpendicular-to-plane giant magnetoresistive (CPP-GMR) devices are promising candidates for next-generation magnetic read heads in HDDs, owing to their low resistance-area (RA) product, which enables compact designs and high-speed operation [1-2]. Co₂FeGa_{0.5}Ge_{0.5} (CFGG) is a prominent half-metallic Heusler alloy known for achieving a high magnetoresistance (MR) ratio in CPP-GMR devices using an Ag spacer [3-4]. However, Ag-based spacers have limitations in achieving MR ratios sufficient for practical use [5-7]. To address this limitation, we systematically explored superior new spacer materials in the B2- and L1₂-type Cu-X binary alloys as alternatives to the conventional Ag spacer. Using firstprinciples calculations and the Landauer formula, we evaluated the majority-spin interface ballistic conductance, which is inversely proportional to the interface resistance in CFGG/Aq/CFGG(001) and CFGG/Cu-X/CFGG(001) trilayers. Our results show that several Cu-X spacer materials outperform Aq in terms of RA reduction, as shown in Figure 1, indicating their potential to enhance the MR ratio. In particular, the RA of the CFGG/CuZn(001) interface is up to ~31% lower than that of CFGG/Ag(001), regardless of interfacial termination, due to superior Fermi surface matching, especially around k_{\parallel} = (0,0) (Fig. 2). These findings highlight the potential of B2-CuZn and various Cu-X binary spacers to improve MR performance, accelerating the development of CPP-GMR read heads for future high-density HDDs.

[1] Diao Z, Chapline M, Zheng Y, Kaiser C, Ghosh Roy A, Chien C J, Shang C, Ding Y, Yang C, Mauri D, Leng Q, Pakala M, Oogane M and Ando Y 2014 Half-metal CPP GMR sensor for magnetic recording *Journal of Magnetism and Magnetic*

Materials 356 73-81

[2] Büker B, Jung J, Sasaki T, Sakuraba Y, Miura Y, Nakatani T, Hütten A and Hono K 2021 Elucidation of the strong effect of an interfacial monolayer on magnetoresistance in giant magnetoresistive devices with current perpendicular to the plane *Phys. Rev. B* 103 L140405

[3] Li S, Takahashi Y K, Furubayashi T and Hono K 2013 Enhancement of giant magnetoresistance by L2₁ ordering in Co₂Fe(Ge_{0.5}Ga_{0.5}) Heusler alloy current-perpendicular-to-plane pseudo spin valves *Applied Physics Letters* 103 042405 [4] Jung J W, Sakuraba Y, Sasaki T T, Miura Y and Hono K 2016 Enhancement of magnetoresistance by inserting thin NiAl layers at the interfaces in

Co₂FeGa_{0.5}/Ag/Co₂FeGa_{0.5}Ge_{0.5} current-perpendicular-toplane pseudo spin valves *Applied Physics Letters* 108 102408 [5] Sakuraba Y, Hattori M, Oogane M, Ando Y, Kato H, Sakuma A, Miyazaki T and Kubota H 2006 Giant tunneling magnetoresistance in Co₂MnSi/Al-O/Co₂MnSi magnetic tunnel junctions *Applied Physics Letters* 88 192508 [6] Tsunegi S, Sakuraba Y, Oogane M, Takanashi K and Ando Y 2008 Large tunnel magnetoresistance in magnetic tunnel junctions using a Co₂MnSi Heusler alloy electrode and a MgO barrier *Applied Physics Letters* 93 112506

[7] Ichinose T, Ikeda J, Onodera Y, Tsuchiya T, Suzuki K Z and Mizukami S 2023 Large tunnel magnetoresistance in magnetic tunnel junctions with magnetic electrodes of metastable body-centered cubic CoMnFe alloys *Journal of Alloys and Compounds* 960 170750

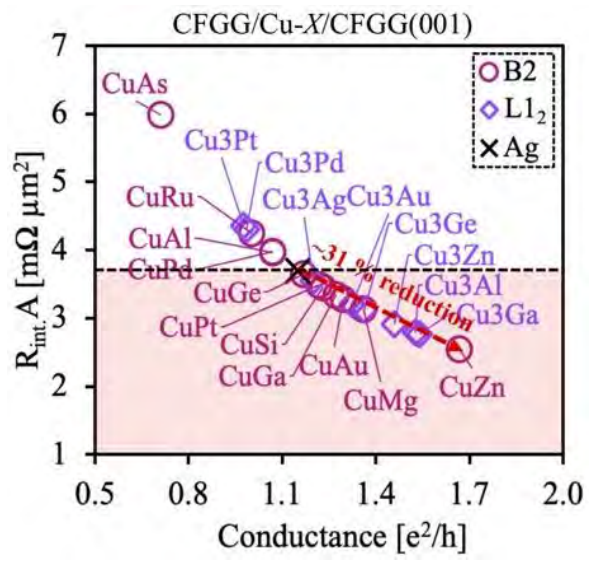


Figure 1 Majority-spin R_{int.}A vs. conductance for various Cu-X and Ag spacers using CFGG electrodes with a FeGa-Cu interface. Several Cu-X spacers (e.g., CuZn, CuMq, CuAu,

CuGa, CuPt in B2; Cu₃Ga, Cu₃Al, Cu₃Zn, Cu₃Ge, Cu₃Au, Cu₃Ag in L1₂) outperform conventional Ag spacer.

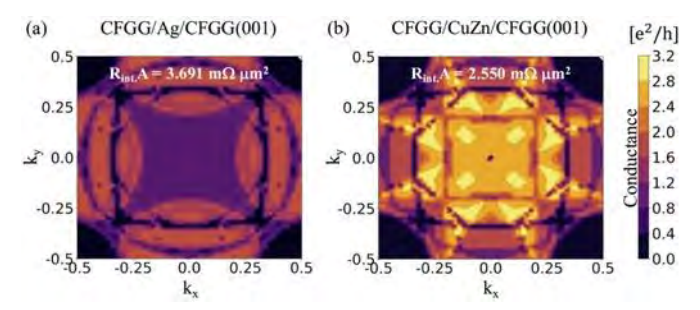


Figure 2 The k_{\parallel} dependence of majority-spin conductance at Fermi level in the parallel magnetization for FeGa termination in (a) CFGG/Ag/CFGG(001) and (b) CFGG/CuZn/CFGG(001) junctions.

EG-09. In-Plane Magnetization Switching in Spin Valves Using Optically Excited Spin Currents

J. Lin¹, Y. L. Guen¹, J. Hohlfeld¹, J. Igarashi¹, Q. Remy², J. Gorchon¹, G. Malinowski¹, S. Mangin¹, T. Hauet¹, M. Hehn¹

¹Institut Jean Lamour, Nancy, France, ²Freie Universität Berlin, Berlin, Germany

Ultrafast magnetization control via laser pulse-induced spin currents, generated through laser-driven demagnetization [1], offers a promising route towards next-generation magnetic memory technologies. By driving the system far from equilibrium, purely longitudinal magnetization dynamics can overcome the precessional limitations of by conventional switching schemes [2]. These optically generated spin current pulses enable ferromagnetic layer reversal within a few hundred femtoseconds in magnetic heterostructures [3,4]. Such switching has predominantly been demonstrated in perpendicularly magnetized spin valve structures [5], where large demagnetization fields inherent to the geometry complicate the investigation of the influence of ferromagnetic (FM) layer thickness. In this work, we employ in-plane magnetized GdCo/Cu/FM spin valves, where the absence of strong perpendicular anisotropy allows us to isolate and systematically study the roles of Curie temperature (T_c) and FM layer thickness on spin-current-induced switching, driven by spin currents originating from the Gd sublattice. We find that, at fixed T_C, increasing the FM layer thickness raises the threshold laser fluence required for switching. Beyond a critical thickness, multiple pulses are needed to fully reverse the magnetization. Moreover, the maximum thickness that can be switched correlates directly with the spin current emitted

by the source layer. These findings [6] provide new insights into ultrafast spin transport and magnetisation switching dynamics.

- [1] G.-M. Choi et al., Nat. Commun., 5, 4334 (2014).
- [2] K. Vahaplar et al., Phys. Rev. Lett., 103, 117201 (2009).
- [3] S. Iihama et al., Adv. Mater., 30, 1804004 (2018).
- [4] Q. Remy et al., Nat. Commun., 14, 445 (2023).
- [5] J. Igarashi et al., Nano Lett., 20, 8654 (2020).
- [6] J.-X. Lin et al., Phys. Rev. Appl., 22, 044051 (2024).

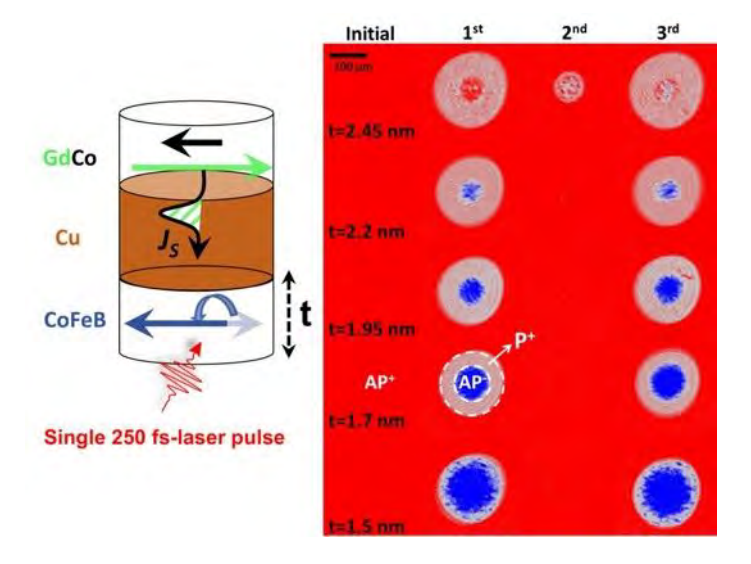


Fig.1 Optically induced magnetization switching in in-plane magnetized spin valves, where GdCo acts as the spin current source (I_s) and CoFeB serves as the switching (free) layer. Kerr microscopy images were recorded after exposure to different numbers of femtosecond single laser pulses, starting from an initial AP+ configuration, where the magnetizations of GdCo and CoFeB are antiparallel. A transition from AP+ to P+ indicates switching of the GdCo layer alone, whereas a transition from AP+ to AP- signifies switching of both the GdCo and CoFeB layers.

EG-10. Magneto-structural characterization and THz emission enhancement in ultrathin Fe/L1 $_0$ -FePt/Pt heterostructures

O. Crisan

National Institute for Materials Physics, Bucharest, Romania

Recent achievements in ultrafast spin physics have enabled the use of heterostructures composed of ferromagnetic (FM)/non-magnetic (NM) thin layers for terahertz (THz) generation. The mechanism of THz emission from FM/NM multilayers has been typically ascribed to the inverse spin Hall effect (ISHE). In this work, we probe the mechanism of the ISHE by inserting a second ferromagnetic layer in the form of an alloy between the FM/NM system. In particular, by utilizing the co-sputtering technique we fabricate Fe/L1₀-FePt/Pt ultra thin heterostructures. We successfully grow the tetragonal phase of FePt (L1₀-phase) as revealed by xrays diffraction- and reflection techniques. We show the strong magnetic coupling between Fe and L1₀-FePt using magnetooptical and Squid magnetometry. Subsequently, by utilizing THz time domain spectroscopy technique we record the THz emission and thus we the reveal the efficiency of spin-to-charge conversion in Fe/L1₀-FePt/Pt. We establish that Fe/L1₀ -FePt/Pt configuration is significantly superior than the Fe/Pt bilayer structure, regarding THz emission amplitude. The unique trilayer structure opens new perspectives in terms of material choices for the future spintronic THz sources.

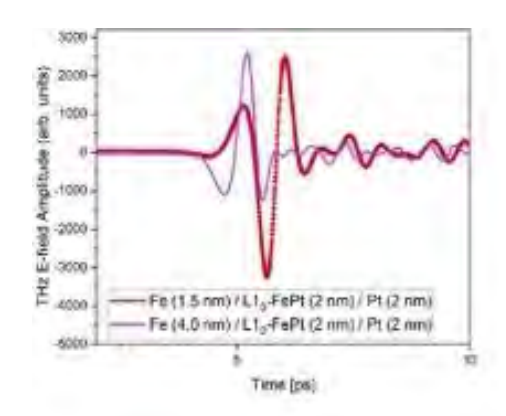


Fig. 1 THz electric field amplitude emitted from two ultrathin Fe/L10-FePt/Pt heterostructures

EG-11. High resolution spin wave based magnetic reader K. Rivkin

RKMAG Corporation, Pacific Grove, California, United States

Magnetic readers currently used in a recording industry rely on a direct observation of a magnetic field. Alternative designs based on a resonant coupling between spin torque oscilator (STO) and recorded magnetization pattern have been proposed, but while they offer an advantage of potentially being able to resolve a magnetization orientation in a multilayer material, i.e. 3D magnetic recording scenario, they have significantly reduced spatial resolution.

We propose an alternative: magnetic reader based on a resonant coupling to localized spin wave modes in the media which are associated with magnetic transitions occuring withinin the recorded magnetization patterns. This allows one to detect the said transitions even if they are associated with exceedingly small spatial distances as well as utilize different spin wave manipulation techniques in order to adjust positioning and resolution of the monitored area, a welcome ability for 2D recording tasks.

EG-12. Laser induced magnetization reversal in Co-Rare Earth alloys

<u>B. Kunyangyuen</u>¹, G. Malinowski¹, D. Lacour¹, J. Lin¹, Y. L. Guen¹, L. D. Buda-Prejbeanu², S. Mangin¹, J. Gorchon¹, M. Hehn¹

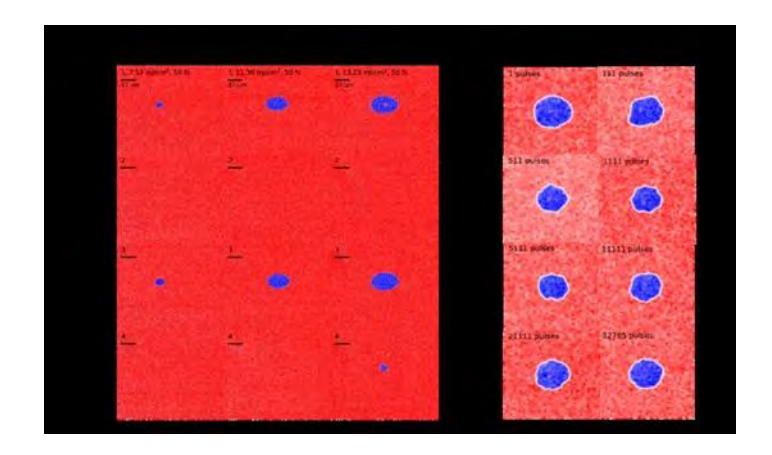
¹Institute Jean-Lamour, Nancy, France, ²SPINTEC, Grenoble, France

Ultrafast All Optical- Helicity Independent switching (AO-HIS) represents the ability to reverse the magnetization of a nanostructure without any applied field with a characteristic time scale to cross zero magnetization of 1 ps. This reversal process, the fastest ever reported for magnetic materials, appears to be of crucial importance for generating smaller, faster and less energy costly storage technologies. First observed in the (FeCo)_xGd_{1-x} ferrimagnetic alloy [1, 2], AO-HIS has been attributed to an ultrafast heating process, characterized by distinct dynamics between the rare earth (RE) and transition metal (TM) elements, and driven by a high transient electron temperature that is out of equilibrium with the lattice. The exchange-driven angular momentum transfer from the rare earth, Gd, and transitions metals, Fe and Co, elements results in total magnetization reversal of (FeCo)_xGd_{1-x} alloy [3, 4].

The extension to other TM-RE alloys single layers failed up

to now. Only a partial single-pulse all-optical switching has been observed only for the first few pulses in case of $Co_{0.75}Dy_{0.25}$ or $Co_{0.75}Tb_{0.25}$ films [5]. On the other hand, AO-HIS could be observed in thin Co/Ho multilayer [6] or adding Gd in Co_xDy_{1-x}, Co_xTb_{1-x} and Co_xHo_{1-x} led to AO-HIS while it fails when Gd concentration is reduced to zero [7]. This presentation will address single-pulse AO-HIS observed in cobalt-rare earth (Co-RE) alloy single layers, specifically where the rare earth elements are Tb, Dy, Ho, or Er. Notably, AO-HIS is observed in Dy- and Ho-based alloys when their composition is near the magnetic compensation point. Conversely, alloys with Tb or Er show only demagnetization. This behavior is counterintuitive, as the reversal mechanism varies significantly with the rare earth element. By studying Hall crosses, we reveal that the reversal process involves the nucleation and propagation of magnetic domain walls, occurring on a microsecond timescale—much slower than in Gd-based materials. I will summarize the current understanding of this intriguing process and its implications for magnetic switching.

- [1] I. Radu, K. Vahaplar, C. Stamm, et al. *Nature*, 472, 205–208 (2011).
- [2] TA. Ostler, J. Barker, R. Evans, et al. *Nature communications*, 3, 666 (2012).
- [3] U. Atxitia, J. Barker, RoyWChantrell, et al. *Physical Review B*, 89, 224421 (2014).
- [4] CS. Davies, T. Janssen, JH. Mentink, et al. *Physical Review Applied*, 13, 024064 (2020).
- [5] Z. Hu, J. Besbas, R. Smith, et al. *Applied Physics Letters*, 120 (2022).
- [6] Y. Peng, G. Malinowski, J. Gorchon, et al. *Physical Review Applied*, 20, 014068 (2023).
- [7] W. Zhang, J. Hohlfeld, TX. Huang, et al. *Physical Review B*, 109, 094412 (2024).



EG-13. CNN/DNN approximation of the recording process coupled with DNN accelerated solution for the magnetization reversal

K. Rivkin

RKMAG, Pacific Grove, California, United States

We propose that using convolution neural network (CNN) layers for magnetic and thermal field profile encoding allows for substantial improvement in both precision and speed of fast AI based recording modeling algorithms. The gains are sufficient enough to enable a coupled recording/magnetic media model capable of resolving both recording and erasure events for a near arbitrary mutli-layer magnetic media configuration.

We demonstrate specifically that for a sub 4.5-5nm grain size there is a substantial shift in the optimal media parameters configuration, from the one based on minimizing the transition (jitter) related parameters to a set of magnetic media layer parameters which allows one to control track width inflation and minimize the erasure tails.

SESSION EP: SPIN AND ORBITAL DYNAMICS (POSTER SESSION)

Chair(s): G. Choi, Department of Energy Science,
Sungkyunkwan University College of Natural Science, Suwon,
Korea (the Republic of)
Thursday, October 30, 2025
09:00 AM-12:00 PM
Exhibit Hall Posters

EP-02-LB. A High Performance Finite Element Approach to Linear and Nonlinear Magnetostatic Modeling

<u>J. Brown</u>, D. Faircloth IERUS Technologies, Inc., Huntsville, Alabama, United States

Current motor and other magnetic system design codes, although sophisticated and accurate for limited scale systems ranging from electric motor design to MRI machines, are not capable of addressing the inherent multilength scale nature of magnetic systems for many applications. At full-scale, these systems have extremely large unknown counts due to the meshing length scales required to model the configuration.

To address the balance between the fidelity of the multiphysics modeling and engineering design optimization for ease of manufacturing, as well as address the multiscale nature of many systems, algorithm and software acceleration via massive parallelization is an absolute

necessity. We present a magnetic modeling solution, named VMP, leveraging DOE's open-source MFEM finite-element libraries, which natively support GPU, HPC, and high-order accuracy in a single package that scales from laptops to HPC environments. The magnetic multiphysics capabilities provided by the MFEM-enhanced VMP unlocks large-scale magnetic field calculations for a wide variety of applications ranging from state of the art magnetic resonance imaging systems used in health care to efficient electric motor design.

We implemented a full nonlinear 3D vector formulation of the magnetic field and flux density, allowing for nonlinear tensor formulations of the relative permeabilities. This work implemented the Jiles-Atherton (JA) hysteresis model to generate realistic hysteresis curves relating the magnetic field to magnetic flux density for input to our software. An example of such a hysteresis model is shown below, where the "loop" around initial magnetization, demagnetization, and remagnetization does not following the same curve. The magnetostatic equation becomes nonlinear and must be solved iteratively. Standard iterative linearization techniques were implemented, including a Newton-Raphson method to iterate through possible values of the permeability which minimized the total configuration energy of the system.

This work demonstrates a fully functional magnetostatic and magneto-quasistatic modeling approach suitable for a large range of user applications. In it, we demonstrate the utility of HPC-based finite element approaches to complex modeling problems, including a representative electric motor (based on a model of the Toyota Prius motor). We demonstrate a user-friendly approach to extend the capabilities of DOE's MFEM libraries to the magnetic modeling community.

Ruoho, S., Dlala, E., & Arkkio, A. (2007). Comparison of demagnetization models for finite-element analysis of permanent-magnet synchronous machines. *IEEE Transactions on magnetics*, *43*(11), 3964-3968.

Jiles, D. C., & Atherton, D. L. (1986). Theory of ferromagnetic hysteresis. *Journal of magnetism and magnetic materials*, 61(1-2), 48-60.

Zirka, S. E., Moroz, Y. I., Harrison, R. G., & Chwastek, K. (2012). On physical aspects of the Jiles-Atherton hysteresis models. *Journal of Applied Physics*, *112*(4).

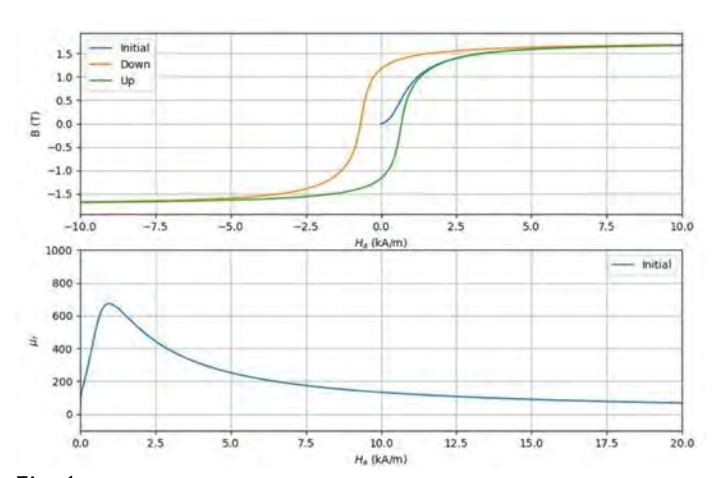


Fig. 1

EP-03-LB. Understanding the Line Shape of Ferromagnetic Resonance Spectrum in a Flip-Chip Measurement

E. D. DeVisscher, A. E. Mays, X. Fan Physics and Astronomy, University of Denver, Denver, Colorado, United States

Flip-chip Ferromagnetic resonance spectrum with a coplanar waveguide has been widely used for studying magnetization dynamics of thin films [1]. Typically, the peak position and linewidth are extrapolated, while the line shape — specifically how far the spectrum deviates from a perfectly symmetric Lorentzian — is neglected. In this work [2], we fit the FMR transmission spectrum using a superposition of a symmetric and antisymmetric Lorentzian. Fig. A shows a representative signal. The pink dots are the data, the purple line is the fit, and the black and gray lines are the symmetric and antisymmetric components of the fit, respectively.

To quantify this deviation, we define a deviation phase angle (DPA), and we find that the DPA of the ferromagnetic resonance spectrum depends on frequency of the microwave (Fig. B), length of the measured sample (Fig. C), impedance mismatch in the transmission line (Fig.D), as well as the material itself. Using a multilayer film consisting of two different ferromagnetic films (Fig. D), we show the possibility to use one ferromagnetic film to calibrate the magnetic susceptibility of the other ferromagnetic film.

[1] Bady, I. (1967). Measurement of linewidth of single crystal ferrites by monitoring the reflected wave in short-circuited transmission line. IEEE

Transactions on Magnetics, 3(3):521–526.

[2] DeVisscher, E., Mays, A., Fan, X. Understanding the Line Shape of Ferromagnetic Resonance Spectrum in a Flip-Chip Measurement. Under review.

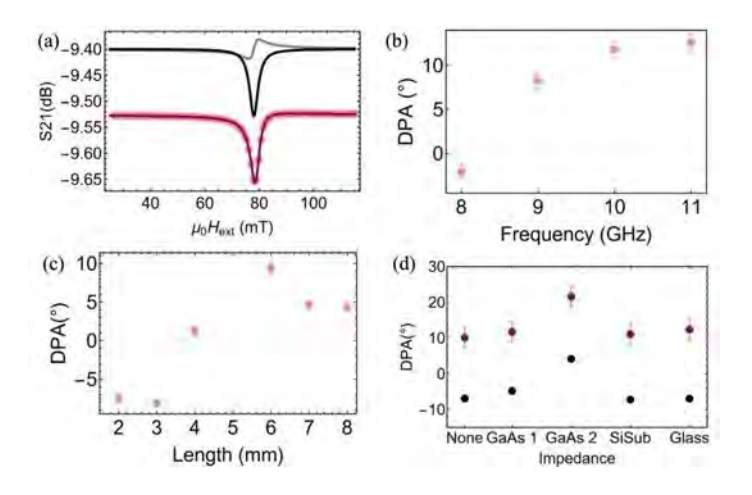


Fig. 1 (A) Typical FMR signal shown with the Lorentzian fit and fit decomposed into symmetric (black) and antisymmetric

(gray) parts. From the measurement of a 4 mm Si/SiO $_2$ /Ni $_{80}$ Fe $_{20}$ (25)/AlO $_x$ (3) film (numbers in parenthesis denoting thickness in

nm) at 10 GHz frequency.

Experimental results for (B) frequency and (C) length dependence of the DPA (degrees). The film was $Si/SiO_2/Ni_{80}Fe_{20}(8)/AlO_x(3)$ with either a constant 10GHz microwave (length dependence) or a constant 6mm length (frequency dependence).

(D) Effect of impedance mismatch on DPA of bilayer signal. The film measured is $% \left(\frac{1}{2}\right) =\frac{1}{2}\left(\frac{1}{2$

 $Si/SiO_2/Ni_{80}Fe_{20}(4)AlO_x(3)Ni_{80}Fe_{20}(8)AlO_x(3)$.

EP-05-LB. Bilinear magnetoresistance in conventional heterostructures

D. Kim¹, K. Kim², J. Jeong³, K. Lee⁴, H. Yang⁵

¹Department of Materials Science and Engineering, Korea
Advanced Institute of Science and Technology (KAIST), Daejeon,
Korea (the Republic of), ²Department of Physics, Yonsei
University, Seoul, Korea (the Republic of), ³Department of
Materials Science and Engineering, Chungnam National
University, Daejeon, Korea (the Republic of), ⁴Department of
Physics, Korea Advanced Institute of Science and Technology
(KAIST), Daejeon, Korea (the Republic of), ⁵Department of

Electrical and Computer Engineering, National University of Singapore (NUS), Singapore, Singapore

Magnetoresistance (MR) is a fundamental spin transport phenomenon essential for reading and writing magnetic states in information storage, novel computing, and sensor applications. Traditionally, MR effects do not scale with an electric field, as they originate from the linear response to an applied field. However, recent studies have extended the understanding of MR beyond the linear response, introducing concepts such as bilinear magnetoelectric resistance (BMER), which scales linearly to both the electric and magnetic fields. BMER has previously been demonstrated only in specific two-dimensional systems exhibiting spin texture in momentum space, such as the surface state of topological insulators and the Rashba systems.

In this study, we demonstrate that BMER is a general phenomenon that can also occur in three-dimensional systems via the spin Hall effect, independent of specific spin-momentum locking mechanisms [1]. The structural asymmetry in spin transport between the top and bottom interfaces of heavy metals enables spin Hall induced-BMER (SH-BMER). This condition is met in bilayers even without a magnetic material, such as Cr/Pt or Ru/Pt bilayers, where we observe BMER. Furthermore, we measure non-linear spin transports and detect the SH-BMER in bilayers composed of an antiferromagnetic insulator a-Fe₂O₃ and a heavy metal. The sign of SH-BMER follows the sign of the spin Hall angle of heavy metals (Pt and Ta), evidencing that the SH-BMER of these bilayers originates from the bulk spin Hall effect, in contrast to previous studies on two-dimensional systems. SH-BMER can play a significant role in overall nonlinear spin transport, particularly in antiferromagnetically coupled systems with negligible magnetization. This discovery provides a crucial framework for accurately understanding nonlinear antiferromagnetic spintronics.

[1] <u>Dong-Jun Kim</u>, Kyung-Whan Kim, Kyusup Lee, Jung Hyun Oh, Xinhou Chen, Shuhan Yang, Yuchen Pu, Yakun Liu, Fanrui Hu, Phuoc Cao Van, Jong-Ryul Jeong, Kyung-Jun Lee, and Hyunsoo Yang, "Spin Hall induced bilinear magnetoelectric resistance" *Nature Materials* 23, 1509-1514 (2024).

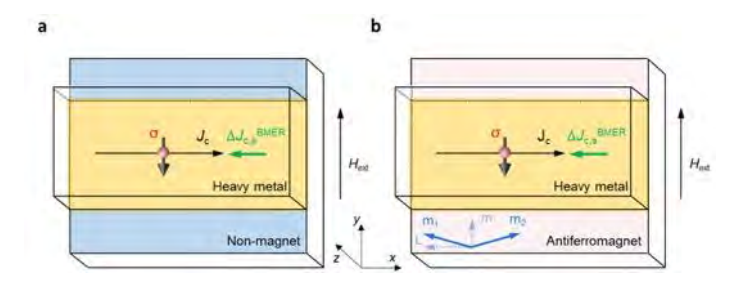


Fig. 1. Spin Hall-induced bilinear magnetoelectric resistances. a,b, Schematic diagrams of the spin Hall-induced bilinear magnetoelectric resistances in non-magnet/heavy metal (HM) and antiferromagnet/HM.

EP-08-LB. Orbital dynamics of hybrid bosonic quasiparticles in magnetic systems

D. To, M. Doty

University of Delaware, Newark, Delaware, United States

We theoretically investigate orbital dynamics in bosonic systems and identify two distinct sources of orbital angular moment (OAM): (i) global rotational motion and (ii) the quantum geometry of wavefunctions. Focusing on the latter, we examine strongly coupled magnon—phonon systems in two-dimensional antiferromagnets and reveal finite OAM arising from quantum geometric effects through two mechanisms: (a) time-parity symmetry breaking, which yields intra-band OAM, and (b) interband coupling, which induces inter-band OAM. Finally, we propose an electrical detection scheme for OAM based on the transverse voltage generated by hybrid magnon—phonon modes.

SESSION EQ: TRANSFORMERS AND POWER ELECTRONICS II (POSTER SESSION)

Chair(s): C. Chinnasamy, Manufacturing Science Division, Oak Ridge National Laboratory, Knoxville, Tennessee, United States and P. Kulik, University of Central Florida, Orlando, Florida, United States

Thursday, October 30, 2025 09:00 AM-12:00 PM Exhibit Hall Posters

EQ-01. Design for AC Loss Reduction in PCB Motors Using Magnet Chamfering

<u>J. Lee</u>, Y. Lee, H. Kim, Y. Lim, W. Kim Gachon University, Seongnamsi, Korea (the Republic of)

This paper studies a magnet chamfering technique to reduce AC loss in coreless, slotless PCB-stator axial flux motors (PCB AFM), which are gaining increasing attention in electrification and robotic applications due to their lightweight construction, minimized axial length, and manufacturing efficiency. By eliminating conventional stator teeth and windings and adopting PCB-etched copper conductors, PCB AFM offer improved compactness and simplified fabrication. However, the absence of cores and slots causes high-frequency time-varying magnetic fields to directly interact with the windings, resulting in significant AC loss—primarily from eddy currents and proximity effects—that degrades overall system efficiency. To address this challenge, this study proposes geometric optimization of the magnet structure through chamfering at the edges of each pole. Chamfering reduces the spatial gradient and temporal variation of the magnetic field near pole transitions, suppressing abrupt flux changes that drive AC loss in the PCB conductors. The technique involves trimming triangular sections at the ends of the magnets. and the removed volume is compensated by increasing magnet thickness to preserve total volume and minimize impacts on flux density and back-EMF.

To identify the optimal configuration, parametric finite element analysis (FEA) is performed by varying chamfer lengths and angles from 20° to 80°. Simulations evaluate their effect on AC loss, current density, and back-EMF under fixed operating conditions and copper usage. The results reveal that increasing chamfer size reduces AC loss by flattening flux transitions, but slightly decreases back-EMF due to non-linear flux behavior. However, volume compensation mitigates this tradeoff and results in a net gain in efficiency.

We further analyze a hybrid method combining magnet chamfering with linear conductor winding. The linear method reduces AC loss by narrowing conductor width near high-gradient regions but increases DC resistance. The hybrid approach balances these effects and achieves greater AC loss reduction while maintaining acceptable back-EMF. The proposed strategy offers a practical design pathway for improving efficiency in PCB AFM.

[1] C. Schmitz, "Performance and Drive Characteristics of Slotless Axial Flux Motors," 2024 IEEE IAS Petroleum and Chemical Industry Technical Conference (PCIC), Orlando, FL, USA, 2024, pp. 1-5, doi:

10.1109/PCIC47799.2024.10832248.

[2] D. -W. Nam, M. -K. Hong, N. -R. Jo, D. -H. Jung and W. -H. Kim, "Design of Coil Patterns for an Axial Flux Permanent Magnet Synchronous Motor With PCB Stator," in IEEE Access, vol. 13, pp. 12936-12944, 2025, doi: 10.1109/ACCESS.2025.3526928.

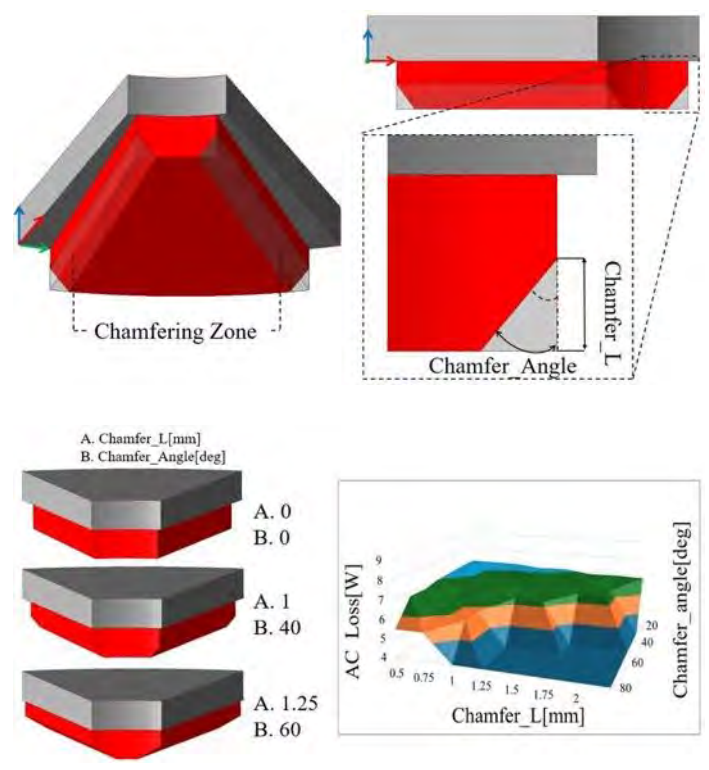


Fig. 1.

EQ-02. Optimal Design of a Support Structure to Enhance Counter-Torque Resistance in a Block-Coil-Type Compact Urban Wind Turbine Generator

H. Kim, Y. Lee, D. Choi, J. Lee, W. Kim

^{*} Best Student Presentation Finalist / LB – Late-breaking Poster

Gachon University, Seongnam-si, Gyeonggi-do, Korea (the Republic of)

This paper proposes a structural support system designed to withstand the counter torque generated by block coil windings in compact urban wind turbine generators. Wind turbines convert wind energy into mechanical rotation of the rotor, which is then converted into electrical energy. While traditional wind farms are typically deployed in offshore or mountainous regions with strong winds, the trend toward miniaturization and decentralization has enabled the installation of small wind power systems within urban environments, such as industrial complexes and building rooftops[1]. These urban applications support the goals of carbon neutrality and energy self-sufficiency. In such compact systems, permanent magnet synchronous generators (PMSGs) are widely used due to their high power density and efficiency. However, conventional core-type PMSGs produce cogging torque, which lowers efficiency and generates noise and vibration[2]. Slotless designs have been explored to address this, and block coil-based generators are gaining attention for their zero cogging characteristics and structural simplicity[3]. In these systems, coils are embedded and fixed inside an injection-molded block, eliminating the stator core. This provides advantages in quiet operation and design flexibility.

Nevertheless, during operation, electromagnetic forces in the stator windings generate counter torque that resists the rotor's motion. Without proper support, this counter torque can compromise structural stability. In response, this study performs 3D coupled electromagnetic-structural analysis to evaluate the torque-induced stress, and proposes a statormounted plate structure that strengthens the system without disturbing the magnetic field.

The proposed approach demonstrates improved mechanical robustness for slotless PMSGs and supports the realization of high-performance compact generators suitable for use in space-constrained urban environments. This research contributes to the design of next-generation urban wind power systems by ensuring both electromagnetic efficiency and structural durability.

[1] V. Ashanin, D. Elinov and O. Birjukova, "Prospects for Using Vertical-Axis Wind Turbines in the Context of Current Urban Development," 2022 International Conference on Industrial Engineering, Applications and Manufacturing (ICIEAM), Sochi, Russian Federation, 2022, pp. 231-235, doi: 10.1109/ICIEAM 54945.2022.9787272.

[2] L. Dosiek and P. Pillay, "Cogging Torque Reduction in

Permanent Magnet Machines," in IEEE Transactions on Industry Applications, vol. 43, no. 6, pp. 1565-1571, Nov.-dec. 2007.

[3] J. Zhao, W. He, W. Fu, Y. Ding and Y. Guo, "Comparative Studies on Performances of Slotted and Slotless High-Speed PMBLDC Motors," in IEEE Access, vol. 12, pp. 13431-13441, 2024.

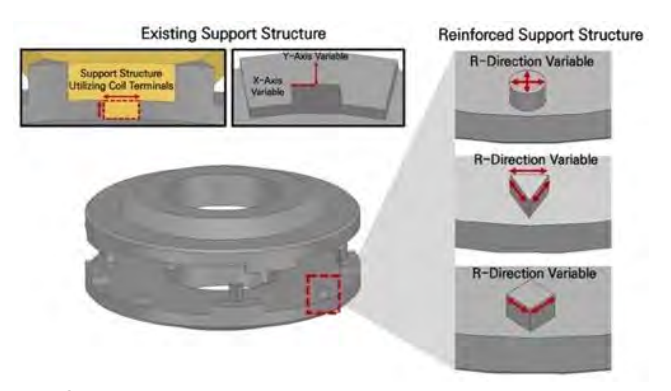


Fig. 2

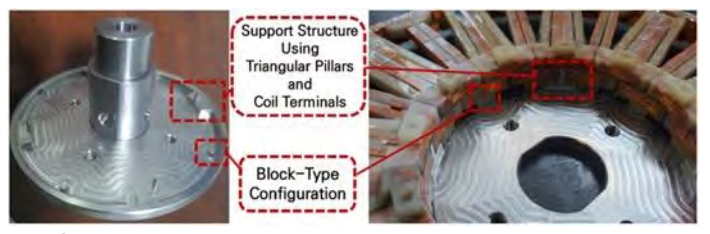


Fig. 2

EQ-03. Force Characterization and Axis Transformation of a Fixed-Bias Flux Three-Phase Magnetic Bearing

S. Noh, <u>S. Byun</u>, J. Kim, J. Park, H. Cho Chungnam National University, Daejeon, Korea (the Republic of)

This study presents the force characterization and axis transformation of a magnetic bearing system that employs permanent magnets to provide a fixed bias flux, in combination with a three-phase electromagnet arrangement for active radial positioning of the rotor. Magnetic bearings offer significant advantages over conventional contact-type bearings, such as maintenance-free operation, elimination of mechanical wear, and extended service life [1–4]. In conventional hybrid magnetic bearings, rotor control is typically achieved by modulating the bias flux generated by permanent magnets together with control currents supplied to the electromagnets. However, this approach does not fully exploit the force contribution of the permanent magnets. To address this limitation, the proposed system is

designed to maximize the utilization of the permanent magnet bias flux. In addition, the adoption of a three-phase winding configuration reduces the number of required power electronic components compared to single-phase full-bridge converter systems, contributing to a more compact and cost-effective implementation.

A 12-pole heteropolar magnetic bearing configured in a three-phase arrangement is applied to both the upper and lower sections of the rotor to realize precise radial position control. The electromagnetic characteristics of the system were evaluated using an equivalent magnetic circuit model, with particular focus on the relationship between rotor eccentricity and the resulting magnetic forces. A schematic representation of the fixed-bias flux three-phase magnetic bearing is shown in Fig. 1.

Force calculations based on the equivalent magnetic circuit model were validated through three-dimensional (3D) finite element analysis (FEA), enabling the development of a comprehensive force model for the system. In addition, the electromagnetic force components of the 12-pole heteropolar magnetic bearing was transformed into an x-y axis coordinate system to facilitate effective radial positioning, and the corresponding force-current characteristics are illustrated in fig.2.

References: [1] N. R. Hemenway and E. L. Severson, "Three-Pole Magnetic Bearing Design and Actuation," IEEE Trans. Ind. Appl., vol. 56, no. 6, pp. 6348-6359, Nov.-Dec. 2020. [2] X. Sun, L. Chen and Z. Yang, "Overview of Bearingless Permanent-Magnet Synchronous Motors," IEEE Trans. Ind. Electron., vol. 60, no. 12, pp. 5528-5538, Dec. 2013. [3] H. Sugimoto, Y. Uemura, A. Chiba and M. A. Rahman, "Design of Homopolar Consequent-Pole Bearingless Motor With Wide Magnetic Gap," IEEE Trans. Magn., vol. 49, no. 5, pp. 2315-2318, May 2013.

[4] W. Zhao and L. Mei, "Reseach on Modular Permanent Magnet Bias Magnetic Bearing," J. Electr. Eng. Technol., vol. 17, pp. 3283-3296, Aug. 2022.

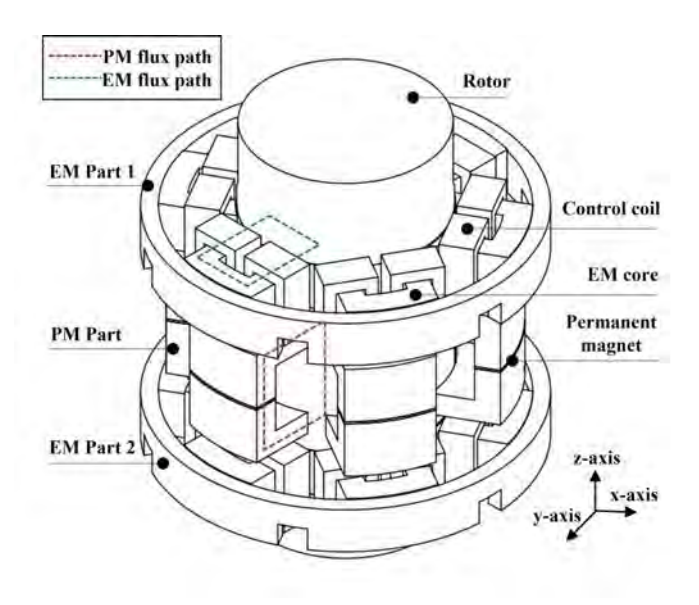


Fig.1 The schematic view of fixed-bias flux three-phase magnetic bearing.

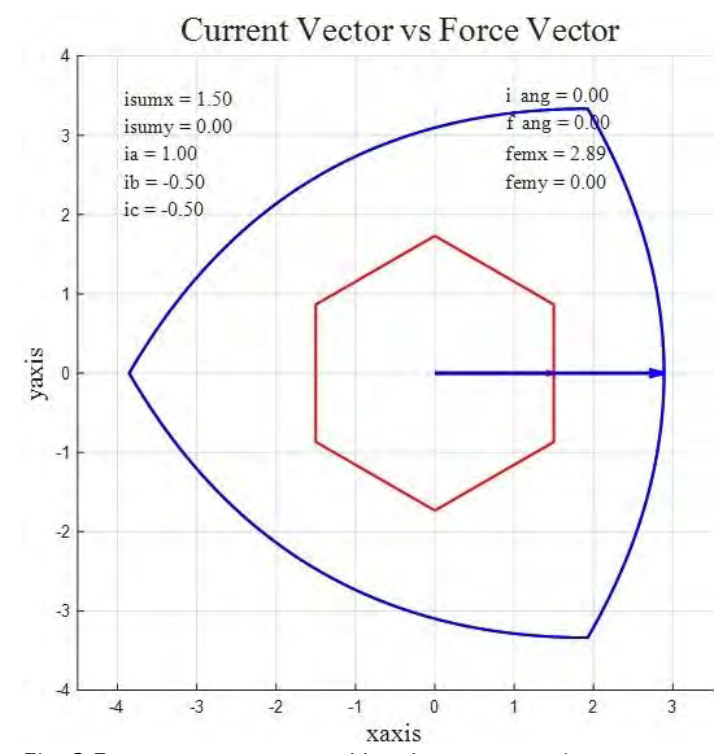


Fig. 2 Force vector generated by electromagnetic part.

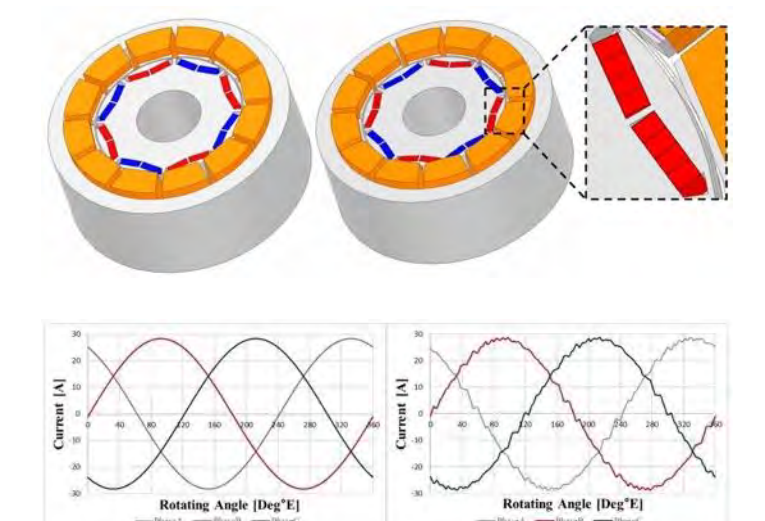
EQ-04. Study on the Reduction of Eddy Current Loss of Permanent Magnet Synchronous Motor considering PWM Y. Lee¹, Y. Lim², J. Lee², H. Kim¹, W. Kim³

¹Department of Next Generation Energy System Convergence, Gachon University, Seongnam-Si, Korea (the Republic of), ²Department of Electrical Engineering, Gachon University, Gyeonggi-do, Korea (the Republic of), ³Department of Electrical Engineering, Gachon University, Seongnam-Si, Korea (the Republic of)

In this study, the effect of PWM (Pulse Width Modulation) current on eddy current loss in permanent magnet synchronous motors (PMSMs) is analyzed, and a method for loss reduction via magnet segmentation is proposed. While traditional motor FEM (Finite Element Method) analysis typically assumes ideal sinusoidal current, PWM control introduces significant harmonic components, which notably increase eddy current loss in permanent magnets[1]. To obtain more accurate predictions of thermal behavior and performance degradation, current waveforms that reflect PWM effects must be applied in the simulation process. Two motor models—one with undivided magnets (ODiv) and one with magnets divided axially into four segments (4Div)—were evaluated under both sinusoidal and PWMcontrolled current waveforms[2]. As shown in Figure 1, the segmented magnet design significantly reduced the eddy current path. The FEM analysis results revealed that, under sinusoidal excitation, eddy current loss was reduced from 5.79 W (0Div) to 0.416 W (4Div). When PWM current was applied, the loss increased to 7.26 W for the undivided model and 0.604 W for the segmented model. This indicates an approximate 34% increase in eddy current loss due to PWM harmonics even after magnet segmentation. Furthermore, Figure 2 compares the ideal sinusoidal current and the actual PWM-shaped current waveform used in the analysis. The Total Harmonic Distortion (THD) of the line-toline voltage under PWM increased by 167%, and torque ripple rose by 33%, emphasizing the necessity of incorporating realistic current waveforms in design stages. This paper confirms that applying PWM-aware current waveforms is essential for accurate eddy current loss estimation. Moreover, magnet segmentation proves to be an effective design strategy, reducing loss by over 90%, thereby enhancing thermal stability and long-term motor performance.

[1] K. Yamazaki, Y. Fukushima and M. Sato, "Loss Analysis of Permanent-Magnet Motors With Concentrated Windings — Variation of Magnet Eddy-Current Loss Due to Stator and Rotor Shapes," in *IEEE Transactions on Industry Applications*, vol. 45, no. 4, pp. 1334-1342, July-aug. 2009 [2] B. -C. Kim, J. -H. Lee and D. -W. Kang, "A Study on the

Effect of Eddy Current Loss and Demagnetization Characteristics of Magnet Division," in IEEE Transactions on Applied Superconductivity, vol. 30, no. 4, pp. 1-5, June 2020.



EQ-05. Design of Magnetization Yoke to Reduce the number of Double Spoke Type PMSM Magnetization Using I-Core D. Choi, J. Lee, H. Kim, Y. Lim, W. Kim Gachon University, Seongnam, Korea (the Republic of)

This paper shows a study on reducing the magnetization cycle and preventing irreversible magnetization in a double spoke motor using an I-core. As interest in spoke-type motors utilizing ferrite permanent magnets increases, there is a growing need for research on magnetization and irreversible magnetization in double spoke rotor configurations. Ferrite magnets offer a significant cost advantage over rare-earth magnets. However, in conventional spoke rotor designs, magnets are deeply embedded within the rotor, making magnetization challenging. As the importance of using permanent magnets that exclude rare-earth materials rises, the application of spoke-type motors becomes more significant, highlighting the necessity of designs that consider magnetization and prevent irreversible magnetization. Therefore, this paper proposes a magnetization voke design that considers magnetization and irreversible magnetization using the Icore in a double spoke PMSM to address these challenges.

[1] H. S. Seol, T. C. Jeong, H. W. Jun, J. Lee, D. W. Kang, "Design of 3-Times Magnetizer and Rotor of Spoke-Type PMSM Considering Post-Assembly Magnetization", IEEE

Transactions on Magnetics, vol. 53, no 11, pp. 1-5, Nov 2017 [2] Q. Wang, H. Ding, H. Zhang, Y. Lv, H. Guo and L. Li, "Study of a Post-Assembly Magnetization Method of a V-Type Rotor of Interior Permanent Magnet Synchronous Motor for Electric Vehicle," in IEEE Transactions on Applied Superconductivity, vol. 30, no. 4, pp. 1-5, June 2020 [3] H. S. Seol, "Design strategy of magnetizer for post-assembly magnetization of spoke-type ferrite magnet motor" J. Electron. Mater. vol. 48 no. 3 Mar. 2019. [4] M. F. Hsieh Y. C. Hsu and D. G. Dorrell "Design of large-power surface-mounted permanent-magnet motors using post assembly magnetization" IEEE Trans. Ind. Electron. vol. 57 no. 10 pp. 3376-3384 Oct. 2010.

EQ-06. A Study on Improvement of Magnetization Performance and Torque Ripple through Magnet Shape Modification in Double-Spoke Type PMSM

S. Kim, H. Kim, <u>D. Choi</u>, J. Lee, W. Kim *Gachon University, Seongnam-si, Korea (the Republic of)*

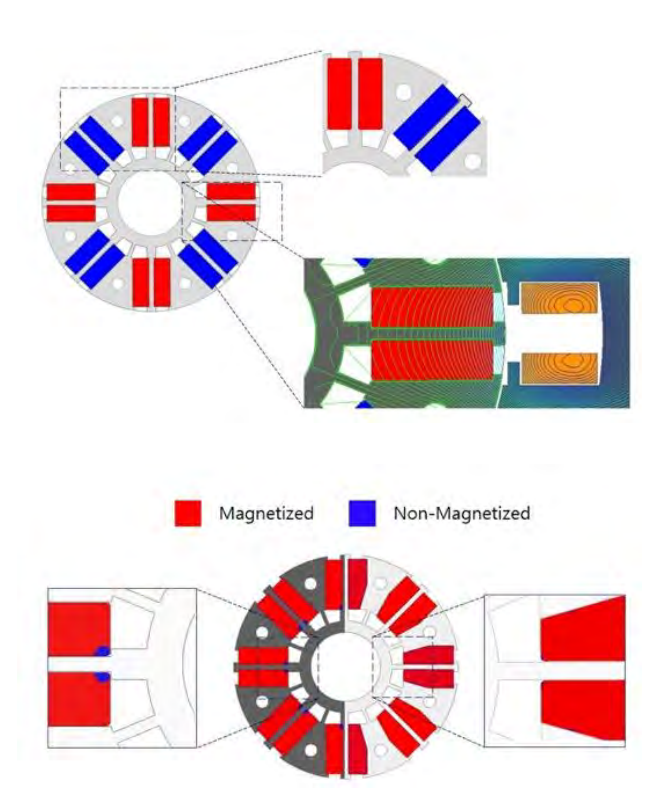
This study aims to improve the magnetization performance and reduce torque ripple by modifying the shape of ferrite magnets in a double-spoke type permanent magnet synchronous motor.

Among the different types of motors, permanent magnet synchronous motors (PMSM) are in ever-increasing demand in applications requiring miniaturization and high power, as they can achieve higher power density compared to motors that do not use permanent magnets[1]. Higher power densities can be achieved with rare earth magnets, but due to supply and demand instability and cost issues caused by export restrictions and trade conflicts in China, a major supplier of rare earth elements, PMSM utilizing ferrite magnets, which are more stable in supply and lower in cost, are being actively researched. Ferrite is a magnetic material composed of various oxides, and these materials have high electrical resistivity and low eddy current losses. However, ferrite magnets have lower coercive force and remanent flux density than rare earth permanent magnets, so spoke-type rotor structures that maximize magnet usage have been developed to secure performance. Spoke and double-spoke rotor structures can maximize magnet usage by inserting the magnets in the longitudinal direction of the motor, but the pole piece becomes narrower the closer it is to the shaft, which is unfavorable for implantation, and torque ripple is also large due to the nature of the flux concentrator structure[2]. Since these problems are directly related to the drive stability, lifespan, and mass production

of electric motors, it is necessary to improve the design of the double-spoke type PMSM in consideration of the engagement performance and torque ripple reduction. Therefore, this study proposes a new rotor geometry that can improve the stiction performance of double-spoke PMSMs and reduce torque ripple at the same time. First, the factors that reduce the magnetization performance of the double spoke type were analyzed, and a structure that improves the magnetization performance and reduces torque ripple was derived from the analysis results. The derived model is compared with the existing double spoke model through FEM and the design feasibility is verified.

[1] M. -J. Jeong, H. -J. Pyo, D. -W. Nam, S. -H. Yang, K. Lee and W. -H. Kim, "The Study on Improving Reluctance Torque and Preventing Irreversible Demagnetization by Modified the Shape of Conventional Ferrite Flux-Concentrated Motor," 2020 IEEE Energy Conversion Congress and Exposition (ECCE), Detroit, MI, USA, 2020, pp. 1386-1391,

[2] Gao, P., Sun, X., Gerada, D., Gerada, C. and Wang, X. (2020), Improved V-shaped interior permanent magnet rotor topology with inward-extended bridges for reduced torque ripple. IET Electr. Power Appl., 14: 2404-2411



EQ-08. Iron Loss Calculation Method for Large-Capacity AC Filter Inductors Considering Non-Uniform Magnetic Flux Density

<u>H. Matsumori</u>¹, T. Yamaguchi¹, N. Kobayashi¹, K. Wada², K. Takano²

¹Nagoya institute of technology, Nagoya, Aichi, Japan, ²Tokyo metropolitan university, Hachioii, Tokyo, Japan

In modern power electronics, achieving higher power density in power converters has become a prominent design goal. While advances in wide-bandgap semiconductors have contributed to this trend, a more pressing issue is the growing impact of magnetic components, such as transformers and inductors. In recent power converter designs, magnetic components account for a significant portion of both system volume and total losses [1-3]. Previous studies have shown that for low-power applications using small inductors, size and loss can be effectively optimized [4-7]. However, in high-power systems using large inductors, challenges arise such as non-uniform magnetic flux density within the core, as shown in Fig. 1 [8]. These issues can introduce significant errors in iron loss estimation, particularly under PWM excitation, where the B-H curve behavior becomes highly nonlinear. Accurate loss prediction is essential for optimal design of magnetic components in large-capacity applications.

This study proposes a method for evaluating the iron loss of AC filter inductors used in PWM inverters, taking into account the radial non-uniformity of flux density within the core shown in Fig. 2. The toroidal core is divided into ten radial sections, and FEM analysis is used to precompute the magnetic flux density and field strength corresponding to the inductor current. Subsequently, the iron losses are estimated by correlating the local magnetic conditions in each switching interval of the PWM excitation with an iron loss map. This loss map, generated in advance using a small test core, assumes uniform flux distribution and serves as a baseline for loss estimation.

To verify the effectiveness of the proposed method, the losses were experimentally measured using the PWM inverter circuit and compared with the calculated results. The 10-section model demonstrated significantly better agreement with the measured values than the conventional undivided model.

A detailed description of the proposed method and its implementation will be provided in the final paper.

1. D. Bortis, D. Neumayr and J. W. Kolar, "ηρ-Pareto optimization and comparative evaluation of inverter

concepts considered for the GOOGLE Little Box Challenge," 2016 IEEE 17th Workshop on Control and Modeling for Power Electronics (COMPEL), Trondheim, Norway, 2016, pp. 1-5, doi: 10.1109/COMPEL.2016.7556767. 2. M. J. Kasper, J. A. Anderson, G. Deboy, Y. Li, M. Haider and J. W. Kolar, "Next Generation GaN-based Architectures: From 240W USB-C Adapters to 11kW EV On-Board Chargers with Ultra-high Power Density and Wide Output Voltage Range," PCIM Europe 2022; International Exhibition and Conference for Power Electronics, Intelligent Motion, Renewable Energy and Energy Management, Nuremberg, Germany, 2022, pp. 1-10, doi: 10.30420/565822004. 3. A. J. Hanson, J. A. Belk, S. Lim, C. R. Sullivan and D. J. Perreault, "Measurements and Performance Factor Comparisons of Magnetic Materials at High Frequency," in IEEE Transactions on Power Electronics, vol. 31, no. 11, pp. 7909-7925, Nov. 2016, doi: 10.1109/TPEL.2015.2514084. 4. R. S. Yang, A. J. Hanson, B. A. Reese, C. R. Sullivan and D. J. Perreault, "A Low-Loss Inductor Structure and Design Guidelines for High-Frequency Applications," in IEEE Transactions on Power Electronics, vol. 34, no. 10, pp. 9993-10005, Oct. 2019, doi: 10.1109/TPEL.2019.2892397. 5. T. Yamaquchi, H.Matsumori, "Proper magnetic materials selection method for AC power inductors under highfrequency rectangular voltage," AIP Advances, vol. 14, no. 1, p. 015132, Jan. 2024. doi: 10.1063/9.0000740. 6. H. Matsumori, T. Shimizu, K. Takano and H. Ishii, "Evaluation of Iron Loss of AC Filter Inductor Used in Three-Phase PWM Inverters Based on an Iron Loss Analyzer," in IEEE Transactions on Power Electronics, vol. 31, no. 4, pp. 3080-3095, April 2016, doi: 10.1109/TPEL.2015.2453055. 7. Bima Nugraha Sanusi, "Advances in High Frequency Inductor Design for Power Converter," Ph.D. thesis, Technical University of Denmark, 2023. 8. H. Sato and T. Shimizu, "Study on an accurate iron loss calculation method considering the non-uniformity of the magnetic flux density," 2015 9th International Conference on Power Electronics and ECCE Asia (ICPE-ECCE Asia), Seoul, Korea (South), 2015, pp. 170-175, doi: 10.1109/ICPE.2015.7167782.

• Magnetic flux density is non-uniform in large cores • BH loops of AC filter inductor in PWM inverter operation • BH loops of AC filter inductor in PWM inverter operation • BH loops of AC filter inductor in PWM inverter operation • BH loops of AC filter inductor in PWM inverter operation • BH loops of AC filter inductor in PWM inverter operation • BH loops of AC filter inductor in PWM inverter operation • BH loops of AC filter inductor in PWM inverter operation • BH loops of AC filter inductor in PWM inverter operation • BH loops of AC filter inductor in PWM inverter operation • BH loops of AC filter inductor in PWM inverter operation • BH loops of AC filter inductor in PWM inverter operation • BH loops of AC filter inductor in PWM inverter operation • BH loops of AC filter inductor in PWM inverter operation • BH loops of AC filter inductor in PWM inverter operation

Figure 1 : Challenges in loss evaluation of large-capacity filter inductors

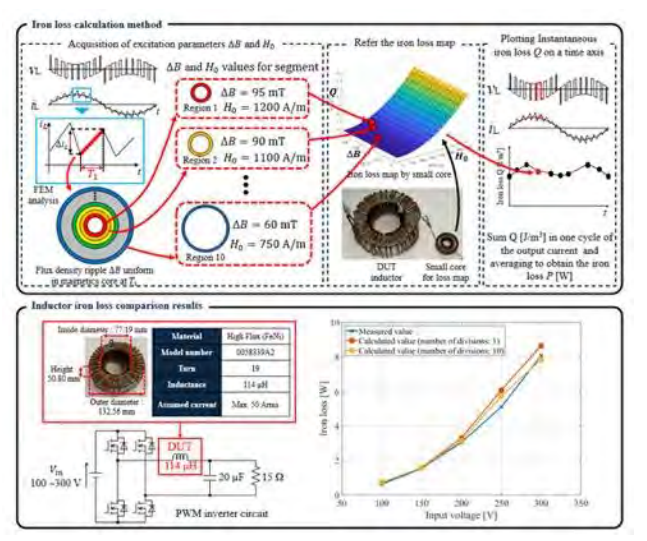


Figure 2: Iron loss calculation method and calculation accuracy

SESSION ER: HARD MAGNETIC MATERIALS II (POSTER SESSION)

Chair(s): S. Okada, Multi-Material Research Institute, National Institute of Advanced Industrial Science and Technology (AIST),
Nagoya, Japan
Thursday, October 30, 2025

Thursday, October 30, 2025 09:00 AM-12:00 PM Exhibit Hall Posters

ER-01. Altering Solidification Kinetics in Nd-Fe-B Alloys through Alloying Additions for 3D-Printable Magnets

S. Krishnan, Q. Guo, J. Shield

MME, University of Nebraska - Lincoln, Lincoln, Nebraska, United States

A significant challenge in additive manufacturing (AM) of Nd-Fe-B-based permanent magnets using laser powder bed fusion (LPBF) is achieving fully dense, crack-free parts due to the material's brittleness and complex thermal behavior. We have established LPBF processing parameters – combinations of laser power, speed, and hatch spacing – that results in fully dense parts (>99% density). Building on this foundation, we designed and fabricated specially developed alloy compositions. Among these, the V+Cmodified composition yielded LPBF parts with isotropic magnetic behavior, with a coercivity as high as 7.5 kOe, remanence of 4.6 kG, and a maximum energy product ((BH)max) of 3.35 MGOe (Figure 1), achieved without the use of a heated build plate or post-processing heat treatment. The alloys were designed using melt spinning as a proxy for the rapid solidification conditions encountered in LPBF and exhibited a broad processing window, with peak coercivity values of 14.98 kOe at 13 m/s for the $(Nd_{15}Fe_{79}B_6)_{88}Ti_6C_6$ alloy and 17.6 kOe at 9 m/s for the $(Nd_{15}Fe_{79}B_6)_{94.6}V_4C_{1.4}$ alloy. These two compositions were selected for LPBF processing. Figure 2 shows identical hysteresis loops of Part 5 (shown in the inset), with the applied magnetic field oriented parallel and perpendicular to the build direction (BD), confirming isotropic magnetic behavior.

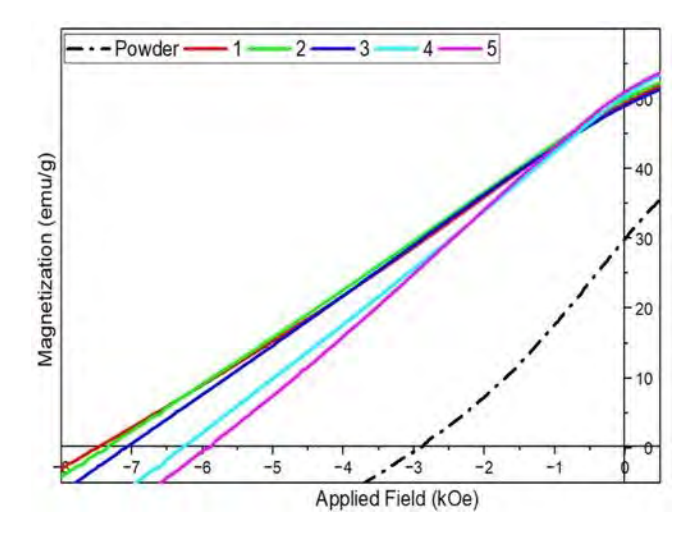


Fig 1 Room temperature demagnetization curves of the LPBF processed parts 1-5 with different combinations of laser power, velocity, and hatch spacing (shown in the inset Fig 2), with Part 1 exhibiting a coercivity of 7.50 kOe without the use of heated bed or post-process heat treatment. The dotted line represents the demagnetization curve of the starting powder.

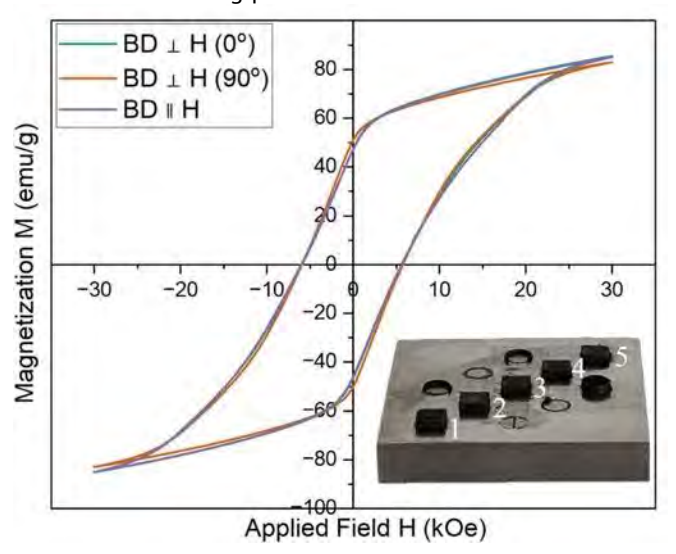


Fig 2 Hysteresis loops of LPBF-processed Nd-Fe-B magnet measured along different orientations relative to the build direction (BD). The data corresponds to Part 5 in the inset. Loops for BD \parallel H and BD \perp H (0° and 90°) indicate isotropic magnetic behavior.

ER-03. Chemical bond and phase stability of Ga-doped $\text{Sm}_2\text{Fe}_{17}\text{C}_x$ Magnet

X. Liu, C. I. Nlebedim

Ames National Laboratory, Ames, Iowa, United States

Alternative to Nd-Fe-B, the interstitial intermetallic compounds Sm₂Fe₁₇X₃ (X=C and N) with a rhombohedral Th₂Zn₁₇-type structure (2:17) display excellent intrinsics hard magnetic properties. While Sm₂Fe₁₇N₃ is metastable and decomposes at a temperature less than 650 °C, $Sm_2Fe_{17}C_x$ can be prepared by arc-melting for x < 1.0 [1]. Doping chemical elements such as Al, Si and Ga enable the formation of 2:17 single phase in arc-melted Sm₂Fe₁₇C_x alloy with x up to 3 [2]. This provides a potential way to prepare fully dense bulk Sm₂Fe₁₇C_x magnets using high temperature processes such as vacuum melting and sintering. To understand the role of these doping elements, we have performed first-principles electronic structure calculations and chemical bond analysis to identify factors contributing to the enhanced phase stability in Sm₂(Fe,Ga)₁₇C₃. Carbon atoms occupy the octahedral 9e site, which is coordinated by two Sm atoms, two Fe atoms at the 18f site, and two Fe atoms at the 18h site. The calculation indicates that Ga prefers to partially replace Fe at the crystallographic site of 9d and 18h in Sm₂Fe₁₇C₃ and Sm₂Fe₁₇, respectively. Doped Ga atoms result in more negative formation energy in Sm₂Fe₁₇C₃, implying a more stable 2:17 structure. Crystal Orbital Hamilton Populations (COHP) calculations indicate that doped Ga atoms induce electron redistribution between different chemical bonds. It enhances the bond strength of Fe(18h)-Sm and Fe(18f)-Sm while slightly reducing that of C-Sm bond (Table 1). The results imply that phase stability and synthesis of Sm₂Fe₁₇C₃ can be enhanced from chemical bond engineering, which is a promising approach to develop novel magnets.

[1] J Coey, Magnetism and Magnetic materials, Cambridge University Press, Cambridge, 2010
[2] B. G. Shen, F. W. Wang, L. S. Kong, L.Cao and W. S. Zhan 1994 J. Appl. Phys. 75, 6253

	Sm-C	Sm-Fe (18f)	Sm-Fe (18h)	C-Fe (18f)	C-Fe (18h)
$Sm_2Fe_{17}C_3$	-2.96	-1.65	-1.95	-5.25	-4.94
Sm ₂ (Fe,Ga) ₁₇ C ₃	-2.93	-1.75	-2.14	-5.27	-4.98

Fig. 1 Integrated COHP (ICOHP, eV/pair) in $Sm_2Fe_{17}C_3$ and $Sm_2(Fe,Ga)_{17}C_3$

^{*} Best Student Presentation Finalist / LB – Late-breaking Poster

ER-04. Tuning the Intrinsic Magnetic Properties of Sm(Fe₁. $_x$ Co_x)₁₀V₂ Compounds with the ThMn₁₂-type Structure X. Zheng, P. Si, B. Zhang, <u>Y. Song</u>, J. Park Korea Institute of Materials Science, Changwon, Korea (the Republic of)

ThMn₁₂-type SmFe-based permanent magnets have gained interest as rare-earth-lean materials due to their high theoretical energy product and lower rare-earth usage compared to Nd–Fe–B magnets [1–3]. Despite excellent theoretical magnetic properties in thin films, their bulk performance is hindered by the thermodynamic instability of the ThMn₁₂ phase [4]. To improve phase stability and coercivity (H_c), elements like Ti, V, Mo, Cr, W, Si, and Zr have been added [5–8], though they often reduce the saturation magnetization (M_s) [6,9,10].

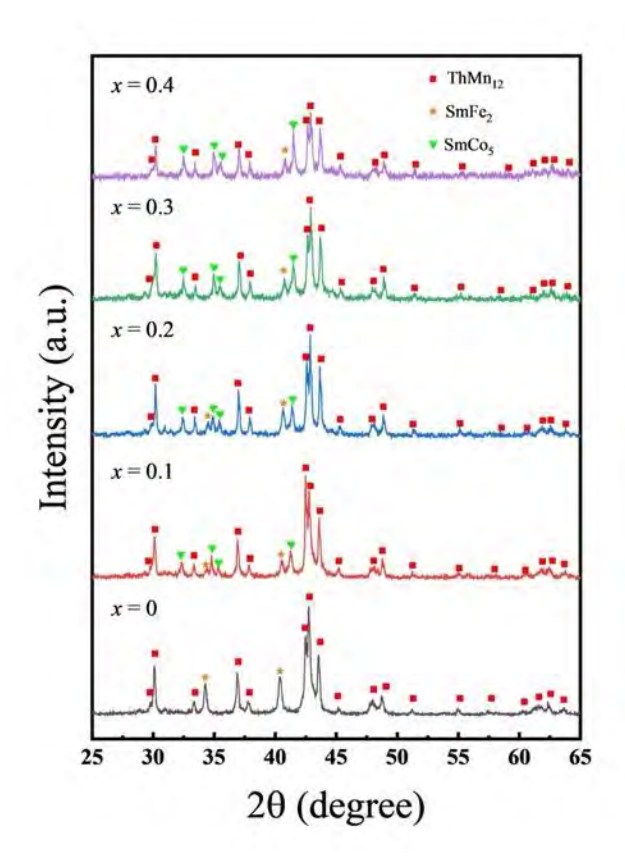
In this study, we investigated the $Sm(Fe_{1-x}Co_x)_{10}V_2$ system (x = 0 - 0.4), where V stabilized the ThMn₁₂ structure and Co tuned the intrinsic magnetic properties. Samples were prepared via arc melting and homogenization. X-ray diffraction confirmed ThMn₁₂-type phase as the primary component in all compositions, with lattice parameters slightly decreasing with Co content due to Co's smaller atomic radius. Magnetic measurements using aligned powder and PPMS revealed that M_s increased with Co addition, peaking at x = 0.2, likely due to Co's high magnetic moment and interaction with the 1:12 matrix. H_a also rose up to x = 0.3, suggesting enhanced magnetocrystalline anisotropy, but both M_s and H_a slightly declined beyond x =0.3, possibly due to secondary phases or structure disruption. Meanwhile, Curie temperature (T_c) gradually increased with more Co, reflecting improved thermal stability.

Sm(Fe_{0.8}Co_{0.2})₁₀V₂ exhibited the most balanced performance, combining high M_s , strong anisotropy, and elevated T_c . These results highlight that moderate Co substitution effectively enhances the intrinsic magnetic performance of the ThMn₁₂-type compounds without compromising structural integrity, offering practical insights for developing advanced, rare-earth-lean permanent magnets.

[1] Y. Hirayama, Y.K. Takahashi, S. Hirosawa, K. Hono, Intrinsic hard magnetic properties of Sm(Fe_{1-x}Co_x)₁₂ compound with the ThMn₁₂ structure, Scripta Materialia 138 (2017) 62–65. https://doi.org/10.1016/j.scriptamat.2017.05.029. [2] P. Tozman, H. Sepehri-Amin, Y.K. Takahashi, S. Hirosawa, K. Hono, Intrinsic magnetic properties of Sm(Fe_{1-x}Co_x)₁₁Ti and Zr-substituted Sm_{1-y}Zr_y(Fe_{0.8}Co_{0.2})_{11.5}Ti_{0.5} compounds with

ThMn₁₂ structure toward the development of permanent magnets, Acta Materialia 153 (2018) 354-363. https://doi.org/10.1016/j.actamat.2018.05.008. [3] P. Tozman, Y.K. Takahashi, H. Sepehri-Amin, D. Ogawa, S. Hirosawa, K. Hono, The effect of Zr substitution on saturation magnetization in $(Sm_{1-x}Zr_x)(Fe_{0.8}Co_{0.2})_{12}$ compound with the ThMn₁₂ structure, Acta Materialia 178 (2019) 114-121. https://doi.org/10.1016/j.actamat.2019.08.003. [4] K. Kobayashi, S. Suzuki, T. Kuno, K. Urushibata, N. Sakuma, M. Yano, T. Shouji, A. Kato, A. Manabe, The stability of newly developed (R,Zr)(Fe,Co)_{12-x}Ti_x alloys for permanent magnets, J. Alloys Compd. 694 (2017) 914-920. https://doi.org/10.1016/j.jallcom.2016.09.311. [5] K.H.J. Buschow, Permanent magnet materials based on tetragonal rare earth compounds of the type $RFe_{12-x}M_x$, J. Magn. Magn. Mater. 100 (1991) 79-89. https://doi.org/10.1016/0304-8853(91)90813-P. [6] R. Madugundo, N.V. Rama Rao, A.M. Schönhöbel, D. Salazar, A.A. El-Gendy, Recent Developments in Nanostructured Permanent Magnet Materials and Their Processing Methods, in: Magn. Nanostructured Mater., Elsevier, 2018: pp. 157-198. https://doi.org/10.1016/B978-0-12-813904-2.00006-1. [7] A.M. Gabay, G.C. Hadjipanayis, Recent developments in RFe₁₂-type compounds for permanent magnets, Scr. Mater. 154 (2018) 284-288. https://doi.org/10.1016/j.scriptamat.2017.10.033. [8] P. Tozman, H. Sepehri-Amin, Y.K. Takahashi, S. Hirosawa, K. Hono, Intrinsic magnetic properties of Sm(Fe_{1-x}Co_x)₁₁Ti and Zr-substituted $Sm_{1-y}Zr_y$ (Fe_{0.8}Co_{0.2})_{11.5}Ti_{0.5} compounds with ThMn₁₂ structure toward the development of permanent magnets, Acta Mater. 153 (2018) 354-363. https://doi.org/10.1016/j.actamat.2018.05.008. [9] R. Verhoef, F.R. de Boer, Z. Zhi-dong, K.H.J. Buschow, Moment reduction in RFe_{12-x}T_x compounds (R=Gd, Y and T=Ti, Cr, V, Mo, W), J. Magn. Magn. Mater. 75 (1988) 319 -322. https://doi.org/10.1016/0304-8853(88)90037-6. [10] X.P. Zhong, F.R. De Boer, D.B. De Mooij, K.H.J. Buschow, Magnetic coupling in the tetragonal rare earth iron compounds of the type R(Fe,V)₁₂, J. Common Met. 163 (1990)

123-132. https://doi.org/10.1016/0022-5088(90)90091-W.



ER-05. Magnetic properties and element site occupation of Zn-substituted W-type hexagonal ferrites

T. Nakagawa, K. Ota, A. Yonaga, S. Seino *The University of Osaka, Suita, Japan*

Ferrite magnets are known for their low cost, stability, and abundance of constituent elements, standing alongside rare-earth magnets in the market. W-type ferrites are promising next-generation materials, with ~10% higher saturation magnetization and similar anisotropy fields compared to M-type. However, their complex structure—where transition metal ions occupy seven possible spin sites—requires detailed understanding of element site occupancy to improve performance.

This study investigates Zn as a key dopant in enhancing saturation magnetization in $SrZn_xMn_{2-x}$ -W, $SrZn_xMg_{2-x}$ -W, and $SrZn_xFe_{2-x}$ -W ferrites. Using techniques like synchrotron X-ray, neutron diffraction, and EXAFS, Zn was found to prefer the down-spin 4e site. In $SrZn_xMn_{2-x}$ -W, Mn mainly occupied 4e and 6g sites. Calculated magnetization based on site occupancy closely matched experimental results, increasing with Zn content. In $SrZn_xMg_{2-x}$ -W, Zn also favored

4e sites, while Mg primarily occupied the 6g site and partly tetrahedral sites. Magnetization rose with Zn content, more than in the Mg- substituted system due to Zn's preference for down-spin sites. Across all ferrites, Zn enhanced magnetization by occupying down-spin sites. Since Zn, Mn, and Mg rarely occupied certain sites (4f_{VI}, 2d, 12k). These positions are likely filled by Fe. Replacing Fe in 4f_{VI} could further boost magnetization. Overall, this study elucidates element-specific site preferences in Zn-substituted W-type ferrites and their impact on magnetic properties.

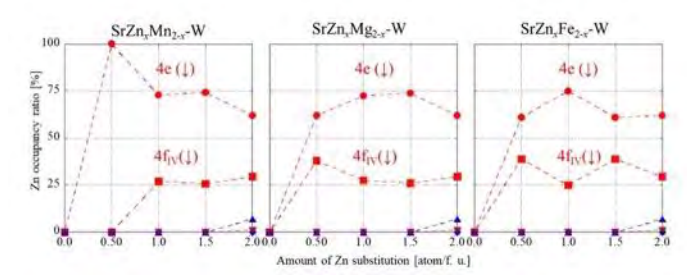


Fig. 1 Change in site occupancy of Mn and Mg with respect to the amount of Zn substitution in $SrZn_xMn_{2-x}$ -W and $SrZn_xMg_{2-x}$ -W ferrites

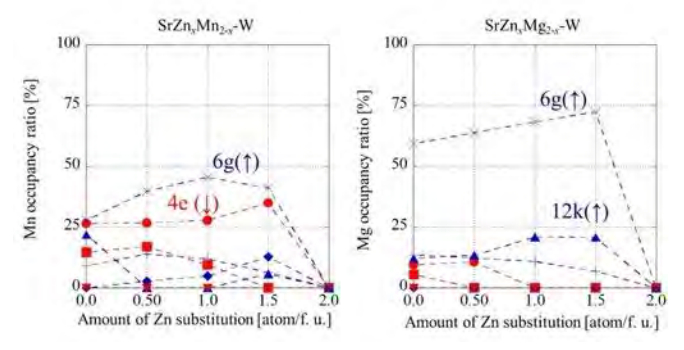


Fig. 2 Change in site occupancy of Zn with respect to the amount of Zn substitution in $SrZn_xMn_{2-x}-W$, $SrZn_xMg_{2-x}-W$ and $SrZn_xFe_{2-x}-W$ type ferrites

ER-06. Process-driven Microstructure Control in Additively Manufactured Alnico Permanent Magnets

<u>A. R. Duong</u>¹, I. M. Smith¹, O. Bishop¹, C. Mayer¹, K. Snyder², R. Barua¹

¹Virginia Commonwealth University, Richmond, Virginia, United States, ²Commonwealth Center for Advanced Manufacturing, Disputanta, Virginia, United States

Among the potential alternatives to rare-earth magnets, Alnico alloys offer compelling advantages for hightemperature applications (>200 °C) due to their thermal stability, corrosion resistance, and reliance on earthabundant elements. Their magnetic performance originates from a spinodally decomposed microstructure consisting of ferromagnetic (Fe-Co)-rich α₁ rods embedded in a nonmagnetic (Al-Ni)-rich α_2 matrix. The processing route critically influences this phase-separated microstructure and, in turn, the magnetic properties of the alloy. This work investigates process-structure-property relationships in Alnico fabricated via Direct Energy Deposition (DED)—a metal additive manufacturing technique that enables directional solidification and microstructure tailoring. Gas-atomized, pre-alloyed Alnico powders were printed into 3 × 5 × 10 mm³ cuboidal specimens using a laser-assisted DED system equipped with real-time monitoring. Key process parameters—including laser power, scan speed, and powder mass flow rate—were evaluated through Global Energy Density (GED) to assess their effect on microstructural evolution and magnetic behavior.

As-built samples exhibited directionally solidified columnar grains with high saturation magnetization (~120 emu/g), while coercivity was highly sensitive to GED. Postdeposition heat treatments involved homogenization at ~850 °C for 10 minutes followed by controlled cooling to 550 °C over 4 hours in an inert atmosphere. This induced spinodal decomposition, refining the α_1/α_2 nanostructure (Fig 1) and enhancing magnetic properties (Fig 2). Transmission electron microscopy and Lorentz imaging revealed that lower GED conditions promoted fine-scale phase separation and improved domain wall pinning via α_1/α_2 interfaces. These findings demonstrate DED's potential as a scalable pathway for manufacturing high-performance Alnico magnets with reduced reliance on post-processing.

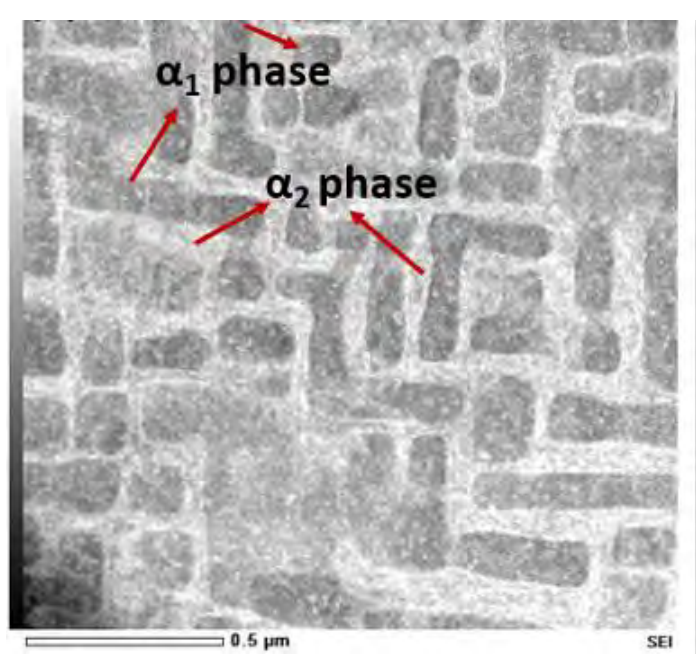


Fig 1. TEM showing Fe-rich α_1 phase and the Ni–Al-rich α_2 phase

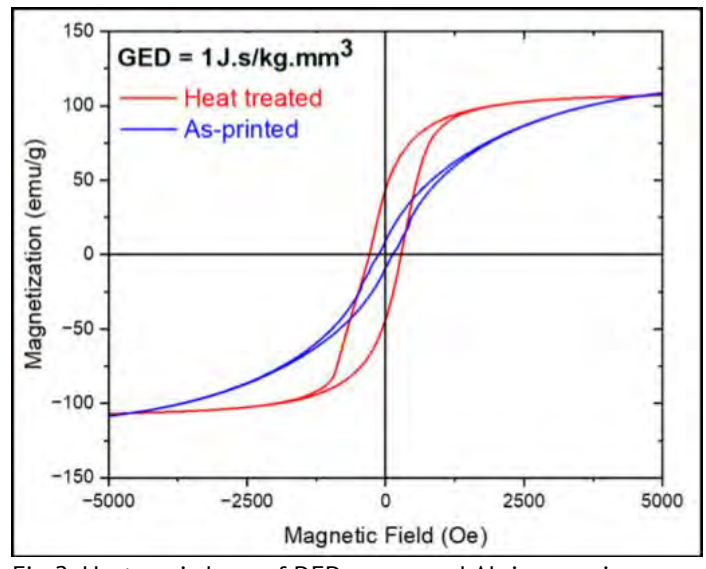


Fig 2. Hysteresis loop of DED-processed Alnico specimen pre- and post-heat treatment

ER-07. Enhanced magnetic anisotropy in $(Fe_{0.7-x}Co_{0.3}Zr_x)_2B$ Nanocrystallites

P. Joshi¹, H. Abbas¹, T. Karki¹, J. Mohapatra¹, X. Liu², P. Liu¹

Physics, The University of Texas at Arlington, Arlington, Texas, United States, ²Ames Laboratory, Critical Materials Institute, Ames, Iowa, United States

Transition metal boride (Fe_{0.7}Co_{0.3})₂B with tetragonal structure is emerging as a strong candidate for rare-earthfree permanent magnet applications due to its inherently high magnetization, magnetocrystalline anisotropy, and Curie temperature [1]. In this study, we developed (Fe_{0.7-} $_{x}Co_{0.3}Zr_{x})_{2}B$ (x = 0, 0.01, 0.02, 0.03, 0.04) hard magnetic phase via arc melting followed by rapid solidification via melt spinning. X-ray diffraction (XRD) confirms the formation of a single phase with the tetragonal structure. with an average crystallite size of 30 nm. Singular point detection (SPD) analysis showed that Zr incorporation enhances magnetocrystalline anisotropy, increasing the anisotropy field from 7.5 to 9.5 kOe with an increase of Zr content from x=0 to x=0.03. Room temperature magnetization loops reveal saturation magnetization (M_S) of 130-140 emu/g and an optimum coercivity of approximately 0.4 kOe. Additionally, Bloch's law fitting of temperature-dependent magnetization data suggests weakened ferromagnetic exchange interactions with increasing Zr content. These findings demonstrate that minor Zr substitution significantly improves magnetic anisotropy, suggesting (Fe_{0.7}Co_{0.3})₂B-based alloys as promising candidates for next-generation, high-performance permanent magnets.

1. Lamichhane, T.N., et al., Reinvestigation of the intrinsic magnetic properties of (Fe1-xCox) 2B alloys and crystallization behavior of ribbons. Journal of Magnetism and Magnetic Materials, 2020. 513: p. 167214.

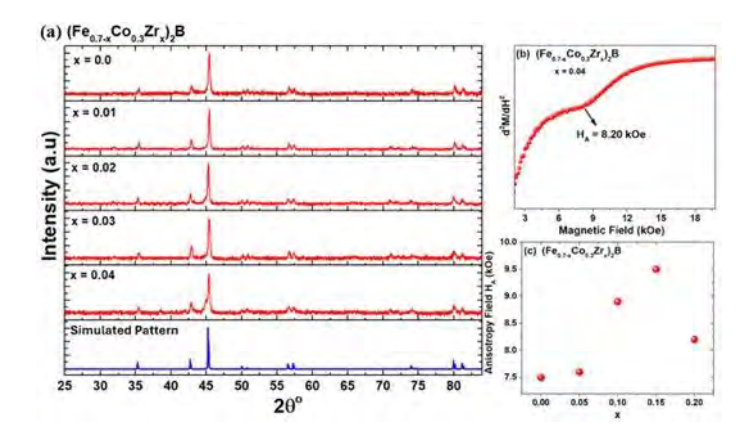


Figure. 1: (a) X-ray diffraction patterns for $(Fe_{0.7-x}Co_{0.3}Zr_x)_2B$ nanocrystallites with $x=0.00,\,0.01,\,0.02,\,0.03,\,$ and 0.04. (b) Anisotropy field at 300 K measured using the singular point detection technique for $(Fe_{0.66}Co_{0.3}Zr_{0.04})_2B$ nanocrystallites. (c) The variation of anisotropy field with Zr content.

ER-08. High Anisotropy Field in Fe₃CoB₂ Nanocrystallite Ribbons

H. Abbas¹, P. Joshi¹, T. Karki¹, J. Mohapatra¹, X. Liu², P. Liu¹

¹Physics, The University of Texas at Arlington, Arlington, Texas, United States, ²Ames Laboratory, Critical Materials Institute, Ames, Iowa, United States

In this study, we developed high magnetic anisotropy in the Fe₃CoB₂ compound via the melt spinning process. X-ray diffraction (XRD) analysis confirmed that the synthesized nanocrystallite ribbons possess an orthorhombic structure [1]. The crystallite size, calculated from the XRD pattern, was observed to be 40 nm. The singular point detection (SPD) technique was used to find the anisotropy field, which was observed to be 10.7 kOe (Fig. 1a). M-H loop at 300 K reveals saturation magnetization of 153 emu/g with a low coercivity of 100 Oe. Temperature-dependent magnetization (M-T) curve indicates a Curie temperature well above 800 K (Fig. 1b), indicating the thermal robustness of this phase. Zero-field-cooled (ZFC) and field-cooled (FC) magnetization curves exhibit a distinct transition near 150 K, likely associated with collective freezing/superspin glass-like behavior (Fig. 1c, d). These results highlight the potential of Fe₃CoB₂ as a thermally stable, rare-earth-free magnetic material with high anisotropy field and thermal stability. [1]. Xia, W., et al., Accelerating the discovery of novel magnetic materials using machine learning-guided adaptive feedback. Proceedings of the National Academy of Sciences, 2022. 119(47): p. e2204485119.

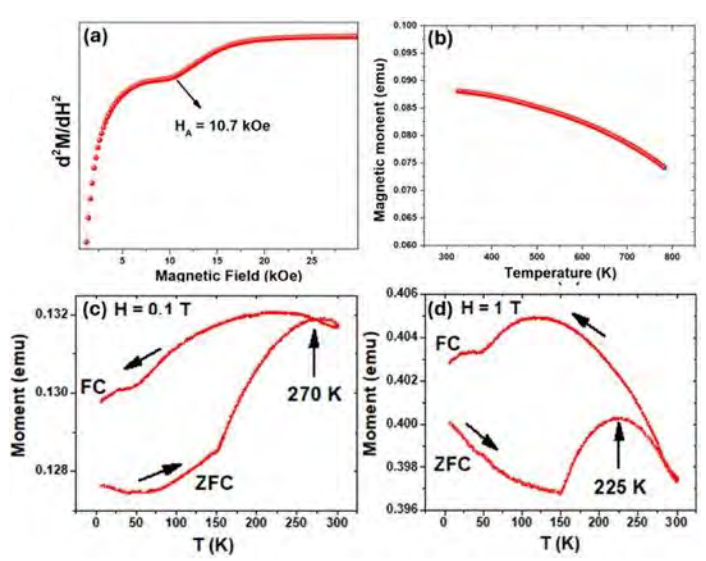


Figure. 1: (a) Anisotropy field for Fe $_3$ CoB $_2$ nanocrystallites using singular detection technique, (b) M-T curve exhibits Curie temperature above 800 K, (c, d) ZFC-FC curves at dc magnetic field of 0.1 and 1 T.

ER-09. Prediction, Synthesis, and Experimental Validation of Magnetic Order and Dimensionality in Cerium-Based Compounds Guided by Structural Characteristics and Tricritical Exponents

J. A. Torres, T. Lamichhane, A. S. Poulo Engineering Physics, University of Central Oklahoma, Oklahoma City, Oklahoma, United States

Ce, the most abundant and chemically versatile lanthanide [3], offers immense potential to address critical shortages in high-performance magnet materials, particularly by discovering novel compounds suitable for gap magnets [1, 2]. Predicting magnetic order and dimensionality in ceriumbased compounds is pivotal due to their unique magnetic and electronic behaviors. In this study, we combine structural characteristics (lattice symmetry, valency, bond lengths, coordination environments) and tri-critical exponents with an Ising Model-based approach to systematically explore and predict magnetic phenomena. Incorporating the Ising Model enhances our ability to simulate spin interactions, refining our predictions of magnetic ordering and dimensionality. By coupling machine learning algorithms with Monte Carlo simulations informed by the Ising Model, we establish a predictive framework that identifies key parameters governing magnetic behavior, such as lattice-induced anisotropy and critical phase

transitions. Furthermore, we synthesize and experimentally test selected cerium-based compounds to validate these theoretical predictions, thereby creating a feedback loop that continuously refines our computational models and enhances prediction accuracy. This integrative approach deepens the fundamental understanding of magnetism in cerium-based compounds and establishes a robust platform for discovering, validating, and engineering next-generation magnetic materials across the broader lanthanide [3] and actinide [4] families.

- 1. Lamichhane, T.N., et al., *Single-Crystal Permanent Magnets: Extraordinary Magnetic Behavior in the Ta, Cu Fe-doped CeCo5 Systems.* Physical Review Applied, 2019. 11(1): p. 014052.
 2. Lamichhane, T.N., et al., *Ce3-xMgxCo9: Transformation of a Pauli Paramagnet into a Strong Permanent Magnet.* Physical Review Applied, 2018. 9(2): p. 024023.
- 3. Churna Bhandari, G.N.N., Jonathan D.H. Smith, Durga Paudyal, *Accurate Machine Learning Predictions of Coercivity in High-Performance Permanent Magnets*. 2023.
- 4. Broyles, C.C., William; Sheng Ran, *Structure-Driven Prediction of Magnetic Order in Uranium Compounds*. 2024.

ER-10. Effect of Mn and V Doping on the Structural and Magnetic Properties of $Fe_{16}N_2$ Thin Films

<u>E. Gokce-Polat</u>¹, A. DeRuiter², W. Echtenkamp¹, H. Kim¹, B. Wolf², J. Wang^{1, 2}

¹Department of Electrical and Computer Engineering, University of Minnesota, Minneapolis, Minnesota, United States, ²Department of Chemical Engineering and Materials Science, University of Minnesota, Minneapolis, Minnesota, United States

Fe $_{16}N_2$ is one of promising permanent magnet candidates due to its high saturation magnetization and relatively high uniaxial anisotropy without critical elements [1]. In this work, we investigate the effects of Mn and V doping (~3 at.%) on the structural and magnetic properties of Fe $_{16}N_2$ thin films [2,3,4]. The films were deposited on MgO(001) substrates by facing target sputtering. The undoped film had a thickness of ~50 nm, while the doped films were ~60 nm thick. X-ray diffraction (XRD) analysis indicates that Mn preserves the Fe $_{16}N_2$ phase with only minor peak broadening, whereas V doping leads to the disappearance of the (002) reflection (Fig.1). The c lattice parameter remains nearly unchanged with Mn doping (6.28 Å), while it is significantly reduced to 6.18 Å with V, suggesting a greater disruption of the tetragonal lattice.

Magnetic hysteresis (M–H) loops (Fig.2) show that Mn doping induces moderate magnetic softening while preserving the magnetic structure. The saturation field is observed to decrease with doping from ~7200 Oe (Fe-N) to ~5900 Oe (Fe-Mn-N) and ~1500 Oe (Fe-V-N), accompanied by a concurrent reduction in coercivity.

These findings are consistent with theoretical predictions that V occupies 8h interstitial sites near nitrogen and couples antiferromagnetically with Fe atoms, thereby weakening magnetic order [3]. Contrary to prior theoretical expectations of enhanced anisotropy, V doping—even at 3.%—significantly disrupts the structural integrity and magnetic functionality of Fe₁₆N₂ [3]. In contrast, Mn preferentially substitutes 4d sites and stabilizes the lattice through ferromagnetic coupling [4]. Mn doping preserves structural and magnetic properties, making it a promising basis for future anisotropy enhancement strategies in Fe₁₆N₂ films.

[1] J. P. Wang, "Environment-friendly bulk Fe $_{16}N_2$ permanent magnet: Review and prospective", Journal of Magnetism and Magnetic Materials Volume 497, 165962 (2020).

[2] M. H. Han, W. J. Kim, E. K. Lee, H. Kim, S. Lebègue, and J. J. Kozak, "Theoretical study of the microscopic origin of magnetocrystalline anisotropy in Fe16N2 and its alloys: Comparison with the other L10 alloys," J. Phys. Condens. Matter 32(3), 035801 (2019).

[3] Peter Stoeckl, Przemyslaw Wojciech Swatek, Jian-Ping Wang; Magnetocrystalline anisotropy in V– and Cu–doped $Fe_{16}N_2$. *AIP Advances* 1 March 2022; 12 (3): 035020. https://doi.org/10.1063/9.0000354

[4] Yanfeng Jiang, Burak Himmetoglu, Matteo Cococcioni, Jian-Ping Wang; DFT calculation and experimental investigation of Mn doping effect in $Fe_{16}N_2$. AIP Advances 1 May 2016; 6 (5): 056007. https://doi.org/10.1063/1.4943059

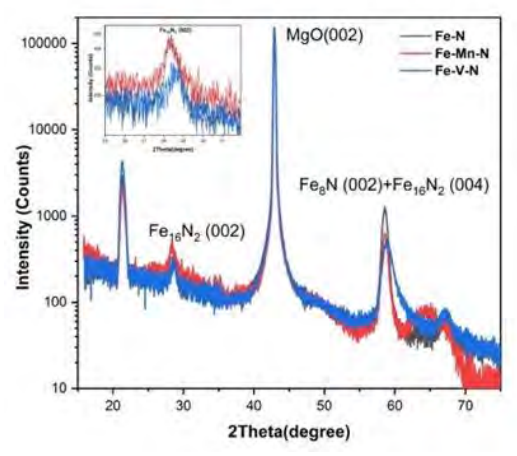


Figure 1. XRD patterns of Fe-N, Fe-Mn-N, and Fe-V-N

thin films.

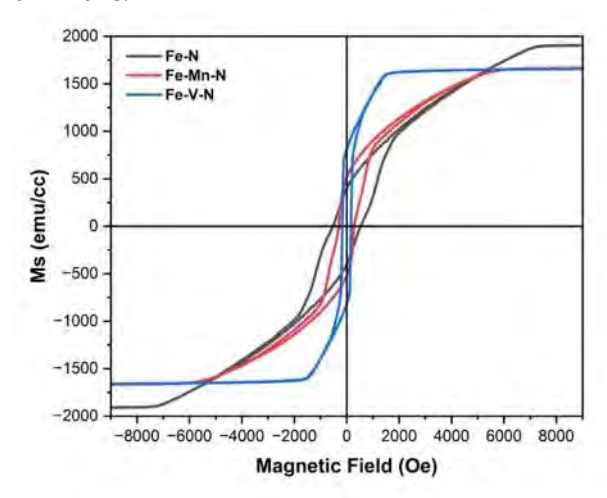


Figure 2. Room-temperature M–H loops of Fe–N, Fe–Mn–N, and Fe–V–N thin films.

ER-12. Controlling $L1_0$ Ordering in the MnAl System Through Cu Elemental Addition

H. Baldino^{1,2}, X. Zhang^{1,3}, G. Hadjipanayis¹, L. H. Lewis^{1,3}
¹Chemical Engineering, Northeastern University, Boston,
Massachusetts, United States, ²Material Science and
Engineering, University of Central Florida, Orlando, Florida,
United States, ³Mechanical and Industrial Engineering,
Northeastern University, Boston, Massachusetts, United States

A high degree of chemical ordering in ferromagnetic L₁₀type compounds donates substantial magnetocrystalline anisotropy, making these materials good candidates for next-generation permanent magnets. While it remains highly challenging to obtain the "holy grail" L10 FeNi compound (aka, tetrataenite), the analogous proxy system of MnAl, with the same L1₀ structure, provides a good testbed for investigating and identifying factors that control chemical ordering. The L1₀-structured τ-MnAl is a nonequilibrium phase that is conventionally formed by heating the metastably retained ε -MnAl phase that has a hexagonal, disordered structure. Here, we present results demonstrating that a small Cu addition (4 at.%) significantly stabilizes the L1₀-ordered structure, enabling a direct formation pathway of τ -MnAl phase distinct from the conventional transformation route.

MnAl-based materials of compositions Mn $_{51}$ Al $_{49}$ ("MnAl") and Mn $_{51}$ Al $_{45}$ Cu $_4$ ("MnAlCu"), synthesized by both regular solidification (arc melting, cooling rate ~ 100 °C/s) and rapid solidification (melt spinning, cooling rate ~ 106 °C/s) approaches, were investigated via structural, magnetic, and

^{*} Best Student Presentation Finalist / LB – Late-breaking Poster

calorimetric probes. While the unmodified MnAl composition adopts the metastable hexagonal ε-phase upon melt spinning, the Cu-containing composition forms phasepure L1₀ τ-MnAl directly, regardless of the solidification rate, Figure 1. In addition, Cu modification alters both the microstructure and the magnetic domain structure of the L₁₀ MnAl phase, transforming it from isotropic grains with globular magnetic domains to poly-twinned crystallographic plates with a pronounced striped magnetic domain structure. The MnAlCu sample also exhibited no loss in magnetocrystalline anisotropy compared to the Cu-free state. These results offer insight into how Cu addition alters the nature of the solidification pathway of MnAl to directly form the L1₀ structure and may have implications in other $L1_0$ -containing systems.[This work was supported by the U.S. Department of Energy, Office of Basic Energy Sciences under Award Number DE SC0022168]

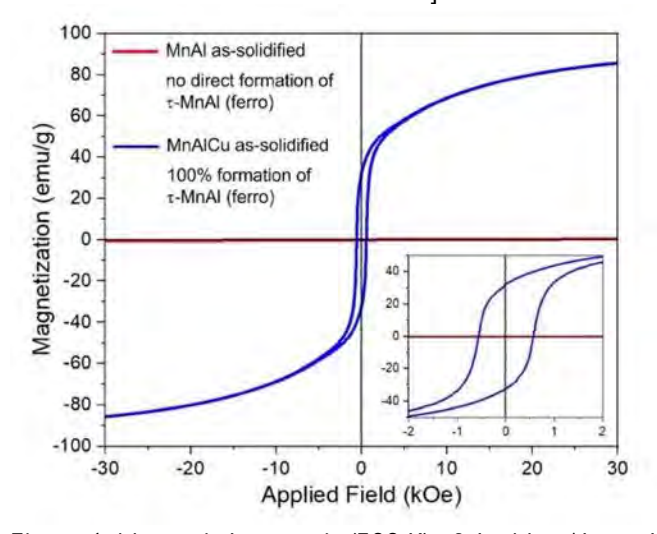


Figure 1. Magnetic hysteresis (300 K) of the $Mn_{51}Al_{49}$ and $Mn_{51}Al_{45}Cu_4$ as-solidified (melt spinning) materials.

ER-13-LB. Tunable magnetic properties for epitaxially grown Co-rich CoPtP films by electrodeposition on Cu(111)/Si substrates: Crossover from non-exchange-spring to exchange spring/coupled magnetic states

S. Seth, <u>S. Roy</u>

Micropower Devices & Nanomagnetics Group, Tyndall National Institute, University College Cork, Cork, Ireland

Typical single layered micro/nano thin ferromagnetic films provide either high coercivity (H_C) with low/moderate saturation magnetization (M_S) (hard magnets) or low H_C with high M_S (soft magnets). Whereas, sandwiched bi/tri layers [1-4] of different materials or in-situ [5,6] (same material)

nano-hetero-structures of hard & soft layers furnish the advantages of both high H_C & M_S , resulting in exchange spring(ES)/exchange coupled(EC) magnets [7-11]. The critical conditions between soft layer thickness (L_S) and hard phase domain wall width (d_h), determine ES/EC behaviour: $L_S > 2d_h$ signifies ES-step hysteresis loop, while $L_S \le 2d_h$ yields EC-rectangular loop [10]. Such ES/EC systems, in which both hard & soft layers can be tuned in nanometer scale by thicknesses, compositions, morphologies, etc., to achieve high energy product (BH_{max}), could be potential candidates for advanced magnetic applications such as recording media [8], spintronics [12,13], electromagnetic energy harvesters, actuators, and so on.

Co-rich Co₈₀Pt₂₀ & Co₈₀(PtP)₂₀ [14-21] alloys are promising candidates for magnetic MEMS/NEMS applications due to their structural and magnetic properties. Here, we investigate the tuneability and enhancement of in plane (IP) & out of plane (OOP) coercivities (e.g. 366 to 3638 Oe in OOP) as well as energy product (e.g. 1.68 to 25.17 kJ/m³ in IP) in electrodeposited CoPtP (cobalt-platinumphosphorous) films (Figure 1). We observe the crossover from non-ES to ES/EC magnetic states in OOP direction (Figure 1) in Co₈₀(PtP)₂₀ films on Cu(111)/Ti/Si substrate, developed by lowering current densities (23, 21, 20, 16 and 13 mA/cm² for 1 hour deposition) during electrodeposition from a stable CoPtP bath of pH 8 at room temperature. XRD patterns in Figure 2 (at $2\theta=43.4^{\circ}$) and corresponding magnetic measurements in Figure 1 (SQUID MPMS3) show the Co(hcp(002)/fcc(111)) mixed phase on Cu(111), confirming epitaxial growth of CoPtP and the gradual increase of Co-hcp(002) (hard magnetic) phase over Cofcc(111) (soft magnetic) phase, as we decrease the deposition current densities.

- 1. K. A. Thórarinsdóttir et al, Physical review B 103, 014440 (2021).
- 2. Y. Liu et al, Applied physics letters 93, 192502 (2008).
- 3. H. D. Chopra et al, Physical Review B 72, 054415 (2005).
- 4. F. Magnus et al, Journal of physics: Condensed matter 33, 445803 (2021).
- 5. A. Samanta et al, Physical review B 107, 214449 (2023).
- 6. A. Samanta et al, APL materials 12, 0223485 (2024).
- 7. E. F. Kneller et al, IEEE transactions on magnetics 27, 3588 (1991).
- 8. M. Dabrowski et al, ACS applied materials & interfaces 12, 52116(2020).
- 9. J. E. Davies et al, Applied physics letters 86, 262503 (2005).
- 10. E. E. Fullerton et al, Physical review B 58, 12193 (1998).

- 11. E. E. Fullerton et al, Journal of magnetism and magnetic materials 200, 392 (1999).
- 12. C. Banerjee et al, RSC advances 6, 80168 (2016).
- 13. T. N. A. Nguyen et al, Physical review applied 2, 044014 (2014).
- 14. I. Zana et al, Electrochemical and solid-state letters 6 (12), C153, 2003.
- 15. J. Mallett et al, Electrochemical and solid-state letters 8 (1), C15, 2004.
- 16. X. Xu et al, Journal of electrochemical society 159, D240, 2012.
- 17. O. D. Oniku et al, ECS transactions 50 (10), 167, 2013.
- 18. I. Zana et al, Journal of magnetism and magnetic materials, 292, 266–280, 2005.
- 19. D. Mallick et al, Journal of applied physics 125, 023902, 2019
- 20. M. Cortés et al, Journal of electroanalytical chemistry, 627,69–75, 2009.
- 21. S. Kulkarni et al, Journal of magnetism and magnetic materials, 322, 1592-1596, 2010.

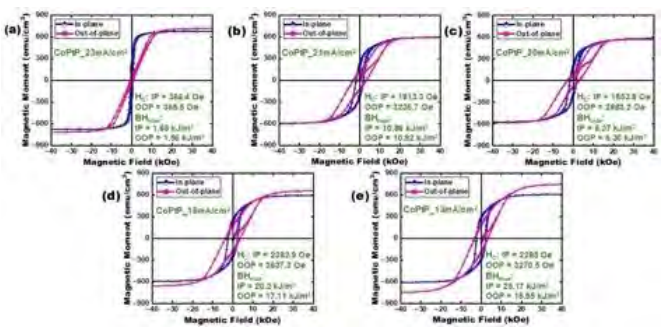


Figure 1. IP & OOP hysteresis loop of electrodeposited CoPtP films developed at: (a) 23 mA/cm², (b) 21 mA/cm², (c) 20 mA/cm², (d) 16 mA/cm² and (e) 13 mA/cm².

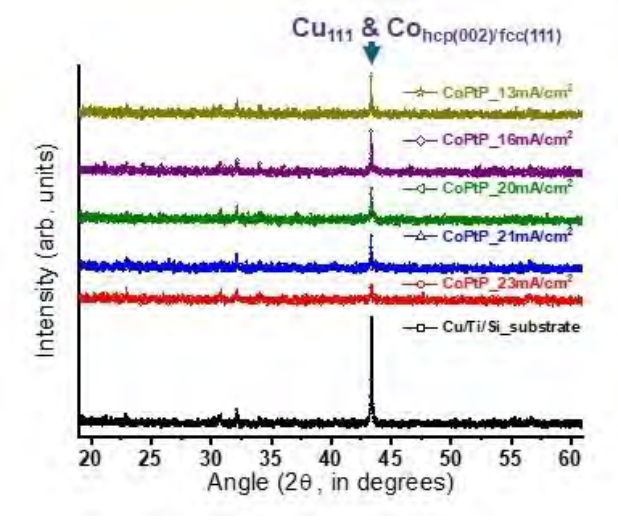


Figure 2. XRD patterns of developed films and Cu/Ti/Si

substrate: Cu(111) peak for substrate and Co-hcp(002)/fcc(111) mixed phase for samples on Cu(111).

ER-14-LB. Measuring initial curves and minor hysteresis loops for high coercivity rare earth magnets using the Pulsed Field Magnetometer (PFM) system

J. Mckenzie, R. Cornelius, J. Wade Hirst Magnetic Instruments Ltd, Falmouth, United Kingdom

This poster will review recent progress and results gained from the Hirst generation 8, Pulsed Field Magnetometers on initial magnetisation curves, minor loops being applied to samples and the implementation of First Order Reversal Curves (FORCs) on a PFM.

The initial curve represents the initial magnetization process of a permanent magnet from when it is completely unmagnetized. This curve is important for understanding the composition, metallurgy, and microstructure of a material. We will present results for NdFeB and SmCo magnets.

Minor Loops are generated when the applied magnetic field is reversed but does not reach the saturation point, creating smaller loops within the main hysteresis loop. This provides information about the reversibility of magnetization within a specific field range and can be used to analyse the stability of a permanent magnet under changing magnetic fields. We will present results for NdFeB magnets.

First order reversal curve (FORC) measurements provide insight into the magnetic properties of materials, information that is not possible to obtain from a full hysteresis loop alone or individual minor loops. FORC curves help in identifying the distribution of switching and interaction fields, and in distinguishing between multiple magnetic phases in composite or hybrid materials containing more than one phase of magnetic materials. This information can be used to analyse magnet production techniques and novel materials. We will present results for NdFeB magnets.

This new option on the latest generation 8 PFMs from Hirst and takes advantage of the full pulsed field that drives the sample through all four quadrants of the hysteresis loop during a measurement.

^{*} Best Student Presentation Finalist / LB – Late-breaking Poster

SESSION FA: ALL-ORBITRONIC CONCEPTS AND DEVICES

Chair(s): A. Kumar, *Physics, University of Gothenburg,*Gothenburg, Sweden

Thursday, October 30, 2025

02:00 PM-05:30 PM

Grand Ballroom

FA-01. Ultrafast Spin-Orbitronics with Terahertz Electromagnetic Pulses

O. Gueckstock

Freie Universität Berlin, Berlin, Germany

To harness electron spin and orbital angular momentum in future electronic devices, it is essential to facilitate their transport and detection. Investigating fundamental processes that generate spin and orbital currents requires launching and measuring their transport on ultrafast time scales. Therefore, we use optical laser pulses with femtosecond duration to generate a transient accumulation of spin [1] and orbital [2] angular momentum in a ferromagnetic metal layer. This spin-orbital current is then injected into an adjacent nonmagnetic metal layer, where it is converted into a transverse charge current and detected via the emitted terahertz electromagnetic pulse [2]. This technique enables the investigation of spin [3] and orbital [2] current transport on their intrinsic ultrafast time scale. Additionally, a reciprocal experimental approach can be employed, using intense terahertz electromagnetic pulses to drive electric currents and manipulate magnetic order on femtosecond time scales via spin and orbital torques, such as Néel spin-orbit torques [4].

- [1] R. Rouzegar et al., Phys. Rev. B 106, 144427 (2022)
- [2] T.S. Seifert et al., Nature Nanotech. 18, 1132-1138 (2023)
- [3] R. Rouzegar et al., Nano Letters 24, 7852-7860 (2024)
- [4] Y. Behovits et al., Nature Commun. 14, 6038 (2023)

FA-02. Lanthanide nitride ferromagnets with large orbital magnetic moments

S. Granville^{1, 2}

¹Robinson Research Institute, Victoria University of Wellington, Wellington, New Zealand, ²MacDiarmid Institute for Advanced Materials and Nanotechnology, Wellington, New Zealand

Unlike transition metal-based magnetic materials, lanthanide-based ferromagnets retain substantial orbital contributions to their magnetic moments, originating from the localised 4f electrons. The rare-earth or lanthanide

nitrides (*LnN*) are a case in point, and in some their magnetisation is dominated by the orbital contribution [1]. Moreover, Hund's rules for spin and orbital angular momentum dictate that several, including SmN and NdN, have opposite sign orbital and spin contributions to their magnetic moments. These factors have generated interest in using the *LnN* to produce large orbital currents for magnetisation switching in neighbouring magnetic layers [2].

In this talk I will present our work demonstrating the spin and orbital contributions to the magnetic properties of a number of *LnN*, including spin-and-orbital compensated ferromagnet SmN [3-4] and orbital dominant ferromagnet NdN [5]. As well as the potential for generating a strong orbital angular momentum, the competing spin and orbital contributions lead to several technologically useful properties such as exchange-spring behaviour in orbital/spin dominant bilayers [6,7] and fully internally magnetised solid solutions of *LnN* with net zero angular momentum [8] or near-zero net magnetisation [4,9,10].

- [1] W. F. Holmes-Hewett, J. D. Miller, H. G. Ahmad, S. Granville, and B. J. Ruck, Rare-Earth Nitrides: Fundamental Advances and Applications in Cryogenic Electronics, J. Phys. D (under review).
- [2] D. Lee et al., Orbital Torque in Magnetic Bilayers, Nat. Commun. 12, 6710 (2021).
- [3] E.-M. Anton, B. J. Ruck, C. Meyer, F. Natali, H. Warring, F. Wilhelm, A. Rogalev, V. N. Antonov, and H. J. Trodahl, Spin/orbit moment imbalance in the near-zero moment ferromagnetic semiconductor SmN, Phys. Rev. B 87, 134414 (2013).
- [4] J. F. McNulty, B. J. Ruck, and H. J. Trodahl, On the ferromagnetic ground state of SmN, Phys. Rev. B 93, 054413 (2016).
- [5] E.-M. Anton, J. F. McNulty, B. J. Ruck, M. Suzuki, M. Mizumaki, V. N. Antonov, J. W. Quilty, N. Strickland, and H. J. Trodahl, NdN: An intrinsic ferromagnetic semiconductor, Phys. Rev. B 93, 064431 (2016).
- [6] J. F. McNulty, E. M. Anton, B. J. Ruck, F. Natali, H. Warring, F. Wilhelm, A. Rogalev, M. M. Soares, N. B. Brookes, and H. J. Trodahl, Twisted phase of the orbital-dominant ferromagnet SmN in a GdN/SmN heterostructure, Phys. Rev. B. 91, 174426 (2015).
- [7] J. F. McNulty, E.-M. Anton, B. J. Ruck, M. Suzuki, M. Mizumaki, and H. J. Trodahl, Tunable magnetic exchange springs in semiconductor GdN/NdN superlattices, Phys. Rev. B 100, 094441 (2019).

[8] J. D. Miller, J. F. McNulty, B. J. Ruck, M. A. Khalfioui, S. Vézian, M. Suzuki, H. Osawa, N. Kawamura, and H. J. Trodahl, Enhanced Sm spin projection in $Gd_xSm_{1-x}N$, Phys. Rev. B 106, 174432 (2022).

[9] J. F. McNulty, K. Temst, M. J. Van Bael, A. Vantomme, and E.-M. Anton, Epitaxial growth of (100)-oriented SmN directly on (100) Si substrates, Phys. Rev. Mater. 5, 113404 (2021). [10] J. D. Miller, H. J. Trodahl, M. Al Khalfioui, S. Vézian, and B. J. Ruck, Complete magnetization compensation in the intrinsic ferromagnetic semiconductor $Gd_xSm_{1-x}N$, Phys. Rev. Materials 9, L041401 (2025).

FA-03. All-Orbitronic Effects and Device Concepts $\underline{\mathsf{M}}.\ \mathsf{Kl\ddot{a}ui^{1,\,2}}$

¹Institute of Physics, Johannes Gutenberg University Mainz, Mainz, Germany, ²Center for Quantum Spintronics and Department of Physics, NTNU, Trondheim, Norway

The current state-of-the-art approach to manipulating magnetization are spin-orbit torques (SOTs), which make use of the electron's spin to switch spin-based magnetic systems in information storage and computing devices. The charge to spin conversion by the Spin Hall Effect and the Rashba-Edelstein Effect leads to enhanced power efficiency, non-volatility, and superior performance compared to other approaches, making this an attractive option for applications [1].

The energy consumption of the device is primarily influenced by the applied current required for magnetization switching. This requirement is directly linked to the charge-to-spin conversion ratio, known as the spin Hall angle (SHA). Traditional bottom electrode materials such as Pt, Ta, and W, however, are often rare, expensive or environmentally unfriendly. Moreover, the SHA values of these heavy metals are limited as the SHE relies on spin-orbit coupling (SOC), which is a small relativistic effect and thus preventing ongoing efforts to optimize and reduce power consumption.

Beyond utilizing spin currents to switch magnetization, recent research has revealed that another fundamental degree of freedom of electron, orbital angular momentum, can also be used to manipulate magnetization. Orbital currents, arising from the orbital Hall effect (OHE) and the orbital Rashba-Edelstein effect (OREE), has been predicted to be a promising mechanism to enhance the charge to angluar momentum conversion efficiency and thus the

resulting torques significantly [2]. As an orbital texture exists even in the absence of relativistic spin-orbit coupling, abundant, cheap and environmentally non-hazardous light materials can be used. A major advantage of using these effects is that the charge to orbital angular momentum conversion is orders of magnitude more efficient compared to the spin-based effects, as the orbital to charge interconversion mechanisms make use of the direct coupling between the crystal momentum of charge carriers and their orbital angular momentum, thereby eliminating the dependence on the typically weak SOC. Finally, orbital angular momentum is not damped by Gilbert damping in the same manner as spin and is expected to be much less sensitive to magnetic disorder making it potentially more robust.

However, as conventional 3d ferromagnets have magnetic moments dominated by spin, one needs to convert the large orbital angular momentum to spin prior to using it. This demonstrates the efficiency of the torques, as for instance in a recent demonstration of magnetic random access cell where using orbital torques one could reduce the switching power only by 50% while the orbital angular momentum generated is expect to lead to manyfold improvement of the torques [3]

So to overcome this shortcoming, one needs to interface the orbital angular momentum layer with a magnetic that has magnetic moments based on orbital angular momentum. This overcomes the requirement of orbital to spin conversion and thus one can use the full efficiency of the huge orbital angular momentum generated. As a materials based, different types of magnets can be exploited: many oxides due to their coordination with oxygen have sizeable orbital moments. Another set of possible materials are mononitrides such as SmN, GdN, etc. We demonstrate that combining strong orbital angular momentum currents and orbital moment magnets leads to an orders of magnitude increased orbitronic effects [4].

- [1] A. Manchon et al., Rev. Mod. Phys. 91, 035004 (2019) [2] D. Go et al., EPL 135, 037001 (2021); S. Ding et al., Phys.
- [2] D. Go et al., EPL 135, 037001 (2021); S. Ding et al., Phy Rev. Lett. 125, 177201 (2020).
- [3] R. Gupta et al., Nature Commun. 16, 130 (2025)].
- [4] C. Schmitt et al., (under review)

FA-04. Chiral Orbitronics

B. Göbel

Martin Luther University Halle-Wittenberg, Halle, Germany

The field of orbitronics is concerned with the orbital angular momentum of particles. Besides charge and spin, an electron can also possess an orbital magnetic moment. However, in most solids, it is suppressed because of the various symmetries of most crystal structures. This situation changes when an electric field is applied. The non-equilibrium orbital magnetization (Edelstein effect) can be considerable and even transverse orbital currents can arise (orbital Hall effect). In this talk, I will present how chirality can enable orbitronic effects. Chirality is a geometrical property of a system that can be distinguished from its mirror image, therefore exhibiting an asymmetry. I will consider (i) chiral magnetic textures and (ii) chiral structures.

- (i) Chiral magnetic textures are non-collinear antiferromagnets such as magnetic skyrmions that look like nano-scale magnetic whirls (review see Ref. [1]). They are topologically non-trivial and exhibit an effective magnetic field, called emergent field, that acts on the conduction electrons. Besides causing a topological Hall effect, they give rise to a considerable orbital magnetization even in equilibrium [2]. As we have shown in Ref. [3], the corresponding orbital angular momentum can be transported. Skyrmions give rise to a topological orbital Hall effect (cf. Fig. 1). Even textures with a compensated emergent field, such as antiferromagnetic skyrmions, exhibit this effect. For hopfions, which are three-dimensional topological solitons, a three-dimensional topological orbital Hall effect arises that can be attributed to the topological invariant called Hopf index [4].
- (ii) Chiral structures can be found as molecules, like the DNA molecule, and solids, such as tellurium. I will present analytical results derived from a simplified model of a helix that exhibits a chirality-dependent orbital Edelstein effect [5]. This effect is caused by intersite contributions to the orbital angular momentum; it is generated by the constrained rotational and translational motion through the helix. We support these analytical results with numerical calculations for tellurium and compare them with the chirality-dependent orbital Edelstein effect in chiral carbon nanotubes [6] (cf. Fig. 2). Even innately achiral systems can become chiral by introducing edges. I will elaborate on this topic by discussing the orbital polarized edge states that

occur at chiral edges of a Kagome lattice [7]. Furthermore, when a strong magnetic field is applied, skipping orbits arise that are chiral and transport not only charge but also orbital angular momentum. As we have shown, the quantum Hall effect is always accompanied by an orbital Hall effect [8].

In summary, I will present that chirality can enable large orbital magnetization and orbital currents that may for example be used to generate orbital torques. This strengthens the potential of orbitronics and might help us to develop more efficient and sustainable devices in the future.

- [1] B. Göbel, I. Mertig, O. Tretiakov, Physics Reports, 895, 1 (2021)
- [2] B. Göbel, A. Mook, J. Henk, I. Mertig. Physical Review B, 99, 060406(R) (2019)
- [3] B. Göbel, L. Schimpf, I. Mertig, Communications Physics, 8, 17 (2025)
- [4] B. Göbel, S. Lounis, arXiv pre-print: 2506.11448 (2025)
- [5] B. Göbel, L. Schimpf, I. Mertig, arXiv pre-print: 2502.04978 (2025)
- [6] B. Göbel, I. Mertig, S. Lounis, arXiv pre-print: 2504.07665 (2025)
- [7] O. Busch, I. Mertig, B. Göbel, Physical Review Research, 5, 043052 (2023)
- [8] B. Göbel, I. Mertig, Physical Review Letters, 133, 146301 (2024)

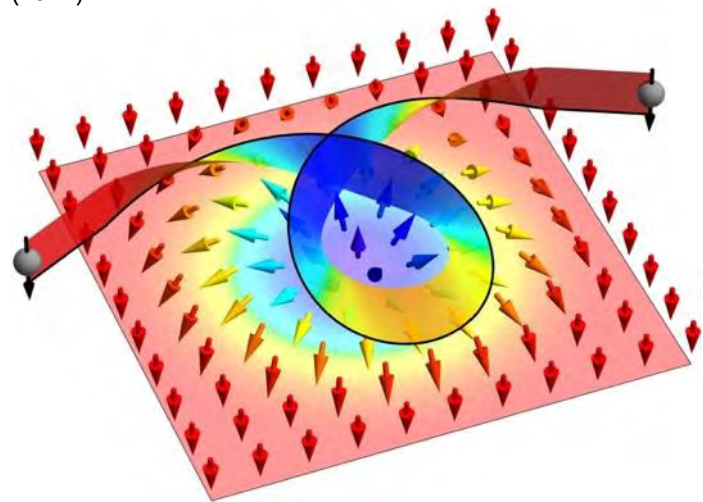


Fig. 1 Topological orbital Hall effect caused by a skyrmion. The emergent field of the skyrmion causes the conduction electron (gray) to exhibit a cycloid trajectory causing the generation and transport of orbital angular momentum. From [3].



Fig. 2 View into a chiral carbon nanotube. The color is assigned based on the underlying graphene layer and visualizes the chirality of the tube. From [6].

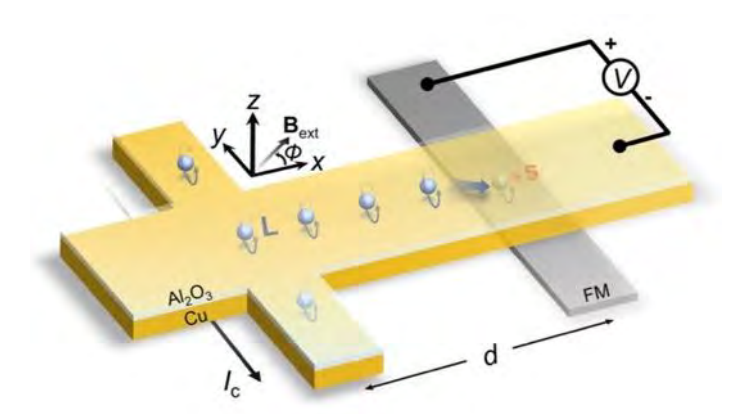
FA-05. Nonlocal Electrical Detection of Reciprocal Orbital Edelstein Effect

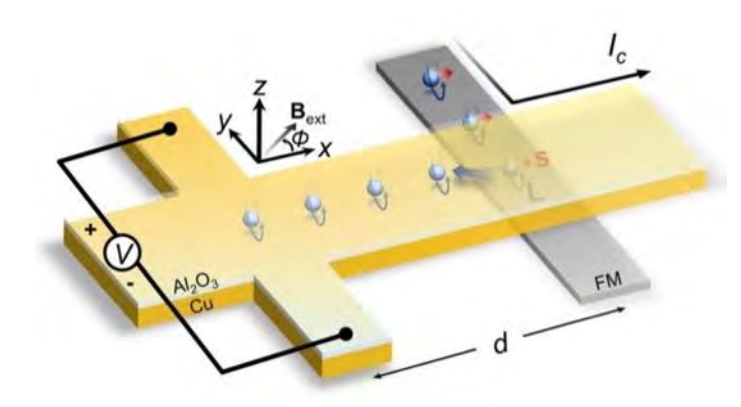
W. Gao, <u>L. Liao</u>, Y. Otani The Institute for Solid State Physics, The University of Tokyo, Kashiwa, Chiba, Japan

Current-induced nonequilibrium orbital angular momentum (OAM) offers a promising method to manipulate nanomagnets efficiently using light elements. Despite extensive research, understanding the Onsager reciprocity of orbital transport—fundamentally rooted in the second law of thermodynamics and time-reversal symmetry remains elusive. In this study, we experimentally test the Onsager reciprocity of orbital transport in an orbital Edelstein system by utilizing nonlocal transport. Identifying the chemical potential generated by the orbital accumulation avoids the limitations associated with orbital torque and pumping measurements. Remarkably, we observe that the direct and inverse orbital-charge conversion processes produce identical electric voltages, confirming Onsager reciprocity in orbital transport. Additionally, we find that the orbital decay length, approximately 100 nm at room temperature, is independent of Cu thickness and decreases with lowering temperature,

revealing a distinct contrast to spin transport behavior. Our findings provide valuable insights into the reciprocity of the charge-orbital interconversion and the nonlocal correlation of the orbital degree of freedom.

W. Gao et al., Nonlocal Electrical Detection of Reciprocal Orbital Edelstein Effect, arXiv:2502.11040.





SESSION FB: COHERENT X-RAY FOR PROBING THE INTERPLAY OF HETEROGENEITY AND SPIN-ELECTRONIC CORRELATIONS

Co-Chair(s): S. Roy, Advanced Light Source, Lawrence Berkeley National Laboratory, Berkeley, California, United States and D. A. Gilbert, University of Tennessee, Knoxville, Tennessee, United States Thursday, October 30, 2025 02:00 PM-05:30 PM Ballroom A

FB-01. Imaging Transient States in Magnetic Materials: Complexity across Space and Time

C. Mazzoli

NSLS-II, Brookhaven National Lab, Upton, New York, United States

The investigation of electronic structures in the space domain is crucial for understanding their hierarchical relationships and functional impact. On the other hand, the study of their evolution in the time domain discloses the underlying energetics thus paving the way to their fundamental modeling. In both domains scaling laws and invariants are of great relevance, thus any attempt of a comprehensive understanding of their complexity has to deal with different length and time scales. However, from an experimental point of view often drastic compromises have to be accepted to push space or time resolution. As a matter of fact, a gain in one domain typically corresponds to a loss in the other. In this talk, different approaches to overcome this apparent intrinsic limitation will be presented, by either exploiting complementary techniques or a different way of approaching data analysis. Some examples based on coherent soft x-ray resonant scattering performed on magnetic materials will be reported, showing how relevant scientific information previously inaccessible can now be retrieved. A generalization will also be porposed, highlighting the potential impact to a variety of systems, sources and techniques.

FB-02. Coherent x-ray studies of spontaneous fluctuations in rare earth nickelates

R. Kukreja

University of California Davis, Davis, California, United States

Rare-earth nickelates (RNiO₃) exhibit a rich interplay of electronic, magnetic, and structural phase transitions, including a metal-to-insulator transition (MIT), charge

ordering, and a symmetry change from orthorhombic to monoclinic structure [1]. While these transitions have been widely studied, the spatio-temporal nature of spontaneous fluctuations across the phase boundary remains largely unexplored. Such fluctuations are increasingly recognized as crucial for stabilizing emergent magnetic textures and for enabling stochastic functionality in neuromorphic computing. Here, we employ X-ray photon correlation spectroscopy (XPCS) [2-3] to directly probe the dynamics of structural and magnetic fluctuations in epitaxial thin films of NdNiO₃ and SmNiO₃. For NdNiO₃, we observe a pronounced slowdown in fluctuation timescales – by an order of magnitude—near the Néel temperature, highlighting strong coupling between structural and magnetic order parameters, independent of epitaxial strain. In contrast, SmNiO₃ shows no such slowdown, emphasizing the distinct dynamics. Unexpectedly, wavevector-dependent measurements reveal that short-range structural fluctuations are significantly slower (by a factor of 3-5) than long-range fluctuations [4]. Our results demonstrate the power of coherent X-ray techniques in capturing nanoscale fluctuation dynamics in quantum materials and provide new insight into the role of fluctuations near phase transitions in complex oxides.

- 1. Middey S., Chakhalian J., Mahadevan P., Freeland J. W., Millis A. J., Sarma D. D. Physics of ultrathin films and heterostructures of rare earth nickelates. Annual Review of Materials Research 46, 305 (2016)
- 2. Sinha S. K., Jiang Z., Lurio L.B. X-ray photon correlation spectroscopy studies of surfaces and thin films. Advanced Materials 26, 7764 (2014)
- 3. Shpyrko O.G. X-ray photon correlation spectroscopy. Journal of Synchrotron Radiation 21, 1057 (2014)
- 4. Zhou Hagstroem, N. et al. Critical slowdown of spontaneous fluctuaitons in the vicinity of metal-insulator transition in rare earth nickelates, in review (2025).

FB-03. Competition between two antiferromagnetic phases in Fe_xNbS₂ studied through Coherent Resonant Scattering A. Frano¹, R. Basak¹, S. Wu²

¹University of California San Diego, La Jolla, California, United States, ²Santa Clara University, Santa Clara, California, United States

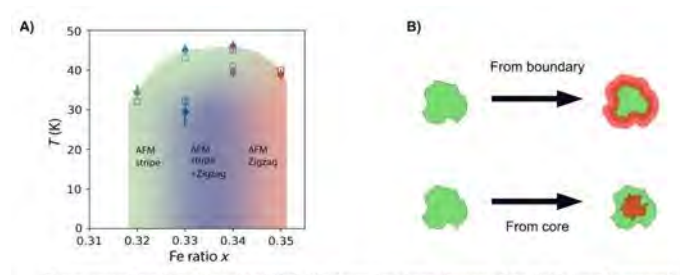
The Fe-intercalated transition metal dichalcogenide Fe_xNbS₂ exhibits a highly tunable antiferromagnetic (AFM) ground state as a function of Fe intercalation ratio (x) near 1/3 [1]. The ground state transitions between two distinct phases: a stripe-AFM phase and a zigzag-AFM phase [2]. Remarkably, at an intermediate doping these two phases coexist and compete as a function of temperature [2]. We asked: how do these two electronic orders compete and evolve in real space within the same material?

During phase competition, the two phases adjust their real-space distributions based on their interaction and relative stability. We focus on whether the competing phase emerges from regions of weak order parameters, such as disordered areas and boundaries in the phase texture, or from regions with strong order parameters, like a topological defect seeded from within the core of an ordered domain. These scenarios suggest distinct real-space phase texture evolution, which we probe using coherent resonant scattering. This technique encodes real-space electronic domain patterns into speckle patterns observed on the Bragg peaks in Fourier space.

We analyze the evolution of these speckle patterns, establishing a connection between the two AFM phases in Fe_xNbS₂ and highlight the unique capability of coherent resonant scattering to study competing and coexisting electronic ground states for the first time.

[1] Sci. Adv. 7, eabd8452 (2021)

[2] Phys. Rev. X 12, 021003 (2022)



Phase competition in Fe intercalated NbS₂ (A) shows the phase diagram of the highly tunable magnetiground state [1] (B) Two different pathways of phase competition unfolding in real space (see text)

Ref: [1] Phys. Rev. X 12, 021003 (2022)

FB-05. Dispersion of Spontaneous Spin Fluctuations measured by MHz X-ray Photon Correlation Spectroscopy L. Shen¹, J. J. Turner¹, S. Roy², Z. Tumbleson², E. Blackburn³ ¹SLAC National Accelerator Laboratory, Menlo Park, California, United States, ²Lawrence Berkeley National Laboratory, Berkeley, California, United States, ³Lund University, Lund, Sweden

Spontaneous fluctuations play a critical role in understanding phase transitions [1], yet their dispersionremains largely unexplored - unlike wellcharacterized quasiparticle excitations such as magnons and phonons, which are routinely studied using inelastic neutron or x-ray scattering [2, 3]. In this work, we investigate the spontaneous fluctuations of spin stripes in a FeGd magnetic superlattice [4, 5] using X-ray Photon Correlation Spectroscopy (XPCS) [6] at a megahertz (MHz) repetitionrate x-ray free-electron laser. Enabled by the significant enhancement in counting statistics at MHz rates, we demonstrate the ability to resolve the dispersion of spin stripe dynamics across a large region in Brillouin zone. Our results establish MHz-XPCS as a powerful and unique tool for probing spontaneous fluctuations and the emergent phenomena they drive in complex materials.

[1] H. E. Stanley, Phase transitions and critical phenomena, Vol. 7 (Clarendon Press, Oxford, 1971).

[2] L. Shen et al., Phys. Rev. B 107, 134425 (2023)

[3] M. Mitrano et al., Phys. Rev. X 14, 040501 (2024)

[4] M. H. Seaberg et al., Phys. Rev. Lett. 119, 067403 (2017)

[5] M. H. Seaberg et al., Phys. Rev. Research 3, 033249 (2021)

[6] L. Shen et al., MRS Advances 6, 221 (2021)

SESSION FC: BIOMAGNETISM AND BIOMEDICAL APPLICATIONS III

Co-Chair(s): R. L. Hadimani, Mechanical and Nuclear Engineering, Virginia Commonwealth University, Richmond, Virginia, United States and J. Gomez-Pastora, Texas Tech University, Lubbock, Texas, United States Thursday, October 30, 2025 02:00 PM-05:30 PM Ballroom C

FC-01. Validation of the Impact of Cylindrical Sensor Arrays on Cardiac Current Source Estimation Performance

W. Shang¹, M. Fushimi², S. Chikaki¹, M. Sekino¹
¹Graduate School of Engineering, The University of Tokyo, Tokyo, Japan, ²Graduate School of Information science and Technology, The University of Tokyo, Tokyo, Japan

In Magnetocardiography (MCG), the current sources generating the magnetic field signal are estimated by solving the electromagnetic inverse problem to locate the abnormal site. Because the conventional MCG devices' sensor array is a flat plane, if the signal sources are far from the sensor plane, the estimation area of excitation will be far from the actual myocardium[1]. In this study, we introduced a cylindrical sensor array to improve the accuracy of current source estimation. The configuration has been shown in Fig. 1. We conducted simulations and animal experiments to compare the performance of current source estimation with planar array and cylindrical array, in order to analyze the influence of sensor array on current source estimation. In the simulations, error levels were evaluated for cylindrical and planar arrays under different distances and radius. We found that the cylindrical array required less proximity and still achieved stable, accurate estimation. In the animal experiments, we designed a custom measurement setup compatible with both planar and cylindrical arrays and conducted comparative tests at the physical distance limits using 10-week-old rats. Measurements were performed five times on each of five rats for both sensor configurations. Source estimation was based on the measured data, and the results were evaluated using both the Goodness of Fit (GoF) and anatomical position. The results showed in Table 1. The GOF for the cylindrical array were between 0.35 and 0.55, whereas those for the planar array ranged from 0.15 to 0.40 (few cases reaching 0.45-0.50). 76% of the cylindrical results had a higher GOF than their planar counterparts, and 52% of them were consistent with anatomical expectations. In contrast, only 24% of the planar array results consistent with

anatomical expectations. These findings suggest that the cylindrical array requires less restrictive sensor-to-subject distance conditions for reliable current source estimation.

[1] W. Sun and K. Kobayashi, *IEEE Transactions on Magnetics*, vol. 53, no. 11, pp. 1–4 (2017)

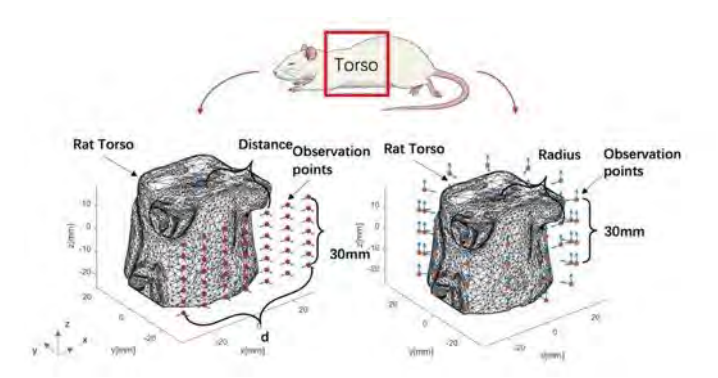


Fig. 1 The planar sensor array and proposed cylindrical sensor array

Rat No.	Method	Data 1	Data 2	Data 3	Data 4	Data 5
Rat 1	Plane	0.4574	0.3658	0.5169	0.4708	0.4964
	Cylinder	0.4027	0.3573	0.3839	0.3878	0.3769
Rat 2	Plane	0.2754	0.214	0.3828	0.2558	0.3556
	Cylinder	0.5615	0.5488	0.4775	0.5133	0.3963
Rat 3	Plane	0.265	0.1629	0.2367	0.236	0.2141
	Cylinder	0.5114	0.4581	0.4148	0.5116	0.4953
Rat 4	Plane	0.4874	0.4516	0.3756	0.2872	0.3938
	Cylinder	0.4186	0.4797	0.4662	0.4431	0.5038
Rat 5	Plane	0.3115	0.3391	0.1668	0.3489	0.3567
	Cylinder	0.4868	0.4946	0.4223	0.4876	0.5017

- Average GOF superiority (Cylinder array): 76%
- Average GOF superiority (Plane array): 24%
- Proportion of estimates in expected region:
 Cylinder array: 52%, Plane array: 24%

Table 1. GOF and anatomical match rates for cylindrical vs. planar arrays.

FC-02. Design of a High-Frequency Magnetic Particle Spectroscopy Instrument for Applications In Vivo

E. Whittier^{1, 2}, J. Beckham^{2, 3, 4}, N. Kent^{2, 4}, P. Anikeeva^{3, 2, 4}
¹EECS, MIT, Cambridge, Massachusetts, United States, ²RLE, MIT, Cambridge, Massachusetts, United States, ³DMSE, MIT, Cambridge, Massachusetts, United States, ⁴McGovern, MIT, Cambridge, Massachusetts, United States

Magnetic hyperthermia has been investigated for several decades for biomedical applications ranging from disease treatment to neuromodulation. Under idealized conditions, magnetohyperthermia utilizes precise temperature control of the local environment surrounding magnetic nanoparticles (MNPs), which serve as magnetothermal transducers. However, our understanding of MNP heating under the relevant experimental conditions is limited by a lack of accurate measurement techniques. design and develop custom magnetic particle spectroscopy (MPS) instrumentation that induces magnetic hyperthermia in MNPs and simultaneously records temperature dependent magnetization dynamics. This measurement is then used to calculate approximate physical properties of the MNPs environment, such as temperature and viscosity.

The MPS instrument consists of a drive coil which applies a 150kHz alternating magnetic field of variable amplitude up to 25mT over a cylindrical volume, diameter 3.2 cm and height 4.3 cm, and a gradiometric receive coil which records the magnetization of MNPs. Despite multiphysics design optimization, inevitable experimental non-idealities create non-uniform conditions throughout large volume samples, such as those used for in vivo studies. We design custom systems to map the drive coil magnetic field in 3D and for determining the spatial sensitivity of the receive coil. We then evaluate the accuracy of the high-frequency MPS for measuring magnetization dynamics by applying it to a broad range of magnetic nanoparticles including colloidallysynthesized isotropic magnetite nanoparticles ranging between ~10-30 nm, ~200 nm magnetite nanodiscs, and lithographically produced (1um x 5 um x 30 nm) permalloy bars, and comparing the measurements to traditional magnetometry, calorimetry, and theoretical estimates.

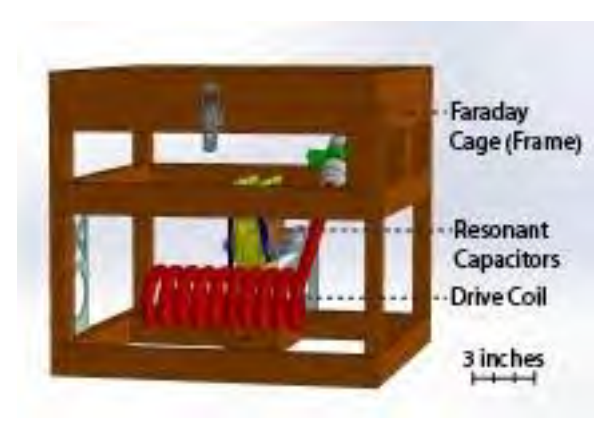


Fig. 1 3D Rendering of MPS Instrument

FC-03. Optimal Operating Condition of a Magnetic Helical Robot to Maximize the Kinetic Energy for Tunneling the Clogged Blood Vessel

S. Lee, J. Kwon, J. Sa, <u>G. Jang</u>

Department of Mechanical Convergence Engineering, Hanyang
Univ., Seoul, Korea (the Republic of)

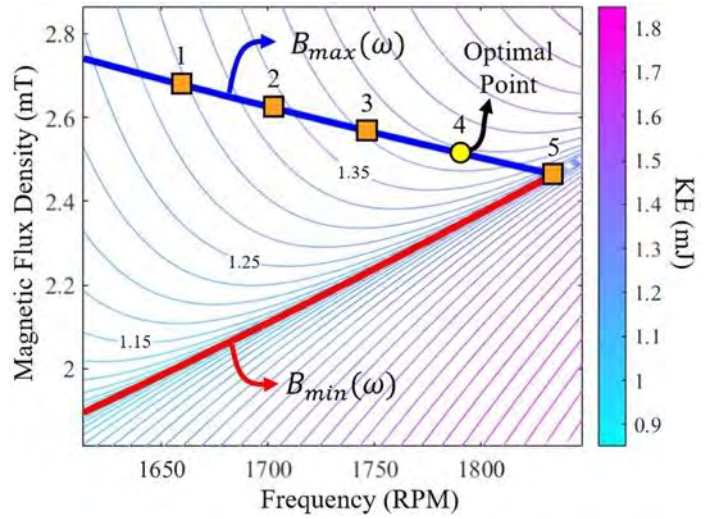
Occlusive vascular disease (OVD), which can cause stroke or a myocardial infarction, occurs when a blood vessel becomes narrowed or blocked due to accumulated blood clots and lipids [1]. Endovascular intervention is performed to treat OVD. But it has 3 major problems; 1) inaccurate procedure, 2) long hours of operation, 3) X-ray radiation exposure of the medical personnel. Robotic endovascular intervention, using a magnetic navigation system (MNS) and magnetic robots, has been introduced to overcome the conventional endovascular intervention [2]. Magnetic helical robots (MHRs) are particularly promising for minimally invasive surgery and targeted therapy. However, these MHRs do not generate sufficient thrust to remove calcified lesions [3]. To improve thrombus removal performance, a high-frequency, high-intensity external magnetic field (EMF) synchronized with MHRs is required. However, such EMF generation is constrained by the power supply voltage, making it necessary to determine the optimal operating conditions for MHR rotation.

We propose a method to determine the optimal magnetic flux density (B_0) and frequency (ω) applied to an MHR to maximize its tunneling performance. First, we derived the analytical solution to the MHR's equation of motion under synchronization with the EMF, and calculated its rotational kinetic energy (KE) based on B_0 and ω of the EMF. Fig. 1 shows the contour lines of simulated KE. $B_{max}(\omega)$ is the

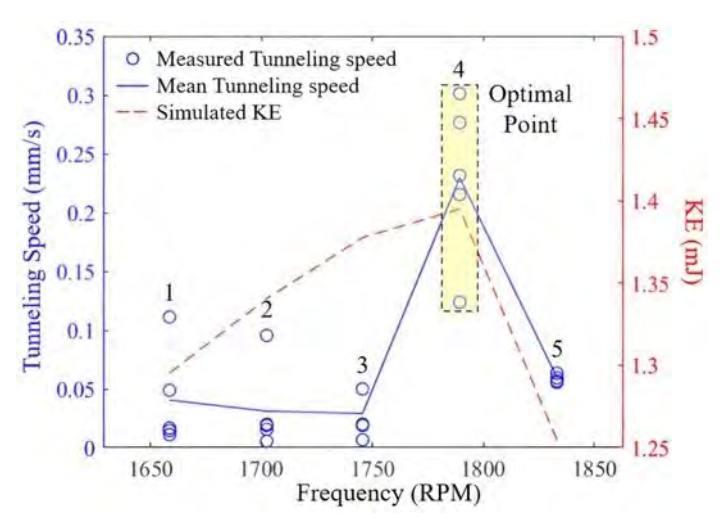
maximum magnetic flux density that the MNS can generate, and $B_{min}(\omega)$ is the minimum magnetic flux density obtained experimentally to synchronize the rotational motion of the MHR by the EMF [4]. It shows that point 4 generates the maximum rotational kinetic energy, representing the optimal operating condition. Fig. 2 presents the measured tunneling speed through an artificial blood clot (0.8 wt%, agar) at five operating points in Fig. 1. It shows that the tunneling speed of the MHR is maximum when the rotational kinetic energy of the MHR is maximized. This paper will contribute to maximizing the tunneling performance of the MHR in the robotic endovascular intervention.

[1] M. S. Kim, J. Hwang and S. Sharfaei, "Global burden of peripheral artery disease and its risk factors, 1990–2019: a systematic analysis for the Global Burden of Disease Study 2019," *Lancet Glob. Health*, Vol. 10, p.e1553–e1565 (2023) [2] J. Hwang, J. Kim and H. Choi, "A review of magnetic actuation systems and magnetically actuated guidewire-and catheter-based microrobots for vascular interventions," *Intelligent Service Robotics*, Vol. 13, p. 1–14 (2020)

[3] Q. Wang, X. Du, and L. Zhang, "Real-time ultrasound doppler tracking and autonomous navigation of a miniature helical robot for accelerating thrombolysis in dynamic blood flow," *ACS nano*, Vol. 16, pp. 604-616 (2022)
[4] J. Kwon, J. Sa, and G. Jang, "Enhanced Tunneling Performance of Magnetic Helical Robots Utilizing Pecking Motion Generated by Alternating Rotating Magnetic Field," *IEEE Transactions on Magnetics*, Vol. 59, pp. 1-5 (2023)



Rotational kinetic energy of the MHR (voltage limitation = 100V)



Measured tunneling speed of the MHR

FC-04. Magnetoencephalographic mapping by optical stimulation of optogenetic rats using Optically pumped magnetometers

<u>K. Komuro</u>¹, M. Fushimi², Y. Kainuma³, T. Zhu¹, S. Funatani¹, S. Chikaki¹, M. Sekino¹

¹Graduate School of Engineering, The University of Tokyo, Tokyo, Japan, ²Graduate School of Information Science and Technology, The University of Tokyo, Tokyo, Japan, ³National Institute of Advanced Industrial Science and Technology, Ibaraki, Japan

Brain function measurements in small animals are essential for studying neural mechanisms and disease models. Optically pumped magnetometers (OPMs) are miniaturized magnetoencephalography (MEG) sensors enabling flexible sensor placement. However, OPM-MEG studies in small animals remain limited and are mostly restricted to singlesensor recordings[1]. In this study, we employed OPMs to conduct multi-channel recordings of somatosensory-evoked responses in small animals, achieving spatial MEG mapping. We used optogenetically modified rats expressing channelrhodopsin-2 (ChR2), in which stimulation of the whisker pad with blue light (473 nm) induces somatosensory-evoked responses[2]. Light stimulation of the whiskers offers high spatiotemporal precision, enabling accurate and selective activation of each individual whisker. We initially explored the stimulation parameters that elicited the strongest brain signal through local field potential (LFP). LFP responses peaked ~40 ms after stimulation. Based on the LFP results, MEG measurements were performed using a stimulation condition of 1 Hz

frequency, 40 ms pulse width, and D3 whisker pad as the stimulation site[2]. We subsequently constructed a fivesensor gradiometric OPM system for MEG measurements (Fig. 1). MEG was recorded at 64 scan points over a 5×5 cm area centered on the bregma. To ensure consistent environmental magnetic conditions, the rat was translated relatively to the stationary sensor array. Data were averaged over 1,000 trials. Fig. 2 shows the MEG results: In Fig. 2(a), magnetic responses peaking at ~120 fT were detected across multiple channels around 40 ms post stimulation. This latency coincides with the peak neural response recorded in the LFP. In Fig. 2(b), spatial mapping of MEG signals was performed. A clear source-sink pattern was visualized around the barrel cortex, providing reliable magnetic field data consistent with neural activation. By creating spatial MEG maps using a multi-channel OPM system, we demonstrated the feasibility and effectiveness of OPM-MEG for small animals.

[1] Yi Ruan, Zhao Xiang , Guanzhong Lu et al., Heliyon, 10(11): e31740(2024)

[2] Tatsuya Honjoh, Zhi-Gang Ji, Yukinobu Yokoyama et al., PLOS ONE, Vol 9, p.1-14(2014)

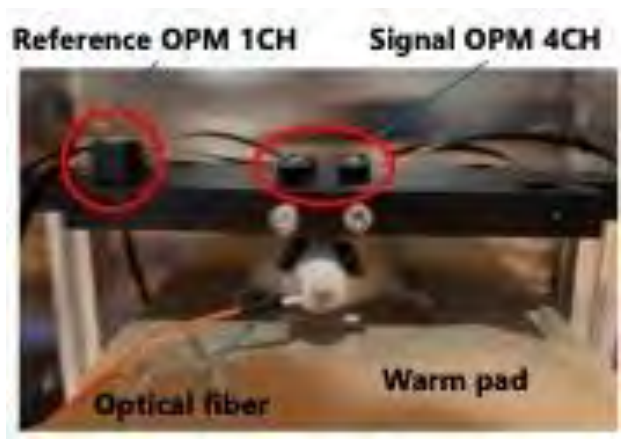


Fig.1 OPM measurement setup

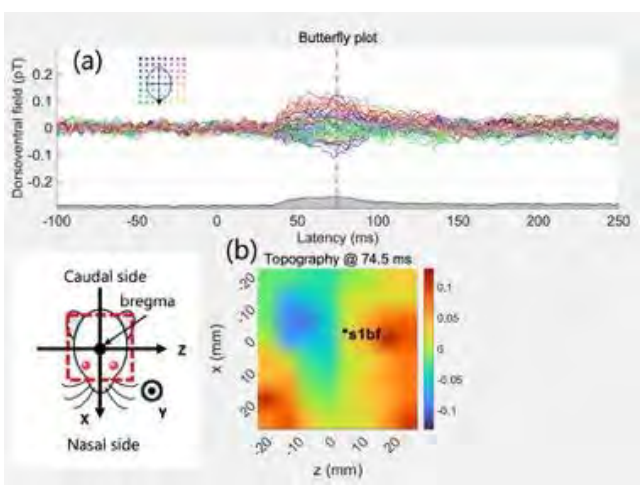


Fig.2 Results of OPM measurements along the Y-axis (a) time waveforms recorded from 64 channels (b) Spatial map at 74.5 ms post-stimulation

FC-05. Exploiting the distinct Fe metabolism of breast cancer cells to analyze and separate stem tumor cells

K. Paz Gonzalez¹, L. Nguyen T. Tran¹, R. Farrell², K. Chen², K. Wu³, J. Chalmers⁴, <u>J. Gomez-Pastora</u>¹

¹Chemical Engineering, Texas Tech University, Lubbock, Texas, United States, ²Department of Biological Science, Texas Tech University, Lubbock, Texas, United States, ³Electrical and Computer Engineering, Texas Tech University, Lubbock, Texas, United States, ⁴William G. Lowrie Department of Chemical and Biomolecular Engineering, The Ohio State University, Columbus, Ohio, United States

Breast cancer is the most common malignancy among women and caused an estimated 670,000 deaths globally in 2022[1]. Despite advances in treatment, cancer heterogeneity and recurrence are closely linked to the presence of cancer stem cells (CSCs). These cells are a distinct subpopulation within tumors, characterized by self-renewal, multipotency, and enhanced resistance to therapy compared to non-stem cancer cells [2, 3]. Identifying and studying CSCs remain challenging due to limited biomarkers and overlapping phenotypes with non-CSCs [2, 3]. Continued research into breast cancer subpopulations is crucial for developing early diagnostics and more effective therapies.

Iron metabolism influences cell survival, proliferation, and therapeutic response. Notably, CSCs exhibit augmented iron uptake and storage, primarily via upregulation of transferrin receptor 1 (TFR1) and ferritin, and downregulation of

ferroportin. This leads to higher intracellular labile iron pools and altered redox states [4-6]. These metabolic changes give CSCs unique biophysical properties, potentially enabling label-free identification and isolation. In this study, we investigate the magnetic properties of breast CSCs and non-CSCs, leveraging differences in iron regulation for cell separation and characterization. We measured differences in magnetic mobility using cell tracking velocimetry, a portable device that tracks cell motion in a microfluidic channel within a defined magnetic field gradient. Based on the observed trajectories, cell properties such as size, volume, and magnetic susceptibility (related to the intracellular Fe content) can be determined. Magnetic separation of the subpopulations of cancer cells is studied in a Quadrupole Magnetic Sorter (QMS). The QMS, with a 10.2mm aperture and maximum magnetic field of 1.36 T, utilizes a quadrupole magnet array that creates a constant magnetic field gradient of 286 T/m. Our work advances the use of magnetic properties as a quantitative, label-free strategy for the identification, isolation, and study of breast cancer stem cells.

- 1. Organization, W. H. (2024). *Breast cancer*. Retrieved from https://www.who.int/news-room/fact-sheets/detail/breast-cancer
- 2. Cosialls, E., El Hage, R., Dos Santos, L., et al., *Cells, Vol.10*(11), p.2981 (2021).
- 3. Marquardt, S., Solanki, M., Spitschak, et al., *Seminars in Cancer Biology, Vol.53*, p.90-109 (2018).
- 4. Mai, T. T., Hamaï, A., Hienzsch, A., et al., *Nature Chemistry, Vol.9*(10), p.1025-1033 (2017).
- 5. Hamaï, A., Tatiana, C., Sebastian, M., et al., *Autophagy, Vol.13*(8), p.1465-1466 (2017).
- 6. El Hout, M., Dos Santos, L., Hamaï, A., et al., *Seminars in Cancer Biology, Vol.53*, p.125-138 (2018).

FC-06. Measurement of the concentration of organic molecules in exhaled gas before and after repetitive magnetic or electrical stimulation of rat hindlimb muscle contractions.

R. Takahashi¹, J. Yang¹, G. Kwoun³, H. Yamada³, H. Yamahara¹, S. Funatani¹, I. Mimura³, M. Fushimi², H. Nishi³, H. Tabata¹, M. Nangaku³, M. Sekino¹
¹Graduate School of Engineering, The University of Tokyo, Bunkyo, Tokyo, Japan, ²Graduate School of Information Science and Technology, The University of Tokyo, Bunkyo, Tokyo, Japan, ³Graduate School of Medicine, The University of Tokyo,

Bunkyo, Tokyo, Japan

Exhaled gas is a non-invasive and repeatedly collectable measure, making it a useful method for evaluating the effects of exercise. Changes in exhaled gas caused by exercise have been widely studied. However, there are few studies on exercise induced by electrical or magnetic stimulation used in exercise therapy. Electrical stimulation in exercise therapy has challenges such as discomfort and limited ability to stimulate deep tissues. Magnetic stimulation causes less discomfort and can stimulate deeper tissues. In this study, the potential of magnetic stimulation as an alternative to electrical stimulation was evaluated. Three types of mixed anesthesia—medetomidine, midazolam, and butorphanol—were administered subcutaneously to the rats. Magnetic stimulation was applied using a circular coil. The output for magnetic stimulation was set at 2.5 times the threshold, with a frequency of 10 Hz, and a total of 18,000 pulses were delivered. For electrical stimulation, the current intensity was also set at 2.5 times the threshold, with a frequency of 10 Hz, and a total of 18,000 pulses were delivered. Exhaled gas was collected at two time points: before stimulation (Pre) and 30 minutes after stimulation (Post). The collected exhaled gas was analyzed using sensor gas chromatography. The results are shown in Figures 1 and 2. Magnetic stimulation significantly increased acetone concentration, consistent with previous studies [1]. This may be due to the longer stimulation duration. Ethanol concentration also increased after magnetic stimulation, possibly reflecting gluconeogenesis or glycogenolysis induced by anesthesia and prolonged stimulation. In contrast, exhaled ethanol concentration significantly decreased after electrical stimulation, which may be due to changes in hepatic metabolic activity. This has not been reported in previous studies. For both magnetic and electrical stimulation, isoprene remained below the minimum detectable concentration (5 ppb). Unlike previous reports [2], this suggests that isoprene is present only in trace amounts in rat exhaled breath.

- [1] Hsuan Chou et al 2024 J. Breath Res. 18 026008
- [2] K F H Hintzen et al 2022 J. Breath Res. 16 027102

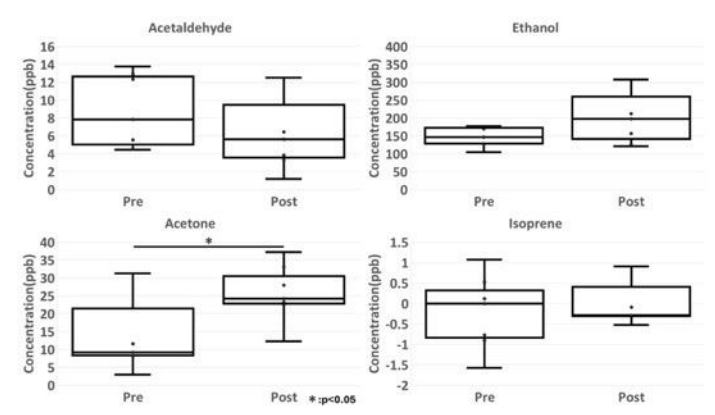


Fig. 1 Exhaled gas about magnetic stimulation (n=7 each)

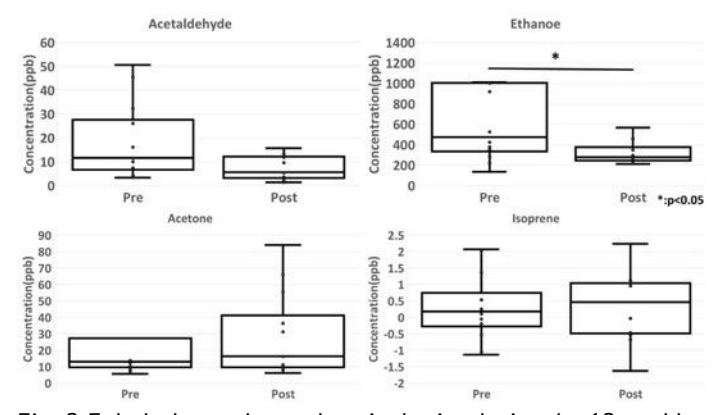


Fig. 2 Exhaled gas about electrical stimulation (n=12 each)

FC-07. Development and Phantom-Based Evaluation of a Deep Transcranial Magnetic Stimulation Coil for the Treatment of Psychiatric Disorders

<u>A. lino</u>¹, W. Lohr², H. M. Kim¹, S. Chikaki¹, M. Fushimi³, R. L. Hadimani⁵, Y. Noda⁴, M. Sekino¹

¹Bioengineering, The University of Tokyo, Tokyo, Japan, ²Biomedical Engineering, Virginia Commonwealth University, Richmond, Virginia, United States, ³Information Physics and Computing, The University of Tokyo, Tokyo, Japan, ⁴Psychiatry, International University of Health and Welfare, Tokyo, Japan, ⁵Mechanical and Nuclear Engineering, Virginia Commonwealth University, Richmond, Virginia, United States

Transcranial magnetic stimulation (TMS) has emerged as a promising non-invasive therapy for neuropsychiatric disorders, including treatment-resistant depression and obsessive-compulsive disorder (OCD). Recent studies have suggested that stimulating deeper brain regions, in addition to the conventional target of the dorsolateral prefrontal

cortex (DLPFC), may improve remission rates [1]. In this study, we aimed to develop a novel deep TMS coil that achieves maximal electric field penetration depth into the brain. To achieve focal deep brain stimulation, we first optimized the electric field to be induced in the brain and derived the coil winding geometry which realizes the optimized electric field using an inverse estimation. The derived coil demonstrated the greatest penetration depth among 50 practical coils [2]. The coil was fabricated by winding hollow conductors according to the derived winding geometry. Fig.1 shows the development pipeline. The coil exhibited an inductance and resistance comparable to commercial TMS coils. To evaluate its stimulation performance, we created a head phantom that replicates the anatomical structures (brain parenchyma, cerebrospinal fluid, skull, and skin) and electrical conductivities based on MRI-derived human head data. Dipole antennas (3 mm in length) were embedded at the two hub target sites: the dorsal anterior cingulate cortex (dACC) for OCD, and the DLPFC for depression. Both the custom coil and a commercial figure-8-coil were tested using the REMED TMS stimulator under the conditions (100% output, 370 µs pulse width). For each coil, the region of maximal winding density was aligned above the dACC position in the phantom (Fig. 2). At the dACC, the measured electric field induced by the figure-8-coil was 76 V/m, while the custom coil generated a higher field of 118 V/m. At the DLPFC, the custom coil induced 638 V/m compared to 155 V/m for the figure-8-coil, indicating a substantial increase in field strength. These improvements may ultimately lead to improved therapeutic outcomes. This study was partly funded by VCU Breakthrough Grant #OP00000431, the VIPC Grant #CCF22-0084-HE, and the AMED Grant 22zf0127006h0001.

[1] L. Carmi et al. Efficacy and Safety of Deep Transcranial Magnetic Stimulation for Obsessive-Compulsive Disorder: A Prospective Multicenter Randomized Double-Blind Placebo-Controlled Trial. Am J Psychiatry., 20(1):152-159, 2022 [2] A. Iino et al. Development of Transcranial Magnetic Stimulator Coils That Physically Achieve the Deepest Stimulation Based on the Inverse Problem Approach. IEEE Trans. Magn., 60, 9, 1-5, 2024

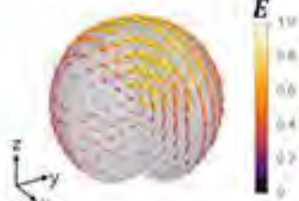
[3] R.A. McGovern and S.A. Sheth. Role of the Dorsal Anterior Cingulate Cortex in Obsessive-Compulsive Disorder: Converging Evidence from Cognitive Neuroscience and Psychiatric Neurosurgery. J Neurosurg., 126, 132, 2017.

2. Derive the coil winding

optimized electric field

which realizes the

1. Optimize the electric field to be induced in the brain



3. Fabricate the coil by winding conductor



Fig. 1 Development pipeline

Locations of dipole antennas implanted in the dACC and DLPFC







Coil position that maximizes the electric field in the dACC





Fig.2 Antenna & coil positions

FC-08. Rapid Detection of Fusobacterium Nucleatum in Saliva using Magnetic Susceptibility

S. Yabukami^{1, 2}, T. Murayama¹, A. Ban¹, K. Okita², S. Tohtake¹, L. Tonthat¹, Y. Ozawa¹, S. Asamitsu¹, H. Okamoto¹, T. Kamei¹,

¹Tohoku University, Sendai, Japan, ²Tohoku-TMIT, Sendai, Japan

There are many other detection methods for bacteria, including polymerase chain reaction (PCR) [1], dielectrophoretic impedance measurement (DEPIM) [2]. We have developed an antigen test that utilizes the antigenantibody reaction between magnetic nanoparticles and biological materials (antigens), which changes the magnetic susceptibility. This method has the following outcomes in bacterial detection: low cost, rapid evaluation, high sensitivity, and reduced influence of contaminants. The magnetic susceptibility of magnetic nanoparticles (MNPs)antigen aggregates decreases as the bacterial concentration increases due to a decrease in the magnetic coupling between the MNPs. Fig. 1 shows the configuration of the measurement system. It consists of a driving coil, a differential pickup coil, a magnetic field coil, a lock-in amplifier, and a signal generator. The driving coil was aircooled to reduce thermal drift, and the size of the differential pickup coil was reduced to achieve a high signal-to-noise ratio in magnetic susceptibility measurements. After the antigen-antibody reaction, the magnetic nanoparticles and antigens are agglutinated by magnetic force, reducing the influence of contaminants and allowing the evaluation of Fusobacterium Nucleatum without washing. Fusobacterium Nucleatum is significantly more prevalent in patients with colorectal cancer and esophageal cancers [3]. Fig. 2 shows the evaluation results of Fusobacterium Nucleatum collected from the saliva of patients, and healthy individuals (28 subjects) admitted to Tohoku University Hospital and compares them with qPCR results. The results showed a strong correlation with qPCR analysis (correlation coefficient = 0.69, p<0.0001), highlighting the accuracy and precision of our method in bacterial quantification. This performance is comparable to that of conventional qPCR systems.

[1] R. K. Saiki, S. Scharf, F. Faloona, Science, 230, p. 1350 (1985). [2] J. Suehiro, R. Hamada, D. Noutomi, Journal of Electrostatics, 57, p. 157 (2003). [3] Yachida, Soga, Fukuda, Yamada, Nature Med. 25, p. 968 (2019).

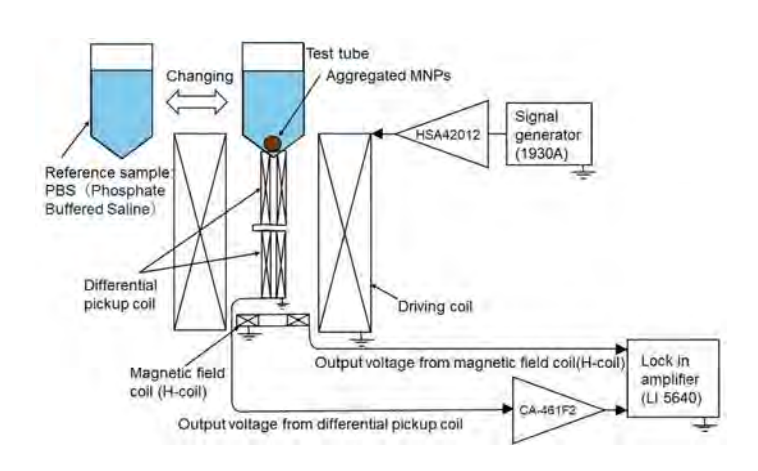


Fig. 1 Schematic view of the portable bacteria detection system.

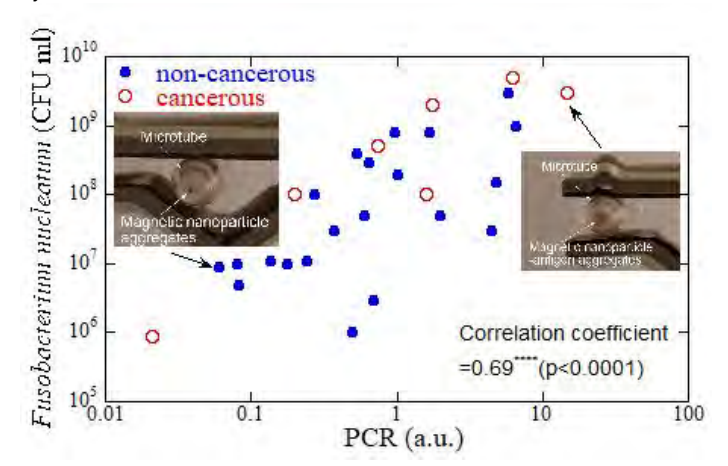


Fig. 2 The evaluation results of Fusobacterium Nucleatum collected from the saliva of patients and healthy individuals (28 subjects) compared against qPCR results. A high correlation coefficient with PCR (0.69, p < 0.0001) was obtained.

FC-09. Superparamagnetic Nanoparticles: bridging traditional Characterization up to 1 GHz and Real-World Biosensing Applications

M. Hauwaert¹, R. Hanus¹, S. Spassov³, V. Pilati², R. B. Goldfarb⁴, L. Lejeune⁵, M. Salvador², S. Hermans⁵, M. Rivas², J. Raskin¹

¹ICTEAM, UCLouvain, Louvain La Neuve, Belgium, ²Dept de Fisica Applicada, Universidad De Oviedo, Gijón, Spain, ³Geophysics Department, IRM-KMI, Dourbes, Belgium, ⁴NIST, Boulder, Colorado, United States, ⁵IMCN, UCLouvain, Louvain La Neuve, Belgium

Superparamagnetic nanoparticles (SPNs) are effective labels in quantitative magnetic (bio)detection applications due to their lack of hysteresis and high susceptibility. Understanding their properties within the sensing platform is key to optimize sensor design and performance. [1] A major challenge lies in the differences between the characterization environment and the actual sensing conditions; affecting their mobility, aggregation, orientation and spacing. These geometrical and mechanical differences alter the DC and AC magnetic properties, questioning the relevance of conventional characterization methods for practical sensing technologies.

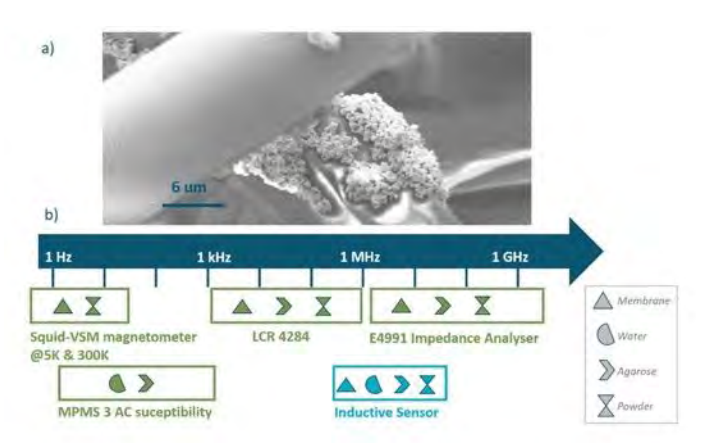
In this work, we focus on the effective AC and DC susceptibility of MnFe $_2$ O $_4$, CoFe $_2$ O $_4$, and Fe $_3$ O $_4$ SPNs and study their specific properties within porous media such as (nitro)cellulose membranes, used in e.g. immunological tests such as Lateral Flow Assays. We compare traditional characterisation results on both SPN powders and distributions in membranes. Magnetization curves, (Z)FC measurements, and low-frequency dynamic susceptibility (up to 1 kHz) are acquired using a SQUID-based magnetometer (MPMS), while complex susceptibility in the 1 MHz $_1$ GHz range is measured with an E4991 impedance analyzer. [2]. SPN analysis up to 1 GHz is rarely found in the literature, providing valuable insights for sensor applications.

Furthermore, we developed an oscillator-based inductive sensor capable of exciting SPNs between 200 kHz and 15 MHz in 4 configurations: microfluidic tubes, powders, agarose suspensions and membranes. Based on these DC to 1 GHz results and relevant models (Neel relaxation, Curie-Weiss and Landau-Lifshitz-Gilbert) the difference between susceptibility properties in traditional characterization setups and real-life biosensing platforms is quantified. The most relevant parameters – such as dipolar interactions- are discussed to allow for a better integration of material physics practices into (bio)sensor design.

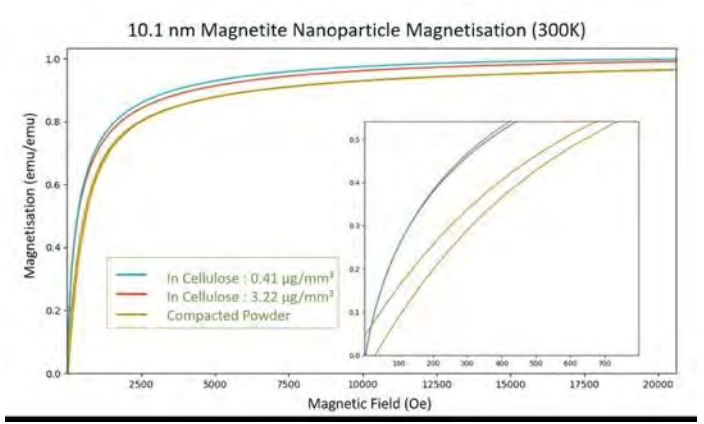
[1] V. Pilati *et al.*, "Mn-ferrite nanoparticles as promising magnetic tags for radiofrequency inductive detection and quantification in lateral flow assays," *Nanoscale Adv.*, Jul. 2024, doi: 10.1039/D4NA00445K.

[2] R. B. Goldfarb and H. E. Bussey, "Method for measuring complex permeability at radio frequencies," *Rev. Sci. Instrum.*, vol. 58, no. 4, pp. 624–627, Apr. 1987, doi: 10.1063/1.1139227.

^{*} Best Student Presentation Finalist / LB – Late-breaking Poster



- (a) SEM image of SNP cluster in glass fiber membrane
- (b) experimental overview



Magnetisation of Fe₃O₄ SPNs. In compacted powder, coercivity is higher. When dispersed in cellulose, initial susceptibility increases when density decreases

FC-10. Additive Manufacturing of Parabolic Ferromagnetic Coils for Transcranial Magnetic Stimulation Using Laser-Based Directed Energy Deposition

D. Mudakavi¹, V. E. Bodur¹, P. J. Udapudi¹, M. Tashli², <u>R. L. Hadimani</u>², S. M. Adinarayanappa¹

¹Additive Manufacturing and 4D Printing lab, Dept of Mechanical Materials and Aerospace Engineering, Indian Institute of Technology, Dharwad, Dharwad, Karnataka, India, ²Biomagnetics lab, Dept of Mechanical and Nuclear Engineering, Virginia Commonwealth University, Virginia, Virginia, United States

Transcranial Magnetic Stimulation (TMS) is a non-invasive technique widely used for the treatment of various neurological and psychological disorders [1]. The core

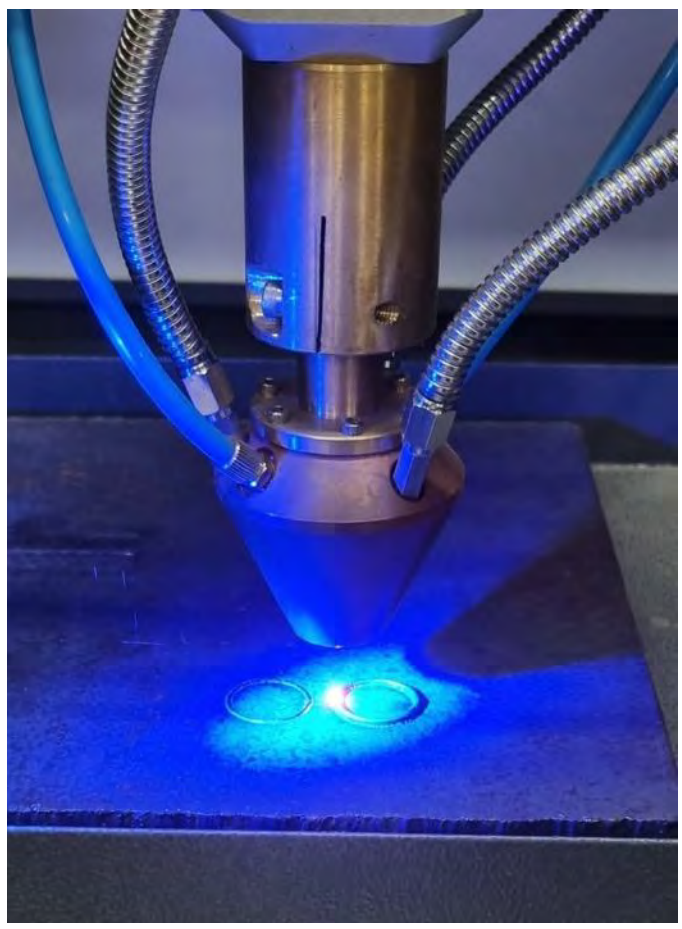
component of any TMS system is the coil, which is responsible for delivering controlled electromagnetic pulses to targeted regions of the brain. Among the different coil designs, Parabolic Ferromagnetic Coils (PFCs) are particularly favored for their ability to focus the electromagnetic field more effectively [2]. However, the fabrication of customized TMS coils using traditional manufacturing methods is both challenging and timeconsuming due to the intricate geometries and tight tolerance requirements. Directed Energy Deposition (DED)based additive manufacturing offers a promising alternative, particularly by enabling control over the material composition and microstructure. Despite these advantages, the DED process also presents several challenges in the context of TMS coil fabrication. The typically complex spiral geometry of PFCs involves significant overhangs, support structures, and precision requirements—all of which are critical for achieving the desired electromagnetic performance. In this study, a premixed powder of Permendur—an iron-cobalt alloy known for its high magnetic saturation—was used as the feedstock material for the design, simulation, and fabrication of TMS coils using a powder-based laser DED process. Finite Element Analysis (FEA) using ANSYS was employed to simulate the thermal profile, estimate the melting temperature range, and predict post-cooling deformation behavior. To evaluate the quality and functional performance of the fabricated coils, a comprehensive material characterization was conducted. This included optical microscopy, scanning electron microscopy (SEM), and energy-dispersive X-ray spectroscopy (EDS) to confirm the composition and microstructural integrity. Furthermore, the inductance of the coil was calculated, and the electric field distribution was experimentally measured. The results were found to be satisfactory, indicating the feasibility of this approach for fabricating high-performance, custom-designed TMS coils. Acknowledgment:

The research at VCU and IIT Dharwad was partly funded by the "2024 VCU Presidential Research Quest Fund" and "Scheme for Promotion of Academic and Research Collaboration (SPARC), Project number P3872, Ministry of Education, Govt. of India," respectively.

[1] M. S. George *et al.*, "Daily left prefrontal transcranial magnetic stimulation therapy for major depressive disorder: a sham-controlled randomized trial.," *Archives of general psychiatry*, vol. 67, no. 5, pp. 507–16, May 2010, doi: 10.1001/archgenpsychiatry.2010.46.

[2] M. Tashli, A. Mhaskar, G. Weistroffer, M. S. Baron, and R.

L. Hadimani, "Novel multi-magnetic material transcranial magnetic stimulation coils for small animals application," *AIP Advances*, vol. 14, no. 1, p. 015324, Jan. 2024, doi: 10.1063/9.0000772.



"3D printing of potential TMS coil magnetic material using directed energy deposition"

FC-11. Evaluation of a Geometrically and Conductively Accurate Brain Phantom for Predicting TMS-Induced Electric Fields

M. Paslar¹, W. Lohr¹, T. J. Taylor¹, T. Atalugama², B. Embree², R. L. Hadimani^{2, 1}, C. L. Peterson¹

¹Biomedical Engineering, Virginia Commonwealth University, Richmond, Virginia, United States, ²Mechanical and Nuclear Engineering, Virginia Commonwealth University, Richmond, Virginia, United States

Non-invasive brain stimulation techniques, such as transcranial magnetic stimulation (TMS), greatly benefit from precise in situ evaluations prior to clinical application.

Developing brain phantoms that closely mimic human brain geometry and tissue properties can significantly enhance electric field (E-field) measurement accuracy, leading to better-tailored and more effective stimulation protocols. In this study, we employed magnetic resonance imaging (MRI) to create a neuroanatomically accurate human brain phantom. Conductive composites were utilized to accurately replicate brain tissue properties, enhancing predictive accuracy of E-field propagation. Triaxial dipole probes (TDPs) embedded within the phantom (Figure 1) allowed precise three-dimensional measurement of the induced E-fields [1]. To validate our phantom, we compared phantom-derived E-field measurements with corresponding in vivo data.

Multimodal data were collected, including electromyography (EMG) to assess muscle activations during TMS (Figure 2), electroencephalography (EEG) for resting-state brain oscillations, and structural MRI scans. MRI data from an individual participant were used to generate a detailed neuroanatomically accurate phantom [2]. We then analyzed E-fields induced by TMS in the phantom and compared these findings to actual TMS-induced responses from the same individual.

Our results demonstrate that neuroanatomically accurate brain phantoms can effectively predict individualized TMS responses, highlighting their potential in enhancing the design and optimization of stimulation protocols. This approach could substantially improve the precision and clinical efficacy of TMS-based therapies and research applications.

- 1. Y.-N. Chen et al., "Stereotaxic atlas of the infant rat brain at postnatal days 7–13," Front. Neuroanat., vol. 16, Aug. 2022, doi: 10.3389/fnana.2022.968320.
- 2. H. Magsood and R. L. Hadimani, "Development of anatomically accurate brain phantom for experimental validation of stimulation strengths during TMS," Materials Science and Engineering: C, vol. 120, p. 111705, Jan. 2021, doi: 10.1016/j.msec.2020.111705.

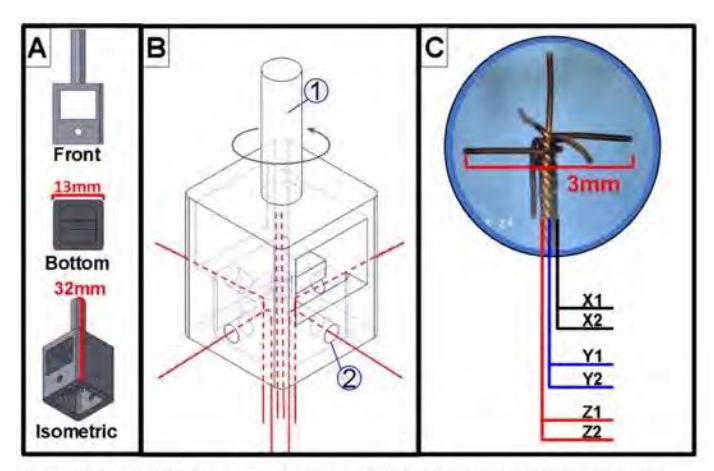


Figure 1. (A) 3D printed TDP winding tool. (B) Six insulated wires were inserted into the 3D printed tool (2), each corresponding to the positive or negative side of a single axis. The tool was then secured into an electric drill using the shaft labelled (1) and the dipoles were wound together. (C) Once wound, the negative Z lead was bent down and the ends were precisely cut to 1.5 mm from the origin. (D) The final result is a TDP with precise axial geometry with known

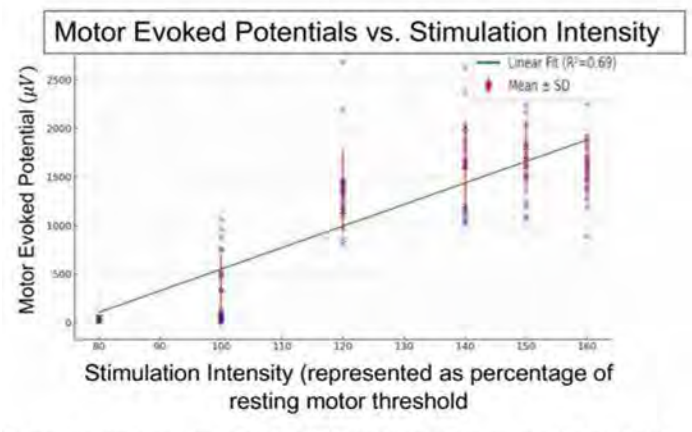


Figure 2: A recruitment curve of MEPs was graphed based on the stimulation intensity. The slope of this curve was estimated to measure the excitability of the primary motor

FC-12. Wearable Magnetic Shielding for the Safe **Application of Transcranial Magnetic Stimulation in Patients** with Brain Implants

W. Lohr¹, T. Atalugama², B. Embree², H. Shah³, J. Chen³, K. Holloway³, R. L. Hadimani²

¹Biomedical Engineering, Virginia Commonwealth University, Richmond, Virginia, United States, ²Mechanical and Nuclear Engineering, Virginia Commonwealth University, Richmond, Virginia, United States, ³Neurosurgery, Virginia Commonwealth University, Richmond, Virginia, United States

Permalloy based composite films serve as effective magnetic shields for low to medium frequency magnetic fields, such as the field generated by transcranial magnetic stimulation (TMS) [1], a neuromodulation technique that is

widely used for the treatment of depression [2, 3]. These shields can help redirect magnetic fields and safeguard implantable devices, reducing overstimulation of cortical areas in TMS procedures. Unlike metallic shields, which generate loud noises due to Lorentz forces, these composites are flexible, allowing for a seamless fit between the TMS coil and the patient's head. The shielding composite is tested using conductively and anatomically accurate neuromodulation phantoms and FEM simulations (Fig. 1). This work investigates the safety of using TMS with implanted devices, such as deep brain stimulation leads, and proposes a wearable shield that may enable multimodal treatment of diseases like Parkinson's disease. Nickel-iron-molybdenum, commercially known as permalloy was purchased from Fushel of concentration 80%, 17%, 3%, and average particle size of 70 nm (Fig. 2). The permalloy powder was mixed with Sylgard 184 PDMS purchased from Dow Chemicals to create a composite of 80 weight percent permalloy and 20 weight percent PDMS. The composite was spin coated to create a thin film followed by a gold sputtered layer to increase shielding effectiveness, layers repeated. DBS probes implanted into a neuromodulation head phantom along with several triaxial dipole probes to measure induced electric fields. The brain phantom is composed of a PDMS and carbon nanotube (CNT) composite mixed at 8 weight percent CNT to mimic brain conductivity. The permalloy composite shielding cap is placed around the head near the insertion point of the DBS lead. TMS is applied to the phantom and induced electric fields are measured using the triaxial dipole probes. This research is partly funded by NSF Grant #2349694, # 2304513 and the Virginia Innovation Partnership

Corporation (VIPC) Grant, #CCF22-0084-HE

- [1] W. Lohr et al., "Novel conformable shielding permalloy composite for controlling field profiles of transcranial magnetic field coils," in IEEE Transactions on Magnetics, doi: 10.1109/TMAG.2025.3562780.
- [2] [M. S. George et al., "Daily left prefrontal transcranial magnetic stimulation therapy for major depressive disorder: a sham-controlled randomized trial," Arch. Gen. Psychiatry, vol. 67, no. 5, pp. 507 – 516, May 2010, doi: 10.1001/archgenpsychiatry.2010.46.
- [3] O. of the Commissioner, "FDA permits marketing of transcranial magnetic stimulation for treatment of obsessive compulsive disorder," FDA. Accessed: Nov. 08, 2024. [Online]. Available: https://www.fda.gov/news-events/pressannouncements/fda-permits-marketing-transcranial-

magnetic-stimulation-treatment-obsessive-compulsive-disorder

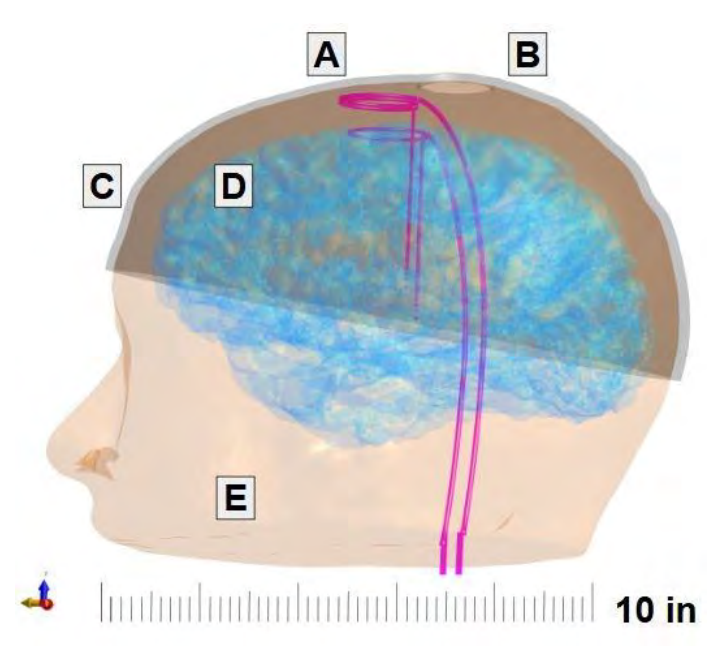


Fig 1: Models of DBS shielding A) DBS lead B) Shield hole C) Shielding cap. D) Grey matter E) Skin

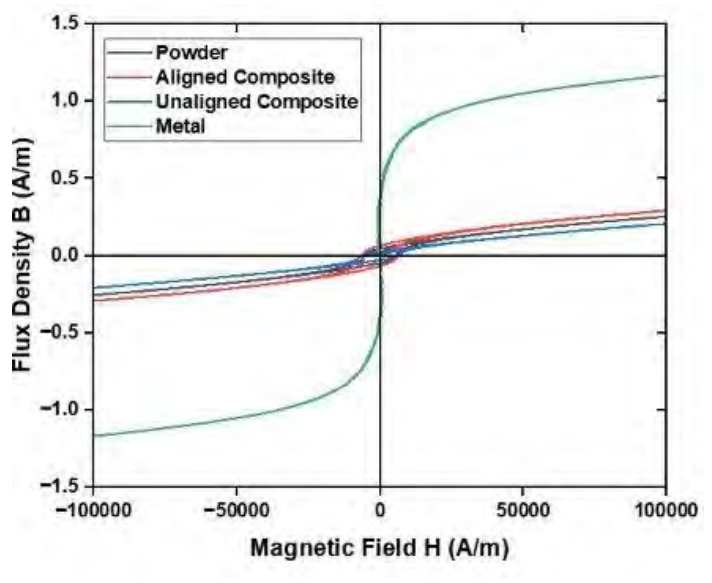


Fig 2: Hysteresis and magnetic properties of permalloy powder, sheet metal, and composite

FC-13. Magnetic Field Gradient Trapping Efficacy on SH-SY5Y Cancer Cells and Total RNA

B. Gungordu¹, N. Gunduz Akdogan^{3, 2}, C. Bagci¹, <u>O. Akdogan^{1, 2}</u>
¹Faculty of Engineering and Natural Sciences, Bahcesehir
University, Istanbul / Besiktas, Istanbul / Besiktas,
Turkey, ²NANOTerial Technology Corporation, Istanbul,
Istanbul, Turkey, ³Faculty of Engineering, Piri Reis University,
Istanbul, Istanbul, Turkey

The extensive implementation of high-performance micromagnets in microfluidics, microchannels, magnetic gradient patches, biomedical microelectromechanical systems (Bio-MEMS), and diagnostic biosensors for disease detection is the reason for the growing demand for these lab-on-a-chip devices [1]. Bio-MEM platforms enhance the efficiency of isolating single cell using magnetic nanoparticles (MNPs) guidance, facilitate targeted drug delivery, and enable the sensitive detection of cancer biomarkers.

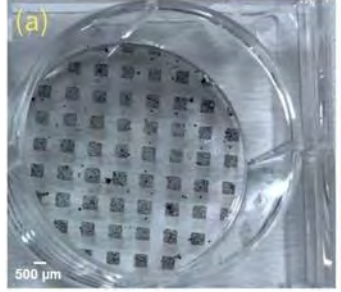
The main objective of the current study was to investigate the interaction between magnetophoretic systems and biological organisms, with a specific focus on brain cancer cells, including the neuroblastoma cell line (SH-SY5Y), and the trapping efficacy of their total RNA. The present work devised a novel and efficient method for synthesizing ordered arrays of Nd-Fe-B and Sr-Fe nanoflakes (NFs) patterns. The surfactant-assisted ball milling technique produced Nd-Fe-B and Sr-Fe NFs exhibiting a high aspect ratio^[1]. A homogeneous combination of negative photoresist was achieved by combining SU-8 with Nd-Fe-B and Sr-Fe NFs at varying concentrations^[2]. 50 wt.% was determined to be the optimal concentration. A photolithography technique was conducted with a spin coating technique at speeds ranging from 1000 to 1500 rpm. Micro-magnets measuring up to 500 µm have been successfully synthesized due to the effective manufacturing of micro-magnets. The main objective was to assess the targeted trapping effectiveness of SH-SY5Y cells and their total RNA utilizing fabricated micro-magnets.Fe₃O₄ MNPs were synthesized by the coprecipitation technique and then coated with polyethylene glycol(PEG)[3]. PEG-coated Fe₃O₄ MNPs were used to label SH-SY5Y cells, and various concentrations were evaluated [4]. The trapping of cells was employed with microfluidic channels incorporating the patterned micro-magnet arrays to evaluate the trapping efficiency^[5]. Furthermore, total RNA was extracted from cells and applied to the micro-magnet arrays. qPCR was conducted to evaluate the trapping efficacy by analyzing gene expression levels.

1. Ozunlu, S., Akdogan, N. G., Bozkurt, M. N., Doganturk, L., Alshammari, H. A., Le Roy, D., & Akdogan, O. (2021, September 16). Innovative technique for patterning Nd – Fe B arrays and development of a microfluidic device with high trapping efficiency. Nanotechnology, 32(49), 495501. https://doi.org/10.1088/1361-6528/ac1dd6
2. Akdogan, N. G., & Akdogan, O. (2019, December 1). Synthesis of Nd- Fe-B/Fe hybrid micro-magnets. AIP Advances, 9(12), 125139. https://doi.org/10.1063/1.5130412

3. Oehlsen, O., Cervantes-Ramírez, S. I., Cervantes-Avilés, P., & Medina-Velo, I. A. (2022, January 21). Approaches on Ferrofluid Synthesis and Applications: Current Status and Future Perspectives. ACS Omega, 7(4), 3134–3150. https://doi.org/10.1021/acsomega.1c05631

4. Domac, B., AlKhatib, S., Zirhli, O., Akdogan, N., Dirican, S. Ö., Bulut, G., & Akdogan, O. (2019). Effects of PEGylated Fe-Fe3O4 core-shell nanoparticles on NIH3T3 and A549 cell lines. Heliyon, 6(1), e03124.

https://doi.org/10.1016/j.heliyon.2019.e03124
5. Ozunlu, S., Akdogan, N. G., Bozkurt, M. N., Doganturk, L., Alshammari, H. A., Le Roy, D., & Akdogan, O. (2021, September 16). Innovative technique for patterning Nd-Fe-B arrays and development of a microfluidic device with high trapping efficiency. Nanotechnology, 32(49), 495501. https://doi.org/10.1088/1361-6528/ac1dd6



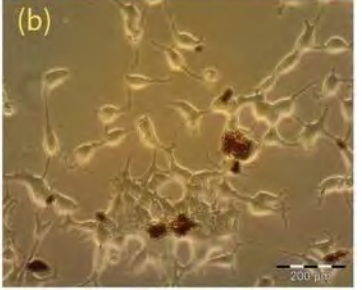


Fig 1. Images of the a. 20 wt.% Nd-Fe-B loaded 500 μ m micro-magnet b. Labelled SH-SY5Y neuroblastoma cells with PEG-Fe₃O₄ NPs.

FC-14. Bioplastics Based on Gelatin-Pectin Blends Enriched with Multifunctional Nanoparticles

B. Gungordu¹, S. Can¹, B. Onat¹, N. Gunduz Akdogan^{2, 3}, <u>O. Akdogan^{1, 3}</u>

¹Bahcesehir University, Istanbul, Turkey, ²Piri Reis University, Istanbul, Turkey, ³NANOTerial Technology Corporation, Istanbul, Turkey

Plastics are widely used due to their low cost and lightweight structure, but their long-lasting and nonbiodegradable nature causes severe environmental and health concerns. Improper destroying of plastics leads to persistent accumulation, particularly in marine ecosystems, where plastics threaten wildlife through ingestion and entanglement [1]. This study aims to develop multifunctional and eco-friendly bioplastics with added properties such as biodegradability, UV resistance, antibacterial and magnetic activity. Gelatin and pectin were chosen as base biopolymers, and glycerin was added as a plasticizer for improved flexibility [2]. The biopolymer matrix was enhanced with silver (AgNPs), zinc oxide (ZnO), titanium dioxide (TiO₂), and iron oxide (Fe₃O₄) nanoparticles. These nanoparticles were produced via chemical co-precipitation, sol-gel, and green synthesis methods [3]. Hazelnut shell extract is used as a natural reducing agent when obtaining silver nanoparticles. This means promoting a more sustainable approach [4]. Nanoparticles were dispersed using an ultrasonic bath, followed by solvent casting to ensure uniform distribution. The resulting bioplastics were characterized by XRD, FTIR, TEM, VSM, and UV-VIS analyses to assess structural, magnetic, and optical features. Mechanical, thermal and antibacterial tests are performed to evaluate performance. Adding ZnO and TiO₂ improved UV blocking and gave the films photocatalytic self-cleaning properties. AgNPs contributed to vigorous antibacterial activity, while the magnetic responsiveness of Fe₃O₄ will increase the functionality of bioplastics. Compared to other bioplastics, these composites were found to be more durable and multifunctional. This study holds promise for producing high-performance smart bioplastics by integrating biobased materials with nanoparticles. The proposed materials could offer sustainable alternatives for use in areas like food packaging and biomedical devices.

[1] United Nations Environment Programme. Everything you need to know about plastic pollution. *UNEP* http://www.unep.org/news-and-stories/story/everything-you-need-know-about-plastic-

pollution (2023).

[2] Mroczkowska, M., Germaine, K., Culliton, D., Kakouli Duarte, T., & Neves, A. C. (2021). Assessment of biodegradation and eco-toxic properties of novel starch and gelatine blend bioplastics. *Recycling*, *6*(4), 81.

[3] Sivri, D., Kurel, A., Baytore, D. I., Akdogan, N. G., & Akdogan, O. (2023c). Recycling of Hazelnut Husk; from Biowaste to Phyto-Assisted Synthesis of Silver Nanoparticles. ChemistrySelect, 8(37).

https://doi.org/10.1002/slct.202302262

[4] Ayrilmis, N., Yurttas, E., Tetik, N., Özdemir, F., Palanisamy, S., Alagarsamy, A., ... & Al-Farraj, S. A. (2024). Antibacterial Performance of Biodegradable Polymer and Hazelnut Husk Flour Antibacterial Biofilm with Silver Nanoparticles. *BioResources*, 19(4).

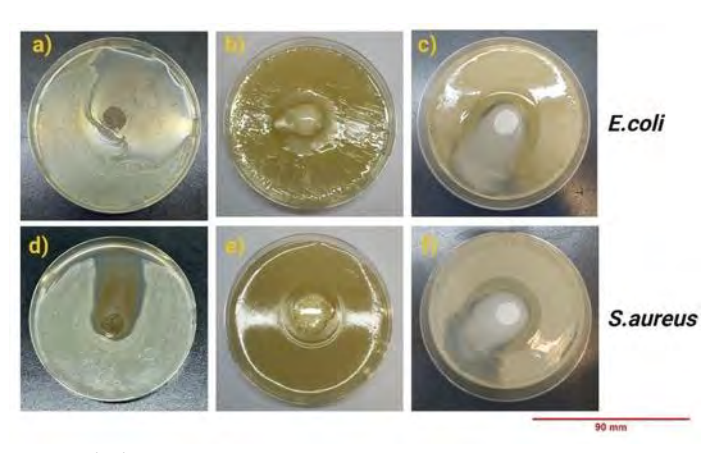


Figure 1. Antibacterial effects of bioplastics with nanoparticles against E. coli (a–c) and S. aureus (d–f). Samples: (a, d) 3% AgNPs, (b, e) 30% TiO_2 , (c, f) 30% ZnO. Clear inhibition zones indicate strong activity.

FC-15. Dual-Mode Detection of Magnetic and Dielectric Responses in Core-Shell Nanoparticles for Biomedical Diagnostics

<u>D. Brown</u>¹, D. Luu¹, K. Hwang¹, M. Nguyen², S. Hoijang², T. Lee², M. Phan¹

¹Department of Physics, University of South Florida, Tampa, Florida, United States, ²Department of Chemistry and the Texas Center for Superconductivity, University of Houston, Houston, Texas, United States

The ability to simultaneously detect magnetic and dielectric signals from core/shell nanoparticles enhances the performance of advanced biosensing platforms. These platforms offer valuable insights into disease markers, cell interactions, and molecular binding events, ultimately

improving diagnostic capabilities [1,2]. Many existing biosensing systems struggle to achieve this dual detection. Through the exploration of magneto-LC resonance (MLCR) sensor technology [2], we demonstrate the exceptional ability to detect both magnetic and dielectric signals from dynamic core/shell nanoparticles. We conducted a systematic study on core/shell Fe₃O₄@SiO₂ nanoparticles. varying both the Fe₃O₄ core diameter (~190 nm and ~340 nm) and the SiO_2 shell thickness (~15 nm - 50 nm). Polycrystalline Fe₃O₄ nanoparticles, each composed of multiple ~9-12 nm nanocrystals, were synthesized using the solvothermal method [3]. A modified Stöber method was then used to coat these Fe₃O₄ nanoparticles with silica to create core/shell nanostructures. While Fe₃O₄ nanostructures have been widely explored for biomedical applications, SiO₂, a non-magnetic dielectric material known for its excellent biocompatibility and a feasible chemical surface for conjugation of biomolecules, is also commonly used in biomedical contexts. The SiO₂ shell not only reduces interference from the magnetic core but also enables the detection of additional signals, such as dielectric properties, which are valuable for biosensing applications. In comparison to the GMI sensor for detecting core/shell nanoparticles, the MLCR sensor demonstrates a remarkable enhancement in detection sensitivity, with a 16fold increase. By varying the SiO₂ shell thickness, we demonstrate how the MLCR sensor can detect dielectric signals from biomarkers while maintaining high magnetic detection sensitivity. These findings provide new insights into how non-magnetic dielectric shells affect the overall detection sensitivity of core/shell nanoparticle-based biosensors. The results have significant implications for medical diagnostics and biosensing, paving the way for more versatile and sensitive detection methods.

- [1] Jimenez, et al., Magnetoimpedance Biosensors and Real-Time Healthcare Monitors: Progress, Opportunities, and Challenges, *Biosensors* 12, 517 (2022)
- [2] Hwang, et al., Signal Differentiation of Moving Magnetic Nanoparticles for Enhanced Biodetection and Diagnostics, *Biosensors* 15, 116 (2025)
- [3] Nguyen, et al., Superparamagnetic Superparticles for Magnetic Hyperthermia Therapy: Overcoming the Particle Size Limit, ACS Applied Materials and Interfaces 17, 19436 (2025)

SESSION FD: LOW DAMPING AND TOPOLOGICAL SYSTEMS

Co-Chair(s): A. I. Ojo, *Physics, University of South Florida, Tampa, Florida, United States* and E. Thareja, *Department of Physics, University of South Florida, Tampa, Florida, United States*

Thursday, October 30, 2025 02:00 PM-05:30 PM Ballroom B

FD-01. Vertically Graded FeNi Alloys with Low Damping and a Sizeable Spin-Orbit Torque

R. E. Maizel¹, S. Wu¹, P. P. Balakrishnan², A. J. Grutter², C. Kinane³, A. Caruana³, P. Nakarmi⁴, B. Nepal⁴, D. A. Smith¹, Y. Lim¹, J. L. Jones¹, W. C. Thomas¹, J. Zhao⁵, M. F. Michel⁵, T. Mewes⁴, S. Emori¹

¹Physics, Virginia Tech, Blacksburg, Virginia, United States, ²National Institute of Standards and Technology, Center for Neutron Research, Gaithersburg, Maryland, United States, ³ISIS-Neutron and Muon Source, STFC Rutherford Appleton Laboratory, Didcot, United Kingdom, ⁴Dept. of Physics and Astronomy, University of Alabama, Tuscaloosa, Alabama, United States, ⁵Geoscience, Virginia Tech, Blacksburg, Virginia, United States

Energy-efficient spintronic devices require a large spin-orbit torque (SOT) and low damping to excite magnetic precession. In conventional devices with heavymetal/ferromagnet bilayers, reducing the ferromagnet thickness to ~1 nm enhances the SOT but dramatically increases damping. Here, we investigate an alternative approach based on a 10 nm thick single-layer ferromagnet to attain both low damping and a sizable SOT. Instead of relying on a single interface, we continuously break the bulk inversion symmetry with a vertical compositional gradient of two ferromagnetic elements: Fe with low intrinsic damping and Ni with sizable spin-orbit coupling. We find low effective damping parameters of α_{eff} < 5 in the FeNi alloy films, despite the steep compositional gradients. Moreover, we reveal a sizable anti-damping SOT efficiency of $|\theta_{AD}| \approx 0.05$ even without an intentional compositional gradient. Through depth-resolved x-ray diffraction, we identify a lattice strain gradient as crucial symmetry breaking that underpins the SOT. Our findings provide fresh insights into damping and SOTs in single-layer ferromagnets for power-efficient spintronic devices. This talk is based on: R.E. Maizel, S. Wu, P. Balakrishnan, et al., Phys. Rev. Appl., 22, 044052 (2024) [1]

[1] R.E. Maizel, S. Wu, P. Balakrishnan, et al., Phys. Rev. Appl., 22, 044052 (2024)

[2] S. Karimeddiny, D.C. Ralph, Phys. Rev. Appl., 15, 064017 (2021)

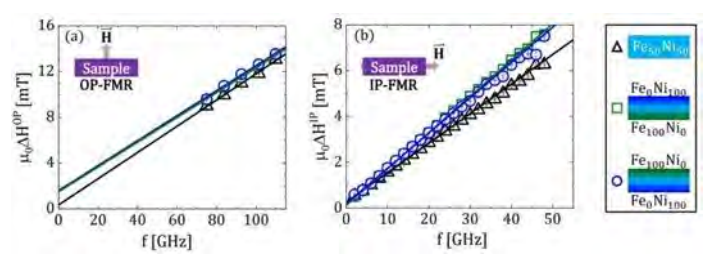


Fig. 1 FMR linewidth vs frequency for $Fe_{50}Ni_{50}$ (black triangle), $Fe_{100-x}Ni_x$ (green square), and Fe_xNi_{100-x} (blue circle) with FMR configuration (a) out-of-plane and (b) in-plane.

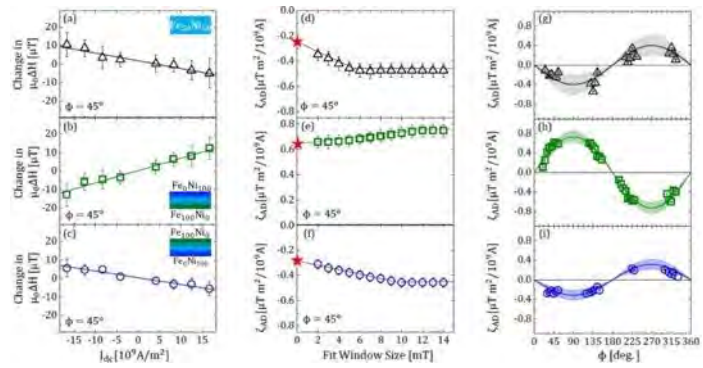


Fig. 2 Left column (a-c): Change in linewidth $\triangle H$ due to dc bias current density J_{dc} at fixed in-plane field angle $\varphi = 45^{\circ}$ for (a) $Fe_{50}Ni_{50}$, (b) $Fe_{100-x}Ni_x$, and (c) Fe_xNi_{100-x} . The line indicates the linear fit to quantify the slope, ξ_{AD} . THe error bars represent the standard deviation of 20 measurements. Center column (d-f): Change in ξ_{AD} with fit window size for (d) $Fe_{50}Ni_{50}$, (e) $Fe_{100-x}Ni_x$, and (f) Fe_xNi_{100-x} . The star at 0 μT indicates ξ_{AD} as the fit window size goes to zero, following the protocol in Ref. [2]. Right column (g-i): ξ_{AD} plotted against in-plane field angle φ for (g) $Fe_{50}Ni_{50}$, (h) $Fe_{100-x}Ni_x$, and (i) Fe_xNi_{100-x} .

FD-02. Low Gilbert damping of canonical frustrated Kagome magnet Fe_3Sn_2

<u>Z. Jin</u>^{1, 2}, E. Lesne³, K. Nukui^{1, 2}, S. Miki², C. Felser³, A. Hirohata^{5, 4, 3}, S. Mizukami^{2, 4}

¹Department of Applied Physics, Graduate School of Engineering, Tohoku Univ., Sendai, Miyagi, Japan, ²WPI-AIMR, Tohoku Univ., Sendai, Miyagi, Japan, ³Max Planck Institute for Chemical Physics of Solids, Dresden, Germany, ⁴CSIS, Tohoku Univ., Sendai, Miyagi, Japan, ⁵RIEC, Tohoku Univ., Sendai, Miyagi, Japan

Kagome magnet materials exhibit a rich array of phenomena, including frustrated magnetism, spin liquids, and skyrmions, as well as topologically nontrivial electronic structures (e.g., Weyl nodes, Dirac cones, and flat bands). These give rise to emergent effects like anomalous Hall effect, anomalous Nernst effect, and chiral anomaly [1-3]. Uniquely, their band structure depends on both lattice and magnetic states. Controlling magnetism provides a route to tune topology, with future efforts focusing on the manipulation of magnetic Kagome's spin dynamics [4,5]. A key indicator of energy dissipation in spin dynamics, magnetic Gilbert damping determines how fast the magnetization relaxes toward the effective magnetic field and plays a central role in spintronics devices. Here we focus on a canonical frustrated Kagome magnet, Fe₃Sn₂, epitaxially grown by magnetron sputtering on (111)-SrTiO₃ substrates. Through time-resolved (TR) magnetooptical Kerr effect (MOKE), we focus on Gilbert damping in Fe₃Sn₂. Figure 1 shows a typical TR-MOKE trace measured under the applied field with the angle of 45deg with respect to the film normal. The out-of-plane component oscillation of Kagome magnetic moments excited by the pump light pulse is clearly detected by polar MOKE geometry with a probe pulse, where the magnetic signal was extracted by taking difference of signals measured with applied high magnetic field of ±2 T. Through the systematic measurements, we found that the effective Gilbert damping of c-plane oriented Fe₃Sn₂ epitaxial films is approximately 0.012, being significantly smaller than the reported values [4]. These findings highlight the potential of topological kagome magnets for spintronic applications. This work is partially supported by JSPS KAKENHI (21H05000, 24K21234), MEXT X-NICS (JPJ011438), and JST ASPIRE (JPMJAP2409). S.M. thanks to Spin-RNJ and Z.J. thanks to JST SPRING and GP-Spin at Tohoku Univ.

[1] Taguchi, Y et al., *Science*, 291, 2573–2576 (2001). [2] Fenner, L. A. et al., *J. Phys.: Condens. Matter*, 21, 452202

(2009). [3] Kacho, I. A. K. et al., *Phys. Rev. Materials*, 4, 084203 (2020). [4] Kuroda, K.; et al., *Sci. Rep.*, 14, 3487 (2024). [5] Igor Lyalin et al., *Nano Lett.*, 21, 6975–6982 (2021)

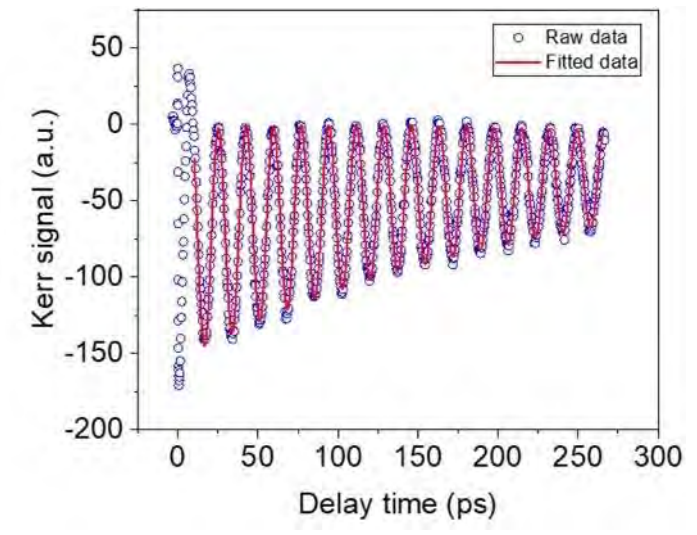


Fig.1: Typical TRMOKE signal obtained for the 10-nm-thick Fe_3Sn_2 epitaxial film.

FD-03. Magnetic Losses in Soft Magnetic Composites and Ferrites under Rectangular Asymmetric Excitation

<u>S. Dobák</u>, F. Onderko, J. Fuzer, P. Kollár Institute of Physics, P. J. Safarik University in Kosice, Kosice, Slovakia

Accurate characterization of magnetic materials is essential for the design of high-frequency power electronic systems, particularly in applications enabled by wide-bandgap semiconductors. Traditional loss estimation methods, which assume sinusoidal excitation, are no longer valid when materials operate under non-sinusoidal conditions with high rates of magnetic field change [1]. In this study, we examine magnetic losses in iron-based composite materials and Mn-Zn ferrites when subjected to rectangular voltage waveforms, as typically found in switched-mode power converters. These excitations generate triangular flux density profiles—either symmetric or asymmetric—which significantly alter the loss behavior compared to sinusoidal operation. These two classes of industrially important materials exhibit distinct energy dissipation mechanisms: eddy currents dominate in iron-based composites due to their structure of insulated conductive particles, while spin damping is predominant in Mn-Zn ferrites, composed of semiconductive grains separated by high-resistance grain

boundaries. We analyze how variations in excitation, specifically changes in duty cycle from 0.1/f to 0.5/f, influence the magnetic losses. Figure 1 presents illustrative measurements at a peak polarization of $J_p = 100 \text{ mT}$ and frequency f = 10 kHz, highlighting the differences between rectangular and sinusoidal excitation. To model these effects, we apply the Statistical Theory of Losses, which allows to separately track the evolution of hysteresis, classical, and excess loss components under realistic operating conditions [2]. The framework enables prediction of losses under arbitrary waveforms using data obtained from standard sinusoidal measurements. This methodology offers a powerful and generalizable approach for assessing magnetic losses in practical, non-ideal excitation scenarios encountered in modern power electronic systems. Funded by the EU NextGenerationEU through the Recovery and Resilience Plan for Slovakia under the project No. 09103-03-V04-00008.

[1] S. Yue, Q. Yang, Y. Li, and C. Zhang, AIP Adv., Vol. 8, Art. No. 056121 (2018).

[2] H. Zhao, C. Ragusa, C. Appino, et al., IEEE Trans. Power Electron., Vol. 34, p. 3655 (2019).

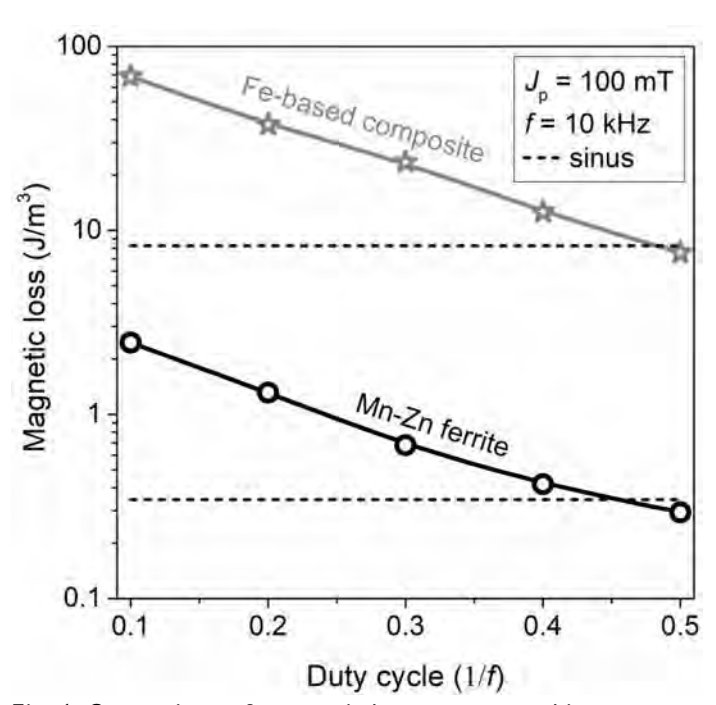


Fig. 1. Comparison of magnetic losses measured in composite material and ferrite core under rectangular excitation waveform with different duty cycle and sinusoidal waveform.

FD-04. Modulation of spin dynamics in Fe thin films induced by adjacent Co/Ni multilayers with perpendicular magnetic anisotropy

<u>S. Baek</u>, T. Izumi, S. Komori, T. Taniyama *Nagoya University, Nagoya, Japan*

Introduction

The Gilbert damping constant α of a ferromagnet is determined by the linear relationship 1) between the ferromagnetic resonance (FMR) linewidth ΔH and the resonance frequency f_r . However, the linear relation often exhibits a sublinear increase due to the extrinsic mechanism originating from two-magnon scattering (TMS): $\Delta H_{TMS}^{1),2}$. A rapid ΔH_{TMS} increase can be observed at a specific resonance frequency (f_{peak}) in certain cases, which could be related to the frequency of the quasi-periodic magnetic structure (ripple) 3). To gain deeper insight into the relation between the rapid ΔH_{TMS} increase and the ripple, in this study, we have investigated a Pt/[Co/Ni]_n/Pt/Fe/MgO(111) structure (Fig. 1), in which a ripple of the Fe layer is tunable via the perpendicular magnetic anisotropy energy of the [Co/Ni]_n multilayer, and have successfully modulated the f_{peak} of the Fe layer.

Experimental details and results

An Fe thin film (30 nm) was first grown on a MgO (111) substrate at 300°C using molecular beam epitaxy, and subsequently, Pt(3 nm)/[Co(0.3 nm)/Ni(0.6 nm)]₈/Pt(10 nm) was deposited on the Fe layer at room temperature. The magnetization was measured by a vibrating sample magnetometer. For FMR measurements, we used a vector network analyzer and a coplanar waveguide. Figure 2 shows the f_r versus ΔH for the sample with the [Co/Ni] multilayer and for the sample without the [Co/Ni] multilayer (a single layer of 30-nm-thick Fe). A clear shift of f_{peak} to lower frequency is observed due to the presence of the [Co/Ni] multilayer. We believe that the perpendicularly magnetized [Co/Ni] multilayer modulates the ripple of the Fe layer magnetized along the in-plane, and as a result, f_{peak} , which is related to the ripple, is modulated and shifted to lower frequency.

This work was supported in part by JSPS KAKENHI Grant Nos. JP24H00380, JP24K21732, JP23KK0086, JP21H04614, JSPS International Joint Research Program with the UK (JRP-LEAD with UKRI) JPJSJRP20241705, JST FOREST JPMJFR212V, JST SPRING, Japan Grant Number JPMJSP2125, the Iketani Science and Technology Foundation 0361214-A.

- 1) K. Lenz et al., Phys. Rev. B 73, 144424 (2006).
- 2) R. Arias et al., Phys. Rev. B 60, 7395 (1999).
- 3) A. V. Izotov et al., J. Magn. Magn. Mater. 529, 167856 (2021).

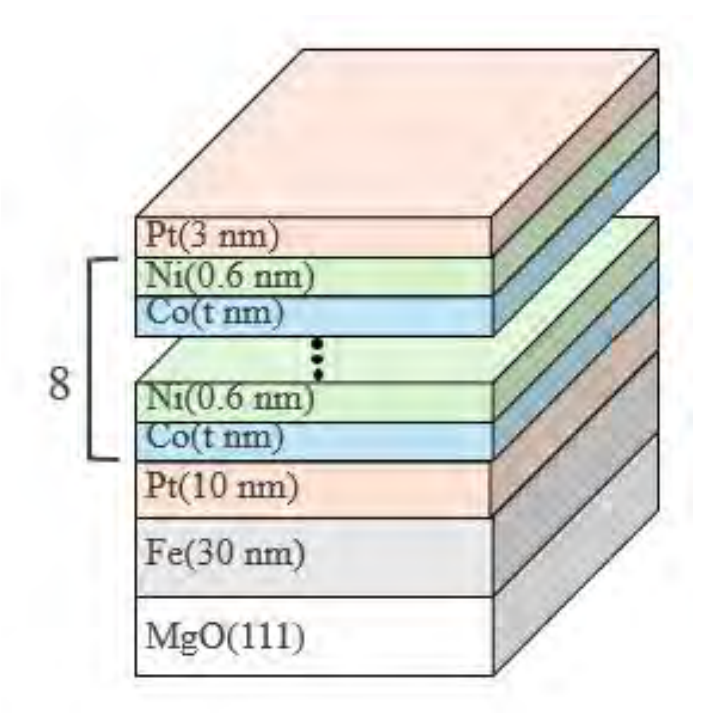


Fig. 1. Sample structure

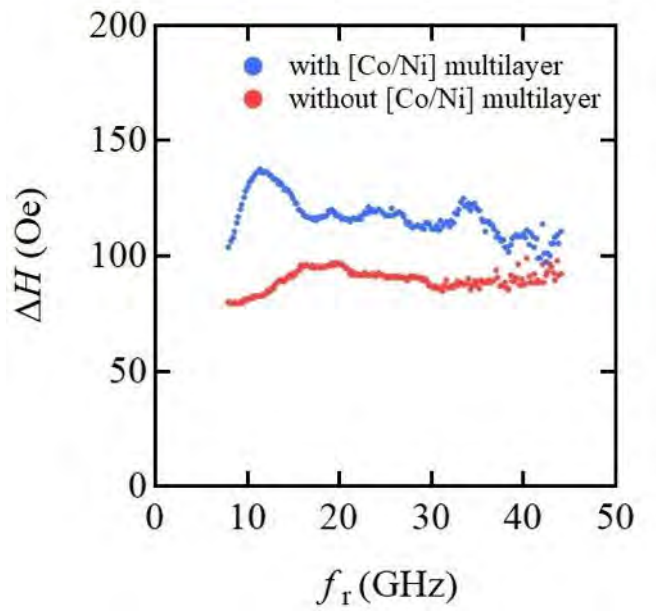


Fig. 2. ΔH vs fr for Fe layers in samples with and without adjacent Co/Ni multilayers

FD-05. Gilbert damping in low-dimensional magnetic systems: Quantum oscillations and symmetry constraint \underline{Z} . Yuan

Interdisciplinary Center for Theoretical Physics and Information Sciences, Fudan University, Shanghai, China

Gilbert damping is a universally important phenomenon in all magnetic materials, determining the time scale and energy consumption of magnetization dynamics. Despite its significance in both fundamental magnetism and spintronic applications, the understanding of Gilbert damping remains unsatifactory, particularly the relationship to microscopic band structure.

To reveal the microscropic picture of Gilbert damping, we theoretically identified the dominant contribution to damping in Fe, elucidating the specific dissipation process from spin to orbital to lattice degrees of freedom. This theoretical prediction was experimentally confirmed through the quantum oscillation of Gilbert damping in ultrathin Fe films at low temperature [1]. It provides a natural explanation for the ultralow Gilbert damping of Febased alloys.

In 2D van der Waals (vdW) ferromagnetic materials, Gilbert damping is found to exhibit strong anisotropy: damping is very low with perpendicular magnetization but remarkably larger with in-plane magnetization. The anisotropy is attributed to the symmetry of 2D lattice structure and the presence of topological electronic states, highlighting the unique characteristics of Gilbert damping in vdW ferromagnets [2].

- [1] Y. Chen et al., Physical Review Letters 134, 136701 (2025).
- [2] W.Z. Chen et al., arXiv:2411.12544.

FD-06. Quantifying Spin-Mixing in Ferrimagnetic Fe-Gd Alloys via XMCD and FMR Spectroscopy

<u>V. Ganepola Arachchige</u>¹, J. J. Wisser², R. Knut³, D. A. Arena¹ Department of Physics, University of South Florida, Tampa, Florida, United States, ²National Institute of Standards and Technology, Boulder, Colorado, United States, ³Department of Physics and Astronomy, Uppsala University, Uppsala, Sweden

Spin-mixing, defined as the quantum admixture of spin-up and spin-down states due to spin-orbit coupling (SOC), plays a crucial role in limiting spin coherence and angular momentum transfer in spintronic systems. Despite its significance, direct experimental quantification of the spin-mixing parameter $\langle b^2 \rangle$ remains rare[1]. This parameter becomes particularly important in complex magnetic systems such as ferrimagnets, where sublattice interactions further cofmplicate spin dynamics.

In this study, we investigate spin-mixing in amorphous ferrimagnetic Fe_xGd_{1-x} thin films by combining X-ray magnetic circular dichroism (XMCD) and broadband ferromagnetic resonance (FMR) spectroscopy. The spin-mixing parameter is estimated by comparing the orbital-to-spin moment ratio (μ_L/μ_S) obtained from XMCD sum rules with effective g-factors extracted from out-of-plane FMR measurements.

Element-specific XMCD spectra were acquired at the Fe $L_{3,2}$ and Gd $M_{5,4}$ absorption edges using the VEKMAG endstation at BESSY-II. Measurements were performed across a composition range (x = 0.3 to 0.9) and temperatures from 10 K to 300 K. Element-specific hysteresis loops were also recorded at the Fe L_3 and Gd M_5 edges to confirm the ferrimagnetic nature of the films.

Figures 1 and 2 show representative absorption spectra and hysteresis loops at both Fe and Gd edges for x=75,80 compositions, respectively. These results extend recent studies on Ni-based ferromagnetic alloys to more complex ferrimagnetic systems, offering valuable experimental input for modeling SOC-related phenomena in technologically relevant spintronic materials.

[1] J. M. Shaw, R. Knut, A. Armstrong, *et al.*, Phys. Rev. Lett. 127, 207201 (2021)

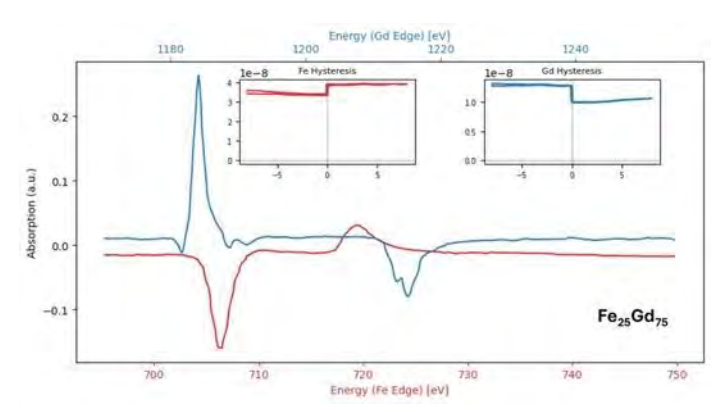


Fig. 1 X-ray absorption spectra and hysteresis loops of $Fe_{75}Gd_{25}$ thin film at the Fe L_3 and Gd M_5 edges.Insets show hysteresis loops recorded at the respective resonance energies.

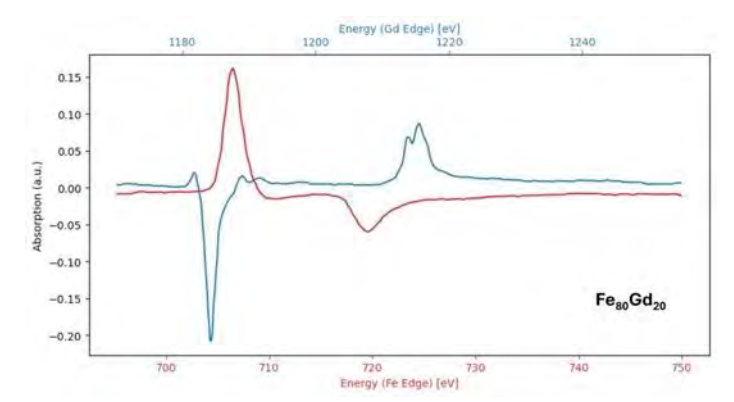


Fig. 2 X-ray absorption spectra of Fe $_{80}\text{Gd}_{20}$ thin film at the Fe L_3 and Gd M_5 edges.

FD-07. Crystal growth and terahertz time-domain spectroscopy in $Sm_{1-x}R_xFeO_3$ orthoferrite

A. Wu¹, Z. Zhang¹, Z. Zhang¹, L. Su¹, L. Luo², J. Wang²
¹State Key Laboratory of Functional Crystals and Devices,
Shanghai Institute of Ceramics, Chinese Academy of Sciences,
Shanghai, China, ²Department of Physics and Astronomy, Iowa
State University, Ames, Iowa, United States

High quality Sm1-xRxFeO3 single crystals with various compounds have been grown by the four-mirror floating zone technique. Sm1-xRxFeO3 samples with a-, b-, and corientation were manufactured by means of Laue photograph. Magnetic properties of Sm1-xRxFeO3 single crystals are studied over a wide temperature range from 2 to 400 K. Spin reorientation transition (SRT) from Γ2 to Γ4 are observed by means of the temperature dependence of magnetization It indicated the reorientation transition temperature of Sm1-xRxFeO3 single crystals is lowered with the contents of R contents rising based on this work and our previous works, thus the spin reorientation transition temperature can be adjusted through changing the compound in orthoferrites materials, which means that we can get orthoferrites single crystals with high magnetism property in various temperature through material design. The dynamics of SRT is studied by terahertz time-domain spectroscopy (THz-TDS). Our results demonstrate that THz-TDS is an effective means to study the dynamical iron ions SRT in RFeO3. Meanwhile, we demonstrate exceptionally high-order THz nonlinear magnonics. It manifests as 7th-order spin-wave-mixing and 6th harmonic magnon generation in an antiferromagnetic orthoferrite.

- 1. A. Wu, B. Wang, X. Zhao, et al., J. Magnetism and Magnetic Materials 426, 721 (2017).
- 2. B. Wang, X. Zhao, A. Wu, et al., J. Magnetism and Magnetic Materials 379, 192 (2015).
- 3. X. Zhao, K. Zhang, X. Liu, et al., AIP ADVANCES 6, 015201 (2016).
- 4. C. Huang, L. Luo, M. Mootz, et al., Nature Communications 15, 3214 (2024)
- 5. A. Wu, X. Zhao, P. Man, et al., J. Crystal Growth 486, 169 (2018)
- 6. X. Zhao, K. Zhang, K. Xu, et al., Solid State Communications 231-232, 43 (2016)

FD-08. Micromagnetic Insights into History-Dependent Domain Behavior in MBE-grown 2D Magnet/Topological Insulator Heterostructure Fe₃GeTe₂/Bi₂Te₃

M. Zhao¹, T. Cham^{6, 2}, A. Koerner¹, E. Berg¹, D. Bergner¹, W. Zhou³, Z. Li³, L. Powalla⁴, S. Wintz⁵, M. Weigand⁵, D. C. Ralph², R. Kawakami³, Y. Luo^{1, 7, 8}

¹Department of Physics and Astronomy, University of Southern California, Los Angeles, California, United States, ²Laboratory of Atomic and Solid State Physics, Cornell University, Ithaca, New York, United States, ³Ohio State University, Columbus, Ohio, United States, ⁴Max Planck Institute for Solid State Research, Stuttgart, Germany, ⁵Helmholtz-Zentrum Berlin für Materialien und Energie, Dresden, Germany, ⁴Division of Physics, Math and Astronomy, California Institute of Technology, Pasadena, California, United States, ⁷USC Mork Family Department of Chemical Engineering and Materials Science, University of Southern California, Los Angeles, California, United States, ⁸Department of Chemistry, University of Southern California, Los Angeles, California, United States

Heterostructures of two-dimensional van der Waals magnets and topological insulators are of substantial interest as candidate materials for efficient spin-torque switching, quantum anomalous Hall effect, and chiral spin textures. Among them, the epitaxial Fe₃GeTe₂/Bi₂Te₃ thin films grown by molecular beam epitaxy (MBE) stand out for their high spin-orbit torque efficiency, strong interfacial coupling, and tunable and high Curie temperature [1,2]. Using magnetic contrast scanning transmission X-ray microscopy (XMCD-STXM), we report the presence of speckled magnetic domain structure in these films (Fig. 1), distinctly different from those in exfoliated Fe₃GeTe₂ crystal [3]. To probe their origin, we simulate proximity effects induced by strain from the Bi₂Te₃ substrate by systematically varying the Dzyaloshinskii - Moriya interaction (DMI) strength across a controlled parameter space (Fig. 2). Comparing experimental observations with simulations, we identify the critical role of interfacial DMI in modulating the competition between short-range exchange and long-range dipolar interactions by analyzing domain size, shape, and density as functions of magnetic field and film thickness. As interfacial DMI increases, magnetization evolves from uniform reversal with circular domains to fragmented speckled patterns and, eventually, to premature switching with stripe-like textures. Finally, we present a phase diagram of domain structures as functions of key magnetic parameters, delineating the regimes associated with distinct morphologies.

[1] W. Zhou, A. J. Bishop, X. S. Zhang, K. Robinson, I. Lyalin,

Z. Li, R. Bailey-Crandell, T. Min, J. Cham, S. Cheng, Y. K. Luo, D. C. Ralph, D. A. Muller, and R. K. Kawakami, *Tuning the Curie temperature of a two-dimensional magnet/topological insulator heterostructure to above room temperature by epitaxial growth*. Phys. Rev. Materials 7, 104004 (2023). [2] Z. Li, W. Zhou, M. Swann, V. Vorona, H. Scott, R. K. Kawakami, *Full-film dry transfer of MBE-grown van der Waals materials*. 2D Materials 12 (3), 035003 (2025) [3] M.T. Birch, L. Powalla, S. Wintz, O. Hovorka, K. Litzius, J.C. Loudon, *History-dependent domain and skyrmion formation in 2D van der Waals magnet Fe*₃*GeTe*₂. Nature communications 13 (1), 3035 (2022)

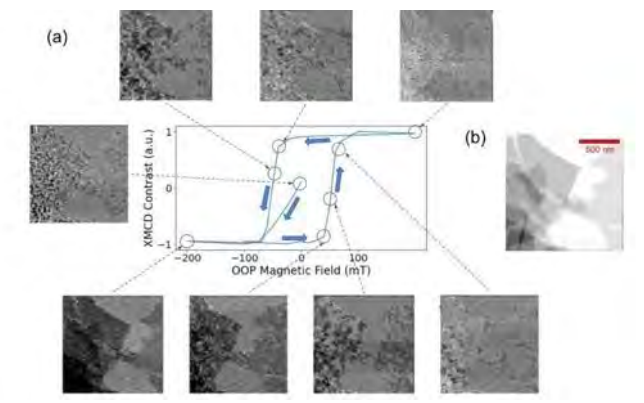


Fig. 1: (a) XMCD-STXM images showing history-dependent magnetic domain behavior in MBE-grown Fe₃GeTe₂/Bi₂Te₃ thin films after zero-field cooling from 300 K to 165 K. (b) Zero-field STXM image highlighting regions of varying film thickness.

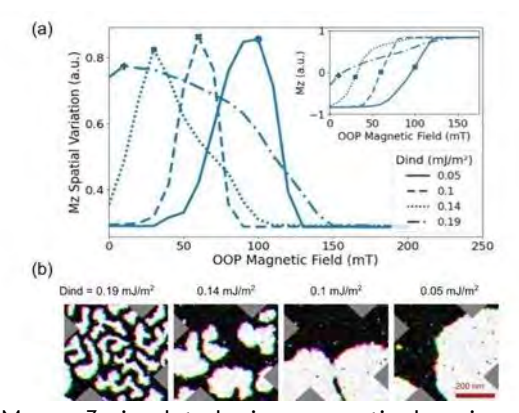


Fig. 2: Mumax3-simulated micromagnetic domain evolution under varying interfacial DMI (Dind) strengths. (a) Out-of-plane (OOP) magnetization (Mz) spatial variations during a field sweep from negative saturation. Inset: average Mz; dots indicate fields with peak spatial variation. (b) Domain snapshots at peak-variation fields.

FD-09. Probing Temperature-dependent Magnetization Dynamics in Co₂MnGa Weyl Semimetal Thin Films

A. I. Ojo¹, V. Ganepola Arachchige¹, D. DeTellem¹, A. Markou², ³, C. Felser³, J. D. Gayles¹, M. Phan¹, D. A. Arena¹
¹Department of Physics, University of South Florida, Tampa, Florida, United States, ²Physics Department, University of Ioannina, Ioannina, Ioannina, Greece, ³Max Planck Institute for Chemical Physics of Solids, Dresden, Germany

Co₂MnGa (CMG), a magnetic Weyl semimetal, exhibits high Curie temperature [1], ultra-low damping [2], and strong spin-dependent transport properties [3,4], favorable for spintronics applications. While its room-temperature magnetization dynamics has been explored, the temperature (T) dependence of key dynamic parameters such as damping and exchange stiffness remains underexplored.

Using broadband ferromagnetic resonance spectroscopy, we investigate the temperature-dependent magnetization dynamics in CMG thin films (20, 60, and 80 nm) with the magnetic field applied perpendicular to the sample plane. X-ray diffraction reveals a strain-induced tetragonal distortion, most pronounced in the 20 nm film. As temperature decreases, the saturation magnetization (M_s) deviates from Bloch's law below 170 K, due to a temperature-dependent tetragonal distortion. Furthermore, the effective magnetization M_{eff} > M_s indicates a net in-plane anisotropy that strengthens with decreasing temperature, while the perpendicular uniaxial anisotropy (K_{u[001]}) also increases, with the 20 nm film exhibiting the highest values across all temperatures. Perpendicular standing spin waves observed in the 60 nm and 80 nm films enable the extraction of the exchange stiffness (A_{ex}) and exchange length (lex), both of which increase with decreasing temperature. Furthermore, A_{ex} follows a T² dependence indicative of a dominant contribution from electron-magnon interactions. All films exhibit ultralow damping at room temperature, with the 80 nm film showing a temperatureindependent behavior.

- [1] P. Webster, Journal of Physics and Chemistry of Solids 32, 1221 (1971).
- [2] C. Guillemard et al., Phys. Rev. Appl. 11, 064009 (2019).
- [3] A. Markou et al., Phys. Rev. B 100, 054422 (2019).
- [4] A. Sakai et al., Nature Physics 14, 1119-1124 (2018).

SESSION FE: MAGNETISM AND SPINTRONICS: LOW-DIMENSIONAL SYSTEMS

Chair(s): Y. Luo, *Physics and Astronomy, University of Southern California, Los Angeles, California, United States*Thursday, October 30, 2025
02:00 PM-05:30 PM
Room 2DE

FE-01. Spin-filter tunneling detection of antiferromagnetic resonance with electrically-tunable damping

T. Cham^{1, 2}, D. G. Chica³, X. Huang¹, K. Watanabe⁴, T. Taniguchi⁵, X. Roy³, Y. Luo^{7, 8, 9}, D. C. Ralph^{1, 6} ¹Laboratory of Atomic and Solid State Physics, Cornell *University, Ithaca, New York, United States, ²Division of Physics,* Math and Astronomy, Caltech, Pasadena, California, United States, ³Department of Chemistry, Columbia University, New York, New York, United States, ⁴Research Center for Electronic and Optical Materials, National Institute for Materials Science, Tsukuba, Ibaraki, Japan, ⁵Research Center for Materials Nanoarchitectonics, National Institute for Materials Science, Tsukuba, Ibaraki, Japan, ⁶Kavli Institute at Cornell, Ithaca, New York, United States, ⁷Department of Physics and Astronomy, University of Southern California, Los Angeles, California, United States, 8 Mork Family Department of Chemical Engineering and Materials Science, University of Southern California, Los Angeles, California, United States, ⁹Department of Chemistry, University of Southern California, Los Angeles, California, United States

Van der Waals (vdW) magnets offer a rich platform to explore spin dynamics in atomically-thin systems and can be engineered into heterostructures for efficient spin-orbit torque (SOT) control. Among these, intrinsic vdW antiferromagnets such as CrSBr promise ultrafast dynamics and zero net moment, but their high-frequency resonance modes remain challenging to detect due to weak signals and the absence of direct electrical probes at the microscale.

Here, we demonstrate spin-filter tunneling detection of antiferromagnetic resonance (AFMR) in bilayer CrSBr using a scalable, three-terminal device geometry (Fig. 1A). CrSBr exhibits strong in-plane triaxial anisotropy and supports multiple gigahertz AFMR modes depending on field orientation, including hybridized chiral (left/right-handed), optical (out-of-phase), and acoustic (in-phase) modes (Fig. 1B) [1]. By rotating the external magnetic field away from high symmetry axes, we access mode hybridization and rich multi-mode dynamics.

To achieve electrical readout, we adapt spin-torque ferromagnetic resonance (ST-FMR) techniques [2] using the c-axis tunneling magnetoresistance of CrSBr, which is sensitive to the relative orientation of spin sublattices [3,4]. AFMR modes are excited via an RF current, and are detected through rectified voltages measured with a lock-in amplifier as the field is swept across resonance. The technique enables detection in micron-sized atomically thin vdW layers, and reveals suppressed interlayer exchange in bilayer CrSBr relative to the bulk [3].

Beyond passive detection, our geometry allows active electrical control of AFMR damping. By passing a dc-bias current through a PtTe $_2$ electrode, we apply spin-orbit torque (SOT) to tune the linewidth of the optical mode. A two-sublattice Landau-Lifshitz-Gilbert-Slonczewski (LLGS) analysis shows that the damping scales linearly with drive current when the spin polarization aligns with one of the canted sublattices. We extract a damping-like SOT efficiency of $\xi = 0.29(2)$ for PtTe $_2$ on CrSBr (Fig. 2), comparable to ferromagnetic heterostructures [2].

Interestingly, we observe a pronounced asymmetry in the linewidth modulation under positive and negative magnetic fields, consistent with a localized spin-orbit torque (SOT) picture in which the torque acts predominantly on the spin sublattice directly adjacent to the PtTe₂electrode. To investigate this effect, we align the easy axis of the CrSBr bilayer at 45° relative to the PtTe₂ electrode, allowing the external magnetic field to cant one of the two sublattices parallel to the spin current polarization from PtTe₂. This configuration maximizes the torque efficiency on that specific sublattice, enabling a clear modulation of damping as a function of dc bias.

Our measurements reveal new information about the differences between antiferromagnetic resonance in thin layers versus bulk samples, including a reduction in interlayer exchange. Most strikingly, we uncover that the SOT in this system is highly local: it acts primarily on the spin sublattice immediately adjacent to the source electrode. This opens a new approach for controlling the dynamics of layered antiferromagnets and provides a strategy for future applications of antiferromagnetic materials as high-frequency detectors, modulators, and signal sources.

[1] T.MJ. Cham, D.C. Ralph, Y.K. Luo et al. *Nano Letters*, *22*(16), pp.6716-6723 (2022).

[2] L. Liu, D.C. Ralph, B.A. Buhrman et al. *Physical review letters* 106, no. 3, 036601 (2011).

[3] T.M.J. Cham, Y.K. Luo, D.C. Ralph et al. *arXiv preprint* arXiv:2407.09462 (2025) (In print, Science).

[4] L. Xue, B.A. Buhrman, D.C. Ralph, et al. *Physical Review Letters* 108, no. 14, 147201 (2012).

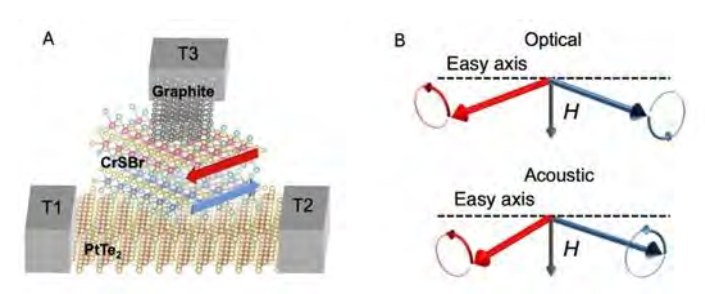


Fig. 1. A) Motion of the two antiferromagnetic sub-lattices for the out-of-phase "Optical" mode and the in-phase "Acoustic" mode. B) Schematic of Graphite/CrSBr/PtTe₂ vdW heterostructure device for ST-AFMR measurements.

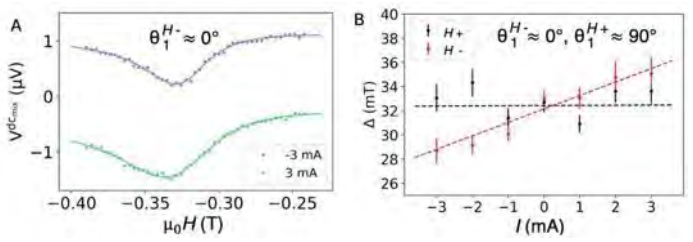


Fig. 2. Spin-orbit torque modulation of antiferromagnetic resonance linewidth. A) ST-AFMR resonance for negative and positive dc-bias currents showing asymmetric linewidth modulation, indicating localized SOT. B) AFMR linewidth versus dc bias. Linear trend reveals tunable damping with SOT efficiency ξ = 0.29 (2), acting primarily on the sublattice of bilayer CrSBr adjacent to PtTe₂.

FE-02. Probing Magnetotransport in 2D Heterostructure of a Weyl Semimetal and a Semiconducting Antiferromagnet R. Posti, R. Bandapelli, I. Kao, Z. Cui, J. Katoch, S. Singh

Department of Physics, Carnegie Mellon University, Pittsburgh, Pennsylvania, United States

The discovery of van der Waals (vdW) materials exhibiting magnetic order down to the two-dimensional (2D) limit has opened exciting opportunities for exploring novel phenomena in spintronics. Particularly, combining 2D magnets with spin source materials, such as 2D Weyl

semimetals, enables the emergence of new functionalities mediated by exchange interactions and interaction of spincurrent with magnetic order. In this work, we present an allvdW heterostructures composed of a 2D A-type antiferromagnet (AFM), CrSBr, and a low-symmetry Weyl semimetal (WSM), TalrTe₄. CrSBr exhibits uniaxial magnetic anisotropy with an easy axis lying within the vdW plane. and its weak interlayer exchange coupling allows for magnetic manipulation with moderate magnetic fields. TalrTe₄, serving as a spin source, provides a unique platform to probe spin-related transport phenomena in AFM. We will present our results wherein in studied heterostructures, magnetic nature of the AFM layer is reflected in the transport response of the WSM layer. We observe clear signatures of magnetic field driven AFM-to-ferromagnetic transitions along both easy and intermediate hard in-plane axis of CrSBr. Moreover, our data suggest a possible proximity-induced magnetization in TalrTe₄ driven by exchange coupling and spin Hall magnetoresistance behaviour arising from interaction of spin-current with magnetic order within the studied heterostructures.

FE-03. Unusual Hall effect in vdW ferromagnetic Fe_3GeTe_2 nanoflake devices

R. Roy Chowdhury^{1, 2}, D. Kurebayashi³, J. Lustikova⁴, O. Tretiakov³, S. Fukami^{5, 4}, R. Singh², <u>S. DuttaGupta</u>^{6, 4, 5}
¹Department of Physics, University of South Florida, Tampa, Florida, United States, ²Department of Physics, Indian Institute of Science Education and Research Bhopal, Bhopal, Madhya Pradesh, India, ³School of Physics, University of New South Wales, Sydney, New South Wales, Australia, ⁴Center for Science and Innovation in Spintronics (CSIS), Tohoku University, Sendai, Miyagi, Japan, ⁵Research Institute of Electrical Communication (RIEC), Tohoku University, Sendai, Miyagi, Japan, ⁶Condensed Matter Physics Division, Saha Institute of Nuclear Physics, Kolkata, West Bengal, India

Two-dimensional (2D) van der Waals (vdW) materials have drawn significant attention owing to their prospect for future spintronic and quantum devices [1]. 2D metallic ferromagnet (FM) Fe₃GeTe₂ (FGT, hereafter) has gathered significant attention owing to its high Curie temperature, large anomalous Hall effect (AHE), and unconventional magnetic ground state comprising of skyrmion-like spin textures, remarkably sensitive to doping at the magnetic (Co-doped FGT) or non-magnetic site (As-doped FGT) [2,3]. First-principles calculations predict a geometrically frustrated spin configuration, manifesting in an intraplanar

antiferromagnet (AFM) state while the interplanar interactions stabilize the overall FM state [4]. However, experimental investigations under applied magnetic fields along easy (H_Z) or hard (H_X) axes in reduced dimensions have remained elusive. Here, we investigate temperature (7) dependent magnetotransport in FGT and

(Co_{0.25}Fe_{0.75})₃GeTe₂ (Co_{0.25}FGT, hereafter) nanoflake devices. Figure 1 shows the optical micrograph of a FGT nanoflake device, fabricated on prepatterned Si/SiO₂ in an inert atmosphere. Atomic force microscopy measurements indicate a thickness of ~29 nm for Co_{0.25}FGT, and ~ 33 nm for FGT, respectively. Transverse resistance measurements under applied $H_{\mathbb{Z}}$ (|| c-axis) and current I (|| ab-plane) show a sizable AHE, originating from topological nodal lines in the band structure. Interestingly, for applied H_X (|| $I \perp c$ -axis), we observe a significantly different behaviour leading to the emergence of a prominent cusp-like feature, invariant with respect to H_X direction (Fig. 2). Atomistic calculations reveal competing intraplanar AFM and interplanar FM interactions resulting in thermally assisted frustrated spin configuration manifesting in a non-zero scalar spin chirality, leading to the unusual magnetotransport behavior. Our study signifies the crucial role of magnetic frustration or fluctuation effects on magnetotransport phenomena in vdW FMs, important for development of 2D spintronic or quantum devices.

[1] B. Zhang, P. Lu, R. Tabrizian *et al.*, npj Spintronics 2, 6 (2024).

[2] R. Roy Chowdhury, S. DuttaGupta, C. Patra *et al.*, Sci. Rep. 11, 14121 (2021).

[3] R. Roy Chowdhury, C. Patra, S. DuttaGupta *et al.*, Phys. Rev. Mater. 6, 014002 (2022).

[4] Z. -X. Shen, X. Bo, K. Cao *et al.*, Phys. Rev. B 103, 085102 (2021).

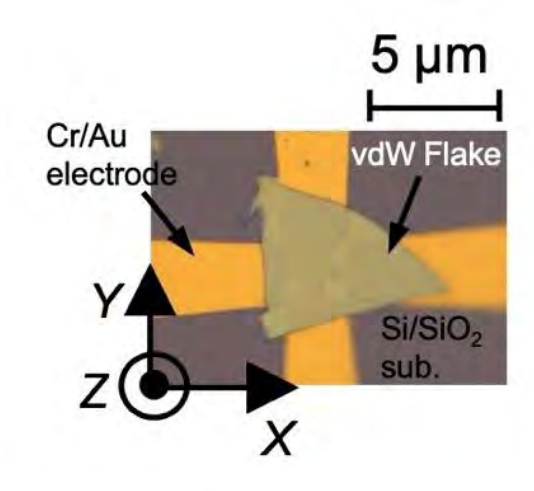


Fig. 1: Optical micrograph of FGT nanoflake device. Scale

bar is 5 µm.

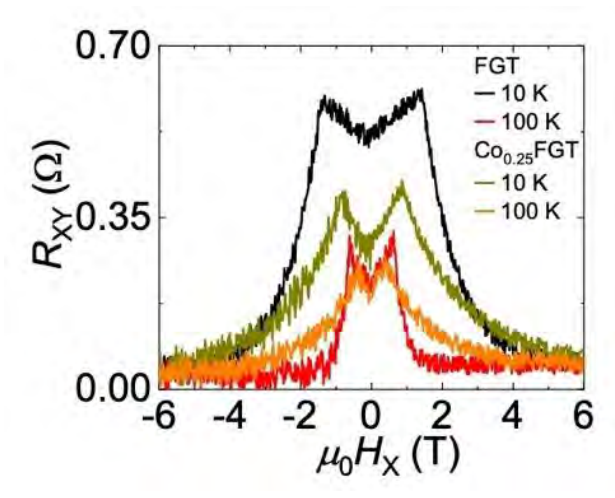


Fig. 2: Experimental results of Hall resistance (R_{XY}) versus H_X for FGT and $Co_{0.25}$ FGT devices at T = 10 and 100 K.

FE-04. Interface Engineering of Exchange Bias in van der Waals Heterostructures

A. Puthirath Balan¹, A. Kumar¹, P. Reiser², J. Vas³, T. Denneulin³, J. Yang⁴, A. Bonanni⁵, B. Lotsch⁶, P. Maletinsky², R. E. Dunin-Borkowski³, M. Kläui^{1,7}

¹Johannes Gutenberg University Mainz, Mainz,

Germany, ²University of Basel, Basel,

Switzerland, ³Forschungszentrum Jülich, Jülich, Germany, ⁴Peking University, Beijing, China, ⁵Johannes Kepler University Linz, Linz, Austria, ⁶Max Planck Institute for Solid State Research, Stuttgart, Germany, ⁷Norwegian University of Science and Technology, Trondheim, Norway

The exchange bias phenomenon observed in exchangecoupled ferromagnetic (FM) and antiferromagnetic (AFM) systems plays a crucial role in stabilising reference layers against magnetic field fluctuations in magnetic tunnel junctions. Recently, van der Waals (vdW) heterostructures have gained attention for their intrinsic layered structure and ability to form atomically well-defined and singlecrystalline interfaces. This research investigates the origin of exchange bias in van der Waals structures, focusing particularly on the FM Fe₃GeTe₂ (FGT) interfaced with three distinct vdW AFMs: CrPS₄,[1] MnPS₃,[2] and CrSBr.[3] CrPS₄ is an A-type AFM with a layered spin structure that can form a fully uncompensated interface, MnPS₃ is a C-type AFM with a fully compensated spin structure, whereas CrSBr forms an uncompensated interface with the sublattice moments oriented perpendicular relative to FM. We further explore

methods to tailor exchange bias by manipulating interface registry, including oxidation and alterations in the intercrystalline distance between the two layers through thermal cycling. A large enhancement of exchange bias is observed by oxidising the interface in the FGT/CrPS₄ heterostructure,[1] and by varying the intercrystalline distance between the two layers in the FGT/MnPS₃ heterostructure.[2] On the other hand, the FGT/CrSBr interface generates exchange bias typical of domain nucleation in FM due to the proximity effects of inplane oriented interfacial spins of CrSBr.[3] These findings highlight the intricate and unique nature of exchange bias in van der Waals heterostructures, emphasising how imperfections at the interface, as well as the nature of the interfacial spin structure, can significantly influence interfacial phenomena, especially exchange bias.

[1] A. P. Balan, A. Kumar, M. Kläui et al., *ACS Nano* 18, 8383–8391 (2024).

[2] A. P. Balan, A. Kumar, M. Kläui et al., *Advanced Materials* 36, 2403685 (2024).

[3] A. P. Balan, A. Kumar, M. Kläui et al., *Unpublished*, *Small* (Under Review)

FE-05. Light-induced orbital and spin magnetism in 3d, 4d, and 5d transition metals

<u>T. Adamantopoulos</u>^{1, 2, 3}, D. Go^{1, 2}, Y. Mokrousov^{2, 1}
¹Johannes Gutenberg University Mainz, Mainz,
Germany, ²Forschungszentrum Jülich, Jülich, Germany, ³RWTH
Aachen University, Aachen, Germany

For many years understanding the coherent interplay of light with the magnetization in metals has been a topic of extensive research in ultrafast magnetism. Although by now it is known that laser light acting on a metal may induce magnetization via the process known as the inverse Faraday effect (IFE), the most basic ingredients of this phenomenon are still largely unexplored. In particular, the strong recent interest in orbital non-equilibrium dynamics and its role in mediating THz emission in transition metals, has made the exploration of distinct features in spin and orbital IFE more relevant than ever. Here, we present a first complete study of the spin and orbital IFE in 3d, 4d and 5d transition metals of groups IV-XI from first-principles. After examining the dependence of IFE on the light polarization and frequency, we showcase that the laser-induced spin and orbital moments may vary significantly both in magnitude and sign. We argue that the key factor which determines the

magnitude and key differences between the spin and orbital responses is the interplay between the crystal field splitting and spin-orbit interaction. Furthermore, we highlight the anisotropy of the effect with respect to the ferromagnetic magnetization and to the crystal structure. The presented complete map of IFE in transition metals may provide a solid foundation for further advances in the fields of orbitronics and THz spintronics.

[1] Adamantopoulos, T., Go, D., Oppeneer, P.M. et al. Light-induced orbital and spin magnetism in 3d, 4d, and 5d transition metals. npj Spintronics 3, 27 (2025).

FE-06. Tunable Moiré Phases in Magnetic Van der Waals Homobilayers

<u>G. Cheng</u>¹, P. Upadhyaya², Y. P. Chen^{1, 2}

¹Tohoku University, Sendai, Japan, ²Purdue University, West Lafayette, Indiana, United States

Moiré superlattices are arising as a new degree of freedom for inducing emergent phases across multiple research fields. While the modulation of electronic states has been extensively explored, research on moiré magnetism remains in its early stages [1-5].

In the first part of this talk, I will present our observations of electrically tunable moiré magnetism in twisted double bilayer CrI₃ [4]. Using magneto-optical Kerr effect microscopy, we observe the coexistence of antiferromagnetic and ferromagnetic orders with nonzero net magnetization---a hallmark of moiré magnetism. We further demonstrate gate-voltage-assisted magnetic switching in these moiré magnetic devices and establish a phase diagram of moiré magnetism.

Beyond exploring the moiré phases in Ising magnets, an even more compelling frontier lies in the XY magnets with spin dimensionality of two, capable of supporting sizable noncollinear spin textures such as the twisted-s phase [6]. In the second part, I will highlight our recent findings regarding the twist engineering in the typical XY magnet, CrCl₃ [7]. By measuring magnetic tunneling conductance though twisted CrCl₃, we are able to track magnetic states, which are closely associated to spin textures. Notably, we observe multiple magnetic transitions and their evolution with magnetic field and temperature. These features are highly sensitive to the twist angle, suggesting the intrinsic origin of magnetic moiré domains. Further bias dependent tunneling conductance implies the electrically tunable transformation of magnetic domains. These findings

demonstrate exotic magnetic states in moiré XY magnets and show their remarkable controllability, offering a novel quantum platform for hosting magnetic excitations and topological spin textures.

- [1] Xu, Y., et al., Nat. Nanotechnol. 17, 143-147 (2021).
- [2] Song, T., et al., Science 374, 1140-1144 (2021).
- [3] Xie, H., et al., Nat. Phys. 18, 30-36 (2021).
- [4] Cheng, G., et al., Nat. Electron. 6, 434-442 (2023).
- [5] Chen, Y., et al., Nature 632, 1045-1051 (2024).
- [6] Hejazi, K., et al., Proc. Natl. Acad. Sci. U.S.A. 117, 10721-10726 (2020).
- [7] Cheng, G., et al., Unpublished.

FE-07. Ultrafast carrier dynamics explored in micron-sized van der Waals materials through spatially localized spintronic terahertz emission spectroscopy

P. Agarwal, M. Jiang, L. Ke, J. Lourembam Institute of Materials Research and Engineering (IMRE), Agency for Science, Technology and Research (A*STAR), Singapore, Singapore

Understanding ultrafast carrier and charge dynamics in twodimensional (2D) materials is pivotal for advancing nextgeneration optoelectronic, quantum, and spintronics technologies. Owing to their high mobility, tunable band structures, and strong quantum confinement, van der Waals materials are promising candidates for devices such as modulators, detectors, and transceivers. While terahertz (THz) spectroscopy techniques, such as THz time-domain spectroscopy (THz-TDS), optical pump THz probe (OPTP), and THz emission spectroscopy (TES) are widely used to probe photoelectric properties, they are fundamentally limited by diffraction due to the long THz wavelengths. These techniques average signals over large areas, obscuring localized phenomena critical to micron-scale flakes and heterostructures. We present a new approach to localized THz emission spectroscopy using spintronic heterostructures integrated with neutral density (ND) optical filters. A spintronic emitter (CoFeB/Pt) is deposited along with a PtTe₂ layer on the opposite faces of the ND filter. The ND filter acts as both mechanical support and high-contrast optical mask, confining femtosecond near-infrared (NIR) excitation while allowing THz transmission. Upon excitation, the spintronic layer generates a spin current via ultrafast demagnetization, which is converted into a transverse charge current through the inverse spin Hall effect (ISHE), producing broadband THz emission from subwavelength regions (~\lambda/10). This configuration transforms the 2D material into an active THz emitter. As such, the emitted THz spectra carry information on charge dynamics, exciton formation, and interfacial transport with femtosecond temporal and micron-scale spatial resolution. Unlike near-field THz methods, our technique preserves the simplicity of tabletop systems while enabling site-specific spectroscopy, grain boundaries, and patterned domains. The work demonstrates the first sub-diffraction spintronic THz emission spectroscopy for probing ultrafast dynamics, offering a scalable platform across quantum materials and heterostructures.

- E. Cinquanta, E. A. A. Pogna, L. Gatto and C. Vozzi, *Advances in Physics: X*, Vol. 8, p. 2120416 (2023)
- C. Chen, Y. Wang and J. Fu, *Optics Letters*, Vol. 49, p. 1864 (2024)
- J. Fu, M. Jiang and P. Suo, *Applied Optics*, Vol. 60, p. 5037 (2021)
- J. Ji, Y. Zhou and B. Zhou et al., *ACS Appl. Mater. Interfaces*, Vol. 15, p. 51319 (2023)
- D. Yagodkin, L. Nádvorník and O. Gueckstock et al., *2D Materials*, Vol. 8, p. 025012 (2021)
- K. Xia, Q. Li and W. Huang, *J. Phys. D: Appl. Phys.*, Vol. 54, p. 314005 (2021)
- A. Liu, npj Quantum Materials, Vol. 10, p. 18 (2025)
- J. Suo, J. Fu and X. Zhang, *Appl. Opt.*, Vol. 60, p. 5037 (2021)

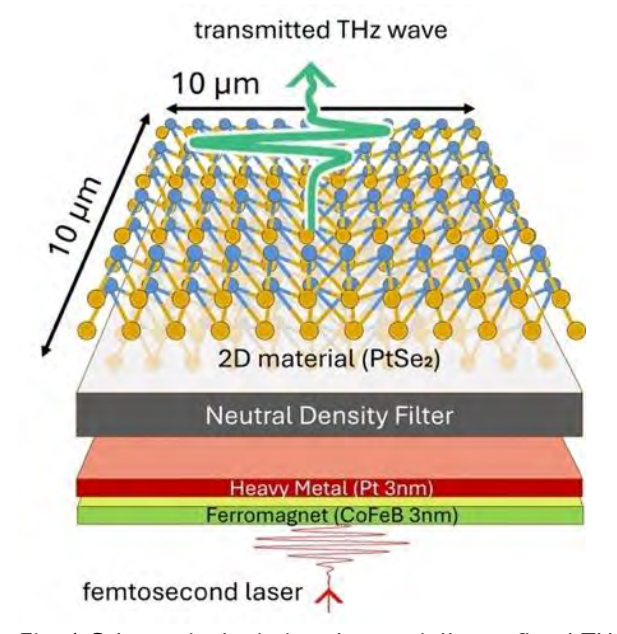


Fig. 1 Schematic depicting the spatially confined THz wave transmitted from the 2D material as a novel method for THz spectroscopy

FE-08. Controllable Synthesis and Modulation of Twodimensional Magnetic Materials

Z. Meng¹, Y. Hou²

¹Peking University, Beijing, China, ²Sun Yat-sen University, Shenzhen, China

Two-dimensional (2D) intercalated materials demonstrate tremendous potential for groundbreaking properties, yet their controllable synthesis and effective modulation continue to pose significant challenges. Recent advancements have enabled the growth of self-intercalated Fe_{1+x}Se₂ nanosheets with varying intercalation ratios through a confinement-assisted chemical potential regulation approach. Systematic structural evolution was observed with increasing intercalation ratio, accompanied by tunable magnetic and electronic transport properties, demonstrating the potential for property engineering through controlled intercalation^[1]. Furthermore, the development of a selective non-uniform nucleation model has allowed precise control over self-intercalated CrTe nanosheets, enabling thickness-controlled design within individual nanosheets for creating tailored artificial antiferromagnetic structures. Using a novel two-step chemical vapor transport and mechanical exfoliation approach, we synthesized heteroatom-intercalated^[2] and heterocrystalline 2D superlattices. These exhibit topological Hall effects, superconductivity, and ferroelectricity, providing a tunable platform for next-generation spintronics and quantum technologies. The developed molten salt method successfully produces vertically-grown high-к Bi₂TeO₅ featuring 2D host lattices intercalated with onedimensional chains, which demonstrate outstanding fieldeffect transistor characteristics with an on/off ratio exceeding 10⁷ and subthreshold swing as low as 65.2 mV/dec[3]. Manipulating spin configurations *via* electric means lies at the core of spintronic functionality. Breakthroughs include highly efficient spin-transfer-torquedriven magnetism modulation in Co₃Sn₂S₂ without external spin injection^[4] and room-temperature ~100% spin-orbit torque switching in Pt/Fe₃GaTe₂ heterostructure with a low current density^[5]. Targeting next-generation highperformance logic circuits, we achieved a milestone in vertical three-dimensional integration with over ten stacked layers of 2D complementary field-effect transistors based on MoS₂-CrOCl heterostructures, highlighting great potential for cutting-edge electronic applications. [6]

[1] Zhao, Z.; Hou, Y., et al. *Natl. Sci. Rev.* 2025, 12(2): nwae430.

- [2] Meng, Z.; Hou, Y., et al. Adv. Funct. Mater. 2025.
- [3] Li, S.; Hou, Y., et al. Nano Lett. 2025, 25(20): 8390.
- [4] Wang, Q.; Hou, Y., et al. Nat. Electron. 2023, 6(2): 119.
- [5] Yun, C.; Hou, Y., et al. Sci. Adv. 2023, 9(49): j3955.
- [6] Guo, Y.; Hou, Y., et al. *Nature* 2024, 630(8016): 346.

FE-09. Twist-angle-programmable magnetism in graphene/CrI₃ heterostructures

F. Sanchez-Ochoa

Instituto de Fisica, Universidad Nacional Autonoma de Mexico, CDMX, Mexico

Graphene monolayer lacks an electronic bandgap and magnetism which limits its application as component in electronics and spintronics devices. Proximity effects in graphene with other two-dimensional materials is a promising route to induce novel properties in van der Waals (vdW) heteorstructures. Here, we build twisted vdW graphene/Crl₃ heterostructures and then calculate their ground state properties as the electronic and magnetic properties using collinear spin-polarized density functional theory (DFT) calculations. Four twisted heterostructures were built with minimal biaxial strain to avoid renormalization of the band structures and possible expansion, shrink or corrugation of the monolayers. We found the same electronic bandwidth in graphene with an induced magnetism by the ferromagnetic and semiconducting monolayer as substrate. Fingerprints of moire effects are observed in the calculated local spindensity, spin-polarization ratio, orbital-resolved density of states and unfolded band structures for graphene. These results show the interlayer rotation angle is an additional degree of freedom to compression and electric fields, for programming magnetism density and switching a Zeeman effect in graphene monolayer.

Acknowledgments: The authors acknowledge the financial support from SECIHTI (CONAHCYT) Grant No. CF-2023-I-336.

FE-10. Giant Odd-Parity Magnetoresistance in α -Sn/(In,Fe)Sb Heterostructures via Magnetic Proximity-Induced Topological States

L. Anh¹, T. Hotta¹, T. Chiba^{2, 3}, Y. Kota⁴, M. Tanaka¹

¹The University of Tokyo, Tokyo, Japan, ²Yamagata University, Yamagata, Japan, ³Tohoku University, Sendai, Japan, ⁴NIT, Fukushima College, Iwaki, Japan

Magnetoresistance (MR) in conventional materials typically displays even symmetry with respect to an applied magnetic field, a consequence of time-reversal symmetry (TRS) and Onsager's reciprocity relations. In systems where TRS is broken, however, odd-parity magnetoresistance (OMR) can emerge. To date, reported OMR values have been modest, usually restricted to a few tens of percent even under high magnetic fields (14 T)[1,2].

In this work, we report the discovery of a giant OMR effect exceeding 1,150% at only 1 Tesla, representing more than three orders of magnitude enhancement over previous reports. This giant OMR is realized in a heterostructure composed of a 3 nm-thick α-Sn film epitaxially grown atop a ferromagnetic semiconductor (In,Fe)Sb on an InSb (001) substrate using molecular beam epitaxy. While α -Sn is a topological Dirac semimetal when thick enough (≥10 nm)[3]. ultrathin α-Sn (≤3 nm) is known to transition into a topologically trivial narrow-gap semiconductor[4]. However, our results including Shubnikov-de Haas oscillations and ab initio calculations show that TRS breaking via magnetic proximity from the (In,Fe)Sb layer reintroduces topological features [4], effectively inducing tilted linear-dispersion topological states even in this ultrathin regime. The observed OMR is quantitatively explained using a semiclassical Boltzmann model incorporating oppositely tilted Weyl cones[5], suggesting the role of topological band geometry in driving the large OMR.

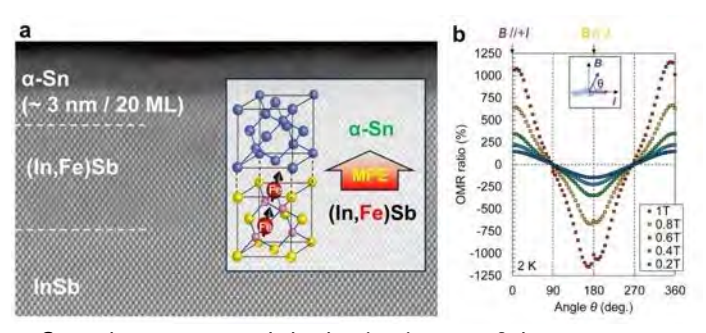
Our findings establish a new paradigm for realizing exceptionally large OMR at low magnetic fields in engineered topologically nontrivial heterostructures. This discovery opens promising avenues for practical applications, including ultra-sensitive magnetic sensors, non-volatile memory, and next-generation spintronic devices.

[1] K. Takiguchi, L.D. Anh, et al., Nature Commun.13, 6538 (2022).

[2] D. Sahani, S. Das, et al., Phys. Rev. Lett. 134, 106301 (2025).

[3] L.D. Anh, K. Takase, et al. Adv. Mater. 33, 2104645 (2021).

[4] S. Fukuoka, L.D. Anh, et al. arXiv:2505.07250.[5] A. Kundu, Z.B. Siu, et al., New J. Phys. 22, 083081 (2020).



a. Crystal structure and the lattice image of the α -Sn/(In,Fe)Sb heterostructure, where time-reversal symmetry in the α -Sn layer is broken via the magnetic proximity effect induced by the underlying ferromagnetic (In,Fe)Sb. b. Angular dependence of the odd-parity magnetoresistance (OMR) ratio as the magnetic field is rotated between the inplane (B // I, ϑ = 0°) and the perpendicular-to-plane ($B \perp I$, ϑ = 90°) directions.

FE-11 is now VP7-13

FE-11. Magnetic properties of $Fe_{5-x}GeTe_2/WSe_2$ van-der-Waals heterostructures

H. Lv¹, J. Herfort¹, <u>T. Shinwari</u>¹, K. Khan¹, M. Hanke¹, A. Trampert¹, R. Engel-Herbert¹, C. Chen², J. M. Redwing², J. J. Lopes¹

¹Paul-Drude Institut für Festkörperelektronik, Berlin, Germany, ²Pennsylvania State University, University Park, Pennsylvania, United States

Van-der-Waals (vdW) heterostructures combining 2D ferromagnets and other nonmagnetic layered materials are highly promising for the realization of novel spintronic devices with integrated magnetic, electronic, and optical functionalities. Among different 2D ferromagnets, $Fe_{5-x}GeTe_2$ (x ~ 0) shows a high potential due to its high Curie temperature T_c . Furthermore, compared to commonly used top-down flake stacking strategies, large-scale, allepitaxial vdW heterostructures are compatible with modern technologies and thus crucial for practical applications. In this work, we study Fe_{5-x}GeTe₂ (FGT) films grown by molecular beam epitaxy on WSe₂ templates, which were epitaxially grown on sapphire substrates. Here, we use the superconducting quantum interference device (SQUID) magnetometry to systematically study the magnetic properties of the all-epitaxial FGT/WSe₂ vdW heterostructures. The clearly larger coercive field H_{C} and smaller saturation field H_5 in out-of-plane (OP) field

configuration compared to those in in-plane (IP) field configuration indicate a pronounced perpendicular magnetic anisotropy (PMA), which is important for low-power spintronic applications. However, the OP-field hysteresis curves at low temperatures display an unusual two-step shape, which can be interpreted by combined contributions from a square-shaped PMA phase caused by the FGT and a zero-coercivity contribution possibly from the oxidized FGT at the surface. The temperature-dependent remanent magnetization M_R was measured at zero field during warming up, where the clearly higher M_R in OP field configuration compared with that in IP field configuration indicates a notably PMA with ferromagnetism up to room temperature, which is consistent with the results of normalized remanent magnetization M_R (divided by the saturation magnetization M_s) that was obtained from the M_s H curves measured at different temperatures. Furthermore, both M-T curve and its derivative dM/dT exhibit two clear magnetic transitions at $T_1 \approx 110 \text{ K}$ and $T_2 \approx 220 \text{ K}$, which can be attributed to the ordering temperatures for the different Fe sublattices in FGT. Finally, we discuss the thickness dependence of the magnetic properties of several FGT/WSe₂ vdW heterostructures.

SESSION FF: UNCONVENTIONAL COMPUTING

Chair(s): P. Talatchian, SPINTEC, Grenoble, Isère, France
Thursday, October 30, 2025
02:00 PM-05:30 PM
Room 2BC

FF-01. Towards All-Electric, Non-volatile Intelligence in Physical Neural Systems

J. Zhou

Institute of Materials Research and Engineering (IMRE), Agency for Science Technology and Research (A*STAR), Singapore, Singapore

Spintronics leverages the interplay of electron's spin and charge degrees of freedom, enabling devices that are non-volatile, non-linear, ultrafast, and intrinsically energy-efficient[1]. Spintronic systems also exhibit rich dynamics, excellent scalability and easy electrical readout, making them promising hardware building blocks for unconventional computing and artificial intelligence (AI)[2]. This talk presents a unified spintronic framework for energy-efficient computing, encompassing the control of spin-orbit torque (SOT), the design of hardware-native algorithms for on-chip applications, and integration with

advanced nanoscale devices such as the magnetic tunnel junction (MTJ). It is organized in two parts. Part I focuses on the material and device engineering of SOT, and its interplay with various field-free switching mechanisms in ferromagnets with perpendicular magnetic anisotropy[3]. We highlight the influences of microscopic domain evolution mechanisms on Al applications. In particular, domain nucleation-dominated switching, enabled by unconventional SOT arising from low crystal symmetry, yields an energy landscape suitable for implementing a hardware-based sigmoidal artificial neuron[4]. In contrast, interlayer exchange coupling (IEC)-mediated field-free switching allows finely controlled domain wall motion, enriched by chiral behaviour and complex temporal dynamics[5]. Notably, IEC is compatible with foundry-ready materials and processes - a key advantage over most fieldfree techniques. Using IEC, we demonstrate scalable allelectric SOT-MTJs with 240-nm cell diameter, fabricated on a 200-mm wafer and integrated with a 180-nm CMOS platform[6]. Part II explores the use of IEC-based systems for hardware-native computing[7]. Most existing hardwarebased computing paradigms remain constrained by the mismatch between analog device responses and abstract Al algorithms, often demanding intensive data pre-processing or model retrofitting. Here, we show that by partially offloading computation processes to spintronic devices, our physical reservoir outperforms the software implementation in terms of simpler network structure, fewer computation steps and lower energy cost. Our approach is rooted in pulse-width-sensitive domain wall motion driven by the combined effects of SOT and IEC. It harnesses the spatiotemporal transformation in magnetic domains, embedding the history dependence of reservoir states into the path dependence of domain evolution (Fig. 1). Our network does not require continuous input streams of specific frequencies, setting it apart from conventional delay-based reservoirs that are essentially volatile[8]. Using a spatial multiplexing scheme, we configure devices activated by distinct pulse-width intervals as artificial neurons, forming a physical reservoir featured by nonvolatility, non-linearity, and rich interconnections. Despite comprising only 14 physical nodes, our prototype system achieves a high recognition rate of 0.903 in written digit recognition and a low error of 0.076 in Mackey-Glass time series prediction (Fig. 2). Moreover, our system consumes 99.6% less energy than its software counterpart, due to low write energy and minimal matrix manipulation. Our approach is adaptable to other memristor technologies, broader physical neural networks, and compact MTJ arrays.

In the latter case, the collective readout of MTJ arrays – where individual MTJ switches coherently and probabilistically – offers an alternative to domain wall motion for building efficient physical reservoirs.

- [1] B. Dieny, I. L. Prejbeanu, K. Garello, Nat. Electron. 3, 8, 446-459 (2020).
- [2] J. Grollier, D. Querlioz, K. Y. Camsari, Nat. Electron. 3, 7, 360-370 (2020).
- [3] J. Zhou, L. Liu, X. Shu, IEEE Trans. Magn. 59, 8, 1-13 (2023).
- [4] J. Zhou, T. Zhao, X. Shu, Adv. Mater. 33, 2103672 (2021).
- [5] J. Zhou, L. Huang, H. J. Chung, ACS Nano, 17, 10, 9049-9058 (2023).
- [6] J. Zhou, L. Huang, S. L. K. Yap, APL Mater. 12, 081105 (2024).
- [7] J. Zhou, J. Xu, L. Huang, Sci. Adv. 11, adr5262 (2025).
- [8] X. Liang, J. Tang, Y. Zhong, Nat. Electron. 7, 3, 193-206 (2024).

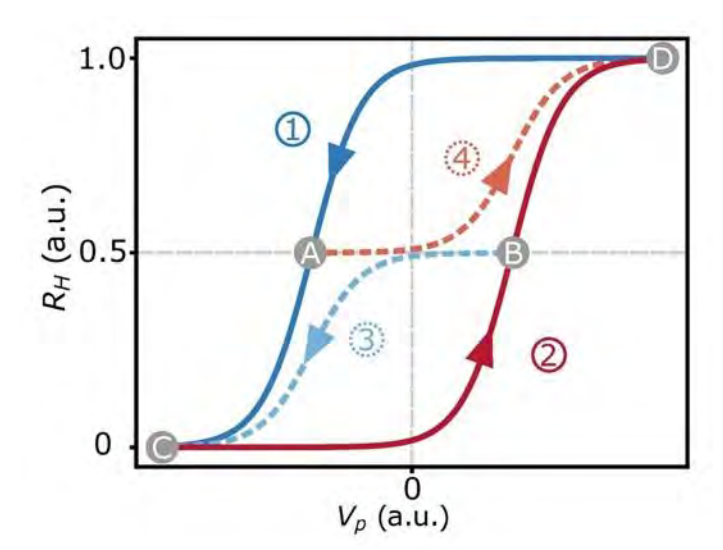


Fig. 1. Path dependence in magnetic hysteresis. State A and B, despite being at the same macroscopic readout of 0.5, will take path 1 and 3 towards state C. R_H : Hall resistance; V_p : pulse amplitude.

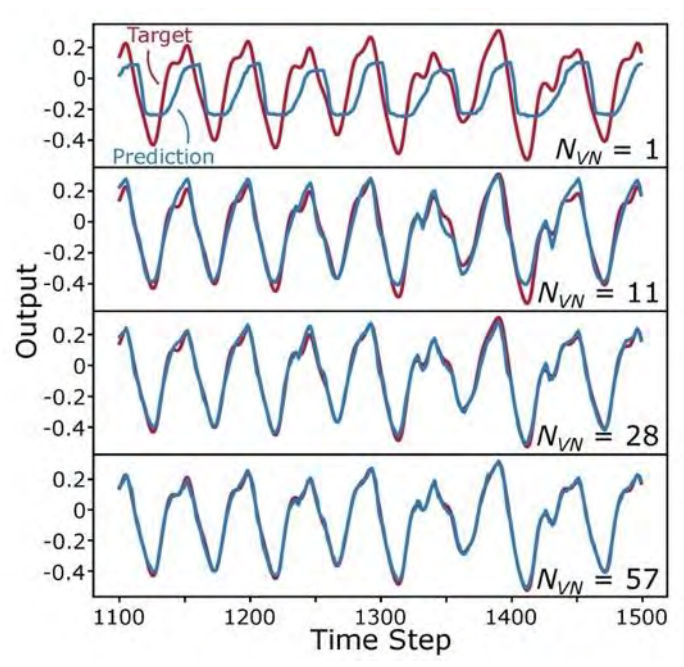


Fig. 2. Chaotic time-series prediction. As number of neurons (N_{VN}) increases, the reservoir produces better prediction.

FF-02. N-ary In-memory Computing in a Crossbar Array of Multistate Magnetic Tunnel Junctions

<u>A. Moureaux</u>, A. Lopes Temporao, F. Abreu Araujo Institute of Condensed Matter and Nanosciences, UCLouvain, Louvain-la-Neuve, Walloon Brabant, Belgium

The recent surge in the use of machine learning has sparked the need for low-power architectures for processing data energy-efficiently without compromising performances. In this regard, growing interest has been observed for inmemory computing, whose strategy consists in processing the data in the memory [1, 2]. More specifically, a strong focus has been made on the so-called multiply-andaccumulate (MAC) operation, a matrix-vector multiplication used extensively in the inference phase of neural networks. So far, the most promising architecture for implementing the MAC operation inside the memory is a crossbar array of cells with distinct levels of conductance (Fig. 1). Several studies have reported on the use of magnetic tunnel junctions (MTJs) for this purpose. However, these solutions are often restricted to the binary encoding of information [2, 3, 4], hence limiting their computing power and scalability.

To overcome this limitation, we investigated the use of multistate magnetic tunnel junctions (M2TJs), which can

encode mutliple conductance states within a single device [5]. This approach allows to perform n-ary in-memory computing, leading to higher data density and computing power. In this work, we present how to perform multi-bit MAC operations using a crossbar array of 16 M2TJs with 4 distinct conductance states. We discuss the multiplexing and weights quantization methods that can be used to leverage the potential of the hardware for real-life applications. Our hardware MAC operation is first benchmarked through simulation with the elementary XOR approximation task, showing excellent results and high robustness to noise and non-idealities. We then confront our solution to the more complex case of MNIST handwritten digits images classification. While the accuracy reached (94.76%) is lower than the software baseline (97.56%), the results show a significant improvement from the binary counterpart (80.41%, Fig. 2).

- [1] A. Sebastian, M. Le Gallo et al., Nature Nanotechnology 15, 529-544 (2020).
- [2] S. Jung, H. Lee et al., Nature 2, 211-216 (2022).
- [3] J. Doevenspeck, K. Garello et al., 2020 IEEE Symposium on VLSI Technology 1-2 (2020).
- [4] T.-N. Pham, Q.-K. Trinh et al., IEEE Journal on Emerging and Selected Topics in Circuits and Systems 12, 569-579 (2022).
- [5] S. Das, A. Zaig, M. Schultz et al., Applied Physics Letters 117, 7 (2020).

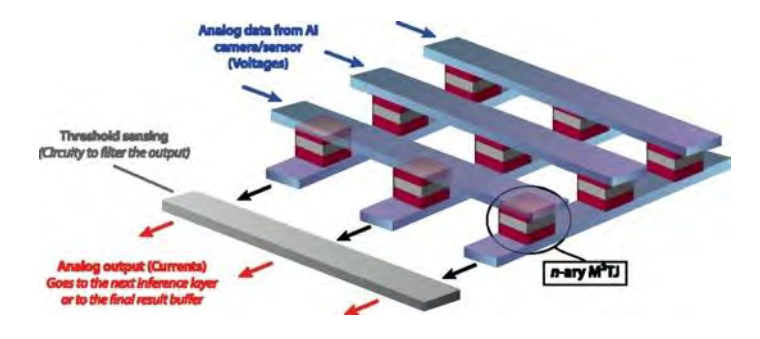


Fig. 1 A crossbar array of 9 M2TJs presenting 4 distinct conductance levels.

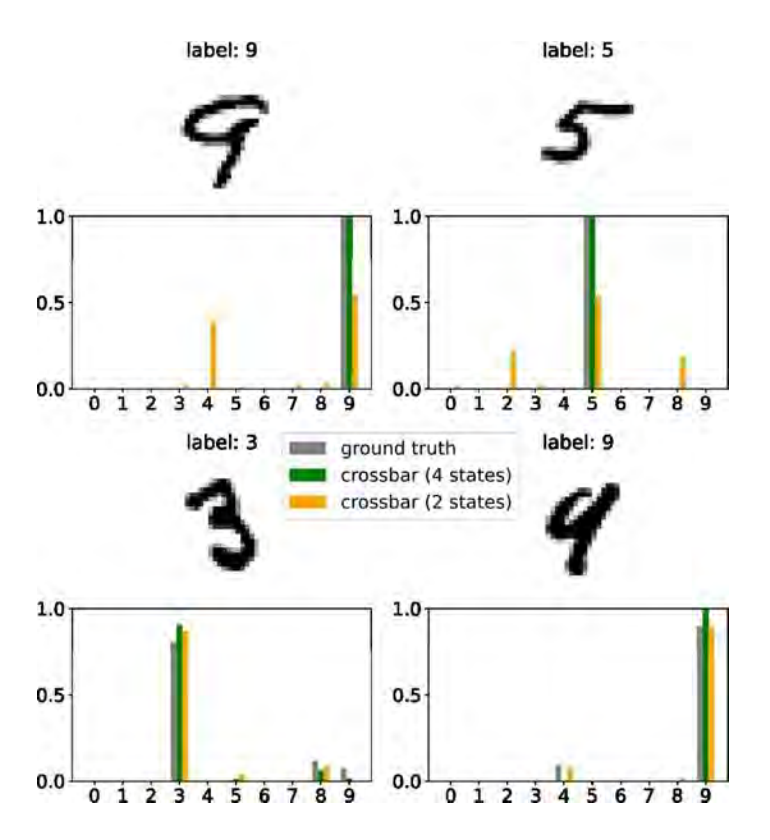


Fig. 2 The hardware MAC operation yields results similar to the software baseline in the case of MNIST handwritten digits recognition when the number of states is 4. The quality obtained in the binary case are significantly worse.

FF-03. Skyrmion based Reservoir Computing for Spatiotemporal Motion Recognition

M. Alam¹, M. Rajib¹, S. Sabyasachi¹, M. Stiles², J. Atulasimha¹,

¹Mechanical and Nuclear Engineering, Virginia Commonwealth University, Richmond, Virginia, United States, ²Alternate Computing Group, NIST, Gaithersburg, Maryland, United States, ³Electrical and Computer Engineering, Virginia Commonwealth University, Richmond, Virginia, United States

Physical reservoir computing (PRC) is a promising computing paradigm that utilizes the nonlinear dynamics of physical systems to perform classification and recognition tasks [1], [2]. In this work, we demonstrate the use of a nanomagnetic system as a reservoir for spatiotemporal skeletal motion recognition. The reservoir consists of a 5×5 array of confined magnetic skyrmions, each occupying a 250×250 nm² region, simulated using mumax3. Human motion data comprising 15-frame sequences of 3D joint positions, are first reduced to 25 spatial features using

principal component analysis (PCA), which are then input into the reservoir as time-varying modulation of local anisotropy. Each feature is applied to its corresponding skyrmion region for 1 ns, resulting in a total simulation window of 15 ns per sample. The nonlinear and coupled magnetization dynamics—driven by inter-skyrmion interaction and time-varying input—are captured by recording the z-component of magnetization of each skyrmion over time, which is indicative of magnetoresistance when such a skyrmion is hosted in the soft layer of a magnetic tunnel junction (MTJ) [3]. A linear readout layer, trained using the Moore-Penrose pseudoinverse, is used to classify the resulting patterns. Although only a small number of training samples are used, the output space shows clear clustering of different action classes, indicating the system's ability to encode spatiotemporal patterns. This study demonstrates the use of magnetic reservoirs for PRC on high-dimensional spatiotemporal data, and highlights the role of dipolecoupled, breathing skyrmions in enabling motion recognition tasks.

Acknowledgement: Convergence Laboratory initiative (CLi) from Airforce: FA865123CA023 REQ F1TBAX3053A002.

[1] K. Nakajima, "Physical reservoir computing—an introductory perspective," *Japanese Journal of Applied Physics*, *59*(6), p.060501, 2020.
[2] D. A. Allwood, M. O. Ellis, D. Griffin, T. J. Hayward, L. Manneschi, M. F. Musameh, S. O'Keefe, S. Stepney, C. Swindells, M. A. Trefzer, and E. Vasilaki, "A perspective on physical reservoir computing with nanomagnetic devices," *Applied Physics Letters*, *122*(4), 2023.
[3] M. M. Rajib, W. A. Misba, M. F. F. Chowdhury, M. S. Alam, and J. Atulasimha, "Skyrmion based energy-efficient straintronic physical reservoir computing," *Neuromorphic Computing and Engineering*, *2*(4), p.044011, 2022.

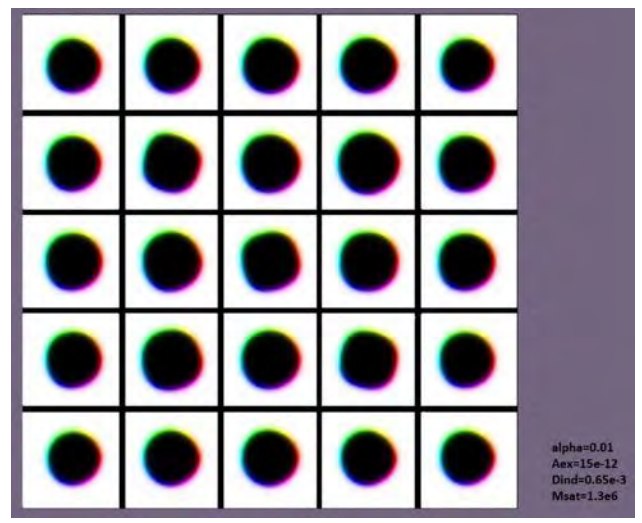


Fig. 1: Schematic of the physical reservoir based on a magnetic thin film hosting confined skyrmion arrays.

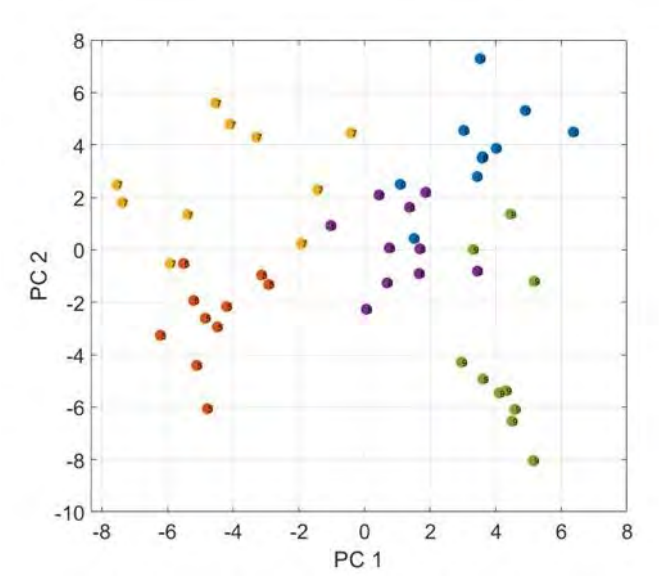


Fig. 2: Principal component projection of reservoir output vectors derived from skyrmion breathing dynamics.

FF-04. Stochastic Multilayer Spintronic Neural Networks Trained using Local-Learning Rules

<u>J. Peters</u>¹, N. Phan^{1, 2}, U. Ebels¹, P. Talatchian¹ ¹Univ. Grenoble Alpes, CEA, CNRS, Grenoble INP, Spintec, Grenoble, France, ²Laboratoire Albert Fert, CNRS, Thales, Université Paris-Saclay, Paris, France

Implementing on-chip learning in physical neural networks is a key step toward developing energy-efficient artificial intelligence systems. Superparamagnetic tunnel junctions (SMTJs) provide a promising hardware platform for such physical networks due to their thermally induced stochastic magnetization fluctuations, which inherently emulate binary stochastic neurons at the nanoscale [1].

In this work, we present the first experimental demonstration of a binary classification task learnt using a network of SMTJ neurons (see Fig. 1). We implement a local hardware-aware learning rule adapted from Equilibrium Propagation (EP), allowing us to avoid the energy-intensive data shuffling typically required in neural network training [2]. By directly interfacing SMTJ arrays with electronic control circuits, we demonstrate the network's ability to learn and classify binary patterns in real time.

Additionally, in simulation, we demonstrate the system's scalability by using deep multi-layer neural networks to perform several complex classification tasks (see Fig. 2). Maximum testing accuracies of 98.1% and 89.8% are achieved on the MNIST and FashionMNIST image recognition tasks after 3000 training epochs.

Our results showcase the potential of spintronic neurons for implementing on-chip learning in physical neural networks, paving the way for scalable, low-power neuromorphic systems.

[1] N.T. Phan et al., Proceedings of the 17th ACM
International Symposium on Nanoscale Architectures (2022)
[2] B. Scellier, Y. Bengio, Frontiers in computational neuroscience, 11, 24 (2017)

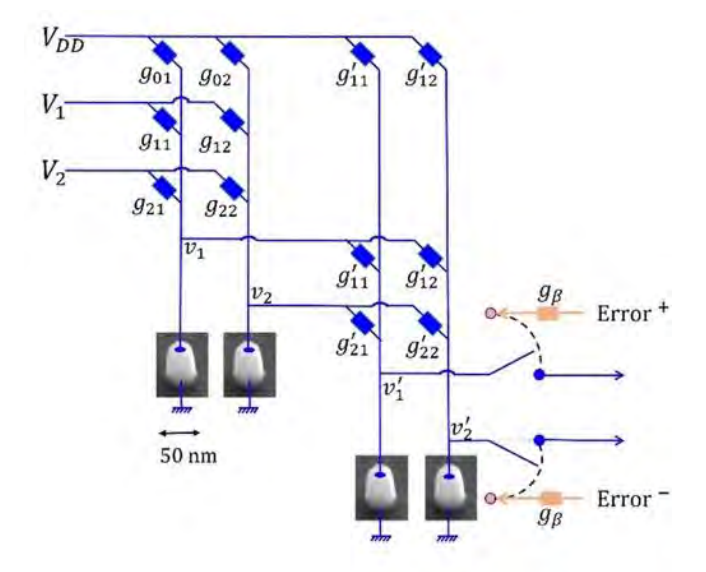


Fig. 1 Schematic of the experimental SMTJ-based neural network architecture, consisting of two input voltage nodes (V) and the corresponding output value (v), for binary classification. Network weights are defined by the conductance matrix (g). The learning process is guided by the error signal (BL) which applies a force on the network depending on the loss function (L) parameterized by the nudging hyperparameter (B). A real SMTJ image represents how the devices are connected within the circuit.

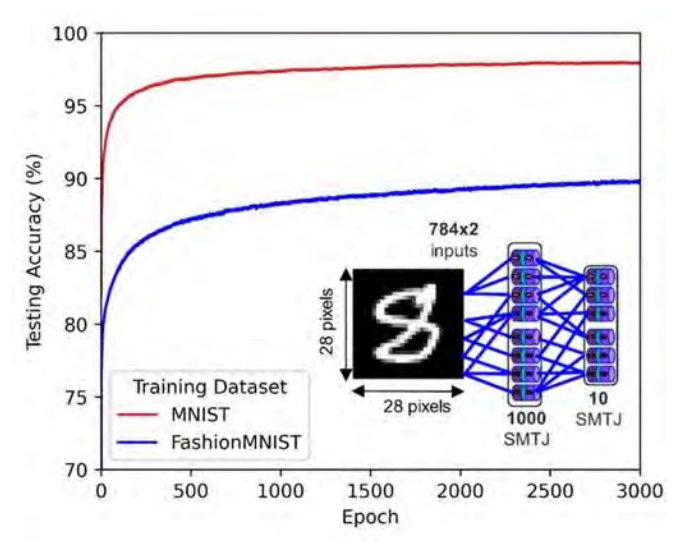


Fig. 2. Testing accuracy curves from simulation for a one hidden layer deep network utilising SMTJs on the MNIST and FashionMNIST datasets. The network configuration is shown on the insert diagram, consisting of layer sizes 1568-1000-10. Maximum testing accuracies of 98.1% and 89.8% are achieved after 3000 training epochs.

FF-05. A Probabilistic Nanomagnetic Logic Network Enabling Reversible Computing

S. Nallan, J. Zhu

Data Storage Systems Center, Carnegie Mellon University, Pittsburgh, Pennsylvania, United States

In this work, we present a new logic-gate architecture comprised of in-plane spin orbit torque magnetoresistive random access memory (SOT-MRAM) cells set by input current pulses. These magnetic discs emanate magnetostatic stray fields in their immediate vicinities, and these fields in turn affect the stochastic switching processes of adjacent magnetic cells, with the sign and magnitude of the resulting bias dependent on system geometry. Using these cell-to-cell interactions - in conjunction with spin transfer torque biases, anisotropy and demagnetization effective fields, and thermal fluctuation effects encapsulated in our Landau-Lifshitz-Gilbert simulation framework - we demonstrate correlated probabilistic switching of SOT-MRAM device networks. Furthermore, by constructing these networks in certain geometries, we form AND, OR, and NOT logic gates with high probabilistic accuracy. These gate-type networks are bidirectional and amenable to both forwards and reverse propagation; they can also be chained through unit-to-unit communications mechanisms to achieve more complex logic operations. Most importantly, in this framework, computation can be reversed to obtain all possible inputs resulting in a given output. Through exhaustive simulations, we quantify key parameters such as switching time, energy use, and gate-bit probabilistic accuracy, and identify relevant tradeoffs and regions of operation. These probabilistic SOT-MRAM units can form the building blocks of a powerful new framework for spintronics-based probabilistic computing.

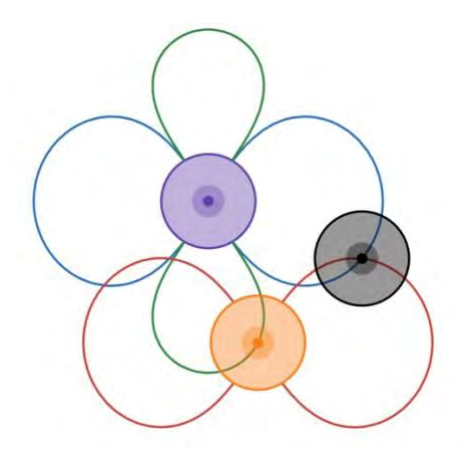


Fig. 1 SOT-MRAM cell arrangement producing the behavior of a probabilistic AND-gate. The lines show clines of

constant magnetostatic stray field in the direction of the inplane anisotropy. All three cells interact with each other through these stray fields, producing a network whose combined state creates AND-gate logic with high probabilistic accuracy.

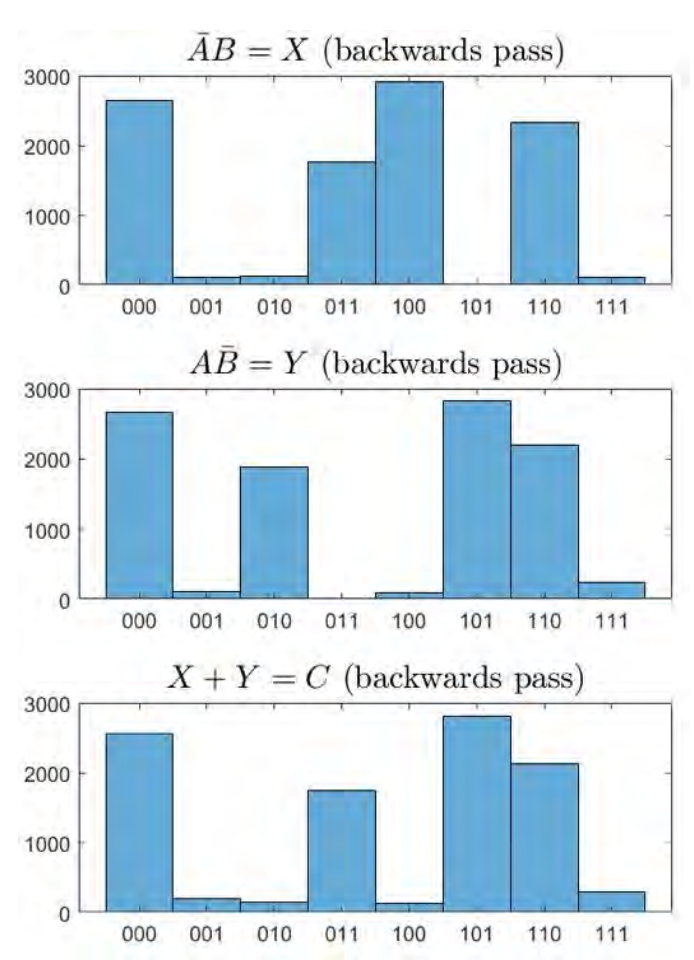


Fig. 2 Backpropagation with a probabilistic XOR network: we produce, with >95% accuracy, network states ABC such that C = A XOR B. This is a complex, non-linearly-separable logic function acheived by chaining multiple smaller gates. The probabilistic nature of the computation and the ability to back-derive inputs from outputs remains unchanged.

FF-06. Field-Free Random Number Generation with Elliptical Voltage-Controlled Magnetic Tunnel Junctions for Probabilistic Computing

J. G. Athas, C. Duffee, T. Neuner, P. Khalili Amiri *Electrical and Computer Engineering, Northwestern University, Chicago, Illinois, United States*

Voltage-controlled magnetic anisotropy (VCMA) in perpendicular magnetic tunnel junctions (pMTJs) enables compact, energy-efficient true random number generators (TRNGs) that are fully compatible with CMOS logic. Prior VCMA-TRNGs relied on external magnetic fields, limiting integration [1-3]. Here, we demonstrate a field-free, CMOS-compatible TRNG using 40 × 80 nm elliptical VCMA-MTJs. The elliptical shape introduces in-plane anisotropy, allowing stochastic thermal relaxation into random states after a short voltage pulse, eliminating the need for magnetic fields or precessional timing circuits and minimizing circuit area.

Random bitstreams were generated with 10 ns pulses, achieving ~1 pJ/bit switching energy and up to 100 Mbps throughput per MTJ. Compared to circular devices from the same stack and measured under identical field-free conditions, elliptical MTJs showed significantly reduced bias due to more symmetric stochastic switching (Fig. 1). While raw bitstreams exhibited some bias and correlation, lightweight LFSR-16 post-processing, implemented in CMOS, produced outputs that passed all NIST SP 800-22 statistical tests (Fig. 2). This hybrid VCMA-MTJ + LFSR architecture offers a scalable, field-free, and area-efficient entropy source for applications in hardware security, probabilistic computing, and low-power embedded systems.

[1] Y. Shao, C. Duffee, P. Khalili Amiri, Nanotechnology, Vol. 34, p. 495203 (2023)

[2] Y Shao, P. Khalili Amiri, Advanced Materials
Technologies, Vol. 8, p. 2300676 (2023)
[3] C. Duffee, J. Athas, P. Khalili Amiri, arXiv:2412.08017 (2024)

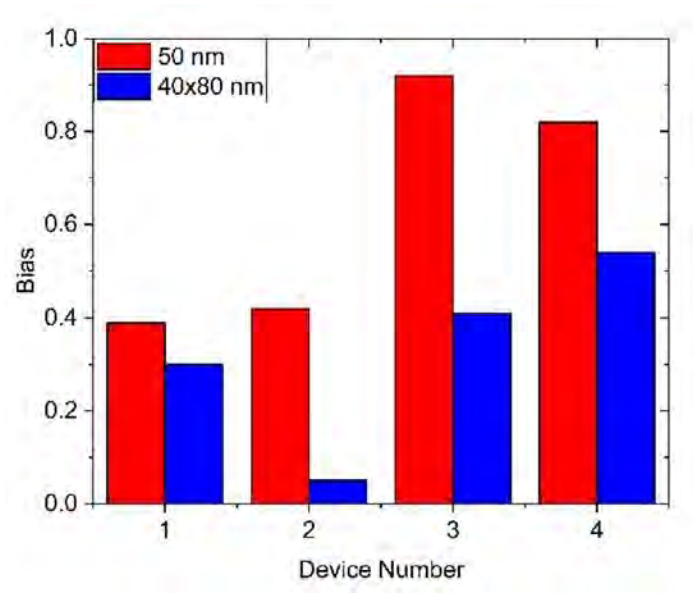


Fig. 1, Bias comparison between 50 nm circular and 40x80 nm elliptical VCMA-MTJs. Each device pair was fabricated adjacently on the wafer. Bias is defined as as |[p(0)-p(1)]/[p(0)+p(1)]|, where p(0) and p(1) are the measured probabilities of 0s and 1s, respectively. Lower Bias values indicate a higher-quality random bit stream.

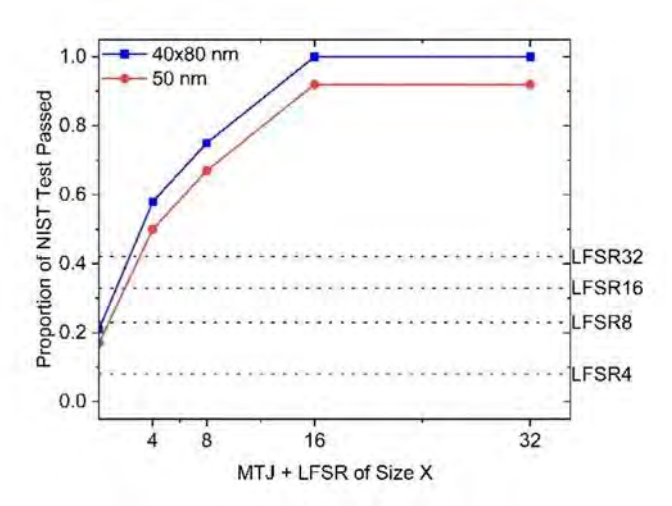


Fig. 2, Proportion of NIST SP 800-22 tests passed for VCMA-MTJs integrated into LFSRs of varying sizes. Elliptical MTJs consistently outperform circular devices. Full NIST test suite passage is achieved with LFSR-16 for the elliptical configuration. Horizontal dashed lines indicate baseline performance of standalone LFSR without MTJ.

FF-07. Exploiting Probabilistic Switching of Magnetic Tunnel Junctions (MTJs) for Near-Memory and In-Memory Computing

S. S. Mugdho, E. Rogers, K. Gupte, <u>C. Wang</u> Electrical and Computer Engineering, Iowa State University, Ames, Iowa, United States

Modern Artificial Intelligence (AI) workloads have become increasingly complex and memory-intensive, posing a significant challenge to computational efficiency. One critical issue in AI computation is the notorious von-Neumann memory wall bottleneck, which is caused by the data movement between the separate processing and memory units. Recently, various emerging computing architectures have been explored to address the von-Neumann memory bottleneck. Particularly, near-memory and in-memory computing have demonstrated immense potential for next-generation AI acceleration. In this work, we show that probabilistic MTJs of various flavour can be exploited to improve the computational efficiency of both in-memory computing (IMC) and near-memory computing (NMC) systems. Specifically, thermally-stable Spin-transfertorque (STT) MTJs with reduced write currents and elevated write error rates (due to probabilistic switching) will enable aggressive scaling down of the access transistor cell in MRAM array, leading to tremendous gain in on-chip memory density that ameoliate the von Neumann memory bottleneck. We exploit the insight that pre-trained DNN models have high heterogeneity in the error resiliency at the bit-level granularity, which provides an optimal tradeoff of error rates for improvement in area and energy efficiency (Fig.1). Moreover, thermally-unstable stochastic spin-orbit-torque (SOT) MTJs can serve as a current-tovoltage converter to connect crossbar arrays in IMC, where the probabilistic switching of SOT-MTJs can also perform analog-to-stochastic digital converter. Our comprehensive evaluation across the stack from device to circuit and system architecture demonstrate significant improvement of hardware efficiency, essentially removing the analog-digital converter (ADC) bottleneck in IMC (Fig.2). Our work demonstrated that probabilistic switching dynamics of MRAM offers a rich avenue for Al hardware acceleration.

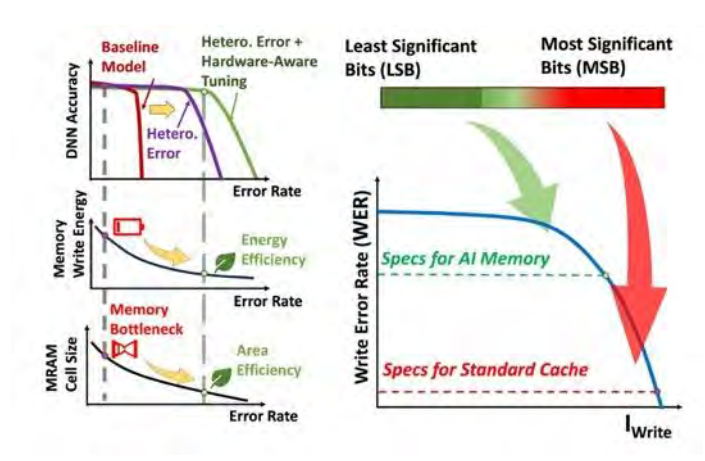


Fig.2 Error-Aware MRAM for Near-Memory Computing

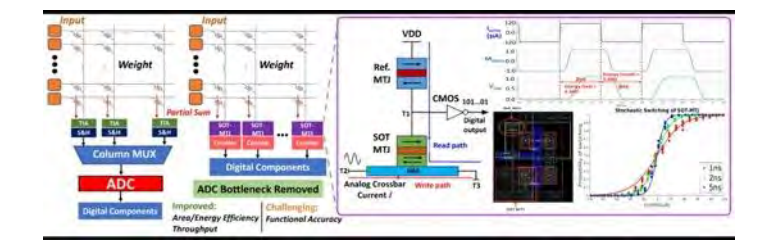


Fig. 2 SOT-MTJ as ADC replacement in In-Memory Computing.

FF-08. Wafer-Scale SOT-MRAM for Energy- and Memory-Efficient Analog Computing

S. Liu¹, M. Song², J. C. Incorvia¹

¹The University of Texas at Austin, Austin, Texas, United States, ²Taiwan Semiconductor Manufacturing Corporation, Hsinchu, Taiwan

Wafer-scale SOT-MRAM is at the cusp of commercialization, showing impressive energy and latency-related metrics for digital memory [1]. Additionally, STT-MRAM has already been demonstrated to be effective elements for analog crossbar arrays, structures that greatly accelerate vector matrix multiplications [2]. Here, we evaluate wafer-scale SOT-MRAM for the low memory analog applications of 2-bit neural network inference, stochastic training of binarized neural networks, and probabilistic graph modeling (PGM).

For edge computing, networks that can be saved in limited precision can be particularly useful. Here, we evaluate and propose an approach for deploying limited-precision neural networks for inference on SOT-MRAM crossbar arrays. We characterize device-to-device switching behavior from a wafer-scale SOT-MRAM from a 4K memory array and project

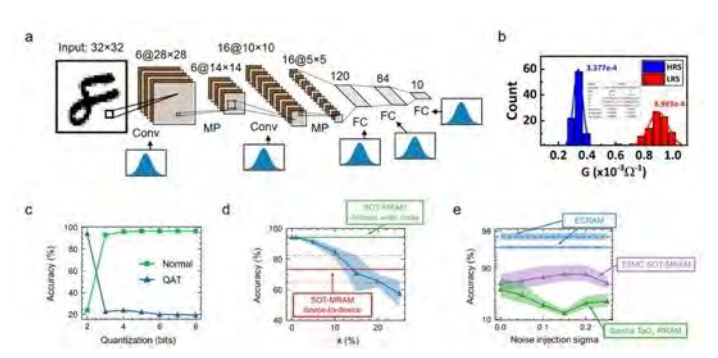
^{*} Best Student Presentation Finalist / LB – Late-breaking Poster

this to network-level behavior using CrossSim [3]. We evaluate approaches such as quantization aware training and noise injection to compensate for limited resistance levels and device-to-device variations. Next, we show that SOT-MRAM is effective for stochastic training of binary networks, with only +1 and -1 allowed for both weights and activations. This stochastic switching behavior can also be leveraged for PGM, where we show that wafer-scale variations in stochastic switching behavior are small enough to effectively utilize large networks.

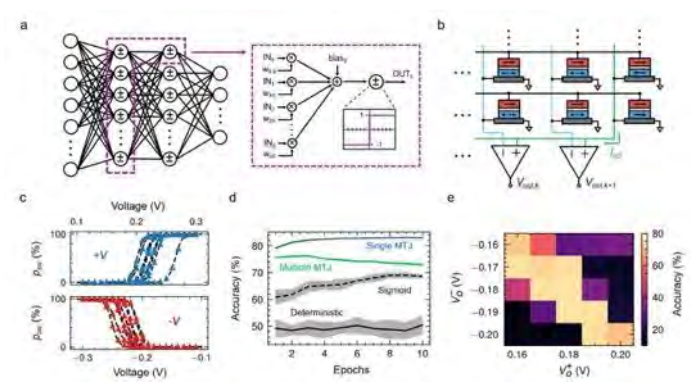
[1] Song, M. Y., Chen, K. L., Chen, K. M., Chang, K. T., Wang, I. J., Hsin, Y. C., Lin, C. Y., Ambrosi, E., Khwa, W.-S., Lu, Y. L., Hu, C. Y., Yang, S. Y., Li, S. H., Wei, J. H., Lee, T. Y., Wang, Y. J., Chang, M. F., Pai, C. F., & Bao, X. Y. (2023). High RA Dual-MTJ SOT-MRAM devices for High Speed (10ns) Compute-in-Memory Applications. 2023 International Electron Devices Meeting (IEDM), 1–4.

[2] Jung, S., Lee, H., Myung, S., Kim, H., Yoon, S. K., Kwon, S.-W., Ju, Y., Kim, M., Yi, W., Han, S., Kwon, B., Seo, B., Lee, K., Koh, G.-H., Lee, K., Song, Y., Choi, C., Ham, D., & Kim, S. J. (2022). A crossbar array of magnetoresistive memory devices for in-memory computing. *Nature*, *601*(7892), 211–216.

[3] Xiao, T. P., Feinberg, B., Bennett, C. H., Prabhakar, V., Saxena, P., Agrawal, V., Agarwal, S., & Marinella, M. J. (2022). On the Accuracy of Analog Neural Network Inference Accelerators. *IEEE Circuits and Systems Magazine*, *22*(4), 26–48.



a) LeNet-5 convolutional neural network architecture. b) Conductance distributions of 100 SOT-MRAM devices from a 4K array. c) Inference accuracy showing differences between normal and quantization aware training (QAT). d) Inference accuracy as a function of proportional noise k. e) Inference accuracy comparison of several device networks with injected noise training.



a) Multilayer perceptron of binarized network. b) Network architecture where single device represents weight. c) Switching distribution of 10 devices in the positive (blue) and negative (red). d) Training accuracy of weights of SOT-MRAM devices compared to ideal stochastic sigmoid and deterministic weight changes. e) Training accuracy map of minimum absolute voltage amplitude for stochastic training.

FF-09. Non-reciprocal phase transitions in kagome artificial spin ice plasmonic metasurfaces

<u>S. Gupta</u>¹, L. Martinez², L. McClintok², Z. Jacob¹, P. Padmanabhan², P. Iyer³

¹Purdue University, West Lafayette, Indiana, United States, ²Los Alamos National Laboratory, Los Almos, New Mexico, United States, ³Sandia National Laboratory, Albuquerque, New Mexico, United States

Artificial spin ice (ASI) metasurfaces, composed of coupled nanomagnets arranged in frustrated lattices, offers significant promise for low-energy information processing by enabling non-reciprocal information flow—an essential feature for emerging in-memory computing paradigms such as probabilistic and neuromorphic architectures [1]. In this work, we introduce a high-sensitivity approach to probe the ultrafast spin dynamics in ASI systems using time-resolved magneto-optic Kerr effect (MOKE) at a plasmonically enhanced wavelength of 900 nm [2]. Our measurements reveal non-reciprocal spin resonances in both longitudinal (L-MOKE) and polar (P-MOKE) configurations. We leverage a metal-insulator-metal (MIM) plasmonic structure to amplify the MOKE signal by two orders of magnitude [3], enabling unprecedented sensitivity in detecting magnetic phase transitions within Kagome nanomagnetic lattices. These observations are consistent with micromagnetic simulations. Our results highlight the potential of ASI systems for all-optical reconfiguration and

readout, offering a viable path toward their integration into stochastic learning models, including directional graph networks and deep reservoir computing [4]. By advancing both the understanding and manipulation of spin dynamics in artificial spin systems, this study lays a foundation for high-performance, energy-efficient computing technologies.

[1] J.C. Gartside, K.D. Stenning, A. Vanstone, et al. Nature Nanotechnology, Vol. 17(5), p.460-469 (2022).

[2] J.A. Schuller, E.S. Barnard, W. Cai. et al. Nature materials, Vol. 9(3), p.193-204 (2010).

[3] I.S. Maksymov. Reviews in Physics, Vol. 1, p.36-51 (2016).
[4] D. Beaini, S. Passaro, V. Létourneau. et al.In International Conference on Machine Learning, p. 748-758 (2021).

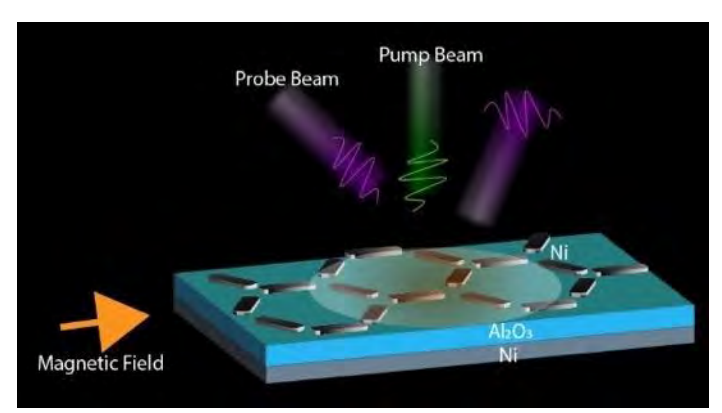


Figure 1. Schematic of the experiment illustrating the structure which is a metal-insulator-metal plasmonic design, with nanomagents arranged in Kagome lattice. Pump-probe Magneto-optic Kerr Effect (MOKE) experiment is utilized to study the magnetization dynamics.

FF-10. Integrated Magnonic Reservoir Computing with Magnetic Metamaterials

C. Swindells¹, I. T. Vidamour^{2, 1}, G. Venkat¹, T. Hayward¹
¹Department of Materials Science and Engineering, University of Sheffield, Sheffield, United Kingdom, ²Department of Computer Science, University of Sheffield, Sheffield, United Kingdom

Reservoir Computing (RC) is a framework in which computation is performed by utilising the non-linear response of a dynamical system. Compared to traditional recurrent neural networks, material-based RC has the potential for large energy savings - provided the material platform has a suitably complex, and energy efficient, response to an input stimulus.

Magnetic materials are ideal candidates for RC due to their

underlying nonlinear and hysteretic properties. Several magnetic systems have been proposed as RC platforms, not limited to spin-oscillators¹, artificial spin ices² and magnonic crystals³.

Recently, we have shown the capabilities of magnetic nanoring arrays⁴ as reservoir computers⁵. However, while competitive performance in a range of tasks was achieved, the demonstration of device-like behaviour was limited by inefficient methods of encoding data with a magnetic field, and single scalar value readout with magnetoresistance, sacrificing useful computational information. Measuring spin wave spectra offers a route to obtaining rich, multidimensional representations of reservoir states, but previous demonstrations were restricted to flip-chip measurements of macroscopic arrays (~mm²) via ferromagnetic resonance (FMR), which lack device compatibility⁶.

Here, we demonstrate an approach which offers an energy efficient method of both encoding information and recording system state, while also more readily device compatible. To achieve this, we integrate a single 100 x 100 μm² nanoring array onto a Pt waveguide. Small bias current (~100 μA) to the waveguides produces transformations of the FMR spectra via spin orbit torque, while measuring the rectified voltage across the device as a function of RF excitation allows for a probe of internal magnetic states. Finally, we show how our device can be used to perform powerful computation in the absence of the external magnetic fields normally used for encoding. We utilise the non-linear, frequency dependent transformations provided by the bias current to classify digits from MNIST dataset. Our work provides a route to realising magnonic fingerprinting as a computational tool in novel neuromorphic devices.

- [1] D.Marković et al., Applied Physics Letters 114.1 (2019)
- [2] J.C. Gartside et al., Nature Nanotechnology 17 (2022)
- [3] A. Papp et al, Nature Communications 12.1 (2021)
- [4] I.T.Vidamour et al., Nanotechnology 33 (2022)
- [5] I.T.Vidamour et al., Communications Physics 6 (1), 230 (2023)
- [6] C. Swindells et al., Spin 15 (2025)



Fig. 1 Example SEM of Device

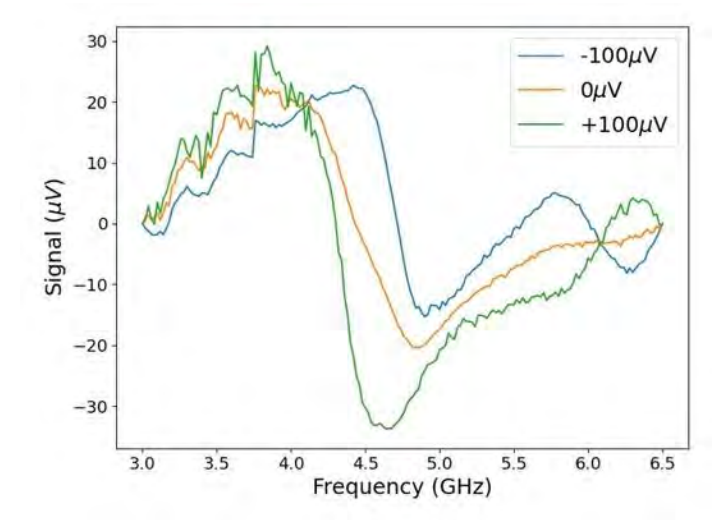


Fig 2. Frequency response to bias current

SESSION FG: THIN FILM AND INTERFACES

Chair(s): P. Tiberto, *INRIM, Torino, Italy*Thursday, October 30, 2025
02:00 PM-05:30 PM
Room 2A

FG-01. Design and Optimization of Thin-film Ferromagnetic Patterns for Ultra-Compact High Frequency Bandstop Filters

H. Yin, A. El-Ghazaly

Electrical and Computer Engineering, Cornell University, Ithaca, New York, United States

Electromagnetic interference is arising as a more serious problem in next-generation microwave front-end devices as the microwave spectrum becomes more crowded [1], [2]. One strategy to suppress the noise is to absorb it with the ferromagnetic resonance (FMR) of thin magnetic films [3], [4]. Such a strategy has tunable FMR frequency, and is also very compact with high permeability ferromagnetic material; but the low FMR frequency of these ferromagnets, typically only sub-gigahertz, greatly limits the widescale use of this method. Attempts have been made to increase the FMR frequency by patterning the ferromagnetic film [5], [6]. However, poor performance including low permeability and small attenuation of many of the designs calls for optimization of the patterns to make this method more practical for microwave applications. In this work, we designed, optimized and fabricated

patterned ferromagnetic thin film integrated ultra-compact bandstop filters operating at 16 GHz under zero bias field, which is the highest among similar filters to the author's best knowledge (Figure 1). Fe₆₅Co₃₅ was selected as the ferromagnetic material for its highest known saturation magnetization, which greatly improved the operating frequency and permeability of the filter. In order to further increase the FMR, shape anisotropy was introduced by patterning the magnets. To alleviate the reduction of permeability and attenuation resulting from patterning, we closely packed the magnet patterns together and thereby increased the total magnetic material volume. With an optimized array spacing, our filter shows a 52.1% percent of increase in attenuation compared to sparsely packed arrays. By simply tuning the spacing of the patterns, the central frequency of our filter can be designed from 15.80 GHz to 18.50 GHz (Figure 2), which demonstrates great frequency agility, while still maintaining high effective permeability of 67. Further tuning can be achieved by applying bias magnetic fields [7] or through magnetoelastic coupling [8]. Thus, our method is highly versatile and can be easily

combined with conventional designs of microwave integrated filters.

- [1] D. J. Simpson, R. Gómez-García, and D. Psychogiou, *IEEE Trans Microw Theory Tech*, vol. 67, no. 5, pp. 1854–1869 (2019)
- [2] Q. Zeng, Z. Shi, W. Wang, and Z. Hu, in *2011 Third International Conference on Communications and Mobile Computing*, pp. 420–423 (2011)
- [3] M. Yamaguchi *et al.*, in *2011 41st European Microwave Conference*, pp. 49–52 (2011)
- [4] Y. He *et al.*, *IEEE Trans Magn*, vol. 54, no. 9, pp. 1–4 (2018)
- [5] T. Wang *et al.*, *IEEE Trans Microw Theory Tech*, vol. 65, no. 2, pp. 504–512 (2017)
- [6] J. Salvia, J. A. Bain, and C. P. Yue, in *IEEE InternationalElectron Devices Meeting, 2005. IEDM Technical Digest.*, pp. 943–946 (2005)
- [7] B. Kuanr *et al.*, *IEEE Trans Magn*, vol. 41, no. 10, pp. 3538–3543 (2005)
- [8] A. El-Ghazaly *et al.*, *Adv Mater Technol*, vol. 2, no. 8, p. 1700062 (2017)

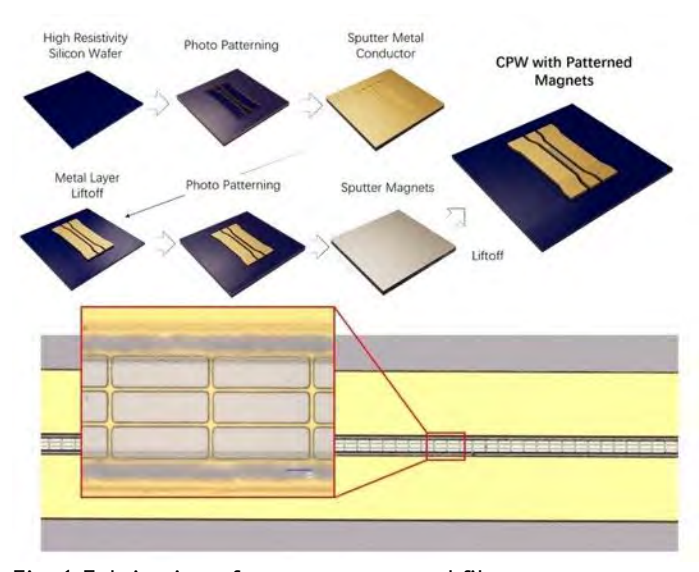


Fig. 1 Fabrication of magnet-patterned filter

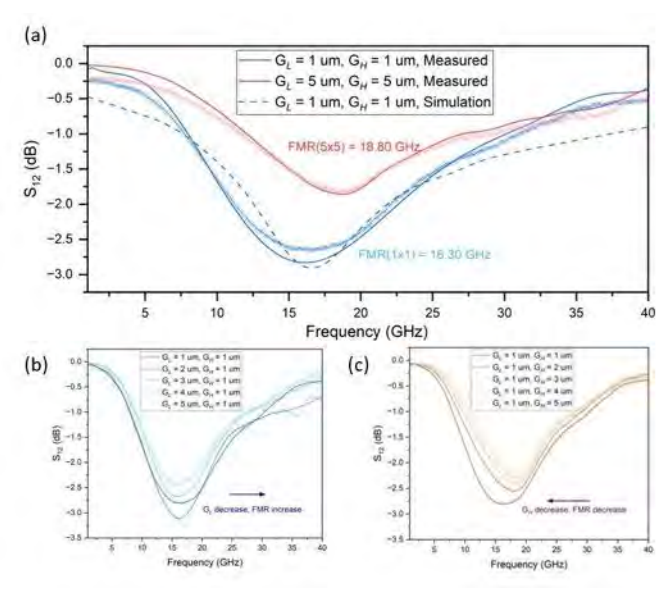


Fig. 2 Simulated and measured S₁₂ parameters of filters

FG-02. Interface-Induced Magnetism in Hybrid Heterostructures Containing Monolayer Transition Metal Dichalcogenide Coated with V_2O_5 Thin Films

Y. Wadumesthri¹, N. Kapuruge¹, R. B. de Oliveira², B. Ipaves², G. S. Fabris², R. Tromer³, K. Lasek¹, N. Schulz¹, H. Srikanth¹, M. Phan¹, D. S. Galvão², H. Rodríguez Gutiérrez¹

¹Department of Physics, University of South Florida, Tampa, Florida, United States, ²Applied Physics Department and Center for Computational Engineering & Sciences, State University of Campinas, Campinas, São Paulo, Brazil, ³Institute of Physics, University of Brasília, Brasília, DF, Brazil

In recent years, magnetism in two-dimensional materials has gained an increasing interest due to the possibility of storing and processing information through the manipulation of both the charge and the spin of electrons (spintronics) [1]. Although intrinsic semiconductor transition metal dichalcogenides (TMDs) are very attractive optoelectronic two-dimensional (2D) materials, they are not magnetic. Different strategies such as defect engineering and magnetic chemical doping have been used to induce long-range magnetic ordering in 2D-TMDs [2]. As an alternative route, here we present a novel hybrid heterostructure, composed of monolayer TMDs (MoSe₂ and WSe₂) covered with a thin overlayer of V₂O₅. Even if the individual materials are not magnetic or weakly magnetic, their combined heterostructure presented enhanced roomtemperature long-range magnetic order, suggesting the

presence of an interface-induced magnetism that has been rarely observed experimentally [1]. The TMD samples were grown by CVD, while the V₂O₅ thin films were deposited in a high-vacuum thermal evaporator. The samples were characterized by Atomic Force Microscopy (AFM), Photoluminescence (PL) and Raman spectroscopies, XPS, VSM and MFM. The coercive field and magnetization vs. temperature and magnetic field orientation (in-plane and out-of-plane) were studied for different V₂O5 film thicknesses. The TMDs photoluminescence in the hybrid structure presents anisotropic peak shape toward lower energies consistent with an increment in trion population. These results are in line with our first-principles calculations of V₂O₅ nanoclusters on TMDs surfaces, suggesting that a charge transfer mechanism at the heterointerface produces a spin redistribution that induces the observed enhanced magnetism in the hybrid system [1]. The synthesis process is compatible with the use of shadow masks, allowing the creation of on-demand 2D structures that laterally connect magnetic and non-magnetic domains.

1] W. Zhang, L. Zhang, P.K.J. Wong, J.R. Yuan, G. Vinai, P. Torelli, G. van der Laan, Y.P. Feng, and A.T.S. Wee, "Magnetic Transition in Monolayer VSe $_2$ via Interface Hybridization," ACS Nano, 13(8), 8997–9004 (2019)

[2] D.L. Duong, S.J. Yun, Y. Kim, S.G. Kim, and Y.H. Lee, "Long-Range Ferromagnetic Ordering in Vanadium-Doped WSe₂ Semiconductor," Applied Physics Letters, 115(24), 242406 (2019)

FG-03. Mechanistic Insights into Anisotropy and Magnetoresistance Control in Cobalt Ferrite Thin Films by Swift Heavy Ion Irradiation

R. Charak¹, <u>S. Gautam</u>^{2, 3}, S. Garg², R. Meena⁴, Y. Kim⁶, K. Chae⁵

¹Energy Research Center, Panjab University, Chandigarh, India, ²Department of Physics, Panjab University, Chandigarh, India, ³Advanced Functional Materials Lab Pvt. Ltd, Panjab University, Chandigarh, India, ⁴Materials Science Centre, Inter University Accelerator Centre, New Delhi, India, ⁵Advanced Analysis & Data Center, Korea Institute of Science and technology, Seoul, Korea (the Republic of), ⁶Pohang Accelerator Lab, Pohang University of Science & Technology, Pohang, Korea (the Republic of)

Swift heavy ion (SHI) irradiation is a highly effective method for defect engineering and modulation of magnetic

properties in ferrimagnetic oxide thin films. Cobalt ferrite $(CoFe_2O_4)$, a spinel oxide with high magnetocrystalline anisotropy and strong spin - orbit coupling, exhibits a high sensitivity to cation redistribution and lattice strain [1-3]. Prior studies have shown that low-fluence SHI enhances anisotropy via domain wall pinning and strain effects, whereas high-fluence irradiation may induce isotropy due to increased structural disorder and randomization of cationic sites [4-5].

In this study, ~ 70 nm CoFe₂O₄ thin films were irradiated with 200 MeV Ag¹⁴⁺ and 75 MeV O⁵⁺ ions at fluences of $5x10^{11}$ and $5x10^{12}$ ions/cm². X-ray magnetic circular dichroism (XMCD) at the Fe L-edge revealed a 13% enhancement in dichroic intensity (from 0.18 to 0.204) for Ag-irradiated films at the lower fluence, indicating increased Fe³⁺ orbital moment localization and hybridization effects. In contrast, higher fluence and oxygen ion irradiation resulted in reduced XMCD intensity, attributed to spin disorder. XMCD measurements at the Co L_{3,2}-edges showed suppression across all irradiated samples, consistent with Co²⁺ site distortion and cation redistribution [5].

Magnetization studies revealed the highest saturation moment at 70 K, with decreasing values at 150 K and 300 K. Remarkably, the Ag 5x10¹¹ ions/cm² sample exhibited enhanced anisotropy at room temperature, in line with the XMCD observations. These modifications did not compromise the tunneling magnetoresistance (TMR), highlighting the scalability of SHI for device applications. This study affirms SHI as a powerful route to precisely tune anisotropy and magnetoresistance in oxide-based spintronic systems.

- [1] Papamihail, K., et al. "Fe+ ion irradiation induced changes in structural and magnetic properties of iron films." *Nuclear Materials and Energy* 9 (2016): 459-464.
 [2] Enayati, Mahnaz, et al. "The role of oxygen defects in magnetic properties of gamma-irradiated reduced graphene oxide." *Journal of Alloys and Compounds* 784 (2019): 134-148.
 [3] Nongjai, Razia, et al. "Modification of magnetic anisotropy induced by swift heavy ion irradiation in cobalt ferrite thin films." *Journal of Magnetism and Magnetic Materials* 394 (2015): 432-438.
- [4] Thien, Jannis, et al. "Cationic ordering and its influence on the magnetic properties of Co-rich cobalt ferrite thin films prepared by reactive solid phase epitaxy on Nb-doped SrTiO3 (001)." *Materials* 15.1 (2021): 46.
- [5] Moya, Carlos, et al. "Crucial role of the Co cations on the destabilization of the ferrimagnetic alignment in Co-ferrite

nanoparticles with tunable structural defects." *The Journal of Physical Chemistry C* 125.1 (2020): 691-701.

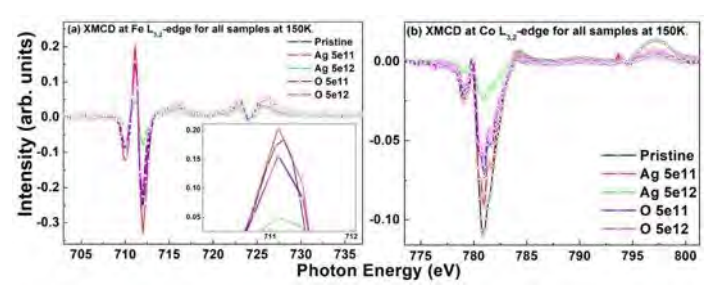


Fig. 1 Irradiation based modification of magnetic properties for cobalt ferrite at 150 K (a) Fe L $_{3,2}$ -edge XMCD spectra showing selective enhancement (0.18 --> 0.204) for Ag $^{+}$ -irradiated samples at 5×10^{11} ions/cm 2 , contrasting with defect-mediated suppression at higher fluences and O-ion irradiation. (b) Co L $_{3,2}$ - edge XMCD spectra reveal universal suppression of intensity across all irradiated samples, indicating irreversible distortion of Co $^{2+}$ octahedral sites.

FG-04. Withdrawn

FG-05. Post-Oxidation Strategy for Reducing Antiphase Boundaries in Spinel Ferrites

<u>H. Yanagihara</u>, K. Takeo, E. Kita *University of Tsukuba, Tsukuba, Japan*

Spinel ferrite thin films grown on MgO (001) substrates tend to develop a high density of antiphase boundaries (APBs) during initial growth, causing magnetic frustration and forming a magnetic "dead layer" near the interface, which degrades magnetic properties [1]. Suppressing APBs is thus crucial for applying spinel-type materials with large unit cells in spintronic devices.

To address this, approaches like epitaxial growth on substrates with the same crystal structure with the film have been explored [2]. In this study, we propose a postoxidation strategy to control cation valence states and reduce APBs in cobalt ferrite (CFO) thin films. CFO was deposited using a Co:Fe = 1:23 alloy target under varying oxygen flows, followed by post-deposition oxidation. CFO films (20-50 nm) were deposited on cleaved MgO (001) substrates using reactive RF magnetron sputtering. Magnetic and structural properties were evaluated by VSM and XRD, respectively. APB density was analyzed via darkfield TEM, and Fe valence states were studied using conversion electron Mössbauer spectroscopy. Post-oxidation was applied to magnetite-like CFO (ML-CFO) grown at 2.0 sccm O₂. Annealing was conducted in situ at 450 °C for 20–60 min in Ar (30 sccm) and O_2 plasma. Process conditions are listed in Table 1. Magnetic hysteresis measurements of 20 nm-thick films showed that post-oxidized CFO (PO-CFO) had increased saturation magnetization, squareness, and coercivity, indicating reduced APB density. As shown in Table 2, TEMbased domain size analysis revealed that PO-CFO exhibited more than double the domain size of the other samples. These improvements are attributed to enlarged magnetic domains and suppressed APBs, likely due to Fe²⁺ oxidation to Fe³⁺, accompanied by cation rearrangement and lattice reconstruction during annealing.

[1] D. T. Margulies et al., Appl. Phys. Lett. 79, 5162 (1997)[2] A. V. Singh et al., J. Appl. Phys. 126, 093902 (2019)

Sample	Preparation process	
γ-Fe2O3 like CFO (GL-CFO)	O2 flow: 4.0 sccm as grown	
Magnetite like CFO (ML-CFO)	O2 flow: 2.0 sccm as grown	
Post oxidized CFO (PO-CFO)	O2 flow: 4.0 sccm post oxidation for MLCFO	

Fig. 1 Sample preparation conditions

Sample	GL-CFO	ML-CFO	PO-CFO
Domain size (nm)	16.0	18.3	38.8

Fig. 2 Anti-phase domain size

FG-07. On the nature of spin reorientation transition thermal hysteresis in AFM/FM bilayers: experiment and phenomenology

M. Slezak¹, E. Swierkosz¹, A. Kwiatkowski¹, M. Szpytma¹, W. Janus¹, M. Zajac², P. Drozdz¹, E. Oles¹, A. Koziol Rachwal¹, T. Slezak¹

¹AGH University of Krakow, Krakow, Poland, ²National Synchrotron Radiation Centre SOLARIS, Jagiellonian University, Krakow, Poland

We report on the temperature driven, in-plane 90 degree magnetization switching of ferromagnetic layer investigated via MOKE, XMC(L)D measurements and supported by phenomenological modeling. The model systems used in this work are AFM/Fe(110) and NM/Fe(110) bilayers epitaxially grown on a W(110), where AFM and nonmagnetic (NM) overlayers were NiO, CoO and Au, Cr, respectively. From the analysis of the temperaturedependent LMOKE loops and XMCD spectra an abrupt switching of the easy axis between the Fe[001] and Fe[1-10] directions as temperature varies, is concluded, see Fig.1 where results for NiO/Fe sample are shown [1]. At ~210 -286 K temperature range there is a thermal hysteresis region where two energy minima (one metastable) coexist at given temperature, see insets in Fig.1a. Complementary simulation (solid line), incorporating temperaturedependent anisotropy constants, successfully reproduce the key features of this process, most importantly the temperature driven hysteresis of magnetization switching. Exemplary results of modelling, including the free energy density landscape spanned across magnetization angletemperature, two-dimensional space is shown in Fig.2. Our

results not only provide a clear picture of the temperature driven SRT phenomenon in FM and AFM/FM thin films but also offer insight into temperature control of magnetic state of these systems. Thermal hysteresis of SRT in exchange biased (EB) CoO/Fe and in EB-free NiO/Fe will be compared and disscussed.

[1] E. Swierkosz,..., M. Slezak, Scientific Reports (2025) accepted

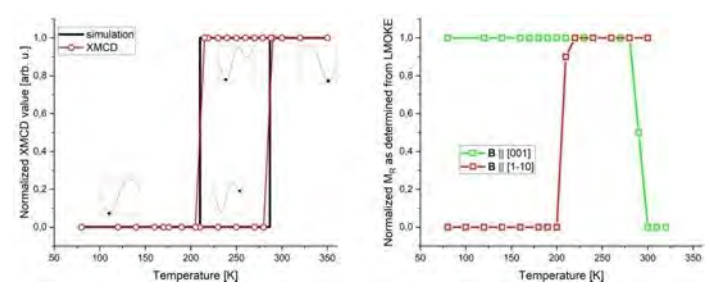


Fig. 1 (a) XMCD results with simulated thermal hysteresis for NiO/Fe. (b) LMOKE results obtained with external magnetic field oriented along two specific in-plane directions.

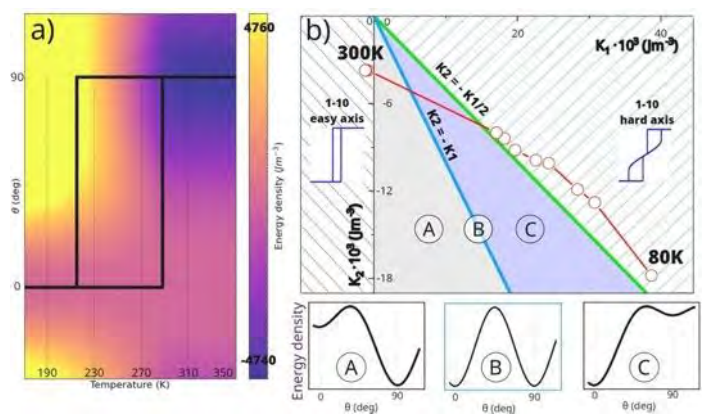


Fig. 2 Simulated free energy density spanned across the two-dimensional angle- temperature (a) and $K_1(K_2)$ in-plane magnetic anisotropy space (b) for NiO/Fe system.

FG-08. Plasma-Treated Perpendicular Magnetic Anisotropy in Sub-Nanometer W/CoFeB/MgO for BEOL Integration G. Hong¹, J. Park¹, J. Pyo¹, J. Yoo¹, S. Lee¹, B. Kang¹, J. An¹, B. Ham¹, J. Choi¹, J. Lee², J. Kwon², S. Ahn¹, R. Baek¹ Department of Electrical Engineering, POSTECH, Pohang, Gyeongbuk, Korea (the Republic of), ²AVP Division, Hyundai Motor Company, Hwaseong, Gyeonggi, Korea (the Republic of)

Perpendicular magnetic anisotropy (PMA) in nonmagnetic transition metal (NM)/CoFeB/MgO heterostructures has

attracted significant attention for the development of highdensity and energy-efficient spintronic devices [1]. In such structures, the NM/CoFeB interface plays a critical role in inducing PMA by providing a structural template and influences spin-orbit interactions [2]. To preserve clean and well-defined interfaces, which are essential for establishing PMA, a continuous in-situ process from the seed to the capping layer is typically required. However, this strict requirement limits process flexibility and poses challenges to integration for CMOS BEOL processes. Here, we introduce a novel process technique that enables robust plasmatreated PMA (pPMA) without the continuous in-situ process for NM deposition. The pPMA stacks were fabricated by applying surface plasma treatment to a sputtered W layer, followed by the deposition of CoFeB/MgO/Ta without vacuum breaking. As shown in Fig. 1, pPMA was observed in the CoFeB layer with a thickness of 5 to 10 Å, indicating that the W/CoFeB interface remains magnetically stable even at sub-nm thickness. Notably, PMA was retained in the pPMA stack even when the W layer was exposed to air, whereas PMA was absent in the pristine stack. Fig. 2 shows cross-sectional TEM images of the pristine and pPMA stack. The pPMA stack exhibits a significantly smoother surface and well-defined [100] MgO crystallinity compared to the pristine stack. This suggests that the plasma treatment reduces defects and roughness of the W surface, thereby enhancing chemically interfacial bonding with the CoFeB layer. To verify this, we conducted additional XPS analysis, which confirmed the formation of a cleaner and chemically stable W/CoFeB interface. Overall, the proposed process represents a promising strategy for BEOL-compatible fabrication of PMA-based spintronic devices. [1] S. Ikeda et al., Nat. Mater., Vol. 9, p. 721-724 (2010). [2] S. Peng et al., Adv. Electron. Mater., Vol. 5, 1900134 (2019).

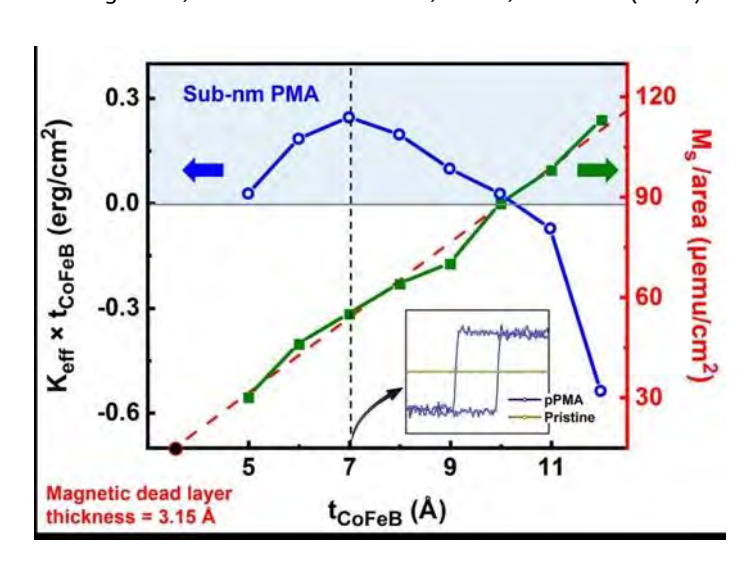


Fig. 1. Saturation magnetization (M_s) and effective magnetic anisotropy constant (K_{eff}) as a function of CoFeB thickness in pPMA stacks. Inset: M-H loops of the pPMA and pristine stack.

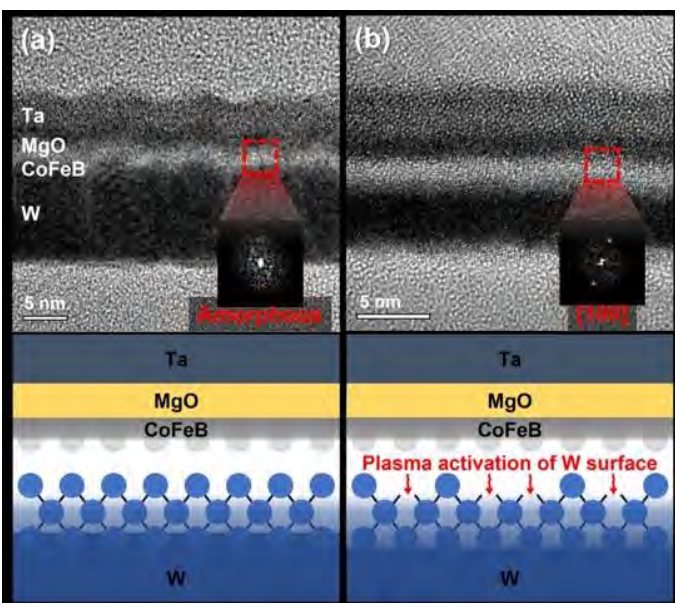


Fig. 2. Cross-sectional TEM images, corresponding FFT analyses, and schematic structures of the (a) pristine and (b) pPMA stack.

FG-09. Growth and Characterization of β -Mn Structured CoZn Thin Films

M. Dearg^{1, 2}, S. Langridge³, G. Burnell¹, <u>C. Marrows</u>¹
¹University of Leeds, Leeds, United Kingdom, ²University of York, York, United Kingdom, ³STFC Rutherford Appleton Laboratory, Didcot, Oxon., United Kingdom

Thin films of polycrystalline β-Mn structure CoZn have been grown on thermally oxidized Si substrates by co-sputtering from elemental targets followed by annealing. A range of films grown with variable Co deposition power and fixed Zn deposition power were produced, so as to vary the proportions of the two elements reaching the substrate. Whilst all films exhibited a (221) β-Mn structure CoZn texture in X-ray diffraction and possessed a ZnO cap, transmission electron microscopy showed that Zn-rich compositions contained large voids. CoZn films deposited at sputter power ratios tuned to give the optimal volume fraction (around 36:25 W Co:Zn) of β-Mn were continuous, with crystallites up to 200 nm in size (Fig. 1). Magnetic measurements show that such optimal CoZn films have a Curie temperature $T_{\rm C} \sim 420~{\rm K}$ and saturation magnetization of 120 emu/cm³, properties close to those reported for bulk crystals (Fig. 2). The Bloch law exponent α and critical exponent β are close to the ideal valies of 3/2 and 1/2. Excess Co beyond this point leads to a significant retained ferromagnetism above the Curie point of the CoZn, suggesting Co-rich aggregates. The β-Mn structure is chiral (P4₁32/P4₃32 space group) and is known to give rise to a Dzyaloshinkii-Moriya interaction (DMI) that stabilizes roomtemperature skyrmions in the bulk [1]. Our thin films [2] are thus a potential materials platform, compatible with planar processing technology, for magnetic skyrmions arising from a bulk DMI.

[1] Y. Tokunaga, X. Z. Yu, J. S. White, H. M. Rønnow, D. Morikawa, Y. Taguchi, and Y. Tokura, Nat. Commun. 6, 7638 (2015).

[2] M. Dearg, S. Langridge, G. Burnell, and C. H. Marrows, Phys. Rev. Mater. (at press).

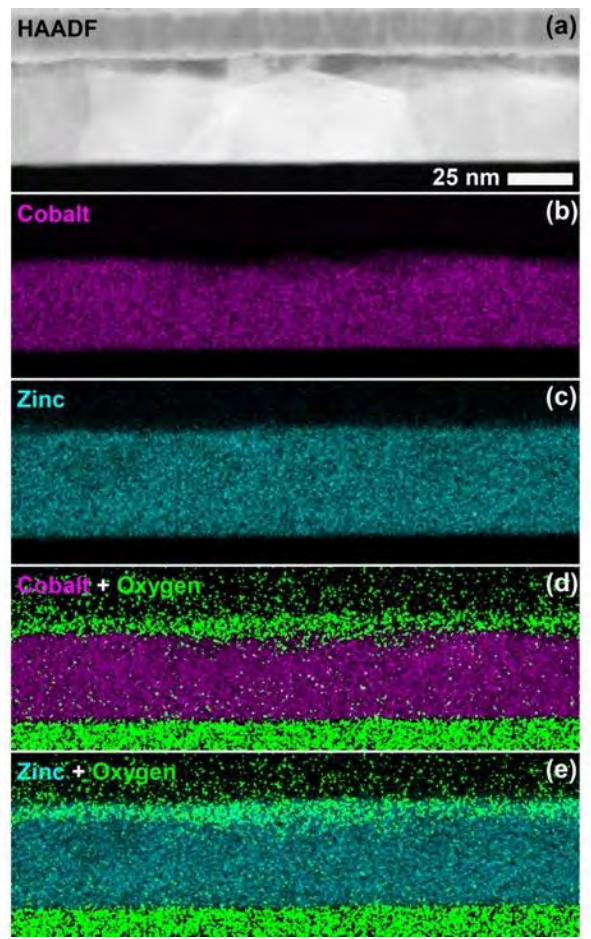


Fig. 1. STEM/EDXS analysis of an annealed 36:25 W Co:Zn alloy sample. (a) HAADF-STEM image of EDXS scan region. (b) Cobalt element signal. (c) Zinc element signal. (d) Oxygen element signal superimposed over Co. (e) Oxygen element signal over Zn.

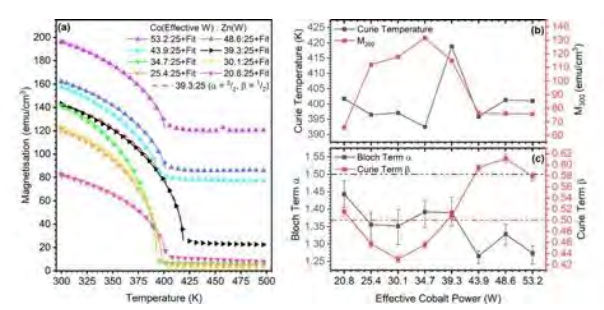


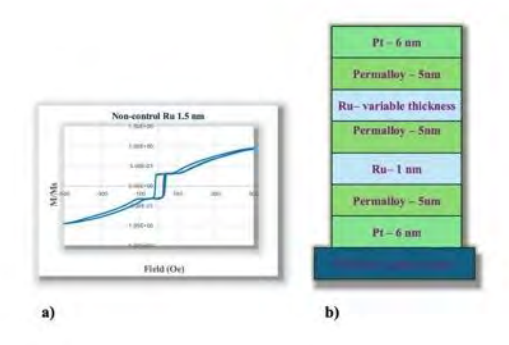
Fig. 2. Temperature dependent magnetic measurements. (a) M(T) results for the CoZn films deposited at effective growth power ratios of 20.8-53.2:25 W Co:Zn. Data points represent experimental results, the solid line shows the result of fitting. (b) $T_{\rm C}$ and $M_{\rm 300}$ versus composition. (c) Empirical Curie-Bloch fitting exponents α and β versus composition.

FG-10. Utilizing a synthetic exchange bias effect to measure ferromagnetic interlayer interactions

<u>I. Hatala</u>, E. Stimpson, J. Sklenar Physics, Wayne State University, Detroit, Michigan, United States

The exchange bias phenomenon is typically attributed to the exchange coupling occurring at the interfaces between ferromagnetic and antiferromagnetic layers. In this study, we introduce a novel manifestation of exchange bias in synthetic antiferromagnet/ferromagnet heterostructures. The structures that we grow are made from three permalloy magnetic layers with two nonmagnetic Ru spacers between them. The thickness of one Ru spacer layer promotes ferromagnetic interactions while the other Ru spacer layer promotes antiferromagnetic interactions between neighboring permalloy layers. This asymmetric trilayer structures, inspired by the exchange bias effect, creates non-collinear magnetization configurations when an external field is applied. This allows experimentalists to measure the strength of the ferromagnetic RKKY interaction with magnetometry. Thus, we demonstrate a new method for measuring ferromagnetic interlayer exchange interactions. In this work, we apply this method to measure the ferromagnetic RKKY interaction mediated by both Ru, RuCo alloy interlayers. By combining these measurements with traditional measurements that measure the antiferromagnetic RKKY interaction [1], we can build a more complete understanding on how the RKKY interaction varies as a function of the thickness of the interlayer. IH and JS acknowledge support from the National Science Foundation under DMR-2328787.

[1] MM Subedi, K Deng, B Flebus, J Sklenar. Journal of Physics: Condensed Matter 36, 375802 (2024).



- a) Magnetometry measurements for trilayer samples with a 1 and 1.5 nm Ru layer thickness.
- b) Represents the sample structure for exchange biased synthetic antiferromagnet.

FG-11. Low-temperature T-ALD HfO₂ for magneto-ionic applications

<u>A. Cataldo^{1, 2}, D. Gouéré³, E. Monteblanco³, D. Ravelosona³, A. Li Bassi⁴, A. Lamperti¹</u>

¹CNR-IMM, Agrate Brianza, Italy, ²Department of Chemistry, Materials and Nanotechnology, Politecnico di Milano, Milan, Italy, ³Spin-Ion Technologies, Palaiseau, France, ⁴Department of Energy, Politecnico di Milano, Milan, Italy

Hafnium dioxide (HfO₂) is a high-k dielectric oxide widely explored for applications in advanced CMOS, neuromorphic, and magneto-ionic devices, owing to its dielectric constant, wide bandgap, and compatibility with Si technologies [1-2]. Among the deposition methods, atomic layer deposition (ALD) offers thickness control, conformality, and atomic-level tunability [3]. However, the integration of HfO₂ with magnetic materials requires low-T processing to avoid interfacial degradation and preserve magnetic properties [4-5]. In this work, we investigate the growth of HfO₂ via thermal ALD using TEMAHf and H₂O from 200 °C to 100 °C, focusing on the effect of growth temperature on physical, chemical and electric properties.

Growth-per-cycle increases from 0.82 Å/cy (200 °C) to 1.10 Å/cy (100 °C). XPS measurements confirm a consistent Hf⁴⁺ chemical state, while O/Hf atomic ratio at high thicknesses decreases from 1.98 (200 °C) to 1.85 (100 °C) (Fig.1). ToF-SIMS shows an increasing incorporation of -OH and -CN groups below 125 °C. C-V measurements report a dielectric constant K \approx 17 \pm 1 across the investigated temperature range. while breakdown voltage analysis shows that low T processes deeply affects the conductive behaviour of HfO₂ and the dielectric breakdown, proving that low-T HfO₂ has the operativity window for magnetoionic devices (Fig. 2).

These findings outline a clear relationship between deposition temperature and film quality, for achieving a high-quality HfO_2 suitable for magneto-ionic and low-power neuromorphic applications. Results from first attempt of T-ALD HfO_2 integration in CoFeB-based stacks reveal a change in coercivity and magnetic saturation evidencing a magneto-ionic mechanism at place.

Financial support from European Union through Horizon Europe EIC Pathfinder METASPIN project (Grant n. 101098651) is acknowledged.

[1] W. Banerjee, A. Kashir and S. Kamba, Small, 18(23), (2022).

[2] M.A. Zidan, J.P. Strachana and W.D. Lu, Nature Electronics, 1(1), pp. 22–29, (2018).

[3] H.A. Hsain, Y. Lee and M. Materano, Journal of Vacuum Science & Technology A, 40(1), (2021).

[4] M. Nichterwitz, S. Honnali and M. Kutuzau, APL Materials, 9(3), (2021).

[5] J. de Rojas, A. Quintana and A. Lopeandía, Advanced Functional Materials, 30(36), (2020).

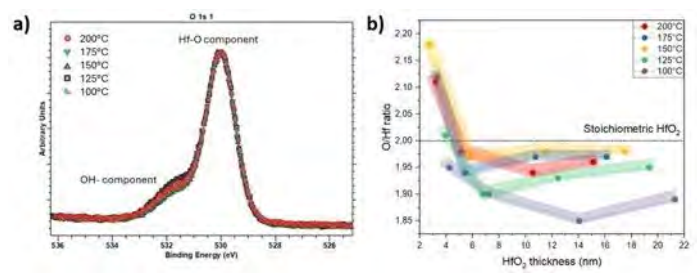


Figure 1 – Panel a) shows the overlapping of O – 1s spectra of HfO_2 grown at 200, 150 and 100°C. Panel c) shows calculated stoichiometry vs HfO_2 thickness over the investigated temperature range.

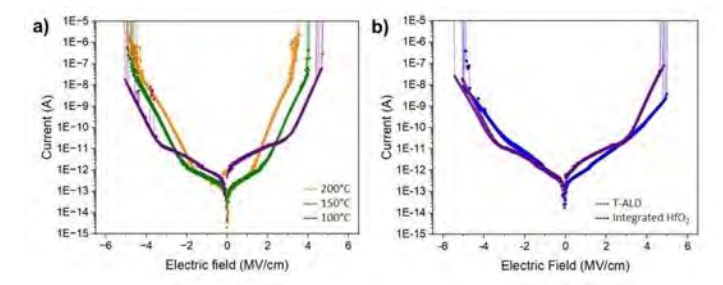


Figure 2 - Panel a) shows I-E curves of HfO_2 based MIMs grown at 200,150 and 100°C. Panel b) shows a comparison between I-E curves of T-ALD HfO_2 and device-integrated HfO_2 .

FG-13. Engineering strong perpendicular magnetic anisotropy in Cu-buffered Co/Pt multilayers grown by moderate vacuum e-beam deposition

<u>J. Porro^{1, 2}, D. Doménech¹, A. Villar¹, C. Redondo³, N. Río-López^{1, 3}, R. Morales^{3, 1, 2}</u>

¹BCMaterials, Bilbao, Spain, ²Ikerbasque, Bilbao, Spain, ³Physical Chemistry, University of the Basque Country, UPV/EHU, Leioa, Spain

Perpendicular magnetic anisotropy (PMA) is fundamental for high-density spintronic, magneto optical, and neuromorphic

devices [1]. While Co/Pt multilayers with strong PMA are traditionally fabricated by ultra-high vacuum sputtering and numerous repeats, we introduce a more accessible method using electron beam (ebeam) evaporation at moderate vacuum conditions.

Our study demonstrates that a Cu buffer layer underlies the success of this method: it induces strong (111) texture in ultrathin [Co/Pt] stacks, enabling full loop squareness and tunable coercivity via Cu and Pt thickness adjustment. Polar MOKE microscopy reveals clear domain contrast even for sub nm Co layers, and adding a second repetition compensates for MOKE signal loss while maximizing effective anisotropy [2].

Structural analysis confirms high crystalline quality and consistent texture (Fig.1). MOKE and vibrating sample magnetometry measurements yield effective anisotropy constants and sharp perpendicular switching comparable to sputtered multilayers [3]. Thermal annealing up to 200 °C preserves PMA, reflecting robust material stability (Fig.2). These properties of our multilayers align with studies of similar materials grown by sputtering deposition [4,5]. Moreover, non-conformal ebeam evaporation has begun to emerge as a favorable deposition technique in moderate vacuum settings.

In summary, we validate that moderate vacuum ebeam evaporation with Cu buffer engineering can achieve Co/Pt films exhibiting PMA and MOKE performance comparable to ultra high vaccuum sputtered samples. Its non conformal geometry supports advanced lithographic processes, reduces layer count and vacuum requirements, and offers a scalable route to next-generation magnetic heterostructures for spintronic and magneto-optical applications.

- [1] Lee, J. S. et al., Appl. Phys. Lett. 113, 103104 (2018).
- [2] Doménech, D. et al., APL Mater. 13, 061110 (2025).
- [3] Cestarollo, L. *et al.*, *J. Magn. Magn. Mater.* 562, 169825 (2022).
- [4] Du, Y. et al., AIP Adv. 10, 105010 (2020).
- [5] Kang, H. et al., J. Appl. Phys. 126, 133901 (2019).

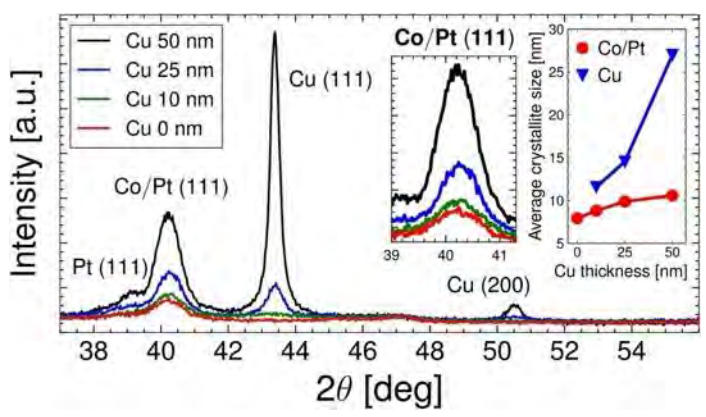


Fig. 1 XRD patterns of e-beam evaporated ultra-thin films of $Cu(t_{Cu})/Pt(4)/Co(0.6)/Pt(5)$ (units in nm). Left inset: zoomed Co/Pt (111) peak. Right inset: estimated average crystallite size of the Co/Pt stack and the Cu buffer using the Scherrer equation and their respective (111) XRD peaks.

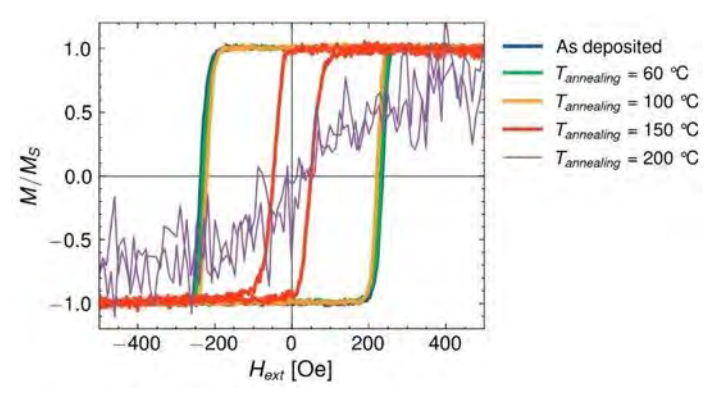


Fig. 2 Normalized polar MOKE hysteresis loops of Cu(10)/Pt(1)/Co(0.6)/Pt(2) after 1h annealing steps in ambient atmosphere at different temperatures.

SESSION FP: SHIELDING AND LEVITATION / STRUCTURED MATERIALS, NANOPARTICLES, AND NANOCOMPOSITES (POSTER SESSION)

Chair(s): S-M. Ahn, POSTECH, Pohang, Korea (the Republic of)
Thursday, October 30, 2025
02:30 PM-05:30 PM
Exhibit Hall Posters

FP-01. Experimental Evaluation of an Active Magnetic Shielding System with a Moving Phantom

X. Cao, T. Zhu, S. Chikaki, M. Sekino Graduate School of Engineering, The University of Tokyo, Tokyo, Japan

Wearable optically pumped magnetometers (OPMs) have relaxed the constraints on subject movement in MEG recordings [1]. However, in non-uniform magnetic fields, sensor displacements will introduce artifacts that degrade signal stability [2]. To cancel these motion-induced artifacts, we developed an active magnetic shielding system capable of adapting to real-time sensor motion, and assessed its effectiveness through controlled phantom experiments. In this study, we built a shielding system combining a magnetic field coil array, a dry phantom with dual-axis OPMs (QuSpin), an optical tracking system (OptiTrack), and a LabVIEW-based controller (Figure 1). The eight coils are arranged to produce three homogeneous and five gradient field components. The phantom and sensors were fixed to a rigid platform and its position and orientation are continuously tracked. The controller uses this pose data to update field mappings and output coil currents via a DAQ device.

As the platform moves, the mapping between coil current and local field at each sensor changes. The conventional approach estimates this mapping via spatial numerical integration, typically requiring ~25 ms per update [3]. We use a precomputed multipole expansion model to compute the mapping matrix algebraically, reducing the update time to ~8 ms.

We performed static tests at different platform poses and dynamic tests by manually moving the platform. Data were filtered and epoch-averaged (Figure 2). In the static condition, processed signals showed clear phantom responses across all tested poses. During movement, low-frequency drift and signal saturation appeared in multiple channels when shielding was disabled. In contrast, with active shielding enabled, magnetic disturbances were suppressed within ±1 nT. The processed waveforms remained discernible even under motion (Figure 2b),

indicating effective suppression of motion-related field changes and preservation of target signals.

[1] E. Boto, N. Holmes and J. Leggett et al., Nature, Vol. 555, p. 657 (2018)

[2] S. Mellor, T. M. Tierney and G. C. O'Neill et al., IEEE Trans. Biomed. Eng., Vol. 69, p. 528 (2022)

[3] N. Holmes, M. Rea and R. M. Hill et al., NeuroImage, Vol. 274, p. 120157 (2023)

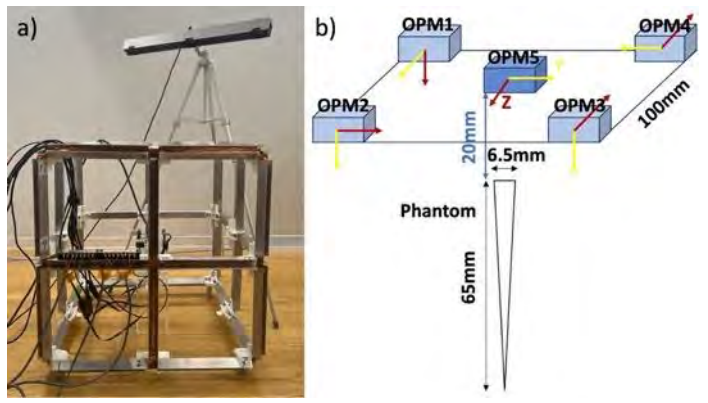


Fig. 1. a) The active shielding coil system. b) The configuration of the dry phantom experiment. OPM1 – OPM4 are reference sensors. OPM5 is for measurement.

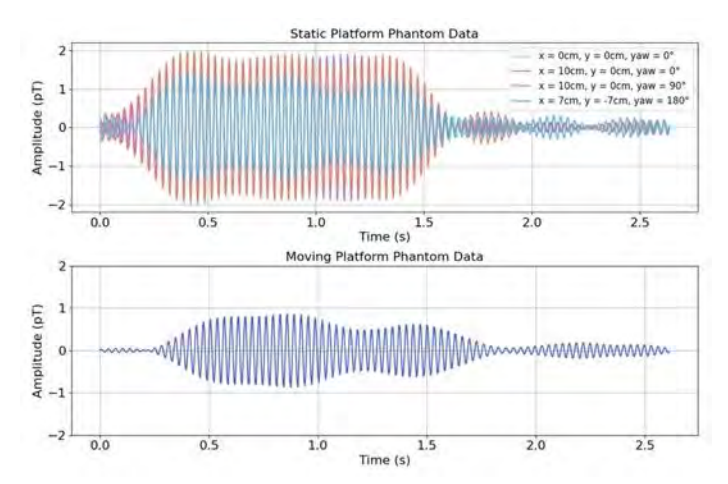


Fig. 2. Processed signals of OPM5 when the phantom was static with varying platform positions and orientations and manually moved.

FP-02. Penetration of Magnetic Field by Long Cables into a Slot on Conducting Plate and Rectangular Enclosure J. Kwon¹, H. Park²

¹Electronics and Telecommunications Research Institute, Daejeon, Korea (the Republic of), ²The University of Suwon, Hwaseong, Korea (the Republic of)

Electromagnetic coupling through apertures such as slots is a key issue in EMI/EMC analysis, especially regarding the interaction between slots and nearby conductors. Early studies primarily focused on how external fields couple through slots in an infinite conducting plate to long and infinite-length wires or cables behind it, often using the integro-differential equations and method of moment [1]. Low-frequency common-mode currents on cables can also act as noise sources that couple through slots and radiate or penetrate into adjacent spaces, posing critical system-level EMI/EMC challenges [2]. While high-frequency coupling has been extensively studied, low-frequency current coupling through slots is relatively underexplored.

This paper analyzes low-frequency current coupling through slots using a two-dimensional (2D) model shown in Fig. 1. A quasi-static magnetic field solution is derived using 2D Green's function and vector magnetic potentials for a semiinfinite plane with Fourier transform and mode-matching [3]. The method extends to low-frequency noise magnetic field penetration from external cables into slotted enclosures (Fig. 1(b)). Fig. 2 shows the vector magnetic potential in region (I) as a superposition of the Green's function for a point current source and a Fourier integral representing the slot. Potentials in regions (II) and (III) use Fourier series for closed regions and integrals for open regions. Magnetic fields are calculated from these, applying continuity and orthogonality conditions to solve coupled mode coefficient equations. Though simplified as 2D, the model approximates practical long cable and slotted enclosure scenarios well. It converges quickly with tens of modes, reducing computation and enhancing physical insight versus conventional methods. Validation against 3D full-wave simulations confirms its accuracy [4].

- 1. K. R. Umashankar and J. R. Wait, "Electromagnetic coupling to an infinite cable placed behind a slot-perforated screen," IEEE Trans. Electromagn. Compat., vol. 20, no. 3, pp. 406-411, Aug. 1978.
- 2. H. Heydari, V. Abbasi, and F. Faghihi, "Impact of switching-induced electromagnetic interference on low-voltage cables in substations," IEEE Trans. Electromagn.

Compat., vol. 51, no. 4, pp. 937 – 944, Nov. 2009. 3. H. J. Eom, "Electromagnetic Wave Theory for Boundary-Value Problems: An Advanced Course on Analytical Methods," Berlin, Germany: Springer, 2004 4. CST Studio Suite (2022) [Online]. Available: https://www.3ds.com/products/simulia/cst-studio-suite

This work was supported by Institute of Information & communications Technology Planning & Evaluation (IITP) grant funded by the Korea government (MSIT) (No. RS-2025-02642985, Development of Identification, Protection, and Detection Technologies for High-Power Electromagnetic Pulse Protection)

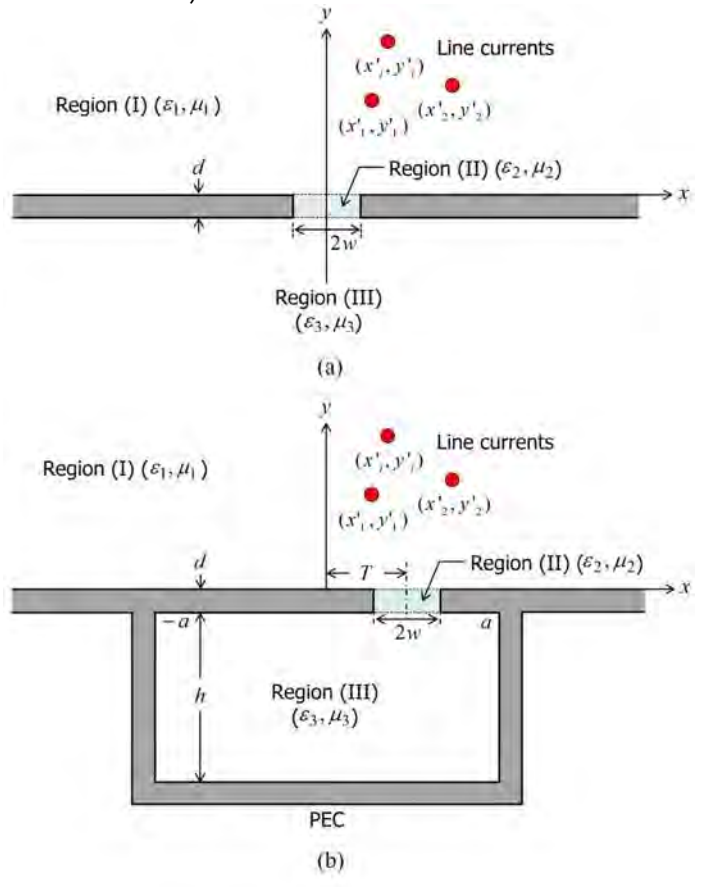


Fig. 1 Configurations of low-frequency magnetic field interference by long cables into a slot on a conducting plate (a) and a rectangular enclosure (b).

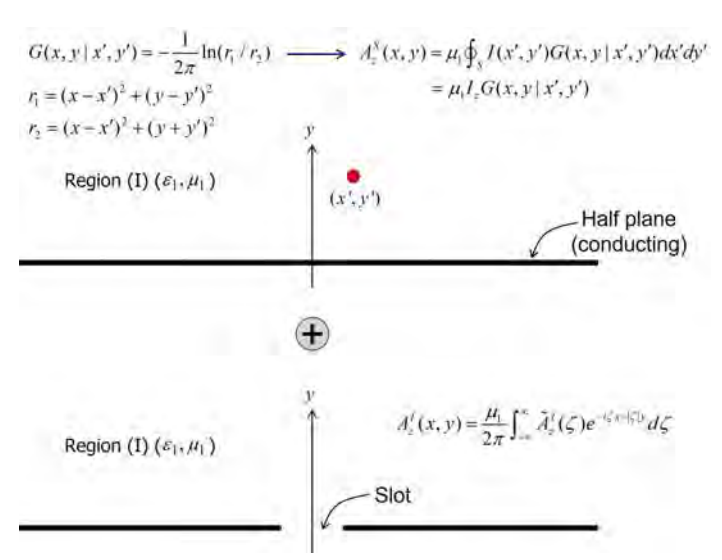


Fig. 2 Vector magnetic potential in Region (I) expressed by superposing the Green's function for the current-carrying long cable and the Fourier integral for the slot effect.

FP-03. Advancing PM Motor Sustainability Through Rapid Computational Evaluation of Alternative Magnet Materials

A. Baghel, I. Nlebedim

Division of Critical Materials, Ames National Laboratory, Ames, Iowa, United States

The growing demand for efficient and sustainable energy solutions is driving innovation in permanent magnet (PM) motor technologies. However, the dependence on critical rare-earth elements in conventional PMs, such as NdFeB, raises concerns over supply chain security and environmental sustainability. This has prompted increasing interest in alternative magnet materials composed of non-or less-critical elements [1-2].

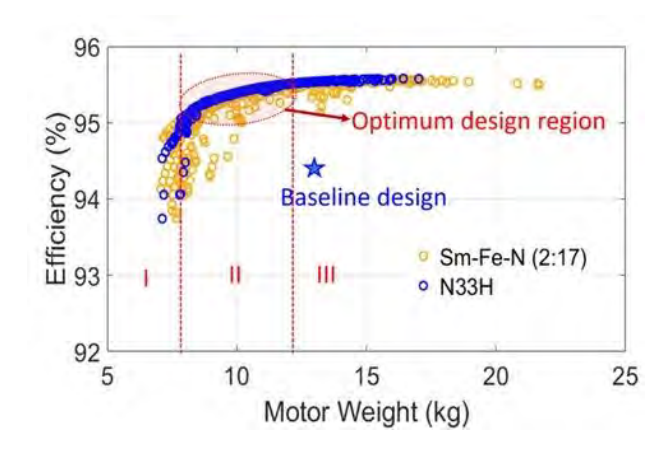
These alternative magnets often exhibit varying magnetic characteristics posing unique design and performance challenges for motor engineers. The development of a computational framework for the rapid evaluation of sustainable magnet materials in PM motors is critical for determining their capability to achieve performance parity with conventional materials under demanding operating conditions [3]. A hybrid approach integrating a recently developed analytical motor modeling framework [4] with multi-objective optimization is employed to evaluate the feasibility of SmFeN magnets as a viable alternative to NdFeB (N33H) in a commercial 5.17 kW, 3000 rpm servo motor (M718), as depicted in Fig. 1.

The developed computational tool enables rapid evaluation

^{*} Best Student Presentation Finalist / LB – Late-breaking Poster

of newly engineered magnetic materials and supports a broad spectrum of design configurations, offering enhanced flexibility and efficiency for electric motor designers. The study aims to support the development of more sustainable magnet technologies and facilitate their integration into advanced PM motor systems, with potential applications in electric vehicles, renewable energy, and other sustainability-driven domains.

- 1. G. Delette, *Journal of Magnetism and Magnetic Materials*, Vol. 577, pp. 170768 (2023)
- 2. R. Kuchi, D. Schlagel, T. Seymour-Cozzini, J. Zaikina, and I. Hlova, *Journal of Alloys and Compounds*, Vol. 980, pp.173532 (2024).
- 3. Y. Cen, H. Shen, X. Wang, W. Yongming, and D. Jingjuan, *Energies*, Vol. 17, pp. 4637 (2024)
- 4. A. P. S. Baghel, B. Sai Ram and I. C. Nlebedim, " *IEEE 21st Biennial Conference on Electromagnetic Field Computation* (CEFC), Jeju, Republic of Korea, pp. 1, (2024).



FP-04. A Link Type Haptic Motor with a Pure Magnetic Spring for Enhanced Lifespan and Performance

Y. Oh¹, K. Park¹, D. Xu², S. Hwang¹

¹School of Mechanical Engineering, Pusan National University, Busan, Korea (the Republic of), ²School of Mechatronic Engineering and Automation, Shanghai University, Shanghai, China

With a growing demand for haptic motors with extended lifespan and superior performance, this paper introduces two novel motor designs incorporating a pure magnetic spring. While linear haptic motors with mechanical springs [1,2] are common, they are limited by poor precision and shorter lifespans. This research focuses on the design and analysis of two distinct types of linear haptic motors

featuring pure magnetic springs: one type utilizes rails and steel balls to support the mover, and the other employs a link structure to support the mover (Fig. 1).

The force profile and acceleration are analyzed using the Maxwell stress tensor and an electromagnetic-mechanical coupling method. In the analysis of the link-type motor, the combined effects of x- and z-cogging forces on the mechanical system due to its swing motion are considered. To precisely model the system's dynamics, these forces were decomposed into their tangential and center-axis components. The total force is then calculated as the sum of this resultant cogging force and the current force, which consists of both Lorentz and solenoid forces.

Based on the analysis results, the rail structure's inherent constraints prevent z-axis displacement, making its resonant frequency (95.0 Hz) significantly lower than the prototype's [3]. In contrast, the link-type motor's distinctive structure allows for z-displacement, which directly impacts both x- and z-cogging forces. This yields resonant frequency of 160.1 Hz, comparable to the prototype's resonant frequency of 163.5 Hz. Additionally, the link-type motor's acceleration performance was comparable to the prototype's (Fig. 2).

For these reasons, the link-type motor emerges as a more competitive design. Its primary advantage, derived from the non-contact magnetic spring, is a significantly extended lifespan, making it a compelling solution for durable, high-performance haptic applications.

[1] Nam J, Yeon T, Jang G. "Development of a linear vibration motor with fast response time for mobile phones." Microsystem technologies, vol.20,pp.1505-10, Aug 2014. [2] Jiang, Z.X., Park, K.H. and Hwang, S.M. "Design and Analysis of Novel Low-Cost Linear Vibration Motor for an Electronic Cigarette." Applied Sciences, vol.10, No. 24, pp.8915, Dec 2020.

[3] Jiang, Z.X, Park, J.H, Xu, D.P, and Hwang, S.M. "Analysis Method Development of Hybrid Linear Motor Considering Cogging Force Effect." In Actuators MDPI, vol. 12, No. 3, pp. 99, Feb 2023.

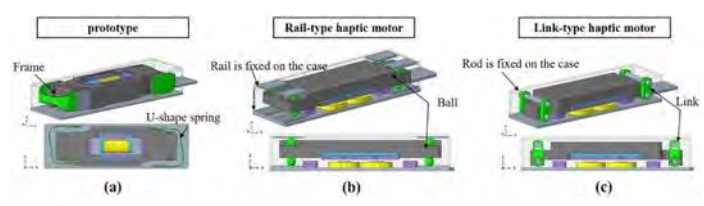


Fig.1 . 3D modeling comparison: (a) prototype, (b) rail-type haptic motor and (c) link-type haptic motor.

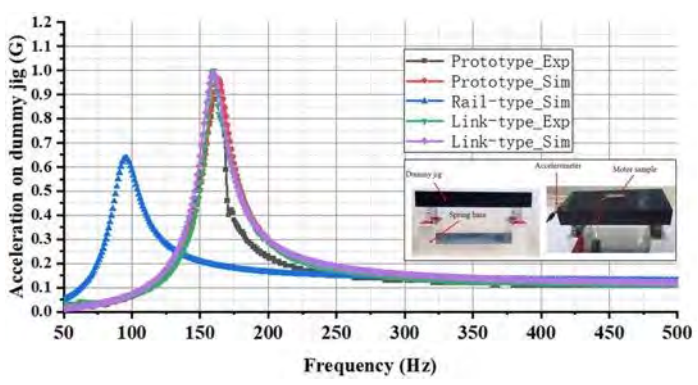


Fig. 2. Acceleration comparison of different haptic motors and the experimental setup.

FP-05. A Railgun Concept for Space Launches and Return Travel from the Moon

M. Trapanese

Dipartimento di Ingegneria, Palermo University, Palermo, Italy

This paper is part of a broader research initiative aimed at exploring innovative electromagnetic launch systems for space missions. In particular, it introduces and begins to develop the concept of a railgun system specifically designed to facilitate the launch of spacecraft from the lunar surface. The idea of electromagnetic space launch has been already proposed. The focus of this initial study is on investigating the fundamental electromagnetic characteristics of such a system, assuming its deployment and operation on the Moon.

The proposed railgun system features a detailed geometric configuration optimized for lunar conditions. The propulsion mechanism is primarily based on the principles of a linear synchronous motor, designed to operate efficiently in the Moon's low-gravity and near-vacuum environment. To minimize mechanical resistance and energy losses due to surface contact, a levitation mechanism is also integrated into the system, significantly reducing frictional forces that could otherwise limit performance and system longevity. An energy assessment is carried out to estimate the total power requirements for launching a vehicle of realistic mass and dimensions from the lunar surface into orbit or on a trajectory toward Earth. This analysis includes a comparative evaluation of two propulsion technologies: the superconducting linear synchronous motor and the permanent magnet synchronous motor. The findings suggest that, due to the Moon's unique environmental conditions—such as the absence of atmospheric drag and reduced thermal dissipation needs—it may be technically

and economically viable to rely on non-superconducting, permanent magnet-based solutions, which are simpler to maintain and implement.

In conclusion, the results obtained from preliminary simulations and calculations are summarized, offering a baseline for determining key design parameters. These findings will serve as the foundation for future phases of the project, which will include more detailed modeling, system integration strategies, and potential applications for both lunar surface-to-orbit transport and future Earth-return missions.

[1] Ian R. McNab, "Launch to Space With an Electromagnetic Railgun", *IEEE Transactions on Magnetics*, VOL. 39, NO. 1, January 2003

FP-06. Asymmetric Magnetization Switching Behavior in FeRh/NiFe Bilayers with Interplay of Competing Exchange Interactions

J. Ahn, M. Jung

Department of Physics, Sogange University, Seoul, Korea (the Republic of)

Magnetic materials with complex phase transitions and interfacial interactions are interesting for advancing spintronic devices [1, 2]. In particular, bilayer systems composed of these magnetic materials can produce diverse exchange interactions, which may compete or synergize, leading to complex phenomena. Systematic studies on these competing exchange effects are poorly understood. This work investigates FeRh/NiFe bilayers to elucidate these mechanisms.

FeRh is a material known for its phase transition at approximately 370 K, transitioning from an antiferromagnetic (AFM) phase at low temperatures to a ferromagnetic (FM) phase at higher temperatures [3]. By adjusting the stoichiometric ratio of FeRh, we achieved an AFM-FM mixed phase, where residual FM moments exist even in the AFM phase of FeRh [4]. Thereby, one can expect intriguing phenomena coming from the two different exchange interactions of AFM-FM and FM-FM in FeRh/NiFe(FM) bilayer system. In this work, we investigated the magnetic properties of FeRh/NiFe bilayers and observed very asymmetric magnetic hysteresis loop with one-step switching in the field-cooled (positive) direction and twostep switching in the negative direction. This asymmetric switching behavior could be understood by the competition between AFM-FM and FM-FM exchange interactions. When the field was swept in the positive-to-negative direction, the

FM moments of FeRh layer first switched and then the FM moments of NiFe layer switched, resulting in two-step switching behavior. This is attributed to the strong exchange bias effect between AFM of FeRh layer and FM of NiFe layer. In contrast, when the field was swept in the opposite direction, only one-step switching behavior was observed. This can be interpreted as a consequence of the strong exchange spring effect between FM of FeRh layer and FM of NiFe layer. These findings highlight the complex interactions at the interface of magnetic bilayers and suggest a novel strategy for tailoring these properties to meet the specific requirements of potential applications in spintronic devices.

[1] J. Meiklejohn, C. P. Bean, Phys. Rev., 102, 1413 (1956)
[2] E. E. Fullerton, J. S. Jiang, S. D. Bader, J. Magn. Magn.
Mater., 200, 392 (1999)
[3] J. S. Kouvel, C. C. Hartelius, J. Appl. Phys., 33, 1343 (1962)
[4] M.-T. Park, J. Yang, M-H Jung, Appl. Surf. Sci., 655, 159539 (2024)

FP-07. Time-resolved and 3-dimensional vector imaging of magnetic materials with coherent soft x-rays

<u>D. M. Burn</u>, L. Turnbull, A. Walters, S. S. Dhesi *Diamond Light Source, Didcot, Oxfordshire, United Kingdom*

Magnetic ordering in nanostructures and in chiral materials gives rise to interesting phenomenon such as the formation of skyrmions, chiral spin structures, domain and domain walls geometries. These features are a key area of research at the forefront of innovation as they provide potential building blocks for future technological devices for data storage, processing and novel computing applications.

The majority of research to date is based on two-dimensional systems, however, the behaviour in the third dimension promises a wealth of opportunities for scientific advancement and technological development [1]. Techniques are now available for experimental fabrication of structures in 3D, along with readily available theoretical and modelling frameworks, however, full understanding is limited by the availability of suitable experimental techniques to measure such systems in 3D.

Here we will outline an instrument which is currently under development at the Coherent Soft X-ray Imaging and Diffraction (CSXID) beamline at Diamond Light Source. This instrument will be tailored towards exploring the three

dimensional spin structuring in nanoscale quantum materials. We will show how cutting-edge developments in synchrotron technology can provide high resolution 3D imaging using coherent soft x-rays[2] with mechanisms to explore temporal resolution in dynamic time resolved processes[3]. Furthermore, we will show how the imaging can be provided along with magnetic fields, temperatures and electrical contacts for a wide variety of relevant research.

[1] Fernández-Pacheco et. al., Nat. Comm. 8, 15756 (2017)
[2] X. Shi et.al. Appl. Phys. Lett. 108, 094103 (2016)
[3] Donnelly, C. et. al. Nat. Nanotechnol. 15, 356-360 (2020).

FP-08. Effect of GO incorporation on microwave characteristics of Zn-Co ferrites nanocomposites

M. Dabla¹, S. Kaushik¹, P. Kumar¹, M. Sharma^{1, 2}, <u>B. K. Kuanr</u>¹

¹Special Centre for Nanoscience, Jawaharlal Nehru University,
New Delhi, Delhi, India, ²Department of Physics, Deshbandhu
College, University of Delhi, New Delhi, Delhi, India

In the present work, we investigate the effect of graphene oxide (GO) concentration on microwave properties of $Zn_{0.3}Co_{0.7}Fe_2O_4$ ferrites (wt%=0.0,2.5,5,7.5,10) synthesized via hummer's and ball-milling method, respectively. The prepared nanoparticles were characterized to determine the structural, morphological, compositional, magnetic and electromagnetic properties. Microwave absorption (RL: Reflection Loss) measurements were performed using vector network analyzer (VNA). XRD pattern of Zn-0.3 and Zn_{0.3}-7.5GO matched with the space group of cubic phase as shown in Figure 1(A). SEM images, depict well dispersed and agglomerated particles with layering of GO. The saturation magnetization decreases and coercivity gradually increases with the increase of GO concentration [Figure 1(B)]. Microwave absorption (RL) parameters were measured using VNA in the range (Ku band) 12–18 GHz are shown in Figure 2(A). It shows different wt% of graphene at a fixed thickness of 2.5 mm indicating that graphene oxide incorporation increases the RL values of GO/Zn_{0.3}Co_{0.7}Fe₂O₄ ferrite nanocomposites (NCs). The value of RL reached - 45 dB for Zn_{0.3}-7.5GO NCs. With further increase of GO, RL decreases to -14 dB for $Zn_{0.3}$ -10GO. The best RL value for $Zn_{0.3}$ -7.5GO resulted from best impedance matching (Z_{in}/Z_0) . The quarter wavelength mechanism governs the appearance of RL peaks at various frequencies. Figure 2(B) shows RL as a function of frequency for Zn_{0.3}-7.5GO ferrites at different thicknesses. It

is interesting to note that $Zn_{0.3}$ -7.5GO exhibits a maximum RL peak of - 45 dB at a frequency of 13.71 GHz and thickness of 2.5 mm with effective absorption bandwidth (EAB) 1.91 GHz. Various applications, including shielding, attenuation, and the fabrication of electromagnetic induction-based flexible absorbing sheets, can be achieved by adjusting the thickness and composition of graphene oxide in Zn doped cobalt ferrites, which in turn allows for tuning of RL as well as EAB of the microwave absorbers [1], [2].

[1] A. Mir, M. Qadeer, R. Waqas, and S. N. Khan, "Study of Morphological, Optical and Microwave Properties of Strontium-Doped Cobalt Ferrites," *J. Electron. Mater.*, vol. 49, no. 8, pp. 4801–4808, 2020, doi: 10.1007/s11664-020-08212-9.

[2] M. Kaur and S. Bahel, "Comparative study of Mn2+ and Zr4+ co-substituted Zn-Co spinel ferrites as microwave absorbing materials in Ku (12.4–18 GHz) and K (18-26.5 GHz) frequency bands," *J. Electroceramics*, vol. 52, no. 1, pp. 29–41, 2024, doi: 10.1007/s10832-023-00341-x.

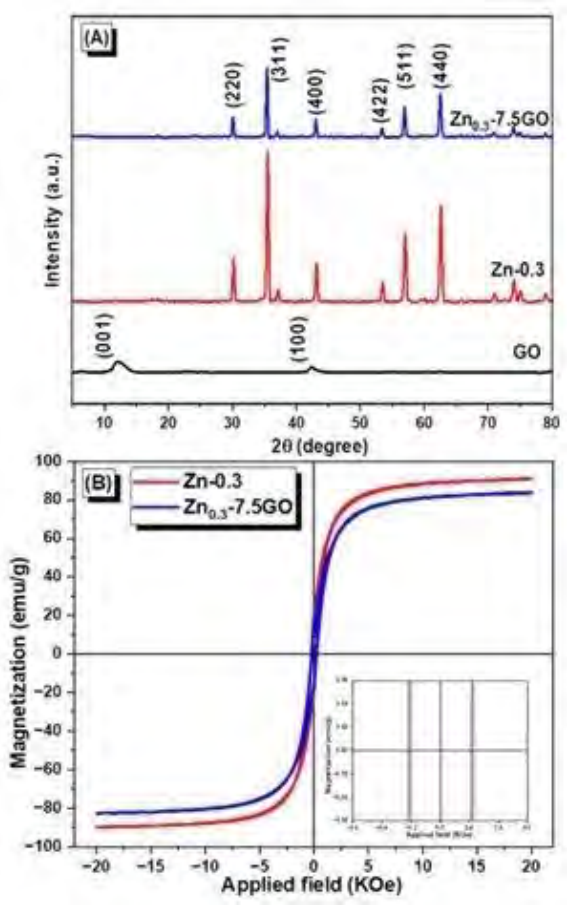


Fig. 1 (A) XRD spectra of GO, Zn-0.3 and Zn_{0.3}-7.5GO (B) Hysteresis loop of Zn-0.3 and Zn_{0.3}-7.5GO

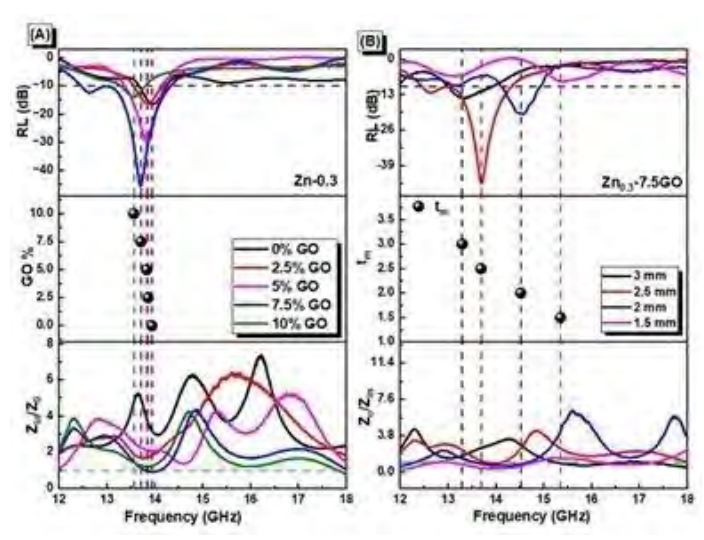


Fig. 2 (A) RL for different wt% of Graphene oxide in $Zn_{0.3}Co_{0.7}Fe_2O_4$ at 2.5 mm thick layer. (B) RL for different thicknesses of $Zn_{0.3}$ -7.5GO nanocomposite.

FP-09. Engineering Next-Generation Magnetic Coupling in Magnetite Core-Shell Nanostructures: The Influence of Advanced Preparation Methods

J. G. Lambe^{3, 1}, M. Gamal^{1, 2}, C. Castaño¹

¹Mechanical and Nuclear Engineering Department, Virginia Commonwealth University, Richmond, Virginia, United States, ²Polymers and Pigments Department, National Research Centre, Cairo, Dokki, Egypt, ³Mechanical Engineering and Physics, Rose-Hulman Institute of Technology, Terre Haute, Indiana, United States

Recent advances in the preparation of magnetite (Fe3O4) core-shell nanostructures have provided unprecedented control over magnetic coupling, positioning these systems as promising candidates for a wide range of magnetic applications. The precise engineering of the interface between the magnetic core and shell is essential for tailoring exchange coupling and for tuning key magnetic parameters, including coercivity, retentivity, and saturation magnetization.

In this study, Fe3O4 nanoparticles with diameters ranging from 30 to 50 nm were prepared using the co-precipitation method. These magnetic cores were subsequently encapsulated with shells of TiO2, CoFe2O4, and NiO. The objective is to establish innovative synthesis strategies for Fe3O4-based core-shell materials with optimized magnetic performance and highly uniform interfaces. Microwave-

assisted synthesis and physical vapor deposition (PVD), specifically sputtering, were utilized to advance conventional approaches, including thermal decomposition and solvothermal synthesis, in the preparation of magnetite core-shell nanostructures.

Comprehensive characterization of the prepared magnetite and core-shell materials was conducted using high-resolution transmission electron microscopy (HRTEM), scanning electron microscopy (SEM), and X-ray diffraction (XRD) to validate enhancements in structure, interface quality, and crystallinity. Additionally, the magnetic properties were assessed through vibrating sample magnetometry (VSM).

FP-10. Fabrication of Fe-B/Epoxy Composite Film via LbL-Assisted Composite Plating Using Silica-Coated Fe-B Particles

<u>T. Nishii</u>¹, I. Tanigawa³, W. K. Tan⁴, H. Muto⁴, Y. Endo¹, M. Izaki², N. Fujita²

¹Tohoku University, Sendai, Miyagi, Japan, ²National Institute of Technology, Nara College, Yamatokoriyama, Nara, Japan, ³Okuno Chemical Industries co., ltd., Osaka, Osaka, Japan, ⁴Toyohashi University of Technology, Toyohashi, Aichi, Japan

In our previous reports, we have demonstrated a novel wet process method for fabricating electromagnetic waveabsorbing thin films. This method, known as layer-by-layer (LbL)-assisted composite plating, is employed to synthesize Fe-B/epoxy composite films, a type of metal-insulator composite thin film [1, 2]. Using this method, charged magnetic ultrafine particles were attracted to the cathode by electrostatic force simultaneously with the deposition of an insulating epoxy thin film. Our findings have shown that coating Fe-B particles with epoxy resin films prevents oxidation during film deposition, which otherwise deteriorates magnetic properties [2].

However, during the epoxy coating process, the Fe-B particles tend to form micro-sized secondary particles, reducing permeability due to eddy current losses. To overcome this issue, in this study, we used silica films fabricated by liquid-phase hydrolysis with ultrasonic agitation to coat the Fe-B particles instead of epoxy films. As shown in Fig. 1, the silica-coated Fe-B particles maintained a monodisperse state with submicron size. Laser scattering particle size analyzer revealed that the silica-coated Fe-B particles exhibited a particle size distribution

centered at 0.2 μ m, indicating that the formation of secondary particles was significantly suppressed. In contrast, the epoxy-coated Fe-B particles showed a size distribution centered around 4 μ m.

Using silica-coated Fe-B particles, we successfully fabricated Fe-B/epoxy composite film with a smooth surface via LbL-assisted composite plating. Fig. 2 shows the complex permeability of the Fe-B/epoxy composite film. The value of μ obtained was 1.5, showing an improvement over previously reported values where μ was 1.3 [2]. Furthermore, broad peaks of μ were observed in the 1-10 GHz range. These results suggest that Fe-B/epoxy composite films can be effectively utilized as electromagnetic wave-absorbing thin films in the GHz band.

[1] N. Fujita, M. Takeuchi, Y. Watanabe, et. al., IEEE Transactions on Magnetics, Vol. 60, No. 4, 2200106 (2024). [2] C. Masumoto, Y. Kumauchi, A. Yokoi, et. al., IEEE Transactions on Magnetics, Vol. 59, No. 11, 2800805 (2023).

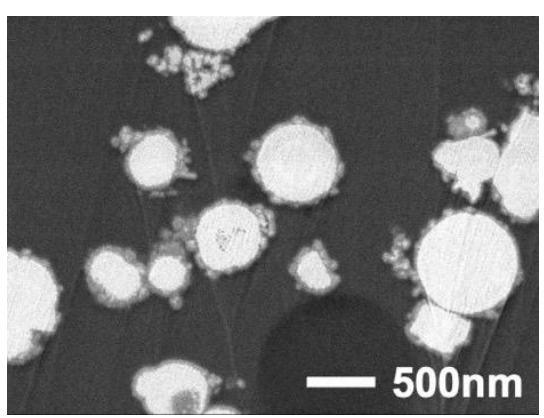


Fig. 1. Cross-sectional SEM image of silica-coated Fe-B particles.

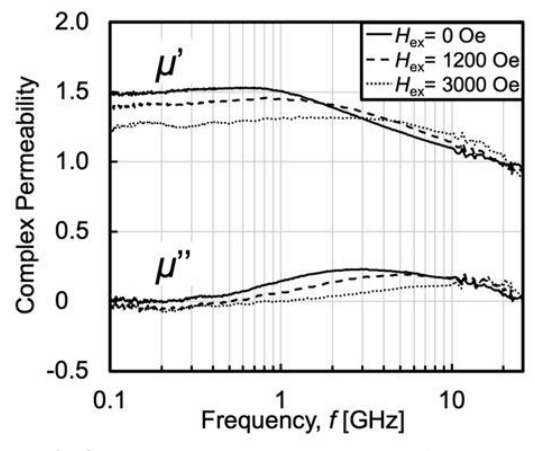


Fig. 2. Complex permeability of Fe-B/Epoxy composite film obtained via LbL-assisted composite plating.

SESSION FQ: ANTIFERROMAGNETS, FERRIMAGNETS & ULTRAFAST SPIN DYNAMICS (POSTER SESSION)

Chair(s): S. Majumder, Department of Physics, University of South Florida, Tampa, Florida, United States Thursday, October 30, 2025 02:30 PM-05:30 PM Exhibit Hall Posters

FQ-01. Observation of magnon polarons in non-local spin transport in an antiferromagnetic crystal Cr_2O_3

O. Gao^{1, 2}, J. Li^{1, 2}

¹Department of Physics, Southern University of Science and Technology, Shenzhen, Guangdong, China, ²Quantum Science Center of Guangdong–Hong Kong–Macao Greater Bay Area (Guangdong), Shenzhen, Guangdong, China

Magnon polarons are hybridized excitations between magnons and phonons due to magnetoelastic coupling in magnetic materials^[1]. Although magnon polarons in antiferromagnetic (AFM) insulator Cr_2O_3 has been observed in spin Seebeck measurements^[2], their impact on long-distance spin current transport in antiferromagnets remains unclear.

Here, we report the observation of AFM magnon polarons in non-local spin current transport in a uniaxial AFM insulator Cr₂O₃. In non-local devices with injector-detector-distance of 1.5 m, the magnon polarons signatures present in second-harmonic channel, instead of first-harmonic channel, of the non-local voltage. Anomalies related to magnon polaron are evident in both field-sweeping and angular-dependent measurements. In field-sweeping measurements, kinks appear at magnetic fields before and after spin-flop transition, as left-handed magnon spectrum shifts down to hybridize with the acoustic phonons to form AFM magnon polarons. Angular-dependent measurements reveal further anomalies when the magnetic field deviates from the easy axis, because field angle could tune the magnon gap as well as the hybridize intensity between lefthanded magnons and acoustic phonons. The magnon polaron signals observed before and after the spin-flop transition disappear at 7 K and 2.2 K, respectively. These results demonstrate a unique way to manipulate the nonlocal spin current transport using AFM magnon polarons. [1] T. Kikkawa, K. Shen, B. Flebus, R. A. Duine, K.-i. Uchida, Z. Qiu, G. E.W. Bauer, and E. Saitoh, Magnon Polarons in the Spin Seebeck Effect, Phys. Rev. Lett. 117, 207203 (2016). [2] J. Li, H. T. Simensen, D. Reitz, Q. Sun, W. Yuan, C. Li, Y.

Tserkovnyak, A. Brataas, and J. Shi, Observation of magnon polarons in a uniaxial antiferromagnetic insulator, *Phys. Rev. Lett.* 125, 217201 (2020).

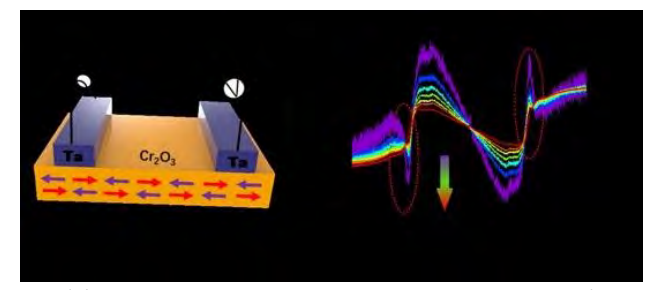


Fig.1 Non-local spin current transport in uniaxial AFM insulators. (a) Device schematics for Non-local measurements in Cr_2O_3/Ta (5nm). (b) Field dependence of magnon-polaron signals in Cr_2O_3/Ta heterostructure at different temperatures. The magnetic field is applied along the easy axis of the AFM insulator.

FQ-02. Enhancing the Magneto-Optical Kerr Effect in Noncollinear Antiferromagnets via a Dielectric Layer

E. Gong^{2,1}, M. Yoo^{2,1}, A. Hoffmann^{2,1}

¹Department of Materials Science and Engineering, The Grainger College of Engineering, University of Illinois Urbana-Champaign, Urbana, Illinois, United States, ²Materials Research Laboratory, University of Illinois Urbana-Champaign, Urbana, Illinois, United States

Non-collinear antiferromagnets such as Mn₃Sn and Mn₃Ge have magnetic moments arranged 120° apart, giving rise to both the anomalous Hall effect and the magneto-optical Kerr effect (MOKE) [1,2]. These materials are promising for spintronics because their magnetic octupole moments couple strongly to electric currents and to light [3]. However, the absence of any net magnetization makes magneto-optical detection inherently difficult. Here, we enhance the Kerr signal by depositing a dielectric MgO cap whose thickness produces constructive interference in the reflected beam. First, we measured the complex refractive index of Mn₃Sn and W by spectroscopic ellipsometry and used these values in a transfer-matrix calculation to predict how Kerr rotation varies with MgO thickness [4]. The model shows a sinusoidal dependence, with a clear maximum at a well-defined thickness. To verify this, we grew Mn₃Sn films, deposited a 120 nm MqO cap, then stepwise thinned the MgO layer via ion milling in 5-10 nm increments while recording polar MOKE loops. The measured Kerr amplitude indeed oscillates, reaching 3.9× the uncapped value at the

optimized MgO thickness (see Figs. 1 and 2), even though the precise thickness for the maximum is higher than theoretically expected. Our calculations further indicate that higher-index caps such as AlN or SiC can enhance the signal by even greater factors. Since the method is purely optical, it leaves the spin order untouched and lets standard MOKE microscopes image antiferromagnetic domains with much higher contrast. This simple approach paves the way for more sensitive studies in antiferromagnetic spintronics. This work was supported by the NSF through the Illinois MRSEC (DMR-1720633).

- [1] S. Nakatsuji et al., *Nature* 527, 212 (2015).
- [2] T. Higo et al., Nat. Photonics 12, 73 (2018).
- [3] T. Chen et al., Nat. Commun. 12, 572 (2021).
- [4] D. Kim et al., Nat Commun., 11, 5937 (2020).

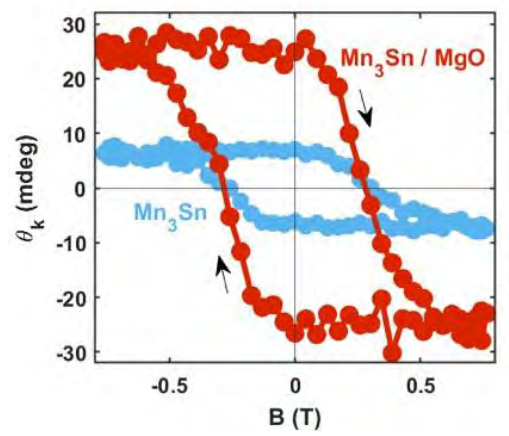


Fig. 1 Kerr rotation as a function of applied field, comparing the bare film (uncapped) and the optimally MgO-capped sample.

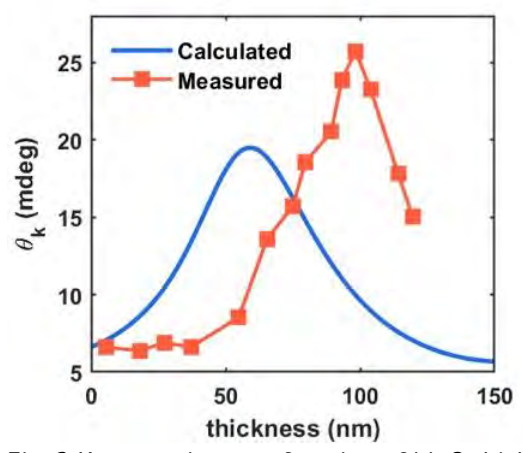


Fig. 2 Kerr rotation as a function of MgO thickness: experimental data and calculations.

FQ-04-LB. Reduction of materials criticality in hybrid manufacturing of Halbach arrays using sintered NdFeB magnets and additively manufactured soft magnet frames

<u>L. Cosgrove</u>¹, T. Lamichhane¹, M. P. Paranthaman², N. Poudel³, T. Charlton²

¹Engineering, University of Central Oklahoma, Edmond, Oklahoma, United States, ²Oakridge National Lab, Oak Ridge, Tennessee, United States, ³Veryst Engineering, Needham, Massachusetts, United States

Using sintered NdFeB N48 magnet cubes and 3D-printed PLA and steel frames, we investigated the enhancement of radial magnetic fields in

cylindrical dipolar Halbach arrays with nested rings. The inner ring contained 8 magnet cubes, while the outer ring had either 24 magnets or a combination of 8 magnets and 16 steel cubes. Results showed a 5% increase in lateral field with the second magnet ring, while adding 16 steel cubes increased the axial field by 27%. Interestingly, the radial field with mixed materials matched that of 24 magnets. Simulations using Ansys Maxwell and COMSOL Multiphysics confirmed optimal geometries for maximizing field strength. This demonstrates the potential of reducing high-quality material usage through additive manufacturing.

FQ-07. Antiferromagnetic-Ferromagnetic Phase Transition in Epitaxial and Non-oriented FeRh Thin Films

<u>F. Efe</u>¹, F. Bakhshizadeh¹, D. Alharbi^{1, 2}, M. Guy¹, M. Davis¹, A. Lisfi¹

¹Physics, Morgan State University, Baltimore, Maryland, United States, ²Physics, The Catholic University of America, Washington DC, District of Columbia, United States

Over the past years, equiatomic FeRh has attracted an increasing interest driven by the fundamental properties of its first order phase transition [1] and its potential technological applications. The occurrence of a temperature or field-induced metamagnetic transition from antiferromagnetic (AFM) order to ferromagnetic (FM) order at 350 K makes this material attractive for technological applications such as thermally assisted magnetic recording [2], magnetocaloric refrigeration [3] and magnetostrictive transduction [4]. The physics behind this transition is still debated and different attempts ranging from an increase in the electronic density of states to spin-wave excitations and instability of the Rh magnetic moment have emerged to explain its origin. Our goal from this study is to investigate the AFM-FM phase transition in epitaxial and randomly

oriented FeRh films. The films of interest were grown with magnetron sputtering from a polycrystalline Fe₅₀Rh₅₀ target on 3 different substrates (MgO, glass and Si) at various temperatures from 25 C to 600 C. The synthesized films were structurally characterized with XRD and atomic force microscopy, whereas magnetic measurements were performed with VSM. The following conclusions were established from the preliminary results of this investigation. (1) Regardless of the substrate nature, films deposited at temperatures below 250 C are amorphous, whereas those deposited at temperatures above 250 C are crystalline. (2) No AFM-FM phase transition was observed in amorphous films. (3) The films deposited on MgO are epitaxial and manifest a narrow AFM-FM transition in the 100-130 C temperature range as portrayed in Fig. 1. (4) The films grown on Si and glass substrates consist of a randomly oriented nanocrystalline structure with a broad AFM-FM transition extending from 60 C to 160 C. All the investigation results will be discussed in the presentation.

[1] L.M. Sandratskii and P. Mavropoulos, "Magnetic excitations and femtomagnetism of FeRh: A first-principles study", Phys. Rev. B 83, 174408 (2011).
[2] J. U. Thiele, S. Maat, and E. E. Fullerton, "FeRh/FePt exchange spring films for thermally assisted magnetic recording media", Appl. Phys. Lett. 82, 2859 (2003).
[3] M. P. Annaorazov, K. A. Asatryan, G. Myalikgulyev, S. A. Nikitin, A. M. Tishin, and A. L. Tyurin, "Alloys of the FeRh system as a new class of working material for magnetic refrigerators", Cryogenics 32, 867 (1992).
[4] M. R. Ibarra and P. A. Algarabel, "Giant volume magnetostriction in the FeRh alloy", Phys. Rev. B 50, 4196 (1994).

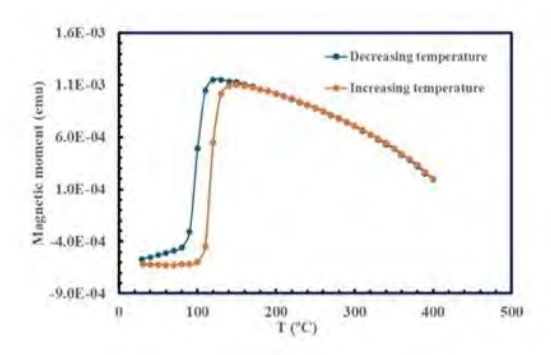


Fig. 1 Magnetization temperature scan of FeRh/MgO film measured at 15 kOe showing a narrow AFM-FM phase transition in the 100-130 C temperature range.

FQ-08. Defect-Mediated Ferromagnetism in Transition Metal-Doped ZnO Thin Films

A. Alsmadi, B. Salameh

Physics, Kuwait University, Kuwait, Kuwait

The search for semiconductor materials exhibiting stable and tunable room-temperature ferromagnetism (RTFM) has become a fundamental challenge in the development of future spintronic devices such as spin LEDs, data storage systems, and logical devices. Previous theoretical and experimental investigations have confirmed the presence of RTFM in ZnO-based magnetic semiconductors [1-3]. In this work, we investigated the interplay between native defect evolution and RTFM in transition metal TM -doped ZnO thin films, modulated by varying TM concentrations and postannealing treatments in different atmospheres (TM = Co, Mn, Ni, and Cu). The doped films exhibited a pure wurtzite phase structure and tunable RTFM. Defect states were characterized using photoluminescence and X-ray photoelectron spectroscopy. The results demonstrated that increasing the TM dopant concentration and annealing in vacuum or hydrogen-rich environments enhanced the formation of zinc interstitials (Zn_i) and oxygen vacancies (V₀), leading to stronger and more tunable RTFM. In contrast, air annealing reduced V₀ and Zn_i, resulting in weaker ferromagnetic behavior. The induced magnetic ordering is well explained by the bound magnetic polaron (BMP) model, wherein a long-range ferromagnetic coupling between TM ions is mediated by intrinsic V₀ and Zn_i defects.

- [1] T. Dietl, et. al.," Science 287, 1019-1022 (2000)
- [2] A. M. Alsmadi, et. al., J. Phys. Chem. C 124, 16116 (2020)
- [3] A. M. Alsmadi, et. al., Phys. Rev. B 108, 054444 (2023)

FQ-09. Deterministic modelling of ultrafast dynamics in magnetic tunnel junctions

P. Thibaudeau¹, M. Fattouhi², L. D. Buda-Prejbeanu² ¹CEA, DAM, Le Ripault, Monts, France, ²SPINtronique et Technologie des Composants, Grenoble, France

We study the ultrafast dynamics of magnetic tunnel junctions (MTJs) using atomistic spin dynamics and femtosecond laser heating. Our method involves solving the dynamical Landau-Lifshitz-Bloch (dLLB) equation in a multispin system [1,2].

To predict the Curie curve during the processes of laser heating, we use the dLLB equation under a RPA for magnetic exchange, combined with a Quantum Fluctuation Dissipation Relation (QFDR). This effectively addresses the

^{*} Best Student Presentation Finalist / LB - Late-breaking Poster

energy transfer derived from the magnon band structure [3]. By simulating the demagnetization of MTJs with laser heating, the energy exchange between different reservoirs is accurately modeled, and we find that the results match the experimental data, as seen from Fig.1(b).

Our method is demonstrated to efficiently model all-optical switching mechanisms in bulk materials, obviating the need for multiple statistical realizations that are inherent in methods based on the stochastic Landau-Lifshitz-Gilbert equation [6]. This is further supported by its ability to effectively simulate not only simple structures, but also complex and realistic devices such as Tb/Co-based ones that are often utilized in advanced all-optical switching schemes [7].

To validate the efficiency of this approach, we proceed to examine key aspects:

- 1) Investigating the magnetic response of multilayer structures upon laser heating.
- 2) Incorporation of spin transfer torques (STTs) and anisotropic energy within the dLLB equation set, which aims to represent the potential for magnetization flipping once triggered by external electrical stress within the layers.
- 3) Investigating the dynamics of magnetization in illuminated layers under the influence of STTs. These cases will be compared to simulations generated by solving the corresponding stochastic precession equations.

In summary, the deterministic atomic spin simulations using the dLLB equation prove valuable and efficient for investigating thermal phenomena in spintronic systems.

Acknowledgments: This work is supported partly by France 2030 government investment plan managed by the French National Research Agency under grant reference PEPR SPIN – [SPINTHEORY] ANR- 22-EXSP-0009, and CEA Exploratory Program, Bottom-Up 2023 ref.59 [THERMOSPIN].

- [1] J. Tranchida, P. Thibaudeau, and S. Nicolis, IEEE Transactions on Magnetics 52, 1 (2016).
- [2] J. Tranchida, P. Thibaudeau, and S. Nicolis, Physical Review E 98, 042101 (2018).
- [3] M. Fattouhi, P. Thibaudeau, and L. D. Buda-Prejbeanu, "Ultrafast dynamics of moments in bulk ferromag- nets," (2025), arXiv:2502.07375 [cond-mat].
- [4] J. Crangle and C. Goodman, Proceedings of the Royal Society of London. A. Mathematical and Physical Sciences 321, 477 (1971).

- [5] B. Koopmans, G. Malinowski, F. Dalla Longa, D. Steiauf, M. Fähnle, T. Roth, M. Cinchetti, and M. Aeschli-mann, Nature Materials 9, 259 (2010).
- [6] O. Eriksson, A. Bergman, L. Bergqvist, and J. Hellsvik, Atomistic Spin Dynamics: Foundations and Appli- cations (Oxford university press, Oxford, 2017).
- [7] D. Salomoni, Y. Peng, L. Farcis, S. Auffret, M. Hehn, G. Malinowski, S. Mangin, B. Dieny, L. Buda- Prejbeanu, R. Sousa, and I. Prejbeanu, Physical Review Applied 20, 034070 (2023).

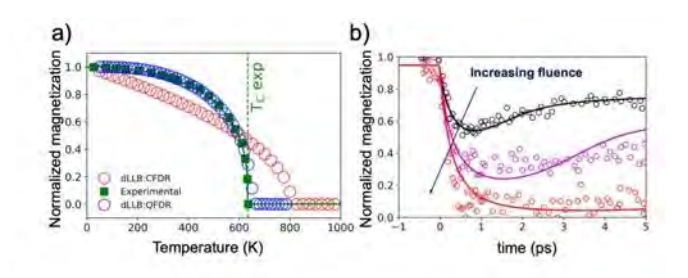


Figure 1. a) Magnetization versus temperature curve of Nickel computed from dLLB with both classical (CFDR) and quantum (QFDR) fluctuation-dissipation relation compared to experimental data from [4]. b) Laser induced ultrafast demagnetization of Nickel. Experimental data are adapted from [5].

FQ-10. Terahertz emission from CoFeB/Pt_{1-x}Cu_x spintronic bilayers

C. Bull^{1,2}, R. Ji^{1,2}, C. Lin^{1,2}, T. Gething^{2,1}, S. M. Hewett^{1,2}, B. Spencer³, H. J. Waring¹, <u>T. Thomson</u>¹, D. M. Graham^{2,4}, P. Nutter¹

¹Dept. of Computer Science, University of Manchester, Manchester, United Kingdom, ²Dept. of Physics and Astronomy, University of Manchester, Manchester, United Kingdom, ³Department of Materials, University of Manchester, Manchester, United Kingdom, ⁴The Cockcroft Institute, Daresbury, United Kingdom

Recent interest in spintronic terahertz (THz) emitters has been driven by their simplicity, low cost and ability to generate high electric field amplitudes over a broad, gapless spectral bandwidth [1, 2]. The mechanism responsible for THz emission is the inverse spin-Hall effect (ISHE) where spin polarized electrons excited by a femtosecond laser pulse are transported directly from the ferromagnetic layer (FM) to an adjacent non-magnetic layer (NM) inducing an oscillating electric field via spin-orbit coupling (SOC) [3]. It is immediately obvious that the efficiency of both the electron transport from the FM to NM layers and SOC in the NM layer are key to controlling the resultant THz electric field.

In this work, we investigate the effect of alloying Pt and Cu in the NM layer on the emission of THz radiation from CoFeB (2.5nm)/Pt_{1-x}Cu_x (2.2nm) spintronic emitters. Fig.1 shows the effect of modifying the NM layer by alloving Cu where at x = 18 at%, the amplitude of the THz emission increases by \sim 7% compared to a similar emitter design without Cu. This increase in emission is coupled with an approximate doubling of the effective spin mixing conductance, $q^{\uparrow\downarrow}$ and an enhancement of the longitudinal DC conductivity by 1.3 x10⁵ S/m. This is consistent with the work of Meinert et al. [4] who observed a similar enhancement for Pt alloyed with Au. Whilst not the only potential mechanism, these results suggest that changes in the interface are most likely responsible for the enhancement in THz emission, since DC conductivity is dominated by interfacial rather than bulk scattering for films of the thickness involved here. These results demonstrate significant potential for improved THz emission by optimising the NM metallic layer via alloying with Cu.

[1] T. Kampfrath, M. Battiato, P. Maldonado, G. Eilers, J. Notzold, S. Mahrlein, V. Zbarsky, F. Freimuth, Y. Mokrousov, S. Blugel, M. Wolf, I. Radu, P. M. Oppeneer, and M. Munzenberg, Nat. Nanotechnol. 8, 256, (2013).
[2] C. Bull, S.M. Hewett, R. Ji, C.-H. Lin, T. Thomson, D.M. Graham, and P.W. Nutter, APL Mater. 9, 090701 (2021).
[3] E. Saitoh, M. Ueda, H. Miyajima, and G. Tatara, Appl. Phys. Lett. 88, 182509 (2006).

[4] M. Meinert, B. Gliniors, O. Gueckstock, T. Seifert, L. Liensberger, M. Weiler, S. Wimmer, H. Ebert, and T. Kampfrath, Phys. Rev. Appl. 14, 064011 (2020).

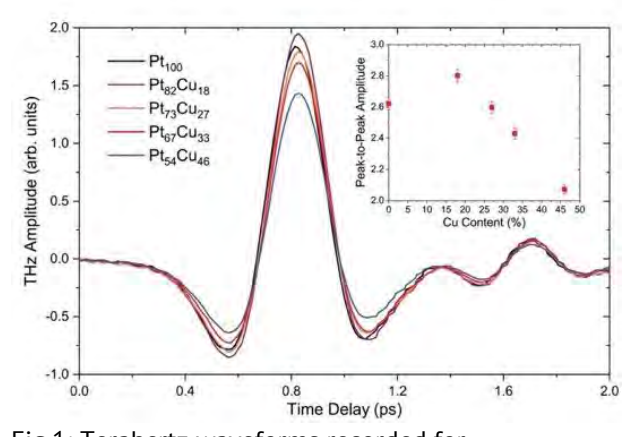


Fig.1: Terahertz waveforms recorded for CoFeB/Pt_{1-x}Cu_x bilayers with x varying from 0 to 46%. Inset shows the peak-to-peak amplitude measured for each waveform as a function of Cu concentration.

SESSION FR: SKYRMIONS AND SPIN-ORBIT TORQUE (POSTER SESSION)

Chair(s): B. Sanyal, *Department of Physics & Astronomy, Uppsala University, Uppsala, Sweden*Thursday, October 30, 2025

02:30 PM-05:30 PM

Exhibit Hall Posters

FR-01. Spin accumulation-induced magneto-photogalvanic effect in metals

<u>A. Kamiryo</u>¹, M. Yamamoto², T. Nishijima², R. Ohshima², M. Shiraishi², Y. Ando¹

¹Osaka Metropolitan Univ., Sakai, Osaka, Japan, ²Kyoto Univ., Kyoto, Kyoto, Japan

We have reported a unidirectional photocurrent generated along the longitudinal direction of a metallic wire when linearly polarized light is irradiated onto its edge, under the application of a DC current¹⁾. This phenomenon is considered to be a manifestation of the magnetophotogalvanic effect (MPGE), which arises in systems where both spatial inversion symmetry and time-reversal symmetry are broken simultaneously²⁾. In general, MPGE emerges in systems with broken spatial inversion symmetry, combined with time-reversal symmetry breaking induced by magnetic fields or magnetization. In contrast, in our study, MPGE is induced by time-reversal symmetry breaking due to spin accumulation arising from the spin Hall effect (SHE), as well as spatial inversion symmetry breaking at the side surfaces of the metallic wire. This effect shows promise as a highly versatile local spin detection technique based on linearly polarized light. However, prior investigations were limited to Pt, W, Cu, and Co/Pt multilayers with perpendicular magnetization. In this study, we evaluated MPGE in a variety of materials to gain insight into its underlying mechanism. Figure 1 shows the mapping results for Ti and Pd. In both samples, a clear optical signal is observed at the edges of the wire. Since we presume that time-reversal symmetry is broken due to spin accumulation from the SHE, the photocurrent is expected to have the same polarity at both edges, which is consistent with the observed results. Differences in signal strength between the left and right edges might be due to variations in focusing or surface geometry. Note that the photocurrent polarity in Pd matches that in Pt, and similarly, Ti matches W. These polarities correspond to the sign of the SHE in each material. In the presentation, we will report on the results obtained from various materials and measurement conditions and discuss our current understanding of the underlying mechanism of

the MPGE observed in metallic systems.

1)T. Nishijima *et al.*, Phys. Rev. B 111, L140406 (2025). 2)M. Matsubara *et al.*, Nat Commun. 13, 6708 (2022).

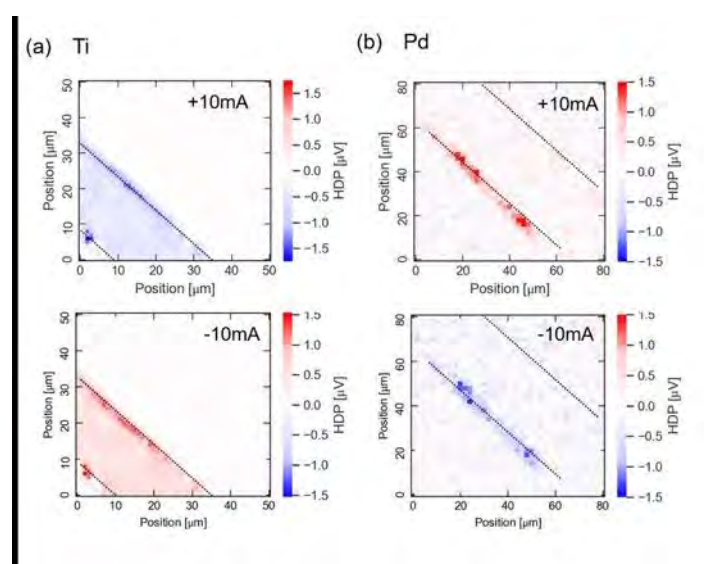


Fig. 1 Spatial two-dimensional maps of the photovoltage in (a) Ti and (b) Pd.

FR-03. Effects of In-Plane Magnetic Fields and Energy Analysis during the Control of Antiskyrmion Formation Y. Machida, M. Taniwaki, A. L. Foggiatto, M. Kotsugi Materials Science and Technology, Tokyo University of Science, Tokyo, Japan

Antiskyrmions, like skyrmions, are topological defects in magnetic textures that have attracted interest due to their potential for high-performance memory devices. While the stability and dynamics of skyrmions are governed by the Dzyaloshinskii-Moriya interaction (DMI), antiskyrmions emerge in systems with anisotropic DMI, where the signs of DMI components differ along orthogonal axes [1]. This property gives rise to complex helicity structures, and antiskyrmions have only been experimentally confirmed in two materials. Various strategies have been explored in previous studies, such as those focusing on the experimental control of antiskyrmion lattices using in-plane fields[2]; however, the role of different energy contributions in this control remains unclear. Therefore, we focus on a mechanism for controlling antiskyrmion lattices based on the sample tilt angle and the associated energy terms using micromagnetic simulations. Formation was simulated using the Landau-Lifshitz-Gilbert equation in MuMax3. As

anisotropic DMI is essential for stabilizing antiskyrmions, we modified the source code to reverse the DMI sign in the ydirection. To simulate in-plane fields, a magnetic field was applied in the [100], [010], and [001] directions, corresponding to a tilt angle θ from the [-1-10] axis. After confirming the transition from the helical state, θ was varied to observe changes in spin textures [3](Fig. 1). We observed a strong dependence of antiskyrmion number on tilt angle. Larger tilt angles, implying stronger in-plane fields, led to earlier transitions and more antiskyrmions. Fig. 2 shows total energy, out-of-plane field, and topological charge (Q), corresponding to textures in Fig. 1 (a – d). Energy showed a local minimum during the helical-to-antiskyrmion transition and a maximum at the onset of the lattice phase. Near the minimum, anisotropy energy dominated, while at the maximum, exchange energy peaked. These results highlight the critical role of energy competition in topological phase transitions and provide a foundation for the controlled manipulation of antiskyrmion structures in future spintronic applications.

- [1] Y. Tokura, N. Kanazawa, Chem. Rev. Vol.121, p.2857-2897, (2021)
- [2] Licong Peng, Rina Takagi, Wataru Koshibae, et al., Nat. Nanotech. Vol.15, p.181-186 (2020)
- [3] Kosuke Karube, Licong Peng, Jan Masell, et al., Nat. Mater. Vol.20, p.335-340 (2021)

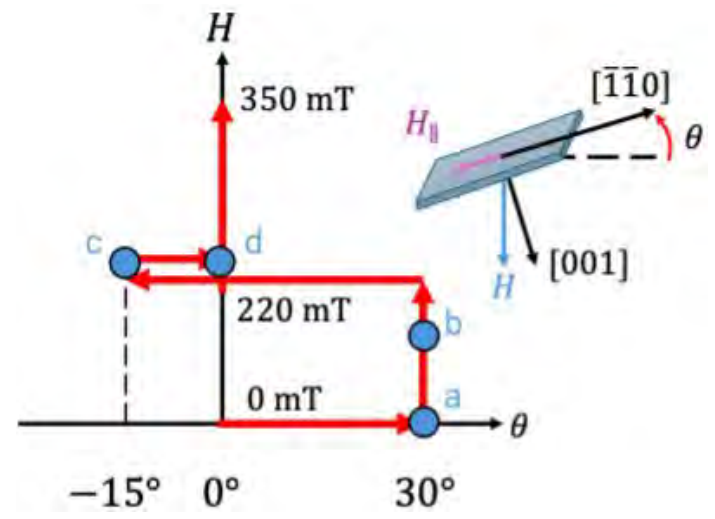


Fig. 1 Simulation process for 30 degree

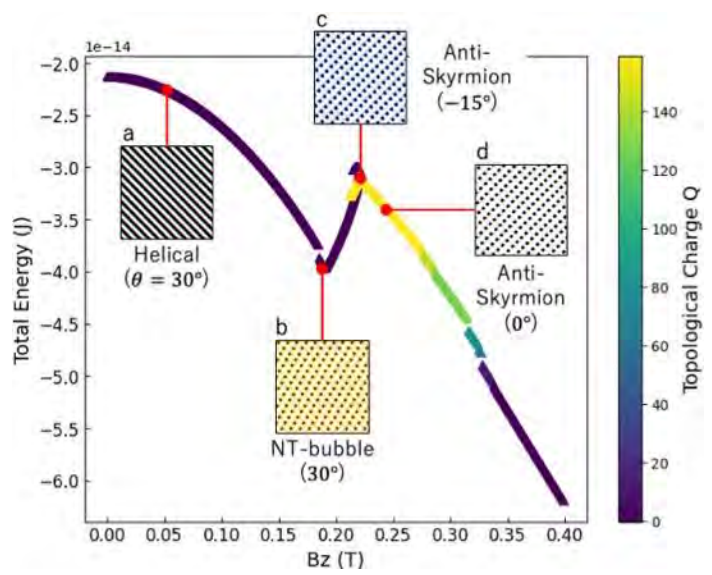


Fig. 2 Q-value color map of OOP field vs total energy

FR-04. Antisymmetric Planar Hall-Induced Artifacts in Second Harmonic Hall SOT Measurements: A Case Study in $RuO_2(101)$

O. Jia, S. Nair, Y. Yang, S. G. Jeong, S. Lee, D. Tonini, S. Liang, Y. Chen, O. Benally, B. Dixit, T. Low, B. Jalan, J. Wang *University of Minnesota, Minneapolis, Minnesota, United States*

Materials with broken in-plane mirror symmetry can generate spin current with out-of-plane spin polarization, enabling field-free spin-orbit torque (SOT) switching. The second harmonic Hall (SHH) method is widely used to electrically quantify such spin components. However, these materials often exhibit an antisymmetric planar Hall effect (APHE), which is typically overlooked in SHH analysis. Using rutile RuO₂(101) as a model system, we demonstrate that APHE introduces a non-negligible artifact in the SHH signal, leading to a maximum of ~20% error in the extracted damping-like z component. This deviation, captured by an analytical model, scales with the APHE-to-PHE ratio and the amplitude of in-plane spin components (S_v or S_x). Our results highlight the necessity of reporting both APHE and PHE contributions to avoid fundamental misinterpretations in SOT z spin quantification.

[1] Y. Cui *et al.*, "Antisymmetric planar Hall effect in rutile oxide films induced by the Lorentz force," *Sci. Bull.*, vol. 69, no. 15, pp. 2362–2369, Aug. 2024, doi: 10.1016/j.scib.2024.06.009.

[2] A. Bose *et al.*, "Tilted spin current generated by the collinear antiferromagnet ruthenium dioxide," *Nat. Electron.*,

vol. 5, no. 5, pp. 267–274, May 2022, doi: 10.1038/s41928-022-00744-8.

[3] Y. Yang *et al.*, "Coexistence of unconventional spin Hall effect and antisymmetric planar Hall effect in IrO2," *Appl. Phys. Lett.*, vol. 126, no. 10, p. 102403, Mar. 2025, doi: 10.1063/5.0240538.

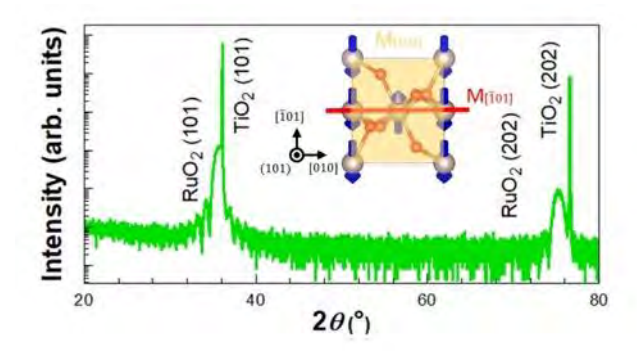


Fig. 1. XRD result of the the single crystal rutile $RuO_2(101)$. The inset figure shows the top view of the unit cell. The broken of the in-plane and out-of-plane mirror symmetry allows both generation of spin current with Sz as well as APHE.

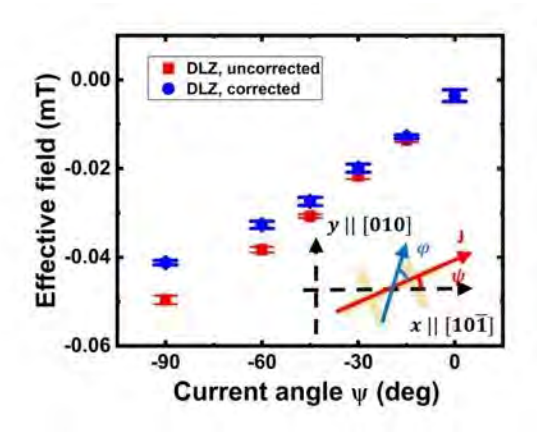


Fig. 2. Extracted damping-like effective magnetic field along the z-direction. Blue and red dots correspond to models with and without accounting for the anomalous planar Hall effect (APHE), respectively.

FR-05. Metallic 2D-MXene: a promising underlayer of SOT device for field-free switching and enhancement of efficiency

P. Kumar¹, H. Abe², Y. Kotani³, A. Sumiyoshiya³, T. Nakamura^{4, 3}, G. K. Shukla¹, <u>S. Isogami</u>¹
¹NIMS, Tsukuba, Japan, ²KEK, Tsukuba, Japan, ³PhoSIC, Sendai, Japan, ⁴Tohoku University, Sendai, Japan

Magnetic memory devices using two-dimensional (2D) materials as spin current channel under layers have been proposed in recent years [1]. However, large-area synthesis remains a bottleneck, making practical implementation difficult. We have successfully synthesized a large-area film of a latest 2D material discovered in 2011, that is, chromium nitride (Cr₂N) MXene [2,3] by reactive sputtering technique. The field-free switching in a spin-orbit torque (SOT) device was demonstrated as shown in Fig. 1, and the possible mechanisms was discussed with X-ray magnetic circular dichroism [4]. In transition metal compounds, the influence of 2p light element of nitrogen has been reported to provide great impacts on the magneto-transport properties such as anomalous Hall conductivity magnetic materials with antiperovskite sructure [5]. A similar effect is considered to contribute to our results of 2D-MXene based SOT devices. In this study, we aimed to further enhance the field-free switching efficiency by intentionally introducing nitrogen into nonequilibrium metastable sites in Cr₂N-MXene. We fabricated a multilayer stacking: C-plane Al₂O₃ substrate $// Cr_2N(5) / [Co(0.35) / Pt(0.3)] \times 3 / MgO(3)$ (in nm), using a magnetron sputtering system. The Cr₂N-MXene layer was deposited at 500 °C, with N_2 partial pressure ($N_2/(Ar+N_2)$) ranging from 0 to 15%. To investigate the local structure with varying nitrogen content, X-ray absorption fine structure (XAFS) of Cr K-edge was measured using beamline BL-7C at KEK-PF.

Figure 2 presents the field-free switching efficiency, quantified as the amplitude ratio of current-induced switching relative to fully saturated magnetization. As the nitrogen composition increases, a clear enhancement is observed, implying that nitrogen atoms at nonequilibrium metastable sites play a crucial role to boost the efficiency due to breaking local spatial symmetry.

- [1] Yang et al., Nature 2022, 606, 663.
- [2] Naguib et al., Adv. Mater. 2011, 23, 4248.
- [3] Ahn et al., Adv. Mater. 2020, 32, 2000919.
- [4] Kumar et al., Small 2025, 2500626.
- [5] Isogami et al., Adv. Electron. Mater. 2023, 9, 2200515

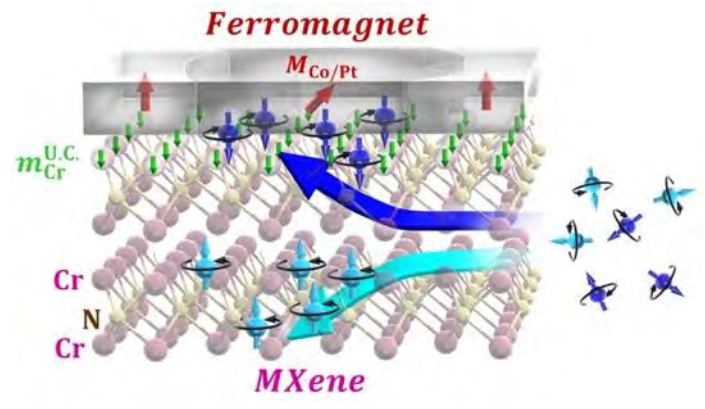


Fig. 1 Schematic illustration showin a spin-orbit torque device with a spin channel of Cr₂N 2D-MXene layer and possible mechanism for field free switching.

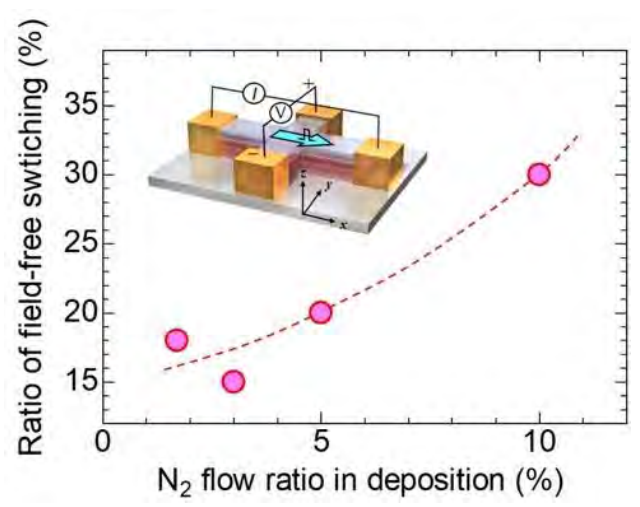


Fig. 2 Variation of field-free magnetization switching ratio that is defined as switching amplitude/amplitude of AHE against the N_2 partial pressure during reactive sputtering deposition.

FR-06. Nonlinear dynamics excited for room-temperature skyrmions by current injection

<u>S. Yadav</u>¹, S. Chatterjee¹, S. Sugimoto², S. Kasai²
¹Physics, IIT Varanasi, Varanasi, India, ²NIMS, Tsukuba, Japan

Magnetic skyrmion is one of the swirling spin textures observed in non-centrosymmetric crystals that lack inversion symmetry [1] and/or magnetic heterostructures under the finite Dzyaloshinskii Moriya interaction (DMI) [2]. Such skyrmion textures, characterized by high stability under the topological protection, have emerged as promising candidates for the next-generation spintronic

devices attributed to their robust manipulation via small electric current density. Recent researches have focused on the single skyrmion dynamics in multilayer thin films and clarified various new functionalities, including the skyrmion Hall effect, Brownian motions, etc. While most of these studies focus on the linear responses of a single skyrmion so far, the nonlinear responses of the collective skyrmions offer other new classes of opportunities, including the base of neuromorphic computing [3].

In this work, we report the current-induced nonlinear dynamics of room-temperature skyrmions for a Pt/Co/Ir multilayer via direct imaging technique utilized by magneto-optical Kerr effect microscopy. The skyrmionics domain morphologies are successfully captured as deformations between bubble and stripe domains, by tuning the perpendicular magnetic anisotropy (PMA) and DMI through the variation of cobalt (Co) and iridium (Ir) thicknesses. Such sub-micron bubbles can be driven by a remarkably lower critical current density (2.5x10¹⁰A/m²) rather than conventional magnetic domains, indicating inherited topological nature known as the skyrmion Hall effect. More interestingly with increasing current densities, these skyrmions exhibited collective segregation phenomena along to the hall directions. Such segregation responses are mediated by spin wave emissions during propagation processes, and regarded as nonlinear dynamics ruled by a topological manner [4]. These nonlinear responses unique to skyrmions have enabled the fast and long-range tuning of domain morphologies, which indicate the potential of skyrmions in developing adaptive neuromorphic-based computing architectures.

- [1] Mühlbauer S. et al, Science 323, 915 (2009).
- [2] Jiang W. et al, Physics Reports 704,1-49 (2017)
- [3] Yokouchi et al., Sci. Adv. 8, 5652 (2022)
- [4] Sugimoto et al., Sci. Rep. 10, 1009 (2020)

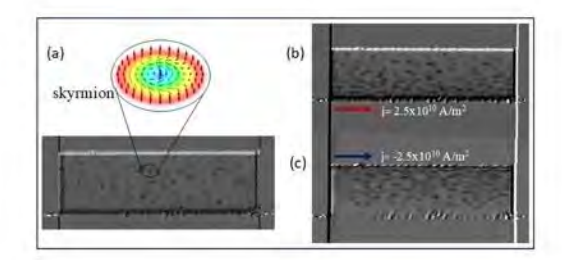


Fig. 1: (a) Room temperature stabilization of skyrmions in Pt/Co/Ir multilayer system. (b) and (c) current-induced skyrmion driving under the opposite current polarities.

FR-07. Skyrmion-like magnetic domain structures in epitaxial [Ru/Co/Pt]_n synthetic antiferromagnets

Y. Hisada, S. Komori, T. Taniyama Dept. Phys., Nagoya Univ., Nagoya, Japan

Antiferromagnetically coupled multilayers, or synthetic antiferromagnets (SAFs), show promise in achieving the nucleation of magnetic skyrmions that are smaller than ferromagnetic skyrmions, with sizes on the order of tens of nanometers. Recent studies have shown that introducing a perpendicularly magnetized multilayer (bias layer) stabilizes small antiferromagnetic skyrmions in SAFs [1]. However, the bias layer impedes the flow of an electric current, thus limiting skyrmion motion. In this study, we demonstrate that skyrmion-like magnetic bubbles with diameters of tens of nanometers can form at zero magnetic field and in the absence of bias layers by investigating the magnetic domain structures of epitaxial [Ru/Co/Pt]_n SAFs. Epitaxial Pt (3)/[Ru (t_{Ru})/Co (2)/Pt (0.5)]_n/Pt (5) multilayers (thickness in nm in parentheses) were grown onto SrTiO₃ (111) substrates by molecular beam epitaxy, where n is the repetition number. The Co thickness was optimized to 2 nm to minimize effective magnetic anisotropy and enable rotation of the magnetization orientation from out-of-plane to in-plane. Figure 1 shows an MFM image of the sample with n=16 and $t_{Ru}=0.8$ nm at zero magnetic field. Magnetic bubble-like domains are clearly visible; one has a diameter of approximately 66 nm (Fig. 2). This bubble size is much smaller than that of conventional magnetic bubble domains or ferromagnetic skyrmions, indicating that the bubble is an antiferromagnetic skyrmion. Micromagnetic simulations also support the nucleation of small-size antiferromagnetic skyrmions in our structures. The n- and t_{Ru} -dependence of the magnetic domain structures in $[Ru(t_{Ru})/Co(2)/Pt(0.5)]_n$ will be discussed in more detail.

This work was supported in part by JSPS KAKENHI Grant Nos. JP24H00380, JP24K21732, JP23KK0086, JP24KJ1306, JSPS JRP-LEAD with UKRI Grant Nos. JPJSJRP20241705, JST FOREST Grant No. JPMJFR212V, and Iketani Science and Technology Foundation Grant Nos. 0361214-A. [1] W. Legrand *et al.*, Nat. Mater. 19, 34 (2020).

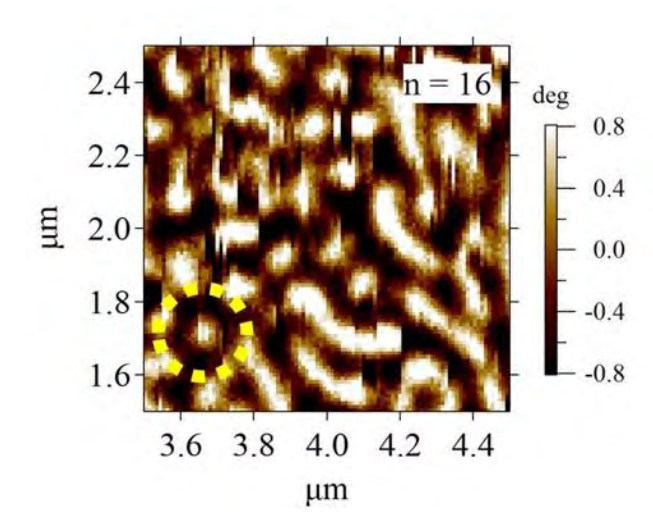


Fig. 1 MFM image of a $[Ru (0.8)/Co (2)/Pt (0.5)]_{16}$ multilayer at zero magnetic field.

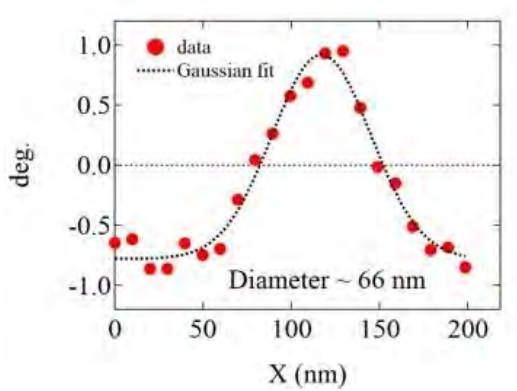


Fig. 2 Line profile of a bubble domain marked by a dotted circle in Fig. 1.

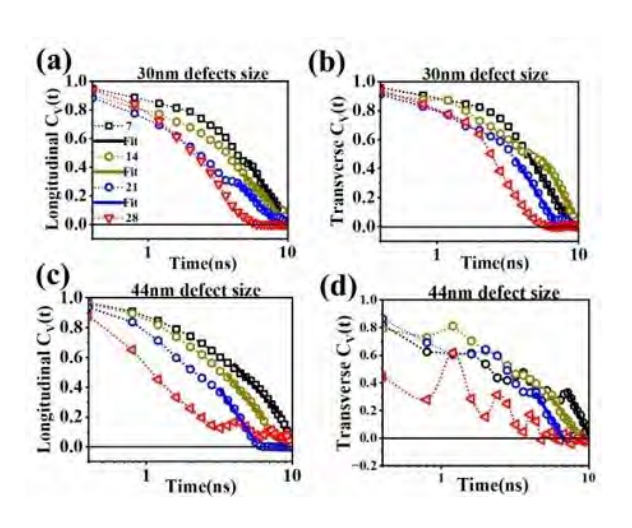
FR-08. Current-driven dynamics of an isolated skyrmion in a racetrack with materialistic defects: Influence of defect size and density

<u>P. Kamal</u>, R. Posti, A. Tripathi Physics, Indian Institute of Technology, Ropar, Department of Physics, Rupnagar, Ropar, Punjab, India

Magnetic skyrmion, characterized by their distinctive topological spin structures, which can be efficiently driven at high speeds using spin-transfer torques and spin-orbit torques at relatively low current densities, found application in racetrack memory devices. However, a comprehensive understanding of their current-induced dynamics in real thin-film environments, where defects are prevalent, remains an open challenge. Here, we examine the influence

of a current-driven dynamics of skyrmion by means of micromagnetic simulation in two types of racetracks: one with defects smaller than the skyrmion and another with defects larger than the skyrmion. Mean square displacement analysis reveals a super-diffusive and sub-diffusive behaviour, governed by defect size and their counts. Using the velocity autocorrelation function as shown in Fig. 1, we identify the origin of these diffusion regimes: superdiffusion arises from sustained velocity correlations, while subdiffusion arises from the anti-persistent skyrmion velocity. Analysis of the Velocity autocorrelation in Fig. 1 reveals a predominance of anomalous diffusion due to current induced motion of skyrmion over normal diffusion exhibited due to thermal energy, with skyrmion motion becoming increasingly hindered as defect density increases. Furthermore, for smaller defect size, as shown in Fig. 2 ,transverse diffusion is consistently lower than longitudinal diffusion, with the difference between them decreasing as the defect count increases. This suggests that mitigating defect size along with their counts in racetracks requires careful control of defect configurations, providing crucial insights for optimizing skyrmion-based memory devices.

- 1. X. Gong, H. Y. Yuan, and X. R. Wang, Current-driven skyrmion motion in granular films, Phys. Rev. B 101, 064421 (2020).
- 2. A. Salimath, A. Abbout, A. Brataas, Current-driven skyrmion depinning in magnetic granular films, Phys. Rev. B 99, 104416 (2019).
- 3. M. Stier, R. Strobel, S. Krause, Role of impurity clusters for the current-driven motion of magnetic skyrmions, Phys. Rev. B 103, 054420 (2021).
- 4. T. Dohi, M. Weißenhofer, N. Kerbe, Enhanced thermally-activated skyrmion diffusion with tunable effective gyrotropic force, Nat. Commun. 14, 5424 (2023).



^{*} Best Student Presentation Finalist / LB - Late-breaking Poster

Fig. 1: Semi-log plot of (a)Longitudinal VAF in presence of 30nm defect size (b) Transverse VAF in presence of 30nm defect size, (c) Longitudinal VAF in presence of 44nm defect size, (d) Transverse VAF in presence of 44nm relative to defect counts 7,14,21,28. Solid lines represents the linear tail fitting of VAF.

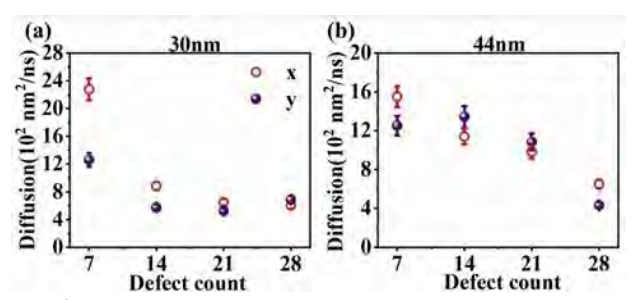


Fig. 2 : Diffusion coefficient of skyrmion in presence of (a) Low disorder racetrack, (b) High disorder racetrack relative to defect count- 7,14,21,28

FR-09. Comparing spin Hall angle in $(Bi_{1-x}Sb_x)_2Te_{3-y}Se_y$ (x = 0.58, y=1) using spin- torque ferromagnetic resonance and non-local voltage measurements

V. Sharma^{1, 2}, S. Jois², G. M. Stephen², T. Hossain³, <u>B. Jungfleisch</u>³, P. J. Taylor⁴, A. T. Hanbicki², A. Friedman²

¹Department of Electrical and Computer Engineering, University of Maryland College Park, College Park, Maryland, United States, ²Laboratory for Physical Sciences, College Park, Maryland, United States, ³Department of Physics and Astronomy, University of Delaware, Newark, Delaware, United States, ⁴Army Research Laboratory, Adelphi, Maryland, United States

Spin to charge conversion processes in thin films are driven by various phenomena such as the spin Hall, Rashba-Edelstein effects¹. The competition between these effects and the quality of the interface governs the spin transport parameters of the film. Here, we compare the spin Hall angle in MBE grown $(Bi_{1-x}Sb_x)_2Te_{3-y}Se_y$ (BSTS, x = 0.58, y = 1) films at room temperature using two complementary techniques: Non-local voltage (NLV) measurements in BSTS Hall bars with DC charge current, and spin-torque ferromagnetic resonance (ST-FMR) measurement in BSTS/Ni₈₀Fe₂₀ heterostructures at GHz frequencies. The NLV measurements are conducted without using ferromagnetic injection contacts, whereas ST-FMR measurements require ferromagnetic Ni₈₀Fe₂₀ for spin injection. The converted charge current in both measurements is analyzed using the spin diffusion model for the spin Hall effect. We observed

that regardless of the differences in the techniques, the spin Hall angle (ϑ_{SH} ~4.71 in ST-FMR and ϑ_{SH} ~3.0 in NLV) in the two cases is comparable. The NLV measurements also show a large spin diffusion length (λ_S ~8 µm) possibly due to the decrease in bulk conduction in this stoichiometric BSTS². Our study leads to more accurate determination of ϑ_{SH} and extends the understanding of one of the most commonly used methods in spin Hall effect measurements.

Acknowledgments

ST-FMR experiments were conducted at the University of Delaware and primarily supported by NSF through the University of Delaware Materials Research Science and Engineering Center, DMR-2011824.

1. Manchon, Aurelien, et al. "Current-induced spin-orbit torques in ferromagnetic and antiferromagnetic systems." *Reviews of Modern Physics* 91.3 (2019): 035004.

2. Ren, Zhi, et al. "Optimizing Bi_{2-x}Sb_xTe_{3-y}Se_y solid solutions to approach the intrinsic topological insulator regime." *Physical Review B—Condensed Matter and Materials Physics* 84.16 (2011): 165311.

FR-10. Static and Dynamic Magnetic Properties of Ultrathin Co Films on MoSe₂/Sapphire Heterostructures for Opto-Spintronic Applications

<u>I. A. Almuhanna</u>, Y. Wadumesthri, A. I. Ojo, H. Rodríguez Gutiérrez, D. A. Arena *University of South Florida, Tampa, Florida, United States*

Van der Waals heterostructures combining ferromagnets and two-dimensional materials enable near-atomic monolayer control of magnetic properties, a key advance for spintronic [1] and opto-spintronic devices [2]. We examine the static and dynamic magnetism of 4 nm Cobalt (Co) films on monolayer and bilayer molybdenum diselenide (MoSe₂) grown by chemical vapor deposition on optically transparent sapphire. MoSe₂ flakes were patterned with TEM grids for further optical studies, and the growth quality and number of layers were verified by photoluminescence and Raman spectroscopy, respectfully. Co was deposited by magnetron sputtering at 14 Å/s and capped with 5 nm Si₃N₄ to prevent oxidization. Reference samples include Co on a 3 nm platinum (Pt) seed layer and Co on bare sapphire. All growth and characterizations were carried out at room temperature.

The in-plane vibrating sample magnetometer (VSM) (Fig. 1) shows that bilayer MoSe₂ yields coercivity H_c comparable to

^{*} Best Student Presentation Finalist / LB – Late-breaking Poster

the Pt-seeded films and nearly doubles the squareness $M_{\text{n}}/M_{\text{s}}$ of the unseeded Co/sapphire. In-plane Ferromagnetic Resonance (FMR) (Fig. 2) reveals that MoSe_2 -seeded samples exhibit moderate Gilbert damping α (\sim 0.018) but maintain inhomogeneous broadening $\Delta H_0 \approx 10$ mT, much lower than Pt / Co, highlighting enhanced spin-orbit coupling with minimal inhomogeneity. Extracted anisotropy fields Hk further indicate interface driven perpendicular anisotropy. These findings demonstrate that MoSe2 can serve as a clean, nonmetallic seed layer capable of tailoring magnetic damping and anisotropy even in soft ferromagnets.

[1] Q. Shao, G. Yu, Y.W. Lan, Y. Shi, M.Y. Li, C. Zheng and K. L. Wang, *Nano letters*, 16.12, 7514-7520 (2016)
[2] L. Cheng, W. Xinbo, Y. Weifeng, C. Jianwei, Y. Ming, C. Mengji, W. Yang, *Nature Physics*, 15.4, 347-351 (2019)

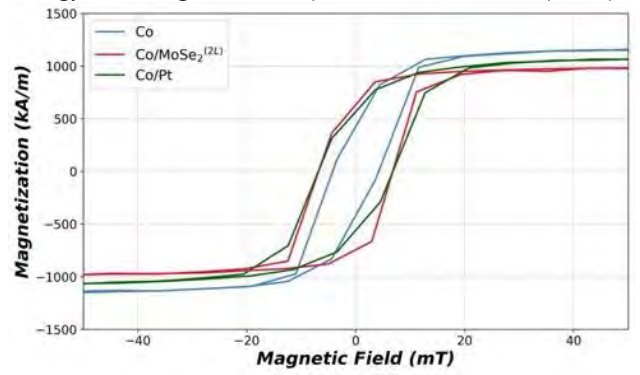


Fig. 1. In-plane H vs. M hysteresis loops (VSM) at room temperature for Co, Co/MoSe₂(bilayer), and Co/Pt, showing enhanced H_c and M_r/M_s .

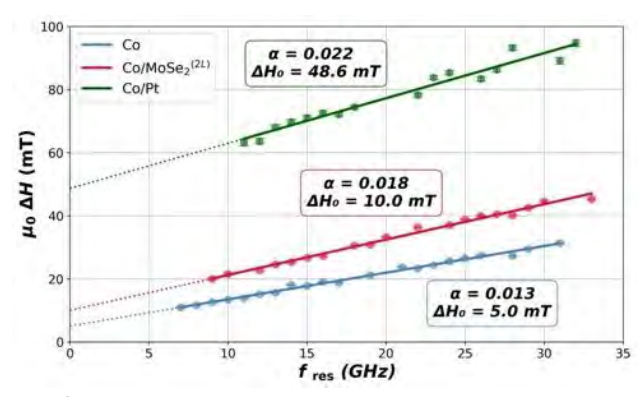


Fig. 2. In-plane FMR linewidth vs. resonance frequency at room temperature, highlighting the changes in Gilbert damping and inhomogeneous broadening without and with metallic and nonmetallic seeding layers.

FR-13. Ultrafast stochastic thermal switching of dipolar skyrmion cores in Fe $_3$ Sn $_2$ nanodisks with perpendicular magnetic anisotropy

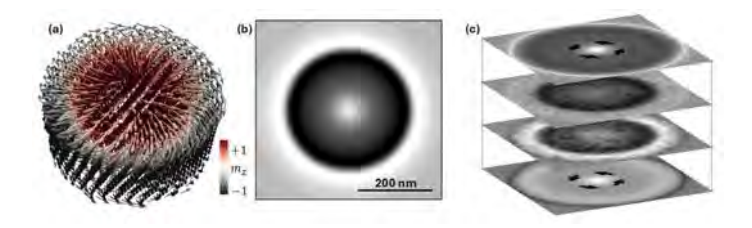
C. M. Nezat, M. Charilaou

Department of Physics, University of Louisiana at Lafayette, Lafayette, Louisiana, United States

Nanoscale magnetization textures, such as skyrmions, are promising for a wide range of applications due to their inherent stability and the ability to encode binary information via their helicity. The prospect of rapidly changing skyrmion states, without the need for strong external magnetic fields or current densities, is promising for future ultrafast and energy-efficient technologies. Recent electron microscopy experiments [1] have demonstrated all-optical switching of magnetization textures in thin films of the Kagome-type Fe₃Sn₂ uniaxial ferromagnet. This work investigates those findings further with micromagnetic simulations of Fe₃Sn₂ nanodisks, where ultrafast (photo)thermal excitation induces stochastic switching of the Néel caps in dipolar skyrmions. The photothermal excitation was modeled as temperature spikes based on a 2-Temperature model profile via a stochastic thermal field. The simulations identified three energy regimes: below a threshold excitation energy, the skyrmions remain stable; in an intermediate energy range, the Néel cap of the skyrmions switch stochastically while the Bloch components remain stable; and at higher energies, both Bloch and Néel components can undergo stochastic reversal. Given that these components can be resolved experimentally by means of high-resolution electron microscopy or holography, we computed images of Lorentz transmission electron microscopy and phase-shift maps of electron holography from the simulated magnetization textures. This enables direct comparison with imaging experiments, as shown in the example figure here. These results provide a quide to the stability of dipolar skyrmions in the uniaxial ferromagnet Fe-Sn at room temperature and the possibility of ultrafast stochastic switching without external magnetic fields or currents.

[1] J. T. Weber, A. Kovács, M. Charilaou, D. Kong, L. Prodan, V. Tsurkan, A. Schröder, N. S. Kiselev, I. Kézsmárki, R. E. Dunin-Borkowski, A. H. Tavabi, S. Schäfer: All-optical stochastic switching of magnetization textures in Fe₃Sn₂. arXiv 2503.05660 (2025)

^{*} Best Student Presentation Finalist / LB - Late-breaking Poster



Snapshot of a micromagnetic simulation of a Fe_3Sn_2 nanodisk showing (a) the vector plot of a stable dipolar skyrmion at room temperature, (b) the phase-shift map of that skyrmion, and (c) the deconstructed layer-dependent phase-shift map. The Bloch and Neel components of the skyrmion can be identified by the overall and center contrast, respectively.

^{*} Best Student Presentation Finalist / LB – Late-breaking Poster

SESSION GA: UNCONVENTIONAL AND NONRECIPROCAL SUPERCONDUCTIVITY

Chair(s): D. Makarov, Helmholtz-Zentrum Dresden-Rossendorf,
Dresden, Germany
Friday, October 31, 2025
08:30 AM-12:00 PM
Grand Ballroom

GA-01. Superconducting Spintronics

S. Parkin

NISE, Max Planck Institute for Microstructure Physics, Halle (Saale), Germany

The interplay of magnetism and superconductivity allows for unconventional superconductivity. Of great interest is proximity induced superconductivity in non-collinear spin textures, both artificially created and naturally formed. Notwithstanding the significant local magnetization that is usually incompatible with conventional superconductivity, such non-collinear spin textures can sustain long range triplet supercurrents that can, in principle, carry angular momentum and could be used manipulate magnetic nanosystems. An important application could be for a cryogenic racetrack memory that could support quantum computing systems. First, I discuss our recent progress in conventional racetrack memory in which we have demonstrated the high speed motion of chiral domain walls in nanoscopic magnetic racetracks less than 50 nm wide [1] as well as the first 3D racetracks [2]. Second, I discuss our recent work demonstrating long range triplet supercurrents in noncollinear spin textures, including a kagome antiferromagnet [3], as well as the observation of a Josephson Diode effect in several distinct materials [4, 5].

- [1] J.-C. Jeon, A. Migliorini, J. Yoon, J. Jeong, and S. S. P. Parkin, "Multi-core memristor from electrically readable nanoscopic racetracks," *Science*, vol. 386, pp. 315-322, 2024, doi: 10.1126/science.adh3419.
- [2] A. M. A. Farinha, S.-H. Yang, J. Yoon, B. Pal, and S. S. P. Parkin, "Interplay of geometrical and spin chiralities in 3D twisted magnetic ribbons," *Nature*, 2025/02/26 2025, doi: 10.1038/s41586-024-08582-8.
- [3] K.-R. Jeon *et al.*, "Chiral antiferromagnetic Josephson junctions as spin-triplet supercurrent spin valves and d.c. SQUIDs," *Nat. Nanotechnol.*, vol. 18, pp. 747-753, 2023. [4] B. Pal *et al.*, "Josephson diode effect from Cooper pair momentum in a topological semimetal," *Nat. Phys.*, vol. 18, pp. 1228-1233, 2022, doi: 10.1038/s41567-022-01699-5. [5] J.-K. Kim *et al.*, "Intrinsic supercurrent non-reciprocity

coupled to the crystal structure of a van der Waals Josephson barrier," *Nat. Commun.*, vol. 15, p. 1120, 2024.

GA-02. Superconducting diode effect in metallic multilayers $\underline{\mathsf{T.Ono}}$

Kyoto University, Uji, Japan

The diode effect is fundamental to electronic devices and is widely used in rectifiers and AC-DC converters. However, conventional diodes suffer from energy loss due to finite resistance. We found the superconducting diode effect (SDE) in Nb/V/Ta superlattices with a polar structure, which is the ultimate diode effect exhibiting a superconducting state in one direction and a normal state in the other [1-3]. The SDE can be considered as the nonreciprocity of the critical current for the metal-superconductor transition. We have also found the reverse effect, i.e., the nonreciprocal critical magnetic field under the application of supercurrent [4]. We also found that the polarity of the superconducting diode shows a sign reversal when the magnetic field is increased [5], which can be considered as the crossover and phase transitions of the theoretically predicted finite-momentum pairing states [6, 7]. SDE in Nb/V/Ta superlattices requires the application of an external magnetic field to break the time-reversal symmetry, which is a drawback in applications. Recently, we have succeeded in demonstrating zero-field SDE by introducing ferromagnetic layers into superlattices [8, 9]. The polarity of the SDE is controlled by the magnetization direction of the ferromagnetic layer, leading to the development of novel non-volatile memories and logic circuits with ultra-low power consumption. This work was partly supported by JSPS KAKENHI Grant Numbers (18H04225, 18H01178, 18H05227, 20H05665, 20H05159, 21K18145), MEXT Initiative to Establish Nextgeneration Novel Integrated Circuits Centers (X-NICS) Grant Number JPJ011438, the Cooperative Research Project Program of the Research Institute of Electrical Communication, Tohoku University, and the Collaborative Research Program of the Institute for Chemical Research, Kyoto University.

- [1] F. Ando et al., J. Magn. Soc. Japan 43, 17 (2019).
- [2] F. Ando et al., Nature 584, 373 (2020).
- [3] F. Ando et al., Jpn. J. Appl. Phys. 60, 060902 (2021).
- [4] Y. Miyasaka et al., Appl. Phys. Express 14, 073003 (2021).
- [5] R. Kawarazaki et. al., Appl. Phys. Express 15 113001 (2022)
- [6] A. Daido et al., Phys. Rev. Lett. 128, 037001 (2022).

- [7] K. Nakamura et al., Phys. Rev. B 109, 094501 2024).
- [8] H. Narita et al., Nat. Nanotechnol. 17, 823 (2022).
- [9] H. Narita et al., Adv. Mater., 10.1002/adma.202304083.

GA-03. Superconductor-Ferromagnet Proximity Coupled Bilayers Leads to Majorana Bound States and Nonreciprocal Critical Current Flow

J. S. Moodera

Physics, Plasma Science and Fusion Center, MIT, Cambridge, Massachusetts. United States

Superconductor (SC)-ferromagnet (FM) proximity coupled system has always been intriguing, while rich in complex physics. Exploring SC/FM has continued to exhibit new phenomena despite the extensive studies for several decades. The prediction of exotic Majorana bound states (MBS) to appear in superconducting proximity coupled (111) Au surface state raised the interest in SC/FM system further. Combined with the ideal Heisenberg semiconducting FM such as EuS and proximity coupled with superconductor V, the (111) Au is an excellent choice of topological SC to seek MBS. Following this direction, we observe the signature of candidate MBS pair by scanning tunnel spectroscopy in superconducting Au (111) surface. Now nanostructured planar junctions are being pursued for further confirmation, to show the highly challenging MBS pair entanglement, a precursor for enabling topological gubits.

In recent times there has been extensive interest and reports of the nonreciprocal critical current flow in many complex structures. It is fascinating to note that the SC/FM platform utilized in our search for MBS has also led us to 'rediscover' the nonreciprocal critical supercurrent flow, called SC diode effect. It turns out that such a phenomenon in superconducting strips with geometrical asymmetry has been around for over 50 years. In thin film bilayers of conventional SC thin film interfaced with a EuS we demonstrate strong SC diode effect, reaching efficiencies ~ 70%, including in zero applied field. This critical supercurrent nonreciprocity in SC thin films is identified to arise from asymmetrical vortex edge/surface barriers and the universal Meissner screening current. We show SC diode full wave rectifiers with high efficiency of >40%. Further tweaking the SC/FM structures we have realized nonvolatile SC memory as well. The evolution of SC order parameter in the SC/FM bilayers and its influence on the magnetic ordering adds richness.

Work is supported by NSF, AFoSR, ARO, ONR and Lincoln Lab ACC grants.

"Signature of a pair of Majorana zero modes in superconducting gold surface states", Sujit Manna, Peng Wei, Yingming Xie, Kam Tuen Law, Patrick A. Lee and Jagadeesh S. Moodera, Proc. Natl. Acad. Sci. 117 (16) 8775-8782 (Apr. 21, 2020); https//doi.10.1073/pnas.1919753117

"Ubiquitous Superconducting Diode Effect in Superconductor Thin Films", [the Editor's Pick], Yasen Hou, Fabrizio Nichele, Hang Chi, A. Lodesani, Yingying Wu, M. F. Ritter, D. Z. Haxell, Margarita Davydova, Stefan Ilić, Ourania Glezakou-Elbert, Amith Varambally, F. Sebastian Bergeret, Akashdeep Kamra, Liang Fu, Patrick A. Lee, and Jagadeesh S. Moodera, Phys. Rev.Lett. Vol. 131, No. 2, 027001 (2023) https://doi.org/10.1103/PhysRevLett.131.027001

"Efficient Superconducting Diodes and Rectifiers for Quantum Circuitry", Josep Ingla-Aynés, Yasen Hou, Sarah Wang, En-De Chu, Oleg A. Mukhanov, Peng Wei & Jagadeesh S. Moodera, Nature Electronics vol. 8, p411–416 (2025), https://doi.org/10.48550/arXiv.2406.12012

GA-05. Magnetic Imaging of Chiral and Magnetic Superconductors

Y. Iguchi^{1, 2}

¹Geballe Laboratory for Advanced Materials, Stanford University, Stanford, California, United States, ²Stanford Institute for Materials and Energy Sciences, SLAC National Accelerator Laboratory, Menlo Park, California, United States

Local magnetism plays a crucial role in studying superconductors with broken time-reversal symmetry, such as chiral superconductors and superconductors that coexist with magnetic orders (magnetic superconductors). Scanning superconducting quantum interference device(SQUID) magnetometry/susceptometry is a powerful technique for microscopically investigating the interplay between magnetism and superconductivity. In this presentation, we will discuss our recent findings using scanning SQUID, highlighting three key results:

- (1) the observation of extrinsically induced chiral edge currents in a spin-triplet superconductor UTe₂[1,2]. Our measurements detected localized magnetic flux at the sample edges consistent with theoretical predictions for chiral edge currents (Fig. 1).
- (2) The discovery of un-quantized vortex in the holeoverdoped $K_xBa_{1-x}Fe_2As_2(x=0.77)$ that breaks time-reversal symmetry[3]. Using scanning SQUID microscopy, we identified vortices carrying fractional magnetic fluxes of the

flux quantum, which vary with temperature and exhibit uniformity over millimeter scales (Fig. 2).

(3) The observation of the suppression of superfluid density near magnetic phase transitions in a helical magnetic superconductor RbEuFe₄As₄, where ferromagnetism also coexists with antiferromagnetism[4]. We also demonstrate the application of scanning SQUID techniques to investigate improved magnetic flux trapping in superconducting devices featuring sub-micron moats.

[1] Y. Iguchi, H. Man, S. M. Thomas, F. Ronning, P.F.S. Rosa, and K. A. Moler, Physical Review Letters 130, 196003 (2023).

[2] Y. Iguchi, H. Man, S. M. Thomas, F. Ronning, J. Ishizuka, M. Sigrist, P.F.S. Rosa, and K. A. Moler, Physical Review B 110, 214505 (2024).

[3] Y. Iguchi, R. A. Shi, K. Kihou, C.-H. Lee, M. Barkman, A. L. Benfenati, V. Grinenko, E. Babaev, and K. A. Moler, Science 380, 1244-1247 (2023).

[4] H. Man, Y. Iguchi, J. Bao, D.Y. Chung, and M.G. Kanatzidis, Nano Letters 24, 9082 (2024).

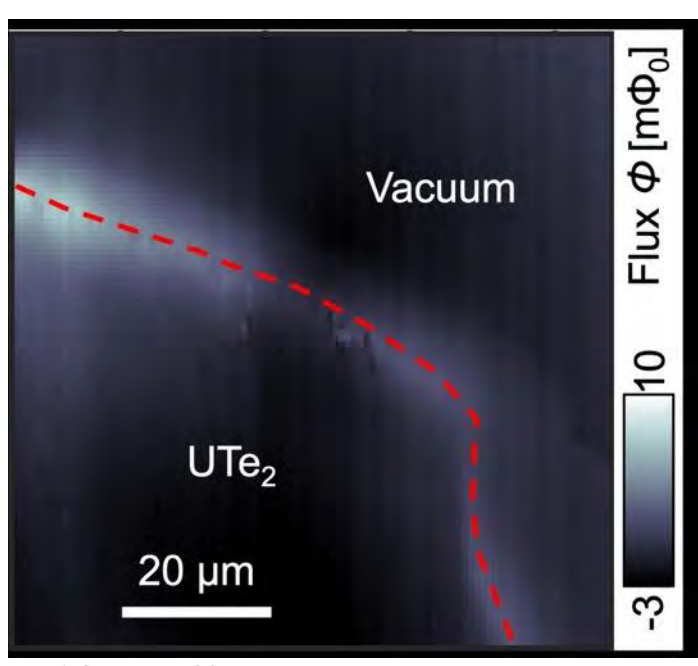


Fig. 1 Scanning SQUID magnetometry detected magnetic edge fields at almost zero background field [2].

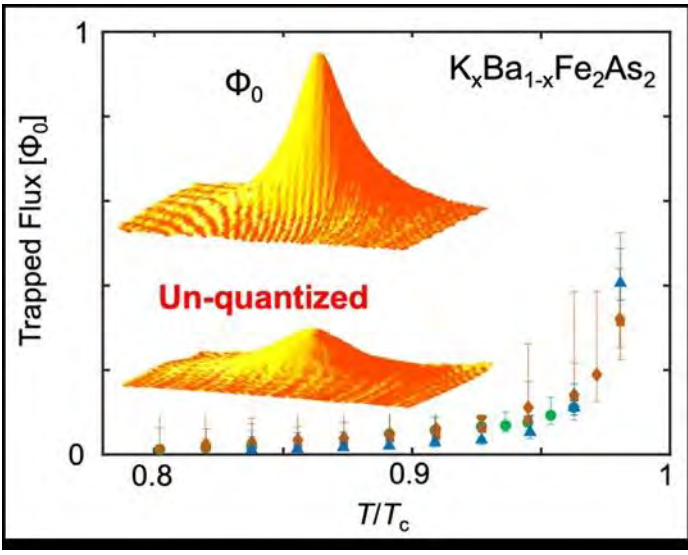


Fig. 2 Un-quantized vortices carry temperature-dependent flux. Insets show magnetic flux scan over a quantized and un-quantized vortices at $0.98T_c$ [3].

SESSION GB: PROBING AND MANIPULATING MAGNETIC ORDER IN 2D SYSTEMS

Chair(s): S. Singh, *Physics, Carnegie Mellon University, Pittsburgh, Pennsylvania, United States*Friday, October 31, 2025

08:30 AM-12:00 PM

Ballroom A

GB-01. Spin-orbit torque in van der Waals magnetic heterostructures: from microscopic domain imaging to ultrasensitive Sagnac Kerr interferometry

<u>Y. Luo</u>^{1, 2, 3}

¹Department of Physics and Astronomy, University of Southern California, Los Angeles, California, United States, ²Mork Family Department of Chemical Engineering and Materials Science, University of Southern California, Los Angeles, California, United States, ³Department of Chemistry, University of Southern California, Los Angeles, California, United States

Spin-orbit torques (SOTs) offer a powerful mechanism to control magnetic order in spintronic devices, and their integration with two-dimensional (2D) van der Waals (vdW) magnetic heterostructures opens new frontiers in both fundamental magnetism studies and device engineering. In this talk, I will present our recent progress in probing and quantifying spin-orbit torques across multiple platforms and scales—spanning microscopic magnetic imaging, optical metrology, and device-level control.

First, we use magnetic contrast scanning transmission X-ray microscopy (XMCD-STXM) at the MAXYMUS beamline of BESSY II synchrotron to visualize nanoscale speckled domain textures in epitaxially grown Fe₃GeTe₂/Bi₂Te₃ heterostructures, features absent in exfoliated Fe₃GeTe₂crystals [1-3]. These nontrivial domain configurations, which deviate from a simple macrospin model, are reproduced in micromagnetic simulations incorporating interfacial Dzyaloshinskii-Moriya interaction (DMI) and supported by first-principles calculations. We attribute the domain evolution to proximity-induced DMI from the Bi₂Te₃ substrate, which alters the balance between short-range exchange and long-range dipolar interactions.

Second, we present our recent advances in spin-orbit torque (SOT) metrology by the development of an ultrasensitive, fiber-based Sagnac magneto-optic interferometer operating under cryogenic temperatures and high magnetic fields [4, Fig 1]. Adapted from designs originally used to detect timereversal symmetry breaking in exotic superconductors [5], our interferometer achieves Kerr sensitivities below 5 µrad/√Hz. This method enables high-precision SOT quantification in both metallic and insulating magnetic systems, including those with low net magnetization or either perpendicular or in-plane anisotropy, where conventional transport-based techniques may suffer from magnetothermal artifacts.

Finally, we demonstrate spin-filtering tunneling detection and manipulation of antiferromagnetic resonance in PtTe₂/bilayer CrSBr/graphite heterostructures using a threeterminal device geometry [6, 7]. This method enables detection of antiferromagnetic dynamics down to atomically thin layers and also selective addressing of individual antiferromagnetic sublattices through SOT. These results establish a scalable platform for manipulating antiferromagnetic order and highlight the synergy between microscopic imaging, optical metrology, and spintronic device engineering in 2D systems.

[1] W. Zhou, A. J. Bishop, X. S. Zhang, K. Robinson, I. Lyalin, Z. Li, R. Bailey-Crandell, T. Min, J. Cham, S. Cheng, Y. K. Luo, D. C. Ralph, D. A. Muller, and R. K. Kawakami, *Tuning the* Curie temperature of a two-dimensional magnet/topological insulator heterostructure to above room temperature by epitaxial growth. Phys. Rev. Materials 7, 104004 (2023).

[2] Z. Li, W. Zhou, M. Swann, V. Vorona, H. Scott, R. K.

Kawakami, Full-film dry transfer of MBE-grown van der Waals materials. 2D Materials 12 (3), 035003 (2025).

- [3] M.T. Birch, L. Powalla, S. Wintz, O. Hovorka, K. Litzius, J.C. Loudon, History-dependent domain and skyrmion formation in 2D van der Waals magnet Fe₃GeTe₂. Nature communications 13 (1), 3035 (2022).
- [4] S. Karimeddiny, T. M. J. Cham, O. Smedley, D. C. Ralph, and Y. K. Luo, Sagnac interferometry for high-sensitivity optical measurements of spin-orbit torque. Science Advances 9, eadi9039 (2023).
- [5] J. Xia, P. T. Beyersdorf, M. M. Fejer, A. Kapitulnik, *Modified* Sagnac interferometer for high-sensitivity magneto-optic measurements at cryogenic temperatures. Applied Physics Letters 89, 062508 (2006).
- [6] T. M. J. Cham, D. G. Chica, X. Huang, K. Watanabe, T. Taniquchi, X. Roy, Y. K. Luo, and D. C. Ralph, Spin-filter tunneling detection of antiferromagnetic resonance with electrically-tunable damping. arXiv preprint arXiv:2407.09462 (In print, Science).
- [7] T. M. J. Cham, S. Karimeddiny, A. H. Dismukes, X. Roy, D. C. Ralph, and Y. K. Luo, Anisotropic gigahertz frequency antiferromagnetic resonance in layered van der Waals semiconductor. Nano Letters, 22, 6716-6723 (2022).

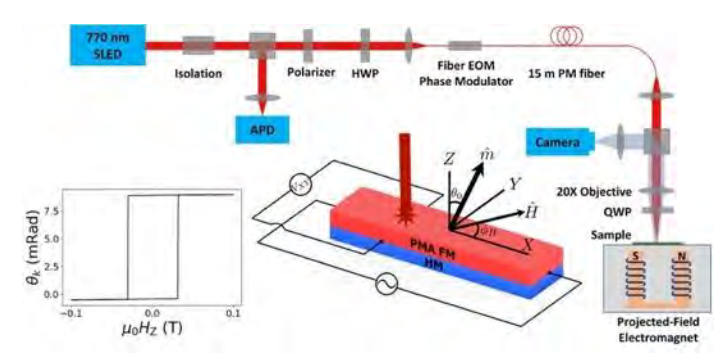


Fig. 1. Schematic of the Sagnac interferometer. The left inset shows the Sagnac signal for out-of-plane magneticfield-swept hysteresis of a Pt(4 nm)/Co(1.15 nm)/MgO device exhibiting strong perpendicular magnetic anisotropy. The measurement achieves a Kerr sensitivity better than 5 µrad/√Hz at an average laser power of 1 µW at the avalanche photodetector over a 10-minute scan.

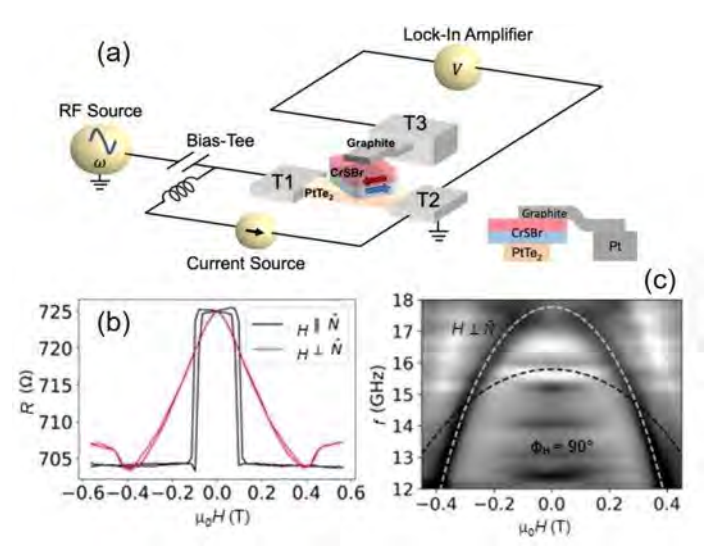


Fig. 2 (a) Schematic of PtTe₂/CrSBr/graphite 3-terminal device and measurement configuration. (b) Spin-filter tunneling magnetoresistance at 85 K measured between the top and bottom contacts (T3-T2 in (a)) as a function of inplane magnetic field H applied parallel to the CrSBr easy axis (H \parallel \tilde{N}) and parallel to the intermediate axis (H \perp \tilde{N}). (c) Spin-torque antiferromagnetic resonance (ST-AFMR) mixing voltage spectra for a magnetic field applied along the intermediate anisotropy axis (Φ H = 90°). Dashed gray line represents fit to the optical magnon field dependence based on a Landau-Lifshitz model for two antiferromagnetically-coupled sublattices. The dashed black line is the corresponding field dependence expected for the acoustic mode, showing that the detection technique is not sensitive to the acoustic mode.

GB-02. Quantum Sensing Using Two-dimensional Hexagonal Boron Nitride

H. Wang, J. Zhou

School of Physics, Georgia Institute of Technology, Atlanta, Georgia, United States

Emergent color centers with optically accessible spins have attracted tremendous research interest in recent years due to their significant potential for implementing transformative quantum sensing applications. Spin defects hosted by hexagonal boron nitride (hBN) represent emerging candidates in this catalog due to their remarkable compatibility with solid-state device integration and multimodal sensing capability of proximal two-dimensional quantum materials/devices [1]. Taking advantage of boron vacancy spin defects in hBN, we report nanoscale quantum imaging of low-dimensional (2D) ferromagnetism sustained

in Fe₃GeTe₂/hBN van der Waals (vdW) heterostructures [2]. Exploiting quantum spin relaxometry methods, we have observed spatially varying magnetic fluctuations in exfoliated Fe₃GeTe₂ nanoflakes, whose magnitude reaches a peak value around the Curie temperature. Using optically detected magnetic resonance measurements, we also show that ferromagnetic resonance and parametric spin excitations in a magnetic insulator Y₃Fe₅O₁₂ (YIG) can be detected by boron vacancy spin defects under various experimental conditions through the off-resonant dipole interaction between YIG magnons and boron vacancy spin defects [3]. We further report hBN-based quantum imaging of field-free deterministic magnetic switching of roomtemperature 2D magnet Fe₃GaTe₂ in an all-vdW spin-orbit torque system [4]. Our results highlight the opportunities offered by novel quantum spin defects in layered vdW materials for investigating microscopic spin behaviors in magnetic solid-state matters.

- [1] A. Gottscholl et al., Nature Materials 19, 540 (2020).
- [2] M. Huang et al., Nature Communications 14, 5259 (2023).
- [3] J. Zhou et al., Science Advances 10, eadk8495 (2024).
- [4] X. Zhang et al., arXiv:2502.04561.

GB-03. Electrostatic and Optical Control over the Magneto-Optics and the Magnetization Dynamics of van der Waals Magnets

M. H. Guimaraes

University of Groningen, Groningen, Netherlands

Van der Waals (vdW) materials are ideal systems for the study of spins and magnetism in low dimensions since they maintain their excellent optical, magnetic and electronic properties down to the atomically-thin limit. Because of their low dimensionality, these materials possess another exciting property, they are extremely sensitive to external stimuli, such as light and electric fields.

In this talk, I will show how we can reveal excitonic features and study the magnetization dynamics of a van der Waals magnetic semiconductor – $Cr_2Ge_2Te_6$ (CGT) – using (timeresolved) magneto-optics. First I will discuss our recent results[1] on the magneto-optic Kerr effect (MOKE) spectroscopy in CGT, which shows a very strong magneto-optic response arising from excitonic effects. The excitonic fingerprint on the MOKE spectrum of CGT is further confirmed by ab-initio calculations. Using electrostatic gating, we demonstrate the control of the magneto-optic

efficiency of CGT, allowing us to modulate the MOKE signals by up to 65%. I will also discuss our recent work on the control of magnetization dynamics in CGT using electrostatic gating[2]. By exploiting opto-magnetic phenomena, we are able to excite magnetization dynamics using ultrafast laser pulses and control, both the excitation process and the dynamics, using electrostatic doping and electric fields.

Our studies illustrate the potential of vdW magnets for combining optics, spintronics and magnetism, making them appealing for new opto-spintronic and opto-magnetic device architectures for future integrated photonic systems.

[1] F. Hendriks, et al., Arxiv 2408.09901 (2024)[2] F. Hendriks, et al., Nature Communications 15, 1298 (2024).

GB-04. Magnetism and spin transport in van der Waals heterostructures with 2D magnets

<u>B. Sanyal</u>, S. Ershadrad, M. Davoudiniya *Uppsala University, Uppsala, Sweden*

During the last few years, the realization of magnetic longrange order at considerably high temperatures in atomically thin 2D materials has opened up a significant potential in spintronic applications in ultrathin magnets along with the possibility of manipulation of magnetism by external fields, strain or proximity effects in van der Waals (vdW) heterostructures. Specifically, the family of 2D metallic magnets Fe_nGeTe₂ (n=3, 4, 5) has attracted a huge attention due to their high Curie temperatures and intriguing structure-property relationship. A systematic study of the electronic structure and magnetism of Fe_nGeTe₂ magnets by ab initio density functional theory, calculations of interatomic exchange interaction parameters and Monte Carlo simulations will be shown highlighting the importance of electron correlation with the aid of dynamical mean field theory [1], spin-orbit coupling and effects of transition metal doping [1-3,5]. Also, results on spinpolarized quantum transport calculations will be presented for PtTe2/Fe4GeTe2/PtTe2 van der Waals heterostructures [4]. Finally, the effects of electrode polytypes on spin transport properties will be shown for a vdW heterostructure comprising of a ferromagnetic monolayer of 1T-VSe\$ 2\$ with two structural polytypes (1T and 2H) of TaS\$ 2\$ electrodes. It will be shown that the 1T-device shows superior performance with lower Gilbert damping,

reduced critical current density and voltage for magnetization switching, compared to the 2H-device, which requires significantly higher current and voltage [6].

- [1] S. Ghosh, S. Ershadrad, V. Borisov, B. Sanyal, *npj comp. mat.* 9, 86 (2023)
- [2] S. Ershadrad, S. Ghosh, D. Wang, Y. Kvashnin, B. Sanyal, *J. Phys. Chem. Lett.* **13**, 4877 (2022)
- [3] S. Ghosh, S. Ershadrad, B. Sanyal, *2D materials* 11 035002 (2024)
- [4] M. Davoudiniya, B. Sanyal, Nanoscale Advances 6, 6278 (2024)
- [5] R. Ngaloy et al., ACS Nano 18, 5240 (2024)
- [6] M. Davoudiniya, B. Sanyal, npj 2D Mater. Appl. 9, 1 (2025)

SESSION GC: QUANTUM MATERIALS AND COOPERATIVE STATES

Chair(s): J. F. Sierra, Catalan Institute of Nanoscience and Nanotechnology (ICN2), Bellaterra, Barcelona, Spain Friday, October 31, 2025 08:30 AM-12:00 PM Ballroom C

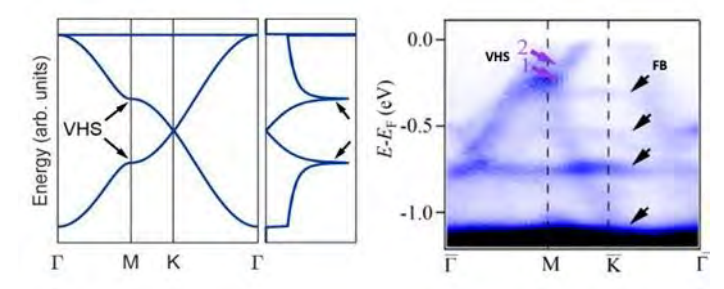
GC-01. Diverse Electronic Landscape of Kagome Motif M. Neupane

Department of Physics, University of Central Florida, Orlando, Florida, United States

Quantum materials with kagome lattice - comprised of corner-sharing triangles forming a hexagon in the crystal structure - have been studied as the potential playgrounds for exploring the interplay among parameters such as geometry, topology, electronic correlations, magnetic, and charge density orders. Recent report on a family of kagome metals of the form ReTi₃Bi₄ (Re = rare-earth) has generated interest due to the combination of highly anisotropic magnetism and a rich electronic structure. We use angleresolved photoemission spectroscopy measurements in combination with density functional theory calculations to investigate the electronic structure of newly discovered kagome metals ReTi₃Bi₄[1-7]. Our results reveal the presence of the multiple van Hove singularities (VHSs), some of which are in the vicinity of the Fermi level (see figure). We observe multiple flat bands, which originate from the destructive interference of wave functions within the Ti kagome motif. These flat bands and VHSs originate from Ti d-orbitals and are very responsive to the polarization of the incident beam. These results

demonstrate that of Ti based kagome materials system is an excellent platform for studying kagome induced flat band physics and its connection with magnetism.

- 1. A. P. Sakhya et al., Commun. Mat. 5, 241 (2024)
- 2. P. Park et al, Nature Commun. 16, 4384 (2025)
- 3. A. P. Sakhya *et al*, arXiv:2503.15759 (2025)
- 4. M. I. Mondal et. al. arXiv:2311.11488v1 (2023)
- 5. S. Regmi et al., Commun. Mater. 3, 100 (2022).
- 6. S. Regmi et al., Phys. Rev. B 108, L121404 (2023)
- 7. Dylan A. Jeff et al, 2D Mater.10 045030 (2023).



(Left) Schematic of electronic band dispersion of the kagome lattice. (Right) Experimental result of the Ti- based kagome material.

GC-03. Withdrawn

GC-04. Molecular Beam Epitaxy Growth of EuIn₂As₂ Thin Films on Sapphire and YAG

<u>M. Abdul Karim</u>, X. Liu, B. A. Assaf Physics, University of Notre Dame, Notre Dame, Indiana, United States

Euln2As2 is an intrinsic antiferromagnetic topological insulator predicted to host the axion insulator state [1]. While previous studies on this material have focused on bulk single crystals, thin films are required to realize its predicted topological edge and surface states. We have recently grown Euln2As2 thin films on both sapphire and yttrium aluminum garnet (YAG) substrates by molecular beam epitaxy (MBE). On sapphire, we found that high substrate temperatures above 680 °C are necessary to stabilize the layered Zintl phase of Euln2As2. We observed a Neel temperature around 17 K and a spin flop transition at 0.25 T. The films exhibit antiferromagnetic order at low temperatures with magnetic and magnetotransport properties consistent with bulk single crystals [2]. However, the large in-plane lattice mismatch between Euln2As2 and

sapphire leads to significant surface roughness and morphological disorder, which limits film quality and enhances resistivity [2]. On YAG, which offers a better lattice match, we achieve c-axis oriented EuIn2As2 thin films at an even lower temperature of 600 °C. X-ray diffraction measurements confirm the formation of the layered Zintl phase, with a lattice constant $c=17.859~\mbox{Å}$ in agreement with what has been reported for bulk crystals. This talk will compare the structural and magnetic properties of EuIn2As2 films grown on both substrates, highlighting the impact of substrate induced strain on magnetic ordering and film quality.

Work supported by NSF-DMR-2313441
[1] Y. Xu et al. Phys. Rev. Lett. 122, 256402 (2019)
[2] M. Abdul Karim et al. Phys. Rev. Mater. 7, 104202 (2023)

GC-05. Fractional Quantum Anomalous Hall Effect and Chiral Superconductivity in Graphene

L. Ju¹, <u>Z. Lu</u>²

¹Physics, Massachusetts Institute of Technology, Cambridge, Massachusetts, United States, ²Department of Physics, Florida State University, Tallahassee, Florida, United States

Fractional quantum Hall effect and superconductivity are two famous examples of emergent quantum phenomena driven by electron topology and correlations. They usually happen in very different materials and experimental settings. In this talk, I will discuss how they can be unified in one crystalline material, known as rhombohedral graphene. More than being hosted by the same materials, the settings challenge the conventional understandings of these phenomena: the fractional quantum Hall effect happens at zero magnetic field[1], while the superconductor behaves as a spin and orbital magnet[2]. I will also discuss the implications of these phenomena in the context of non-Abelian quasiparticles.

[1] Lu, Z., Han, T., Yao, Y., Reddy, A. P., Yang, J., Seo, J., ... & Ju, L. (2024). Fractional quantum anom-alous Hall effect in multilayer graphene. Nature, 626(8000), 759-764.
[2] Han, T., Lu, Z., Hadjri, Z., Shi, L., Wu, Z., Xu, W., ... & Ju, L. (2024). Signatures of chiral supercon-ductivity in rhombohedral graphene. *Nature* (2025). https://doi.org/10.1038/s41586-025-09169-7

GC-07. Fate of entanglement in quantum spin liquid under Lindbladian or non-Markovian dynamics induced by sudden coupling to dissipative bosonic environment

<u>F. E. García Gaitan</u>, B. Nikolić Department of Physics, University of Delaware, Newark, Delaware, United States

We investigate the stability of long-range entanglement in the Kitaev model of quantum spin liquid (QSL) that is suddenly coupled to a dissipative bosonic environment of Caldeira-Leggett type and time-evolved using Markovian [1,2,3] (i.e., Lindblad) or non-Markovian (via reaction coordinate mapping with the polaron transformation [4]) quantum master equation for weak or strong coupling, respectively. Using such a time-evolved density matrix of spins within QSL, we compute spin-spin correlation functions, logarithmic negativity, and Wilson loop expectation values for the interplay between local correlations and flux-sector stability. These quantities reveal dissipation-induced transitions of topological order and identify conditions under which QSL features will persist in the long-time limit, as relevant for building OSL-based topological quantum computer operating under realistic conditions and at finite temperature.

- [1] K. Yang, S. C. Morampudi, and E. J. Bergholtz, Exceptional spin liquids from couplings to the environment, Phys. Rev. Lett. 126, 077201 (2021).
- [2] K. Fukui, Y. Kato, and Y. Motome, Magnetic field effects on the Kitaev model coupled to environment, Phys. Rev. B 110, 024429 (2024).
- [3] K. Hwang, Mixed-state quantum spin liquids and dynamical anyon condensations in Kitaev Lindbladians, Quantum 8, 1412 (2024).
- [4] N. Anto-Sztrikacs, B. Min, M. Brenes, and D. Segal, Effective Hamiltonian theory: An approximation to the equilibrium state of open quantum systems, Phys. Rev. B 108, 115437 (2023).

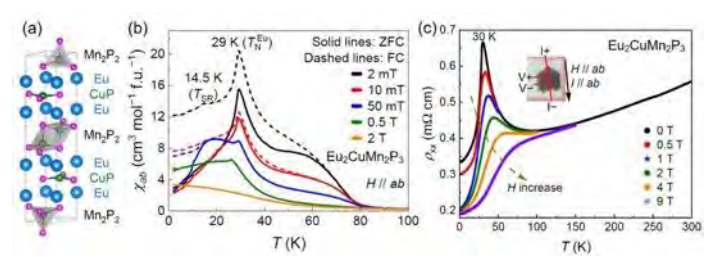
GC-08. Structural design and multiple magnetic orderings of the intergrowth compound Eu $_2$ CuMn $_2$ P $_3$

X. Chen¹, Z. Wang¹, W. Yang², J. Lu³, Z. Zhou¹, Z. Ren², G. Cao³, S. Dong¹, Z. Wang¹

¹Southeast University, Nanjing, China, ²Westlake University, Hangzhou, China, ³Zhejiang University, Hangzhou, China

We report the design, synthesis, crystal structure, and physical properties of the layered intergrowth compound Eu₂CuMn₂P₃. The structure of Eu₂CuMn₂P₃ features an alternating arrangement of hexagonal EuCuP block layers and trigonal EuMn₂P₂ block layers, interconnected through shared Eu planes. This structural hybridization leads to multiple magnetic orderings in Eu₂CuMn₂P₃: weak antiferromagnetic (AFM) ordering of Mn at $T^{Mn}_{N} = 80$ K, AFM ordering of Eu at T^{Eu}_{N} = 29 K, a spin-reorientation transition at T_{SR} = 14.5 K, and weak ferromagnetism below T_{N}^{Mn} . The spin configurations in different temperature regions are discussed based on the calculations of magnetic energies for various collinear arrangements. Resistivity measurements reveal a pronounced transition peak at T^{Eu}_{N} , which is suppressed in the presence of a magnetic field, resulting in a significant negative magnetoresistance effect. The computed semimetallic band structure, characterized by a small density of states at the Fermi level, aligns well with experimental observations. The successful synthesis of Eu₂CuMn₂P₃ and its fascinating magnetic properties highlight the effectiveness of our block-layer design strategy. By assembling magnetic block layers of compounds with compatible crystal symmetries and closely matched lattice parameters, this approach opens exciting avenues for discovering layered materials with unique magnetic behaviors.

[1] Xiyu Chen, Ziwen Wang, Wuzhang Yang, Jia-Yi Lu, Zhiyu Zhou, Zhi Ren, Guang-Han Cao, Shuai Dong, and Zhi-Cheng Wang, Structural design and multiple magnetic orderings of the intergrowth compound Eu₂CuMn₂P₃, Phys. Rev. B 111, 184441 (2025)



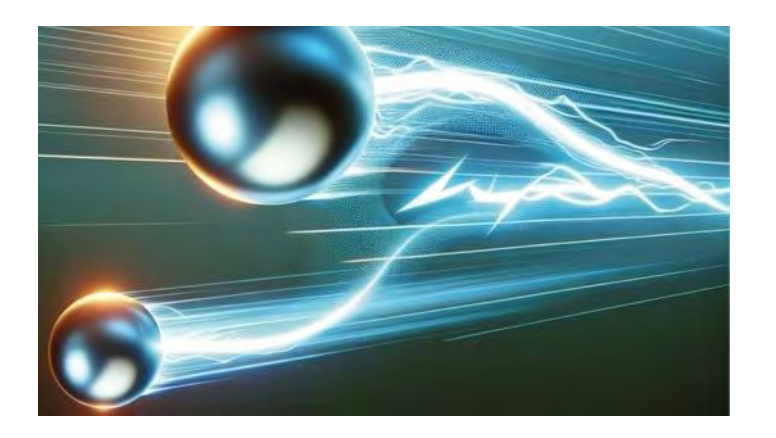
(a) The crystal structure of $Eu_2CuMn_2P_3$. Temperature-dependent magnetic suceptibility (b) and resistivity (c) under various fields.

GC-09. Evidence for electron fractionalization in a kagome metal

G. Aeppli^{1, 2, 3}, S. Ekahana³, <u>Y. Soh</u>³, Z. Wenliang³, T. Schmitt³ ¹ETH, Zurich, Switzerland, ²EPFL, Lausanne, Switzerland, ³PSI, Villigen, Switzerland

There are long-standing ideas and experiments concerning the emergence of unconventional quasiparticles in strongly interacting Fermi systems. The most dramatic are the fractional states originally observed for the two-dimensional electron gases in semiconductor heterostructures subjected to perpendicular magnetic fields, and explained shortly thereafter by Laughlin. Others found in zero field are more subtle in the sense that their peculiarity is reflected in their scattering rates which rise linearly together with their energies; these are the "marginal" fermions first conjectured for the layered cuprates also displaying high temperature superconductivity. Here we describe experiments revealing signatures of both types of anomalous quasiparticles in zero applied field. The material is Fe3Sn2, a ferromagnetic "kagome" metal, with numerous Weyl nodes near the Fermi level, and a high Curie temperature of ca. 640K. We investigated the compound using microfocused, laser-based angle-resolved photoemission, together with density functional theory (DFT) and machine learning-based analysis of images. Inelastic X-ray scattering measurements reveal that the correct starting point for understanding this material is not a single kagome layer, but rather a triangular lattice of Fe octahedra.

S. A. Ekahana et al., Nature 627, 67-72 (2024)
S. A. Ekahana et al., Mach. Learn.: Sci. Technol. 4 035021 https://doi.org/10.1088/2632- 2153/aced7d(2023)
M. Yao et al. arXiv:1810.01514
W. Zhang et al., Nature Comm. 15, Article number: 8905 (2024)



SESSION GD: MAGNETOELECTRIC AND MULTIFERROICS III

Chair(s): S. Husain, Material Science and Engineering, University of California, Berkeley, Berkeley, California, United States Friday, October 31, 2025

Friday, October 31, 2025 08:30 AM-12:00 PM Ballroom B

GD-01. Magnetoelectric Coupling Reprogrammed Magnonic Logic in Multiferroic Heterostructure

<u>P. Che</u>¹, A. Abdelsamie¹, Á. Papp², S. Salama³, A. Thiaville⁴, R. Lebrun¹, S. Fusil¹, V. Garcia¹, A. Vecchiola¹, K. Bouzehouane¹, M. Bibes¹, A. Barthelemy¹, J. Adam³, V. E. Demidov⁵, P. Bortolotti¹, A. Anane¹, I. Boventer¹

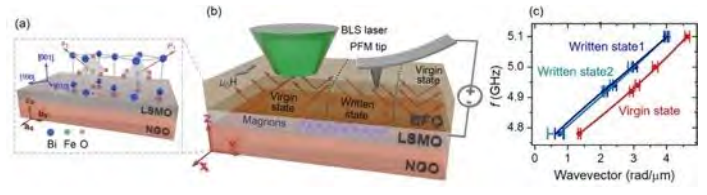
¹Laboratoire Albert Fert, CNRS, Thales, Université Paris-Saclay, Palaiseau, Île-de-France, France, ²Faculty of Information Technology and Bionics, Pazmany Peter Catholic University, Budapest, Hungary, ³Centre de Nanosciences et de Nanotechnologies, CNRS, Université Paris-Saclay, Palaiseau, Île-de-France, France, ⁴Laboratoire de Physique des Solides, Université Paris-Saclay, CNRS, Orsay, Île-de-France, France, ⁵Institute of Applied Physics, University of Muenster, Muenster, Germany

The increasing demand for high-performance and artificial intelligence (AI)-driven computing is causing a great increase in power consumption. Meanwhile, traditional CMOS-based semiconductor technology is reaching its limits in terms of size and energy efficiency. A new approach to constructing logic devices is needed. Magnons, the quanta of spin waves, are the quasiparticles of collective excitations in magnetically ordered materials. Information is encoded and processed using spin rather than electronic charge, which significantly reduces Joule heating, especially in magnetic insulators [1]. Therefore, magnonic logic devices have been identified as promising candidates for next-generation computing, offering both improved performance and energy efficiency while scaling down to the nanoscale and operating across a wide frequency range from GHz to THz [2,3]. The key step is the realization of fully reconfigurable, voltage-controlled, and programmable onchip magnonic devices.

Here, we utilize multiferroic heterostructures consisting of a BiFeO $_3$ (BFO) layer as a ferroelectric (FE) control element to manipulate magnonic properties in the ferromagnetic La $_{0.67}$ Sr $_{0.33}$ MnO $_3$ (LSMO) layer, epitaxially grown on NdGaO $_3$ (NGO) substrates (Fig. 1(a) and (b)). Using microfocus Brillouin light scattering (BLS), we observe controlled magnon propagation in the magnetostatic surface spin wave

configuration along programmable wavequides formed by magnetoelectric (ME) coupling in the multiferroic layer. The FE polarization is reconfigurable with up to seven switching cycles, with no fatique observed. Thermal magnon spectra show that the internal magnetic fields at the interface are modified by FE domain imprinting in BFO. The magnon dispersion relations are downshifted in frequency within the FE-domain-controlled waveguides as displayed in Fig. 1(c), and it is confirmed by micromagnetic simulations. This mechanism is further used for inverse design, and logic circuits such as majority gates are efficiently constructed in the multiferroic BFO/LSMO heterostructure. Our results open a new avenue for using multiferroic heterostructures and magnetoelectric coupling to build magnonic logic, with potential for future reservoir and neuromorphic computing applications.

- [1] B. Flebus, D. Grundler, B. Rana, et al. The 2024 magnonics roadmap. *J. Phys.: Condens. Matter* 36, 363501 (2024).
- [2] Q. Wang, M. Kewenig, M. Schneider, et al. A magnonic directional coupler for integrated magnonic half-adders. *Nat. Electron.* 3, 765–774 (2020).
- [3] J. Cheng, R. Yu, L. Sun, et al. A nonvolatile magnon field effect transistor at room temperature. *Nat. Commun.* 15, 9314 (2024).



(a) Schematic diagram of the epitaxial grown $BiFeO_3$ (BFO) on $La_{0.7}Sr_{0.3}MnO_3$ (LSMO) and $(001)_o$ -NdGaO $_3$ (NGO) substrate. Green arrows indicate the cryostalline orientation of BFO. Red arrows P_1 and P_2 show the ground state of the ferroelectric (FE) polarization directions. (b) Illustration of scanning Brillouin light scattering (BLS) detecting thermal magnons in LSMO and piezoresponse force microscopy (PFM) writing of FE domains in BFO layer. Electric field was applied between the PFM tip and the LSMO layer serving as bottom electrode for FE domain writing. In the written region, the FE polarization is switched from P_1 and P_2 to P_w (opposite direction of P_2) as marked by the red arrows. (c) Magnon dispersion relations of LSMO layer extracted from the phase-resolved BLS spectra modified by ferroelectric domains in the BFO layer.

GD-02. Ferroelectric-Control of Magnetotransport in Ruddlesden-Popper Strontium Iridates

X. Hong

Department of Physics and Astronomy, University of Nebraska-Lincoln, Lincoln, Nebraska, United States

The Ruddlesden-Popper 5d iridates $Sr_{n+1}Ir_nO_{3n+1}$ represents a model system where the electronic and magnetic states can by systematically tuned by the competition between strong spin-orbit coupling and onsite Coulomb energy. Voltage control of their electronic and magnetic properties is of intense fundamental and technological interests but remains to be demonstrated. This talk discusses the tuning of magnetotransport properties of ultrathin $Sr_{n+1}Ir_nO_{3n+1}$ (n = 1, 2, ∞) films via interfacial ferroelectric PbZr_{0.2}Ti_{0.8}O₃ (PZT). Nonvolatile polarization control of metal-insulator transition (MIT) has been achieved in SrIrO₃ and Sr₃Ir₂O₇. The former exhibits weak localization and weak antilocalization [1] that are modulated via PZT polarization reversal. Anomalous Hall effect and topological Hall effect are observed in PZT/SrIrO₃close to the MIT, signaling emergent magnetism. The latter can account for the enhanced electroresistance observed in Sr₃Ir₂O₇-based ferroelectric tunnel junctions [2]. Compared with the bulk Mott insulator state of Sr₂IrO₄, the PZT/Sr₂IrO₄ heterostructure exhibits transport characteristic of a 2D correlated metal [3], which can be attributed to interfacial charge transfer. The in-plane magnetoresistance and out-of-plane anisotropic magnetoresistance of the heterostructure sample show distinct temperature and magnetic field dependences compared with those of single layer Sr₂IrO₄, suggesting possible emergence of incipient ferromagnetism and polarization controlled magnetic anisotropy. These results shed new light on the intricate interplay of interface lattice coupling, charge doping, symmetry breaking, and magnetism in 5d iridates, opening new avenues for exploring correlated phenomena and designing voltage-controlled functionalities in this intriguing material system.

This work was supported by NSF through Grant No. DMR-1710461 and EPSCoR EQUATE center Award No. OIA-2044049, the UNL Grand Challenges catalyst award, and the Nebraska Center for Energy Sciences Research.

[1] L. Zhang, X. Jiang, X. Xu and X. Hong, *APL Materials*, Vol. 8, p. 051108 (2020).

[2] Y. Zhang, Y. Hao, L. Zhang, K. Wang and X. Hong, *Applied Physics Letters*, Vol. 125, p. 102904 (2024).

^{*} Best Student Presentation Finalist / LB - Late-breaking Poster

[3] Y. Zhang, Q. Wu, Y. Hao and X. Hong, *Advanced Physics Research*, Article No. 2400208 (2025).

GD-03. Stress-Coupled Nonlinear Magneto-Thermo-Mechanical Behaviour of Magnetostrictive and Magnetoelectric Composites under Combined Loads

S. Somavarapu¹, P. Kondaiah¹, K. Deepak²

¹Department of Aerospace and Mechanical Engineering,
Mahindra University, Hyderabad, Telangana, India, ²Department
of Metallurgical Engineering, Indian Institute of Technology
(BHU) Varanasi, Varanasi, Uttar Pradesh, India

Magnetoelectric (ME) composites are ever-increasing attention due to the coupling of magnetostrictive and piezoelectric materials, which are giving promising applications[1,2]. The nonlinear ME behaviour of composites with nanoscale has unique advantages and the studies when soft ferromagnetic magnetostrictive material with magnetoelectric composite when subjected to stresscoupled combined loads such as prestress, temperature and bias magnetic field are unexplored[3,4]. This study focuses on investigating these nonlinear magnetostrictive and ME magneto-thermo-mechanical responses using a finite element method. Metglas as soft ferromagnetic magnetostrictive material, and PZT 5H as piezoelectric material are used in the present work. he present model quantitatively predicts the nonlinear isotropic magnetostrictive and magnetoelectric behaviour when subjected to stress-coupled combined loads of prestress and temperature along with the external bias field. Results show that the magnetostrictive strain increases with increase in the prestress and the magnetization is equal at the saturation level. The ME coupling coefficient initially decreases with external stress up to an optimum magnetic field, and subsequently increases until reaching the saturation field. In contrast, with increase in temperature, all remaining preoperies are reduce linearly. Further, Main effects plots are employed to understand the influence of individual parameters across 396 and 576 simulation combinations for magnetostrictive and ME responses, respectively. The main effects plots shows that a nonlinear variation of ME coupling coefficient with increasing external stress, while temperature leads to a linear reduction. Additionally, optimization of the ME composite is performed by varying the geometry of piezoelectric and magnetostrictive layers to maximize the ME coefficient. The developed nonlinear magneto-thermo-mechanical behaviour of magnetoelectric composite may provide a

theoretical basis and geometry optimization for regulating the stress-coupled, temperature, and bias magnetic field during the device fabrication applications such as ultrasensitive biomedical devices.

[1] Z. Chu, M. PourhosseiniAsl and S. Dong, *J. Phys. D: Appl. Phys.*, Vol. 51, p. 243001 (2018).

[2]S. Zuo, Y. Wang, L. Liu, Q. Fang and Y. Gao, *IEEE Trans. Biomed. Circuits Syst.*, Vol. 14, pp. 971–984 (2020)

[3] X. J. Zheng and X. E. Liu, *Journal of Applied Physics.*, Vol. 97, p.053901 (2005)

[4]X. J. Zheng and L. Sun, *Journal of Applied Physics.*, Vol. 100, p. 063906 (2006)

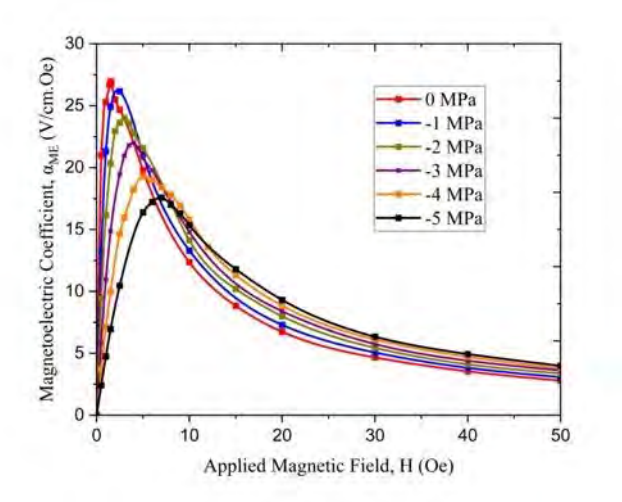


Fig.1. ME coefficient with varying prestress

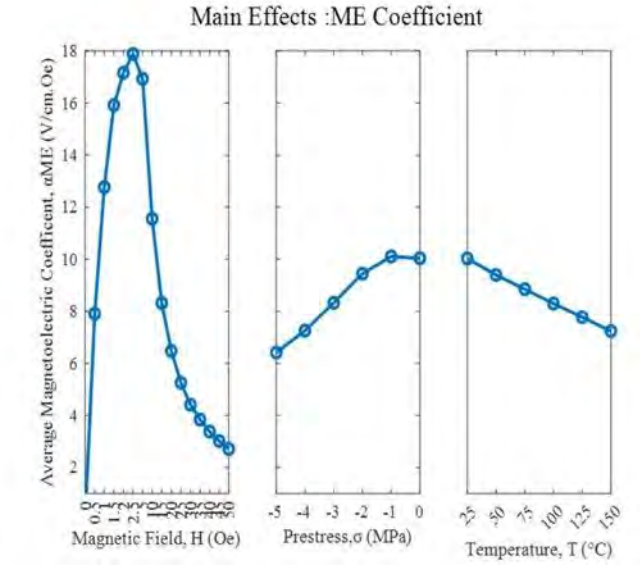


Fig. 2 ME Main Effects plots

GD-04. Withdrawn

GD-05. Swift Heavy Ion-Induced Modifications in the Magnetic and Electronic Properties of LaMn_{0.8}Co_{0.2}O₃ Thin Film

F. H. Bhat¹, <u>A. Jan</u>¹, G. Anjum²
¹Department of Physics, Islamic University of Science and Technology, Kashmir, Pulwama, India, ²Department of Physics, Govt. SAM Degree College Budgam, Budgam, India

Perovskite manganites are well known for their diverse electrical, magnetic, and electronic properties, including mixed valence states, ferromagnetism/anti-ferromagnetism [1-2], metal-insulator transition, and colossal magnetoresistance (CMR) [3], in addition to spin, orbital, and charge ordering properties [4]. These characteristics make them promising materials for applications in read heads, storage media, and magnetic sensors [5]. In this study, LaMn_{0.8}Co_{0.2}O₃ (LMCO2) thin film was synthesized using the Pulsed Laser Deposition (PLD) technique on (100) oriented LaAlO₃ substrates. To explore the effects of swift heavy ion (SHI) irradiation, the films were irradiated with 100 MeV Ag ions at a fluence of 5×10¹² ions/cm². Structural analysis was performed using X- ray diffraction (XRD) and magnetic properties were studied using a SOUID magnetometer. To gain insights into the electronic structure and the underlying physics, X-ray absorption spectroscopy (XAS) measurements were carried out at the Mn L_{2.3}-edge and Co L_{2.3}-edge. The XAS results indicate that SHI irradiation induces the formation of oxygen vacancies and introduces significant structural disorder and strain, thereby modifying the hybridization between Mn/Co 3d and O 2p orbitals. Magnetic measurements revealed paramagnetic to ferromagnetic transition with a reduced Curie temperature compared to the bulk counterpart. These results highlight the substantial impact of SHI irradiation on the electronic and magnetic properties of LMCO2 thin films and provide valuable insights into the mechanisms governing phase transitions and magnetic interactions in these systems.

[1] S. Chauhan, S. Kumari, and P. K. Siwach, Physica E: Low-dimensional sys. And Nanost. 128, 114573 (2021).
[2] F. H. Bhat, G. Anjum, and R. Kumar, Ceramics International 47 (5), 6753-6763 (2021).
[3] R. M. Kusters, J. Singleton, and D. A. Keen, Physica B 155, 362 (1989).

[4] C. N. R. Rao, A. Arulraj, and A. K. Cheetham, J. Phys. Condens. Matter 12, R83 (2000).

[5] N. Adeela, U. Khan, and S. Naz, Applied Surface Science 422, 184-191 (2017).

GD-06. Boosting Magneto-Ionic Effects in CoFeB/MgO/HfO₂/LiPON Stacks by Ion Irradiation

<u>Y. Sassi</u>¹, R. Mansell², D. Gouéré¹, E. Monteblanco¹, S. van Dijken², D. Ravelosona¹

¹Spin-Ion Technologies, Centre de Nanosciences et Nanotechnologies, Palaiseau, France, ²NanoSpin, Department of Applied Physics, Aalto University School of Science, FI-00076 Aalto, Finland

Magneto-ionics offers a promising route for developing energy-efficient spintronic devices by enabling low-power voltage-driven ion motion for non-volatile tuning of magnetic properties such as perpendicular magnetic anisotropy (PMA) [1-4] . However, current implementations are often limited by high voltage thresholds and poor reversibility.

In this study, we enhance the magneto-ionic effect in all-solid-state stacks using ion irradiation (Fig. 1). The device architecture is based on a Ta/CoFeB/MgO/HfO₂/LiPON/Pt multilayer structure grown on a silicon substrate. A key advantage of using a LiPON ionic gate lies in its supercapacitive behavior [5,6]. To enable parallel testing of multiple devices, the multilayer was patterned into an array of crossbar junctions, featuring Ta/CoFeB/MgO/HfO₂ as grounded bottom electrodes and LiPON/Pt as top electrodes (Fig. 1).

We observe that applying negative voltage pulses reduces PMA toward an in-plane magnetic state, while positive pulses reverse this effect (Fig. 2). This behavior is attributed to Li⁺ ion migration out of the CoFeB layer and the redistribution of oxygen ions, altering the oxidation state and the magnetic anisotropy of the layer [7]. Initially, the voltage required to trigger this effect exceeds 4 V. To reduce this, we introduced ion irradiation either before or after top electrodes deposition. Our results (Fig. 2) show that increasing the irradiation fluence significantly enhances the magneto-ionic response and lowers the voltage threshold by up to a factor of two.

[1] T. da Câmara Santa Clara Gomes, T. Bhatnagar-Schöffmann, S. Krishnia, Y. Sassi, D. Sanz-Hernández, N. Reyren, M.-B. Martin, F. Brunnett, S. Collin, F. Godel, S. Ono, D. Querlioz, D. Ravelosona, V. Cros, J. Grollier, P. Seneor, L. Herrera Diez, Phys. Rev. Applied 21, 024010 (2024)

[2] A. J. Tan, C. O. Avci, F. Büttner, M. Mann, W. Hu, C. Mazzoli, S. Wilkins, H. L. Tuller, G. S. D. Beach, Nature Mat. 18, 35-41 (2019)

[3] S. Chen, E. Monteblanco, B. Borie, S. Ono, D. Ravelosona, arXiv 2502.18248 (2025)

[4] M. Ameziane, R. Mansell, V. Havu, P. Rinke, S. van Dijken, Adv. Funct. Mater. 32, 2113118 (2022)

[5] M. Ameziane, J. Huhtasalo, L. Flajšman, R. Mansell, S. van Dijken, Nano. Lett., 23, 8, 3167-3173 (2023)

[6] S. Das, R. Mansell, L. Flajšman, M.A. Syskaki, R. Langer, S. van Dijken, Phys. Rev. Applied 23, 054043 (2025)

[7] I. Benguettat-El Mokhtari, R. Pachat, V. Porée, A. Lamperti, Y. Roussigné, M.-A. Syskaki, J. Wrona, G. Bernard, A. Cataldo, A. Resta, A. Nicolaou, S. Ono, S. M. Chérif, J. Langer, D. Ravelosona, M. Belmeguenai, A. Solignac, L. Herrera Diez, Appl. Phys. Lett. 9 (2025)

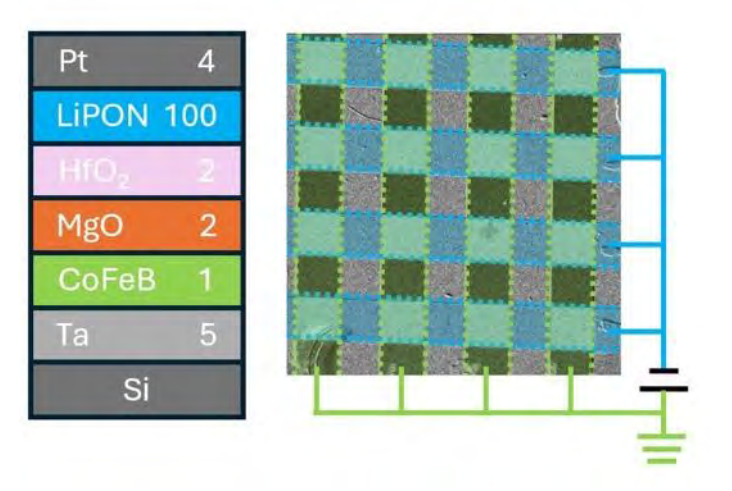


Figure 1. *Left*: Schematic of the all-solid-state multilayer stack (thickness in nanometers). *Right*: Polar-MOKE image of the array of crossbar junctions. Green regions indicate bottom electrodes, while blue regions correspond to the LiPON/Pt top layers. Electrodes are 200 µm wide.

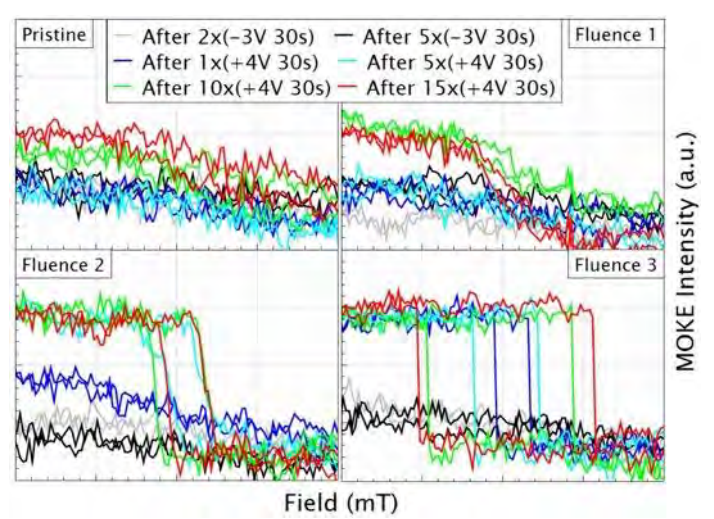


Figure 2._Comparison of polar MOKE hysteresis loops measured on samples irradiated at the same energy but with increasing fluence (F1 < F2 < F3). The CoFeB magnetization is initially set to an in-plane state using negative voltage pulses. Subsequently, sequences of positive pulses are applied to progressively reorient the magnetization out of plane.

GD-07. Precession-Field-Free Voltage Controlled Magnetic Anisotropy Switching of Magnetic Tunnel Junction

<u>D. Favaro^{2, 1}</u>, D. Narducci², J. Chatterjee², M. Gama Monteiro², S. Rao², R. Carpenter², J. Van Houdt^{2, 1}, K. Temst^{1, 2}, W. Kim² ¹Physics and Astronomy, KU Leuven, Leuven, Belgium, ²Imec, Leuven, Belgium

The voltage controlled magnetic anisotropy (VCMA) effect has been extensively studied as a low power alternative to spin transfer torque (STT) for switching magnetic tunnel junctions (MTJs) [1]. However, VCMA driven precessional switching faces three major limitations: (i) it typically requires an external in plane magnetic field to control precession and a pre read operation due to its unipolar and non deterministic nature [2,3]; (ii) the pulse width operating window is narrow, making it difficult to define a common operating window across devices; and (iii) offset fields favor one switching direction, reducing switching probability in the opposite direction [4,5]. Here we propose and demonstrate, via micromagnetic simulations, a deterministic VCMA based switching scheme called Precession Field Free VCMA, which eliminates the need for external magnetic fields and pre read. This approach introduces a second VCMA sensitive magnetic layer, named driver layer (DL), which enables free layer (FL) switching through offset field

433

modulation. Figure 1 illustrates the MTJ simplified stack and FL switching mechanism. At low bias, the DL magnetization remains out of plane, producing a negative offset field on the FL. In this state, the paralle to antiparallel (P to AP) switching field is negative and only the AP state is stable at remanence. At higher bias, the DL is driven in plane, reversing the offset field polarity; now the AP to P switching field is positive and only the P state is stable at remanence. Figure 2 shows the FL dynamics: with DL out of plane the FL either switches to AP (if initially P, described by the solid red line) or remains AP (dashed red line); with DL in plane it either switches to P or remains P (blue solid line and dashed blue line, respectively).

- [1] Nozaki, Takayuki, et al., *Micromachines* 10.5 (2019): 327. [2] Shao, Yixin, et al., *Communications Materials* 3.1 (2022): 87.
- [3] Kanai, S., et al., *Applied Physics Letters* 103.7 (2013).
 [4] Wu, Y. C., et al., *2020 IEEE Symposium on VLSI Technology*.
 IEEE, 2020.
- [5] Carpenter, Robert, et al., *IEEE Transactions on Nanotechnology* 22 (2023): 564-568.

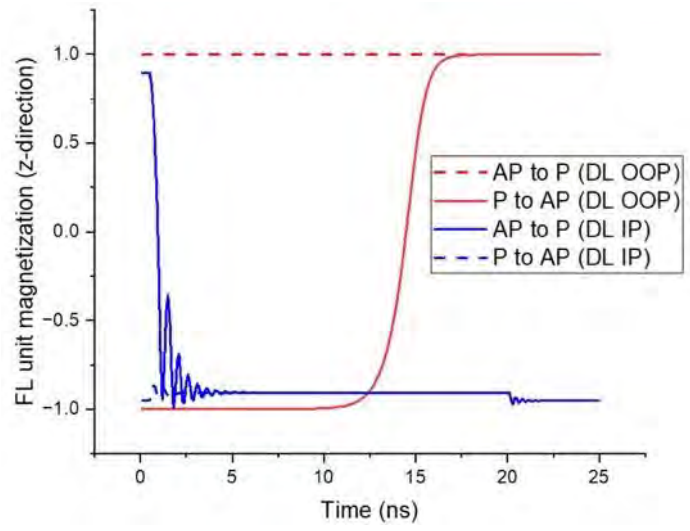


Fig. 1 FL unit magnetization dynamics: with DL out of plane only AP state is stable, if FL is in P it switches to AP (solid red curve) while if it is in AP it remains in AP (dashed red curve). Vice versa for the case of DL in plane (blue curves).

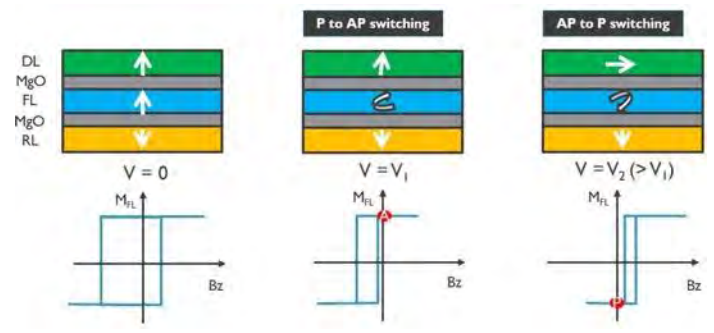


Fig. 2 Schematic of the PFF VCMA operation and FL hysteresis loop at remanence, for P to AP and AP to P switching. The corresponding DL magnetization states and a simplified MTJ stack structure are also illustrated.

GD-08. Large Room-Temperature Anomalous Nernst Effect in a Magnetic Equiatomic Heusler Alloy for Spin-Caloritronic Applications

R. Roy Chowdhury¹, <u>P. Sharma</u>¹, A. Bera², J. Nag^{2, 3}, A. Alam², K. G. Suresh², M. Phan¹, H. Srikanth¹

¹Department of Physics, University of South Florida, Tampa, Florida, United States, ²Department of Physics, Indian Institute of Technology Bombay, Mumbai, Maharashtra, India, ³Pennsylvania State University, University Park, Pennsylvania, United States

Equiatomic Heusler alloys (EQHAs) are a fascinating class of intermetallic compounds that have garnered significant attention due to their diverse and exotic electronic and magnetic characteristics that can be engineered for specific applications [1]. These alloys comprise of 1:1:1:1 elemental ratio of the constituent elements (XX'YZ, X and Y: transition metals and Z: main group element). Notably, EQHAs often host half-metallicity and large spin polarization, ideal for spin valves, magnetic tunnel junctions, and spin-transfer torque-based magnetic memory devices [2]. Here, we present the first experimental realization of CoRuMnSn as a room temperature magnetic Heusler alloy with novel spindependent thermal transport properties. CoRuMnSn crystallizes in a cubic crystal structure with a lattice parameter of 6.12 Å. Magnetometry measurements reveal high-temperature ferromagnetic ordering, with a Curie temperature exceeding 400 K. The longitudinal resistivity of CoRuMnSn exhibits metallic behavior. Thermoelectric investigations reveal a total thermal conductivity ~ 4.62 and 0.35 W/K.m at 300 K and 5 K, respectively. Interestingly, the longitudinal Seebeck coefficient (Sxx) undergoes a sign crossover from negative (400 K-143 K) to positive (< 143 K) values, indicating a transition of majority carriers from

electrons to holes. The spin-dependent transverse magnetothermoelectric transport properties of CoRuMnSn are particularly remarkable, with a large Anomalous Nernst voltage (V_{XY}^{ANE}) ~ 4.5 V and a corresponding Nernst coefficient (S_{xy}^{ANE}) of ~ 63 nV/K at 295 K. This transverse voltage arises perpendicular to both the applied in-plane magnetic field and the temperature gradient [3]. Furthermore, V_{XY}^{ANE} exhibits opposite polarity compared to the anomalous Hall effect, suggesting distinct underlying mechanisms. Our findings highlight CoRuMnSn as a promising magnetic Heusler compound with exceptional thermal and electronic characteristics, paving the way for further exploration of its potential in tunable, highefficiency spin-caloritronic applications. Our study contributes to the emerging field of spin-caloritronics, which explores the interplay of spin, charge, and heat in magnetic materials [4].

[1] L. Bainsla, and K. G. Suresh, "Equiatomic quaternary Heusler alloys: A material perspective for spintronic applications", *Appl. Phys. Rev.* 3, 031101 (2016).

[2] V. Barwal, H. Suto, R. Toyama, K. Simalaotao, T. Sasaki, Y. Miura, and Y. Sakuraba, "Large magnetoresistance and high spin-transfer torque efficiency of $Co_2Mn_xFe_{1-x}Ge$ ($0 \le x \le 1$) Heusler alloy thin films obtained by high-throughput compositional optimization using combinatorially sputtered composition-gradient film", *APL Mater.* 12, 111114 (2024).

[3] A. Chanda, J. Nag, N. Schulz, D. DeTellem, A. Alam, K. G. Suresh, M.H. Phan, and H. Srikanth, "Robust Nernst magnetothermoelectricity in the topological spin semimetal FeCrRhX (X = Si, Ge)", *Phys. Rev. B.* 111, 094416 (2025).

SESSION GE: MAGNONICS III: MATERIALS & SPIN TEXTURE DYNAMICS

Chair(s): B. Jungfleisch, *University of Delaware, Newark,*Delaware, United States

Friday, October 31, 2025

08:30 AM-12:00 PM

Room 2DE

GE-01. Magnetic Properties of CoFeB Films in the Ultrathin Limit

W. K. Peria¹, J. J. Wisser¹, <u>C. Swindells</u>^{2, 4}, M. Tanksalvala¹, M. Kiechle², G. Hu³, M. Pufall¹, H. T. Nembach¹

¹Applied Physics Division, National Institute of Standards and Technology, Boulder, Colorado, United States, ²Associate,

Physical Measurement Laboratory, National Institute of Standards and Technology, Boulder, Colorado, United States, ³IBM T. J. Watson Research Center, Yorktown Heights, New York, United States, ⁴Department of Electrical Engineering, University of Colorado Denver, Denver, Colorado, United States

In magnetic memory applications, among the critical material parameters that impact device performance are the magnetic moment, the magnetic anisotropy, the Gilbert damping, and the Heisenberg exchange parameter. The Heisenberg exchange is one quantity for which there has been disagreement about how to obtain reliable values in ultrathin films. For instance, the common method of measuring perpendicular standing spin waves (PSSW) in films of thickness ~100 nm is not possible for ultrathin films due to the high frequencies of the PSSW's accompanied by weak signal strength.

In this work, we use Brillouin light scattering (BLS) measurements to map the spin wave manifold of ultrathin (~1 nm) CoFeB films to determine the Heisenberg exchange parameter (see Figure 1). This method is an extension of previous BLS measurements on thicker films [1]. The BLS measurements were complemented by values for the effective magnetization and *q*-factor determined from ferromagnetic resonance and saturation magnetization determined from SOUID magnetometry. For films with thicknesses ranging from 0.7 to 1.5 nm, we obtain values of the exchange parameter A_{ex} ranging from approximately 5 – 9 pJ/m (compare to bulk value of ~27.5 pJ/m [2]) and observe a trend where A_{ex} decreases with film thickness (see Figure 2). Our work establishes a method for determining the exchange parameter in application-relevant ultrathin films and demonstrates that the exchange parameter can deviate significantly from the bulk value in the ultrathin limit.

- 1. Riley et al., Appl. Phys. Lett., Vol. 120, p.112405 (2020)
- 2. Devolder et al., J. Appl. Phys., Vol. 120, p.183902 (2016)

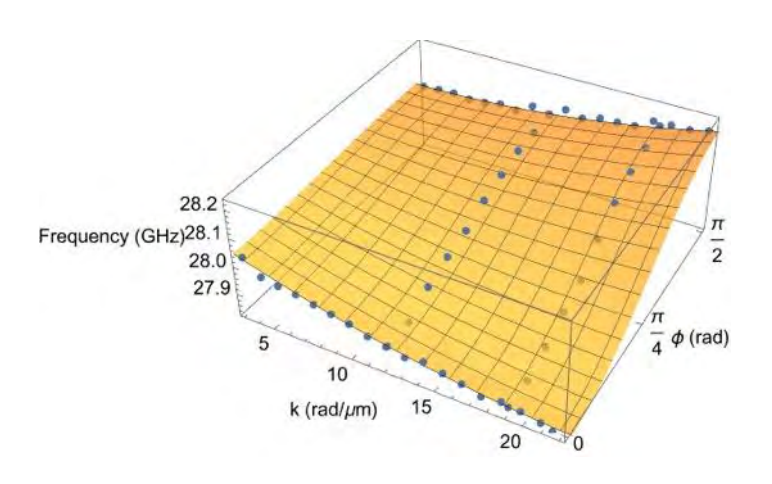


Fig. 1: Spin wave frequency of a 1.1 nm CoFeB film as a function of wavevector magnitude k and angle φ , where φ is the angle between the film magnetization and spin wave wavevector. The orange surface is a fit to the blue data points.

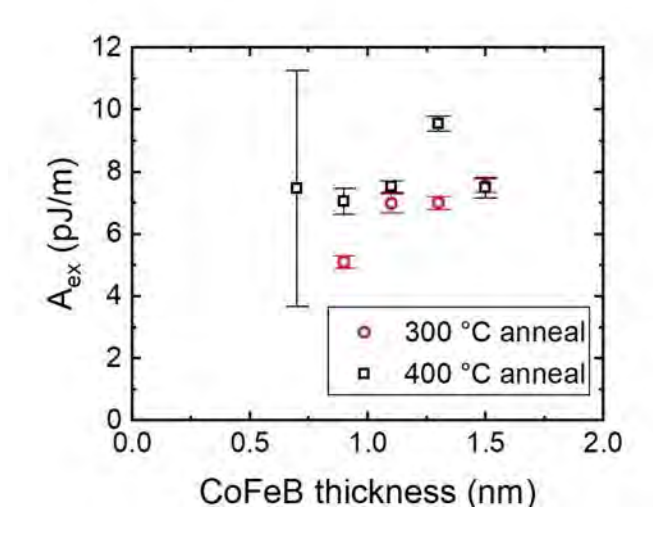


Fig. 2: Exchange parameter A_{ex} as a function of CoFeB thickness for annealing temperatures of 300 °C (red circles) and 400 °C (black squares).

$\label{eq:GE-02.Emulating 2D Materials with Magnonic Crystals} \textbf{GE-02. Emulating 2D Materials with Magnonic Crystals}$

B. Kaman, J. Lim, A. Hoffmann

Materials Research Laboratory and Department of Materials Science and Engineering, The Grainger College of Engineering, University of Illinois Urbana-Champaign, Urbana, Illinois, United States

Magnons in 2D and layered materials have received increased interest due to their unique spin dynamics. However, many interesting features occur at high energies near Brillouin zone boundaries, limiting experimental probes and potential applications. Here, we study a 2D magnonic crystal formed by holes in a perpendicularly magnetized yttium iron garnet (YIG) film. Through simulation, we find that its band structure mimics that of graphene, but additionally has kagome-like character and includes a few flat bands. Surprisingly, its nature can be understood using a tight binding model. This simple understanding enables us to engineer band gaps in analog to the 2D insulator boron nitride and exploit band topology to create localized states along 1D channels. Notably, the topological nature of these 1D excitations allows access to the valley degree of freedom in a magnonic analog of the quantum valley-Hall effect. Overall, this system brings a few unique features of 2D magnets to more accessible scales. Aside from applications in rf signal control, it may provide a platform for analogs of graphene physics like pseudo-Landau levels and magnon valley-tronics.

This work was supported by the NSF through the MRSEC award DMR-2309037.

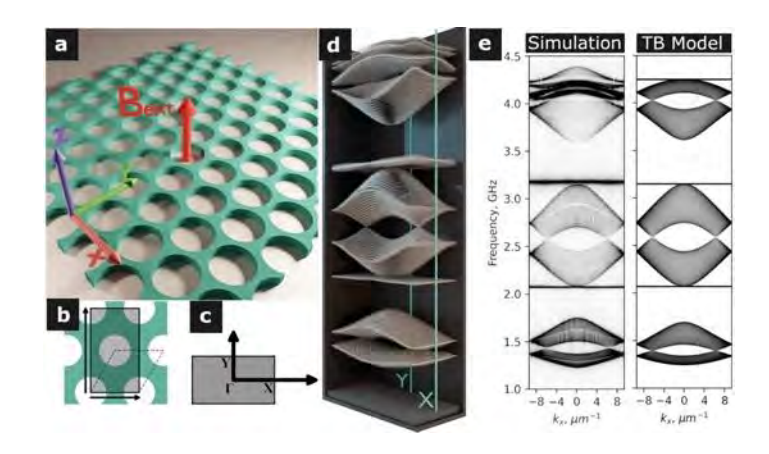


Fig. 1 Geometry and band structure. (a) 15 nm-thick YIG film (b) Unit cell, with hole spacing a=333 nm and diameter d/a=0.8. We adopt a rectangular cell, and (c) a rectangular Brillouin zone. (d) 3D band structure with

special points marked under a field of 185mT. (e) The same band structure as a projection in the (Γ -X, f) plane: (left) simulation, and (right) tight-binding (TB) model of the same, which is based on s-like and p-like modes. A working TB model implies simple, manipulable physics.

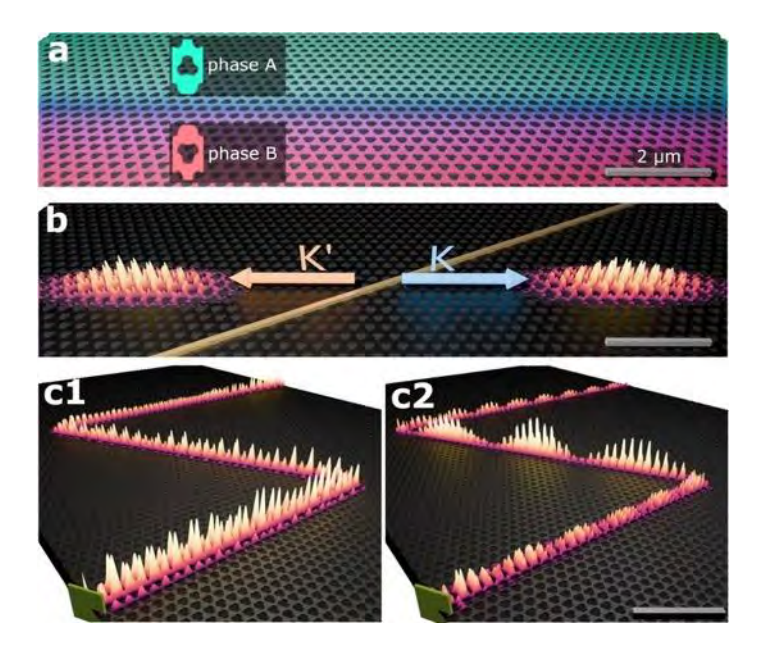


Fig. 2 Boundaries between gapped phases in analogy to the 2D insulator boron nitride. (a) the unit cell gradually changes between two distinct phases. (b) a large antenna can excite a localized mode. These can be considered quantum valley-Hall edge states, so wave packets are valley-polarized. (c) A different geometry: boundary modes stay well-localized when the boundary has reduced width and makes turns. This is true for both (c1) the low-frequency *s*-like modes, and (c2) the high-frequency *p*-like modes.

GE-03. Magnon-Magnon Coupling in a Pinned Synthetic Antiferromagnet

D. Backes

Diamond Light Source, Didcot, United Kingdom

Magnon-magnon coupling garnered considerable interest lately because of the novel spin- wave states that can be observed, coherently overlapping over a large volume. A synthetic antiferromagnet (SAF) is the ideal model system to study such coupling effects, as it can harbor both optical and acoustic magnon modes. Under certain circumstances, these modes can mix or hybridize into magnon bands exhibiting a band gap, a measure for the

coupling strength.

We demonstrate magnon-magnon coupling in a SAF using a home-built, VNA-based ferromagnetic resonance spectroscopy setup. Exciting both modes at the same time can be tedious, posing special requirements at the waveguide [1] or cavity design [2]. Our method is compatible with any given FMR setup and relies on pinning the SAF to an antiferromagnet. We show that, even in the weak pinning case, a magnon band gap of several GHz can be produced. This band gap is independent of the sample orientation with respect to the waveguide, requires no cooling and just a moderate magnetic field of <0.5T. A coupling rate η of 0.5 has been achieved, very close to the maximum of 1 for ultrastrong coupling.

Highly coherent magnon-magnon coupling states have the potential to be integrated and entangled with quantum platforms including superconducting qubits, nitrogen-vacancy centers, cavity photons, and phonons for coherent information transfer and collaborative information processing [3]. Our work thus paths the way towards applications in quantum computing, quantum memories and high-precision measurements.

- [1] S. Shiota et al., PRL 125, 17203 (2020)
- [2] A. Sud et al., Phys. Rev. B 102, 100403(R) (2020)
- [3] D. D. Awschalom et al., IEEE Trans. Quantum Eng. 2, 5500836 (2021)

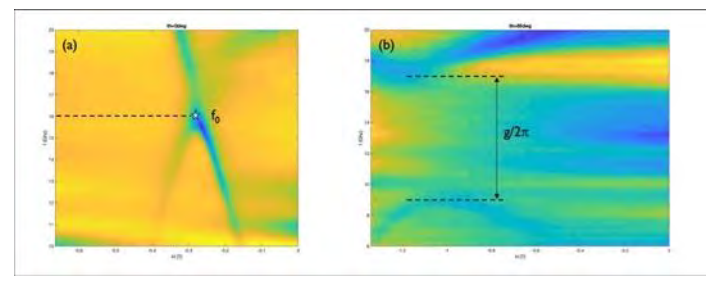


Fig. 1 Spectral map of a coupled optical and acoustic mode for a rotation angle θ of (a) 0° and (b) 85°. The hybridization of the two modes leads to the opening of a band gap. The coupling rate η , the ratio between band gap and intrinsic excitation frequency, as measured in (b) is 0.5. A value of η =1 marks the ultrastrong coupling regime.

GE-04. Experimental study of magnon-magnon interaction in bilayer, tetralayer, hexlayer, octlayer, and decalayer synthetic antiferromagnets (SAFs)

^{*} Best Student Presentation Finalist / LB – Late-breaking Poster

M. M. Subedi¹, K. Deng², Y. Xiong^{3,4,5}, J. Mongeon², T. Hossain⁶, P. Meisenheimer⁷, E. T. Zhou¹, J. Heron⁷, B. Jungfleisch⁶, W. Zhang^{3,4}, B. Flebus³, J. Sklenar¹

¹Physics and Astronomy, Wayne State University, Detroit, Michigan, United States, ²Department of Physics, Boston College, Chestnut Hill, Massachusetts, United States, ³Department of Physics and Astronomy, University of North Carolina, Chapel Hill, North Carolina, United States, ⁴Department of Physics, Oakland University, Rochester, Michigan, United States, ⁵Department of Electronic and Computer Engineering, Oakland University, Rochester, Michigan, United States, ⁶Department of Physics and Astronomy, University of Delaware, Newark, Delaware, United States, ⁷Department of Materials Science and Engineering, University of Michiqan, Ann Arbor, Michiqan, United States

Spin pumping has been an effective source to generate pure spin currents in spintronics and extensively studied in collinear magnetic systems [3, 4]. In this work, we discover a novel manifestation of spin pumping in non-collinear magnetic configurations which requires a theoretical expansion of the Landau-Lifshiz-Gilbert (LLG) formalism. Specifically, by incorporating both damping like and field like torques we explain an experimentally observed doublegap in the magnon spectrum of tetralayer synthetic antiferromagnets. Motivated by this foundational published work [1] and original theoretical work on magnon hybridization [2], additional study goes to hexlayer, octlayer, and decalayer SAFs. Microwave spectroscopic measurements reveal an interesting trait of level attraction feature in the magnon spectrum in hexlayer SAF. We do not see this same anomaly on the magnon spectrum in octlayers, and decalayers. This study not only provides a foundational understanding of magnon spectrum in these structures but also signifies an unprecedented role of spin pumping in magnon-magnon interactions in magnetic heterostructures, thereby contributing significantly towards providing flexibility in developing highly tunable, ultrafast, magnonic devices. M.M.S. and J.S. acknowledge support from the National Science Foundation under DMR-2328787. [1] M.M. Subedi et al., Phys. Rev. Appl., 23, L031003 (2025). [2] J. Sklenar, W. Zhang, *Phys. Rev. Appl.*, 15, 044008 (2021). [3] B. Heinrich, Y. Tserkovnyak, G. Woltersdorf, A. Brataas, R. Urban, G. Bauer, "Dynamic exchange coupling in magnetic bilayers," Phys. Rev. Lett., 90, 187601 (2003).

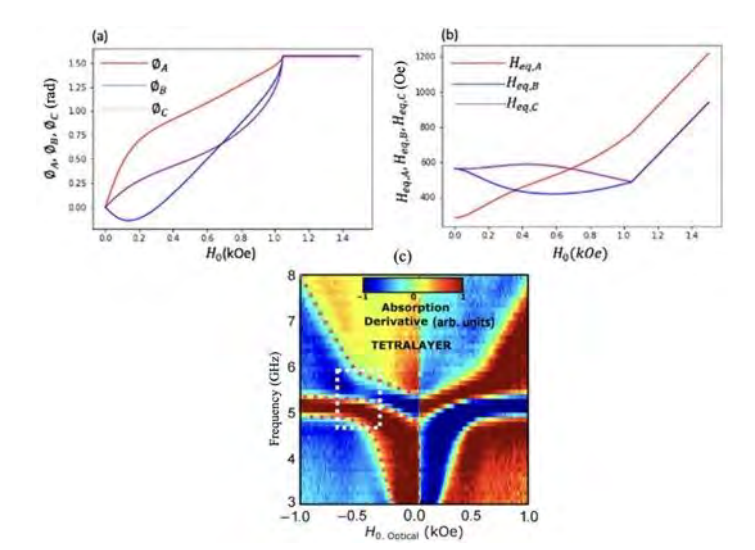


Figure 1. (a) Variation of equilibrium angles as a function of external field in a hexlayer synthetic antiferromagnetic. (b) Variation of effective (net) fields experienced by individual layers as a function of external field, for a fixed value of interlayer exchange field constant, in a hexlayer synthetic antiferromagnetic. (c) Experimentally observed doublegapped magnon spectrum in a tetralayer synthetic antiferromagnetic.

GE-05. Soliton Formation and Topological Transitions during Stripe Collapse in Fe/Gd Multilayers

J. A. Reddinger¹, E. Fullerton², S. Montoya², B. McMorran¹
¹Department of Physics, University of Oregon, Eugene, Oregon, United States, ²Center for Memory and Recording Research, University of California San Diego, San Diego, California, United States

Interest in magnetic skyrmions for spintronics applications has led to the development of a wide variety of magnetic materials. Certain approaches stabilize skyrmions not with the Dzyaloshinskii-Moriya interaction but through competition between short-range exchange and the longrange dipolar interactions. Without a symmetry-breaking interaction, these textures exhibit achiral, depth-varying domain wall structures. Fe/Gd multilayers, one such system, hosts a wide variety of magnetic structures including stripe domains and Type-I (skyrmions) and Type-II bubbles [1]. One method for forming both types of bubbles involves a field sweep from positive saturation to negative saturation at low sample tilt (α = 4°). This process is recreated in micromagnetic simulation enabling the investigation of nanosecond scale dynamics and energetics [2]. Achiral

[4] J. Slonczewski, "Current-driven excitation of magnetic

multilayers," Phys. Rev. Lett., 67, 3172

(1991).

stripe domains form oriented parallel (anti-parallel) to the in-plane component of the external magnetic field before (after) crossing remanence. At critical field strengths, the stripes collapse into various bubbles (Fig. 1). Due to the anti-alignment to the weak in-plane magnetic field, the Type-II bubbles minimize total energy via one of the following mechanisms depending on neighboring textures:

1) collapse into a skyrmion, 2) 180° rotation, 3) formation of Néel caps. The structure formed by the third mechanism is a Type-III bubble: a hybrid bubble with skyrmion closure domains and a Type-II core [3]. Analysis of the system's energetics (Fig. 2) reveals the factors driving a bubble to favor a transition and provides direction for improving the longevity of Type-III bubbles in future experiments.

[1] S.G. Je, H.S. Han, and J.I. Hong, ACS Nano, 14, p.3251-3258 (2020)

[2] A. Vansteenkiste, J. Leliaert, and B. Van Waeyenberge, AIP Advances, 4 (2014)

[3] L. Kong, J. Tang and H. Du, Physical Review B, 107, p.174425 (2023)

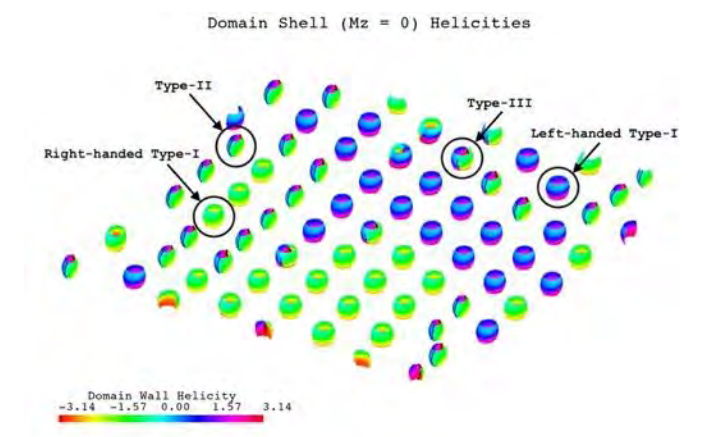


Fig. 1 Simulation depicting domain walls (mz=0) of Type-I, Type-II, and Type-III bubbles after stripe collapse. The colormap shows the angle between the domain wall magnetization and the gradient of the out-of-plane magnetization (helicity). Black lines show inversions in the domain wall chirality (Bloch line).

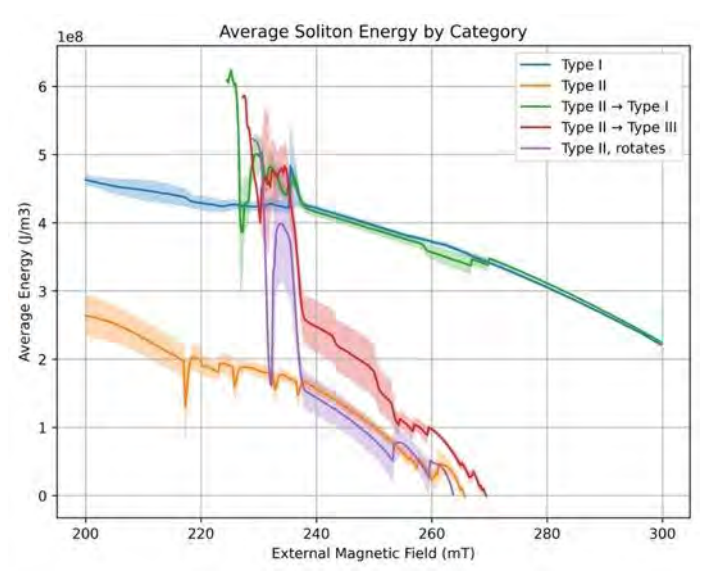


Fig. 2 Average energy of simulated soliton by category. Type-I (blue) and Type-II (orange) maintained topology for the duration of the simulation. Type-II \rightarrow Type-I (green) and Type-II \rightarrow Type-III (red) switch topology. Type-II, rotates (purple) rotated without a change in topology.

GE-06. Skyrmion Dynamics Probed with Neutron and X-ray Scattering and in situ Excitations

N. Tang¹, N. Liyanage¹, C. C. Buchanan¹, S. A. Morley², S. Roy², E. Fullerton³, S. Montoya³, L. DeBeer-Schmitt⁴, <u>D. A. Gilbert</u>¹

¹University of Tennessee, Knoxville, Tennessee, United States, ²Lawrence Berkeley National Laboratory, Berkeley, California, United States, ³University of California, San Diego, San Diego, California, United States, ⁴Oak Ridge National Laboratory, Oak Ridge, Tennessee, United States

Neutron and X-ray scattering remain gold-standard techniques for investigating nanoscale magnetic structures, from atomic ordering to mesoscopic textures. Skyrmions and other chiral spin configurations are no exception—their initial discovery was achieved via small-angle neutron scattering (SANS) [1]. These techniques are especially powerful due to their compatibility with a wide range of in situ sample environments [2,3], enabling studies under applied fields, temperature gradients, and RF excitation. We recently extended this capability through ferromagnetic resonance SANS (FMR-SANS), where skyrmions are driven into dynamic modes—such as gyration and breathing—using gigahertz RF fields, while their scattering signatures are captured simultaneously using SANS and small-angle X-ray scattering (SAXS) [4]. This allows direct observation of

skyrmion lattice dynamics, spin-wave excitations, and, under strong drive, lattice instability and collapse. These measurements have been demonstrated in both achiral skyrmions hosted by Gd/Fe multilayers and chiral skyrmions in Cu2OSeO3. Comparing these systems provides new insights into the fundamentals of high-frequency magnetic behavior and interactions between magnetic quasiparticles.

- [1] Science 336.6078, 198 (2012).
- [2] Physical Review Materials 2, 104402 (2018).
- [3] Nanoscale 16, 10715 (2024).
- [4] Advanced Materials 2300416 (2023).

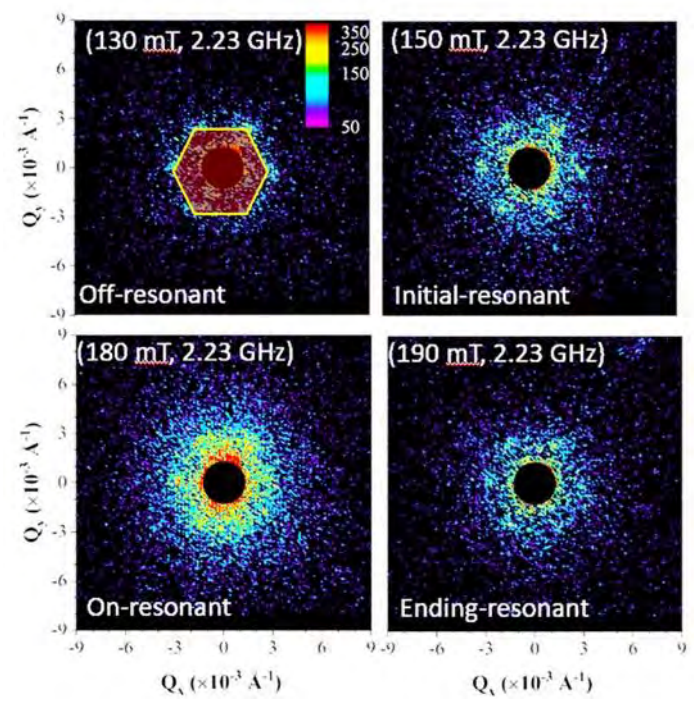


Fig. 1

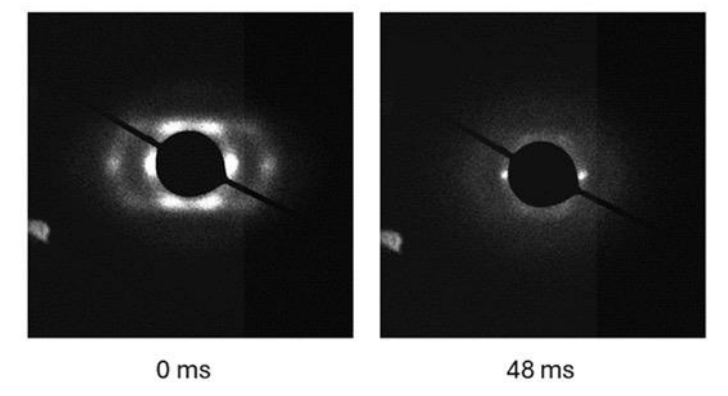


Fig. 2

GE-08. Coherent phonon excitation by phonon-magnon coupling in stripe domains

N. Arora¹, D. Prestwood^{1, 2, 3}, T. Kikkawa⁴, E. Saitoh^{4, 5, 6}, W. R. Branford^{3, 7}, J. Gartside^{3, 7}, H. Kurebayashi^{1, 2, 8}

¹London Centre for Nanotechnology, University College London, London, United Kingdom, ²Department of Electronic and Electrical Engineering, University College London, London, United Kingdom, ³Blackett Laboratory, Imperial College London, London, United Kingdom, ⁴Advanced Science Research Center, Japan Atomic Energy Agency, London, United Kingdom, ⁵Institute for AI and Beyond, The University of Tokyo, Tokyo, Japan, ⁶Department of Physics and Astronomy & Nebraska Center for Materials and Nanoscience, University of Nebraska, Lincoln, Nebraska, United States, ⁷London Centre for Nanotechnology, Imperial College London, London, United Kingdom, ⁸WPI-Advanced Institute for Material Research, Tohoku University, Sendai, Japan

The interplay between spin waves (magnons) and lattice vibrations (phonons) in magnetic materials offers pathways to novel hybrid excitations and energy transfer mechanisms, pivotal for advancements in spintronics and magnonics [1, 2]. In this study, we explore the coherent excitation of shear acoustic phonon modes induced by magnetisation dynamics within the stripe domain regime of single-crystal yttrium iron garnet (YIG) thin films on a (111)-oriented gadolinium gallium garnet (GGG) substrate. Stripe domains emerge under low in-plane magnetic fields (<6 mT) due to the combined effects of weak perpendicular magnetic anisotropy and cubic magnetocrystalline anisotropy [3]. Broadband ferromagnetic resonance (FMR) spectroscopy reveals rich spin-wave spectra in this regime, which is corroborated by micromagnetic simulations identifying bulk, edge, and domain wall modes. Notably, coherent excitation of shear acoustic phonon modes is observed and coupled to specific low-frequency spin-wave modes within the stripe domain phase. The magnon-phonon coupling manifests as sharp phonon mode contribution to individual magnon modes. We analyse this mode hybridisation by a coupled harmonic oscillator model [4] and extract the collective coupling strength (q_{eff}), placing the system in the intermediate coupling regime. Furthermore, the dependence of $g_{\rm eff}$ on individual dynamic magnetisation components is investigated, with which we discuss coupling mechanisms that govern selective magnon-phonon mode coupling observed in complex micromagnetic structures.

[1] An, K., Litvinenko, A. N., et al., Phys. Rev. B, 101, 060407 (2020).

^{*} Best Student Presentation Finalist / LB - Late-breaking Poster

[2] Hioki, T., Hashimoto, Y., *et al.*, *Comm. Phys.*, 5, 115 (2022). [3] Prestwood, D., Barker, C., *et al.*, (2025). arXiv preprint arXiv:2505.08431.

[4] Zollitsch, C.W., Khan, S., et al. Nat Commun 14, 2619 (2023).

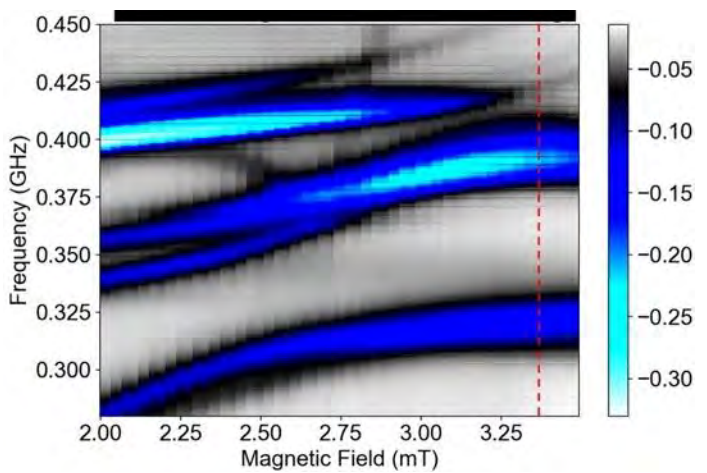


Fig. 1 Measured magnetic resonance spectra for YIG sample for rf $\perp H_{ext}$ which is directed along the [110] axis.

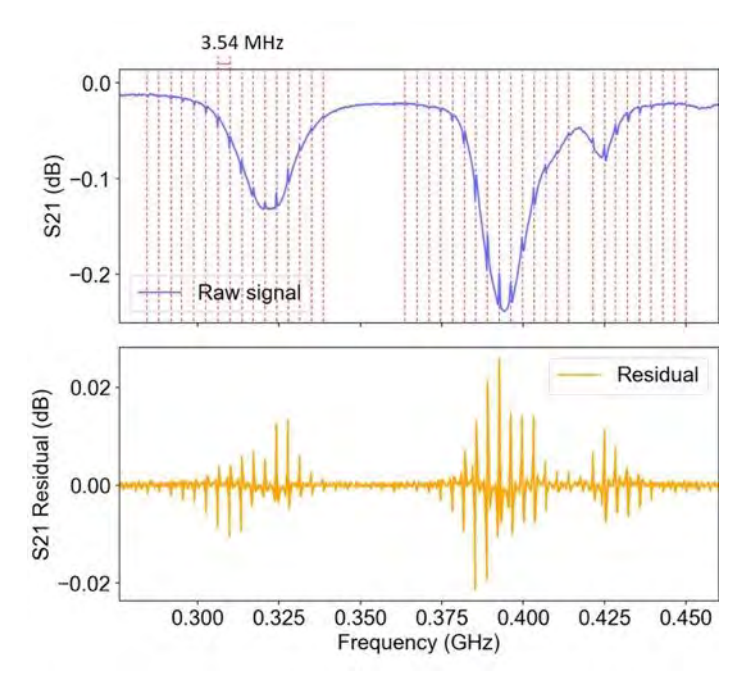


Fig. 2 Top: Resonance spectra at $\mu_0 H_{ext} = 3.31$ mT (red dashed line in Fig. 1), with vertical red markers denoting magnon-phonon anticrossings on the magnon envelope. Bottom: Residual FMR signal after subtracting a smoothed magnon background, highlighting the hybridized modes and their splittings.

GE-09. Spin-torque skyrmion resonance in a frustrated Fe_3Sn_2 kagome magnet

N. Bernstein¹, <u>B. J. Assouline</u>¹, H. Li², Y. Lau², I. Rozhansky³, A. Capua¹

¹Applied Physics, The Hebrew University of Jerusalem, Jerusalem, Israel, ²Physics, Beijing National Laboratory for Condensed Matter Physics, Beijing, China, ³National Graphene Institute, University of Manchester, Manchester, United Kingdom

Magnetic skyrmions are nanoscale, vortex-like spin textures characterized by a nontrivial topological charge that endows them with remarkable stability. Owing to these properties, skyrmions are considered promising candidates for next-generation magnetic information technologies. A key requirement for skyrmion-based transport and control is the efficient generation of spin torques within the host crystal, and the underlying mechanisms require further exploration. Here, we introduce an experimental technique for studying the microwave resonance dynamics in textured magnetic systems using a spin-torque drive that is generated inherently in the material [1]. To this end, we drive the dynamics using an RF spin torugue and probe them using time-resolved magneto-optical Kerr effect (TR-MOKE) setup, as depicted in the figure. The optical method offers high sensitivity, making it especially effective for detecting the multitude of exited modes associated with skyrmion resonance. The temporal resolution enables to distinguish between the different resonance modes. Additionally, TR-MOKE's sensitivity to evolving spin structures makes it an effective technique for identifying magnetic phase transitions. We apply this method to the frustrated kagome magnetic crystal Fe₃Sn₂. Our measurements reveal the excitation of only the breathing and counterclockwise rotational modes, unlike the three characteristic modes typically observed in skyrmion systems governed by Dzyaloshinskii-Moriya interactions [2-3]. Furthermore, we observed that, when a DC current is applied, it modulates the skyrmion resonance linewidth, indicating the presence of spin currents in the crystal. Our measurements uncovered a previously unobserved torque originating from the skyrmion's internal spin texture, which plays a significant role in its dynamics. Our findings indicate that skyrmion dynamics can be used to understand the spin electrodynamics related to the generation of spin currents. These results open new pathways to exploring the interplay between real-space and momentum-space chiralities in the generation of spin torques in textured magnets.

- [1] Bernstein, N., Li, H. and Capua, A., Spin-torque skyrmion resonance in a frustrated magnet. Nat Commun 16, 4616 (2025)
- [2] M. Mochizuki, "Spin-Wave Modes and Their Intense Excitation Effects in Skyrmion Crystals", Physical Review Letters 108, 017601 (2012).
- [3] Schwarze, T., Waizner, J., Garst, and D. Grundler, Universal helimagnon and skyrmion excitations in metallic, semiconducting and insulating chiral magnets. Nature Mater 14, 478–483 (2015).

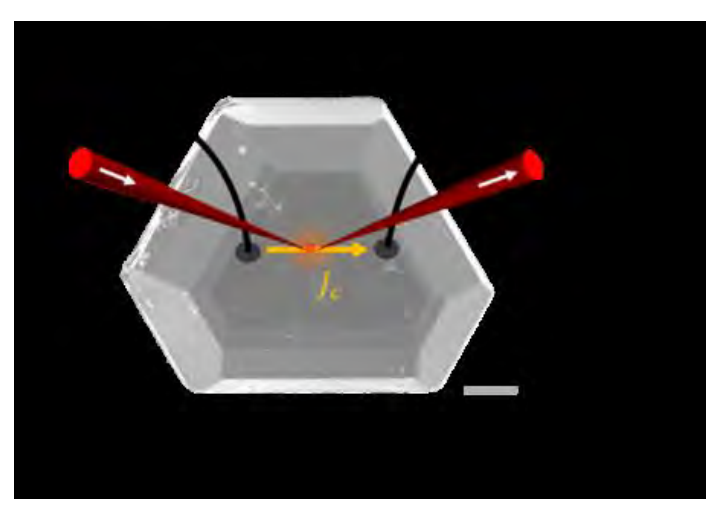


Figure 1

GE-10. All-optical stochastic switching of magnetization textures in Fe₃Sn₂

A. Kovács¹, J. T. Weber², M. Charilaou³, D. Kong¹, N. Kiselev⁴, I. Kezsmarki⁵, R. E. Dunin-Borkowski¹, A. Tavabi¹, S. Schäfer²¹Ernst Ruska Centre, Forschungszentrum Juelich, Juelich, Germany, ²Department of Physics, University of Regensburg, Regensburg, Germany, ³Department of Physics, University of Louisiana at Lafayette, Lafayette, Louisiana, United States, ⁴Peter Gruenberg Institute, Forschungszentrum Juelich, Juelich, Germany, ⁵Experimental Physics V, University of Augsburg, Augsburg, Germany

Magnetization textures with non-zero topological charge, such as skyrmions, are promising for a wide range of applications in data storage, spintronics, logic devices, and probabilistic computing, due to their quasiparticle nature and inherent stability. The prospect of controlling skyrmion states without strong external magnetic fields or high current densities has the potential to open new pathways for their application. Specifically, the possibility of controlling magnetization textures at room temperature by

purely optical means in short time scales can unlock new prospects for future ultrafast energy-efficient applications. In this work [1], we tested femtosecond optical pulses as a means to change the helicity of the spin configuration in dipolar skyrmions formed in the kagome magnet Fe₃Sn₂ in the absence of an external magnetic field and at room temperature. In situ Lorentz transmission electron microscopy revealed that the optical pulses induced stochastic switching of chiral Néel caps, while the internal Bloch component of the dipolar skyrmions remained unchanged. In addition to this switching process, we observed the interconversion between type I skyrmionic and type II bubble configurations depending on the initial and illumination conditions during the experiments. To corroborate the spin states and the light-induced magnetization dynamics, micromagnetic modelling and simulations of the resulting electron phase shift maps were conducted to elucidate the spin rearrangement induced by individual femtosecond optical pulses.

[1] J. T. Weber, A. Kovács, M. Charilaou, D. Kong, L. Prodan, V. Tsurkan, A. Schröder, N. S. Kiselev, I. Kézsmárki, R. E. Dunin-Borkowski, A. H. Tavabi, S. Schäfer: All-optical stochastic switching of magnetization textures in Fe₃Sn₂. arXiv 2503.05660 (2025)

GE-11. Non-Abelian Gauge Theory for Magnons in Topologically Textured Frustrated Magnets

R. Zarzuela¹, S. Kim²

¹Institut für Physik, Johannes Gutenberg Universität Mainz, Mainz, Germany, ²Department of Physics, Korean Advanced Institute of Science and Technology, Daejeon, Korea (the Republic of)

We develop an effective gauge theory for three-flavored magnons in frustrated magnets hosting topological textures with the aid of the quaternion representation of the SO(3) order parameter [1]. We find that the effect of topological solitons on magnons is captured generally by the non-Abelian emergent electromagnetic fields, distinct from the previously established gauge theory for magnons in collinear magnets where the gauge theory is often restricted to be Abelian. As concrete examples, 4π vortices in two-and three-dimensional magnets and Shankar skyrmions in three-dimensional magnets are discussed in detail, which are shown to induce, respectively, the Abelian and the non-Abelian topological magnetic field on magnons, and thereby engender the topological Hall transport in textured

frustrated magnets. We also discuss the effect of magnon-magnon interactions on our effective theory. Our work is applicable to a broad class of magnetic materials whose low-energy manifold is described by the SO(3) order parameter. We envision that the discovery of the non-Abelian magnonic gauge theory will enrich the field of magnonics as well as prompt the study of magnon transport in textured frustrated magnets.

[1] Ricardo Zarzuela and Se Kwon Kim, "Non-Abelian Gauge Theory for Magnons in Topologically Textured Frustrated Magnets," Phys. Rev. Lett. 134, 186701 (2025)

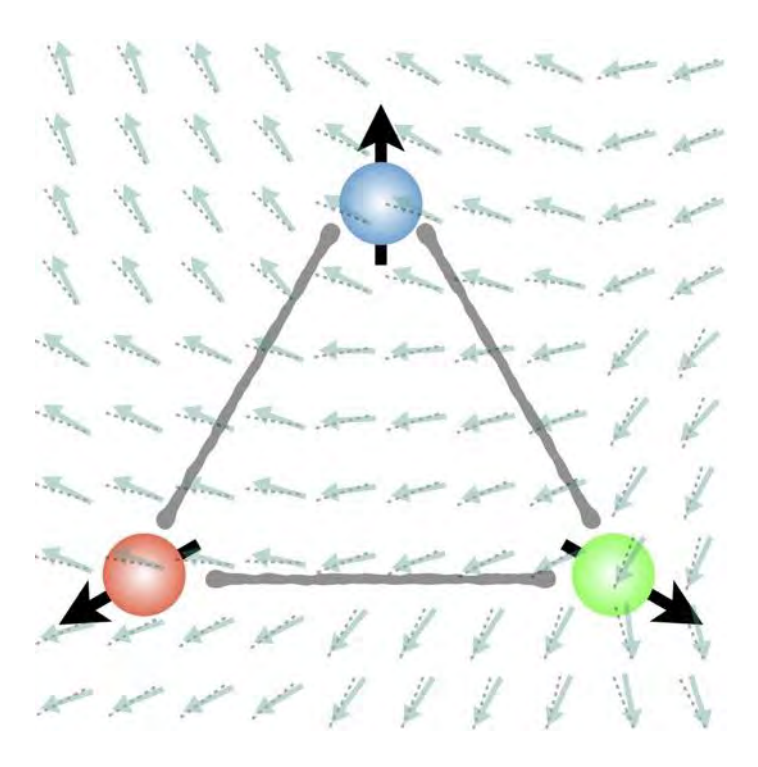


Fig. 1 The schematic figure of QCD-like interactions of three-flavored magnons in frustrated spin systems.

SESSION GF: ALTER- / ANTI-FERROMAGNETISM IN RUO2 AND OTHER MATERIALS

Chair(s): O. Amin, *University of Nottingham, Nottingham, United Kingdom*Friday, October 31, 2025
08:30 AM-12:00 PM
Room 2BC

GF-01. Revisiting Spin Transport in RuO₂: Distinguishing Anisotropic Spin Hall from Altermagnetic Spin Splitting Effects

<u>D. Ou</u>¹, Y. Wang², C. Liao², Z. Shen², C. Lin², W. Hsu², Y. Chen¹, Y. Tien², Y. Chin³, A. Singh⁴, W. Lee⁴, S. Huang²
¹Center for Condensed Matter Sciences, National Taiwan University, Taipei, Taiwan, ²Department of Physics, National Taiwan University, Taipei, Taiwan, ³Department of Physics, National Chung Cheng University, Chia-Yi, Taiwan, ⁴Institute of Physics, Academia Sinica, Taipei, Taiwan

Altermagnetism has emerged as a new class of magnetism that distinguishes from ferromagnetism and antiferromagnetism. Among the materials proposed, the rutile RuO_2 has attracted considerable attention, since it is metallic and predicted to be a d-wave altermagnet with strong spin-splitting energy. However, recent studies have revealed a puzzling discrepancy between spectroscopic and transport measurements in this material. On one hand, neutron scattering and spin-resolved angle-resolved photoemission spectroscopy have shown no clear evidence of magnetic order and spin-splitting in the band structure of RuO_2 , casting doubt on its altermagnetic nature. On the other hand, spin transport experiments have reported anisotropic or unconventional spin-dependent transport behaviors that are typically attributed to spin-splitting.

This contradiction raises an important question: Can the observed transport signatures in RuO_2 be explained without invoking altermagnetic spin-splitting? In our two most recent studies [1, 2], we address this question by systematically investigating the anisotropic spin-to-charge conversion in epitaxially grown RuO_2 films. We show in ref [1], an epitaxial RuO_2 film is crucial in observing the anisotropic spin-to-charge conversion. In ref [2], by comparing the anisotropic voltage ratios for epitaxial RuO_2 with three different crystal orientations [(100), (110), and (101)], we conclusively rule out the presence of spin-splitting features, and attribute this anisotropy to the anisotropic spin Hall effect which originates from spin-orbit interaction modulated by the crystallographic anisotropy,

independent of any magnetic ordering or spin-split band structure.

These results provide a quantitative explanation for the transport behavior in RuO_2 , without requiring the presence of altermagnetic spin-splitting. Our study thus helps reconcile the apparent conflict between spectroscopic and transport data. Moreover, it highlights the broader importance of crystalline symmetry in governing spin transport phenomena, especially in systems with low crystalline symmetry.

Overall, our work offers a new perspective on spin-charge interconversion in RuO_2 and suggests that similar effects may exist in other low-symmetry materials, even in the absence of altermagnetic order. This underscores the need for careful symmetry and orientation analyses in spintronic materials and opens new avenues for exploring functional spin phenomena beyond conventional magnetic paradigms.

[1] C.-T. Liao, Y.-C. Wang, Y.-C. Tien, S.-Y. Huang, and \underline{D} . \underline{Qu} , "Separation of Inverse Altermagnetic Spin-Splitting Effect from Inverse Spin Hall Effect in RuO_2 ", Phys. Rev. Lett. 133, 056701 with Editors' suggestion (2024)

[2] Y.-C. Wang, Z.-Y. Shen, C.-H. Lin, W.-C. Hsu, Y.-S. Chen, Y.-Y. Chin, A. K. Singh, W.-L. Lee, S.-Y. Huang, and D. Ou, "Robust Anisotropic Spin Hall Effect in Rutile RuO_2 ", arXiv:2503.07985 (2025)

GF-02. Negative and Large Spin Hall Angle in RuO₂

Y. Wang^{1,2}, Z. Shen¹, C. Lin¹, W. Hsu¹, Y. Chen², Y. Chin³, A. Singh⁴, W. Lee⁴, S. Huang^{1,5}, D. Qu^{2,5}

¹Department of Physics, National Taiwan University, Taipei, Taiwan, ²Center for Condensed Matter Sciences, National Taiwan University, Taipei, Taiwan, ³Department of Physics, National Chung Cheng University, Chia-Yi, Taiwan, ⁴Institute of Physics, Academia Sinica, Taipei, Taiwan, ⁵Center of Atomic Initiatives for New Materials, National Taiwan University, Taipei, Taiwan

Altermagnetic materials have spin-splitting bands in the momentum space and zero magnetic moment in the real space [1]. Among a few candidates, ruthenium dioxide (RuO_2) has attracted significant attention as a prototypical altermagnetic material theoretically, but faces intensive debates on its magnetic order experimentally. On the other hand, in the spin-dependent transport studies, one of the

key features for altermagnetism is the altermagnetic spinsplitting effect (ASSE) that converts a charge current to a transverse spin current without spin-orbit coupling (SOC). However, detecting and isolating the ASSE is extremely difficult, since it is often mixed with the spin Hall effect (SHE) in materials with SOC.

In our recent work [2], through the thermal spin injection from yttrium iron garnet (YIG) into a few different crystal planes of the epitaxial RuO2 films, we show that the anisotropic and unconventional spin-to-charge conversion in this material, that are often taken as evidence for ASSE, are solely caused by the anisotropic inverse spin Hall effect. These phenomena result from the three independent spin Hall conductivity tensors for the rutile structure with low crystal symmetry. Moreover, with a careful analysis of the sign for the spin Hall angle (ϑ_{SH}) for RuO₂, we show that it is negative when RuO₂ is in contact with YIG, but is positive when in contact with Py. This sign discrepancy is confirmed by not only the spin Seebeck measurement as demonstrated in ref. [2], but also the spin pumping measurement as shown in Fig. 1. The hard X-ray photoemission spectroscopy (HAXPES) reveals that about 10 % of Ru⁴⁺ is reduced to the Ru⁰ at the interface, when RuO₂ is in contact with Py but not YIG, suggesting the interfacial reduced Ru may be responsible for the sign change. Through a RuO₂ thicknessdependent measurement, we further extrapolate the large but also anisotropic ϑ_{SH} for RuO₂ Our study provides a comprehensive understanding of the spin-to-charge conversion in this highly controversial material.

[1] L. Šmejkal, J. Sinova, and T. Jungwirth, Phys. Rev. X 12, 040501 (2022).

[2] Y. C. Wang et al., arXiv:2503.07985 (2025)

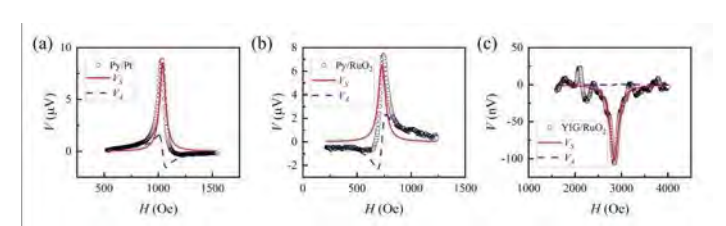


Fig. 1. The spin pumping voltage as a function of magnetic field for (a) Py/Pt, (b) Py/RuO₂, and (c) YIG/RuO₂. Solid and dashed lines fit symmetric Lorentzian V_S and antisymmetric Lorentzian V_A , respectively.

GF-03. Enhanced Transport of Altermagnet Grain Boundaries Between Crystallographic Domains of Opposite Handedness

<u>S. Tkacik</u>, G. M. Pantano, E. Thareja, J. D. Gayles *University of South Florida, Tampa, Florida, United States*

Altermagnetism was introduced by Šmejkal et al. [1] when they demonstrated its contributions to the crystal Hall effect (CHE) in a symmetry-based tight-binding model. Properties like the CHE and spin Hall effect have also been shown to be enhanced by interfaces such as those in magnetic multilayer materials [2]. Šmejkal and others have stated minimal models for bulk altermagnets and we build on this to study symmetry-reducing environments, such as material interfaces, essential to understanding topological features and device applications. We model material grains and boundaries in which the anisotropy of the crystal field and on-site magnetic exchange produce altermagnetism. These features modify local magnetization densities and reduce symmetries relating spin sublattices from a combined inversion and time-reversal operation to a combined timereversal and rotation operation. Symmetry can be further reduced by interfaces between grains of opposite handedness, which can be determined with a SOC term that simplifies configurations of noncentrosymmetric, nonmagnetic atoms [1]. Such interfaces form during crystal growth, and it is essential to identify when they enhance, rather than hinder, properties like the CHE. We fit tightbinding parameters to first-principles calculations to accurately model these materials such as RuO₂ and its grain boundaries. Our model facilitates both inclusion of multiple boundaries and variation of real space parameters such as distances between them. Distance-dependent interactions between boundaries and impacts on electronic band structure are demonstrated simultaneously with interfacial and external field modifications in real space. We calculate Berry curvature to identify conditions for which emergent states are non-trivial in their topology. Conductance calculations also support that the CHE is enhanced by various grain boundary environments and contributions from the anomalous Hall effect produced by interfacial conditions with a magnetic moment. Our results suggest highly tunable transport along the interface and motivate further prediction of electromagnetic responses via chemical constituents, symmetries, and electronic band structure in altermagnetic grain boundaries.

[1] Šmejkal, Libor, et al. "Crystal time-reversal symmetry breaking and spontaneous Hall effect in collinear

antiferromagnets." Science advances 6.23 (2020): eaaz8809. [2] Sinova, Jairo, et al. "Spin hall effects." Reviews of modern physics 87.4 (2015): 1213-1260.

GF-04. Spin-to-charge current conversion in altermagnet candidate RuO₂ probed by terahertz emission spectroscopy J. Jechumtal¹, O. Gueckstock², K. Jasenský¹, Z. Kašpar^{1, 3}, K. Olejník³, M. Gaerner⁴, G. Reiss⁴, S. Moser⁵, P. Kessler⁵, G. De Luca⁶, S. Ganguly⁷, J. Santiso⁷, D. Scheffler³, J. Zázvorka¹, P. Kubascik¹, H. Reichlova³, E. Schmoranzerova¹, P. Nemec¹, T. Jungwirth³, P. Kuzel³, T. Kampfrath², L. Nadvornik¹ ¹Faculty of Mathematics and Physics, Charles University, Prague, Czechia, ²Department of Physics, Freie Universität Berlin, Berlin, Germany, ³Institute of Physics, Czech Academy of Science, Prague, Czechia, ⁴Faculty of Physics, Bielefeld University, Bielefeld, Germany, 5Physikalisches Institut and Würzburg-Dresden Cluster of Excellence ct.gmat, Universität Würzburg, Würzburg, Germany, ⁶Materials Science Institute of Barcelona (ICMAB-CSIC), Barcelona, Spain, ⁷Catalan Institute of Nanoscience and Nanotechnology, Barcelona, Spain

The emerging physics of the altermagnetic (AM) phase [1] has garnered significant interest due to the strong nonrelativistic spin splitting in band structure without net magnetization, offering potential for THz and ultra-dense memory technologies beyond traditional ferromagnet-based technologies. Evidence for such spin splitting exists in MnTe, CrSb and RuO₂ thanks to the spin-resolved ARPES experiments [2,3] and several transport phenomena which were attributed to altermagnetism in MnTe, Mn₅Si₃, and RuO₂ [4-6]. However, recent studies [7] have challenged the magnetic order in RuO₂, casting doubt on its magnetic character in its bulk and thick-layer form. In this study, we employ THz emission spectroscopy to investigate the theoretically predicted AM spin splitting in RuO₂ in the ultrafast regime. This technique is based on a scheme in which an optically excited ferromagnet (FM)/conversion metal (CM) bilayer emits THz pulses via the conversion of spin current pumped from the FM layer into the CM layer [8]. Using RuO₂ as the CM layer, we study the THz spin-to-charge current conversion (SCCC) [1,6], as illustrated in Fig. 1. THz emission was measured for different angles between the injected spin and the crystal orientation of RuO2 at several temperatures. Symmetry of signals, affected also by anisotropy of THz outcoupling, was compared with the expected AM symmetry shown in Fig. 2. Our findings suggest that the observed SCCC in RuO₂ originates in the inverse spin Hall effect (ISHE), which

is strongly anisotropic with the modulation ~ 30%. Moreover, any contribution from AM spin-splitter effect appears negligible compared to the ISHE.

- L. Smejkal et al., *Phys. Rev. X* 12 040501 (2022)
- J. Krempaský et al., *Nature* 626 517 (2024)
- S. Reimers et al., *Nat. Comm* 15, 2116 (2024)
- R.D.G. Betancourt et al., Phys. Rev. Lett. 130, 036702 (2023)
- H. Reichlova et al., Nat. Comm. 15, 4961 (2024)
- A. Bose et al., Nat. Electron. 5, 263 (2022).
- P. Keßler et al., Npj Spintron. 2, 50 (2024)
- T. Seifert et al., Nat Photonics 10 483 (2016)

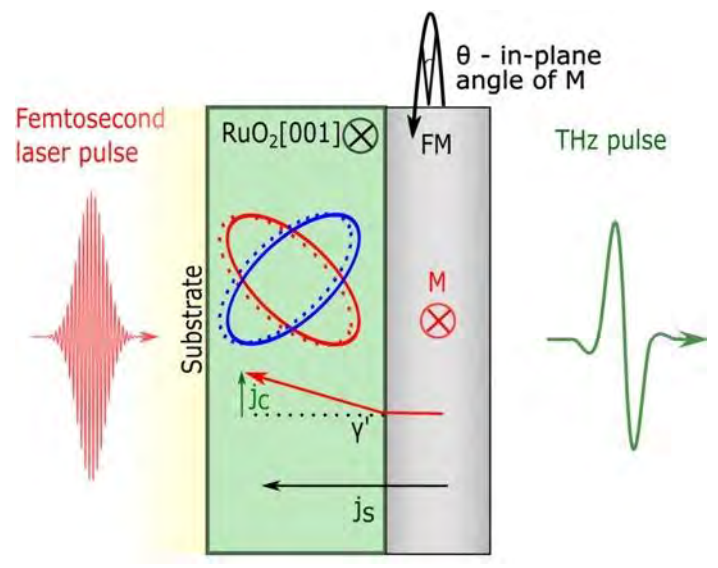


Figure 1. A femtosecond laser pulse excites a ferromagnetic layer (FM) with an in-plane magnetization M, whose angle θ is controlled by an external field. This generates a spin current js (black arrow) into RuO₂, where it is converted via the AM SCCC into a transverse charge current jc, emitting a THz pulse.

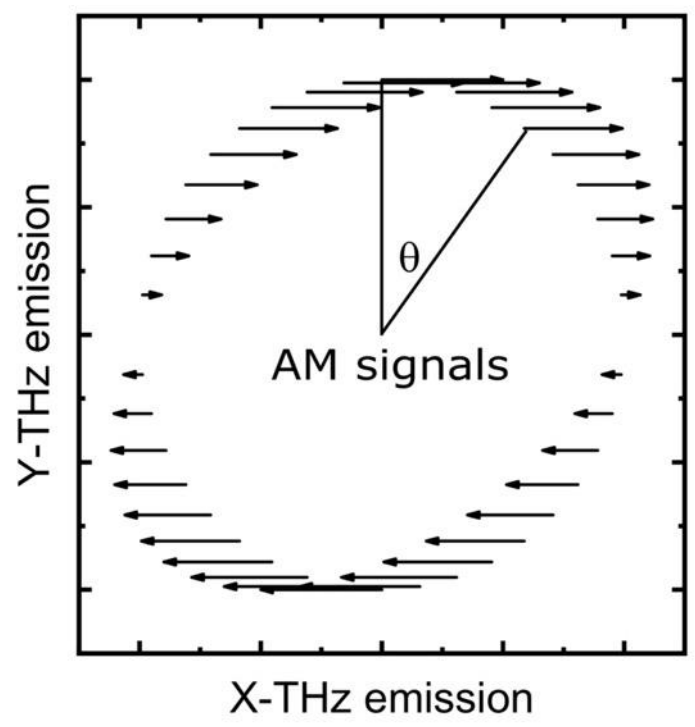


Figure 2. Symmetry of THz emission expected within an AM-type response is a cosine dependence on θ , with emission only along the x-direction. The signal magnitude is $|\cos(\theta)|$, with $\theta=0$ when M is parallel to the RuO₂ expected Neél vector.

GF-05. Indications of Terahertz Spin Transport in the Altermagnet Candidate RuO₂

<u>O. Gueckstock</u>¹, J. Jechumtal², M. Gaerner³, C. Simons¹, Z. Kaspar^{2, 4}, T. Seifert¹, T. Kuschel^{3, 5}, G. Reiss³, L. Nadvornik², T. Kampfrath¹

¹Department of Physics, Freie Universität Berlin, Berlin, Germany, ²Faculty of Mathematics and Physics, Charles University, Prague, Czechia, ³Faculty of Physics, Bielefeld University, Bielefeld, Germany, ⁴Institute of Physics, Czech Academy of Sciences, Prague, Czechia, ⁵Institute of Physics, Johannes Gutenberg University Mainz, Mainz, Germany

The recently emerging material class of altermagnets has large potential to offer properties such as strong spin splitting, which are so far rather typical for classical ferromagnets [1]. RuO_2 appears to be a promising metallic altermagnet candidate with huge spin splitting in the electronic band structure and for photoinduced spin and orbital transport with a Néel temperature above room temperature [1,2]. Here, we apply femtosecond laser pulses to $RuO_2(110)|HM$ stacks consisting of a structurally twinned

RuO₂ layer and a heavy-metal layer HM of Pt or W. We observe THz emission signals with distinct pumppolarization dependence. The signals change sign when HM=Pt is replaced by W and exhibit a marked temperature dependence, thereby suggesting a magnetism-related signal origin. We discuss possible mechanisms of THz-signal generation, including an ultrafast photoinduced spin current from RuO₂ to HM and its conversion into in-plane charge in HM, which gives rise to the emission of a THz electromagnetic pulse.

- [1] Smejkal et al., Phys Rev. X 12, 040501 (2022)
- [2] Adamantopoulos et al., npj spintronics 2, 46 (2024)

GF-06. Surface roughness effect on dynamic magnetic properties of RuO₂/CoFeB stack

T. Nguyen^{1, 2}, H. Naganuma^{3, 4}, Y. Saito², S. Maruyama⁵, T. Nguyen⁶, D. Vu⁶, S. Ikeda^{2, 1}, T. Endoh^{2, 1, 5} ¹Center for Science and Innovation in Spintronics, Tohoku University, Sendai, Miyaqi, Japan, ²Center for Innovative Integrated Electronic Systems, Tohoku University, Sendai, Miyaqi, Japan, ³Institute for Advanced Study, Nagoya University, Nagoya, Aichi, Japan, ⁴Institute of Materials and Systems for Sustainability, Nagoya University, Nagoya, Aichi, Japan, ⁵Graduate School of Engineering, Tohoku University, Sendai, Miyagi, Japan, ⁶Institute of Physics, Vietnam Academy of Science and Technology, Hanoi, Hanoi, Viet Nam

RuO₂ is an emerging oxide showing peculiar properties such as the collinear antiferromagnetic-induced spin-split band in the momentum space under the applied electric field [1-3]. The spin current by spin-split effect (SSE) is generated [1], which would trigger the magnetization reversal in RuO₂/ferromagnet stack by the induced-spin-orbit torque (SOT) [2,3]. The anisotropic behavior of SSE-induced SOT was proposed [1] and observed [3,4], implying the importance of investigating the relationship between the RuO₂ crystalline structure and magnetic properties. Herein, we prepared RuO₂ films on different substrates and investigated the magnetic properties in the RuO₂/CoFeB stacks.

Stack A, B, and C with RuO₂/CoFeB bilayer were prepared on TiO_2 (001), α -Al₂O₃ (0001), and TiO_2 (110) substrates by DC/RF sputtering [4]. The roughness of the surface was evaluated by AFM, and the epitaxial growth of the RuO₂ films was characterized using RHEED. The static and dynamic magnetic properties were investigated by VSM and a broadband FMR technique.

Fig. 1 shows the RHEED and AFM images for the RuO₂ films on different substrates. The dots/streaks patterns in the RHEED images are observed for all samples, implying their epitaxial growth and good surface. The RMS roughness evaluated from AFM images is 0.2 nm, 0.3 nm, and 0.56 nm for Stacks A, B, and C, respectively. Fig. 2 shows the damping constant and the effective magnetization (4p $M_{\rm S,eff}$) evaluated from the FMR. The damping constant for Stacks A, B is close, while it becomes higher for Stack C, implying the impact of surface roughness. The 4pM_{s.eff} is close for all samples, suggesting their close interfacial anisotropy energy. Both VSM and FMR data measured at different azimuthal angles of the in-plane magnetic field showed that Stack A is isotropic, while Stacks B and C possess uniaxial anisotropy. The experimental findings would contribute to the development of oxide-based spintronics. The authors acknowledge JSPS Core-to-Core Program: JPJSCCA20230005, X-NICS: JPJ011438, JSPS KAKENHI Grants: 23H03803, 24H00030, the Core Research Cluster

program, and CIES Consortium.

- [1] R. González-Hernáldez et al., Phys. Rev. B 126, 127701 (2021).
- [2] A. Bose et al., Nature Electronics 5, 267 (2022).
- [3] H. Bai et al., Phys. Rev. Lett. 128, 197202 (2022).
- [4] T.V.A. Nguyen et al., Adv. Science 2413165 (2025).

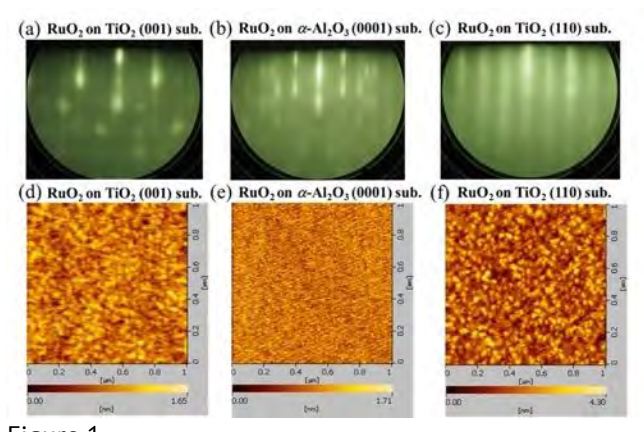


Figure 1

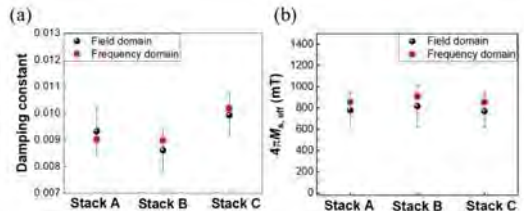


Figure 2

447

MMM 2025 Conference, Palm Beach, Florida, USA

GF-07. Giant Tunneling Magnetoresistance in Antiferromagnetic Tunnel Junctions with Non-collinear Mn₃NiN Electrodes

M. A. Elekhtiar¹, G. Gurung², D. Shao³, E. Y. Tsymbal¹
¹Physics and Astronomy, University of Nebraska-Lincoln,
Lincoln, Nebraska, United States, ²Trinity College, University of
Oxford, Oxford, United Kingdom, ³Institute of Solid-State
Physics, Chinese Academy of Sciences, Hefei, China

Antiferromagnetic tunnel junctions (AFMTJs) have emerged as a promising platform for antiferromagnetic (AFM) spintronics due to a sizable tunneling magnetoresistance (TMR) effect that is determined by the relative orientation of the AFM Néel vector of the two electrodes [1]. It has been demonstrated that non-collinear antiferromagnets can produce exceptionally large TMR in AFTJs due to their momentum-dependent spin polarization effectively approaching 100% [2]. In this work, we employ firstprinciples calculations to investigate the performance of the non-collinear antiferromagnet Mn₃NiN in its Γ_{4q} AFM phase (Fig. 1a), as an electrode material in AFMTJs. We demonstrate that, owing to the spin-split electronic structure, Mn₃NiN exhibits highly spin-polarized conduction channels within its (001) 2D Brillouin zone. When integrated with the wide band gap insulator LaAlO₃ into a Mn₃NiN/LaAlO₃/Mn₃NiN (001) AFMTJ (Fig. 1b), this results in a giant TMR effect exceeding 2000%. By decomposing transmission into conduction channels differed by transverse wave vector k_{\parallel} , we observe a significant enhancement of transmission for parallel Néel vector configuration, T_P , compared to antiparallel, T_{AP} , near the center of the Brillouin zone (Fig. 1c). We attribute this behavior to the nearly perfect spin polarization of Mn₃NiN in this k_{\parallel} region, which coincides with the low tunneling decay rates of the evanescent states in LaAlO₃. A detailed band-toband transmission analysis allows us to elucidate the key features of the transmission spectra, where the matching of k_1 -group symmetries of the propagating and evanescent states control tunneling pathways. Due to a similar cubic perovskite structure with a comparable lattice parameter, epitaxial growth of Mn₃NiN and LaAlO₃ is feasible in practice, providing the necessary condition of a fully crystalline AFMTJ for observing the predicted giant TMR. These findings highlight the potential of Mn₃NiN-based AFMTJs as a robust platform for next-generation highperformance spintronic devices.

D.-F. Shao and E. Y. Tsymbal, *npj Spintronics* 2, 13 (2024).
 G. Gurung, M. Elekhtiar, Q. Q. Luo, D.-F. Shao, E. Y. Tsymbal, *Nat. Comm.* 15, 10242 (2024).

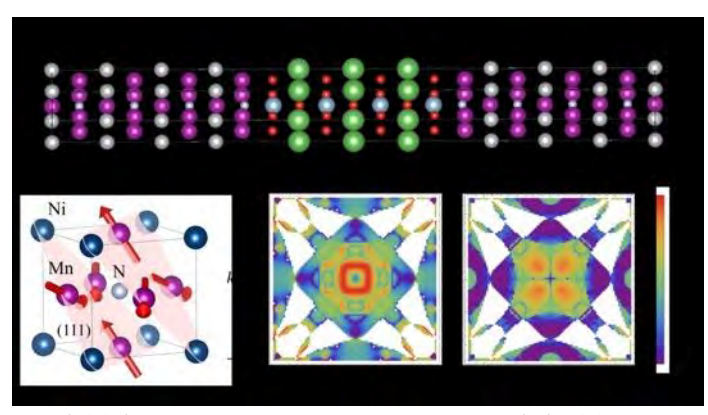


Fig. 1 (a) Atomic and magnetic structure Mn_3NiN . (b) Schematic of $Mn_3NiN/LaAlO_3/Mn_3NiN$ (001) AFMTJ. (c) k_{\parallel} -resolved transmission spectra for parallel (T_{P}) and antiparallel (T_{AP}) Néel vector.

GF-08. Spintronics in "dirty" antiferromagnetic materials B. L. Zink

Physics & Astronomy, University of Denver, Denver, Colorado, United States

The promise of anitferromagnetic spintronics, including nominally zero stray fields and rapid magnetization dynamics, comes with challenges in quantifying the magnetic state. Real materials have complications such as defects, oxidation, interdiffusion, grain boundaries and strain, that are far beyond the simple models that typically quide our intuition of fundamental spintronic effects. These material realities often make the task of quantifying and understanding the magnetic states in systems featuring antiferromagnetic (AF) exchange interactions more difficult. This talk will overview several recent examples where the inevitable realities in materials complicate understanding of spintronic effects in these systems. The first example focuses on the interface between YIG thin films and GGG substrates [1]. Comparing polarized neutron reflectivity with quantitative SOUID magnetometry sheds light on significant complications that arise in this now ubiquitous system for spintronics. The second example highlights growthtechnique dependent spin conversion in antiferromagnetic chromium thin films probed via spin Seebeck and spin Hall magnetoresistance techniques [2,3]. The third example concerns comparison of magnetometry and transport effects

in synthetic ferrimagnet Co/Gd heterostructures [4], where particularly divergent effects, most likely due to sample imperfections, shed light on the presence of magnetically active, but electrically "silent" spins in metallic ferrimagnets. This work highlights that advances in antiferromagnetic spintronics will be enabled by gaining a better view of the realities of the materials.

- 1) Roos, et al. PRM 6 034401 (2022)
- 2) Bleser, et al. JAP 131 113904 (2022)
- 3) Bleser, et al. PRM 8 124411 (2024)
- 4) Hernandez et al. PRApp (in review)

GF-09. Temperature dependence of current-induced switching in epitaxial Mn₃Sn thin films

<u>K. Nihei</u>^{1, 2}, T. Uchimura^{1, 2}, J. Han^{1, 3}, S. Kanai^{1, 3}, H. Ohno^{1, 4}, S. Fukami^{1, 4}

¹RIEC, Tohoku Univ., Sendai, Miyagi, Japan, ²Grad School of Eng., Tohoku Univ., Sendai, Miyagi, Japan, ³AIMR, Tohoku Univ., Sendai, Miyagi, Japan, ⁴CSIS, Tohoku Univ., Sendai, Miyagi, Japan

Non-collinear antiferromagnets, represented by Mn₃Sn, have attracted considerable interest in spintronics due to the capability of electrically probing the magnetic order by the anomalous Hall effect [1] and electrically manipulating the magnetic order by the current-induced spin-orbit torque (SOT) [2-5]. While a model based on the SOT provides a self-consistent explanation of the current-induced magnetic switching in epitaxial Mn₃Sn thin films [3-5], some studies with polycrystalline Mn₃Sn thin films reveal an important role of Joule heating [6-8], suggesting that the switching process involves a step that heats the sample close to or above the Néel temperature (T_N) of Mn₃Sn [6]. In this study, we employ an epitaxial heterostructure of W/Ta/Mn₃Sn on the MqO (110) single-crystal substrate, where the W/Ta layers support the epitaxial growth of (10-10)-oriented Mn₃Sn and source the SOT (Fig. 1a). We evaluate the role of SOT and Joule heating by investigating the temperature dependence of the current-induced switching. From the deterministic switching loops under inplane bias magnetic fields (Fig. 1b), we extract the switching current I_{sw} at different temperatures (red dots in Fig. 1c). On the other hand, by comparing the longitudinal resistance as functions of T and current, we calibrate the current-induced temperature increase and, accordingly, determine $I(T \rightarrow T_N)$, the threshold current that heats the sample to the Néel temperature (black dots in Fig. 1c). We

* Best Student Presentation Finalist / LB – Late-breaking Poster

can see that $I_{\rm sw}$ is well below I ($T{
ightharpoonup }T_{\rm N}$) through the temperature range of 140~300 K, indicating that the sample maintains the non-collinear antiferromagnetic order during the switching and thus the Joule heating plays a less dominant role than that in polycrystalline samples. Our results suggest the major role of SOT in the current-induced switching in the epitaxial films of non-collinear antiferromagnets.

[1] S. Nakatsuji, et al. *Nature* 527, 212 (2015). [2] Tsai, et al. *Nature* 580, 608 (2020). [3] Y. Takeuchi, et al. *Nat. Mater.* 20, 1364 (2021). [4] T. Higo, et al. *Nature* 607, 474 (2022). [5] J.-Y. Yoon, et al. *Nat. Mater.* 22, 1106 (2023). [6] B. Pal, et al. *Sci. Adv.* 8, eabo5930 (2022). [7] G. Krishnaswamy, et al. *Phys. Rev. Appl.* 18, 024064 (2022). [8] M.-W. Yoo, et al. *APL Mater.* 12, 081107 (2024).

A portion of this study was supported by JSPS KAKENHI (Grant Nos. 23KJ0216, 24K16999, 24H00039, and 24H02235) and the MEXT X-NICS (Grant No. JPJ011438).

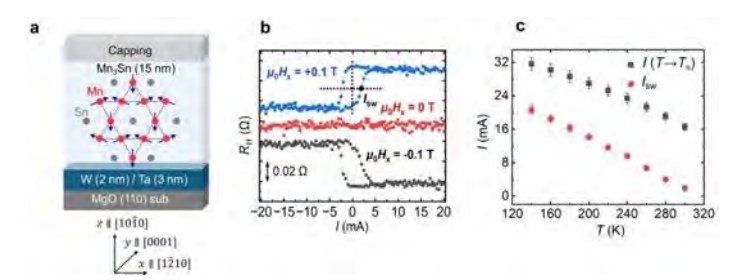


Fig. 1. (a) Sample structure. (b) Hall resistance $R_{\rm H}$ as a function of the applied pulse current under different magnetic fields at 300 K. The current and the magnetic field are along the x axis. (c) Temperature dependence of the switching current $I_{\rm SW}$ and the current that heats the sample to the Néel temperature, I ($T \rightarrow T_{\rm N}$).

GF-10. Distinct pulse-width dependence of two threshold currents driving a noncollinear antiferromagnetic nanodot via spin-orbit torque

<u>Y. Sato</u>^{1, 2}, Y. Takeuchi^{3, 4}, Y. Yamane^{1, 5}, S. Kanai^{1, 4}, H. Ohno^{6, 7}, S. Fukami^{1, 6}

¹Laboratory for Nanoelectronics and Spintronics, RIEC, Tohoku Univ., Sendai, Japan, ²Graduate School of Engineering, Tohoku Univ., Sendai, Japan, ³CMSM, NIMS, Tsukuba, Japan, ⁴WPI-AIMR, Tohoku Univ., Sendai, Japan, ⁵FRIS, Tohoku Univ., Sendai, Japan, ⁶CSIS, Tohoku Univ., Sendai, Japan, ⁷CIES, Tohoku Univ., Sendai, Japan

Manipulation of the collective spins in antiferromagnets (AFMs) is a key ingredient in AFM spintronics [1,2]. Bidirectional switching by spin-orbit torque (SOT) has been reported for epitaxial [3,4] and polycrystalline [5,6] films of a noncollinear AFM Mn₃Sn. In epitaxial films, a competition between the chiral-spin rotation driven by the current [3] and the reorientation of the uncompensated magnetization caused by the magnetic field has been attributed as the underlying mechanism of the switching [4]. Here we study the SOT-driven dynamics in an epitaxial Mn₃Sn(20nm) nanodot [7] as a function of the pulse width and find two threshold currents having distinct pulse-width dependence. The Mn₃Sn nanodot sample with Ta(3nm)/W(2nm) Hall bar is fabricated on the MgO(110) substrate [Fig. 1(a) and (b)]. Figure 2(a)-(d) show the switching probability (P) versus current density into the W/Ta layer (J_{HM}) , with various pulse widths τ_p , under an in-plane field of 100 mT. We find that, with a given τ_p , P initially increases with J_{HM} , reaches the unity, and then starts decreasing upon further increasing J_{HM} . We define the two threshold current densities: J_{c1} and J_{c2} at which P hits 0.5 in the switching process and 0.75 in the switching-back process, respectively. J_{c1} decreases with τ_{p} , which can be understood in a straightforward manner: the Mn₃Sn nanodot is exposed to the thermal fluctuation for a longer time with a longer τ_p , hence a better chance of completing the switching at a lower J_{HM} with the thermal assistance. In contrast, J_{c2} is insensitive to τ_{D} , which defies a simple interpretation with no similar phenomenon known in ferromagnets. These experimental results are reproduced well by LLG simulations. In the talk, we discuss potential mechanism of the unconventional switching behavior. This work not only sheds a new light on the noncollinear antiferromagnetic dynamics but also could lead to unique functionalities of AFM-based SOT devices.

- [1] T. Jungwirth et al., Nat. Nanotechnol. 11, 231 (2016).
- [2] V. Baltz et al., Rev. Mod. Phys. 90, 015005 (2018).

- [3] Y. Takeuchi et al., Nat. Mater. 20, 1364 (2021).
- [4] T. Higo et al., Nature 607, 474 (2022).
- [5] H. Tsai et al., Nature 580, 608 (2020).
- [6] B. Pal et al., Sci. Adv. 8, 24 (2022).
- [7] Y. Sato et al., Appl. Phys. Lett. 122, 122404 (2023).

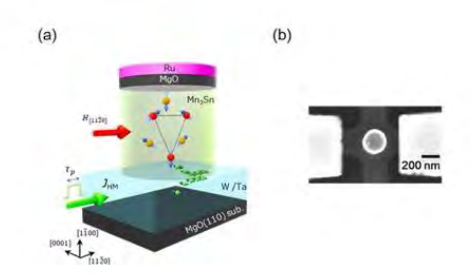


Fig.1 (a) Schematic of the switching measurement of Hall device with a Mn₃Sn nanodot. (b) The scanning electron microscope image of the fabricated device. The nominal dot diameter is 200 nm.

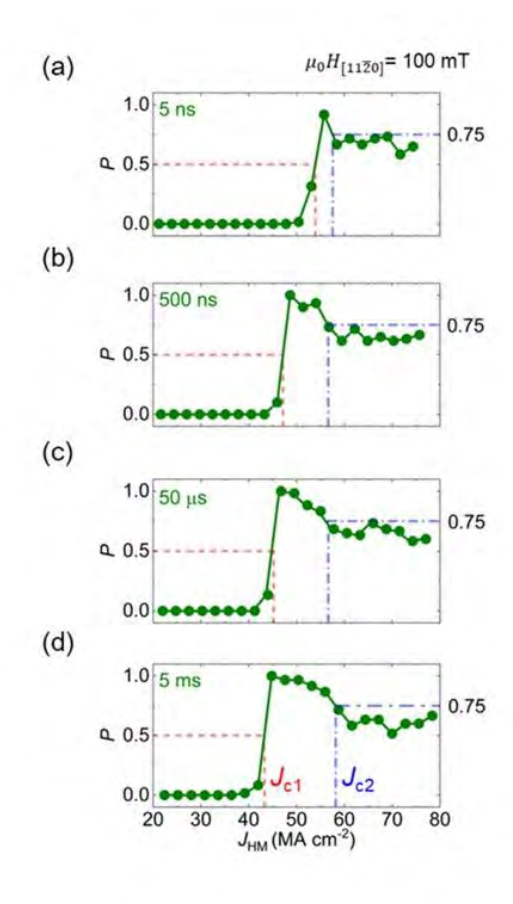


Fig. 2(a)-(d) P versus J_{HM} for various τ_p .

SESSION GG: MAGNETORESISTANCE IN HETEROSTRUCTURES (GMR, TMR, TAMR)

Co-Chair(s): H. Li, Analog Devices, Hillsboro, Oregon, United States and G. Yu, Institute of Physics, Chinese Academy of Sciences, Beijing, China and Y. Fan, Western Digital, San Jose, California, United States Friday, October 31, 2025 08:30 AM-12:00 PM Room 2A

GG-01. Enhancing and Decoupling Magnetic Anisotropy and Tunnel Magnetoresistance in CoFe₂O₄/MgO Bilayers via Swift Heavy Ion Irradiation

R. Charak^{1,2}, <u>S. Gautam</u>^{2,3}, S. Garg², Y. Kim⁴, K. Chae⁵
¹Energy Research Centre, Panjab University, Chandigarh, India, ²Dr. SSB Univ Inst of Chemical Engineering & Technology, Panjab University, Chandigarh, India, ³Advanced Functional Materials Lab Pvt. Ltd., Panjab University, Chandigarh, India, ⁴Pohang Accelerator Lab, Pohang University of Science and Technology, Pohang, Korea (the Republic of), ⁵Advanced Analysis & Data Center, Korea Institute of Science & Technology, Seoul, Korea (the Republic of)

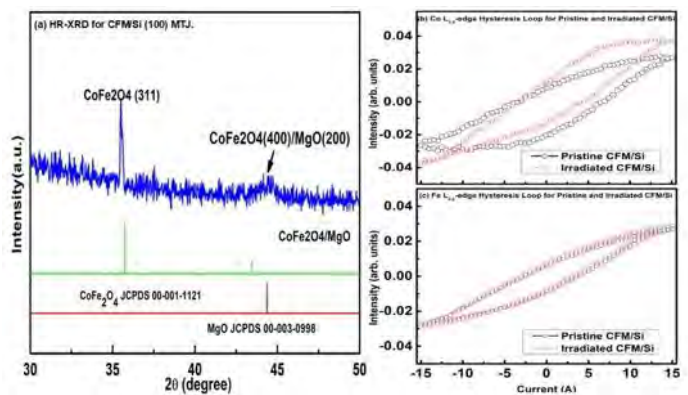
Magnetic tunnel junctions (MTJs) based on CoFe₂O₄/MgO bilayers are pivotal for high-density magnetoresistive random-access memory (MRAM), where perpendicular magnetic anisotropy (PMA) ensures thermal stability, and tunnel magnetoresistance (TMR) governs readout efficiency [1]. However, optimizing these competing properties remains a critical challenge. This study demonstrates how swift heavy ion (SHI) irradiation - a post-deposition processing technique - selectively enhances PMA and TMR in CoFe₂O₄/MgO bilayers, offering a pathway to tailor device performance [2].

Bilayers were fabricated via RF magnetron sputtering on MgO (001) substrates and annealed at 600 °C. Irradiation with 100 MeV ${\rm Ag^{+7}}$ ions (fluence: $1{\rm x}10^{12}$ - $1{\rm x}10^{14}$ ions/cm²) induced a 40% PMA enhancement ($1.2{\rm x}10^6$ erg/cm³ --> $1.7{\rm x}10^6$ erg/cm³) at $5{\rm x}10^{13}$ ions/cm², attributed to lattice strain and interfacial orbital hybridization via XMCD analysis. TMR increased from 180% to 250% at lower fluences (${\rm x}10^{13}$ ions/cm²) but declined to 210% at higher fluences ($1{\rm x}10^{14}$ ions/cm²) due to interfacial atomic intermixing, as confirmed by HR-TEM, which may be inverse PMA-TMR correlation challenges conventional design paradigms.

The study identifies a fluence "sweet spot" (5x10¹³ ions/cm²) where PMA and TMR are maximized concurrently (1.7x10⁶ erg/cm³ and 230%, respectively). SHI-induced

structural modifications - strain, defect density, and interfacial coherence - are mechanistically linked to functional property enhancements, providing a roadmap for engineering MTJs with application-specific performance. By bridging materials engineering (interface control) and device physics (anisotropy-transport coupling), this work establishes SHI irradiation as a scalable method to optimize spintronic devices. The findings advance the fundamental understanding of competing mechanisms in MTJs while offering practical strategies for next-generation MRAM development.

- 1. Niizeki, T., et al. Extraordinarily large perpendicular magnetic anisotropy in epitaxially strained cobalt-ferrite $Co_xFe_{3-x}O_4(001)$ (x=0.75, 1.0) thin films. Applied Physics Letters 103.16 (2013).
- 2. Garg, S., et al. Dissolution of $Mg(OH)_2$ by swift heavy ion irradiation in $CoFe_2O_4/MgO/ZnFe_2O_4$ multilayer thin films. Materials Letters 349 (2023): 134738.
- 3. Lou, K., et al. Perpendicular magnetic anisotropy in asdeposited CoFeB/MgO thin films. Applied Physics Letters 121.12 (2022).
- 4. Yang, C. Y., et al. Competing anisotropy-tunneling correlation of the CoFeB/MgO perpendicular magnetic tunnel junction: An electronic approach. Scientific Reports 5.1 (2015): 17169.



(a) HR-XRD data for CFM/Si(100) showing characteristic peaks for $CoFe_2O_4$ (311) and MgO (200). (b) Element specific hyteresis measurements at Co L-edge for pristine and Agion irradiated CFM/Si (c) Element specific hyteresis measurements at Fe L-edge for pristine and Agion irradiated CFM/Si .

451

GG-03. Magnetic Tunnel Junctions utilizing metastable cubic GaN tunnel barrier

<u>H. Kwon^{1, 2}</u>, K. Suzuki^{1, 2}, D. Kumar², M. Tsujikawa³, T. Roy^{4, 3}, S. Miki², M. Shirai^{3, 4}, S. Mizukami^{2, 4}

¹School of engineering, Tohoku University, Sendai, Japan, ²WPI-Advanced Institute for Materials Research, Tohoku University, Sendai, Japan, ³Research Institute of Electrical Communication, Tohoku University, Sendai, Japan, ⁴Center for Science and Innovation in Spintronics, Tohoku University, Sendai, Japan

Magnetic tunnel junction (MTJ) is a key device of spintronics, in which a MgO(001) barrier has been used since MgO-MTJs exhibit high tunnel magnetoresistance (TMR) owing to the orbital-symmetry filtering effect [1,2]. Other barrier materials are being explored to gain lower device resistance area product (RA) with keeping high TMR, such as wide-bandgap oxide semiconductors [3-5]. Here, we study metastable cubic GaN(001) as a tunnel barrier in MTJs. Our first-principles calculations suggest that zinc-blende (ZB) GaN supports coherent tunneling via Δ_1 symmetry channels, being similar to the case of MgO. Combined with its relatively narrow bandgap (~3.3 eV), ZB-GaN is expected to enable low RA while maintaining high TMR, making it a promising alternative tunnel barrier material.

Film deposition was carried out using ultra-high vacuum magnetron sputtering. The MTJ film structure was MgO(001) single crystalline substrate/ Cr (40)/ CoMnFe (10)/ Mg (0.5)/ MgO (0.6)/ GaN (d=0.4-1.5)/ MgO (0.6)/ CoMnFe (8)/ IrMn (10)/ Ru (10), with thicknesses in nanometers. Here, metastable bcc Co-Mn-Fe alloys are used for ferromagnetic electrodes [6,7]. To mitigate the large lattice mismatch (~13%) between the magnetic CoMnFe layers and the ZB-GaN barrier, thin MgO seed layers were inserted above and below the GaN(001) layer.

The transport properties were evaluated using both current-in-plane tunneling (CIPT) in unpatterned MTJ films and four-probe measurements in patterned MTJs. We observed the RA values lower than those of MgO-MTJs (Fig. 1). Although the TMR ratio decreases with increasing GaN thickness, it remained reasonably high, reaching ~80% for thicker GaN(001) barriers (Fig. 2). X-ray diffraction and transmission electron microscopy (TEM) measurements indicated epitaxial growth of GaN(001) barrier layer with some imperfections. Such imperfections introduced into GaN(001) may influence the TMR ratio observed in GaN-MTJs in this study.

This work was supported by KAKENHI (No. 21H05000), JST CREST (No. JPMJCR17J5), and X-NICS of MEXT (No.

347JPJ011438). SM and MS acknowledge Spin-RNJ. H.K thanks GP-Spin at Tohoku Univ.

- 1)S. Yuasa et al., Nat. Mater. 3, 868 (2004).
- 2)S. S. P. Parkin et al., Nat. Mater. 3, 862 (2004).
- 3)H. Sukegawa et al, Appl. Phys. Lett. 110, 122404 (2017).
- 4)S. Mertens et al., Appl. Phys. Lett. 118, 172402 (2021).
- 5)R. R. Sihombing et al., Appl. Phys. Lett. 126, 022407 (2025).
- 6)T. Ichinose et al., J. Alloy. Compound. 960, 170757 (2023).
- 7)D. Kumar et al. Sci. Tech. Adv. Mater., 25, 2421746 (2024).

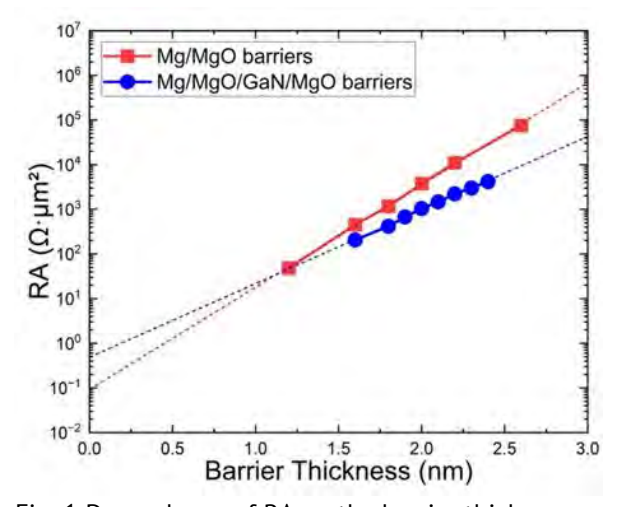


Fig. 1 Dependence of RA on the barrier thickness.

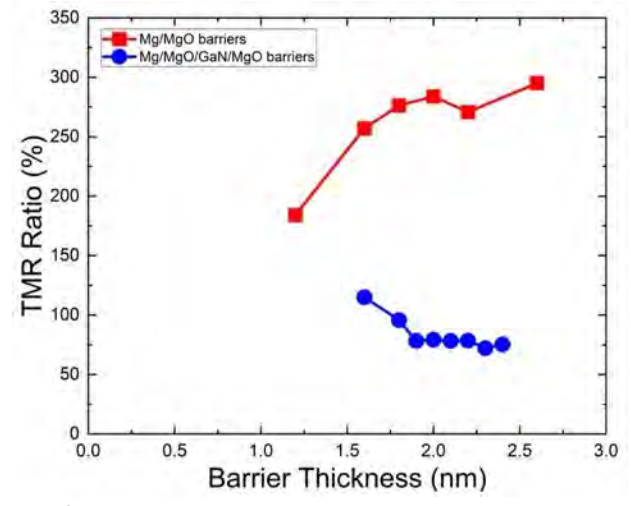


Fig. 2 Dependence of TMR on the barrier thickness.

GG-05. Magnetically Modulated Electrical Switching in an Antiferromagnetic Transistor

<u>C. Chou</u>¹, E. Park¹, J. Ingla-Aynes¹, J. Klein¹, K. Mosina², J. S. Moodera¹, Z. Sofer², F. Ross¹, L. Liu¹

¹MIT, Cambridge, Massachusetts, United States, ²University of Chemistry and Technology Prague, Prague, Czechia

We present a magnetic field-effect transistor (FET) using the van der Waals antiferromagnetic semiconductor CrSBr as the channel material. The channel current is efficiently modulated by both gate voltage and magnetic order, with magnetoresistance (MR) highly sensitive to carrier density. While MR remains weak at high carrier densities, we observe a pronounced enhancement up to 1500% in the low-carrier-density regime. Combined experimental and theoretical analyses reveal that magnetic transitions modulate both carrier density and mobility, introducing a distinct mechanism from conventional MR effects. The strong gate voltage dependence of MR is consistent with a spin-induced conduction band shift, further supported by temperature-dependent measurements that yield an activation energy of 9 meV - in agreement with optical spectroscopy.

This spin-modulated transport enables a magnetic subthreshold swing as low as 2 µeV/decade at 40 K, surpassing the Boltzmann thermal limit of conventional MOSFETs by over three orders of magnitude. Additionally, we uncover a two-step magnetic transition observable only at high carrier densities, likely arising from interface-specific effects. These results establish a new approach to energy-efficient spintronic devices by combining magnetic and electric control in a single FET architecture, with implications for logic, memory, and sensing applications. C.-T. Chou, et al., arXiv preprint arXiv:2505.09019 (2025)

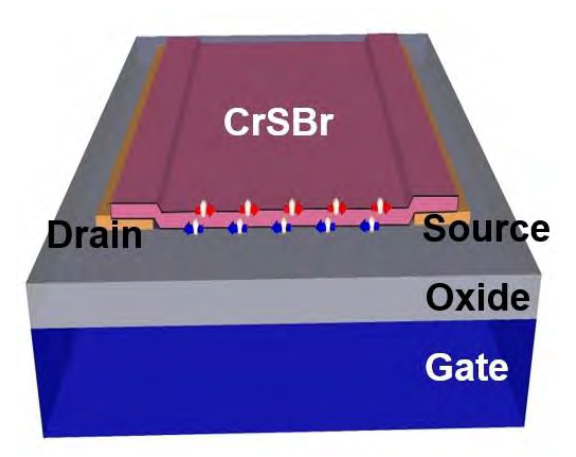


Fig. 1 Schematic of a CrSBr-based magnetic transistor.

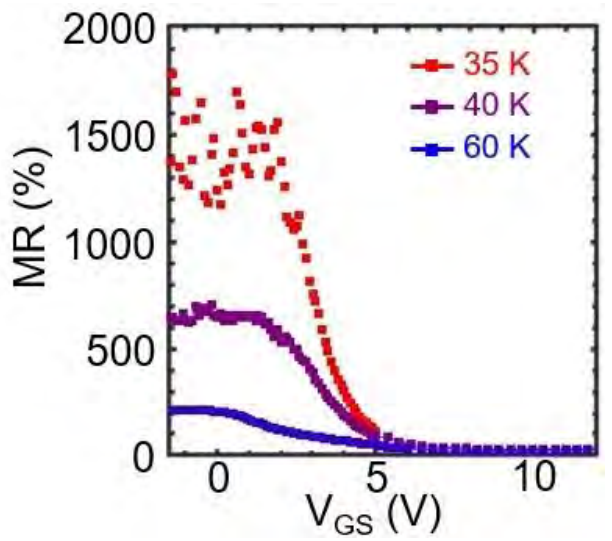


Fig. 2 Magnetoresistance ratio (MR) of magnetic transistor vs. gate voltage (V_{GS}) at different temperatures.

GG-06. Metastable Spin Canting Lifetimes in Magnetic Tunnel Junction Artificial Spin Ice

C. Sullivan¹, H. Chen², S. Majetich²

¹Materials Science and Engineering, Carnegie Mellon University, Pittsburgh, Pennsylvania, United States, ²Physics, Carnegie Mellon University, Pittsburgh, Pennsylvania, United States

The field and time-dependent magnetization dynamics of magnetostatically frustrated magnetic tunnel junctions (MTJs) were characterized via tunnel magnetoresistance (TMR) using conductive atomic force microscopy. Circular 60 nm MTJs were arranged in a square artificial spin ice (ASI) array with 25 nm edge-to-edge spacing. TMR(Hx) revealed a checkerboard pattern of alternating magnetization along $\pm x$ and $\pm y$ ($\phi = \pm 90^{\circ}$). At zero field, TMR(t) showed X-oriented devices exhibiting two-state telegraphing with distinct dwell times, while Y-oriented devices displayed spikes of a few ms, followed by relaxation to metastable baselines. Fig. 1 shows histograms from 200 ms TMR(t) windows for a Y device, revealing discrete metastable states with different canting angles.

Dwell times within individual metastable states were determined from 60s continuous TMR traces. For an X device, this is the time between switching events; for a Y device, the time before leaving the baseline. Fig. 2 shows representative histograms for a single X and Y device, revealing differences shaped by local magnetostatic environments. All distributions deviate from single

exponential decay, indicating a spread of energy barriers from collective interactions. Y devices with canting from $\pm 90^{\circ}$ toward the parallel orientation ($\phi < 90^{\circ}$) exhibited more long dwell times. A baseline dwell time was defined as the time in a single metastable state before leaving, including spikes that relaxed back to baseline. Dwell times ranged from 4-2500 ms. Baselines with $\phi < 90^{\circ}$ were longer lived, on average. This anisotropy results from weak coupling to the fixed layer.

In contrast to isolated MTJs of similar size, which relax in $\sim\!1.35~\mu s$ [2], MTJ-based ASI exhibits a hierarchy of metastable states and collective dynamics that slow relaxation. This enables short-term memory independent of individual switching. Excited canted baselines in Y devices, analogous to emergent magnetic monopole configurations, can persist locally.

[1] J. S. Moodera and L. R. Kinder, Journal of Applied Physics 79, 4724 (1996).

[2] B. Parks et al., Physical Review Applied 13, 014063 (2020).

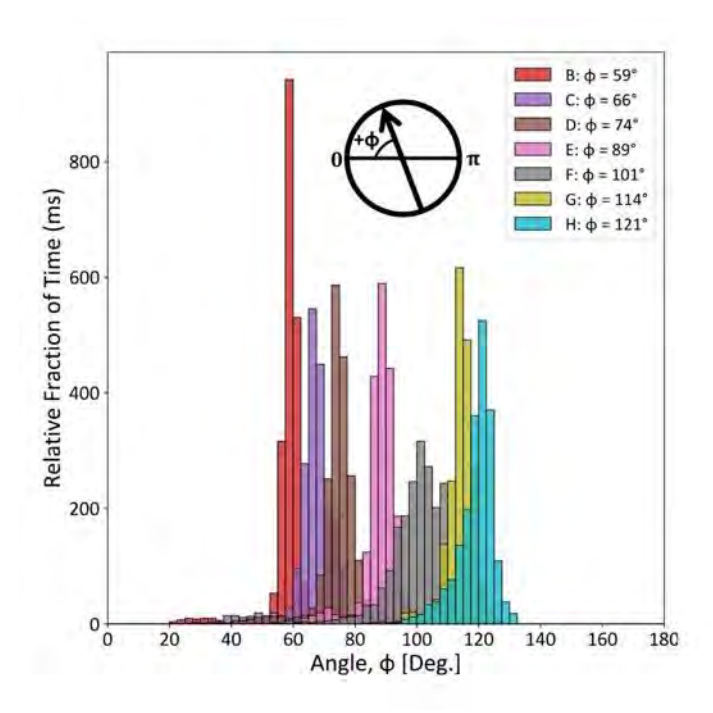


Fig. 1. Zero field histogram for TMR-converted angle [1] for select 200 ms TMR windows from the same Y device

recorded continuously.

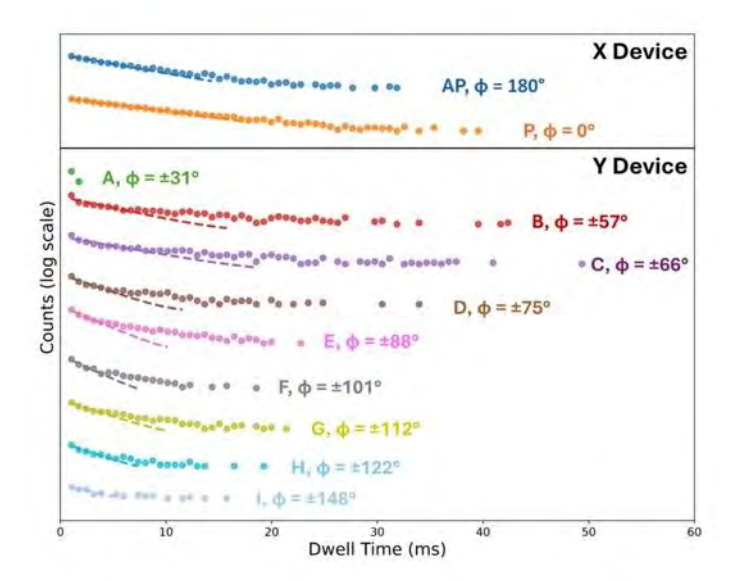


Fig. 2. Empirical dwell time distributions for X and Y devices. State A was observed, but its dwell times were short.

GG-07. Impact of Synthetic Ferrimagnetic Free Layers on Current-in-Plane Giant Magnetoresistance

S. Abdizadeh Kalan¹, V. Amin², S. Emori¹
¹Physics, Virginia Tech, Blacksburg, Virginia, United
States, ²Physics, School of Science, Indiana University – Purdue
University Indianapolis (IUPUI), Indianapolis, Indiana, United
States

Giant magnetoresistance (GMR) in spin valves, with broad applications in sensing and computing technologies, depends sensitively on the constituent layers. While spin valves with simple ferromagnetic free layers have been studied extensively [1,2], the GMR response with more complex structures - e.g., synthetic ferrimagnetic (SF) free layers - remains less well understood. Such current-inplane spin valves with SF free layers are attractive for devices leveraging large cone-angle dynamics [3]. Here, we investigate how the current-in-plane GMR ratio is influenced by the degree of compensation in the SF free layers in a series of spin valves. As illustrated in Fig. 1, each spin valve consists of a Co(3)/Cr(1)/Co(3) synthetic antiferromagnet hard layer, a Cu(3) spacer, and a Co(x)/Cr(1)/Co(6-x) SF free layer with the tuned thickness x from 0 to 6 nm. Altering x across compensation (x = 3 nm) changes the polarity of the GMR loop [Fig. 1]. Figure 2 summarizes the magnitude of the GMR ratio

against x. The measured GMR ratio vanishes near compensation (x = 3 nm) as the SF becomes hard to switch. We also observe that increasing x (i.e., reducing the thickness of the Co sublayer adjacent to the Cu spacer) leads to, on average, a decrease in the GMR ratio. More intriguingly, the GMR ratio oscillates with a periodicity of ≈ 0.4 nm in x, varying by up to a factor of 2 between peaks and troughs. We tentatively attribute the GMR oscillations to quantum interference of spin-polarized conduction electrons. While GMR oscillations with spacer thickness were previously reported [4], our experiment is distinct in demonstrating such oscillations with magnetic layer thickness. Moreover, our findings reveal the need to carefully tune the ferromagnet thicknesses of the SF free layer at the angstrom scale to maximize the GMR ratio for practical device applications [5].

- [1] Kim, S. N., Choi, J. W., & Lim, S. H, Scientific Reports 9, Article 1617 (2019).
- [2] Yao, F., Multian, V., Watanabe, K., et al. Nano Letters, 25(9), 3549-3555 (2025).
- [3] Skarsvåg, H., Holmqvist, C., & Brataas, A., Physical Review Letters, 115(23), 237201 (2015).
- [4] Kim, S. N., Choi, J. W., & Lim, S. H., Scientific Reports, 9, Article 1617(2019).
- [5] Kübler, D., Smith, D. A., Nguyen, T., et al. Physical Review B, 111(5), 054425 (2025).

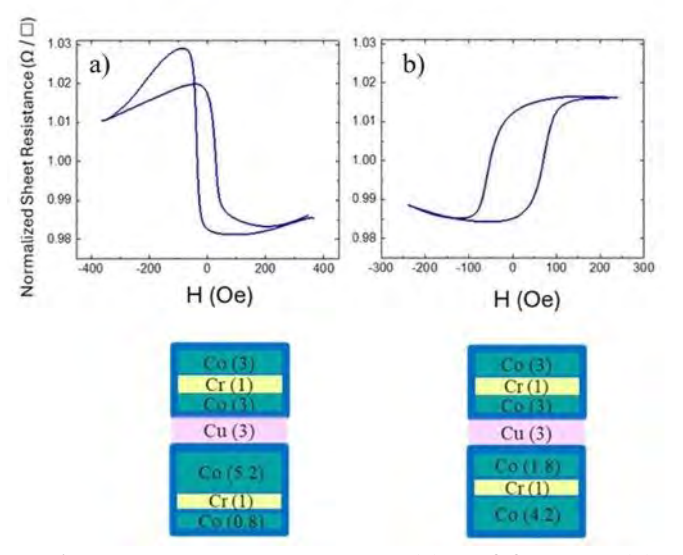


Fig. 1. Magnetoresistance loops for (a) x = 0.8 nm and (b) x =4.2 nm.

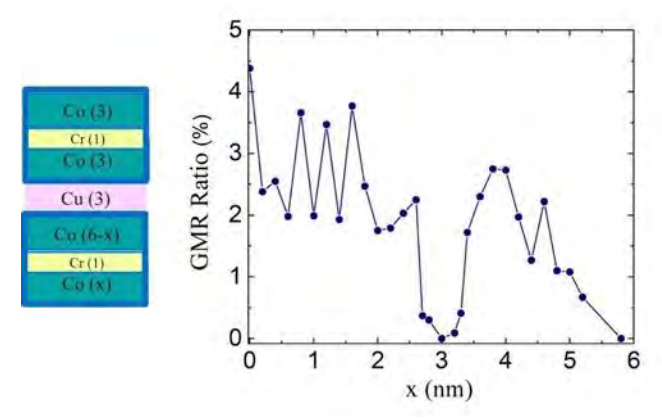


Fig. 2. GMR ratio vs Co sublayer thickness (x) in SF free layer.

GG-08. Co-Sputtered Diluted Magnetic Layers for Thermal **Compensation in Vortex Magnetic Tunnel Junction Sensors**

T. Fernandes¹, P. Araujo¹, R. Macedo¹, P. Freitas^{1, 2}, S. Cardoso^{1, 2}

¹INESC Microssistemas e Nanotecnologias, Lisboa, Portugal, ²Instituto Superior Técnico, Lisboa, Portugal

Magnetic tunnel junction (MTJ) sensors using the vortex state for the free layer (FL) are viable sensing solutions for applications that require a wide linear range and low magnetic noise [1,2]. Some applications require operating temperatures of up to 150°C [3] where the loss of sensitivity with increasing temperature is critical. The temperature resilience of these systems can be improved by engineering the reference layers [4], but the devices still show sensitivity degradation with increasing temperature.

A strategy to reduce the temperature coefficient of sensitivity in vortex-based structures includes the FL (typically CoFeB/NiFe) dilution with a non-magnetic metal (e.g. Ta/Ru). By controlling the FL magnetization (M_{sat}) decay with temperature, a stable sensitivity across the whole temperature range can be achieved. This method was proposed in [5], with sequential depositions of the magnetic material and dusting layers. Here, we report on diluted CoFeB/NiFe-based FLs deposited through co-sputtering of the magnetic and dilution elements. The co-sputtering allows complete tunability of the FL dilution ratio while ensuring a uniform composition across thickness. To illustrate this, CoFeB and Ru co-sputtered films were prepared in a Nordiko 8800 tool, with Ru ratios from 0-30%.

Temperature dependent magnetometry measurements of these films show the decrease in M_{sat} with the dilution ratio,

from 1280 to 572 emu/cc. Additionally, the decrease in magnetization with temperature was accentuated with the dilution, with M_{sat} at 150°C dropping from 97% to 69% of the M_{sat} at RT (fig.1). These results demonstrate the cosputtering of magnetic layers as a viable strategy that enables a degree of freedom to tune the decay of M_{sat} and ultimately compensate for thermal degradation.

The film uniformity and thermal stability will be assessed in vortex MTJ devices based on CoFeB/MgO/CoFeB/Diluted FL, patterned on 200mm wafers. The impact of the FL dilution on the sensor sensitivity and linearity will be further discussed and compared with other optimization strategies towards a thermally resilient MTJ sensor.

- [1] Suess, Dieter, et al. Nature Electronics 1.6 (2018): 362-370.
- [2] Matos, F., et al. AIP Advances 13.2 (2023).
- [3] Iwata-Harms, Jodi M., et al. Scientific reports 8.1 (2018): 14409.
- [4] Hua Lv, et.al., J.Magn.Magn. Mat. 477, 68-73 (2019)
- [5] Timopheev, Andrey, Clarisse Ducruet, and Jeffrey Childress. U.S. Patent Application No. 18/294,283.

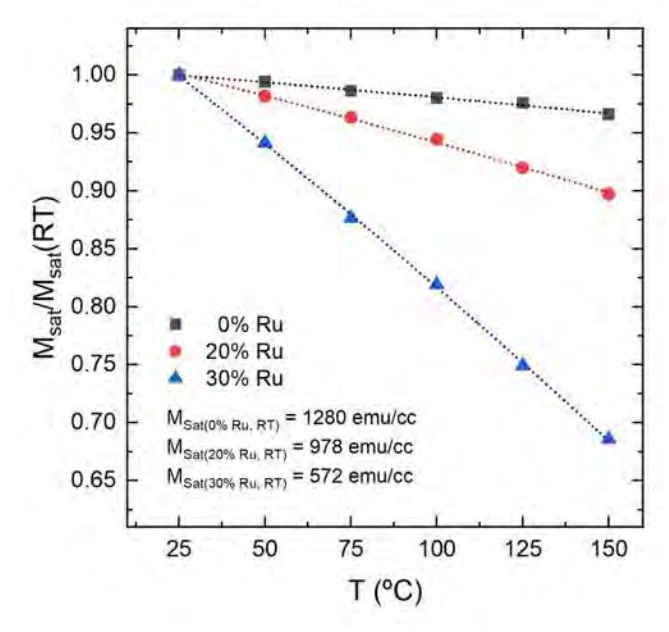


Fig.1: Normalized M_{sat} vs T for co-sputtered CoFeB films with varying Ru content, fitted by $T^{3/2}$ law (dashed lines).

GG-10. Anomalous Spin Canting and Monopole-Like Excitations in Artificial Spin Ice

S. Majetich¹, C. Sullivan²

¹Physics, Carnegie Mellon University, Pittsburgh, Pennsylvania, United States, ²Materials Science and Engineering, Carnegie Mellon University, Pittsburgh, Pennsylvania, United States

Micromagnetic simulations were used to understand anomalous spin canting directions in artificial spin ice (ASI) made from magnetic tunnel junctions (MTJs). Traditional square lattice ASI has nanomagnet moments oriented at 0°/180° or at ±90°, depending on shape anisotropy. Here the nanomagnets are the free layers of MTJs with a shared fixed layer. Though the free layers are circular, symmetry is broken by the fixed layer. Half the MTJs telegraph between parallel (0°) and antiparallel (180°) states. The other half have a range of angles, not just ±90°.

The canting angles were predicted based on the magnetostatic fields generated by neighboring 60 nm CoFeB discs with 85 nm pitch. Good agreement with the nine experimentally observed angles was obtained when nearest and next nearest neighbor contributions were included (Table 1). 88% of the data for a single device measured over 60 s could be assigned to one of the nine canting angles.

Because the observed TMR baselines can be related to specific spin configurations, they can also be used to determine if a nanomagnet is part of an emergent magnetic monopole (EMM). In traditional ASI, EMMs are identified by calculating the net magnetic charge at a node between four nanomagnets [1], treating the north and south poles of the moment as fictitious magnetic charges. With this definition the MTJs with canted states would have non-integer but non-zero charges, and are therefore part of EMM excitations. Figure 1 shows examples of local configurations where the central spin is part of two nodes. In e₁ the two in, two out ice rule is followed in both nodes, and there are no EMMs. This is also true for the top node of e_2 but the bottom has a nonzero net magnetic charge. a_P, b_P, and q_{1P} all have fractional magnetic charges at both nodes. While TMR cannot distinguish monopole-containing e2 from nonmonopole e₁, monopole-like excitations with canted spins can be detected. Based on the relative abundance of these states, the majority of the MTJs are part of these excitations at any given time.

1. R. F. Wang, et al., Nature 446, 102 (2007).

^{*} Best Student Presentation Finalist / LB - Late-breaking Poster

Near Neighbor Model Label	Φ _{pred} C)	Experiment Empirical Label	Normalized TMR (0-1)	(PleuC)	Relative Abundance %
ар	27.0	A	0.07	31	0.3
bp	57.0	В	0.23	57	19.8
gp	68.6	C	0.30	66	24.4
dp	74.4	D	0.37	75	9.5
e	90.0	E	0.48	88	16.1
dap	105.6	F	0.60	101	6.3
BAP	111.4	G	0.68	112	7.7
hAP	123.0	H	0.76	122	3.1
aAP	153.0	- 1.	0.92	148	1.6

Table 1. Near Neighbor Model Predictions and Measured Canting Angles

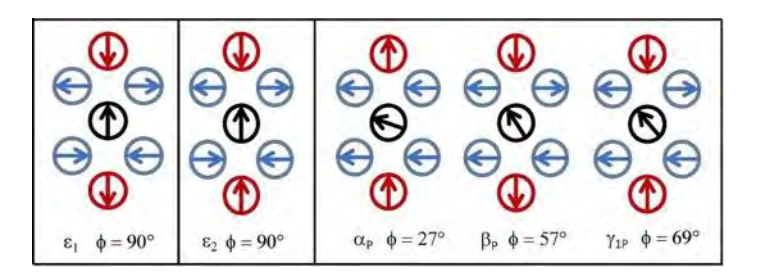


Fig. 1. Schematics of near neighbors (blue, red) around a central spin (black) that is part of two nodes.

GG-11. Predicting Novel Tunnel Barrier Materials for Magnetic Tunnel Junctions using Language Models and First-Principles Screening

<u>S. Islam</u>¹, W. Rogers¹, C. Hu², M. Song², X. Bao², S. Sayed³, J. Incorvia¹

¹Chandra Family Department of Electrical and Computer Engineering, University of Texas at Austin, Austin, Texas, United States, ²Taiwan Semiconductor Manufacturing Company, Taipei, Taiwan, ³Headway Technologies Inc., Milpitas, California, United States

The use of magnetic tunnel junctions (MTJs) in modern computing paradigms is limited by the constraints of magnesium oxide (MgO) tunnel barriers. While providing spin filtering and good interfacing with Fe-based electrodes, MgO-based MTJs have challenges of high resistance area (RA) product resulting in vulnerabilities due to the needed ultrathin thicknesses. To discover alternative materials, we developed a hybrid framework that employs machine learning large language models (LLMs) followed by screening based on first principles, illustrated in Fig. 1. Using Word2Vec [1], a word embedding model, correlations were extracted from a corpus of materials science literature

to identify promising candidates [2]. This led to the discovery of materials such as NbN and hybrid nitride-based barriers as tunnel barrier candidates. Additionally, a MaterialsBERT [3] masked language model was further trained on the same corpus to capture deeper contextual relationships. The model functions as a heuristic filter for potential materials, and identified NiO, BaO, and TiN as barrier material candidates.

The LLM-predicted materials were subsequently screened via density functional theory (DFT) simulations using QuantumATK [4], with the predicted materials' TMR and RA product benchmarked against MgO in Fig. 2. Results indicate that hybrid tunnel barrier MTJs featuring a monolayer dusting of ScN [5] or TiN on either side of the MgO barrier are predicted to have similar RA products and higher TMR ratios than MTJs with pure MgO of identical number of layers. Remarkably, when sweeping thicknesses, an 8-layer ScN configuration achieved both a lower RA product and a higher TMR ratio than the 6-layer MgO reference. Furthermore, the NiFe/6NiO/NiFe MTJ outperformed the Fe/6ScN/Fe structure, demonstrating superior TMR and reduced RA. This integrated LLM-DFT pipeline provides a scalable path toward discovering new tunnel barrier materials and advancing MTJ performance for emerging memory and neuromorphic computing technologies.

- [1] T. Mikolov, K. Chen, G. Corrado, and J. Dean, ArXiv:1301.3781 (2013).
- [2] S. Sayed, H. C. Kleidermacher, G. Hashemi-Asasi, C.-H. Hsu, and S. Salahuddin, *npj Comput. Mater.* 11, 167 (2025). [3] P. Shetty, A. C. Rajan, C. Kuenneth, S. Gupta, L. P. Panchumarti, L. Holm, C. Zhang, and R. Ramprasad, *npj Comput. Mater.* 9, 52 (2023).
- [4] S. Smidstrup, K. Stokbro, A. Blom, T. Markussen, J. Wellendorff, J. Schneider, T. Gunst, B. Verstichel, P. A. Khomyakov, U. G. Vej-Hansen, M. Brandbyge et al., *J. Phys.: Condens. Matter.* 32, 015901 (2020).
- [5] S. Karki, V. Rogers, P. Jadaun, D. S. Marshall, and J. A. C. Incorvia, *Adv. Theory Simul.* 4, 2100309 (2021).

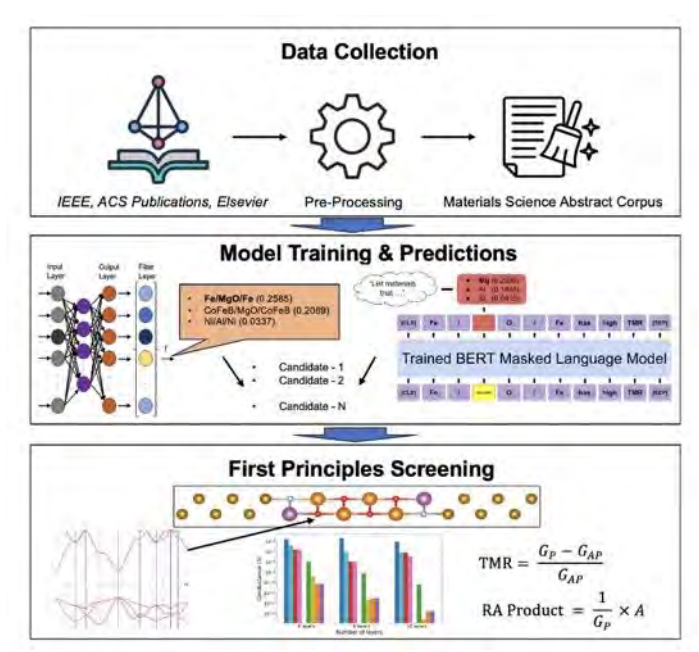


Fig. 1. Schematic representation of the overall materials discovery workflow.

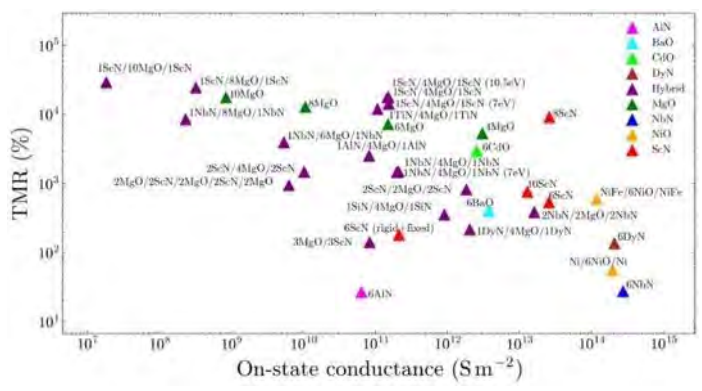


Fig. 2. TMR ratios plotted against on-state conductance for each simulated MTJ.

GG-12. Phase-resolved Ultrabroadband Terahertz Spectroscopy of Giant Magnetoresistance

Z. Kaspar^{1, 2}, O. Gueckstock³, B. D. Mohapatra⁴, G. Schmidt⁴, P. Kubascik², J. Jechumtal², P. Kuzel¹, L. Nadvornik², T. Kampfrath³

¹FZU - Institute of Physics of the Czech Academy of Sciences, Prague, Czechia, ²Charles University, Prague, Czechia, ³Freie Universität Berlin, Berlin, Germany, ⁴Martin-Luther-Universität Halle-Wittenberg, Halle, Germany

Understanding ultrafast spin transport and magnetoresistive phenomena on femtosecond timescales is crucial for developing future high-speed spintronic devices $^{[1,2]}$. In this work, we employ ultrabroadband terahertz time-domain spectroscopy (THz-TDS) to investigate giant magnetoresistance (GMR) in metallic trilayers of the form $F_A|Cu(d)|F_B$, where F_A and F_B are ferromagnetic thin films with collinear in-plane magnetization aligned either parallel $(\uparrow\uparrow)$ or antiparallel $(\uparrow\downarrow)$, and separated by a non-magnetic copper layer of varying thickness d.

Our measurements are performed in a current-in-plane (CIP) geometry using broadband, single-cycle THz electric-field pulse with spectral coverage from 1 to 25 THz. We obtain a magnetoresistive response as the difference in transmission between the $\uparrow\uparrow$ and $\uparrow\downarrow$ magnetic states [3], with particular focus on high temporal resolution. This quantity allows us to access not only the amplitude, but also phase shifts of the GMR signal.

We observe a notable decrease in GMR contrast from the DC value of 3% to 2% at 25 THz. Remarkably, we detect a nearly frequency-independent time delay of 14 fs (d_{Cu} = 3 nm) in the GMR response relative to the driving THz field. This behavior suggests that the observed phase shift arises from electron propagation across the Cu layer and subsequent spin-dependent scattering at the F_A/Cu and Cu/F_B interfaces. To further investigate the origin of this delay, we systematically vary the Cu thickness and find that delay scales with the spacer thickness.

Our findings demonstrate that phase-sensitive THz spectroscopy is a powerful tool for probing femtosecond spin transport in layered magnetic heterostructures, revealing ultrafast transport delays inaccessible to conventional DC or frequency-domain techniques.

[1] Leitenstorfer, A. et al. The 2023 terahertz science and technology roadmap. J. Phys. D: Appl. Phys. 56, 223001

(2023).

[2] Jin, Z. et al. Accessing the fundamentals of magnetotransport in metals with terahertz probes. Nature Phys11, 761-766 (2015).

[3] Nádvorník, L. et al. Broadband Terahertz Probes of AMR Disentangle Extrinsic and Intrinsic Contributions. Phys. Rev. X 11, 021030 (2021).

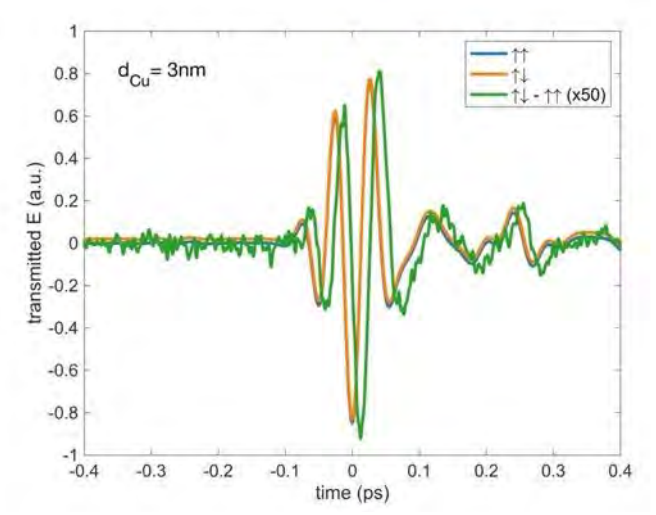


Fig. 1 Waveforms of the transmitted THz electric field for parallel $(\uparrow\uparrow)$ and antiparallel $(\uparrow\downarrow)$ magnetization. The difference waveform follows the spectral shape of the transmitted pulse and is temporally delayed by 14 fs.

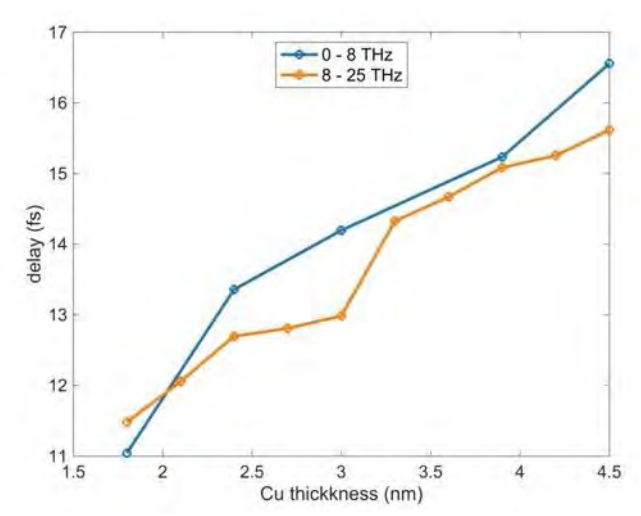


Fig. 2 Temporal delay of the difference waveform as a function of the thickness of the non-magnetic copper spacer.

GG-13. Terahertz spectroscopy of spin-Hall magnetoresistance: case study of YIG|Pt and CoFeB|Pt

P. Kubascik¹, R. Schlitz², O. Gueckstock^{3,4}, O. L. Franke³, D. Reiss³, M. Borchert⁵, M. Busina¹, G. Jakob⁶, K. Olejník⁷, A. Farkas^{1,7}, Z. Kaspar^{1,7}, J. Jechumtal¹, E. Schmoranzerova¹, P. Nemec¹, M. Wolf⁴, Y. Wu^{8, 9}, G. Woltersdorf¹⁰, M. Kläui⁶, P. Brouwer³, S. Goennenwein², T. Kampfrath^{3,4}, L. Nadvornik¹ ¹Department of chemical physics and optics, Charles University, Prague, Czechia, ²Department of Physics, University of Konstanz, Konstanz, Germany, ³Department of Physics, Freie Universität Berlin, Berlin, Germany, ⁴Department of Physical Chemistry, Fritz Haber Institute of the Max Planck Society, Berlin, Germany, ⁵Max Born Institute for Nonlinear Optics and Short Pulse Spectroscopy, Berlin, Germany, ⁶Institut für Physik, Johannes Gutenberg-Universität Mainz, Mainz, Germany, ⁷Insitute of Physics, Czech Academy of Sciences, Prague, Czechia, ⁸Department of Physics, State Key Laboratory of Surface Physics, Fudan University, Shanghai, China, ⁹Shanghai Research Center for Ouantum Sciences. Shanghai, China, ¹⁰Institut für Physik, Martin-Luther-Universität, Halle, Germany

Spin-Hall magnetoresistance (SMR) is a novel magnetoresistive phenomenon observed in bilayers consisting of a heavy metal (HM) and a magnetically ordered layer (M). SMR originates from the coupling between SHE driven spin accumulation in the HM and the magnetization in M through interfacial spin-orbit torque[1], [2] and spin-transport in M (e.g.through magnons[3] or electrons [4]). Although SMR has been studied in the DC[5] and GHz spectral range[6], the ultrafast response of this phenomenon and the associated spin-sink channels remain unclear.

We report a terahertz investigation of spin-Hall magnetoresistance (SMR) in the frequency range from 0.2 to 25 THz in YIG|Pt and CoFeB|Pt bilayers. By combining sensitive THz detection with high-frequency magnetic field modulation, we observed pronounced magnonic spectral low-pass behavior in YIG|Pt, in contrast to a frequencyindependent SMR response up to 25 THz in CoFeBIPt. Modelling attributes the spectral filtering to the finite response time of a magnon chemical potential that builds up in M due to the time-dependent spin accumulation in HM at the interface [7], [8], whereas the broadband response in CoFeB|Pt arises from efficient, fast electronic spin-sink channels.

459

Our results highlight the importance of thermal magnon transport in SMR devices. Furthermore, we show that to faster spin relaxation of electrons, the magnonic low-pass filter can be deteriorated by electronic spin relaxation. This implies that metallic structures are more suitable for high-frequency applications, while THz spectroscopy of SMR in insulating systems enables the investigation of various magnonic phenomena.

- [1] S. Cho et al. *Scientific Reports*, Vol. 5, p. 14668(2015).
- [2] Y.-T. Chen et al. Physical Review B—Condensed Matter and Materials Physics, Vol. 87, p. 144411(2013).
- [3] L. J. Cornelissen et al. *Physical Review B*, Vol. 94, p. 014412(2016).
- [4] J. Kim et al. Phys Rev Lett, vol. 116, p. 097201(2016).
- [5] M. Althammer *et al. Physical Review B—Condensed Matter and Materials Physics*, Vol. 87, p. 224401(2013).
- [6] J. Lotze et al. *Physical Review B*, Vol. 90, p. 174419(2014).
- [7] D. A. Reiss, T. Kampfrath, and P. W. Brouwer. *Physical Review B*, Vol. 104, p. 024415(2021).
- [8] O. Franke, et al. arXiv preprint arXiv:2408.13099, 2024.

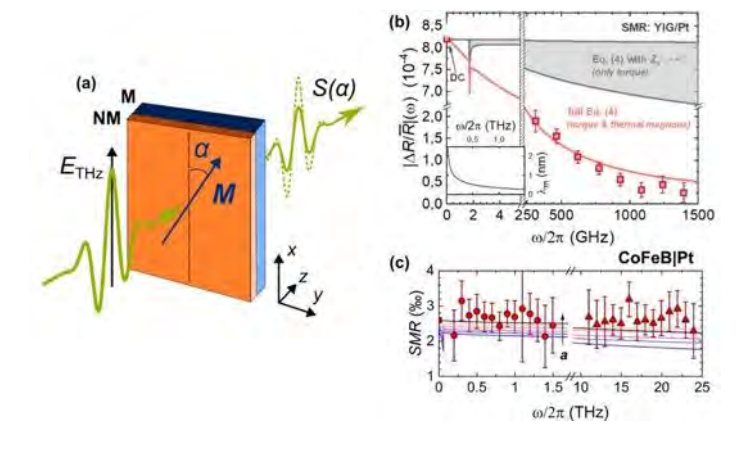


Fig. 1: (a) Sketch of the experiment. Depending on the mutual orientation of THz polarisation and magnetisation, the conductivity/resistivity changes, which reflects in THz absorption. Low-pass filter in SMR spectrum in YIG|Pt is in (b). SMR spectrum of CoFeB|Pt from 0.2 up to 25 THz is in (c). In both, (b) and (c), solid Lines shows various theoretical models of SMR.

SESSION GP: ANTIFERROMAGNETS AND 2D MATERIALS (POSTER SESSION)

Chair(s): Z. Yuan, Interdisciplinary Center for Theoretical Physics and Information Sciences, Fudan University, Shanghai, China Friday, October 31, 2025

riday, October 31, 2025 09:00 AM-12:00 PM Exhibit Hall Posters

GP-01-LB. Highly Tunable Electronic States near Chiralityreversed Planar Defect with Magnetic Interstitial Atomic Layer in Magnetic Weyl Semimetals

E. Thareja¹, G. M. Pantano¹, I. Vekhter², <u>J. D. Gayles¹</u>
¹Physics, University of South Florida, Tampa, Florida, United States, ²Physics, Louisiana State University, Baton Rouge, Louisiana, United States

Topological features of the electronic band structure are robust against many types of disorder, which makes materials such as topological insulators and Weyl semimetals promising for low-power spintronics and quantum computing. Weyl semimetals possess topologically protected linear band crossings, called Weyl nodes, that always arise in pairs. The electronic excitations near these nodes have spin-momentum locking that can be characterized by a chiral charge, with individual nodes having opposite chirality [1]. While non-magnetic candidates for Weyl semimetals have been known for about a decade, their magnetic counterparts (typically having fewer Weyl node pairs) have only been identified recently [2,3,4]. Weyl semimetals, like other materials, have planar defects such as twin boundaries. Additionally, planar defects can be intentionally induced via an interstitial atomic layer. In this work, we show using a continuum model that a planar defect between chirality-reversed (due to magnetization-reversal) regions will host bound states, in agreement with Araki et. al. [5]. Moreover, we demonstrate the dispersion, and the spin texture of these states are highly tunable in the presence of a magnetic interstitial atomic layer at the planar defect. These properties have a periodic dependence on defect electrostatic potential, due to the emergent Weyl character of the electronic states, in agreement with similar result for topological insulators [6]. Another consequence of the Weyl character is that interstitial magnetic potential pointing out of the defect plane does not affect physical observables. Meanwhile, the in-plane magnetic potential parallel to the Weyl node split direction affects the spatial distribution of the states, and

strongly blocks the bulk states from being transmitted across the defect [7]. The other in-plane component perpendicular to the Weyl node split direction affects the shape of the fermi-arc-like bound states and spin selects the bulk states scattering off the defect [7]. Hence, we provide a comprehensive picture of how electrostatic and magnetic potentials from the interstitial layer can tune chirality-reversed planar defect states in magnetic Weyl semimetals.

[1] N. P. Armitage, E. J. Mele, and A. Vishwanath, Rev. Mod. Phys. 90, 015001 (2018).

[2] D. F. Liu, A. J. Liang, E. K. Liu, et al. Science 365, 6459 (2019).

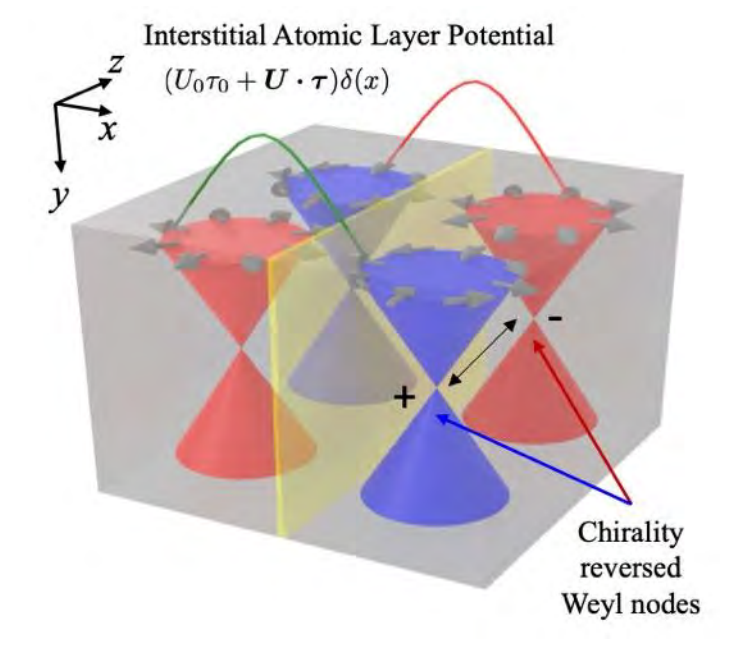
[3] S. Nie, T. Hashimoto, and F. B. Prinz, Phys. Rev. Lett. 128, 176401 (2022)

[4] X. Yao, J. Gaudet, R. Verma, Phys. Rev. X 13, 011035 (2023).

[5] Y. Araki, A. Yoshida, and K. Nomura, Phys. Rev. B 98, 045302 (2018).

[6] E. Thareja and I. Vekhter, Phys. Rev. B 107, 144205 (2023).

[7] Eklavya Thareja, Gina Pantano, Ilya Vekhter, Jacob Gayles arXiv:2501.05594 (2025).



GP-02-LB. Topological Magnetic Insulators for Dissipationless Monostructural Adiabatic Spintronics

<u>J. Hanson-Flores</u>¹, A. Regmi¹, J. Tang², J. Keum⁴, J. Park⁴, R. Cheng³, E. del Barco¹

¹Physics, University of Central Florida, Orlando, Florida, United States, ²Physics, University of California, Riverside, Riverside, California, United States, ³Electrical Engineering, University of California, Riverside, Riverside, California, United States, ⁴Physics and Astronomy, Seoul National University, Seoul, Korea (the Republic of)

Adiabatic electric currents offer a promising route toward energy-efficient computation. Unlike conventional ohmic currents that dissipate energy through Joule heating, adiabatic transport can, in theory, enable lossless electron flow with perfect mechanical efficiency. A recently developed theory reveals that Néel-type spin-orbit torque (NSOT) can be driven by an electric field, enabling efficient control of antiferromagnetic (AFM) dynamics without the use of conduction currents. In this work, we experimentally verify this prediction by demonstrating an unconventional AFM resonance driven purely by an electric field in a bulk crystal of layered AFM insulator. This electric field driven resonance is characterized though a spectroscopic study at a variety of frequencies using a quasi-optical CW EPR system. Rotation of the microwave polarization in the Voigt geometry provides selectivity between magnetic and electric-field driven resonance mechanisms, enabling the isolated study of each. This novel electric field driven resonance is a signature of the exotic NSOT which holds the potential to revolutionize data processing and dramatically reduce energy dissipation in such processes.

GP-04-LB. Octupole-driven spin-transfer torque switching in all-antiferromagnetic tunnel junctions

J. Kang¹, M. Hamdi¹, S. Cheung¹, L. Yuan¹, M. A. Elekhtiar², W. Rogers¹, A. Meo³, P. G. Lim¹, M. N. Tey¹, A. D'Addario⁴, S. Konakanchi⁵, E. Matt¹, J. G. Athas¹, S. Arpaci¹, L. Wan⁶, S. Mehta⁶, P. Upadhyaya⁵, M. Carpentieri³, V. P. Dravid¹, M. C. Hersam¹, J. Katine⁶, G. Fuchs⁴, G. Finocchio⁷, E. Y. Tsymbal², J. M. Rondinelli¹, P. Khalili Amiri¹

¹Northwestern University, Evanston, Illinois, United States, ²University of Nebraska, Lincoln, Nebraska, United States, ³Politecnico di Bari, Bari, Italy, ⁴Cornell University, Ithaca, New York, United States, ⁵Purdue University, West Lafayette, Indiana, United States, ⁶Western Digital Corporation, San Jose, California, United States, ⁷University of Messina, Messina, Italy

Magnetic tunnel junctions (MTJs) based on ferromagnets are canonical devices in spintronics, with a wide range of applications in data storage, computing, and sensing. This was enabled by well-established mechanisms for electrical detection and manipulation of magnetic order through the tunneling magnetoresistance (TMR)¹⁻⁴, and reciprocally, through the spin-transfer torque (STT) effect⁵⁻⁷. It was long assumed that neither of these effects could be present in tunnel junctions based on antiferromagnetic materials due to their zero net magnetization. Recently, however, it was shown that noncollinear antiferromagnets host a spin-split band structure and associated non-relativistic momentumdependent spin polarization and cluster magnetic octupole moment, thereby leading to non-zero TMR in allantiferromagnetic tunnel junctions (AFMTJs)8-10. However, the reciprocal effect, i.e., the antiferromagnetic counterpart of STT driven by currents through the AFMTJ, has been assumed nonexistent due to the total electric current being spin-neutral.

Here, in contrast to this common expectation, we report nanoscale AFMTJs exhibiting this reciprocal effect, which we term octupole-driven spin-transfer torque (OTT)¹¹. We demonstrate current-induced OTT switching in PtMn₃|MqO|PtMn₃ AFMTJs, fabricated on a thermally oxidized silicon substrate, exhibiting a TMR value of up to 363% at room temperature and switching current densities on the order of 10 MA/cm². Our theoretical modeling reveals that the imbalance between intra- and inter-sublattice spin currents across the AFMTJ, and equivalently, the non-zero net cluster magnetic octupole polarization of each PtMn₃ layer, give rise to the torque and associated switching dynamics. Our findings lay the foundation for antiferromagnetic spintronics based on a new AFMTJ material platform, paving the way for deeply scaled magnetic memory and room-temperature terahertz technologies.

- 1. Moodera, J. S., Kinder, L. R., Wong, T. M. & Meservey, R. Large magnetoresistance at room temperature in ferromagnetic thin film tunnel junctions. *Phys. Rev. Lett.* 74, 3273-3276 (1995).
- 2. Miyazaki, T. & Tezuka, N. Giant magnetic tunneling effect in Fe/Al2O3/Fe junction. J. Magn. Magn. Mater. 139, L231-L234 (1995).
- 3. Parkin, S. S. et al. Giant tunnelling magnetoresistance at room temperature with MgO (100) tunnel barriers. Nat. Mater. 3, 862-867 (2004).
- 4. Yuasa, S., Nagahama, T., Fukushima, A., Suzuki, Y. & Ando, K. Giant room-temperature magnetoresistance in single-

- crystal Fe/MgO/Fe magnetic tunnel junctions. Nat. Mater. 3, 868-871 (2004).
- 5. Slonczewski, J. C. Current-driven excitation of magnetic multilayers. *J. Magn. Magn. Mater.* 159, L1-L7 (1996).
- 6. Berger, L. Emission of spin waves by a magnetic multilayer traversed by a current. Phys. Rev. B 54, 9353 (1996).
- 7. Katine, J. A., Albert, F. J. & Buhrman, R. A. Current-driven magnetization reversal and spin-wave excitations in Co/Cu/Co pillars. Phys. Rev. Lett. 84, 3149 (2000).
- 8. Qin, P. et al. Room-temperature magnetoresistance in an all-antiferromagnetic tunnel junction. *Nature* 613, 485-489 (2023).
- 9. Chen, X. et al. Octupole-driven magnetoresistance in an antiferromagnetic tunnel junction. *Nature* 613, 490-495 (2023).
- 10. Shi, J. et al. Electrically controlled all-antiferromagnetic tunnel junctions on silicon with large room-temperature magnetoresistance. Adv. Mater. 36, e2312008 (2024). 11. Kang, J., Hamdi, M. et al. Octupole-driven spin-transfer torque switching of all-antiferromagnetic tunnel junctions. arXiv:2509.03026 (2025).

GP-06-LB. Altermagnetism and Strain Induced Altermagnetic Transition in Cairo Pentagonal Monolayer

<u>S. Li</u>, Y. Zhang, A. Bahri, X. Zhang, C. Jia *Physics, University of Florida, Gainesville, Florida, United States*

Altermagnetism, a recently recognized form of magnetic order with vanishing net magnetization and spin-split band structures, has become a focus of intense research [1,2]. In this work [3], we propose a two-dimensional system that realizes \$q\$-wave altermagnetism and exhibits a straindriven transition to a \$d\$-wave state. This behavior arises in a monolayer Cairo pentagonal lattice, described by a realistic tight-binding model including both magnetic and non-magnetic sites. We further demonstrate that breaking the symmetry protecting spin-polarized nodal points can induce non-trivial band topology. Finally, we present \emph{ab initio} results on candidate materials such as FeS\$ 2\$ and Nb\$ 2\$FeB\$ 2\$, which contain the required lattice symmetry and are consistent with our model. These results broaden the landscape of altermagnetic systems and suggest new opportunities for spintronic applications.

[1] Šmejkal, L., Sinova, J. and Jungwirth, T., 2022. Beyond conventional ferromagnetism and antiferromagnetism: A phase with nonrelativistic spin and crystal rotation

symmetry. Physical Review X, 12(3), p.031042.

[2] Šmejkal, L., Sinova, J. and Jungwirth, T., 2022. Emerging research landscape of altermagnetism. Physical Review X, 12(4), p.040501.

[3] Li, S., Zhang, Y., Bahri, A., Zhang, X. and Jia, C., 2025. Altermagnetism and strain induced altermagnetic transition in Cairo pentagonal monolayer. npj Quantum Materials, 10(1), p.83.

GP-08-LB. Sub-Terahertz Spin Pumping in Easy Plane Canted Antiferromagnet $\alpha\text{-Fe}_2\text{O}_3$

A. Regmi¹, G. Fritjofson¹, J. Hanson-Flores¹, J. Michel², J. Tang³, F. Yang², R. Cheng³, E. del Barco¹

¹Physics, University of Central Florida, Orlando, Florida, United States, ²Department of Physics, The Ohio State University, Columbus, Ohio, United States, ³Department of Physics and Astronomy, University of California, Riverside, California, United States

Antiferromagnets (AFs) offer intrinsic advantages for ultrafast spintronic devices due to their high-frequency dynamics, negligible stray fields, and immunity to magnetic crosstalk. Easy-plane and canted AFs are particularly promising, as their room-temperature optical modes extend into the sub-terahertz regime, enabling operation speeds beyond conventional ferromagnets and antiferromagnets accessible at room temperature. α -Fe₂O₃ is a prototypical canted, easy-plane AF with Dzyaloshinskii-Moriya interaction inducing weak ferromagnetism, allowing simultaneous access to acoustic and optical resonances. We investigate coherent spin pumping from both modes in α -Fe₂O₃/Pt bilayers, comparing a bulk single crystal and a thin-film geometry. Microwave excitation, in a 9 T split-coil magnet, reveals distinct frequency-field dispersions for the two resonances, supporting the principle of spin mixing conductance in antiferromagnetic/non-magnetic interfaces [1]. Spin-current detection via the inverse spin Hall effect in Pt confirms efficient spin transport from both modes, with the amplitude tunable by the excitation geometry. The optical mode, associated with Neel order dynamics, appears at higher frequencies for hac ||m, while the acoustic mode, corresponding to magnetization dynamics, appears at lower frequencies for hac im [2]. Interestingly, the optical spin pumping was observed in the bulk sample but vanished in thin films, likely due to increased inhomogeneities or insufficient thickness to fully sustain the mode. These results clarify the selection rules governing mode excitation in canted AFs and demonstrate polarization-based control over their dynamics [3].

- 1. Tang, J.; Cheng, R. Absence of cross-sublattice spin pumping and spin-transfer torques in collinear antiferromagnets. *APL Materials* 2023, *11* (11).

 2. Fritjofson, G.; Regmi, A.; Hanson-Flores, J.; Michel, J.; Tang, J.; Yang, F.; Cheng, R.; Del Barco, E. Coherent Spin Pumping Originated from Sub-Terahertz Neel Vector Dynamics in Easy Plane {\alpha}-Fe2O3/Pt. *arXiv preprint arXiv:2502.11281* (2025).
- 3. Fritjofson, G.; Regmi, A.; Hanson-Flores, J.; Michel, J.; Tang, J.; Yang, F.; Cheng, R.; Del Barco, E. Probing polarization-tunable sub-terahertz spin pumping in bimodal α -Fe2O3/Pt. *npj Spintronics* 2O25, *3* (1), 24.

GP-09-LB. Magnetoresistance in RuO₂(001)/Co Bilayers<u>S. Yoon¹</u>, S. Ko², D. Woo¹, H. Jeon¹, H. Cho¹, W. Kim¹, G. Jung¹, K. Kim², J. Jeong³, B. Park⁴, S. Lee¹

¹Semiconductor Engineering, Gachon university, Seong, Korea (the Republic of), ²Physics, KAIST, Dae jeon, Korea (the Republic of), ³Materials Science and Engineering, Chungnam National university, Daejoen, Korea (the Republic of), ⁴Materials Science and Engineering, KAIST, Daejoen, Korea (the Republic of)

Altermagnets, combining the essential characteristics of both ferromagnets and antiferromagnets, have recently emerged as a new class of materials that exhibit pronounced spin splitting while maintaining long-range antiferromagnetic order [1]. This unusual coexistence provides a fundamentally different platform compared to conventional antiferromagnets, where spin-degenerate electronic band structures typically suppress spin transport and limit spin-charge conversion. Owing to its large spin splitting and high critical temperature, RuO2 is regarded as a promising candidate. The investigation of its magnetoresistance (MR) is essential, as the various MR mechanisms serve as indicators of spin polarization and magnetic ordering in materials. [2,3]. In this study, we measured the MR in a RuO_{<span} style="fontsize:10.8333px">2 (001) (15 nm)/Co (4 nm) bilayer. The RuO₂ film was epitaxially grown on a TiO₂(001) substate using pulsed laser deposition (PLD), and the Co layer was deposited by sputtering. Figure 1 shows a schematic of MR measurement geometry with the Hall-bar patterned sample, where I represent the charge current applied along the xdirection, b and q denote the angles between I and the magnetic field. MR measurements were performed at

various temperatures by rotating the magnetic field within the xz-plane and yz-plane. Figure 2 presents the MR measurement results for the RuO2/Co, where the current is applied along the [110] crystallographic direction. The measurement was performed at 4K under 9 T magnetic field. R_{xx} and R_{xx} are indicate the longitudinal resistance and the angle-averaged longitudinal resistance, respectively. As the magnetic field increases, the MR of this bilayer exhibits an enhancement of negative MR. This distinct evolution of transport properties is not merely a trivial resistance change but rather reflects the underlying spin-orbit-coupled electronic structure of RuO₂. The observed enhancement can be attributed to the anisotropic magnetoresistance (AMR) contribution that arises from the spin-flop transition of the Néel vector, a characteristic reorientation inherent to antiferromagnetic materials under applied magnetic fields. [2]. Our results provide insights into the magnetic structure of RuO₂, advancing the development of altermagnet-based spintronic devices.

- [1] L. Smejkal et al., Phys. Rev. X, 12, 040501 (2020)
- [2] Y. Kobayashi et al., AIP Adv, 14, 115120 (2024)
- [3] C. Avci et al., Nat. Phys., 11, 570-575 (2015)

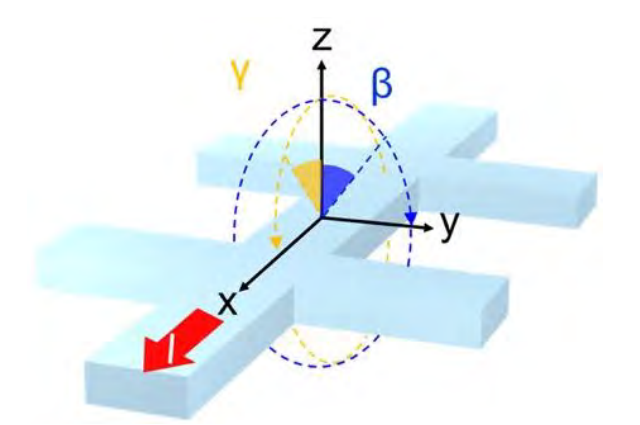


Fig. 2

GP-10-LB. Angle-Resolved Sub-THz Resonant Absorptions in $\alpha\text{-Fe}_2\text{O}_3$

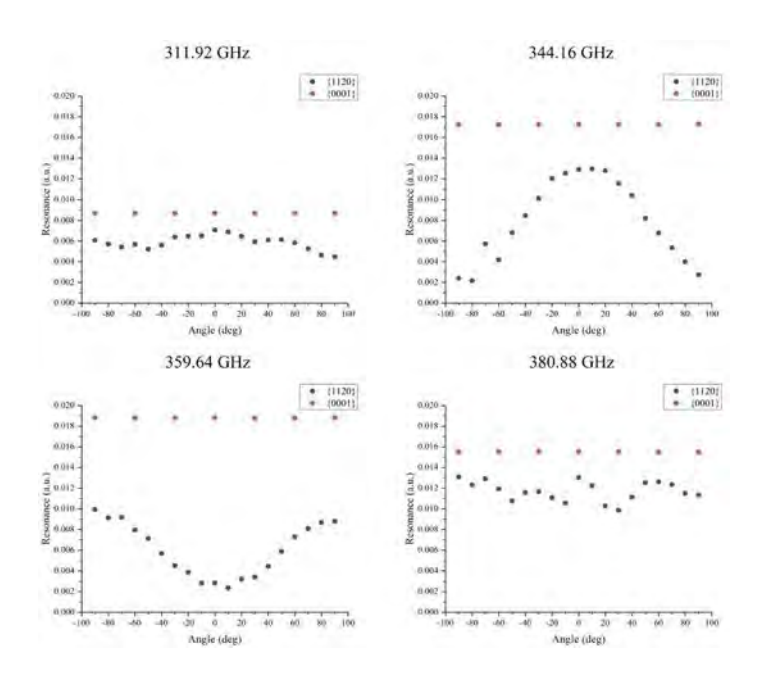
S. Zhou¹, Y. Xiong¹, J. Wu¹, E. Kwao², B. Yang², W. Zhang¹

¹Physics and Astronomy, University of North Carolina at Chapel Hill, Chapel Hill, North Carolina, United States, ²Electrical and Computer Engineering, North Carolina Agricultural and Technical State University, Greensboro, North Carolina, United States

Antiferromagnetic resonances have recently received increasing attention due to both fundamental interests and technological leverage pertinent to the sub-THz frequencies [1,2]. We report a systematic investigation of angle-resolved terahertz (THz) absorption in single-crystal α -Fe O over the 200 500 GHz range. Under constant temperature, the resonance strength of {1120} oriented crystal exhibits strong angular dependence at specific frequencies, with certain modes increasing while others decrease in intensity upon crystal rotation. Particularly, at 344.16 GHz and 359.64 GHz, the angular response shows opposite trends, revealing a directional-selective response that suggests anisotropic magnetic mode activation. In contrast, {0001} oriented crystal shows strong resonance under all frequencies. This distinct angular behavior is attributed to the excitation of quasi-antiferromagnetic resonance (qAFMR) modes that couple asymmetrically to the incident THz polarization under crystal rotation. The interplay between spin dynamics and anisotropic dielectric response appears critical in shaping this non-reciprocal resonance strength. Further experiments with extent frequencies and time-domain spectroscopy reveal more special antiferromagnetic characteristics of α Fe O under sub-THz region. Our results will help establish α -Fe O as a versatile model system for anisotropic spin-photon interactions in the THz regime.

- [1] M. Bialek, J. Zhang, and et al.. Applied Physics Letter, Vol. 121, p. 032401 (2022)
- [2] M. Bialek, J. Zhang, and et al.. Physical Review Applied, Vol. 15, p. 044018 (2021)

^{*} Best Student Presentation Finalist / LB – Late-breaking Poster



SESSION GQ: MULTI-FUNCTIONAL MAGNETIC MATERIALS AND OTHER EMERGING TOPICS (POSTER SESSION)

Co-Chair(s): H. Arava, Argonne National Laboratory, Lemont, Illinois, United States and Y. Wu, Electrical and Computer Engineering, University of Florida, Gainesville, Florida, United States

Friday, October 31, 2025 09:00 AM-12:00 PM Exhibit Hall Posters

GQ-01. Investigation of Magnetic Field-Induced Phase Transition Ni₅₀Mn₂₈Ga₂₂, Ferromagnetic Shape Memory Alloy

P. Chaitanya¹, S. Smith³, M. Staruch⁴, <u>R. L. Hadimani</u>^{1,2}
¹Department of Mechanical and Nuclear Engineering, Virginia Commonwealth University, Richmond, Virginia, United States, ²Department of Biomedical Engineering, Virginia Commonwealth University, Richmond, Virginia, United States, ³Department of Chemical and Life Sciences Engineering, Virginia Commonwealth University, Richmond, Virginia, United States, ⁴Materials Science and Technology Division, US Naval Research Laboratory, Washington DC, District of Columbia, United States

Ferromagnetic shape memory alloys (FSMAs) exhibit magnetic-field-induced strain (MFIS) through a reversible martensitic transformation. Among these, Nickel-Manganese-Gallium (Ni-Mn-Ga) alloys have drawn significant attention due to their large MFIS (up to ~10% in

single crystals) under moderate magnetic fields, far surpassing even the best magnetostrictive materials such as Terfenol [1, 2]. Such a large axial strain change in single-crystal Ni-Mn-Ga arises from a coupled structural and magnetic phase transition. This enables rapid, reversible deformation without mechanical loading, making these materials promising for compact actuators, sensors, and energy harvesters [3]. Their transformation temperatures and magnetic properties are tunable via composition, offering flexibility for several device applications.

Our research focuses on the investigation of Ni50Mn28Ga22 FSMA for the development of a core-shell structure with the MFIS materials as a core and piezoelectric material as the shell for biomedical applications such as imaging and stimulation. As a first step, we purchased two samples of Ni50Mn28Ga22 FSMAs at VCU and NRL from 2 independent vendors and investigated their magnetic and magnetostrictive properties. Fig. 1 shows MT graphs at different applied magnetic fields for both samples, and Fig. 2 shows hysteresis graphs at 295K for both VCU and NRL samples. The MT graphs show that there is a first-order-like phase transition at 300K for applied field from 0 to 0.6T. The phase transition then changes to a second-order-like broader phase transition from 0.6T to 9T. A large transitional strain is demonstrated while cycling through the transition with temperature, but at all temperatures, only a magnetostrictive-like strain is observed with field. The magnetic field-induced phase transition was not observed experimentally in either sample.

The Authors acknowledge the funding support of VCU Presidential Quest Funds and the Breakthrough grant awarded to RLH. The Authors also acknowledge the ONR Summer Faculty Fellowship funds awarded to RLH and MS.

- [1] Ullakko, K., Huang, J. K., Kantner, C., O'Handley, R. C., & Kokorin, V. V. (1996). Large magnetic-field-induced strains in Ni2MnGa single crystals. *Applied Physics Letters*, 69(13), 1966–1968.
- [2] Sozinov, A., et al. (2002). Giant magnetic-field-induced strain in NiMnGa seven-layered martensitic phase. *Applied Physics Letters*, 80(10), 1746–1748.
- [3] Tickle, R., & James, R. D. (1999). Magnetic and magnetomechanical properties of Ni2MnGa. *Journal of Magnetism and Magnetic Materials*, 195(3), 627–638.

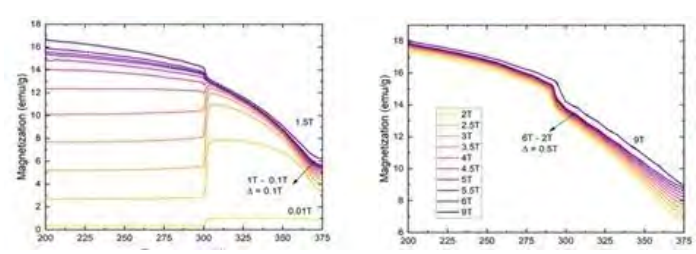


Fig. 1 Magnetization as a function of temperature at different magnetic fields; 0.01-1.5T (left) 2T-9T (right).

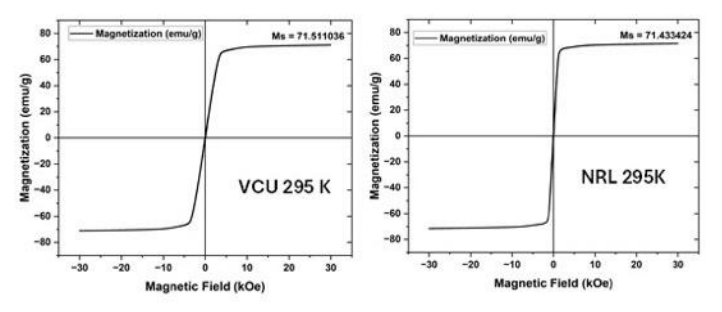


Fig. 2 Hysteresis graph of NRL and VCU Samples at 295K.

GQ-02. Influence of Cu Partial Substitution on Saturation Magnetostriction Constant of Polycrystalline CoFe₂O₄

<u>S. Kosugi</u>¹, M. Hisamatsu¹, S. Fujieda², Y. Ohishi¹, H. Muta¹, S. Seino¹, T. Nakagawa¹

¹Graduate School of Engineering, Osaka University, Suita, Osaka, Japan, ²IAMR&D, Shimane University, Matsue, Shimane, Japan

Magnetostrictive materials are used in various technologies such as sensors, actuators and vibration energy harvesting. Cobalt ferrite (CoFe₂O₄) has attracted attention due to its large negative magnetostriction. Recently, it has been reported that magnetostrictive properties of CoFe₂O₄ are significantly enhanced by the partial substitution of Cu for Co [1]. The strain of Cu_{0.6}Co_{0.4}Fe₂O₄ at 1 T is approximately 1.6 times larger than that of Galfenol, a commercial magnetostrictive material [1]. Magnetostrictive properties are influenced not only by magnetostriction constants but also by various factors such as microstructure and internal stress. It is important to clarify whether the enhancement of magnetostrictive properties is caused by changes in the saturation magnetostriction constant (λ_s) or by other factors. This study investigates the influence of the partial substitution of Cu for Co on λ_S of polycrystalline CoFe₂O₄. Cu-substituted cobalt ferrite (Cu_xCo_{1-x}Fe₂O₄) polycrystalline samples were synthesized by a solid-state reaction method.

Magnetostrictive properties were measured by the strain gauge method at room temperature. Magnetic fields were applied parallel and perpendicular to the measurement direction of the strain. Fig. 1 shows the magnetic field dependence of the strain ($\Delta L/L$) of CoFe₂O₄ and $Cu_{0.6}Co_{0.4}Fe_2O_4$ up to 7 T. The $\Delta L/L-H$ curves of both samples exhibit characteristics of negative magnetostriction and a tendency to saturate at 7 T. The λ_S values were determined from the $\Delta L/L$ values at 7 T. Fig. 2 shows the $|\lambda_s|$ values of CoFe₂O₄ and Cu_{0.6}Co_{0.4}Fe₂O₄, superimposed on the Cu substitution amount x dependence of $|\Delta L/L_{\parallel} - \Delta L/L_{\perp}|$ at 1 T, reported in our previous study [1]. The λ_S of CoFe₂O₄ is enhanced by the partial substitution of Cu for Co. As with $|\Delta L/L_{\parallel} - \Delta L/L_{\perp}|$ values, the $|\lambda_{\rm S}|$ value of Cu_{0.6}Co_{0.4}Fe₂O₄ is more than 1.5 times that of CoFe₂O₄. Therefore, the enhancement of the magnetostrictive properties of Cu_xCo_{1-x}Fe₂O₄ is mainly attributed to an increase in the $|\lambda_S|$ value.

[1] S. Kosugi, M. Hisamatsu and Y. Ohishi *et al.*, *Mater. Trans.*, Vol. 64, pp. 2014–2017 (2023)

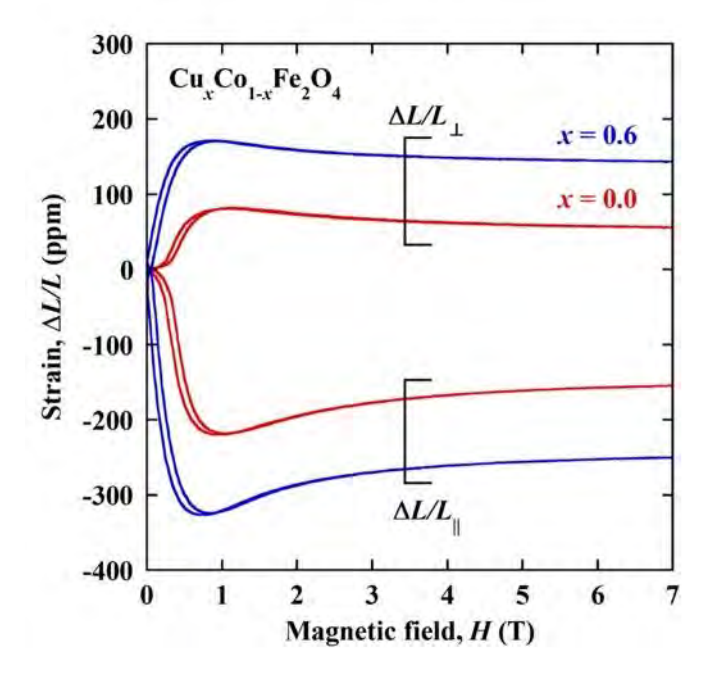


Fig. 1 Magnetic field dependence of $\Delta L/L$ of CoFe₂O₄ and Cu_{0.6}Co_{0.4}Fe₂O₄ up to 7 T

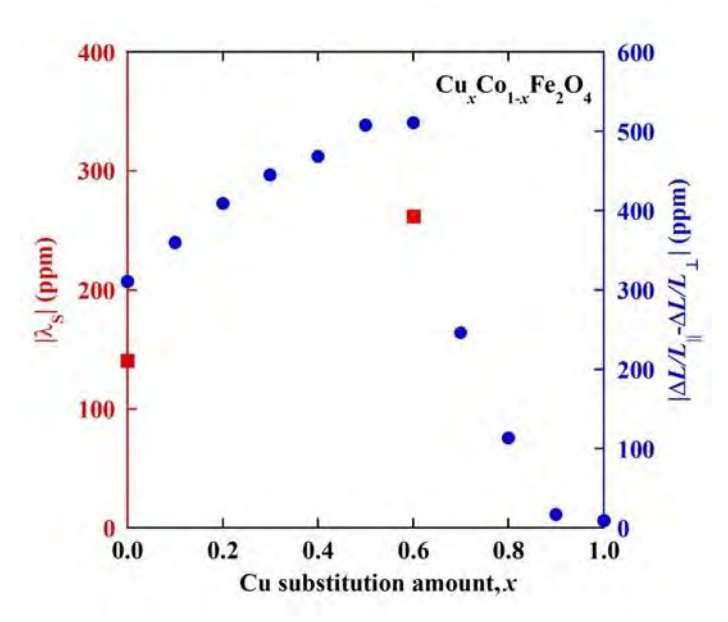


Fig. 2 Cu substitution amount x dependence of $|\lambda_s|$ and $|\Delta L/L_{\parallel} - \Delta L/L_{\perp}|$ at 1 T [1]

GQ-03. Enhanced Superparamagnetism and Emergent Phenomena at $C_{60}/PdCo$ Interface

V. H. Bui¹, Y. T. Pham¹, T. A. Ngo², N. Schulz¹, <u>D. Le¹</u>, T. D. Nguyen², M. Phan¹

¹Department of Physics, University of South Florida, Tampa, Florida, United States, ²Department of Physics, University of Georgia, Athens, Georgia, United States

Organic semiconductors, characterized by low spin-orbit coupling and mechanical flexibility, have garnered significant attention for their potential in spintronic applications. Among them, buckminsterfullerene (C₆₀) stands out due to its unique molecular structure and high electron affinity. Interfacing a magnetic material with a C₆₀ layer can lead to hybridized interfacial magnetic states and mediate magnetic interactions [1,2]. In this study, 15 nm-thick Pd₈₀Co₂₀ (PdCo) films and hole arrays were grown using the air/water interface method and electron beam deposition [3]. The thin films and hole arrays are deposited on bare glass or on 50 nm-thick C₆₀ on glass substrate. We demonstrate that stacking a C60 layer on a PdCo thin film significantly increases the blocking temperature compared to the bare PdCo film. The C₆₀/PdCo interface also exhibits enhanced magnetic anisotropy and, consequently, increased coercivity in the ferromagnetic regime. Additionally, the C₆₀ overlayer leads to a substantial reduction in both remanent and saturation magnetization of the PdCo film in

the ferromagnetic regime, while having negligible effect in the superparamagnetic regime. The observed enhancement in blocking temperature is attributed to the C_{60} -induced increase in magnetic anisotropy. Furthermore, low-field magnetization switching below 100 K [4] suggests that rotational freezing of C_{60} molecules strongly influences surface magnetization at the C_{60} /PdCo interface. These findings offer a promising strategy for enhancing magnetic hardness in thin films and for tuning magnetism in low-dimensional systems via molecular interfacing with C_{60} .

- 1. V. Kalappattil et al., Materials Horizons 7, 1413 (2020).
- 2. K. Bairagi et al., Physical Review Letters 114, 247203 (2015).
- 3. M.T. Pham et al., ACS Applied Nano Materials 4, 3664 (2021).
- 4. T. Moorsom et al., Physical Review B 101, 060408 (2020).

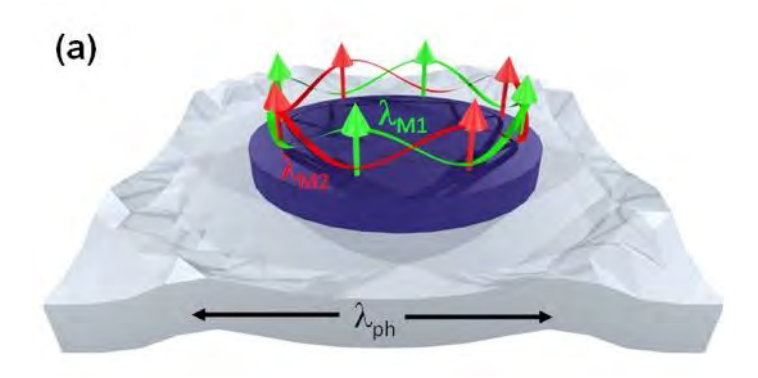
GQ-04. Binary Magnon-Polaron Formation in a twodimensional Artificial Magneto-Elastic Crystal

S. Majumder¹, J. L. Drobitch², S. Bandyopadhyay², A. Barman¹ Department of Condensed Matter and Materials Physics, S. N. Bose National Centre for Basic Sciences, Kolkata, West Bengal, India, ²Department of Electrical and Computer Engineering, Virginia Commonwealth University, Richmond, Virginia, United States

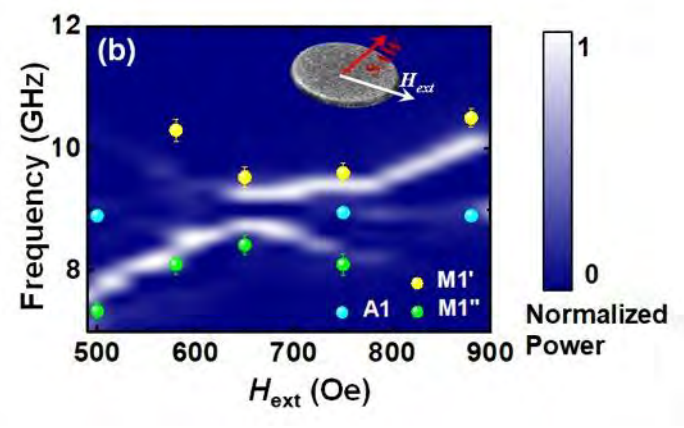
Strong coupling between different quasiparticles enables precise control of physical phenomena through hybridized states. We report (1) strong tripartite magnon-phononmagnon coupling (2) in a two-dimensional array of magnetostrictive nanomagnets on a piezoelectric substrate, forming a magneto-elastic crystal. This involves coupling between two Kittel-type spin wave (magnon) modes and a non-Kittel magneto-elastic mode generated by a surface acoustic wave (SAW). Maximum coupling occurs under phase-matched conditions - when the frequencies and wavevectors of all three modes align. This was achieved through careful tuning of the SAW frequency, nanomagnet geometry, and external magnetic field. The resulting coupling, with a cooperativity factor greater than one, gives rise to a novel hybrid quasiparticle: a binary magnonpolaron (3). This state facilitates nearly complete (~100%) energy transfer from the magneto-elastic mode to the two magnon modes. The coupling strength is highly anisotropic due to the spatial asymmetry of the nanomagnet array. Our experimental results show strong agreement with

theoretical predictions, demonstrating the potential of engineered magneto-elastic crystals for controlling energy and information transfer at the nanoscale.

- 1. S. Majumder, NPG Asia Materials 15 (1), 51 (2023).
- 2. F. Godejohann, Physical Review B 102, 144438 (2020).
- 3. D. Vaclavkova, Physical Review B 104, 134437 (2021).



Schematic Representation of Magnon-Phonon-Magnon Coupling in a Nanodot Structure.



Bias field dependence of the experimental and simulated spin wave (SW) spectra of the nanomagnet near the anticrossing point. In this case, the surface acoustic wave (SAW) propagates along the minor axis of the nanomagnets. The corresponding color scales are shown in the figure.

GQ-05. Optimizing Magnetostrictive Films for Surface Acoustic Wave Devices

Z. Zhang, J. Lim, H. Ni, J. Zuo, A. Hoffmann Materials Science and Engineering, University of Illinois Urbana-Champaign, Urbana, Illinois, United States

Owing to their short wavelength and long propagation distance, surface acoustic waves (SAW) are promising for miniaturizing microwave devices such as isolators, which rely on large nonreciprocity facilitated by magnetoelastic coupling. Fe₈₀Ga₂₀ is a popular choice for the magnetoelastic layer due to its high magnetoelasticity. In this work, we studied boron concentration effect on magnetoelastic coupling and temperature dependent damping in (Fe₈₀Ga₂₀)₁₋ _xB_xthin films in order to optimize such SAW devices for cryogenic temperature operation. We integrated (Fe₈₀Ga₂₀)₉₀B₁₀ films, which demonstrated high magnetostriction of 50 ppm and low damping of 6×10⁻³ into SAW devices and studied magnon-phonon interactions. First, (Fe₈₀Ga₂₀)_{1-x}B_x films with boron contents varying from 2% to 16% were synthesized by magnetron sputtering. X-ray diffraction revealed a suppressed diffraction peaks in high boron doping regime, consistent with the vanishing of the lattice fringes observed in HRTEM, indicating a polycrystalline to amorphous structural transition. Significant enhancement of magnetostriction [Fig. 1(a)] and reduction of Gilbert damping were observed in the amorphous regime. Gilbert damping at cryogenic temperatures showed a peak at around 40 K [Fig. 1(b)]. It is noticed that the relative peak intensity followed a similar trend with the magnetostriction, indicating potential magnetoelastic contribution to the damping peak at 40 K [1]. Interdigital transducers (IDTs) were patterned on the LiNbO₃ substrate to excite SAW with GHz frequencies and magnetoelastic (Fe₈₀Ga₂₀)₉₀B₁₀ film was incorporated in the SAW propagation path [Fig. 2(a)]. SAW transmission measurements showed an absorption peak, indicating a coupled magnon-phonon system with the strongest coupling measured at 45° field angle relative to the SAW propagation direction [Fig. 2(b)]. This work was supported by DOE BES under contract No.

This work was supported by DOE BES under contract No DE-SC0022060.

[1] Z. Zhang, et al., arXiv:2505.11472.

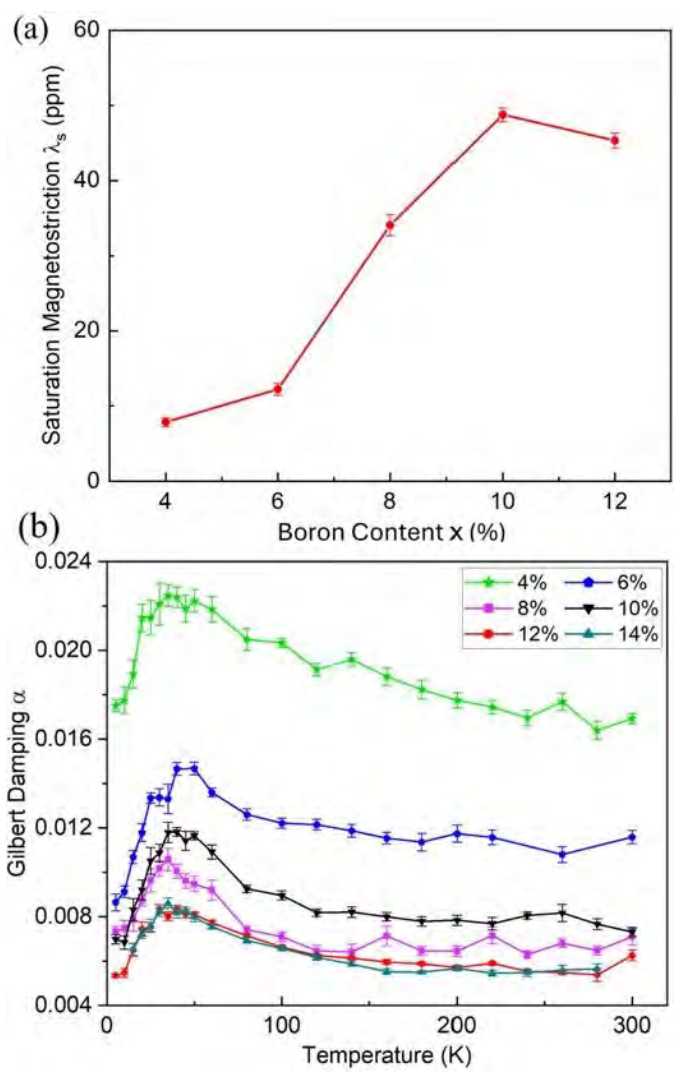
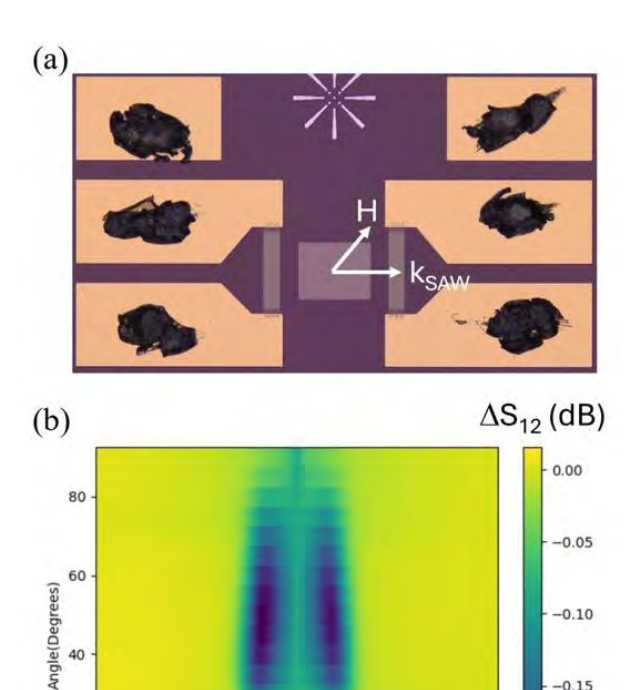


Fig. 1: (a) Saturation magnetostriction as a function of B concentration. (b) Gilbert damping as a function of temperature for 20-nm ($Fe_{80}Ga_{20}$)_{1-x} B_x films.



-1000 1000 Field(Oe) Fig. 2(a) Microscope image of IDTs and (Fe₈₀Ga₂₀)₉₀B₁₀ film. (b) SAW absorption as a function of magnetic field measured at different field angles.

-0.15

-0.20

GQ-07. Silicon Nitride Integrated Magneto-Optical Isolator based on Mach-Zehnder Interferometer

B. Moghal¹, B. Stadler²

40

20

¹Electrical and Computer Engineering, University of Minnesota, Minneapolis, Minnesota, United States, ²Electrical and Computer Engineering, University of Minnesota, Minneapolis, Minnesota, United States

Waveguide integrated optical isolators are an integral part of photonic integrated circuits (PIC) due to their unique capability of blocking the back-reflected light travelling into the laser cavity. This unidirectional light propagation is called optical non-reciprocity, which can be attained by a time-reversal asymmetry. For a long time, rare-earth magneto-optical garnets have been used as the ideal candidate to achieve non-reciprocity which can be explained by their non-zero off-diagonal dielectric tensor elements generated by Zeeman splitting. In this work, we propose a novel silicon nitride (SiN) waveguide-integrated

isolator device that employs cerium-substituted yttrium-iron garnet (Ce:YIG) as the non-reciprocal material. This isolator device is designed based on the Mach-Zehnder interferometer principle, where Ce:YIG will function as a cladding/core material to demonstrate both transverse magnetic (TM)/transverse electric (TE) mode of light input at 1550 nm wavelength. A thin YIG seedlayer (Faraday rotation +200°/cm) is deposited on top of the SiN waveguide to provide a platform for high-quality Ce:YIG growth. The optical isolator device exhibits non-reciprocal phase shift (NRPS) by demonstrating constructive/destructive interference in forward/backward light propagation direction. This NRPS phenomenon is achieved by applying opposite-direction magnetic fields in the interferometric isolator branches containing the Ce:YIG/YIG layers; perpendicular to the direction of light propagation. The Faraday rotation of the Ce:YIG has been chosen to -4500 ⁰/cm at 1550 nm [2]. The Finite-Difference Eigenmode (FDE) solver is used to design and simulate to identify the appropriate device dimensions. The isolator design is presented for both TM and TE modes of light input shown in Fig. 1. Finally, a high-performance magneto-optic isolator will be presented that exhibits low loss with a small device footprint.

- [1] Srinivasan, Karthik, and Bethanie JH Stadler. "Magneto-optical materials and designs for integrated TE-and TM-mode planar waveguide isolators: a review." Optical Materials Express 8, no. 11 (2018): 3307-3318.
- [2] Shintaku, Toshihiro, and Takehiko Uno. "Optical waveguide isolator based on nonreciprocal radiation." Journal of Applied Physics 76, no. 12 (1994): 8155-8159.

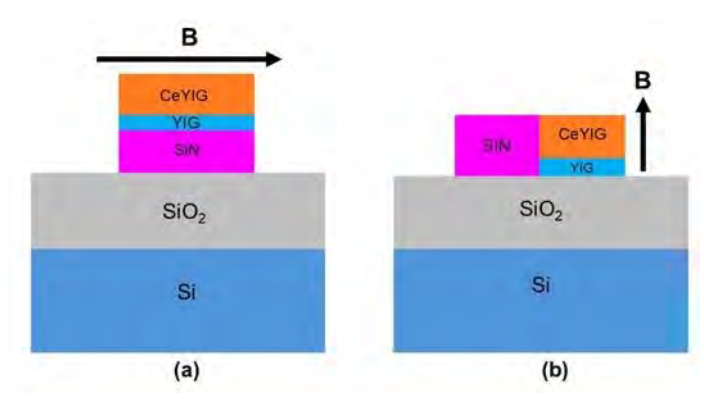


Fig. 1: The optical isolator design side-views for (a) Transverse magnetic (TM) and (b) Transverse electric (TE) modes of light input

GQ-08. Transport of Paramagnetic Ions in Porous Materials P. Andrei^{1, 2}, P. Wang¹

¹Department of Electrical and Computer Engineering, Florida State University, Tallahassee, Florida, United States, ²Center for Rare Earths, Critical Minerals, and Industrial Byproducts, National High Magnetic Field Laboratory, Tallahassee, Florida, United States

The transport of paramagnetic ions in porous materials has received increased attention recently because of the potential of magnetic separation techniques to extract metal ions of critical elements from non-magnetic material. (Notice that although the magnetic separation of ferromagnetic or superparamagnetic clusters of particles has been studied extensively in the literature since the classical works of Watson [1] and others [2], the transport of small paramagnetic particles such as ions of rare earth elements of Cu²⁺, Mn2+, etc. has become a major research topic only recently [3-5].) The porous media can be either a magnetic matrix like in the case of high-gradient magnetic separation experiments [2], nonmagnetic like in the case transition metal ions in silica gel [6], or both like in the case of paramagnetic particles in spent batteries recycled residues [7].

In this presentation we develop a mathematical model for the transport of paramagnetic ions in nonmagnetic porous media. The model is based on a continuum description of the magnetic particles and solvent that satisfy the classical fluid transport equations (mass continuity and Navier-Stokes equations) and a solid and fixed non-magnetic matrix of specified porosity and tortuosity. The magnetic particles (ions or small ion clusters in our case) are moving in an aqueous solution reacting according to a Langmuir isotherm with the solid matrix. The model equations are relatively similar to the transport of ions in porous materials such as the transport of Li ions in anode and cathodes in electrochemical systems, however, a number of notable differences related to interaction of magnetic particles in the solid particles still exist.

After developing the mathematical model and compare our numerical predictions with experimental results currently published in the literature, we investigate the possibility to use magnetophoresis in porous media for the separation of single metal ions.

- [1] J. H. P. Watson, Magnetic Filtration, J. Appl. Phys. 44, 4209 (1973).
- [2] R. Gerber and R. Birss, High Gradient Magnetic

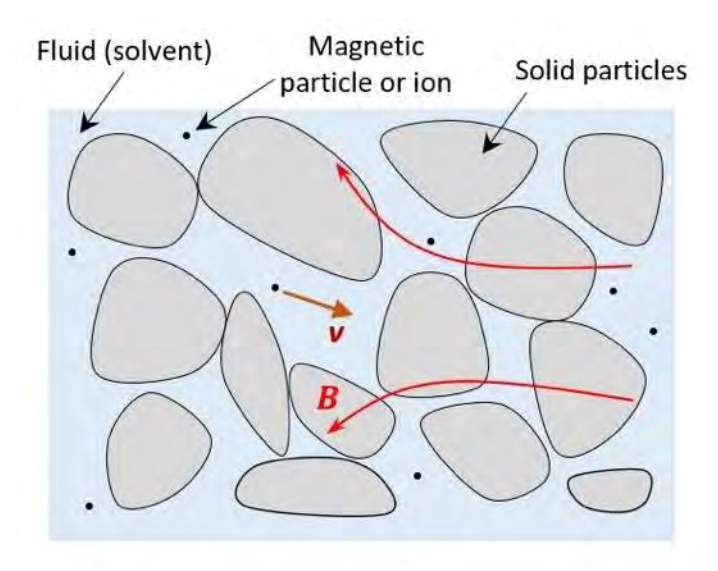
Separation (Research Studies Pr Ltd, Chichester; New York, 1983).

[3] L. Kuger and M. Franzreb, Design of a Magnetic Field-Controlled Chromatography Process for Efficient and Selective Fractionation of Rare Earth Phosphors from Endof-Life Fluorescent Lamps, ACS Sustain. Chem. Eng. 12, 2988 (2024).

[4] B. Pulko, X. Yang, Z. Lei, S. Odenbach, and K. Eckert, Magnetic Separation of Dy(III) Ions From Homogeneous Aqueous Solutions, Appl. Phys. Lett. 105, 232407 (2014). [5] Z. Lei, B. Fritzsche, R. Salikhov, K. Schwarzenberger, O. Hellwig, and K. Eckert, Magnetic Separation of Rare-Earth Ions: Property Database and Kelvin Force Distribution, J. Phys. Chem. C 126, 2226 (2022).

[6] M. Fujiwara, K. Mitsuda, and Y. Tanimoto, Movement and Diffusion of Paramagnetic Ions in a Magnetic Field, J. Phys. Chem. B 110, 13965 (2006).

[7] High-Intensity Magnetic Separation for Recovery of LiFePO4 and Graphite From Spent Lithium-Ion Batteries, Sep. Purif. Technol. 297, 121486 (2022).



Magnetophoresis of magnetic particle or ions in a porous media.

GQ-09. Processing of Functional Magnetic Composite Filaments for Additive Manufacturing of Broadband Electromagnetic Absorbers

K. Bhandari, M. Patel, R. Barua Mechanical and Nuclear Engineering, Virginia Commonwealth University, Richmond, Virginia, United States

The Internet of Things (IoT) involves billions of devices exchanging data, creating a congested electromagnetic environment. This requires ultra-efficient materials to control electronic pollution by blocking or absorbing electromagnetic waves. Additive manufacturing (AM) offers a transformative solution, overcoming traditional absorbers' limitations in flexibility and integration. AM enables precise microstructure tailoring to optimize absorption efficiency for specific frequencies. Multi-material capabilities allow advanced graded or composite absorbers essential for stealth, high-frequency communication, and shielding. Additionally, AM supports rapid prototyping, lightweight designs, and scalable production, driving high-performance.

Fused filament fabrication (FFF) is a popular form of additive manufacturing, using a melted extrusion method where a feedstock material is pulled through a hot nozzle at 200-300°C and extruded layer by layer on a build platform to create a 3D object. However, commercially sourced filaments are limited to a narrow range of metals/alloys. including aluminum, bronze, copper, stainless steel, highcarbon iron, tungsten, and more recently, titanium [2]. By combining microwave-absorbing ferrites with 3D printed polymers, high-performance structures for wave-absorbing devices can be produced, opening up new possibilities in electromagnetic shielding [1]. This study aims to develop an innovative electromagnetic shielding composite using ferromagnetic ferrite nanoparticles and 2D carbon nanostructures embedded in a thermally conductive polymer matrix, creating a lightweight, weather-resistant EM shield for broadband absorption (4-40 GHz). We will present research on optimizing FFF parameters, including extrusion temperature, layer height, printing speed, nozzle diameter, bed temperature, cooling control, fill density, path orientation, and retraction, all affecting adhesion, stability, strength, and surface finish. Optimizing these variables ensures enhanced precision and performance, advancing strategies for practical, customized EMI shielding solutions.

^[1] Kuznetsov, E. A., & Mikhailov, E. A. (2024), Mathematics, 12(5), 677;

^[2] Martins, L.C, . et.al. Polymers, 15(24), 4649

GQ-10-LB. Dynamic Phase Transitions in Mean-Field Ginzburg—Landau Models: Conjugate Fields and Fourier-Mode Scaling

L. Satynska, D. T. Robb

Physics, Roanoke College, Salem, Virginia, United States

Dynamic phase transitions of periodically forced mean-field ferromagnets are often described by a single order parameter and a scalar conjugate field h(t). Building from 2014 Robb-Ostrander paper, we show that, at the critical period P_c of the mean-field Ginzburg-Landau (MFGL) dynamics with energy $F(m) = am^2 + bm^4 - hm$, the correct conjugate field is the entire even-Fourier component part of the applied field. The correct order parameter is $z_k = \sqrt{\|m_k\|^2}$ $|m_{k,c}|^2$), where m_k is the k^{th} Fourier component of the magntization m(t), and m_{k,c} indicates the value of the kth Fourier component at the critical period. Using highaccuracy limit-cycle integration and Fourier analysis, we find or confirm from Robb 2014 paper three robust facts. (1) For periodic fields that contain only odd components, the symmetry-broken branch below P_c exhibits $z_k \sim \varepsilon^{1/2}$, computationally tested for Fourier modes $k \le 30$, where $\epsilon =$ (P_c - P)/P_c. This provides strong evidence that the 1/2 scaling holds for all Fourier modes. (2) Exactly at Pc, adding a small perturbation composed of even Fourier components with an overall field multiplier h_{mult} produces $z_k \sim (h_{mult})^{1/3}$ scaling across many values of k. This holds even when the constant term h_0 is absent. (3) For $P > P_c$ and small h_{mult} , z_k crosses over from $z_k \sim (h_{mult})^{1/3}$ to $z_k \sim h_{mult}$ as $h_{mult} \rightarrow 0$; the crossover point shifts to smaller h_{mult} as $P \rightarrow (P_c)^+$. The findings persist in MFGL models where an m⁶ replaces the m⁴ term and come with simple period-integral criteria to locate P_c.

Aaron Ostrander, Daniel T. Robb. Extended order parameter and conjugate field for the dynamic phase transition in a Ginzburg-Landau Mean-Field Model in an Oscillating Field. 2014

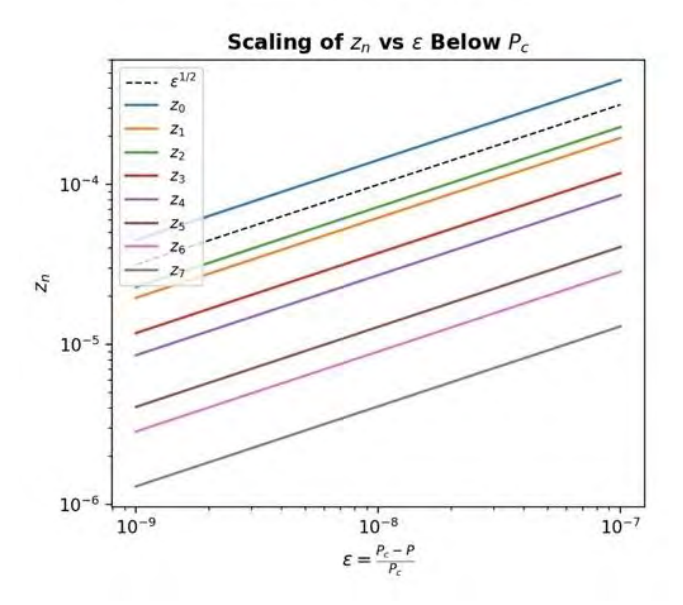


Fig. 1 z_n vs ϵ Scaling Below P_c

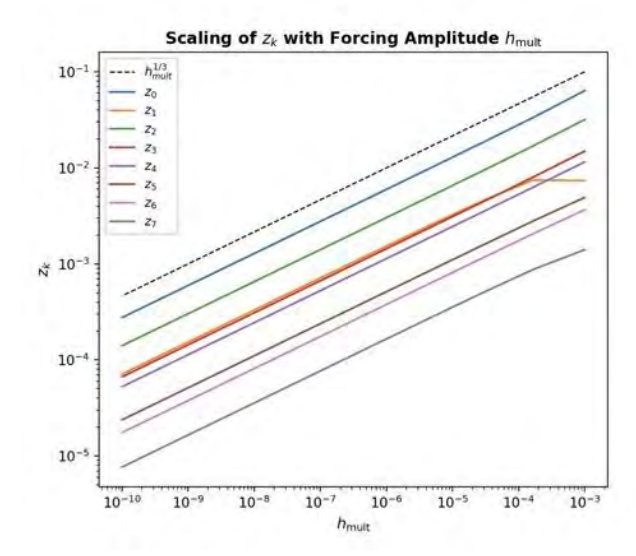


Fig. 2 Scaling of z_k vs h_{mult} at P_c

SESSION GR: FUNDAMENTAL PROPERTIES AND COOPERATIVE PHENOMENA (POSTER SESSION)

Co-Chair(s): D. Chakraborty, *Physics & Astronomy, University*of Nebraska, Kearney, Nebraska, United States and R.
Chopdekar, Western Digital, San Jose, California, United States
Friday, October 31, 2025
09:00 AM-12:00 PM
Exhibit Hall Posters

GR-01. Coexistence of superconductivity and antiferromagnetism in GdNi_{0.7}Bi₂

J. Moon¹, M. Jung¹, Y. Choi¹, T. Park², S. Yousuf²
¹Department of Physics, Sogang University, Seoul, Korea (the Republic of), ²Department of Physics, Sungkyunkwan University, Suwon, Korea (the Republic of)

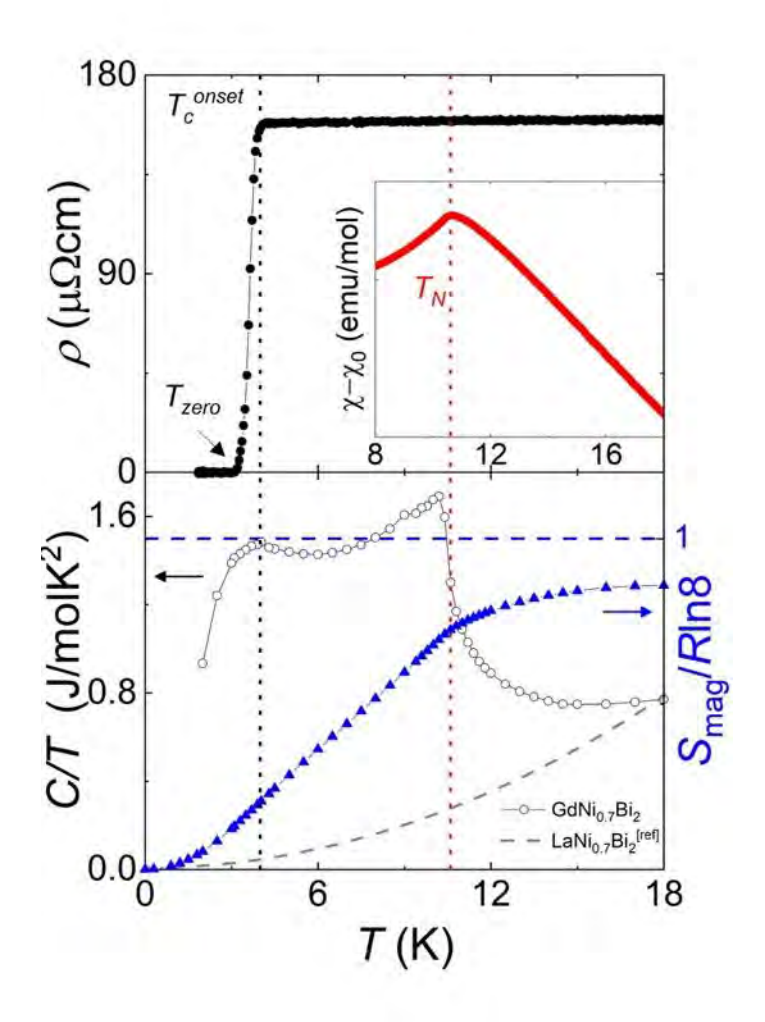
The RNiBi $_2$ (R = rare earth) family, with a ZrCuSi $_2$ -type structure composed of alternating Bi square nets and RNiBi layers, has garnered attention because of the coexistence of superconductivity (SC) and antiferromagnetism (AFM). In particular, studies on polycrystalline CeNi $_{0.8}$ Bi $_2$ have indicated that the light electrons from the Bi square net are responsible for SC with $T_c \sim 4.2$ K and the heavy electrons from Ce in the CeNi $_{0.8}$ Bi layer are contribute to AFM with $T_N \sim 5.0$ K. However, single crystal investigations of CeNi $_{0.8}$ Bi $_{2.03}$ have suggested that the observed superconductivity is related to secondary Ni-Bi binary phases. $^{[2]}$

To elucidate the origin of SC and its relationship with AFM, we examine the transport and magnetic properties of GdNi_{0.7}Bi₂ single crystals. Gd was chosen instead of Ce due to its larger magnetic moments, enhancing AFM characteristics, and its higher AFM transition temperature, more separating the SC and AFM phases. X-ray diffraction results reveal no secondary phases related to Ni-Bi binaries, and the energy dispersive spectroscopy confirms a GdNi_{0.7}Bi₂ stoichiometry. We observe the SC transition at $T_c \sim$ 3.6 K in the electrical resistivity and the diamagnetic signal below T_c in the magnetic susceptibility. The magnetic data identify the AFM transition at $T_N \sim 10.8$ K with easy magnetic axis parallel to the ab plane. Specific heat data exhibit two distinct anomalies corresponding to the SC and AFM transitions, supporting the coexistence of SC and AFM. In the SC state, upper critical fields are anisotropic, with $H_{c2}^{ab} \sim 22.5$ T and $H_{c2}^{c} \sim 6.6$ T, yielding coherence lengths of $\xi^{ab} \sim 7.2$ nm and $\xi^{c} \sim 2.0$ nm. The larger H_{c2} and ξ in the ab plane reflect the layered crystal structure, where Cooper pairs seem to be more easily generated within the NiBi layer, as suggested by band

calculations. SC volume fractions (VF) at 10 Oe show anisotropy, with VF ab ~ 5% for H//ab and VF c ~ 90% for H//c. The smaller VF for the ab plane is linked to the easy magnetization parallel to the plane, providing strong evidence of the SC and AFM coexistence in GdNi $_{0.7}$ Bi $_{2}$. These findings offer insights into the interplay of these competing phenomena in layered rare-earth compounds.

[1] H. Mizoguchi, S. Matsuishi and H. Hosono, *Phys. Rev. Lett.*, 106, 057002 (2011).

[2] X. Lin, W.E. Straszheim and S.L. Bud'ko, *J. Alloys Comp.*, 554, 304 (2013).



GR-02. Competing Magnetic Interactions and Functional Implications in Disordered $\text{Co}_2\text{TiSi}_{0.5}\text{Al}_{0.5}$ Heusler Alloy

P. Yadav, B. K. Mani, R. S. Dhaka

Physics, Indian Institute of Technology Delhi, New Delhi, Delhi, India

We present a comprehensive experimental and theoretical investigation of the Co₂TiSi_{0.5}Al_{0.5} Heusler alloy, highlighting the role of antisite disorder in tuning the functional properties. Structural analysis revealed a partial B2-type order amid the L2₁ main cubic phase, ~29% Ti-Al antisite disorder. Thermo-magnetic measurements reveal two distinct ferromagnetic transitions at $T_{C1} \approx 278$ K and $T_{C2} \approx$ 270 K. At low fields ($\mu_0 H \leq 0.03$ T), T_{C1} dominates, while T_{C2} becomes prominent under higher fields, indicating competing exchange interactions linked to structural disorder. Inverse susceptibility data show a pronounced downward deviation from Curie-Weiss behavior, marking the onset of a robust Griffiths-like phase. Power-law analysis yields a critical exponent $\lambda \approx 0.87$, confirming short-range ferromagnetic cluster formation above T_c . The magnetocaloric response displays two non-identical peaks at low fields, corresponding to T_{C1} and T_{C2} , with a maximum $\Delta S_{\rm M} \approx 2.22$ J/kg-K at 7 T and a relative cooling power of 64.4 J/kg. Critical scaling analysis yields exponents $\beta = 0.361$, $\gamma =$ 1.108, and δ = 3.943, which deviate from mean-field values toward the 3D Heisenberg model. The exchange interactions decay as $J(r) \sim r^{4.6}$, indicating an intermediaterange character consistent with extended-type exhange interactions and magnetic inhomogeneity. This study demonstrates how antisite disorder in Co-based Heusler alloys governs phase competition, critical behavior, and entropy response, offering insight into designing materials with tunable magnetocaloric and spintronic functionalities driven by defect-engineered exchange

[1] P. Yadav, B.K. Mani, R.S. Dhaka, Exploring the role of disorder in Griffith-like magnetic phase transition in Co₂TiSi_{0.5}Al_{0.5} Heusler alloy for magnetocaloric and spintronic applications, J. Magn. Magn. Mat. 628,173093 (2025).

interactions.

[2] P. Nehla, Y. Kareri, G.D. Gupt, J. Hester, P.D. Babu, C. Ulrich, R.S. Dhaka, Neutron diffraction and magnetic properties of Co₂Cr_{1-x}Ti_xAl Heusler alloys, Phys. Rev. B 100, 144444 (2019).

[3] R.B. Griffiths, Nonanalytic behavior above the critical point in a random Ising ferromagnet, Phys. Rev. Lett. 23, 17–19 (1969).

GR-03-LB. Permanent Magnet Repulsive Force Based Floor structure to mitigate Floor Impact Noise

J. Kim¹, <u>S. Byun</u>¹, S. Noh², W. Lee³, J. Han³, S. Lee³, H. Cho¹

¹Electric., Electron. & Comm. Engineering Education, Chungnam National University, Daejeon, Korea (the Republic of), ²Korea Research Institute of Ships & Ocean Engineering, Daejeon, Korea (the Republic of), ³Floor Impact Noise Laboratory, Samsung C&T, Seoul, Korea (the Republic of)

Floor impact noise has emerged as a critical social issue in recent years. This problem has become a major source of resident conflict and psychological stress, thereby necessitating effective noise mitigation strategies[1]. Previous studies have suggested various approaches, such as increasing the thickness of the floor or applying elastic cushioning materials. Among these, the application of Ethylene Vinyl Acetate (EVA) foam has shown the most effective mitigation. However, this approach presents limitations in long-term reliability and is characterized by a relatively low damping ratio[2]. To overcome these issues, this study proposes permanent magnet repulsive force based floor structure. This approach suppresses energy transfer by minimizing direct physical contact between the upper and lower layers, while ensuring superior long-term performance[3-4].

The proposed floor structure is illustrated in Fig. 1 (left). Cylindrical magnets with identical polarity face each other inside the upper and lower cases. The cases are mechanically fastened using mounting screws, and the maximum gap between the cases is 4 mm. The 4 mm gap facilitates the repulsive force of the permanent magnets. Finite element analysis (FEA) determined the mechanical parameters of the permanent magnets. As shown in Fig. 1 (right), damping performance tests (impact hammer and ball tests) evaluated heavy impact noise and damping ratio. Experimental groups were categorized into three types based on repulsive force. For comparison, a bare reinforced slab and a floor structure incorporating EVA foam—certified as the highest grade for floor impact noise reduction by the Korea Conformity Laboratories (KCL) – were used as control groups.

Table 1 presents the results of the damping performance tests. The experimental groups (Model 1 – Model 3) have significantly higher damping ratios than the EVA foam structure. Regarding the noise reduction performance, Models 2 and 3, which had sufficient repulsive force, achieved mitigation rates of 20.14% and 20.99%,

respectively. Taking into account both the damping ratio and noise reduction performance, the permanent magnet repulsive force based floor structure achieved superior damping performance compared with the EVA foam structure.

- [1] S. H. Park and P. J. Lee, "Effects of floor impact noise on psychophysiological responses," Building and Environment, vol. 116, pp. 173–181, May 2017.
- [2] J.-Y. Lee, J.-M. Kim, J. Kim, and J. Kim, "Evaluation of the long-term sound reduction performance of resilient materials in floating floor systems," *J. Sound Vib.*, vol. 366, pp. 199–210, Mar. 2016.
- [3] T. Mizuno, M. Takasaki, D. Kishita, and K. Hirakawa, "Vibration isolation system combining zero-power magnetic suspension with springs," *Control Eng. Pract.*, vol. 15, no. 2, pp. 187–196, Feb. 2007.
- [4] T. Zhu, B. Cazzolato, W. S. P. Robertson, and A. Zander, "Vibration isolation using six degree-of-freedom quasi-zero stiffness magnetic levitation," *Journal of Sound and Vibration*, vol. 358, pp. 48–73, Dec. 2015.

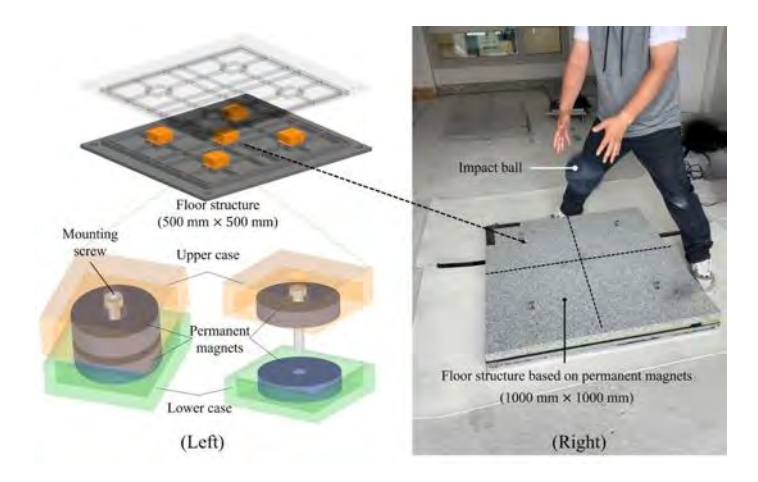


Fig. 1. Floor structure with Permanent magnets and damping test

Model types	Natural frequency (H2)	Damping ratio	Heavy impact noise (dB)
Bare reinforced concrete slab			56.2
Floor with EVA foam	12.5	10	44,6
Model 1 (Repulsive force : 57 N)	6.7	28	48.0
Model 2 (Repulsive force : 72 N)	8.3	32.5	44.9
Model 3 (Repulsive force : 92 N)	30	40	44.4

Table 1. Impact ball test result

GR-04. Magnetic Field-Modulated Critical Phenomena in van der Waals Ferromagnets

N. T. Duc¹, N. Mudiyanselage¹, <u>D. Le</u>¹, H. Srikanth¹, L. Balicas², M. Phan¹

¹Department of Physics, University of South Florida, Tampa, Florida, United States, ²National High Magnetic Field Laboratory, Florida State University, Tampa, Florida, United States

Fe₃GeTe₂ is an intriguing material primarily due to its unique electronic and topological properties, near roomtemperature ferromagnetism, and giant magnetoresistance (GMR) for perspective applications in spintronics and quantum computing [1]. Its properties can also be tuned through strain engineering, doping, and applying external fields, which opens opportunities for tailoring its functionalities to specific application requirements [2,3]. One of the significant challenges associated with Fe₃GeTe₂ is its instability when exposed to air or moisture. This can lead to degradation and alterations in its intrinsic magnetic and electronic properties, which is a considerable drawback for practical applications. In this study, we observed significant alterations in the magnetic properties of Fe₃GeTe₂ single crystals upon exposure to ambient air for varying durations. Initially, these changes manifested rapidly, followed by a relatively stable phase. A comprehensive analysis of critical exponents revealed magnetic field-modulated critical behavior, especially below its Curie temperature. When subjected to strong magnetic fields, the system tends to develop long-range ferromagnetic order, consistent with predictions from the mean-field model rather than the 3D Heisenberg model. Our findings illuminate the time-dependent magnetic intricacies of van der Waals ferromagnets like Fe₃GeTe₂, providing insights that elucidate discrepancies in reported critical exponent values observed by other researchers [4,5].

- 1. B. Huang et al., Nature Materials 19, 1276 (2020).
- 2. N.T. Dang et al., Advanced Science 10, 2206842 (2023).
- 3. M.H. Phan et al., J. Alloys and Compounds 937, 168375 (2023).
- 4. Y. Liu et al., Phys. Rev. B 96, 144429 (2017).
- 5. A. Tiwari et al., Phys. Rev. B 109, L020407 (2024).

GR-05. Magnetic ground states in Sc-Fe-Ge kagome systems Z. Zhang¹, K. Belashchenko², V. Antropov¹

¹Iowa State University, Ames, Iowa, United States, ²University of Nebraska-Lincoln, Lincoln, Nebraska, United States

The electronic structure and magnetic properties of Sc-Fe-Ge kagome systems have been studied using first-principles calculations. Initially, we optimized structures using the density functional approach for the ScFe₆Ge₆ compound and two closely related ternary kagome materials, ScFe₆Ge₅ and ScFe₆Ge₄. Using a noncollinear density functional approach, we determined the magnetic ground states for these materials. In all three cases, ground states appear collinear with mono- or bilayer A-type antiferromagnetic structures. The calculated RKKY Heisenberg exchange coupling parameters confirm the stability of the obtained magnetic ground states and the high value of the Néel temperatures in all materials. Using these parameters, the spin wave spectra have been obtained. The applicability of both the electronic and magnonic spectra was analyzed for the topological magnetism applications.

Further, we studied the disordered substitutional alloy $Sc(Fe_{1-x}Co_x)_6Ge_6$ and determined the dependence of the electronic and magnetic properties as a function of the electronic substitution. The A-type antiferromagnetism appears to be stable in the whole concentration range, while for x=1, the system becomes non-magnetic. The magnetic moment on the Fe atom appears to be local at all concentrations.

Acknowledgment

This work is supported by the U.S. Department of Energy (DOE) Established Program to Stimulate Competitive Research (EPSCoR) Grant No. DE-SC0024284. The Ames National Laboratory is operated for the U.S. DOE by Iowa State University under Contract No. DE-AC02-07CH11358.

GR-06. Magnetic properties of the quaternary Heusler alloy CoFeTiSn

<u>I. Shigeta</u>¹, K. Kuma¹, H. Aoshima¹, T. Yamauchi², R. Umetsu³, T. Kanomata⁴, M. Hiroi¹

¹Kagoshima University, Kagoshima, Japan, ²The University of Tokyo, Kashiwa, Japan, ³Tohoku University, Sendai, Japan, ⁴Tohoku Gakuin University, Tagajo, Japan

First-principles band calculations indicate that several quaternary Heusler alloys have a density of states characteristic of half-metals or spin-gapless semiconductors. CoFeTiSn is expected to be a half-metal because its band gap structure appears at the Fermi energy in the minority spin density [1]. Therefore, we have studied the magnetic properties of the quaternary Heusler alloy CoFeTiSn.

Magnetization measurements for CoFeTiSn were performed using a SQUID magnetometer. Figure 1 shows the magnetic field dependence of magnetization M(H) with the spontaneous magnetization $M_s = 1.06 \mu_B/f.u.$ Figure 2 represents the temperature dependence of magnetization M(T) with the Curie temperature $T_C = 173.6$ K. Using spin fluctuation theory [2], we can quantitatively estimate the energy scale of the spin fluctuation spectrum [3]. The parameters for CoFeTiSn are $F_1/k_B = 5.51 \times 10^4$ K, $T_0 =$ 7.45×10^{2} , $T_{A} = 1.24 \times 10^{4}$, and $\eta = 0.615$. Very weak itinerant electron ferromagnets are characterized by small n values. In contrast, magnets with localized magnetic moments usually have large η values because T_0 is roughly comparable to T_c . Moreover, for weak itinerant electron ferromagnets, spin fluctuation theory predicts the following magnetic behaviors depending on η : (1) For small η , the Arrott plot shows a linear relation over a wide temperature range, while for larger η , this relation does not hold at finite temperatures. (2) For small η , the squared spontaneous magnetization follows a $T^{4/3}$ dependence, whereas for larger η , it more closely follows a T^2 dependence. These theoretical predictions are in good agreement with the behavior observed in CoFeTiSn. The electronic state of CoFeTiSn is considered to lie between the ferromagnetic limit of very weak itinerant electrons and an intermediate case similar to Fe and Ni. Hence, the spin fluctuation theory for weakly ferromagnetic itinerant electron systems remains applicable to the highly spin-polarized Heusler alloy CoFeTiSn, which exhibits somewhat localized Co and Fe moments.

- [1] Y. Zhang et al., J. Alloys Compd. 842 (2020) 155977.
- [2] Y. Takahashi, J. Phys. Soc. Jpn. 55 (1986) 3553.
- [3] T. Sasaki et al., J. Alloys Compd. 317-318 (2001) 406.

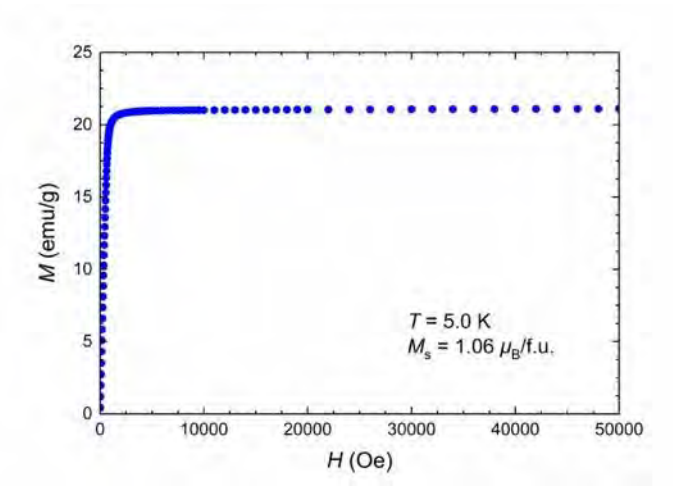


Fig. 1 Magnetic field dependence of the magnetization M(H) for the quaternary Heusler alloy CoFeTiSn.

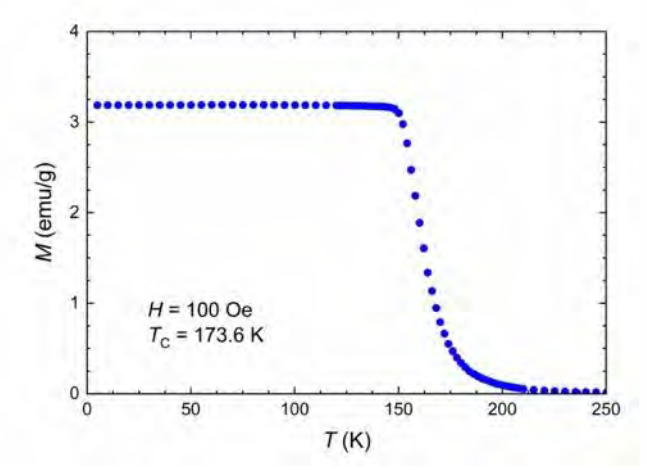


Fig. 2 Temperature dependence of the magnetization M(T) for the quaternary Heusler alloy CoFeTiSn

GR-07. Unconventional magnetic glassiness in noncentrosymmetric Sm₇Pd₃

<u>A. Kumar</u>, A. Biswas, Y. Mudryk Ames National Laboratory, U.S. Department of Energy, Iowa State University, Ames, Iowa, United States

The complex magnetic relaxation in systems exhibiting non-ergodic, metastable states, whether due to FM-AFM phase separation or strong magnetocrystalline anisotropy, has led to the identification of a distinct "magnetic glass" state, different from conventional spin glass behavior [1, 2]. Clarifying the origin of such glassiness is crucial for understanding spin dynamics in these systems. In this work, we investigate Sm₇Pd₃, a compound that exhibits dominant FM behavior coupled with weak AFM interactions and hosts significant magnetocrystalline anisotropy [3]. Thus, it resides at the crossroads of spin-glass, domain-glass, and ferromagnetic behaviors. Detailed ac and dc magnetization measurements under various protocols were performed to explore the nature of magnetic glassiness in this compound. Our findings establish two distinct types of glassiness in the ordered state of Sm₇Pd₃: one stemming from intrinsic magnetic frustration due to competing FM-AFM interactions arising from the compound's complex non-centrosymmetric nature, and the other induced by field-driven metastable states [4]. We attribute the former to conventional spinglass behavior and the latter to domain-glass behavior, both of which are distinct from the magnetic glass behavior observed in phase-separated compounds. Magnetism in Sm-based compounds is highly sensitive to the strength of the crystal field, which governs the degree of mixing between the ground state J = 5/2 and the first excited J = 7/2 states of Sm^{3+} , due to their small energy separation. Magnetization measurements reveal a separation of 965 K between these levels in Sm₇Pd₃, with the J = 7/2 state significantly influencing the paramagnetic susceptibility of the compound. Moreover, specific heat measurements indicate the further splitting of the 3sixfold degenerate J = 5/2 ground state into a doublet ground state and an excited fourfold-degenerate state located 255 K above it [4].

Acknowledgment

This work was performed at Ames National Laboratory and supported by DMSE, BES, Office of Science, U.S. DOE. Ames Lab is operated for the DOE by Iowa State University under Contract No. DE-AC02-07CH11358.

- [1] K. Sengupta and E. V. Sampathkumaran, Phys. Rev. B 73, 020406(R) (2006).
- [2] S. Pal, K. Kumar, and A. Banerjee, Phys. Rev. B 103, 144434 (2021).
- [3] A. Biswas, R. K. Chouhan, O. Dolotko, P. Manfrinetti, S. Lapidus, D. L. Schlagel, and Y. Mudryk, Acta Mater. 265, 119630 (2024).
- [4] Ajay Kumar, A. Biswas, and Y. Mudryk, Phys. Rev. B 111, 174448 (2025).

GR-08. Effect of Second-Neighbor Hopping on Weyl points in the Antiferromagnetic Phase of Rashba-Hubbard Model A. Jain, D. K. Singh

Department of Physics and Material Science, Thapar Institute of Engineering and Technology, Patiala, Punjab, India

The interplay of spin-orbit coupling (SOC) and strong electronic correlations in non-centrosymmetric systems has emerged as a fertile ground for realizing novel quantum phases [1]. In particular, the Rashba-Hubbard model offers a rich platform to explore the coexistence of magnetic ordering and nontrivial band topology. In such systems time-reversal and inversion symmetries are inherently broken, making them ideal hosts for realizing topological semimetals [2-6].

Prior studies on the Rashba-Hubbard model with nearestneighbor hopping have reported the stabilization of an antiferromagnetic (AFM) phase featuring two-dimensional Weyl points (WPs) at half-filling [5]. In another work [6], the inclusion of second-neighbor hopping was shown to restrict AFM stability to weak SOC regimes for same filling, though its topological consequences remained largely unaddressed. In this work, we examine the AFM phase in the presence of both Rashba SOC and second-neighbor hopping using a self-consistent Hartree-Fock mean-field framework. While AFM order survives at half-filling above a critical Coulomb interaction [6], our results reveal that the inclusion of second-neighbor hopping breaks particle-hole symmetry, leading to a displacement of Weyl points away from the Fermi level, thereby the Weyl semimetallic phase is lost. Nevertheless, the band crossings retain topological character, as verified through calculation of Berry connections and quantized winding numbers with opposite chiralities for each WP pair.

These findings demonstrate the delicate sensitivity of topological states to microscopic hopping pathways in correlated systems with Rashba SOC. These insights are valuable for engineering Weyl physics in artificial or real materials, with potential applications in spintronics and topological quantum devices.

- 1. A. Manchon, H. C. Koo, J. Nitta, S. M. Frolov, and R. A. Duine, Nat. Mater., Vol. 14, 871 (2015).
- 2. W. Kennedy, S. A. Sousa-Jr., N. C. Costa, and R. R. Santos, Phys. Rev. B, Vol. 106, 165121 (2022).
- 3. M. Kawano and C. Hotta, Phys. Rev. B, Vol. 107, 045123 (2023).
- 4. K. Kubo, J. Phys. Soc. Jpn., Vol. 93, 024708 (2024).
- 5. A. Jain, G. Goyal, and D. K. Singh, Phys. Rev. B, Vol. 110, 075134 (2024).
- 6. A. Greco, M. Bejas, and A. P. Schnyder, Phys. Rev. B, Vol. 101, 174420 (2020).

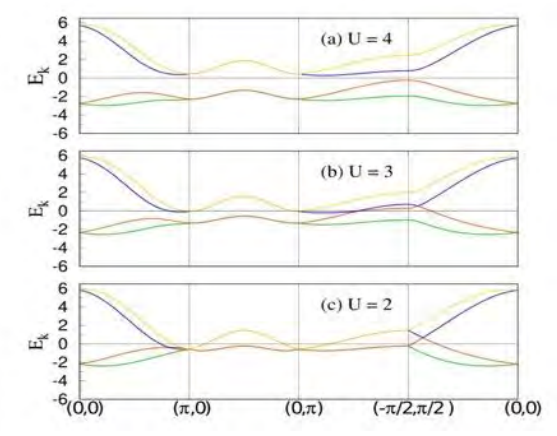


Fig. 1 At half-filling, electronic dispersions are plotted, depicting shifted Weyl crossings.

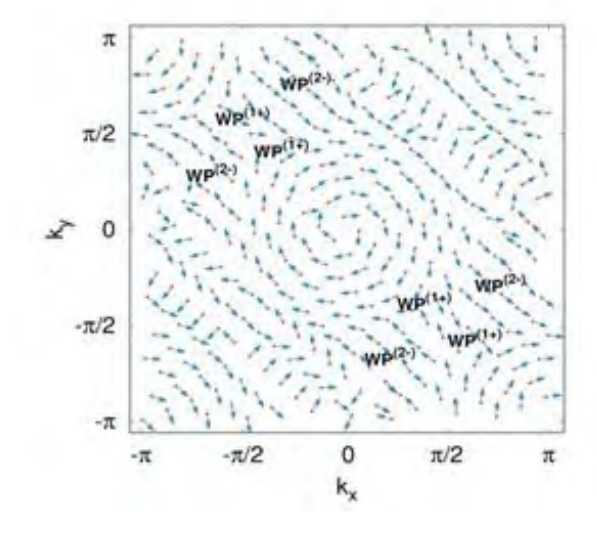


Fig. 2 For full Brillouin zone, Berry connection at U = 3 and RSOC = t' = 0.3 is shown.

GR-09. Observation of an Odd-Symmetric Planar Hall Effect in α'' -Fe₁₆N₂ Thin Films

O. Jia, E. Gokce-Polat, A. DeRuiter, Y. Chen, W. Echtenkamp, B. Wolf, J. Wang

University of Minnesota, Minneapolis, Minnesota, United States

Planar Hall effect (PHE) in ferromagnets is conventionally even under magnetization reversal, reflecting the preservation of two-fold rotational symmetry. Here, we report the emergence of an odd-symmetric PHE component in α'' -Fe₁₆N₂ ferromagnetic thin films, manifested as a sin ϕ term that reverses sign with magnetization. Measurements on two thicknesses (26 nm and 49 nm) reveal that the odd component becomes significantly stronger in the thinner film. Moreover, the $\sin \phi$ component exhibits a fixed orientation dictated by the crystal axis, rather than by the applied current, indicating a possible origin in lattice distortion or interfacial symmetry breaking. This behavior suggests a previously unexplored symmetry-breaking mechanism in planar magnetotransport and provides a new approach for magnetic state readout in spintronic devices based on the odd PHE.

- 1. Gokce-Polat, E. *et al.* Unusually high coercivity of sputtered Fe16N2 thin films on MgO (001) substrate. *AIP Adv.* 15, (2025).
- 2. Cui, Y. *et al.* Antisymmetric planar Hall effect in rutile oxide films induced by the Lorentz force. *Sci. Bull.* 69, 2362–2369 (2024).

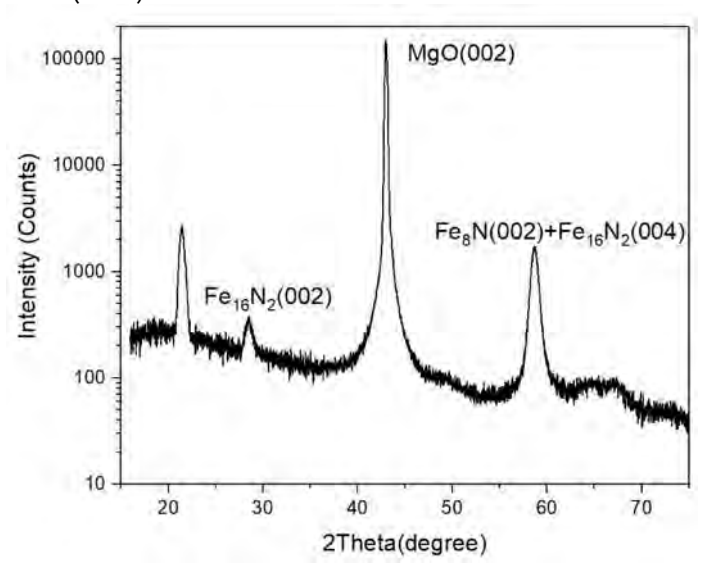


Fig. 1. XRD of the α'' -Fe₁₆N₂ (49 nm) deposited on MgO(001)/Fe(3.7 nm).

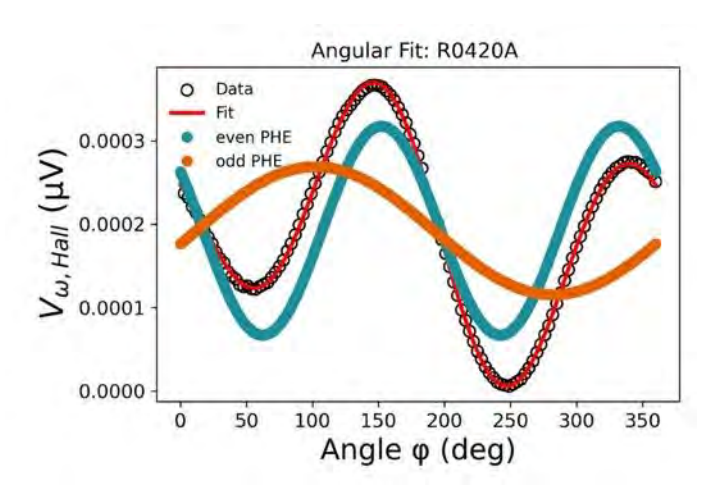


Fig. 2. Angular-dependent first harmonic Hall signal of α'' -Fe₁₆N₂ (49 nm) thin film. An odd-symmetric planar Hall component appears superimposed on the conventional even PHE, indicating broken in-plane symmetry.

GR-10. Emergent Low-Temperature Magnetic Properties of [2.2.2] Cryptand (DHS)-MnBr₄ Compound

D. Le¹, K. Nassar², M. Elolimy², G. M. Pantano¹, I. Spanopoulos², J. D. Gayles¹, M. Phan¹

¹Department of Physics, University of South Florida, Tampa, Florida, United States, ²Department of Chemistry, University of South Florida, Tampa, Florida, United States

Organic-inorganic hybrid metal halides have emerged as promising lead-free materials for spintronic and optoelectronic applications [1]. In these systems, organic components serve as structure-directing agents, while inorganic moieties contribute to tunable magnetic and optical properties through the incorporation of transition metal atoms and bandgap engineering [1-3]. Among these, manganese-based clusters, particularly [MnBr₄]²⁻, offer favorable conditions for strong paramagnetic behavior due to the fully occupied spin states of Mn²⁺ ions. Previous studies have reported spin-spin interactions affecting relaxation rates at room temperature [4] and magnetic fieldinduced ordering at low temperatures [5]. However, the role of thermal fluctuations in suppressing such magnetic ordering remains poorly understood. In this work, we investigate the low-temperature magnetic properties of the hybrid compound [2.2.2]cryptand (DHS)[MnBr₄], featuring paramagnetic [MnBr₄]²⁻ clusters. Brillouin fitting confirms the compound's paramagnetic nature, while magnetization versus magnetic field (M-H) measurements at low temperatures (e.g., 2 K) reveal magnetic field-modulated antiferromagnetic-like behavior. The successful fit of the

M–H data to the Langevin function suggests minimal magnetic interactions among [MnBr₄]²⁻ clusters. Density functional theory (DFT) calculations provide further insight into Mn orbital contributions to the electronic structure and magnetic moments. Notably, magnetic ordering becomes apparent only below 20 K, when thermal fluctuations are significantly reduced. These findings highlight [MnBr₄]²⁻-based hybrids as a promising class of materials for probing quantum critical fluctuation phenomena and multifunctional device applications.

- [1] Asensio et al. "Engineering magnetism in hybrid organicinorganic metal halide perovskites." Materials Horizons 12, 2414 (2025).
- [2] Azmy et al. "Synthesis, optical, electronic and magnetic studies of air-stable chiral Cu(II) chlorides" Journal of Materials Chemistry A 12, 25730 (2024).
- [3] Li et al. "Lead-free hybrid metal halides with a greenemissive [MnBr₄] unit as a selective turn-on fluorescent sensor for acetone." Inorganic Chemistry 58, 13464 (2019). [4] Lynds, Lahmer, et al. "Electron Spin Relaxation Studies of Manganese (II) Complexes in Acetonitrile." The Journal of Chemical Physics 57, 5216 (1972).
- [5] Panda, et al. "Photophysical and Magnetic Properties in Zero-Dimensional (H_2DABCO) MX_4n H_2O)." The Journal of Physical Chemistry C 126, 13291 (2022).

GR-11. A Comparative Study of Static and Dynamic Magnetic Responses in Equiatomic Heusler Alloys CoRuXGe (X = Co, Mn)

P. Sharma¹, R. Roy Chowdhury¹, J. Nag², A. Alam², K. G. Suresh², S. Witanachchi¹, M. Phan¹, H. Srikanth¹

Department of Physics, University of South Florida, Tampa, Florida, United States, ²Department of Physics, Indian Institute of Technology Bombay, Mumbai, Maharashtra, India

Equiatomic Quaternary Heusler alloys are versatile intermetallic compounds with diverse properties, viz. half-metallicity and high Curie temperatures, making them attractive for spintronic applications. The compositional tunability of 3d/4d transition metals (e.g., Cr, Ru, Co, Mn) in these alloys gives rise to complex magnetic phenomena such as magnetic frustration, spin glass behavior, and spin freezing; however, a comprehensive understanding of the mechanisms driving these states remains elusive. In this study, we investigate the static and dynamic magnetic properties of CrRuXGe (X = Co, Mn), which crystallize in the cubic LiMgPdSn-type structure with a lattice parameter of ~

5.90 Å [1,2]. Magnetometry measurements reveal that CrRuMnGe exhibits soft ferromagnetism with a saturation magnetization (M_S) of ~ 0.98 $\mu_B/f.u.$ at 10 K, consistent with Slater-Pauling predictions. In contrast, CrRuCoGe shows a glassy magnetic ground state, with coexisting ferromagnetic and antiferromagnetic phases, and a higher M_S of ~ 1.65 μ_B/f.u. at 10 K. In order to delve deeper into the underlying spin dynamics, we performed radio-frequency transverse susceptibility (TS) measurements using the tunnel diode oscillator (TDO) technique. For CrRuCoGe, TS spectra exhibit peak broadening and asymmetric features in bipolar DC field scans below ~ 140 K, indicative of spin freezing and enhanced magnetic anisotropy at low temperatures. These observations align with magnetization data showing a broad peak near 140 K and a drop around 40 K, hallmark features of a glassy magnetic state. The effective magnetic anisotropy field (H_{Keff}) exhibits a non-monotonic temperature and field dependence above 140 K, evidencing the interplay between ferromagnetic and antiferromagnetic interactions, while a marked increase in H_{Keff} below ~ 40 K further confirms spin freezing. In contrast, CrRuMnGe displays relatively sharper TS peaks, reaffirming its soft ferromagnetic nature. This comparative analysis presented in this work highlights that the role of subtle changes in composition, such as substituting manganese with cobalt, can precisely tune magnetic frustration and anisotropy in these Ouaternary Heusler alloys.

[1] Chanda, A., Nag, J., Schulz, N., Alam, A., Suresh, K. G., Phan, M.-H., & Srikanth, H. Large anomalous Nernst effect and its bipolarity in the quaternary equiatomic Heusler alloys CrRuXGe (X = Co and Mn). *Phys. Rev. B.* 109, 224415 (2024).

[2] Idrissi, S., Labrim, H., Bahmad, L., & Benyoussef, A. Structural, electronic, and magnetic properties of the equiatomic quaternary Heusler CoRuMnGe alloy: a DFT study. *Ferroelectrics*, 582(1), 155–166 (2021).

GR-12. Frequency-Dependent Nonlinear Hall Response in Focused-Ion-Beam-Deposited Platinum Cross-Bar Devices

J. Wu¹, S. Zhou¹, R. Sun², S. Lei³, D. Sun², W. Zhang¹
¹Physics and Astronomy, University of North Carolina at Chapel Hill, Chapel Hill, North Carolina, United States, ²Department of Physics, North Carolina State University, Raleigh, North Carolina, United States, ³Materials Science and Engineering, University of Central Florida, Orlando, Florida, United States

The nonlinear Hall effect (NLHE) has emerged as a powerful probe of broken inversion symmetry in both topological and non-topological materials.[1] While most experimental studies of NLHE have focused on DC and low-frequency transport regimes, its frequency-dependent behavior—particularly in disordered metallic systems—remains largely unexplored.[2]

In this work, we report the observation of frequencydependent nonlinear Hall responses in platinum (Pt) crossbar devices fabricated by focused ion beam (FIB) deposition. The devices exhibit clear second- and third-harmonic Hall voltages under amplitude-modulated AC excitation in the frequency range from 1 kHz to 100 kHz. The second-order transverse Hall voltage emerges above 1 kHz and increases with frequency, reaching a maximum near 15 kHz before gradually declining. Similarly, a third-harmonic response becomes prominent in the same frequency range, peaking at ~15 kHz. In contrast, the rectified DC Hall voltage displays a distinct maximum at a higher frequency of approximately 25 kHz. The frequency-dependence property is also observed in DC and third harmonic signal of Fe₃GeTe₂—an intrinsic ferromagnetic van der Waals material, as a comparative investigation. These results demonstrate that the nonlinear Hall effect in FIBD-Pt is highly frequencysensitive and governed by a complex interplay between AC current dynamics and geometric asymmetry within the nanostructured Pt.

The observation of multiple harmonic components and their distinct frequency profiles establishes FIBD-Pt as a promising platform for nonlinear signal processing, including frequency-selective rectification and harmonic generation. This work provides new insights into the dynamic transport properties of disordered metallic systems and highlights the potential of engineered Pt nanostructures for device applications operating in the kHz regime.

[1]B. Arka, J. Nesta, N. Awadhesh, Materials Today Electronics., Vol 8, 100101 (2024)[2] L. Min, Y. Zhang, Z. Xie, *Nat. Mater.* 23, 1671–1677 (2024)

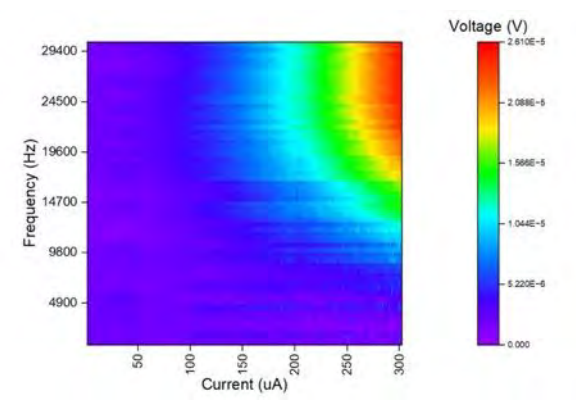


Fig. 1 Frequency-dependence of rectified DC signal

GR-13-LB. Sub 10 mK Refrigeration and Enhanced Magnetocaloric Effects

<u>A. M. Donald</u>¹, A. G. Duque¹, S. Li¹, C. J. Ollmann¹, R. Schanen², C. Huan¹, R. P. Haley², M. W. Meisel¹, C. Jia¹, R. Gazizulin¹

¹Physics, University of Florida, Gainesville, Florida, United States, ²Physics, Lancaster University, Lancaster, United Kingdom

This research investigates future magnetic refrigerants with magnetocaloric effects enhanced by quantum phase transitions and their application as refrigerants for cryogenic systems. The motivation for this work is guided by the development of adiabatic demagnetization refrigeration (ADR) cells compatible with cryogen free systems [1]. Experiments with a prototype ADR cell achieved temperatures down to 2 mK and used copper powder as the refrigerant. However, the design of this cell supports the utilization of materials beyond non-interacting paramagnetic spins, such as copper, and this research explores the potential future of magnetic refrigerants. The thermodynamics for these interacting quantum spin materials with field induced quantum phase transitions are under investigation using computational simulation methods. This study focuses on spin-1 Heisenberg antiferromagnetic chains (HAFC) as a potential candidate for magnetic refrigeration [2]. Computational models such as minimally entangled typical thermal states (METTS), density matrix renormalization group (DMRG), and Exact Diagonalization (ED) provide a method for calculating the

optimal parameters a refrigerant could possess [3]. This presentation reports on the explored thermodynamic phase space of these spin materials and presents some of the optimal characteristics for a magnetic refrigerant such as entropy and minimum temperature.

[1] D.I. Bradley et al. J Low Temp Phys 57 (1984) 359.

DOI: 10.1016/0011-2275(94)90217-8

[2] T. Liu et al. Phys Rev Research 3 (2021) 033094.

DOI: 10.1103/PhysRevResearch.3.033094

[3] E M Stoudenmire and Steven R White. New Journal of

Physics 12 (2010) 055026

DOI: 10.1088/1367-2630/12/5/055026

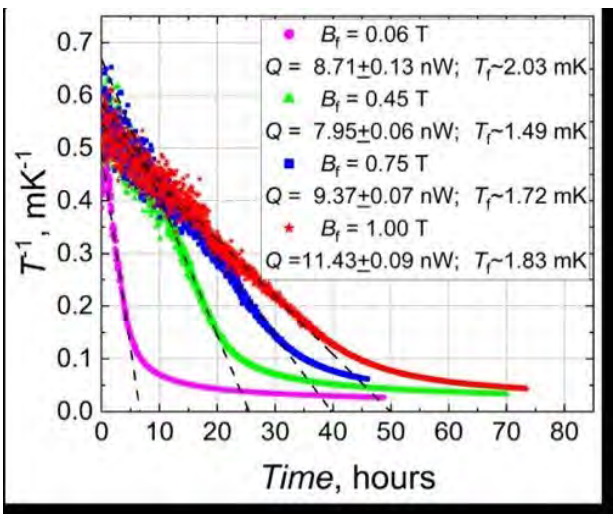


Figure 1. Warming curves at different final magnetic fields after demagnetization. Dashed lines are fits used to get Odot and $T_{\rm f}$ values.

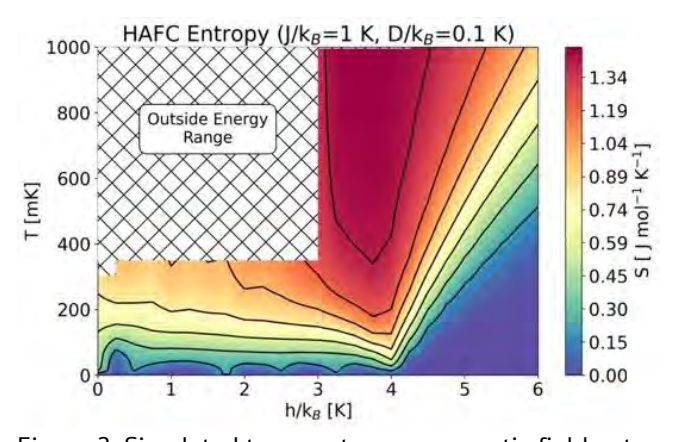


Figure 2. Simulated temperature vs magnetic field entropy contours of a 1-D Heisenberg anti-ferromagnetic chain using DMRG. Crossed region shows DMRG simulation limitations.

GR-14-LB. Multiferroic heterostructured devices for energy efficient electronics and biomedical applications J. Hong

Hubei University of Technology, Wuhan, Hubei, China

Recent strides in electrically controlled spin devices have been enabled through the utilization of multiferroic systems integrating ferroelectric (FE) and ferromagnetic (FM) materials. In this talk, we investigated multiferroic heterostructures which have a magnetic order parameter and are being fabricated for various device applications. In this poster, I will discuss about 1) nano-cracking, 2) straincontrolled racetracks, 3)

spin orbit torque mechanisms, and 4) flexible multiferroic sensors for energy efficient electronics and medical applications. First, the controlled nano-cracking in MnPt/PMN-PT heterostructures achieved non-volatile switching: Resistive Load (RL) was demonstrated through complementary crack switching. Second, nanowire based racetrack using magnetic domain wall (DW)-based logic devices were demonstrated

to manipulate magnetization through an electric field, enabling all-electrical logic operations. Third, spin orbit torque (SOT) devices modulate magnetization switching via induced strain in multiferroic heterostructures. Last, we demonstrated flexible multiferroic heterostructures enabling nanotechnology for sensing and actuating devices. Nanoparticles' responses to stimuli can be monitored for sensing the physical environment. A methodology using piezo-magnetoelectric properties of nanoparticles enables strain sensing and actuation in a flexible patch. These structures unveil a device platform for energy-efficient electronics and medical applications

^{*} Best Student Presentation Finalist / LB – Late-breaking Poster

SESSION VP1: COMPUTATIONAL METHODS

Chair(s): R. Hertel, *Insitut de Physique et Chimie des Matériaux de Strasbourg, Centre National de la Recherche Scientifique, Strasbourg, France*Conference Resource Center

VP1-01. Impact of Surface Termination on Magnetic Anisotropy and Gilbert Damping in L1₀-MnAl Thin Films R. R. Sheikh, R. K. Ghosh

Electronics and Communication Engineering, Indraprastha Institute of Information Technology Delhi, New Delhi, India

The magnetic properties of L1₀-MnAl thin films are of significant interest due to the combination of high magnetic anisotropy energy and low Gilbert damping, which play critical roles in thermal stability and low switching current (I_C) for spintronic applications like STT-MRAM. In this study, we employ density functional theory (DFT) to investigate the impact of different surface terminations – Mnterminated, Al-terminated, and Mn-Al terminated configurations on the magnetic anisotropy energy (MAE) and Gilbert damping constant (α) of L1₀-MnAl thin films, both in bare form and in MgO/MnAl/MgO heterostructures. The MAE was evaluated using the force theorem (FT) and α using Kambersky's torque-torque correlation model. We demonstrate that surface termination plays a crucial role in defining the magnetic properties of L1₀-MnAl thin films. Our calculations reveal that surface anisotropy is influenced not only by the film thickness but also by the atomic environment of the surface layer. We found that the perpendicular magnetic anisotropy of L1₀-MnAl thin films is enhanced with Al-termination compared to Mn-termination. Furthermore, the calculated Gilbert damping, a key factor in spin relaxation dynamics, indicate that the density of states (DOS), hybridization, and spin-orbit coupling (SOC) at the interface significantly affect spin relaxation mechanisms. These findings provide fundamental insights into tailoring interfacial properties in L1₀-MnAl-based devices and emphasize the importance of surface terminations in enhancing magnetic performance, an essential factor for the development of high-efficiency STT-MRAM devices.

- 1. R. R. Sheikh and R. K. Ghosh, J. Appl. Phys. 137, (2025).
- 2. X. Zhang et al., Appl. Phys. Lett. 110, (2017).
- 3. K. Hammar et al., Surf. Sci. 717, (2022)
- 4. E. Barati et al., Phys. Rev. B Condens. Matter Mater. Phys. 90, (2014).
- 5. G. H. O. Daalderop, P. J. Kelly, and M. F. H. Schuurmans, Phys. Rev. B 41, 11919 (1990).

6. K. Gilmore, Y. U. Idzerda, and M. D. Stiles, Phys. Rev. Lett. 99, (2007).

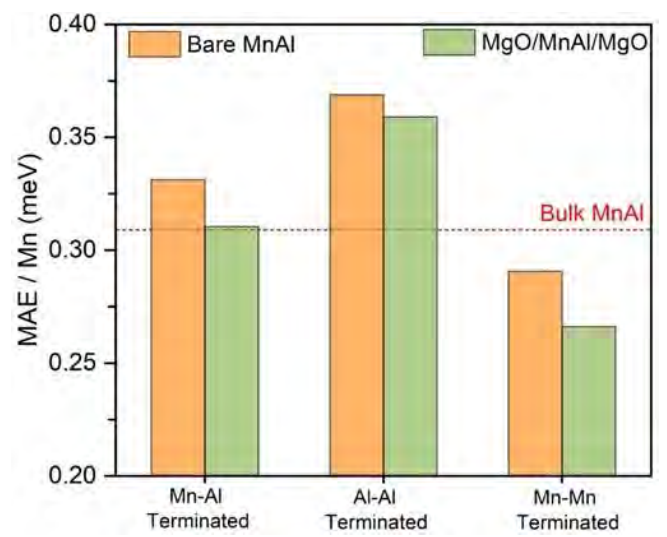


Fig.1. Magnetic anisotropy energy per Mn (MAE/Mn) of various surface terminations of bare and MgO capped MnAl (nL) thin films. Here nL, the number of layers, is 12 for Mn-Al and 13 for Al-Al and Mn-Mn terminated structure, respectively. The horizontal line marks the bulk value of MAE.

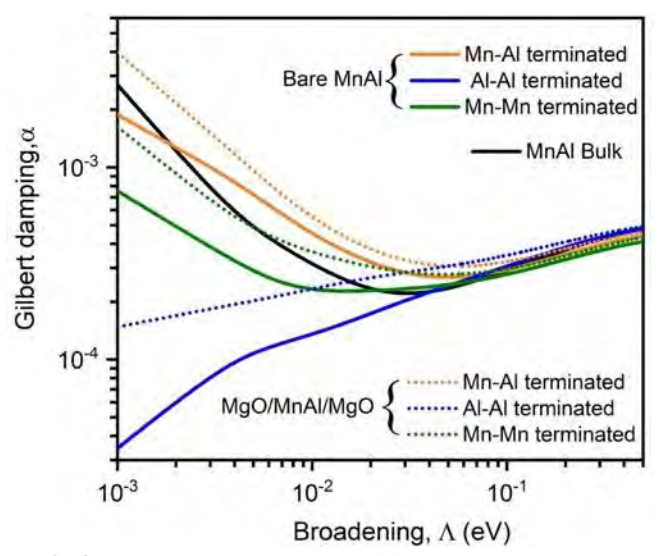


Fig.2. Gilbert damping constant (α) of various surface terminations of bare and MgO capped MnAl (nL) thin films, along with the bulk α value, as a function of lifetime broadening (Λ). Here nL, the number of layers, is 12 for MnAl and 13 for Al-Al and Mn-Mn terminated structure, respectively.

VP1-02. Prediction of Hysteresis Behavior in Soft Magnetic Materials Based on Neural Networks and Preisach Model

<u>Y. Qin</u>¹, Z. Li¹, R. Pei^{1, 2}, Y. Li¹, J. Li¹, L. Zeng²

¹Department of Electric Engineering, Shenyang University of Technology, Shenyang, China, ²Suzhou Inn-Mag New Energy Ltd, Suzhou, China

Soft magnetic materials have low coercivity and are easy to magnetize and demagnetize, so they are widely used in the core of electrical equipment such as electric motors. However, their nonlinear hysteretic behavior has a significant impact on the power and efficiency of electrical equipment. Therefore, dynamic hysteresis calculation is crucial to the performance prediction of equipment. This paper proposes a physical-constraint neural network method integrated with the analytical Preisach forward hysteresis model, aiming to improve the accuracy of hysteresis calculation and prediction, as well as the universality of the model for novel soft magnetic materials.T his method embeds the Preisach model into the neural network as a physical loss function, which can accurately calculate the ascending and descending branches of the hysteresis loop. In addition, the model efficiently identifies the six core parameters of the Preisach model based on magnetic measurement data, enabling the prediction of hysteresis loops at different frequencies. The model was verified by silicon steel, iron-cobalt alloy and amorphous alloy. The results show that the proposed method exhibits higher accuracy and faster convergence speed than the traditional model in the fitting of hysteresis behavior in silicon steel materials. Moreover, the hysteresis calculation and prediction of iron-cobalt alloys and amorphous alloys can also be realized, which expands the application range and accuracy of the Preisach model. The physically constrained neural network method proposed in this paper not only addresses the challenges of complex parameter calculation and limited applicability in the Preisach model but also overcomes the limitation of the "black-box" nature of neural networks that lack physical interpretability. This approach can enhance the calculation accuracy for the design and optimization of electrical equipment, holding significant significance for the engineering applications of different soft magnetic materials.

[1] Grech, Christian, et al. "Dynamic ferromagnetic hysteresis modelling using a Preisach-recurrent neural network model." Materials 13.11 (2020): 2561.

[2] Semenov, M. E., et al. "The Preisach model of hysteresis: fundamentals and applications." Physica Scripta 99.6 (2024):

062008.

[3] Liu, R., et al. "Derivation and modification of analytical forward Preisach hysteresis model." Proc. CSEE 43 (2023): 2070-2079.

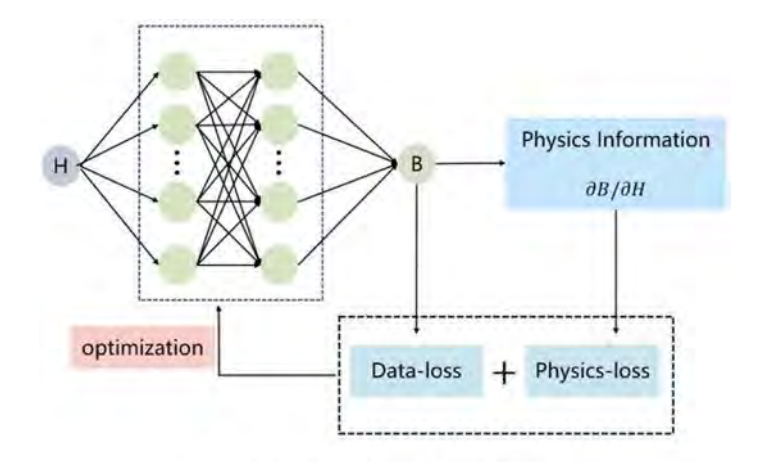


Fig.1 Calculation flow chart

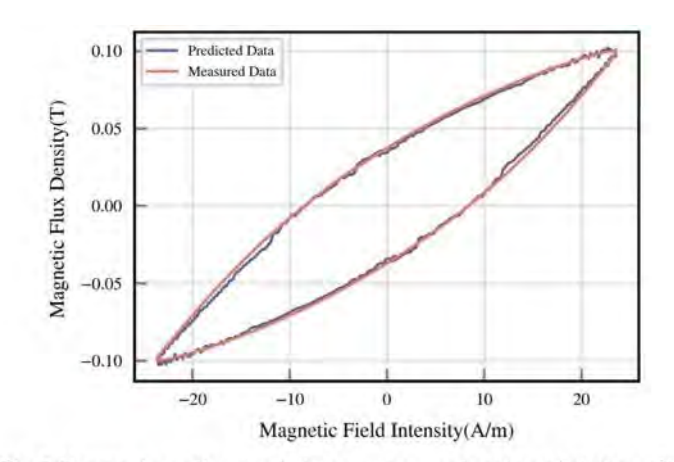


Fig.2 Comparison diagram between measured and predicted results

VP1-03. Application of DeepONet Based on Multi-branch Residual Structure and Physical Priors in Magnetic Field Prediction

L. Chen, <u>Z. Yang</u>, T. Ben, W. Ke China Three Gorges University, Yichang, China

Neural networks have demonstrated significant potential in magnetic field prediction research and have become an important alternative to finite element methods. However, most methods still rely on fixed input conditions and struggle to handle transient changes in geometric structures or operating conditions. PINN and DeepONet networks, representing physically driven modeling, also have limitations. PINN has difficulty converging during training when solving magnetic field problems and requires a long training time [1]. DeepONet can generalize different input functions but is highly dependent on data and has difficulty fully capturing nonlinear behavior in magnetic fields [2].

To address the challenge of predicting magnetic fields caused by transient changes under different geometric structures or operating conditions in physics-driven modeling, this paper proposes a DeepONet framework based on physical information, which incorporates physical prior knowledge. Based on finite element simulation data, a multi-branch residual DeepONet architecture is constructed using spatiotemporal sampling and current waveform inputs. The main network processes spatial coordinates, while two residual branches, respectively, encode phaseencoded temporal features and three-phase current waveforms. Additionally, a double-period constraint is introduced to guide training and ensure physical consistency. The model is trained in stages, gradually introducing physics-based loss functions to enhance learning stability. This method provides a structured and physically interpretable solution for predicting transient magnetic fields under different geometric structures or operating conditions.

After training, predictions can be made by directly inputting parameters, with calculations completed in seconds. Compared to PINN, training is faster. As shown in Figure 2, the average percentage error of the predicted Epstein's square circle is 3%, while the average error of the unimproved DeepOneNet network is 5%.

[1]Z. Gong, Y. Chu, and S. Yang, Physics-Informed Neural Networks for Solving 2-D Magnetostatic Fields, Vol. 59, no. 11, pp. 1–5, Nov. (2023)

[2]S. Wang, H. Wang, and P. Perdikaris, Learning the solution operator of parametric partial differential equations with physics-informed DeepONets, Vol. 7, no. 40, p. eabi8605, Oct. (2021)

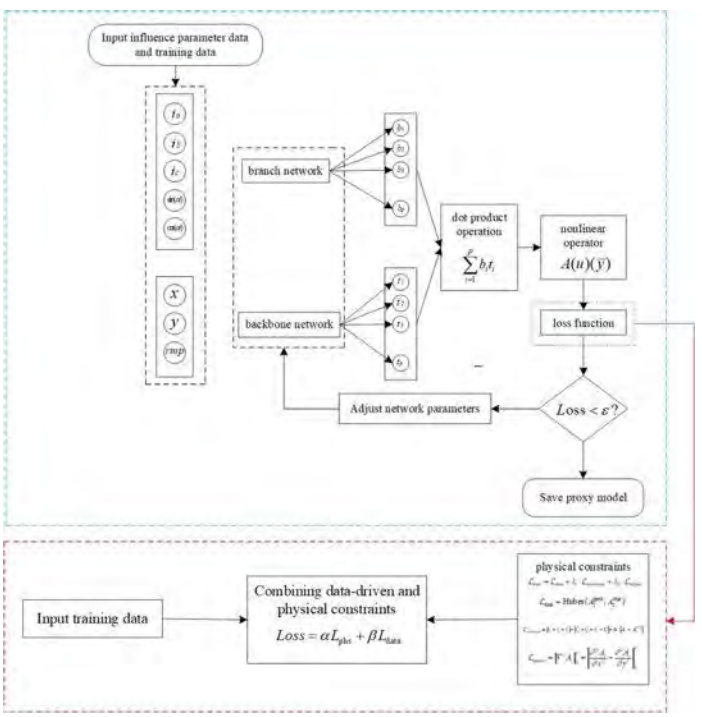


Fig. 1 Flowchart of improved transient magnetic field numerical prediction using DeepNet

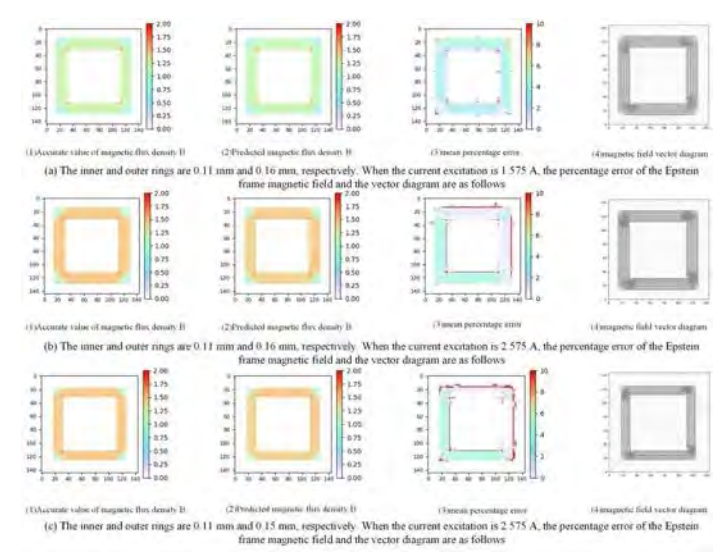


Fig. 2 Magnetic field prediction of Epstein's square circle under different structural incentives

VP1-04. Optimizing Recoil Damping in Artillery Systems Using Magnetorheological Fluid

K. Feng, Y. Li

National Defense University, Chung-Cheng Institute of Technology, Taoyuan, Taiwan

This study numerically explores the feasibility of integrating magnetorheological fluid (MRF) technology into artillery recoil systems for adaptive and fail-safe damping control. MRF-based dampers can adjust damping force in real time by varying the applied magnetic field, enabling optimized recoil absorption depending on firing conditions. Figure 1 illustrates the magnetic field distribution in the recoil damper under externally applied fields generated by a pair of adjustable-current electromagnetic coils. The recoil system is filled with hydraulic oil having a density of 849 kg/m³ and a dynamic viscosity of 0.0134 Pas. The two subfigures compare magnetic field response without (left) and with (right) MRF inclusion. In the right figure, MRF with a volume fraction of 22.8% is incorporated near the recoil rod. MRF properties are referenced from commercially available Dynabeads M-450 magnetic microspheres (4.5 µm diameter, 1390 kg/m³ density). The MRF enhances the magnetic field strength around the recoil rod from approximately 0.7 T to 1 T. Denser magnetic flux lines are observed around the rod, particularly near the damping chamber. This is due to the higher magnetic permeability of the MRF, which locally concentrates and guides field lines. The intensified field in the MRF region enhances the magnetorheological effect, increasing yield stress under the same current. As a result, less energy is needed to produce the required damping force, improving system efficiency and control precision. Figure 2 shows the displacementdamping response under varying currents (0A to 200A) when the damper is subjected to a 100 kN force. Displacement decreases significantly from 0A to 150A, indicating effective modulation. However, the curves for 150A and 200A show minimal difference, suggesting magnetic saturation near 150A at 22.8% MRF. This defines an optimal operating range for current input. Further discussion on particle size, density, volume fraction, and energy dissipation will be presented in the full manuscript.

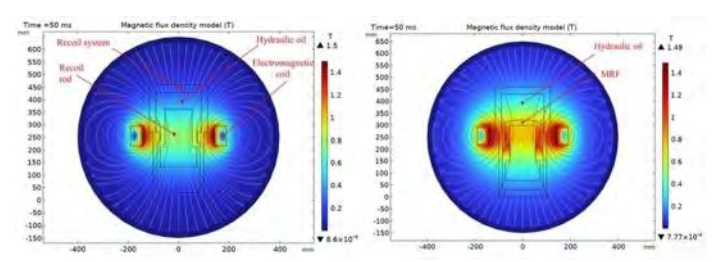


Fig. 1 The magnetic field distribution within the recoil damper under an external magnetic field strength of 1.5T

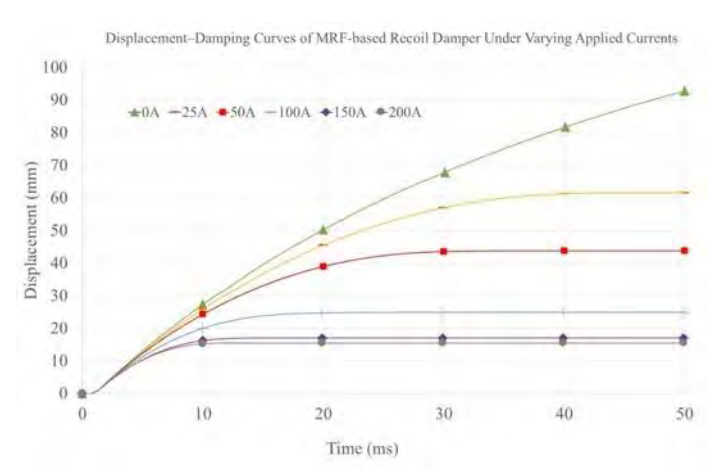


Fig. 2 Displacement-damping response curves of the MRF-based recoil damper under varying applied currents.

VP1-05. Manipulation of the spiking activity of Hodgkin-Huxley-analogue spintronic neuron based on magnetoimpedance thin-film structure

G. D. Demin, N. A. Djuzhev

R&D Center "MEMSEC", National Research University of Electronic Technology (MIET), Moscow, Zelenograd, Russian Federation

Currently, modern spintronics technology offers great potential for hardware implementation of the concept of miniature neuromorphic devices [1]. This is due to the similar behavior of biological neurons and synapses in the presence of an external stimulus and the nonlinear nature of the magnetization dynamics in magnetic heterostructures induced by magnetic field or electric current. A number of neuron models based on magnetic tunnel junctions (MTJs) have recently been demonstrated: neuron models with simple activation functions [2], more realistic leaky integrate-and-fire (LIF) [3] and biologically plausible FitzHugh-Nagumo [4] and Hodgkin-Huxley [5] spiking neuron models.

However, imitation of bio-realistic spike behavior of MTJ requires its operation in stochastic mode, which is necessary for the reverse switching after spike firing. Such stochasticity of magnetization dynamics is often realized by thermal effects and can lead to random errors.

The dependence of the magnetic permeability of amorphous ferromagnetic (FM) structures on the frequency and amplitude of the exciting alternating current (AC) in a non-magnetic (NM) bus of magnetoimpedance (MI) thin-film structures allows us to implement a simpler approach to mimic the neural functionality without the need of MTJ and stochastic switching of the FM layer [6].

In this work, we propose a Hodgkin-Huxley (HH)-analogue spintronic neuron model based on the AC-excited magnetization dynamics of the FM-insulator-NM-insulator-FM magnetic stack, which exhibit the MI effect under magnetic field H_{DC} aligned parallel/perpendicular (TT/TL) to the easy magnetic anisotropy axis of the FM film (Fig. 1). According to micromagnetic simulation, by adjusting the frequency f_{AC} and the amplitude I_{AC} of the excited current, as well as the magnetic field H_{DC} , it is possible to obtain different shapes of the output voltage and bring the spike activity of the GMI-based HH neuron closer to the biorealistic level (Fig. 2). This work was supported by State Assignment No. FSMR-2023-0003.

- [1] C.H. Marrows, et al., Npj Spintronics, Vol. 2, p. 12 (2024)
- [2] H. Tu, et al., Appl. Phys. Lett., Vol. 122, p. 122402 (2023)
- [3] A. H. Lone, et al., Adv. Elect. Materials, p. 2500091 (2025)
- [4] A. H. Lone, et al., APL Materials, Vol. 5, p. 051119 (2025)
- [5] D. R. Rodrigues, et al., Phys. Rev. Applied, Vol. 19, p. 064010 (2023)
- [6] L. Jamilpanah, et al., Sci. Rep., Vol. 13, p. 8635 (2023)

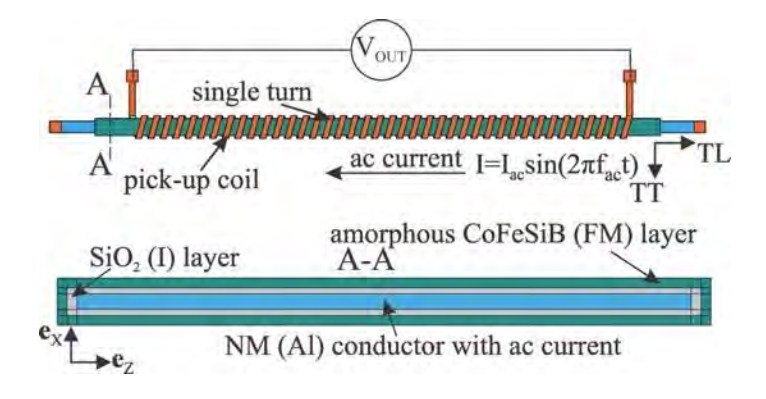


Fig. 1. Sketch of FM-insulator-NM-insulator-FM GMI thin-film structure.

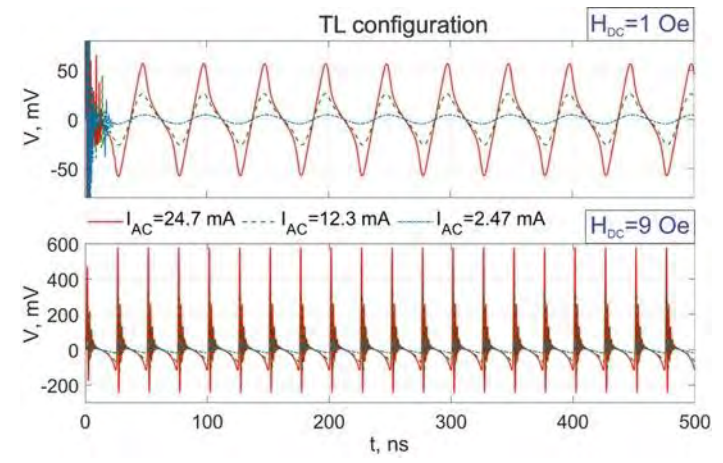


Fig. 2. The output voltage of the GMI structure for different I_{AC} and H_{DC} (f_{AC} =20 MHz).

VP1-06. Integrating Domain Knowledge with Machine Learning for Property Prediction from Chemical Composition

M. Shabir, A. Bashir, F. H. Bhat

Department of Physics, Islamic University of Science and technology, Kashmir, Awantipora, Jammu and Kashmir, India

Inorganic semiconductors are fundamental to modern electronics, optoelectronics, and energy conversion, with their band gap serving as a crucial parameter that dictates their electrical and optical properties [1]. Traditionally, band gap determination relies on experimental methods such as spectroscopy and first-principle calculations, which, while accurate, can be time-consuming and resource-intensive. This study leverages machine learning techniques as an efficient complement to traditional approaches, accelerating the discovery and tailoring of inorganic semiconductors for technological applications. Using an available dataset of inorganic semiconductors [2], domain knowledge is incorporated via the Magpie [3] feature generation tool, which converts chemical formulas into trainable features. To refine the dataset, two feature selection methods – SelectKBest and Recursive Feature Elimination (RFE) are applied, yielding optimal sets of 45 and 13 features, respectively. Several machine learning models, including Decision Tree (DT), Support Vector Machine (SVM), K-Nearest Neighbors (KNN), Random Forest (RF), Extra Trees (ET), and Gradient Boosting (GB), are trained and evaluated using five-fold cross-validation, ensuring robust performance assessment. Among the tested models, Extra Trees achieved the highest accuracy on unseen data, with R² scores of 0.85 and 0.82 for features selected via SelectKBest and RFE, respectively, while Gradient Boosting

^{*} Best Student Presentation Finalist / LB - Late-breaking Poster

followed closely with R² scores of 0.83 and 0.80. Hyperparameter tuning further enhanced performance, particularly improving SVM, which initially lagged behind. By integrating machine learning into band gap prediction, this study contributes to efficient screening and selection of inorganic semiconductors, significantly reducing computational and experimental effort while enhancing material design for targeted electronic and optoelectronic applications.

References:

[1] S. Morab, M. M. Sundaram, and A. Pivrikas, *Coatings*13, 1657 (2023).

[2] Y. Zhuo, A. Mansouri Tehrani, and J. Brgoch, *J. Phys. Chem. Lett.* 9, 1668 (2018).

[3] L. Ward, A. Agrawal, A. Choudhary, and C. Wolverton, *npjComput. Mater.*2, 16028 (2016).

Table 1: Model Performance Summary for R2 Scores on Test Set

Model	R ² Score SelectKBest	R2 Score RFE
Decision Tree (DT)	0.7007	0.5454
Support Vector Machine (SVM)	0.5915	0.5448
k-Nearest Neighbors (KNN)	0.6530	0.6219
Random Forest (RF)	0.8210	0.7943
Extra Trees (ET)	0.8504	0.8219
Gradient Boosting (GB)	0.8313	0.7956

SESSION VP2: FUNDAMENTAL PROPERTIES AND COOPERATIVE PHENOMENA

Chair(s): Y. Wu, *Electrical and Computer Engineering, University of Florida, Gainesville, Florida, United States*Conference Resource Center

VP2-02. Spin Nematic Phase of the Ferromagnetic Dimer System on the Shastry-Sutherland Lattice

T. Sakai^{1, 2}

¹School of Science, University of Hyogo, Kamigori, Hyogo, Japan, ²Institutes for Quantum Science and Technology, SPring-8, Sayo, Hyogo, Japan

The spin nematic order has attracted a lot of interest in the field of magnetism. It is the quadrupole order of spins, which is described by the four spin correlation function and is characterized by the two-magnon bound state. Most previous theoretical works about the spin nematic order were based on the mechanism of the frustration or the biquadratic interaction. Recently the spin nematic liquid realized by the anisotropy was theoretically proposed for several one-dimensional quantum spin systems[1,2]. Thus it would be interesting to consider the possibilty of the anisotropy induced spin nematic phase in two-dimensional systems. In the present work, a spin-1/2 magnetic system with the ferromagnetic and antiferromagnetic interactions on the Shastry-Sutherland lattice is investigated using the numerical diagonalization of finite-size clusters. We introduce the easy-axis coupling anisotropy at the ferromagnetic interaction of this system and study the magnetization process in the external magnetic field along the easy axis. It is found that the two-magnon bound state appears at higher magnetization region, after the spin flop transition. The calculated spin correlation function indicated that the quadrupole (nematic) spin correlation is enhanced in the two-magnon bound phase. Based on the analogy to the previous study on the one-dimensional systems[1,2], the spin nematic order perpendicular to the external field would be expected to appear in this two-magnon bound phase.

[1]T. Sakai, R. Nakanishi, T. Yamada, R. Furuchi, H. Nakano, H. Kaneyasu, K. Okamoto and T. Tonegawa, Phys. Rev. B 106, 064433 (2022)

[2]T. Sakai, R. Furuchi, H. Nakano, K. Okamoto, SciPost Physics Proceedings 11, 011 (2023)

VP2-03. Magnetization Plateau of the S=1 Spin Ladder with Anisotropies

<u>Y. Hamazaki</u>, R. Hasegawa, T. Kawatsu, H. Suzuki, T. Houda, H. Nakano, T. Sakai, K. Okamoto

School of Science, University of Hyogo, Kamigouri, Hyogo, Japan

The magnetization plateau has attracted a lot of interest as a macroscopic quantum phenomenon in the field of magnetism. It was proposed as the spin gap induced by the external magnetic field[1]. The previous magnetization measurement of the organic S=1 spin ladder material[2], abreviated as BIP-TENO, observed a magnetization plateau at 1/4 of the saturation magnetization. According to the rigorous theory[1], this 1/4 plateau can appear only when the ground state has the two-fold degenracy due to the spontaneous translational symmetry breakdown. The spin frustration due to the second or third nearest neighbor interaction was proposed, but the correct origon of the 14 plateau ob BIP-TENO has not been clarified. Recently the numerical diagonalization and the density matrix renormalization group analysis indicated the two competing anisotropies can induce the translational symmetry broken magnetization plateau in the S=1 antiferromagnetic chain[3]. Thus it would be interesting to consider the possibility of the translational symmetry broken magnetization plateau based on such conpeting anisotropies in the S=1 spin ladder system. In the present research we investigate the magnetization process of the S=1 spin ladder with the easy-axis anisotropy at the leg intearction and the easy-plane single ion one at each site. The numerical diagonalization of finite-size clusters and the level spectroscopy analysis indicated that the translational symmetry broken plateau would appear at 1/4 and 3/4 of the saturation magnetization. In addition the translationally symmetric plateau is revealed to appear at the 1/2 magnetization. The phase diagrams for the two anisotropies at 1/4, 1/2, and 3/4 of the saturation magnetization are presented. In addition the magnetization curves for several typical parameters are obtained.

[1]M. Oshikawa, M. Yamanaka and I. Affleck, Phys. Rev. Lett. 78, 1984 (1997).

[2]T. Sakai, N. Okazaki, K. Okamoto, K. Kindo, Y. Narumi, Y. Hosokoshi, K. Kato, K. Inoue, T. Goto, Phsica B 329-333, 1203 (2003).

[3]T. Sakai, K. Okamoto, K. Okunishi, M. Hashimoto, T. Houda, R. Furuchi, H. Nakano, Phys. Rev. B 108, 174435 (2023).

VP2-04. Field-Induced Spin Nematic Liquid of the S=1/2 Kondo Necklace Spin Chain

R. Hasegawa, Y. Hamazaki, T. Kawatsu, H. Suzuki, T. Houda, H. Nakano, K. Okamoto, T. Sakai

School of science, University of Hyogo, Kamigori, Hyogo, Japan

The low-dimensional quantum spin systems exhibits various interesting phenomena. In the one-dimensional quantum antiferromagnets the quasi-long-range order characterized by the power-law decay of the spin correlation function sometimes appears due to strong quantum fluctuations. Such a quasilong-range ordered phase is called the Tomonaga-Luttinger liquid (TLL) phase[1]. The recent theoretical study[2] on the S=1/2 spin ladder system with the anisotropic ferromagnetic rung interaction indicated that the TLL phase where the two-magnon bound state is a quasiparticle would appear in the magnetization process. In this work the conformal field theory approach[3] suggested that the quasilong-range spin nematic order is dominant in the two-magnon TLL phase at higher magnetization. Such a spin nematic liquid was also theoretically predicted in the ferromagnetic and antiferromagnetic bond alternating spin chain[4]. The field-induced spin nematic liquid based on the same mechanism is expected to occur in the S=1/2 Kondo necklace spin chain with the anisotropic ferromagnetic interaction. In the present work we investigate the magnetization process of the S=1/2 Kondo necklace spin chain using the numerical diagonalization of finite-size clusters. As a result it is found that the two-magnon TLL phase would appear in the magnetization process for sufficiently large anisotropy and the quasilong-range spin nematic order dominant region appears in this phase. The phase diagram for the anisotropy and the magnetization is presented.

[1]F. D. M. Haldane, J. Phys. C 14, 2585 (1981).

[2]T. Sakai, R. Nakanishi, T. Yamada, R. Furuchi, H. Nakano, H. Kaneyasu,

K. Okamoto, T. Tonegawa, Phys. Rev. B 106, 064433 (2022).[3]J. L. Cardy, J. Phsy. A 17, L385 (1984).

[4]R. Nakanishi, T. Yamada, R. Furuchi, H. Nakano, H. Kaneyasu, K.

Okamoto, T. Tonegawa and T. Sakai, JPS Conf. Proc. 38, 011155 (2023).

VP2-05. Application of Screened Range-Separated Hybrid Functional to Antiferromagnetic 3*d*-oxides

A. B. Shick^{1, 2}, L. Kronik²

¹Department of Condensed Matter Theory, Institute of Physics, Czech Academy of Sciences, Prague, Czechia, ²Department of Molecular Chemistry and Materials Science, Weizmann Institute of Science, Rehovoth, Israel

A recently developed Wannier-localized, optimally tuned, screened range-separated hybrid (WOT-SRSH) functional [1] is applied to bulk antiferromagnetic insulators. The results are compared to calculations based on well-established empirical hybrid functionals [2,3], as well as to DFT+U [4], self-consistent quasiparticle GW [5], and experiment. It is found that WOT-SRSH provides a good quantitative description for experimental band gaps, spin magnetic moments, photoemission, and optical absorption spectra for selected magnetically ordered transition metal oxides, specifically MnO, NiO, and hematite (Fe₂O₃). This study demonstrates that the WOT-SRSH approach establishes a uniform framework for electronic, magnetic, and optical properties of magnetic insulators and can provide a starting point for subsequent many-body perturbation theory calculations. Partial support by the European Union and the Czech Ministry of Education, Youth and Sports (Project TERAFIT - CZ.02.01.01/00/22_008/0004594) is acknowleged.

- [1] D. Wing et al., Proc. Natl. Acad. Sci. 118, e2104556118 (2021).
- [2] J. P. Perdew, M. Ernzerhof, and K. Burke, J. Chem. Phys. 105, 9982 (1996).
- [3] J. Heyd, G. E. Scuseria, and M. Ernzerhof, J. Chem. Phys. 124.
- 219905 (2006).
- [4] V. I. Anisimov, J. Zaanen, and O. K. Andersen, Phys. Rev. B 44, 943 (1991).
- [5] M. S. Abdallah, and A. Pasquarello, Phys. Rev. B 110, 155105 (2024).

VP2-06. Magnetism of rare earth intermetallic compound Pr₃Te₄: a neutron diffraction study

R. Nirmala¹, G. Jangam², T. A², A. Morozkin³

¹Physics, Indian Institute of Technology Madras, Chennai, India, ²Tata Institute of Fundamental Research, Mumbai, India, ³Moscow Lomonosov State University, Moscow, Russian Federation

While a few members of rare earth chalcogenide family R_3Te_4 (R = rare-earth) with the cubic Th_3P_4 -type structure (space group 1-43d, No. 220, c128) are known as potential thermoelectric materials [1], some of them exhibit fieldinduced magnetic behaviour at low temperatures. The rare earth intermetallic compound Pr₃Te₄ compound has a cubic Th₃P₄-type structure, where the Pr atoms occupy 12a site (3/8, 0, 1/4) and the Te atoms occupy the 16c site and the unit cell dimension indicates contraction when compared with that of La₃Te₄ and Ce₃Te₄ compounds, in accordance with the trivalent state of rare earths. Temperature dependent magnetization data of Pr₃Te₄ compound shows a slope change and a tendency to order ferromagnetically at ~5 K (T_C) [Fig. 1a]. The magnetization value at 5 K in 70 kOe field is about 1.77 μ_B/Pr^{3+} [inset in Fig. 1a]. Neutron powder diffraction experiments were carried out from about 100 K to 1.5 K in zero magnetic field (wavelength l = 2.52 Å). Down to 3 K, Pr₃Te₄ does not show any signature of magnetic order. A slight (112) magnetic reflection is observed at 1.5 K and this may correspond to a collinear ferromagnetic ordering of Pr_3Te_4 (wave vector $K_0 = [0, 0, 0]$), similar to that in Ce₃Te₄ and Nd₃Te₄ compounds [2] [Fig. 1b] The magnetic moment of about $0.61(5) \mu_B/Pr^{3+}$ is obtained at 1.5 K and this is significantly less than that is gotten from the magnetization data. Indeed, it is substantially smaller than the theoretical gJ value of 3.2 µ_B for Pr³⁺. The large Pr-Pr distances of ~ 4.435 Å (while Pr atomic radius is only 1.828 Å) may lead to the incomplete magnetic ordering of Pr-8Pr clusters in Pr₃Te₄ compound. The bulk magnetization behaviour at 5 K is mainly field-induced.

References

- 1. Andrew F. May, Jean-Pierre Fleurial, and G. Jeffrey Snyder, Phys. Rev. B 78 (2008) 125205
- 2. A.V. Morozkin, R. Nirmala, O. Isnard, S.K. Malik, Jinlei Yao, Yu. Mozharivskyj and S.A. Granovsky, Intermetallics 19 (2011) 1794

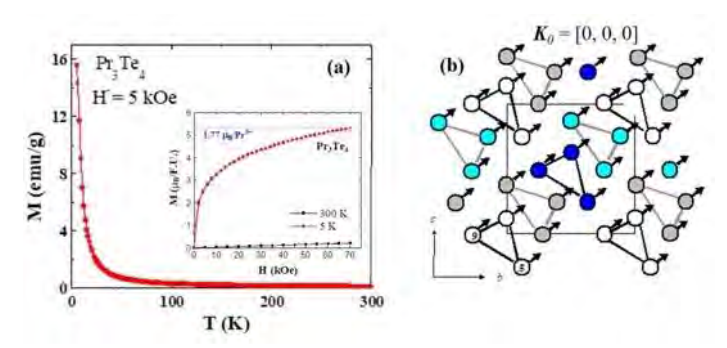


Figure 1 (a) Magnetization vs temperature of Pr_3Te_4 in applied field of 5 kOe. Inset: Magnetization vs field at 5 K. (b) Magnetic structure of Pr_3Te_4 at 1.5 K.

VP2-07. Low symmetry inter-orbital pairing states in Sr₂RuO₄ from DFT+DMFT

C. Moon

Korea Research Institute of Standards and Science, Daejeon, Korea (the Republic of)

We investigate the superconducting pairing symmetries in Sr₂RuO₄ by solving the frequency-dependent linearized Eliashberg equation within the DFT+DMFT framework. It is found that the 'SPOT' classification of the gap symmetry does not apply to inter-orbital pairing solutions in general, since the inter-orbital pairing interaction is not invariant under the orbital or frequency exchange. In the imaginary frequency domain, an inter-orbital paring interaction component transforms to its complex conjugate under the frequency exchange, so that its gap solution components with opposite frequency signs are also the complex conjugate to each other. These considerations lead to the conclusion that the gap solutions are either purely real or imaginary in the real frequency domain, each preserving the time reversal symmetry. Meanwhile, we find a pair of interorbital gap solutions one of which has positive imaginary frequency components only and the other has negative frequency components only in the numerical solutions of Sr₂RuO₄. We show that this unique property translates to the gap functions having real and imaginary components both non-zero in the real frequency domain, implying the inherently time-reversal symmetry broken pairing state. We arque that this unique property is associated with the Hundness of the material

SESSION VP3: HARD MAGNETS AND FUNCTIONAL MAGNETIC MATERIALS

Chair(s): T. Gottschall, *Dresden High Magnetic Field Laboratory, Dresden, Germany*Conference Resource Center

VP3-01. Effect of Solution Temperature on the Microstructures and Magnetic Properties of Fe-Rich Sm-Co-Fe-Cu-Zr Permanent Magnets

J. Yang¹, D. Zhang², H. Li¹, H. Sun¹, Z. Wang¹
¹Anyang Institute of Technology, Anyang, Henan,
China, ²Beijing University of Technology, Beijing, China

Fe-rich Sm-Co-Fe-Cu-Zr magnets are preferred for high-

temperature applications due to their excellent magnetic properties, high Curie temperature, good temperature stability, and corrosion resistance. They are widely used in aerospace, military defense, rail transportation, highefficiency shafts. Solution treatment is crucial for magnet homogenization. This study, the 2:17-type Sm-Co permanent material was homogenized by controlling the solution temperature, and the microstructure and magnetic properties were systematically investigated. The magnets were prepared using the powder metallurgy method. The sintering temperature was 1489K, and the solution temperatures (Ts) were 1433-1453K. Fig. 1 shows the BSE images and element distribution of Sm, Fe, Cu, and Zr in the aged magnets. At lower solution temperatures, Ts=1438K [Fig. 1(a)], and 1443K [Fig. 1(b)], Fe and Cu distributions were inhomogeneous, with Fe depletion and Cu enrichment in some areas. At Ts=1448K [Fig. 1(c)], the elements were uniformly distributed, as confirmed by WDS analysis. However, at Ts=1453K [Fig. 1(d)], contrast differences increased, grain boundaries became discontinuous, and Fe depletion/Cu enrichment and white oxide contrast phases appeared. Adjusting the solution temperature can homogenize element distribution, benefiting magnetic performance. Fig. 2 presents the demagnetization curves for magnets with Ts ranging from 11433K to 1453K. As Ts increased, remanence (Br) remained around 11.53-11.56kG. coercivity (Hcj), squareness (Sr), and maximum energy product [(BH)max] first increased and then decreased, peaking at Ts=1448K (Br=11.56kG, Hcj=23.35kOe, (BH)max=31.15MGOe, Hk/Hcj=51.4%). The coercivity was significantly affected by Ts. From Fig. 1 and 2, solution treatment is key for homogenizing Fe-rich Sm-Co-Fe-Cu-Zr permanent magnets. An appropriate solution temperature ensures a uniform microstructure across scales, leading to superior magnetic

properties. Subsequently, we will further observe the microstructure at the nanoscale.

[1] J. Cao, T. L. Zhang and J. H. Liu. Journal of Materials Science & Technology., VOL 85, P56-61(2021). [2] J. J. Yang, D. T. Zang and H. G. Zhang. Acta Materialia., VOL251, No.118901(2023).

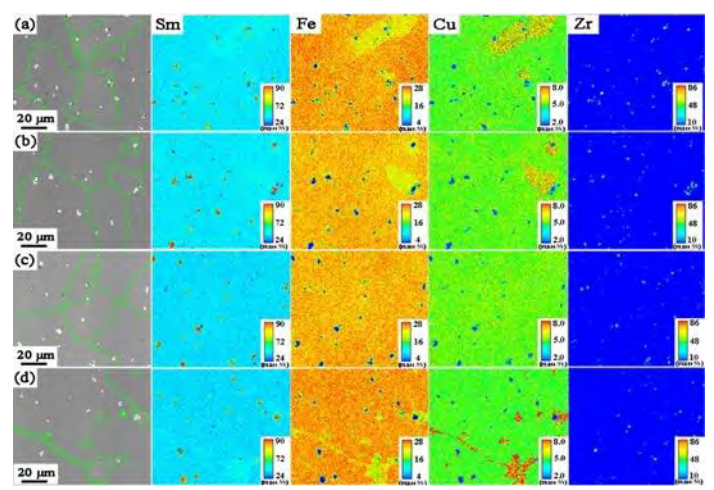


Fig. 1 BSE images and corresponding Sm, Fe, Cu Zr mapping of magnets after aging. (a) T_s =1438K, (b) T_s =1443K, (c) T_s =1448K, (d) T_s =1453K

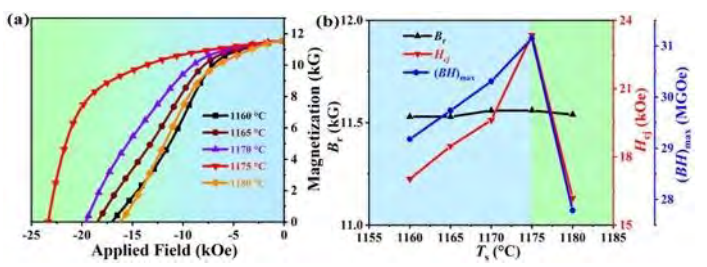


Fig. 2 Demagnetizing curves of magnets with different solution temperatures

VP3-02. Hard magnetic properties of Sm-Fe-Ga-C melt-spun ribbons with SmFe $_5$ phase

<u>T. Saito</u>¹, D. Nishio-Hamane²
¹Chiba Institute of Technology, Narashino, Japan, ²University of Tokyo, Kashiwa, Japan

It is known that the $Sm_2Fe_{17}N_3$ phase possesses a high saturation magnetization with a large anisotropy field and a high Curie temperature [1]. Many fundamental investigations have been made to produce $Sm_2Fe_{17}N_3$ magnets [2-5], but the development of high-performance $Sm_2Fe_{17}N_3$ magnets is still ongoing. Thus,

another Sm-Fe phase, the SmFe₅ phase, was investigated. We aim to enhance the magnetic properties of the SmFe₅ phase by incorporating Ga and C. In this study, we discuss the structures and magnetic properties of SmFe₅, SmFe₅C, SmFe₅Ga, and SmFe₅GaC alloys produced by meltspinning and subsequent annealing. Sm-Fe-Ga-C melt-spun ribbons were prepared by melt-spinning under an argon atmosphere. The Sm-Fe-Ga-C melt-spun ribbons were subsequently annealed under an argon atmosphere at 973 – 1173 K. The specimens were examined by an X-ray diffraction (XRD) system, transmission electron microscope (TEM), and vibrating sample magnetometer (VSM). The Sm-Fe-Ga-C melt-spun ribbons did not show high coercivity in the as-quenched state. After annealing, the SmFe₅and SmFe₅C melt-spun ribbons exhibited low coercivity values regardless of the annealing temperature. On the other hand, the coercivity of the SmFe₅Ga melt-spun ribbon was slightly improved, and that of the SmFe₅GaC melt-spun ribbon was greatly enhanced by annealing. The SmFe₅Ga melt-spun ribbon with the Sm(Fe,Ga)₅ phase showed a coercivity of 1.12 kOe, and the SmFe₅GaC melt-spun ribbon with the Sm(Fe,Ga)₅ phase exhibited a high coercivity of 12.2 kOe when annealed at 1073 K.

[1] J. M. D. Coey and H. Sun, J. Magn. Magn. Mater. 87, L251 (1990). [2] K. Schnitzke, L. Schultz, J. Wecker, and M. Katter, Appl. Phys. Lett. 57, 2853 (1990). [3] J. P. Liu, K. Bakker, P. R. de Boer, T. H. Jacobs, D. B. de Mooij, and K. H. J. Buschow, J. Less-Common Met. 170,109 (1991). [4] S. Miraglia, J. L. Soubeyroux, C. Kolbeck, O. Isnard, and D. Fruchrat, J. Less-Common Met. 171, 51 (1991). [5] T. Iriyama, K. Kobayashi, and H. Imai, IEEE Trans. Magn. 28, 2326 (1992).

^{*} Best Student Presentation Finalist / LB – Late-breaking Poster

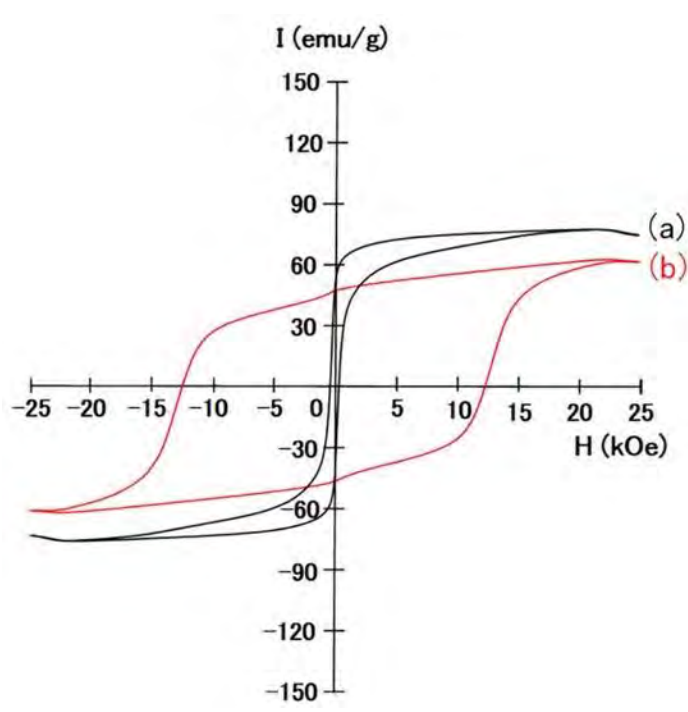


Fig.1 Hysteresis loops of the (a) as-quenched and (b) annealed SmFe₅GaC melt-spun ribbons.

VP3-03. (Nd,Ce)-Fe-B core-shell magnet simulation using mumax3 software

<u>C. Li</u>, J. Zuo, Y. Li, M. Zhang School of Science, Inner Mongolia University of Science and Technology, Baotou, China

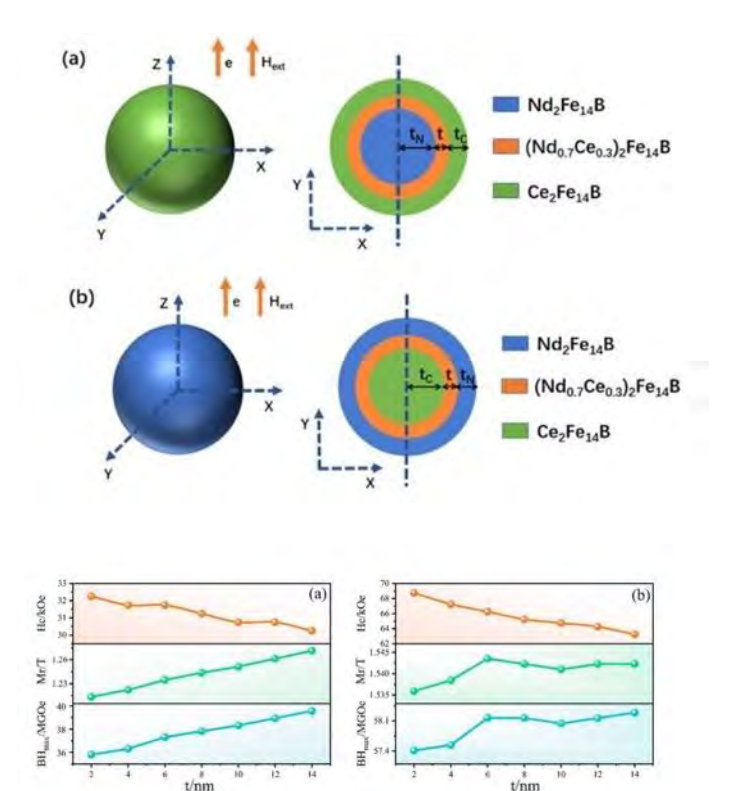
As the demanding of the Nd-Fe-B based permanent materials is further rising, huge consumption of Nd, Pr and Dy becomes a great concern which would result in the imbalance utilization of rare earth resource. Developing technologies of using high abundance rare earth elements such as Ce in permanent magnetic materials has been proposed. This study employs the micromagnetic method by using Mumax3 software to simulate a three-layer nested core-shell structure (Fig. 1). The thickness of the Nd2Fe14B layer and Ce2Fe14B layer were denoted as tN and tC respectively, which were fixed at 10 nm; the thickness of the transition layer set as a variable t. the influence of transition layer thickness variation on the magnetic properties of the magnet is investigated.

The total demagnetization energy ($E_{\rm d}$) of both model rose as the thickness of the transition layer gradually increases. For the magnetic properties, for model a, the remanence and

maximum magnetic energy product were both increased while the coercivity was decreased; for model b, the remanence and maximum magnetic energy product were firstly increased and then decreased peaking at t=6nm, the coercivity exhibited the same variation as the model a. Comparing the calculation results of two models, at the same grain size and Neodymium content, model b exhibited better coercivity and can achieve superior magnetic properties.

The magnetic moment changes of two models under different magnetic fields were also studied

[1]Zhu M,Li W,Wang J, Zheng L, Li Y, Zhang K, Feng H, Liu T.Influence of Ce Content on the Rectangularity of Demagnetization Curves and Magnetic Properties of Re-Fe-B Magnets Sintered by Double Main Phase Alloy Method[J].IEEE Transactions on Magnetics,2014,50(1):1-4. [2]Li L,Dong S,Chen H, Jiang R, Li D, Han R, Zhou D, Zhu M, Li W, Sun W.Micromagnetic simulations of reversal magnetization in cerium-containing magnets[J]. Chinese Physics B. 2019 Mar 1;28(3):037502.



^{*} Best Student Presentation Finalist / LB – Late-breaking Poster

VP3-05. Influence of ytterbium-doping on the structural, magnetic and dielectric properties of gallium ferrite nanoparticles

T. Han, <u>C. Lai</u>, Y. Chen Department of Applied Physics, National University of Kaohsiung, Kaohsiung, Taiwan

Gallium ferrite, GaFeO₃ (GFO), has ferrimagnetic and piezoelectric orderings and has been intensively studied recently for its potential application as a magnetoelectric ferrimagnet [1]. Site-disorder in bulk GFO is reported to be induced by adopting different preparation methods and conditions, which are shown to affect the magnetic properties significantly [1-3]. Moreover, the physical properties of GFO at reduced grain sizes remain underexplored due to the challenges associated with their synthesis with a proper control over the crystalline phase. However, the origin of the replacement of Ga by a larger trivalent ion on the correlation between the site-disorder and magnetism in the nanosized GFO system has not yet been completely established. In this work, Ga₁₋ $_{x}Yb_{x}FeO_{3}$ (GYFx) (x = 0, 0.05, 0.01) nanoparticles were prepared by a sol-qel method to systematically study the effect of Yb-doping on their structural, magnetic, and dielectric properties. The structural parameters of the samples were determined using the GSAS program based on the Rietveld refinement methodology. The cation distribution across the four crystallographic sites in GFO lattice was determined. The integration of ytterbium into the lattice results in alterations in cation distribution, inducing distortions in the bond lengths and angles of tetrahedral and octahedral structure. In general, the distortions of octahedrons tend to increase with Yb-doping. In addition, the magnetic transition temperature increased with increasing Yb-content in GFO. The coercivity of the doped samples increased due to decreasing the grain size. Moreover, the dielectric characterization also indicates that the sample of Ga_{0.95}Yb_{0.05}FeO₃ exhibits the largest dielectric constant. Furthermore, the dielectric constant of each GYFx sample is strongly perturbed by the external magnetic field. It is to be noted that the value of magnetodielectric (MD) increases in the Yb-doped samples for different applied magnetic fields. Our studies show that despite the increasing of magnetic transition temperature, coercivity and dielectric permittivity can be optimized in GYFx, which may help further optimization of nanosized GFO.

[1]. T. Arima, D. Higashiyama, Y. Kaneko, J. P. He, T. Goto, S. Miyasaka, T. Kimura, K. Oikawa, T. Kamiyama, R. Kumai and

Y. Tokura, Phys. Rev. B 70, 064426 (2004).
[2]. M. B. Mohamed, A. Senyshyn, H. Ehrenberg and H. Fuess, J. Alloys Compd. 492, L20 (2010).

[3]. T. C. Han, Y. C. Lee and Y. T. Chu, Appl. Phys. Lett. 105, 212407 (2014).

VP3-06. Influence of device structure on magnetoelectric coupling in laminate composites of textured Fe-Ga thin sheet and PZT

J. Liu^{1,2}, Z. He^{1,2}, S. Hu^{1,2}, Y. Sha³, L. Chen^{1,2}, L. Zuo³
¹School of Materials Science and Engineering, Shenyang
University of Technology, Shenyang, China, ²Shenyang Key
Laboratory of Advanced Structural Materials and Applications,
Shenyang University of Technology, Shenyang, China, ³Key
Laboratory for Anisotropy and Texture of Materials (Ministry of Education), Northeastern University, Shenyang, China

Magnetoelectric (ME) coupling devices using magnetostrictive Fe-Ga alloy sheets and piezoelectric materials have been used in magneto-mechanical-electrical (MME) sensors. The ME response can be tailored by the geometry and phase fractions of the constituent layers. In this paper, seven MME generators with different geometries were prepared using laminated Fe-Ga/PZT sandwich structures. The effect of geometries on the ME responses was investigated by the comparison of the output voltage and the ME coupling coefficients of the ME-coupled device. The ME-coupled device with Fe-Ga/PZT/Fe-Ga structure (the lower layer is a short Fe-Ga thin sheet) exhibits excellent output performance with an output voltage of 2.88 V and the ME coupling coefficient of 47.95 V/(cm×Oe) at a resonant frequency of 42 Hz.

Fe-Ga alloy sheets with a thickness of 0.3 mm are obtained by hot rolling and cold rolling. Isothermal annealing was performed on Fe₈₁Ga₁₉ alloy sheets at 950°C for 120 minutes to obtain nearly Goss-oriented single-crystal Fe-Ga sheets. The saturation magnetostriction of Fe-Ga alloy sheets reaches 190 mm with a saturation magnetic field of 300 Oe. Figure 1 illustrates the schematic diagram of seven ME generators. Figure 2 compares the electrical output of the ME-coupled devices. Figure 2(a) illustrates the ratio of induced voltage to actual voltage for device structure A. The induced voltage due to the coil varies with frequency and is $0.057 \pm 0.001 \text{ V}$ in the range of 0 to 50 Hz. The output voltage of the device increases gradually with increasing frequency at a resonant frequency of 49 Hz, the maximum total output voltage is 0.191 V, while the maximum actual output voltage is 0.135 V. Based on the analysis of seven

sets of comparison experiments, the ME coupled device with device structure g has the largest output voltage and ME conversion factor of 2.88 V and 47.95 V/(cm×Oe), respectively. This phenomenon has been confirmed by the simulation of stress distribution on the piezoelectric layer of the ME-coupled device.

[1] G. T. Hwang, V. Annapureddy, J. H. Han, D. J. Joe, C. Baek, D. Y. Park, D. H. Kim, J. H. Park, C. K. Jeong, K. Park, J. J. Choi, D. K. Kim, J. Ryu and K. J. Lee, Adv. Energy Mater. 6, 1600237 (2016).

[2] S. Dong, J. Zhai, N. Wang, F. Bai, J. Li, D. Viehland and T. A. Lograsso, Appl. Phys. Lett. 87, 022504 (2005).

[3] S. Dong, J. Zhai, J. Li and D. Viehland, Appl. Phys. Lett. 89, 252904 (2006).

[4] S. Dong, J. Zhai, F. Bai, J. Li, D. Viehland and T. A. Lograsso, Appl. Phys. Lett. 97, 103902 (2005)

[5] T. Fitchorov, Y. Chen, B. Hu, S. M. Gillette, A. Geiler, C. Vittoria and V. G. Harris, J. Appl. Phys. 110, 1239156 (2011).

[6] H. Song, M. Peddigari, A. Kumar, S. Lee, D. Kim, N. Park, J. Li, D. R. Patil and J. Ryu, J. Alloys Compd. 834, 155124 (2020).

[7] H. Palneedi, S. M. Na, G. T. Hwang, M. Peddigari, K. W. Shin, K. H. Kim, K. H. Kim and J. Ryu, J. Alloys Compd. 765, 764 (2018).

[8] V. Annapureddy, S. M. Na, G. T.Hwang, M. G. Kang, R. Sriramdas, H. Palneedi, W. H. Yoon, B. D. Hahn, J. W. Kim, C. W. Ahn, D. S. Park, J. J. Choi, D. Y. Jeong, A. B. Flatau, M. Peddigari, S. Priya, K. H. Kim and J. Ryu, Energy Environ. Sci. 11, 818 (2018).

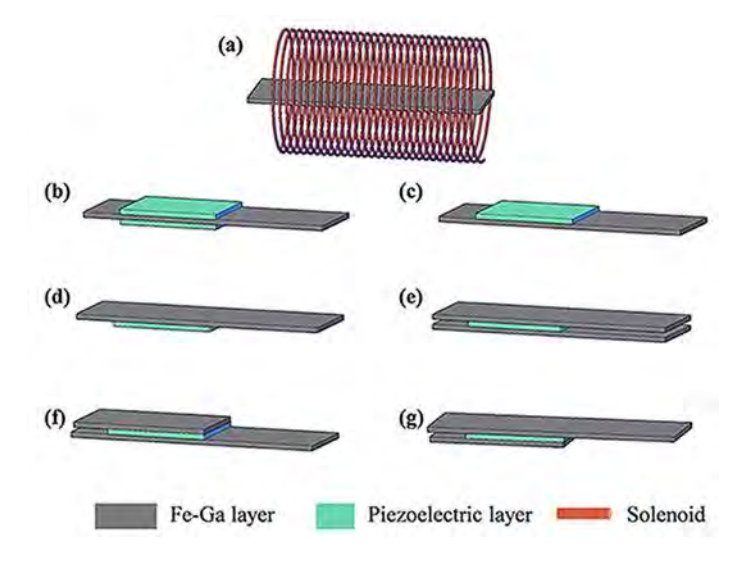


Fig. 1. Schematic diagram of (a~g) MME generator

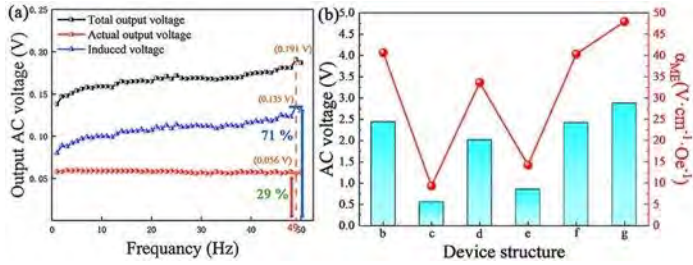


Fig. 2. Output AC voltage and ME coupling coefficient of devices with different structures, (a)structure a, (b)structure (b~q)

VP3-08. Structural, magnetic and electrical transport properties of YMnAl

P. Kharel, M. Anas

Chemistry, Biochemistry and Physics, South Dakota State University, Brookings, South Dakota, United States

The AB₂ type Laves phase materials can crystallize in different structural forms, including the hexagonal C14 and C36 phases, as well as the cubic C15 phase. These compounds often exhibit spin-glassy behavior and magnetic properties that are governed by magnetic exchange interactions within the unit cell. In our study, we investigated one such material, YMnAl, which crystallizes in the MqCu₂ type cubic structure (space group Fd-3m). The sample was synthesized using arc-melting followed by annealing. In this compound, Mn is the only magnetic atom present in the unit cell. The refined lattice parameter is a = 7.816(1) Å. The Y, Mn, and Al atoms occupy the Wyckoff positions 8b, 16c, and 16c, respectively. YMnAl exhibits antiferromagnetic ordering with a Néel temperature of approximately 38 K. Above this temperature, the temperature dependence of magnetization shows a deviation from Curie-Weiss behavior, indicating non-linear magnetic susceptibility. In the high-temperature linear region, the effective magnetic moment is found to be 6.06 μ_B/f.u., and the Curie-Weiss temperature is -79 K, consistent with antiferromagnetic interactions. Isothermal magnetization measurements below the Néel temperature do not show saturation up to 9 T, with a maximum magnetization of 0.09 µ_B/f.u. In addition to magnetic characterization, we will discuss the electrical transport properties of YMnAl, which provide insights into the theoretically proposed altermagnetic behavior in this compound.

This work is supported by the U.S. Department of Energy (DOE) Established Program to Stimulate Competitive Research (EPSCoR) grant no. DE-SC0024284.

VP3-09. Carbon-Driven Enhancement of Magnetic Response in Pyrolyzed Copper-Porphyrin Nanocomposites

<u>S. Figueroa</u>, V. Pena Perez, F. Iglesias, A. Khodagulyan, O. Bernal, A. N. Kocharian

Physics and Astronomy, California State University Los Angeles, Los Angeles, California, United States

The magnetic properties of carbon-based nanocomposites synthesized by pyrolyzing metal-organic complexes containing copper and porphyrin ligands are conducted. Specifically, Copper(II) Phthalocyanine (CuPc), Copper(II) Tetraphenylporphyrin (CuTPP), and control ligands (Pc and TPP) were incorporated into a carbon matrix by pyrolysis under inert atmosphere at temperatures up to 900 °C. Magnetic characteristics of nanocomposites were measured using VSM at 300 K. Resulting magnetization vs H and T measurements reveal that increasing carbon content through dilution of the copper-containing complex—results in a marked enhancement of magnetization per gram of copper in both CuTPP and CuPc samples. This effect is especially pronounced in 0.5-2 wt% CuTPP and CuPc nanocomposites, which exhibit clear ferromagnetic hysteresis, whereas undiluted or pure metal-organic complexes show only weak magnetic responses [1]. Normalization by Cu mass highlights the significant role of the carbon (C) matrix in mediating magnetic interactions, possibly through improved nanoparticle dispersion, size confinement, or carbon-induced magnetic ordering. Control experiments using Pc and TPP without copper show predominantly diamagnetic or linear paramagnetic behavior, underscoring the role of Cu and C synergy in driving ferromagnetic behavior. These findings, shown in Fig. 1, suggest that increasing the relative carbon content during pyrolysis not only dilutes the metal component but actively enhances the magnetic response of copper nanoparticles embedded in the C matrix. These results provide a path toward tunable carbon-metal nanocomposites consisting also of non-magnetic elements such as Pd and Zn, and compounds with functionalized surfaces within the range of 0.1-20 nm with potential applications in spintronics, magnetic data storage, and biomedical technologies. Ongoing work includes HR-STEM, SEM, XRD, and FTIR analyses to correlate structural, and chemical changes with the observed magnetic behavior.

This work is supported by grants from the NSF, Catsus Grant No. HRD-1547723 and No. HRD-2112554..

[1] A. Manukyan, H. Gyulasaryan, A. Kocharian, et al., JMMM, 488 165336 (2019).

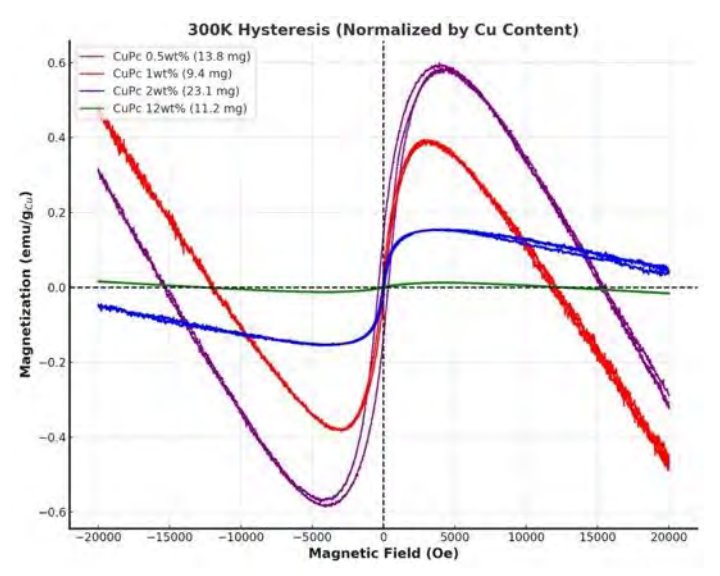


Fig. 1 Room temperature magnetization versus H in CuPc series with different weight percentage of copper of Cu_m/C (m = 0.5, 1, 2, and 12 wt%).

VP3-10. Characterization of Magnetic Core-shell Nanoparticles in Different Carbon Matrices under Annealing by Oxygen and Nitrogen

V. Pena Perez, S. Figueroa, F. Iglesias, A. Khodagulyan, O. Bernal, <u>A. N. Kocharian</u>

Physics and Astronomy, California State University Los Angeles, Los Angeles, California, United States

Metallic and organometallic nanoparticles exhibit intriguing size- and morphology-dependent magnetic properties that differ markedly from their bulk counterparts. Here, we report a detailed synthesis and characterization of magnetic iron (Fe), nickel (Ni), and cobalt (Co) nanoparticles and non-magnetic zinc and copper (Zn, Cu), embedded in different carbon matrices such as phthalocyanine (Pc), tetrakis(4-carboxyphenyl)porphyrin (TCPP) and tetrakis(4-carboxyphenyl)porphyrin (TPP). Using powder X-ray diffraction (PXRD), scanning electron microscopy (SEM), high-resolution transmission electron microscopy (HR-TEM), and Raman spectroscopy, we systematically investigate how precursor composition, annealing conditions, and nanostructure formation impact the resulting magnetic

behaviors. We introduce a novel algorithm for morphological analysis that identifies crystallinity and amorphous content at the nanoscale with enhanced accuracy. Hysteresis measurements at low temperatures reveal that iron-based compounds—particularly iron phthalocyanine (FePc) and iron tetrakis(4carboxyphenyl)porphyrin (FeTCPP)—exhibit notable saturation magnetization and stronger coercivity, respectively, whereas other precursors (e.g., Cu tetraphenylporphyrin, CuTPP) show diamagnetic responses. These changes in behaviors underscore the importance of understanding how phase composition (e.g., metallic cores, graphite, or iron carbide phases) correlates with magnetic characteristics of core-shell nanoparticles [1]. Our findings highlight the feasibility of optimizing characteristics of carbon matrixwith sp2-sp3 hybridization under annealing, magnetic and nonmagnetic metal nanocomposites for targeted applications in biomedicine such as magnetic hyperthermia or drug delivery. The developed advanced image-analysis algorithm offers a robust framework for future studies seeking to tailor nanoparticle size, morphology, and magnetic properties through controlled synthesis and post-annealing processes.

This work is supported by grants from NSF, Catsus Grant No. HRD-1547723 and No. HRD-2112554. [1] V. P.Perez, C. R. Gonzalez, E. Villegas, et al., AIP Advances 15, 035226 (2025).

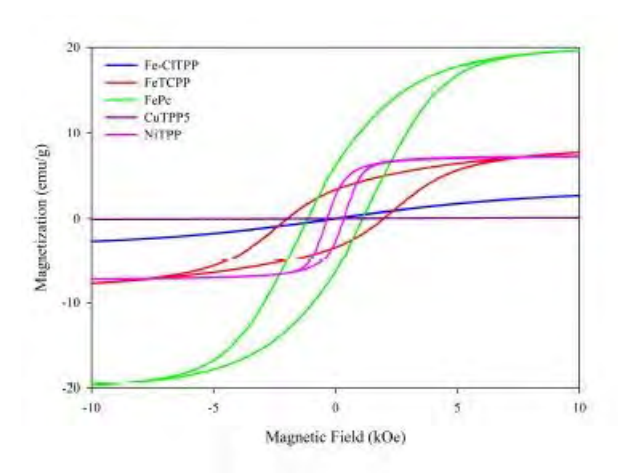


Fig. 1 Magnetic hysteresis loops at T=10 K for Fe-CITPP, FeTCPP, FePc, CuTPP5, and NiTPP nanoparticles synthesized by pyrolysis at 900 C for 60 minutes.

SESSION VP4: MAGNETIC SENSORS, HIGH FREQUENCY **DEVICES. AND POWER ELECTRONICS II**

Co-Chair(s): S. Ajia, Department of Electrical Engineering, Tohoku University, Sendai, Miyagi, Japan and K. Srinivasan, *Electrical and Computer Engineering*, *Boise State* University, Boise, Idaho, United States Conference Resource Center

VP4-01. Measurement of added mass of a spherical model in water using Magnetic Suspension and Balance System

N. Riho, H. Fujiwara

Mechanical engineering, National Defense Academy, Yokosuka, Kanagawa, Japan

In conventional wind tunnel testing, scaled aircraft models are supported by struts, which interfere with accurate measurement of aerodynamic forces. To address this, a Magnetic Suspension and Balance System (MSBS) was developed to levitate models without physical supports using magnetic force. While MSBS has been applied extensively in airflow environments, its use in liquids remains limited due to the difficulty of magnetic levitation under high-density conditions. This study explores the measurement of added mass in water using a MSBS by exciting the model using electromagnetic forces rather than relying on fluid flow. A spherical DURACON® model embedded with a permanent magnet was levitated in water using the MSBS consisted of a coil, a current controller, a permanent magnet, a control computer, and a laser displacement sensor. The model levitated in water using the MSBS is shown in Fig. 1. The model's vertical position was detected by the sensor and stabilized via feedback control. The system was modeled as a single-degree-of-freedom spring-mass-damper system. The added mass (m*) was calculated from the natural frequency (fn), mass (m), and spring constant (k), via fn = $(1/2\pi)^*$ sgrt(k/(m+m*)). Theoretical added mass from a reference book is (m* = 0.5 * density * Volume). The experimentally obtained added mass had an error of 0.82%. This confirms that the MSBS method enables accurate added mass estimation without fluid flow. Future work will examine models of various sizes and shapes, including those with unknown theoretical values, to further validate applicability.

The Japan Society of Mechanical Engineers, JSME Mechanical Engineers' Handbook., pp. 123 (1987)



Fig. 1

VP4-02. Flyback Converter Design for Satellite Data Server Auxiliary Power Systems

Z. Lin, K. Zheng, <u>T. Zhang</u>, Y. Zhuang, Y. Zhang College of Electrical Engineering and Automation, Fuzhou University, Fuzhou, Fujian, China

Satellite data server auxiliary power supply design plays a critical role in modern data-driven applications. It serves not only as the "lifeline" for stable system operation but also as a key foundation ensuring data integrity, system reliability, and mission success. Designing a satellite data server auxiliary power supply demands extreme miniaturization to maximize power output within minimal volume, ensuring system reliability and margin. Challenges include stringent space constraints, sufficient power delivery, and high efficiency to minimize heat. Traditional linear supplies, while stable and low-ripple, are too bulky due to powerfrequency transformers, making them unsuitable. Switching supplies, offering small size, low weight, and reduced dissipation, are essential. Comparing types, forward converters suit medium-high power but have complex peripherals, output filter inductors, larger volume, and higher cost [1]. Consequently, the flyback converter, with its

simpler structure and lower cost [2], is the preferred topology for this satellite application.

This design employs a flyback converter to achieve high power density and miniaturization [3]. To further minimize volume within the confined space environment, it utilizes high-voltage MOSFETs and replaces the conventional wirewound transformer with a planar transformer structure. This maximizes power density in an extremely compact footprint. Careful design of the winding distribution across different PCB layers enhances inter-layer isolation characteristics.

[1] M. A. K. A. Biabani, "Simulation, mathematical calculation and comparison of power factor and efficiency for forward, fly back and proposed forward-flyback converter," 2016 International Conference on Electrical, Electronics, and Optimization Techniques (ICEEOT), Chennai, India, pp.1583-1589, (2016).

[2] A. Bose and P. C. Sekhar, "Flyback Converters for Electric Vehicle Applications- A Review," 2025 3rd IEEE International Conference on Industrial Electronics: Developments & Applications (ICIDeA), Bhubaneswar, India, pp. 1-6, (2025).
[3] N. Coruh, S. Urgun and T. Erfidan, "Design and implementation of flyback converters," 2010 5th IEEE Conference on Industrial Electronics and Applications, Taichung, Taiwan, pp. 1189-1193, (2010).

VP4-03. Analysis and Design of a Dual-Output Wireless Power Transfer System

J. Wang¹, D. Ahn², C. Liu¹, <u>H. Xie</u>¹, X. Mao¹, Y. Zhang¹
¹College of Electrical Engineering and Automation, Fuzhou University, Fuzhou, China, ²Department of Electrical Engineering, Incheon National University, Incheon, Korea (the Republic of)

By leveraging magnetic coupling within electromagnetic fields, Wireless power transfer (WPT) systems facilitate efficient and convenient power transfer across short to medium distances, supporting a wide range of applications, including consumer electronics, biomedical implant and electric vehicles. To meet the power supply needs of load devices requiring different types of outputs, this study introduces a WPT system that features a single-input multiple-output (SIMO) configuration. The circuit topology and magnetic coupler structure of the proposed dual-type constant output WPT system are shown in Fig. 1. This system adopts a single transmitting coil and receiving coil setup, thereby preventing additional cross-coupling interference between the coils. Furthermore, the receiver

only contains a compensation inductor and capacitor, which ensures both the lightweight and cost-effectiveness. To thoroughly validate the performance of the proposed system, a simulink platform is established to analyze waveform characteristics. Fig. 2 presents both the circuit simulation waveforms and efficiency testing results. Specifically, Figs. 2(a), (b), and (c) display the simulated waveforms of $U_{\rm l}$, $I_{\rm l}$, $I_{\rm B1}$, and $U_{\rm B2}$ under zero-phase-angle (ZPA) conditions when $R_{\rm B1}$ and $R_{\rm B2}$ are set to (a) 10 Ω , 25 Ω , (b) 15 Ω , 50 Ω , and (c) 20 Ω , 75 Ω . The fact that $I_{\rm B1}$ and $U_{\rm B2}$ remain essentially unchanged under different load conditions confirms that the proposed system can simultaneously provide both CC and CV characteristics. Moreover, $U_{\rm l}$ and $I_{\rm l}$ are basically in phase, which validates

Moreover, U_1 and I_1 are basically in phase, which validates that the system has achieved ZPA operation. The simulated DC-DC efficiency of the proposed SIMO system is shown in Fig. 2(d). The system demonstrates a relatively high overall efficiency, with a peak value of 92.5%.

R. Xie *et al.*, "A Strongly Coupled Vehicle-to-Vehicle Wireless Charging System for Emergency Charging Purposes With Constant-Current and Constant-Voltage Charging Capabilities," *IEEE Transactions on Power Electronics*, vol. 39, no. 4, pp. 3985-3989, (2024)

R. Xie *et al.*, "An Interoperable Wireless Power Transmitter for Unipolar and Bipolar Receiving Coils Based on Three-Switch Dual-Output Inverter," *IEEE Transactions on Power Electronics*, vol. 39, no. 2, pp. 1985-1989, (2024)

Y. Zhang *et al.*, "An Interoperable Dynamic Wireless Charging System With Stable Output Based on a Self-Adaptive Two-Pole Receiver," *IEEE Transactions on Power Electronics*, vol. 39, no. 10, pp. 11943-11947, (2024)

W. Pan *et al.*,"An Interoperable Electric Vehicle Wireless Charging System Based on Mutually Spliced Double-D Coil," *IEEE Transactions on Power Electronics*, vol. 39, no. 3, pp. 3864-3872, (2024)

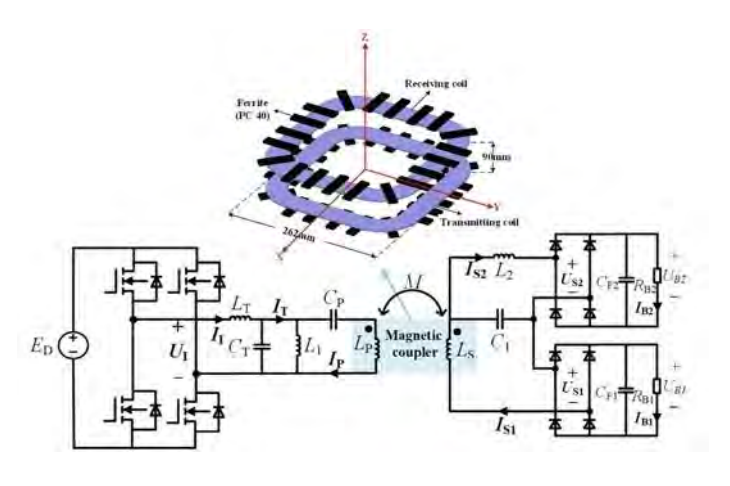


Fig. 1. Circuit topology and magnetic coupler structure of the proposed dual-type constant output WPT system.

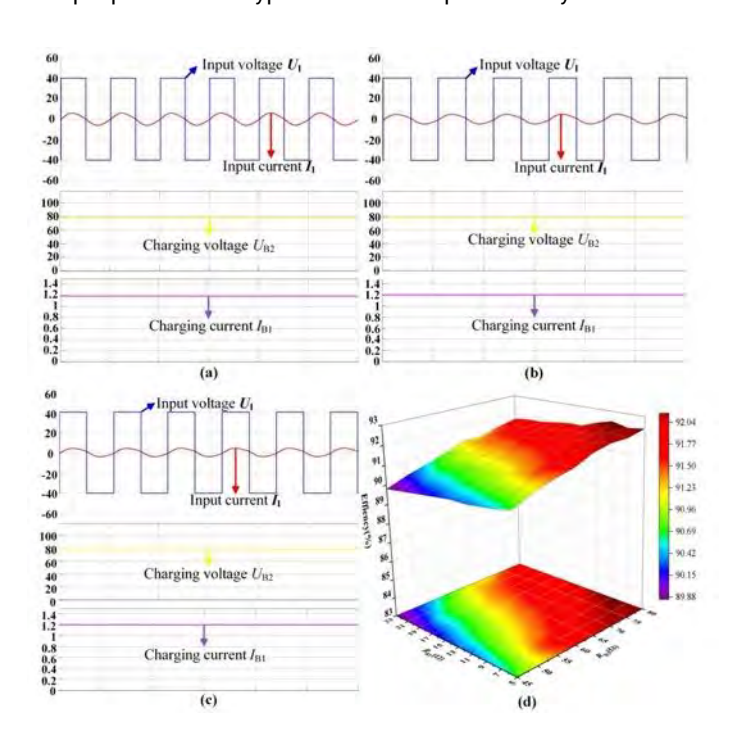


Fig. 2. Simulink waveforms of $U_{\rm l}$, $I_{\rm l}$, $I_{\rm B1}$, and $U_{\rm B2}$ when $R_{\rm B1}$ and $R_{\rm B2}$ are set to (a) 10 Ω , 25 Ω , (b) 15 Ω , 50 Ω , and (c) 20 Ω , 75 Ω . (d) DC-DC efficiency.

499

VP4-04. Electromagnetic Shielding Analysis of Canned Magnetic Bearings

H. Jianq^{1, 2}, Z. Su^{1, 2}, Y. Wei^{1, 2}

¹Naval University of Engineering, Wuhan, Hubei, China, ²East Lake Laboratory, Wuhan, Hubei, China

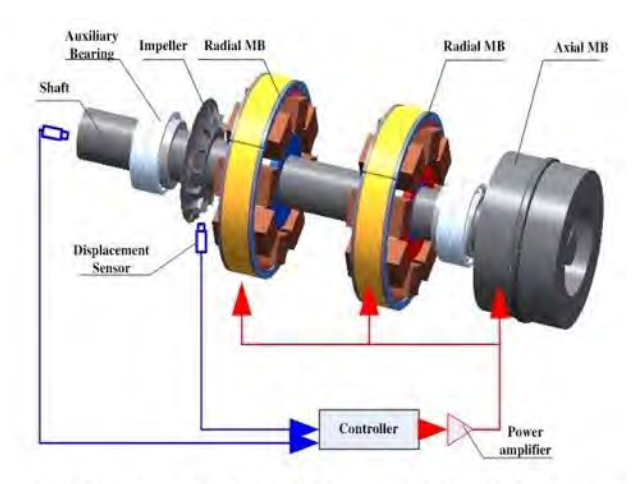
Magnetic bearings (MBs), offering advantages such as no wear and no need for lubrication, have been widely used in turbomachinery, flywheel energy storage, and other fields [1]. Due to their low noise and maintenance-free operation, MBs also demonstrate significant application potential in pumping equipment. However, unlike vacuum or air environments, pump equipment operating in liquid media typically cannot employ conventional corrosion prevention methods. Ordinary anti-corrosion measures often fail to achieve complete physical isolation between these components and the liquid. To enhance the anti-corrosion performance and reliability of pumping equipment, researchers have proposed using a shielding sleeve to improve both corrosion resistance and sealing [2-3]. As a mechatronic device, adding a metal shielding sleeve significantly impacts not only the electromagnetic performance of the MBs but also their control system performance [4]. Therefore, it is essential to quantitatively assess the influence of the shielding sleeve on MBs' performance.

To address this challenge, this paper proposes canned MBs structure, utilizing a high-strength, corrosion-resistant metal shielding sleeve to protect the MBs core from corrosion and prevent liquid media ingress. Building upon this design, and considering the eddy current effects induced by the shielding sleeve, a model for the canned MBs is established. This model is used to analyze the influence of the sleeve's material and thickness on the performance of the canned MBs. Based on the derived influence patterns, an optimal sleeve material and thickness were selected. A prototype was then manufactured to validate the performance of the canned MBs. Experimental results demonstrate that the canned MBs meet the expected performance requirements. Furthermore, the prototype exhibits excellent long-term operational stability, with no signs of rust or corrosion. This canned MBs solution effectively addresses the need for long-term, rust-free, corrosion-free, and leak-free operation in magnetic levitation pumps and similar equipment, providing a viable approach for safe and stable performance.

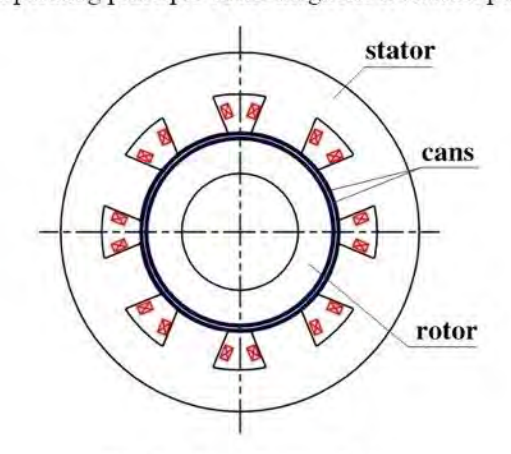
[1]Maslen E H, Schweitzer G, Bleuler H, et al. Magnetic Bearings - Theory, Design, and Application to Rotating Machinery [M]. 2009.

[2]Ai L, Lu Y, Han J, et al. Simulation of the temperature of a shielding induction motor of the nuclear main pump under different turbulence models[J]. Energies, 2023, 16(6): 2792. [3]Wang, DongmeiLiang, YanpingLi, CangxueYang, PeipeiZhou, ChunleiGao, Lianlian.Thermal equivalent network method for calculating stator temperature of a shielding induction motor[J].International Journal of Thermal Sciences, 2020, 147.

[4]Yu Q , Chu S , Li W ,et al. Electromagnetic Shielding Analysis of a Canned Permanent Magnet Motor[J]. IEEE Transactions on Industrial Electronics, 2020, 67(10):8123-8130.



(a) Operating principle of the magnetic levitation pump

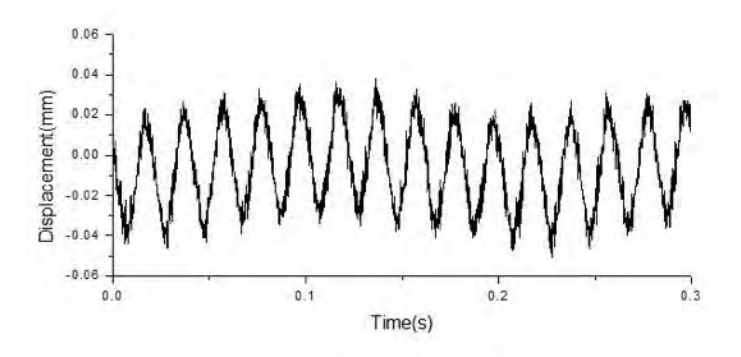


(b) Structure of canned MBs

Fig. 1 Operating principle of the magnetic levitation pump and structure of canned MBs



(a) Prototype of canned MBs



(b) Displacement curve of rotor at rated speed
 Fig. 2 Prototype of canned MBs and displacement curve of rotor at rated speed

VP4-06. Novel Design of Dual-Coil Microspeaker for Low-Frequency Sound Pressure Level Improvement in Tablet

J. Park¹, K. Park¹, D. Xu², S. Hwang¹
¹Department of Mechanical Engineering, Pusan National University, Busan, Korea (the Republic of), ²School of Mechatronic Engineering and Automation, Shanghai University, Shanghai, China

As portable smart devices such as smartphones and tablets continue to become thinner and more functionally integrated, the demand for compact and high-performance acoustic microspeakers has significantly increased. A microspeaker drives the diaphragm through the Lorentz force generated when current flows through the voice coil, and the efficiency of the magnetic circuit critically affects its performances[1]. Microspeaker architectures have evolved from circular to rectangular geometries to improve space utilization, and the adoption of variable magnet structures has improved the magnetic circuit efficiency and low-frequency response[2,3]. However, as the device thickness

decreases, achieving sufficient low-frequency performance remains a technical challenge.

This study proposes a tablet microspeaker with a novel dual-coil magnetic circuit to enhance the low-frequency performance within a constrained thickness limit. All the tablet speakers used in this study shared external dimensions of $25.0 \times 16.0 \times 1.9$ mm. Fig. 1 compares the magnetic circuit structure of a single-coil tablet speaker with those of short-axis, long-axis and nested dual-coil designs. The force factor, a critical parameter in micorspeakers, is defined as the product of total coil length (L) and the average magnetic flux density at the coil (B). The dual-coil configuration exhibited higher efficiency than the single-coil, and the nested dual-coil exhibited the best performance, by increasing the force factor from 1.392 to 1.891 N/A, a 35.8% improvement.

The finite element method was used to validate the coupled electromagnetic–mechanical–acoustic design, and the sound pressure level performance was measured using B&K equipment. Both simulation and measurement results in Fig. 2 show that the nested dual-coil speaker outperforms the single-coil version by approximately 3.0 dB in the 100–500 Hz range and by 0.1 dB in the 2–10 kHz range. These results demonstrate the potential of the proposed design to effectively enhance acoustic performance under limited thickness constraints.

[1] Zhi-Xiong Jiang, Ji-Hun Park and Sang-Moon Hwang,
Sensors and Actuators A: Physical., p.113853 (2022)
[2] Joong-Hak Kwon, Sang-Moon Hwang and Kwang-Seok
Kim, IEEE Transactions on Magnetics., Vol. 43, p. 2704 (2007)

[3] Ki-Hong Park, Zhi-Xiong Jiang and Sang-Moon Hwang, Appl. Sci., Vol.10, p.8902 (2020)

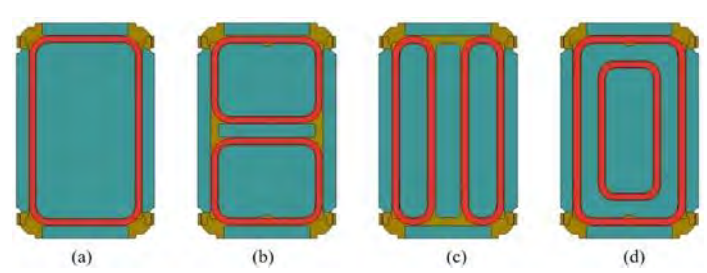


Fig. 1 Speaker magnetic part design comparison (a) Single coil, (b) Short-axis dual coil, (c) Long-axis dual coil, (d) Nested dual coil

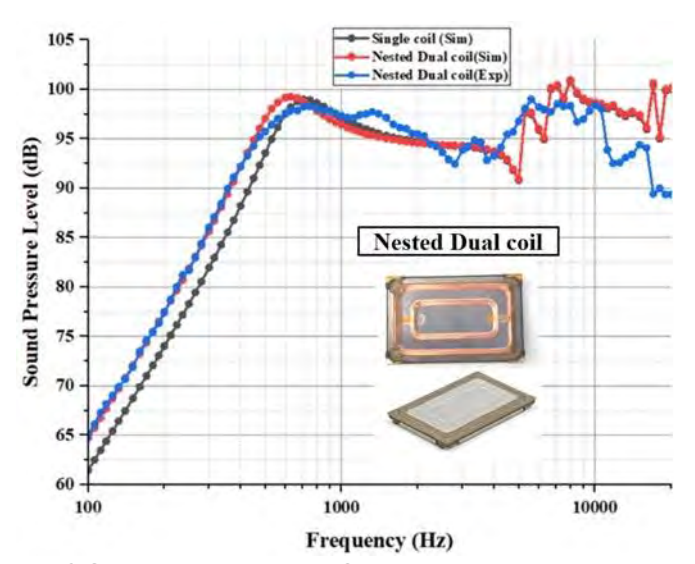


Fig. 2 Sound Pressure Level Comparison

VP4-07. Fundamental Consideration related to the Construction of a Bi-directional Wireless Power Transfer System for Independent Operation of Flying Drones.
T. Nitta, Y. Osaki, F. Sato, S. Miyahara, O. Ito

<u>T. Nitta,</u> Y. Osaki, F. Sato, S. Miyahara, O. Ito *Tohoku Gakuin University, Sendai, Miyagi, Japan*

In recent years, according to reports published by market research companies, the drone industry is expected to develop rapidly in the future. However, the problem with industrial drones is their short operating time and distance. The operating time of an industrial drone is about 30 minutes, which decreases to less than half depending on flight conditions, such as payload and weather conditions. Therefore, it could lead to lost drones due to loss of power and limitation of the range of operations.

To solve these problems, we would like to propose a drone capable of bi-directional wireless power transfer using electromagnetic field resonance.

By forming an "airspace power network" that allows power to be transferred between drones, it will be possible to extend operating hours as appropriate.

For the independent operation of the drone, wireless power transfer was applied to charge the battery without the need for human assistance. In addition, the electromagnetic induction method was adopted, which is highly efficient and capable of high-power transmission in principle. To enable mutual transmission and reception of power, full-wave rectifiers and DC/AC converter circuits were incorporated in both.

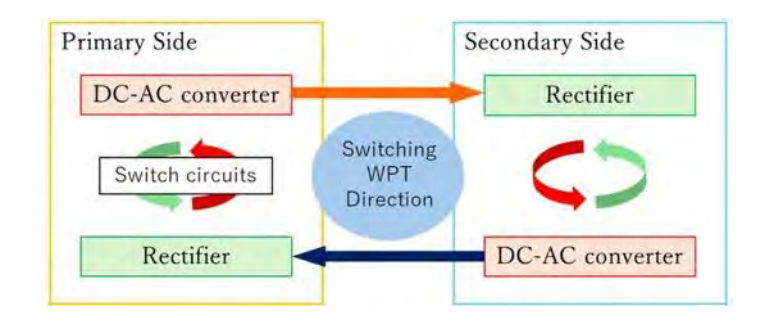
The circuit was created by combining a power receiving circuit and a full bridge circuit.

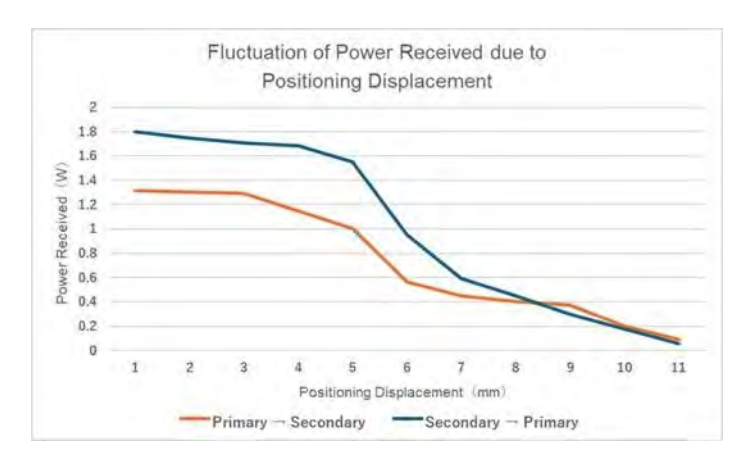
Using this circuit, a demonstration experiment was conducted on the variation of a received voltage and current with the direction of power transmission.

Measurements were taken while shifting the position to consider the effect of positional displacement that occurs when wireless power transfer is applied.

This confirmed that bidirectional wireless power transfer works properly. However, the issue remained of reduced power-feeding efficiency due to positioning displacement. In the proper position, a highly efficient and stable wireless power transfer was confirmed and worked to improve it. [1]Ministry of Economy, Trade and Industry of Japan. *Drone Route Map.* (2025)

[2]Prime Minister's Office of Japan. *Realization of LEVEL 4 Flight and Status of Subsequent institutional development.* (2024)





^{*} Best Student Presentation Finalist / LB - Late-breaking Poster

VP4-08. Construction of Transformer Equivalent Circuit Model Based on Piecewise Linear Reluctance

Z. Ye, Y. Wang

School of Mechanical and Electrical Engineering, China University of Mining and Technology-Beijing, Beijing, China

This paper presents a nonlinear transient transformer model based on the Unified Magnetic Equivalent Circuit (UMEC), using piecewise linear reluctance to capture magnetic nonlinearity, implemented in C++ for efficient time-domain simulation. Traditional equivalent circuits like the T-type inadequately represent saturation, magnetic coupling, and frequency-dependent effects. The UMEC approach constructs a permeance-based magnetic circuit topology reflecting the transformer's physical structure (see Figure 1), with parameters derived from standard open- and short-circuit tests, enabling accurate conductance matrix formation without detailed geometry.

To handle core nonlinearity, the B-H curve is segmented into linear intervals with constant permeability, allowing simple calculation and dynamic updating of reluctance via a lookup table during simulation. This piecewise linearization switches magnetic parameters efficiently without modifying the global system matrix, enhancing speed and accuracy. Implemented in C++ with a time-stepping algorithm, the model computes flux, updates reluctance, and solves for winding currents, supporting real-time and parallel computation due to segment-wise magnetic branch independence. Figure 2 shows primary current distortion near voltage peaks under nonlinear conditions, reflecting core saturation and reduced magnetic conductance at high flux densities.

Simulation results confirm the model's accuracy in reproducing smooth sinusoidal currents in linear regimes and capturing saturation-induced waveform distortion, providing a computationally efficient and scalable solution for engineering-level transient transformer analysis.

References

[1] Power Systems Electromagnetic Transients Simulation, Springer, 2016, pp. 137–141.

[2] Y. Zhang, T. Maguire, and P. Forsyth, "UMEC transformer model for the real time digital simulator," in *Proc. Int. Conf. Power System Transients*, Montreal, Canada, 2005, pp. 19–23. [3] Q. Li, S. Zhang, and S. Sun, "Study of DC bias of power transformer based on UMEC model," *Proc. 7th Asia-Pacific Conf. on Environmental Electromagnetics (CEEM)*, Xi'an, China, 2015.

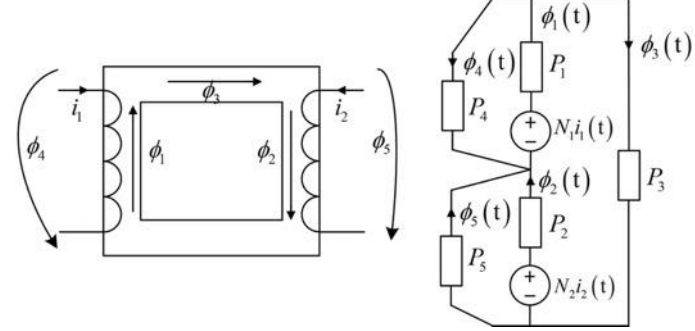


Fig. 1. Single phase double winding magnetic circuit topology

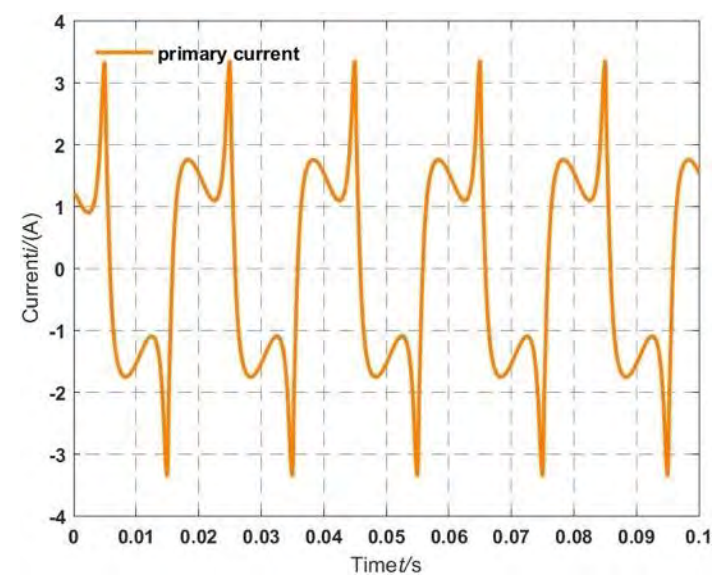


Fig. 2. Primary current waveform under nonlinear conditions.

503

VP4-09. Remanence Evaluation of Transformer Core Based on Magnetic Barkhausen Noise

L. Chen^{1,2}, <u>L. Wu</u>¹, T. Ben¹, H. Huang¹
¹College of Electrical Engineering and New Energy, China Three Gorges University, Yichang, Hubei, China, ²Hubei Provincial Engineering Technology Research Center for Power

Transmission Line, China Three Gorges University, Yichang, Hubei, China

Due to the hysteresis phenomenon in transformer cores, an unknown remanence B_R will be generated in cores after transformers are cut off[1]. When the remanence is high, it will cause an inrush current and seriously harm electrical equipment. To suppress the inrush current, evaluating the remanence in transformer cores is very important[2]. Therefore, a new remanence evaluation method based on Magnetic Barkhausen Noise (MBN) is proposed.

The primary process of the method is shown in Fig.1. In the determination of the remanence evaluation method, firstly, according to the J-A magnetization theory, a relationship between the MBN peak voltage and the stress is obtained. Then, according to the magnetic domain theory, a relationship between the stress and the remanence is established. Finally, the relationship between the MBN peak voltage and the remanence is derived by using the stress as an intermediate quantity. There is a nonlinear inverse relationship between the MBN peak voltage and the remanence because magnetostriction λ_{S} , demagnetization factors N_2 , N_1 , proportional coefficient p, b', average factor A, and vacuum permeability μ_0 can be regarded as constants. In the remanence evaluation process, the direction and value of remanence can be determined and calculated by the MBN voltage intensity and the measured MBN peak voltage, respectively. The experimental platform and results are shown in Fig.2. In Fig.2(b), the MBN voltage intensity decreases as the remanence increases, which is consistent with the trend shown by the constructed remanence evaluation model. The remanence evaluation accuracy method can be proven by Fig.2(c). In Fig.2(d), the MBN voltage intensity is reduced under the positive remanence compared to its negative counterpart, which can determine the remanence direction. Based on the above results, this method can serve as a basis for the remanence evaluation.

In this paper, a new remanence evaluation method based on MBN is proposed. The full paper will systematically analyze the principle and process of this method.

[1] Y. Z. Gerdroodbari, M. Davarpanah, and S. Farhangi, IEEE Transactions on Power Delivery., Vol. 33, p.2938 – 2945(2018)

[2] C. L. Huo, Y. H. Wang, and S. P. Wu, IEEE Transactions on Instrumentation and Measurement., Vol. 70, 3117087(2021)

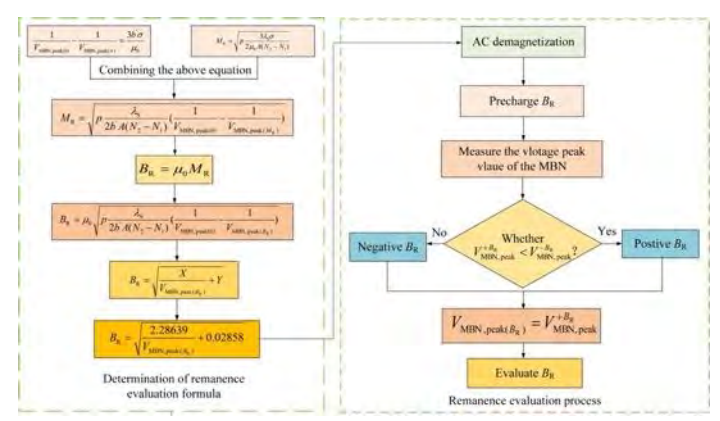


Fig. 1 The primary process of the remanence evaluation

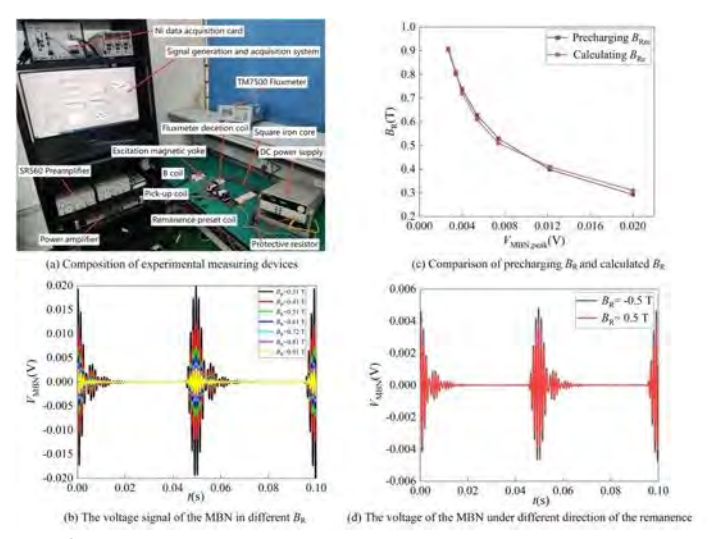


Fig. 2 Experimental platform and results of the remanence evaluation

VP4-10. Basic Consideration about Constructing Cell-culture Management System by Functionalized Petri Dishes with Wireless Power Transfer

<u>Y. Hara</u>¹, F. Sato¹, O. Ito¹, S. Miyahara¹, K. Sagara², S. Sasaki², T. Abe³, K. Inada³

¹Tohoku Gakuin University, Sendai, Miyagi, Japan, ²Hikaridenshi Co., Ltd., Osaki, Miyagi, Japan, ³NITTOKU Co., Ltd., Fukushima, Japan

In recent years, cell culture has become critical to research fields like drug discovery and tissue engineering. However, its quality remains acutely sensitive to uncontrolled external factors, as no standardized management methods exist. Standard techniques depend heavily on technicians' expertise, compromising reproducibility and reliability. This study proposes a solution: a cell-culture management system leveraging functionalized petri dishes integrated with wireless power transfer to address these challenges.

Fig.1 shows the concept of the system we propose. This system comprises three integrated components:

- 1. Identification: Embedded trackers enable unique monitoring of individual units.
- 2. Environmental Monitoring: Continuous temperature/humidity sensing ensures real-time environmental tracking.
- 3. Temperature Optimization: Adaptive heaters, guided by localized sensors and oven integration, dynamically regulate conditions for optimal culture medium performance. And wireless power transfer (WPT) is selected as a power solution due to the need to eliminate physical connectors, optimize spatial efficiency, and ensure consistent energy delivery for extended operational periods.

We consider WPT technology using electromagnetic induction, with a pair of coils as transmitter and receiver. The transmitter is a square Helmholtz-like coil, adapted to shape of a constant-temperature oven. The receivers, wrapping around each dish, are designed to make it easier to see the inside.

We tested whether all receivers could get the same voltage at the same time using the model: the transmitter with face-to-face distance of 170 mm was installed, and the voltage of each of 4 receivers obtained was measured at 9 locations separated by 10 mm from the bottom coil to 90 mm the middle. The result is shown in Fig.2.

At any height, voltage measurements across all positions showed negligible variation between receivers, validating the system's feasibility for concurrent voltage transfer. Y.Kanda, K.Nakamura and M.K.Furue, Proposal for "Fundamental principles of cell culture", Tissue Culture Research Communications, 36, Vol. 2, p. 13-19 (2017)

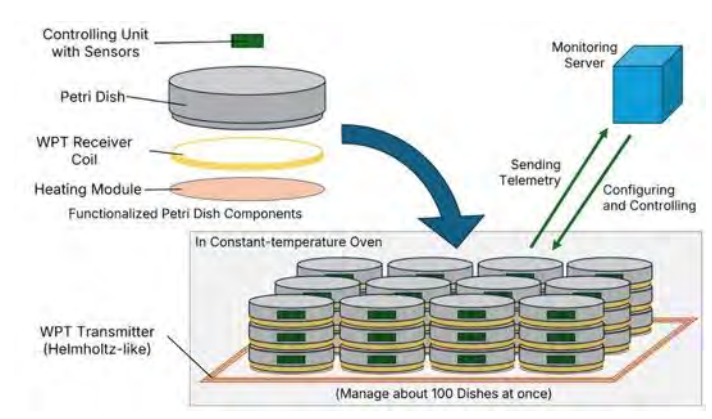


Fig.1: The system's concept

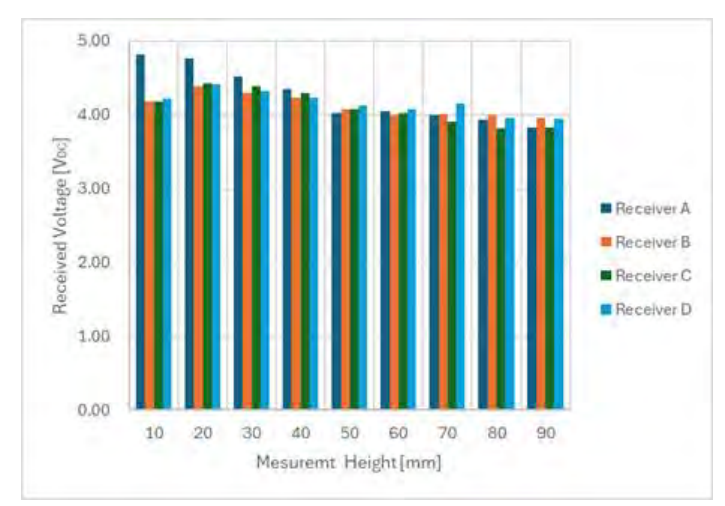


Fig.2: The result of WPT test

VP4-12. Calculation and Optimization Design of Parasitic Capacitance in High-Frequency Transformers

<u>J. Liu</u>, Y. Li, S. Yue, Z. Wan, Z. Cao Hebei University of Technology, Tianjin, China

With the increase in operating frequency, the parasitic capacitance of high-frequency transformers causes the capacitive reactance of its equivalent circuit to decrease, weakening magnetic coupling and energy transfer efficiency, and affecting the overall performance of the transformer. Therefore, efficient calculation of parasitic capacitance parameters and optimized design during transformer design are of great significance. Aiming at the defects of low calculation accuracy of the analytical method and complex calculation steps of the finite element method [1-3], this paper proposes a semianalytical calculation method based on a partitioned solution strategy, extracts the distribution laws of different types of capacitances (Fig. 1), and divides the winding capacitance parameters into two parts: inter-turn capacitance and ground capacitance: 1. For inter-turn capacitance, analytical calculation formulas for C-type, Ztype, segmented, and progressive winding structures are derived, and a 2D simulation model is built to verify the accuracy of the formulas; 2. For ground capacitance, a 3D simulation model is constructed, and the overall winding is plate-equivalent to achieve rapid solution of ground parasitic capacitance.

Using the above calculation method, parametric scanning is employed to analyze the influence of core structure, winding arrangement, winding spacing, and conductor gauge on the values of each parasitic capacitance. The study finds that selecting EP, RM, PM type cores, constructing progressive or segmented winding arrangements, and preferentially increasing the interlayer distance under the same window size can effectively reduce parasitic capacitance. In addition, building a shielding layer can effectively reduce inter-turn parasitic capacitance but will increase ground capacitance to a certain extent. After optimized design of each influencing parameter, the value of parasitic capacitance can be reduced by more than 90%. Finally, the complete 3D simulation model and physical prototype of the high-frequency transformer are built for verification (Fig. 2).

[1]Le D ,Quqin S ,Fan J.Modeling and Analysis of Parasitic Capacitance of Secondary Winding in High-Frequency High-Voltage Transformer Using Finite-Element Method. IEEE Transactions on Applied Superconductivity,vol.28,pp.1-

5(2018)

[2]C. A. Valdivieso, G. Meunier, B. Ramdane, Capacitance Computation of Multi-Turn Windings via Elementary Neighbor-Conductor Models, IEEE Journal on Multiscale and Multiphysics Computational Techniques, vol.6, pp. 125-131(2021)

[3]A. K. Das and B. G. Fernandes, Estimation of the Resonance Frequencies Using an Electrostatic Energy Based Capacitance Model of a Two-Winding Medium/High-Frequency Transformer, IEEE Transactions on Industry Applications, vol. 58, pp. 5301-5316(2022)

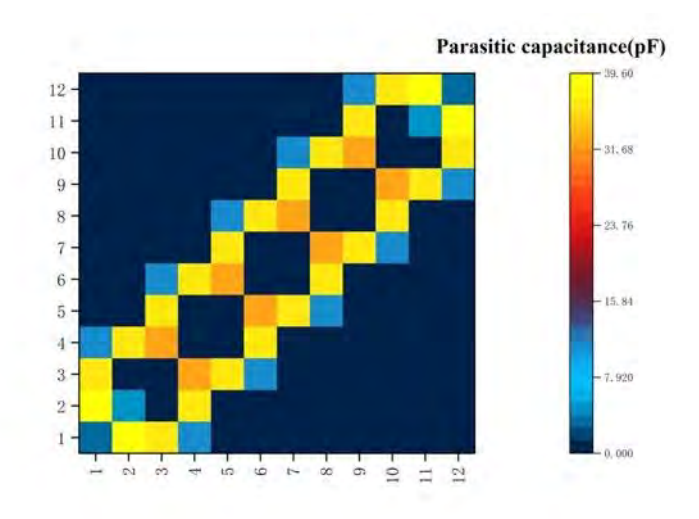


Fig. 1 Extraction Example of Capacitance Matrix

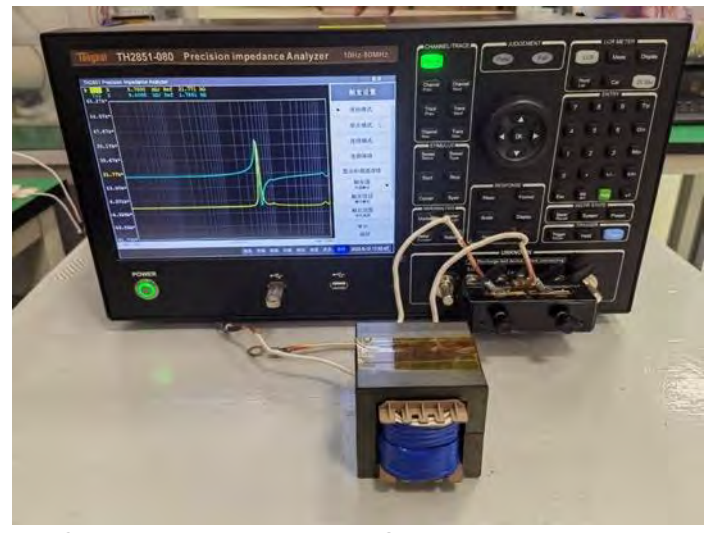


Fig. 2 Measurement of Parasitic Capacitance in High-Frequency Transformer

VP4-15. Energy Harvester Based on FeCoV-PZT Laminated Magnetoelectric Composite for Transformer Temperature Monitoring System

C. Zhang, <u>Z. Wang</u>
Faculty of Electrical Engineering, Hebei University of
Technology, Tianjin, China

FeCoV alloy is a soft magnetic material with low coercivity, high magnetic permeability, and a high magnetostrictive coefficient ($\lambda \sim 70$ ppm). PZT ceramic is a piezoelectric ceramic with strong piezoelectric effects. The laminated magnetoelectric composite made of FeCoV sheets and PZT ceramics exhibits a high magnetoelectric coefficient. Due to the excellent soft magnetic properties of FeCoV, the FeCoV-PZT magnetoelectric composite demonstrates superior lowfrequency response. Transformer temperature monitoring systems are typically powered by disposable batteries, which have disadvantages such as environmental pollution, inconvenient replacement, and short service life[2]. The energy harvester based on FeCoV-PZT laminated magnetoelectric composites offers advantages such as excellent low-frequency response, low cost, self-powering capability, and compact size[3]. It converts stray magnetic field energy generated by transformers into electrical energy to power temperature sensors, thereby replacing disposable batteries in transformer temperature monitoring systems.

In this study, the FeCoV-PZT laminated magnetoelectric composite was prepared using the bonding method. The magnetoelectric performance of the composite was tested under different DC bias magnetic fields and at different frequencies. The output voltage and power density of the energy harvester based on the FeCoV-PZT composite were measured under weak power-frequency magnetic fields, demonstrating its capability to drive low-power temperature sensors. The AC signal output from the energy harvester is converted into a DC signal through an AC-DC rectifier circuit to charge a storage capacitor, ensuring reliable power supply. The harvested energy can sustain the operation of low-power temperature sensors, enabling them to wake up every ten seconds.

[1]Qiu J ,Gao Y ,Xu X , et al.A high-sensitivity zero-biased magnetoelectric sensor using five-phase laminate composites based on FeCoV nanocrystalline soft magnetic alloy[J].AIP Advances,2017,7(5):056623.
[2]Fayang W ,Meitong Z ,Pengfan W , et al.Self-powered transformer intelligent wireless temperature monitoring system based on an ultra-low acceleration piezoelectric

vibration energy harvester[J].Nano Energy,2023,114 [3]Na Y ,Xuan L ,Qian Z , et al.Current Detection and Energy Harvesting Integrated Magnetoelectric Sensor with Flexibility and Heat Resistance Based on Polylactide/VB2 Composites and FeCoV[J].Advanced Materials Interfaces,2022,9(9):

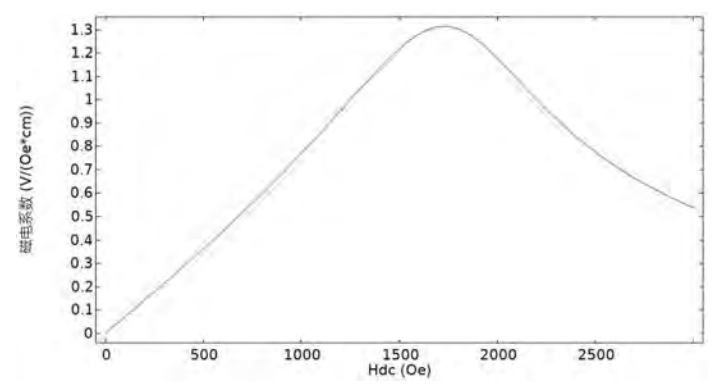


Fig.1 Magnetoelectric effect under different DC bias magnetic fields

VP4-17. Noninvasive Current Measurement in Multiconductor Cables with TMR Sensor Array

C. Zhang, S. Zhao

School of Electrical Engineering, Hebei University of Technology, Tianjin, China

Multi-core cables, with their high transmission efficiency and strong insulation, have become the core carriers for electric energy transmission in distribution networks[1]. However, their unique multi-conductor composite structure poses challenges to traditional single-conductor current measurement technologies, making it difficult to obtain comprehensive and accurate cable currents profiles. This severely affects power system operations such as fault location, harmonic analysis, and energy efficiency optimization^[2].Therefore, the non-intrusive TMR sensor array measurement technology provides a new solution for current inversion of multi-conductor cables, but it faces substantial challenges in practice. On one hand, the interference of external magnetic fields with the measured field of the target conductor increases the complexity of inversion, seriously weakening the scenario adaptability of the measurement method^[3].On the other hand, changes in the spatial conductor posture, such as position and conductor tilt angle, cause magnetic field distortion, leading to measurement deviations and a significant decline in current inversion accuracy^[4]. Aiming at the above problems,

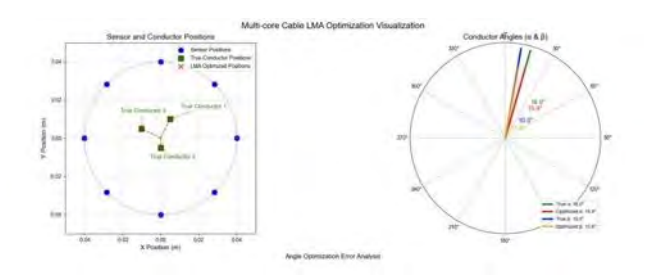
this study begins with TMR sensor sensitivity calibration for accurate data measurement. Then, a uniformly distributed ring-shaped TMR sensor array was constructed. By integrating wavelet transform and adaptive filtering algorithms, feature extraction of complex magnetic fields was performed to separate the target magnetic field signals from ambient electromagnetic interference, thereby enhancing magnetic field measurement stability in complex scenarios. Finally, for the multi-conductor decoupling, a hybrid optimization strategy combining Particle Swarm Optimization (PSO) and Levenberg-Marquardt Algorithm (LMA) is adopted.PSO is used for global optimization of the spatial positions and tilt angles of multi-conductors firstly, and then LMA is employed for fine iterative optimization to construct a coefficient matrix for current inversion. This dual-error-controlled method enables highprecision current inversion, improving accuracy in complex scenarios. As Fig. 1 and Fig. 2 show, optimized multiconductor parameters facilitate precise current inversion calculations.

Xuyang Liu, Chunhua Liu, Wei Han, et al. Design and Implementation of a Multi-Purpose TMR Sensor Matrix for Wireless Electric Vehicle Charging[J]. IEEE Sensors Journal, 2019, 19(5): 1683-1692.

A. Kadechkar, J.-R. Riba, M. Moreno-Eguilaz, et al. Real-Time Wireless, Contactless, and Coreless Monitoring of the Current Distribution in Substation Conductors for Fault Diagnosis[J]. IEEE Sensors Journal, 2019, 19(05): 1693 – 1700.

Alexander Itzke, Roland Weiss, et al. The Influence of Interference Sources on a Magnetic Field-Based Current Sensor for Multiconductor Measurement[J]. IEEE Sensors Journal, 2018, 18(16): 6782-6787.

Alexander Itzke, Roland Weiss, Robert Weigel. Influence of the Conductor Position on a Circular Array of Hall Sensors for Current Measurement[J]. IEEE Transactions on Industrial Electronics, 2019, 66(01): 580-585.



VP4-18. Quantifying Magnetic Degradation in Laser-Cut Electrical Steel: A Domain-Level Study with Angle-Dependent Magnetization

R. Shahbaz^{1, 2}, <u>C. Zhang</u>¹, H. Fatima³, H. Zhang¹
¹Electrical Engineering, State Key Laboratory of Reliability and Intelligence of Electrical Equipment, Hebei University of Technology, Tianjin, Hebei, China, ²Electrical Engineering, Hebei Key Laboratory of Equipment and Technology Demonstration of Flexible DC Transmission, Hebei University of Technology, Tianjin, Hebei, China, ³Physics, Xidian University, Xi'an, Shaanxi, China

Laser cutting is a precise manufacturing process widely used across industries for cutting and shaping materials, including electrical steel parts.[1] This method has gained popularity for producing intricate designs with minimal waste. However, laser cutting in transformer and motor core production raises concerns about its impact on material properties.[2] The localized heat during cutting can create mechanical stresses that may affect the magnetic properties of electrical steel.[3]

This research investigates changes in magnetic domains and their effects on surface magnetic characteristics of nonoriented silicon steel.[4] Magnetization was performed at various angles to analyze local hysteresis characteristics. The magneto-optic Kerr effect [5] was used to study magnetic properties by examining light polarization changes from magnetized surfaces. Results show that laser cutting creates fluctuations in domain orientations near the cutting edge, increasing core losses and decreasing magnetic susceptibility. The observed hysteresis loss near the cutting edge was 10% greater in the longitudinal direction compared to the loss from the center sample of the sheet. In the transverse direction, the loss near the cutting edge is 1.5 times greater than that at the center, signifying a substantial increase in energy dissipation. These findings suggest that the cutting edge may experience different microstructural or stress-induced changes compared to the center of the sheet. The multi-angle application of the magnetic field (at 0°, 30°, 45°, 60°, 90°) further emphasizes that the laser-induced changes in material properties vary with the direction of the applied field, with the transverse direction being more sensitive to these changes.

[1] P. Li, J. Zhang, Y. Gao, X. Xia, and G. J. Weng, "Effect of magnetic field on macroscopic hysteresis and microscopic magnetic domains for different ferromagnetic materials," *J. Mater. Res. Technol.*, vol. 31, pp. 458–471, Jul. 2024.

- [2] S. Wu, W. Wang, C. Yue, and H. Li, "Effect of Processing Methods on the Magnetic Properties of Non-oriented Electrical Steel," in *TMS 2024 153rd Annual Meeting & Exhibition Supplemental Proceedings*, Cham: Springer Nature Switzerland, 2024.
- [3] C. Backes, M. Kahlert and M. Vollmer, "Microstructure and magnetic domain structure of additively manufactured Fe–Si soft magnetic alloys with 3 and 9 wt.-% Si," *J. Mater. Res. Technol.*, vol. 29, pp. 1691–1702, Mar. 2024.
- [4] Q. Xiang, L. Cheng, and K. Wu, "Influencing Factors of the Specific Total Loss of Non-Oriented Electrical Steels Processed by Laser Cutting," *Metals*, vol. 13, no. 3, Art. no. 3, Mar. 2023.
- [5] Q. Xiang, L. Cheng, and K. Wu, "Effects of Laser Cutting Parameters on the Magnetic Properties of 50W350 High-Grade Non-Oriented Electrical Steel," *Materials*, vol. 16, no. 4, Art. no. 4, Jan. 2023.

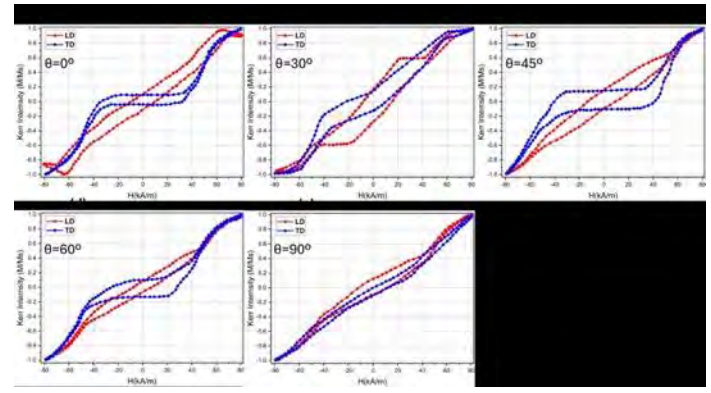


Fig. 1 Surface magnetization curves along LD and TD directions at 80kA/m field in (0,30,45,60,90) degrees angles from (a-e) near the cutting edge

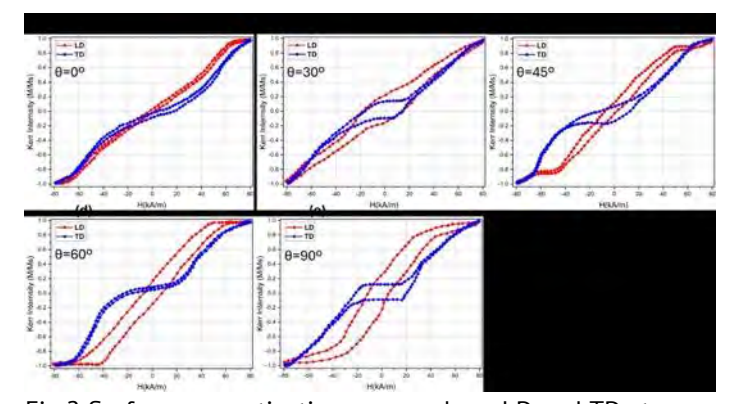


Fig.2 Surface magnetization curves along LD and TD at 80kA/m field in (0,30,45,60,90) degree angles from (a-e) at sample center

VP4-19. Damping Capacitor for Suppression of Ringing Caused by Parasitic Components in PCBs and EMI Reduction

H. Park¹, J. Cheon¹, S. Kim², D. Kim¹

¹Yeungnam University, Gyeongsan-si, Gyeongsangbuk-do, Korea (the Republic of), ²Gyeongbuk Technopark, Gyeongsan-si, Gyeongsangbuk-do, Korea (the Republic of)

Recently, power conversion modules have been widely adopted, as a variety of electronic devices require different power consumption levels. The power conversion module is composed of resistance, inductance, and switches, and the combination of these components can give rise to ringing [1-2].

However, ringing can be a source of electromagnetic interference (EMI) [3]. Therefore, the reduction and control of the ringing phenomenon are important. Practically, printed circuit boards (PCBs) are widely used in circuit design, and due to their physical dimensions, PCBs have parasitic inductance, resistance, and capacitance, which affect the ringing phenomenon and result in EMI. In this research, a theoretical analysis of the ringing phenomenon in power electronics circuits, including the parasitic components of the PCB, is conducted. To control the ringing effect, a damping capacitor is included to reduce it. Fig. 1(a) shows the parasitic inductance (L_{para}) and resistance (R_{para}), which arise from the PCB trace included in the buck converter circuit. The parasitic inductance and resistance are assumed as 50 nH and 20 m Ω respectively. As noted in C_{M1} and C_{M2}, each MOSFET has parasitic capacitance inside it, and therefore ringing can be observed during the transition time as illustrated in Fig. 1(b), and the FFT result is shown in Fig. 1(c). In order to reduce this ringing, the frequency response analysis of this circuit have conducted and the evaluated damping capacitor, which is 420uF, is included in front of M1 as shown in Fig. 2(a). The transient response and FFT results of V_{AB} are illustrated in Fig. 2 (b) and Fig. 2(c) respectively. Compared to the case in Fig. 1, it is noticeable that both the ringing and harmonic components are dramatically reduced. These results support that the theoretically derived damping capacitor reduces the ringing and also improves EMI performance.

[1] Z. Zhang, et al., "Evaluation of Switching Loss Contributed by Parasitic Ringing for Fast Switching Wide Band-Gap Devices," IEEE Trans. Power Electron., Vol. 34, No. 9, pp. 9082-9094, Nov. 2018.

[2] S. Walder, et al., "Effect of load parasitics on the losses and ringing in high switching speed SiC MOSFET based power converters," Proc. IEEE Energy Convers. Congr. Expo., pp. 6161-6168, Sep. 2015.

[3] J. Kim, D. Shin, and S.-K. Sul, "A Damping Scheme for Switching Ringing of Full SiC MOSFET by Air Core PCB Circuit," IEEE Trans. Power Electron., Vol. 33, No.6, pp. 4605-4615, June 2018.

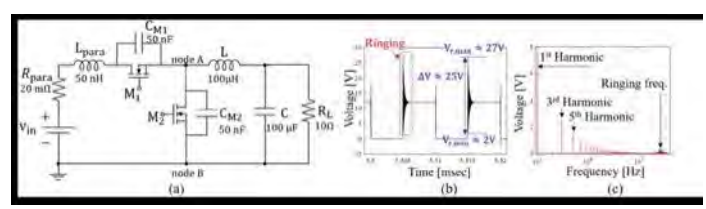


Fig. 1 Simulation setup and results. (a) Circuit including parasitic components of PCB trace (L_{para}&R_{para}) (b) transient response and (c) FFT results of V_{AB}.

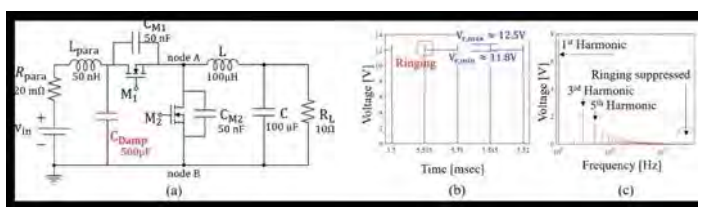


Fig. 2. Circuit diagram for simulation and results. (a) Circuit model including a damping capacitor (C_{Damp}), (b) transient response and (c) FFT results of V_{AB}.

510

SESSION VP5: NEW APPLICATIONS AND OTHER EMERGING TOPICS II

Chair(s): K. Sriram, Electronics and Electrical Engineering, IIT

Guwahatti, Assam, India

Conference Resource Center

VP5-01. Machine Learning Estimation of Curie Temperature for Ferromagnetic Perovskites

M. Shabir, F. H. Bhat Physics, Islamic University of Science and Technology, Pulwama, Jammu and Kashmir, India

Perovskites, possessing a crystal structure similar to calcium titanium oxide (CaTiO₃), exhibit diverse properties, including ferromagnetism, colossal magnetoresistance, metalinsulator transition, and the magnetocaloric effect, making them highly valuable for various technological applications [1]. Rapid estimation of the Curie temperature (T_C) of ferromagnetic perovskites prior to synthesis, characterization, or computationally intensive simulations can significantly enhance research efficiency [2]. This study employs a machine learning approach utilizing a manually curated dataset of 300 perovskites with their corresponding T_C values. Domain knowledge is leveraged to generate features using MAGPIE [3]. Several machine learning algorithms, including Decision Trees (DT), Support Vector Regressor (SVR), K-Nearest Neighbors (KNN), Random Forest (RF), Extra Trees (ET), and Gradient Boosting (GB), are used to train predictive models. Feature selection techniques such as SelectKBest and Recursive Feature Elimination are applied to identify the most relevant features. An average R² score of 0.80 through five-fold cross-validation and an R² value of 0.74 on unseen Perovskites has been achieved. The methodologies presented in this work offer insights into the exploration of material properties through machine learning, facilitating the accelerated design of materials for advanced technological applications.

- [1] B. Raveau, Phil. Trans. R. Soc. A, 2008, 366: 83–92.[2] A. Jain, Curr. Opin. Solid State Mater. Sci., 2024, 33: 101189.
- [3] L. Ward, A. Agrawal, A. Choudhary, et al., npj Comput Mater, 2016, 2: 16028.

VP5-02. Loss research of graphene copper flat wire electrical machinery considering deformation and temperature effects

J. Li¹, Z. Li¹, R. Pei^{1, 2}, Y. An¹

¹Electrical Engineering, Shenyang University of Technology, Shenyang, China, ²Suzhou INN-MAG New Energy Technology Co.. Ltd., Suzhou, China

The development of new energy vehicles has increasingly highlighted the demand for high power density of flat-wire electrical machinery, however, the deterioration of iron and copper losses of motor core materials and winding materials under multi-physical field coupling has seriously affected the motor modeling accuracy. For this reason, this paper investigates the magnetic property evolution law of silicon steel material under the coupling of temperature, pressure and tensile force by means of a multi-physical field coupling test system to reveal its loss mechanism. Based on the experimental data, an iron loss correction model considering force and temperature variables is established, and the relative error of the final test results is controlled within 3% by comparing and analyzing with the physical prototype.

In order to further enhance the power density and alleviate the loss generated by the skin effect of the motor at high frequency, the influence of bending temperature on the conductivity of the winding is clarified. Using high conductivity graphene copper composite material, through the bending - stretching - variable temperature multi-field coupling experiment to quantify its conductivity degradation characteristics, test data are shown in Figure 1. According to the measured data for the graphene copper material to consider the temperature and molding bending of the copper loss modification model[2], and prototype of the physical test values for comparison, the maximum relative error is controlled within 6%.

[1]Ou, J., Liu, Y., Breining, P., Gietzelt, T., Wunsch, T., & Doppelbauer, M. (2020). Experimental characterization and feasibility study on high mechanical strength electrical steels for high-speed motors application. IEEE Transactions on Industry Applications, 57(1), 284-293.

[2]Fujisaki, K., Hirayama, R., Kawachi, T., Satou, S., Kaidou, C., Yabumoto, M., & Kubota, T. (2007). Motor core iron loss analysis evaluating shrink fitting and stam** by finite-element method. IEEE Transactions on Magnetics, 43(5), 1950-1954.

[3] Miyagi, D., Maeda, N., Ozeki, Y., Miki, K., & Takahashi, N. (2009). Estimation of iron loss in motor core with shrink

fitting using FEM analysis. IEEE Transactions on Magnetics, 45(3), 1704-1707.

[4]Liu, G., Liu, M., Zhang, Y., Wang, H., & Gerada, C. (2019). High-speed permanent magnet synchronous motor iron loss calculation method considering multiphysics factors. IEEE Transactions on Industrial Electronics, 67(7), 5360-5368. [5]Sato, M., Kaneko, S., Tomita, M., Doki, S., & Okuma, S. (2005). Reducing efficiency loss cased by shrink fit in compressor motor for air-conditioners. In 2005 Annual Meeting record, IEEJ (No. 5-101, pp. 132-133).

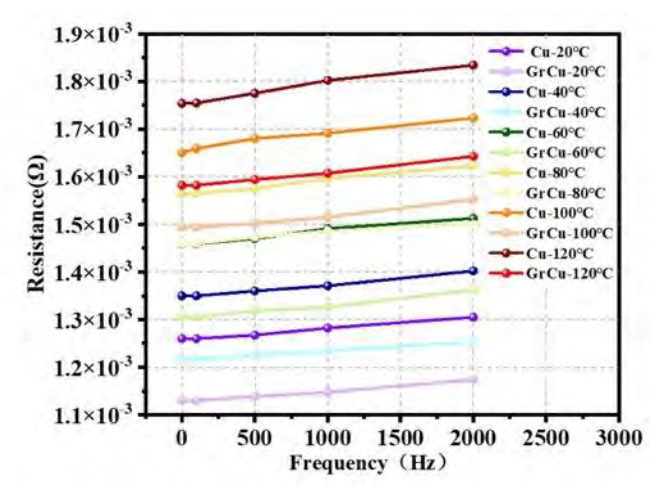


Fig.1 Effect of temperature and current frequency on the resistance of graphene-copper composites and copper materials

VP5-03. High-Tc SQUID-Based Ultra-Low Field MRI in Unshielded Environments

S. Liao, H. Huang

Institute of Electro-Optical Engineering, National Taiwan Normal University, Taipei city, Taiwan

A high- T_c SQUID based ultra low field MRI system in unshield environments is reported in this work. The technique of NMR/MRI was optimized to study MRI of water phantoms and fingers. An SNR of 62 in image contrast was achieved for a water column of 200 μ L at magnetic fields of 98 μ T using a pre-polarization field of ~55 mT and a gradient field of ~52.6 μ T/m. The MRI showed high image contrast and demonstrated a spatial resolution of 2 mm for samples in magnetically unshielded environments. A clear image of fingers was demonstrated which shows promise for biological or clinical applications



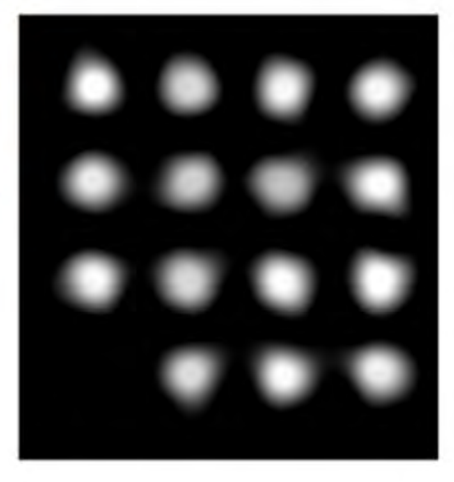


Fig. 1 The photograph and MRI of the water specimen.



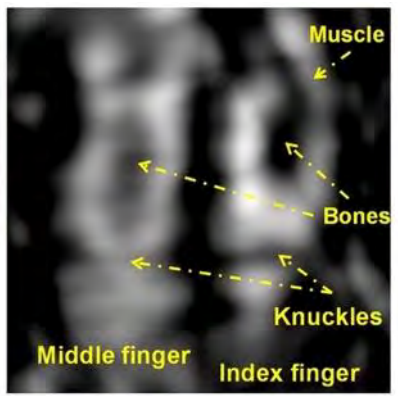


Fig. 2 The photograph and 2D MRI of index and middle fingers.

VP5-04. Multi-harmonic Response of Superparamagnetic Nanoparticles As a Function of Particle Size and Concentration Across Multiple Optical Configurations

M. Syed, C. Su, S. Reza

Physics, Optical Engineering and NanoEngineering, Rose-Hulman Institute of Tech, Terre Haute, Indiana, United States

Superparamagnetic nanoparticles (SNPs) play an increasingly important role in biomedical applications like MRI contrast imaging, magnetic hyperthermia, drug delivery, etc. [1-2]. We have investigated the magneto-optical response of dilute aqueous and non-aqueous suspensions of single-domain iron oxide nanoparticles under the influence of a resonant AC magnetic field [3-5]. We present results from a Michelson interferometer-based measurement setup. Interferometric measurements enhance the measurement

^{*} Best Student Presentation Finalist / LB - Late-breaking Poster

sensitivity of the induced magnetization response of the nanoparticle samples. Further, the signal-to-noise ratio of the measurements is improved with a lock-in detection scheme. Our experimental setup captures both even and odd harmonics of the magneto-optic response. In this work we focus on the contrasting outcomes of "small" (10 nm or less in diameter) vs. "medium" (15 to 20 nm diameter) sized particles in terms of the spectral composition of the detected optical signal. All our SNPs have ligands that keep these particles from aggregating. Our results provide important insight into the role of the applied magnetic field in generating dipole interactions that result in new equilibrium configurations consisting of loosely assembled aggregates (clusters) of these SNPs, compared to the case when there is no applied magnetic field. This approach allows us to investigate how formation of the aforementioned aggregates modify the effective magnetic moment and the scattering due to the formation of SNP aggregates. In addition to highlighting the role of SNP size (both, the hydrodynamic radius as well as the Neel radius), we also discuss the role of starting concentrations of the SNP samples.

- [1] R. Hergt, S. Dutz, and M. Zeisberger, "Validity limits of the Neel relaxation model of magnetic nanoparticles for hyperthermia," Nanotechnology, vol. 21, (2010).
- [2] Y. Xiao and J. Du, "Superparamagnetic nanoparticles for biomedical applications," J. Mater. Chem. B, vol. 8, 3, 354–367, (2020).
- [3] S. Vandendriessche, W. Brullot, D. Slavov, V. Valev, and T. Verbiest, "Magneto-optical harmonic susceptometry of superparamagnetic materials," Appl. Phys. Lett., vol. 102, (2013).
- [4] C. Patterson, M. Syed, Y. Takemaura, "Harmonic decomposition of magneto-optical signal from suspensions of superparamagnetic nanoparticles," JMMM, 451, 248-253 (2018).
- [5] M. Syed, W. Li, N. Fried, and C. Patterson, "Magneto-optical investigation of scattering by superparamagnetic nanoparticles using multi-harmonic analysis," AIP Advances 11, 015328 (2021).

VP5-05. Research on Magnetic Anomaly Noise Suppression Method Based on Magnetic Fields Induced by Threedimensional Short Peak Ocean Waves

<u>Y. Xu</u>, J. Qiu, C. Cao, H. Sun, B. Fan, X. Zeng College of Optoelectronic Engineering, Chongqing University, Chongqing, China

Marine magnetic anomaly detection is one of the important means in the fields of marine scientific observation and seabed resource exploration, etc[1]. Since the seawater motion noise is very close to the target magnetic anomaly signal in terms of magnitude and frequency band, the noise suppression method based on the wave magnetic field can achieve better results. To date, the wave magnetic field model has been delineated into two categories: the magnetic field generated by two-dimensional regular waves and the magnetic field generated by three-dimensional irregular waves. The latter model takes into account the randomness and multi-directionality of the wind, which is more in line with the actual situation. Nevertheless, the current state of research on this remains nascent. This study introduces a dynamic three-dimensional short-peak wave magnetic field model, which solves the problems that the three-dimensional wave magnetic field cannot describe the magnetic field generated by the diffuse harmonics outside the main wave[2], and the non-time-varying magnetic field is inconsistent with the energy diffusion and dissipation. The proposed method based on the random wave theory and Maxswell's equation system can obtain the analytical solutions of the wave-induced magnetic field, so as to have a more accurate estimation of the noise of the wave magnetic field, and the simulation results are shown in Fig. 1. Moreover, on the basis of the solutions, the influence of water depth and wind fields on the distribution of the spectrum and time series of the induced fields was simulated using a typical wave spectrum and directional spectrum. Ultimately, the ocean noise is suppressed by spectral subtraction and the residual noise such as geomagnetic noise is suppressed by wavelet denoising. The experimental results show that the signal-to-noise ratio is improved by 12.01 dB, as shown in Fig. 2, which realizes the effective noise suppression in the detection of marine magnetic anomalies.

[1]Supeng Li, Jing Zhao*, Yi Wang, et al. IEEE Sensors Journal., Vol. 23, p.10694-10705(2023) [2]Ronghua Tao, Baoqing Zhang*, Chun Zhou, et al. IEEE Access., Vol. 12, p.64927-64936(2024)

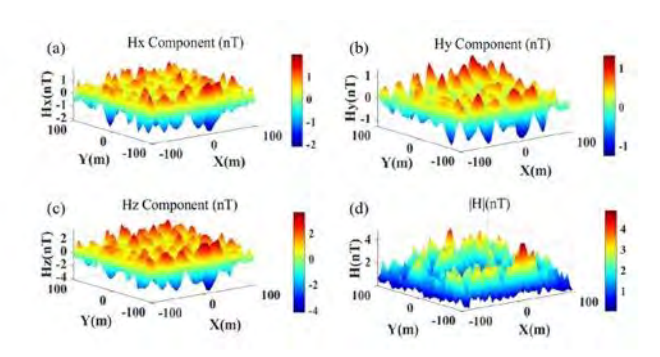


Fig. 1 Wave magnetic field modeling with geomagnetic parameters: strength 43.334 μ T, declination 23.785°, inclination offset -1.452°. (a) Hx, (b) Hy, (c) Hz, (d) |H|.

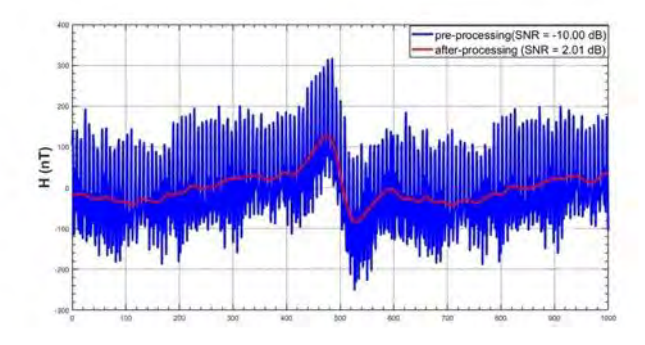


Fig. 2 Waveform and SNR of the signal before and after noise suppression.

VP5-06. Mutual Suppression of Polar and Magnetic Orders in Charge-Compensated Fe-Substituted Bi_{0.5}Na_{0.5}TiO₃: Evidence of inverse Magnetoelectric Coupling

M. Kumari^{1, 2}, R. Chatterjee¹

The realization and control of magnetoelectric (ME) coupling in single-phase multiferroics remain key challenges in the development of next-generation spintronic and multifunctional devices [1]. While positive ME coupling is well established, the inverse phenomenon wherein electric poling suppresses magnetization, remains largely unexplored [2]. In this work, we demonstrate a rare and robust case of negative ME coupling in charge-compensated Fe-substituted $Bi_{0.5}Na_{0.5}TiO_3$ (BNFT) system. A systematic investigation of $Bi_{0.5}Na_{0.5}(Fe_xTi_{(1-3x/4)})O_3$ compositions ($0 \le x \le 0.2$) reveals single-phase

rhombohedral perovskite structures confirmed by both laboratory and synchrotron X-ray diffraction. X-Ray near edge spectroscopy confirms the incorporation of Fe³⁺ at Ti⁴⁺ sites without secondary phases. Increasing Fe content leads to a progressive reduction in remanent polarization and a transition from ferroelectric to mixed ferroelectric antiferroelectric behavior in this system. Magnetic measurements reveal that while pristine BNT is diamagnetic, Fe-substituted variants display compensated antiferromagnetic states. Notably, for x = 0.05 (BNFT0.05), electric poling induces ~19% magnetization reduction – clear evidence of inverse ME coupling. This reproducible, intrinsic behavior is confirmed by a newly developed labbased poling method. Magnetocapacitance results further show bidirectional suppression of ferroic orders under crossfields (Fig. 1(a) and (b)). To interpret this, we developed a Landau-Devonshire free-energy model with coupled polarization and magnetization terms. The model captures experimental trends and predicts inverse ME coupling. These insights broaden the ME material design space and offer opportunities for devices where electric-field-driven magnetization suppression is advantageous.

[1] Vinai *et.al.*, APL Mater. 3, 116107 (2015). [2] Gianluca Giovannetti, Sanjeev Kumar, Carmine Ortix, Massimo Capone, and Jeroen van den Brink, PRL 109, 107601 (2012).

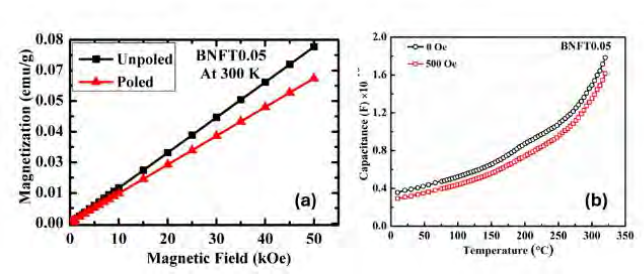


Fig. 1 Room temperature M–H curves and temperature-dependent magnetocapacitance for BNFT0.05: (a) Poled and unpoled magnetization curves showing inverse ME coupling; (b) dielectric response under 0 and 500 Oe fields confirming bidirectional coupling.

¹Physics, Indian Institute of Technology, New Delhi, New Delhi, India, ²HDD, Western Digital Corporation, San Jose, California, United States

SESSION VP6: SOFT MAGNETIC MATERIALS III

Co-Chair(s): S. C. Mills, Materials Science and Technology, US Naval Research Laboratory, Washington, District of Columbia, United States and D. Hedlund, Department of Electrical and Computing Engineering, University of Central Florida, Orlando, Florida, United States

Conference Resource Center

VP6-01. Role of Surfactants in Enhancing Colloidal Stability and Magnetic Hyperthermia Efficiency of Fe_3O_4 Nanoparticles.

<u>S. Singh</u>¹, Y. Kaur², B. Chudasama¹

¹Physics, Thapar Institute of engineering and Technology, Patiala, Punjab, India, ²Physics, Maharishi Markandeshwar University, Mullana, Ambala Cantt, Haryana, India

In recent years, magnetic hyperthermia has emerged as promising therapy for the treatment of cancer. Use of Fe₃O₄ nanoparticles (NPs) for *in-vivo* magnetic hyperthermia therapy has been approved by US food and drug administration. Dipolar interactions between nanocrystallites further promote aggregation in Fe₃O₄ NPs due to their high surface energy. To minimize effect of dipolar interactions between NPs, they are sterically stabilized by small chain surfactants and could deteriorate their magnetic hyperthermia performance. In this study we have studied effect of anionic (oleic acid) and cationic (Cetrimonium bromide (CTAB)) surfactants on colloidal stability and hyperthermia performance of Fe₃O₄ NPs. Bilayer oleic acid (OA) or CTAB- Fe₃O₄ NPs were synthesized by chemical coprecipitation method. As-synthesized Fe₃O₄ NPs are superparamagnetic in nature. The hydrodynamic size of OA-Fe₃O₄ NPs show minimal change in 30 days aging. It increases from 40.5 nm to 41.7 nm, while their zeta potential changes from -65 mV to -52.50. In case of CTAB-Fe₃O₄ NPs, hydrodynamic size increases from 64.6 nm to 73.8 nm and zeta potential also increases to 56 mV from 40 mV. Magnetic hyperthermia measurements of OA and CTAB-Fe₃O₄ NPs were established by performing measurements as a function of magnetic field strength (2-10 mT), field frequency (162-935.6 kHz) and NPs concentration for 10 mins. Specific loss power (SLP) of OA- Fe₃O₄ decreases from 14.94 W/g to 10.05 W/g while it remains almost constant (9.67 W/g to 9.39 W/g) in CTAB- Fe₃O₄ aged for 30 days. Thus, CTAB- Fe₃O₄ NPs possess better colloidal stability and hence more suitable for magnetic hyperthermia applications.

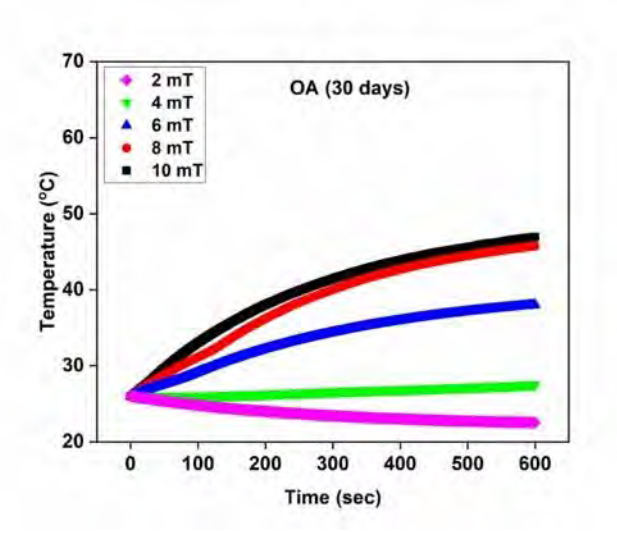


Fig. 1 Temperature - time plots of aqueous dispersion of OA coated Fe_3O_4 (OA- Fe_3O_4) nanoparticles recorded as a function of magnetic field strength at constant magnetic field frequency (f = 935.6 kHz) and nanoparticle concentration (C= 35 mg/mL) for 30 days

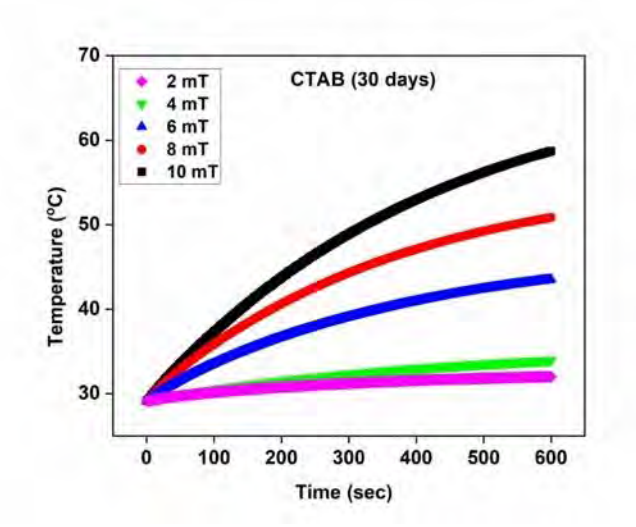


Fig. 2 Temperature - time plots of aqueous dispersion of CTAB coated Fe $_3O_4$ (CTAB-Fe $_3O_4$) nanoparticles recorded as a function of magnetic field strength at constant magnetic field frequency (f = 935.6 kHz) and nanoparticle concentration (C= 35 mg/mL) for 30 days

VP6-04. Giant Magnetoimpedance and Magneto-optical Characterization of Amorphous Alloys

<u>C. S. Martins</u>¹, V. Bellintani¹, F. A. Albuquerque², A. D. Santos³, J. H. Severo⁴

¹DEG, FATEC, São Paulo, SP, Brazil, ²Energy and Nuclear Research Institute, IPEN/CNEN, São Paulo, SP, Brazil, ³Institute of Physics, University of Sao Paulo, São Paulo, SP, Brazil, ⁴Institute of Physics, university of Sao Paulo, São Paulo, SP, Brazil

Giant Magnetoimpedance (GMI) refers to the significant change in the impedance of magnetic materials when exposed to an external magnetic field [1,2]. This study focuses on the analysis of amorphous magnetic samples, specifically CoFeSiB ribbons produced by the melt-spinning technique. GMI measurements were performed across low and moderate frequency regimes. The observed increase in impedance with frequency is attributed to the enhanced contribution of the imaginary component of the impedance. The peak GMI value was found to be highly frequencydependent. A maximum GMI ratio of 75% was recorded at 10 Oe for a frequency of 1 MHz, resulting in a sensitivity of 7.5%/Oe, as shown in Fig. 1. This property makes the material suitable for a wide range of technological applications. Additionally, magnetic susceptibility measured via the magneto-optical Kerr effect (MOKE) exhibited a similar trend to that of the GMI response, as depicted in Fig. 2. Through MOKE microscopy, the domain structure of the ribbons was visualized, revealing domain widths on the order of 100 µm. An inclined magnetic structure, deviating from the longitudinal axis of the ribbon, was also observed. This feature is associated with a significant transverse component of the magnetic susceptibility tensor, a necessary condition for the observation of the GMI effect [3].

[1] F. L. A. Machado, B. L. da Silva, S. M. Rezende, C.S. Martins. "Giant ac magnetoresistance in the soft ferromagnet Co70.4Fe4.6Si15B10" J. Appl. Phys, Vol.75, p.6563 (1994). [2] R. S. Beach, A. E. Berkowitz, "Sensitive field and frequency dependent impedance spectra of amorphous FeCoSiB wire and ribbon (invited)", J. Appl Phys. Vol 76, p. 6209(1994).

[3] P. Corte-Leon et al. "Giant magnetoimpedance and magneto-optical Kerr effects in (Co63Ni37)75Si15B10 amorphous ribbon", Intermetallics, Vol.125, p.106925(2020).

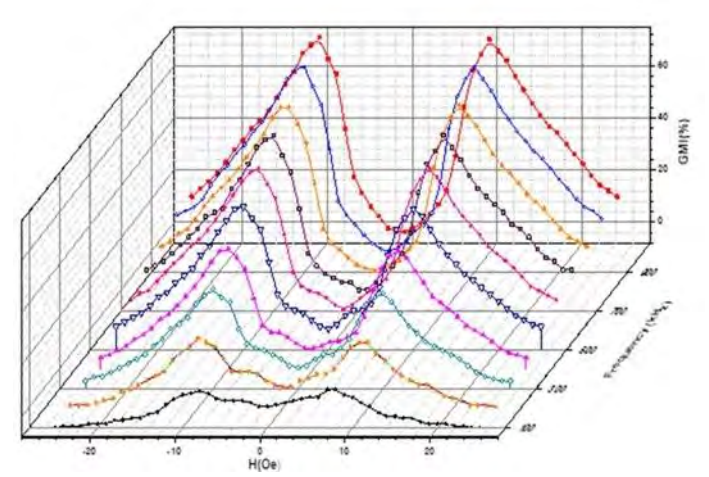


Fig. 1- Magnetoimpedance as a function of magnetic field for various frequencies.

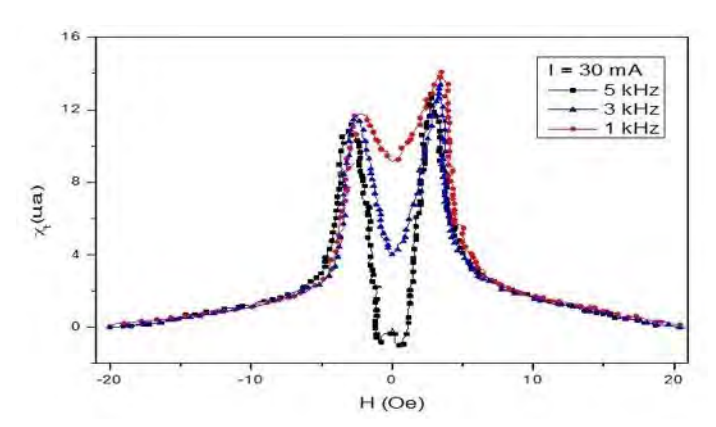


Fig. 2 – Susceptibility as a function of magnetic field for three frequency.

VP6-06. Analysis and Calculation of Magnetostrictive Properties of Thin-gauge Low-loss Electrical Steel Sheets Considering Stress Effects

J. Wang¹, D. Ma¹, Z. Chen², P. Meng¹, L. Zeng³, R. Pei^{1,3}
¹Shenyang University of Technology, ShenYang, China, ²Hunan CRRC Times Electric Drive Technology Co., Ltd., ZhuZhou, China, ³SuZhou Inn-Mag New Energy Ltd, SuZhou, China

The magnetostriction phenomenon occurs in electrical steel sheets under an external magnetic field, and this phenomenon is one of the main causes of vibration and noise in motors and transformers [1]. In actual motor operation, electrical steel sheets are subjected to complex mechanical stresses formed by the coupling of assembly and electromagnetic forces, while traditional

magnetostriction models struggle to accurately predict core deformation [2]. Therefore, calculating the magnetostriction of electrical steel sheets considering stress effects is particularly important.

In the second part of this paper, an electrical steel magnetostriction measurement device (as shown in Fig. 1(a)) is used to measure the magnetostriction phenomena of ultra-thin silicon steel (ST100), high-silicon steel, and amorphous alloy electrical steel sheets under different stresses (-3 MPa to 3 MPa). The samples were processed by wire-cutting and laser-cutting methods, respectively, as shown in Fig. 1(b). Partial measurement results are presented in Fig. 2(a)-(b). The test results reveal the stressinduced variation law of magnetostriction in electrical steel sheets and explain this phenomenon from the perspective of microscopic magnetic domain structures. In the third part, based on existing classical magnetostriction models, we establish a stress-dependent magnetostriction calculation model by introducing a stress influence factor. By comparing experimental magnetostriction data, traditional model calculations, and the proposed model calculations, we analyze the error accuracy. The results verify that the proposed model demonstrates higher accuracy in calculating magnetostriction for electrical steel sheets. Finally, this paper will carry out magnetostriction tests on three electrical steel sheets, establish a stress-involved magnetostriction model, and verify its accuracy. The results will aid in subsequent research on suppressing motor vibration and noise, offering practical guidance for enhancing motor and transformer performance.

[1] Z. Lihua, L. Jingjing, Y. Qingxin, Z. Jianguo and C. -S. Koh, "An Improved Magnetostriction Model for Electrical Steel Sheet Based on Jiles—Atherton Model," in IEEE Transactions on Magnetics, vol. 56, no. 3, pp. 1-4, March 2020, Art no. 7514604, doi: 10.1109/TMAG.2019.2951824.
[2]D. Ma et al., "Effect of Si Content on Magnetostrictive Properties of Electrical Steel Sheet Considering Tensile Stress," in IEEE Transactions on Magnetics, vol. 60, no. 9, pp. 1-5, Sept. 2024, Art no. 2100905, doi: 10.1109/TMAG.2024.3408219.

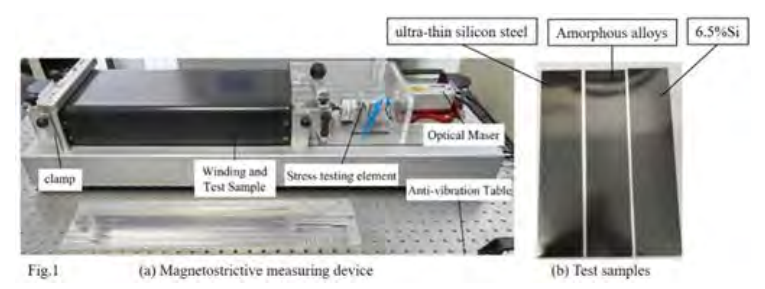


Fig. 1

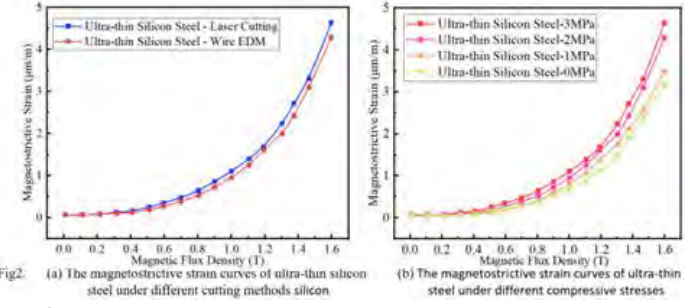


Fig. 2

VP6-07. Comparative Research on the Magnetic Properties of High Permeability Soft Magnetic Materials and Conventional Silicon Steel Under Stress-electromagnetic Coupling

X. Liu¹, J. Li¹, Z. Li¹, S. Zhang¹, Z. Chen², R. Pei^{3,1}, L. Zeng³
¹Shenyang University of Technology, Shenyang, China, ²Hunan CRRC Times Electric Drive Technology Co., Ltd., Zhuzhou, China, ³Suzhou InnMaq New Energy Ltd., Suzhou, China

Magnetic flux density is low in ultra-high-speed permanent magnet motors, so high permeability materials are urgently demanded in order to increase the torque and power of the motor. However, when the motor is fabricated and operated, stator shrink fitting force and rotor centrifugal force are introduced, and the stresses will affect the magnetic properties of soft magnetic materials, so it is very important to study the effect of stresses on soft magnetic materials. In this paper, by designing experiments, the performance changes of materials with different magnetic permeability are investigated when different compressive and tensile stresses are coupled with magnetic field. The experimental results show that the high permeability material Fe-Ni alloy (1J50) is more likely to reach the operating point (1.2T \sim 1.4T) of ultra-high-speed permanent magnet motors within a limited range of magnetic fields. When compressive stress is applied to the test specimen, as shown in Fig. 1, the

magnetic permeability of the soft magnetic material changes significantly, and the magnetic permeability decreases with the increase of the compressive stress, and this phenomenon is more obvious in the high permeability material, when the magnetic flux density is 1.1T, the magnetic permeability of the conventional silicon steel decreases by 44.41%, and the magnetic permeability of 1J50 decreases by 85.35%. We will show more details of the content of tensile stress comparison experiments in the subsequent full text. Experiments show that high permeability materials are more sensitive to stress, this paper analyzes the reasons from the material structural properties, and studies the soft magnetic material permeability change rule with stress, and finally brings the above experimental data into the finite element model for the feasibility analysis of the application of high permeability material 1J50 in high-speed motors.

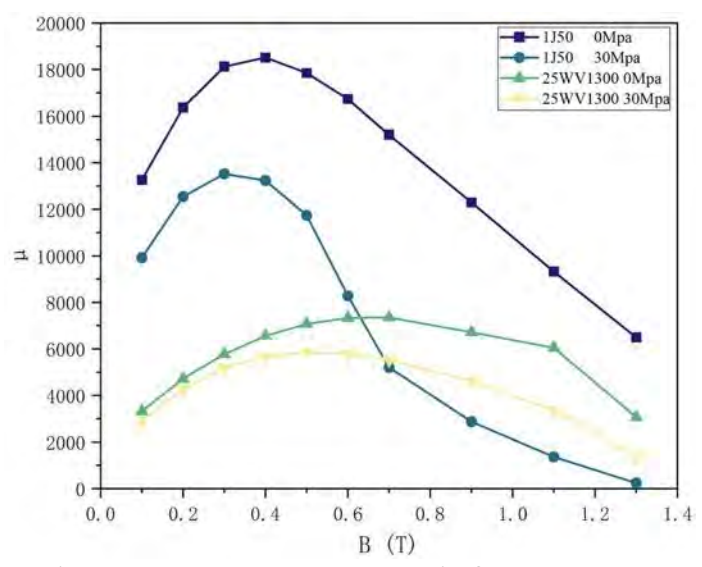


Fig. 1 Relative permeability curves of 1J50 and conventional silicon steel under compressive stress test

VP6-08. Research on Magnetic Properties in Soft Magnetic Composites Considering Temperature and Stress Effect Y. Li¹, Z. Li¹, B. Yang¹, R. Pei¹, L. Zeng²

¹Shenyang University of Technology, Shenyang, Liaoning, China, ²Suzhou InnMag New Energy Ltd, Suzhou, China

Due to the compression molding process, soft magnetic composites (SMCs) enable customization of magnetic circuit structures for specific applications. The unique feature of SMCs to realize three-dimensional magnetic circuits has

aroused extensive interest among electric motor researchers. During electric motor manufacturing and operation, the iron core is subjected to stress, temperature, and magnetic field environments, which affect the magnetic properties of soft magnetic materials, whether SMCs or conventional silicon steel. However, as SMCs are formed by pressing insulated ferromagnetic particles, its magnetic properties responses differ from those of conventional silicon steel. Therefore, this paper investigates the influence of temperature and stress on the magnetic properties of SMCs.

This paper first designs the test specimens for SMCs to enable magnetic properties testing under temperature and stress, with its structure is shown in Fig. 1. The magnetization curves and loss curves of SMCs are then tested within the ambient temperature range of -70°C to 120°C and stress variation range of 0 MPa to 20 MPa. A 0.35mm silicon steel sheet was set as the control group. Partial test results are presented in Fig. 2. Based on the test results, the magnetic properties variation laws of SMCs and conventional silicon steel under temperature and stress are compared and analyzed. It is found that temperature rise reduces material losses, but SMCs exhibit higher temperature sensitivity. Compared with conventional silicon steel, SMCs can withstand smaller tensile stress, and their magnetic properties are more significantly affected by tensile stress. Finally, the influence of temperature and stress factors on the magnetic properties of SMCs is summarized. The research content of this paper is of certain significance for the application of SMCs in electric motors and the design of magnetic circuit structures.

- [1] Muthusamy M, Abdel-Mageed BS, Bernier F, et al.Impact of Soft Magnetic Composite Materials for Traction Applications[J].IEEE Transactions on Industry Applications, vol. 61, no. 3, pp. 3737-3752.
- [2] Ballestin-Bernad V , Kulan M C , Baker N J ,et al.Power Analysis in an SMC-Based Aerospace Transverse Flux Generator for Different Load and Speed Conditions[J].IEEE Transactions on Transportation Electrification, vol. 11, no. 2, pp. 5700-5708.
- [3] Liu C, Du H, Lei G, et al.Design and Analysis of Modular Permanent Magnet Claw Pole Machines With Hybrid Cores for Electric Vehicles[J].IEEE Transactions on Energy Conversion, vol. 40, no. 2, pp. 1047-1061.

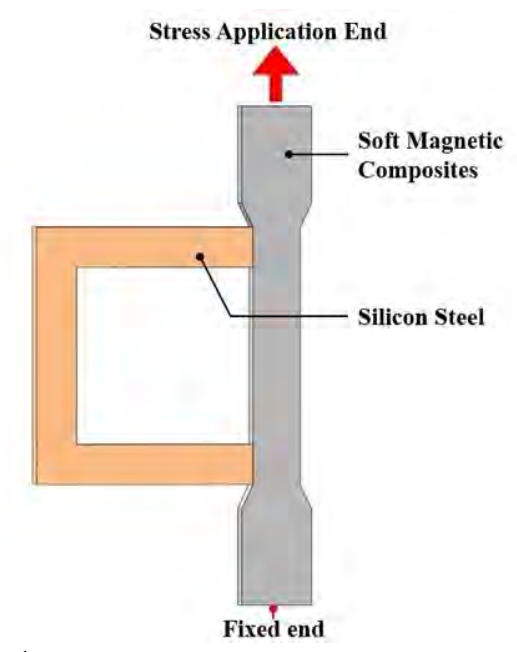


Fig. 1

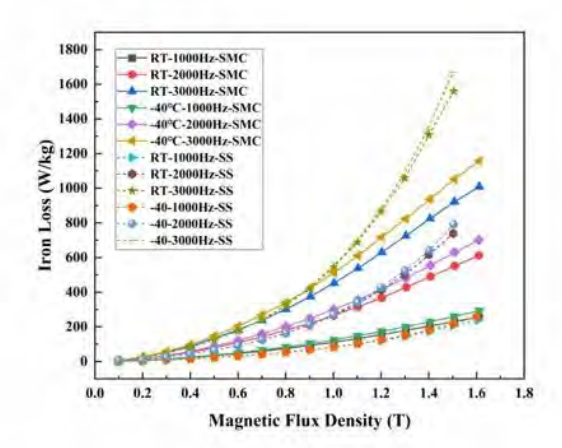


Fig. 2

VP6-09. Analysis of Amorphous Alloy-Ultra-Thin Silicon Steel Hybrid Iron Core for High-Speed Electrical Machine J. Feng¹, X. Lu¹, Z. Li¹, J. Wang¹, L. Zeng², R. Pei^{1, 2} ¹Shenyang University of Technology, Shenyang, Liaoning,

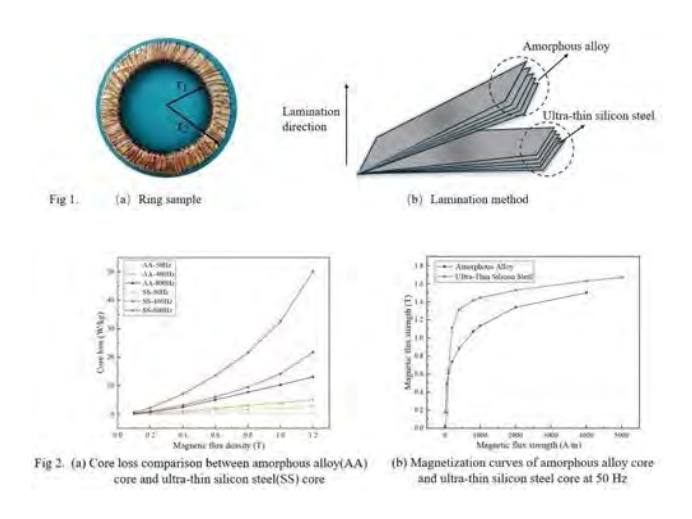
¹Shenyang University of Technology, Shenyang, Liaoning, China, ²Suzhou InnMag New Energy Ltd, Suzhou, Jiangsu, China

Currently, improving the torque of high-speed electrical machine has been the focus of the industry. Silicon steel has a large saturation flux density, but its losses are larger than those of amorphous alloy^[1]. The saturation magnetic flux density directly determines the torque and power of the equipment, while the magnetic loss characteristics are related to the overall operating efficiency^[2]. However, soft magnetic materials with both high saturation flux density and low losses have been a major challenge in the materials field

Therefore, this paper proposes a hybrid laminated core that aims to synthesize the advantages of high saturation flux density of silicon steel and low core loss of amorphous alloy. By performing finite element analysis of the hybrid core, and the core with potential for application is selected from a variety of schemes for fabrication of samples and actual testing. The test validation results show that the lamination of an odd number of layers is more suitable for such a hybrid core because the Maxwell stresses in the direction of the lamination can be canceled to some extent. In addition, the measured results show that the number of laminated layers is a key factor affecting the magnetic properties of the core. The higher the number of layers, the better the magnetic field distribution uniformity in the core, but it will bring the problem of increased process complexity and longer fabrication cycle time. The lower the number of layers, the smaller the magnetic field across the interface between the two materials, and therefore the lower the core loss. Through simulation and testing, this paper finds that the cores with 5, 7, and 9 laminated layers perform as expected, with the 7-layer core being the most satisfactory. In order to verify the performance of this hybrid cores in electrical machine, this paper performs performance calculations for electrical machine with silicon steel, amorphous alloy and hybrid cores, and the results show that combining the two materials not only improves the efficiency of the core, but the torque is also satisfactory.

[1] Ismagilov, Flyur R., et al. "Design and performance of a high-speed permanent magnet generator with amorphous alloy magnetic core for aerospace applications." *IEEE Transactions on Industrial Electronics* 67.3 (2019): 1750-1758. [2] Tong, Wenming, et al. "Performance comparison

between an amorphous metal PMSM and a silicon steel PMSM." *IEEE Transactions on Magnetics* 55.6 (2019): 1-5.



VP6-10. Measuring Magnetostriction in Electric Motor Stator Cores Considering Manufacturing Factors and Material Anisotropy

L. Chen¹, H. Huang¹, T. Ben^{1, 2}, L. Wu¹
¹College of Electrical Engineering and New Energy, China Three Gorges University, Yichang City, China, ²Hubei Provincial Research Center on Microgrid Engineering Technology, China Three Gorges University, Yichang City, China

Magnetostriction refers to the dimensional change that occurs when ferromagnetic materials are magnetized. It is one of the significant sources of vibration and noise in electric motors [1]. The stator core of the electric motor is composed of non-oriented silicon steel sheets, and its inherent magnetostrictive anisotropy is caused by the differences in grain size and crystal structure. In addition, residual stresses introduced by manufacturing processes such as stamping, lamination, and welding can also alter its magnetostrictive properties [2]. To investigate the effects of these factors, a measurement system has been established to measure and analyze their impact on the magnetostriction properties of the stator core.

To investigate the magnetostriction characteristics of stator core under alternating magnetic field, strain gauges are used to measure the slight strain in the core caused by magnetostriction. Figure 1 shows the measurement system used to analyze the influence of material anisotropy and manufacturing process on the magnetostriction characteristics of the stator core. Figure 2 compares the strain amplitudes in the circumferential, radial, and axial

directions of the welded and unwelded areas of the motor stator. The results show that with the increase of magnetic flux density, the magnetostriction coefficients of the two areas increase in all three directions. However, the peak values of the radial and axial strain curves in the welded area are significantly higher than those in the unwelded area.

This paper systematically investigates the impact of degradation effects during the manufacturing process and the anisotropy of magnetic materials on the magnetostriction characteristics of the stator core. It is found that material anisotropy results in significant differences in the strain amplitude of the core at different angles, while degradation effects in the manufacturing process further exacerbate the strain magnitude. The paper will present more test results and delve into the underlying physical mechanisms.

[1] Y. Cai, F. S. El-Faouri, and N. Saikawa, IEEE Transactions on Industry Applications., Vol. 61, p.2983-2995(2025) [2] M. Oka, T. Ogasawara, and N. Kawano, IEEE Transactions on Magnetics., Vol. 50, 8202904(2014)

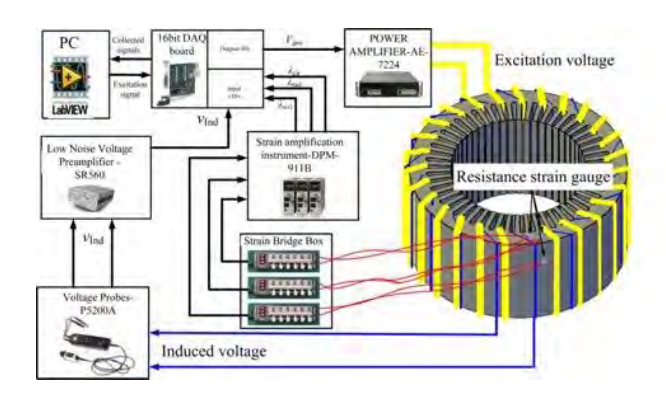


Fig. 1 Control loops for the hardware of the measurement system

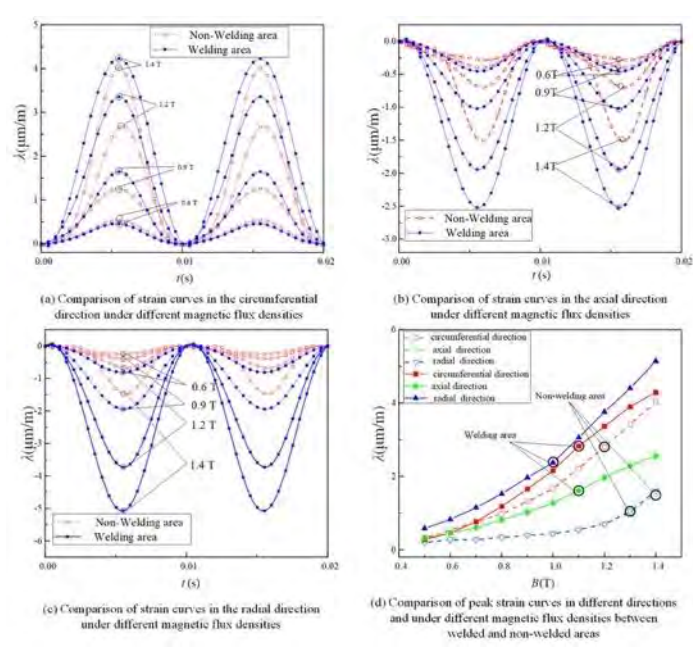


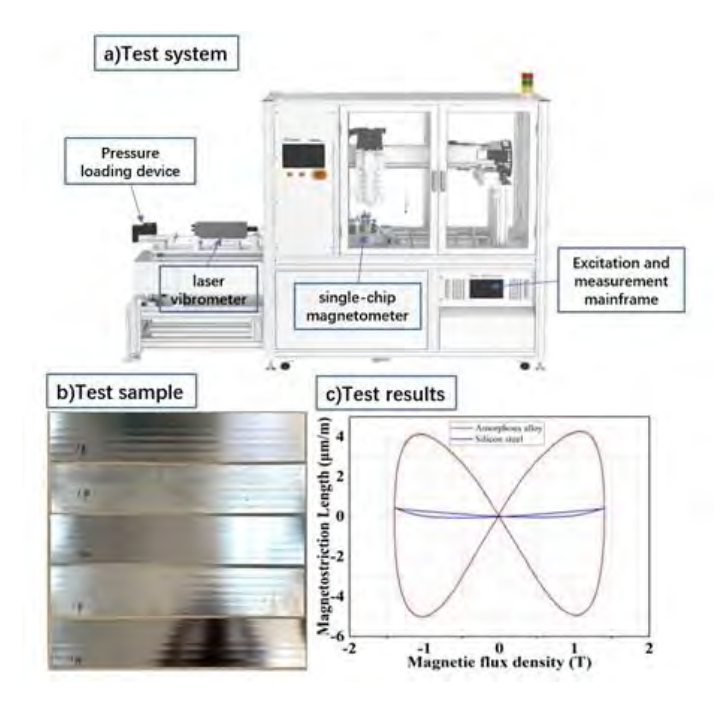
Fig. 2 Magnetostriction comparison between welded and non-welded areas

VP6-11. Optimization of amorphous magnetostriction prediction model considering the effect of stresses X. Liu¹, X. Lu¹, Z. Li¹, J. Feng¹, L. Zeng², R. Pei^{1, 2} ¹Shenyang University of Technology, Shenyang, Liaoning, China, ²Suzhou InnMag New Energy Ltd, Suzhou, Jiangsu, China

Amorphous soft magnetic materials are characterized by high permeability and low magnetic losses, which have attracted the interest of motor scholars and manufacturers. However, the magnetostrictive deformation of amorphous alloys is very large compared to ordinary electrical steel, which causes vibration and noise in electric machines. Magnetostriction can be regarded as an internal stress. which can be measured and modeled and calculated experimentally. However, during electric machines fabrication and operation, the core is subjected to external forces from a rich variety of sources, for example, compressive stresses induced by the thermal jacket, rotor centrifugal forces and Maxwell stresses. In order to investigate the law of magnetostriction and stress interaction, in this paper, we design experiments to investigate the magnetostriction of amorphous alloys under different stresses. At the same time, we noticed that layers need to be stacked and bonded with adhesive during the core molding process, so we comparatively tested the magnetostrictive effect of multilayer amorphous containing adhesive. The results show that the magnetostriction of

amorphous alloys is more sensitive to external stress than that of ordinary electrical steel. The degree of core loss and magnetic flux density decrease in amorphous alloys under the same stress is also greater than that of ordinary electrical steel. This indicates that the deformation caused by stress and magnetostriction must be accurately calculated when making electric machines from amorphous alloys. Based on the magnetostriction experiments under stress, this paper proposes a magnetostriction model for amorphous alloys based on the piezomagnetic equation. The model can accurately predict the amorphous magnetostriction under different stresses, which is informative for electric machines design and performance calculation.

Wu, Shengnan, et al. "Analytical model for predicting vibration due to magnetostriction in axial flux permanent magnet machines with amorphous metal cores." IEEE Transactions on Magnetics 53.8 (2017): 1-8.



^{*} Best Student Presentation Finalist / LB - Late-breaking Poster

VP6-12. Analysis of Stator Core Losses in Motors Made of Amorphous Alloy Materials Considering Temperature and Compressive Stress Factors

X. Lu¹, D. Ma¹, J. Feng¹, N. Zhang¹, L. Zeng², R. Pei^{1, 2}
¹Department of Electrical Engineering, Shenyang University of Technology, Shenyang, Liaoning, China, ²Suzhou INN-MAG New Energy Technology Co., Ltd., Suzhou, Jiangsu, China

Iron-based amorphous strips are considered to be the core material that may be effective in reducing the losses of electric motors due to their low loss characteristics. During the operation of the motor, the core is often affected by the coupling of mechanical stress, temperature, magnetic field and other complex factors. It has been demonstrated that the residual stresses during core processing can have a large impact on the core losses. Further, the study of amorphous core loss considering the coupling effects of temperature and stress is essential, which will directly affect the accuracy of motor modeling. Currently, there are fewer experimental investigations for this aspect. In this paper, in order to understand the amorphous and conventional silicon steel in the temperature, stress coupling loss difference and explore the amorphous loss change rule, first of all, the amorphous (1K101) and conventional very thin silicon steel (ST-100) two materials for the temperature and stress coupling iron loss test, and analyze the difference between the 1K101 loss change rule. The self-research system for the test contains a magnetic property measurement device, a mechanical property test device and a high and low temperature alternating device.

Further, an amorphous iron loss calculation model considering the effects of temperature and stress coupling is proposed with the aim of improving the iron loss calculation accuracy of amorphous motors, and the measured values, the classical iron loss model and the innovative model in this paper are compared to verify its accuracy. Meanwhile, a high-speed permanent magnet motor is modeled and finite element simulated to analyze the temperature rise and stress distribution of the motor under the two methods to verify the accuracy and advantages of the temperature and stress coupling magnetic performance test results.

[1] Zhang, Changgeng, et al. "Testing of magnetic properties of amorphous and nanocrystalline alloys applied out-of-plane stress at wide frequency range." *Journal of Magnetism and Magnetic Materials* 623 (2025): 173013.

[2] Zhao, Zhixiao, et al. "Research on Performance Degradation Mechanism and Correction of Core Loss Model of Amorphous Alloys Based on Wire Cutting." *IEEE Transactions on Magnetics* (2025).

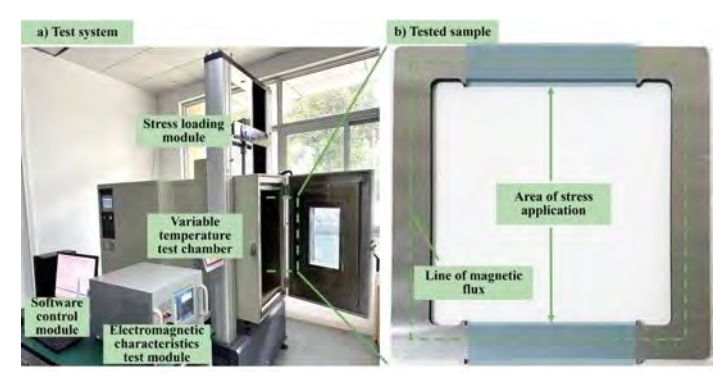


Fig.1 a) Temperature and stress coupled magnetic property measurement system and b) The developed test sample

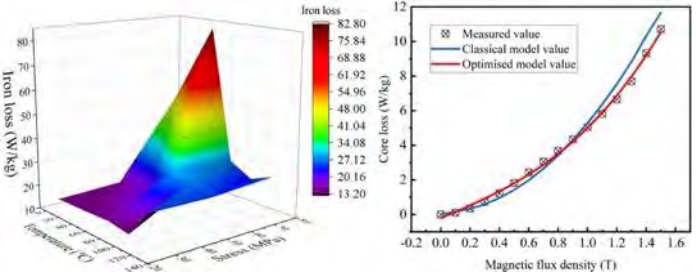


Fig.2 a) Amorphous loss variation considering temperature and stress (1T&400Hz) and b) Comparison chart of three types of iron losses

VP6-13. Effect of Ytterbium substitution on the structural and magnetic properties of cobalt ferrite nanoparticles

T. Han, <u>F. Huang</u>, T. Du

Department of Applied Physics, National University of Kaohsiung, Kaohsiung, Taiwan

Cobalt ferrite, CoFe₂O₄ (CFO), has received much attention due to its numerous functional properties. It is a hard magnet with considerable magnetic anisotropy, high chemical stability, and mechanical hardness [1]. Researchers have been trying to optimize the properties of cobalt ferrite in various ways, including doping it with various elements [1,2]. The low coercivity of spinel ferrites is a significant barrier limiting their use in high-density magnetic recording applications. The large magnitude of the magnetocrystalline anisotropy of the rare earth group elements can lead to a high coercivity field by doping the magnetic ferrites with these elements. Moreover, the physical properties of CFO at reduced grain sizes remain

underexplored due to the challenges associated with their synthesis with a proper control over the crystalline phase. Therefore, in this work, we prepared a series of CoFe₂₋ $_{x}Yb_{x}O_{4}$ nanoparticle samples with x = 0.05, 0.10, 0.15, and 0.20 by the sol-gel method, and systematically study the effect of ytterbium (Yb) substitution on their structural and magnetic properties. The X-ray diffraction pattern (XRD) analysis using the Rietveld refinement method indicated that all samples have a spinel structure. The lattice parameter was estimated to be in the range of 0.835 nm to 0.838 nm. The average crystallite size and lattice strain was estimated by using Debye-Scherrer formula and Williamson-Hall (W-H) method. It has shown also by increasing Ybcontent, the average crystallite size decrease, while the lattice strain increases. The Raman spectroscopy data from the samples showed a mixed spinel structure for Yb doped samples. Raman spectroscopy analysis also reveals that Yb3+ is substituting Fe3+ in both the tetrahedral and octahedral sites. Hysteresis loops at room temperature obtained by the vibrating sample magnetometer (VSM) indicate that the coercivity field (H_c) increases significantly from 171 to 1002 Oe by decreasing Yb doping from x = 0.20to 0.05. Furthermore, the analysis of the anisotropy constants showed that the anisotropy share of the magnetocrystalline anisotropy of the nanoparticles is cubic and not uniaxial.

Sharma, G. Chandra, S. K. Upadhyay, J. Magn. Magn.
 Mater. 606, 172397 (2024).
 X. Jing, M. Guo, Z. Li, C. Qin, Z. Chen, Z. Li and H. Gong,
 Ceram. Int. 49, 14046 (2023).

VP6-15. Withdrawn

VP6-16. On the analysis of the skin effect on the loss evaluation of soft magnetic materials under broadband magnetization

L. Chen^{1,2}, <u>L. Tan</u>¹, T. Ben¹, H. Huang¹, B. Huang¹
¹College of Electrical Engineering and New Energy, China Three Gorges University, Yichang, Hubei, China, ²Hubei Provincial Research Center on Microgrid Engineering Technology, China Three Gorges University, Yichang, Hubei, China

Accurate modeling of skin effect impact on soft magnetic core losses is critical for electrical equipment analysis[1]. Recent high-frequency loss models for laminated materials exhibit significant discrepancies, with analytic (Steinmetz, loss separation) and numerical (FDTD/FEM) approaches remaining divergent due to material parameter variations. This study proposes a coupled-hysteresis 1D FEM framework to establish material-specific skin effect criteria for grain-oriented silicon steel[2], non-oriented silicon steel, and nanocrystalline alloy, delineating operational boundaries where skin effect necessitates inclusion in dynamic loss computations.

As shown in Fig. 1, a time-domain solution was implemented on a 1D laminated sheet model to establish effective skin effect application criteria. The formulation incorporates hysteretic effects and excess loss magnetic fields, with the hysteretic field component resolved via an inverse Preisach model.

As demonstrated in Fig. 2(a)-(f), varying degrees of skin effect manifestation occur across different materials under distinct flux densities and excitation frequencies. Consequently, generalized claims regarding skin effect inclusion requirements for specific materials at given frequencies are unsubstantiated. Consequently, a skin effect factor λ incorporating frequency, material thickness, permeability, and flux density magnitude is proposed as a quantitative metric to evaluate the significance level of skin effect at arbitrary operating points. Obtained results shows that the skin effect needs to be considered for grain-oriented silicon steel λ of 0.83, and nanocrystalline alloy λ of 1.62.

In this paper, methodologies for determining skin effect criteria across diverse soft magnetic materials have been thoroughly investigated. Calculated results show that the criteria for considering skin effect are not consistent across materials and conditions.

[1] H. Zhao, J. Tu, Y. Zhang, F. Zheng and Y. An, IEEE Transactions on Magnetics, Vol. 59, 6300904(2023).
[2] S. Quondam Antonio, A. Faba, H. P. Rimal and E. Cardelli, IEEE Transactions on Magnetics, Vol. 56, p.1-15, April(2020)

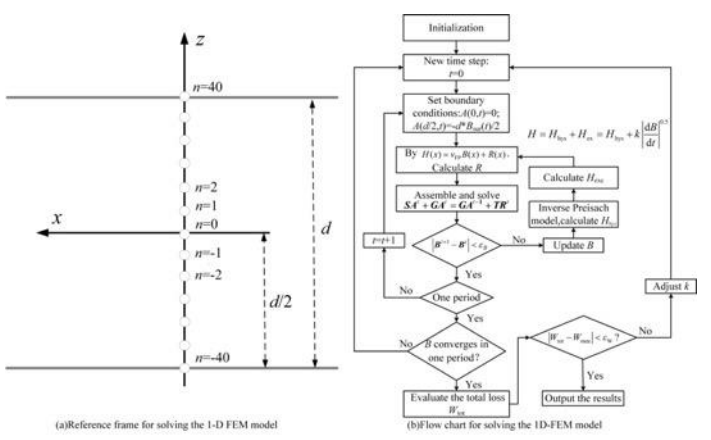


Fig.1. Time-domain solution procedure for a onedimensional laminated model with coupled dynamic hysteresis

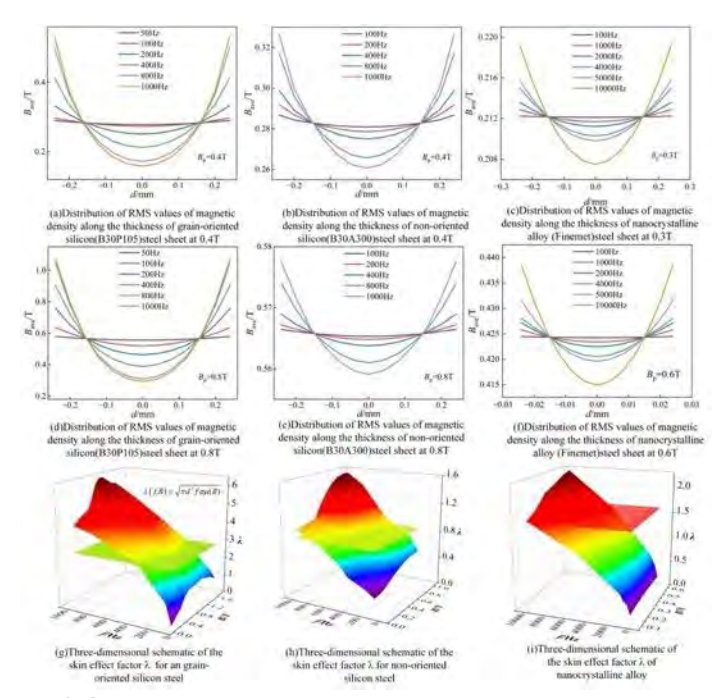


Fig.2 Comparison of skin effect of different materials under different working conditions

VP6-17. Structural and Magnetic Investigation of Fe doped $Mn_{3-x}Fe_xO_4$ ($x\leq0.1$)

S. Yoon

Department of Physics, Gunsan National University, Gunsan, Korea (the Republic of)

Zhang et al. [1] has reported an unusual structural-magnetic interplay in FeMn₂O polyhedral distortion. Since the Mn³⁺ ion in the octahedral (B) site is Jahn-Teller active, there is a cubic to tetragonal transition with lowering the temperature. Unit cell stretched along c-axis and accordingly the tetragonality (c/a) increased as the temperature lowerd. Through their elaborate neutron diffraction analysis, they clarified that the B site was finally divided into two different sublattices B1 and B2, among which B2 showed spin canting below T_{N2}. Inspired by their work, the spin structure of Mn-rich ferrite was explored by small-amount substitution of Fe for Mn in this work. According to their conjecture, we could control the tetragonality and spin structure not only by lowering the temperature but also by gradually adding non-Jahn-Teller Mössbauer ion into Mn₃O₄.

In this study, structural and magnetic properties of Fe ion containing manganese ferrites Mn_{3-x}Fe_xO₄ have been investigated by using X-ray diffraction (XRD), neutron diffraction(ND), vibrating sample magnetometer (VSM) and Mössbauer spectroscopy. ⁵⁷Fe doped Mn_{3-x}Fe_xO₄(0≤x≤0.1) powders were prepared by conventional ceramic method followed by liquid-nitrogen quenching. GSAS refinement of XRD profiles has been done (space group I4 /amd) to obtain lattice constants and tetragonality of the samples (right of Figure 1). Left of Fig. 1 shows that magnetic peaks near 20° (arrow) disappears across T≈60 K. Figure 2 depicts ⁵⁷Fe Mössbauer spectra of the samples taken at room temperature. When x<0.75, the tetragonality is large and the spectra consist of three quadrupole doublets stemming from tetrahedral (A), octahedral B1 and B2, respectively. Ratio of absorption area of A, B2 and B1 is 10:1:1. Isomer shift values of all subspectra correspond to +3 state. The tetragonality decreased with further substitution of Fe. When x≥0.1 (c/a=1.628), B2 phase disappeared and merged into B1. As a result, we can conclude that B2 subspectra came from the B2 crystallographic site of $Mn_{3-x}Fe_xO_4$ (x ≤ 0.075). The quadrupole splitting of B2 was ~2.3 mm/s. [1] Qiang Zhang, Wei Tian, Roshan Nepal, Ashfia Hug, Stephen Nagler, J. F. DiTusa, and Rongying Jin, Chem. Mater. <u>35</u>, 2330 (2023).

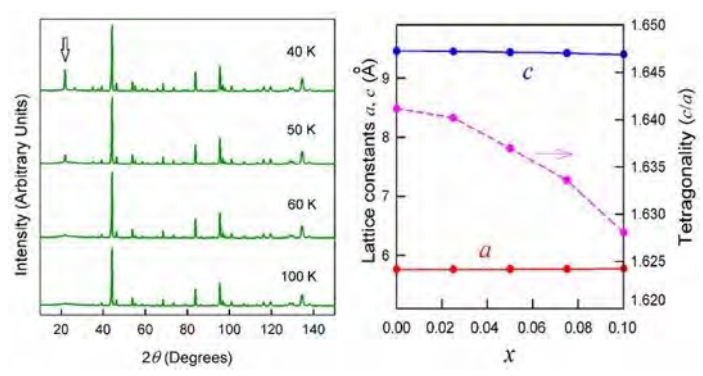


Fig. 1 ND profile for x=0.05 (left) and change of lattice constants and tetragonality(right).

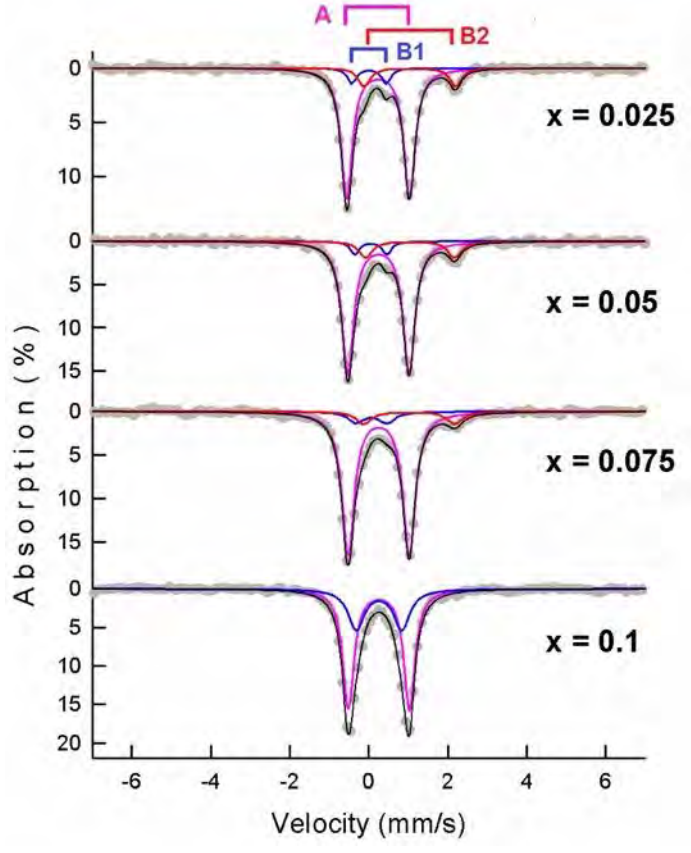


Fig. 2 Room-temperature Mossbauer spectra of Mn_{3-x}Fe_xO₄.

VP6-18. Research and Analysis of Different Thickness Silicon Steels for an Ultra High-Speed PMSM

M. Cheng, Z. Li, Y. Li, R. Pei

Shenyang University of Technology, Shenyang, Liaoning, China

Ultra-high speed permanent magnet synchronous motors (UHSPMSMs) have the advantages of small size, light weight and high efficiency. However, the high rotational speed of the electric motor leads to a high working frequency, in turn causing significant core loss, particularly eddy current loss. Reducing the thickness of silicon steel sheet has become a prevalent technique. Thus, this paper investigates the impact of reducing the thickness of silicon steel sheets on the core loss of UHSPMMs. To this end, four types of silicon steel (0.1 mm, 0.15 mm, 0.2 mm, and 0.25 mm) in three states (steel sheet, iron core, and electric motor) are researched. The experimental and finite element analysis approach was employed to investigate the core loss and its proportion in the total loss of the four silicon steels, particularly under high frequencies. Based on Bertotti's iron loss model, the iron loss is divided into the hysteresis loss, eddy current loss and additional loss. The results indicate that thin silicon steel cores exhibit reduced losses. However, this conclusion is contingent upon the assumption that the frequency must attain a specific value and that the thickness of the silicon steel strip exerts an influence on this frequency. The results of the iron loss separation indicate that compared with thicker silicon steel, thin silicon steel has more obvious hysteresis loss and additional loss at low frequencies, which are also applicable to silicon steel sheets and stator cores. However, due to the processes of shearing and laminating when manufacturing silicon steel sheets into cores, significant differences in losses appear in numerical values. In this paper, a 25kW, 95krpm permanent magnet synchronous motor is taken as the research object. The results show that the reduction of stator iron loss is proportional to the thickness, but this reduction is accompanied by an increase in copper loss and rotor eddy current loss. Therefore, in practical engineering applications and material selection, the distribution of losses needs to be comprehensively considered.

M. Leandro, N. Elloumi, A. Tessarolo, and J. K. Noland, Analytical Iron Loss Evaluation in the Stator Yoke of Slotless Surface-Mounted PM Machines, *IEEE Trans. on Ind. Applicat.*, vol. 58, no. 4, pp. 4602–4613, Jul (2022)

Zi-Qiang. Zhu, Shaoshen Xue, Wenqiang Chu, Jianghua Feng *et al.*, Evaluation of Iron Loss Models in Electrical

^{*} Best Student Presentation Finalist / LB - Late-breaking Poster

Physics, Iasi, Romania

Machines, *IEEE Trans. on Ind. Applicat.*, vol. 55, no. 2, pp. 1461–1472, Mar (2019)

Guanghui Du, Wei Xu, Jianguo Zhu, and Na Huang, Power Loss and Thermal Analysis for High-Power High-Speed Permanent Magnet Machines, *IEEE Trans. Ind. Electron*, vol. 67, no. 4 (2020)

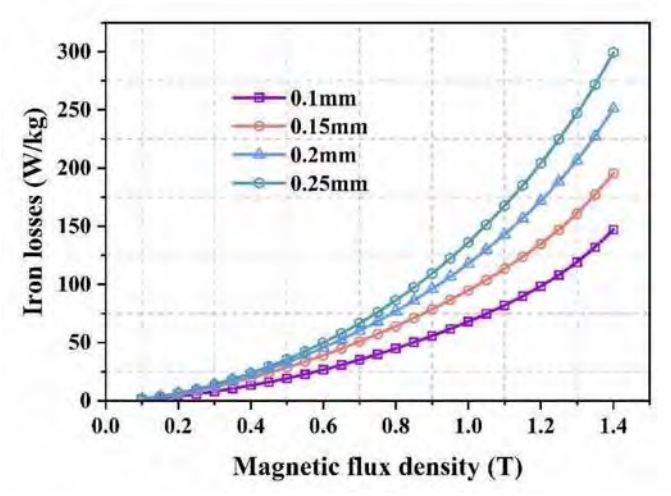


Fig.1 Measured *B-P* curves of various ultra-thin silicon steels at 2000Hz.

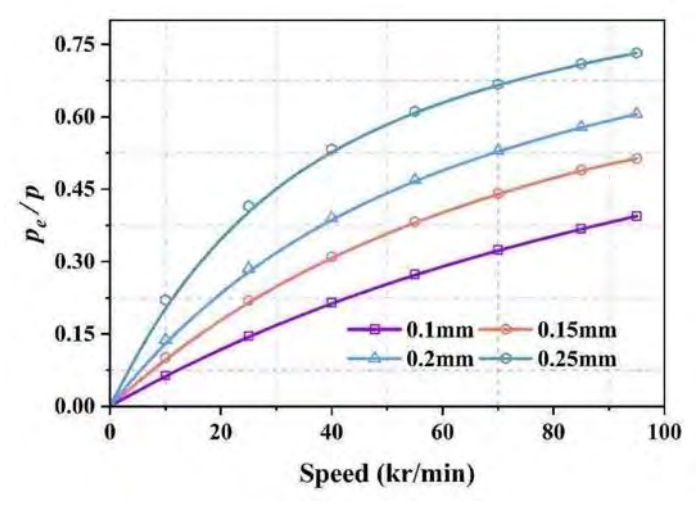


Fig.2 The ratio of eddy current loss to iron loss.

VP6-19. Magneto-Optical Investigation of Magnetization Reversal and Anisotropy in Amorphous Co-Based Microwires M. Lostun, I. Murgulescu, H. Chiriac, T. A. Ovari, N. Lupu National Institute of Research and Development for Technical

Magnetic amorphous microwires are of great interest for both technological applications and fundamental research. Thanks to their cylindrical symmetry, they can exhibit longitudinal magnetization desirable for practical applications.

In this study, we present a magneto-optical Kerr effect (MOKE) investigation of the surface magnetization reversal process in amorphous $Co_{68.15}Fe_{4.35}Si_{12.5}B_{15}$ microwires, with diameters of 120 µm and saturation magnetization of 0.68 T, fabricated by in-rotating water spinning. Our main objective is to understand how annealing under longitudinal stress influences surface magnetic behavior. The magnetostriction coefficient changes from slightly negative values ($\lambda_s = -0.8 \times 10^{-6}$) in the as-cast state to slightly positive values ($\lambda_s = +0.2 \times 10^{-6}$) after thermal treatment, inducing specific magnetic anisotropy.

MOKE measurements on as-quenched samples reveal that longitudinal magnetization reversal results in narrow, inclined hysteresis loops with low remanence and coercivity. This indicates that the longitudinal direction on the wire surface (LMOKE) acts as a relatively hard magnetic axis. As the field is reduced from saturation, magnetization initially rotates toward the local easy axis, followed by domain wall motion. In the transverse MOKE (TMOKE) configuration, hysteresis loops show discrete jumps, linked to redistribution of circumferential domains on the wire surface (noting the microscope's observed area is limited relative to the wire's total length). The helical-type anisotropy observed in annealed wires is attributed to two factors: (i) magnetoelastic anisotropy that gives rise to circumferential easy axes due to negative magnetostriction and tensile stresses; (ii) precipitation of very small Co clusters (up to 5 nm) that contributes significantly to the experimentally observed helical-type anisotropy (Fig. 1). Acknowledgements. Financial support from the NUCLEU Programme - Contract No. 18N/01.01.2023, project PN 23 11 01 01, is gratefully acknowledged.

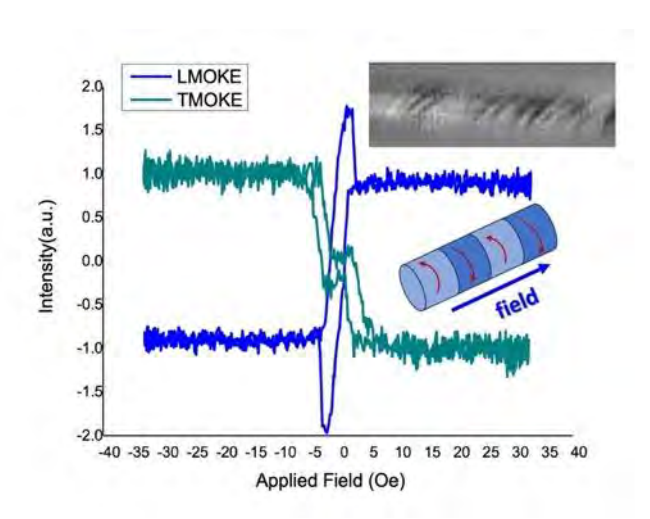


Fig. 1. MOKE hysteresis loops measured at the surface of $Co_{68.15}Fe_{4.35}Si_{12.5}B_{15}$ microwires after thermal treatments under longitudinal stress.

VP6-20. Effect of Lamination Forming Process on the Magnetic Properties of Electrical Steel Core

W. Li¹, Y. Li¹, Z. Xie¹, L. Zeng², R. Pei^{1, 2}
¹Shenyang University of Technology, Shenyang, China, ²Suzhou Inn-Mag New Energy Ltd., Suzhou, China

Iron core lamination forming process is one of the necessary process of motor manufacturing, core lamination way, being widely used, is worth to cite the clamping, welding or gluing technologies, these have a greater impact on the motor performance [1]. Ref. [2] studied the effect of welding on the performance of the core, and Ref. [3] investigated the application of self-bonding material with a thickness of 0.35 mm, which has made great improvements in coating in recent years, in an external rotor permanent magnet synchronous motor with a speed of 1500 rpm. At present, the effect of different core lamination processes on the magnetic properties of materials over a wide range of variable frequencies has rarely been investigated. Tests were performed to fabricate three rings and three cores, as shown in Fig. 1. Ring 1 is based on a self-bonding core (ZZ25WV1300), which is stacked by placing it under 1.5 MPa pressure for 1h at 180°C; Ring 2 is made of the same material with a conventional coating (25WV1300), which is applied by dispensing; Ring 3 is made of the same material as ring 2, but it is welded, with 5 weld seams set up. Three stator cores were fabricated and tested for magnetic properties to compare with the performance of the circular samples. Core 1 corresponds to the self-bonding process,

core 2 corresponds to the dispensing ring process, and core 3 corresponds to the welded ring process (8 weld seams). The magnetic performance tests of three process rings at 50Hz-1000Hz were completed, the Magnetic field strength-Flux density curves (B-H curves) at 50Hz are shown in Fig. 2. It can be seen that the magnetic density of the self-bonding sample is about 1.32 T at 800 A/m, which is higher than the values of dispensing and welding samples of 7.32% and 1.54%, respectively. It is worth noting that the B-H of the two processes of dispensing, and welding produce an intersection point at a flux density of about 1.2 T, which is just the intersection point between the irreversible magnetic domain wall movement and the dominant phase of domain rotation (the migration behaviour of the magnetic domain wall decreases gradually), which will be analysed in the full paper.

- [1] Z. Gmyrek, and A. Cavagnino, Influence of punching, welding, and Clamping on magnetic cores of fractional kilowatt motors. IEEE Transactions on Industry Applications, 54 (5): 4123-4132. (2018).
- [2] H. Wang and Y. Zhang. Modeling of Eddy-Current Losses of Welded Laminated Electrical Steels. IEEE Transactions on Industrial Electronics, 64(4), 2992-3000 (2017).
- [3] Z. Yu, J. Wan, Y. Li, et al. Application analysis of self-bonding electrical steel sheet in high power density PMSM for all-electric aircraft. Energy Reports, 9, 514-521 (2023).

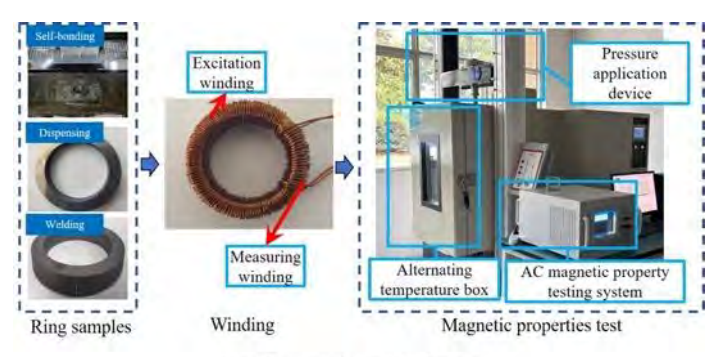


Fig. 1 Test samples and equipment

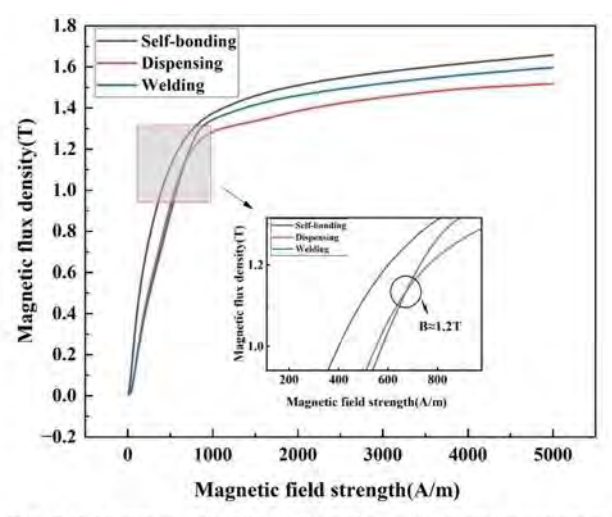


Fig. 2 B-H curves of self-bonding, dispensing, and welding at 50Hz

VP6-21. A Mean Field Approach to Analyzing the Magnetization of Interacting Ferrimagnetic Particles under Superparamagnetic Conditions

S. Rajput, S. Tiwari

Department of Physics and Materials Science, Thapar institute of Engineering and Technology, Patiala, Punjab, India

The magnetic behavior of ferrimagnetic nanoparticles is strongly influenced by interparticle and dipolar interactions, especially under superparamagnetic conditions where thermal fluctuations dominate. The magnetization of superparamagnetic particles has been also described by the Langevin function for last few decades which assumes the moments are non-interacting which is not correct for any superparamagnetic system. According to Mean field approach, each particle is assumed to experience both the externally applied magnetic field and the averaged impact of its surrounding magnetic particles. The internal magnetic field generated by interactions with neighboring particles is directly related to the overall magnetization of the system. Nanoparticles of magnetite are synthesized via coprecipitation method. These particles are divided in to two parts. One part is uncoated nanoparticles and rest of the particles are coated with a monolayer of non-magnetic oleic acid. The samples are characterized by x-ray diffractometer, TEM and VSM. FTIR confirms the coating around the magnetite nanoparticles. Mean crystallite size of the magnetic material is 6.5 nm. The magnetite particles are superparamagnetic in nature. The ZFC susceptibility of uncoated particles peaks at 110 K, while the ZFC and FC curves get bifurcate at 185 K. For the case of coated

particles, the ZFC susceptibility peaks at 85 K, while the ZFC and FC curves get bifurcate at 175 K. The Langevin function is used to describe the magnetization of the samples. But these results overestimated value for the mean particle magnetic moment. The Langevin function does not consider any dipolar interactions among particles. Concept of Mean field theory is used with the Langevin function and this proposed function describes the magnetization of interacting particles well and results sensible values for the mean particles magnetic moment. This work contributes to a deeper understanding in high-performance applications such as magnetic hyperthermia, targeted drug delivery, and high-density magnetic storage.

- 1. I.S. Jacobs, C.P.Bean, in Magnetism, Vol. III edited by G.T. Rado, H. Suhl (Academic Press Inc., New York, 1963).
- 2. M.S. Seehra, H. Shim, P. Dutta, A. Manivannan, J. Bonevich, J. Appl. Phys. 97, 10J509 (2005).
- 3. M. Tadic, S. Kralj, Y. Lalatonne, L. Motte, Appl. Surf. Sci. 476, 641 (2019).
- 4. S. Rajput, S.D. Tiwari, J. Magn. Magn. Mater. 611, 172603 (2024).

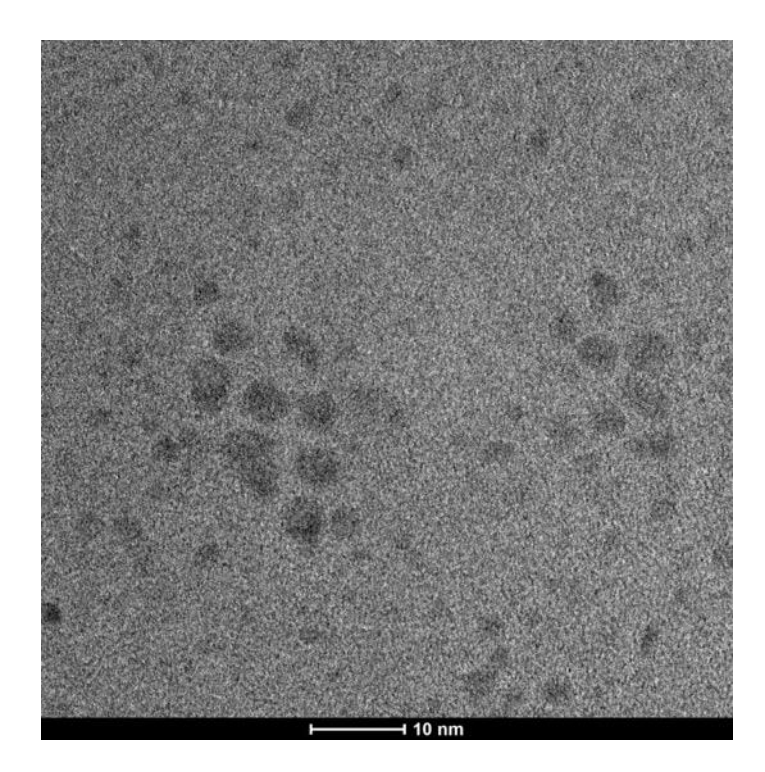


Fig. 1 TEM image of magnetite nanoparticles

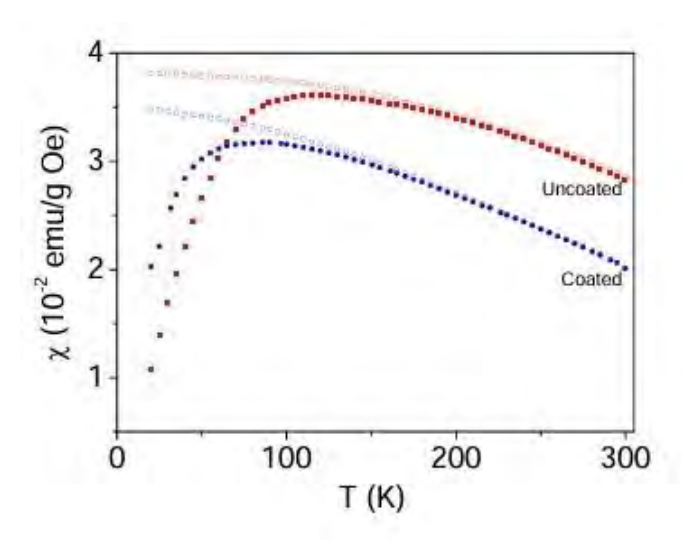


Fig. 2 Temperature variation of ZFC and FC magnetic susceptibility in 350 G magnetic field for the uncoated and the coated particles.

SESSION VP7: SPINTRONIC MATERIALS AND DEVICES

Chair(s): S. Husain, Material Science and Engineering, University of California, Berkeley, Berkeley, California, United States

Conference Resource Center

VP7-01. Spin-orbit torque magnetization switching in CoFeB/Ta/CoFeB tri-layer thin films

K. Okada, M. Matsuura, Y. Saito, N. Tezuka Tohoku University, Sendai, Miyagi, Japan

Spin-orbit torque magnetoresistive random-access memory (SOT-MRAM) is a promising technology for low-power and high-performance electronics. However, one problem for SOT-MRAM with perpendicular magnetization is needing an external in-plane magnetic field for reliable switching. To achieve field-free switching, composite structures using a perpendicularly magnetized ferromagnet (PMF), a nonmagnetic metal (NM), and an in-plane magnetized ferromagnet (IFM) have been proposed [1]. While previous studies have used Ti for the NM layer, this study utilizes Tantalum (Ta), which is known for its large spin Hall angle, to enhance SOT efficiency. This study aims to demonstrate SOT magnetization switching in a CoFeB(PMF)/Ta/CoFeB(IFM) trilayer system without an external magnetic field, and to clarify the relationship between layer thickness and the required switching current density.

We fabricated SOT devices realized as CoFeB(PMF)/Ta/CoFeB(IMF), systematically varying the thickness of the IFM layer (t_{IMF}). Figure 1 shows the relationship between applied current and anomalous Hall resistance for the device with t_{IMF} =4.0 nm. From the clear hysteresis loop in the figure, we confirmed that magnetization switching occurred without an external magnetic field.

Figure 2 shows the relation between the switching current density (J_c) and the external magnetic field (H_{ex}). As t_{IMF} was reduced, J_c under zero-field conditions decreased, reaching a minimum of $8.6\times10^{10}\,\text{Am}^{-2}$ at $t_{\text{IMF}}\text{=}2.0$ nm. This device also exhibited a 30% reduction in an applied field compared to a conventional Ta/CoFeB bilayer.

These findings demonstrate that the CoFeB/Ta/CoFeB trilayer structure is a viable solution for achieving both field-free operation and lower power consumption in SOT-MRAM, offering a promising path toward high-performance and energy-efficient memory systems.

This work was partly supported by the MEXT Initiative to Establish Next-generation Novel Integrated Circuits Centers (X-NICS) Grant Number JPJ011438, JSPS KAKENHI Grant Number 21K18189, and BRIDGE.

[1] S. C. Baek, et al., Nature Materials, Vol. 17, p.509-513 (2018)

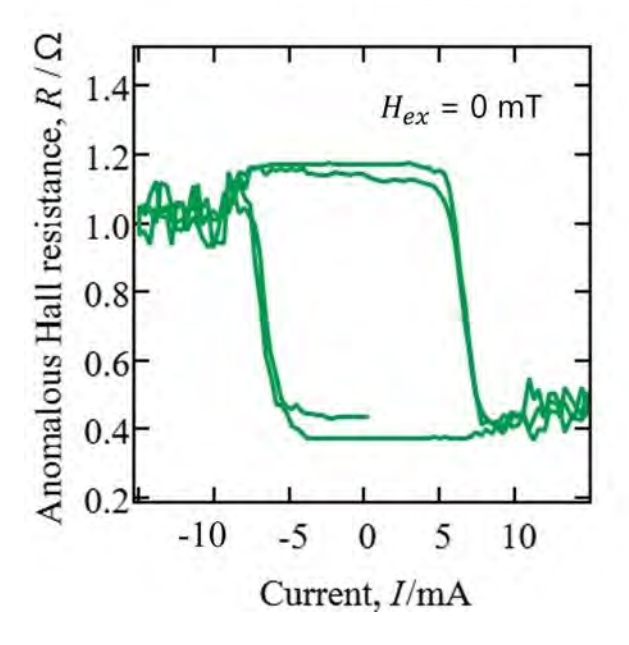


Fig. 1 Anomalous Hall resistance vs. applied current for the device with t_{IMF} =4.0 nm without an external field.

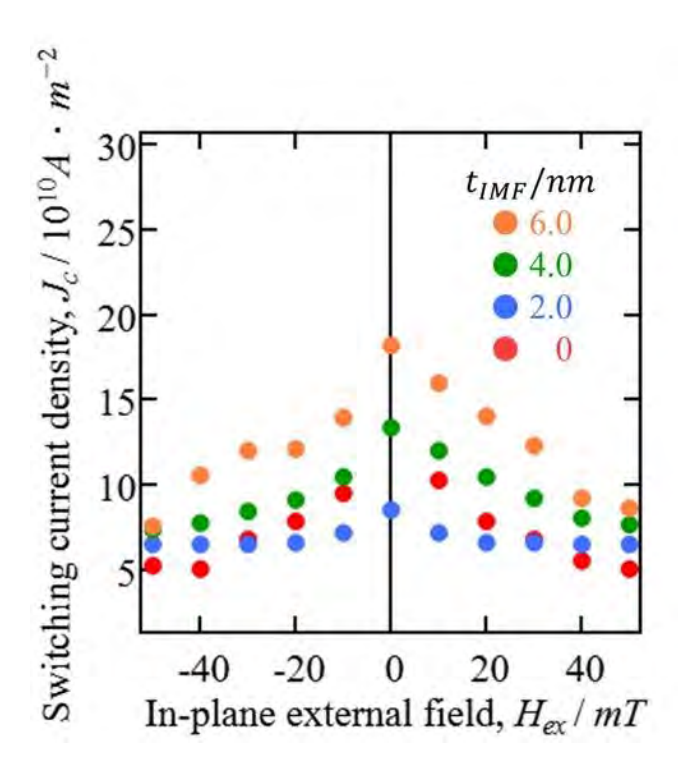


Fig. 2 Switching current density vs. external in-plane magnetic field for various t_{IMF} .

VP7-02. Thermal noise induced probability switching in SOT-MTJs based on spin-circuit simulation

T. Huang, <u>S. Hu</u> Shenzhen Technology University, Shenzhen, Guangdong, China

Spin-orbit torque magnetoresistive random access memory (SOT-MRAM) is emerging as a promising non-volatile memory technology characterized by low power consumption and high performance. The core structure of SOT-MRAM consists of magnetic tunnel junctions (MTJs) and heavy metal layer, as illustrated in Fig.1(a). However, practical performance of spintronic devices, including MTJs, is significantly influenced by magnetization noise. Particularly, under thermally activated switching conditions, thermal noise becomes the dominant factor due to its pronounced effect in modifying the effective temperature and lowering the energy barrier for magnetization reversal. When the applied current pulse approaches the critical switching current of the MTJ, thermal noise enables probabilistic magnetization switching. Such probabilistic behavior of MTJs facilitates their application in probabilistic computing. However, current simulation techniques primarily employ compact mathematical models, which lack

physical-level fidelity. Consequently, these models inadequately account for the influence of pulse duration and circuit density effects on switching behavior, limiting their accuracy and predictive capabilities.

This study employs a physics-based simulation framework fully implemented in SPICE, designed for hybrid spintronic and conventional electronic circuits. This framework provides notable advantages, including high accuracy, rapid simulation speed, seamless compatibility with existing MOSFET SPICE models, straightforward implementation, and excellent usability. To explore the probabilistic switching behavior in SOT-MTJs induced by thermal noise, we developed a spin circuit composed of an MTJ module, non-magnetic (NM) module, a Landau-Lifshitz-Gilbert (LLG) module, and a spin Hall module, as illustrated in Fig. 1(b). Our findings reveal that thermal noise markedly impacts the probabilistic switching behavior, especially with varying pulse durations. Furthermore, the developed spincircuit model serves as a robust foundation for future design and implementation of circuit systems leveraging SOTbased MTJ devices, including true random number generators and neural network computing applications.

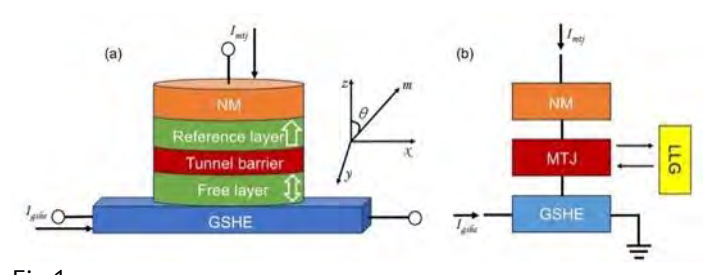


Fig.1

VP7-03. High-Throughput SEM Imaging of Nanoscale Metal Grains for Heat Assisted Magnetic Recording

M. Hauwiller, C. Mann, P. Mach, T. Zhao, T. Gao, A. Abdurahman, S. Hernandez, K. Terry, M. Kautzky Seagate Technology, Bloomington, Minnesota, United States

Development of nanoscale magnetic and plasmonic materials for applications such as Heat Assisted Magnetic Recording (HAMR) requires precise control and understanding of the materials' microstructure. Scanning Electron Microscopy (SEM) has the speed and resolution to characterize grain structure with high throughput, but there is little precedence for imaging sub-50 nm, crystallographically-aligned metal grains in a traditional SEM without specialized detectors or optics. Imaging

ungrounded micron-scale metal structures on wafers presents further challenges due to charging. By optimizing imaging parameters for each sample, sub-50 nm and sub-25 nm metal grains were captured. Monte Carlo simulations were used to understand the depth of backscattered electron signal for the stacks of materials and the effect of grain boundary tilt on grain boundary contrast. Highthroughput SEM grain imaging as demonstrated in this work yields large materials characterization datasets without expensive detectors or specialized hardware. Translating the qualitative SEM grain images to quantitative characterization requires continued algorithm development, yet there are significant opportunities for automated materials development and structure-property elucidation for SEM grain imaging combined with computer vision. The present and future of magnetic devices requires nanoscale materials control, and high-throughput SEM grain imaging is a promising metrology route for understanding and producing those structures.

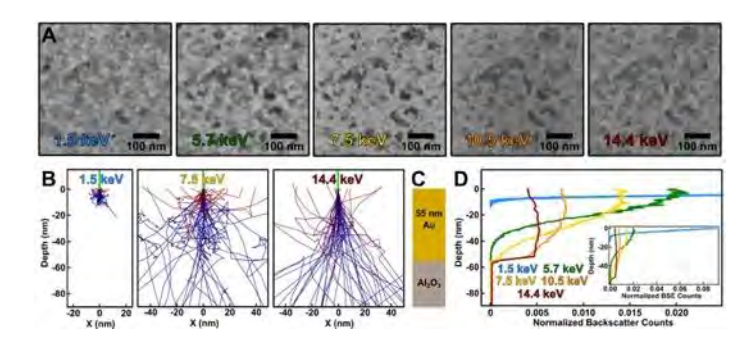


Fig. 1. The effect of Landing Energy on grain imaging. A) Imaging the same region of a 55 nm thick Au film on Al_2O_3 at varying landing energies. B) Monte Carlo simulations of electron trajectories in the film stack at varying landing energies. Red electron trajectories represent backscattered electrons that reach the surface (for detection) and blue electron trajectories represent electrons that remained buried in the sample. C) Schematic of the film stack of 55 nm Au on Al_2O_3 , scaled to align with 4B and 4D. D) Depth of backscattered electrons from Monte Carlo simulations for the film stack at the imaged landing energies. Inset shows the full 1.5 keV normalized counts.

VP7-05. Field-free magnetic resonance detection in the terahertz band using $Gd_{3/2}Yb_{1/2}BiFe_5O_{12}$

<u>T. Tsuchida</u>¹, Y. Ishikawa², T. Ito², K. Kawagita², Y. Goto², K. Yabushita², H. Fukumoto², Y. Fujii², K. Mikuni³, T. Satoh³, M. Goto^{1, 4}

¹Department of Electrical and Electronics Engineering, University of Fukui, Fukui, Japan, ²Research Center for Development of Far-Infrared Region, University of Fukui, Fukui, Japan, ³Department of Physics, Institute of Science Tokyo, Tokyo, Japan, ⁴Center for Spintronics Research Network (CSRN-Osaka), Osaka, Japan

Ferrimagnetic and antiferromagnetic materials have resonance frequencies in the terahertz band, and are considered promising for use in next-generation communication devices such as Beyond 5G and 6G. However, terahertz-band magnetic resonance needs a large external magnetic field of several Tesla, which limits the downsizing of devices. Therefore, we focused on the fact that $Gd_{3/2}Yb_{1/2}BiFe_5O_{12}$ has strong magnetic anisotropy at a specific temperature. We used this magnetic anisotropy as an effective magnetic field to detect terahertz magnetic resonance.

As shown in Fig. 1, Pt film of 6 nm was deposited on the side of the $Gd_{3/2}Yb_{1/2}BiFe_5O_{12}[1-2]$ substrate, and electrodes were connected to both ends of the Pt film using silver paste and thin copper wire. Gyrotron was also used as the electromagnetic wave source. The irradiated electromagnetic wave was modulated to a repetition rate of 5 Hz and an irradiation time of 10 ms. The modulation signal was also used as the reference signal for the lock-in amplifier. The external magnetic field was swept out of plane while irradiating the sample with the electromagnetic wave from the gyrotron, and a potential difference generated at both ends of the sample was measured by the lock-in amplifier.

At various temperatures, the magnetic field was swept from 0 T to 4 T while irradiating the sample with electromagnetic waves of 135 GHz frequency. As a result, the voltage signal shown in Figure 2 was obtained. In particular, voltage peaks were observed at zero magnetic field at 50 K and 80 K. This result represents successful magnetic field-free magnetic resonance detection in the terahertz range, and will serve as the foundational technology for terahertz spin devices.

- [1] S. Parchenko et al., IEEE Trans.Magn. 50, 6000904 (2014).
- [2] K. Mikuni et al., arXiv:2411.14792 (2024).

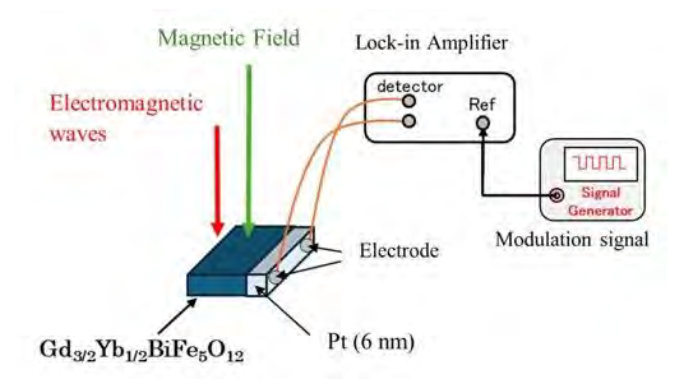


Fig. 1 Schematic of sample and measurement setup

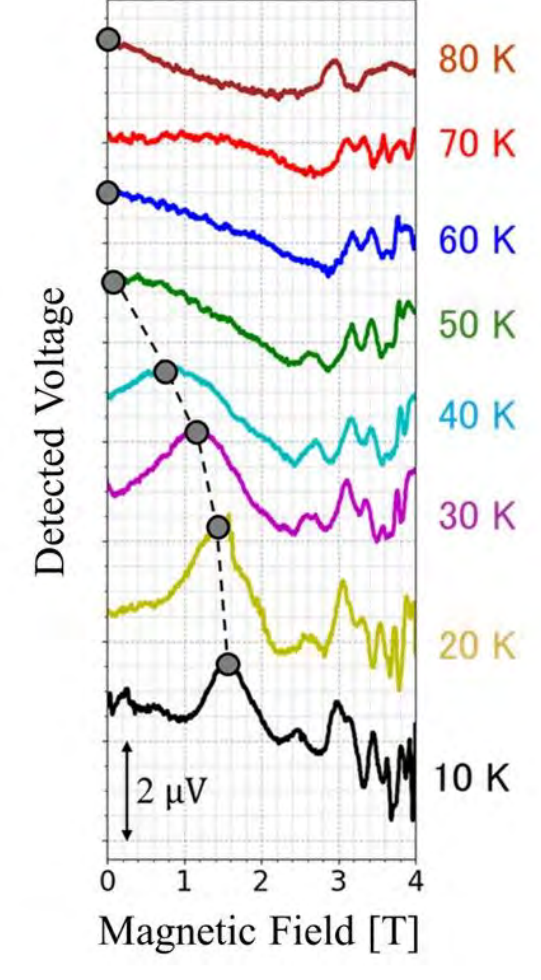


Fig. 2 Voltage peaks and their temperature dependence observed when the sample is irradiated with electromagnetic waves at a frequency of 135 GHz while the magnetic field is swept in the out of plane direction. The color represents the measurement temperature. The resonant magnetic field where the voltage peak is maximum is indicated by a gray circle, and these are connected by a dashed line.

VP7-06. Micromagnetic study of spin wave transmission in bent ferrimagnetic strips.

L. Sánchez-Tejerina, L. M. Moreno-Ramírez, <u>O. Alejos</u> *Universidad de Valladolid, Valladolid, Valladolid, Valladolid, Spain*

Recently, disruptive spintronic logic device concepts have been based on spin waves (SWs) as information carriers [1]. Such devices can be implemented on antiferro- and ferrimagnetic materials, presenting significant advantages in terms of speed and energy efficiency as compared to conventional electronic ones. Some devices rely on the interference of SWs travelling along different waveguides with geometries containing various bends. Their feasibility requires a thorough understanding of the transmission and propagation phenomena of SWs in these geometries.

A comprehensive study is made here of the transmission of SWs in bent waveguides made of ferrimagnetic material, with the geometry shown in Fig. 1. The guide is excited by spin currents in the area marked I and the transmission of SWs in the area marked O is measured. The excitation frequency of the guide is chosen according to typical values of the micromagnetic parameters of ferrimagnetic materials to obtain a propagation wavelength of $\lambda = 128$ nm [2], the width w_a being chosen equal to $\lambda/4$. Wave absorption zones at the ends of the guide have been stated to prevent reflections at these ends from affecting the propagation from I to O. At its center, the quide has two bends d_2 apart. Both the angle α of the bends and the distance d_2 determine the transmission coefficient (T) of the SW, defined from the quotient between the amplitude of the SW at O and the amplitude at a point at the same distance as that measurement point with respect to the excitation point in a strip without bends, i.e., without reflections associated with the geometry.

A summary of this study is seen in Fig.2. The dependence of T on d_2 is shown for different α , the values computed for d_2 equal to multiples of $\lambda/8$ (lines are only a guide for the eye). Transmission minima for d_2 equal to multiples of $\lambda/2$ and maxima for odd multiples of $\lambda/4$ are shown, which is reminiscent of interferometry results for other waveguides, but only explainable here through an imaginary reflection coefficient at both bends.

[1] A. Mahmoud et al., J. Appl. Phys. 128, 161101 (2020) [2] L. Sánchez-Tejerina, D. Osuna Ruiz, V. Raposo, E. Martínez, L. López Díaz, and Ó. Alejos, Physical Review B (in preparation)

^{*} Best Student Presentation Finalist / LB - Late-breaking Poster

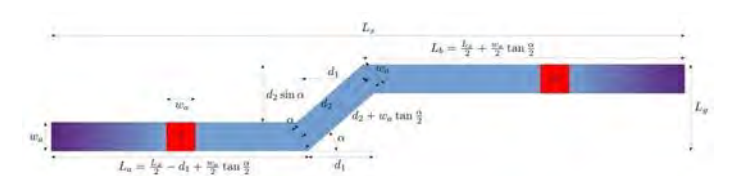


Fig. 1 Geometry of the device under study. The geometric relevant parameters are here shown.

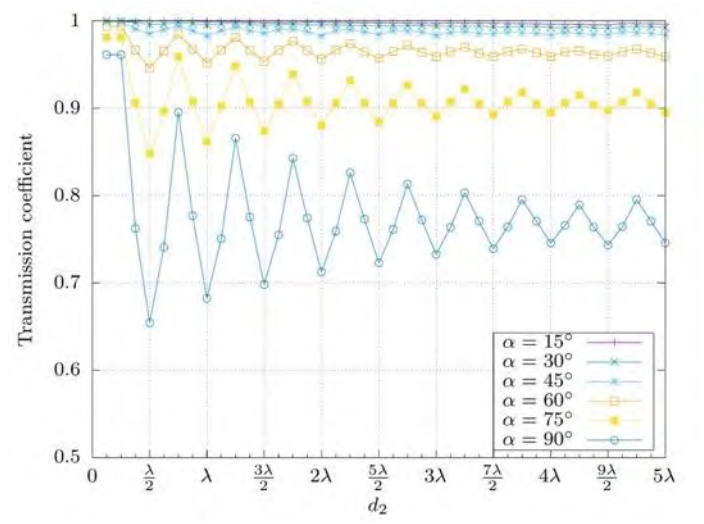


Fig. 2 Dependence of the transmission coefficient on distance d_2 with the angle α as a parameter.

VP7-07. Theoretical Insights Into Room-temperature Ferromagnetism of Metal-doped MoSe₂ Monolayer B. Narangerel, M. Adiya, D. Odkhuu

Physics, Incheon National University, Incheon, Korea (the Republic of)

The unique structure of transition metal dichalcogenides, characterized by strong intralayer covalent bonds and weak interlayer van der Waals forces, makes them ideal for modification through substitutional and intercalation of guest metal atoms, which in turn creates novel properties. Herein, we perform density functional theory, Monte Carlo, and molecular dynamic simulations to systematically investigate the intrinsic magnetic properties and Curie temperature of MoSe₂ monolayer doped with Fe and Co atoms. Both substitutional and intercalation doping approaches have been considered against various amounts of doping concentration. It is found that Fe and Co atoms preferentially replace for Mo over Se site, in agreement with the experimental and previous theoretical studies. Furthermore, our results demonstrate that the magnetic

moments and magnetic exchange interactions are highly dependent on the substitutional configurations and interatomic distance of dopant atoms. Remarkably, while interactions at shorter distances are suppressed with doping concentration, the interaction at a longer distance is significantly enhanced, reaching up to ~30 meV. This long-range strong interaction is illustrated as the dominant factor in stabilizing room-temperature ferromagnetism found in the experiments. These results are further supported by the micromagnetic simulations. The physical insights on temperature dependent intrinsic magnetic properties and Curie temperature will be discussed in comparison with the available experimental results.

This work is supported by the US DOD Office of Naval Research Global under award No. N62909-23-1-2035.

VP7-09. Withdrawn

VP7-10. Spin-Damping Dynamics Inspired Optimizer for Neural Networks

S. Ghaderi, A. D. Kent

Physics, New York University, New York, New York, United States

This work introduces a new class of physics-grounded optimizer for neural networks, directly inspired by the precession and damping dynamics central to magnetization in ferromagnets. The update rule parallels the relaxation of a spin toward equilibrium in an effective field, embedding the same physical principles that underlie phenomena from ferromagnetic resonance to spin-torque oscillators. The method combines a transverse, exploration-oriented motion with a dissipative relaxation that stabilizes learning trajectories on ill-conditioned, saddle-rich, and plateaued objectives.

Across representative benchmarks, the approach demonstrates more reliable convergence, lower final loss, and improved generalization than baselines (e.g., Adam, SGD) under matched budgets. The analogy with magnetic relaxation provides an intuitive physical explanation for robust saddle escape and efficient stabilization. Importantly, the framework also suggests a hardware pathway: magnetic tunnel junctions (MTJs) naturally embody precession and Gilbert damping as tunable device primitives. Leveraging these spintronic effects, the method could enable compact and energy-efficient optimization engines, bridging

- fundamental magnetization physics with modern machinelearning practice. Representative results will be shown.
- [1] D. Chen, A. D. Kent, D. Sels, and F. Morone, "Solving combinatorial optimization problems through stochastic Landau-Lifshitz-Gilbert dynamical systems," Physical Review Research, vol. 7, p. 013129, 2025. DOI: 10.1103/PhysRevResearch.7.013129.
- [2] W. F. Brown, Jr., "Thermal Fluctuations of a Single-Domain Particle," Physical Review, vol. 130, p. 1677, 1963.
- [3] C. Kittel, "On the Theory of Ferromagnetic Resonance Absorption," Physical Review, vol. 73, p. 155, 1948.
- [4] M. Lakshmanan, "The fascinating world of the Landau Lifshitz Gilbert equation: an overview," Philosophical Transactions of the Royal Society A, vol. 369, pp. 1280 1300, 2011.
- [5] J. C. Slonczewski, "Current-driven excitation of magnetic multilayers," Journal of Magnetism and Magnetic Materials, vol. 159, pp. L1–L7, 1996.
- [6] L. Berger, "Emission of spin waves by a magnetic multilayer traversed by a current," Physical Review B, vol. 54, pp. 9353–9358, 1996.
- [7] D. C. Ralph and M. D. Stiles, "Spin Transfer Torques," Journal of Magnetism and Magnetic Materials, vol. 320, no. 7–8, pp. 1190–1216, 2008.
- [8] A. Brataas, A. D. Kent, and H. Ohno, "Current-induced torques in magnetic materials," Nature Materials, vol. 11, no. 5, pp. 372–381, 2012.
- [9] A. Manchon, J. Zelezny, I. M. Miron, T. Jungwirth, J. Sinova, A. Thiaville, K. Garello, and P. Gambardella, "Current-induced spin-orbit torques in ferromagnetic and antiferromagnetic systems," Reviews of Modern Physics, vol. 91, p. 035004, 2019.
- [10] M. Jullière, "Tunneling between ferromagnetic films," Physics Letters A, vol. 54, no. 3, pp. 225–226, 1975.
- [11] J. S. Moodera, L. R. Kinder, T. M. Wong, and R. Meservey, "Large Magnetoresistance at Room Temperature in Ferromagnetic Thin Film Tunnel Junctions," Physical Review Letters, vol. 74, pp. 3273–3276, 1995.

- [12] S. Yuasa, T. Nagahama, A. Fukushima, Y. Suzuki, and K. Ando, "Giant room-temperature magnetoresistance in single-crystal Fe/MgO/Fe magnetic tunnel junctions," Nature Materials, vol. 3, pp. 868–871, 2004.
- [13] S. S. P. Parkin et al., "Giant tunnelling magnetoresistance at room temperature with MgO (100) tunnel barriers," Nature Materials, vol. 3, pp. 862–867, 2004.
- [14] S. Ikeda et al., "A perpendicular-anisotropy CoFeB-MgO magnetic tunnel junction," Nature Materials, vol. 9, pp. 721–724, 2010.
- [15] A. D. Kent and D. C. Worledge, "A new spin on magnetic memories," Nature Nanotechnology, vol. 10, pp. 187–191, 2015.
- [17] M. J. Donahue and D. G. Porter, OOMMF User's Guide, Version 1.0, NIST Interagency/Internal Report (NISTIR) 6376, 1999.
- [18] A. Vansteenkiste, J. Leliaert, M. Dvornik, F. Garcia-Sanchez, and B. Van Waeyenberge, "The design and verification of MuMax3," AIP Advances, vol. 4, p. 107133, 2014.
- [19] M. d'Aquino, C. Serpico, G. Miano, I. D. Mayergoyz, and G. Bertotti, "Numerical integration of Landau–Lifshitz–Gilbert equation based on the midpoint rule," Journal of Applied Physics, vol. 97, p. 10E319, 2005.
- [20] J. L. García-Palacios and F. J. Lázaro, "Langevindynamics study of the dynamical properties of small magnetic particles," Physical Review B, vol. 58, pp. 14937 14958, 1998.
- [21] J. H. Mentink, M. V. Tretyakov, A. Fasolino, M. I. Katsnelson, and Th. Rasing, "Stable and fast semi-implicit integration of the stochastic Landau–Lifshitz equation," Journal of Physics: Condensed Matter, vol. 22, p. 176001, 2010.
- [22] D. P. Kingma and J. Ba, "Adam: A Method for Stochastic Optimization," Proc. ICLR, 2015; arXiv:1412.6980.
- [23] J. Duchi, E. Hazan, and Y. Singer, "Adaptive Subgradient Methods for Online Learning and Stochastic Optimization,"

- Journal of Machine Learning Research, vol. 12, pp. 2121–2159, 2011.
- [24] T. Tieleman and G. Hinton, "Lecture 6.5—rmsprop: Divide the gradient by a running average of its recent magnitude," Coursera: Neural Networks for Machine Learning, 2012.
- [25] S. J. Reddi, S. Kale, and S. Kumar, "On the Convergence of Adam and Beyond," Proc. ICLR, 2018; arXiv:1904.09237.
- [26] L. Bottou, F. E. Curtis, and J. Nocedal, "Optimization Methods for Large-Scale Machine Learning," SIAM Review, vol. 60, no. 2, pp. 223–311, 2018.
- [27] Y. N. Dauphin, R. Pascanu, C. Gulcehre, K. Cho, S. Ganguli, and Y. Bengio, "Identifying and attacking the saddle point problem in high-dimensional non-convex optimization," Proc. NeurIPS, 2014.
- [28] C. Jin, R. Ge, P. Netrapalli, S. M. Kakade, and M. I. Jordan, "How to Escape Saddle Points Efficiently," Proc. ICML, 2017.
- [29] A. Choromanska, M. Henaff, M. Mathieu, G. B. Arous, and Y. LeCun, "The Loss Surfaces of Multilayer Networks," Proc. ICML, 2015.
- [30] N. S. Keskar, D. Mudigere, J. Nocedal, M. Smelyanskiy, and P. T. P. Tang, "On Large-Batch Training for Deep Learning: Generalization Gap and Sharp Minima," Proc. ICLR, 2017.
- [31] C. Zhang, S. Bengio, M. Hardt, B. Recht, and O. Vinyals, "Understanding deep learning requires rethinking generalization," Proc. ICLR, 2017.
- [32] A. C. Wilson, R. Roelofs, M. Stern, N. Srebro, and B. Recht, "The Marginal Value of Adaptive Gradient Methods in Machine Learning," Proc. NeurIPS, 2017.
- [33] S. Hochreiter and J. Schmidhuber, "Flat Minima," Neural Computation, vol. 9, no. 1, pp. 1–42, 1997.
- [34] P. Foret, A. Kleiner, H. Mobahi, and B. Neyshabur, "Sharpness-Aware Minimization for Efficiently Improving Generalization," Proc. ICLR, 2021.
- [35] J. Grollier, D. Querlioz, and M. D. Stiles, "Spintronic nanodevices for bioinspired computing," Proceedings of the

- IEEE, vol. 104, no. 10, pp. 2024-2039, 2016.
- [36] D. Marković, A. Mizrahi, D. Querlioz, and J. Grollier, "Physics for neuromorphic computing," Nature Reviews Physics, vol. 2, pp. 499–510, 2020.
- [37] H. H. Rosenbrock, "An automatic method for finding the greatest or least value of a function," The Computer Journal, vol. 3, no. 3, pp. 175–184, 1960.
- [38] L. A. Rastrigin, Systems of Extremal Control, Mir, Moscow, 1974.
- [39] J. E. Hirsch, "Spin Hall Effect," Physical Review Letters, vol. 83, pp. 1834–1837, 1999.
- [40] J. Sinova, S. O. Valenzuela, J. Wunderlich, C. H. Back, and T. Jungwirth, "Spin Hall effects," Reviews of Modern Physics, vol. 87, pp. 1213–1260, 2015.
- [41] D. Apalkov, B. Dieny, and J. M. Slaughter, "Magnetoresistive Random Access Memory," Proceedings of the IEEE, vol. 104, no. 10, pp. 1796–1830, 2016.

VP7-11. Magnetic Multilayer (MMLs) Domain Wall-Driven dynamically coupled hybrid vortex structures for mobile Majorana zero modes

K. K. Mishra

Physics & Astrophysics, University of Delhi, Delhi, Delhi, India

The pursuit of robust and controllable platforms for Majorana zero modes (MZMs) remains a central challenge in condensed matter physics and topological quantum computing [1]. MZMs, quasiparticle excitations exhibiting non-Abelian braiding statistics, hold great promise as building blocks for fault-tolerant quantum computation due to their intrinsic topological protection against local perturbations [2]. Theoretical proposals [3,4] predict their emergence in one-dimensional systems as edge states or in two-dimensional topological superconductors at vortex cores [5].

While unambiguous detection remains a major bottleneck, recent theoretical advances suggest that experimental verification via non-Abelian statistics offers the most definitive evidence of MZMs. As a result, hybrid heterostructures combining superconductivity and magnetism have emerged as promising platforms, though

prior studies focus predominantly on static vortex configurations [6,7,8].

In this work, we propose a novel dynamic platform where domain wall (DW) motion drives superconducting vortex dynamics, enabling active control over the position of bound MZMs in hybrid multilayer structures. DW spin textures in magnetic multilayers have been widely studied for their remarkable stability and current-driven mobility. Using micromagnetic simulations, we demonstrate that a moving DW drags a superconducting vortex, which oscillates and moves while following the DW trajectory. We analyze the coupling mechanism, dynamics, and stability of this hybrid vortex system. This coupled dynamics provides a unique handle to manipulate MZMs, where an emergent gauge field generated by the inhomogeneous magnetization texture induces a topological superconducting gap. This leads to topological phases akin to conventional topological superconductors, hosting robust zero-energy modes at vortex cores.

- 1. Jason Alicea, "New directions in the pursuit of majorana fermions in solid state systems," Reports on Progress in Physics 75, 076501 (2012).
- 2. Chetan Nayak, Steven H. Simon, Ady Stern, Michael Freedman, and Sankar Das Sarma, "Non-abelian anyons and topological quantum computation," Rev. Mod. Phys. 80, 1083–1159 (2008).
- 3. Roman M. Lutchyn, Jay D. Sau, and S. Das Sarma, "Majorana fermions and a topological phase transition in semiconductor-superconductor heterostructures," Phys. Rev. Lett. 105, 077001 (2010).
- 4. T.-P. Choy, J. M. Edge, A. R. Akhmerov, and C. W. J. Beenakker, "Majorana fermions emerging from magnetic nanoparticles on a superconductor without spin-orbit coupling," Phys. Rev. B 84, 195442 (2011)
- 5. Sho Nakosai, Yukio Tanaka, and Naoto Nagaosa, "Two-dimensional p-wave superconducting states with magnetic moments on a conventional s-wave superconductor," Phys. Rev. B 88, 180503 (2013).
- 6. Pathak, Vedangi, Sayak Dasgupta, and Marcel Franz. "Majorana zero modes in a magnetic and superconducting hybrid vortex." *Physical Review B* 106.22 (2022): 224518.
- 7. Sergey S. Pershoguba, Kristofer Bjornson, Annica M. Black-Schaffer, and Alexander V. Balatsky, "Currents induced by magnetic impurities in superconductors with spin-orbit coupling," Phys. Rev. Lett. 115, 116602 (2015).
- 8. Kjetil M. D. Hals, Michael Schecter, and Mark S. Rudner, "Composite topological excitations in ferromagnet

superconductor heterostructures," Phys. Rev. Lett. 117, 017001 (2016).

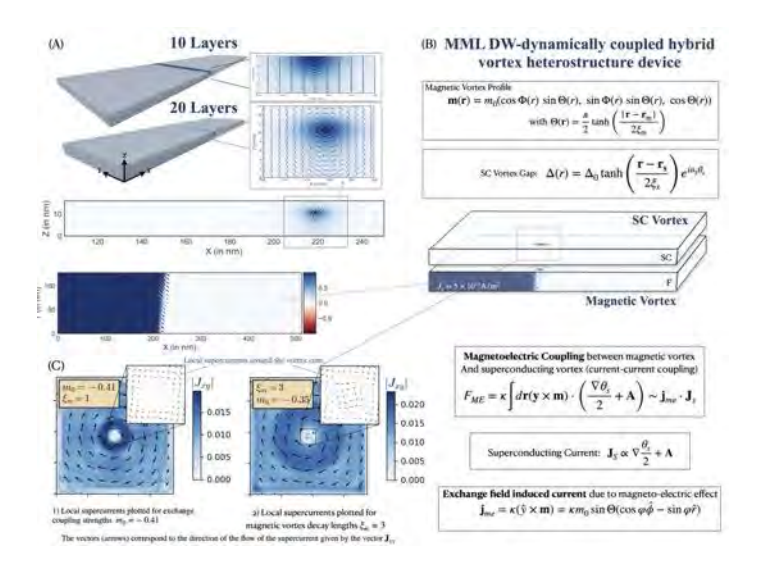


Fig. 1 (A) Multilayer micromagnetic simulation results depicting the vortex formation as the number of layers increased to 20. DW (xy-plane) nucleates and stabilises a dynamically-coupled Vortex at the edge-wall (x-z plane) (B) MML coupled hybrid heterostructure device having thin MML proximity coupled with SC with vortex (C) Due to magnetoelectric coupling, current-current interaction stabilises the hybrid vortex structure

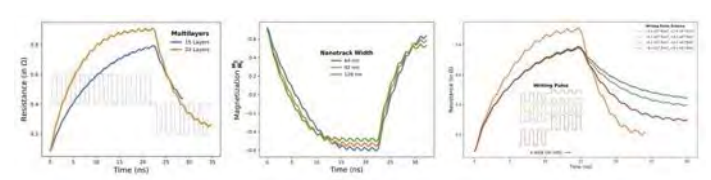


Fig. 2 Micromagnetic analysis of the MML device for different thickness and measured resistance

VP7-12. Revisiting the Role of Symmetry for High Performance Magnetic Tunnel Junctions

S. Chakraborti¹, A. Sharma²

¹Electrical Engineering, Indian Institute Of Technology Ropar, Rupnagar, Punjab, India, ²School of Computing and Electrical Engineering, Indian Institute of Technology, Mandi, Mandi, Himachal Pradesh, India

We present a novel idea of symmetry-dependent resonance of the electrons associated with the Δ_1 states of the Fe(001)/MqO(001)/ZnO(001)/MqO(001)/Fe(001) heterostructures, opening up a new horizon to engineer magnetic tunnel junctions (MTJs) that provide a sizable tunnel magnetoresistance(TMR) reaching 3.5×10⁴% and a resistance area(RA)-product that drops to a minimum of $0.05\Omega-\mu m^2$, with a high ($\approx 99\%$) spin polarization[1]. Our calculations are premised on the self-consistent coupling of the density functional theory with the non-equilibrium Green's function formalism. We present this study in light of the zero bias TMR(%) and the RA-product of a complete ensemble of resonant tunneling MTJs, abbreviated as the Δ^{R}_{1} -MTJs. Here we show the zero-bias k-avg transmission with energy and k-resolved transmission at the Fermi energy of a sample(s)- Δ^{R}_{1} -MTJ comprising the Fe/2 layers(l)-MgO/3l-ZnO/2l-MgO/Fe that offers a TMR(%) of 6000% and provides a momentous reduction of 150 times in the RA product compared to a Fe/6l-MgO/Fe MTJs with nearly 100% spin polarisation, promising a massive increase of spin transfer torque(STT). The physics of symmetrydependent tunnelling is elucidated by corroborating the spectral density, transmission eigenchannels, and band structure of the unit cell comprising the Fe electrodes[1]. State-of-the-art MTJs with 4l-MgO layers can be switched with a critical current density of ≈ 10⁶ A/cm²[2] at an RA product of 0.9 Ω - μ m², whereas the s- Δ ₁^R-MTJ is found to offer an RA-product of 0.14 Ω - μ m² at the same point, ensuring a reduction in the power consumption by 6.5 times while keeping the window for high-speed switching wide open. This work relies on the stability of the MqO-ZnO stack and ticks the box of BEOL compatibility [3], making the Δ_1^R -MTJs highly relevant in the era of spintronics-coupled silicon CMOS technology.

[1] Symphony of Symmetry Selective Resonances in Fe-MgO-ZnO-MgO-Fe, S. Chakraborti, A. Kashyap, A. Sharma, arXiv:2504.09842v2

[2] Jun Hayakawa *et al* 2005 *Jpn. J. Appl. Phys.* 44 L1267 [3] H. Saito *et al.*, "Tunneling Magnetoresistance and Spin-Dependent Diode Performance in Fully Epitaxial Magnetic

Tunnel Junctions With a Rocksalt ZnO/MgO Bilayer Tunnel Barrier," *Phys. Rev. Applied*, vol. 11, no. 6, p. 064032, Jun. 2019.

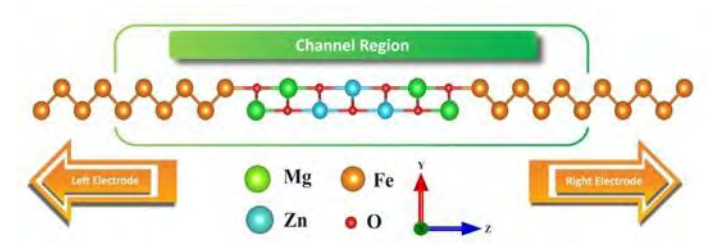


Fig. 1 Device schemtic of the $s-\Delta_1^R$ -MTJ comprising Fe(001)/MgO(001)/ZnO(001)/MgO(001)/Fe(001).

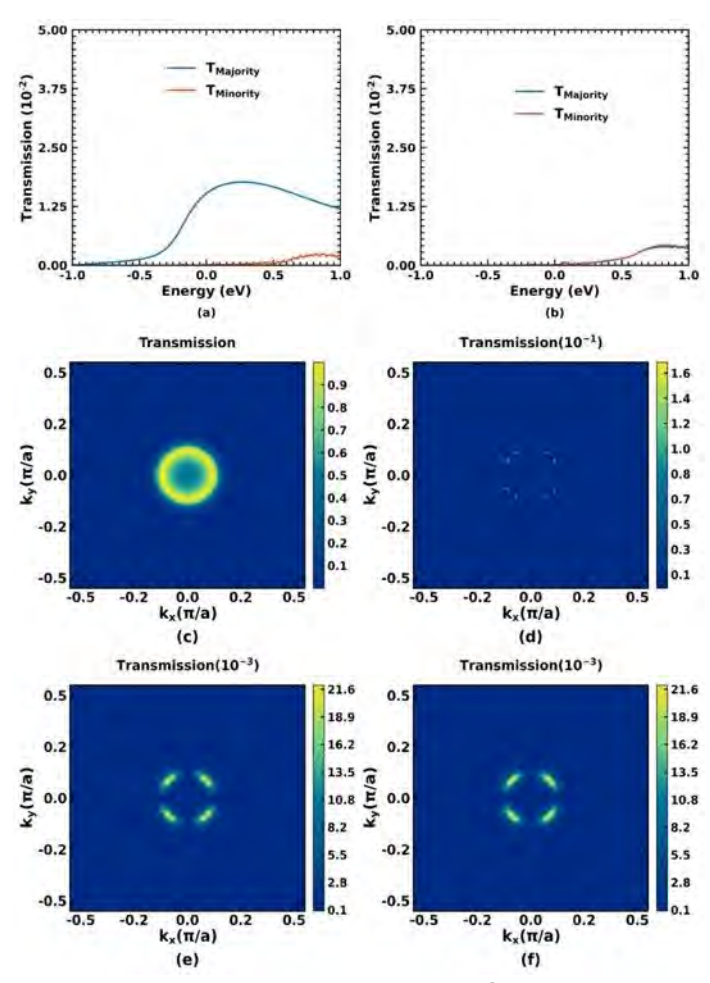


Fig. 2 k-averaged transmission of the $s-\Delta_1^R$ -MTJ in the (a) parallel(PC) and the (b) antiparallel(APC) configuration; k-resolved transmission of the (c) upspin and (d) downspin electronss in the PC, (e) upspin and the (f) downspin electrons in the APC.

A A. T: VP2-06

Ababneh, E M.: DR-09

Abad, A: DC-07

Abbas, H: CF-03, CF-10, ER-07, ER-08

Abbott, C: EE-05 Abdelhafiz, H: **DR-12** Abdel-Mottaleb, M: BB-03 Abdelsamie, A: GD-01 Abdizadeh Kalan, S: **GG-07** Abdul Karim, M: **GC-04** Abdurahman, A: VP7-03

Abe, H: FR-05 Abe, S: **BD-04** Abe, T: AP-03, FC-08 Abe, T: VP4-10 Abels, E: DE-07 Abramson, M: DR-13 Abreu Araujo, F: FF-02 Achinuq, B: CD-08 Aczel, A: AG-06

Adamantopoulos, T: **FE-05** Adedo, H A.: DQ-02, DQ-03 Adinarayanappa, S M.: FC-10 Adiya, M: BG-13, VP7-07

Aeppli, G: GC-09 Agarwal, P: **FE-07** Ahmad, S: DF-04, **EF-09**

Ahn, D: VP4-03 Ahn, J: **AF-09** Ahn, J: AP-10-LB Ahn, J: **FP-06**

Adam, J: GD-01

Ahn, S: **BP-10**, **CF-04**, FG-08

Aihemaiti, H: CR-02 Ajantiwalay, T: BD-06 Ajia, S: BD-13, CR-03, DG-08

Akamatsu, J: BD-04

Akdogan, O: CG-10, **FC-13**, **FC-14** Akerman, J: AF-08, DF-06, EE-03

Akita, Y: BG-08 Alaei, S: BP-03 Alam, A: GD-08, GR-11 Alam, M: **FF-03** Alatawneh, N: **AE-11** Alatteili, G: DB-01 Albert, M S.: DQ-09 Albisetti, E: **DB-02**

Albrecht, M: EA-05

Albuquerque, F A.: VP6-04

Alejos, O: **VP7-06** Alexandrov, A: DQ-09

Alharbi, D: **BR-06**, CR-07, FQ-07

Ali, Z: **DG-05**Al Janaideh, M: AE-11
Almuhanna, I A.: **FR-10**Alonso Masa, J: **DC-07**Al Saaideh, M: AE-11
Alsmadi, A: **FQ-08**Althammer, M: **CC-01**

Amanatiadis, S: DG-11

Amara, S: AE-06, AE-08, DE-03

Ambal, K: EF-10 Ambaye, H: CE-05 Amemiya, K: AD-05 Amiie, D: **DR-07** Amin, O: **CG-11**, EB-01 Amin, V: DR-09, GG-07 Amoo, F: **DQ-05** Am-Shalom, N: CG-04

An, J: FG-08 An, T: EF-05 An, Y: VP5-02

Anane, A: CH-08, EE-06, GD-01 Anantharaman, M: AE-10 Anas, M: CD-05, DO-10, VP3-08

Ando, Y: DG-01 Ando, Y: DR-04, FR-01 Andoni, I: CB-02 Andre, V: BB-03

Andrei, P: AE-02, **GQ-08**

Andrew, J: BB-01

Anh, L: FE-10

Angayarkanni Ramamurthy, D: EG-05

Anikeeva, P: FC-02
Anil Kumar, P: DG-02
Anjum, G: GD-05
Anjum, R: BD-08
Antropov, V: GR-05
Aoshima, H: GR-06
Apiñaniz, E: AE-12
Arakawa, Y: AP-01, AP-02
Araki, Y: DF-08, DF-10
Araujo, P: GG-08
Arauzo, A: BE-04
Arena, D. A: AP-04, AR-08

Arena, D A.: AP-04, AR-08, BP-03, CR-13, CR-14, DC-10, FD-06, FD-09, FR-

10

Ariando, A: CG-06 Arisawa, H: BC-03 Arita, R: BA-04 Arora, N: **GE-08** Arpaci, S: GP-04-LB Arterburn, S: DE-04 Asamitsu, S: FC-08 Asari, Y: **BD-02**, DD-03 Aseguinolaza, I: BE-10 Ashokan.K, A: AF-02 Assaf, B A.: CE-05, GC-04

Assouline, B J.: **CG-04**, **CH-11**, **GE-09** Atalugama, T: AP-06, CQ-09, FC-11,

FC-12

Atalugama, T V.: AP-08

Athas, J G.: **BF-02**, **FF-06**, GP-04-LB Atulasimha, J: CH-03, DF-05, FF-03

Awad, A A.: DF-06, EE-03

Awano, H: DR-01 Azizi, E: AR-05

В

Bacani, M: **CG-01** Bachmann, S: CR-05 Backes, D: **EF-11**, **GE-03** Badie, L: CD-09

Badie, L: CD-09 Badura, A: EB-02 Baek, R: FG-08 Baek, S: **FD-04** Bagci, C: FC-13 Baghel, A: **FP-03** Bahri, A: GP-06-LB

Baiao De Albuguerque, G: CB-02

Bakare, O A.: AF-06

Bakhshizadeh, F: BR-06, CR-07, FQ-07

Balakrishnan, G: EF-11 Balakrishnan, P P.: FD-01 Baldino, H: **BG-02**, DE-07, **ER-12**

Balicas, L: GR-04 Baltz, V: EB-02 Balz, C: CE-08 Ban, A: FC-08

Bandapelli, R: CE-09, FE-02

Bandyopadhyay, S: BF-10, CH-09, GQ-

04

Banerjee, T: AE-03, CD-06

Bansil, A: AG-03 Bao, X: GG-11 Barick, K C.: CF-09

^{*} Best Student Presentation Finalist / LB - Late-breaking Poster

Barker, J: DD-07, DF-02 Barman, A: BF-10, GQ-04

Barrera, A: CD-01 Barrera, G: DE-01 Barthelemy, A: GD-01 Bartolomé, E: **BE-04**

Barua, R: BG-05, ER-06, GQ-09

Basak, R: FB-03
Bashir, A: VP1-06
Basker, M: CQ-09
Batarchuk, V: DQ-09
Bauer, L: BE-03, DG-03
Bazso, G: DD-01
Beach, G: BC-11, ED-09
Beard, M C.: AA-01
Beckert, S: EB-02
Beckham, J: FC-02
Beekman, C: **DE-08**Beeson, W: BG-01
Behera, N: AF-08, EE-03

Belkhou, R: DC-01 Bellintani, V: VP6-04

Belmeguenai, M: AD-09, CD-04 Ben, T: VP1-03, VP4-09, VP6-10, VP6-

Benally, O: BF-01, CD-10, FR-04

Belashchenko, K: DR-12, GR-05

Ben Chroud, M: CA-01

Benguettat- El Mokhtari, I: CD-04 Ben Mbarek, S: **AE-06**, AE-08, **DE-03**

Bennett, C H.: BF-08 Bennett, S P.: CE-05 Ben Youssef, J: EE-06 Bera, A: GD-08 Berg, E: FD-08 Bergman, A: CR-02 Bergner, D: FD-08

Bernal, O: VP3-09, VP3-10

Bernard, E: **BC-09**Bernard, G: AD-09
Bernard, G: CD-04
Bernstein, N: CG-0

Bernstein, N: CG-04, GE-09 Bertacco, R: DB-02

Bessas, D: DD-01 Bey, S: **CE-05**

Bezsmertna, O: DC-02, DC-04

Bhaduri, I: **CD-06** Bhandari, K: **GQ-09** Bhat, F H.: VP1-06, VP5-01 Bhat, F H.: GD-05 Bhat, V: DB-01

Bhatnagar-Schöffmann, T: AD-09 Bhattacharya, D: BG-01, DC-02, DC-04

Biagi, M: **ED-02** Biancardi, I: DB-02 Bibes, M: GD-01

Bidouba-Sanvany, D: AD-03

Biedinger, J: BC-07 Binnie, I: **CG-05** Bishop, O: **BG-05**, ER-06

Bishop, O: **BG-05**, ER-06 Bishop, S R.: BD-07 Bista, D: BG-01

Biswas, A: **DQ-01**, GR-07 Bitla, Y: CF-02, DE-10 Blackburn, E: FB-05

Blanco Rodríguez, J Á.: AR-08

Blonski, P S.: AR-13 Blügel, S: AC-08 Bodur, V E.: FC-10 Böhm, D: BE-07 Boissiere, J D.: BD-07 Bonanni, A: FE-04 Bonetti, S: BC-09 Bono, D: BC-11 Borah, D P.: BD-05 Borchers, J: EF-06 Borchert, M: GG-13 Boris, A V.: CH-01

Bortolotti, P: EE-06, GD-01 Bosomtwi, D: BD-07 Bossini, D: **BA-05**

Bouzehouane, K: CG-03, GD-01 Boventer, I: EE-06, GD-01

Bowman, R M.: BR-03, CH-06, CH-10

Bovd. N: DR-09

Bozhko, D A.: DC-05, DE-07, EE-05, **EE-**

12

Bradley, H: DR-13 Brajpuriya, R: AR-01

Bramerdorfer, G: BR-09, BR-10

Branford, W R.: GE-08 Branford, W: DB-01 Breitbach, D: DB-02 Brevis, F: DB-04 Brock, J A.: BC-09 Brock, S: DQ-05 Brockie, R: EG-03 Broders, M: DD-12 Brown, C: DQ-10

Brown, D: AP-07, BR-07, FC-15

Brown, J: **EP-02-LB**Brown, S: XA-03
Bruley, J: XA-03
Bruno, N M.: BD-11
Buchanan, C C.: GE-06
Buchanan, K: CD-01

Buda-Prejbeanu, L D.: EG-12, FQ-09

Bui, V H.: GQ-03 Bull, C: FQ-10

Burn, D M.: **CG-02**, CH-06, **FP-07**

Burnell, G: DF-02, FG-09

Busina, M: GG-13

Byun, S: **EQ-03**, **GR-03-LB**

C

Camley, R E.: EE-05 Camosi, L: EF-01

Campion, R: CG-02, CG-11

Can, S: FC-14
Canavan, E R.: BE-13
Candler, R: DG-13
Canlas, D: DG-01
Canvel, Y: BC-14
Cao, C: VP5-05
Cao, G: GC-08
Cao, X: FP-01
Cao, Z: VP4-12
Capotondi, F: BC-09
Capraro, B: CR-05

Capriata, C C.: ED-02

Capua, A: CG-04, CH-11, GE-09

Cardoso, S: GG-08
Cardwell, S G.: BF-08
Carfagno, H: DB-01
Carlomagno, I: FG-04
Caron, L: BC-07
Carpenter, E E.: BG-05
Carpenter, R: **CA-01**, GD-07

Carpentieri, M: AR-10, DA-04, GP-04-

LB

Caruana, A: FD-01 Carva, K: **EF-03** Castaño, C: FP-09

Cataldo, A: **CD-03**, **CD-04**, **FG-11** Cating-Subramanian, E: CG-05

Celebi, D: CG-10

^{*} Best Student Presentation Finalist / LB - Late-breaking Poster

Celegato, F: CD-01, DE-01 Chae, K: FG-03, GG-01 Chaitanya, P: BE-13, GQ-01 Chakraborti, S: **VP7-12**

Chalmers, J: AQ-05, CF-07, FC-05

Cham, T: FD-08, **FE-01**Chan, P: **AP-09-LB**Chance, F: BF-08
Chang, H: **EA-05**Chang, H: AC-12
Chang, J: **EG-04**

Charak, R: FG-03, GG-01 Charilaou, M: **FR-13**, **GE-10**

Charlton, T: BC-02, EF-06, FQ-04-LB

Chatterjee, J: BC-14, GD-07 Chatterjee, R: VP5-06 Chatterjee, S: FR-06 Chaturvedi, A: AC-11 Chaurasiya, A: EE-03 Che, P: EE-06, **GD-01**

Chen, C: FE-11 Chen, H: GG-06 Chen, J: FC-12 Chen, K: FC-05 Chen, L: VP3-06

Chen, L: VP1-03, VP4-09, VP6-10,

VP6-16

Chen, L: BC-02, GC-03 Chen, S: AC-11 Chen, S: BB-03 Chen, S: CD-03 Chen, T: CD-09

Chen, V: AP-09-LB Chen, X: BQ-05 Chen, X: CG-06 Chen, X: GC-08 Chen, X: AQ-08 Chen, Y: VP3-05 Chen, Y: DF-09 Chen, Y: AC-12 Chen, Y: EG-02

Chen, Y P.: FE-06

Chen, Y: GF-01, GF-02 Chen, Y: AD-04, BF-01, CD-10, FR-04,

GR-09

Chen, Z: BP-05-LB Chen, Z: VP6-06, VP6-07

Chen, Z: DC-02 Cheng, B: **CQ-02** Cheng, G: **FE-06** Cheng, M: **VP6-18**

Cheng, R: GP-02-LB, GP-08-LB

Cheon, J: VP4-19 Cherif, S: CD-04 Chern, G: **EC-08**

Chesnel, K: **DC-11**, **DC-12** Cheung, S: GP-04-LB Chhabra, H: AE-03 Chi, H: **EF-08** Chiappini, M: DA-04 Chiba, T: **EE-13**, FE-10 Chica. D G.: FE-01

Chikaki, S: FC-01, FC-04, FC-07, FP-01

Chiku, H: DF-11

Chin, Y: GC-03, GF-01, GF-02 Chinnasamy, C: **BD-06** Chinnathambi, K: BD-11 Chiriac, H: VP6-19 Cho, H: EQ-03, GR-03-LB Cho, H: AF-04, GP-09-LB

Cho, S: AF-09 Choe, H: AQ-05, CF-07 choi, J: AF-08

Choi, C: BG-03

Choi, D: BQ-02, EQ-02, EQ-05, EQ-06

Choi, G: **BA-03** Choi, J: FG-08 Choi, W: **DF-01** Choi, Y: GR-01

Chopdekar, R V.: BF-03, BF-04

Chou, C: CA-02, GG-05
Chou, H: BC-02, GC-03
Chowdhury, M F.: CH-03
Chshiev, M: CD-09
Chudasama, B: VP6-01
Chugh, V K.: AR-05
Chumak, H: DQ-09
Chumakov, A I.: DD-01
Cierpial, M: BF-05
Coisson, M: DE-01
Collin, S: CG-03
Collins, K: DE-07
Cong, A: ED-10
Cong, G: AA-01
Connell, S: DF-02

Consolo, G: AR-02

Cornelius, R: ER-14-LB

Copus, M: EE-05

Corrielli, G: DB-02 Cortie, D: GC-03

Cosgrove, L: DR-05, **EC-02**, **FQ-04-LB** Cottam, M G.: AR-04, BP-01, BP-07

Cousins, R: CG-11 Cress, C: EF-05 Cresswell, Z: BF-01 Crisan, O: **EG-10** Cros, V: CG-03 Cui, B: BG-02, **DD-08** Cui, J: DD-08, DD-14 Cui, Z: CE-09, FE-02

D

d'Aquino, M: CH-08, EC-12, EE-09

Dabla, M: CR-11, FP-08 Dabrowski, M: CH-06 Da Costa, A: CD-09 Dainone, A: AA-01 Dal Din, A: CG-11

Damatopoulou, T: AQ-09, DD-05

Dandeu, E: AD-03 Das, H: BD-06 Das, P: **DF-05** Das, R: DC-10 Das, S: AF-07, ED-08 Dastanpour, E: CR-02 Daurer, B: CG-02 Davies, C S.: CH-01

Davila, N: BF-02

Davis, M: BR-06, CR-07, FQ-07 Davoudiniya, M: GB-04 Davydov, A: BG-01 Deak, A: DD-01 De Angelis, D: BC-09 Dearg, M: FG-09

DeBeer-Schmitt, L: GE-06

Deepak, K: GD-03 DeFeo, J R.: DQ-02, DQ-03

Deka, A: **BE-03**, DG-03

Deka, J: DQ-07

De la Torre Duran, A: CE-01

Delaunay, R: EA-03

del Barco, E: GP-02-LB, GP-08-LB

Del Giacco, A: DB-02 Delord, T: EF-05 de Loubens, G: CH-08 De Luca, G: GF-04 Demidov, V E.: GD-01

^{*} Best Student Presentation Finalist / LB – Late-breaking Poster

Demin, G D.: VP1-05 De Negri, S: BE-10 Deng, K: GE-04 Denneulin, T: FE-04 de Oliveira, R B.: FG-02 Deroo, M: BR-12, CD-03 DeRuiter, A: ER-10, GR-09 Desfeux, R: CD-09

DeTellem, D: CR-14, **DQ-06**, FD-09

Devaux, X: AA-01, CD-09 DeVisscher, E D.: EP-03-LB De Zoysa, K: BA-02, DF-06

Dhagat, P: EE-08 Dhaka, R S.: GR-02 Dhapola, S: BG-06

Dhesi, S S.: CG-02, CG-11, EF-11, FP-

07

Diao, Y: DF-09

Dias Nakashima, A T.: BE-08

Diez, LH.: CD-04 Dil, H: CG-11 Dimitrov, D: EF-01 Di Napoli, D: CF-06 Dion, T C.: DB-01 Dipirro, M J.: BE-13 Divan, R: DE-06, EE-04 Divyanshu, D: AE-08

Dixit, B: AD-04, AR-03, BF-01, FR-04

Djuzhev, N A.: VP1-05 Do, N: AR-11-LB Dobák, S: FD-03 Dobler, C: BR-10 Dohi, T: DF-06, DF-11 Dolui, S: AR-02 Doménech, D: FG-13 Donald, A M.: GR-13-LB Dong, S: AD-06, GC-08 Donnelly, C: DB-02, DC-01 Doty, M: DB-01, EP-08-LB Dravid, V P.: GP-04-LB Drobitch, J L.: GQ-04

Drozdz, P: AC-07, CE-03, FG-07

Du. T: VP6-13 Duan, J: **BD-10**

Drouhin, M: BR-12

Duarte de Melo, R: DQ-04

Dubois, J: EA-03 Duc, N T.: GR-04 Duffee, C: BF-02, FF-06 Dunin-Borkowski, R E.: AD-09, FE-04,

GF-10

Duong, A R.: BG-05, ER-06 Duque, A G.: GR-13-LB Duquesne, J: EC-11 Durnez, A: AD-09 Dutta, R: AG-06, EF-06 DuttaGupta, S: FE-03 Dwivedi, S: AR-02 D'Addario, A: GP-04-LB

Ε

Ebels, U: FF-04

Echtenkamp, W: BD-07, ER-10, GR-09

Eddrief, M: EA-03

Edmonds, K: CG-02, CG-11 Efe, F: BR-06, CR-07, FQ-07

Egan, S: DR-02 Eichenfield, M: DE-04 Ekahana, S: GC-09

Elekhtiar, M A.: EF-10, GF-07, GP-04-

LB

El-Ghazaly, A: FG-01 Elo, M: EE-05 Elolimy, M: GR-10

Embree, B: AP-06, FC-11, FC-12 Emori, S: AF-06, DF-07, FD-01, GG-07

Endo, M: BR-08, DG-01

Endo, Y: BD-13, CR-03, DG-08, FP-10

Endoh, T: AF-10, GF-06 Engel-Herbert, R: FE-11 Engelke, F: AG-02 Enoki, M: BD-02 Eom, K: AF-04 Eppler, W R.: EG-01 Erickson, A: EF-05 Ershadrad, S: GB-04 Espeso, J: DC-07

F

Fabiha, R: BF-10 Fabris, G S.: FG-02 Faircloth, D: EP-02-LB Fan. B: VP5-05

Fan, X: **CC-03**, DR-09, EP-03-LB

Fan, Y: **AF-05** Fan, Y: EG-06 Fan, Y: BF-01 Fan, Y: EC-08

Fanq, C: **DQ-07** Fang, H: CG-05 Farkas, A: GG-13 Farrell, R: FC-05 Fatima, H: VP4-18 Fattouhi, M: FQ-09 Favaro, D: GD-07 Fecher, G: CR-09 Feggeler, T: CG-05 Felser, C: FD-02, FD-09

Feng, J: **VP6-09**, VP6-11, VP6-12

Feng, K: **VP1-04** Fernandes. T: GG-08 Fernandez, V V.: BC-12 Fernández Barquín, L: DC-07

Fernandez-Gonzalez, C: BC-12, DC-02

Fernandez Gubieda, M: DC-07 Fernández-Pacheco, A: DC-01

Ferrer, S: BC-12 Ferri, A: CD-09 Ferson, N: BB-01 Fescenko, I: EF-05 Fidelis Peixer, G: BE-08

Fields, C: CG-11 Fields, S: CE-05

Figueiredo-Prestes, N: AA-01 Figueroa, S: **VP3-09**, VP3-10

Filippou, P C.: CA-03 Finco, A: CG-03 Finizio, S: DB-02

Finocchio, G: AR-10, DA-04, GP-04-LB

Fischer, P: DC-02, DC-04 Flebus, B: **AB-04**, GE-04 Fleischmann, C: BF-06

Flores, J: CE-07 Florio, P: DB-02 Foerster, M: CD-01

Foggiatto, A L.: CR-01, FR-03

Fonesca, J: EF-05 Fortuna, F: EA-03 Frame, M: CD-08 Francesca, K: CD-09 Franchina Vergel, N: CA-01

Frandsen, B: CE-08 Franke, O L.: GG-13 Frano, A: FB-03 Freitag, J M.: CB-02 Freitas, P: GG-08 Friedman, A: FR-09

^{*} Best Student Presentation Finalist / LB – Late-breaking Poster

Friedmann, T: DE-04 Gopman, D B.: CA-04 Garcia, V: GD-01 Fritjofson, G: GP-08-LB García-Arribas, A: DC-07 Gorchon, J: EG-09, EG-12 Fromage, S: CG-11 Garcia-Barriocanal, J: BF-01 Gorria, P: AR-08 Frost, A: BP-01 García Gaitan, F E.: GC-07 Goto, M: DR-04, VP7-05 Fuchs, G: **CF-01**, GP-04-LB García-Prieto, A: DC-07 Goto, Y: VP7-05 Fugetta, B: DC-02, DC-04 Garello, K: ED-02 Gotoh, Y: BR-13 Fujieda, S: GO-02 Garg, S: FG-03, GG-01 Gottwald, MG.: XA-03 Fujii, Y: VP7-05 Garshev, A: AE-12 Gouéré, D: BR-12, CH-08, FG-11, GD-Gartside, J: DB-01, GE-08 06 Fujisawa, Y: CG-06 Fujita, N: FP-10 Gas-osoth, T: EF-05 Grab, J L.: CB-02 Fujita, R: EF-11 Gautam, R: DC-11 Gracheva, M A.: DD-01 Gautam, S: FG-03, GG-01 Fujiwara, H: VP4-01 Grafov, A: AQ-10 Fujiwara, K: BR-08, DG-01 Gavles, J D.: AC-03, AC-04, FD-09, GF-Graham, DM.: FQ-10 Fukami, S: BA-02, DF-06, DF-11, FE-03, **GP-01-LB**, GR-10 Graning, S: DD-01 Gazizulin, R: GR-13-LB Granville, S: FA-02 03, GF-09, GF-10 Fukumoto, H: VP7-05 Gensbittel, A: AD-03 Gray, A X.: AG-06, EF-06 Fukushima, H: DG-01 George, J: AA-01 Greaves, S: BR-02 Fukushima, T: AD-05 Gerhardt, N: AA-01 Grelier, M: BR-12 Fukuzaki, T: CR-08 Gething, T: FO-10 Gribik, A K.: EG-04 Fullerton, E: BC-09, CG-05, GE-05, GE-Ghaderi, S: VP7-10 Grier, A: **CB-01** 06 Ghosh, B: AG-03 Gries, T: CD-09 Fullerton, J: **DC-01** Ghosh, R K.: VP1-01 Grimaldi, A: DA-04 Funatani, S: FC-04, FC-06 Ghosh, S: AF-08 Grobis, M: BF-04 Fushimi, M: BB-05, FC-01, FC-04, FC-Gibbons, J: AF-05 Grochot, K: BF-05 06, FC-07 Gilbert, D A.: GE-06 Gross, M J.: CH-03 Fusil, S: GD-01 Gili, M: AP-07, BR-07 Grundler, D: DB-05 Fuzer, J: FD-03 Giner-Planas, J: BE-04 Gruszecki, P: AR-07 Giordano, A: AR-10, DA-04 Grutter, A J.: BC-02, EF-06, FD-01, GC-G Girardi, D: DB-02 03 G. Suresh, K: GD-08, GR-11 Giuliano, D: BF-06 Grynko, V: DQ-09 Gadbois, J: EG-01, EG-06 Go, D: FE-05 Gstöttenbauer, N: BR-09, BR-10 Gaerner, M: BC-07, CC-02, GF-04, GF-Göbel, B: FA-04 Gu, K: AC-05 Godel, F: CG-03 Gubala, K: BF-05 05 Galkin, V: DD-10 Goennenwein, S: EB-02, GG-13 Gubbiotti, G: DB-01, EE-02 Gallardo, R: DB-04, ED-07 Gokce-Polat, E: ER-10, GR-09 Gubieda, A G.: DC-07 Galvão. D S.: FG-02 Goldfarb, R B.: FC-09 Gueckstock, O: **FA-01**, GF-04, **GF-05**, Gamal, M: FP-09 Golias, E: CG-11 GG-12, GG-13 Gama Monteiro, M: BF-06, CA-01, GD-Gomes, A: DQ-04 Guen, Y L.: EG-09, EG-12 07 Gomez-Pastora, J: AQ-05, CF-07, CQ-Guillet, T: EF-01 Gandarias, L: DC-07 06, CQ-07, **FC-05** Guimaraes, M H.: GB-03 Gandia, D: DC-07 Gomonay, O: BC-07, EB-02 Gunduz Akdogan, N: CG-10, FC-13, FC-Ganepola Arachchige, V: BP-03, FD-Goncharov, A: EG-03 06, FD-09 Gong, C: **BE-01** Gungordu, B: FC-13, FC-14 Ganguly, S: GF-04 Gong, E: FQ-02 Guo. G: DR-11 Gao, Q: ED-10, FQ-01 Gonzalez, J W.: ED-07 Guo, O: ER-01 Gonzalez, V: EE-03 Gao, T: VP7-03 Guo, X: AQ-08 Gao, W: FA-05 González de la Vega, M: AR-08 Gupta, A: AR-01, FG-04

Gonzalez-Fuentes, C: ED-07

Goodman, M: DR-05

Gao, Y: CC-05

Garcia, I: AE-03

Gupta, J: CF-09

Gupta, M: AR-01

^{*} Best Student Presentation Finalist / LB – Late-breaking Poster

Gupta, R: AF-08 Hauet, T: EG-09 Hloskovsky, A: CR-09, FG-04 Gupta, S: **DG-03**, **FF-09** Haugstad, G: BF-01 Hodason, A: DO-09 Gupte, K: FF-07 Hauwaert, M: FC-09 Hoffmann, A: DE-06, DF-09, EE-04, Gurung, G: GF-07 Hauwiller, M: VP7-03 FO-02, GE-02, GO-05 Guy, M: BR-06, CR-07, FO-07 Hayward, T: FF-10 Hohlfeld, J: EG-09 Gwalani, B: BD-06, BG-10 Hazarika, K: BD-05 Hoijang, S: FC-15 He, H: BO-10 Hojo, T: CR-10, DG-01, DR-07, DR-08 He, H: DR-08 Holder, H: DB-01 Ha, J: DF-01 Holloway, K: FC-12 He, R: AR-05 Haaq, J: BD-06 He, Z: VP3-06 Hong, G: **FG-08** Hackett, L: DE-04 He, Z: CA-02 Hong, J: GR-14-LB Hadimani, R L.: AP-05, AP-06, AP-08, Hedlund, D: BG-02, BQ-03, **DE-07** Hong, J: AF-04 BE-13, CO-03, CO-09, FC-07, **FC-10**, Heaedus, G: DD-01 Hong, J: DF-01 FC-11, FC-12, **GQ-01** Hehn, M: EG-09, EG-12 Hong, X: EF-05, **GD-02** Heiliger, C: AG-02 Hadjipanayis, G: ER-12 Hong, Y: CB-02 Hai, N: AC-12 Heiman, D: BG-02, DE-07 Hono, K: EG-06 Hait, S: DF-02 Heinsohn, C: XA-03 Horaquchi, T: AR-06 Haley, R P.: GR-13-LB Hendren, W R.: BR-03, CH-06, CH-10 Horiuchi, H: DF-08 Ham, B: FG-08 Hennes, M: EA-03 Horst, O: CR-05 Hamasaki, A: AQ-04, AQ-07, CQ-01, Herfort, J: EF-02, FE-11 Horvath, Z E.: DD-01 CQ-08 Herquedas, A: BC-12 Hosen, K: EG-07 Hamasaki, H: CR-10 Herling, F: EF-01 Hosomi, M: BR-08 Hamazaki, Y: VP2-03, VP2-04 Hermans, S: FC-09 Hossain, T: FR-09, GE-04 Hamdi, M: GP-04-LB Hernandez, S: VP7-03 Hotta, T: FE-10 Hamrle, J: CC-02 Heron, J: GE-04 Hou, D: CC-05 Herrera, S: DE-04 Hou, J: BQ-09, BQ-10 Han, D: DF-01 Han, D: **DR-03** Herrera Diez, L: AD-09 Hou, Y: FE-08 Houda, T: VP2-03, VP2-04 Han, J: BA-02, GF-09 Herrero, A: AE-12, BE-10 Han, J: GR-03-LB Hersam, M C.: GP-04-LB Hristoforou, EV.: AQ-09, DD-05 Han, T: VP3-05, VP6-13 Hertel, R: DB-03 Hrushko, O: CH-07 Han, X: AA-01 Hesjedal, T: CH-06, EF-11 Hsu, W: GF-01, GF-02 Hanbicki, AT.: FR-09 Hewett, S M.: FQ-10 Hu, C: GG-11 Haney, P: DF-04 Heywood, S: CG-11 Hu, G: GE-01, XA-03 Hibino, Y: BA-04 Hanke, M: EF-02, FE-11 Hu, S: VP3-06 Hanna, D: DR-13 Hicken, R: CH-03, CH-06 Hu, S: **VP7-02** Hanson-Flores, J: GP-02-LB, GP-08-LB Hidaka, K: BQ-06 Hu. Y: AE-05 Hanus, R: FC-09 Hidalgo Gonzalez, J: CR-12 Hu, Z: AB-03 Hao, R: CB-03 Hierro-Rodriguez/, A: BC-12, DC-01 Huan, C: GR-13-LB Hao, Y: CD-09 Higo, T: BA-04, ED-11 Huang, A: AR-14 Hara, Y: **VP4-10** Hillebrands, B: EE-12 Huang, B: VP6-16 Hirama, R: BR-08 Huang, D: AC-13 Harouri, A: AD-09 Harrison, R: DC-11 Hirata, Y: BC-03 Huang, F: **VP6-13** Hirayama, Y: BG-08, BG-12 Hasan, A: AR-10 Huang, H: VP4-09, VP6-10, VP6-16 Hasegawa, R: VP2-03, VP2-04 Hirohata, A: AC-09, FD-02 Huang, H: VP5-03 Hashemi, P: XA-03 Hiroi, M: GR-06 Huang, K: CE-04, EF-10 Hata, S: CQ-02 Hisada, Y: FR-07 Huang, L: DF-02

Hisamatsu, M: GO-02

Hisatomi, R: ED-05

Hiura, S: AA-03

Hatala, I: FG-10

Hatt, S: CE-08

Hatano, M: BB-05

Huang, S: DR-11, GF-01, GF-02

Huang, S: BC-11

Huang, T: GC-03

^{*} Best Student Presentation Finalist / LB – Late-breaking Poster

Huang, T: VP7-02 Jiang, H: **VP4-04** Isogami, S: AF-03, **EG-06**, **FR-05** Huang, T: AD-03 Itai, S: CH-04 Jiang, M: FE-07 Huang, X: FE-01 Ito, O: BQ-06, VP4-07, VP4-10 Jiang, T: AC-05 Huang, Y: AD-04, CD-10 Ito, T: VP7-05 Jin, H: BF-08 Huang, Y: BF-01 Iwasaki, H: CB-05 Jin, Z: **FD-02** Hubble, Z: EF-10 Iyer, P: AQ-05, CF-07 Jinno, J: DG-01 Huber, J W.: CH-09 Iver, P: FF-09 Ji Omar, G: CG-06 Jois, S: FR-09 Hui, H: AE-05 Izaki, M: FP-10 Huligerepura Shankaregowda, R: CR-Izumi, T: FD-04 Jones, J L.: FD-01 Jong-Woo, K: BG-03 Hullahalli, A: BP-06 J Josephy, S: EF-02 J. Lopes, J: EF-02, FE-11 Husain, S: AD-01 Joshi, P: **CF-03**, CF-10, **ER-07**, ER-08 Hussain, B: AR-04, BP-01, BP-07 Jaberolansar, E: AP-04 Joshi, V: BD-06 Hussain, S: **BP-07** Jacob, Z: BE-03, DG-03, FF-09 Jossart, N: CA-01 Hutin, L: ED-02 Jaffrès, H: AA-01 Ju, L: GC-05 Hwang, J: CE-07 Jahjah, W: CD-09 Jubert, P: EG-03 Hwang, K: FC-15 Jung, G: AF-04, GP-09-LB Jain, A: GR-08 Hwang, S: BQ-04, FP-04, VP4-06 Jain, P: CE-08 Jung, M: DF-01 Hwang, S: BA-03 Jain, R: AC-12 Jung, M: FP-06, GR-01 Jakob, G: GG-13 Jung, W: BF-04 ı Jal, E: EA-03 Jungfleisch, B: DB-01, EE-02, FR-09, Iacocca, E: DB-01, DC-05, EE-05 Jalan, B: FR-04 **GE-04** Ibrahim, F: CD-09 Jaman, A: AE-03 Jungwirth, T: CG-11, EB-01, EB-02, GF-Ichinose, T: AD-05 Jamshed, B: AF-07, **ED-08** Idachi, S: DG-06 Jan, A: **GD-05** Jurczyk, J: DC-01 leda, J: BA-02, DF-08, DF-10 Jan, S: AP-04, AP-07, AR-08, DC-10 Ievlev, A: CE-05 K Jander, A: EE-08 Igarashi, J: EG-09 Jang, G: **FC-03** Kaffash, M T.: DB-01, EE-02 Iglesias, F: VP3-09, VP3-10 Jang, H: DF-01 Kailas, L: DF-02 Iquchi, Y: GA-05 Jangam, G: VP2-06 Kainuma, Y: FC-04 lida, H: DF-06 Janqid, R: BC-09 Kákay, A: DB-04 lino, A: FC-07 Janus, W: FG-07 Kalkavan, D: CG-10 Ikeda, S: AF-10, GF-06 Jasenský, K: GF-04 Kalouni, C: AF-02 Illes, L: DD-01 Kalsar, R: BD-06 Jayathilake, UM.: AG-06, EF-06 Imaoka, N: BD-04 Jechumtal, J: GF-04, GF-05, GG-12, GG-Kamal, P: FR-08 Inada, K: VP4-10 Kaman, B: GE-02 Incorvia, J C.: FF-08 Jeffrey, T: **BP-09**, DQ-05 Kamei, T: FC-08 Incorvia, J: BF-08, GG-11 Jensen, C: EF-06 Kamiryo, A: **AR-06**, **FR-01** Jeon, H: AF-04, GP-09-LB Kampfrath, T: GF-04, GF-05, GG-12, Ingla-Aynes, J: GG-05 Inoue, M: AP-01, AP-02 Jeon, J: AF-09 GG-13 Inoue, T: CR-08 Jeon, S: DF-09 Kanai, S: BA-02, **DA-01**, DF-06, DF-11, Ipaves, B: FG-02 Jeong, J: EP-05-LB, GP-09-LB GF-09, GF-10 Ishida, M: DG-01 Jeong, S G.: FR-04 Kanai, Y: BR-02, **DG-11** Ishikawa, R: AC-09 Kanematsu, T: CR-08 Jeong, Y: **BQ-04** Ishikawa, Y: VP7-05 Ji, R: FO-10 Kaneta-Takada, S: DF-08 Ishrak, F: BG-10 Ji, Y: DB-01, EE-02 Kang, B: FG-08 Ishraque, Z: BP-03 Jia, C: GP-06-LB, GR-13-LB Kang, J: **GP-04-LB** Kang, M: BF-07 Islam, K: DR-10 Jia, Q: AD-04, BF-01, **CD-10**, **DR-02**,

FR-04, GR-09

Islam, S: **GG-11**

Kanno, Y: BA-02

^{*} Best Student Presentation Finalist / LB - Late-breaking Poster

Kanomata, T: GR-06 Kantartzis, N V.: DG-11 Kao, I: CE-09, FE-02 Kapteyn, H C.: AQ-10, CG-05

Kapuruge, N: FG-02

Karampelas, I H.: CF-07, CQ-06, CQ-07

Karki, P: EF-10

Karki, T: CF-03, CF-10, ER-07, ER-08

Karmakar, P: AR-01 Karrai, K: CG-01 Karube, S: AF-10, **ED-05**

Kasai, S: DF-10 Kasai, S: FR-06 Kashyap, A: BG-06

Kaspar, Z: GF-05, **GG-12**, GG-13

Kašpar, Z: GF-04 Kassa, A: EF-02 Kateel, V: BF-06

Katine, J: AF-05, BF-02, GP-04-LB

Katoch, J: CE-09, FE-02 Kaur, Y: VP6-01

Kaushik, S: CR-11, FP-08
Kautzky, M: VP7-03
Kawagita, K: VP7-05
Kawaguchi, H: AQ-07, CQ-01
Kawakami, R: **EA-04**, FD-08, **TU-03**Kawatsu, T: VP2-03, VP2-04

Ke, L: FE-07 Ke, W: VP1-03

Keatley, PS.: CH-03, CH-06

Keller, M: BC-09

Kent, A D.: **DA-02**, VP7-10

Kent, N: FC-02 Kern, L: AC-02 Kesler, M K.: DD-11 Kessler, P: GF-04 Keum, J: GP-02-LB Keylin, V: BD-11 Kezsmarki, I: GE-10 Kfir, O: EA-05

Khalili Amiri, P: BF-02, DA-03, FF-06,

GP-04-LB

Khan, K: EF-02, FE-11 Khan, M: DQ-02, DQ-03 Khan, R M.: AP-05 Khanna, M K.: CH-05

Kharel, P: CD-05, DQ-10, VP3-08

Khizroev, S: BB-03

Khodagulyan, A: VP3-09, VP3-10

Khorwal, A K.: DE-10 Khymyn, R: EE-03 Kiechle, M: GE-01 Kiehl, C: EE-04 Kikkawa, T: BC-03 Kikkawa, T: GE-08 Kim, B: AP-10-LB

Kim, D: **AP-10-LB**, BF-07, **EP-05-LB**

Kim, D: **DD-10** Kim, D: VP4-19 Kim, G: XA-03 Kim, H M.: FC-07

Kim, H: EQ-01, **EQ-02**, EQ-04, EQ-05,

EQ-06 Kim, H: ER-10 Kim, H: AR-11-LB Kim, J: AR-11-LB Kim, J: EQ-03, GR-03-LB

Kim, J: DF-01

Kim, J: XA-03

Kim, K: AF-04, GP-09-LB Kim, K: DF-01, EP-05-LB

Kim, S: **GE-11** Kim, S: DF-01 Kim, S: EQ-06 Kim, S: AR-11-LB Kim, S: VP4-19 Kim, T: **AR-11-LB**

Kim, W: BQ-02, EQ-01, EQ-02, EQ-04,

EQ-05, EQ-06

Kim, W: AF-04, GD-07, GP-09-LB

Kimák, J: CC-04 Kimoto, R: AQ-04 Kimura, T: DB-01 Kinane, C: FD-01 Kino, K: **DF-11** Kioussis, N: DR-12 Kiraly, B: CG-11 Kirilyuk, A: CH-01 Kiselev, N: GE-10 Kita, E: FG-05 Kitcher, M D.: **ED-09**

Kim, Y: FG-03, GG-01

Kläui, M: DF-01, **FA-03**, FE-04, GG-13

Klein, J: GG-05 Klewe, C: AF-06 Kluck Graham, H: DR-05

Knut, R: BP-03, FD-06

Ko, H: AR-11-LB

Ko, H: BA-03

Ko, S: AF-04, GP-09-LB Kobayashi, N: BD-01 Kobayashi, N: EQ-08

Kocharian, A N.: VP3-09, VP3-10

Kodama, Y: BD-13 Koerner, A: FD-08 Koh, D: **BF-07** Koi, K: CH-04 Koizumi, H: AC-09 Koll, M: **BR-09**, **BR-10** Kollár, P: FD-03 Kolli, A: CH-08 Komaili, J: DG-01 Komeda, T: **CF-05** Komori, S: FD-04, FR-07

Komuro, K: **FC-04**Konakanchi, S: GP-04-LB
Kondaiah, P: GD-03
Kondou, K: ED-11
Kong, D: GE-10
Koo, H: AF-09, DF-01
Kopcansky, P: CQ-04
Körber, L: DB-04
Kosaki, H: BA-04
Koshino, Y: **DR-04**Kosma, A: **AC-08**

Kosogor, A: **BE-07**, CH-07

Koster, M: EE-12 Kosugi, S: **GQ-02** Kota, Y: FE-10

Kotani, Y: BA-04, FR-05 Kotsugi, M: CR-01, FR-03

Kounta, I: EB-02

Kovács, A: AD-09, GE-10

Koziol Rachwal, A: AC-07, CE-03, FG-

07

Kramer, M J.: DD-11 Krempaský, J: CG-11 Kriegner, D: CG-11, EB-02 Krishnan, S: **ER-01** Krishnaswamy, G: CG-06 Krivorotov, I: DR-13 Krockenberger, Y: DF-08 Kronast, F: CE-09 Kronik, L: VP2-05

Kronik, L: VP2-05 Krylyuk, S: BG-01 Ku, M: EE-07

Kuanr, B K.: CH-05, CR-11

^{*} Best Student Presentation Finalist / LB – Late-breaking Poster

Kuanr, B K .: FP-08 Lee, S: AF-04 Lagarrique, A: DF-06 Kubascik, P: CC-04, GF-04, GG-12, GG-LaGasse, S: EF-05 Lee. S: AF-09 Lai, C: **VP3-05** Lee, T: AP-07, FC-15 Kubota, T: BR-08, **DG-01** Lambe, J G.: FP-09 Lee, T: AG-06 Kubota, Y: EG-06 Lambert, G: EA-03 Lee, W: GF-01, GF-02 Kukreja, R: BC-09, BG-01, FB-02 Lamichhane, A: DQ-02, DQ-03 Lee, W: BA-03 Kulik, P: BG-02, BO-03, DE-07 Lamichhane, S: EF-05, EF-10 Lee, W: GR-03-LB Kulkarni, PD.: CB-05 Lamichhane, T: **BG-04**, **DD-06**, DR-05, Lee, Y: BQ-02, EQ-01, EQ-02, EQ-04 Kuma, K: GR-06 EC-02, ER-09, FQ-04-LB Lee, Y: CH-04 Kumagai, S: DG-01 Lamperti, A: AD-09, CD-03, CD-04, FG-Lei, N: GD-04 Kumar, A: AF-02 Lei, S: GR-12 Kumar, A: FE-04 Landeros, P: DB-04, ED-07 Leighton, C: CE-08 Kumar, A: BE-13, DQ-01, GR-07 Langer, J: AD-09, BF-05, CD-04 Leiviska, M: EB-02 Kumar, A: AF-08, DF-06, **EE-03** Langridge, S: FG-09 Lejeune, L: FC-09 Kumar, A: AC-11 Langton, C: **DC-02**, **DC-04** Lemaitre, A: AA-01 Kumar, A: **DO-08** Lanier, J: CE-07 Lengyel, A: **DD-01** Kumar, D: GG-03 Laraoui, A: **EF-05**, **EF-10** Lenk, S: DD-01 Kumar, D: ED-08 Largeau, L: AD-09 Lenz, J: **DC-03** Lasek, K: FG-02 Kumar, J: EF-10 Leo, N: DC-01 Kumar, P: FR-05 Lasheras, A: DG-12 Le Pottier, A: CD-09 Kumar, P: CH-05 Lasthofer, F: CH-07 Lesne, E: FD-02 Kumar, P: CH-05, CR-11, FP-08 Lastovich, M: BG-10 Lethole, N L.: EC-03 Kumar, R: EF-05 Lau, Y: GE-09 Levati, V: DB-02 Kumari, M: VP5-06 Laughlin, D E.: EG-04 Lewis, L H.: ER-12 Kumay, A: AG-03 Lauter, V: CE-05 Li, C: **VP3-03** Kunca, B: BD-12 Lauterbach, H: CR-05 Li, H: GE-09 Kuninski, N: BR-03, CH-06, CH-10 Lawati, DR.: EF-10 Li, H: VP3-01 Laxmeesha, PM.: AG-06, EF-06 Kunyangyuen, B: **EG-12** Li, J: BF-03 Kurebayashi, D: FE-03 Le, D: AC-03, AC-04, GQ-03, GR-04, Li, J: **VP5-02 GR-10** Li, J: VP1-02, VP6-07 Kurebayashi, H: DB-01, GE-08 Kurniawan, I: EG-08 Leary, A: BD-11 Li, J: **BC-13**, **ED-10**, FQ-01 Kuschel, T: BC-07, CC-02, GF-05 Lebrat, M: AQ-10 Li, L: BD-06 Le Breton, J: CD-09 Li, L: BG-02 Kuwahara, Y: BR-13 Kuwahata, A: **AP-01**, **AP-02**, BB-05, Lebrun, R: EE-06, GD-01 Li, N: AQ-10 CQ-05 Le Chin, J: DR-05 Li, S: **DF-09** Kuzel, P: GF-04, GG-12 Lee, B: ED-09 Li, S: **GP-06-LB**, GR-13-LB Kwao, E: GP-10-LB Lee, J: FG-08 Li, T: EF-05 Kwiatkowski, A: AC-07, CE-03, FG-07 Lee, J: BO-02, **EQ-01**, EO-02, EO-04, Li, T: AB-02 EQ-05, EQ-06 Li, W: VP6-20 Kwon, H: **GG-03** Kwon, J: **FP-02** Lee, J: DR-03 Li, W: **DR-11** Kwon, J: FG-08 Lee, K: BG-03 Li, X: CD-09 Kwon, J: FC-03 Lee, K: BA-03, EP-05-LB Li, X: BQ-09, BQ-10 Kwoun, G: FC-06 Lee, O: AF-09, DF-01 Li, Y: BC-14 Lee. S: FG-08 Li. Y: VP1-04 Lee, S: FC-03 Li, Y: DE-06, **EE-04** Lacour, D: EG-12 Lee, S: BF-01, FR-04 Li, Y: VP3-03 Lee, S: GR-03-LB Li, Y: VP4-12, VP6-15 Ladak, S: DC-03 Lafosse, X: AD-09 Lee, S: **AC-12** Li, Y: VP6-20

Lee, S: AF-04, GP-09-LB

Lagarde, D: AA-01

Li, Y: VP1-02, **VP6-08**, VP6-18

^{*} Best Student Presentation Finalist / LB - Late-breaking Poster

Li, Z: BE-04	Liu, X: VP6-11	Ma, G: BQ-10
Li, Z: VP1-02, VP5-02, VP6-07, VP6-08,	Liu, X: BE-04	Ma, H: AC-09
VP6-09, VP6-11, VP6-18	Liu, X: CB-02	Ma, T: AQ-08
Li, Z: FD-08	Liu, X: VP6-07	Ma, T: AA-01
Liang, B: ED-10	Liu, X: CE-05, GC-04	Ma, X: AQ-08
Liang, J: XA-03	Liu, X: CF-03, DD-08, DD-11, DD-12,	Ma, Z: CD-01, CD-03
Liang, J: AC-12	ER-03 , ER-07, ER-08	Maccari, F: DD-01
Liang, P: BB-03	Liu, Y: AQ-08, EB-03	Maccherozzi, F: CG-11
Liang, S: AD-04, BF-01, BR-11, CD-10,	Liu, Y: BP-05-LB	Macedo, R: GG-08
FR-04	Liu, Y: AE-05	Mach, P: VP7-03
Liao, B: BE-13	Liu, Z: BG-12, CC-05	Machida, Y: FR-03
Liao, C: GF-01	Liyanage, N: GE-06	MacLaren, D: DC-01
Liao, L: FA-05	Lohr, W: AP-05 , AP-06, AP-08, CQ-03,	Madami, M: DB-02
Liao, S: VP5-03	CQ-09 , FC-07, FC-11, FC-12	Madej, E: CE-03
Li Bassi, A: DB-02, FG-11	Lomakin, V: BD-10, EC-05	Maekawa, H: CH-04
Licwinko, G: AP-09-LB	Lombez, L: AA-01	Magni, A: CD-01
Lille, J: BF-04	Lopes, A: DG-12	Mahfouzi, F: DF-04, DR-12
Lim, J: EE-04, GE-02, GQ-05	Lopes Seeger, R: EB-02	Maity, S: AR-02
Lim, P G.: GP-04-LB	Lopes Temporao, A: FF-02	Maizel, R E.: AF-06, FD-01
Lim, Y: EQ-05	Lorenzoni, A: BE-08	Majetich, S: GG-06, GG-10
Lim, Y: BQ-02 , EQ-01, EQ-04	Lostun, M: VP6-19	Major, M: DD-01
Lim, Y: FD-01	Lotsch, B: FE-04	Majumder, S: GQ-04
Lin, C: FQ-10	Louis, S: DR-13	Makarov, D: DC-02, DC-04
Lin, C: DR-11, GF-01, GF-02	Lourembam, J: AC-11, FE-07	Maletinsky, P: FE-04
Lin, H: AG-04	Loven, J: EG-01	Malik, V K.: AF-02
Lin, J: EG-09 , EG-12	Low, T: BF-01, FR-04	Malinowski, G: EG-09, EG-12
Lin, W: ED-06	Lozano, J A.: BE-08	Manago, T: AR-06
Lin, Z: VP4-02	Lu, J: GC-08	Manchon, A: AC-13 , ED-04
Lindemann, M: AA-01	Lu, J: DG-07	Mancias, M F.: BD-11
Liou, S: EF-05, EF-10	Lu, X: VP6-09, VP6-11, VP6-12	Manfrinetti, P: BE-10
Liou, Y: AC-12	Lu, Y: AA-01, CD-09	Mangin, S: AA-01, EG-09, EG-12
Lisfi, A: BR-06, CR-07, FQ-07	Lu, Z: GC-05	Mani, B K.: GR-02
Liu, B: CE-07	Luepke, G: EC-07	Manikketh, M: CB-05
Liu, C: VP4-03	Lukashev, P: CD-05 , DQ-10	Mann, C: VP7-03
Liu, C: CD-09	Luo, C: EF-02	Mansell, R: GD-06
Liu, C: CG-07	Luo, L: FD-07	Mansueto, M: BF-09
Liu, H: BQ-10	Luo, Y K.: AC-03	Mantion, S: EE-06
Liu, J: BQ-07	Luo, Y: FD-08, FE-01, GB-01	Manuel, W: AP-07, BR-07
Liu, J: VP3-06	Lupu, N: VP6-19	Mao, X: VP4-03
Liu, J L.: BQ-07	Lustikova, J: FE-03	Marangolo, M: AD-03, EA-03, EC-11
Liu, J: VP4-12	Luu, D: AP-07, BR-07, FC-15	Marcano, L: DC-07
Liu, J: ED-10	Lv, H: EF-02, FE-11	Marcin, J: BD-12
Liu, J: CB-02	Lv, Y: AR-03, BF-01, CD-10, DR-02	Marie, X: AA-01
Liu, K: BG-01 , DC-02, DC-04	Lynn, J: BC-02, GC-03	Marinova, V: EF-01
Liu, L: AB-03 , CA-02, GG-05	Lyu, D: AD-04, BF-01, CD-10	Markou, A: FD-09
Liu, P: BD-09		Marotta, A R.: BD-07
I: D. CE 07 CE 10 ED 07 ED 00	M	Marausa II . DD 04

M. Jefremovas, E: DC-07

Ma, D: VP6-06, VP6-12

Liu, P: CF-03, CF-10, ER-07, ER-08

Liu, Q: AG-08

Liu, S: **FF-08**

Marques, J L.: BB-04

Martella, D: DE-01

Marrows, C: DF-02, FG-09

^{*} Best Student Presentation Finalist / LB – Late-breaking Poster

Martinez, L: FF-09 Martinez, V: DB-01

Martinez-Garcia, J C.: BB-04
Martins, C S.: **VP6-04**Martins, P: EE-06
Maruyama, S: GF-06
Maslanka, D: BF-05
Masood, A: BD-08
Maspero, F: DB-02
Masuda, K: CB-05
Masumoto, C: BD-13

Matsubara, D: CF-11

Matsuda, T: ED-11

Matsueda, H: EE-13

Matsumori, H: BQ-01, EQ-08

Matsuo, T: **ED-11**Matsuura, M: VP7-01
Matsuzaki, H: DG-01
Matt, E: GP-04-LB
Matutes, J: CR-12
Matzelle, M: AG-03
Mavani, H: **CE-04**Mavropoulos, P: AC-08
May, S: AG-06, **EF-06**Mayer, C: ER-06
Mayoh, D: EF-11
Mays, A E.: EP-03-LB
Mazzoli, C: **FB-01**McAllister, K H.: **EE-05**McClintok, L: FF-09

McCormack, T E.: **BR-03**, CH-06, CH-10

Mckenzie, J: **ER-14-LB** McMorran, B: GE-05 Meena, R: FG-03 Meera, F: BC-09 Mehta, S: GP-04-LB Meier, F: BC-07

Meisel, M W.: GR-13-LB Meisenheimer, P: GE-04 Mendonsa, R A.: **BR-11** Meneghini, C: FG-04 Menéndez, E: CD-03 Meng, P: VP6-06 Meng, W: VP6-15 Meng, Z: FE-08

Merbouche, H: CH-08, EE-06

Meriles, C: EF-05

Mentink, J H.: EA-05

Meo, A: GP-04-LB

Merkel, D G.: DD-01 Mertens, S: CA-01 Messner, L: AQ-03 Mewes, T: FD-01 Meyerheim, H: AC-05 Miao, B: AF-01 Miao, G: AE-07

Miao, J: CG-05

Michel, J: CE-07, GP-08-LB Michel, M F.: FD-01 Michez, L: **EB-02** Migot, S: CD-09

Mihajlović, G: AF-05, BF-04 Miki, S: FD-02, GG-03 Mikuni, K: VP7-05 Milano, J: EA-03 Mille, N: DC-01 Miller, M: DE-04 Millo, F: **EC-11**

Mimica-Figari, B: DB-04 Mimura, I: FC-06 Min, B: DF-01 Mishra, K K.: **VP7-11** Mishra, V: CR-14 Mitsui, N: BD-04 Mitsumata, C: CR-01 Miura, Y: EG-08

Miwa, S: BA-04, ED-11 Miyahara, S: BQ-06, VP4-07, VP4-10

Miyazaki, D: BR-04, **BR-05** Miyazaki, T: BD-13, CR-03 Miyazawa, M: CR-04 Mizukami, S: FD-02, GG-03

Mo, Z: BQ-09

Moghal, B: BD-09, **GQ-07** Mohammadi, M: DR-01 Mohammed, R: **DQ-09** Mohapatra, B D.: GG-12

Mohapatra, J: CF-03, CF-10, ER-07, ER-

80

Mohapatra, S: AP-04 Mojsiejuk, J: BF-05

Mokrousov, Y: AC-08, FE-05

Mondal, A: BF-10 Mondal, M: AG-03 Monem, Z: BG-02 Mongeon, J: GE-04

Monteblanco, E: BR-12, CD-03, CG-03,

FG-11, GD-06

Montoncello, F: DB-01, EE-02 Montoya, S: CG-05, GE-05, GE-06 Moodera, J S.: **GA-03**, GG-05, **XA-01**

Moon, C: **VP2-07** Moon, J: **GR-01** Morales, A: CG-01 Morales, R: FG-13 Morassi, M: AA-01

Moreno-Ramírez, L M.: VP7-06

Morley, S A.: GE-06

Morozkin, A: AE-12, VP2-06

Moser, S: GF-04 Mosina, K: GG-05

Mostufa, S: **AQ-06**, **CQ-06**, CQ-07

Moureaux, A: **FF-02**Mousa, M: BE-03
Moussi, K: DE-03
Mudakavi, D: FC-10
Mudiyanselage, N: GR-04
Mudryk, Y: BE-13, DQ-01, GR-07

Mugdho, S S.: FF-07 Mukherjee, D: DD-01 Muller, D: BG-02 Müller, J: BF-09 Munnik, F: EF-02 Muñoz, M: CH-08

Murayama, T: AP-03, FC-08 Murqulescu, I: VP6-19

Murnane, M M.: AQ-10, CG-05, **EA-01** Muroga, S: BD-13, CR-03, DG-08

Muta, H: GQ-02 Muto, H: FP-10

Ν

N'Diaye, A T.: BG-01, CH-06 Nachawaty, A: CD-09

Nadvornik, L: CC-04, GF-04, GF-05,

GG-12, GG-13

Nag, J: GD-08, GR-11

Naganuma, H: AD-05, DG-05, GF-06

Nagayoshi, K: BQ-01 Nagy, D L.: DD-01 Nair, S: FR-04

Nakagawa, T: **ER-05**, GQ-02 Nakamura, K: BD-01 Nakamura, T: BA-04, FR-05 Nakano, H: VP2-03, VP2-04 Nakano, T: DR-06, DR-08

Nakarmi, P: FD-01

^{*} Best Student Presentation Finalist / LB - Late-breaking Poster

Nakasato, N: DG-01 Nakashinden, H: CR-04 Nakatani, T: **CB-05** Nakatani, Y: DR-01

Nakatsuji, S: BA-04, CA-05, ED-11

Nakayama, M: CH-04 Nallan, S: EE-07, **FF-05** Nan, T: BF-05 Nangaku, M: FC-06

Nara, T: BR-13

Narangerel, B: BG-13, VP7-07 Narasimhan, K S.: DG-02 Narducci, D: GD-07 Nassar, K: GR-10 Natekar, N A.: EG-03 Naushin, N: BG-01

Navratil, J: AR-13 Nawa, K: AD-05

Negrello, R: DB-01

Nembach, H T.: DD-07, GE-01 Nemec, P: CC-04, GF-04, GG-13

Nemes, N M.: DD-01 Nemeth, A: DD-01 Nepal, B: FD-01 Netzer, J: EE-05 Neuefeind, J: CE-08 Neuner, T: BF-02, FF-06 Neupane, M: AG-03, **GC-01**

Newburger, M: DE-07 Newman, D G.: CH-06 Nezat, C M.: FR-13 Ngo, T A.: GQ-03 Nguyen, M: AP-07, FC-15

Nguyen, M: AP-07, FC-15 Nguyen, T: GF-06

Nguyen, T. **GF-06** Nguyen, T D.: GQ-03 Nguyen, V: BC-14, BF-06

Nguyen T. Tran, L: AQ-05, FC-05

Ni, H: GQ-05 Nicolau, A: CD-04 Nihal, I: CD-08 Nihei, K: **GF-09** Nii, S: DR-08

Nikolić, B: EE-11, GC-07 Nirmala, R: **VP2-06** Nishi, H: FC-06 Nishii, T: **FP-10** Nishijima, T: FR-01 Nishikura, A: **CR-04** Nishio-Hamane, D: BA-04, ED-11, VP3-

02

Nitta, T: **VP4-07** Niu, Q: CC-05 Niu, W: DQ-07 Niu, Y: CG-11

Nlebedim, C I.: DD-12, ER-03 Nlebedim, I: DD-08, **DD-11**, FP-03

Noack, T B.: EE-12 Noda, Y: FC-07 Noebe, R D.: BD-11 Noh, S: EQ-03, GR-03-LB

Nomoto, T: BA-04

Noujima, M: BD-02, DD-03 Novosad, V: DE-06, EE-04

Nozaki, T: BA-04 Nozaki, Y: DF-03 Nukui, K: FD-02 Nunez, J P.: BE-13 Nutter, P: FQ-10

0

O'Shea, K: AR-09

Odkhuu, D: **BG-13**, VP7-07

Odlyzko, M: BF-01 Ogawa, T: **BD-01**, BD-02

Oh, A: CG-05 Oh, Y: **FP-04** Ohishi, Y: GQ-02

Ohno, H: BA-02, DF-06, DF-11, GF-09,

GF-10

Ohshima, R: DR-04, FR-01

Ohtani, T: DG-11 Ohtani, T: BP-04-LB Ohya, S: CF-11, DF-08

Ojo, A I.: AR-08, CR-13, CR-14, DC-10,

FD-09, FR-10 Oka, C: CQ-02 Okada, K: **VP7-01** Okada, S: BD-04, **BG-11** Okada, Y: CG-06 Okamoto, H: FC-08

Okamoto, K: VP2-03, VP2-04

Okamoto, S: AQ-02 Okita, K: AP-03, FC-08 Oleaga, A: **AE-12, BE-10** Olejník, K: GF-04, GG-13 Oles, E: AC-07, CE-03, FG-07 Ollmann, C J.: GR-13-LB Olson, T: EG-03 Onat, B: FC-14 Onderko, F: FD-03 Onishi, K: DG-01

Ono, H: DG-01

Ono, N: AQ-02 Ono, S: AD-09, CD-03, CD-04

Ono, T: ED-05, GA-02

Oogane, M: AR-12, BR-08, CR-10, DR-

06, DR-07, DR-08 Orlova, T: CE-05 Oropesa, A E.: **CR-12** Ortiz, B: AG-03 Orue, I: DC-07 Osaki, Y: VP4-07 Osellame, R: DB-02 Ostapyuk, V: DQ-05 Ostatnicky, T: CC-04

Ota, K: ER-05 Otaki, T: EE-13 Otani, Y: ED-11, FA-05 Otsuka, R: DG-01 Otyepka, M: AR-13 Oulton, R: DB-01 Ourdani, D: AD-09 Ovari, T A.: VP6-19 Oyagi, S: DG-01

Ozaki, K: BD-04 Ozawa, Y: FC-08

Oyarzún, S: ED-07

Ρ

P. Chhetri, T: BD-06 Pachat, R: CD-04 Padgett, A S.: **BD-07** Padmanabhan, P: FF-09

Page, M: DE-07 Pal, P: **BF-10**, **DE-06** Palai, D: DQ-08 Palanivel, U: AR-11-LB Palau, A: CD-01

Palomino Lopez, A: CA-01

Pan, C: DD-14

Panagopoulos, C: BP-06 Pancaldi, M: BC-09 Pané, S: BB-03

Pantano, G M.: AC-04, GF-03, GP-01-

LB, GR-10 Panzeri, M: DB-02

Papp, Á: GD-01

Paranthaman, M P.: FQ-04-LB Pardo-Almanza, M: CG-06

Parekh, K: CO-04

Park, B: AF-04, AP-10-LB, BA-03, BF-

07, GP-09-LB Park, E: GG-05 Park, H: **VP4-19** Park, H: FP-02

Park, J: GP-02-LB, **TU-02** Park, J: BG-03, ER-04 Park, J: BQ-04, **VP4-06**

Park, J: FG-08 Park, J: EQ-03 Park, K: **BG-08**

Park, K: FP-04, VP4-06

Park, T: GR-01

Parkin, S: AC-05, DQ-07, **GA-01**

Parmar, H: **DD-12**Parmenter, C: CG-02
Paslar, M: AP-06, **FC-11**Patel, H H.: **CQ-04**Patel, M: GQ-09

Pathak, A: DQ-02, DQ-03 Pathak, S: AR-01, FG-04 Pathare, S: DG-01 Patil, S: CE-09 Patra, A K.: DE-10

Patra, L: BE-13 Paul, A: **DD-13**

Paz Gonzalez, K: AQ-05, FC-05

Peddis, D: BE-10 Pedersoli, E: BC-09 Peer, M: BR-10

Pei, R: VP1-02, VP5-02, VP6-06, VP6-07, VP6-08, VP6-09, VP6-11, VP6-12,

VP6-18, VP6-20 Pekarek, T M.: **AR-09** Pellizzi, N: DB-02

Pena Perez, V: VP3-09, VP3-10

Peng, B: BQ-05 Percival, S: BD-07 Pérez-Álvarez, L: DG-12 Peria, W K.: DD-07, GE-01 Perna, S: **CH-08**, **EC-12**, **EE-09** Peroor, R: **DC-05**, DE-07

Peters, F: BC-07 Peters, J: **FF-04**

Peterson, C L.: AP-06, FC-11

Peterson, O R.: EG-04 Peterson, T: AD-04, BF-01

Petit, M: EB-02 Petrik, P: DD-01 Petti, D: DB-02 Pham, Y T.: GQ-03

Phan, M: AC-03, AP-07, **BB-02**, BR-07, CR-14, DQ-06, FC-15, FD-09, FG-02, GD-08, GQ-03, GR-04, GR-10, GR-11

Phan, N: FF-04

Phatak, C: DC-01, EE-04 Phelan, D: CE-08 Piao X: CA-01

Piao, X: CA-01 Piccolo, E: AR-10 Pilati, V: BB-04, FC-09

Piramanayagam, S: AF-07, ED-08

Pirro, P: DB-02 Pitt, W: DC-11 Pokhrel, H: DR-10 Pokhrel, K: EF-03 Polakovic, T: EE-04 Polkotuwa, P: BP-04-LB Pollard, S: DR-10 Poon, A: DG-05 Popov, M: DQ-09

Poree, V: CD-04

Porro, J: FG-13

Posti, R: CE-09, **FE-02**, FR-08 Pothuganti, J: AP-09-LB Poulo, A.S.: **DP-05**, FR-09

Poulo, A S.: **DR-05**, ER-09 Powalla, L: FD-08 Pradhan, G: DE-01 Pramanik, P: VP7-09 Prasad, B: BE-03 Prasad, K: EF-10 Prestwood, D: GE-08 Priese, C: BD-03 Proscia, N: EF-05 Provino, A: BE-10 Psaroudaki, C: BP-06 Puebla-Hellmann, G: CG-01 Puente-Orench, I: AE-12

Pulickel M., A: AE-10 Pulse, M: CD-05

Pufall, M: DD-07, GE-01

Puthirath Balan, A: AE-10, FE-04

Pyo, J: FG-08

Q

Qian, S: **EC-04** Qin, Y: **VP1-02** Qiu, J: VP5-05

Qu, D: DR-11, **GF-01**, GF-02

Quirós, C: BC-12 Qureshi, P: EF-03

R

Raabe, J: DB-02 Rackham, J: DC-12 Radhakrishnan, S: AE-10 Radnoczi, G Z.: DD-01 Rado, J: DQ-09

Radu, F: EF-02 Radulov, I: DD-01

Raftrey, D W.: DC-02, DC-04

Rahaman, H: ED-08 Rahman, R: CH-09 Rai, R K.: EF-06 Raimondo, E: **DA-04**

Rajib, M: CH-03, DF-05, FF-03

Rajnak, M: CQ-04 Rajput, S: **VP6-21** Rakheja, S: EC-04 Ralph, D C.: FD-08, FE-01

Ramos, L: **CR-13** Ramu, M: AF-07, ED-08

Rana, K: **DG-10**

Rao, S: BC-14, BF-06, CA-01, GD-07

Raskin, J: FC-09

Ravelosona, D: AD-09, BR-12, CD-03,

CG-03, GD-06

Ravelosona, D: CD-04, FG-11

Ray, S: EF-03 Raznjevic, S: CH-07 Reddinger, J A.: **GE-05** Reddy, V: AR-01 Redondo, C: FG-13 Redwing, J M.: FE-11 Reese, B L.: EG-04

Regmi, A: GP-02-LB, GP-08-LB

Rego, S: BG-02 Rehm, L: XA-03

Reichlova, H: EB-02, GF-04

Reif, D D.: BE-08 Reisbick, S: CG-07 Reiser, P: FE-04

Reisinger, J: BR-09, BR-10

^{*} Best Student Presentation Finalist / LB – Late-breaking Poster

Reiss, D: GG-13
Reiss, G: GF-04, GF-05
Remy, Q: EG-09
Ren, Z: GC-08
Renucci, P: AA-01
Reparaz, J: EF-01
Resta, A: AD-09, CD-04
Retterer, S: CD-08
Reyes-Osorio, F: EE-11
Reyren, N: CG-03
Reza, S: VP5-04

Rezaei, B: AQ-06, CQ-06, CQ-07

Reznik, A: DQ-09 Rhensius, J: CG-01 Rial, J: EB-02 Richards, D: BD-07 Richter, H J.: BF-03 Rickhaus, P: DC-03 Riho, N: **VP4-01** Riley, C R.: BD-07 Rinaldi, C: **ED-01** Río-López, N: FG-13 Riso Barbosa Jr., J: BE-08

Rivard, C: EE-08

Rivas, M: **BB-04**, FC-09

Rivkin, K: BR-01, CG-09, DR-14, EC-

06, EG-11, EG-13 Robb, D T.: GQ-10-LB Robbins, M: XA-03 Rockwell, K: BC-09 Rodrigues, C L.: DQ-04 Rodrigues, D: AR-10 Rodriguez, R: ED-07

Rodríguez Gutiérrez, H: CR-13, DC-10,

FG-02, FR-10 Rogers, D: **AE-02** Rogers, E: FF-07

Rogers, W: GG-11, GP-04-LB Rojas-Sanchez, J: AA-01 Rondinelli, J M.: GP-04-LB

Ropers, C: EA-05 Rosenkranz, S: CE-08 Ross, C A.: BC-11, CH-03

Ross, F: GG-05

Roussigné, Y: AD-09, CD-04

Royillain, P: EC-11 Roy, D: AF-02 Roy, S: **ER-13-LB** Roy, S: FB-05, GE-06 Roy, T: GG-03 Roy, X: FE-01

Roy Chowdhury, M: VP7-09

Roy Chowdhury, R: AP-04, AR-08, CR-14, DC-10, FE-03, GD-08, GR-11

Rozhansky, I: GE-09 Ruiz Gómez, S: CD-01 Rushforth, A: CG-11 Russell, D: CE-07 Rüßmann, P: AC-08 Russo, V: DB-02

Š

Šmejkal, L: CG-11 Šturm, S: CH-07

S

Sa, J: FC-03

Sabyasachi, S: FF-03 Sadeghi, Z: CC-04 Sadler, C: CD-05, **DQ-10** Sadowski, J: BC-11 Safranski, C: XA-03 Sagar, D: BG-06 Sagara, K: VP4-10 Saha, S: **DE-10** Sahoo, M: DC-06 Sahoo, T: CD-08 Sai, R: **BD-08** Sain, R: **DC-06**

Saito, S: BR-04, BR-05, CR-04

Saito, T: **VP3-02**

Sait, C: CH-06

Saito, Y: AF-10, ED-05, GF-06, VP7-01

Saitoh, E: BC-03, GE-08 Sajerman, K: DD-01 Sajti, S: DD-01 Sakai, L: BR-08

Sakai, T: VP2-02, VP2-03, VP2-04

Sakamoto, S: **BA-04** Sakhya, A: AG-03

Sakuraba, Y: CB-05, EG-08

Sakurai, J: CQ-02 Salama, S: GD-01 Salameh, B: FQ-08 Salazar, H T.: **BC-02** Salazar, H: GC-03

Salvador, M: BB-04, FC-09

Samal, D: DQ-08

Samanta, K: CE-04 Samanta, T: BC-07 Samarth, N: **CE-06** Sampson, E: EC-07 Sánchez, S P.: CR-12 Sanchez Hazen, D: BF-09 Sanchez-Ochoa, F: **FE-09** Sánchez-Tejerina, L: VP7-06

Sands, J: DC-02 Sankar, R: AC-12 Sankaran, K: CA-01 Santhosh, P: DQ-08 Santiso, J: GF-04 Santos, A D.: VP6-04

Santos, T: AF-05, BF-03, BF-04

Sanyal, B: GB-04

Sanz Hernandez, D: DC-01

Sarkar, T: VP7-09 Sarker, S: **CH-03** Sasaki, D: CD-08 Sasaki, S: BR-08

Sasaki, S: BQ-06, VP4-10

Sasaki, T: CB-05 Sasaki, Y: EG-06

Sassi, Y: BR-12, **CG-03**, **GD-06** Satapathy, S: DC-02, DC-04 Sato, F: BO-06, VP4-07, VP4-10

Sato, K: **CR-03**Sato, K: AQ-07
Sato, Y: AD-05, DF-08
Sato, Y: BA-02, **GF-10**Satoh, T: VP7-05
Satynska, L: **GQ-10-LB**Savero-Torres, W: EF-01
Savostin, E: **EC-05**Sawruk, E: AQ-10

Saxena, A: **AQ-01**Sayed, S: GG-11
Scafuri, L A.: DC-05

Schaeffer, K: **DQ-02**, DQ-03

Schäfer, S: GE-10 Schäfermeier, C: CG-01 Schäffer, M: CC-02 Schandler, L: AP-05 Schanen, R: GR-13-LB Scharf, P: BF-09 Scheffler, D: GF-04

Scheiblhofer, S: BR-09, BR-10

Scheike, T: CB-04

^{*} Best Student Presentation Finalist / LB - Late-breaking Poster

Schieffer, P: CD-09 Schlaphof, F: BF-09 Schlitz, R: GG-13

Schlueter, C: CR-09, FG-04

Schmidt, G: GG-12 Schmidt, T: EA-05 Schmitt, T: GC-09

Schmoranzerova, E: EB-02, GF-04, GG-

13

Schmoranzerová, E: **CC-04**Schneider, M: DD-07
Schnitzer, N: BG-02
Schoener, B: **AE-05**Schöffmann, P: AD-09
Schorr, L: **CQ-03**Schrefl, T: BE-07, CH-07
Schulz, N: AR-08, FG-02, GQ-03
Schuster, S: BR-09, BR-10
Schweizer, M R.: EE-12

Seagar, A: DG-07 Seal, A: AG-03 Seehra, M S.: VP7-09 Seifert, T: GF-05 Seino, S: ER-05, GQ-02 Sekertekin, Y: **DE-05**

Scott, J N.: CH-10

Scott, J: BR-03, CH-06

Scott-Vandeusen, A: BB-03

Sekino, M: BB-05, FC-01, FC-04, FC-

06, FC-07, FP-01 Sepehri-Amin, H: EG-05 Serga, A A.: EE-12

Serpico, C: CH-08, EC-12, EE-09

Seth, S: ER-13-LB

Setti, G: AE-06, AE-08, DE-03

Severo, J H.: VP6-04 Sha, Y: VP3-06

Shabir, M: VP1-06, VP5-01

Shah, H: FC-12 Shahbaz, R: VP4-18 Shahee, A: DF-01 Shaji, M: DG-12 Shalabi, J: DG-03 Shand, P: CD-05, DQ-10 Shang, W: FC-01 Shao, D: GF-07 Shao, Q: BP-05-LB Shapiro, D: CG-05

Sharma, A: VP7-12

Sharma, A: **AR-01** Sharma, A: EC-11 Sharma, M: CR-11, FP-08 Sharma, P: **EC-07**

Sharma, P: CR-14, GD-08, GR-11

Sharma, V: **DG-13**Sharma, V: FR-09
Sharma, V: CH-05
Shashank, U: AF-08
Shearer, B: CG-05
Sheikh, R R.: **VP1-01**Sheikh, S: AG-06, EF-06

Shen, K: ED-10 Shen, L: **FB-05** Shen, Z: GF-01, GF-02 Shepelytskyi, Y: DQ-09 Shick, A B.: **VP2-05**

Shield, J: BG-06, DD-13, ER-01

Shiga, M: BA-04 Shigematsu, N: BR-13 Shigeta, I: **GR-06** Shiku, K: **BR-13** Shima, Y: **CR-01** Shimizu, K: EC-08 Shinoda, T: DF-11 Shinohara, R: CQ-05 Shinwari, T: **EF-02**, **FE-11**

Shiota, Y: ED-05 Shirai, M: GG-03

Shiraishi, M: DR-04, FR-01 Shiraishi, T: AD-05 Shotbolt, M: BB-03 Shukla, A: EC-04

Shukla, G K.: **AF-03**, FR-05

Shukla, S: BD-06 Si, P: ER-04 Sierra, J F.: **EF-01** Silber, R: CC-02 Silva, T: BC-09 Silvani, R: DB-02 Silva Teixeira, C: BE-08

Sim, M: CG-06 Simalaotao, K: EG-08 Simon, M: DG-13 Simons, C: GF-05 Singh, A: GF-01, GF-02 Singh, D K.: GR-08 Singh, H: VP7-09 Singh, M: FG-04 Singh, P: DQ-01 Singh, R: FE-03 Singh, S: **VP6-01** Singh, S: **CE-09**, FE-02 Singh, U: BE-03 Sinova, J: EB-02

Sklenar, J: BP-09, DQ-05, FG-10, GE-04

Skobjin, G: EB-02 Skoric, L: DC-01 Skorvanek, I: **BD-12** Skowronski, W: **BF-05** Slavin, A N.: DR-13

Sivis, M: EA-05

Slezak, M: AC-07, CE-03, **FG-07** Slezak, T: AC-07, CE-03, FG-07

Smejkal, L: EB-02 Smekhova, A: CE-09 Smith, D A.: FD-01 Smith, I M.: BG-05, ER-06

Smith, S: GQ-01 Snijder, S: CD-06 Snowden, I: CD-08 Snyder, J: **BG-07** Snyder, K: BG-05, ER

Snyder, K: BG-05, ER-06 Sobucki, K W.: **AR-07** Sofer, Z: GG-05 Soh, Y: **EF-07**, **GC-09**

Solignac, A: AD-09, CD-03, CD-04

Somavarapu, S: GD-03

Son, K: DR-03 Song, M: FF-08, GG-11 Song, Y: **BC-11** Song, Y: **BG-03**, **ER-04** Sonkusale, S: DE-05

Sorrentino, A: BC-12, DC-02, DC-04

Sort, J: CD-01, CD-03 Soss, S: BF-09

Sorée, B: BC-14

Soumyanarayanan, A: AC-11, CG-06

Sousa, D: BF-01 Sousa, R: ED-02 Spanopoulos, I: GR-10 Spasojević, I: **CD-01** Spassov, S: FC-09 Spencer, B: FQ-10 Spraque, M: AG-03

Srikanth, H: AP-04, AP-07, AR-08, CR-14, DC-10, FG-02, GD-08, GR-04, GR-

11

^{*} Best Student Presentation Finalist / LB – Late-breaking Poster

Srinivasan, K: BD-11 Srivastava, A: AC-05 Sršan, V: CH-07 Stach, E A.: EF-06 Stadler, B: BD-09, GO-07 Stamenov, P S.: AG-05 Stamenova, M T.: AG-05 Stanescu, S: DC-01 Staruch, M: GQ-01 Stenning, K D.: DB-01 Stephen, G M.: FR-09 Stevenson, P: AD-08 Stiles, M: FF-03

Stimpson, E: BP-09, FG-10 Stoeffler, D: EC-11 Stoffel, M: AA-01 Straßburger, J: BC-07 Street, G T.: AF-06, **DF-07**

Ström, P: DE-07 Su, C: VP5-04 Su, L: FD-07 Su, Z: VP4-04

Suarez-Blanco, P: BC-12 Subedi, M M.: GE-04 Subhani, N: DG-07 Sud, A: DF-06 Sudo, R: AR-12

Sugimoto, S: **DF-10**, FR-06

Suh, P: **BC-01**

Sukegawa, H: CB-04, XA-02 Sullivan, C: **GG-06**, GG-10 Sultana, R: DB-01, **EE-02** Sultana, S: BQ-03

Sumi, S: **DR-01**

Sumiyoshiya, A: FR-05

Sun. C: ED-04 Sun, D: GR-12 Sun, G: VP6-15 Sun, H: VP5-05 Sun, H: VP3-01 Sun, R: GR-12 Sun, S: BC-02, GC-03 Sun, Y: BQ-07 Suto, H: CB-05

Suwa, T: **AQ-02** Suwannaharn, N: CB-05 Suzuki, H: VP2-03, VP2-04

Suzuki, I: EG-05 Suzuki, K: GG-03 Suzuki, R: EE-13 Suzuki, Y: AC-09 Suzuki, Y: BP-03 Svec, P: BD-12 Svec ir., P: BD-12 Svetlik, J: EF-01 Swierkosz, E: FG-07

Swindells, C: **DD-07**, **FF-10**, **GE-01**

Syed, M: **VP5-04** Syskaki, M: AD-09, CD-04 Szilagyi, E O.: DD-01 Szpytma, M: CE-03, FG-07

Т

Tabata, H: FC-06

Tabata, T: BD-02, **DD-03**

Tacchi, S: DB-02 Takagi, S: DF-03 Takahashi, R: FC-06

Takahashi, Y K.: DF-10, EG-05, EG-06

Takamura, Y: CD-08 Takano, K: EQ-08 Takashima, R: CH-04 Takasu, T: DG-08 Takeda, T: CF-11 Takeo, K: FG-05

Takeuchi, Y: AQ-04, AQ-07, CQ-01,

CQ-08

Takeuchi, Y: BA-02, GF-10 Talapatra, A: BF-09

Talatchian, P: DA-05, FF-04

Talleb, H: AD-03

Talmelli, G: BC-14, BF-06 Tamaru, S: BA-04, CR-01

Tan, H: CG-06 Tan. L: **VP6-16** Tan, W K.: FP-10 Tanabe, K: DR-01 Tanahashi, K: EG-03

Tanaka, M: CF-11, DF-08, FE-10

Tanaka, S: BP-04-LB Tandon, T: AG-06, EF-06 Tang, J: GP-02-LB, GP-08-LB

Tang, N: GE-06

Tang, W: DD-08, **DD-14** Tanigawa, I: FP-10 Taniquchi, T: FE-01 Taniwaki, M: FR-03 Taniyama, T: FD-04, FR-07 Taniyasu, Y: DF-08 Tanksalvala, M: GE-01

Tao, Y: CE-08 Tapon, I: DG-12 Tashli, M: FC-10 Tatetsu, Y: BG-09 Tavabi, A: GE-10 Taylor, PJ.: FR-09 Taylor, T J.: **AP-06**, FC-11

Teano, E: CD-08

Temst, K: BC-14, BF-06, GD-07

Tener, Z: DD-11

Terada, S: BD-02, DD-03

Terry, K: VP7-03 Tey, M N.: GP-04-LB Tezuka, N: VP7-01 Thakur, A: DG-10 Tham, K: **BR-04**, BR-05

Thareja, E: AC-03, AC-04, GF-03, GP-

01-LB

Thayer, A: DQ-01 Thiaville, A: GD-01 Thibaudeau, P: FQ-09 Thomas, A: EB-02 Thomas, W C.: FD-01 Thompson, T: DG-01 Thomson, T: FO-10 Thota, S: VP7-09 Tian, J: BB-03

Tiberto, P: CD-01, DE-01

Tian, W: AG-06

Tien, Y: GF-01 Tiwari. A: CE-09 Tiwari, B: EF-10 Tiwari, S: VP6-21 Tiwary, C: AE-10 Tkacik, S: GF-03 To, D: **EP-08-LB** Tobise, M: CR-04 Tohtake, S: FC-08 Toko, M: CH-04 Tomar, M: DG-10 Tomasello, R: DA-04 Tonini. D: FR-04

Tonthat, L: AP-03, FC-08

Töpfer, J: BD-03 Topolnicki, R: AR-13 Torres, J A.: DR-05, ER-09

Toyama, R: CB-05

^{*} Best Student Presentation Finalist / LB – Late-breaking Poster

Trampert, A: EF-02, FE-11 Wang, J: AA-01, AD-04, AR-03, BD-07, Vattathurvalappil, S: CF-06 Tran, T: CA-01 Vayalil, S K.: FG-04 **BF-01**, BR-11, CD-10, DR-02, ER-10, Trapanese, M: DG-09, FP-05 Vecchiola, A: GD-01 FR-04, GR-09 Tretiakov, O: FE-03 Vedmedenko, E Y.: EC-14 Wang, J: FD-07 Trevillian, C: DR-13 Vega, M: AP-07, BR-07 Wang, J: DD-14 Tripathi, A: FR-08 Veiga, L: EF-11 Wang, J: **VP6-06**, VP6-09 Tromer, R: FG-02 Veis, M: CC-02 Wang, P: AC-05, AE-02, GO-08 Trouilloud, P L.: XA-03 Vekhter, I: GP-01-LB Wang, Q: BQ-05 Tsai, F: BG-10 Velez, M: BC-12 Wang, Q: AB-03 Tsai, H: ED-11 Velic, A: EF-06 Wang, S X.: DG-05 Tsai, L: AC-12 Venkat, G: FF-10 Wang, Y: BQ-09 Tsai, Y: BC-02, GC-03 Venner, A: CD-05 Wang, Y: EF-05 Tsuchida, T: VP7-05 Vergnat, M: AA-01 Wang, Y: VP4-08 Tsujikawa, M: GG-03 Verma, M: CF-02 Wang, Y: CD-09 Vermeulen, B: BC-14, BF-06 Tsunoda, M: CR-10 Wang, Y: GF-01, **GF-02** Tsymbal, E Y.: **BA-01**, CE-04, EF-10, Viala, B: ED-02 Wang, Y: DR-08 GF-07, GP-04-LB Victora, R H.: CB-03, EG-02, EG-07 Wang, Z: GC-08 Tucker, T D.: AG-06 Vidamour, I T.: FF-10 Wang, Z: VP3-01 Tumbleson, Z: FB-05 Wang, Z: GC-08 Vilas-Vilela, J: DG-12 Turnbull, L: FP-07 Villar, A: FG-13 Wang, Z: **VP4-15** Turner, J J.: FB-05 Vitali, M: DB-02 Waring, H J.: FQ-10 Tutt, F: CE-08 Vitor de Faria, P: BE-08 Watanabe, K: FE-01 Tyaqi, P: CD-09 Vitos, L: CR-02 Watanabe, K: DR-06 Tyberkevych, V: DR-13 Vodungbo, B: EA-03 Watt, J: EF-10 von Freymann, G: EE-12 Webb, C M.: **EC-01** Vourna, X: AQ-09 Weber, J T.: GE-10 Uchimura, T: BA-02, GF-09 Vu, D: GF-06 Weck, PF.: BD-07 Uchiyama, T: DG-06 Wei, G: BD-08 Udapudi, PJ.: FC-10 W Wei, M: CC-05 Uddin, M: BG-10 Wachs, R: CR-05 Wei, Y: VP4-04 Ueda, Y: **BQ-01** Wada, K: EQ-08 Weigand, M: FD-08 Ueno, T: AR-12 Wade, J: ER-14-LB Weiler, M: EE-12 Ukleev, V: EF-02 Wadley, P: CG-02, CG-11, **EB-01** Weir, VJ.: AP-05 Welp, U: DE-06, EE-04 Umetsu, R: GR-06 Wadumesthri, Y: CR-13, DC-10, FG-02, FR-10 Upadhyay, C: DC-06 Wenliang, Z: GC-09 Upadhyaya, P: FE-06, GP-04-LB Wagatsuma, H: DG-01 Whittier, E: FC-02 Wakabayashi, K: CR-03 Wilgocka-Slezak, D: CE-03 Wakabayashi, Y K.: DF-08 Will-Cole, A R.: DE-04 Vaczi, T: DD-01 Wallace, P: DG-05 William, MM.: AP-05 Valenzuela, S O.: EF-01 Walters, A: FP-07 Winkler, R: ED-13 van den Berg, A: DC-03 Wan, L: AF-05, GP-04-LB Wintz, S: BP-03, FD-08 van der Laan, G: CH-06, EF-11 Wan, Z: VP4-12 Wisser, J J.: DD-07, FD-06, GE-01 van Dijken, S: GD-06 Witanachchi, S: CR-14, DQ-06, GR-11 Wang, C: **FF-07** Van Houdt, J: GD-07 Wang, C: AQ-08 Withrington, J: DG-01 Vanstone, A: DB-01 Wang, H: **GB-02** Wöckinger, D: BR-09, BR-10 Wang, H: GD-04 Wohlrath, V: CC-04 Varma, Y: DD-14 Varshney, K: AF-02 Wang, H: BO-05 Wojnar, T: AE-05

Wang, J: VP4-03

Wang, J: EF-10

Vas, J: FE-04

Vasyuchka, V I.: EE-12

Wolf, B: ER-10, GR-09

Wolf, M: GG-13

^{*} Best Student Presentation Finalist / LB - Late-breaking Poster

Woltersdorf, G: GG-13 Yamane, I: DG-01 Yu, X: AG-04 Woo, D: AF-04, GP-09-LB Yamane, Y: BA-02, GF-10 Yuan, J: AQ-08, BQ-05, BQ-07, BQ-09, Wood, G: EF-11 Yamanoi, K: DF-03 BO-10, CR-06 Worledge, D: XA-03 Yamanouchi, M: DF-08 Yuan, L: GP-04-LB Wrona, J: BF-05, CD-04 Yamashita, S: AR-12 Yuan, Z: **FD-05** Wu, A: FD-07 Yamauchi, T: GR-06 Yue, S: VP4-12 Wu, J: GP-10-LB, **GR-12** Yamazaki, A: CO-05 Yunker, B: CF-07 Wu, K: AQ-05, AQ-06, AR-05, CF-07, Yamazaki, T: CR-01 Yutaka, H: BR-08 CQ-06, **CQ-07**, FC-05 Yanaqihara, H: FG-05 Wu, L: **VP4-09**, VP6-10 Yang, B: GP-10-LB Z Wu, Q: CR-06 Yang, B: VP6-08 Zajac, M: FG-07 Wu, S: FB-03 Yang, B: BP-02, EE-07 Zaka, A: BF-09 Wu. S: ED-10 Yang, F: **CE-07**, GP-08-LB Zakharov. A: CG-11 Wu, S: FD-01 Yang, F: AQ-08 Zalewski, T: CH-01 Wu, X: AQ-05, CF-07 Yang, G: **EB-03** Zappala, E: CE-08 Wu, Y: **TU-01** Yang, H: AP-10-LB, EP-05-LB Zarzuela, R: GE-11 Wu, Y: GG-13 Yang, J: FC-06 Zayko, S: EA-05 Yang, J: **VP3-01** Zázvorka, J: GF-04 Χ Yang, J: FE-04 Zeng, H: AE-05 Xiao, F: AQ-08 Yang, L: GD-04 Zeng, L: VP1-02, VP6-06, VP6-07, VP6-Xie, B: AC-11 Yang, M: BC-13, ED-10 08, VP6-09, VP6-11, VP6-12, VP6-20 Xie, H: **VP4-03** Yang, S: **AG-04** Zeng, W: AC-09 Xie, Z: VP6-20 Zeng, X: VP5-05 Yang, W: GC-08 Xiong, J: AE-05 Yang, Y: AD-04, BF-01, CD-10, FR-04 Zhang, B: BG-03, ER-04 Xiong, Y: GE-04, GP-10-LB Yang, Z: **VP1-03** Zhang, C: VP4-15, VP4-17, **VP4-18**, **VP6-15** Xu, B: AA-01 Yang, Z: DG-03 Xu, D: BO-04, FP-04, VP4-06 Yao, W: DG-07 Zhang, C: DR-08 Xu, K: EF-01 Zhanq, D: AQ-08, BQ-07 Yapaskurt, V: AE-12 Xu, Y: **VP5-05** Yazdi, S: CG-05 Zhang, D: CD-10 Xue, F: **DF-04**, EF-09 Ye, Z: VP4-08 Zhang, D: VP3-01 Yemeli, I N.: CH-08 Zhang, E: BB-03 Υ Yenugonda, V: DQ-02, DQ-03 Zhang, E: BP-02, **EE-07** Yabukami, S: AP-01, AP-02, AP-03, Yin, G: BG-01, DC-02, DC-04 Zhang, H: VP4-18 CQ-05, FC-08 Yin, H: **FG-01** Zhang, H: BG-01 Yin, Z: AC-05 Yabushita, K: VP7-05 Zhang, M: VP3-03 Yadav, P: GR-02 Yokoi, K: DG-01 Zhang, N: VP6-12 Yadav, S: FR-06 Yokota, N: AA-05 Zhang, R: ED-06 Yahaqi, Y: ED-05 Yonaga, A: ER-05 Zhang, S: EC-08 Yakushiji, K: BA-04 Yoo, J: FG-08 Zhang, S: VP6-07 Yamada, H: FC-06 Yoo, M: DF-09, FQ-02 Zhang, S: EC-01 Yamada, T: CQ-01 Yoon, J: BA-02 Zhang, T: **VP4-02** Yamaquchi, T: EQ-08 Yoon, S: AF-04, GP-09-LB Zhang, W: BQ-07 Yoon, S: **VP6-17** Yamaguchi, W: BG-12 Zhang, W: GE-04, GP-10-LB, GR-12 Yamahara, H: FC-06 Yoshida, Y: DF-06 Zhang, X: GP-06-LB Yamamoto, H: DF-08 Yoshimoto, T: CR-08 Zhang, X: GD-04 Yamamoto, H: BD-01 Yousuf, S: GR-01 Zhang, X: AA-02 Yamamoto, M: FR-01 Yu, C: CB-02 Zhang, X: ER-12 Zhang, Y: CE-08 Yamamoto, S: BD-01 Yu, G: BF-01

Yu, W: AP-09-LB

Yamamoto, T: BA-04

Zhang, Y: VP4-02, VP4-03

^{*} Best Student Presentation Finalist / LB - Late-breaking Poster

Zhang, Y: GP-06-LB

Zhang, Z: FD-07, GR-05

Zhang, Z: **GQ-05**

Zhang, Z: FD-07

Zhao, J: FD-01

Zhao, M: FD-08

Zhao, S: **VP4-17**

Zhao, T: VP7-03

Zheng, K: VP4-02

Zheng, S: **EG-01**

Zheng, T: **BP-02**, EE-07

Zheng, X: BG-03, ER-04

Zheng, Y: AD-03

Zhou, B: **AB-01**

Zhou, ET.: GE-04

Zhou, H: AQ-08, BQ-05, BQ-07, BQ-09,

BO-10, CR-06

Zhou, J: **AC-11**, **FF-01**

Zhou, J: GB-02

Zhou, S: **GP-10-LB**, GR-12

Zhou, W: FD-08

Zhou, Y: AD-06

Zhou, Z: GC-08

Zhou Hagström, N: BC-09

Zhu, E: BB-03

Zhu, J: BP-02, EE-07, EG-04, FF-05

Zhu, T: FC-04, FP-01

Zhu, Y: CG-07

Zhu, Y: DG-07

Zhuang, Y: VP4-02

Zhukovskyi, M: CE-05

Zink, B L.: **GF-08**

Zink, B: AD-04, BF-01, CD-10

Zolla, H G.: **CB-02**

Zolnai, Z: DD-01

Zülicke, U: ED-13

Zuo, H: AR-05

Zuo, J: VP3-03

Zuo, J: EE-04, GQ-05

Zuo, L: VP3-06

Zutic, I: AA-01, AE-05

Zuzek Rozman, K: CH-07

Zygiridis, T: DG-11

^{*} Best Student Presentation Finalist / LB - Late-breaking Poster